Data-Driven Construction of an Imine Reductase Library Capable of Broad-Scope Reductive Amination at Equimolar Substrate Concentrations

Sarah A. Berger, Christopher Grimm, Marco Cespugli, Andreas Krassnigg, Tobias Schopper, Irene Marzuoli, Isabel Oroz-Guinea, Stephan Vrabl, Lukas Roemer, Melanie A. Weber, Fabian M. Kulier, Yuliya Orel, Bettina M. Nestl, Christian C. Gruber, Georg Steinkellner, Serena Bisagni, Francis Gosselin, Hans Iding, Kurt Puentener, Dennis Wetzl, Wolfgang Kroutil, Joerg H. Schrittwieser*

*e-mail: joerg.schrittwieser@uni-graz.at

Supplementary Information

Contents:

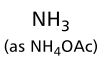
Table of Screening Substrates 2
Supplementary Data 3
- Chemoinformatic Analysis of the Substrate Panel 3
- Bioinformatic Analysis of the IRED Panel 10
- Activity Prediction Using Machine-Learning Models 15
- Selection of Enzymes for the Diversification Screening 19
- Protein Sequence–Activity Analysis 20
- Protein Structure–Activity and Structure–Selectivity Analysis 26
- Biotransformations 36

Supplementary Methods 57
- Tabular Overview of Screening Phases 57
- Chemoinformatic Analysis of the Substrate Panel 58
- Bioinformatic Analysis of the IRED Panel 58
- Activity Prediction Using Machine-Learning Models 60
- Protein Sequence/Structure–Activity and Structure–Selectivity Analysis 60
- Sequence Selection, Gene Synthesis, and Subcloning 61
- Preparation of Biocatalysts 65
- Determination of Expression Level 66
- Photometric IRED Activity Assay: Overview Screening 69
- Photometric IRED Activity Assay: Diversification Screening 73
- FIA–MS Activity Assay: Diversification Screening 76
- Data Transformation for Generating z-Score Heatmaps 81
- Synthesis of Reference Compounds 83
- Analytical Methods 129

NMR and MS Spectra 235
Supplementary References 386

Table of Screening Substrates

Overview Screening



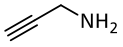
a1



a2



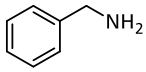
a3



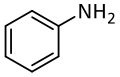
a4



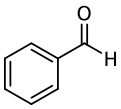
a5



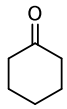
a6



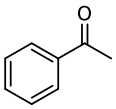
a7



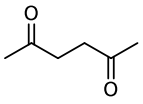
c1



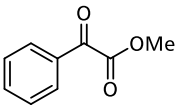
c2



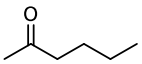
c3



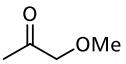
c4



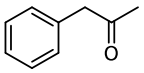
c5



c6

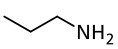


c7

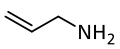


c8

Diversification Screening: Amine Scope



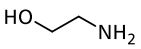
a8



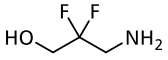
a9



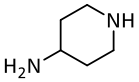
a10



a11



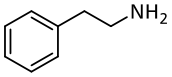
a12



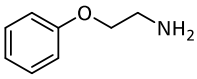
a13



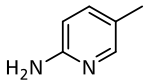
a14



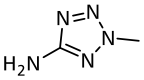
a15



a16



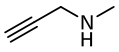
a17



a18



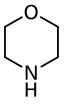
a19



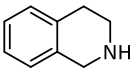
a20



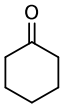
a21



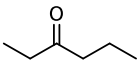
a22



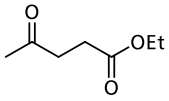
a23



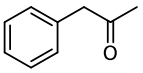
c2



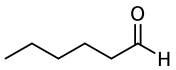
c9



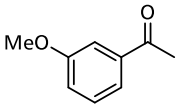
c10



c8



c11

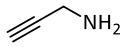


c12

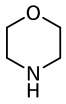
Diversification Screening: Carbonyl Scope



a2



a4



a22

a24

c13

c14

c15

c16

c17

c18

c19

c20

c21

c22

c23

c24

c25

c26

c27

c28

c29

c30

c31

c32

c33

c34

c35

c36

Supplementary Data

Chemoinformatic Analysis of the Substrate Panel

To identify representative screening substrates, 191 compounds (137 carbonyls and 54 amines, comprising 136 literature-known IRED substrates and 55 additional structures of interest; see Table S1) were subjected to chemoinformatic diversity analysis.

Table S1. Amines and carbonyls subjected to chemoinformatic analysis (*continued on next pages*).

IUPAC name	SMILES	CAS number
Ammonia	N	7664-41-7
Methanamine	CN	74-89-5
Ethanamine	CCN	75-04-7
Propan-1-amine	NCCC	107-10-8
Butan-1-amine	NCCCC	109-73-9
Propan-2-amine	CC(N)C	75-31-0
Butan-2-amine	NC(CC)C	33966-50-6
2-Methylpropan-1-amine	NCC(C)C	78-81-9
2-Methylpropan-2-amine	NC(C)(C)C	75-64-9
Prop-2-en-1-amine	NCC=C	107-11-9
Prop-2-yn-1-amine	NCC#C	2450-71-7
Cyclopropanamine	NC1CC1	765-30-0
2-Aminoethan-1-ol	NCCO	141-43-5
3-Amino-2,2-difluoropropan-1-ol	NCC(F)(F)CO	155310-11-5
Cyclohexanamine	NC1CCCCC1	108-91-8
Ethane-1,2-diamine	NCCN	107-15-3
Hexane-1,6-diamine	NCCCCCCN	124-09-4
2-Methylpentane-1,5-diamine	NCCCC(C)CN	15520-10-2
Dimethylamine	CNC	124-40-3
N-Methylethanamine	CCNC	624-78-2
Diethylamine	CCNCC	109-89-7
N-Methylprop-2-yn-1-amine	CNCC#C	35161-71-8
N-Methylprop-1-yn-1-amine	CNC#CC	90990-89-9
Pyrrolidine	C1CNCC1	123-75-1
Piperidine	C1CNCCC1	110-89-4
4-Methylpiperidine	CC1CCNCC1	626-58-4
Morpholine	C1CNCCO1	110-91-8
Azepane	C1CNCCCC1	111-49-9
Piperidin-4-amine	NC1CCNCC1	13035-19-3
Phenylmethanamine	NCC1=CC=CC=C1	100-46-9
Thiophen-3-ylmethanamine	NCC1=CSC=C1	27757-86-4
2-Phenylethan-1-amine	NCCC1=CC=CC=C1	64-04-0
2-Phenoxyethan-1-amine	NCCOC1=CC=CC=C1	1758-46-9
1,2,3,4-Tetrahydroisoquinoline	C12=CC=CC=C1CCNC2	91-21-4
2-Phenylcyclopropan-1-amine	NC1CC1C2=CC=CC=C2	54-97-7
Aniline	NC1=CC=CC=C1	62-53-3
2-Aminophenol	NC1=C(O)C=CC=C1	95-55-6
2-Methoxyaniline	NC1=C(OC)C=CC=C1	90-04-0
3-Methoxyaniline	NC1=CC(OC)=CC=C1	536-90-3
3-Methylaniline	NC1=CC(C)=CC=C1	108-44-1
4-Aminophenol	NC1=CC=C(O)C=C1	123-30-8
4-Methoxyaniline	NC1=CC=C(OC)C=C1	104-94-9
4-Chloroaniline	NC1=CC=C(Cl)C=C1	106-47-8
4-Nitroaniline	NC1=CC=C([N+]([O-])=O)C=C1	100-01-6
Benzene-1,4-diamine	NC1=CC=C(N)C=C1	106-50-3

Table S1. Amines and carbonyls subjected to chemoinformatic analysis (*continued from previous page*).

IUPAC name	SMILES	CAS number
3-Methylaniline	NC1=CC(C)=CC=C1	108-44-1
4-Aminophenol	NC1=CC=C(O)C=C1	123-30-8
4-Methoxyaniline	NC1=CC=C(OC)C=C1	104-94-9
4-Chloroaniline	NC1=CC=C(Cl)C=C1	106-47-8
4-Nitroaniline	NC1=CC=C([N+]([O-])=O)C=C1	100-01-6
Benzene-1,4-diamine	NC1=CC=C(N)C=C1	106-50-3
2,6-Difluoro-4-methylaniline	NC1=C(F)C=C(C)C=C1F	1379028-84-8
4-Bromo-2,6-difluoroaniline	NC1=C(F)C=C(Br)C=C1F	67567-26-4
Pyridin-3-amine	NC1=CN=CC=C1	462-08-8
Thiophen-3-amine	NC1=CSC=C1	17721-06-1
2-Methyl-2*H*-tetrazol-5-amine	CN1N=C(N)N=N1	6154-04-7
N-Methylhydroxylamine	CNO	593-77-1
N-Methylcyclohexanamine	CNC1CCCCC1	100-60-7
Cyclopentanamine	NC1CCCC1	1003-03-8
p-Tolylmethanamine	CC1=CC=C(CN)C=C1	104-84-7
Cyclobutanone	O=C1CCC1	1191-95-3
Cyclopentanone	O=C1CCCC1	120-92-3
Cyclohexanone	O=C1CCCCC1	108-94-1
2-Methylcyclohexan-1-one	CC1CCCCC1=O	583-60-8
2-Chlorocyclohexan-1-one	ClC1CCCCC1=O	822-87-7
2-Allylcyclohexan-1-one	O=C1C(CC=C)CCCC1	94-66-6
2-(Benzyloxy)cyclohexan-1-one	O=C1C(OCC2=CC=CC=C2)CCCC1	36713-55-0
3-Methylcyclohexan-1-one	O=C1CC(C)CCC1	591-24-2
3-Phenylcyclohexan-1-one	O=C1CC(C2=CC=CC=C2)CCC1	20795-53-3
4-Methylcyclohexan-1-one	O=C1CCC(C)CC1	589-92-4
4-Hydroxycyclohexan-1-one	O=C1CCC(O)CC1	13482-22-9
4-Aminocyclohexan-1-one	O=C1CCC(N)CC1	
4-Phenylcyclohexan-1-one	O=C1CCC(C2=CC=CC=C2)CC1	4894-75-1
3,3-Dimethyl-1,5-dioxaspiro[5.5]-undecan-9-one	O=C1CCC2(OCC(C)(C)CO2)CC1	69225-59-8
Benzyl 3-oxopyrrolidine-1-carboxylate	O=C1CCN(C(OCC2=CC=CC=C2)=O)C1	130312-02-6
tert-Butyl 3-oxopyrrolidine-1-carboxylate	O=C1CCN(C(OC(C)(C)C)=O)C1	101385-93-7
1-Benzyl-4-methylpiperidin-3-one	O=C1CN(CC2=CC=CC=C2)CCC1C	32018-96-5
Cyclohex-2-en-1-one	O=C1C=CCCC1	930-68-7
Cyclohexane-1,4-dione	O=C(CC1)CCC1=O	637-88-7
Cycloheptanone	O=C1CCCCCC1	502-42-1
Cyclooctanone	O=C1CCCCCCC1	502-49-8
Propan-2-one	CC(C)=O	67-64-1
Butan-2-one	CCC(C)=O	78-93-3
1-Hydroxybutan-2-one	CCC(CO)=O	5077-67-8
Pentan-2-one	CC(CCC)=O	107-87-9
3-Methylpentan-2-one	CC(C(C)CC)=O	565-61-7
4-Methylpentan-2-one	CC(CC(C)C)=O	108-10-1
Hexan-2-one	CC(CCCC)=O	591-78-6
Hexan-3-one	CCC(CCC)=O	589-38-8
Heptan-2-one	CC(CCCCC)=O	110-43-0
Heptan-4-one	CCCC(CCC)=O	123-19-3
Octan-2-one	CC(CCCCCC)=O	111-13-7

Table S1. Amines and carbonyls subjected to chemoinformatic analysis (*continued from previous page*).

IUPAC name	SMILES	CAS number
Octan-3-one	CCC(CCCCC)=O	106-68-3
Nonan-2-one	CC(CCCCCCC)=O	821-55-6
Decan-2-one	CC(CCCCCCCC)=O	693-54-9
1-Cyclohexylethan-1-one	O=C(C)C1CCCCC1	823-76-7
1-Methoxypropan-2-one	CC(COC)=O	5878-19-3
5-Chloropentan-2-one	CC(CCCCl)=O	5891-21-4
4-(2,6,6-Trimethylcyclohex-1-en-1-yl)-butan-2-one	CC(CCC1=C(C)CCCC1(C)C)=O	17283-81-7
4-(2,6,6-Trimethylcyclohex-1-en-1-yl)-but-3-en-2-one	CC(C=CC1=C(C)CCCC1(C)C)=O	14901-07-6
4-(2,6,6-Trimethylcyclohex-2-en-1-yl)-but-3-en-2-one	CC(C=CC1C(C)(C)CCC=C1C)=O	127-41-3
Hexane-2,5-dione	CC(CCC(C)=O)=O	110-13-4
Methyl 3-oxobutanoate	CC(CC(OC)=O)=O	105-45-3
Ethyl 3-oxobutanoate	O=C(OCC)CC(C)=O	141-97-9
Methyl 4-oxopentanoate	CC(CCC(OC)=O)=O	624-45-3
Ethyl 4-oxopentanoate	CC(CCC(OCC)=O)=O	539-88-8
Ethyl 5-oxohexanoate	O=C(OCC)CCCC(C)=O	13984-57-1
Methyl 4-methoxy-3-oxobutanoate	COC(CC(COC)=O)=O	41051-15-4
Ethyl 3-oxopentanoate	CCC(CC(OCC)=O)=O	4949-44-4
Ethyl 4-methyl-3-oxopentanoate	CC(C)C(CC(OCC)=O)=O	7152-15-0
Ethyl 3-oxohexanoate	O=C(OCC)CC(CCC)=O	3249-68-1
Ethyl 2-oxocyclopentane-1-carboxylate	O=C(OCC)C1C(CCC1)=O	611-10-9
Ethyl 2-oxocyclohexane-1-carboxylate	O=C(OCC)C1C(CCCC1)=O	1655-07-8
1-Phenylpropan-2-one	CC(CC1=CC=CC=C1)=O	103-79-7
1-(4-Fluorophenyl)propan-2-one	CC(CC1=CC=C(F)C=C1)=O	459-03-0
1-(4-Hydroxyphenyl)propan-2-one	O=C(C)CC1=CC=C(O)C=C1	770-39-8
1-(4-Methoxyphenyl)propan-2-one	O=C(C)CC1=CC=C(OC)C=C1	122-84-9
1-(4-Bromo-3-chlorophenyl)propan-2-one	CC(CC1=CC(Cl)=C(Br)C=C1)=O	
4-Phenylbutan-2-one	CC(CCC1=CC=CC=C1)=O	2550-26-7
1-Phenylbutan-2-one	O=C(CC)CC1=CC=CC=C1	1007-32-5
1-(1*H*-Indol-3-yl)propan-2-one	O=C(C)CC1=CNC2=CC=CC=C21	1201-26-9
1-(5-Fluoro-1*H*-indol-3-yl)propan-2-one	O=C(C)CC1=CNC2=CC=C(F)C=C21	
1,3-Dihydro-2*H*-inden-2-one	O=C1CC2=C(C=CC=C2)C1	615-13-4
3,4-Dihydronaphthalen-2(1*H*)-one	O=C1CCC2=C(C=CC=C2)C1	530-93-8
4,4-Diphenylbutan-2-one	CC(CC(C1=CC=CC=C1)C2=CC=CC=C2)=O	5409-60-9
2-Amino-4,7-dihydrobenzo[*d*]thiazol-6(5*H*)-one	O=C1CC2=C(N=C(N)S2)CC1	113030-24-3
1-Phenylethan-1-one	CC(C1=CC=CC=C1)=O	98-86-2
1-(4-Methoxyphenyl)ethan-1-one	CC(C1=CC=C(OC)C=C1)=O	100-06-1
1-(4-Nitrophenyl)ethan-1-one	CC(C1=CC=C([N+]([O-])=O)C=C1)=O	100-19-6
1-(3,5-Bis(trifluoromethyl)phenyl)-ethan-1-one	CC(C1=CC(C(F)(F)F)=CC(C(F)(F)F)=C1)=O	30071-93-3
2-Fluoro-1-phenylethan-1-one	FCC(C1=CC=CC=C1)=O	450-95-3
2-Fluoro-1-(4-fluorophenyl)ethan-1-one	FCC(C1=CC=C(F)C=C1)=O	369-41-5
1-(4-Chlorophenyl)-2-fluoroethan-1-one	FCC(C1=CC=C(Cl)C=C1)=O	329-78-2
1-(4-Bromophenyl)-2-fluoroethan-1-one	FCC(C1=CC=C(Br)C=C1)=O	403-30-5
2-Fluoro-1-(4-iodophenyl)ethan-1-one	FCC(C1=CC=C(I)C=C1)=O	369-42-6
2-Fluoro-1-(*p*-tolyl)ethan-1-one	FCC(C1=CC=C(C)C=C1)=O	37032-34-1

Table S1. Amines and carbonyls subjected to chemoinformatic analysis (*continued from previous page*).

IUPAC name	SMILES	CAS number
2-Chloro-1-phenylethan-1-one	O=C(CCl)C1=CC=CC=C1	532-27-4
2,2-Difluoro-1-phenylethan-1-one	O=C(C(F)F)C1=CC=CC=C1	395-01-7
2,2,2-Trifluoro-1-phenylethan-1-one	O=C(C(F)(F)F)C1=CC=CC=C1	434-45-7
2-Hydroxy-1-phenylethan-1-one	OCC(C1=CC=CC=C1)=O	582-24-1
1-Phenylpropan-1-one	O=C(CC)C1=CC=CC=C1	93-55-0
2,2-Dimethyl-1-phenylpropan-1-one	O=C(C(C)(C)C)C1=CC=CC=C1	938-16-9
3-Methyl-1-phenylbutan-1-one	O=C(CC(C)C)C1=CC=CC=C1	582-62-7
2,3-Dihydro-1*H*-inden-1-one	O=C1CCC2=CC=CC=C21	83-33-0
3,4-Dihydronaphthalen-1(2*H*)-one	O=C1C2=CC=CC=C2CCC1	529-34-0
Phenyl(*p*-tolyl)methanone	O=C(C1=CC=CC=C1)C2=CC=C(C)C=C2	134-84-9
1-(Naphthalen-1-yl)ethan-1-one	CC(C1=CC=CC2=CC=CC=C21)=O	941-98-0
Methyl 7-methyl-5-oxo-2,3,4,5-tetrahydro-1*H*-benzo[*b*]azepine-1-carboxylate	O=C(OC)N(CCC1)C2=CC=C(C)C=C2C1=O	
6,7-Dihydrobenzofuran-4(5*H*)-one	O=C1C(C=CO2)=C2CCC1	16806-93-2
Ethyl 3-oxo-3-phenylpropanoate	O=C(CC(OCC)=O)C1=CC=CC=C1	94-02-0
Ethyl 3-(3-fluorophenyl)-3-oxo-propanoate	O=C(CC(OCC)=O)C1=CC(F)=CC=C1	33166-77-7
Ethyl 3-(4-aminophenyl)-3-oxo-propanoate	O=C(CC(OCC)=O)C1=CC=C(N)C=C1	61252-00-4
Methyl 2-oxo-2-phenylacetate	O=C(C(OC)=O)C1=CC=CC=C1	15206-55-0
2-(4-Methoxyphenyl)-*N*-methyl-2-oxoacetamide	O=C(C(NC)=O)C1=CC=C(OC)C=C1	244264-57-1
1-(Pyridine-2-yl)ethan-1-one	CC(C1=NC=CC=C1)=O	1122-62-9
1-(Pyridine-3-yl)ethan-1-one	CC(C1=CN=CC=C1)=O	350-03-8
Ethanal	CC=O	75-07-0
Propanal	O=CCC	123-38-6
3,3,3-Trifluoro-2-methylpropanal	O=CC(C)C(F)(F)F	58928-28-2
3-Methoxy-2-methylpropanal	O=CC(C)COC	13141-08-7
2,3-Dihydroxypropanal	O=CC(O)CO	56-82-6
Butanal	O=CCCC	123-72-8
Pentanal	O=CCCCC	110-62-3
2-Methylpentanal	O=CC(C)CCC	123-15-9
Hexanal	CCCCCC=O	66-25-1
Heptanal	O=CCCCCCC	111-71-7
Octanal	O=CCCCCCCC	124-13-0
2-Methylbut-2-enal	O=CC(C)=CC	1115-11-3
Cyclohexanecarbaldehyde	O=CC1CCCCC1	2043-61-0
2-Methylcyclohexane-1-carbaldehyde	CC1CCCCC1C=O	13076-15-8
2-Cyclohexylacetaldehyde	O=CCC1CCCCC1	5664-21-1
3-Cyclohexyl-2-methylpropanal	O=CC(C)CC1CCCCC1	20514-52-7
2-Phenylacetaldehyde	O=CCC1=CC=CC=C1	122-78-1
2-Phenylpropanal	CC(C=O)C1=CC=CC=C1	34713-70-7
3-Phenylpropanal	O=CCCC1=CC=CC=C1	104-53-0
2-Methyl-3-phenylpropanal	O=CC(C)CC1=CC=CC=C1	5445-77-2
3-Phenylprop-2-enal	O=CC=CC1=CC=CC=C1	104-55-2
3-(Benzo[*d*][1,3]dioxol-5-yl)-2-methyl-propanal	O=CC(C)CC1=CC(OCO2)=C2C=C1	1205-17-0
2-(*p*-Tolyl)propanedial	CC1=CC=C(C=C1)C(C=O)C=O	27956-35-0

Table S1. Amines and carbonyls subjected to chemoinformatic analysis (*continued from previous page*).

IUPAC name	SMILES	CAS number
2-(4-Chlorophenyl)-3-oxopropanenitrile	ClC1=CC=C(C=C1)C(C=O)C#N	62538-21-0
2,2-Diphenylethanal	O=CC(C1=CC=CC=C1)C2=CC=CC=C2	947-91-1
Benzaldehyde	O=CC1=CC=CC=C1	100-52-7
2-Methoxybenzaldehyde	O=CC1=C(OC)C=CC=C1	135-02-4
2-Bromo-6-(methylsulfanyl)benzaldehyde	O=CC1=C(SC)C=CC=C1Br	1289264-36-3
Furan-2-carbaldehyde	O=CC1=CC=CO1	98-01-1
2-Oxopropanoic acid	CC(C(O)=O)=O	127-17-3
4-Oxopentanoic acid	OC(CCC(C)=O)=O	123-76-2
2-Oxo-3-phenylpropanoic acid	OC(C(CC1=CC=CC=C1)=O)=O	156-06-9
Ethyl 2-oxo-4-phenylbutanoate	O=C(C(OCC)=O)CCC1=CC=CC=C1	64920-29-2
Ethyl 4-(2-fluorophenyl)-2-oxobutanoate	O=C(C(OCC)=O)CCC1=C(F)C=CC=C1	
Ethyl 4-(3-fluorophenyl)-2-oxobutanoate	O=C(C(OCC)=O)CCC1=CC(F)=CC=C1	
Ethyl 4-(4-fluorophenyl)-2-oxobutanoate	O=C(C(OCC)=O)CCC1=CC=C(F)C=C1	85918-77-0
Ethyl 2-oxo-3-phenylpropanoate	O=C(C(OCC)=O)CC1=CC=CC=C1	6613-41-8
Ethyl 2-oxopropanoate	CC(C(OCC)=O)=O	617-35-6
Ethyl 2-oxopentanoate	O=C(C(OCC)=O)CCC	50461-74-0
Ethyl 4-methyl-2-oxopentanoate	O=C(C(OCC)=O)CC(C)C	26073-09-6
Ethyl 2-oxoheptanoate	O=C(C(OCC)=O)CCCCC	13088-50-1

Ten descriptors based on two-dimensional or three-dimensional structure were calculated for the carbonyl compounds and amines (see Table S28, *Supplementary Methods*), and a feature correlation analysis highlighted which descriptors carry a similar information, for example the radius of gyration and the number of heavy atoms, as they are both related to compound size (Figure S1).

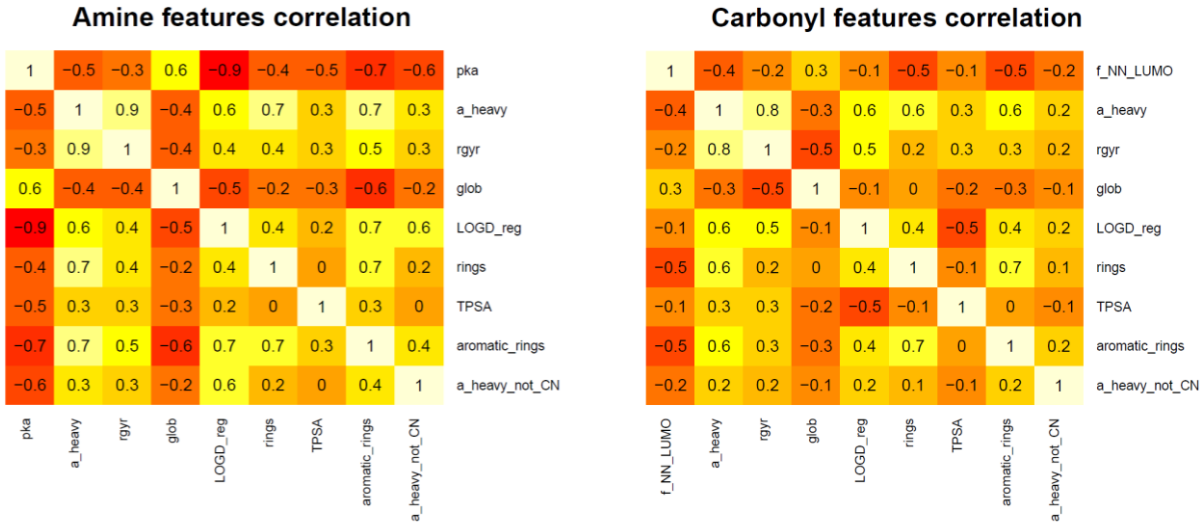


Figure S1. Feature correlation analysis of amine and carbonyl descriptors. *Abbreviations:* a_heavy, number of heavy atoms; a_heavy_not_CN, number of heavy atoms (not C or N); aromatic_rings, number of aromatic rings; f_NN_LUMO, LUMO energy; glob, globularity; LOGD_reg, logD value; pka, p*K*a value; rgyr, radius of gyration; rings, number of rings (total); TPSA, topological polar surface area

A principal component analysis (PCA) was then performed, separately for amines and carbonyl compounds, and the distribution of the substrates in the space of the first four principal components (PCs) was graphically evaluated. Figure S2 and Figure S3 show the distribution in

the respective PC1–PC2 space for the two groups of substrates. The coloured points indicate substrates selected for the Overview Screening and Diversification Screening (see below), while grey points represent substrates reported in the literature, but not investigated experimentally in the present study.

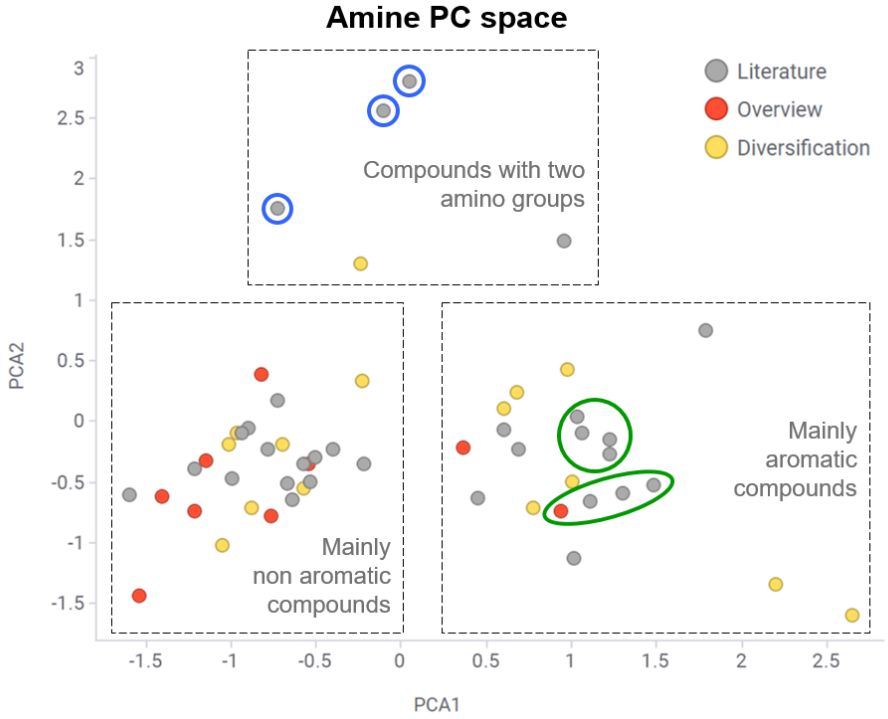


Figure S2. Amine substrates represented in the principal component (PC) 1 and 2 space. The colour of the points reflects whether the compound was part of the Overview Screening or the Diversification Screening, or whether it is known from literature, but not tested experimentally in the present study. Blue circles highlight substrates bearing aliphatic chains with terminal amino groups on both sides and green circles highlight aniline compounds with different decorations.

The amine substrates cluster roughly based on the presence of aromatic rings and of the number of amino groups (Figure S2). Aliphatic chains with terminal amino groups on both sides (circled in blue in Figure S2) were deemed of less interest for the screening and hence not included in the panels for experimental investigation. Furthermore, previous studies have often focused on decorations of aniline (compounds circled in green), only some of which were selected for the present study. The other regions are more thoroughly sampled by the substrate selection of the Overview Screening and Diversification Screening.

Carbonyl compounds are distributed in the PC1–PC2 space roughly by size and linearity of the structure (Figure S3, overleaf). In particular, lower values of PC1 encode smaller molecules, and higher values encode structures of higher molecular weight. Linear compounds occupy the top-left region of the PC1–PC2 space, and compounds with two rings (either aromatic or aliphatic) cluster in the bottom-right region. Very small, aliphatic carbonyl compounds, such as acetone, butan-2-one, propanal, butanal and cyclopropanone (grey rectangle, Figure S3, left) were deemed of less interest for the screening. The central region is occupied by compounds such as 3-phenylpropanal and 3-cyclohexylpropanal, including variations of the group attached to the ring, as well as by α- and β-keto esters, only some of which have been sampled.

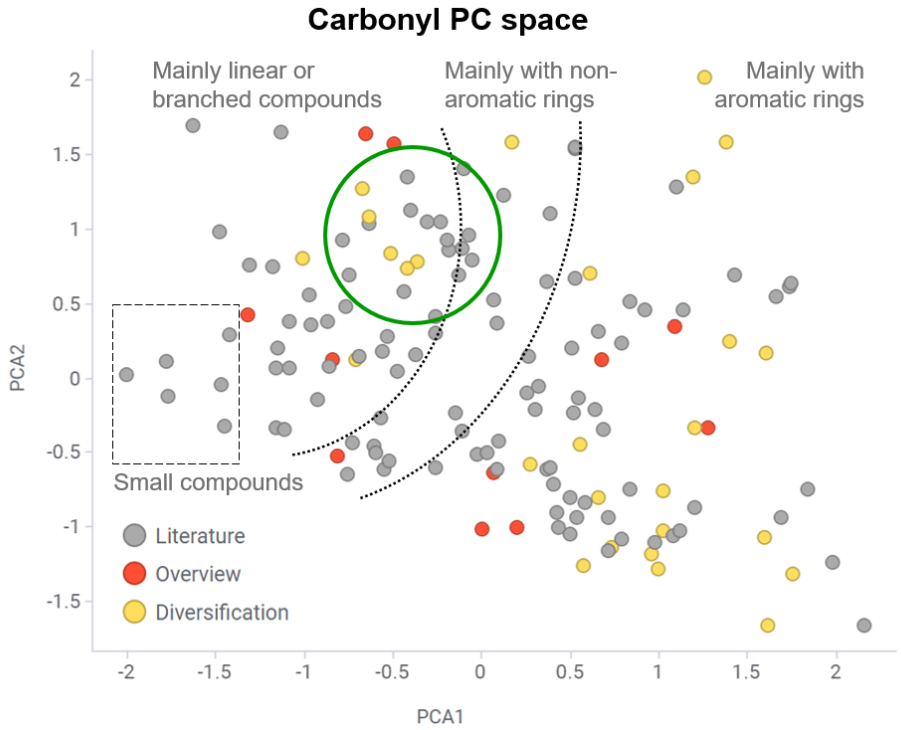


Figure S3. Carbonyl substrates represented in the principal component (PC) 1 and 2 space. The colour of the points reflects whether the compound was part of the Overview Screening or the Diversification Screening, or whether it is known from literature, but not tested experimentally in the present study. The green circle highlights keto esters.

Classic multidimensional scaling (MDS), available from the standard statistics package in R,[1] confirmed the findings of the principal component analysis, suggesting a similar distribution of the substrates (Figure S4, Figure S5).

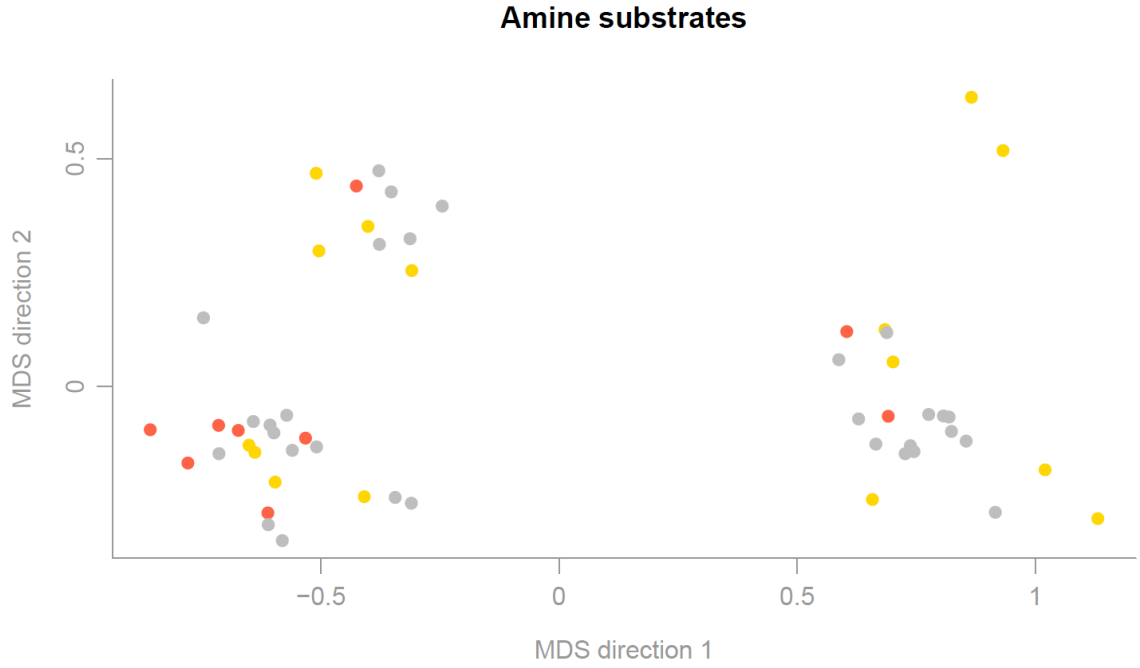


Figure S4. Multidimensional scaling of amine substrates. The colour of the points reflects whether the compound was part of the Overview Screening (red) or the Diversification Screening (yellow), or whether it is known from literature, but not tested experimentally in the present study (grey).

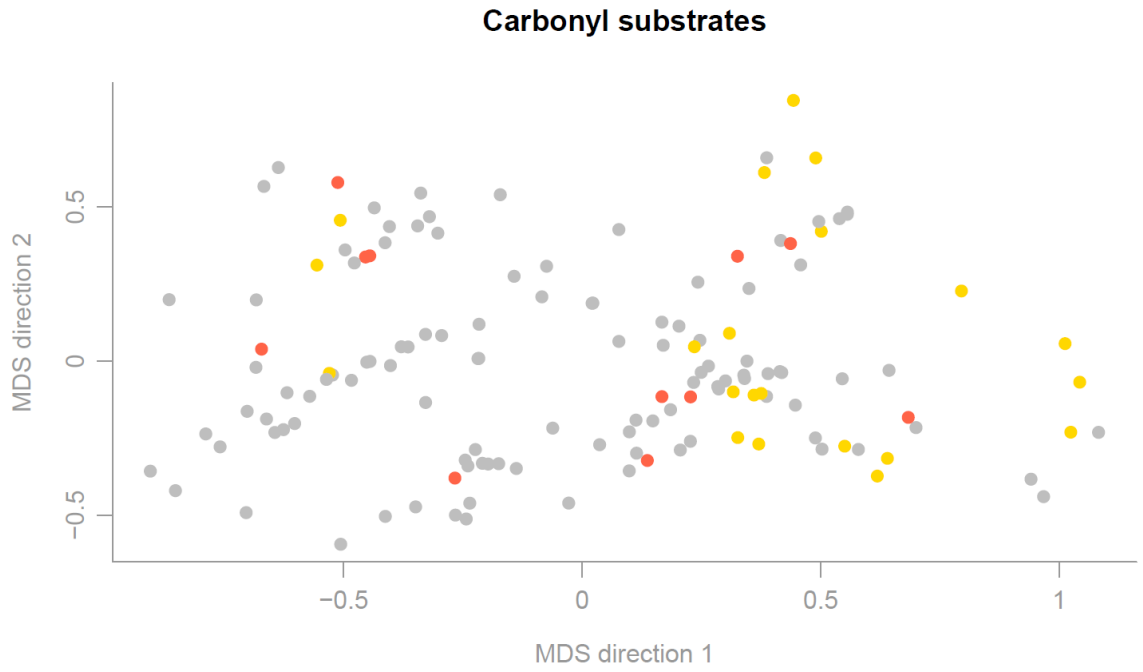


Figure S5. Multidimensional scaling of carbonyl substrates. The colour of the points reflects whether the compound was part of the Overview Screening (red) or the Diversification Screening (yellow), or whether it is known from literature, but not tested experimentally in the present study (grey).

The substrates for the Overview Screening and Diversification Screening (see *Table of Screening Substrates*) were selected so as to achieve a good coverage of the principal component space and of more general structural categories (alicyclic ketones, aliphatic ketones, aryl-aliphatic ketones, aromatic ketones, aliphatic aldehydes, aromatic aldehydes; primary aliphatic amines, primary aryl-aliphatic amines, primary aromatic amines, secondary amines, and amino alcohols). Commercial availability and reported acceptance by known IREDs were also taken into account.

Bioinformatic Analysis of the IRED Panel

Collection of IRED sequences:

An *in-silico* panel of IRED sequences was generated by collecting protein sequence information of IREDs previously investigated at *Roche* and at the *University of Graz*,[2-4] enzymes from published reductive amination screening campaigns,[5-12] and entries of the BioCatNet IRED database (*v*. 3). Additional candidate sequences were identified by BLAST searches on the NCBI nr (non-redundant) database, whereby nine query sequences (Table S2, overleaf) were selected based on their phylogenetic distance, as shown in Figure S6 (overleaf). To obtain the largest number of sequences closely related to the query, sequence identity cut-offs were adjusted on a case-by-case basis. The sequences were also filtered for length by setting an 80% bidirectional coverage. Redundancy with the original IRED data set was removed using a 99% identity cut-off; that is, only sequences with an identity less than 99% to any sequence in the original data set were retained. In total, 318 sequences were appended to the original IRED panel. After removal of 68 β-hydroxyacid dehydrogenases (β-HADs) based on their different acid–base catalytic residue in the active site (lysine, in contrast to aspartate and tyrosine commonly found in IREDs),[13-16] the resulting panel of 1620 sequences was subjected to homology modelling (see following section).

Table S2. IRED sequences used as BLAST search queries, identity cut-offs used and number of sequences arising from each search that were added to the initial data set.

			Identity cut-offs [%]			
Query	**PDB**[a]	**Source organism**	Min	Max	**Seq.**[b]	**Ref.**
IR1294		*Saccharothrix espanaensis*	60	99	15	17
IR0070		*Streptomyces viridochromogenes*	80	99	72	8 (IR-75)
IR0051	5A9S	*Amycolatopsis orientalis*	60	99	11	8 (IR-84), 18 (*Ao*IRED)
IR0020		*Streptomyces* sp.	65	99	61	2,3 (IR_20)
IR0037	5G6R	*Aspergillus oryzae*	60	99	22	8 (IR-72), 7 (*Asp*RedAm)
IR1134		*Salinispora pacifica*	60	99	66	10 (IR47)
IR0063	6TO4	*Myxococcus stipitatus*	60	99	10	8 (IR-01)
IR0033		*Aeromonas veronii*	60	95	16	3 (IR_33)
IR0023		*Streptomyces viridochromogenes*	75	99	45	2,3 (IR_23)
Total					**318**	

[a] Accession codes for X-ray crystal structures in the RCSB Protein Data Bank. [b] Number of BLAST results added to the IRED panel.

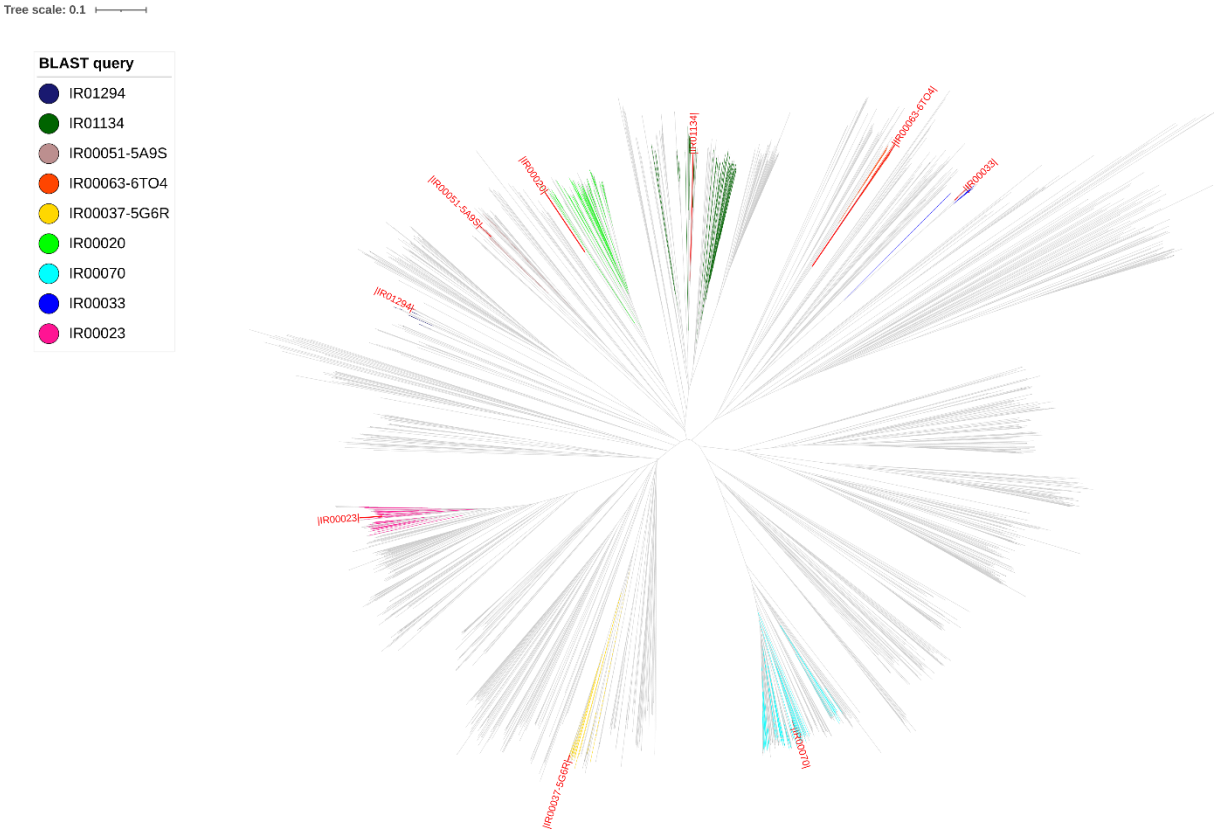


Figure S6. Phylogenetic tree depicting the initially sampled IRED sequence space. Sequences obtained from public databases and literature sources are shown in grey. Labelled branches indicate the query sequences used for the BLAST searches on the NCBI NR database, and sequences identified in these searches are coloured according to the query sequence from which they originate.

Homology modelling:
High-throughput homology modelling of the collected IRED sequences was performed using YASARA Structure (*v*. 21.6.2) and a curated list of 12 template structures available in the RCSB Protein Data Bank (PDB), ensuring that all the templates contain cofactor molecules and possess the homodimeric fold typical of imine reductases. As shown in Figure S7, most sequences were modelled on the PDB structures 5OCM, 6SMT, 5G6S, 6JIZ, 6TO4, and 5A9S.

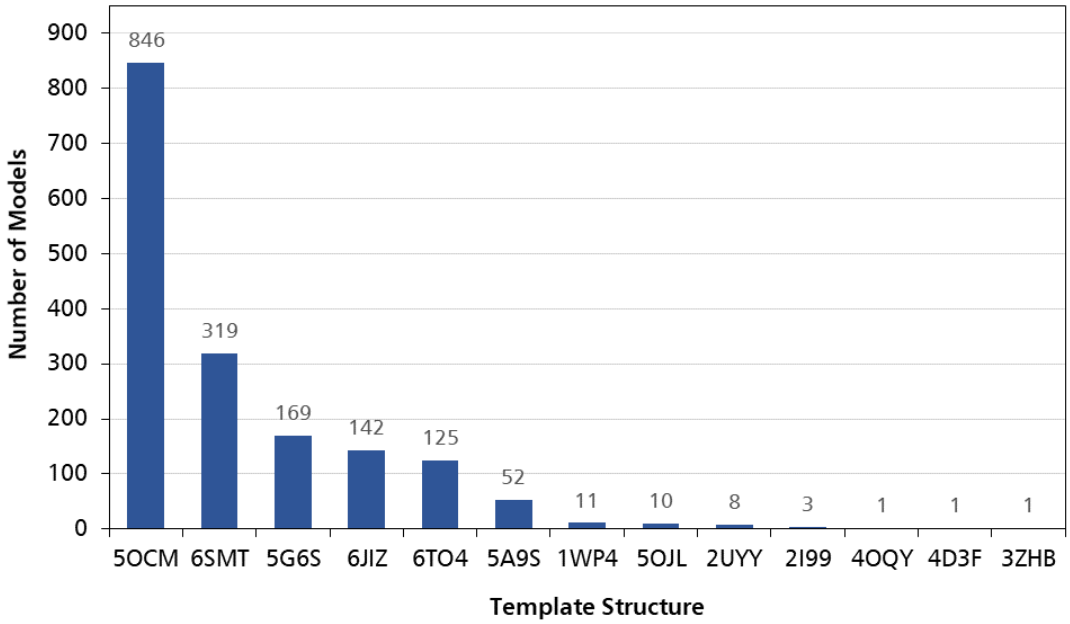


Figure S7. Number of models built on each template structure. The templates are referred to by their PDB identifiers. Source data are provided as a Source Data file.

Generation of point clouds on *Innophore*'s Catalophore™ platform:
Innophore's proprietary Catalophore™ technology was used to generate active-site point clouds that map the physicochemical environment of the active site in terms of specific features like hydrophobicity, electrostatic interactions, H-bond capabilities and shape. The identified cavities were refined using a dummy ligand approach to arrive at a realistic representation of the substrate binding site (Figure S8).

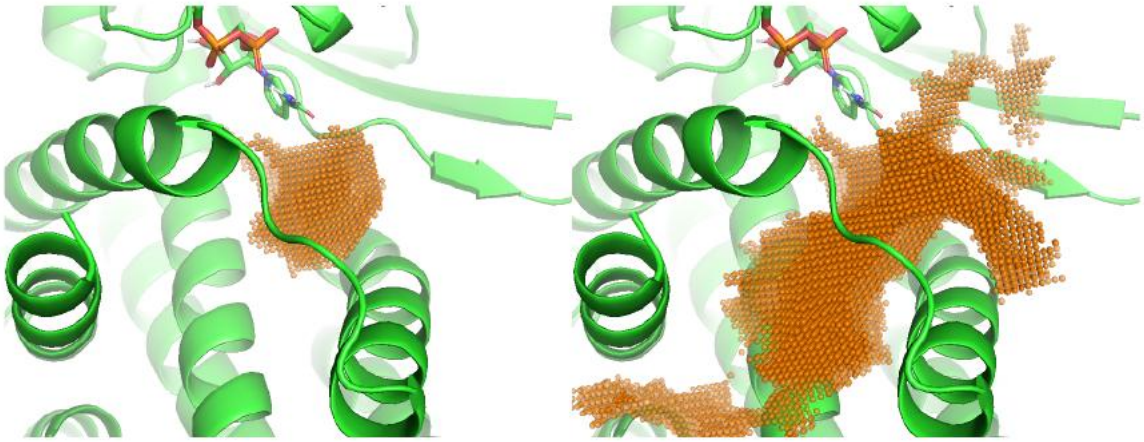


Figure S8. Exemplary Catalophore™ active-site point cloud after (left) and before (right) active-site shaping *via* a dummy ligand approach. The nicotinamide cofactor is shown in stick representation.

Selection of IREDs for the Overview Screening:
A total of 85 IREDs from the combined *Roche* and *University of Graz* enzyme collections were selected for screening because the required expression plasmids were already available. Thirty additional sequences were selected by *Innophore* to ensure an even sampling of the sequence space, visualised using multi-dimensional scaling (Figure S9).

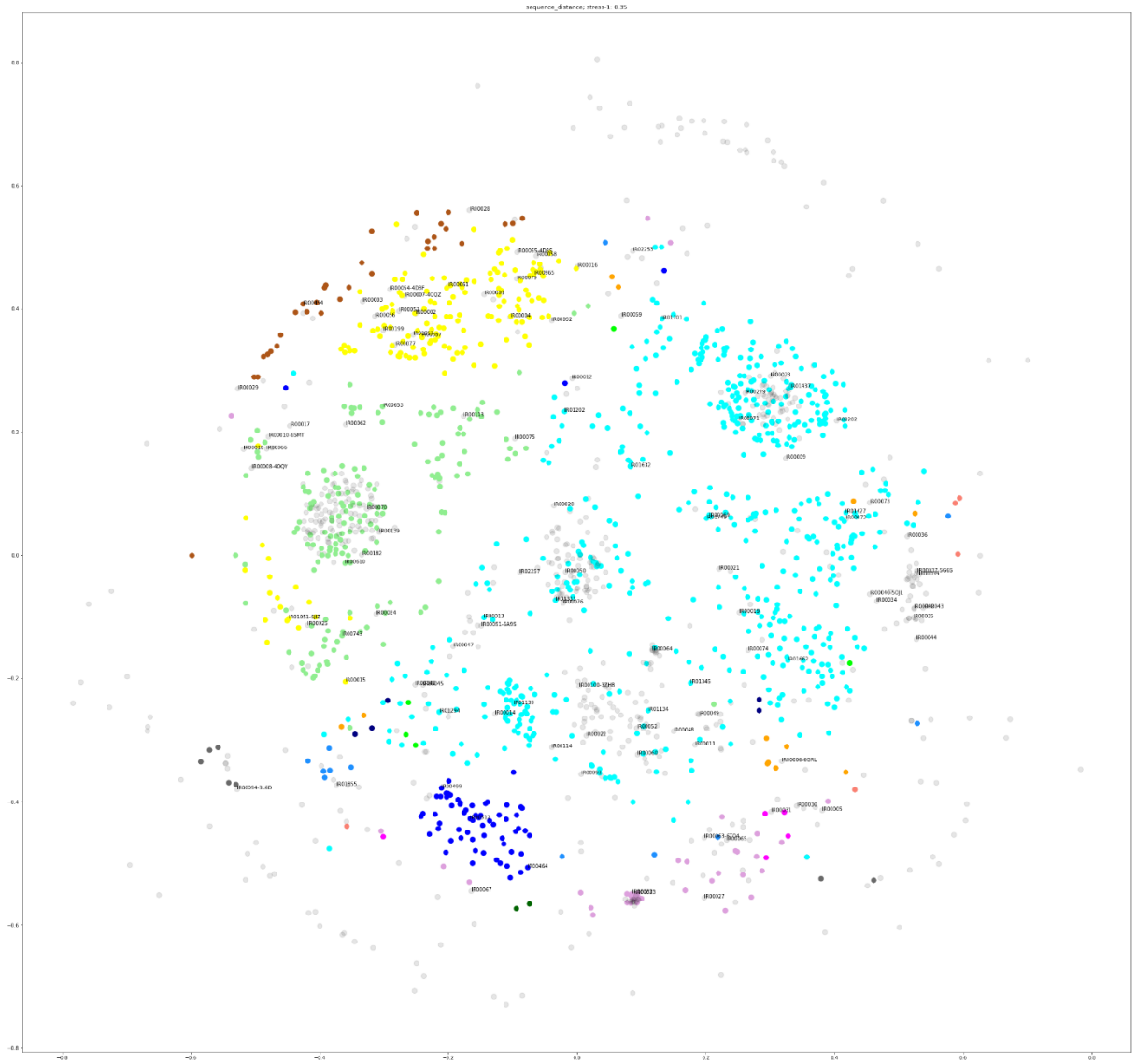


Figure S9. Multidimensional scaling of the IRED panel based on overall sequence similarity, coloured according to the BioCatNet Database classification. S_type_IREDs are shown in yellow, R_type_IREDs in cyan; other colours represent smaller families from SFAM3 to SFAM14. Sequences not present in the BioCatNet Database are shown in grey. IREDs selected for the Overview Screening are labelled. The axes have no physical meaning. Source data are provided as a Source Data file.

As a basis for choosing these additional sequences, we performed an active-site clustering of the IRED panel with respect to eight hotspot residues in the active site that show variable conservation levels, leading to representative sequences with diverse active-site composition (Table S3, overleaf). The reductive aminase from *Aspergillus oryzae* (*Asp*RedAm, PDB identifiers 5G6S and 5G6R) was used as a reference, and the chosen hotspots correspond to positions 120, 176, 177, 180, 210, 242, 244, 281 in *Asp*RedAm numbering (Figure S10).

Table S3. Thirty IREDs selected for the Overview Screening based on active-site clustering. Each enzyme is representative of a sequence cluster of varied size.

			Active-site residues[b]							
IRED	**Items[a]**	**Source**	120	176	177	180	210	242	244	281
IR0610	127	BioCatNet SFAM3	T	F	W	M	I	T	T	F
IR0182	127	IR-77, Ref. 8	T	F	W	M	I	A	A	F
IR1311	91	BioCatNet R_type_IRED	T	M	W	M	W	Q	A	Y
IR2257	91	NCBI nr	T	M	W	M	W	Q	T	F
IR1139	37	BioCatNet R_type_IRED	A	M	W	L	I	D	A	Y
IR1134	34	IR47, Ref. 10	A	M	W	L	M	H	A	Y
IR0139	31	IR-29, Ref. 8	T	F	W	M	I	G	S	F
IR0199	28	IR-94, Ref. 8	V	F	L	L	S	M	T	W
IR1202	26	BioCatNet R_type_IRED	V	M	Y	M	W	N	A	Y
IR0887	26	BioCatNet S_type_IRED	V	F	W	M	T	G	S	F
IR0512	26	BioCatNet SFAM8	N	L	L	L	W	G	H	I
IR0279	25	pIR79, Ref. 12	A	M	Y	F	W	–	S	T
IR1437	22	BioCatNet, R_type_IRED	A	M	S	F	W	–	N	G
IR1749	22	BioCatNet, R_type_IRED	A	M	Y	F	W	–	Y	L
IR0202	21	pIR2, Ref. 12	A	M	T	F	W	–	N	T
IR0653	20	BioCatNet, SFAM3	V	F	Y	M	I	M	S	W
IR0743	20	BioCatNet, SFAM3	V	F	Y	M	I	M	S	W
IR1701	19	BioCatNet, R_type_IRED	A	M	Y	F	W	A	I	L
IR0965	19	BioCatNet, S_type_IRED	V	F	L	L	L	M	T	W
IR1345	18	BioCatNet, R_type_IRED	T	M	W	L	W	H	T	Y
IR1294	16	Ref. 17	S	L	W	L	W	G	K	L
IR1855	15	IR77, Ref. 10	A	–	W	L	A	H	A	F
IR0454	15	BioCatNet SFAM9	T	F	H	L	S	M	G	P
IR0464	11	BioCatNet SFAM8	N	L	L	L	W	A	D	I
IR1662	11	BioCatNet R_type_IRED	A	M	Y	F	W	A	L	F
IR1427	10	BioCatNet R_type_IRED	A	M	Y	F	W	D	Y	L
IR0499	8	BioCatNet SFAM8	N	L	L	L	W	G	A	I
IR2253	8	NCBI nr	G	–	W	L	T	H	A	F
IR1632	7	BioCatNet R_type_IRED	A	M	Y	F	W	A	V	F
IR1051	1	PDB 6JIZ	T	F	L	L	M	M	T	W

[a] Number of sequences in the corresponding cluster. [b] Residue positions are numbered according to the sequence of *Asp*RedAm.[7]

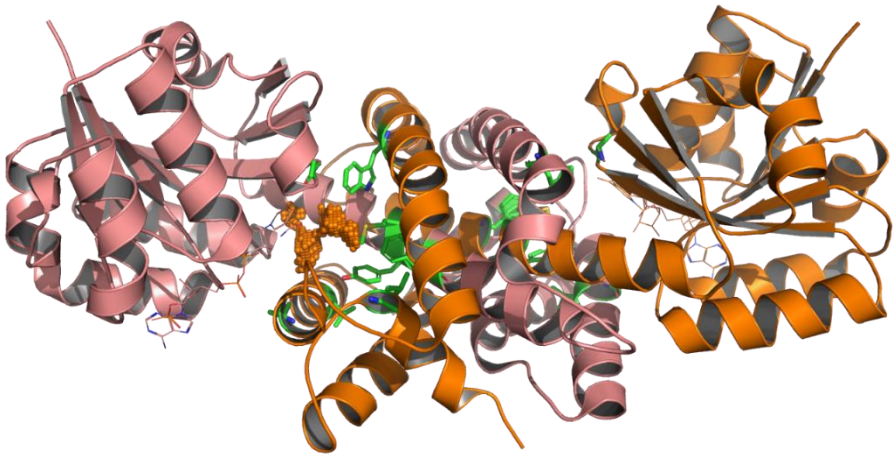


Figure S10. Crystal structure of reductive aminase from *Aspergillus oryzae* (*Asp*RedAm, PDB: 5G6S). Residues selected for active-site clustering are shown as green sticks, NADP cofactors are represented in line mode. The point cloud generated by *Innophore* for mapping physicochemical properties of the active site is shown as spheres representation (orange) in one of the two active sites.

Overall, 115 IRED sequences were initially selected for experimental testing in the *Overview Screening*, but five of them (IR0037, IR0038, IR0044, IR0512, IR1311) could not be expressed in soluble form. Hence, screening data could only be collected for 110 enzymes. 65 additional IREDs (in batches of 45 and 20) were later added to the panel based on predictions obtained using machine-learning models trained on the original data set (see following section).

Activity Prediction Using Machine-Learning Models

We used machine learning to combine knowledge from experimental reductive amination activity measurements on the one hand and the dissimilarity scores from an all-to-all matching of Catalophore™ point clouds on the other hand with the aim of predicting activities for IRED–substrate combinations not tested experimentally before.

Prioritisation of IRED candidates for the Overview Screening:
Within the scope of the Overview Screening, our goal was to identify promising additional IREDs for experimental testing based on the activity data collected for the 110 enzymes of the starting panel. To this end, we predicted the reductive amination performance of 1491 candidate IREDs across all 54 substrate combinations investigated in the screening. The underlying assumption for this is that based on Catalophore™ similarity among the IRED active-site set, and considering the entire array of substrate combinations, similar Catalophores™ do in general correlate with similar levels of activity.

In order to achieve concrete predictions for the activity grid (*cf*. Figure S12) of a candidate IRED, we first computed the dissimilarity score of its active-site point cloud to the point clouds of all IREDs for which activity data had been collected. This led to a comprehensive table of all-to-all matching scores (Figure S11, overleaf), indicating how similar or dissimilar the IRED's active site is to that of each experimentally characterised enzyme and all others in the list.

While the most direct approach to predict activity values from such a matching score table would be to use the known activity values from the most similar IRED in the measured data set, this would suffer from two main shortcomings: First, such an approach would introduce a strong bias towards a single data point, and second, it would be independent of the actual value of the similarity between the candidate and the most similar IRED. Therefore, we analysed the results *via* a weighted *k*-nearest neighbour algorithm in order to arrive at suitably chosen weighted averages as predicted activity values. The situation discussed above, where only the most similar IRED would have been used for the basis of each prediction, corresponds to $k = 1$ in such an algorithmic setup. The opposite extreme is to use the entire data set as the basis for each prediction, in which case k is equal to the size of the known data set.

To find a suitable middle ground between these two extremes, we used the similarity score of the candidate to each experimentally characterised IRED for weighting the contributions of the *k*-nearest neighbours in such a way that domination of the prediction by a single IRED was avoided, but at the same time actual similarity was taken into account to a large enough extent. To this end, in the first step, we used the results from $k = 1$, 3, 5, 10, 15, 25, 50, and 100 to generate predicted activity grids for all candidate IREDs (see Figure S12, overleaf, for an exemplary prediction output). Note that while $k = 1$ is still present here, its effect is mitigated by the subsequent analysis.

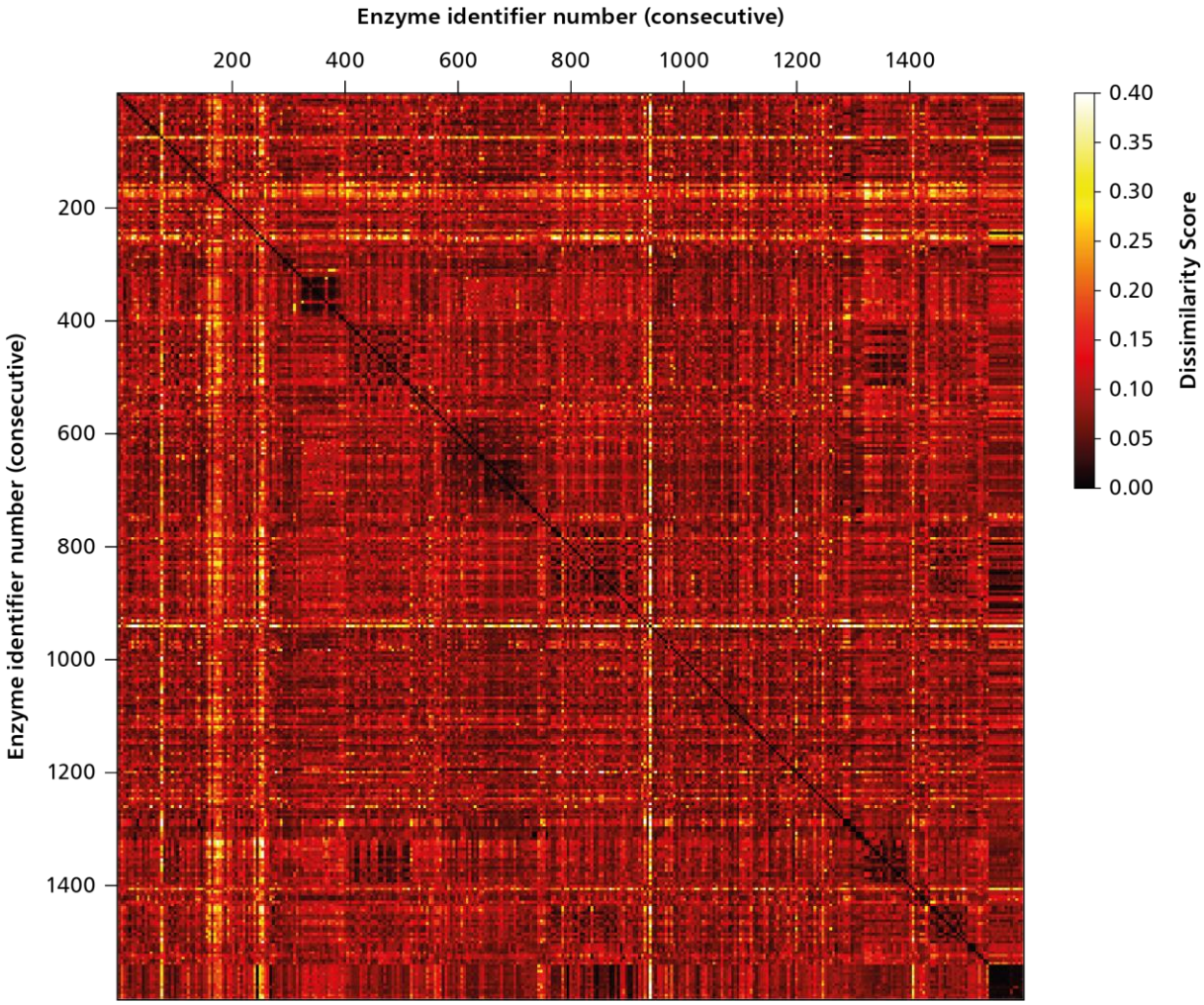


Figure S11. Heatmap representation of the all-to-all matching scores computed for the entire IRED library (candidate sequences and experimentally characterised IREDs), using the standard combined (total) dissimilarity score of the Catalophore™ active-site point clouds. Low values (dark colours) indicate high similarity.

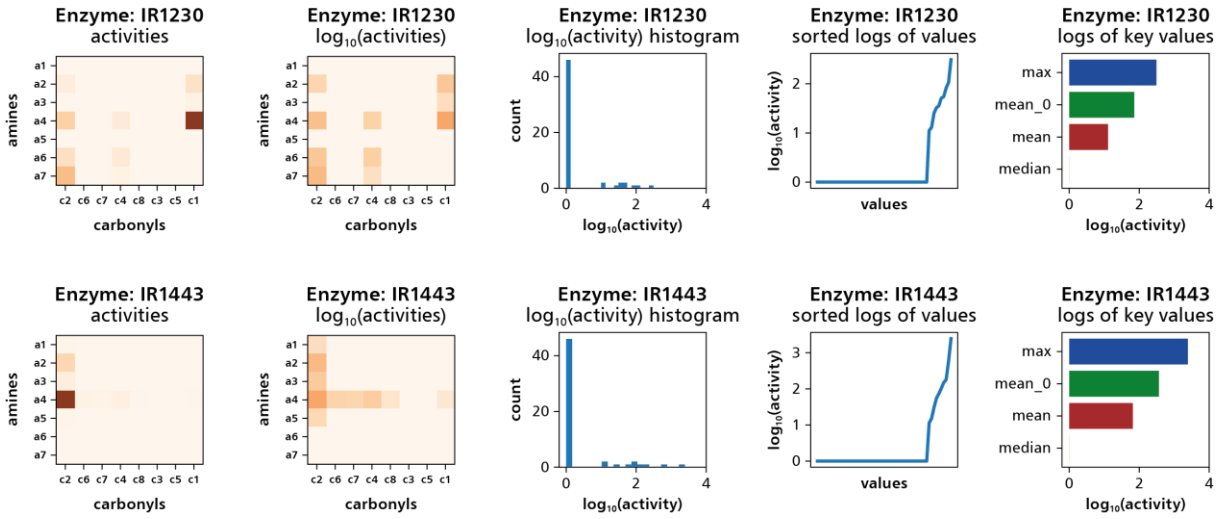


Figure S12. Exemplary activity predictions for IR1230 and IR1443, using $k = 15$. Left to right: activity heatmap on a linear scale, activity heatmap on a logarithmic scale, activity histogram on a logarithmic scale, activity values sorted ascendingly on a logarithmic scale, key statistical parameters on a logarithmic scale (max, maximum; mean_0, arithmetic mean of non-zero values).

In a second step, the resulting predictions were consolidated into two types of ranked lists of candidate IREDs: one ranked according to the likely diversity, *i.e.*, the predicted number of active substrate combinations (beyond levels of 1 mU/mg_{IRED} for avoiding noise and then 10 mU/mg_{IRED} to strengthen contributions from larger values), and another ranked according to the predicted maximum absolute activity of any given substrate combination. We explored combinations of different physico-chemical properties in the Catalophore™ point clouds, namely electrostatic, hydrophobicity, aromatic carbon, and non-hydrogen-bonding nitrogen point clouds, in order to make the resulting ranked lists of candidates diverse. Subsequent clustering based on active-site residues (*cf. Bioinformatic Analysis of the IRED Panel*) was used to ensure that new candidates were different enough from each other and from the established set of IREDs to warrant inclusion in the next round of testing. In this way, batches of 50 (first additions; 45 solubly expressed and experimentally characterised) and 20 (second additions; all solubly expressed and experimentally characterised) additional IREDs were identified as promising candidates for the Overview Screening.

For completeness, we also include two notes on the limitations of such a model: One limitation of this approach is that it does not easily deal with changes in or additions to the array of substrate combinations considered. Another limitation is that the model, since it is based on weighted averages, does not (by construction) predict activity values outside the maximum and minimum already found in the data set. Therefore, it tends towards conservative predictions for high values and optimistic predictions for low values, which likely contributes to the observed bias for moderate scope and high maximum activity in the recruited IREDs. However, as indicated by the results shown in Figure 3d (main paper), these limitations did not compromise the outcome of the subsequent experimental testing rounds.

Prioritisation of IREDs for testing with novel substrate combinations:
Building on the results from the Overview Screening and Diversification Screening, our goal was to predict activity on substrate combinations that had not been investigated experimentally yet. This required a more elaborate machine learning model that takes information on substrate structure into account. We started by using Catalophore™ cavity features of the IREDs combined with molecular descriptors of the substrates and z-transformed activity data as a training set. On the combined features, a gradient-boosted random forest was used as a predictor for activity. Subsequently, to test the predictive performance on unseen substrate combinations, we employed a group-k-fold cross validation scheme, where the 54 substrate combinations of the Overview Screening were used as groups and split into twenty folds. Furthermore, all combinations containing features from the held-out folds were excluded from the training set, effectively making the task the prediction of entirely unseen substrates.

To optimise the model's extrapolation ability for unseen substrate combinations, we employed the Catalophore™ FeatureEngineer, which manipulates molecular features in such a way that spurious information leading to overfitting is trimmed or obscured. For predicting activity on unseen substrate combinations, we again split the training set into folds based on substrate combinations. For every new substrate combination to be predicted, we kept all substrate combinations that contained one of the substrates from the new combination for validation. The validation substrates were not used for further optimisation of the training or early stopping, but only for monitoring. This way we emulated the task of predicting combinations of previously unseen substrates. We observed that the ranking of enzymes did not change significantly when predicting whether an enzyme was active at all or highly active, only the confidences were shifted, meaning that even when binning high- and low-activity values into the same classes, the confidence values output from the prediction model still correlated with the expected activity.

The predictive performance of the model was evaluated using receiver operating characteristic (ROC) curves (Figure S13). These visualise the rates of true positive and false positive predictions dependent on the confidence threshold used to distinguish between active and inactive enzymes, with a higher area under the curve (AUC) indicating higher model quality. The model performs remarkably well for substrate combinations of which the constituent substrates are included in the training set (Figure S13, top; AUC = 0.83 ± 0.08) and shows lower but still sufficient performance for the above-described extrapolation case (Figure S13, bottom; AUC = 0.73 ± 0.11). For the latter scenario, six out of seven substrate combinations would be expected to produce 70% true positive predictions in the worst case, and well over 90% on average. The higher the confidence cut-off, the more accurate the model becomes: Taking only the top 10 predicted enzymes from our panel of 175 would be expected to produce almost exclusively true positives. In the four cases where predictions of the model were tested experimentally, 12–14 of the 15 top-ranked IREDs (80–93%) were indeed found to be active (see *Performance of DL-Selected IREDs for Novel Substrate Combinations*, Table S23–Table S26).

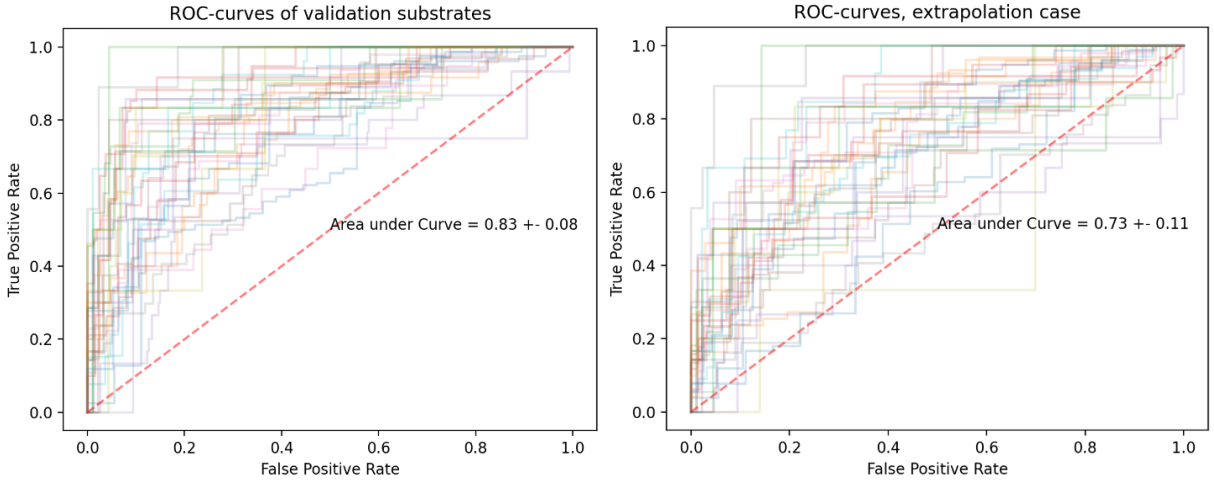


Figure S13. Receiver operating characteristic (ROC) curves of the validation substrate groups. Each line represents a single substrate combination. The median area under the curve (AUC) is reported, and the diagonal – corresponding to random classification – is drawn for comparison. Left: Combinations containing one of the substrates from the validation example are included in the training set. Right: These substrates are removed to emulate the "extrapolation" into substrate space, dealing with entirely novel structures.

Additionally, we determined enrichment factors (EFs) for the case of predicting new enzymes using leave-one-enzyme-out cross validation and comparing the relative rankings within their respective training folds. As shown in Table S4, EFs above 200% were found within the top-15 predictions for substrate–enzyme combinations with >2.5, >5, and >10 U/mg specific activity. Hence, the model is more than three times as likely to identify IREDs surpassing these activity cut-offs compared to a random selection. Conversely, activities <10 mU/mg were reduced 10-fold and activities <50 U/mg 6-fold, which helps to avoid the unfruitful screening of negatives. This is reflected in the results of the wet-lab experiments, where the bottom five predictions generally showed no or only trace activity (Table S23–Table S26).

Table S4. Enrichment factors at top 15 (out of 150) of predicted enzymes.

Activity [mU/mg$_{IRED}$]	**Enrichment at top 15 [%]**
>10,000	230
>5,000	245
>2,500	230

Selection of Enzymes for the Diversification Screening

For the Diversification Screening, the set of tested IREDs was narrowed down from 175 to 100 by excluding enzymes that showed poor substrate scope and/or activity in the Overview Screening. The cut-off criteria used were slightly different for the three sub-panels of our IRED collection: From the 110 enzymes of the initial panel, 52 were excluded from further screening based on their restricted substrate scope (≤7 positive combinations, corresponding to the bottom 47%), while one (IR0100) was removed because it had shown poor temperature stability in a previous study,[4] and two were dropped because of their limited maximum activity (IR0053, 189 mU/mg_{IRED}; IR0376, 275 mU/mg_{IRED}). For the first panel of additional enzymes identified by machine learning (45 IREDs), the diversity cut-off was again set to ≤7 substrate combinations (bottom 36%), but IR0273 (6 positive combinations) was included in the Diversification Screening because of its high maximum activity (5.2 U/mg_{IRED}). The second panel of additional enzymes generally had shown lower substrate diversity but high maximum activities in the Overview Screening, so excluding the 25% (5/20) least substrate-diverse IREDs (≤1 positive combination) resulted in the inclusion of several enzymes that were active on only 2–4 substrate pairs. We deemed this acceptable in view of the substantial maximum activities of these IREDs (>1 U/mg_{IRED}, except for IR1136: 600 mU/mg_{IRED}).

Despite the slightly more relaxed selection criterion for IREDs from the second addition panel compared to the other two, the aggregated data of the Diversification Screening (expressed as *z*-scores; see *Data Transformation for Generating z-Score Heatmaps*) show the enzymes selected from the three panels to have similar reductive amination performance (Figure S14). Hence, our iterative screening approach was able to identify IREDs of comparable quality from three source panels varying considerably in size (110, 45, and 20 enzymes for the starting panel and the first and second additions, respectively).

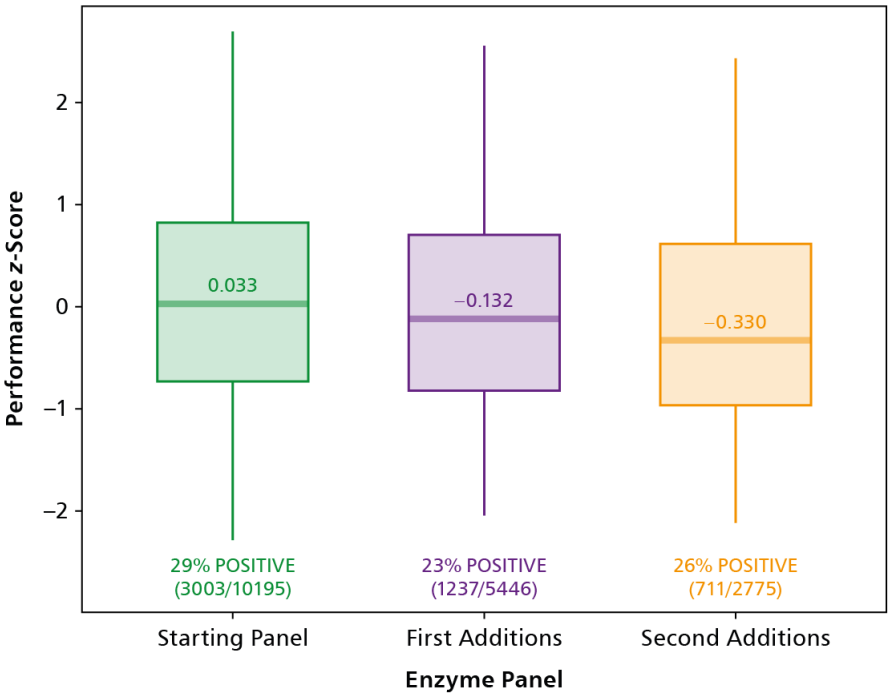


Figure S14. Box plot of non-zero activities (expressed as *z*-scores) found in the Diversification Screening (amine scope and carbonyl scope combined), grouped by the panel from which the investigated enzymes were sourced. The median values are reported in each box. Source data are provided as a Source Data file.

Protein Sequence–Activity Analysis

Overview Screening:

The enzymes showing the best performance in the Overview Screening according to the substrate scope *vs*. maximum activity scatter plot (Figure 3c, main paper) were compared to each other and to a prototypical reductive aminase, *Asp*RedAm, based on their protein sequence. To this end, a multiple-sequence alignment was performed in CLC Workbench (*v*. 22.0.2) and a pair-wise identity matrix was generated. As shown in Figure S15, the 24 enzymes are fairly dissimilar from each other (average pairwise identity: 46%), with only few exceptions: The *Aspergillaceae* proteins IR0035, IR0041, IR0043, and IR2021 share 87–96% pairwise identity, while being only moderately similar to *Asp*RedAm (57–59% pairwise identity). The *Streptomyces* IREDs IR0069, IR1749, and IR1760 (91–94% pairwise identity) as well as IR1437, IR1453, and IR2150 (92–96% pairwise identity) are also closely related.

	*Asp*RedAm	IR0023	IR0035	IR0036	IR0040	IR0041	IR0043	IR0063	IR0069	IR0233	IR0279	IR0343	IR1395	IR1427	IR1437	IR1453	IR1589	IR1674	IR1738	IR1749	IR1760	IR1855	IR2021	IR2150
*Asp*RedAm		36	57	58	56	57	57	29	47	50	40	38	39	42	37	40	41	42	39	45	46	28	59	39
IR0023	36		36	38	38	37	36	30	49	34	65	33	58	42	72	72	63	49	67	48	50	26	36	72
IR0035	57	36		55	56	94	90	31	44	46	38	35	40	47	37	37	37	40	38	43	44	29	91	36
IR0036	58	38	55		54	56	55	30	46	46	41	37	41	44	38	40	39	43	40	44	45	32	56	39
IR0040	56	38	56	54		55	54	33	47	51	42	38	42	45	40	41	42	44	41	45	46	29	55	41
IR0041	57	37	94	56	55		96	30	44	46	39	36	41	47	38	38	38	40	40	42	43	30	91	37
IR0043	57	36	90	55	54	96		29	44	46	38	35	39	45	38	37	37	38	38	43	44	29	87	36
IR0063	29	30	31	30	33	30	29		34	31	31	30	33	32	30	29	30	30	32	33	33	50	31	31
IR0069	47	49	44	46	47	44	44	34		48	48	39	50	52	50	51	53	60	52	91	94	32	44	50
IR0233	50	34	46	46	51	46	46	31	48		38	37	39	42	38	39	39	44	41	47	48	29	47	38
IR0279	40	65	38	41	42	39	38	31	48	38		36	63	45	70	71	65	49	69	47	49	27	39	71
IR0343	38	33	35	37	38	36	35	30	39	37	36		35	39	33	32	35	39	37	38	39	29	36	33
IR1395	39	58	40	41	42	41	39	33	50	39	63	35		43	65	63	63	45	66	48	50	29	41	65
IR1427	42	42	47	44	45	47	45	32	52	42	45	39	43		44	45	43	55	44	51	51	29	46	44
IR1437	37	72	37	38	40	38	38	30	50	38	70	33	65	44		92	68	50	72	49	51	28	38	96
IR1453	40	72	37	40	41	38	37	29	51	39	71	32	63	45	92		67	53	70	50	52	29	38	93
IR1589	41	63	37	39	42	38	37	30	53	39	65	35	63	43	68	67		53	69	52	54	26	36	67
IR1674	42	49	40	43	44	40	38	30	60	44	49	39	45	55	50	53	53		49	57	58	29	40	50
IR1738	39	67	38	40	41	40	38	32	52	41	69	37	66	44	72	70	69	49		51	53	29	38	70
IR1749	45	48	43	44	45	42	43	33	91	47	47	38	48	51	49	50	52	57	51		94	32	42	50
IR1760	46	50	44	45	46	43	44	33	94	48	49	39	50	51	51	52	54	58	53	94		32	43	51
IR1855	28	26	29	32	29	30	29	50	32	29	27	29	29	29	28	29	26	29	29	32	32		29	29
IR2021	59	36	91	56	55	91	87	31	44	47	39	36	41	46	38	38	36	40	38	42	43	29		36
IR2150	39	72	36	39	41	37	36	31	50	38	71	33	65	44	96	93	67	50	70	50	51	29	36	

Figure S15. Pairwise protein sequence identities of top-performing IREDs identified in the Overview Screening and *Asp*RedAm, the prototypical fungal reductive aminase. Source data are provided as a Source Data file.

The presence or absence of key active-site residues is likely to be a more useful predictor of reductive amination performance than is global sequence similarity. Turner, Grogan, and co-workers have identified three conserved residues in fungal reductive aminases that appear to be directly involved in catalysis: Asn93 (*Asp*RedAm numbering) and Asp169 have been assigned roles in amine binding and activation, while Tyr177 seems to be important for binding of the carbonyl substrate.[7,19] Screening studies that focused on or at least included bacterial enzymes found Asn93 to be replaceable with other polar residues (serine, threonine) in IREDs showing good reductive amination performance.[10,20] Similarly, Tyr177 can be replaced with tryptophan or phenylalanine, although these residues likely cannot fulfil the same catalytic role as a tyrosine residue in the same position.[10,20,21] In Table S5 (overleaf), the top-performing IREDs

of the Overview Screening and *Asp*RedAm are analysed for the presence of these key residues. Twelve enzymes contain all three of them (N–D–Y) and six contain two plus one "acceptable" replacement (T/S–D–Y), indicating that the presence of active-site residues with a putative catalytic role in fungal reductive aminases is a useful indicator for reductive amination performance in the wider IRED enzyme family, irrespective of the phylogenetic background.

Table S5. Source organisms and partial sequence alignments of top-performing IREDs identified in the Overview Screening and *Asp*RedAm, the prototypical fungal reductive aminase.

IRED	Source organism[a]	Partial sequence alignment[b]
*Asp*RedAm	*Aspergillus oryzae*	91 LTN 93 ... 169 DLALLSGMYGLF 180
IR0023	*S. viridochromogenes*	107 LTT 109 ... 186 DVALLSAMYGMF 197
IR0035	*Neosartorya fischeri*	90 LTN 92 ... 167 DLALLSGMYGLF 178
IR0036	*Aspergillus nidulans*	92 LTN 94 ... 172 DLALLSGMYGLF 183
IR0040 (*At*RedAm)	*Aspergillus terreus*	96 LTN 98 ... 175 DLALLSGMYGLF 186
IR0041 (*Nf*RedAm)	*Neosartorya fumigata*	90 LTN 92 ... 167 DLALLSGMYGLF 178
IR0043	*Aspergillus fumigatus*	90 LTN 92 ... 167 DLALLSGMYGLF 178
IR0063	*Myxococcus stipitatus*	93 LTS 95 ... 171 DSALLFQMWGTL 182
IR0069	*Streptomyces* sp.	92 LTN 94 ... 169 DIALLSAMYGMF 180
IR0233	*Emergomyces pasteurianus*	92 LTN 94 ... 169 DLALLSGMYGLF 180
IR0279	*S. chattanoogensis*	102 LTT 104 ... 181 DVALLSAMYGMF 192
IR0343	*Brevibacillus brevis*	96 LTT 98 ... 174 DLSLLTMMYGAW 185
IR1395	*Streptomyces* sp.	94 LTT 96 ... 173 DVALLSAMYGLF 184
IR1427	*Mesorhizobium* sp.	90 LTN 92 ... 167 DISLLTGMYGMF 178
IR1437	*Streptomyces* sp.	99 LTT 101 ... 178 DVALLSAMSGMF 189
IR1453	*Streptomyces* sp.	96 LTT 98 ... 175 DVALLSAMSGMF 186
IR1589	*Streptomyces* sp.	94 LVT 96 ... 173 DVALLSAMYGMF 184
IR1674	*Amycolatopsis lurida*	95 LTN 97 ... 172 DIALLSGMYGYF 183
IR1738	*Streptomyces toyocaensis*	95 LTT 97 ... 174 DVALLSAMYGMF 185
IR1749	*Streptomyces iranensis*	92 LTN 94 ... 169 DIALLSAMYGMF 180
IR1760	*Streptomyces rapamycinicus*	92 LTN 94 ... 169 DIALLSAMYGMF 180
IR1855	*Ensifer adhaerens*	93 LTS 95 ... 171 DSAVLALMWGAL 182
IR2021	*Aspergillus udagawae*	90 LTN 92 ... 167 DLALLSGMYGLF 178
IR2150	*Streptomyces luteogriseus*	102 LTT 104 ... 181 DVALLSAMSGMF 192

[a] *Abbreviation: S.*, *Streptomyces*. [b] Residues directly involved in catalysis according to the proposed reductive amination mechanism of fungal RedAms[7,19] are highlighted in red; an orange highlight is used for residues that are known to be an accepted replacement of the *Asp*RedAm residue in the corresponding position.

This conclusion was further corroborated when we classified all 175 enzymes tested in the Overview Screening according to the presence of the RedAm catalytic residues. 60 IREDs featured the complete three-residue motif (N/S/T93, D169, Y177; *Asp*RedAm numbering), 61 retained part of the motif (D169 and one of the other two key residues), and 54 did not contain the motif at all (either no D169, or D169 without the other two key residues). Of these three groups, the enzymes containing a complete or partial RedAm motif performed similarly well, showing the same rate of positives (18%) and a similar median of non-zero values (141 and 97 mU/mg$_{IRED}$, respectively). In contrast, enzymes from which the RedAm motif is absent achieved a significantly lower hit rate (10% positives) and a lower median of non-zero values (44 mU/mg$_{IRED}$, Figure S16a, overleaf).

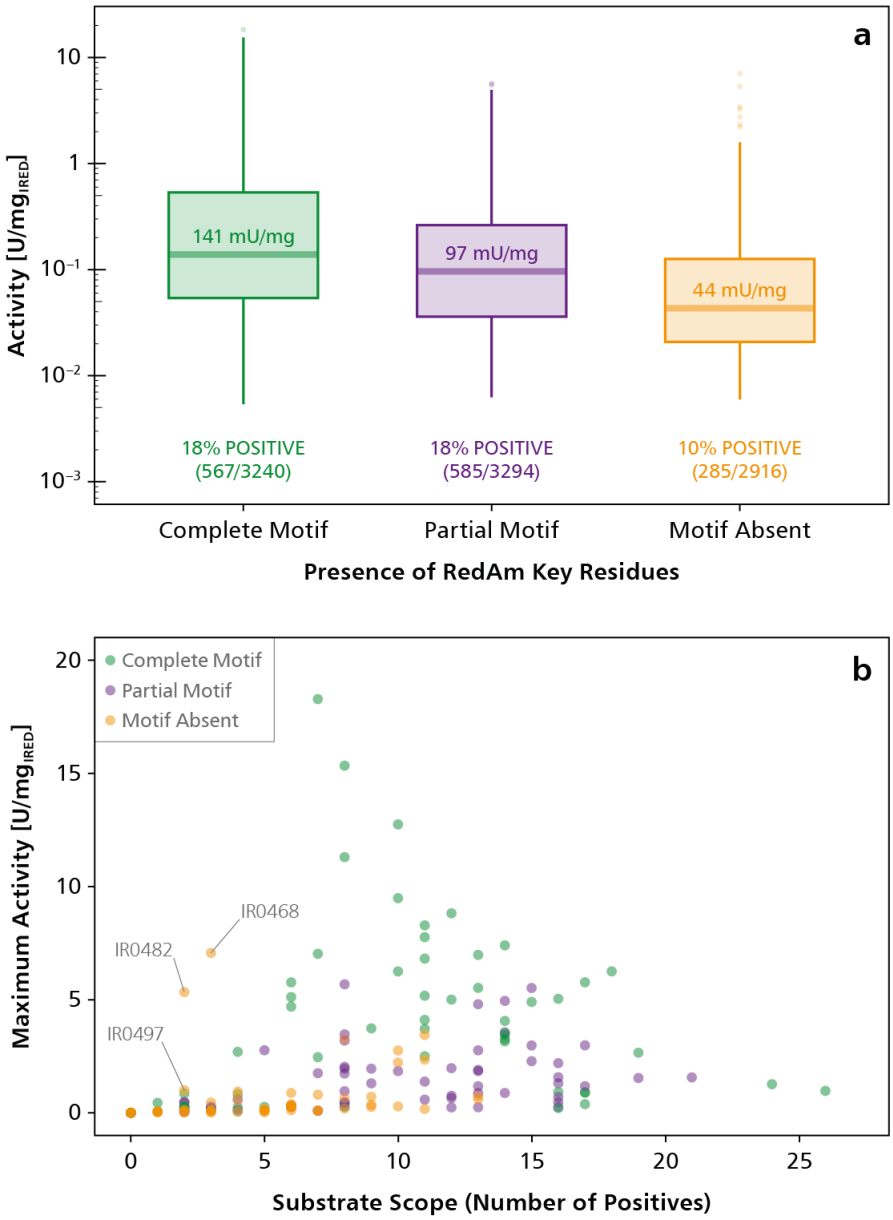


Figure S16. Analysis of data collected in the Overview Screening with respect to the presence of reductive aminase key residues in the investigated IREDs. **(a)** Box plot of non-zero activities (scaled logarithmically). Extreme values (data points farther than 1.5 times the inter-quartile range from the hinges) are shown as semi-transparent circles, and median values are reported in each box. **(b)** Scatter plot of maximum activity *vs*. number of positive substrate combinations for each tested enzyme. All data represent the mean of three experiments (n = 3). Source data are provided as a Source Data file.

In view of these differences, it is not surprising that IREDs containing a complete or partial RedAm motif cluster towards the top-right front of the substrate scope *vs*. maximum activity scatter plot (Figure S16b); *i.e.*, they represent the most versatile and active enzymes identified in our screening. Nevertheless, some IREDs lacking the RedAm motif can rival the reductive amination performance of the other two groups for a few individual substrate combinations. This is illustrated by IR0468, IR0482, and IR0497 (labelled in Figure S16b), which present an interesting case of medium-fast specialists. They are only active on two to three of the tested substrate combinations, but achieve maximum activities of 1–7 U/mg for the best combination, which in all three cases is cyclohexanone (**c2**) and benzylamine (**a6**). The three IREDs are close relatives on a sequence basis (58–75% overall sequence identity) and share a glutamate residue in position 169 (*Asp*RedAm numbering), where fungal RedAms possess the conserved aspartate.

Diversification Screening:
As discussed above, IREDs containing key active-site residues reported to have a direct catalytic role in fungal RedAms (N/S/T93, D169, Y177; *Asp*RedAm numbering) showed a significantly better performance in the Overview Screening compared to enzymes that do not contain these residues. Since we used this performance as the basis for selecting IREDs for further testing in the Diversification Screening, enzymes containing a complete or partial RedAm motif are enriched in the set of 100 enzymes investigated in this second screening phase (Table S6). However, their performance advantage in the Diversification Screening is less pronounced than it was in the Overview Screening. For instance, the hit rates (percentage of positive assay reactions) of all three groups of enzymes are very similar in the amine scope part of the screening, and in the carbonyl scope, the IREDs featuring a partial RedAm motif even have a higher rate of positives than those featuring the complete motif. Nevertheless, the median of non-zero values is highest for enzymes containing a complete RedAm motif and lowest for those from which the motif is absent, irrespective of whether the data are analysed separately for the amine and carbonyl scope (Table S6) or aggregated for all substrate combinations of the Diversification Screening (expressed as *z*-scores, Figure S17).

Table S6. Analysis of data collected in the Diversification Screening with respect to the presence of reductive aminase key residues in the investigated IREDs.

		Rate of positives		Median non-zero value	
RedAm residues	**IREDs**[a]	Amine scope	Carbonyl scope	Amine scope	Carb. scope[b]
Complete motif	42	30% (1115/3743)	24% (972/3990)	930 mU/mg	17.5
Partial motif	42	27% (1010/3740)	29% (1141/3990)	730 mU/mg	11.2
Motif absent	16	28% (404/1433)	20% (309/1520)	440 mU/mg	9.5
Total	100	28% (2529/8916)	25% (2422/9500)	732 mU/mg	12.8

[a] Number of enzymes in each group. [b] Target/buffer integral ratio, corrected for IRED expression level.

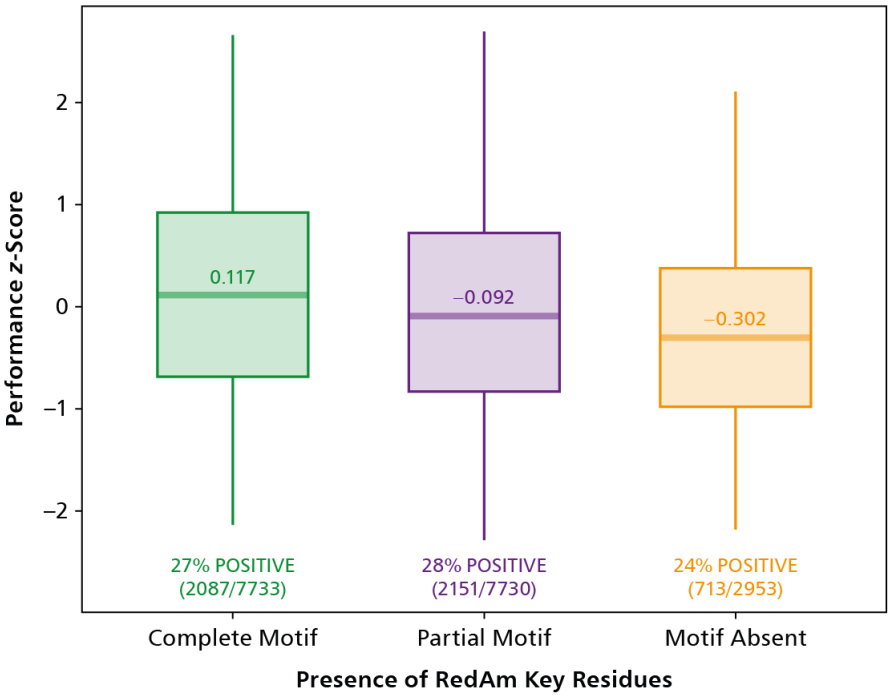


Figure S17. Box plot of non-zero activities (expressed as *z*-scores) found in the Diversification Screening (amine scope and carbonyl scope combined), grouped according to the presence of reductive aminase key residues in the investigated IREDs. The median values are reported in each box. Source data are provided as a Source Data file.

In contrast to the Overview Screening, where a trade-off seemed to exist between the substrate scope of an enzyme and its maximum activity (*cf*. Figure 3c, main paper; Figure S16b), the aggregated data of the Diversification Screening do not indicate such a limitation. The IREDs accepting the largest number of substrate combinations show maximum activities (expressed as z-scores) that are on a par with less substrate-diverse enzymes tested in the screening (Figure S18a). Plotting the data individually for the amine scope and the carbonyl scope (before z-transformation) even reveals a weak positive correlation between the number of accepted substrate pairs and the maximum activity or target/buffer integral ratio (Amine: $r = 0.42$, $p < 0.01$; Carbonyl: $r = 0.31$, $p < 0.01$; Figure S18b,c). We attribute this difference to the significantly larger and more structurally diverse panel of substrates used in the Diversification Screening, which is more likely to contain at least one particularly favourable substrate pair for any broad-scope IRED than the panel of generic model substrates used in the Overview Screening.

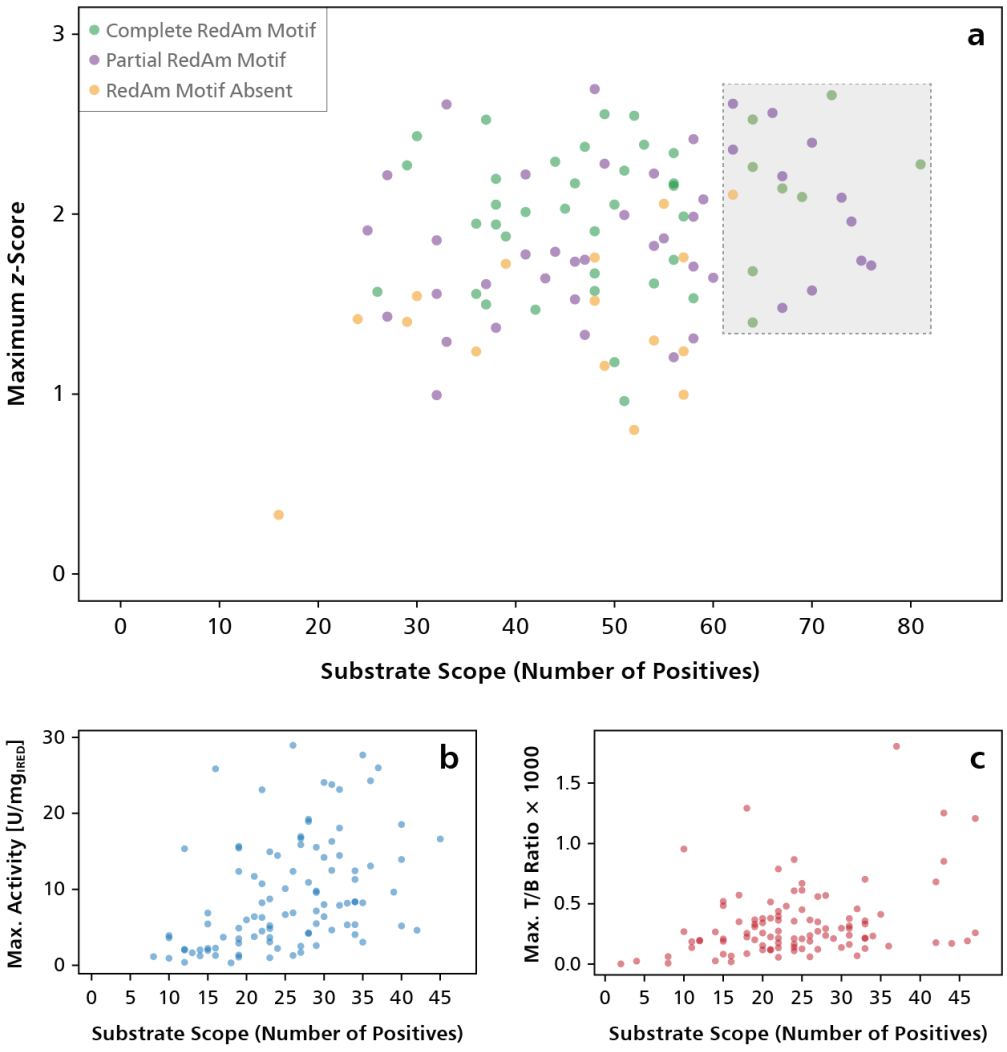


Figure S18. Visualisation of substrate scope and maximum activity of the 100 IREDs tested in the Diversification Screening. **(a)** Scatter plot of maximum z-score *vs*. number of positive substrate combinations across the entire screening (amine scope and carbonyl scope combined) for each tested enzyme. The top-performing IREDs highlighted by the grey box are listed in Table S7. **(b,c)** Individual scatter plots based on data of the two sub-screenings: Maximum activity *vs*. number of positive substrate combinations in the amine scope (**b**, blue); maximum target/buffer integral ratio (corrected for IRED expression level) *vs*. number of positive substrate combinations in the carbonyl scope (**c**, red). All data are from single experiments ($n = 1$). Source data are provided as a Source Data file.

The twenty enzymes showing the broadest substrate scope (highlighted by the grey box in Figure S18a) are listed in Table S7. They cover 62–81 of the 185 interpretable substrate combinations tested (34–44%) and reach *z*-scores of 1.40–2.66 for their most favourable individual combination, corresponding to the top 7–1% of scores among all positives found in the screening. With one exception (IR0066, A–D–W), all of these IREDs contain a complete or partial RedAm active-site motif (N/S/T93, D169, Y177; *Asp*RedAm numbering), suggesting that this simple sequence-based criterion possesses some predictive value for reductive amination performance in general. Nevertheless, the 16 non-RedAm enzymes included in the Diversification Screening spread out quite evenly in the substrate scope *vs*. maximum *z*-score scatter plot (Figure S18a), which demonstrates that they can rival the catalytic performance of RedAms even in reductive amination reactions performed at equimolar substrate concentrations.

Table S7. Substrate scope and maximum activity performance scores of the twenty broadest-scope IREDs identified in the Diversification Screening. The enzymes are sorted by the total number of positive substrate combinations.

		Number of positives[a]			Maximum score[b]		
IRED	**RedAm residues**	Amine	Carbonyl	Total	Act. [U/mg$_{IRED}$]	T/B	*z*-Score
IR0035	Complete motif	45	36	81	16.6	150	2.28
IR0064	Partial motif	32	44	76	7.9	172	1.71
IR0063	Partial motif	33	42	75	8.2	178	1.74
IR0052	Partial motif	28	46	74	10.9	193	1.96
IR0065	Partial motif	31	42	73	12.5	682	2.09
IR2021	Complete motif	35	37	72	27.7	1804	2.66
IR1105	Partial motif	23	47	70	1.0	1206	2.40
IR1134	Partial motif	23	47	70	5.2	259	1.58
IR0041	Complete motif	36	33	69	13.1	214	2.10
IR0043	Complete motif	40	27	67	13.9	272	2.14
IR0060	Partial motif	34	33	67	5.4	217	1.48
IR1136	Partial motif	24	43	67	2.2	852	2.21
IR0030	Partial motif	36	30	66	24.3	298	2.56
IR0023	Complete motif	40	24	64	5.2	111	1.40
IR1427	Complete motif	31	33	64	16.3	359	2.26
IR1632	Complete motif	33	31	64	5.3	317	1.68
IR1805	Complete motif	32	32	64	23.1	458	2.53
IR0066	Motif absent	29	33	62	9.6	703	2.11
IR0202	Partial motif	37	25	62	26.0	452	2.61
IR1855	Partial motif	40	22	62	16.6	398	2.36

[a] Number of positive substrate combinations in the amine scope screening (Amine), the carbonyl scope screening (Carbonyl), and in both sub-screenings combined (Total). [b] Maximum value of specific activity in the amine scope screening (Act. [U/mg$_{IRED}$]), of target/buffer integral ratio in the carbonyl scope screening (T/B; corrected for IRED expression level), and of *z*-score across both sub-screenings combined (*z*-Score).

Protein Structure–Activity and Structure–Selectivity Analysis

We identified correlations of the collected screening data with IRED structural features through a combination of several *in-silico* analysis methods, including multiple-sequence alignments, residue conservation analysis, and protein–ligand docking. Recent studies that attempt to pinpoint key residues governing activity and selectivity in IRED-catalysed reductive amination provided valuable guidance for these efforts.[22,23]

In particular, we address the following questions: (1) Can high reductive amination performance be linked to specific structural features of the top-ranked IREDs? (2) Can the poor reactivity of aromatic ketones and amines be explained by steric factors (poor binding of the corresponding imines in the IREDs' active site) or does it result from other properties of these substrates? (3) Can the observed stereoselectivity in IRED-catalysed reductive amination be rationalised, or even predicted, based on active-site structure or enzyme sequence?

General reductive amination performance:

We identified residues that are linked to high reductive amination performance by analysing differences in sequence conservation between the top-20 IREDs of the Diversification Screening (see Table S7, *Protein Sequence–Activity Analysis*) and two control groups: the remaining 155 enzymes we had studied experimentally and the complete set of 1,555 curated IRED sequences we had collected at the outset of the study. Three cases of interest were considered in this analysis: (1) *Strong enrichment:* High conservation (≥85%) in the top-20 *vs*. low conservation (≤50%) in at least one of the other groups, with no difference in the modal (most frequent) amino acid at the respective position. (2) *Moderate enrichment:* ≥30% increase of conservation rate in the top-20 *vs*. at least one of the other groups, with no difference in the modal residue and no restrictions on the extent of conservation in each group. (3) *Modal change:* Substantial conservation (≥70%) in the top-20 of a modal residue different from that of the other groups. No positions were found to satisfy the third condition, but two cases of strong enrichment and ten of moderate enrichment were identified, as summarised in Table S8.

Table S8. Summary of positional sequence conservation differences between top-20 performing IREDs identified in our screening and two control groups.

	Modal Residue / Frequency[b]			Difference[c]	
Position[a]	*Top-20*	*Ex-155*	*Cur-1555*	*vs Ex-155*	*vs Cur-1555*
Leu133	L / 0.850	L / 0.419	L / 0.516	0.431	0.334
Gly178	G / 0.900	G / 0.477	G / 0.386	0.423	0.514
Ala120	A / 0.950	A / 0.503	A / 0.465	0.447	0.485
Leu184	L / 0.750	L / 0.374	L / 0.442	0.376	0.308
Val272	V / 0.700	V / 0.335	V / 0.345	0.365	0.335
Leu284	L / 0.750	L / 0.413	L / 0.406	0.337	0.344
Ser144	A / 0.600	A / 0.265	A / 0.292	0.335	0.308
Gly243	A / 0.650	A / 0.323	A / 0.360	0.327	0.290
Leu206	L / 0.650	L / 0.335	L / 0.295	0.315	0.355
Leu48	L / 0.550	L / 0.239	L / 0.273	0.311	0.277
Ser258	A / 0.600	A / 0.290	A / 0.316	0.310	0.284
Met176	M / 0.850	M / 0.548	M / 0.534	0.302	0.316

[a] Amino acid position according to *Asp*RedAm numbering. [b] Modal (most frequent) residue at the corresponding position in the top-20 performing IREDs from our screening (*Top-20*), the remaining 155 IREDs studied experimentally in our work (*Ex-155*), and the complete panel of 1,555 curated IRED sequences (*Cur-1555*). The reported frequency is calculated relative to the total number of sequences in the group. [c] Difference in modal frequency at the respective position between the top-20 IREDs and either of the two control groups.

The location of these twelve residues in the X-ray crystal structure of *Asp*RedAm is shown in Figure S19. Only one of them, Met176, is an active-site residue whose side chain points towards the substrate binding pocket, making a direct role in substrate recognition likely. Most of the other identified positions are amino acids with apolar side chains (Leu, Val) engaging in hydrophobic interactions (C…C distances 3.9–4.4 Å) in the protein core (for examples, see Figure S20, panels c, d; overleaf). Their enrichment in the top-performing IREDs might hence translate to a general stability advantage for these enzymes. The same is plausible for conservation of Gly178, which sits at the point of closest inter-subunit contact (C…C distance 3.3 Å) in the domain-swapping helix of the *Asp*RedAm crystal structure (Figure S20b). Any exchange with a larger residue is hence likely to disturb the dense packing of the domain interface.

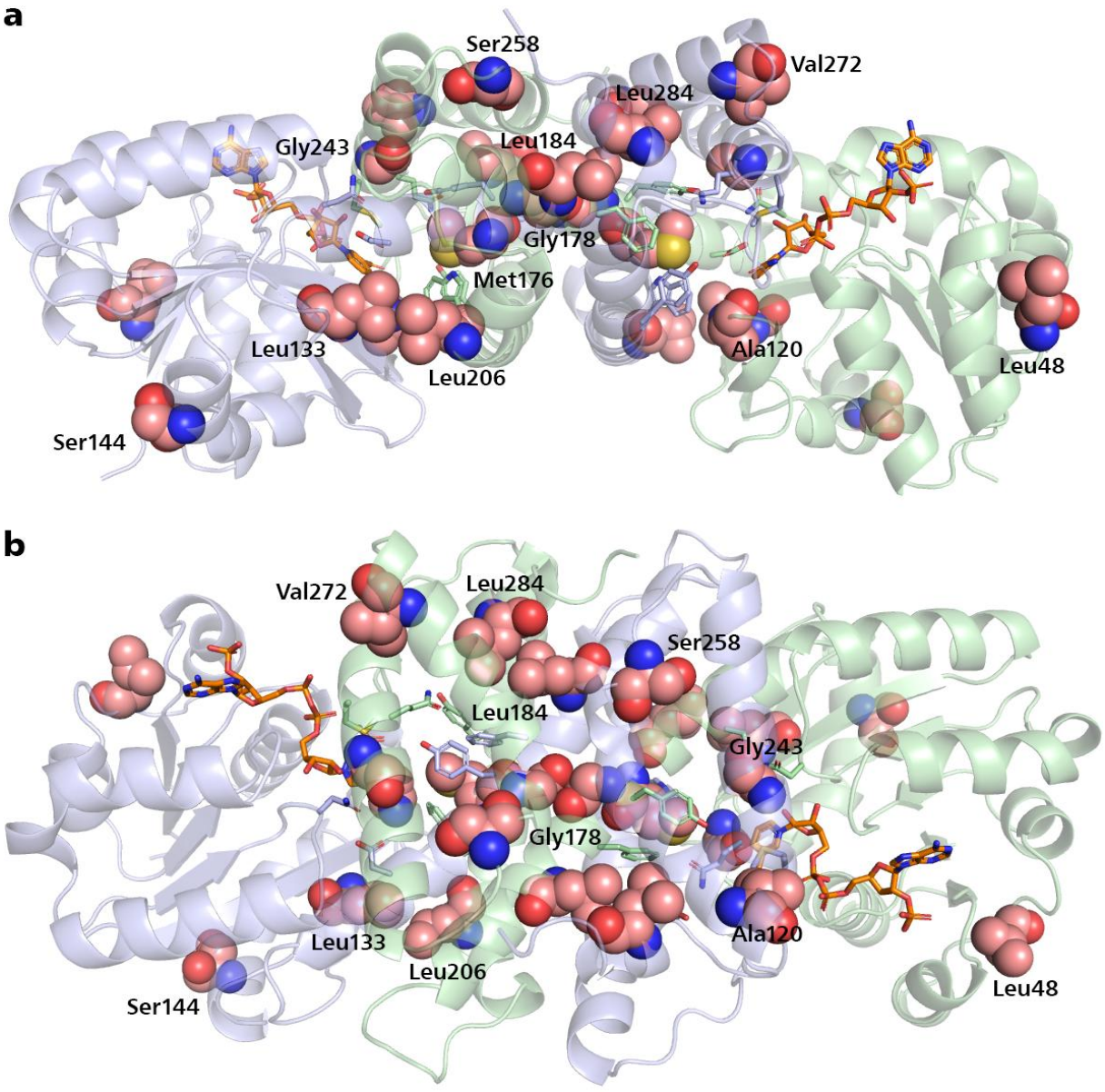


Figure S19. Residues with a substantial conservation difference between top-20 performing IREDs and the general IRED/RedAm family mapped onto the X-ray crystal structure of *Asp*RedAm (PDB: 5g6s, rasagiline ligand removed for clarity). Active-site residues and the NADP cofactor are shown in stick representation. A-Chain residues are rendered in green, B-chain residues in blue, and NADP in orange. Residues enriched in top-20 enzymes are shown as pink spheres and labelled in one of the two chains. **(a)** Front view, **(b)** top view.

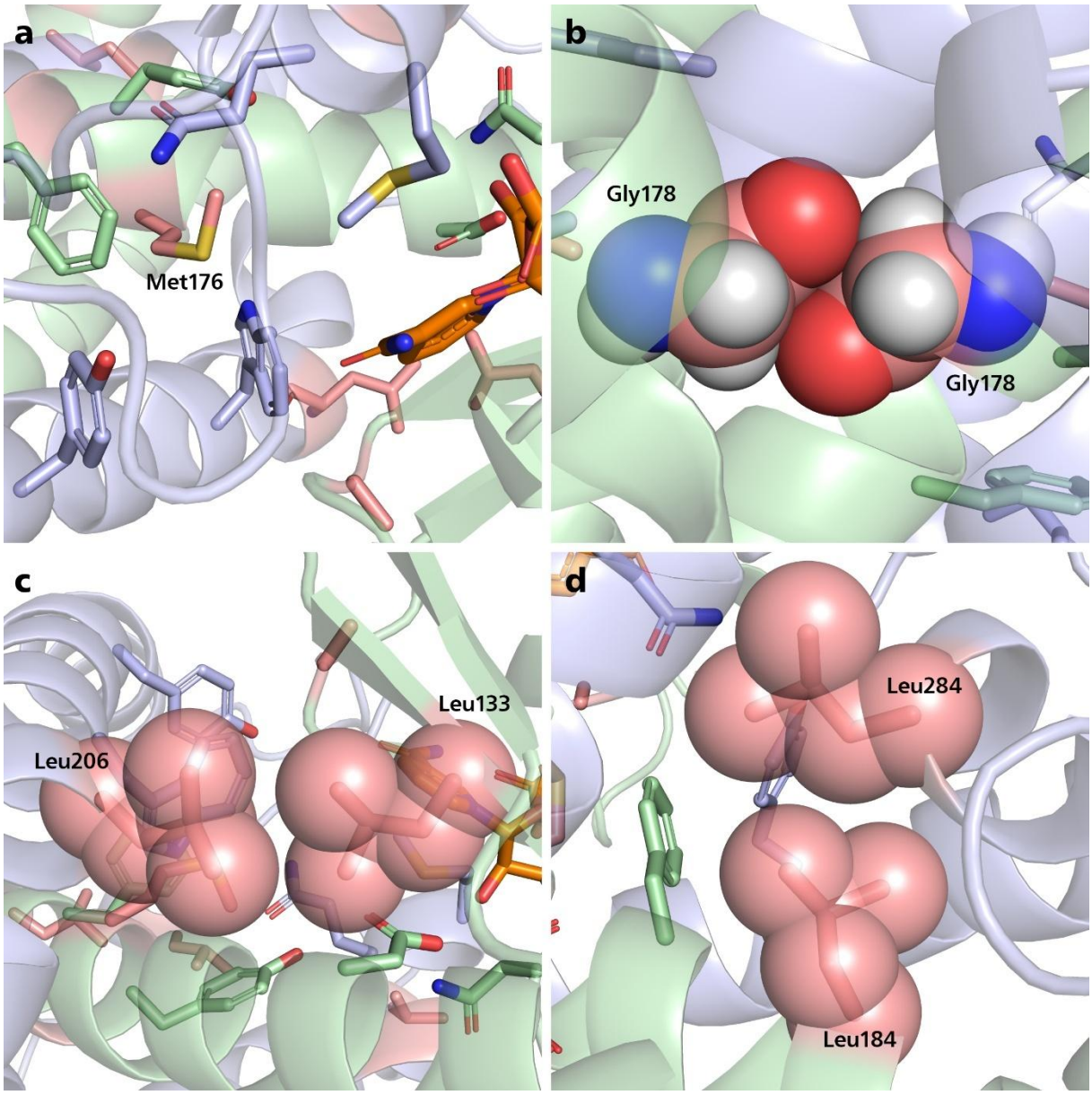


Figure S20. Exemplary residues enriched in top-20 performing IREDs and their protein environment in the X-ray crystal structure of *Asp*RedAm (PDB: 5g6s, rasagiline ligand removed for clarity). Active-site residues and the NADP cofactor are shown in stick representation. A-Chain residues are rendered in green, B-chain residues in blue, NADP in orange, and enriched residues in pink. **(a)** Environment of Met176 in the active-site pocket, **(b)** close contact of Gly178 residues from the two protein chains in the inter-domain helix, **(c)** Leu133 and Leu206 engaging in hydrophobic interactions, **(d)** Leu184 and Leu284 engaging in hydrophobic interactions.

The observed influence of distant residues on substrate scope agrees with results of a recent study aimed at identifying RedAms with broad activity towards arylamines, where increased conservation was found mainly for positions involved in NADPH binding, but not in substrate binding.[24] On the other hand, there is only limited overlap between the 12 residues identified in our analysis and positions reported as hotspots for broad substrate scope in a recent site-saturation mutagenesis study.[23] The eight residues listed there (Arg33, Thr95, Tyr134, Leu170, Met176, Tyr177, Trp210, and Gln240 in *Asp*RedAm numbering) include only one position for which we observe conservational enrichment in our top-20 IREDs (Met176), but they overlap considerably with residues we found to influence stereoselectivity (see below).

Poor reactivity of aromatic ketones and amines:
In line with previous reports,[25] our screening found aromatic ketones (**c3**, **c12**, **c27**–**c36**) and aromatic amines (**a7**, **a17**, **a18**, **a24**) to be poor substrates. While some low-level activities could be observed when these compounds were combined with a favourable reaction partner (*e.g.*, **a4** for ketones, **c2** for amines), the reductive amination of two aromatic partners (ketone *and* amine) was not achieved under the investigated reaction conditions, despite screening 100–175 IREDs for each substrate pair.

Steric constraints might play a role in the poor acceptance of aromatic compounds, but given that arylaliphatic molecules (*e.g.*, **c8**, **c24**, **a15**, **a16**, **a23**) and alicyclic ketones carrying bulky substituents (**c16**–**c18**) were tolerated comparably well, we consider steric demand alone insufficient for explaining the inability of IREDs to achieve reductive amination of aromatic substrate pairs. To assess whether the active sites of typical IREDs provide sufficient space to accommodate the bulky, aromatic imines in a catalytically productive conformation, we docked several representative structures (**c28=a24** and **c33=a24** as examples of imines with aromatic substituents on both ends of the C=N bond, and **c2=a14**, **c2=a17**, and **c32=a2** as examples with only one bulky group) into five broad-scope IREDs (IR0035, IR0041, IR0060, IR1136, IR2021) identified in our screening. All dockings were performed with rigid receptor structures (X-ray crystal structures or homology models) and Meeko-prepared ligands[26] in AutoDock Vina,[27,28] sampling 20 poses per docking run. A pose was classified as productive if the distance between the imine carbon atom and the nicotinamide C4 atom (C4N) of the NADPH cofactor was below 4.5 Å. This cut-off is intentionally generous, as experimentally observed C4N–C(sp^2) distances in ternary complexes of IREDs and other NAD(P)H-dependent oxidoreductases are typically lower, at 3.5–4.0 Å. As shown in Table S9, all five bulky imines reach productive conformations in at least one of the five investigated IREDs by this criterion.

Table S9. Results of protein–ligand docking of bulky imines.

	Productive Poses[b]					
Ligand[a]	*IR0035*	*IR0041*	*IR0060*	*IR1136*	*IR2021*	*Overall*
c2=a14	6/20	4/20	0/20	0/20	4/20	14/100
c2=a17	3/20	2/20	0/20	0/20	2/20	7/100
c32=a2	1/20	2/20	0/20	0/20	0/20	3/100
c28=a24	0/20	1/20	0/20	0/20	0/20	1/100
c33=a24	1/20	0/20	0/20	0/20	0/20	1/100

[a] The imines resulting from condensation of the specified carbonyl and amine substrates were used as ligands, and the equal sign represents the C=N double bond. [b] Number of productive docking poses (out of total poses) for each investigated IRED and overall.

Although the two imines bearing aromatic substituents on both sides of the C=N bond (**c28=a24**, **c33=a24**) reach only a single productive conformation each, inspection of these poses confirms that they are geometrically plausible (Figure S21, overleaf). This suggests that even the largest aromatic structures covered in our screening find sufficient space in the IREDs' active site to bind productively. Indeed, in an independent study we found that both these imines (and several others, including **c3=a7**, **c5=a7**, and **c32=a24**) are often accepted as substrates if they are pre-formed chemically and supplied to IREDs for reduction.[29] We interpret this as a strong indication that direct reductive amination of the corresponding ketone–amine pairs is limited by the low reactivity of the substrates for imine formation, not by imine binding or reduction.

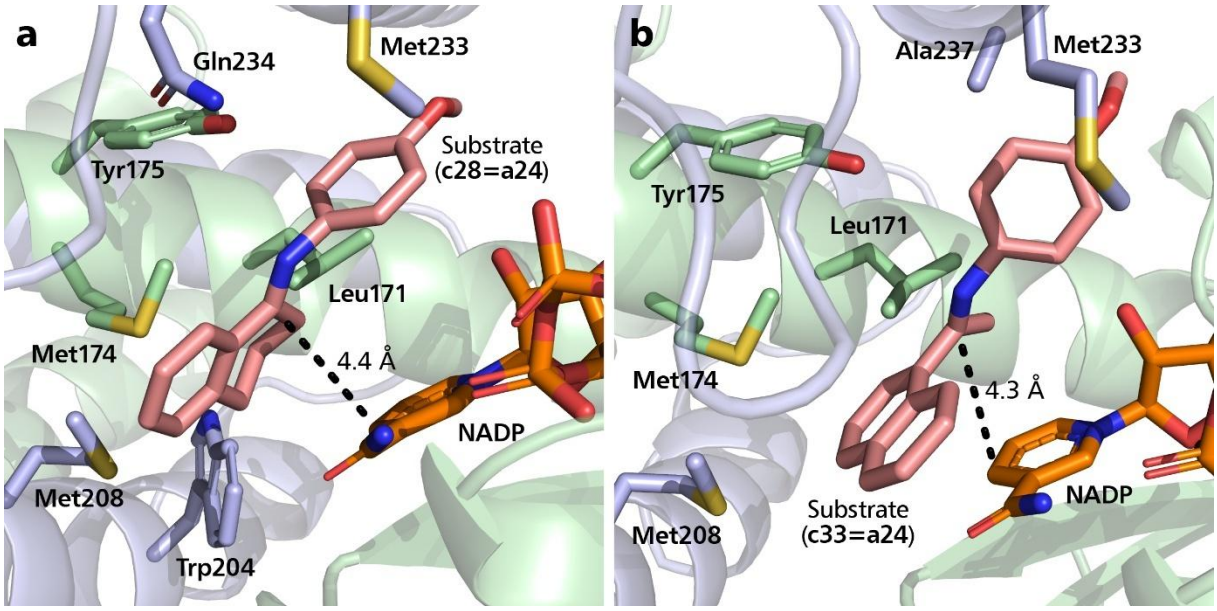


Figure S21. Plausible productive docking poses of bulky aromatic imines. Residues in close contact with the substrate are shown in stick representation. A-Chain residues are rendered in green, B-chain residues in blue, NADP in orange, and substrates in pink. The distances between the imine carbon atom and the nicotinamide C4 atom are shown as dashed black lines. **(a)** Imine **c28=a24** in IR0041. **(b)** Imine **c33=a24** in IR0035.

This notion is further supported by a correlation between the substrates' median z-scores (as a measure of general substrate acceptance) and two parameters from our set of chemoinformatic descriptors that serve as proxies for reactivity (Figure S22): Carbonyl z-scores are correlated with the relative LUMO energy level (expressed as Jaguar-calculated eigenvalues; $r = 0.39$, $p < 0.05$), a measure of electrophilicity. Amine z-scores, on the other hand, tend to increase with the pK_{aH} value, a proxy for nucleophilicity, although this correlation is not statistically significant because of the relatively small sample size (24 amines) and the *tert*-butylamine (**a14**) outlier ($r = 0.37$, $p = 0.068$). It becomes statistically significant when *tert*-butylamine is removed from the analysis ($r = 0.55$, $p < 0.01$).

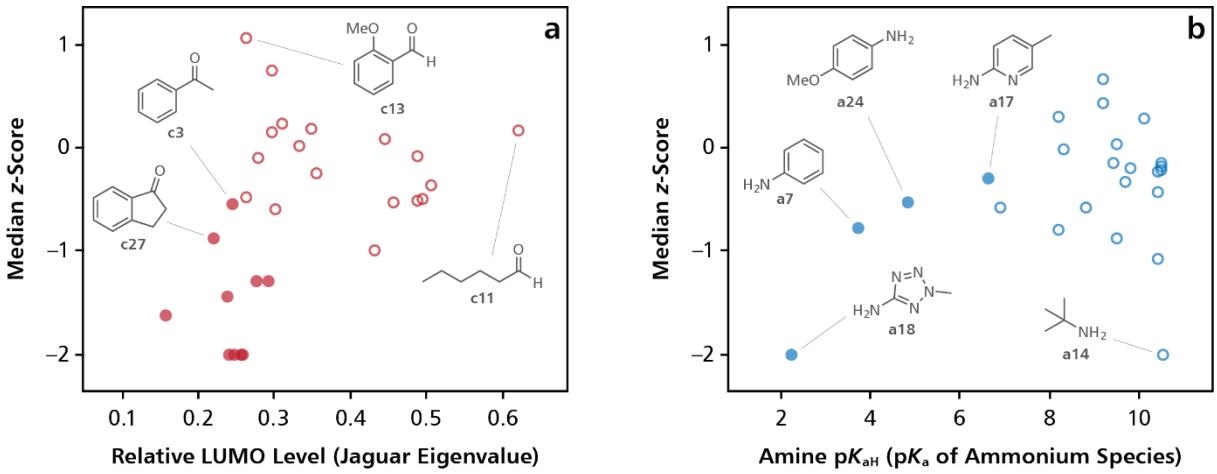


Figure S22. Correlation between median z-scores and chemoinformatic descriptors of reactivity. Substrates with no positive screening results were assigned a z-score of –2 for this analysis. Aromatic ketones and amines are shown as filled circles, other substrates as empty circles, and selected compounds are labelled. **(a)** Relative LUMO levels and median z-scores of carbonyl substrates, **(b)** pK_{aH} values and median z-scores of amine substrates. Source data are provided as a Source Data file.

Structural determinants of stereoselectivity:
As a first step in rationalising the stereoselectivity of the investigated IREDs, we tried to replicate the observed enantiopreference of six example reactions (Table S10) by protein–ligand docking. The imines corresponding to the chosen substrate combinations were docked into the rigid protein structures (X-ray crystal structures or homology models) using AutoDock Vina, sampling a total of 80 poses (two independent seeds with 40 poses each) per receptor–ligand pair. For each productive pose (imine carbon within 4.5 Å of nicotinamide C4), the imine face presented to the nicotinamide ring was identified, and Boltzmann weighting of poses by their Vina docking score was used to generate an aggregated stereoselectivity call for each example. As shown in Table S10, the stereopreference prediction generated in this way matched the observed enantiomer in five of the six test cases. The negative case (**c16=a4**, IR0041) was re-investigated using protein structures generated by two alternative methods (X-ray crystal structure of a homologue with grafted side chains, Boltz-2[30] *ab-initio* model); however, these failed to give productive docking poses. In all five positive cases, the stereochemical prediction was robust over two independent Boltzmann seeds. Overall, these results suggest that IRED stereoselectivity in reductive amination reactions can in many cases be modelled by simple protein–ligand docking.

Table S10. Rationalisation of observed stereoselectivity by protein–ligand docking.

			Stereoselectivity[c]		
Ligand[a]	**Receptor**	**Poses**[b]	ee_{exp} [%]	*Pred.*	*Match*
c8=a10	IR0068 (homology model)	7/80	>99 (*R*)	(*R*) / (*R*)	yes
c8=a10	IR1855 (PDB: 8a3x)	22/80	>99 (*S*)	(*S*) / (*S*)	yes
c16=a4	IR0041 (homology model)	6/80	>99 (*R*)	(*S*) / (*S*)	no
c16=a4	IR0041 (PDB: 6sle, with side-chain graft)	0/80	>99 (*R*)	–	–
c16=a4	IR0041 (Boltz *ab-initio* model)	0/80	>99 (*R*)	–	–
c16=a4	IR0065 (homology model)	9/80	99 (*S*)	(*S*) / (*S*)	yes
c22=a4	IR0068 (homology model)	8/80	>99 (*R*)	(*R*) / (*R*)	yes
c22=a4	IR1855 (PDB: 8a3x)	23/80	>99 (*S*)	(*S*) / (*S*)	yes

[a] The imines resulting from condensation of the specified carbonyl and amine substrates were used as ligands, and the equal sign represents the C=N double bond. [b] Number of productive docking poses used for analysis (out of total poses). [c] Experimentally observed enantiomeric excess and absolute configuration (ee_{exp}), predicted enantiopreference reported for two independent Boltzmann seeds (*Pred.*), and agreement between observed and predicted absolute configuration (*Match*).

Visual inspection of representative docking poses showed the side chains of residues Asn94, Leu173, Met176, Trp208, Ser233, Met235 and Gln238 in (*R*)-selective IR0068 (corresponding to Asn93, Leu173, Met176, Trp210, Ser235, Met239, and Gln240 in *Asp*RedAm numbering) to be in direct contact with the imine ligands (Figure S23, panels a, c; overleaf). In the (*S*)-selective enzymes IR0065 and IR1855, the position corresponding to Trp210 is occupied by significantly smaller residues (Met219 and Val212, respectively), leading to a flipped substrate-binding mode, a tighter arrangement of the active site, and strongly altered protein–ligand interactions in the docking poses (Figure S23b,d): The N-terminal, NADP-binding domain closes in on the substrate, which occupies some of the space created by the absence of the bulky tryptophan side chain. Consequently, interactions with A-chain residues Leu175 and Leu/Met178 (equivalent to Leu173 and Met176 in IR0068) and B-chain residue His242/His244 (replacement of IR0068's Gln238) are intensified, while contacts with other B-chain residues are weakened or lost.

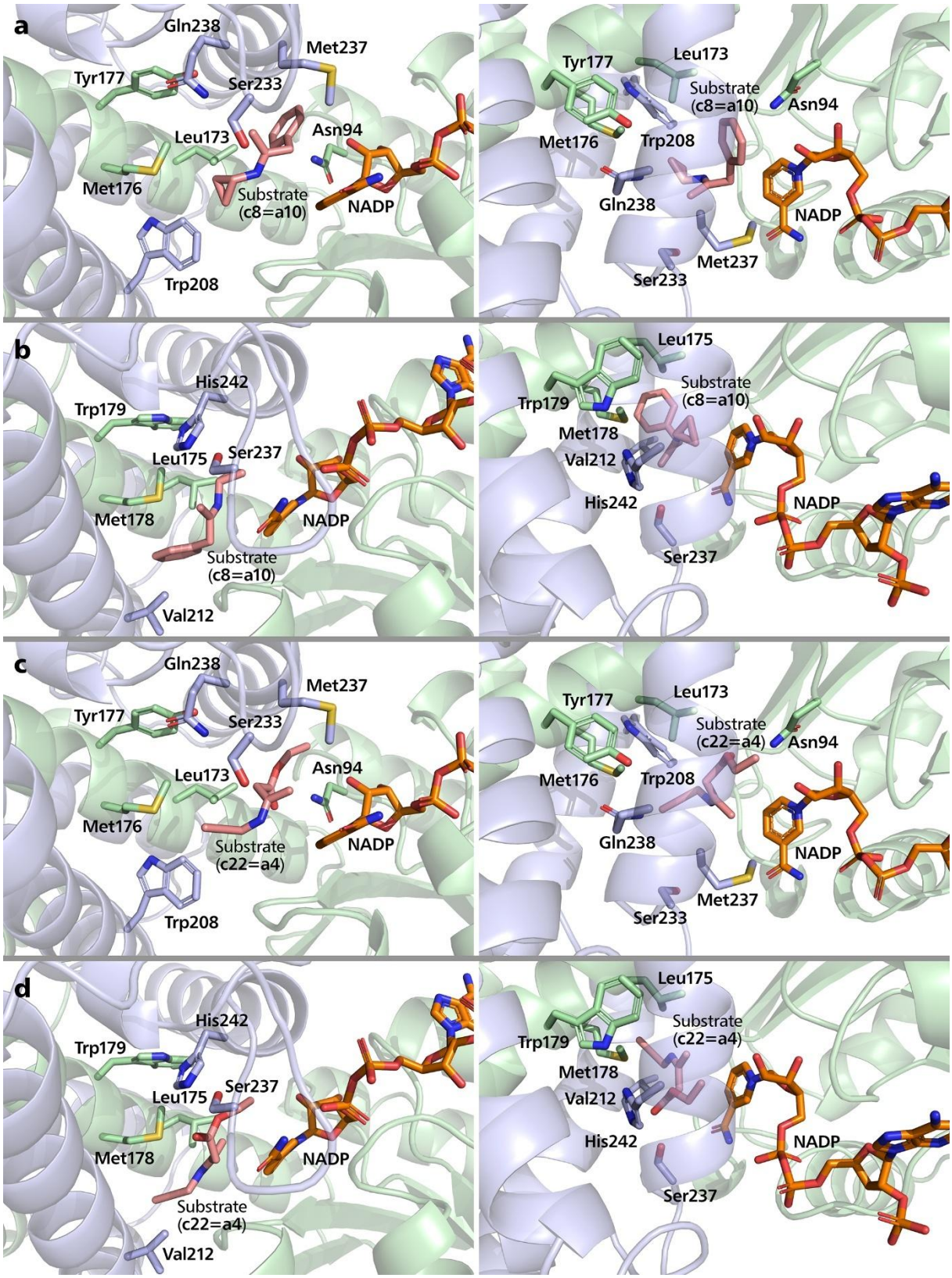


Figure S23. Representative docking poses used to rationalise enantioselectivity differences between IREDs, showing two view angles (front view, left; top view, right) for each pose. Residues in close contact with the substrate as well as the second-shell residue Tyr177/Trp179 are shown in stick representation. A-Chain residues are rendered in green, B-chain residues in blue, NADP in orange, and substrates in pink. **(a)** Pro-(*R*)-conformation of imine **c8=a10** in IR0068. **(b)** Pro-(*S*)-conformation of imine **c8=a10** in IR1855. **(c)** Pro-(*R*)-conformation of imine **c22=a4** in IR0068. **(d)** Pro-(*S*)-conformation of imine **c22=a4** in IR1855.

To better understand whether this observation has wider significance, we generated multiple-sequence alignments of 10 IREDs that had reliably shown canonical RedAm stereoselectivity in our screening – that is, (*R*) for most model substrates – and of 10 enzymes that had tended to provide the opposite product enantiomer. As shown in Table S11 (blue and green highlights), these two groups of IREDs conserve different amino acid residues in two of the active-site positions that directly interact with the substrate. Most notably, Trp210 (*Asp*RedAm numbering) is fully conserved in the ten enzymes showing canonical selectivity, but consistently replaced with smaller residues in the non-canonical group. Similarly, Gln240 is fully conserved in the canonical group, but replaced with different amino acids (most frequently histidine) in the IREDs showing non-canonical selectivity. Other residues in direct contact with the substrate show no or a less pronounced conservation difference between (*R*)- and (*S*)-selective enzymes: Met176 and Ser235 are fully conserved in IREDs with canonical and partly conserved in IREDs with non-canonical selectivity, while Leu173 is a highly conserved position in both groups. Interestingly, Tyr177, a second-shell residue implicated in catalysis (see *Protein Sequence–Activity Analysis*), is highly conserved in IREDs with canonical RedAm selectivity, but frequently replaced with tryptophan in the non-canonical group. As shown in the top view (right-hand side of all panels) in Figure S23, this exchange counterintuitively increases the space available for substrate binding, as the indole moiety of tryptophan bends back towards the core of the α-helix on which the residue is located.

Table S11. Partial sequence alignments of ten IREDs showing canonical RedAm stereoselectivity in our screening (IR0035–IR2021), ten IREDs showing opposite stereoselectivity (IR0010–IR1855), and *Asp*RedAm, the prototypical fungal reductive aminase.

IRED	Partial sequence alignment[a]																								
*Asp*RedAm	170	L	A	L	L	S	G	M	Y	G	L	F	180	...	210	W	L	S	A	M	T	G	Y	L	S	S	I	A	K	Q	I	D	D	G	D	Y	A	T	Q	G	-	S	N	L	G	M	Q	240
IR0035	168	L	A	L	L	S	G	M	Y	G	L	F	178	...	204	W	L	G	A	M	T	E	Y	T	K	G	M	A	R	Q	I	D	E	G	N	Y	A	S	E	G	-	S	N	L	G	M	Q	234
IR0040	176	L	A	L	L	S	G	M	Y	G	L	F	186	...	215	W	L	Q	A	M	T	G	Y	L	G	L	L	A	R	Q	I	D	D	G	V	Y	T	A	Q	T	-	S	N	L	E	M	Q	245
IR0041	168	L	A	L	L	S	G	M	Y	G	L	F	178	...	204	W	L	G	A	M	T	E	Y	T	K	G	M	A	K	Q	I	D	E	G	K	Y	T	S	E	G	-	S	N	L	A	M	Q	234
IR0043	168	L	A	L	L	S	G	M	Y	G	L	F	178	...	204	W	L	G	A	M	T	E	Y	T	K	G	M	A	K	Q	I	D	E	G	K	Y	T	S	E	G	-	S	N	L	A	M	Q	234
IR0068	170	L	A	L	L	S	G	M	Y	G	L	F	180	...	208	W	L	T	A	M	T	Q	H	L	N	L	L	A	T	Q	V	D	E	K	D	Y	G	D	G	G	-	S	S	L	D	M	Q	238
IR0233	170	L	A	L	L	S	G	M	Y	G	L	F	180	...	208	W	L	T	A	M	T	Q	H	L	N	M	L	A	K	Q	V	D	D	E	D	F	G	D	G	G	-	S	S	L	E	M	Q	238
IR1395	174	V	A	L	L	S	A	M	Y	G	L	F	184	...	211	W	L	G	A	M	G	F	F	V	G	N	A	A	E	R	L	T	S	R	D	F	T	S	G	V	V	S	N	L	A	M	Q	242
IR1453	176	V	A	L	L	S	A	M	S	G	M	F	186	...	213	W	L	A	A	M	A	P	A	V	H	Q	S	A	D	Q	L	Q	S	G	D	Y	T	R	N	V	V	S	N	L	A	M	Q	244
IR1738	175	V	A	L	L	S	A	M	Y	G	M	F	185	...	212	W	L	V	A	M	A	P	A	V	H	Q	T	A	D	R	L	R	S	G	D	Y	T	K	G	V	V	S	S	L	A	M	Q	243
IR2021	168	L	A	L	L	S	G	M	Y	G	L	F	178	...	204	W	L	G	A	M	T	E	Y	T	K	G	M	A	K	Q	I	D	E	G	K	Y	A	S	E	G	-	S	N	L	A	M	Q	234
IR0010	171	M	A	L	L	D	L	F	W	T	S	V	181	...	208	I	V	G	I	L	S	P	I	215	...	228	H	S	D	A	S	A	S	V	S	S	V	238
IR0015	167	Q	A	Q	L	Y	L	F	W	S	T	L	177	...	207	S	L	G	V	D	G	P	M	214	...	229	S	P	G	G	E	N	S	M	L	M	M	239
IR0032	169	C	A	V	A	A	Y	F	A	G	G	L	179	...	209	I	L	G	G	D	V	A	H	216	...	226	F	D	H	P	Y	A	S	L	K	T	W	236
IR0065	172	S	A	I	L	F	Q	L	W	G	S	L	182	...	212	M	I	Q	F	S	M	K	D	219	...	232	D	P	Q	S	P	A	T	L	D	T	H	242
IR0066	167	V	A	L	L	D	L	F	W	T	S	V	177	...	204	I	S	E	I	L	P	A	I	211	...	224	H	D	D	A	S	A	P	V	S	S	V	234
IR0199	186	Q	A	Q	L	A	V	F	L	T	T	L	196	...	226	S	I	G	D	I	L	R	A	233	...	247	H	P	G	H	L	S	T	V	T	M	M	257
IR0395	172	V	A	G	L	A	M	M	W	S	I	L	182	...	209	L	A	S	V	V	V	E	W	216	...	229	F	P	A	E	V	S	A	L	E	T	D	239
IR1134	177	M	A	L	L	G	L	M	W	G	I	L	187	...	214	M	I	K	E	V	T	E	Y	221	...	234	Y	P	A	T	D	A	T	L	T	V	H	244
IR1136	177	L	S	V	L	S	I	M	W	G	V	L	187	...	214	A	I	N	V	T	A	E	Y	221	...	234	Y	P	A	T	D	A	T	V	N	V	H	244
IR1855	172	S	A	V	L	A	L	M	W	G	A	L	182	...	212	V	V	E	G	L	V	A	D	219	...	232	D	A	E	T	L	S	S	I	S	P	H	242

[a] First-shell active-site residues with a clear conservation difference between IREDs of opposite stereoselectivity are highlighted in blue for the canonical and green for the non-canonical group, while residues with no clear conservation difference are highlighted in grey. A red highlight is used for the second-shell residue Tyr177 (canonical) and an orange highlight for its frequent non-canonical replacement, tryptophan.

These conservation trends are intriguing in the context of earlier studies that used site-directed mutagenesis to modify RedAm stereoselectivity. Already in the original *Asp*RedAm paper,[7] the W210A, W210S and Q240A mutations were shown to strongly impact the stereoselectivity of the reductive amination reaction across several substrate combinations, with both Trp210 replacements leading to a pronounced switch from (*R*)- to (*S*)-selectivity. The equivalent position (W204) in an IRED from *Aspergillus lentulus* (IR-09) was later targeted to engineer the enzyme for the enantio- and diastereoselective synthesis of a medicinal chemistry building block featuring three contiguous stereocentres.[31] Again, initial replacement with alanine or serine revealed a profound impact on stereoselectivity, and site-saturation mutagenesis identified the W204R variant as the most selective for the desired absolute configuration (*S*,*S*,*S*). Recently, Aleku and co-workers used alanine scanning of multiple bulky active-site residues in a reductive aminase from *Mortierella antarctica* (*Ma*RedAm) to identify positions that govern stereoselectivity.[22] Once again, replacement of the very same tryptophan residue (W211A) had the strongest impact, resulting in a switch from (*R*)- to (*S*)-selectivity. Targeting the catalytically important Tyr181 residue of *Ma*RedAm (equivalent to Tyr177 in *Asp*RedAm) negatively affected activity in the Y181A variant, but led to improved (*R*)-stereoselectivity. Taken together, these site-directed mutagenesis studies pinpoint Tyr177, Trp210 and Gln240 (*Asp*RedAm numbering) as active-site positions that are key to modulating the stereoselectivity of IREDs and RedAms in reductive amination. Our observation of marked conservation differences for these residues between (*R*)- and (*S*)-selective wild-type IREDs reveals that natural evolution has explored the same positions for generating enzymes with non-canonical stereoselectivity. However, we also note that other residues identified as influential in the recent alanine scanning study (W31, R33, Y113, and Y134 in *Asp*RedAm numbering) do not appear indicative for stereopreference in wild-type IREDs, as they are highly conserved in both (*R*)- and (*S*)-selective enzymes.

The conservation trends and docking results discussed above strongly suggest that the enantiopreference of an IRED in reductive amination can be predicted based on its amino acids in positions 177, 210 and 240 (*Asp*RedAm numbering). To assess whether these positions indeed have predictive value, we analysed four representative model reactions (substrate combinations **c6-a4**, **c10-a10**, **c16-a2**, **c22-a4**) of eight enzymes from our top-20 panel (*cf*. Table S7) for which we had not previously collected any stereoselectivity data. Based on the three key residues, two of these IREDs (IR1632, IR1805) are expected to show canonical (*R*)-selectivity in the investigated reactions, as they conserve the Tyr177 and Trp210 positions of *Asp*RedAm and replace Gln240 with a chemically similar amino acid, asparagine. The other six enzymes (IR0030, IR0052, IR0060, IR0063, IR0064, IR1105) are expected to be (*S*)-selective, as they all have Trp210 replaced with a significantly smaller residue. With the exception of IR1105, they also match the modal pattern of non-canonical selectivity on the remaining two positions, with Tyr177 and Gln240 changed for tryptophan and histidine, respectively. As summarised in Table S12 (overleaf), 29 of the 32 investigated reactions gave sufficient levels of product to determine its enantiomeric excess and absolute configuration. Of these, 23 (79%) match the expected enantiopreference, with five enzymes showing consistent selectivity in all model reactions. The most significant deviations from expected behaviour are observed for IR1105, whose stereoselectivity is inconsistent and generally low to moderate, and IR0030, which is poorly active towards the investigated substrate pairs (as expected based on the activity screening results), but shows (*R*)-enantiopreference in the two reactions for which an *ee* could be determined. Overall, these results indicate that wild-type IREDs can be categorised as (*R*)- or (*S*)-selective in reductive amination with a useful but not absolute confidence based on only three active-site key residues. This complements the sequence-based enantiopreference classification of IREDs in imine reduction developed in earlier studies.[13]

Table S12. Predictive value of active-site key residues for IRED enantiopreference.

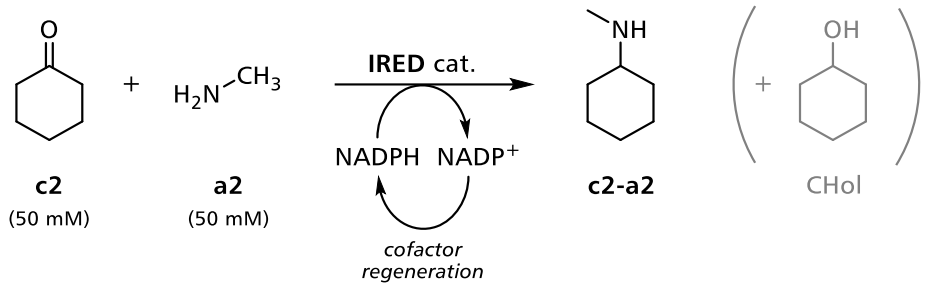
		Conversion [%], *ee* [%][a,b]			
IRED	**Key Residues**	**c6-a4**	**c10-a10**	**c16-a2**	**c22-a4**
IR1632	Y...W...N	40, 84 (*R*)	39, 75 (*R*)	1, >99 (*R*)	9, 97 (*R*)
IR1805	Y...W...N	37, 91 (*R*)	32, 56 (*R*)	2, 28 (*S*)	2, 74 (*R*)
IR0030	W...V...H	18, 98 (*R*)	1, n.d.[c]	–, n.d.[c]	1, 36 (*R*)
IR0052	W...M...H	26, 88 (*S*)	71, 97 (*S*)	–, n.d.[c]	4, 84 (*S*)
IR0060	W...A...H	13, 85 (*S*)	86, >99 (*S*)	4, 95 (*S*)	1, 93 (*S*)
IR0063	W...V...H	49, 42 (*S*)	86, >99 (*S*)	trace, >99 (*S*)	34, 90 (*S*)
IR0064	W...M...H	40, 98 (*S*)	79, 93 (*S*)	2, 77 (*S*)	6, 98 (*S*)
IR1105	F...V...C	46, 80 (*R*)	75, 33 (*S*)	6, 66 (*R*)	19, 77 (*R*)

[a] Conversion into the expected reductive amination product determined by GC–FID analysis using *n*-decane or *n*-dodecane as internal standard. For **c10-a10**, the sum of lactam and open-chain amino ester products is reported. [b] Enantiomeric excess determined by GC analysis on a chiral stationary phase. Absolute configurations that agree with the expectation based on active-site key residues are highlighted in green. [c] n.d., not determined. *Reaction conditions:* Carbonyl compound (50 mM), amine (50 mM), $NADP^+$ (1 mM), $Na_2HPO_3 \cdot 5\ H_2O$ (100 mM), IRED preparation (4 mg/mL lyophilised cell lysate), PtDH preparation (4 mg/mL lyophilised cell lysate), bicine–NaOH buffer (100 mM, pH 8.0), DMSO (10% v/v), reaction volume 500 μL, 30 °C, 120 rpm, 24 h.

Biotransformations

Comparison of different cofactor regeneration systems:

For regeneration of the NADPH cofactor required by the IREDs, we tested six NADP-dependent auxiliary enzymes available in our group: three formate dehydrogenases (FDHs), two glucose dehydrogenases (GDHs), and a phosphite dehydrogenase (PtDH; for details on these auxiliary enzymes, see *Supplementary Methods*, Table S31). The reductive amination of cyclohexanone (**c2**) with methylamine (**a2**) catalysed by IREDs IR0071 and IR0076 was used as a model reaction, and the six cofactor regeneration systems were compared regarding the formation of the desired product, *N*-methylcyclohexanamine (**c2-a2**), and of the side product resulting from competing C=O reduction, cyclohexanol (Scheme S1). As shown in Table S13, the use of PtDH led to the highest conversions into the desired product (29% with IR0071 and 83% with IR0076 after 4 h), along with only minor formation of cyclohexanol (0.3% after 4 h). In comparison, the tested FDHs gave lower levels of **c2-a2** (22–28% with IR0071 after 4 h) with comparable alcohol formation (0.1–0.2% after 4 h), while *Bm*-GDH showed relatively pronounced C=O reduction (2.1% after 4 h) and *Bs*-GDH was entirely inactive, resulting in no consumption at all of cyclohexanone (**c2**). Therefore, we chose phosphite dehydrogenase (PtDH) as the auxiliary enzyme for NADPH regeneration in all further experiments.



Scheme S1. IRED-catalysed reductive amination of cyclohexanone (**c2**) with methylamine (**a2**), leading to *N*-methylcyclohexanamine (**c2-a2**) as the desired product and cyclohexanol (CHol) as carbonyl reduction side product.

Table S13. Comparison of six auxiliary enzymes for the regeneration of NADPH.

			Conversion[a] (4 h) [%]		Conversion[a] (24 h) [%]	
IRED	**Auxiliary enzyme**	**Co-substrate**	**c2-a2**	CHol	**c2-a2**	CHol
IR0071	PtDH	$Na_2HPO_3 \cdot 5\ H_2O$	29.2	0.3		
IR0071	NADP-FDH-var	$HCOONH_4$	27.5	0.2		
IR0071	*Myc*-FDH	$HCOONH_4$	24.0	0.1		
IR0071	*Pse*-FDH-V13	$HCOONH_4$	21.8	0.1		
IR0071	*Bm*-GDH	D-glucose	14.7	2.1		
IR0071	*Bs*-GDH	D-glucose	–	–		
IR0076	PtDH	$Na_2HPO_3 \cdot 5\ H_2O$	83.3	0.3	92.9	1.5
IR0076	NADP-FDH-var	$HCOONH_4$	64.0	0.2	84.7	1.2

[a] Conversion into the expected reductive amination product (**c2-a2**) and into cyclohexanol (CHol) determined by GC–FID analysis using *n*-decane as internal standard. *Reaction conditions:* **c2** (50 mM), **a2** (50 mM), $NADP^+$ (1 mM), co-substrate (100 mM), IRED preparation (4 mg/mL lyophilised cell lysate), auxiliary enzyme preparation (4 mg/mL lyophilised cell lysate), bicine–NaOH buffer (100 mM, pH 8.0), DMSO (10% v/v), reaction volume 500 μL, 30 °C, 800 rpm, 4–24 h.

Validation experiments for the Overview Screening:

The results of the photometric NADPH consumption assay used in the Overview Screening and, in particular, the statistical criterion for hit identification (equation 3, see *Photometric IRED Activity Assay: Overview Screening*) were validated by three series of small-scale biotransformations that were analysed by GC–MS or HPLC–MS. First, the false-positive rate (type I error, α) and false-negative rate (type II error, β) of the hit criterion were estimated based on 50 randomly selected substrate–enzyme combinations (25 positives and 25 negatives), picked using a random-number generator in *Microsoft* Excel. As shown in Table S14 and Table S15 (overleaf), the expected reductive amination product could be detected in 23 of the photometric hits and in only one of the photometric non-hits, corresponding to false-positive and false-negative rates of α = 8% and β = 4%. All three false results occurred at low activity levels (76–12 mU/mg_{IRED}) and with ammonia (**a1**) as the amine substrate.

Table S14. Photometric activity levels and chromatographically determined levels of product formation for 50 randomly selected IRED–substrate combinations of the Overview Screening.

Photometric positives					*Photometric negatives*				
IRED	**Substrates**		**Activity**[a]	**Conv.**[b]	**IRED**	**Substrates**		**Activity**	**Conv.**
	Carb.	*Am.*	[mU/mg_{IRED}]	[%]		*Carb.*	*Am.*	[mU/mg_{IRED}]	[%]
IR1738	**c2**	**a4**	15354 ± 236	>99	IR0196	**c2**	**a3**	–39 ± 17	–
IR2010	**c4**	**a4**	1635 ± 352	27	IR0202	**c2**	**a1**	76 ± 5	16
IR1460	**c2**	**a6**	1509 ± 176	93	IR0002	**c6**	**a7**	–3 ± 1	–
IR0059	**c1**	**a4**	1045 ± 114	26	IR0039	**c6**	**a3**	10 ± 1	–
IR1662	**c1**	**a2**	422 ± 15	34	IR0482	**c6**	**a2**	–15 ± 3	–
IR2145	**c1**	**a4**	306 ± 21	45	IR2092	**c6**	**a5**	–10 ± 4	–
IR2147	**c6**	**a6**	280 ± 9	92	IR0497	**c7**	**a4**	–24 ± 4	–
IR2159	**c1**	**a2**	199 ± 13	10	IR1662	**c7**	**a5**	9 ± 2	–
IR0499	**c4**	**a6**	199 ± 15	15	IR0049	**c4**	**a3**	–6 ± 3	–
IR0041	**c6**	**a4**	192 ± 18	96	IR0058	**c4**	**a5**	–8 ± 2	–
IR1662	**c4**	**a4**	148 ± 10	2	IR1136	**c4**	**a7**	–21 ± 2	–
IR0869	**c2**	**a2**	87 ± 4	42	IR1664	**c4**	**a2**	–48 ± 8	–
IR0902	**c2**	**a2**	61 ± 5	44	IR1749	**c4**	**a7**	–33 ± 2	–
IR0070	**c2**	**a6**	51 ± 5	74	IR2114	**c8**	**a5**	–142 ± 38	–
IR0199	**c2**	**a4**	49 ± 7	90	IR0015	**c3**	**a6**	2 ± 4	–
IR0376	**c4**	**a2**	45 ± 2	2	IR0058	**c3**	**a3**	–24 ± 3	–
IR1805	**c6**	**a2**	40 ± 3	12	IR0392	**c3**	**a7**	–7 ± 1	–
IR0023	**c8**	**a4**	30 ± 7	1	IR0034	**c5**	**a4**	75 ± 27	–
IR2253	**c3**	**a1**	27 ± 2	1	IR0312	**c5**	**a4**	46 ± 85	–
IR0056	**c6**	**a1**	27 ± 4	trace	IR2036	**c5**	**a1**	–28 ± 3	–
IR0021	**c1**	**a1**	25 ± 2	33	IR2137	**c5**	**a7**	–39 ± 6	–
IR2022	**c4**	**a7**	20 ± 3	9	IR0018	**c1**	**a2**	–2 ± 11	–
IR1392	**c7**	**a6**	20 ± 3	23	IR0065	**c1**	**a1**	–41 ± 2	–
IR0392	**c4**	**a1**	14 ± 1	–	IR0196	**c1**	**a3**	–8 ± 10	–
IR0887	**c2**	**a1**	12 ± 3	–	IR0869	**c1**	**a3**	–6 ± 1	–

[a] Specific activity (mean ± standard deviation, corrected for background absorbance decrease, prior to data consolidation) determined by a photometric NADPH consumption assay. *Assay conditions:* Carbonyl compound (50 mM), amine (50 mM; except **a1**: 500 mM), NADPH (2 mM), IRED preparation (2 mg/mL lyophilised cell lysate), bicine–NaOH buffer (100 mM, pH 8.0), DMSO (10% v/v), reaction volume 100 μL, 30 °C. [b] Conversion into the expected reductive amination product determined by uncalibrated GC–MS analysis. *Reaction conditions:* Carbonyl compound (50 mM), amine (50 mM; except **a1**: 500 mM), $NADP^+$ (1 mM), $Na_2HPO_3 \cdot 5\ H_2O$ (100 mM), IRED preparation (4 mg/mL lyophilised cell lysate), PtDH preparation (4 mg/mL lyophilised cell lysate), bicine–NaOH buffer (100 mM, pH 8.0), DMSO (10% v/v), reaction volume 500 μL, 30 °C, 120 rpm, 24 h.

Table S15. Result matrix for the photometric screening and chromatographic validation of 50 randomly selected IRED–substrate combinations of the Overview Screening.

		Result of photometric assay		
		positive	negative	total
Result of chromatographic analysis	positive	23 (92%)	1 (4%)	24 (48%)
	negative	2 (8%)	24 (96%)	26 (52%)
	total	25 (50%)	25 (50%)	50 (100%)

We considered an overall false-negative rate of 4% unproblematic, but decided to take further steps to reduce the rate of false positives (8%). To this end, we next performed a chromatographic re-screening of all substrate pairs for which at least one hit had been identified, focussing on the IREDs showing the highest activities in each case. The results are summarised in Table S16 and are reassuring in that they confirm the formation of the expected reductive amination product for 36 of the 44 investigated substrate combinations (100 of 116 performed biotransformations).

Table S16. Photometric activity levels and chromatographically determined levels of product formation for selected photometric positives of the Overview Screening (*continued on next page*).

IRED	**Substrates**		**Activity**[a]	**Conv.**[b]	**IRED**	**Substrates**		**Activity**[a]	**Conv.**[b]
	Carb.	*Am.*	[mU/mg$_{IRED}$]	[%]		*Carb.*	*Am.*	[mU/mg$_{IRED}$]	[%]
IR0010	**c1**	**a1**	67 ± 14	27	IR0036	**c2**	**a5**	140 ± 6	–
IR0043	**c1**	**a1**	38 ± 11	1	IR0035	**c2**	**a5**	123 ± 9	–
IR0005	**c1**	**a2**	1666 ± 67	>99	IR1446	**c2**	**a5**	48 ± 11	trace
IR0013	**c1**	**a2**	935 ± 15	>99	IR0058	**c2**	**a6**	3443 ± 208	98
IR0073	**c1**	**a2**	887 ± 45	81	IR0499	**c2**	**a6**	2757 ± 16	99
IR0005	**c1**	**a3**	1247 ± 88	>99	IR0497	**c2**	**a6**	1000 ± 42	86
IR0032	**c1**	**a3**	897 ± 26	91	IR0395	**c2**	**a7**	614 ± 16	51
IR0064	**c1**	**a3**	699 ± 32	28	IR0005	**c2**	**a7**	497 ± 51	86
IR2173	**c1**	**a3**	319 ± 53	trace	IR2159	**c2**	**a7**	463 ± 31	89
IR0032	**c1**	**a4**	3558 ± 240	>99	IR1105	**c2**	**a7**	423 ± 103	74
IR0005	**c1**	**a4**	3453 ± 285	>99	IR0066	**c3**	**a1**	85 ± 3	1
IR0073	**c1**	**a4**	2458 ± 228	>99	IR0610	**c3**	**a1**	35 ± 5	trace
IR0005	**c1**	**a5**	91 ± 7	23	IR2253	**c3**	**a1**	27 ± 2	trace
IR0066	**c2**	**a1**	1536 ± 129	>99	IR0011	**c3**	**a2**	155 ± 30	trace
IR0076	**c2**	**a1**	263 ± 29	>99	IR0041	**c3**	**a2**	150 ± 37	trace
IR0279	**c2**	**a1**	180 ± 15	35	IR1427	**c3**	**a2**	127 ± 33	trace
IR2021	**c2**	**a2**	3872 ± 167	88	IR0043	**c3**	**a3**	114 ± 27	–
IR0202	**c2**	**a2**	2286 ± 127	83	IR0059	**c3**	**a4**	1759 ± 41	1
IR1674	**c2**	**a3**	1845 ± 8	4	IR0041	**c3**	**a4**	1264 ± 162	10
IR1427	**c2**	**a3**	1141 ± 158	2	IR1427	**c3**	**a4**	1124 ± 284	trace
IR1805	**c2**	**a3**	110 ± 16	15	IR0043	**c3**	**a5**	102 ± 22	–
IR1749	**c2**	**a4**	9493 ± 279	>99	IR0464	**c3**	**a6**	546 ± 29	1
IR2021	**c2**	**a4**	8825 ± 156	>99	IR0499	**c3**	**a6**	311 ± 16	1
IR0069	**c2**	**a4**	8291 ± 1017	>99	IR0395	**c3**	**a6**	95 ± 19	1
IR1413	**c2**	**a4**	441 ± 20	32	IR0052	**c3**	**a7**	16 ± 3	–

[a] Specific activity (mean ± standard deviation, corrected for background absorbance decrease, prior to data consolidation) determined by a photometric NADPH consumption assay. *Assay conditions:* Carbonyl compound (50 mM), amine (50 mM; except **a1**: 500 mM), NADPH (2 mM), IRED preparation (2 mg/mL lyophilised cell lysate), bicine–NaOH buffer (100 mM, pH 8.0), DMSO (10% v/v), reaction volume 100 μL, 30 °C. [b] Conversion into the expected reductive amination product determined by uncalibrated GC–MS. *Reaction conditions:* Carbonyl compound (50 mM), amine (50 mM; except **a1**: 500 mM), $NADP^+$ (1 mM), $Na_2HPO_3 \cdot 5\ H_2O$ (100 mM), IRED preparation (4 mg/mL lyophilised cell lysate), PtDH preparation (4 mg/mL lyophilised cell lysate), bicine–NaOH buffer (100 mM, pH 8.0), DMSO (10% v/v), reaction volume 500 μL, 30 °C, 800 rpm, 24 h.

Table S16. Photometric activity levels and chromatographically determined levels of product formation for selected photometric positives of the Overview Screening (*continued from previous page*).

IRED	Substrates		Activity[a]	Conv.[b]	IRED	Substrates		Activity[a]	Conv.[b]
	Carb.	*Am.*	[mU/mg$_{IRED}$]	[%]		*Carb.*	*Am.*	[mU/mg$_{IRED}$]	[%]
IR0066	**c4**	**a1**	103 ± 15	yes[c]	IR1743	**c7**	**a1**	138 ± 38	–[c]
IR1855	**c4**	**a1**	34 ± 5	yes[c]	IR0279	**c7**	**a1**	102 ± 31	–[c]
IR1743	**c4**	**a1**	24 ± 2	–[c]	IR2021	**c7**	**a2**	108 ± 23	yes[c]
IR1392	**c4**	**a2**	179 ± 3	1	IR0032	**c7**	**a2**	49 ± 9	yes[c]
IR0041	**c4**	**a2**	130 ± 1	12	IR1855	**c7**	**a2**	41 ± 2	yes[c]
IR0043	**c4**	**a3**	70 ± 14	–	IR0204	**c7**	**a3**	28 ± 2	–
IR2021	**c4**	**a4**	2316 ± 115	38	IR2021	**c7**	**a4**	682 ± 72	99
IR0068	**c4**	**a4**	1955 ± 230	23	IR0068	**c7**	**a4**	569 ± 72	>99
IR0036	**c4**	**a4**	1636 ± 42	29	IR0202	**c7**	**a4**	460 ± 43	91
IR0043	**c4**	**a5**	62 ± 10	–	IR0041	**c7**	**a4**	189 ± 13	96
IR2147	**c4**	**a6**	277 ± 1	29	IR0009	**c7**	**a6**	117 ± 8	4
IR0015	**c4**	**a6**	215 ± 28	12	IR1437	**c7**	**a6**	106 ± 7	87
IR0464	**c4**	**a6**	202 ± 18	18	IR1855	**c7**	**a6**	97 ± 2	76
IR0033	**c4**	**a7**	37 ± 7	14	IR0005	**c7**	**a7**	41 ± 6	1
IR2022	**c4**	**a7**	20 ± 3	4	IR0033	**c7**	**a7**	30 ± 3	6
IR1059	**c5**	**a1**	142 ± 8	–[d]	IR0063	**c8**	**a1**	31 ± 1	trace
IR0041	**c5**	**a4**	72 ± 10	yes[d]	IR0107	**c8**	**a1**	28 ± 9	trace
IR0035	**c5**	**a4**	62 ± 3	yes[d]	IR0063	**c8**	**a2**	79 ± 3	trace
IR2036	**c5**	**a5**	76 ± 16	–[d]	IR1134	**c8**	**a2**	51 ± 2	28
IR0742	**c6**	**a1**	100 ± 10	–[c]	IR0052	**c8**	**a2**	42 ± 1	13
IR0068	**c6**	**a1**	66 ± 3	yes[c]	IR0068	**c8**	**a4**	346 ± 42	48
IR2021	**c6**	**a2**	182 ± 5	59	IR0036	**c8**	**a4**	277 ± 9	36
IR0068	**c6**	**a2**	102 ± 1	53	IR0041	**c8**	**a4**	271 ± 48	71
IR0032	**c6**	**a2**	60 ± 4	18	IR2021	**c8**	**a4**	233 ± 11	38
IR2021	**c6**	**a4**	1549 ± 77	95	IR0204	**c8**	**a4**	206 ± 26	5
IR0068	**c6**	**a4**	752 ± 68	95	IR2173	**c8**	**a6**	231 ± 9	–
IR0023	**c6**	**a4**	174 ± 1	93	IR1855	**c8**	**a6**	40 ± 2	trace
IR1460	**c6**	**a6**	382 ± 42	72	IR0064	**c8**	**a6**	37 ± 9	trace
IR2147	**c6**	**a6**	280 ± 9	77	IR0464	**c8**	**a6**	31 ± 5	trace
IR0202	**c6**	**a6**	134 ± 18	48	IR1136	**c8**	**a7**	600 ± 21	trace
IR0032	**c6**	**a7**	29 ± 5	18	IR1105	**c8**	**a7**	200 ± 30	–
IR0041	**c6**	**a7**	19 ± 1	6	IR2137	**c8**	**a7**	157 ± 11	trace
IR0043	**c6**	**a7**	7 ± 1	2	IR0033	**c8**	**a7**	27 ± 7	1

[a] Specific activity (mean ± standard deviation, corrected for background absorbance decrease, prior to data consolidation) determined by a photometric NADPH consumption assay. *Assay conditions:* Carbonyl compound (50 mM), amine (50 mM; except **a1**: 500 mM), NADPH (2 mM), IRED preparation (2 mg/mL lyophilised cell lysate), bicine–NaOH buffer (100 mM, pH 8.0), DMSO (10% v/v), reaction volume 100 μL, 30 °C. [b] Conversion into the expected reductive amination product determined by uncalibrated GC–MS or HPLC–MS analysis. *Reaction conditions:* Carbonyl compound (50 mM), amine (50 mM; except **a1**: 500 mM), $NADP^+$ (1 mM), $Na_2HPO_3 \cdot 5\ H_2O$ (100 mM), IRED preparation (4 mg/mL lyophilised cell lysate), PtDH preparation (4 mg/mL lyophilised cell lysate), bicine–NaOH buffer (100 mM, pH 8.0), DMSO (10% v/v), reaction volume 500 μL, 30 °C, 800 rpm, 24 h. [c] Product formation determined qualitatively after acetylation due to the volatility of substrates and product. [d] Product formation determined qualitatively because of competing substrate hydrolysis.

Finally, we re-screened 84 low-level photometric hits with the aim to identify and eliminate false positives within the fraction of our data set that is most susceptible to a type I error. As shown in Table S17 (overleaf), we could remove 39 false positives in this way, while confirming 45 low-level hits.

Table S17. Photometric activity levels and chromatographically determined levels of product formation for selected low-level photometric positives of the Overview Screening.

IRED	Substrates		Activity[a]	Conv.[b]	IRED	Substrates		Activity[a]	Conv.[b]
	Carb.	*Am.*	[mU/mg$_{IRED}$]	[%]		*Carb.*	*Am.*	[mU/mg$_{IRED}$]	[%]
IR1743	**c1**	**a1**	116 ± 11	–	IR1392	**c3**	**a6**	41 ± 5	trace
IR1674	**c1**	**a1**	48 ± 10	–	IR0041	**c3**	**a6**	13 ± 2	trace
IR1589	**c1**	**a1**	34 ± 1	–	IR1743	**c4**	**a1**	24 ± 2	–[c]
IR0027	**c1**	**a1**	10 ± 1	trace	IR0068	**c4**	**a2**	141 ± 14	trace
IR1738	**c1**	**a2**	79 ± 20	–	IR0059	**c4**	**a2**	115 ± 11	trace
IR0343	**c1**	**a2**	53 ± 7	–	IR1773	**c4**	**a4**	23 ± 3	1
IR1743	**c1**	**a2**	33 ± 5	–	IR0043	**c4**	**a5**	62 ± 10	–
IR1446	**c1**	**a3**	79 ± 10	trace	IR1855	**c4**	**a6**	42 ± 2	–
IR1805	**c1**	**a3**	67 ± 8	trace	IR0043	**c4**	**a6**	16 ± 2	trace
IR1598	**c1**	**a3**	30 ± 10	trace	IR1674	**c5**	**a2**	157 ± 37	–[d]
IR0468	**c1**	**a4**	166 ± 14	trace	IR0204	**c5**	**a2**	77 ± 8	–[d]
IR1743	**c1**	**a4**	130 ± 8	trace	IR2145	**c5**	**a4**	62 ± 12	–[d]
IR1369	**c1**	**a4**	113 ± 17	trace	IR1793	**c5**	**a4**	39 ± 7	–[d]
IR1630	**c1**	**a4**	71 ± 12	trace	IR1760	**c5**	**a4**	26 ± 3	–[d]
IR1100	**c1**	**a4**	42 ± 8	–	IR0039	**c6**	**a1**	28 ± 1	yes[c]
IR1662	**c1**	**a5**	69 ± 4	2	IR0020	**c6**	**a1**	18 ± 1	yes[c]
IR1446	**c1**	**a5**	54 ± 4	trace	IR0023	**c6**	**a1**	9 ± 2	–[c]
IR0030	**c1**	**a5**	19 ± 3	trace	IR1105	**c6**	**a2**	62 ± 6	9
IR0279	**c2**	**a1**	180 ± 15	35	IR0032	**c6**	**a2**	60 ± 4	trace
IR1773	**c2**	**a1**	60 ± 4	11	IR0023	**c6**	**a2**	11 ± 1	trace
IR1743	**c2**	**a1**	49 ± 4	–	IR0343	**c6**	**a4**	140 ± 5	50
IR0073	**c2**	**a2**	310 ± 24	44	IR0030	**c6**	**a4**	64 ± 2	60
IR1630	**c2**	**a2**	177 ± 6	54	IR1136	**c6**	**a4**	32 ± 3	23
IR0077	**c2**	**a2**	37 ± 4	21	IR1134	**c6**	**a4**	24 ± 1	60
IR1788	**c2**	**a3**	117 ± 11	trace	IR0053	**c6**	**a4**	17 ± 5	15
IR0343	**c2**	**a3**	100 ± 5	trace	IR0031	**c6**	**a4**	7 ± 1	trace
IR0063	**c2**	**a3**	92 ± 28	41	IR1589	**c6**	**a6**	126 ± 5	65
IR2145	**c2**	**a3**	57 ± 5	5	IR0482	**c6**	**a6**	42 ± 1	–
IR1630	**c2**	**a3**	47 ± 5	–	IR1385	**c6**	**a7**	4 ± 1	–
IR1793	**c2**	**a3**	34 ± 4	trace	IR1674	**c7**	**a1**	34 ± 4	–[c]
IR1136	**c2**	**a4**	97 ± 4	83	IR2159	**c7**	**a2**	243 ± 34	–[c]
IR0497	**c2**	**a4**	70 ± 2	51	IR1805	**c7**	**a2**	77 ± 20	–[c]
IR1630	**c2**	**a5**	45 ± 3	–	IR0204	**c7**	**a2**	75 ± 16	–[c]
IR0343	**c2**	**a5**	117 ± 18	trace	IR2252	**c7**	**a2**	58 ± 17	–[c]
IR1773	**c2**	**a5**	95 ± 5	–	IR1136	**c7**	**a4**	100 ± 3	trace
IR1743	**c2**	**a5**	58 ± 5	–	IR0139	**c7**	**a5**	14 ± 4	–
IR0010	**c3**	**a1**	20 ± 5	trace	IR0031	**c8**	**a4**	3 ± 1	–
IR2252	**c3**	**a2**	58 ± 16	–	IR1446	**c8**	**a6**	43 ± 10	–
IR2159	**c3**	**a2**	56 ± 12	–	IR0395	**c8**	**a6**	35 ± 4	trace
IR1369	**c3**	**a4**	106 ± 25	–	IR2159	**c8**	**a7**	130 ± 33	–
IR2252	**c3**	**a4**	58 ± 16	–	IR0030	**c8**	**a7**	30 ± 5	–
IR1743	**c3**	**a4**	51 ± 12	–	IR0032	**c8**	**a7**	27 ± 4	–

[a] Specific activity (mean ± standard deviation, corrected for background absorbance decrease, prior to data consolidation) determined by a photometric NADPH consumption assay. *Assay conditions:* Carbonyl compound (50 mM), amine (50 mM; except **a1**: 500 mM), NADPH (2 mM), IRED preparation (2 mg/mL lyophilised cell lysate), bicine–NaOH buffer (100 mM, pH 8.0), DMSO (10% v/v), reaction volume 100 μL, 30 °C. [b] Conversion into the expected reductive amination product determined by uncalibrated GC–MS or HPLC–MS analysis. *Reaction conditions:* Carbonyl compound (50 mM), amine (50 mM; except **a1**: 500 mM), $NADP^+$ (1 mM), $Na_2HPO_3 \cdot 5\ H_2O$ (100 mM), IRED preparation (4 mg/mL lyophilised cell lysate), PtDH preparation (4 mg/mL lyophilised cell lysate), bicine–NaOH buffer (100 mM, pH 8.0), DMSO (10% v/v), reaction volume 500 μL, 30 °C, 800 rpm, 24 h. [c] Product formation determined qualitatively after acetylation due to the volatility of substrates and product. [d] Product formation determined qualitatively because of competing substrate hydrolysis.

Validation experiments for the Diversification Screening:
Within the amine scope part of the Diversification Screening, we followed a similar strategy for validating the photometric assay results as described above for the Overview Screening. Each positive substrate combination was re-screened chromatographically at least once, focussing on the most active IREDs in each case, and low-level photometric hits were re-investigated to identify and eliminate false positives. The results of these validation experiments are summarised in Table S18. Most hits could be confirmed, but several substrate combinations (**c2-a14**, **c8-a14**, **c8-a16**, **c9-a14**, **c9-a23**, **c11-a14**, **c12-a12**, **c12-a14**, **c12-a20**, **c12-a22**) seemed to systematically produce false positives and were manually flagged as non-hits for all investigated enzymes after validation of the strongest photometric positives had failed.

Table S18. Photometric activity levels and chromatographically determined levels of product formation for selected photometric positives of the amine scope part of the Diversification Screening (*continued on next page*).

IRED	Substrates		Activity[a]	Conv.[b]	IRED	Substrates		Activity[a]	Conv.[b]
	Carb.	*Am.*	[mU/mg$_{IRED}$]	[%]		*Carb.*	*Am.*	[mU/mg$_{IRED}$]	[%]
IR0261	**c2**	**a8**	354	2	IR0052	**c2**	**a19**	283	4
IR0040	**c2**	**a8**	190	5	IR0001	**c2**	**a20**	1560	trace
IR0020	**c2**	**a8**	187	10	IR0001	**c2**	**a21**	321	71
IR2114	**c2**	**a8**	145	8	IR1139	**c2**	**a22**	4133	2
IR2010	**c2**	**a9**	3851	91	IR2137	**c2**	**a23**	7608	92
IR0020	**c2**	**a9**	1099	78	IR1737	**c2**	**a23**	7578	91
IR0001	**c2**	**a9**	995	65	IR0068	**c8**	**a8**	5166	yes[c]
IR0039	**c2**	**a9**	866	89	IR0043	**c8**	**a8**	4913	yes[c]
IR0033	**c2**	**a9**	182	21	IR0035	**c8**	**a9**	7237	yes[c]
IR0011	**c2**	**a10**	15531	>99	IR0068	**c8**	**a9**	5696	yes[c]
IR0023	**c2**	**a10**	3424	>99	IR1855	**c8**	**a10**	7816	93
IR2173	**c2**	**a10**	502	77	IR0052	**c8**	**a10**	4319	72
IR2128	**c2**	**a11**	466	yes[c]	IR1855	**c8**	**a11**	4743	3
IR0049	**c2**	**a11**	312	yes[c]	IR0035	**c8**	**a11**	4533	5
IR2022	**c2**	**a11**	241	yes[c]	IR0063	**c8**	**a12**	1585	3
IR1674	**c2**	**a12**	162	yes[c]	IR0035	**c8**	**a14**	2015	–
IR0499	**c2**	**a13**	4182	trace	IR0036	**c8**	**a14**	437	–
IR1855	**c2**	**a13**	833	trace	IR0499	**c8**	**a15**	4500	5
IR0041	**c2**	**a14**	1319	–	IR0027	**c8**	**a15**	546	10
IR1632	**c2**	**a14**	1171	–	IR0035	**c8**	**a16**	14984	–
IR0023	**c2**	**a14**	806	–	IR0464	**c8**	**a16**	9475	–
IR0001	**c2**	**a14**	154	–	IR0011	**c8**	**a17**	294	–
IR0464	**c2**	**a15**	8365	98	IR0035	**c8**	**a23**	4256	trace
IR0035	**c2**	**a15**	8430	79	IR2137	**c8**	**a23**	4023	trace
IR0468	**c2**	**a15**	2387	81	IR0068	**c9**	**a8**	1193	yes[c]
IR0464	**c2**	**a16**	4687	96	IR0131	**c9**	**a8**	927	yes[c]
IR0499	**c2**	**a16**	1016	93	IR0131	**c9**	**a9**	2563	trace
IR1738	**c2**	**a16**	592	77	IR0071	**c9**	**a9**	1010	7
IR0464	**c2**	**a17**	805	–	IR0052	**c9**	**a10**	10144	78

[a] Specific activity (corrected for background absorbance decrease, prior to data consolidation) determined by photometric NADPH consumption assay. *Assay conditions:* Carbonyl compound (50 mM), amine (50 mM), NADPH (2 mM), IRED preparation (1 mg/mL lyophilised cell lysate), bicine–NaOH buffer (100 mM, pH 8.0), DMSO (10% v/v), reaction volume 100 μL, 30 °C. [b] Conversion into the expected reductive amination product determined by uncalibrated GC–MS or HPLC–MS analysis. *Reaction conditions:* Carbonyl compound (50 mM), amine (50 mM), $NADP^+$ (1 mM), $Na_2HPO_3 \cdot 5\ H_2O$ (100 mM), IRED preparation (4 mg/mL lyophilised cell lysate), PtDH preparation (4 mg/mL lyophilised cell lysate), bicine–NaOH buffer (100 mM, pH 8.0), DMSO (10% v/v), reaction volume 500 μL, 30 °C, 800 rpm, 24 h. [c] Product formation determined qualitatively by HPLC–MS analysis.

Table S18. Photometric activity levels and chromatographically determined levels of product formation for selected photometric positives of the amine scope part of the Diversification Screening (*continued from previous page*).

IRED	Substrates		Activity[a]	Conv.[b]	IRED	Substrates		Activity[a]	Conv.[b]
	Carb.	*Am.*	[mU/mg$_{IRED}$]	[%]		*Carb.*	*Am.*	[mU/mg$_{IRED}$]	[%]
IR1855	**c9**	**a11**	11359	yes[c]	IR0023	**c11**	**a8**	634	94
IR1427	**c9**	**a11**	6676	yes[c]	IR0393	**c11**	**a9**	19859	>99
IR0279	**c9**	**a12**	4027	yes[c]	IR0069	**c11**	**a9**	14195	>99
IR0041	**c9**	**a14**	790	–	IR0464	**c11**	**a9**	637	1
IR0035	**c9**	**a14**	921	–	IR0009	**c11**	**a10**	1827	78
IR0464	**c9**	**a15**	1465	yes[c]	IR0032	**c11**	**a10**	1379	95
IR1437	**c9**	**a15**	1212	yes[c]	IR1437	**c11**	**a11**	3324	yes[c]
IR0009	**c9**	**a16**	25850	yes[c]	IR1437	**c11**	**a12**	1775	yes[c]
IR1437	**c9**	**a16**	3506	yes[c]	IR0464	**c11**	**a12**	1620	yes[c]
IR0001	**c9**	**a21**	3793	yes[c]	IR0035	**c11**	**a14**	18502	–
IR1139	**c9**	**a21**	2771	yes[c]	IR1855	**c11**	**a14**	3822	–
IR1139	**c9**	**a22**	3573	yes[c]	IR0816	**c11**	**a17**	816	2
IR0131	**c9**	**a22**	1264	yes[c]	IR0015	**c11**	**a19**	296	trace
IR2010	**c9**	**a23**	5854	–	IR0063	**c11**	**a19**	181	trace
IR2114	**c9**	**a23**	4275	–	IR2010	**c11**	**a20**	316	yes[c]
IR0393	**c10**	**a8**	1891	trace	IR1674	**c11**	**a20**	137	yes[c]
IR0068	**c10**	**a8**	1549	6	IR1805	**c11**	**a21**	1046	yes[c]
IR0043	**c10**	**a9**	8383	16	IR2173	**c11**	**a22**	1423	yes[c]
IR0035	**c10**	**a9**	5449	14	IR1805	**c11**	**a22**	572	yes[c]
IR0069	**c10**	**a9**	4713	trace	IR0027	**c11**	**a23**	3044	9
IR2021	**c10**	**a10**	14248	56	IR0043	**c12**	**a8**	1845	trace
IR1855	**c10**	**a10**	10219	96	IR0015	**c12**	**a8**	438	trace
IR0041	**c10**	**a10**	9507	40	IR1773	**c12**	**a8**	142	trace
IR0052	**c10**	**a10**	5857	62	IR1855	**c12**	**a9**	5010	yes[c]
IR0072	**c10**	**a11**	4907	yes[c]	IR0499	**c12**	**a9**	1263	yes[c]
IR1855	**c10**	**a11**	3689	yes[c]	IR0464	**c12**	**a9**	176	yes[c]
IR1421	**c10**	**a12**	3264	yes[c]	IR0011	**c12**	**a10**	2924	2
IR0043	**c10**	**a12**	2901	yes[c]	IR2173	**c12**	**a10**	759	9
IR0499	**c10**	**a12**	2513	yes[c]	IR1855	**c12**	**a11**	2041	yes[c]
IR0202	**c10**	**a15**	4025	trace	IR0035	**c12**	**a11**	355	yes[c]
IR1437	**c10**	**a15**	828	trace	IR1460	**c12**	**a12**	801	–
IR0902	**c10**	**a15**	947	trace	IR0063	**c12**	**a12**	577	–
IR1460	**c10**	**a16**	6876	12	IR1855	**c12**	**a14**	2074	–
IR0464	**c10**	**a16**	4670	8	IR2137	**c12**	**a19**	1133	–
IR0035	**c10**	**a20**	494	–	IR2253	**c12**	**a20**	1812	–
IR0053	**c10**	**a20**	338	–	IR0035	**c12**	**a20**	912	–
IR1139	**c10**	**a21**	3400	yes[c]	IR0041	**c12**	**a21**	1734	–
IR0058	**c10**	**a21**	2387	yes[c]	IR0499	**c12**	**a22**	18255	–
IR1855	**c10**	**a22**	4700	yes[c]	IR1139	**c12**	**a22**	3392	–
IR0001	**c10**	**a22**	2427	yes[c]	IR2010	**c12**	**a23**	2076	yes[c]
IR1674	**c10**	**a23**	4766	35	IR2150	**c12**	**a23**	2240	yes[c]
IR2128	**c10**	**a23**	4481	34	IR1437	**c12**	**a23**	912	–

[a] Specific activity (corrected for background absorbance decrease, prior to data consolidation) determined by photometric NADPH consumption assay. *Assay conditions:* Carbonyl compound (50 mM), amine (50 mM), NADPH (2 mM), IRED preparation (1 mg/mL lyophilised cell lysate), bicine–NaOH buffer (100 mM, pH 8.0), DMSO (10% v/v), reaction volume 100 μL, 30 °C. [b] Conversion into the expected reductive amination product determined by uncalibrated GC–MS or HPLC–MS analysis. *Reaction conditions:* Carbonyl compound (50 mM), amine (50 mM), $NADP^+$ (1 mM), $Na_2HPO_3 \cdot 5\ H_2O$ (100 mM), IRED preparation (4 mg/mL lyophilised cell lysate), PtDH preparation (4 mg/mL lyophilised cell lysate), bicine–NaOH buffer (100 mM, pH 8.0), DMSO (10% v/v), reaction volume 500 μL, 30 °C, 800 rpm, 24 h. [c] Product formation determined qualitatively by HPLC–MS analysis.

Validation of the carbonyl scope part of the Diversification Screening focussed on confirming each positive substrate combination at least once and on finding a suitable cut-off value for the target/buffer integral ratio above which the target amine could be reliably detected by GC–MS or HPLC–MS analysis. Based on the data summarised in Table S19, we chose 0.02 as a base value for the target/buffer cut-off, but adjusted this value for some combinations that showed a higher detection limit (*e.g.*, **c23-a2**, 0.1; **c25-a4**, 0.5).

Table S19. FIA–MS target/buffer integral ratios and chromatographically determined levels of product formation for selected FIA–MS positives of the carbonyl scope part of the Diversification Screening (*continued on next page*).

IRED	Substrates		FIA–MS[a]		Conv.[b]	IRED	Substrates		FIA–MS[a]		Conv.[b]
	Carb.	*Am.*	*T/B*	*S/N*	[%]		*Carb.*	*Am.*	*T/B*	*S/N*	[%]
IR0005	**c13**	**a2**	10.32	413	>99	IR0040	**c20**	**a2**	3.90	1503	57
IR0005	**c13**	**a4**	10.83	211	>99	IR2010	**c20**	**a2**	0.20	77	49
IR0052	**c13**	**a22**	0.50	16	8	IR0273	**c20**	**a2**	0.04	14	11
IR0005	**c13**	**a24**	2.54	31	75	IR0877	**c20**	**a2**	0.02	7	–
IR2021	**c14**	**a2**	4.57	146	17	IR2021	**c20**	**a4**	13.46	1473	57
IR0001	**c14**	**a4**	5.02	815	74	IR0005	**c20**	**a22**	0.19	190	3
IR0052	**c14**	**a22**	1.38	108	51	IR0033	**c20**	**a24**	1.19	382	63
IR0033	**c14**	**a22**	0.47	36	20	IR0033	**c21**	**a2**	1.20	1200	18
IR0033	**c14**	**a24**	0.60	183	15	IR2021	**c21**	**a2**	0.98	976	8
IR2021	**c15**	**a2**	7.57	7570	53	IR2021	**c21**	**a4**	7.21	1616	>99
IR2021	**c15**	**a4**	13.49	244	>99	IR0131	**c21**	**a22**	0.14	70	yes[c]
IR0005	**c15**	**a22**	4.57	4567	16	IR0049	**c21**	**a22**	0.12	63	yes[c]
IR0058	**c15**	**a22**	0.15	152	5	IR0052	**c21**	**a24**	1.63	16	90
IR1139	**c15**	**a22**	0.07	69	9	IR0035	**c21**	**a24**	0.91	8	91
IR0005	**c15**	**a24**	2.02	137	44	IR0034	**c22**	**a2**	1.81	1811	50
IR2021	**c16**	**a2**	3.44	1086	33	IR2021	**c22**	**a4**	15.58	1975	84
IR2021	**c16**	**a4**	10.61	5795	96	IR1105	**c22**	**a22**	0.10	18	trace
IR0065	**c16**	**a22**	0.49	98	3	IR2252	**c22**	**a22**	0.07	12	trace
IR0036	**c16**	**a24**	0.11	110	1	IR0030	**c22**	**a24**	0.08	84	38
IR0052	**c17**	**a2**	1.05	564	25	IR0063	**c23**	**a2**	1.69	1694	32
IR0035	**c17**	**a4**	0.73	270	63	IR1446	**c23**	**a2**	0.31	309	2
IR0005	**c17**	**a22**	0.80	799	29	IR2147	**c23**	**a2**	0.11	105	trace
IR2022	**c17**	**a24**	0.16	36	trace	IR2021	**c23**	**a4**	7.65	636	79
IR0060	**c17**	**a24**	0.05	9	trace	IR0005	**c23**	**a22**	0.10	104	–
IR0027	**c18**	**a2**	5.65	474	45	IR1632	**c23**	**a24**	0.02	23	trace
IR0035	**c18**	**a4**	2.25	70	16	IR2021	**c24**	**a2**	4.61	4611	39
IR1134	**c18**	**a22**	0.07	54	trace	IR0041	**c24**	**a2**	1.90	1902	55
IR0052	**c18**	**a22**	0.05	43	trace	IR2021	**c24**	**a4**	6.57	322	95
IR0030	**c18**	**a24**	0.09	93	1	IR0001	**c24**	**a22**	0.02	23	4
IR0005	**c19**	**a2**	3.26	183	16	IR0064	**c24**	**a24**	0.11	112	9
IR2021	**c19**	**a4**	11.03	151	92	IR0052	**c25**	**a2**	0.65	176	22
IR0063	**c19**	**a22**	0.29	287	1	IR0035	**c25**	**a2**	0.53	135	16
IR0064	**c19**	**a22**	0.08	83	1	IR0202	**c25**	**a4**	0.20	173	2
IR1139	**c19**	**a22**	0.08	81	trace	IR1427	**c25**	**a4**	0.68	596	trace
IR0011	**c19**	**a24**	2.26	98	23	IR2021	**c25**	**a4**	0.04	33	–

[a] Target/buffer integral ratio (T/B) and signal/noise ratio relative to empty-vector control (S/N) determined by flow-injection mass spectrometry (FIA–MS). [b] Conversion into the expected reductive amination product determined by uncalibrated GC–MS or HPLC–MS analysis. *Reaction conditions:* Carbonyl compound (50 mM), amine (50 mM), $NADP^+$ (1 mM), $Na_2HPO_3 \cdot 5\ H_2O$ (100 mM), IRED preparation (4 mg/mL lyophilised cell lysate), PtDH preparation (4 mg/mL lyophilised cell lysate), bicine–NaOH buffer (100 mM, pH 8.0), DMSO (10% v/v), reaction volume 500 μL, 30 °C, 800 rpm, 24 h. [c] Product formation determined qualitatively by HPLC–MS analysis.

Table S19. FIA–MS target/buffer integral ratios and chromatographically determined levels of product formation for selected FIA–MS positives of the carbonyl scope part of the Diversification Screening (*continued from previous page*).

IRED	Substrates		FIA–MS[a]		Conv.[b]	IRED	Substrates		FIA–MS[a]		Conv.[b]
	Carb.	*Am.*	*T/B*	*S/N*	[%]		*Carb.*	*Am.*	*T/B*	*S/N*	[%]
IR0023	**c25**	**a24**	0.04	45	trace	IR0041	**c31**	**a2**	0.10	97	5
IR1793	**c25**	**a24**	0.04	44	trace	IR0052	**c31**	**a2**	0.08	76	8
IR1136	**c25**	**a24**	0.03	32	trace	IR0041	**c31**	**a4**	0.05	54	–
IR0063	**c26**	**a2**	0.43	113	trace	IR0035	**c31**	**a4**	0.05	46	–
IR2147	**c26**	**a2**	0.36	92	trace	IR0049	**c31**	**a24**	0.10	96	3
IR0041	**c26**	**a4**	0.38	378	1	IR0010	**c32**	**a2**	0.01	11	–
IR2128	**c26**	**a24**	0.04	42	trace	IR0052	**c32**	**a2**	0.01	11	–
IR1632	**c26**	**a24**	0.04	42	trace	IR2150	**c32**	**a4**	0.11	14	–
IR1136	**c26**	**a24**	0.03	26	trace	IR1475	**c32**	**a24**	0.02	18	–
IR0005	**c27**	**a2**	0.24	242	trace	IR1392	**c32**	**a24**	0.02	17	–
IR1134	**c27**	**a2**	0.14	139	trace	IR1760	**c33**	**a2**	0.27	8	–
IR0035	**c27**	**a2**	0.13	126	trace	IR2022	**c33**	**a4**	0.03	10	trace
IR0041	**c27**	**a4**	0.38	383	9	IR2173	**c33**	**a24**	0.06	62	–
IR2150	**c27**	**a4**	0.34	343	1	IR1136	**c33**	**a24**	0.03	32	–
IR2021	**c27**	**a4**	0.26	261	4	IR0005	**c34**	**a2**	0.06	10	–
IR0052	**c27**	**a24**	0.07	67	trace	IR0005	**c34**	**a4**	0.08	30	–
IR0065	**c27**	**a24**	0.03	28	trace	IR1788	**c34**	**a42**	0.01	5	–
IR0063	**c28**	**a2**	0.02	22	trace	IR0005	**c35**	**a2**	0.02	19	–
IR1760	**c28**	**a4**	0.28	12	–	IR0033	**c35**	**a2**	0.02	17	–
IR1136	**c28**	**a24**	0.02	18	–	IR0005	**c35**	**a4**	0.03	57	–
IR1632	**c29**	**a4**	0.07	51	–	IR0005	**c35**	**a22**	0.01	9	–
IR0041	**c29**	**a4**	0.05	40	–	IR0343	**c35**	**a24**	0.02	17	–
IR1136	**c29**	**a4**	0.04	31	–	IR0005	**c36**	**a2**	0.08	80	–
IR1136	**c29**	**a24**	0.02	23	–	IR0395	**c36**	**a2**	0.05	51	trace
IR1855	**c30**	**a2**	0.05	16	–	IR0343	**c36**	**a2**	0.12	121	–
IR2022	**c30**	**a2**	0.04	14	–	IR0395	**c36**	**a4**	0.04	39	trace
IR2010	**c30**	**a4**	0.03	31	–	IR0343	**c36**	**a4**	5.29	5077	–
IR0041	**c30**	**a4**	0.02	23	–	IR0343	**c36**	**a24**	4.98	1056	–

[a] Target/buffer integral ratio (T/B) and signal/noise ratio relative to empty-vector control (S/N) determined by flow-injection mass spectrometry (FIA–MS). [b] Conversion into the expected reductive amination product determined by uncalibrated GC–MS or HPLC–MS analysis. *Reaction conditions:* Carbonyl compound (50 mM), amine (50 mM), $NADP^+$ (1 mM), $Na_2HPO_3 \cdot 5\ H_2O$ (100 mM), IRED preparation (4 mg/mL lyophilised cell lysate), PtDH preparation (4 mg/mL lyophilised cell lysate), bicine–NaOH buffer (100 mM, pH 8.0), DMSO (10% v/v), reaction volume 500 μL, 30 °C, 800 rpm, 24 h.

Translation of carbonyl scope *z*-scores into conversion values:
In contrast to the amine scope part of the Diversification Screening, where *z*-scores correspond directly to the photometrically determined specific activity values, translating the *z*-scores of the carbonyl scope into an easily interpretable performance parameter is non-trivial, as they are based on the dimensionless target/buffer integral ratio determined by uncalibrated FIA–MS. In particular, the ESI-MS detector response of the analyte, the level of background mass signal at the analyte's *m/z* ratio, and the IRED expression level will influence how a given target/buffer ratio (and, hence, a *z*-score) corresponds to conversion into the desired product. Nevertheless, as higher *z*-scores will generally correlate with higher levels of conversion, analysing multiple reductive amination reactions across diverse substrate pairs and IREDs should allow at least an approximate translation of carbonyl scope *z*-scores into conversion values.

To establish such a translation, we performed small-scale biotransformations of 25 substrate–enzyme combinations whose *z*-scores are close to integer values (–2, –1, 0, 1, 2) and determined their conversions by GC–MS analysis. Sorting the resulting conversion values at each *z*-score level ascendingly and taking the arithmetic mean of the three central data points provided an estimate of the mean conversion that can be expected for the respective *z*-score (Table S20). Only for the $z = -2$ level, where product formation was barely above the detection limit in all five cases, we report "trace" (product just detectable) as the most likely reaction outcome.

Table S20. Estimation of the mean conversion values corresponding to integer *z*-scores (–2, –1, 0, 1, 2) for the carbonyl scope part of the Diversification Screening.

IRED	Carbonyl	Amine	*z*-Score	Conv.[a] [%]	Estimate[b]
IR1134	**c26**	**a4**	–2.01	trace	
IR0064	**c25**	**a24**	–1.99	trace	
IR0902	**c20**	**a22**	–2.04	1	trace
IR0027	**c20**	**a24**	–2.00	2	
IR0060	**c17**	**a22**	–1.99	2	
IR0057	**c20**	**a2**	–0.99	trace	
IR0064	**c27**	**a4**	–1.00	1	
IR0393	**c31**	**a24**	–0.99	2	3%
IR0040	**c16**	**a24**	–0.99	5	
IR0020	**c15**	**a2**	–1.00	54	
IR0261	**c16**	**a2**	0.01	9	
IR2128	**c25**	**a4**	0.01	9	
IR0055	**c20**	**a4**	–0.01	10	11%
IR0027	**c20**	**a2**	0.00	15	
IR0063	**c15**	**a22**	0.00	80	
IR0039	**c22**	**a4**	1.00	32	
IR0011	**c15**	**a2**	1.00	32	
IR1460	**c18**	**a2**	1.01	37	46%
IR0261	**c16**	**a4**	1.00	69	
IR0005	**c15**	**a22**	1.01	86	
IR1105	**c18**	**a4**	2.04	39	
IR0066	**c13**	**a24**	2.00	49	
IR0009	**c15**	**a4**	2.00	81	73%
IR0233	**c14**	**a4**	2.03	87	
IR1105	**c13**	**a24**	2.04	98	

[a] Conversion into the expected reductive amination product determined by GC–MS analysis. [b] Estimated mean conversion for the corresponding integer *z*-score. Except for the –2 level, the estimate is the mean of the three middle values. *Reaction conditions:* Carbonyl compound (50 mM), amine (50 mM), $NADP^+$ (1 mM), $Na_2HPO_3 \cdot 5\ H_2O$ (100 mM), IRED preparation (4 mg/mL lyophilised cell lysate), PtDH preparation (4 mg/mL lyophilised cell lysate), bicine–NaOH buffer (100 mM, pH 8.0), DMSO (10% v/v), reaction volume 500 µL, 30 °C, 800 rpm, 24 h.

Consolidated data of the Diversification Screening – Product heatmaps:
To complement the *z*-score heatmaps used to visualise the outcome of all 18,416 assay reactions performed within the Diversification Screening (Figures 4 and 5, main paper) with intuitive graphs based on aggregated data, we prepared product heatmaps that show the number of hits found for each investigated reductive amination reaction in the same way as Figure 2 (main paper) summarises the outcome of the Overview Screening.

For the carbonyl scope, Figure S24 reveals good acceptance of alicyclic and open-chain aliphatic ketones, even when they carry sterically demanding substituents, as do substrates **c18** and **c19**. α,α-Difluoroacetophenone (**c31**) is accepted to some extent, but in agreement with previous findings[32] its reductive amination is accompanied by carbonyl reduction as a competing side reaction. Products derived from bulky aromatic ketones or keto esters (**c32**, **c33–c35**) are virtually inaccessible under our reaction conditions, particularly when using challenging amine coupling partners such as morpholine (**a22**) or *p*-anisidine (**a24**).

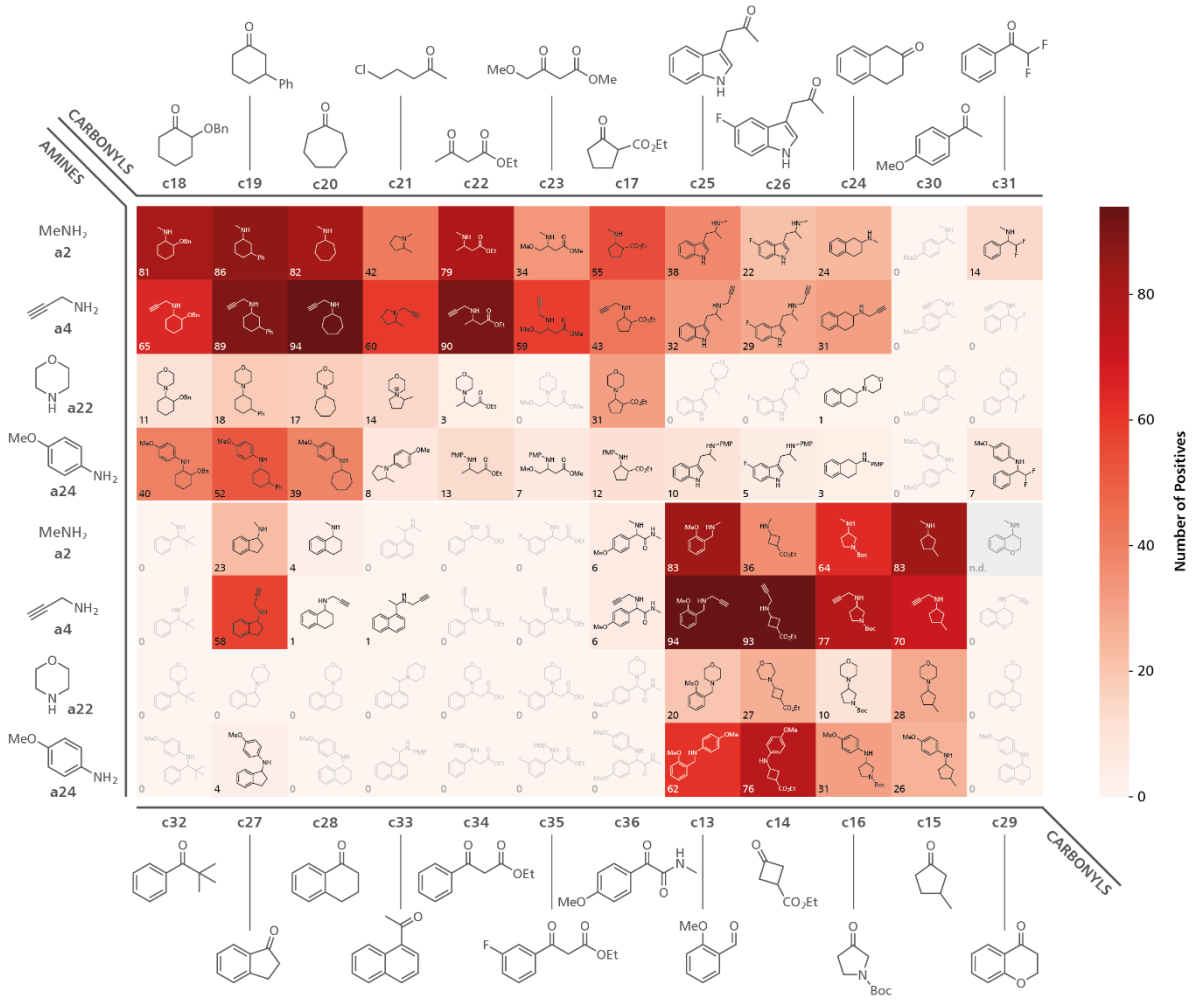


Figure S24. Summary of hits identified in the carbonyl scope part of the Diversification Screening. The tiles show the products resulting from the 96 tested substrate combinations along with the number of active IREDs for the respective combination given in the bottom-left corner of each tile. Activity was assayed by flow-injection analysis mass spectrometry (FIA–MS), monitoring the mass signals ($M+H^+$) of the expected product and bicine buffer, and confirmed by re-screening of selected positives using GC–MS or HPLC–MS analysis. The colour scale represents the number of consolidated hits identified for each substrate combination. One reaction that could not be assayed by FIA–MS due to identical masses of product (**c29–a2**) and bicine is shown as a grey tile. Source data are provided as a Source Data file. *Abbreviations:* Boc, *tert*-butyloxycarbonyl; PMP, *para*-methoxyphenyl

The aggregated results for the amine scope part of the Diversification Screening (Figure S25) indicate broad acceptance of primary aliphatic amines, including amino alcohols **a11** and **a12**, but no activity with the primary but α-branched *tert*-butylamine (**a14**). Aryl-aliphatic primary amines **a15** and **a16** are challenging substrates accepted in less than one-third of the investigated reactions, as are secondary amines **a19–a22**. This lower reactivity of secondary compared to primary amines is in line with the findings of the Overview Screening (Figure 3b, main paper) and with previous reports.[33] The heteroaromatic primary amines **a17** and **a18** proved to be particularly poor substrates.

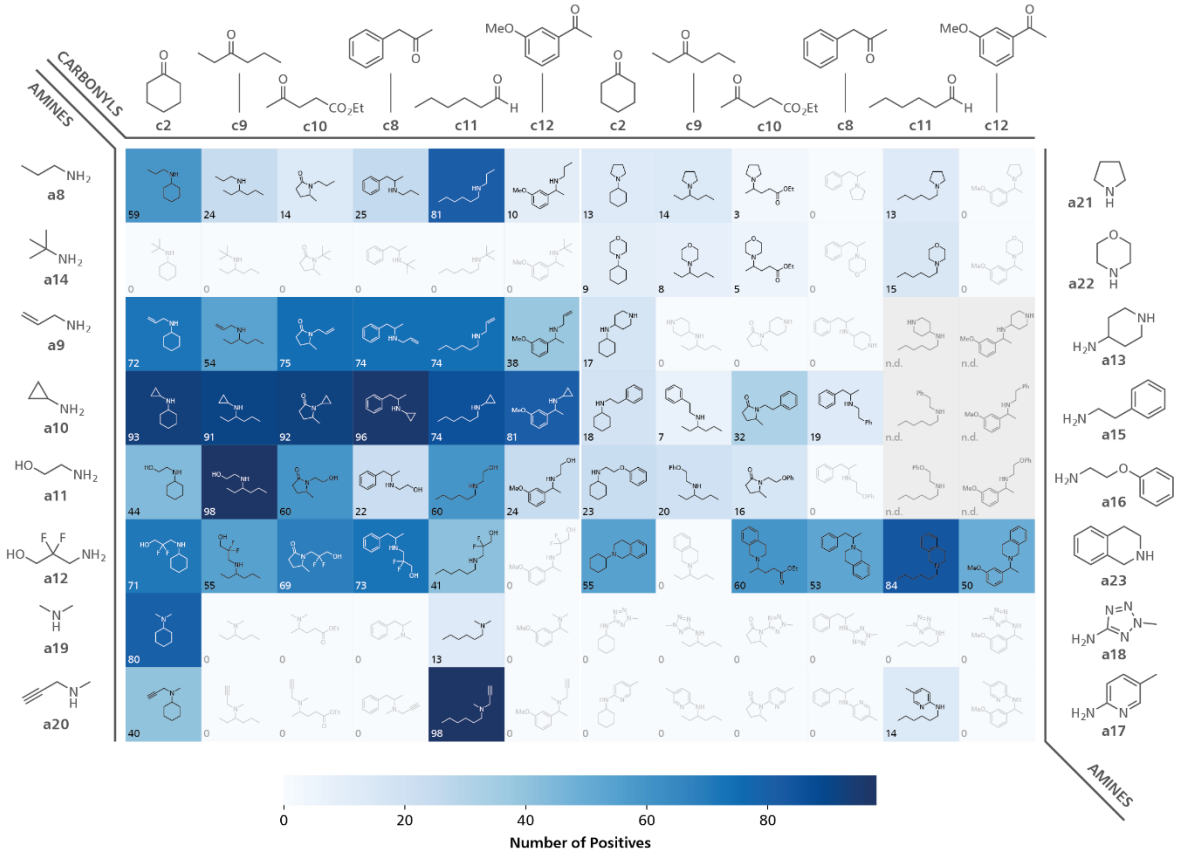
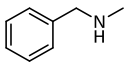
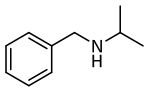
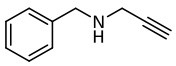
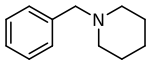
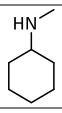
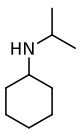
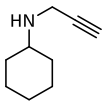
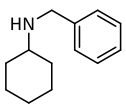
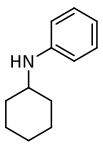


Figure S25. Summary of hits identified in the amine scope part of the Diversification Screening. The tiles show the products resulting from the 96 tested substrate combinations along with the number of active IREDs for the respective combination given in the bottom-left corner of each tile. Activity was assayed spectrophotometrically by following the consumption of the IREDs' cofactor, NADPH, and confirmed by re-screening of selected positives using GC–MS or HPLC–MS analysis. The colour scale represents the number of consolidated hits identified for each substrate combination. Six reactions that could not be assayed spectrophotometrically due to formation of turbidity (**c11–a13**, **c11–a15, c11–a16**, **c12–a13, c12–a15**, **c12–a16**) are shown as grey tiles. Source data are provided as a Source Data file.

Conversion and stereoselectivity data:

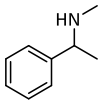
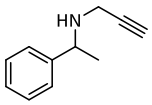
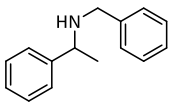
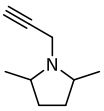
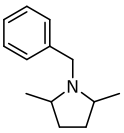
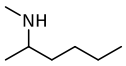
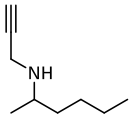
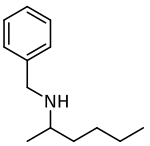
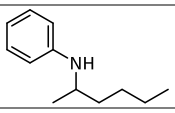
Selected, confirmed positives from the photometric and FIA–MS screenings were re-investigated in analytical-scale biotransformations (500 μL reaction volume) to determine conversion and, where applicable, the enantiomeric excess (*ee*) and/or diastereomeric ratio (*dr*) of the product. Table S21 (overleaf) lists these data for substrate combinations of the Overview Screening, while Table S22 summarises the conversion, *ee*, and *dr* values for substrate combinations of the Diversification Screening.

Table S21. Conversions (into the expected product and any side products) and stereoselectivities (enantiomeric excess, diastereomeric ratio) of IRED-catalysed reductive amination reactions of the Overview Screening (*continued on next pages*).

Carb.	Am.	IRED	Product	Conv.[a] [%]	Other[a] [%]	*ee*[b] [%]	*dr*[a]
c1	**a2**	IR0005		>99			
c1	**a2**	IR0073		>99			
c1	**a2**	IR0013		94	2 (imine)		
c1	**a2**	IR1805		87	4 (imine)		
c1	**a2**	IR2252		25	30 (imine)		
c1	**a3**	IR0064		>99			
c1	**a3**	IR0005		98	1 (imine)		
c1	**a3**	IR2173		86	4 (imine)		
c1	**a3**	IR0032		65	9 (imine)		
c1	**a3**	IR1421		2	44 (imine)		
c1	**a4**	IR0005		>99			
c1	**a4**	IR0073		>99			
c1	**a4**	IR0032		99			
c1	**a4**	IR2022		98			
c1	**a4**	IR2159		58	11 (imine)		
c1	**a5**	IR0005		13			
c1	**a5**	IR1632		1			
c1	**a5**	IR0030		1			
c2	**a1**	IR0020		>99			
c2	**a1**	IR0066		>99			
c2	**a1**	IR0076		>99			
c2	**a1**	IR0035		82			
c2	**a1**	IR1760		51			
c2	**a2**	IR0076		88			
c2	**a2**	IR2021		88			
c2	**a2**	IR0202		83			
c2	**a3**	IR0063		26			
c2	**a3**	IR1674		6			
c2	**a3**	IR2021		2			
c2	**a3**	IR1427		1			
c2	**a3**	IR2150		1			
c2	**a4**	IR0069		>99			
c2	**a4**	IR0233		>99			
c2	**a4**	IR1453		>99			
c2	**a4**	IR1738		>99			
c2	**a4**	IR1749		94			
c2	**a6**	IR0499		95			
c2	**a6**	IR2128		95			
c2	**a6**	IR0464		94			
c2	**a6**	IR0063		93			
c2	**a6**	IR0468		85			
c2	**a7**	IR2022		84			
c2	**a7**	IR0060		76			
c2	**a7**	IR0395		70			
c2	**a7**	IR0014		67			
c2	**a7**	IR0005		52			

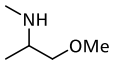
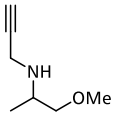
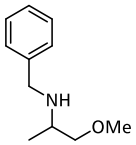
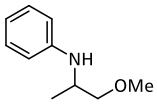
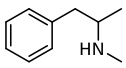
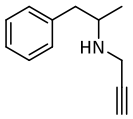
[a] Conversion into the expected reductive amination product (Conv.) and any side products (Other) as well as diastereomeric ratio (*dr*) determined by GC–FID analysis using *n*-decane or *n*-dodecane as internal standard. [b] Enantiomeric excess determined by GC or HPLC analysis on a chiral stationary phase. *Reaction conditions:* Carbonyl compound (50 mM), amine (50 mM; except **a1**: 500 mM), $NADP^+$ (1 mM), $Na_2HPO_3 \cdot 5\ H_2O$ (100 mM), IRED preparation (4 mg/mL lyophilised cell lysate), PtDH preparation (4 mg/mL lyophilised cell lysate), bicine–NaOH buffer (100 mM, pH 8.0), DMSO (10% v/v), reaction volume 500 µL, 30 °C, 800 rpm, 24 h.

Table S21. Conversions (into the expected product and any side products) and stereoselectivities (enantiomeric excess, diastereomeric ratio) of IRED-catalysed reductive amination reactions of the Overview Screening (*continued from previous page*).

Carb.	Am.	IRED	Product	Conv.[a] [%]	Other[a] [%]	*ee*[b] [%]	*dr*[a]
c3	**a2**	IR0041		2		80 (*R*)	
c3	**a2**	IR2253		1		88 (*S*)	
c3	**a2**	IR0011		trace		n.d.[c]	
c3	**a2**	IR1392		trace		n.d.[c]	
c3	**a4**	IR0041		16		85 (*R*)	
c3	**a4**	IR0043		4		99 (*R*)	
c3	**a4**	IR0068		3		94 (*R*)	
c3	**a4**	IR0059		1		98 (*S*)	
c3	**a6**	IR0464		3		n.d.[c]	
c3	**a6**	IR0395		1		n.d.[c]	
c3	**a6**	IR0499		trace		n.d.[c]	
c3	**a6**	IR0041		trace		n.d.[c]	
c4	**a4**	IR0035		21	46 (pyrroline)	>99 (*B*)[d]	85:15
c4	**a4**	IR0041		13	53 (pyrroline)	>99 (*B*)[d]	67:33
c4	**a4**	IR0015		12		*rac*	72:28
c4	**a4**	IR2010		10	55 (pyrroline)	>99 (*B*)[d]	90:10
c4	**a4**	IR2021		10	47 (pyrroline)	>99 (*B*)[d]	80:20
c4	**a4**	IR0066		7		>99 (*B*)[d]	23:77
c4	**a6**	IR2147		13	22 (pyrrole)	>99 (*A*)[d]	9:91
c4	**a6**	IR0499		8	11 (pyrrole)	>99 (*A*)[d]	7:93
c4	**a6**	IR2128		5	24 (pyrrole)	>99 (*A*)[d]	19:81
c4	**a6**	IR0015		4	7 (pyrrole)	91 (*B*)[d]	21:79
c4	**a6**	IR0063		2	6 (pyrrole)	n.d.[c]	2:98
c6	**a2**	IR2021		56		95 (*R*)	
c6	**a2**	IR0068		48		99 (*R*)	
c6	**a2**	IR1855		39		>99 (*S*)	
c6	**a2**	IR1674		33		98 (*R*)	
c6	**a2**	IR1476		26		96 (*R*)	
c6	**a2**	IR0032		9		>99 (*S*)	
c6	**a4**	IR0068		93		>99 (*R*)	
c6	**a4**	IR2021		93		98 (*R*)	
c6	**a4**	IR1395		92		99 (*R*)	
c6	**a4**	IR1738		90		99 (*R*)	
c6	**a4**	IR1760		85		>99 (*R*)	
c6	**a4**	IR1749		41		>99 (*R*)	
c6	**a4**	IR0395		36		99 (*S*)	
c6	**a4**	IR0015		28		93 (*S*)	
c6	**a6**	IR1453		65		99 (*R*)	
c6	**a6**	IR2147		58		>99 (*R*)	
c6	**a6**	IR1460		43		>99 (*R*)	
c6	**a6**	IR0279		39		99 (*R*)	
c6	**a6**	IR1855		6		>99 (*R*)	
c6	**a7**	IR0032		3		32 (*R*)	
c6	**a7**	IR0041		1		>99 (*R*)	
c6	**a7**	IR0043		trace		>99 (*R*)	

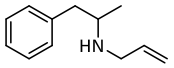
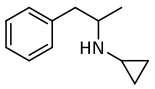
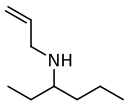
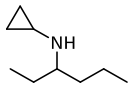
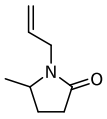
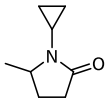
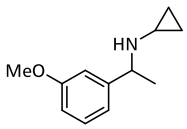
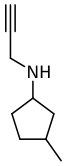
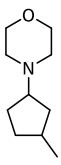
[a] Conversion into the expected reductive amination product (Conv.) and any side products (Other) as well as diastereomeric ratio (*dr*) determined by GC–FID analysis using *n*-decane or *n*-dodecane as internal standard. [b] Enantiomeric excess determined by GC or HPLC analysis on a chiral stationary phase. [c] n.d., not determined. [d] (*A*) and (*B*) refer to the first-eluting and second-eluting enantiomer, respectively, where absolute configurations are unknown. *Reaction conditions:* Carbonyl compound (50 mM), amine (50 mM), $NADP^+$ (1 mM), $Na_2HPO_3 \cdot 5\ H_2O$ (100 mM), IRED preparation (4 mg/mL lyophilised cell lysate), PtDH preparation (4 mg/mL lyophilised cell lysate), bicine–NaOH buffer (100 mM, pH 8.0), DMSO (10% v/v), reaction volume 500 µL, 30 °C, 800 rpm, 24 h.

Table S21. Conversions (into the expected product and any side products) and stereoselectivities (enantiomeric excess, diastereomeric ratio) of IRED-catalysed reductive amination reactions of the Overview Screening (*continued from previous page*).

Carb.	Am.	IRED	Product	Conv.[a] [%]	Other[a] [%]	*ee*[b] [%]	*dr*[a]
c7	**a2**	IR0063		55		89 (*S*)	
c7	**a2**	IR0020		50		83 (*R*)	
c7	**a2**	IR1855		46		87 (*S*)	
c7	**a2**	IR0032		10		>99 (*S*)	
c7	**a2**	IR2021		9		37 (*R*)	
c7	**a4**	IR2010		86		95 (*R*)	
c7	**a4**	IR0068		79		97 (*R*)	
c7	**a4**	IR0204		73		78 (*R*)	
c7	**a4**	IR1395		64		82 (*R*)	
c7	**a4**	IR2021		64		80 (*R*)	
c7	**a4**	IR0233		46		>99 (*R*)	
c7	**a4**	IR1855		27		29 (*R*)	
c7	**a4**	IR0032		4		98 (*S*)	
c7	**a6**	IR2147		91		95 (*R*)	
c7	**a6**	IR1453		77		88 (*R*)	
c7	**a6**	IR1855		68		94 (*R*)	
c7	**a6**	IR2114		65		91 (*R*)	
c7	**a6**	IR0279		12		92 (*R*)	
c7	**a7**	IR1855		3		96 (*R*)	
c7	**a7**	IR0033		2		56 (*R*)	
c7	**a7**	IR0041		1		>99 (*R*)	
c7	**a7**	IR1453		trace		n.d.[c]	
c8	**a2**	IR0052		20		68 (*R*)	
c8	**a2**	IR0035		9		98 (*R*)	
c8	**a2**	IR0063		8		94 (*R*)	
c8	**a2**	IR1134		1		58 (*R*)	
c8	**a2**	IR0041		trace		97 (*R*)	
c8	**a4**	IR0041		58		95 (*R*)	
c8	**a4**	IR0035		55		97 (*R*)	
c8	**a4**	IR0068		34		97 (*R*)	
c8	**a4**	IR2021		24		95 (*R*)	
c8	**a4**	IR0069		22		97 (*R*)	
c8	**a4**	IR1855		17		>99 (*S*)	
c8	**a4**	IR0036		16		99 (*R*)	
c8	**a4**	IR2173		9		56 (*R*)	
c8	**a4**	IR0204		5		92 (*R*)	
c8	**a4**	IR0032		1		98 (*S*)	

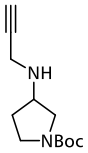
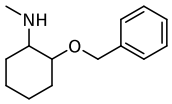
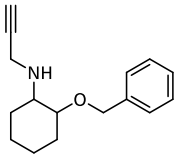
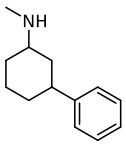
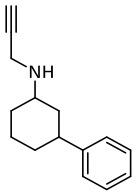
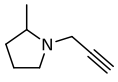
[a] Conversion into the expected reductive amination product (Conv.) and any side products (Other) as well as diastereomeric ratio (*dr*) determined by GC–FID analysis using *n*-decane or *n*-dodecane as internal standard. [b] Enantiomeric excess determined by GC or HPLC analysis on a chiral stationary phase. [c] n.d., not determined. *Reaction conditions:* Carbonyl compound (50 mM), amine (50 mM), $NADP^+$ (1 mM), $Na_2HPO_3 \cdot 5\ H_2O$ (100 mM), IRED preparation (4 mg/mL lyophilised cell lysate), PtDH preparation (4 mg/mL lyophilised cell lysate), bicine–NaOH buffer (100 mM, pH 8.0), DMSO (10% v/v), reaction volume 500 μL, 30 °C, 800 rpm, 24 h.

Table S22. Conversions (into the expected product and any side products) and stereoselectivities (enantiomeric excess, diastereomeric ratio) of IRED-catalysed reductive amination reactions of the Diversification Screening (*continued on next pages*).

Carb.	Am.	IRED	Product	Conv.[a] [%]	Other[a] [%]	*ee*[b] [%]	*dr*[a]
c8	**a9**	IR1855		19		>99 (*S*)	
c8	**a9**	IR0041		12		>99 (*R*)	
c8	**a9**	IR0043		3		>99 (*R*)	
c8	**a10**	IR1855		91		>99 (*S*)	
c8	**a10**	IR0068		17		>99 (*R*)	
c8	**a10**	IR2021		12		91 (*R*)	
c8	**a10**	IR1674		5		99 (*S*)	
c9	**a9**	IR0043		25		83 (*A*)[c]	
c9	**a9**	IR1674		15		99 (*A*)[c]	
c9	**a9**	IR1855		8		32 (*B*)[c]	
c9	**a9**	IR2021		8		51 (*B*)[c]	
c9	**a9**	IR0279		2		90 (*A*)[c]	
c9	**a10**	IR1855		80		97 (*B*)[c]	
c9	**a10**	IR1674		79		99 (*A*)[c]	
c9	**a10**	IR2010		72		98 (*A*)[c]	
c9	**a10**	IR0393		54		83 (*A*)[c]	
c9	**a10**	IR1134		48		89 (*B*)[c]	
c10	**a9**	IR0041		4	36 (am.-ester)	92 (*S*)	
c10	**a9**	IR1855		4	38 (am.-ester)	>99 (*S*)	
c10	**a9**	IR0043		3	27 (am.-ester)	94 (*S*)	
c10	**a9**	IR0065		3	25 (am.-ester)	95 (*S*)	
c10	**a9**	IR0068		2	19 (am.-ester)	73 (*R*)	
c10	**a10**	IR1855		7	79 (am.-ester)	>99 (*S*)	
c10	**a10**	IR0041		4	46 (am.-ester)	49 (*S*)	
c10	**a10**	IR1139		4	52 (am.-ester)	>99 (*S*)	
c10	**a10**	IR2021		4	47 (am.-ester)	55 (*S*)	
c10	**a10**	IR1427		2	24 (am.-ester)	68 (*R*)	
c12	**a10**	IR1855		16		>99 (*B*)[c]	
c12	**a10**	IR2253		12		>99 (*B*)[c]	
c12	**a10**	IR0065		9		>99 (*B*)[c]	
c12	**a10**	IR0011		2		>99 (*B*)[c]	
c12	**a10**	IR1805		2		>99 (*B*)[c]	
c15	**a4**	IR0039		87		n.d.[d]	96:4
c15	**a4**	IR2021		87		n.d.[d]	86:14
c15	**a4**	IR0043		86		n.d.[d]	74:26
c15	**a4**	IR0071		85		n.d.[d]	97:3
c15	**a4**	IR0015		80		n.d.[d]	2:98
c15	**a4**	IR1369		76		n.d.[d]	97:3
c15	**a22**	IR0005		43		91 (*A*)[c]	84:16
c15	**a22**	IR1855		32		40 (*B*)[c]	86:14
c15	**a22**	IR0064		30		36 (*A*)[c]	78:22
c15	**a22**	IR0063		27		62 (*A*)[c]	84:16
c15	**a22**	IR1136		12		71 (*A*)[c]	78:22
c15	**a22**	IR0015		9		62 (*B*)[c]	87:13

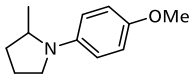
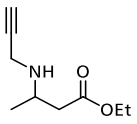
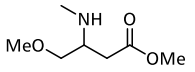
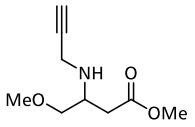
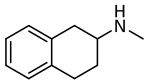
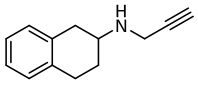
[a] Conversion into the expected reductive amination product (Conv.) and any side products (Other) as well as diastereomeric ratio (*dr*) determined by GC–FID analysis using *n*-decane or *n*-dodecane as internal standard. [b] Enantiomeric excess determined by GC or HPLC analysis on a chiral stationary phase. For compounds with two stereogenic centres, *ee* is reported for the major diastereomer. [c] (*A*) and (*B*) refer to the first-eluting and second-eluting enantiomer, respectively, where absolute configurations are unknown. [d] n.d., not determined. *Reaction conditions:* Carbonyl compound (50 mM), amine (50 mM), $NADP^+$ (1 mM), $Na_2HPO_3 \cdot 5\ H_2O$ (100 mM), IRED preparation (4 mg/mL lyophilised cell lysate), PtDH preparation (4 mg/mL lyophilised cell lysate), bicine–NaOH buffer (100 mM, pH 8.0), DMSO (10% v/v), reaction volume 500 µL, 30 °C, 800 rpm, 24 h.

Table S22. Conversions (into the expected product and any side products) and stereoselectivities (enantiomeric excess, diastereomeric ratio) of IRED-catalysed reductive amination reactions of the Diversification Screening (*continued from previous page*).

Carb.	Am.	IRED	Product	Conv.[a] [%]	Other[a] [%]	ee[b] [%]	dr[a]
c16	**a2**	IR0035		86		>99 (*R*)	
c16	**a2**	IR1662		68		99 (*R*)	
c16	**a2**	IR0041		30		>99 (*R*)	
c16	**a2**	IR2021		25		>99 (*R*)	
c16	**a2**	IR0065		24		99 (*S*)	
c16	**a2**	IR1136		11		91 (*S*)	
c16	**a4**	IR0041		99		>99 (*R*)	
c16	**a4**	IR2021		91		99 (*R*)	
c16	**a4**	IR0343		82		>99 (*R*)	
c16	**a4**	IR2150		81		>99 (*R*)	
c16	**a2**	IR2128		79		99 (*R*)	
c16	**a4**	IR0065		49		99 (*S*)	
c18	**a2**	IR0065		84		>99 (*B*)[c]	48:52
c18	**a2**	IR0052		78		>99 (*B*)[c]	44:56
c18	**a2**	IR1855		73		>99 (*B*)[c]	39:61
c18	**a2**	IR1134		66		>99 (*B*)[c]	39:61
c18	**a2**	IR2159		42		>99 (*B*)[c]	37:63
c18	**a2**	IR2128		35		>99 (*B*)[c]	86:14
c18	**a4**	IR0064		96		>99 (*A*)[c]	50:50
c18	**a4**	IR1136		94		>99 (*A*)[c]	51:49
c18	**a4**	IR0065		74		86 (*A*)[c]	68:32
c18	**a4**	IR0395		40		>99 (*A*)[c]	6:94
c18	**a4**	IR0058		29		95 (*A*)[c]	3:97
c18	**a4**	IR1105		19		>99 (*A*)[c]	97:3
c19	**a2**	IR1105		49		72 (*A*)[c]	83:17
c19	**a2**	IR0065		31		>99 (*B*)[c]	35:65
c19	**a2**	IR0035		28		>99 (*B*)[c]	44:56
c19	**a2**	IR1855		22		>99 (*A*)[c]	56:44
c19	**a2**	IR2114		15		>99 (*A*)[c]	14:86
c19	**a2**	IR0063		12		96 (*A*)[c]	66:34
c19	**a2**	IR1134		8		90 (*A*)[c]	92:8
c19	**a4**	IR2021		80		69 (*A*)[c]	59:41
c19	**a4**	IR1105		64		41 (*B*)[c]	94:6
c19	**a4**	IR0065		62		92 (*B*)[c]	68:32
c19	**a4**	IR2159		50		28 (*B*)[c]	99:1
c19	**a4**	IR1136		49		89 (*B*)[c]	82:18
c19	**a4**	IR1134		42		64 (*B*)[c]	98:2
c19	**a4**	IR0233		24		98 (*B*)[c]	19:81
c21	**a4**	IR2021		99		>99 (*R*)	
c21	**a4**	IR0043		99		99 (*R*)	
c21	**a4**	IR0039		97		>99 (*R*)	
c21	**a4**	IR0032		66		14 (*S*)	
c21	**a4**	IR0015		57		46 (*R*)	
c21	**a4**	IR0010		56		97 (*R*)	

[a] Conversion into the expected reductive amination product (Conv.) and any side products (Other) as well as diastereomeric ratio (*dr*) determined by GC–FID analysis using *n*-decane or *n*-dodecane as internal standard. [b] Enantiomeric excess determined by GC or HPLC analysis on a chiral stationary phase. For compounds with two stereogenic centres, *ee* is reported for the major diastereomer. [c] (*A*) and (*B*) refer to the first-eluting and second-eluting enantiomer, respectively, where absolute configurations are unknown. *Reaction conditions:* Carbonyl compound (50 mM), amine (50 mM), $NADP^+$ (1 mM), $Na_2HPO_3 \cdot 5\ H_2O$ (100 mM), IRED preparation (4 mg/mL lyophilised cell lysate), PtDH preparation (4 mg/mL lyophilised cell lysate), bicine–NaOH buffer (100 mM, pH 8.0), DMSO (10% v/v), reaction volume 500 µL, 30 °C, 800 rpm, 24 h.

Table S22. Conversions (into the expected product and any side products) and stereoselectivities (enantiomeric excess, diastereomeric ratio) of IRED-catalysed reductive amination reactions of the Diversification Screening (*continued from previous page*).

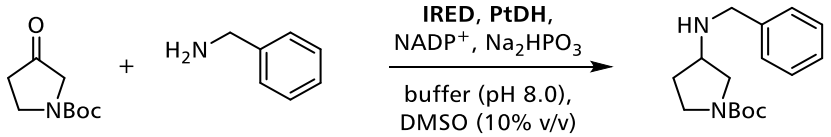
Carb.	Am.	IRED	Product	Conv.[a] [%]	Other[a] [%]	ee[b] [%]	dr[a]
c21	**a24**	IR0010		19		89 (*R*)	
c21	**a24**	IR0066		16		78 (*R*)	
c21	**a24**	IR0005		12		20 (*R*)	
c21	**a24**	IR2021		10		47 (*S*)	
c21	**a24**	IR0052		9		16 (*S*)	
c21	**a24**	IR0005		8		5 (*S*)	
c22	**a4**	IR0041		67		10 (*R*)	
c22	**a4**	IR0068		64		>99 (*R*)	
c22	**a4**	IR1630		59		>99 (*R*)	
c22	**a4**	IR2021		55		87 (*R*)	
c22	**a4**	IR1395		52		80 (*R*)	
c22	**a4**	IR0233		30		>99 (*R*)	
c22	**a4**	IR1738		21		98 (*R*)	
c22	**a4**	IR1855		18		>99 (*S*)	
c23	**a2**	IR1105		4		79 (*B*)[c]	
c23	**a2**	IR0063		3		12 (*A*)[c]	
c23	**a2**	IR1446		2		>99 (*A*)[c]	
c23	**a2**	IR2257		1		76 (*B*)[c]	
c23	**a2**	IR0041		1		n.d.[d]	
c23	**a4**	IR0041		44		>99 (*S*)	
c23	**a4**	IR0035		42		>99 (*S*)	
c23	**a4**	IR0043		29		>99 (*S*)	
c23	**a4**	IR2021		26		>99 (*S*)	
c23	**a4**	IR1395		5		>99 (*S*)	
c23	**a4**	IR0343		2		>99 (*S*)	
c24	**a2**	IR0035		48		99 (*R*)	
c24	**a2**	IR0041		39		>99 (*R*)	
c24	**a2**	IR0043		23		99 (*R*)	
c24	**a2**	IR2021		15		88 (*R*)	
c24	**a2**	IR0034		12		97 (*R*)	
c24	**a2**	IR1589		11		>99 (*R*)	
c24	**a2**	IR0069		8		>99 (*R*)	
c24	**a2**	IR1738		6		>99 (*R*)	
c24	**a4**	IR0035		78		>99 (*R*)	
c24	**a4**	IR1589		78		>99 (*R*)	
c24	**a4**	IR1738		62		98 (*R*)	
c24	**a4**	IR0279		61		97 (*R*)	
c24	**a2**	IR2021		48		>99 (*R*)	
c24	**a2**	IR0233		32		>99 (*R*)	
c24	**a2**	IR1630		27		75 (*R*)	
c24	**a4**	IR0343		25		42 (*R*)	

[a] Conversion into the expected reductive amination product (Conv.) and any side products (Other) as well as diastereomeric ratio (*dr*) determined by GC–FID analysis using *n*-decane or *n*-dodecane as internal standard. [b] Enantiomeric excess determined by GC or HPLC analysis on a chiral stationary phase. [c] (*A*) and (*B*) refer to the first-eluting and second-eluting enantiomer, respectively, where absolute configurations are unknown. [d] n.d., not determined. *Reaction conditions:* Carbonyl compound (50 mM), amine (50 mM), $NADP^+$ (1 mM), $Na_2HPO_3 \cdot 5\ H_2O$ (100 mM), IRED preparation (4 mg/mL lyophilised cell lysate), PtDH preparation (4 mg/mL lyophilised cell lysate), bicine–NaOH buffer (100 mM, pH 8.0), DMSO (10% v/v), reaction volume 500 µL, 30 °C, 800 rpm, 24 h.

Performance of DL-selected IREDs for novel substrate combinations:
As discussed above (see *Activity Prediction Using Machine-Learning Models*), we used the combined data collected in the Overview and Diversification Screenings, along with physico-chemical descriptors of the substrates and the IREDs' active sites, to train a deep-learning (DL) model for predicting IRED activity on novel combinations of substrates. These predictions were generated in the form of lists, in which the 100 IREDs included in the Diversification Screening are ranked by a confidence score (in the range of 0–1) for each novel substrate combination to be investigated. A higher confidence score indicates a higher likelihood of the respective IRED showing activity for the substrate combination under question.

We evaluated the performance of the DL model experimentally using four novel substrate combinations (**c16-a6**, **c16-a15**, **c23-a10**, **c24-a6**) as test cases. For each of these substrate pairs, analytical-scale biotransformations (500 μL reaction volume) were set up with the top 15 and bottom 5 IREDs in the DL-generated list. The confidence scores for the top-15 enzymes span ranges of 0.94–0.77 (**c23-a10**) to 0.28–0.14 (**c24-a6**), indicating significant differences in the likelihood of success of these reactions. Product formation was verified qualitatively by GC–MS and quantified by calibrated GC–FID, and the enantiomeric excess (*ee*) of the product was determined by HPLC analysis on a chiral stationary phase.

The results of these experiments are summarised in Table S23 to Table S26. In all four examples, the majority of the top-15 picks are active, while the bottom-5 IREDs afforded no or only trace amounts of product. The conversions attained in the hit cases don't exceed 37%, but the stereoselectivities are often excellent (>99% *ee* in 11 reactions). Hence, by testing only the top suggestions of the model, useful starting points for further optimisation (*e.g.*, by protein engineering) can be generated with a minimal screening effort.

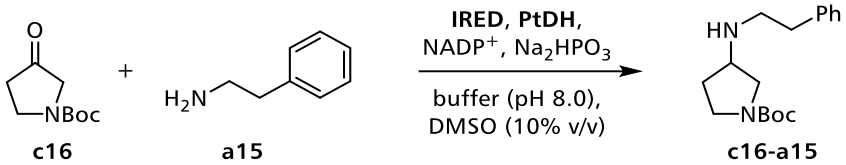


c16 **a6** **c16-a6**

Table S23. Confidence scores, conversions and stereoselectivities obtained for the substrate pair **c16-a6** with the top 15 and bottom 5 IREDs identified by the deep-learning (DL) model.

IRED	Conf.[a]	MS[b]	Conv.[c] [%]	*ee*[d] [%]	IRED	Conf.[a]	MS[b]	Conv.[c] [%]	*ee*[d] [%]
IR2128	0.74	+	22	40 (*R*)	IR0065	0.56	trace	–	–
IR2150	0.74	+	17	>99 (*R*)	IR0063	0.55	–	–	–
IR1437	0.68	+	23	>99 (*R*)	IR0202	0.55	+	3	n.d.[e]
IR0035	0.63	–	–	–	IR1632	0.53	+	1	n.d.[e]
IR2147	0.62	+	12	84 (*R*)	IR1855	0.52	–	–	–
IR1453	0.61	+	15	>99 (*R*)	IR0006	0.04	–	–	–
IR2114	0.60	+	9	>99 (*R*)	IR1587	0.03	–	–	–
IR1460	0.59	+	2	n.d.[e]	IR0381	0.03	–	–	–
IR0064	0.58	+	1	n.d.[e]	IR0742	0.02	–	–	–
IR0043	0.58	+	10	>99 (*R*)	IR1664	0.02	–	–	–

[a] Confidence score (0–1, higher values mean a higher likelihood of the enzyme being active) assigned by the DL model. [b] Presence or absence of product determined by GC–MS analysis. [c] Conversion into the expected reductive amination product determined by GC–FID analysis using *n*-dodecane as internal standard. [d] Enantiomeric excess determined by HPLC analysis on a chiral stationary phase. [e] n.d., not determined. *Reaction conditions:* **c16** (50 mM), **a6** (50 mM), $NADP^+$ (1 mM), $Na_2HPO_3 \cdot 5\ H_2O$ (100 mM), IRED preparation (4 mg/mL lyophilised cell lysate), PtDH preparation (4 mg/mL lyophilised cell lysate), bicine–NaOH buffer (100 mM, pH 8.0), DMSO (10% v/v), reaction volume 500 μL, 30 °C, 120 rpm, 24 h.

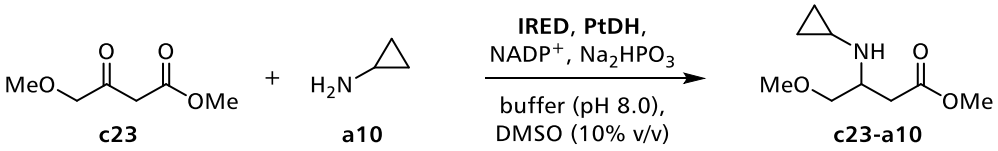


c16 **a15** **c16-a15**

Table S24. Confidence scores, conversions and stereoselectivities obtained for the substrate pair **c16-a15** with the top 15 and bottom 5 IREDs identified by the deep-learning (DL) model.

IRED	Conf.[a]	MS[b]	Conv.[c] [%]	*ee*[d] [%]	IRED	Conf.[a]	MS[b]	Conv.[c] [%]	*ee*[d] [%]
IR0202	0.59	trace	1	n.d.[e]	IR1855	0.29	trace	–	–
IR0499	0.53	+	3	n.d.[e]	IR0468	0.29	trace	–	–
IR2021	0.42	–	–	–	IR0001	0.25	trace	–	–
IR2128	0.37	+	1	n.d.[e]	IR2137	0.25	+	2	n.d.[e]
IR0464	0.36	+	9	71 (*R*)	IR2114	0.24	+	2	n.d.[e]
IR2150	0.36	+	1	n.d.[e]	IR0743	0.02	–	–	–
IR0035	0.36	trace	–	–	IR0131	0.02	–	–	–
IR1437	0.30	+	2	n.d.[e]	IR2036	0.02	–	–	–
IR0043	0.30	trace	–	–	IR0381	0.01	–	–	–
IR0009	0.29	–	–	–	IR0020	0.01	trace	–	–

[a] Confidence score (0–1, higher values mean a higher likelihood of the enzyme being active) assigned by the DL model. [b] Presence or absence of product determined by GC–MS analysis. [c] Conversion into the expected reductive amination product determined by GC–FID analysis using *n*-dodecane as internal standard. [d] Enantiomeric excess determined by HPLC analysis on a chiral stationary phase. [e] n.d., not determined. *Reaction conditions:* **c16** (50 mM), **a15** (50 mM), $NADP^+$ (1 mM), $Na_2HPO_3 \cdot 5\ H_2O$ (100 mM), IRED preparation (4 mg/mL lyophilised cell lysate), PtDH preparation (4 mg/mL lyophilised cell lysate), bicine–NaOH buffer (100 mM, pH 8.0), DMSO (10% v/v), reaction volume 500 µL, 30 °C, 120 rpm, 24 h.

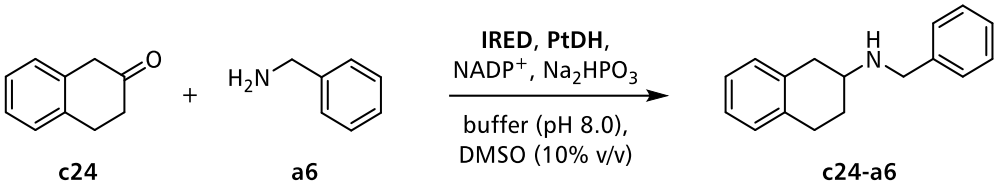


c23 **a10** **c23-a10**

Table S25. Confidence scores, conversions and stereoselectivities obtained for the substrate pair **c23-a10** with the top 15 and bottom 5 IREDs identified by the deep-learning (DL) model.

IRED	Conf.[a]	MS[b]	Conv.[c] [%]	*ee*[d] [%]	IRED	Conf.[a]	MS[b]	Conv.[c] [%]	*ee*[d] [%]
IR0035	0.94	+	16	>99 (*S*)	IR0072	0.79	trace	–	–
IR2021	0.94	+	7	>99 (*S*)	IR1395	0.79	+	4	>99 (*S*)
IR0043	0.94	+	2	>99 (*S*)	IR2159	0.79	+	9	47 (*S*)
IR0063	0.91	+	30	8 (*R*)	IR0064	0.77	+	4	25 (*S*)
IR1427	0.89	+	1	n.d.[e]	IR2010	0.77	+	2	>99 (*S*)
IR0030	0.87	–	–	–	IR0468	0.15	–	–	–
IR0065	0.85	+	4	39 (*R*)	IR0610	0.14	–	–	–
IR0202	0.85	–	–	–	IR1587	0.13	–	–	–
IR1855	0.85	+	6	6 (*S*)	IR0482	0.11	–	–	–
IR0071	0.80	trace	–	–	IR0497	0.09	–	–	–

[a] Confidence score (0–1, higher values mean a higher likelihood of the enzyme being active) assigned by the DL model. [b] Presence or absence of product determined by GC–MS analysis. [c] Conversion into the expected reductive amination product determined by GC–FID analysis using *n*-decane as internal standard. [d] Enantiomeric excess determined by HPLC analysis on a chiral stationary phase after Fmoc derivatisation. *Reaction conditions:* **c23** (50 mM), **a10** (50 mM), $NADP^+$ (1 mM), $Na_2HPO_3 \cdot 5\ H_2O$ (100 mM), IRED preparation (4 mg/mL lyophilised cell lysate), PtDH preparation (4 mg/mL lyophilised cell lysate), bicine–NaOH buffer (100 mM, pH 8.0), DMSO (10% v/v), reaction volume 500 µL, 30 °C, 120 rpm, 24 h.



c24 **a6** **c24-a6**

Table S26. Confidence scores, conversions and stereoselectivities obtained for the substrate pair **c24-a6** with the top 15 and bottom 5 IREDs identified by the deep-learning (DL) model.

IRED	Conf.[a]	MS[b]	Conv.[c] [%]	*ee*[d] [%]	IRED	Conf.[a]	MS[b]	Conv.[c] [%]	*ee*[d] [%]
IR0035	0.28	trace	–	–	IR2114	0.17	+	11	n.d.[e]
IR1437	0.27	+	26	99 (*R*)	IR0043	0.17	+	9	n.d.[e]
IR0202	0.24	+	20	14 (*R*)	IR0023	0.15	+	7	n.d.[e]
IR0464	0.23	+	27	97 (*R*)	IR1855	0.14	trace	–	–
IR0063	0.22	–	–	–	IR0058	0.14	+	10	n.d.[e]
IR2128	0.22	+	24	99 (*R*)	IR0006	0.01	–	–	–
IR2150	0.21	+	23	99 (*R*)	IR0742	0.01	–	–	–
IR2147	0.20	+	37	>99 (*R*)	IR1100	0.00	–	–	–
IR0279	0.18	+	17	96 (*R*)	IR1587	0.00	trace	–	–
IR1632	0.18	trace	1	n.d.[e]	IR1664	0.00	–	–	–

[a] Confidence score (0–1, higher values mean a higher likelihood of the enzyme being active) assigned by the DL model. [b] Presence or absence of product determined by GC–MS analysis. [c] Conversion into the expected reductive amination product determined by GC–FID analysis using *n*-decane as internal standard. [d] Enantiomeric excess determined by HPLC analysis on a chiral stationary phase. [e] n.d., not determined. *Reaction conditions:* **c24** (50 mM), **a6** (50 mM), $NADP^+$ (1 mM), $Na_2HPO_3 \cdot 5\ H_2O$ (100 mM), IRED preparation (4 mg/mL lyophilised cell lysate), PtDH preparation (4 mg/mL lyophilised cell lysate), bicine–NaOH buffer (100 mM, pH 8.0), DMSO (10% v/v), reaction volume 500 μL, 30 °C, 120 rpm, 24 h.

Supplementary Methods

Tabular Overview of Screening Phases

The computational and experimental contributions to the present study were completed in a heavily intertwined way over a time span of roughly three years. While Figure 1c (main paper) gives a general visual outline of the study design, Table S27 below provides detailed information on the main tasks at a more specific level. For each sub-task, we report the chemical space (Scope) and IRED sequence space (Enzymes) covered, as well as the approximate time span required to complete the sub-task. For screenings, the hit rate (percentage of positives) is also reported. Note that the Overview Screening was carried out in three iterations that all used the same assay setup but covered IRED panels of different size: 110 enzymes in the initial panel, 45 in the first panel of additional enzymes identified by machine learning (ML), and 20 in the second panel of ML additions. The Diversification Screening, on the other hand, was performed in a single iteration, but required two different assay setups (amine scope, carbonyl scope).

Table S27. Summary of computational and experimental contributions to the screening workflow.

Type of contribution	Scope[a]	Enzymes	Hit rate	Time required
COMPUTATIONAL WORK				
Chemoinformatic analysis of substrate panel	191	–	–	6 weeks
Bioinformatic analysis of enzyme panel	–	1555	–	3 months
IRED activity prediction for Overview Screening	54	1491	–	3 months
IRED activity prediction using DL pipeline	239	100	–	9 months
EXPERIMENTAL WORK				
Overview Screening	54	175	15%	9 months[b]
– Enzyme expression and lyophilisation	–	180	–	6 months
– Method development (plate reader)	–	–	–	2 weeks
– Screening initial IRED panel	54	110	16%	6 months
– Screening first ML additions	54	45	16%	2 months
– Screening second ML additions	54	20	8%	1 month
– Data validation (GC–MS, HPLC–MS)	51	101	–	3 months
– Synthesis of reference compounds[c]	39	–	–	6 months
– Collecting conversion and *ee* data	25	57	–	6 months
Diversification Screening	185	100	27%	18 months[b]
– Method development (plate reader)	–	–	–	1 week
– Method development (FIA–MS)	–	–	–	1 month
– Screening amine scope	90	100	28%	10 months
– Screening carbonyl scope	95	100	25%	12 months
– Data validation (GC–MS, HPLC–MS)	153	77	–	6 months
– Synthesis of reference compounds[c]	110	–	–	12 months
– Collecting conversion and *ee* data	22	47	–	12 months
Testing DL predictions	4	20	70%	4 weeks[b]
– Method development (GC–FID)	–	–	–	1 week
– Synthesis of reference compounds[c]	7	–	–	2 weeks
– Collecting conversion and *ee* data	4	45	70%	2 weeks

[a] Number of substrates or substrate combinations investigated: For the chemoinformatic analysis, the number of individual compounds; for predictive models, the number of combinations in the training data set; for experimental work, the number of combinations with interpretable screening data. [b] The total time required for completing a screening phase is not necessarily identical to the sum of the time spans reported for its constituent tasks, as several tasks were worked on in parallel. [c] Total of achiral, racemic, and non-racemic reference compounds.

Chemoinformatic Analysis of the Substrate Panel

The carbonyl and amine compounds were characterised by ten descriptors each (Table S28). For generating descriptors that required a three-dimensional structure, the substrates were energy-minimised in MOE (Molecular Operating Environment)[34] with the 2D Extended Hueckel Theory (EHT),[35] applying an implicit solvation reaction field model (ε = 80), with cut-offs of 8 and 10 Å. pK_a values were computed with MoKα.[36] The energy of the LUMO orbitals was computed using Jaguar at the DFT level with the B3LYP-D3 functional and 6-31G++* basis set.[37,38] logD values were predicted by a machine learning algorithm trained on proprietary *Roche* molecules.[39] All other descriptors were computed in MOE.

Table S28. Summary of descriptors used in the chemoinformatic analysis of the substrate panel.

Descriptor	Source	Category	Amine[a]	Carbonyl[a]
Radius of gyration (Rg)	MOE	3D	●	●
Globularity	MOE	3D	●	●
Number of heavy atoms	MOE	2D	●	●
Number of heavy atoms (not C or N)	MOE	2D	●	●
Number of amino groups	MOE	2D	●	
Number of carbonyl groups	MOE	2D		●
Number of rings (total)	MOE	2D	●	●
Number of aromatic rings	MOE	2D	●	●
Topological polar surface area	MOE	2D	●	●
pK_a value	MoKα	3D	●	
LUMO energy	Jaguar	3D		●
logD value	*Roche* predictor	3D	●	●

[a] The circle indicates that the respective descriptor was used for this type of substrate.

The amine and carbonyl descriptors were subjected to correlation analysis in R (*v*. 4.0.5)[1] and the results were plotted as correlation tables directly from R. Principal component analysis (PCA) and multidimensional scaling (MDS) were performed in R, and the results were exported to *Microsoft* Excel and graphically evaluated using *TIBCO* Spotfire (*v*. 12.0.6).

Bioinformatic Analysis of the IRED Panel

Collection of IRED sequences:

Protein sequence information of IREDs from the existing *Roche* and *University of Graz* enzyme panels was collected manually from in-house documents. The protein sequences of IREDs reported in published screening campaigns of other groups were extracted manually from the Supporting Information of the respective journal publications. The complete collection of protein sequences of the BioCatNet IRED database (*v*. 3) was downloaded from the project website (https://ired.biocatnet.de/). The curated sequence data set was stored in a FASTA format. Redundancy filtering and removal of β-hydroxyacid dehydrogenases was carried out in Jalview (*v*. 2.11)[40] based on a multiple-sequence alignment performed using Clustal Omega (*v*. 1.2).[41] The phylogenetic tree (Figure S6) was generated using the iTOL online tool (*v*. 5).[42]

Homology modelling:

The template crystal structures selected for homology modelling comprised all the IRED and RedAm structures deposited in the RCSB Protein Data Bank (PDB) at the time of early 2020, as well as four structurally related proteins of other function. The list was manually curated by

selecting just one representative out of very similar sequences, prioritizing structure resolution and presence of cofactors (Table S29). The template structures were prepared for modelling by keeping just the two chains representing the enzyme in dimeric form, removing all the ligands except for the cofactors, removing bound crystal water, and setting the protonation at pH 7. High-throughput homology modelling of the collected IRED sequences based on the selected templates was performed using YASARA Structure (*v*. 21.6.2) implemented on *Innophore*'s proprietary Catalophore™ platform.

Table S29. X-ray crystal structures used as templates for homology modelling.

PDB ID	Enzyme	Bound Cofactor	Resolution	Ref.
5OCM	IRED from *Streptosporangium roseum*	$NADP^+$	1.81 Å	14
6SMT	IRED from *Mycobacterium smegmatis*	NADPH	1.55 Å	43
5G6S	RedAm from *Aspergillus oryzae*	NADPH	2.35 Å	7
6JIZ	IRED from *Stackebrandtia nassauensis*	$NADP^+$	1.76 Å	
6TO4	IRED from *Myxococcus stipitatus*	$NADP^+$	2.29 Å	44
5A9S	IRED from *Amycolatopsis orientalis*	$NADP^+$	2.06 Å	18
1WP4	HIBADH from *Thermus thermophilus*	NADPH	2.00 Å	45
5OJL	RedAm from *Aspergillus terreus*	$NADPH_4$[b]	1.56 Å	46
2UYY	human cytokine-like nuclear factor	ADPRP[c]	2.50 Å	
2I99	human μ-crystallin	NADPH	2.60 Å	47
4OQY	IRED from *Streptomyces* sp. GF3546	NADPH	1.90 Å	48
4BV9	mouse μ-crystallin	NADPH	2.19 Å	49

[a] HIBADH, 3-Hydroxyisobutyrate dehydrogenase. [b] $NADPH_4$, 1,4,5,6-tetrahydronicotinamide adenine dinucleotide phosphate. [c] ADPRP, adenosine-5'-*O*-diphosphoribose phosphate.

Generation of point clouds on *Innophore*'s Catalophore™ platform:

Active-site point clouds were generated using *Innophore*'s proprietary Catalophore™ platform. Protein structures were protonated at pH 7, and the grid resolution was set to 0.0375 nm with a probe radius of 0.14 nm. The identified pockets were shaped around 0.5 nm from dummy ligands placed in the active site, occupying the catalytic centre.

Selection of IREDs for the Overview Screening:

The active-site clustering was performed using MMseqs2 (release 11)[50] by means of clustering masked sequences representing active-site residues only. The representative sequences generated by MMseqs2 were selected as candidates for the Overview Screening, and for the most populated clusters, one additional sequence was picked to avoid underrepresenting highly populated clusters. Only clusters containing at least two sequences were considered, with the exception of IR1051, which attracted our attention as it was the single item from a cluster with a crystal structure available (PDB code: 6JIZ). To graphically represent the results and to confirm a balanced coverage of the sequence space, the sequence distance was visualised as a scatter plot by means of multidimensional scaling (MDS) of the sequence distance matrix. The Python libraries Scikit-learn and Plotly were used to obtain the MDS, and to generate the scatter plot, respectively.

Activity Prediction Using Machine-Learning Models

Prioritisation of IRED candidates for the Overview Screening:
All-to-all matching of active-site point clouds was performed using *Innophore*'s proprietary Catalophore™ platform. The matching results were exported in CSV format and further processed using standard Python and freely available Python libraries. In particular, we used Pandas for data processing and filtering, Numpy for numerical operations such as the nearest-neighbour algorithm and weighted averages, and Matplotlib for visualisations.

The creation of the consolidated, ranked candidate lists was done by a subsequent Python script using Pandas and Numpy. The final clustering check was performed with the same software setup as the one used in preparation of the initial screening candidates (see *Selection of IREDs for the Overview Screening*).

Each data output was stored in CSV format for easy further processing. Visualisations were stored as JPG and PDF graphic files for later use.

Prioritisation of IREDs for testing with novel substrate combinations:
Point cloud features were extracted from the IREDs' active-site point clouds using *Innophore*'s proprietary deep learning models. A subset of 22 features was determined to be sufficient to fully distinguish all IREDs. Molecular features of the substrates were extracted using Mordred.[51] The pre-processing and feature engineering of molecular features was performed using *Innophore*'s FeatureEngineer. We used Pandas and Numpy for pre- and post-processing. ScikitLearn (*v*. 1.3.0)[52] was used for the group-*k*-fold validation during the feature engineering phase; for the prediction of novel substrate combinations the splitting into folds was done manually. XGBoost (*v*. 2.0.3)[53] was used for the gradient-boosted random forest.

Protein Sequence/Structure–Activity and Structure–Selectivity Analysis

Multiple-sequence alignments: The multiple-sequence alignments of IRED subsets shown in Table S5 and Table S7 and the pairwise identity matrix shown in Figure S15 were generated in CLC Workbench (*v*. 22.0.2) using default settings. The complete alignment of all 1,555 curated sequences that formed the basis for residue conservation analysis was generated by MAFFT (*v*. 7.525) using the `--auto` strategy, resulting in selection of the FFT–NS–2 progressive method.[53,54]

Conservation analysis: The conservation analysis is based on determining the modal (most frequent) amino acid and its frequency for every position of the MAFFT-generated alignment and was implemented using standard Python.

Protein–ligand docking: IRED receptors (homology models, X-ray crystal structures, or *ab-initio* models; polar hydrogens added, waters removed) and RDKit-generated imine ligands were parametrised with Meeko[26] and docked with AutoDock Vina (*v*. 1.2.6),[27,28] using a rigid receptor geometry. For each receptor, the search box was centred on the A-chain NADPH binding pocket and sized to enclose the catalytic residues. Dockings of bulky imines (Table S9) used a single seed, exhaustiveness = 16 and 20 sampled poses per run, while stereoselectivity dockings (Table S10) used two independent seeds (12345 and 54321) with exhaustiveness = 32 and 40 sampled poses per run. A pose was called productive when the imine carbon lay within 4.5 Å of C4N of the A-chain NADPH cofactor. Stereoselectivity calls were generated by determining the imine face (*Re/Si*) presented to the nicotinamide C4 atom from the CIP-ranked substituents of the sp^2 imine carbon, mapping *Re* → (*S*) and *Si* → (*R*). Pairwise calls were aggregated over productive poses by Boltzmann weighting on the Vina score at 298 K.

Sequence Selection, Gene Synthesis, and Subcloning

IREDs IR0001–IR00033 were described in two publications from *F. Hoffmann–La Roche* and are referred to there as IR_1 to IR_33.[2,3] An additional 60 IREDs used in the present study were described in publications from various groups, including our own. 98 IRED sequences were recruited from the *Imine Reductase Engineering Database* (https://ired.biocatnet.de/)[13] and have not been studied experimentally before, to the best of our knowledge. FASTA files containing the protein and DNA sequences of the studied IREDs are openly available in the Mendeley Data repository (https://data.mendeley.com/) at https://doi.org/10.17632/jn4sfsrz8x.2.

All expression constructs were obtained from commercial suppliers as synthetic genes that have been codon-optimised for *E. coli* expression and sub-cloned into the desired plasmid vectors. References to relevant publications, enzyme identifiers used in the original studies, and the most important properties of the expression plasmids used in the present study are summarised in Table S30.

Table S30. IRED expression vectors used in the present study (*continued on next pages*).

				Restriction Sites		
Enzyme	**Lit. ID**[a]	**Source Organism**	**Vector**	5′	3′	**Ref.**
IR0001	IR_1	*Streptomyces* sp. Mg1	pET22b(+)	*Nde*I	*Bam*HI	2
IR0002	IR_2	*Streptomyces fulvissimus*	pET22b(+)	*Nde*I	*Bam*HI	2
IR0003	IR_3	*Paenibacillus lactis*	pET22b(+)	*Nde*I	*Bam*HI	2
IR0004	IR_4	*Kribbella flavida* DSM 17836	pET22b(+)	*Nde*I	*Bam*HI	2
IR0005	IR_5	*Cupriavidus* sp. HPC(L)	pET22b(+)	*Nde*I	*Bam*HI	2
IR0006	IR_6	*Saccharomonospora xinjiangensis*	pET22b(+)	*Nde*I	*Bam*HI	2
IR0009	IR_9	*Frankia* sp. QA3	pET22b(+)	*Nde*I	*Bam*HI	2
IR0010	IR_10	*Mycobacterium smegmatis*	pET22b(+)	*Nde*I	*Bam*HI	2
IR0011	IR_11	*Verrucosispora maris*	pET22b(+)	*Nde*I	*Bam*HI	2
IR0012	IR_12	*Streptomyces* sp. CNB091	pET22b(+)	*Nde*I	*Bam*HI	2
IR0013	IR_13	*Saccharopolyspora erythraea*	pET22b(+)	*Nde*I	*Bam*HI	2
IR0014	IR_14	*Nocardia cyriacigeorgica* GUH-2	pET22b(+)	*Nde*I	*Bam*HI	2
IR0015	IR_15	*Actinomadura rifamycini*	pET22b(+)	*Nde*I	*Bam*HI	2
IR0017	IR_17	*Mycobacterium vaccae*	pET22b(+)	*Nde*I	*Bam*HI	2
IR0018	IR_18	*Mycobacterium* sp. JLS	pET22b(+)	*Nde*I	*Bam*HI	2
IR0019	IR_19	*Cellulosimicrobium cellulans*	pET22b(+)	*Nde*I	*Bam*HI	2
IR0020	IR_20	*Streptomyces tsukubaensis*	pET22b(+)	*Nde*I	*Bam*HI	2
IR0021	IR_21	*Paenibacillus ehimensis*	pET22b(+)	*Nde*I	*Bam*HI	2
IR0022	IR_22	*Streptomyces* sp. CNH287	pET22b(+)	*Nde*I	*Bam*HI	2
IR0023	IR_23	*Streptomyces viridochromogenes*	pET22b(+)	*Nde*I	*Bam*HI	2
IR0025	IR_25	*Paenibacillus* sp. HGF5	pET22b(+)	*Nde*I	*Bam*HI	3
IR0027	IR_27	*Chitinophaga* sp. JGI 0001002-D04	pET22b(+)	*Nde*I	*Bam*HI	3
IR0028	IR_28	*Glycomyces tenuis*	pET22b(+)	*Nde*I	*Bam*HI	3
IR0029	IR_29	*Nocardia brasiliensis*	pET22b(+)	*Nde*I	*Bam*HI	3
IR0030	IR_30	*Nitratireductor pacificus*	pET22b(+)	*Nde*I	*Bam*HI	3
IR0031	IR_31	*Mesorhizobium* sp. L48C026A00	pET22b(+)	*Nde*I	*Bam*HI	3
IR0032	IR_32	*Aeromonas veronii*	pET22b(+)	*Nde*I	*Bam*HI	3
IR0033	IR_33	*Aeromonas veronii*	pET22b(+)	*Nde*I	*Bam*HI	3
IR0034	pIR355	*Blastomyces gilchristii* SLH14081	pET22b(+)	*Nde*I	*Bam*HI	12
IR0035		*Neosartorya fischeri* ATCC 1020	pET22b(+)	*Nde*I	*Bam*HI	
IR0036	pIR12	*Aspergillus nidulans* FGSC A4	pET22b(+)	*Nde*I	*Bam*HI	12
IR0037	*Asp*RedAm	*Aspergillus oryzae*	pET22b(+)	*Nde*I	*Bam*HI	7
IR0038		*Aspergillus oryzae*	pET22b(+)	*Nde*I	*Bam*HI	
IR0039	pIR207	*Aspergillus parasiticus*	pET22b(+)	*Nde*I	*Bam*HI	12
IR0040	*At*RedAm	*Aspergillus terreus*	pET22b(+)	*Nde*I	*Bam*HI	7

[a] Enzyme identifier used in the original publication. Entries typeset in grey indicate proteins for which no soluble expression could be achieved.

Table S30. IRED expression vectors used in the present study (*continued from previous page*).

Enzyme	Lit. ID[a]	Source Organism	Vector	Restriction Sites 5′	Restriction Sites 3′	Ref.
IR0041	*Nf*RedAm	*Neosartorya fumigata*	pET22b(+)	*Nde*I	*Bam*HI	11
IR0042		*Aspergillus fumigatus* A1163	pET22b(+)	*Nde*I	*Bam*HI	
IR0043		*Aspergillus fumigatus* var. RP-2014	pET22b(+)	*Nde*I	*Bam*HI	
IR0044		*Aspergillus clavatus*	pET22b(+)	*Nde*I	*Bam*HI	12
IR0045		*Streptomyces virginiae*	pET22b(+)	*Nde*I	*Bam*HI	
IR0046		*Streptomyces* sp.	pET22b(+)	*Nde*I	*Bam*HI	
IR0049	IR43	*Streptomyces* sp. AA0539	pET22b(+)	*Nde*I	*Bam*HI	9
IR0051	*Ao*IRED	*Amycolatopsis orientalis*	pET21a(+)	*Bgl*II	*Xho*I	18
IR0052	RIR-Sip	*Streptomyces ipomoeae*	pET21a(+)	*Bgl*II	*Xho*I	5
IR0053	IR-08	*Paenibacillus elgii*	pET21a(+)	*Bgl*II	*Xho*I	8
IR0054	*Bc*IRED	*Bacillus cereus*	pET21a(+)	*Bgl*II	*Xho*I	6
IR0055	*Nh*IRED	*Nocardiopsis halophila*	pET21a(+)	*Bgl*II	*Xho*I	6
IR0056		*Paenibacillus lactis*	pET21a(+)	*Bgl*II	*Xho*I	
IR0057		*Kribbella flavida*	pET21a(+)	*Bgl*II	*Xho*I	
IR0058	IR-73	*Amycolatopsis azurea*	pET21a(+)	*Bgl*II	*Xho*I	8
IR0059		*Brevibacillus* sp.	pET21a(+)	*Bgl*II	*Xho*I	
IR0060		*Saccharothrix espanaensis*	pET21a(+)	*Bgl*II	*Xho*I	
IR0061		*Streptomyces viridochromogenes*	pET21a(+)	*Bgl*II	*Xho*I	
IR0062	pIR232	*Paenibacillus lactis*	pET21a(+)	*Bgl*II	*Xho*I	12
IR0063	IR-01	*Myxococcus stipitatus*	pET21a(+)	*Bgl*II	*Xho*I	8
IR0064	IR-10	*Streptomyces albidoflavus*	pET21a(+)	*Bgl*II	*Xho*I	8
IR0065	IR-13	*Myxococcus fulvus*	pET21a(+)	*Bgl*II	*Xho*I	8
IR0066	IR-22	*Mycolicibacterium mageritense*	pET21a(+)	*Bgl*II	*Xho*I	8
IR0067	IR-49	*Paenibacillus beijingensis*	pET21a(+)	*Bgl*II	*Xho*I	8
IR0068	IR-59	*Blastomyces dermatitidis* ER-3	pET21a(+)	*Bgl*II	*Xho*I	8
IR0069	IR-69	*Streptomyces* sp. PRh5	pET21a(+)	*Bgl*II	*Xho*I	8
IR0070	IR-75	*Streptomyces viridochromogenes*	pET21a(+)	*Bgl*II	*Xho*I	8
IR0071	IRED-**C**	*Micromonospora* sp. M42	pET21a(+)	*Bgl*II	*Xho*I	4
IR0072	IRED-**D**	*Mesorhizobium* sp. L2C089B000	pET21a(+)	*Bgl*II	*Xho*I	4
IR0073	IRED-**E**	*Nocardiopsis alba*	pET21a(+)	*Bgl*II	*Xho*I	4
IR0074	IRED-**F**	*Streptomyces niveus* NCIMB 11891	pET21a(+)	*Bgl*II	*Xho*I	4
IR0075	IRED-**G**	*Streptomyces rimosus* ATCC 10970	pET21a(+)	*Bgl*II	*Xho*I	4
IR0076	IRED-**H**	*Frankia* sp. QA3	pET21a(+)	*Bgl*II	*Xho*I	4
IR0077	IRED-**K**	*Streptosporangium roseum* DSM 43201	pET21a(+)	*Bgl*II	*Xho*I	4
IR0079	IRED-**M**	*Saccharothrix espanaensis* ATCC 51144	pET21a(+)	*Bgl*II	*Xho*I	4
IR0096		*Escherichia coli*	pET19b	*Nde*I	*Bam*HI	
IR0097		*Candida parapsilosis*	pET19b	*Nde*I	*Bam*HI	
IR0100	IRED-**B**	*Streptomyces kanamyceticus*	pET28a(+)	*Nde*I	*Xho*I	4
IR0107	IRED-**I**	*Streptomyces* sp. GF3546	pET28a(+)	*Nde*I	*Xho*I	4
IR0131	IR-20	*Streptosporangium roseum*	pET21a(+)	*Nde*I	*Bam*HI	8
IR0139	IR-29		pET21a(+)	*Nde*I	*Xho*I	8
IR0182	IR-77		pET21a(+)	*Nde*I	*Xho*I	8
IR0196	IR-91		pET21a(+)	*Nde*I	*Xho*I	8
IR0199	IR-94		pET21a(+)	*Nde*I	*Xho*I	8
IR0202	pIR2		pET21a(+)	*Nde*I	*Xho*I	12
IR0204	pIR4	*Aspergillus calidoustus*	pET21a(+)	*Nde*I	*Xho*I	12
IR0205	pIR5		pET21a(+)	*Nde*I	*Xho*I	12
IR0233	pIR33	*Emergomyces pasteurianus* Ep9510	pET21a(+)	*Nde*I	*Xho*I	12
IR0235	pIR35		pET21a(+)	*Nde*I	*Xho*I	12
IR0261	pIR61	*Penicillium arizonense*	pET21a(+)	*Nde*I	*Xho*I	12
IR0273	pIR73	*Streptomyces albus*	pET21a(+)	*Nde*I	*Xho*I	12
IR0279	pIR79		pET21a(+)	*Nde*I	*Xho*I	12

[a] Enzyme identifier used in the original publication. Entries typeset in grey indicate proteins for which no soluble expression could be achieved.

Table S30. IRED expression vectors used in the present study (*continued from previous page*).

Enzyme	Lit. ID[a]	Source Organism	Vector	Restriction Sites 5′	Restriction Sites 3′	Ref.
IR0301	pIR115		pET21a(+)	*Nde*I	*Xho*I	12
IR0312	pIR147		pET21a(+)	*Nde*I	*Xho*I	12
IR0327	pIR208		pET21a(+)	*Nde*I	*Xho*I	12
IR0343	pIR246		pET21a(+)	*Nde*I	*Xho*I	12
IR0371	pIR338		pET21a(+)	*Nde*I	*Xho*I	12
IR0376	pIR351		pET21a(+)	*Nde*I	*Xho*I	12
IR0381	pIR360		pET21a(+)	*Nde*I	*Xho*I	12
IR0392	IR_7	*Streptomyces aurantiacus*	pET21a(+)	*Nde*I	*Xho*I	2
IR0393	IRED-**A**	*Streptomyces* sp. GF3587	pET21a(+)	*Nde*I	*Xho*I	4
IR0394	IR45-W191A	*Streptomyces aurantiacus*	pET21a(+)	*Nde*I	*Xho*I	9
IR0395	IR2	*Actinomadura madurae*	pET21a(+)	*Nde*I	*Xho*I	9
IR0427		*Nocardia vinacea*	pET21a(+)	*Nde*I	*Xho*I	
IR0454		*Glycomyces* sp.	pET21a(+)	*Nde*I	*Xho*I	
IR0464		*Nocardia testacea*	pET21a(+)	*Nde*I	*Xho*I	
IR0468			pET21a(+)	*Nde*I	*Xho*I	
IR0482			pET21a(+)	*Nde*I	*Xho*I	
IR0497			pET21a(+)	*Nde*I	*Xho*I	
IR0499		*Streptomyces purpureus*	pET21a(+)	*Nde*I	*Xho*I	
IR0512		*Streptomyces peruviensis*	pET21a(+)	*Nde*I	*Xho*I	
IR0610		*Streptomyces* sp.	pET21a(+)	*Nde*I	*Xho*I	
IR0653		*Streptomyces tsukubaensis*	pET21a(+)	*Nde*I	*Xho*I	
IR0742		*Streptomyces griseus*	pET21a(+)	*Nde*I	*Xho*I	
IR0743		*Streptomyces griseus* subsp. *griseus*	pET21a(+)	*Nde*I	*Xho*I	
IR0856		*Streptomyces* sp. NRRL S-920	pET21a(+)	*Nde*I	*Xho*I	
IR0869			pET21a(+)	*Nde*I	*Xho*I	
IR0887		*Streptomyces* sp.	pET21a(+)	*Nde*I	*Xho*I	
IR0895		*Streptomyces mobaraensis*	pET21a(+)	*Nde*I	*Xho*I	
IR0902			pET21a(+)	*Nde*I	*Xho*I	
IR0965		*Brachybacterium phenoliresistens*	pET21a(+)	*Nde*I	*Xho*I	
IR1029		*Actinoalloteichus caeruleus*	pET21a(+)	*Nde*I	*Xho*I	
IR1051	SnIR	*Stackebrandtia nassauensis*	pET21a(+)	*Nde*I	*Xho*I	54
IR1059		*Actinomadura oligospora*	pET21a(+)	*Nde*I	*Xho*I	
IR1100		*Lysinibacillus varians*	pET21a(+)	*Nde*I	*Xho*I	
IR1105			pET21a(+)	*Nde*I	*Xho*I	
IR1134	IR47	*Salinispora pacifica*	pET21a(+)	*Nde*I	*Xho*I	10
IR1136			pET21a(+)	*Nde*I	*Xho*I	
IR1139		*Nocardia vulneris*	pET21a(+)	*Nde*I	*Xho*I	
IR1202		*Streptomyces rimosus*	pET21a(+)	*Nde*I	*Xho*I	
IR1294	IR-46	*Saccharothrix espanaensis*	pET21a(+)	*Nde*I	*Xho*I	17
IR1311		*Streptomyces afghaniensis*	pET21a(+)	*Nde*I	*Xho*I	
IR1345		*Kitasatospora azatica*	pET21a(+)	*Nde*I	*Xho*I	
IR1369			pET21a(+)	*Nde*I	*Xho*I	
IR1385			pET21a(+)	*Nde*I	*Xho*I	
IR1392			pET21a(+)	*Nde*I	*Xho*I	
IR1395			pET21a(+)	*Nde*I	*Xho*I	
IR1413		*Paenibacillus* sp. HGF5	pET21a(+)	*Nde*I	*Xho*I	
IR1421			pET21a(+)	*Nde*I	*Xho*I	
IR1427		*Mesorhizobium* sp.	pET21a(+)	*Nde*I	*Xho*I	
IR1437		*Streptomyces* sp.	pET21a(+)	*Nde*I	*Xho*I	
IR1446			pET21a(+)	*Nde*I	*Xho*I	
IR1453			pET21a(+)	*Nde*I	*Xho*I	
IR1460			pET21a(+)	*Nde*I	*Xho*I	

[a] Enzyme identifier used in the original publication. Entries typeset in grey indicate proteins for which no soluble expression could be achieved.

Table S30. IRED expression vectors used in the present study (*continued from previous page*).

Enzyme	Lit. ID[a]	Source Organism	Vector	Restriction Sites 5′	Restriction Sites 3′	Ref.
IR1475			pET21a(+)	*Nde*I	*Xho*I	
IR1476			pET21a(+)	*Nde*I	*Xho*I	
IR1491		*Amycolatopsis lurida NRRL 2430*	pET21a(+)	*Nde*I	*Xho*I	
IR1587			pET21a(+)	*Nde*I	*Xho*I	
IR1589			pET21a(+)	*Nde*I	*Xho*I	
IR1597		*Mycolicibacterium* sp.	pET21a(+)	*Nde*I	*Xho*I	
IR1598			pET21a(+)	*Nde*I	*Xho*I	
IR1612		*Actinoalloteichus spitiensis*	pET21a(+)	*Nde*I	*Xho*I	
IR1624		*Pseudonocardia spinosispora*	pET21a(+)	*Nde*I	*Xho*I	
IR1629		*Nocardia transvalensis*	pET21a(+)	*Nde*I	*Xho*I	
IR1630			pET21a(+)	*Nde*I	*Xho*I	
IR1632		*Streptomyces rimosus*	pET21a(+)	*Nde*I	*Xho*I	
IR1662		*Nocardia veterana*	pET21a(+)	*Nde*I	*Xho*I	
IR1664		*Actinomadura flavalba*	pET21a(+)	*Nde*I	*Xho*I	
IR1674			pET21a(+)	*Nde*I	*Xho*I	
IR1701		*Nocardia brasiliensis*	pET21a(+)	*Nde*I	*Xho*I	
IR1723			pET21a(+)	*Nde*I	*Xho*I	
IR1728		*Mesorhizobium sp.*	pET21a(+)	*Nde*I	*Xho*I	
IR1730		*Streptomyces cyaneogriseus*	pET21a(+)	*Nde*I	*Xho*I	
IR1737			pET21a(+)	*Nde*I	*Xho*I	
IR1738		*Streptomyces toyocaensis*	pET21a(+)	*Nde*I	*Xho*I	
IR1743			pET21a(+)	*Nde*I	*Xho*I	
IR1749		*Streptomyces iranensis*	pET21a(+)	*Nde*I	*Xho*I	
IR1757			pET21a(+)	*Nde*I	*Xho*I	
IR1760			pET21a(+)	*Nde*I	*Xho*I	
IR1773			pET21a(+)	*Nde*I	*Xho*I	
IR1788			pET21a(+)	*Nde*I	*Xho*I	
IR1793			pET21a(+)	*Nde*I	*Xho*I	
IR1805			pET21a(+)	*Nde*I	*Xho*I	
IR1855	IR077	*Ensifer adhaerens*	pET21a(+)	*Nde*I	*Xho*I	10
IR2010		*Aspergillus nomiae*	pET21a(+)	*Nde*I	*Xho*I	
IR2020		*Aspergillus nanangensis*	pET21a(+)	*Nde*I	*Xho*I	
IR2021		*Aspergillus udagawae*	pET21a(+)	*Nde*I	*Xho*I	
IR2022		*Plesiomonas shigelloides*	pET21a(+)	*Nde*I	*Xho*I	
IR2036		*Plesiomonas shigelloides*	pET21a(+)	*Nde*I	*Xho*I	
IR2092			pET21a(+)	*Nde*I	*Xho*I	
IR2095			pET21a(+)	*Nde*I	*Xho*I	
IR2114		*Streptomyces* sp. SA15	pET21a(+)	*Nde*I	*Xho*I	
IR2128		*Streptomyces qaidamensis*	pET21a(+)	*Nde*I	*Xho*I	
IR2137		*Streptomyces lomondensis*	pET21a(+)	*Nde*I	*Xho*I	
IR2145		*Streptomyces* sp. S3	pET21a(+)	*Nde*I	*Xho*I	
IR2147		*Streptomyces* sp.	pET21a(+)	*Nde*I	*Xho*I	
IR2150			pET21a(+)	*Nde*I	*Xho*I	
IR2159			pET21a(+)	*Nde*I	*Xho*I	
IR2173		*Nonomuraea jabiensis*	pET21a(+)	*Nde*I	*Xho*I	
IR2252			pET21a(+)	*Nde*I	*Xho*I	
IR2253		*Corallococcus* sp.	pET21a(+)	*Nde*I	*Xho*I	
IR2257		*Streptomyces qinzhouensis*	pET21a(+)	*Nde*I	*Xho*I	

[a] Enzyme identifier used in the original publication. Entries typeset in grey indicate proteins for which no soluble expression could be achieved.

For regeneration of the NADPH cofactor required by the IREDs, we tested six NADP-dependent auxiliary enzymes available in our group: three formate dehydrogenases (FDHs), two glucose dehydrogenases (GDHs), and a phosphite dehydrogenase (PtDH). The tested FDHs are a variant of the enzyme from *Mycobacterium vaccae* N10 (*Myc*-FDH, C145S/A198G/D221Q/C255V),[55] and two variants of the enzyme from *Pseudomonas* sp. 101 (NADP-FDH-var, D221Q/H223N; *Pse*-FDH-V13, A198G/D221Q/C255T/H379K/S380V),[56,57] which have been engineered for acceptance of $NADP^+$. The GDHs are the wild-type enzymes from *Bacillus megaterium*[58] and from *Bacillus subtilis*.[59] The PtDH is the 12× variant of the enzyme from *Pseudomonas stutzeri* reported by Zhao and co-workers (engineered for improved thermostability).[60]

FASTA files containing the protein and DNA sequences of these enzymes are openly available in the Mendeley Data repository (https://data.mendeley.com/) at https://doi.org/10.17632/jn4sfsrz8x.2, and the most important properties of the used expression plasmids are summarised in Table S31.

Table S31. Expression vectors of cofactor regeneration enzymes used in the present study.

			Restriction Sites				
Internal ID	**Vector**	**Insert**	5′	3′	**Antibiotic**	**Inducer**[a]	**Ref.**
pEG40	pET21a(+)	*Bm*-GDH	*Nde*I	*Xho*I	Ampicillin	IPTG	58
pEG299	pET28a(+)	PtDH	*Nde*I	*Xho*I	Kanamycin	IPTG	60
pEG494	pET28a(+)	*Myc*-FDH	*Nde*I	*Bam*HI	Kanamycin	IPTG	55
pEG521	pET28a(+)	*Bs*-GDH	*Nde*I	*Xho*I	Kanamycin	IPTG	59
pEG522	pET28a(+)	NADP-FDH-var	*Nde*I	*Xho*I	Kanamycin	IPTG	56
pEG606	pET28a(+)	*Pse*-FDH-V13	*Nde*I	*Xho*I	Kanamycin	IPTG	57

[a] IPTG, isopropyl β-D-1-thiogalactopyranoside

Preparation of Biocatalysts

Chemically competent cells of *E. coli* BL21(DE3) (*New England Biolabs*) were transformed with the plasmids encoding the investigated IREDs (or cofactor regeneration enzymes) according to the cell supplier's instructions. A single colony from a transformant agar plate was used to inoculate LB medium (15 mL, cont. the appropriate antibiotic: 100 μg/mL ampicillin or 50 μg/mL kanamycin) and the resulting culture was incubated at 37 °C and 120 rpm overnight in a closed plastic tube (50 mL). Glycerol stocks were prepared by diluting the cell suspension of the overnight culture (800 μL) with sterile 60% (v/v) aqueous glycerol (800 μL) and were stored at –80 °C. For expression, LB medium (15 mL, cont. the appropriate antibiotic: 100 μg/mL ampicillin or 50 μg/mL kanamycin) was inoculated with 50 μL of cell suspension from a glycerol stock and the resulting culture was incubated at 37 °C and 120 rpm overnight in a closed plastic tube (50 mL). 5 mL of this overnight culture was used to inoculate TB medium (500 mL, cont. the appropriate antibiotic: 100 μg/mL ampicillin or 50 μg/mL kanamycin) and the resulting culture was incubated at 37 °C and 120 rpm in a baffled Erlenmeyer flask (2 L). Samples (1 mL) of the culture were taken at regular intervals and analysed for their optical density at 600 nm (OD_{600}). When the OD_{600} reached a value of 0.8–1.0 (approx. after 3.5 h), protein expression was induced by the addition of IPTG (1 mM) and incubation was continued at 20 °C and 120 rpm overnight. The culture was transferred to a centrifuge beaker (500 mL) and centrifuged (5,000 rpm, 4,696 × g, 4 °C, 10 min) to pellet the cells. The supernatant was discarded and the cell pellet was resuspended in bicine–NaOH buffer (10 mL per 1 g wet cells; 100 mM, pH 7.5) and disrupted by ultrasonication on ice (20% amplitude = 50 W, 2 s pulse, 4 s pause, total pulse time 2:30 min, 75 cycles) using a *Sonics & Materials* Vibra Cell CV26 ultrasonicator (13 mm tip). The cell debris was removed by

centrifugation (14,000 rpm, 23,519 × g, 4 °C, 30 min), and the supernatant was transferred to a round-bottom flask (250 mL), flash-frozen in liquid nitrogen and lyophilised overnight (*Christ* Alpha 1–4 LSCbasic) to obtain the lyophilised cell-free extract (typically 0.5–0.9 g), which was stored at –20 °C until use.

Determination of Expression Level

The IRED expression level in the obtained cell-free extracts was determined by a combination of two measurements: First, the total protein content of the lyophilised cell-free extract was quantified using the Bradford method.[61] Then, the cell-free extract was subjected to SDS-PAGE and the ratio of IRED to total protein was quantified by pixel densitometry of a digital image of the gel. The results of the two measurements were combined to calculate the IRED content of the cell-free extract:

$$c_{\mathrm{IRED}} = c_{\mathrm{prot}} \cdot x_{\mathrm{IRED}} \tag{1}$$

where c_{IRED} [$\mathrm{mg_{IRED} \cdot mg_{CFE}^{-1}}$] … relative IRED content of the lyophilised cell-free extract; c_{prot} [$\mathrm{mg_{prot} \cdot mg_{CFE}^{-1}}$] … relative protein content of the lyophilised cell-free extract (determined by Bradford assay); x_{IRED} [dimensionless] … ratio of IRED to total protein (determined by pixel densitometry)

Bradford protein assay: The lyophilised cell-free extracts (3.0–6.0 mg) were dissolved in bicine-NaOH buffer (100 mM, pH 8.0; 250 μL) and dilutions (1:50) were prepared using the same buffer. Solutions of bovine serum albumin (BSA, *Sigma–Aldrich*; 0.05–0.5 mg/mL) in the same buffer were used as reference series. Commercial Bradford reagent (*Bio-Rad* Protein Assay Dye Reagent) was diluted five-fold with deionised water. The protein-containing samples (diluted IRED solutions or BSA solutions; 10 μL) were mixed with the diluted Bradford reagent (200 μL) in a 96-well microtiter plate (*Greiner*, clear polystyrene, flat bottom) and incubated at room temperature for 10–30 min. The absorbance at 590 nm was measured using a microtiter plate reader (*Molecular Devices* SpectraMax M2), and the linear fit of protein concentration and absorbance values obtained for the BSA reference series was used to calculate the protein concentration in the cell-free extract solutions.

SDS-PAGE and pixel densitometry: Solutions of the lyophilised cell-free extracts prepared as described above were diluted with bicine-NaOH buffer (100 mM, pH 8.0) to give a total protein concentration of *ca*. 1 mg/mL. The diluted samples (10 μL) were mixed with Laemmli buffer (10 μL, *Sigma–Aldrich*), heated to 95 °C for 10 min, and centrifuged (14,000 rpm, 23,519 × g, 1 min). The samples (20 μL) and a molecular weight marker (*Thermo Scientific* PageRuler™ Prestained Protein Ladder, 10–180 kDa; 10 μL) were loaded onto commercial, pre-cast SDS gels (*GenScript* SurePAGE™ Bis-Tris gels, 10% polyacrylamide, 12 or 15 wells), and the gels were developed at 120 V for 60 min in commercial Tris–MOPS–SDS running buffer (*GenScript*). Afterwards, the gels were removed from their plastic frames, washed with deionised water, stained with Coomassie solution (110 mg Coomassie Brilliant Blue G-250 and 10 g β-cyclodextrin in 850 mL H_2O, 50 mL EtOH and 80 mL phosphoric acid) for at least 2 h, and destained with deionised water overnight.

The gels were digitalised using a colour image scanner (*Canon* LiDE 110) and loaded into the ImageJ software,[62] where they were converted to black-and-white (Image > Type > 32-bit) and inverted (Edit > Invert Image). The lane and IRED pixel densities were determined by selecting the entire protein lane and IRED spot, respectively, with the polygon shape tool and measuring their density values (Analyse > Measure). The ratio of IRED to total protein (x_{IRED}) was obtained by simple division.

The image conversion and densitometry process is illustrated for an exemplary SDS gel in Figure S26, and the determined expression levels are summarised in Table S32.

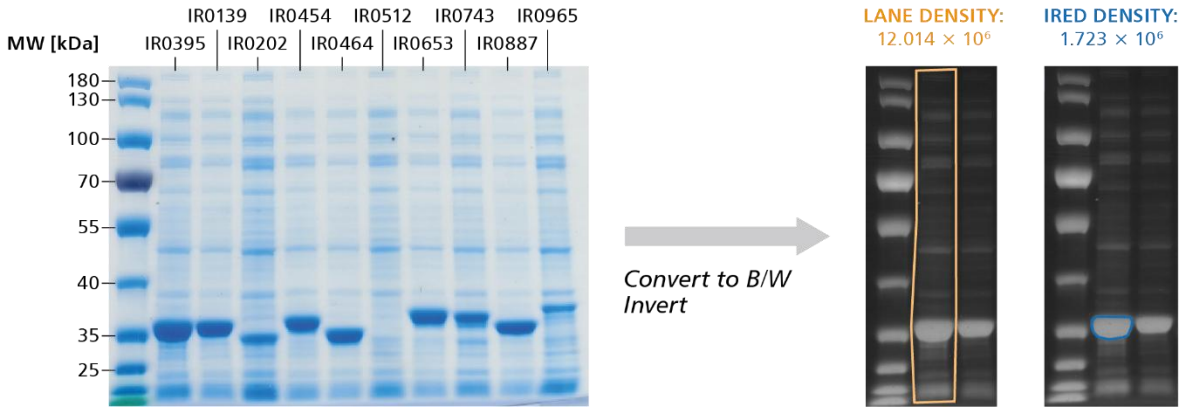


Figure S26. Quantification of the IRED to total protein ratio by pixel densitometry.

Table S32. Expression levels of the IREDs used in the present study (*continued on next page*).

IRED	c_{prot} [%]	x_{IRED}	c_{IRED} [%]	IRED	c_{prot} [%]	x_{IRED}	c_{IRED} [%]
IR0001	34.9	0.105	3.7	IR0042	43.5	0.046	2.0
IR0002	85.6	0.050	4.2	IR0043	45.9	0.057	2.6
IR0003	34.0	0.127	4.3	IR0045	76.6	0.049	3.7
IR0004	28.2	0.101	2.8	IR0046	74.6	0.135	10.1
IR0005	39.3	0.130	5.1	IR0049	24.5	0.168	4.1
IR0006	43.2	0.117	5.0	IR0051	73.8	0.114	8.4
IR0009	32.6	0.027	0.9	IR0052	32.2	0.173	5.6
IR0010	55.6	0.074	4.1	IR0053	19.5	0.223	4.4
IR0011	27.1	0.131	3.5	IR0054	21.3	0.197	4.2
IR0012	40.3	0.126	5.1	IR0055	53.6	0.158	8.5
IR0013	46.7	0.119	5.6	IR0056	26.8	0.132	3.5
IR0014	60.7	0.126	7.7	IR0057	30.8	0.159	4.9
IR0015	35.5	0.135	4.8	IR0058	27.1	0.109	3.0
IR0017	42.9	0.048	2.1	IR0059	26.8	0.129	3.4
IR0018	47.4	0.040	1.9	IR0060	64.4	0.097	6.2
IR0019	45.9	0.044	2.0	IR0061	62.7	0.136	8.5
IR0020	44.4	0.157	7.0	IR0062	84.7	0.108	9.2
IR0021	31.4	0.207	6.5	IR0063	51.9	0.116	6.0
IR0022	58.4	0.082	4.8	IR0064	41.0	0.154	6.3
IR0023	40.3	0.151	6.1	IR0065	80.0	0.052	4.2
IR0025	73.2	0.073	5.4	IR0066	13.9	0.091	1.3
IR0027	71.7	0.138	9.9	IR0067	70.9	0.081	5.8
IR0028	74.4	0.127	9.4	IR0068	49.0	0.033	1.6
IR0029	18.9	0.163	3.1	IR0069	49.5	0.086	4.3
IR0030	45.9	0.039	1.8	IR0070	43.6	0.089	3.9
IR0031	71.4	0.136	9.7	IR0071	33.8	0.111	3.8
IR0032	38.8	0.123	4.8	IR0072	51.3	0.082	4.2
IR0033	40.7	0.147	6.0	IR0073	49.5	0.078	3.9
IR0034	67.3	0.095	6.4	IR0074	40.6	0.057	2.3
IR0035	52.3	0.067	3.5	IR0075	36.5	0.098	3.6
IR0036	49.7	0.065	3.2	IR0076	29.6	0.140	4.1
IR0039	83.4	0.029	2.4	IR0077	26.8	0.200	5.4
IR0040	88.4	0.122	10.8	IR0079	33.3	0.136	4.5
IR0041	57.3	0.063	3.6	IR0096	22.9	0.049	1.1

The relative protein content (c_{prot}) and IRED content (c_{IRED}) of the cell-free extract have the dimensions [$mg_{prot} \cdot mg_{CFE}^{-1}$] and [$mg_{IRED} \cdot mg_{CFE}^{-1}$], respectively, but are reported as percentages for convenience.

Table S32. Expression levels of the IREDs used in the present study (*continued from previous page*).

IRED	c_{prot} [%]	x_{IRED}	c_{IRED} [%]	IRED	c_{prot} [%]	x_{IRED}	c_{IRED} [%]
IR0097	22.8	0.105	2.4	IR1385	32.1	0.038	1.2
IR0100	24.6	0.122	3.0	IR1392	87.7	0.051	4.5
IR0107	33.8	0.149	5.0	IR1395	26.0	0.082	2.1
IR0131	49.4	0.192	9.5	IR1413	30.4	0.029	0.9
IR0139	56.3	0.117	6.6	IR1421	43.2	0.075	3.3
IR0182	63.1	0.112	7.1	IR1427	26.6	0.089	2.4
IR0196	24.6	0.070	1.7	IR1437	66.5	0.164	10.9
IR0199	20.0	0.243	4.9	IR1446	77.5	0.047	3.7
IR0202	25.0	0.047	1.2	IR1453	83.1	0.042	3.5
IR0204	25.6	0.148	3.8	IR1460	34.3	0.128	4.4
IR0205	19.5	0.052	1.0	IR1475	79.3	0.042	3.3
IR0233	32.1	0.040	1.3	IR1476	42.3	0.147	6.2
IR0261	24.0	0.069	1.7	IR1587	49.3	0.029	1.4
IR0273	27.2	0.086	2.3	IR1589	68.1	0.045	3.0
IR0279	30.1	0.141	4.2	IR1597	50.9	0.055	2.8
IR0301	22.7	0.066	1.5	IR1598	39.0	0.064	2.5
IR0312	31.7	0.136	4.3	IR1612	39.3	0.062	2.4
IR0343	43.0	0.065	2.8	IR1629	51.3	0.060	3.1
IR0371	70.9	0.050	3.5	IR1630	61.7	0.069	4.2
IR0376	75.6	0.132	10.0	IR1632	79.2	0.065	5.1
IR0381	20.6	0.028	0.6	IR1662	45.6	0.055	2.5
IR0392	55.0	0.121	6.7	IR1664	19.9	0.042	0.8
IR0393	37.5	0.052	1.9	IR1674	41.6	0.092	3.8
IR0394	25.4	0.099	2.5	IR1701	46.6	0.052	2.4
IR0395	33.9	0.134	4.6	IR1723	50.0	0.026	1.3
IR0427	72.0	0.055	4.0	IR1737	49.4	0.063	3.1
IR0454	69.1	0.105	7.2	IR1738	66.7	0.039	2.6
IR0464	70.9	0.115	8.2	IR1743	46.0	0.076	3.5
IR0468	31.5	0.048	1.5	IR1749	25.4	0.023	0.6
IR0482	40.3	0.055	2.2	IR1757	51.5	0.078	4.0
IR0497	46.8	0.051	2.4	IR1760	41.6	0.042	1.7
IR0499	35.1	0.048	1.7	IR1773	29.9	0.133	4.0
IR0610	44.1	0.055	2.4	IR1788	46.5	0.037	1.7
IR0653	60.9	0.118	7.2	IR1793	90.0	0.058	5.2
IR0742	27.6	0.059	1.6	IR1805	33.7	0.060	2.0
IR0743	47.9	0.066	3.2	IR1855	46.7	0.059	2.8
IR0856	84.1	0.044	3.7	IR2010	47.0	0.077	3.6
IR0869	50.0	0.074	3.7	IR2021	24.5	0.035	0.9
IR0887	57.5	0.116	6.7	IR2022	62.4	0.063	3.9
IR0895	40.8	0.124	5.1	IR2036	77.3	0.056	4.4
IR0902	43.3	0.161	7.0	IR2092	74.7	0.080	6.0
IR0965	29.3	0.044	1.3	IR2095	48.6	0.068	3.3
IR1029	54.2	0.057	3.1	IR2114	86.7	0.046	4.0
IR1051	51.7	0.121	6.3	IR2128	81.3	0.041	3.3
IR1059	44.5	0.068	3.0	IR2137	49.0	0.052	2.6
IR1100	35.7	0.062	2.2	IR2145	57.7	0.055	3.2
IR1105	42.0	0.057	2.4	IR2147	90.7	0.035	3.2
IR1134	49.5	0.150	7.4	IR2150	61.2	0.072	4.4
IR1136	42.4	0.088	3.7	IR2159	24.0	0.054	1.3
IR1139	60.4	0.070	4.2	IR2173	39.6	0.066	2.6
IR1202	47.7	0.126	6.0	IR2252	41.7	0.047	2.0
IR1294	42.5	0.084	3.6	IR2253	40.0	0.055	2.2
IR1345	48.5	0.063	3.0	IR2257	14.0	0.059	0.8
IR1369	30.5	0.048	1.5				

The relative protein content (c_{prot}) and IRED content (c_{IRED}) of the cell-free extract have the dimensions [$mg_{prot} \cdot mg_{CFE}^{-1}$] and [$mg_{IRED} \cdot mg_{CFE}^{-1}$], respectively, but are reported as percentages for convenience.

Photometric IRED Activity Assay: Overview Screening

The reductive amination activities of 175 IREDs for the 56 substrate combinations (8 carbonyls × 7 amines) of the Overview Screening were determined by following the consumption of NADPH photometrically using a microtiter plate reader (*Molecular Devices* SpectraMax M2). A wavelength of 370 nm (ϵ_{NADPH} = 2,216 M^{-1} cm^{-1}) was chosen for this photometric assay instead of the more common 340 nm to enable using a higher NADPH concentration while maintaining linear absorbance response and to reduce background absorbance by the substrates. The optical path length in each well was determined using the PathCheck feature of the plate reader, which compares the absorbance values at 900 nm and 1000 nm to those of a reference solution (buffer/DMSO 9:1) placed in the cuvette port (known path length: 1 cm) of the reader.

Stock solutions: The following stock solutions were used for setting up the assay reactions:

- *500 mM Carbonyl stock:* carbonyl compounds **c1–c8** (500 μmol) in DMSO (1.0 mL)
- *1 M Ammonia stock:* Ammonium acetate (3.08 g, 40 mmol) in bicine–NaOH buffer (100 mM, pH 8.0; 40 mL), pH re-adjusted to 8.0±0.1 by addition of 10 M NaOH solution
- *100 mM Amine stock:* Amines **a2–a7** (4.0 mmol) in bicine–NaOH buffer (100 mM, pH 8.0; 40 mL), pH re-adjusted to 8.0±0.1 by addition of acetic acid
- *10 mM NADPH stock:* NADPH tetrasodium salt (41.7 mg, 50 μmol) in bicine–NaOH buffer (100 mM, pH 8.0; 5 mL)
- *5× IRED stock (10 mg/mL):* lyophilised IRED preparation (cell-free extract, 50 mg) in bicine–NaOH buffer (100 mM, pH 8.0; 5 mL)

Aniline (**a7**) was purified by short-path distillation (Kugelrohr) directly before preparing the stock solution. Amine stock solutions were prepared on a monthly basis and stored in plastic tubes (50 mL) at 4 °C. Carbonyl stock solutions were also prepared on a monthly basis and stored in a 96-deep-well plate (*Ritter* Riplate SW 96; polypropylene, 2 mL, round bottom) covered with a rubber lid at room temperature and in the dark. The NADPH and IRED stock solutions were prepared freshly before setting up the assay.

Assay setup and data collection: Each well of a 96-well microtiter plate (*Greiner*, clear polystyrene, flat bottom) was charged with amine stock solution (50 μL; replaced with bicine–NaOH buffer for the 'no amine' condition), carbonyl stock solution (10 μL), NADPH stock solution (20 μL), and IRED stock solution (20 μL) according to one of the two plate layouts shown in Figure S27 (overleaf), resulting in final concentrations of 50 mM carbonyl compound, 50 mM amine (except ammonia: 500 mM), 2 mM NADPH, 2 mg/mL lyophilised IRED preparation (cell-free extract), and 10% (v/v) DMSO in a total volume of 100 μL. The required pipetting operations were performed using electronic multi-channel pipettes (*Sartorius* Picus 8-channel 10–300 μL and 50–1200 μL). Directly after adding the last component (IRED stock), the plate was closed with a transparent polystyrene lid and placed into the reader, which had been pre-equilibrated to an internal chamber temperature of 30 °C for at least 15 min. After an initial shaking step (5 s), the assay reactions were followed by measuring the absorbance at 370 nm every 30 s over a period of 1 h (121 data points). To maximise the number of interpretable data points for fast reactions, the PathCheck endpoint measurement was performed after completion of the kinetic series.

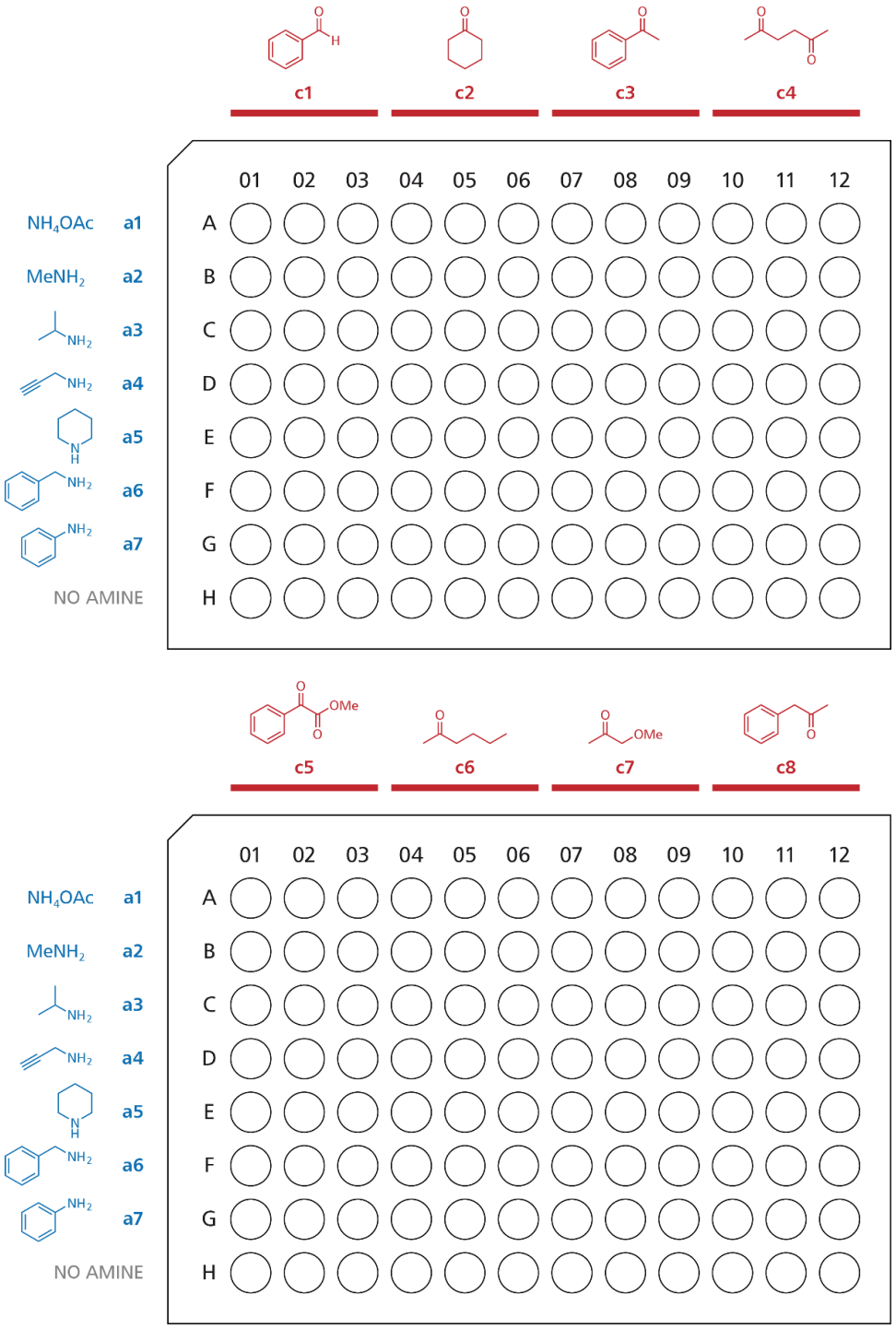


Figure S27. Plate layouts for the Overview Screening.

Data analysis: The slopes of absorbance decrease were determined by applying a linear fit to the linear range of the absorbance curves using the built-in function of the plate reader's *Molecular Devices* Softmax Pro (*v*. 6.4) software. Two standard fits were used for the majority of the reactions: maximum slope over 10 data points (for fast reactions), and maximum slope over 30 data points with 600 s lag time (for slower reactions that showed random noise in the initial phase of the measurement). In cases where neither of the two standard fits represented the data well, custom fits were employed. Path length data (in units of cm) and slope data (in units of mAU/min), arranged in a plate format (12 columns × 8 rows), were exported to *Microsoft* Excel for further processing.

After importing the data into *Microsoft* Excel, all slopes were corrected for path length, experimental multiplicates were aggregated to give a mean and standard deviation (SD) for each experimental condition, and the mean values were corrected for the background rate of absorbance decrease (obtained from the 'no amine' control reactions), followed by conversion into specific activity values according to the following equation:

$$A_{\mathrm{CFE}} = \frac{\Delta OD}{\epsilon_{\mathrm{NADPH}} \cdot l \cdot c_{\mathrm{CFE}}} \tag{2}$$

where A_{CFE} [U·mg$_{\mathrm{CFE}}^{-1}$] … specific activity (based on cell-free extract); ΔOD [mAU·min^{-1}] … slope of absorbance decrease; $\epsilon_{\mathrm{NADPH}}$ [L·mol^{-1}·cm^{-1}] … extinction coefficient of NADPH (2,216 at 370 nm); l [cm] … path length; c_{CFE} [mg·mL^{-1}] … concentration of enzyme preparation (cell-free extract) in the assay mixture

Hit identification: Since a low but noticeable background activity (*i.e.*, a decrease in absorbance that is independent of the target reaction) was observed in all negative-control reactions, and since the handling of small volumes required for a plate-based assay inevitably introduces random error, not all corrected means that are positive should be interpreted as a true positive, indicative of enzyme activity. Instead, positives ('hits') were identified based on a simple statistical criterion:

$$[mean_{\mathrm{reaction}} > 3 \cdot SD_{\mathrm{reaction}}] \wedge [mean_{\mathrm{reaction}} > \frac{1}{2} \cdot mean_{\mathrm{control}}] \tag{3}$$

where $mean_{\mathrm{reaction}}$ … mean activity value of the assay reactions (corrected for background); SD_{reaction} … standard deviation of the activity values of the assay reactions; $mean_{\mathrm{control}}$ … mean activity value of the corresponding negative-control reactions (uncorrected)

Figure S28 illustrates how the triplication of assay reactions and blanks allowed the detection of low-level positives despite the non-zero background activity.

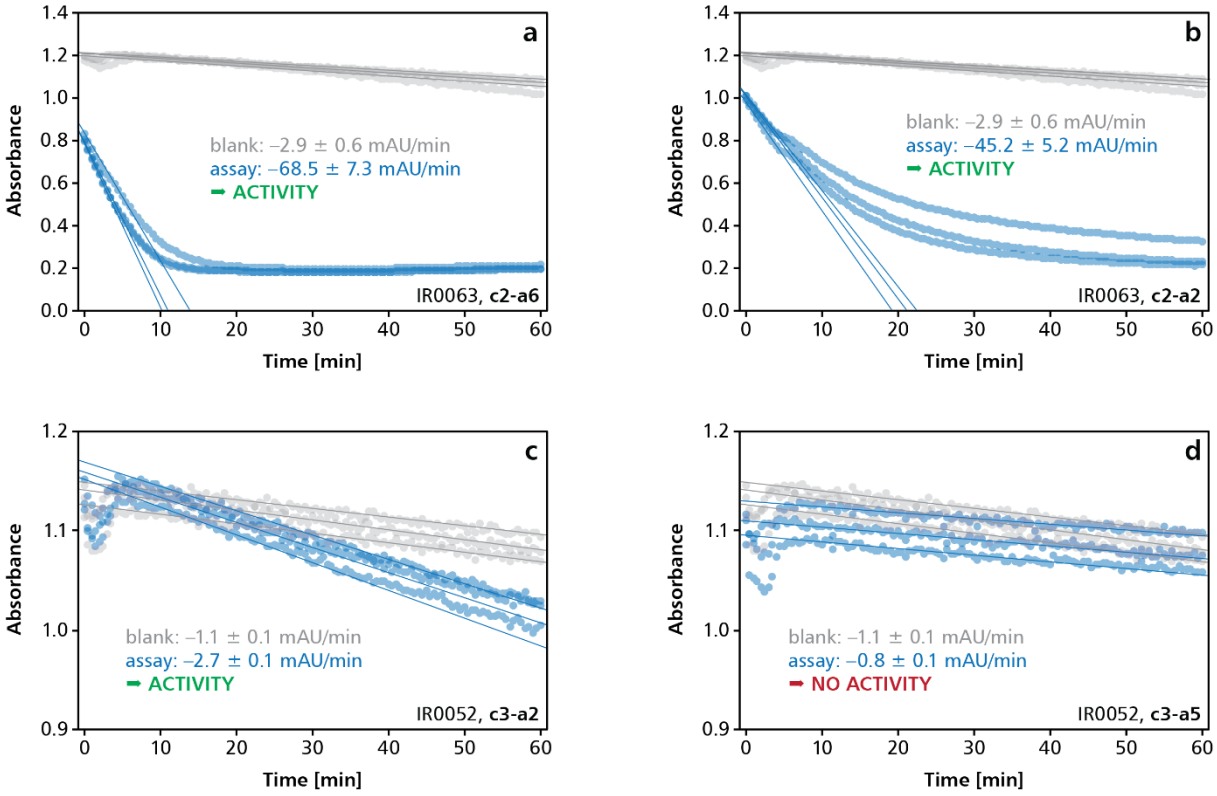


Figure S28. Exemplary photometric absorbance curves collected during the Overview Screening. Blank reactions (no amine) are shown in grey and complete assay reactions in blue, with semi-transparent circles showing absorbance reads at different time points and lines showing linear fits. Note the different *y*-axis scales for panels **a** and **b** *vs*. **c** and **d**.

The identification of hits based on this criterion was implemented in *Microsoft* Excel using an if-condition. In cases where re-screening using GC–MS or HPLC–MS (see *Validation Experiments for the Overview Screening*) failed to reproduce a hit (which was the case only at low activity levels), the corresponding substrate combination was manually flagged as non-hit in the Excel file.

Collation of data into a single matrix: After photometric data collection and analysis in *Microsoft* Excel had been completed for all investigated enzymes, a Python script (available at: https://github.com/saberger/Screening_for_Generality/tree/main/Initial_Screening) was used to collate the activity data from the individual Excel files (one per enzyme, containing two sheets each) into a single matrix comprising the following columns: IRED identifier, amine identifier, carbonyl identifier, activity mean, activity SD. During this collation process, the activity mean and SD of non-hits ("negatives") were set to zero, and non-interpretable assay reactions (**c1-a6** and **c1-a7**, which were affected by turbidity) were removed from the data set entirely. This data clean-up process is visualised in Figure S29.

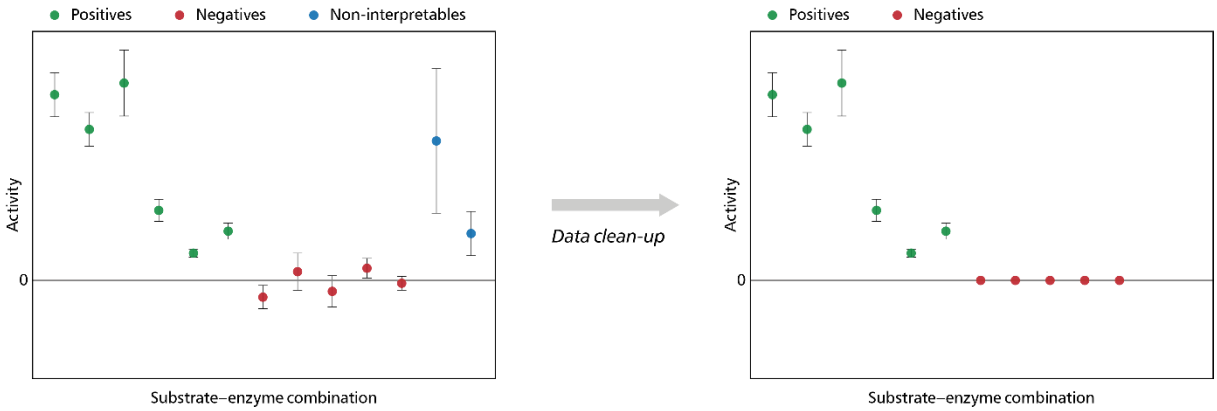


Figure S29. Illustration of the data clean-up steps implemented during collation of the activity data.

Normalisation of data for IRED expression level: For the purpose of activity prediction using machine-learning models (see above), the collected activity data needed to be normalised for IRED expression level to eliminate differences in expression as a source of activity variance in the data set. Therefore, as a final data processing step, the activity mean and SD in the collated matrix were normalised using the expression data obtained as described above (see *Determination of Expression Level*) according to the following equation:

$$A_{\mathrm{IRED}} = A_{\mathrm{CFE}} / c_{\mathrm{IRED}} \tag{4}$$

where A_{IRED} [U·mg$_{\mathrm{IRED}}^{-1}$] … specific activity (based on IRED); A_{CFE} [U·mg$_{\mathrm{CFE}}^{-1}$] … specific activity (based on cell-free extract); c_{IRED} [mg$_{\mathrm{IRED}}$·mg$_{\mathrm{CFE}}^{-1}$] … relative IRED content of the lyophilised cell-free extract

This transformation was implemented in LibreOffice Calc using the VLOOKUP function (equivalent to XLOOKUP in *Microsoft* Excel), and the final matrix containing the IRED-based activity data is openly available in the Mendeley Data repository (https://data.mendeley.com/) at https://doi.org/10.17632/jn4sfsrz8x.2.

Photometric IRED Activity Assay: Diversification Screening

The reductive amination activities of 100 IREDs for the 96 substrate combinations (6 carbonyls × 16 amines) of the amine scope part of the Diversification Screening were determined by following the consumption of NADPH photometrically in a similar way as described above for the Overview Screening, but with the following modifications: (1) The required pipetting operations were performed by a liquid-handling robot (*Beckman-Coulter* Biomek i7), (2) the absorbance measurements were performed using a microtiter plate reader integrated in the robotic platform (*BMG Labtech* FLUOstar Omega), and (3) an average optical path length for all wells (obtained from previous data) was used instead of an individual path length for each well, as the FLUOstar Omega reader does not allow a correction of photometric path length measurements for the influence of the organic co-solvent (DMSO) present in the sample.

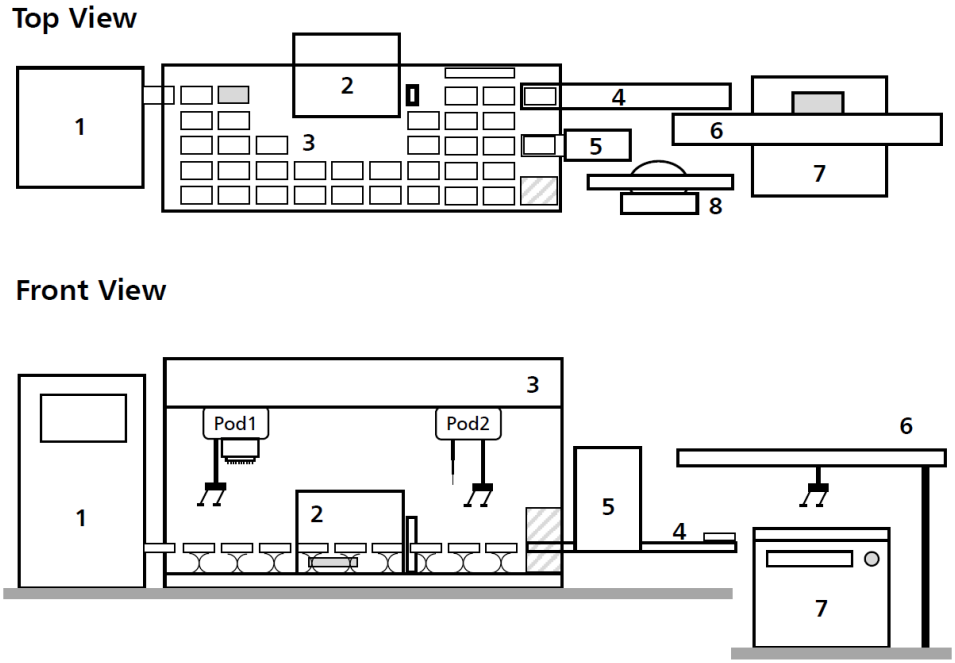


Figure S30. Schematic overview of the robotic liquid-handling and screening platform. **1**, SBS-format plate incubator (*Thermo Scientific* Cytomat 2 C450 LiN); **2**, UV/Vis and fluorescence microtiter plate reader (*BMG Labtech* FLUOstar Omega); **3**, liquid-handling robot (*Beckman-Coulter* Biomek i7); **4**, microtiter plate shuttle (*Beckman-Coulter* Servo Shuttle); **5**, colony detection module (*Amplius* Visual ALP); **6**, robotic arm (*Beckman-Coulter* BRT II); **7**, refrigerated centrifuge (*Hettich* Rotana 460 Robotic); Pod1, 96-multichannel pipetting head; Pod2, Span8 pipetting head. The devices are controlled and integrated by a personal computer (**8**) running Biomek and DART 2.0 software. Representation of the computer in front view is avoided for clarity.

Stock solutions: The following stock solutions were used for setting up the assay reactions:

- *500 mM Carbonyl stock:* carbonyl compounds **c2** and **c8–c12** (500 μmol) in DMSO (1.0 mL)
- *100 mM Amine stock:* Amines **a8–a23** (4.0 mmol) in bicine–NaOH buffer (100 mM, pH 8.0; 40 mL), pH re-adjusted to 8.0±0.1 by addition of acetic acid
- *10 mM NADPH stock:* NADPH tetrasodium salt (41.7 mg, 50 μmol) in bicine–NaOH buffer (100 mM, pH 8.0; 5 mL)
- *5× IRED stock (5 mg/mL):* lyophilised IRED preparation (cell-free extract, 25 mg) in bicine–NaOH buffer (100 mM, pH 8.0; 5 mL)

Amine stock solutions were prepared on a monthly basis, stored in plastic tubes (50 mL) at 4 °C, and aliquots of 2 mL were transferred to a 96-deep-well plate (*Thermo Scientific* Matrix™

DeepWell™ Storage Blocks, polypropylene, 2200 μl, square well, conical bottom) used as reservoir in the robotic platform. Carbonyl stock solutions were also prepared on a monthly basis and stored in a 96-deep-well plate (*Thermo Scientific* Matrix™ DeepWell™ Storage Blocks, polypropylene, 2200 μl, square well, conical bottom) covered with a rubber lid at room temperature and in the dark. The NADPH and IRED stock solutions were prepared freshly before setting up the assay and transferred to a 96-deep-well plate (*Thermo Scientific* Matrix™ DeepWell™ Storage Blocks, polypropylene, 2200 μl, square well, conical bottom) used as reservoir in the robotic platform.

Assay setup and data collection: Each well of a 96-well microtiter plate (*Greiner*, clear polystyrene, flat bottom) was charged with amine stock solution (50 μL), carbonyl stock solution (10 μL), IRED stock solution (20 μL), and NADPH stock solution (20 μL), according to the plate layout shown in Figure S31, resulting in final concentrations of 50 mM carbonyl compound, 50 mM amine, 2 mM NADPH, 1 mg/mL lyophilised IRED preparation (cell-free extract), and 10% (v/v) DMSO in a total volume of 100 μL. The carbonyl and amine substrates, as well as the cofactor, were dispensed using the 96-multichannel head (96-MC, Pod1), while the enzyme preparation was pipetted by the Span8 head (S8, Pod2). Directly after adding the last component (NADPH stock), the plate was robotically transferred into the reader, which had been pre-equilibrated to an internal chamber temperature of 30 °C for at least 15 min. After an initial shaking step (5 s), the assay reactions were followed by measuring the absorbance at 370 nm every 30 s over a period of 1 h (121 data points).

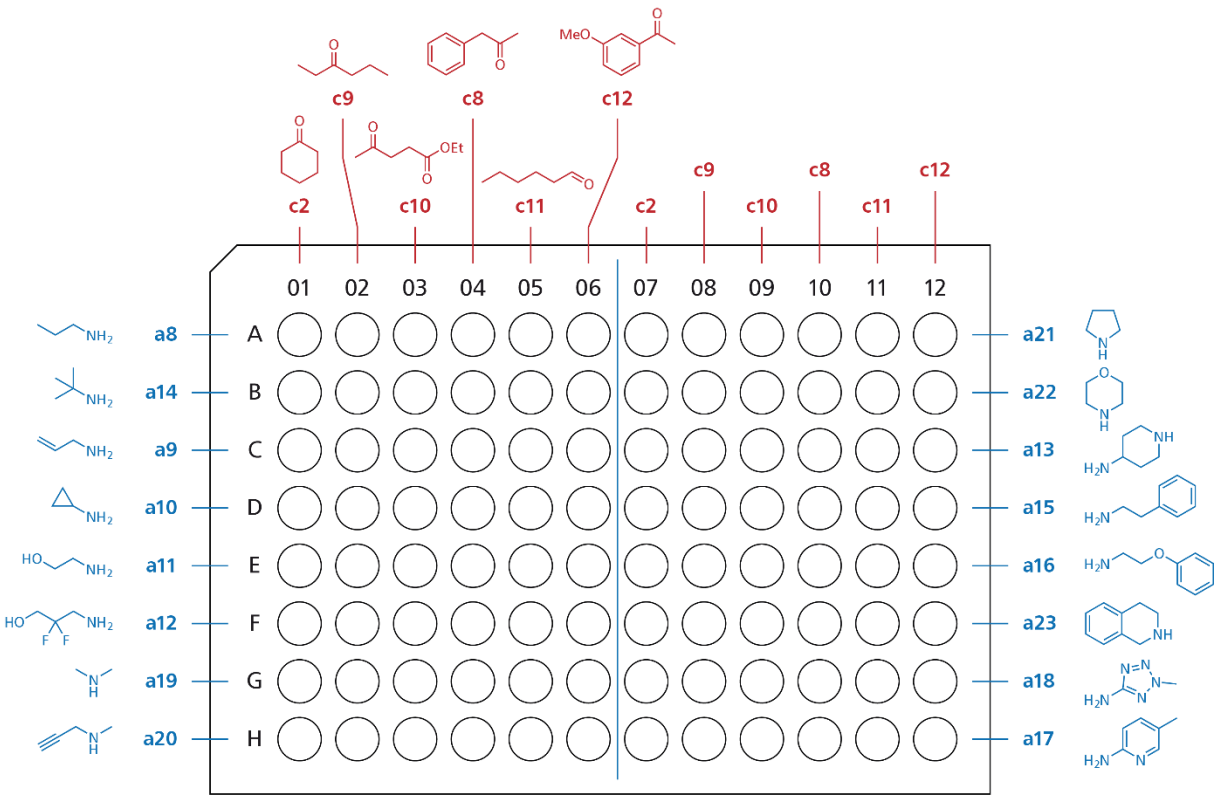


Figure S31. Plate layout for the amine scope part of the Diversification Screening.

Data analysis: The raw absorbance data were exported to *Microsoft* Excel and the slopes of absorbance decrease were determined using a Python script (available at: https://github.com/saberger/Screening_for_Generality/tree/main/Diversification_Screening/Amine-Scope) that fits the data to a Legendre polynomial and returns the maximum of its first derivative (maximum slope). Two standard fits were used for the majority of the reactions: maximum slope within

data points 6 to 60 (for fast reactions), and maximum slope within data points 31 to 121 (for slower reactions that showed random noise in the initial phase of the measurement). In cases where neither of the two standard fits represented the data well, custom fits were employed. For further details on the curve fitting process, see the README file in the Github repository. Slope data (in units of mAU/min), arranged in a plate format (12 columns × 8 rows), were exported to *Microsoft* Excel for further processing.

After importing the data into *Microsoft* Excel, all slopes were corrected for path length and for the background rate of absorbance decrease (obtained from the empty-vector control reactions, see below), followed by conversion into specific activity values according to equation 2 (see *Photometric* IRED Activity Assay: Overview Screening).

Hit identification: To enable the identification of hits based on a statistical criterion without having to replicate every experimental condition, we performed the photometric assay reactions of all substrate–enzyme combinations as single determinations but collected multiplicate negative control data. These were obtained as nine replicates spread out over the time span of the entire screening process (10 months) using the same plate layout and replacing the IRED preparation with cell-free extract of *E. coli* BL21 (DE3) transformed with an "empty" pET22b(+) plasmid (empty-vector controls, EVCs). Positives were identified by comparing the activity value obtained for each substrate combination, corrected for background activity (mean of EVCs), to the standard deviation of the EVCs according to the following criterion:

$$(A_{\text{reaction}} - mean_{\text{EVC}}) > 5 \cdot SD_{\text{EVC}} \tag{5}$$

where A_{reaction} … activity value of the assay reaction; $mean_{\text{EVC}}$ … mean activity value of the corresponding empty-vector control reactions; SD_{EVC} … standard deviation of the activity values of the corresponding empty-vector control reactions

The identification of hits based on this criterion was implemented in *Microsoft* Excel using an if-condition. In cases where re-screening using GC–MS or HPLC–MS (see *Validation Experiments for the Diversification Screening*) failed to reproduce a hit, the corresponding substrate combination was manually flagged as non-hit in the Excel file.

Collation of data into a single matrix: After photometric data collection and analysis in *Microsoft* Excel had been completed for all investigated enzymes, a Python script (available at: https://github.com/saberger/Screening_for_Generality) was used to collate the activity data from the individual Excel files (one per enzyme) into a single matrix comprising the following columns: IRED identifier, amine identifier, carbonyl identifier, activity. During this collation process, the activity of non-hits ("negatives") was set to zero, and non-interpretable assay reactions (**c11-a13**, **c11-a15**, **c11-a16**, **c12-a13**, **c12-a15**, and **c12-a16**, which were affected by turbidity) were removed from the data set entirely.

Normalisation of data for IRED expression level: In a similar way as described above for the Overview Screening, the activity data in the collated matrix were normalised for IRED expression level according to equation 4 (see *Photometric* IRED Activity Assay: Overview Screening). This transformation was implemented in LibreOffice Calc using the VLOOKUP function (equivalent to XLOOKUP in *Microsoft* Excel), and the final matrix containing the IRED-based activity data is openly available in the Mendeley Data repository (https://data.mendeley.com/) at https://doi.org/10.17632/jn4sfsrz8x.2.

FIA–MS Activity Assay: Diversification Screening

The 96 substrate combinations (24 carbonyls × 4 amines) of the carbonyl scope part of the Diversification Screening were assayed by flow-injection analysis mass spectrometry (FIA–MS), using uncalibrated integral ratios of target amine over bicine buffer to quantify product formation.[63] The required pipetting, incubation, and centrifugation steps for setting up the assay, quenching the reactions, removing precipitated protein, and transferring the supernatant to HPLC glass vials were performed by a liquid-handling robot (*Beckman-Coulter* Biomek i7) coupled to an automated incubator (*Thermo Scientific* Cytomat 2 C450-LiN) and a table-top centrifuge (*Hettich* Rotana 460 Robotic).

Stock solutions: The following stock solutions were used for setting up the assay reactions:

- *500 mM Carbonyl stock:* carbonyl compounds **c13–c35** (500 μmol) in DMSO (1.0 mL)
- *100 mM Amine stock:* Amines **a2**, **a4**, **a17**, and **a24** (4.0 mmol) in bicine–NaOH buffer (100 mM, pH 8.0; 40 mL), pH re-adjusted to 8.0±0.1 by addition of acetic acid
- *5× NADP–phosphite stock:* $NADP^+$ sodium salt (76.5 mg, 100 μmol) and $Na_2HPO_3 \cdot 5\ H_2O$ (2.16 g, 10 mmol) in bicine–NaOH buffer (100 mM, pH 8.0; 20 mL)
- *5× IRED–PtDH stock (20 mg/mL):* lyophilised IRED preparation (cell-free extract, 100 mg) and lyophilised PtDH preparation (cell-free extract, 100 mg) in bicine–NaOH buffer (100 mM, pH 8.0; 5 mL)

Amine stock solutions were prepared on a monthly basis, stored in plastic tubes (50 mL) at 4 °C, and aliquots of 2 mL were transferred to a 96-deep-well plate (*Thermo Scientific* Matrix™ DeepWell™ Storage Blocks, polypropylene, 2200 μl, square well, conical bottom) used as reservoir in the robotic platform. Carbonyl stock solutions were also prepared on a monthly basis and stored in a 96-deep-well plate (*Thermo Scientific* Matrix™ DeepWell™ Storage Blocks, polypropylene, 2200 μl, square well, conical bottom) covered with a rubber lid at room temperature and in the dark. The NADP–phosphite and IRED–PtDH stock solutions were prepared freshly before setting up the assay and transferred to a 96-deep-well plate (*Thermo Scientific* Matrix™ DeepWell™ Storage Blocks, polypropylene, 2200 μl, square well, conical bottom) used as reservoir in the robotic platform.

Biotransformation setup: Each well of a 96-deep-well plate (*Thermo Scientific* Matrix™ DeepWell™ Storage Blocks, polypropylene, 2200 μl, square well, conical bottom) was charged with amine stock solution (50 μL), carbonyl stock solution (10 μL), IRED–PtDH stock solution (20 μL), and NADP–phosphite stock solution (20 μL), according to the plate layout shown in Figure S32 (overleaf), resulting in final concentrations of 50 mM carbonyl compound, 50 mM amine, 1 mM $NADP^+$, 100 mM phosphite, 4 mg/mL lyophilised IRED preparation (cell-free extract), 4 mg/mL lyophilised PtDH preparation (cell-free extract), and 10% (v/v) DMSO in a total volume of 100 μL. The carbonyl and amine substrates, as well as the NADP–phosphite solution, were dispensed using the 96-MC (Pod1), while the IRED–PtDH stock was pipetted by the S8 (Pod2). After adding the last component (NADP–phosphite stock), the plate was closed with a plastic lid (*Greiner*, clear polystyrene, high profile) and robotically transferred to the automated incubator, where it was shaken at 800 rpm and 30 °C for 24 h.

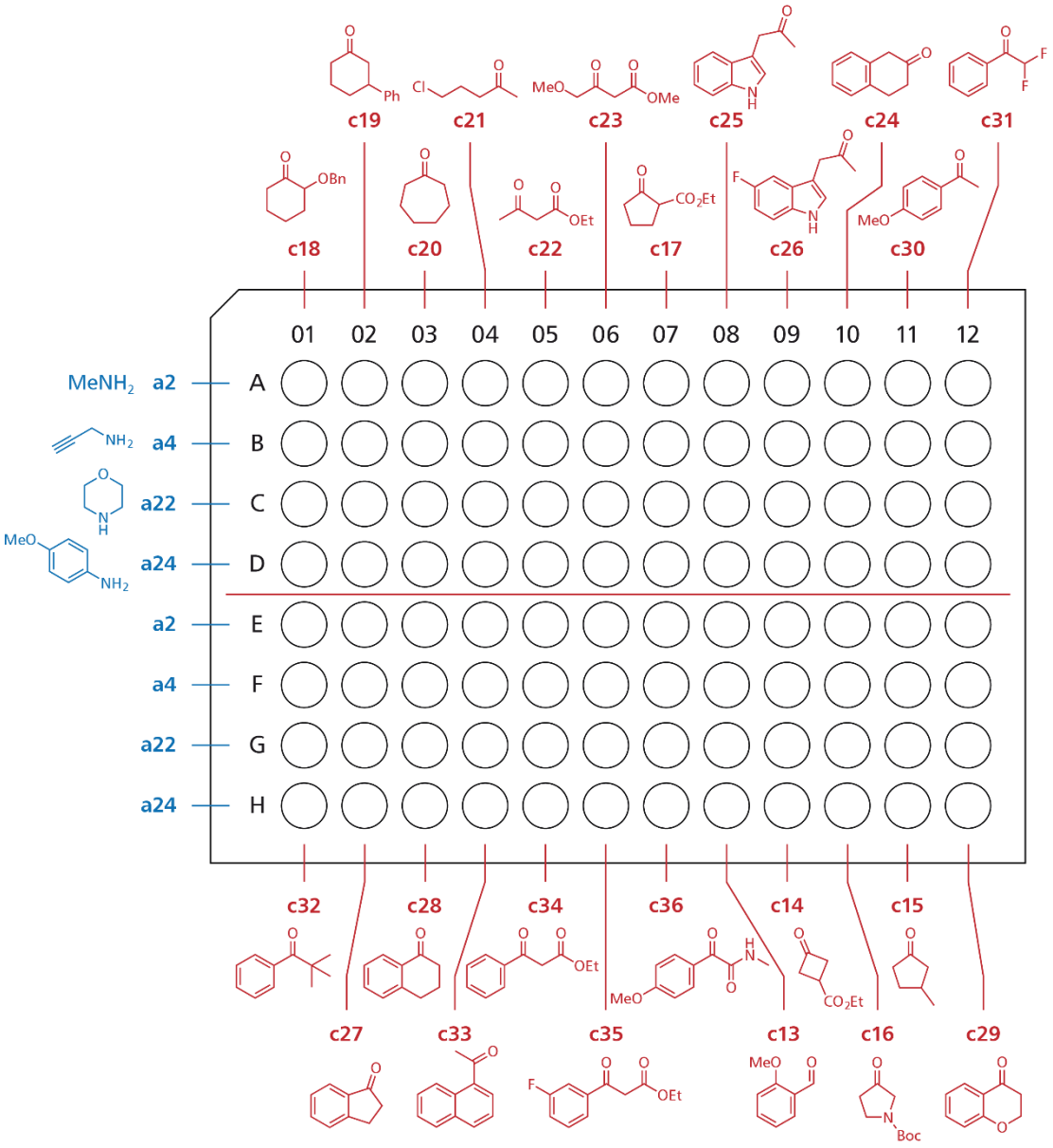


Figure S32. Plate layout for the carbonyl scope part of the Diversification Screening.

Work-up for FIA–MS: The assay reactions were quenched by addition of acetonitrile (900 μL) and precipitated protein was pelleted by centrifugation (4,500 rpm, 4,300 × g, 30 min). Part of the supernatant (700 μL) from each well was transferred to a glass HPLC vial for flow-injection MS analysis. The first pipetting operation (MeCN quench) was carried out using the 96-MC (Pod1), while the sample transfer to vials was carried out using the S8 (Pod2).

Flow-injection MS analysis: Flow-injection MS analysis was carried out on an *Agilent* 1260 Infinity HPLC system (G1311B quaternary pump, G1329B autosampler, G1316A thermostatted column compartment, G1314F variable wavelength detector) equipped with a *Phenomenex* SecurityGuard™ C18 cartridge and coupled to an *Agilent* 6120 single-quadrupole MS detector, using method FIA-MS1 described below.

Method FIA-MS1 (used for all analytes)

Column:	no column, SecurityGuard™ C18 cartridge
Column temperature:	not controlled
Eluent composition:	H_2O/MeCN = 50:50 (+ 0.1% formic acid), isocratic
Eluent flow rate:	0.5 mL/min
Run time:	1 min, with overlapping injection cycle (0.3 min)
Injection volume:	1 μL
Ionisation mode:	API-ES, positive polarity
Drying gas temperature:	300 °C
Drying gas flow:	6.0 L/min
Nebuliser pressure:	15 psig (2.0 bar)
Capillary voltage:	3000 V
Signal 1 (scan):	40% cycle time mass range 50–500 fragmentor 70 V
Signal 2 (bicine buffer):	30% cycle time SIM masses 164.10 $[M+H]^+$ fragmentor 70 V
Signal 3 (target):	30% cycle time SIM on target mass fragmentor 70 V

The target masses of the expected amine products were specified individually for each sample in the sequence table and are summarised in Table S33.

Table S33. Target masses of amine products analysed by FIA–MS (*continued on next page*).

Target	Well	Mass (*m/z*)	Target	Well	Mass (*m/z*)
c18-a2	A01	220.2 $[M+H]^+$	**c18-a4**	B01	244.2 $[M+H]^+$
c19-a2	A02	190.2 $[M+H]^+$	**c19-a4**	B02	214.2 $[M+H]^+$
c20-a2	A03	128.1 $[M+H]^+$	**c20-a4**	B03	152.1 $[M+H]^+$
c21-a2	A04	100.2 $[M+H]^+$	**c21-a4**	B04	124.1 $[M+H]^+$
c22-a2	A05	146.1 $[M+H]^+$	**c22-a4**	B05	170.1 $[M+H]^+$
c23-a2	A06	162.1 $[M+H]^+$	**c23-a4**	B06	186.1 $[M+H]^+$
c17-a2	A07	172.1 $[M+H]^+$	**c17-a4**	B07	196.1 $[M+H]^+$
c25-a2	A08	189.1 $[M+H]^+$	**c25-a4**	B08	213.1 $[M+H]^+$
c26-a2	A09	207.1 $[M+H]^+$	**c26-a4**	B09	231.1 $[M+H]^+$
c24-a2	A10	162.1 $[M+H]^+$	**c24-a4**	B10	186.1 $[M+H]^+$
c30-a2	A11	166.1 $[M+H]^+$	**c30-a4**	B11	190.1 $[M+H]^+$
c31-a2	A12	172.1 $[M+H]^+$	**c31-a4**	B12	196.1 $[M+H]^+$
c18-a22	C01	276.2 $[M+H]^+$	**c18-a24**	D01	312.2 $[M+H]^+$
c19-a22	C02	246.2 $[M+H]^+$	**c19-a24**	D02	282.2 $[M+H]^+$
c20-a22	C03	184.2 $[M+H]^+$	**c20-a24**	D03	220.2 $[M+H]^+$
c21-a22	C04	156.1 $[M]^+$	**c21-a24**	D04	192.1 $[M+H]^+$
c22-a22	C05	202.1 $[M+H]^+$	**c22-a24**	D05	238.1 $[M+H]^+$
c23-a22	C06	218.1 $[M+H]^+$	**c23-a24**	D06	254.1 $[M+H]^+$
c17-a22	C07	228.2 $[M+H]^+$	**c17-a24**	D07	264.2 $[M+H]^+$
c25-a22	C08	245.2 $[M+H]^+$	**c25-a24**	D08	281.2 $[M+H]^+$
c26-a22	C09	263.2 $[M+H]^+$	**c26-a24**	D09	299.2 $[M+H]^+$
c24-a22	C10	218.2 $[M+H]^+$	**c24-a24**	D10	254.2 $[M+H]^+$
c30-a22	C11	222.1 $[M+H]^+$	**c30-a24**	D11	258.1 $[M+H]^+$
c31-a22	C12	228.1 $[M+H]^+$	**c31-a24**	D12	264.1 $[M+H]^+$

Table S33. Target masses of amine products analysed by FIA–MS (*continued from previous page*).

Target	Well	Mass (*m/z*)	Target	Well	Mass (*m/z*)
c32-a2	E01	178.2 $[M+H]^+$	**c32-a4**	F01	202.2 $[M+H]^+$
c27-a2	E02	148.1 $[M+H]^+$	**c27-a4**	F02	172.1 $[M+H]^+$
c28-a2	E03	162.1 $[M+H]^+$	**c28-a4**	F03	186.1 $[M+H]^+$
c33-a2	E04	186.1 $[M+H]^+$	**c33-a4**	F04	210.1 $[M+H]^+$
c34-a2	E05	208.1 $[M+H]^+$	**c34-a4**	F05	232.1 $[M+H]^+$
c35-a2	E06	226.1 $[M+H]^+$	**c35-a4**	F06	250.1 $[M+H]^+$
c36-a2	E07	209.1 $[M+H]^+$	**c36-a4**	F07	233.1 $[M+H]^+$
c13-a2	E08	152.1 $[M+H]^+$	**c13-a4**	F08	176.1 $[M+H]^+$
c14-a2	E09	158.1 $[M+H]^+$	**c14-a4**	F09	182.1 $[M+H]^+$
c16-a2	E10	201.2 $[M+H]^+$	**c16-a4**	F10	225.2 $[M+H]^+$
c15-a2	E11	114.1 $[M+H]^+$	**c15-a4**	F11	138.1 $[M+H]^+$
c29-a2	E12	164.1 $[M+H]^+$ [a]	**c29-a4**	F12	188.1 $[M+H]^+$
c32-a22	G01	234.2 $[M+H]^+$	**c32-a24**	H01	270.2 $[M+H]^+$
c27-a22	G02	204.1 $[M+H]^+$	**c27-a24**	H02	240.1 $[M+H]^+$
c28-a22	G03	218.2 $[M+H]^+$	**c28-a24**	H03	254.2 $[M+H]^+$
c33-a22	G04	242.2 $[M+H]^+$	**c33-a24**	H04	278.2 $[M+H]^+$
c34-a22	G05	264.2 $[M+H]^+$	**c34-a24**	H05	300.2 $[M+H]^+$
c35-a22	G06	282.1 $[M+H]^+$	**c35-a24**	H06	318.1 $[M+H]^+$
c36-a22	G07	265.2 $[M+H]^+$	**c36-a24**	H07	301.2 $[M+H]^+$
c13-a22	G08	208.1 $[M+H]^+$	**c13-a24**	H08	244.1 $[M+H]^+$
c14-a22	G09	214.1 $[M+H]^+$	**c14-a24**	H09	250.1 $[M+H]^+$
c16-a22	G10	257.2 $[M+H]^+$	**c16-a24**	H10	293.2 $[M+H]^+$
c15-a22	G11	170.2 $[M+H]^+$	**c15-a24**	H11	206.2 $[M+H]^+$
c29-a22	G12	220.1 $[M+H]^+$	**c29-a24**	H12	256.1 $[M+H]^+$

[a] This analyte mass coincides with the mass of bicine (used as reaction buffer and internal standard), making quantification of this product by FIA–MS impossible.

Data analysis: The peak areas of the buffer and target SIM signals were determined by automated integration in the *Agilent* LC/MS ChemStation B.04.03 software and exported as a PDF report (one file per well). The buffer and target integrals were extracted from the individual PDF files using a Python script (available at: https://github.com/saberger/Screening_for_Generality/tree/main/Diversification_Screening/Carbonyl-Scope) and collated into a single comma-separated value (CSV) file per measurement series.

After importing the CSV file into *Microsoft* Excel, the integrals were converted into a target/buffer ratio (T/B) according to the following equation:

$$T/B = \frac{int_{\text{target}}}{int_{\text{buffer}}} \tag{6}$$

where T/B [dimensionless] … target/buffer ratio; int_{target} [counts·min] … integral area of target SIM signal; int_{buffer} [counts·min] … integral area of buffer SIM signal

Hit identification: To enable the identification of hits based on a statistical criterion without having to replicate every experimental condition, we performed the FIA–MS assay reactions of all substrate–enzyme combinations as single determinations but collected multiplicate negative control data. These were obtained as nine replicates spread out over the time span of the entire screening process (14 months) using the same plate layout and replacing the IRED preparation with cell-free extract of *E. coli* BL21 (DE3) transformed with an "empty" pET22b(+) plasmid (empty-vector controls, EVCs). Positives were identified by comparing the target/buffer ratio obtained for each substrate combination, corrected for background signal (mean of EVCs), to the standard deviation of the EVCs according to the following criterion:

$$[(T/B_{\text{reaction}} - mean_{\text{EVC}}) > 5 \cdot SD_{\text{EVC}}] \wedge [T/B_{\text{reaction}} > 0.02] \quad (7)$$

where T/B_{reaction} [dimensionless] … target/buffer ratio of the assay reaction; $mean_{\text{EVC}}$ [dimensionless] … mean target/buffer ratio of the corresponding empty-vector control reactions; SD_{EVC} [dimensionless] … standard deviation of the target/buffer ratios of the corresponding empty-vector control reactions

We refer to the quotient of background-corrected target/buffer ratio divided by the standard deviation of the empty-vector controls as the signal/noise ratio:

$$S/N = (T/B_{\text{reaction}} - mean_{\text{EVC}})/SD_{\text{EVC}} \quad (8)$$

where S/N [dimensionless] … signal/noise ratio of the assay reaction; T/B_{reaction} [dimensionless] … target/buffer ratio of the assay reaction; $mean_{\text{EVC}}$ [dimensionless] … mean target/buffer ratio of the corresponding empty-vector control reactions; SD_{EVC} [dimensionless] … standard deviation of the target/buffer ratios of the corresponding empty-vector control reactions

Hence, the hit criterion expressed in equation 7 is fulfilled if an assay reaction has a signal/noise ratio of greater than 5 and a target/buffer ratio of greater than 0.02. The identification of hits based on this criterion was implemented in *Microsoft* Excel using an if-condition. In cases where re-screening using GC–MS or HPLC–MS (see *Validation Experiments for the Diversification Screening*) failed to reproduce a hit, the threshold value for the target/buffer ratio (0.02 in equation 7) was raised until the lowest hit could be confirmed.

Collation of data into a single matrix: After FIA–MS data collection and analysis in *Microsoft* Excel had been completed for all investigated enzymes, a Python script (available at: https://github.com/saberger/Screening_for_Generality) was used to collate the activity data from the individual Excel files (one per enzyme) into a single matrix comprising the following columns: IRED identifier, amine identifier, carbonyl identifier, target/buffer ratio, hit. During this collation process, non-interpretable assay reactions (**c29-a2**, for which the target mass coincides with the buffer mass) were removed from the data set entirely.

Normalisation of data for IRED expression level: Although the collected target/buffer ratios, being derived from endpoint measurements, are not as directly influenced by IRED expression level as are the activity values collected in the Overview Screening and in the amine scope part of the Diversification Screening, we still decided to correct the values for expression level for better comparability. Therefore, as a final data processing step, the target/buffer ratios in the collated matrix were normalised using the expression data obtained as described above (see *Determination of Expression Level*) according to the following equation:

$$T/B_{\text{IRED}} = T/B_{\text{CFE}}/c_{\text{IRED}} \quad (9)$$

where T/B_{IRED} [dimensionless] … target/buffer ratio (based on IRED); T/B_{CFE} [dimensionless] … target/buffer ratio (based on cell-free extract); c_{IRED} [$mg_{\text{IRED}} \cdot mg_{\text{CFE}}^{-1}$] … relative IRED content of the lyophilised cell-free extract

This transformation was implemented in *Microsoft* Excel, and the final matrix containing the IRED-based target/buffer ratios is openly available in the Mendeley Data repository (https://data.mendeley.com/) at https://doi.org/10.17632/jn4sfsrz8x.2.

Data Transformation for Generating *z*-Score Heatmaps

The two-pronged approach used for the Diversification Screening resulted in two data sets based on different measures of enzyme performance: For the amine scope, initial enzyme activity is quantified in mU/mg_{IRED}, while for the carbonyl scope, product formation after 24 h of reaction is quantified through the target/buffer integral ratio (corrected for IRED expression level) as a dimensionless number. To make the two data sets more comparable and allow data visualisation on a common scale, we explored several mathematical transformation options using R and finally opted for a logarithmic transformation, followed by conversion into *z*-scores (distance from mean in units of standard deviation).

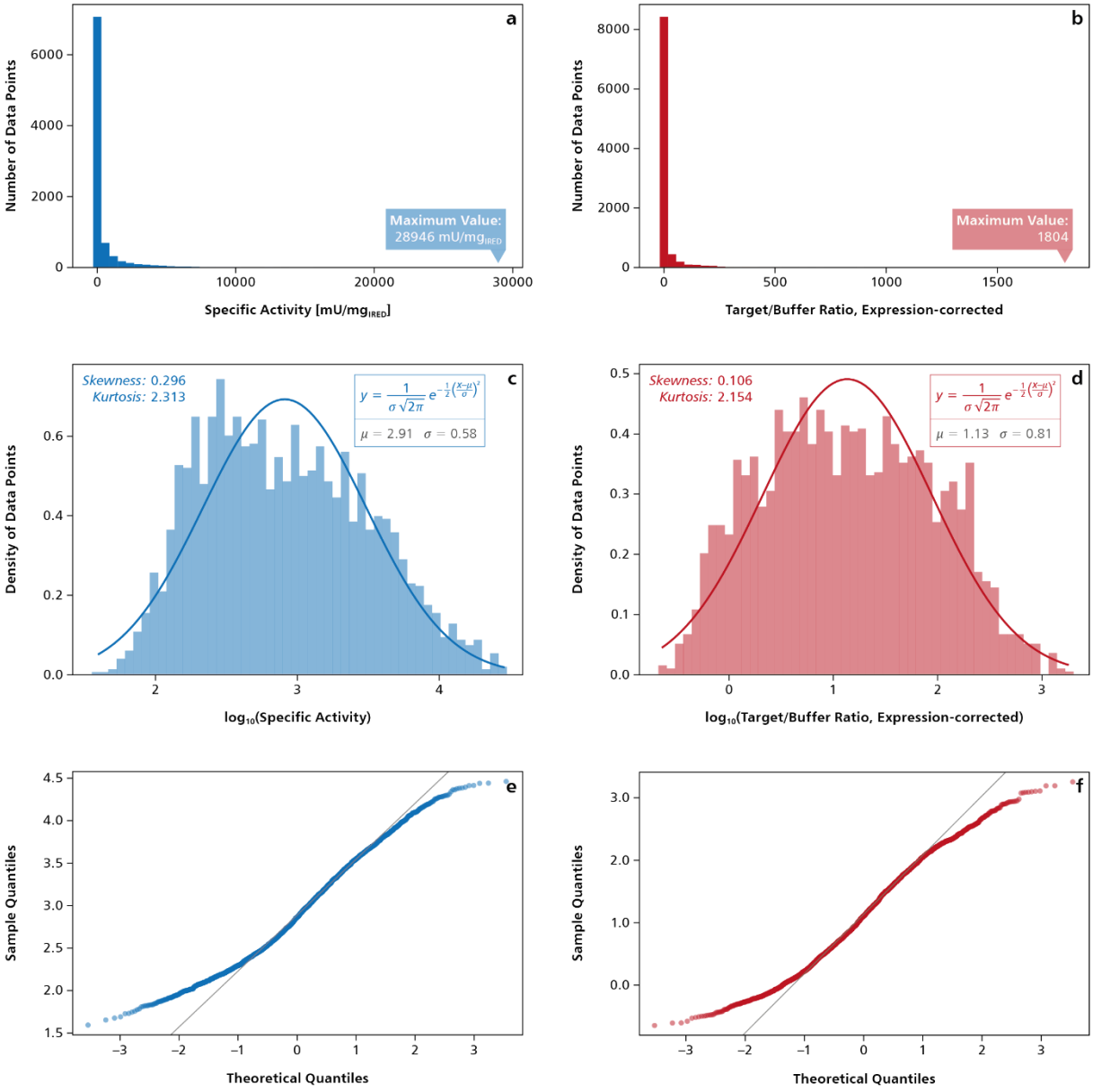


Figure S33. Visualisation of exploratory data analysis and *z*-score transformation of the data obtained in the Diversification Screening (amine scope: left column, blue; carbonyl scope: right column, red). **(a,b)** Histogram representations (50 bins) of all data points on a linear scale. The maximum values are indicated to illustrate the large span of both data sets. **(c,d)** Histogram representations (50 bins) of non-zero data points on a logarithmic scale. The skewness and kurtosis of the distributions are given in the upper-left corner, and the parameters of the Gaussian fits (μ, mean; σ, standard deviation) are reported in a box in the top-right corner. **(e,f)** Normal Q–Q plots visualising the deviation of the value distribution in each data set from a theoretical normal distribution.

Both data sets contain a large number of zero and near-zero data points (72% of the amine scope reactions and 75% of the carbonyl scope reactions are non-hits), while the non-zero values span three to four orders of magnitude (amine scope: A_{IRED} = 39–28946 mU/mg$_{\mathrm{IRED}}$, carbonyl scope: T/B_{IRED} = 0.23–1804). As a result, histograms plotted on a linear scale show heavy positive skew (Figure S33a,b). However, on a logarithmic scale, both data sets are essentially symmetric and reasonably well-described by a Gaussian distribution (Figure S33c,d). Statistical normality tests (Jarque–Bera, Shapiro–Wilk)[64,65] performed in R turned out negative (indicating statistically significant deviations from a normal distribution) as a result of the large sample size, but quantile–quantile (Q–Q) plots show a good agreement with a Gaussian distribution within at least –1 to +2 standard deviations from the mean for the amine scope data and ±1 standard deviation from the mean for the carbonyl scope data (Figure S33e,f). Therefore, we concluded that Gaussian distributions based on the mean (μ) and standard deviation (σ) values reported in Figure S33c,d are a suitable approximation of the two data sets, and we used these μ and σ values to convert the data points into z-scores according to the following equation:

$$z = (x - \mu)/\sigma \tag{10}$$

where z [dimensionless] … z-score (standard score); x [dimensionless] … raw score (logarithmised activity or target/buffer value); μ [dimensionless] … mean of raw scores (logarithmised activity or target/buffer values); σ … standard deviation of raw scores (logarithmised activity or target/buffer values)

Later, the data collected in the Overview Screening were subjected to z-score transformation in the same way to enable their inclusion in the training data set for the deep-learning model (see *Activity Prediction Using Machine-Learning Models*). As shown in Figure S34, the distribution of activity values is not as well described by a Gaussian function as it was in the case of the data from the Diversification Screening. Nevertheless, the fit is still reasonable within ±1 standard deviation from the mean, and we concluded that the benefit of adding these z-scores to the training data (thus increasing the size of the training set by 51% from 18416 to 27866 data points) would outweigh the error introduced by their deviation from a true Gaussian distribution.

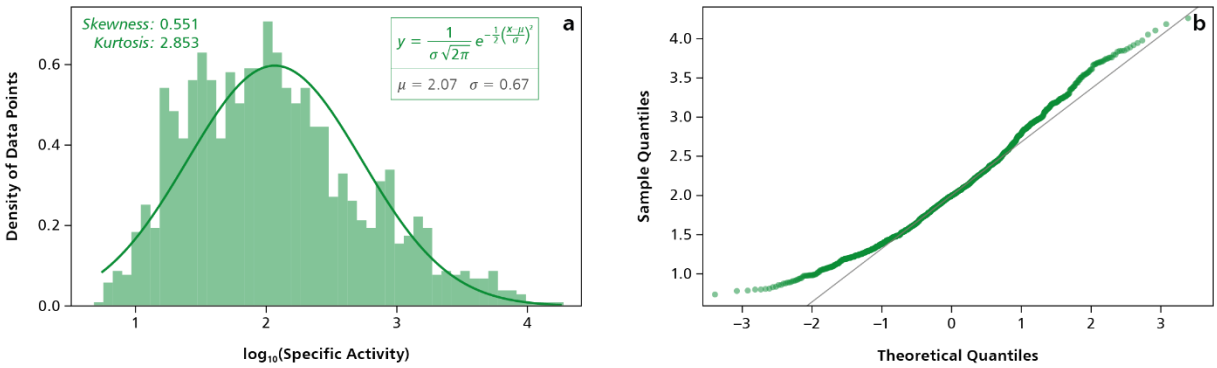


Figure S34. Visualisation of z-score transformation of the data obtained in the Overview Screening. **(a)** Histogram representation (50 bins) of non-zero data points on a logarithmic scale. The skewness and kurtosis of the distribution is given in the upper-left corner, and the parameters of the Gaussian fit (μ, mean; σ, standard deviation) are reported in a box in the top-right corner. **(b)** Normal Q–Q plot visualising the deviation of the value distribution from a theoretical normal distribution.

Synthesis of Reference Compounds

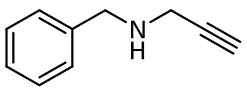
Achiral and racemic product reference compounds:

Most product reference compounds were synthesised from the corresponding amine and carbonyl substrates by reductive amination according to modified literature procedures.[66,67]

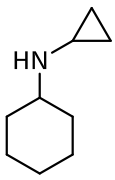
General procedure A:[66] In a round-bottom flask (50 mL) with magnetic stirring bar, the desired carbonyl compound (3 mmol, 1 eq.) and amine (30 mmol, 10 eq.) were dissolved in MeOH (15 mL), and acetic acid (1.72 mL, 1.80 g, 30 mmol, 10 eq.) was added. Sodium cyanoborohydride (566 mg, 9 mmol, 3 eq.) was added in portions to the stirred solution, the flask was closed with a bubbler, and the reaction mixture was stirred at room temperature for 24 h. After confirming completion of the reaction by TLC analysis, the reaction mixture was basified (pH ≥12) by addition of half-saturated aqueous Na_2CO_3 solution (50 mL) and extracted with EtOAc (3 × 45 mL). The combined organic phases were dried over Na_2SO_4, filtered, and the solvent was removed under reduced pressure to give the crude amine product. If necessary, the amine was purified by traditional column chromatography or automated flash chromatography (*Biotage* Selekt) on silica gel 60.

Variations of the general procedure: In several cases, the reaction was performed in a smaller batch size (1 mmol carbonyl compound, 10 mL MeOH), but with the same stoichiometric ratios of reagents. In other cases, the molar excess of amine substrate and acetic acid was lowered to 5 eq. or 3 eq. For the preparation of primary amines, ammonium acetate (10 eq.) was used as substrate and no acetic acid was added. With carbonyl substrates that contain ethyl ester groups (**c10**, **c14**, **c17**, **c34**, **c35**), transesterification was observed when the reaction was performed in methanol. Ethanol was used instead for these substrates. For reactions that afford volatile products (*e.g.*, **c4-a4**, **c6-a2**, **c21-a4**), Et_2O was used for extraction instead of EtOAc to minimize product loss during rotary evaporation. For the most volatile products (*e.g.*, **c7-a2**, **c7-a4**, **c15-a2**, **c15-a4**), we found it advantageous to acetylate the amine and isolate the acetamide. To this end, the combined organic phases obtained by the general work-up were treated with acetic anhydride (2.83 mL, 3.06 g, 30 mmol, 10 eq.) and saturated aqueous Na_2CO_3 solution (25 mL) for 2 h. Afterwards, the phases were separated, the organic phase was dried over a mixture of Na_2SO_4 and K_2CO_3, filtered, and the solvent was removed under reduced pressure to give the crude acetamide product.

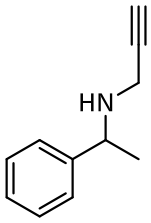
General procedure B:[67] A dry, two-necked round-bottom flask (50 mL) equipped with a magnetic stirring bar was flushed with argon and charged with anhydrous MeOH (8 mL), followed by the desired carbonyl compound (3 mmol, 1 eq.), amine (9 mmol, 3 eq.), and titanium(IV) isopropoxide (1.17 mL, 1.12 g, 4.0 mmol, 1.3 eq.). The reaction mixture was allowed to stir at room temperature overnight. Afterwards, the reaction mixture was cooled to 0 °C in an ice bath, and $NaBH_4$ (113 mg, 3 mmol, 1 eq.) was added in portions to the stirred solution. After another 2 h of stirring at room temperature, the reaction was quenched by addition of water (1.5 mL) and was allowed to stir for further 10 min. For reactions using ethanolamine as amine substrate, the reaction mixture was then acidified with hydrochloric acid (1 M, 6 mL) and filtered through Celite, followed by washing the Celite layer with EtOAc (20 mL) and water (20 mL). The organic phase was separated, dried over Na_2SO_4, and evaporated under reduced pressure to give the crude amino alcohol product. For reactions with other amines, the reaction mixture was basified with saturated aqueous Na_2CO_3 solution (5 mL) and filtered through Celite, followed by washing the Celite layer with EtOAc (20 mL) and water (20 mL). The organic phase was separated, dried over Na_2SO_4, and evaporated under reduced pressure to give the crude amine product. If necessary, the product was purified by traditional column chromatography or automated flash chromatography (*Biotage* Selekt) on silica gel 60.



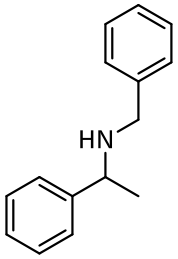
***N*-Benzylprop-2-yn-1-amine (c1-a4) [CAS 1197-51-9].** Prepared from benzaldehyde (**c1**, 306 μL, 319 mg, 3.0 mmol) and propargylamine (**a4**, 1.92 mL, 1.65 g, 30.0 mmol) in MeOH according to *General procedure A*. Purification by column chromatography (silica gel 60, cyclohexane/EtOAc = 3:1) gave 189 mg (0.77 mmol, 26%) of a colourless liquid. TLC (silica gel 60, cyclohexane/EtOAc = 3:1, UV visualisation): R_f = 0.20. ^{1}H NMR (300 MHz, $CDCl_3$): δ [ppm] = 7.40–7.26 (5H, m), 3.88 (2H, s), 3.42 (2H, d, J = 2.4 Hz), 2.26 (1H, t, J = 2.4 Hz), 1.54 (1H, s). ^{13}C NMR (75 MHz, $CDCl_3$): δ [ppm] = 139.4, 128.5, 128.5, 127.2, 82.1, 71.7, 52.3, 37.4. GC–MS (EI, 70 eV): *m/z* = 145 (M^+, 22), 144 (100), 130 (6), 115 (17), 104 (23), 91 (75), 77 (15), 68 (32), 54 (32), 39 (18). The characterisation data are in agreement with literature values.[68]



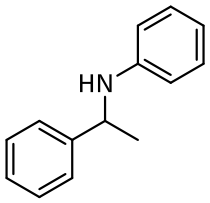
***N*-Cyclopropylcyclohexanamine (c2-a10) [CAS 824-82-8].** Prepared from cyclohexanone (**c2**, 311 μL, 292 mg, 3.0 mmol) and cyclopropylamine (**a10**, 2.10 mL, 1.72 g, 30.2 mmol) in MeOH according to *General procedure A*. Purification by column chromatography (silica gel 60, MTBE/MeOH/NH_4OH = 96:3:1) gave 124 mg (0.91 mmol, 30%) of an orange liquid. TLC (silica gel 60, cyclohexane/EtOAc = 1:1, $KMnO_4$ staining): R_f = 0.62. ^{1}H NMR (300 MHz, $CDCl_3$): δ [ppm] = 2.56 (1H, tt, J = 10.5, 3.8 Hz), 2.13 (1H, tt, J = 6.6, 3.7 Hz), 2.00–1.89 (3H, m), 1.71 (1H, dt, J = 12.9, 3.7 Hz), 1.65–1.56 (1H, m), 1.36–0.99 (5H, m), 0.47–0.30 (4H, m). ^{13}C NMR (75 MHz, $CDCl_3$): δ [ppm] = 57.5, 33.9, 28.3, 26.3, 25.2, 6.5. GC–MS (EI, 70 eV): *m/z* = 139 (M^+, 45), 138 (14), 124 (78), 110 (62), 96 (100), 82 (27), 68 (32), 58 (37), 56 (48), 41 (43), 39 (22). The characterisation data are in agreement with literature values.[68]



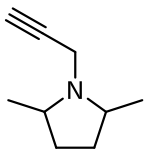
***rac*-*N*-(1-Phenylethyl)prop-2-yn-1-amine (c3-a4) [CAS 56862-34-1].** Prepared from acetophenone (**c3**, 354 μL, 361 mg, 3.0 mmol) and propargylamine (**a4**, 1.92 mL, 1.65 g, 30.0 mmol) in MeOH according to *General procedure A*. The crude product was used without purification. 356 mg (2.24 mmol, 74%) of a pale-yellow liquid. TLC (silica gel 60, cyclohexane/EtOAc = 2:1, $KMnO_4$ staining): R_f = 0.46. ^{1}H NMR (300 MHz, $CDCl_3$): δ [ppm] = 7.43–7.27 (5H, m), 4.03 (1H, q, J = 6.6 Hz), 3.36 (1H, dd, J = 17.1, 2.4 Hz), 3.16 (1H, dd, J = 17.1, 2.3 Hz), 2.24 (1H, t, J = 2.4 Hz), 2.06 (1H, br s), 1.37 (3H, d, J = 6.6 Hz). ^{13}C NMR (75 MHz, $CDCl_3$): δ [ppm] = 144.2, 128.3, 127.0, 126.7, 82.1, 71.3, 56.1, 35.7, 23.8. GC–MS (EI, 70 eV): *m/z* = 159 (M^+, <1), 144 (100) 143 (8), 115 (11), 105 (11), 91 (6), 77 (11). The characterisation data are in agreement with literature values.[69]



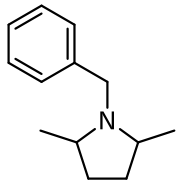
***rac*-*N*-Benzyl-1-phenylethan-1-amine (c3-a6) [CAS 3193-62-2].** Prepared from acetophenone (**c3**, 354 μL, 361 mg, 3.0 mmol) and benzylamine (**a6**, 3.28 mL, 3.21 g, 30.0 mmol) in MeOH according to *General procedure A*. Purification by automated flash chromatography (silica gel 60, *Biotage* SFär Duo 25 g cartridge; cyclohexane/EtOAc = 85:15) gave 460 mg (2.17 mmol, 72%) of a colourless liquid. TLC (silica gel 60, cyclohexane/EtOAc = 5:1, ninhydrin staining): R_f = 0.59. ^{1}H NMR (300 MHz, $CDCl_3$): δ [ppm] = 7.46–7.25 (10H, m), 3.87 (1H, q, J = 6.6 Hz), 3.72 (1H, d, J = 13.1 Hz), 3.64 (1H, d, J = 13.1 Hz), 1.72 (1H, br s), 1.42 (1H, d, J = 6.6 Hz, 1H). ^{13}C NMR (75 MHz, $CDCl_3$): δ [ppm] = 145.7, 140.7, 128.6, 128.5, 128.3, 127.1, 127.0, 126.8, 57.6, 51.8, 24.6. GC–MS (EI, 70 eV): *m/z* = 211 (M^+, 1), 196 (100), 134 (6), 105 (14), 91 (91), 79 (6), 77 (10), 65 (8). The characterisation data are in agreement with literature values.[70]



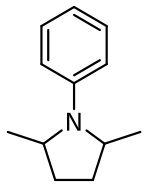
***rac-N*-(1-Phenylethyl)aniline (c3-a7) [CAS 779-54-4].** Prepared from acetophenone (**c3**, 354 μL, 361 mg, 3.0 mmol) and aniline (**a7**, 2.74 mL, 2.79 g, 30.0 mmol) in MeOH according to *General procedure A*. Purification by automated flash chromatography (silica gel 60, *Biotage* SFär Duo 25 g cartridge; gradient of cyclohexane/EtOAc = 95:5 to cyclohexane/EtOAc = 70:30) gave 512 mg (2.59 mmol, 86%) of a pale-yellowish liquid. TLC (silica gel 60, cyclohexane/EtOAc = 8:1, CAM staining): R_f = 0.56. ^{1}H NMR (300 MHz, $CDCl_3$): δ [ppm] = 7.42–7.17 (7H, m), 7.08 (2H, t, J = 7.9 Hz), 6.63 (1H, t, J = 7.3 Hz), 6.50 (2H, d, J = 7.7 Hz), 4.47 (1H, q, J = 6.7 Hz), 4.00 (1H, br s), 1.50 (3H, d, J = 6.7 Hz). ^{13}C NMR (75 MHz, $CDCl_3$): δ [ppm] = 147.4, 145.3, 129.2, 128.8, 127.0, 126.0, 117.3, 113.4, 53.6, 25.2. GC–MS (EI, 70 eV): m/z = 197 (M^+, 43), 182 (100), 120 (8), 105 (63), 93 (39), 79 (12), 77 (36), 65 (6), 51 (10). The characterisation data are in agreement with literature values.[71]



***all-rac*-2,5-Dimethyl-1-(prop-2-yn-1-yl)pyrrolidine (c4-a4).** Prepared from hexane-2,5-dione (**c4**, 706 μL, 685 mg, 6.0 mmol) and propargylamine (**a4**, 3.84 mL, 3.30 g, 60.0 mmol) in MeOH according to *General procedure A* (double batch size). Diethyl ether was used for extraction, and evaporation of the solvent was performed very carefully (40 °C, 180 mbar). Purification by automated flash chromatography (silica gel 60, *Biotage* SFär Duo 25 g cartridge; gradient of cyclohexane/EtOAc = 95:5 to cyclohexane/EtOAc = 50:50) gave 279 mg (2.04 mmol, 34%) of a pale-yellowish liquid. The product is a mixture of diastereomers in a ratio of approx. 96:4. TLC (silica gel 60, cyclohexane/EtOAc = 2:1, $KMnO_4$ staining): R_f = 0.50, 0.32. ^{1}H NMR (300 MHz, $CDCl_3$): δ [ppm] = 3.55 (2H, d, J = 2.4 Hz), 2.85–2.69 (2H, m), 2.11 (1H, t, J = 2.4 Hz), 1.91–1.77 (2H, m), 1.44–1.28 (2H, m), 1.08 (6H, d, J = 6.1 Hz). ^{13}C NMR (75 MHz, $CDCl_3$): δ [ppm] = 77.9, 72.7, 56.8, 36.9, 30.8, 19.1. GC–MS (EI, 70 eV): m/z = 137 (M^+, 6), 136 (6), 122 (100), 80 (7), 39 (12). No NMR and MS reference data were available for this compound.

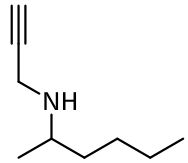


***all-rac*-1-Benzyl-2,5-dimethylpyrrolidine (c4-a6) [CAS 72753-12-9].** Prepared from hexane-2,5-dione (**c4**, 353 μL, 342 mg, 3.0 mmol) and benzylamine (**a6**, 3.28 mL, 3.21 g, 30.0 mmol) in MeOH according to *General procedure A*. Purification by automated flash chromatography (silica gel 60, *Biotage* SFär Duo 25 g cartridge; gradient of cyclohexane/EtOAc = 95:5 to cyclohexane/EtOAc = 50:50) gave 334 mg (1.77 mmol, 59%) of a colourless liquid. The product is a mixture of diastereomers in a ratio of approx. 55:45. TLC (silica gel 60, EtOAc, $KMnO_4$ staining): R_f = 0.56. ^{1}H NMR (300 MHz, $CDCl_3$): δ [ppm] = 7.52–6.88 (10H, m), 3.83 (1H, d, J = 13.8 Hz), 3.74 (2H, s), 3.51 (1H, d, J = 13.8 Hz), 3.02 (2H, sext, J = 6.6 Hz), 2.57 (2H, q, J = 5.6 Hz), 2.07–1.92 (2H, m), 1.85–1.69 (2H, m), 1.44–1.30 (4H, m), 1.05 (6H, d, J = 6.1 Hz), 0.97 (6H, d, J = 6.3 Hz). ^{13}C NMR (75 MHz, $CDCl_3$): δ [ppm] = 140.9, 139.4, 129.4, 128.6, 128.2, 128.0, 126.7, 126.5, 59.7, 55.2, 55.0, 51.8, 31.4, 31.1, 20.7, 17.2. GC–MS (EI, 70 eV): m/z = 189 (M^+, 7), 174 (100), 91 (89), 65 (7). The characterisation data are in agreement with literature values.[72]

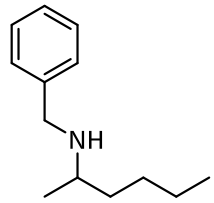


***all-rac*-2,5-Dimethyl-1-phenylpyrrolidine (c4-a7) [CAS 37035-03-3].** Prepared from hexane-2,5-dione (**c4**, 353 μL, 342 mg, 3.0 mmol) and aniline (**a7**, 2.74 mL, 2.79 g, 30.0 mmol) in MeOH according to *General procedure A*. Purification by automated flash chromatography (silica gel 60, *Biotage* SFär Duo 25 g cartridge; gradient of cyclohexane/EtOAc = 95:5 to cyclohexane/EtOAc = 65:35) gave 177 mg (1.01 mmol, 33%) of an orange liquid. The product is a mixture of diastereomers in a ratio of approx. 58:42. TLC (silica gel 60, cyclohexane/EtOAc = 8:1, UV visualisation): R_f = 0.80. ^{1}H NMR (300 MHz, $CDCl_3$): δ [ppm] = 7.25–7.11 (4H, m), 6.68–6.50

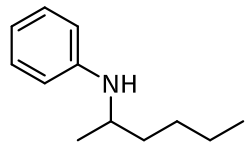
(6H, m), 3.98 (2H, pent, J = 6.1 Hz), 3.76 (2H, sext, J = 6.6 Hz), 2.30–2.13 (2H, m), 2.09–1.96 (2H, m), 1.77–1.63 (2H, m), 1.64–1.53 (2H, m), 1.26 (6H, d, J = 6.1 Hz), 1.08 (6H, d, J = 6.1 Hz). ^{13}C NMR (75 MHz, $CDCl_3$): δ [ppm] = 147.4, 145.3, 129.2, 115.4, 114.6, 113.4, 112.0, 56.0, 52.8, 32.4, 30.4, 21.9, 18.2. GC–MS (EI, 70 eV): m/z = 175 (M^+, 19), 160 (100), 118 (9), 104 (10), 77 (16). The characterisation data are in agreement with literature values.[73]



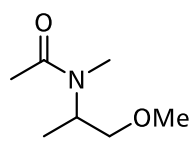
***rac-N*-(Prop-2-yn-1-yl)hexan-2-amine (c6-a4) [CAS 1158062-10-2].** Prepared from hexan-2-one (**c6**, 369 μL, 299 mg, 3.0 mmol) and propargylamine (**a4**, 1.92 mL, 1.65 g, 30.0 mmol) in MeOH according to *General procedure A*. Purification by column chromatography (silica gel 60, cyclohexane/EtOAc = 2:1) gave 333 mg (2.39 mmol, 80%) of a yellowish liquid. TLC (silica gel 60, cyclohexane/EtOAc = 3:1, $KMnO_4$ staining): R_f = 0.27. ^{1}H NMR (300 MHz, $CDCl_3$): δ [ppm] = 3.46 (1H, dd, J = 17.1, 2.4 Hz), 3.38 (1H, dd, J = 17.1, 2.4 Hz), 2.83 (1H, sext, J = 6.0 Hz), 2.18 (1H, t, J = 2.4 Hz), 1.50–1.16 (7H, m), 1.01 (3H, d, J = 6.2 Hz), 0.89 (3H, t, J = 6.8 Hz). ^{13}C NMR (75 MHz, $CDCl_3$): δ [ppm] = 74.6, 52.5, 34.8, 34.4, 27.7, 22.6, 17.8, 13.9. GC–MS (EI, 70 eV): m/z = 139 (M^+, <1), 124 (8), 82 (100), 42 (7), 39 (8). No NMR and MS reference data were available for this compound.



***rac-N*-Benzylhexan-2-amine (c6-a6) [CAS 61806-77-7].** Prepared from hexan-2-one (**c6**, 369 μL, 299 mg, 3.0 mmol) and benzylamine (**a6**, 3.28 mL, 3.21 g, 30.0 mmol) in MeOH according to *General procedure A*. Purification by automated flash chromatography (silica gel 60, *Biotage* SFär Duo 25 g cartridge; gradient of cyclohexane/EtOAc = 95:5 to cyclohexane/EtOAc = 50:50) gave 160 mg (0.84 mmol, 28%) of a yellow liquid. TLC (silica gel 60, cyclohexane/EtOAc = 4:1, UV visualisation): R_f = 0.31. ^{1}H NMR (300 MHz, $CDCl_3$): δ [ppm] = 7.39–7.16 (5H, m), 3.84 (1H, d, J = 13.1 Hz), 3.75 (1H, d, J = 13.0 Hz), 2.68 (1H, sext, J = 6.2 Hz), 1.84 (1H, br s), 1.56–1.44 (1H, m), 1.39–1.22 (5H, m), 1.10 (3H, d, J = 6.3 Hz), 0.90 (3H, t, J = 6.7 Hz). ^{13}C NMR (75 MHz, $CDCl_3$): δ [ppm] = 140.6, 128.5, 128.3, 127.0, 52.6, 51.4, 36.8, 28.3, 23.0, 20.3, 14.2. GC–MS (EI, 70 eV): m/z = 191 (M^+, <1), 176 (5), 134 (76), 91 (100), 65 (7). The characterisation data are in agreement with literature values.[74]

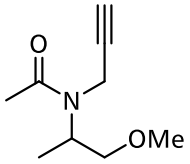


***rac-N*-(Hexan-2-yl)aniline (c6-a7) [CAS 80865-89-0].** Prepared from hexan-2-one (**c6**, 369 μL, 299 mg, 3.0 mmol) and aniline (**a7**, 2.74 mL, 2.79 g, 30.0 mmol) in MeOH according to *General procedure A*. Purification by column chromatography (silica gel 60, cyclohexane/EtOAc = 20:1) gave 116 mg (0.65 mmol, 22%) of an orange liquid. TLC (silica gel 60, cyclohexane/EtOAc = 20:1, UV visualisation): R_f = 0.50. ^{1}H NMR (300 MHz, $CDCl_3$): δ [ppm] = 7.21–7.07 (2H, m), 6.65 (1H, t, J = 7.3 Hz), 6.56 (2H, d, J = 7.6 Hz), 3.51–3.33 (2H, m), 1.65–1.51 (1H, m), 1.48–1.24 (5H, m), 1.16 (3H, *d*, J = 6.1 Hz), 0.90 (3H, t, J = 6.8 Hz). ^{13}C NMR (75 MHz, $CDCl_3$): δ [ppm] = 147.9, 129.4, 116.8, 113.2, 77.2, 48.5, 37.1, 28.5, 22.9, 20.9, 14.2. GC–MS (EI, 70 eV): m/z = 177 (M^+, 13), 162 (7), 120 (100), 77 (7). The characterisation data are in agreement with literature values.[75]

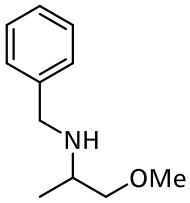


***rac-N*-(1-Methoxypropan-2-yl)-*N*-methylacetamide (c7-a2-Ac).** Prepared from methoxyacetone (**c7**, 278 μL, 264 mg, 3.0 mmol) and methylamine (**a2**, 3.07 mL of a 40% w/w solution in MeOH; 0.93 g $MeNH_2$, 30.0 mmol) in MeOH according to *General procedure A*, followed by derivatisation with acetic anhydride. The crude product was used without purification. 226 mg (1.74 mmol, 58%) of a yellowish liquid. The product is a mixture of amide rotamers in a ratio of approx. 54:46. TLC (silica gel 60, EtOAc, $KMnO_4$ staining): R_f = 0.12. ^{1}H NMR (300 MHz,

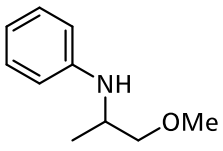
$CDCl_3$): δ [ppm] = 4.93–4.74 (1H, m), 4.00 (1H, dqd, J = 8.4, 6.8, 5.0 Hz), 3.40–3.20 (4H, m), 3.27 (3H, s), 3.27 (3H, s), 2.81 (3H, s), 2.72 (3H, s), 2.07 (3H, s), 2.04 (3H, s), 1.10 (3H, d, J = 6.8 Hz), 1.03 (3H, d, J = 7.0 Hz). ^{13}C NMR (75 MHz, $CDCl_3$): δ [ppm] = 171.1, 171.0, 73.8, 73.8, 59.0, 58.8, 52.8, 47.1, 30.2, 26.1, 22.5, 21.8, 15.2, 14.1. GC–MS (EI, 70 eV): *m/z* = 130 (M^+–CH_3, <1), 113 (13), 100 (43), 72 (6), 58 (100), 43 (13). HRMS calcd for $C_7H_{16}NO_2^+$ [M+H^+]: 146.1176, found: 146.1182. No NMR and MS reference data were available for this compound.



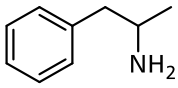
***rac*-*N*-(1-Methoxypropan-2-yl)-*N*-(prop-2-yn-1-yl)acetamide (c7-a4-Ac).** Prepared from methoxyacetone (**c7**, 278 μL, 264 mg, 3.0 mmol) and propargylamine (**a4**, 960 μL, 826 mg, 15.0 mmol) in MeOH according to *General procedure A* (5 eq. amine and AcOH), followed by derivatisation with acetic anhydride. The excess of propargylamine was also acetylated and the resulting *N*-propargylacetamide could not be removed by column chromatography. Therefore, the product was taken up in CH_2Cl_2, washed with aqueous NaOH solution (10 M, 20 mL), the organic phase was dried over Na_2SO_4, filtered, and the solvent was removed under reduced pressure. Purification by column chromatography (silica gel 60, cyclohexane/EtOAc = 1:4) gave 273 mg (1.61 mmol, 54%) of a pale-yellow liquid. The product is a mixture of amide rotamers in a ratio of approx. 55:45. TLC (silica gel 60, cyclohexane/EtOAc = 1:4, $KMnO_4$ staining): R_f = 0.30. ^{1}H NMR (300 MHz, $CDCl_3$): δ [ppm] = 4.90–4.72 (1H, m), 4.19–3.92 (5H, m), 3.56–3.36 (4H, m), 3.34 (3H, s), 3.32 (3H, s), 2.27 (1H, t, J = 2.5 Hz), 2.22 (3H, s), 2.17 (3H, s), 2.14 (1H, t, J = 2.5 Hz), 1.29 (3H, d, J = 6.9 Hz), 1.23 (3H, d, J = 7.0 Hz). ^{13}C NMR (75 MHz, $CDCl_3$): δ [ppm] = 171.1, 170.8, 81.2, 80.4, 74.6, 74.3, 71.7, 69.9, 59.0, 58.9, 53.5, 48.6, 34.2, 29.6, 22.4, 22.0, 16.0, 14.9. GC–MS (EI, 70 eV): *m/z* = 169 (M^+, <1%), 124 (42), 82 (100), 72 (6), 56 (6), 43 (18). HRMS calcd for $C_9H_{16}NO_2^+$ [M+H^+]: 170.1176, found: 170.1173. No NMR and MS reference data were available for this compound.



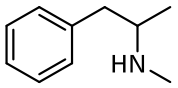
***rac*-*N*-Benzyl-1-methoxypropan-2-amine (c7-a6) [CAS 256473-98-0].** Prepared from methoxyacetone (**c7**, 278 μL, 264 mg, 3.0 mmol) and benzylamine (**a6**, 987 μL, 967 mg, 9.0 mmol) in MeOH according to *General procedure A* (3 eq. amine and AcOH). Purification by column chromatography (silica gel 60, cyclohexane/EtOAc = 1:2) gave 246 mg (1.37 mmol, 46%) of a pae-yellowish liquid. TLC (silica gel 60, EtOAc, UV visualisation): R_f = 0.15. ^{1}H NMR (300 MHz, $CDCl_3$): δ [ppm] = 7.42–7.17 (5H, m), 3.89 (1H, d, J = 13.0 Hz), 3.73 (1H, d, J = 13.0 Hz), 3.32 (3H, s), 3.45–3.19 (2H, m), 3.07–2.85 (1H, m), 1.07 (3H, d, J = 6.4 Hz). ^{13}C NMR (75 MHz, $CDCl_3$): δ [ppm] = 140.0, 128.6, 128.3, 127.1, 77.0, 58.9, 52.0, 51.3, 16.9. GC–MS (EI, 70 eV): *m/z* = 179 (M^+, <1%), 134 (56), 91 (100), 65 (8), 56 (11). No NMR and MS reference data were available for this compound.



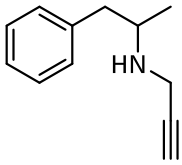
***rac*-*N*-(1-Methoxypropan-2-yl)aniline (c7-a7) [CAS 78923-90-7].** Prepared from methoxyacetone (**c7**, 278 μL, 264 mg, 3.0 mmol) and aniline (**a7**, 2.74 mL, 2.79 g, 30.0 mmol) in MeOH according to *General procedure A*. Purification by automated flash chromatography (silica gel 60, *Biotage* SFär Duo 25 g cartridge; gradient of cyclohexane/EtOAc = 95:5 to cyclohexane/EtOAc = 50:50) gave 185 mg (1.12 mmol, 37%) of an orange liquid. TLC (silica gel 60, cyclohexane/EtOAc = 1:2, UV visualisation): R_f = 0.82. ^{1}H NMR (300 MHz, $CDCl_3$): δ [ppm] = 7.19 (2H, dd, J = 8.5, 7.3 Hz), 6.71 (1H, tt, J = 7.4, 1.1 Hz), 6.64 (2H, dd, J = 8.5, 1.1 Hz), 3.76 (1H, br s), 3.75–3.58 (1H, m), 3.53–3.29 (2H, m), 3.39 (3H, s), 1.25 (3H, d, J = 6.4 Hz). ^{13}C NMR (75 MHz, $CDCl_3$): δ [ppm] = 147.5, 129.4, 117.4, 113.5, 76.2, 59.2, 48.3, 18.0. GC–MS (EI, 70 eV): *m/z* = 165 (M^+, 11), 120 (100), 91 (9), 77 (19). The characterisation data are in agreement with literature values.[76]



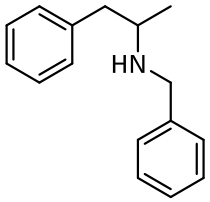
***rac*-1-Phenylpropan-2-amine (c8-a1) [CAS 300-62-9].** Prepared from phenylacetone (**c8**, 399 μL, 403 mg, 3.0 mmol) and ammonium acetate (**a1**·HOAc, 2.33 g, 30.0 mmol) in MeOH according to *General procedure A*. Purification by automated flash chromatography (silica gel 60, *Biotage* SFär Duo 25 g cartridge; gradient of cyclohexane/EtOAc = 50:50 to EtOAc) gave 47 mg (0.35 mmol, 12%) of a colourless liquid. TLC (silica gel 60, cyclohexane/EtOAc = 4:1, UV visualisation): R_f = 0.29. ^{1}H NMR (300 MHz, $CDCl_3$): δ [ppm] = 7.36–6.95 (5H, m), 3.99 (sext, J = 6.1 Hz), 2.76 (1H, dd, J = 13.4, 5.0 Hz), 2.68 (1H, dd, J = 13.4, 7.8 Hz), 1.76 (1H, br s), 1.22 (3H, d, J = 6.2 Hz). ^{13}C NMR (75 MHz, $CDCl_3$): δ [ppm] = 138.6, 129.5, 128.6, 126.5, 68.9, 45.9, 22.9. GC–MS (EI, 70 eV): m/z = 135 (M^+, <1), 92 (100), 91 (74), 65 (12), 45 (15). The characterisation data are in agreement with literature values.[77]



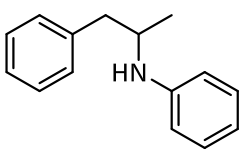
***rac*-*N*-Methyl-1-phenylpropan-2-amine (c8-a2) [CAS 7632-10-2].** Prepared from phenylacetone (**c8**, 399 μL, 403 mg, 3.0 mmol) and methylamine (**a2**, 3.07 mL of a 40% w/w solution in MeOH; 0.93 g $MeNH_2$, 30.0 mmol) in MeOH according to *General procedure A*. The crude product was used without purification. 705 mg (quant.) of an orange liquid. TLC (silica gel 60, MTBE/MeOH/NH_4OH = 90:9:1, $KMnO_4$ staining): R_f = 0.22. ^{1}H NMR (300 MHz, $CDCl_3$): δ [ppm] = 7.32–7.12 (5H, m), 3.08–2.94 (1H, m), 2.91 (1H, dd, J = 13.2, 5.8 Hz), 2.63 (1H, dd, J = 13.1, 7.8 Hz), 2.46 (3H, s), 1.11 (3H, d, J = 6.3 Hz). ^{13}C NMR (75 MHz, $CDCl_3$): δ [ppm] = 137.4, 129.2, 128.5, 126.6, 56.5, 41.2, 32.1, 17.6. GC–MS (EI, 70 eV): m/z = 149 (M^+, <1), 134 (M^+–CH_3, 2), 91 (10), 65 (5), 58 (100), 42 (5). The characterisation data are in agreement with literature values.[78]



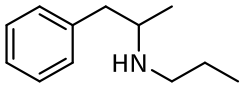
***rac*-*N*-(1-Phenylpropan-2-yl)prop-2-yn-1-amine (c8-a4) [CAS 18913-84-3].** Prepared from phenylacetone (**c8**, 134 μL, 135 mg, 1.0 mmol) and propargylamine (**a4**, 640 μL, 550 mg, 10.0 mmol) in MeOH according to *General procedure A* (one-third of the usual batch size). The crude product was used without purification. 126 mg (0.73 mmol, 73%) of a yellow liquid. TLC (silica gel 60, cyclohexane/EtOAc = 2:1, $KMnO_4$ staining): R_f = 0.22. ^{1}H NMR (300 MHz, $CDCl_3$): δ [ppm] = 7.34–7.13 (5H, m), 3.48 (1H, dd, J = 17.2, 2.4 Hz), 3.40 (1H, dd, J = 17.2, 2.4 Hz), 3.17 (1H, sext, J = 6.4 Hz), 2.72 (1H, dd, J = 13.4, 7.1 Hz), 2.64 (1H, dd, J = 13.4, 6.6 Hz), 2.18 (1H, t, J = 2.4 Hz), 1.07 (3H, d, J = 6.2 Hz). ^{13}C NMR (75 MHz, $CDCl_3$): δ [ppm] = 139.1, 129.4, 128.6, 126.4, 81.9, 71.5, 52.7, 43.5, 35.6, 19.6. GC–MS (EI, 70 eV): m/z = 173 (M^+, <1), 91 (17), 82 (100), 65 (7), 56 (5), 39 (11). The characterisation data are in agreement with literature values.[79]



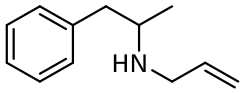
***rac*-*N*-Benzyl-1-phenylpropan-2-amine (c8-a6) [CAS 1085-42-3].** Prepared from phenylacetone (**c8**, 399 μL, 403 mg, 3.0 mmol) and benzylamine (**a6**, 3.28 mL, 3.21 g, 30.0 mmol) in MeOH according to *General procedure A*. Purification by automated flash chromatography (silica gel 60, *Biotage* SFär Duo 25 g cartridge; gradient of cyclohexane/EtOAc = 95:5 to cyclohexane/EtOAc = 50:50) gave 232 mg (1.03 mmol, 34%) of an orange liquid. TLC (silica gel 60, cyclohexane/EtOAc = 1:2, UV visualisation): R_f = 0.40. ^{1}H NMR (300 MHz, $CDCl_3$): δ [ppm] = 8.20–6.29 (5H, m), 3.94 (1H, d, J = 13.3 Hz), 3.82 (1H, d, J = 13.3 Hz), 3.03 (1H, sext, J = 6.4 Hz), 2.87 (1H, dd, J = 13.3, 7.0 Hz), 2.73 (1H, dd, J = 13.3, 6.5 Hz), 1.71 (1H, br s), 1.19 (3H, d, J = 6.2 Hz). ^{13}C NMR (75 MHz, $CDCl_3$): δ [ppm] = 140.5, 139.4, 129.3, 128.4, 128.0, 126.8, 126.2, 53.7, 51.3, 43.6, 20.2. GC–MS (EI, 70 eV): m/z = 225 (M^+, <1), 134 (58), 132 (15), 91 (100), 65 (12). The characterisation data are in agreement with literature values.[77]



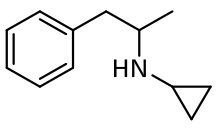
***rac-N*-(1-Phenylpropan-2-yl)aniline (c8-a7) [CAS 75859-35-7].** Prepared from phenylacetone (**c8**, 399 μL, 403 mg, 3.0 mmol) and aniline (**a7**, 2.74 mL, 2.79 g, 30.0 mmol) in MeOH according to *General procedure A*. Purification by automated flash chromatography (silica gel 60, *Biotage* SFär Duo 25 g cartridge; gradient of cyclohexane/EtOAc = 95:5 to cyclohexane/EtOAc = 50:50) gave 524 mg (2.48 mmol, 83%) of an orange liquid. TLC (silica gel 60, cyclohexane/EtOAc = 1:2, UV visualisation): R_f = 0.91. ^{1}H NMR (300 MHz, $CDCl_3$): δ [ppm] = 7.41–7.16 (7H, m), 6.77 (1H, t, J = 7.3 Hz), 6.70 (2H, d, J = 7.8 Hz), 3.83 (1H, sext, J = 6.4 Hz), 3.61 (1H, br s), 3.01 (1H, dd, J = 13.4, 4.6 Hz), 2.76 (1H, dd, J = 13.4, 7.3 Hz), 1.21 (3H, d, J = 6.4 Hz). ^{13}C NMR (75 MHz, $CDCl_3$): δ [ppm] = 147.3, 138.6, 129.6, 129.5, 128.4, 126.4, 117.3, 113.5, 49.4, 42.4, 20.3. GC–MS (EI, 70 eV): m/z = 211 (M^+, 4), 120 (100), 91 (12), 77 (11), 65 (5). The characterisation data are in agreement with literature values.[80]



***rac-N*-(1-Phenylpropan-2-yl)propan-1-amine (c8-a8) [CAS 51799-32-7].** Prepared from phenylacetone (**c8**, 399 μL, 403 mg, 3.0 mmol) and propylamine (**a8**, 2.50 mL, 1.80 g, 30.5 mmol) in MeOH according to *General procedure A*. Purification by automated flash chromatography (silica gel 60, *Biotage* SFär Duo 25 g cartridge; gradient of cyclohexane/EtOAc = 50:50 to EtOAc) gave 458 mg (2.58 mmol, 86%) of a colourless liquid. TLC (silica gel 60, cyclohexane/EtOAc = 1:5, UV visualisation): R_f = 0.73. ^{1}H NMR (300 MHz, CD_3OD): δ [ppm] = 7.75–6.99 (5H, m), 3.57–3.42 (1H, m), 3.21 (1H, dd, J = 13.2, 4.6 Hz), 3.13–2.95 (2H, m), 2.70 (1H, dd, J = 13.2, 10.0 Hz), 1.81–1.61 (2H, m), 1.22 (3H, d, J = 6.5 Hz), 1.04 (3H, t, J = 7.4 Hz). ^{13}C NMR (75 MHz, CD_3OD): δ [ppm] = 137.2, 130.4, 130.0, 128.3, 56.9, 47.9, 40.3, 21.0, 16.0, 11.3. GC–MS (EI, 70 eV): m/z = 177 (M^+, 1), 91 (20), 86 (100), 44 (24). No NMR and MS reference data were available for this compound.

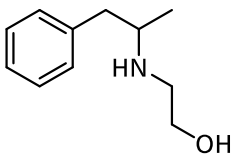


***rac-N*-(1-Phenylpropan-2-yl)prop-2-en-1-amine (c8-a9) [CAS 33236-68-9].** Prepared from phenylacetone (**c8**, 399 μL, 403 mg, 3.0 mmol) and allylamine (**a9**, 2.30 mL, 1.75 g, 30.6 mmol) in MeOH according to *General procedure A*. Purification by automated flash chromatography (silica gel 60, *Biotage* SFär Duo 10 g cartridge; gradient of cyclohexane/EtOAc = 95:5 to cyclohexane/EtOAc = 60:40) gave 17 mg (0.10 mmol, 3%) of a colourless liquid. TLC (silica gel 60, cyclohexane/EtOAc = 4:1, UV visualisation): R_f = 0.30. ^{1}H NMR (300 MHz, $CDCl_3$): δ [ppm] = 7.28–6.99 (5H, m), 5.78 (1H, ddt, J = 17.1, 10.2, 6.0 Hz), 5.06 (1H, dq, J = 17.0, 1.5 Hz), 4.99 (1H, dq, J = 10.2, 1.4 Hz), 3.26 (1H, ddt, J = 14.0, 5.8, 1.5 Hz), 3.14 (1H, ddt, J = 14.0, 6.3, 1.4 Hz), 2.89 (1H, sext, J = 6.4 Hz), 2.71 (1H, dd, J = 13.3, 6.7 Hz), 2.54 (1H, dd, J = 13.3, 6.7 Hz), 1.69 (1H, br s), 1.00 (3H, d, J = 6.2 Hz). ^{13}C NMR (75 MHz, $CDCl_3$): δ [ppm] = 139.4, 136.8, 129.4, 128.5, 126.3, 116.1, 54.0, 49.9, 43.6, 20.1. GC–MS (EI, 70 eV): m/z = 175 (M^+, <1), 91 (16), 84 (100), 65 (8), 41 (23), 39 (8). The characterisation data are in agreement with literature values.[81]

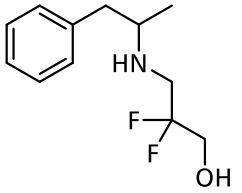


***rac-N*-(1-Phenylpropan-2-yl)cyclopropanamine (c8-a10) [CAS 18381-61-8].** Prepared from phenylacetone (**c8**, 399 μL, 403 mg, 3.0 mmol) and cyclopropanamine (**a10**, 2.10 mL, 1.72 g, 30.2 mmol) in MeOH according to *General procedure A*. Purification by automated flash chromatography (silica gel 60, *Biotage* SFär Duo 25 g cartridge; gradient of cyclohexane/EtOAc = 95:5 to cyclohexane/EtOAc = 60:40) gave 87 mg (0.50 mmol, 17%) of a pale-yellowish liquid. TLC (silica gel 60, cyclohexane/EtOAc = 4:1, UV visualisation): R_f = 0.29. ^{1}H NMR (300 MHz, $CDCl_3$): δ [ppm] = 7.43–6.79 (5H, m), 3.04 (1H, sext, J = 6.5 Hz), 2.79 (1H, dd, J = 13.3, 6.9 Hz), 2.58 (1H, dd, J = 13.3, 6.7 Hz), 2.06 (1H, tt, J = 6.7, 3.7 Hz), 1.67 (1H, br s),

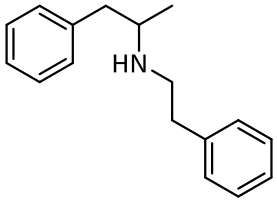
1.10 (3H, d, J = 6.3 Hz), 0.55–0.16 (4H, m). ^{13}C NMR (75 MHz, $CDCl_3$): δ [ppm] = 139.8, 129.4, 128.5, 126.2, 55.6, 43.9, 28.9, 20.8, 7.4, 6.0. GC–MS (EI, 70 eV): m/z = 175 (M^+, 2), 160 (7), 146 (8), 117 (10), 91 (34), 84 (100), 65 (6), 56 (6), 41 (13). No NMR and MS reference data were available for this compound.



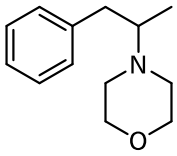
***rac*-2-((1-Phenylpropan-2-yl)amino)ethan-1-ol (c8-a11) [CAS 63918-85-4].** Prepared from phenylacetone (**c8**, 399 μL, 403 mg, 3.0 mmol) and ethanolamine (**a11**, 543 μL, 554 mg, 9.1 mmol) according to *General procedure B*. The crude product was used without purification. 105 mg (0.59 mmol, 20%) of a yellowish liquid. TLC (silica gel 60, EtOAc, $KMnO_4$ staining): R_f = 0.10. ^{1}H NMR (300 MHz, $CDCl_3$): δ [ppm] = 7.47–7.09 (5H, m), 3.88 (2H, br s), 3.71 (2H, t, J = 5.2 Hz), 3.17–2.80 (4H, m), 2.75–2.59 (1H, m), 1.16 (3H, d, J = 6.3 Hz). ^{13}C NMR (75 MHz, $CDCl_3$): δ [ppm] = 138.5, 129.4, 128.7, 126.6, 60.3, 55.0, 48.2, 42.6, 19.2. GC–MS (EI, 70 eV): m/z = 179 (M^+, <1), 148 (4), 130 (100), 119 (5), 91 (35), 87 (64), 70 (28), 65 (6), 56 (6), 43 (21). The characterisation data are in agreement with literature values.[67]



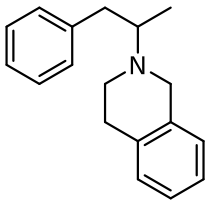
***rac*-2,2-Difluoro-3-((1-phenylpropan-2-yl)amino)propan-1-ol (c8-a12) [CAS 1692603-76-1].** Prepared from phenylacetone (**c8**, 134 μL, 135 mg, 1.0 mmol) and 3-amino-2,2-difluoropropan-1-ol (**a12**, 116 mg, 1.0 mmol) in MeOH according to *General procedure A* (one-third of the usual batch size, 1 eq. of amine and AcOH). Purification by automated flash chromatography (silica gel 60, *Biotage* SFär Duo 5 g cartridge; gradient of cyclohexane/EtOAc = 85:15 to EtOAc) gave 145 mg (0.63 mmol, 63%) of a colourless solid. TLC (silica gel 60, cyclohexane/EtOAc = 1:1, ninhydrin staining): R_f = 0.47. mp: 56–57 °C. ^{1}H NMR (300 MHz, $CDCl_3$): δ [ppm] = 7.38–7.32 (2H, m), 7.27 (1H, tt, J = 6.8, 1.4 Hz), 7.23–7.19 (2H, m), 3.84 (2H, dd, J = 13.3, 11.7 Hz), 3.20 (1H, dt, J = 15.4, 12.4 Hz), 3.14–3.04 (1H, m), 3.01 (1H, sext, J = 6.5 Hz), 2.94 (1H, br s), 2.76 (1H, dd, J = 13.5, 6.9 Hz), 2.68 (1H, dd, J = 13.5, 6.6 Hz), 1.13 (3H, d, J = 6.4 Hz). ^{13}C NMR (75 MHz, $CDCl_3$): δ [ppm] = 138.7, 129.3, 128.6, 126.5, 121.2 (t, J_{CF} = 243.8 Hz), 64.0 (t, J_{CF} = 31.5 Hz), 54.8, 49.7 (t, J_{CF} = 28.3 Hz), 43.3, 19.9. GC–MS (EI, 70 eV): m/z = 229 (M^+, <1), 138 (100), 120 (14), 91 (20), 88 (10), 56 (13). No NMR and MS reference data were available for this compound.



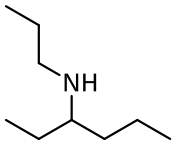
***rac-N*-Phenethyl-1-phenylpropan-2-amine (c8-a15) [CAS 21026-75-5].** Prepared from phenylacetone (**c8**, 134 μL, 135 mg, 1.0 mmol) and 2-phenylethylamine (**a15**, 1.26 mL, 1.22 g, 10.1 mmol) in MeOH according to *General procedure A* (one-third of the usual batch size). Purification by automated flash chromatography (silica gel 60, *Biotage* SFär Duo 25 g cartridge; gradient of cyclohexane/EtOAc = 95:5 to cyclohexane/EtOAc = 45:65) gave 94 mg (0.39 mmol, 39%) of a yellow liquid. The product contains the amine substrate, 2-phenylethylamine, as residual impurity and was used as GC reference material without further purification. TLC (silica gel 60, cyclohexane/EtOAc = 1:1, ninhydrin staining): R_f = 0.33. ^{1}H NMR (300 MHz, $CDCl_3$): δ [ppm] = 7.39–7.09 (10H, m), 3.10 (1H, quint, J = 6.8 Hz), 3.01–2.72 (5H, m), 2.61 (1H, dd, J = 13.3, 6.7 Hz), 2.15 (1H, br s), 1.08 (3H, d, J = 6.3 Hz). ^{13}C NMR (75 MHz, $CDCl_3$): δ [ppm] = 139.8, 139.2, 129.3, 128.7, 128.6, 128.5, 126.3, 126.3, 54.7, 48.5, 43.4, 36.2, 20.0. GC–MS (EI, 70 eV): m/z = 239 (M^+, <1), 148 (100), 119 (9), 105 (54), 91 (30), 77 (8), 65 (5). The characterisation data are in agreement with literature values.[82]



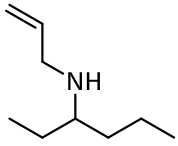
***rac*-4-(1-Phenylpropan-2-yl)morpholine (c8-a22) [CAS 18341-10-1].** Prepared from phenylacetone (**c8**, 399 μL, 403 mg, 3.0 mmol) and morpholine (**a22**, 2.64 mL, 2.66 g, 30.5 mmol) in MeOH according to *General procedure A*. Purification by automated flash chromatography (silica gel 60, *Biotage* SFär Duo 25 g cartridge; gradient of cyclohexane/EtOAc = 95:5 to EtOAc) gave 361 mg (1.76 mmol, 60%) of a pale-yellowish liquid. TLC (silica gel 60, cyclohexane/EtOAc = 5:1, UV visualisation): R_f = 0.12. ^{1}H NMR (300 MHz, $CDCl_3$): δ [ppm] = 7.37–7.04 (5H, m), 3.83–3.53 (4H, m), 3.01 (1H, dd, J = 13.0, 4.3 Hz), 2.87–2.69 (1H, m), 2.69–2.50 (4H, m), 2.41 (1H, dd, J = 12.9, 9.6 Hz), 0.96 (3H, d, J = 6.6 Hz). ^{13}C NMR (75 MHz, $CDCl_3$): δ [ppm] = 140.6, 129.4, 128.4, 126.0, 67.6, 61.8, 49.2, 39.4, 14.5. GC–MS (EI, 70 eV): m/z = 205 (M^+, <1), 114 (100), 91 (10), 70 (6). The characterisation data are in agreement with literature values.[83]



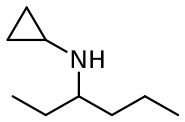
***rac*-2-(1-Phenylpropan-2-yl)-1,2,3,4-tetrahydroisoquinoline (c8-a23).** Prepared from phenylacetone (**c8**, 134 μL, 135 mg, 1.0 mmol) and 1,2,3,4-tetrahydroisoquinoline (**a23**, 1.31 mL, 1.39 g, 10.4 mmol) in MeOH according to *General procedure A* (one-third of the usual batch size). Purification by automated flash chromatography (silica gel 60, *Biotage* SFär Duo 25 g cartridge; gradient of cyclohexane/EtOAc = 95:5 to cyclohexane/EtOAc = 40:60) gave 110 mg (0.44 mmol, 44%) of an orange liquid. TLC (silica gel 60, cyclohexane/EtOAc = 3:1, $KMnO_4$ staining): R_f = 0.43. ^{1}H NMR (500 MHz, $CDCl_3$): δ [ppm] = 7.28–7.23 (2H, m), 7.21–7.14 (3H, m), 7.12–7.06 (3H, m), 7.04–6.97 (1H, m), 3.81 (2H, s), 3.08 (1H, dd, J = 12.9, 4.1 Hz), 3.05–2.97 (1H, m), 2.93–2.87 (2H, m), 2.86–2.78 (2H, m), 2.50 (1H, dd, J = 12.9, 9.6 Hz), 1.03 (3H, d, J = 6.6 Hz). ^{13}C NMR (126 MHz, $CDCl_3$): δ [ppm] = 140.7, 135.6, 134.8, 129.3, 128.8, 128.4, 126.8, 126.0, 125.9, 125.6, 61.3, 51.6, 46.2, 39.5, 30.0, 14.3. GC–MS (EI, 70 eV): m/z = 251 (M^+, <1), 160 (100), 117 (10), 91 (11), 56 (9). HRMS calcd for $C_{18}H_{22}N^+$ [M+H$^+$]: 252.1747, found: 252.1749. No NMR and MS reference data were available for this compound.



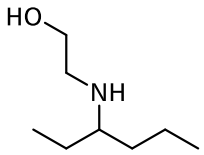
***rac*-*N*-Propylhexan-3-amine (c9-a8) [CAS 151490-32-3].** Prepared from hexan-3-one (**c9**, 366 μL, 300 mg, 3.0 mmol) and propylamine (**a8**, 1.23 mL, 887 mg, 15.0 mmol) in MeOH according to *General procedure A* (5 eq. of amine and AcOH). Purification by column chromatography (silica gel 60, MTBE/MeOH/NH_4OH = 95:4:1) gave 192 mg (1.34 mmol, 45%) of a pale-yellowish liquid. TLC (silica gel 60, MTBE/MeOH/NH_4OH = 90:9:1, $KMnO_4$ staining): R_f = 0.72. ^{1}H NMR (300 MHz, $CDCl_3$): δ [ppm] = 2.99 (1H, quint, J = 6.1 Hz), 2.91–2.83 (2H, m), 1.88–1.60 (6H, m), 1.47–1.31 (2H, m), 1.00 (3H, t, J = 7.4 Hz), 0.99 (3H, t, J = 7.5 Hz), 0.96 (3H, t, J = 7.3 Hz). ^{13}C NMR (75 MHz, $CDCl_3$): δ [ppm] = 60.0, 47.4, 31.9, 23.1, 19.9, 18.5, 14.0, 11.4, 9.4. GC–MS (EI, 70 eV): m/z = 143 (M^+, 14), 128 (20), 112 (100), 98 (13), 84 (33), 67 (9), 55 (19), 41 (16). No NMR and MS reference data were available for this compound.



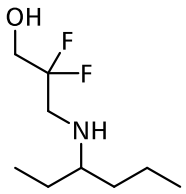
***rac*-*N*-Allylhexan-3-amine (c9-a9) [CAS 1248736-23-3].** Prepared from hexan-3-one (**c9**, 366 μL, 300 mg, 3.0 mmol) and allylamine (**a9**, 2.29 mL, 1.74 g, 30.5 mmol) in MeOH according to *General procedure A*. The crude product was used without purification. 430 mg (quant.) of a colourless liquid. TLC (silica gel 60, cyclohexane/EtOAc = 5:1, ninhydrin staining): R_f = 0.38. ^{1}H NMR (300 MHz, $CDCl_3$): δ [ppm] = 5.97 (1H, ddt, J = 17.1, 10.2, 6.8 Hz), 5.54–5.42 (2H, m), 3.58 (2H, dt, J = 6.9, 1.2 Hz), 3.01 (1H, quint, J = 6.0 Hz), 1.79–1.58 (4H, m), 1.47–1.32 (2H, m), 1.03–0.92 (6H, m). ^{13}C NMR (75 MHz, $CDCl_3$): δ [ppm] = 128.3, 123.6, 58.6, 47.8, 31.7, 22.9, 18.3, 13.9, 9.1. GC–MS (EI, 70 eV): m/z = 141 (M^+, <1), 112 (97), 98 (100), 70 (13), 56 (14), 41 (35). No NMR and MS reference data were available for this compound.



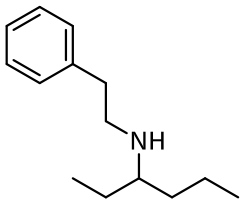
***rac-N*-(Hexan-3-yl)cyclopropanamine (c9-a10) [CAS 1856410-74-6].** Prepared from hexan-3-one (**c9**, 366 μL, 300 mg, 3.0 mmol) and cyclopropanamine (**a10**, 2.08 mL, 1.71 g, 29.9 mmol) in MeOH according to *General procedure A*. The crude product was used without purification. 226 mg (1.60 mmol, 53%) of a pale-yellowish liquid. TLC (silica gel 60, cyclohexane/EtOAc = 5:1, ninhydrin staining): R_f = 0.28. ^{1}H NMR (300 MHz, $CDCl_3$): δ [ppm] = 2.94 (1H, quint, J = 6.1 Hz), 2.37 (1H, tt, J = 7.3, 4.0 Hz), 1.77–1.52 (4H, m), 1.45–1.30 (2H, m), 0.96 (3H, t, J = 7.5 Hz), 0.94 (3H, t, J = 7.3 Hz), 0.89–0.82 (2H, m), 0.80–0.70 (2H, m). ^{13}C NMR (75 MHz, $CDCl_3$): δ [ppm] = 60.9, 32.8, 28.8, 23.9, 18.6, 14.2, 9.5, 4.9, 4.8. GC–MS (EI, 70 eV): *m/z* = 141 (M^+, 12), 126 (33), 112 (100), 98 (84), 84 (17), 70 (22), 56 (60), 41 (36). No NMR and MS reference data were available for this compound.



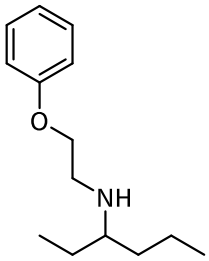
***rac*-2-(Hexan-3-ylamino)ethan-1-ol (c9-a11) [CAS 1005310-34-8].** Prepared from hexan-3-one (**c9**, 366 μL, 300 mg, 3.0 mmol) and ethanolamine (**a11**, 543 μL, 554 mg, 9.1 mmol) according to *General procedure B*. Purification by column chromatography (silica gel 60, methanol) gave 160 mg (1.10 mmol, 37%) of a colourless liquid. TLC (silica gel 60, methanol, ninhydrin staining): R_f = 0.36. ^{1}H NMR (300 MHz, $CDCl_3$): δ [ppm] = 3.61 (2H, t, J = 5.2 Hz), 2.74 (2H, dd, J = 6.1, 4.4 Hz), 2.43 (1H, quint, J = 5.8 Hz), 1.49–1.23 (6H, m), 0.97–0.82 (6H, m). ^{13}C NMR (75 MHz, $CDCl_3$): δ [ppm] = 61.3, 58.3, 48.3, 36.1, 26.5, 19.1, 14.4, 9.9. GC–MS (EI, 70 eV): *m/z* = 145 (M^+, <1), 116 (98), 114 (17), 102 (100), 84 (15), 70 (10), 56 (28), 41 (22). No NMR and MS reference data were available for this compound.



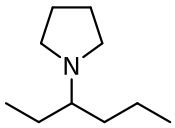
***rac*-2,2-Difluoro-3-(hexan-3-ylamino)propan-1-ol (c9-a12) [CAS 1699196-54-7].** Prepared from hexan-3-one (**c9**, 122 μL, 100 mg, 1.0 mmol) and 3-amino-2,2-difluoropropan-1-ol (**a12**, 213 mg, 1.9 mmol) in MeOH according to *General procedure A* (one-third of the usual batch size, 2 eq. of amine and AcOH). The crude product was dissolved in $CHCl_3$, dried over Na_2SO_4, filtered, and concentrated under reduced pressure to give 159 mg (0.81 mmol, 81%) of a yellowish liquid. TLC (silica gel 60, MeOH, $KMnO_4$ staining): R_f = 0.76. ^{1}H NMR (300 MHz, $CDCl_3$): δ [ppm] = 3.89 (2H, t, J = 12.2 Hz), 3.11 (2H, td, J = 12.8, 1.1 Hz), 2.95 (1H, br s), 2.50 (1H, quint, J = 5.7 Hz), 1.50–1.19 (6H, m), 0.92 (3H, t, J = 7.0 Hz), 0.88 (3H, t, J = 7.5 Hz). ^{13}C NMR (75 MHz, $CDCl_3$): δ [ppm] = 120.6 (t, J_{CF} = 243.4 Hz), 65.2 (t, J_{CF} = 31.6 Hz), 58.7, 50.4 (t, J_{CF} = 29.2 Hz), 35.5, 26.0, 19.0, 14.4, 9.7. GC–MS (EI, 70 eV): *m/z* = 195 [M^+, <1%)], 166 (93), 152 (100), 134 (10), 124 (8), 102 (8), 70 (10), 56 (12), 43 (10). No NMR and MS reference data were available for this compound.



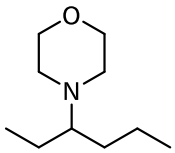
***rac-N*-Phenethylhexan-3-amine (c9-a15) [CAS 416847-82-0].** Prepared from hexan-3-one (**c9**, 366 μL, 300 mg, 3.0 mmol) and 2-phenylethylamine (**a15**, 3.77 mL, 3.66 g, 30.2 mmol) in MeOH according to *General procedure A*. Purification by automated flash chromatography (silica gel 60, *Biotage* SFär Duo 50 g cartridge; gradient of cyclohexane/EtOAc = 95:5 to cyclohexane/EtOAc = 60:40) gave 180 mg (0.87 mmol, 29%) of a yellowish liquid. TLC (silica gel 60, cyclohexane/EtOAc = 4:1, ninhydrin staining): R_f = 0.26. ^{1}H NMR (300 MHz, $CDCl_3$): δ [ppm] = 7.34–7.13 (5H, m), 2.91–2.73 (4H, m), 2.42 (1H, quint, J = 5.8 Hz), 1.47–1.11 (7H, m), 0.88 (3H, t, J = 6.9 Hz), 0.82 (3H, t, J = 7.5 Hz). ^{13}C NMR (75 MHz, $CDCl_3$): δ [ppm] = 140.4, 128.8, 128.5, 126.2, 58.6, 48.6, 36.8, 36.0, 26.4, 19.1, 14.5, 9.9. GC–MS (EI, 70 eV): *m/z* = 205 (M^+, <1), 176 (42), 162 (41), 114 (100), 105 (78), 91 (13), 77 (12), 72 (10), 56 (7), 43 (12). The characterisation data are in agreement with literature values.[84]



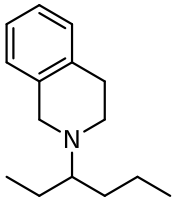
***rac*-*N*-(2-Phenoxyethyl)hexan-3-amine (c9-a16) [CAS 1343107-62-9].** Prepared from hexan-3-one (**c9**, 366 μL, 300 mg, 3.0 mmol) and 2-phenoxyethylamine (**a16**, 1.96 mL, 2.06 g, 15.0 mmol) in MeOH according to *General procedure A* (5 eq. of amine and AcOH). Purification by automated flash chromatography (silica gel 60, *Biotage* SFär Duo 25 g cartridge; gradient of cyclohexane/EtOAc = 90:10 to EtOAc) gave 196 mg (1.34 mmol, 45%) of a yellowish liquid. TLC (silica gel 60, cyclohexane/EtOAc = 1:1, ninhydrin staining): R_f = 0.44. ^{1}H NMR (300 MHz, $CDCl_3$): δ [ppm] = 7.27 (2H, dd, J = 8.6, 7.2 Hz), 6.97–6.83 (3H, m), 4.06 (2H, t, J = 5.3 Hz), 2.97 (2H, dd, J = 6.0, 4.7 Hz), 2.50 (1H, quint, J = 5.7 Hz), 1.66 (1H, br s), 1.53–1.22 (6H, m), 0.99–0.73 (6H, m). ^{13}C NMR (75 MHz, $CDCl_3$): δ [ppm] = 159.0, 129.5, 120.9, 114.7, 67.7, 58.4, 46.1, 36.1, 26.5, 19.1, 14.5, 9.9. GC–MS (EI, 70 eV): *m/z* = 221 (M^+, <1), 192 (100), 178 (99), 121 (9), 114 (54), 98 (8), 84 (19), 77 (19), 70 (12), 65 (13), 56 (25), 43 (19). No NMR and MS reference data were available for this compound.



***rac*-1-(Hexan-3-yl)pyrrolidine (c9-a21) [CAS 111735-03-6].** Prepared from hexan-3-one (**c9**, 122 μL, 100 mg, 1.0 mmol) and pyrrolidine (**a21**, 837 μL, 711 mg, 10.0 mmol) in MeOH according to *General procedure A* (one-third of the usual batch size). Purification by column chromatography (silica gel 60, MTBE/MeOH/NH_4OH = 95:4:1) gave 274 mg (1.76 mmol, 59%) of a pale-yellowish liquid. TLC (silica gel 60, MTBE/MeOH/NH_4OH = 90:9:1, $KMnO_4$ staining): R_f = 0.76. ^{1}H NMR (300 MHz, $CDCl_3$): δ [ppm] = 2.59–2.49 (4H, m), 2.07 (1H, tt, J = 6.9, 4.1 Hz), 1.81–1.68 (4H, m), 1.62–1.21 (6H, m), 0.89 (3H, t, J = 7.1 Hz), 0.86 (3H, t, J = 7.1 Hz). ^{13}C NMR (75 MHz, $CDCl_3$): δ [ppm] = 64.9, 51.5, 33.4, 24.1, 23.5, 19.0, 14.7, 9.9. GC–MS (EI, 70 eV): *m/z* = 155 (M^+, 8), 126 (100), 112 (92), 97 (7), 84 (5), 70 (9), 55 (5). No NMR and MS reference data were available for this compound.

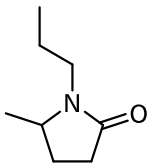


***rac*-4-(Hexan-3-yl)morpholine (c9-a22).** Prepared from hexan-3-one (**c9**, 366 μL, 300 mg, 3.0 mmol) and morpholine (**a22**, 2.61 mL, 2.63 g, 30.2 mmol) in MeOH according to *General procedure A*. Purification by automated flash chromatography (silica gel 60, *Biotage* SFär Duo 10 g cartridge; gradient of cyclohexane/EtOAc = 90:10 to EtOAc) gave 35 mg (0.20 mmol, 7%) of a yellowish liquid. TLC (silica gel 60, cyclohexane/EtOAc = 1:1, $KMnO_4$ staining): R_f = 0.35. ^{1}H NMR (300 MHz, $CDCl_3$): δ [ppm] = 3.72–3.62 (4H, m), 2.55–2.41 (4H, m), 2.20 (1H, quint, J = 6.4 Hz), 1.57–1.16 (6H, m), 0.90 (3H, t, J = 7.2 Hz). ^{13}C NMR (75 MHz, $CDCl_3$): δ [ppm] = 67.8, 65.8, 49.1, 31.8, 22.6, 20.4, 14.5, 11.8. GC–MS (EI, 70 eV): *m/z* = 171 (M^+, 4), 142 (100), 128 (96), 56 (8), 41 (8). HRMS calcd for $C_{10}H_{22}NO^+$ [M+H^+]: 172.1696, found: 172.1694. No NMR and MS reference data were available for this compound.

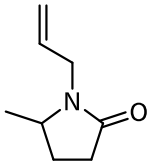


***rac*-2-(Hexan-3-yl)-1,2,3,4-tetrahydroisoquinoline (c9-a23).** Prepared from hexan-3-one (**c9**, 122 μL, 100 mg, 1.0 mmol) and 1,2,3,4-tetrahydroisoquinoline (**a23**, 1.31 mL, 1.39 g, 10.4 mmol) in MeOH according to *General procedure A* (one-third of the usual batch size). Purification by automated flash chromatography (silica gel 60, *Biotage* SFär Duo 25 g cartridge; gradient of cyclohexane/EtOAc = 95:5 to cyclohexane/EtOAc = 50:50) gave 72 mg (0.33 mmol, 33%) of an orange liquid. TLC (silica gel 60, cyclohexane/EtOAc = 3:1, $KMnO_4$ staining): R_f = 0.57. ^{1}H NMR (500 MHz, $CDCl_3$): δ [ppm] = 7.11–7.05 (3H, m), 7.03–6.98 (1H, m), 3.73 (2H, s), 2.83 (2H, t, J = 5.7 Hz), 2.78–2.69 (2H, m), 2.44 (1H, quint, J = 6.5 Hz), 1.64–1.48 (2H, m), 1.42–1.25 (4H, m), 0.93 (3H, t, J = 7.5 Hz), 0.91 (3H, t, J = 7.2 Hz). ^{13}C NMR (126 MHz, $CDCl_3$): δ [ppm] = 136.4, 135.4, 128.9, 126.7, 125.8, 125.4, 65.3, 51.6, 45.8, 32.1, 30.4, 22.8, 20.6, 14.5, 12.1. GC–MS (EI, 70 eV):

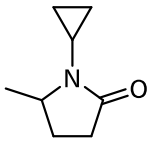
m/z = 217 (M^+, 3), 188 (98), 174 (100), 158 (5), 132 (7), 117 (12), 105 (7). HRMS calcd for $C_{15}H_{24}N^+$ [M+H^+]: 218.1903, found: 218.1878. No NMR and MS reference data were available for this compound.



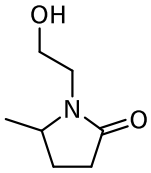
***rac*-5-Methyl-1-propylpyrrolidin-2-one (c10-a8) [CAS 38286-46-3].** Prepared from ethyl levulinate (**c10**, 428 μL, 437 mg, 3.0 mmol) and propylamine (**a8**, 2.50 mL, 1.80 g, 30.5 mmol) in MeOH according to *General procedure A*. Purification by automated flash chromatography (silica gel 60, *Biotage* SFär Duo 25 g cartridge; gradient of cyclohexane/EtOAc = 80:20 to EtOAc) gave 224 mg (1.59 mmol, 53%) of a pale-yellowish liquid. The product contains the title compound and the corresponding open-chain amino ester, ethyl 4-(propylamino)-pentanoate in a ratio of approx. 85:15 and was used as GC reference material without further purification. TLC (silica gel 60, cyclohexane/EtOAc = 1:1, $KMnO_4$ staining): R_f = 0.17. ^{1}H NMR (300 MHz, $CDCl_3$): δ [ppm] = 3.65 (1H, dquint, *J* = 7.4, 6.2 Hz), 3.49 (1H, ddd, *J* = 13.7, 9.0, 7.2 Hz), 2.86 (1H, dddd, *J* = 13.8, 8.8, 5.1, 1.0 Hz), 2.44–2.23 (2H, m), 2.14 (1H, dddd, *J* = 12.6, 9.1, 7.4, 6.1 Hz), 1.60–1.35 (3H, m), 1.16 (3H, d, *J* = 6.3 Hz), 0.85 (3H, t, *J* = 7.4 Hz). ^{13}C NMR (75 MHz, $CDCl_3$): δ [ppm] = 174.9, 53.4, 41.7, 30.4, 26.8, 20.7, 19.8, 11.4. GC–MS (EI, 70 eV): *m/z* = 141 (M^+, 51), 126 (42), 112 (100), 98 (8), 84 (53), 67 (7), 55 (19), 41 (16). The characterisation data are in agreement with literature values.[85]



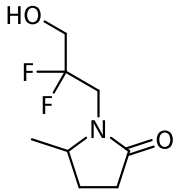
***rac*-1-Allyl-5-methylpyrrolidin-2-one (c10-a9) [CAS 1425041-26-4].** Prepared from ethyl levulinate (**c10**, 143 μL, 146 mg, 1.0 mmol) and allylamine (**a9**, 766 μL, 582 mg, 10.2 mmol) in MeOH according to *General procedure A* (one-third of the usual batch size). Purification by column chromatography (silica gel 60, cyclohexane/EtOAc = 1:1) gave 47 mg (0.38 mmol, 38%) of a colourless liquid. TLC (silica gel 60, EtOAc, $KMnO_4$ staining): R_f = 0.36. ^{1}H NMR (300 MHz, $CDCl_3$): δ [ppm] = 5.69 (1H, dddd, *J* = 17.3, 10.1, 7.3, 4.8 Hz), 5.20–5.10 (2H, m), 4.24 (1H, ddt, *J* = 15.5, 4.8, 1.7 Hz), 3.67 (1H, dquint, *J* = 7.5, 6.2 Hz), 3.50 (1H, ddd, *J* = 15.5, 7.3, 1.2 Hz), 2.49–2.27 (2H, m), 2.17 (1H, dddd, *J* = 12.7, 9.3, 7.5, 6.2 Hz), 1.57 (1H, dddd, *J* = 12.8, 9.5, 7.1, 5.7 Hz), 1.16 (3H, d, *J* = 6.3 Hz). ^{13}C NMR (75 MHz, $CDCl_3$): δ [ppm] = 174.8, 132.9, 117.6, 53.4, 43.0, 30.3, 26.8, 19.8. GC–MS (EI, 70 eV): *m/z* = 139 (M^+, 44), 124 (100), 112 (6), 96 (9), 84 (27), 68 (9), 55 (18), 41 (44). No NMR reference data were available for this compound.



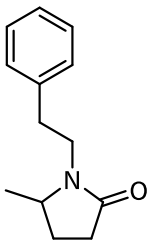
***rac*-1-Cyclopropyl-5-methylpyrrolidin-2-one (c10-a10) [CAS 1351473-78-3].** Prepared from ethyl levulinate (**c10**, 428 μL, 437 mg, 3.0 mmol) and cyclopropanamine (**a10**, 2.08 mL, 1.71 g, 29.9 mmol) in MeOH according to *General procedure A*. Purification by automated flash chromatography (silica gel 60, *Biotage* SFär Duo 50 g cartridge; gradient of cyclohexane/EtOAc = 80:20 to EtOAc) gave 229 mg (1.65 mmol, 55%) of a red liquid. TLC (silica gel 60, cyclohexane/EtOAc = 1:1, $KMnO_4$ staining): R_f = 0.12. ^{1}H NMR (300 MHz, $CDCl_3$): δ [ppm] = 3.54 (1H, dqd, *J* = 7.7, 6.3, 4.5 Hz), 2.45–2.18 (3H, m), 2.07 (1H, ddt, *J* = 12.7, 9.5, 7.4 Hz), 1.55 (1H, dddd, *J* = 12.7, 9.5, 6.0, 4.5 Hz), 1.22 (3H, d, *J* = 6.2 Hz), 0.91 (1H, dtd, *J* = 9.7, 7.0, 5.4 Hz), 0.77 (1H, dddd, *J* = 10.4, 6.8, 5.4, 3.9 Hz), 0.63 (1H, dtd, *J* = 9.8, 6.9, 5.2 Hz), 0.54–0.43 (1H, m). ^{13}C NMR (75 MHz, $CDCl_3$): δ [ppm] = 176.0, 55.1, 30.7, 26.3, 23.1, 20.1, 7.5, 4.2. GC–MS (EI, 70 eV): *m/z* = 139 (M^+, 43), 124 (100), 96 (18), 84 (41), 68 (21), 55 (28), 41 (27). The characterisation data are in agreement with literature values.[86]



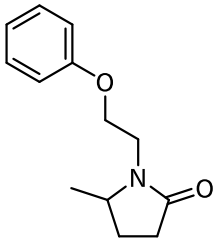
***rac*-1-(2-Hydroxyethyl)-5-methylpyrrolidin-2-one (c10-a11) [CAS 59941-34-3].** Prepared from ethyl levulinate (**c10**, 143 μL, 146 mg, 1.0 mmol) and ethanolamine (**a11**, 598 μL, 610 mg, 10.0 mmol) in MeOH according to *General procedure A* (one-third of the usual batch size). Purification by column chromatography (silica gel 60, EtOAc) gave 118 mg (0.83 mmol, 83%) of a pale-yellowish liquid. TLC (silica gel 60, MeOH, $KMnO_4$ staining): R_f = 0.55. ^{1}H NMR (300 MHz, $CDCl_3$): δ [ppm] = 3.81–3.68 (3H, m), 3.56 (1H, ddd, J = 14.5, 6.8, 4.2 Hz), 3.23 (1H, dt, J = 14.5, 4.5 Hz), 2.99 (1H, br s), 2.34–2.18 (3H, m), 1.71–1.51 (1H, m), 1.22 (3H, d, J = 6.3 Hz). ^{13}C NMR (75 MHz, $CDCl_3$): δ [ppm] = 177.3, 61.2, 55.2, 44.0, 30.4, 27.1, 20.1. GC–MS (EI, 70 eV): m/z = 143 (M^+, 14), 128 (20), 112 (100), 98 (13), 84 (33), 67 (9), 55 (19), 41 (16). No NMR reference data were available for this compound.



***rac*-1-(2,2-Difluoro-3-hydroxypropyl)-5-methylpyrrolidin-2-one (c10-a12).** Prepared from ethyl levulinate (**c10**, 143 μL, 146 mg, 1.0 mmol) and 3-amino-2,2-difluoropropan-1-ol (**a12**, 320 mg, 2.9 mmol) in MeOH according to *General procedure A* (one-third of the usual batch size, 3 eq. of amine and AcOH). Purification by column chromatography (silica gel 60, EtOAc) gave 115 mg (0.60 mmol, 60%) of a yellowish liquid. TLC (silica gel 60, EtOAc, $KMnO_4$ staining): R_f = 0.53. ^{1}H NMR (300 MHz, $CDCl_3$): δ [ppm] = 4.33 (1H, br s), 3.91 (1H, ddd, J = 25.0, 15.1, 5.0 Hz), 3.82–3.72 (1H, m), 3.67–3.46 (2H, m), 3.40 (1H, ddd, J = 15.1, 11.5, 8.1 Hz), 2.54–2.33 (2H, m), 2.25 (1H, dddd, J = 13.1, 8.9, 7.2, 6.0 Hz), 1.65 (1H, dddd, J = 12.7, 9.5, 7.5, 6.2 Hz), 1.25 (3H, dd, J = 6.3, 0.8 Hz). ^{13}C NMR (75 MHz, $CDCl_3$): δ [ppm] = 177.9, 121.7 (dd, J_{CF} = 248.8, 245.8 Hz), 61.4 (dd, J_{CF} = 34.6, 29.7 Hz), 55.7, 41.7 (dd, J_{CF} = 36.1, 28.7 Hz), 29.9, 27.3, 19.4. GC–MS (EI, 70 eV): m/z = 193 (M^+, 2), 178 (53), 173 (38), 150 (16), 112 (100), 84 (30), 55 (17), 41 (10). No NMR and MS reference data were available for this compound.

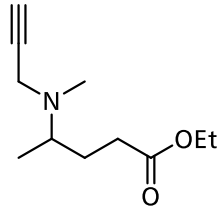


***rac*-5-Methyl-1-phenethylpyrrolidin-2-one (c10-a15) [CAS 175166-14-0].** Prepared from ethyl levulinate (**c10**, 143 μL, 146 mg, 1.0 mmol) and 2-phenylethylamine (**a15**, 1.26 mL, 1.22 g, 10.0 mmol) in MeOH according to *General procedure A* (one-third of the usual batch size). Purification by automated flash chromatography (silica gel 60, *Biotage* SFär Duo 25 g cartridge; gradient of cyclohexane/EtOAc = 90:10 to cyclohexane/EtOAc = 20:80) gave 168 mg (0.83 mmol, 83%) of a pale-yellowish liquid. TLC (silica gel 60, cyclohexane/EtOAc = 1:1, $KMnO_4$ staining): R_f = 0.19. ^{1}H NMR (500 MHz, $CDCl_3$): δ [ppm] = 7.27 (2H, t, J = 7.6 Hz), 7.23–7.14 (3H, m), 3.80 (1H, ddd, J = 13.9, 9.2, 6.3 Hz), 3.51 (1H, sext, J = 6.3 Hz), 3.14 (1H, ddd, J = 14.3, 8.9, 6.2 Hz), 2.86 (1H, ddd, J = 13.3, 9.2, 6.1 Hz), 2.75 (1H, ddd, J = 13.6, 8.9, 6.3 Hz), 2.36 (1H, ddd, J = 15.8, 9.5, 5.9 Hz), 2.26 (1H, ddd, J = 16.8, 9.5, 7.3 Hz), 2.09 (1H, dddd, J = 13.1, 9.5, 7.4, 5.9 Hz), 1.51 (1H, dddd, J = 12.8, 9.5, 7.2, 5.9 Hz), 1.13 (3H, d, J = 6.4 Hz). ^{13}C NMR (126 MHz, $CDCl_3$): δ [ppm] = 174.6, 138.8, 128.5, 128.3, 126.2, 53.5, 41.5, 33.7, 30.0, 26.6, 19.5. GC–MS (EI, 70 eV): m/z = 203 (M^+, 15), 112 (100), 104 (11), 91 (7), 84 (12), 55 (9). The characterisation data are in agreement with literature values.[87]

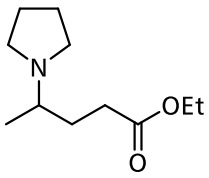


***rac*-5-Methyl-1-(2-phenoxyethyl)pyrrolidin-2-one (c10-a16).** Prepared from ethyl levulinate (**c10**, 213 μL, 217 mg, 1.5 mmol) and 2-phenoxyethylamine (**a16**, 1.96 mL, 2.06 g, 15.0 mmol) in MeOH according to *General procedure A* (half of the usual batch size). Purification by automated flash chromatography (silica gel 60, *Biotage* SFär Duo 50 g cartridge; gradient of cyclohexane/EtOAc = 95:5 to EtOAc) gave 78 mg of a pale-yellowish liquid. TLC (silica gel 60, cyclohexane/EtOAc = 1:1, $KMnO_4$

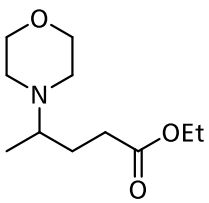
staining): R_f = 0.21. ^{1}H NMR (300 MHz, $CDCl_3$): δ [ppm] = 7.31–7.23 (2H, m), 6.94 (1H, tt, J = 7.3, 1.1 Hz), 6.89–6.83 (2H, m), 4.09 (2H, dd, J = 5.9, 4.7 Hz), 3.92 (1H, dd, J = 14.5, 4.6 Hz), 3.87 (1H, ddt, J = 12.3, 7.1, 6.2 Hz), 3.39 (1H, dddd, J = 14.4, 6.4, 5.6, 0.8 Hz), 2.50–2.27 (2H, m), 2.18 (1H, dddd, J = 12.6, 9.2, 7.3, 6.0 Hz), 1.67–1.51 (1H, m), 1.28 (3H, d, J = 6.2 Hz). ^{13}C NMR (75 MHz, $CDCl_3$): δ [ppm] = 175.5, 158.5, 129.6, 121.1, 114.4, 66.3, 55.0, 40.0, 30.2, 27.1, 19.9. GC–MS (EI, 70 eV): m/z = 219 (M^+, <1), 126 (100), 120 (25), 112 (25), 91 (8), 83 (18), 77 (11), 55 (15), 42 (5). HRMS calcd. for $C_{13}H_{18}NO_2^+$ [M+H$^+$]: 220.1332, found: 220.1335.



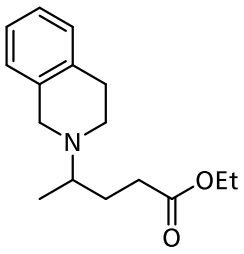
Ethyl *rac*-4-(methyl(prop-2-yn-1-yl)amino)pentanoate (c10-a20) [CAS 1348977-94-5 (hydrochloride)]. Prepared from ethyl levulinate (**c10**, 428 μL, 437 mg, 3.0 mmol) and *N*-methylpropargylamine (**a20**, 760 μL, 623 mg, 9.0 mmol) in EtOH according to *General procedure A* (3 eq. of amine and AcOH). Purification by automated flash chromatography (silica gel 60, *Biotage* SFär Duo 25 g cartridge; gradient of cyclohexane/EtOAc = 75:25 to EtOAc) gave 260 mg (1.32 mmol, 44%) of a pale-yellowish liquid. TLC (silica gel 60, EtOAc, $KMnO_4$ staining): R_f = 0.79. ^{1}H NMR (300 MHz, CD_3OD): δ [ppm] = 4.10 (2H, q, J = 7.2 Hz), 3.35–3.26 (2H, m), 2.77 (1H, sext, J = 6.5 Hz), 2.58 (1H, t, J = 2.5 Hz), 2.40–2.29 (2H, m), 2.27 (3H, s), 1.92–1.78 (1H, m), 1.67–1.50 (1H, m), 1.24 (3H, t, J = 7.1 Hz), 1.02 (3H, d, J = 6.6 Hz). ^{13}C NMR (75 MHz, CD_3OD): δ [ppm] = 175.4, 80.7, 74.2, 61.5, 57.7, 43.6, 37.1, 32.1, 29.7, 14.7, 14.5. GC–MS (EI, 70 eV): m/z = 197 (M^+, <1), 182 (10), 152 (18), 108 (9), 96 (100), 68 (13), 56 (19), 42 (12). No NMR and MS reference data were available for this compound.



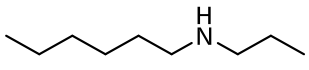
Ethyl *rac*-4-(pyrrolidin-1-yl)pentanoate (c10-a21) [CAS 874496-84-1]. Prepared from ethyl levulinate (**c10**, 143 μL, 146 mg, 1.0 mmol) and pyrrolidine (**a21**, 837 μL, 711 mg, 10.0 mmol) in EtOH according to *General procedure A* (one-third of the usual batch size). Purification by column chromatography (silica gel 60, 2-propanol) gave 42 mg (0.21 mmol, 21%) of a pale-yellowish liquid. TLC (silica gel 60, 2-propanol, $KMnO_4$ staining): R_f = 0.19. ^{1}H NMR (300 MHz, $CDCl_3$): δ [ppm] = 4.16 (2H, q, J = 7.1 Hz), 3.36–3.12 (5H, m), 2.52 (1H, ddd, J = 17.0, 7.7, 5.8 Hz), 2.45–2.30 (1H, m), 2.19 (1H, ddd, J = 13.8, 7.9, 3.4 Hz), 2.14–2.03 (4H, m), 1.85 (1H, dddd, J = 13.4, 9.6, 7.2, 5.8 Hz), 1.37 (3H, d, J = 6.6 Hz), 1.28 (3H, t, J = 7.2 Hz). ^{13}C NMR (75 MHz, $CDCl_3$): δ [ppm] = 172.5, 61.2, 60.1, 51.5, 30.0, 27.5, 23.5, 15.8, 14.2. GC–MS (EI, 70 eV): m/z = 199 (M^+, <1), 184 (7), 154 (12), 110 (7), 98 (100), 56 (6). No NMR and MS reference data were available for this compound.



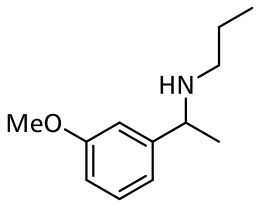
Ethyl *rac*-4-morpholinopentanoate (c10-a22). Prepared from ethyl levulinate (**c10**, 428 μL, 437 mg, 3.0 mmol) and morpholine (**a22**, 2.61 mL, 2.63 g, 30.2 mmol) in EtOH according to *General procedure A*. The crude product was used without purification. 765 mg (quant.) of a pale-yellowish liquid. TLC (silica gel 60, EtOAc, $KMnO_4$ staining): R_f = 0.41. ^{1}H NMR (500 MHz, $CDCl_3$): δ [ppm] = 4.11 (2H, qd, J = 7.1, 1.5 Hz), 3.71–3.57 (4H, m), 2.61–2.48 (3H, m), 2.44–2.31 (4H, m), 1.81 (1H, dq, J = 14.0, 7.6 Hz), 1.59 (1H, dtd, J = 14.9, 7.2, 5.8 Hz), 1.25 (3H, t, J = 7.3 Hz), 0.97 (3H, d, J = 6.7 Hz). ^{13}C NMR (126 MHz, $CDCl_3$): δ [ppm] = 173.4, 66.9, 59.6, 58.3, 48.2, 31.0, 28.0, 13.8, 13.1. GC–MS (EI, 70 eV): m/z = 215 (M^+, 2), 200 (6), 170 (12), 114 (100), 55 (6). HRMS calcd for $C_{11}H_{22}NO_3^+$ [M+H$^+$]: 216.1594, found: 216.1595. No NMR and MS reference data were available for this compound.



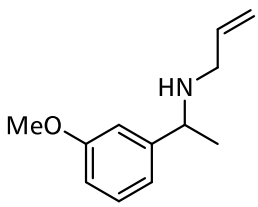
Ethyl 4-(3,4-dihydroisoquinolin-2(1*H*)-yl)pentanoate (c10-a23). Prepared from ethyl levulinate (**c10**, 428 μL, 437 mg, 3.0 mmol) and 1,2,3,4-tetrahydroisoquinoline (**a23**, 3.78 mL, 3.99 g, 30.0 mmol) in EtOH according to *General procedure A*. Purification by automated flash chromatography (silica gel 60, *Biotage* SFär Duo 25 g cartridge; gradient of cyclohexane/EtOAc = 90:10 to EtOAc) gave 139 mg (0.53 mmol, 18%) of an orange liquid. TLC (silica gel 60, cyclohexane/EtOAc = 1:1, $KMnO_4$ staining): R_f = 0.63. ^{1}H NMR (500 MHz, $CDCl_3$): δ [ppm] = 7.11–7.04 (3H, m), 7.02–6.96 (1H, m), 4.08–3.97 (2H, m), 3.75 (1H, d, J = 14.7 Hz), 3.61 (1H, d, J = 14.7 Hz), 2.86–2.71 (4H, m), 2.66–2.58 (1H, m), 2.44–2.28 (2H, m), 1.93 (1H, dtd, J = 13.9, 8.1, 6.9 Hz), 1.66 (1H, ddt, J = 14.1, 8.0, 6.4 Hz), 1.18 (3H, t, J = 7.2 Hz), 1.04 (3H, d, J = 6.7 Hz). ^{13}C NMR (126 MHz, $CDCl_3$): δ [ppm] = 174.0, 135.7, 134.9, 128.7, 126.6, 125.8, 125.4, 60.1, 58.3, 51.2, 45.7, 31.8, 29.9, 28.9, 14.2, 13.5. GC–MS (EI, 70 eV): *m/z* = 261 (M^+, <1), 246 (7), 216 (8), 160 (100), 132 (32), 117 (9), 104 (5), 56 (6). HRMS calcd for $C_{16}H_{24}NO_2^+$ [M+H$^+$]: 262.1802, found: 262.1802. No NMR and MS reference data were available for this compound.



***N*-Propylhexan-1-amine (c11-a8) [CAS 20193-23-1].** Prepared from hexanal (**c11**, 333 μL, 266 mg, 3.1 mmol) and propylamine (**a8**, 2.50 mL, 1.80 g, 30.5 mmol) in MeOH according to *General procedure A*. Purification by automated flash chromatography (silica gel 60, *Biotage* SFär Duo 25 g cartridge; gradient of cyclohexane/EtOAc = 90:10 to EtOAc) gave 255 mg (1.78 mmol, 58%) of a colourless liquid. TLC (silica gel 60, cyclohexane/EtOAc = 1:1, ninhydrin staining): R_f = 0.30. ^{1}H NMR (300 MHz, $CDCl_3$): δ [ppm] = 7.13 (1H, br s), 3.18–2.78 (4H, m), 1.92–1.65 (4H, m), 1.48–1.18 (6H, m), 1.03 (3H, t, J = 7.4 Hz), 0.90 (3H, t, J = 6.1 Hz). ^{13}C NMR (75 MHz, $CDCl_3$): δ [ppm] = 49.9, 48.4, 30.8, 25.9, 25.6, 22.1, 19.2, 13.7, 10.8. GC–MS (EI, 70 eV): *m/z* = 143 (M^+, 9), 114 (26), 72 (100), 44 (28). The characterisation data are in agreement with literature values.[88]

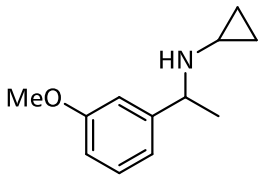


***rac-N*-(1-(3-Methoxyphenyl)ethyl)propan-1-amine (c12-a8) [CAS 727968-53-8].** Prepared from 3-methoxyacetophenone (**c12**, 412 μL, 449 mg, 3.0 mmol) and propylamine (**a8**, 2.50 mL, 1.80 g, 30.5 mmol) in MeOH according to *General procedure A*. Purification by automated flash chromatography (silica gel 60, *Biotage* SFär Duo 25 g cartridge; gradient of cyclohexane/EtOAc = 95:5 to EtOAc) gave 505 mg (2.61 mmol, 87%) of a colourless liquid. TLC (silica gel 60, cyclohexane/EtOAc = 3:1, UV visualisation): R_f = 0.50. ^{1}H NMR (300 MHz, $CDCl_3$): δ [ppm] = 7.34 (1H, dd, J = 8.3, 7.5 Hz), 7.06–7.02 (1H, m), 6.98 (1H, dt, J = 7.7, 1.2 Hz), 6.93 (1H, ddd, J = 8.3, 2.5, 0.9 Hz), 4.14 (1H, q, J = 6.8 Hz), 3.85 (3H, s), 2.75–2.53 (2H, m), 1.88–1.66 (2H, m), 1.74 (3H, d, J = 6.9 Hz), 0.93 (3H, t, J = 7.4 Hz). ^{13}C NMR (75 MHz, $CDCl_3$): δ [ppm] = 160.6, 137.9, 130.7, 119.9, 115.8, 112.2, 59.8, 55.7, 48.3, 20.6, 20.0, 11.3. GC–MS (EI, 70 eV): *m/z* = 193 (M^+, 1), 178 (93), 164 (7), 135 (100), 105 (12), 91 (11), 86 (12), 77 (10), 58 (10). No NMR and MS reference data were available for this compound.

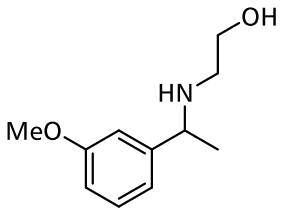


***rac-N*-(1-(3-Methoxyphenyl)ethyl)prop-2-en-1-amine (c12-a9) [CAS 1019537-68-8].** Prepared from 3-methoxyacetophenone (**c12**, 412 μL, 449 mg, 3.0 mmol) and allylamine (**a9**, 2.25 mL, 1.71 g, 30.0 mmol) in MeOH according to *General procedure A*. Purification by automated flash chromatography (silica gel 60, *Biotage* SFär Duo 25 g cartridge; gradient of cyclohexane/EtOAc = 90:10 to EtOAc) gave 140 mg (0.73 mmol, 24%) of a colourless liquid. TLC (silica gel 60, cyclohexane/EtOAc = 4:1, UV visualisation): R_f = 0.28. ^{1}H NMR (300 MHz, $CDCl_3$): δ [ppm] = 7.29–7.18 (1H, m), 6.92–

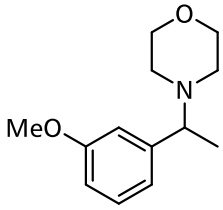
6.86 (2H, m), 6.81–6.74 (1H, m), 5.89 (1H, ddt, J = 17.1, 10.2, 6.0 Hz), 5.13 (1H, dq, J = 17.2, 1.7 Hz), 5.09–5.04 (1H, m), 3.81 (3H, s), 3.78 (1H, q, J = 6.6 Hz), 3.11 (2H, dq, J = 6.1, 1.4 Hz), 1.35 (3H, d, J = 6.6 Hz). ^{13}C NMR (75 MHz, $CDCl_3$): δ [ppm] = 159.9, 147.4, 137.1, 129.5, 119.1, 115.9, 112.3, 112.3, 57.7, 55.3, 50.4, 24.3. GC–MS (EI, 70 eV): m/z = 191 (M^+, 2), 176 (100), 144 (7), 136 (38), 121 (13), 105 (9), 91 (11), 84 (14), 77 (9), 56 (11), 41 (11). No NMR and MS reference data were available for this compound.



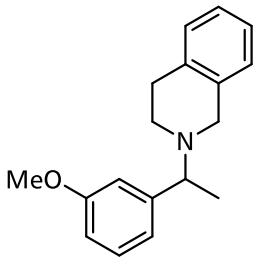
***rac-N*-(1-(3-Methoxyphenyl)ethyl)cyclopropanamine (c12-a10) [CAS 926195-59-7].** Prepared from 3-methoxyacetophenone (**c12**, 412 μL, 449 mg, 3.0 mmol) and cyclopropanamine (**a10**, 2.10 mL, 1.72 g, 30.2 mmol) in MeOH according to *General procedure A*. Purification by automated flash chromatography (silica gel 60, *Biotage* SFär Duo 25 g cartridge; gradient of cyclohexane/EtOAc = 95:5 to cyclohexane/EtOAc = 60:40) gave 87 mg (0.50 mmol, 17%) of a pale-yellowish liquid. TLC (silica gel 60, cyclohexane/EtOAc = 4:1, UV visualisation): R_f = 0.29. ^{1}H NMR (300 MHz, $CDCl_3$): δ [ppm] = 7.24 (1H, t, J = 7.8 Hz), 6.94–6.84 (2H, m), 6.78 (1H, ddd, J = 8.2, 2.6, 1.0 Hz), 3.83 (1H, q, J = 6.7 Hz), 3.81 (3H, s), 2.03–1.93 (1H, m), 1.85 (1H, br s), 1.35 (3H, d, J = 6.7 Hz), 0.46–0.22 (4H, m). ^{13}C NMR (75 MHz, $CDCl_3$): δ [ppm] = 159.8, 148.0, 129.5, 119.1, 112.4, 112.1, 58.5, 55.3, 29.0, 23.8, 6.6, 6.5. GC–MS (EI, 70 eV): m/z = 191 (M^+, 16), 190 (69), 176 (22), 160 (8), 148 (7), 135 (100), 120 (11), 105 (31), 91 (20), 77 (13), 65 (6), 57 (5). No NMR and MS reference data were available for this compound.



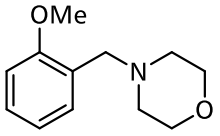
***rac*-2-((1-(3-Methoxyphenyl)ethyl)amino)ethan-1-ol (c12-a11) [CAS 1038707-90-2].** Prepared from 3-methoxyacetophenone (**c12**, 412 μL, 449 mg, 3.0 mmol) and ethanolamine (**a11**, 539 μL, 550 mg, 9.0 mmol) according to *General procedure B*. The crude product was used without purification. 304 mg (quant.) of an orange liquid. TLC (silica gel 60, cyclohexane/EtOAc = 1:1, $KMnO_4$ staining): R_f = 0.22. ^{1}H NMR (300 MHz, CD_3OD): δ [ppm] = 7.22 (1H, t, J = 7.8 Hz), 6.98–6.86 (2H, m), 6.79 (1H, ddd, J = 8.2, 2.6, 1.0 Hz), 3.76 (3H, s), 3.74 (1H, q, J = 6.7 Hz), 3.61 (2H, td, J = 5.5, 1.3 Hz), 2.63–2.45 (2H, m), 1.36 (3H, d, J = 6.7 Hz). ^{13}C NMR (75 MHz, $CDCl_3$): δ [ppm] = 161.3, 147.3, 130.6, 120.0, 113.6, 113.2, 61.5, 59.2, 55.6, 50.2, 23.8. GC–MS (EI, 70 eV): m/z = 195 (M^+, <1)], 180 (27), 164 (27), 135 (100), 105 (14), 91 (10), 77 (8). No NMR and MS reference data were available for this compound.



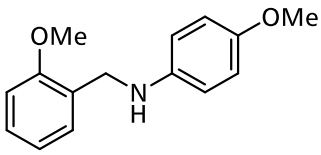
***rac*-4-(1-(3-Methoxyphenyl)ethyl)morpholine (c12-a21) [CAS 865874-23-3].** Prepared from 3-methoxyacetophenone (**c12**, 412 μL, 449 mg, 3.0 mmol) and morpholine (**a22**, 3.89 mL, 3.92 g, 45.0 mmol) in MeOH according to *General procedure A* (15 eq. of amine and AcOH). Purification by automated flash chromatography (silica gel 60, *Biotage* SFär Duo 25 g cartridge; gradient of cyclohexane/EtOAc = 95:5 to EtOAc) gave 400 mg (1.81 mmol, 60%) of a colourless liquid. TLC (silica gel 60, cyclohexane/EtOAc = 4:1, UV visualisation): R_f = 0.32. ^{1}H NMR (300 MHz, $CDCl_3$): δ [ppm] = 7.22 (1H, t, J = 8.1 Hz), 6.93–6.86 (2H, m), 6.78 (1H, ddd, J = 8.2, 2.5, 1.1 Hz), 3.81 (3H, s), 3.69 (4H, t, J = 4.7 Hz), 3.26 (1H, q, J = 6.6 Hz), 2.55–2.44 (2H, m), 2.42–2.30 (2H, m), 1.33 (3H, d, J = 6.7 Hz). ^{13}C NMR (75 MHz, $CDCl_3$): δ [ppm] = 159.8, 146.0, 129.4, 120.2, 113.4, 112.2, 67.4, 65.6, 55.3, 51.5, 20.0. GC–MS (EI, 70 eV): m/z = 221 (M^+, 10), 206 (100), 135 (42), 121 (8), 114 (26), 105 (12), 91 (14), 86 (15), 77 (10), 56 (13). No NMR and MS reference data were available for this compound.



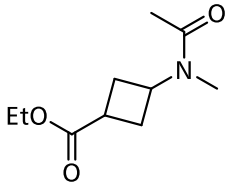
***rac*-2-(1-(3-Methoxyphenyl)ethyl)-1,2,3,4-tetrahydroisoquinoline (c12-a23) [CAS 1348702-50-0].** Prepared from 3-methoxyacetophenone (**c12**, 142 μL, 155 mg, 1.0 mmol) and 1,2,3,4-tetrahydroisoquinoline (**a23**, 1.31 mL, 1.39 g, 10.4 mmol) in MeOH according to *General procedure A* (one-third of the usual batch size). Purification by automated flash chromatography (silica gel 60, *Biotage* SFär Duo 25 g cartridge; gradient of cyclohexane/EtOAc = 95:5 to cyclohexane/EtOAc = 50:50) gave 142 mg (0.53 mmol, 53%) of a yellow liquid. TLC (silica gel 60, cyclohexane/EtOAc = 3:1, $KMnO_4$ staining): R_f = 0.42. ^{1}H NMR (500 MHz, $CDCl_3$): δ [ppm] = 7.22 (1H, t, J = 8.0 Hz), 7.12–7.03 (3H, m), 7.00–6.93 (3H, m), 6.81–6.76 (1H, m), 3.82 (1H, d, J = 14.8 Hz), 3.78 (3H, s), 3.56 (1H, d, J = 14.8 Hz), 3.50 (1H, q, J = 6.7 Hz), 2.91–2.82 (1H, m), 2.81–2.73 (2H, m), 2.62–2.55 (1H, m), 1.44 (3H, d, J = 6.7 Hz). ^{13}C NMR (126 MHz, $CDCl_3$): δ [ppm] = 159.8, 146.3, 135.3, 134.7, 129.3, 128.7, 126.9, 126.1, 125.6, 120.1, 113.1, 112.4, 64.6, 55.3, 53.7, 48.2, 29.5, 20.4. GC–MS (EI, 70 eV): m/z = 267 (M^+, 2), 252 (72), 160 (27), 136 (49), 132 (100), 121 (15), 117 (10), 105 (18), 91 (16), 77 (15). No NMR and MS reference data were available for this compound.



4-(2-Methoxybenzyl)morpholine (c13-a22) [CAS 29175-54-0]. Prepared from 2-methoxybenzaldehyde (**c13**, 408 mg, 3.0 mmol) and morpholine (**a22**, 2.61 mL, 2.63 g, 30.2 mmol) in MeOH according to *General procedure A*. Purification by automated flash chromatography (silica gel 60, *Biotage* SFär Duo 25 g cartridge; gradient of cyclohexane/EtOAc = 95:5 to EtOAc) gave 26 mg (0.13 mmol, 4%) of a colourless liquid. TLC (silica gel 60, cyclohexane/EtOAc = 1:1, ninhydrin staining): R_f = 0.29. ^{1}H NMR (300 MHz, $CDCl_3$): δ [ppm] = 7.35 (1H, dd, J = 7.5, 2.0 Hz), 7.28–7.17 (1H, m), 6.93 (1H, td, J = 7.5, 1.2 Hz), 6.87 (1H, dd, J = 8.3, 1.0 Hz), 3.82 (3H, s), 3.75–3.67 (4H, m), 3.56 (2H, s), 2.54–2.46 (4H, m). ^{13}C NMR (75 MHz, $CDCl_3$): δ [ppm] = 158.0, 130.6, 128.2, 126.0, 120.4, 110.6, 67.2, 56.6, 55.6, 53.8. GC–MS (EI, 70 eV): m/z = 207 (M^+, 62), 176 (18), 146 (55), 121 (100), 100 (7), 91 (62), 86 (20), 78 (10), 65 (12), 56 (10). The characterisation data are in agreement with literature values.[89]

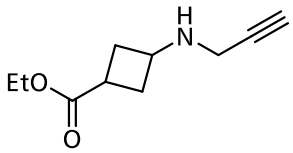


4-Methoxy-*N*-(2-methoxybenzyl)aniline (c13-a24) [CAS 862604-21-5]. Prepared from 2-methoxybenzaldehyde (**c13**, 408 mg, 3.0 mmol) and *p*-anisidine (**a24**, 3.69 g, 30.0 mmol) in MeOH according to *General procedure A*. Purification by automated flash chromatography (silica gel 60, *Biotage* SFär Duo 25 g cartridge; gradient of cyclohexane/EtOAc = 95:5 to EtOAc) gave 440 mg (1.81 mmol, 60%) of a red liquid. TLC (silica gel 60, cyclohexane/EtOAc = 2:1, ninhydrin staining): R_f = 0.67. ^{1}H NMR (300 MHz, $CDCl_3$): δ [ppm] = 7.29 (1H, dd, J = 7.4, 1.8 Hz), 7.23 (1H, td, J = 7.8, 1.8 Hz), 6.93–6.84 (2H, m, 1H), 6.79–6.72 (2H, m), 6.64–6.58 (2H, m), 4.27 (2H, s), 3.84 (3H, s), 3.71 (3H, s). ^{13}C NMR (75 MHz, $CDCl_3$): δ [ppm] = 157.5, 152.2, 142.8, 129.1, 128.4, 127.7, 120.6, 114.9, 114.5, 110.3, 55.9, 55.4, 44.6. GC–MS (EI, 70 eV): m/z = 243 (M^+, 93), 121 (100), 91 (61), 77 (7), 65 (10). The characterisation data are in agreement with literature values.[90]

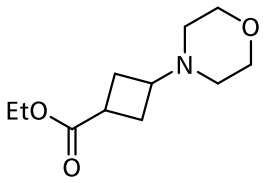


Ethyl 3-(N-methylacetamido)cyclobutane-1-carboxylate (c14-a2-Ac). Prepared from ethyl 3-oxocyclobutane-1-carboxylate (**c146**, 182 μL, 213 mg, 1.5 mmol) and methylamine (**a2**, 1.29 mL of a 40% w/w aqueous solution; 0.47 g $MeNH_2$, 15.0 mmol) in EtOH according to *General procedure A* (half of the usual batch size), followed by derivatisation with acetic anhydride. Purification by automated flash chromatography (silica gel 60, *Biotage* SFär Duo 25 g cartridge; gradient of cyclohexane/EtOAc = 75:25 to EtOAc)

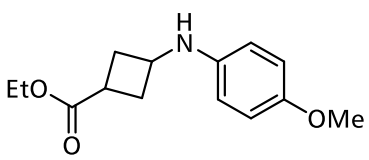
gave 52 mg (0.26 mmol, 17%) of a colourless liquid. TLC (silica gel 60, EtOAc, ninhydrin staining): R_f = 0.20. GC–MS (EI, 70 eV): *m/z* = 199 (M^+, <1), 154 (16), 99 (75), 84 (12), 57 (100), 43 (20). HRMS calcd for $C_{10}H_{18}NO_3^+$ [M+H$^+$]: 200.1281, found: 200.1284. The NMR spectra reveal the presence of significant residual impurities, but the spectral data are in agreement with the proposed product structure.



Ethyl 3-(prop-2-yn-1-ylamino)cyclobutane-1-carboxylate (c14-a4). Prepared from ethyl 3-oxocyclobutane-1-carboxylate (**c14**, 121 μL, 142 mg, 1.0 mmol) and propargylamine (**a4**, 640 μL, 550 mg, 10.0 mmol) in EtOH according to *General procedure A* (one-third of the usual batch size). Purification by column chromatography (silica gel 60, EtOH) gave 92 mg (0.51 mmol, 51%) of a colourless liquid. The product is a mixture of diastereomers in a ratio of approx. 68:32. TLC (silica gel 60, EtOH, $KMnO_4$ staining): R_f = 0.77. ^{1}H NMR (300 MHz, $CDCl_3$): δ [ppm] = 4.15 (2H minor, q, J = 7.2 Hz), 4.13 (2H, major, q, J = 7.1 Hz), 3.72–3.58 (1H minor, m), 3.38 (2H major, d, J = 2.5 Hz), 3.36 (2H minor, d, J = 2.4 Hz), 3.40–3.28 (1H major, m), 3.07 (1H minor, ttd, J = 9.6, 4.6, 1.2 Hz), 2.84–2.66 (1H major, m), 2.62–2.42 (2H major + minor, m), 2.20 (1H minor, t, J = 2.5 Hz), 2.19 (1H major, t, J = 2.5 Hz), 2.12–1.93 (2H major + minor, m), 1.65 (1H major + minor, br s), 1.27 (3H minor, t, J = 7.1 Hz), 1.25 (3H major, t, J = 7.2 Hz). ^{13}C NMR (75 MHz, $CDCl_3$): δ [ppm] = 176.1 (minor), 175.0 (major), 82.5 (major), 82.3 (minor), 71.4 (minor), 71.3 (major), 60.6 (major + minor), 51.0 (minor), 49.5 (major), 35.9 (major), 35.8 (minor), 34.6 (major), 33.3 (minor), 32.9 (minor), 31.6 (major), 14.3 (major + minor). GC–MS (EI, 70 eV): *m/z* = 181 (M^+, <1), 136 (11), 81 (39), 80 (100), 53 (5), 39 (9). HRMS calcd for $C_{10}H_{16}NO_2^+$ [M+H$^+$]: 182.1176, found: 182.1177. No NMR and MS reference data were available for this compound.

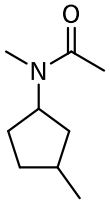


Ethyl 3-morpholinocyclobutane-1-carboxylate (c14-a22). Prepared from ethyl 3-oxocyclobutane-1-carboxylate (**c146**, 182 μL, 213 mg, 1.5 mmol) and morpholine (**a22**, 1.31 mL, 1.32 g, 15.1 mmol) in EtOH according to *General procedure A* (half of the usual batch size). Purification by automated flash chromatography (silica gel 60, *Biotage* SFär Duo 25 g cartridge; gradient of cyclohexane/EtOAc = 90:10 to EtOAc) gave 176 mg (0.83 mmol, 55%) of a colourless liquid. The product is a mixture of diastereomers in a ratio of approx. 83:17. TLC (silica gel 60, cyclohexane/EtOAc = 1:1, ninhydrin staining): R_f = 0.08. ^{1}H NMR (300 MHz, $CDCl_3$): δ [ppm] = 4.16 (2H minor, q, J = 7.1 Hz), 4.12 (2H major, q, J = 7.1 Hz), 3.75–3.67 (4H major + minor, m), 3.05–2.93 (2H minor, m), 2.85–2.64 (2H major, m), 2.39–2.26 (6H major + minor, m), 2.20–2.06 (2H, major + minor, m), 1.27 (3H minor, t, J = 7.1 Hz), 1.25 (3H, major, t, J = 7.1 Hz). ^{13}C NMR (75 MHz, $CDCl_3$): δ [ppm] = 176.1 (minor), 174.6 (major), 66.8 (minor), 66.8 (major), 60.7 (minor), 60.5 (major), 58.0 (minor), 56.1 (major), 49.9 (minor), 49.8 (major), 32.3 (minor), 31.0 (major), 30.2 (minor), 29.5 (major), 14.3 (major + minor). GC–MS (EI, 70 eV): *m/z* = 213 (M^+, <1), 168 (29), 140 (15), 113 (100), 98 (32), 83 (20), 55 (30), 41 (9). HRMS calcd for $C_{11}H_{20}NO_3^+$ [M+H$^+$]: 252.1747, found: 252.1749. No NMR and MS reference data were available for this compound.

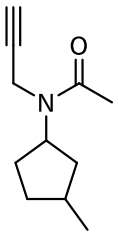


Ethyl 3-((4-methoxyphenyl)amino)cyclobutane-1-carboxylate (c14-a24). Prepared from ethyl 3-oxocyclobutane-1-carboxylate (**c146**, 182 μL, 213 mg, 1.5 mmol) and *p*-anisidine (**a24**, 1.85 g, 15.0 mmol) in EtOH according to *General procedure A* (half of the usual batch size). Purification by automated flash chromatography (silica gel 60, *Biotage* SFär Duo 25 g cartridge; gradient of cyclohexane/EtOAc = 90:10 to cyclohexane/EtOAc = 35:65) gave 91 mg (0.37 mmol, 24%) of a red liquid. The product is a mixture of diastereomers in a ratio of approx. 59:41. TLC (silica

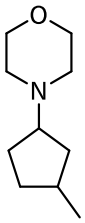
gel 60, cyclohexane/EtOAc = 1:1, ninhydrin staining): R_f = 0.46. ^{1}H NMR (300 MHz, $CDCl_3$): δ [ppm] = 6.80–6.72 (2H major + minor, m), 6.58–6.47 (2H major + minor, m), 4.18 (2H minor, q, J = 7.1 Hz), 4.13 (2H major, q, J = 7.1 Hz), 4.11–4.03 (1H minor, m), 3.89–3.77 (1H major, m), 3.73 (3H major + minor, s), 3.11 (1H minor, dddd, J = 14.4, 9.8, 4.6, 1.2 Hz), 2.92–2.78 (1H major, m), 2.74–2.61 (2H major + minor, m), 2.17–1.99 (2H major + minor, m), 1.28 (3 H minor, t, J = 7.1 Hz), 1.25 (3H major, t, J = 7.1 Hz). ^{13}C NMR (75 MHz, $CDCl_3$): δ [ppm] = 176.0 (minor), 175.0 (major), 152.5 (major + minor), 141.1 (minor), 140.9 (major), 115.0 (major + minor), 114.7 (major), 114.6 (minor), 60.7 (major + minor), 55.9 (major + minor), 47.6 (minor), 45.8 (major), 34.7 (major), 33.6 (minor), 33.3 (minor), 31.7 (major), 14.3 (major + minor). GC–MS (EI, 70 eV): m/z = 249 (M^+, 22), 204 (9), 176 (14), 149 (100), 134 (40), 122 (8), 107 (12), 77 (5). HRMS calcd for $C_{14}H_{20}NO_3^+$ [M+H$^+$]: 250.1438, found: 250.1440. No NMR and MS reference data were available for this compound.



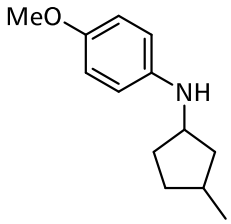
***all-rac-N*-Methyl-*N*-(3-methylcyclopentyl)acetamide (c15-a2-Ac) [CAS 1852077-76-9].** Prepared from 3-methylcyclopentanone (**c15**, 327 μL, 298 mg, 3.0 mmol) and methylamine (**a2**, 3.07 mL of a 40% w/w solution in MeOH; 0.93 g $MeNH_2$, 30.0 mmol) in MeOH according to *General procedure A*, followed by derivatisation with acetic anhydride. Purification by automated flash chromatography (silica gel 60, *Biotage* SFär Duo 25 g cartridge; gradient of cyclohexane/EtOAc = 88:12 to EtOAc) gave 132 mg (0.85 mmol, 28%) of a colourless liquid. The product is a mixture of diastereomers and amide rotamers in a ratio of approx. 26:26:24:24. TLC (silica gel 60, EtOAc, $KMnO_4$ staining): R_f = 0.20. ^{1}H NMR (300 MHz, $CDCl_3$): δ [ppm] = 5.19–4.92 (1H minor, m), 4.37–4.07 (1H major, m), 2.85, 2.85 (3H minor, 2 × s), 2.80, 2.79 (3H major, 2 × s), 2.13, 2.13 (3H major, 2 × s), 2.08, 2.07 (3H minor, 2 × s), 1.99–1.10 (7H major + minor, m), 1.11–0.94 (3H major + minor, m). ^{13}C NMR (75 MHz, $CDCl_3$): δ [ppm] = 171.0, 170.9, 170.6, 170.6, 59.2, 58.4, 53.9, 53.2, 38.5, 37.8, 37.1, 36.2, 33.9, 33.9, 33.6, 33.5, 33.0, 32.9, 32.8, 30.6, 30.4, 30.4, 29.5, 28.3, 27.5, 27.4, 27.3, 22.6, 22.6, 21.8, 21.8, 21.0, 20.9, 20.7, 20.5. GC–MS (EI, 70 eV): m/z = 155 (M^+, 51), 140 (13), 126 (7), 112 (28), 98 (54), 84 (39), 74 (100), 70 (70), 67 (10), 56 (16), 43 (31), 39 (8). No NMR and MS reference data were available for this compound.



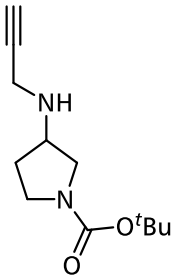
***all-rac-N*-(3-Methylcyclopentyl)-*N*-(prop-2-yn-1-yl)acetamide (c15-a4-Ac).** Prepared from 3-methylcyclopentanone (**c15**, 327 μL, 298 mg, 3.0 mmol) and propargylamine (**a4**, 960 μL, 826 mg, 15.0 mmol) in MeOH according to *General procedure A* (5 eq. amine and AcOH), followed by derivatisation with acetic anhydride. Purification by automated flash chromatography (silica gel 60, *Biotage* SFär Duo 25 g cartridge; gradient of cyclohexane/EtOAc = 88:12 to EtOAc) gave 170 mg (0.95 mmol, 32%) of a yellowish liquid. The product is a mixture of diastereomers and amide rotamers in a ratio of approx. 26:26:24:24. TLC (silica gel 60, cyclohexane/EtOAc = 1:1, $KMnO_4$ staining): R_f = 0.37. ^{1}H NMR (300 MHz, $CDCl_3$): δ [ppm] = 5.05–4.81 (1H minor, m), 4.31–4.06 (1H major, m), 4.01, 4.00 (2H major, 2 × s), 3.88 (2H minor, s), 2.26 (1H minor, s), 2.17 (3H minor, s), 2.12 (4H major, 2 × s overlap), 2.03–1.07 (7H major + minor, m), 1.07–0.94 (3H major + minor, m). ^{13}C NMR (75 MHz, $CDCl_3$): δ [ppm] = 171.0, 170.2, 81.1, 80.2, 72.2, 70.3, 59.5, 58.7, 54.8, 54.1, 39.2, 38.4, 37.5, 36.6, 34.0, 33.7, 33.0, 33.0, 32.5, 32.4, 32.3, 32.3, 31.1, 30.7, 30.4, 30.2, 28.9, 28.0, 22.4, 21.9, 20.7, 20.6. GC–MS (EI, 70 eV): m/z = 179 (M^+, 16), 164 (21), 150 (7), 140 (47), 136 (22), 122 (22), 108 (41), 105 (12), 98 (100), 94 (83), 80 (62), 67 (20), 56 (28), 43 (59), 39 (37). HRMS calcd for $C_{11}H_{18}NO^+$ [M+H$^+$]: 180.1383, found: 180.1385. No NMR and MS reference data were available for this compound.



***all-rac*-4-(3-Methylcyclopentyl)morpholine (c15-a22) [CAS 31130-68-4].** Prepared from 3-methylcyclopentanone (**c15**, 327 μL, 298 mg, 3.0 mmol) and morpholine (**a22**, 2.61 mL, 2.63 g, 30.2 mmol) in MeOH according to *General procedure A*. Purification by automated flash chromatography (silica gel 60, *Biotage* SFär Duo 25 g cartridge; gradient of cyclohexane/EtOAc = 75:25 to EtOAc) gave 244 mg (1.44 mmol, 48%) of a colourless liquid. The product is a mixture of diastereomers in a ratio of approx. 70:30. TLC (silica gel 60, EtOAc, $KMnO_4$ staining): R_f = 0.51. ^{1}H NMR (300 MHz, $CDCl_3$): δ [ppm] = 3.73 (4H major + minor, t, J = 4.8 Hz), 2.68 (1H minor, tt, J = 9.2, 7.3 Hz), 2.62–2.55 (1H major, m), 2.55–2.48 (4H major + minor, m), 2.09 (1H minor, dtd, J = 13.1, 9.2, 6.6 Hz), 1.99 (1H major, ddt, J = 11.1, 4.7, 1.2 Hz), 1.95–1.68 (3H major + minor, m), 1.64–1.04 (3H major + minor, m), 0.99 (3H major, d, J = 6.3 Hz), 0.95 (3H minor, d, J = 6.8 Hz). ^{13}C NMR (75 MHz, $CDCl_3$): δ [ppm] = 67.9 (major), 67.0 (minor), 66.7 (major), 66.6 (minor), 52.7 (major), 52.6 (minor), 39.6 (major), 37.5 (minor), 33.6 (minor), 33.0 (major), 32.6 (minor), 32.3 (major), 30.7 (minor), 29.1 (major), 21.6 (minor), 20.8 (major). GC–MS (EI, 70 eV): m/z = 169 (M^+, 32), 154 (12), 140 (84), 126 (100), 112 (22), 96 (7), 82 (22), 68 (8), 55 (19), 41 (15). No NMR and MS reference data were available for this compound.

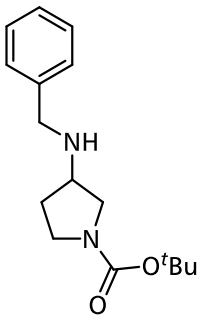


***all-rac*-4-Methoxy-*N*-(3-methylcyclopentyl)aniline (c15-a24) [CAS 1343471-28-2].** Prepared from 3-methylcyclopentanone (**c15**, 327 μL, 298 mg, 3.0 mmol) and *p*-anisidine (**a24**, 3.69 g, 30.0 mmol) in MeOH according to *General procedure A*. Purification by automated flash chromatography (silica gel 60, *Biotage* SFär Duo 25 g cartridge; gradient of cyclohexane/EtOAc = 95:5 to EtOAc) gave 211 mg (1.03 mmol, 34%) of a brownish liquid. The product is a mixture of diastereomers in a ratio of approx. 52:48. TLC (silica gel 60, cyclohexane/EtOAc = 3:1, ninhydrin staining): R_f = 0.63. ^{1}H NMR (300 MHz, $CDCl_3$): δ [ppm] = 6.80–6.72 (2H major + minor, m), 6.60–6.52 (2H major + minor, m), 3.85–3.65 (1H major + minor, m), 3.74 (3H major + minor, s), 3.28 (1H major + minor, br s), 2.31 (1H major, dt, J = 13.2, 6.9 Hz), 2.24–1.65 (3H major + 4H minor, m), 1.58–1.10 (2H major + 3H minor, m), 1.04 (3H major, d, J = 6.6 Hz), 1.01 (3H minor, d, J = 6.7 Hz), 0.98–0.89 (1H major, m). ^{13}C NMR (75 MHz, $CDCl_3$): δ [ppm] = 152.0 (major + minor), 142.5 (major), 142.4 (minor), 115.0 (major + minor), 114.7 (major), 114.7 (minor), 56.0 (major + minor), 55.8 (major), 55.2 (minor), 43.3 (major), 42.2 (minor), 34.1 (minor), 33.6 (major), 33.5 (major + minor), 33.0 (major), 32.8 (minor), 21.0 (major), 20.8 (minor). GC–MS (EI, 70 eV): m/z = 205 (M^+, 100), 190 (18), 176 (41), 162 (60), 149 (58), 134 (26), 122 (10), 108 (32), 77 (7), 55 (6), 41 (8). No NMR and MS reference data were available for this compound.

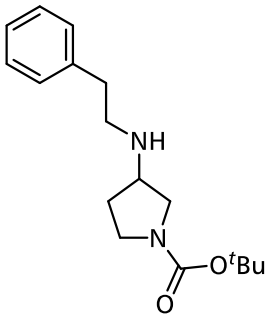


***tert*-Butyl *rac*-3-(prop-2-yn-1-ylamino)pyrrolidine-1-carboxylate (c16-a4) [CAS 1504422-31-4].** Prepared from *tert*-butyl 3-oxopyrrolidine-1-carboxylate (**c16**, 185 mg, 1.0 mmol) and propargylamine (**a4**, 640 μL, 550 mg, 10.0 mmol) in MeOH according to *General procedure A* (one-third of the usual batch size). Purification by automated flash chromatography (silica gel 60, *Biotage* SFär Duo 25 g cartridge; gradient of cyclohexane/EtOAc = 75:25 to EtOAc) gave 46 mg (0.21 mmol, 21%) of a yellow liquid. The product is a mixture of carbamate rotamers in nearly equal amounts. TLC (silica gel 60, EtOAc, ninhydrin staining): R_f = 0.57. ^{1}H NMR (300 MHz, $CDCl_3$): δ [ppm] = 3.63–3.30 (6H, m), 3.24–3.06 (1H, m), 2.25 (1H, t, J = 2.4 H), 2.16–1.93 (2H, m), 1.82–1.63 (1H, m), 1.46 (9H, s). ^{13}C NMR (75 MHz, $CDCl_3$): δ [ppm] = 154.8, 81.7, 81.7, 79.8, 79.7, 72.0, 71.9, 56.2, 55.4, 51.8, 51.4, 44.6, 44.2, 36.5, 31.6, 31.1, 28.6. GC–MS (EI, 70 eV): m/z = 167 (M^+–^{t}Bu,

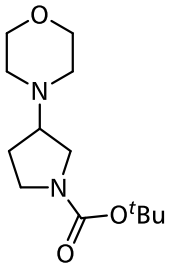
23), 151 (26), 129 (20), 123 (65), 113 (42), 94 (89), 80 (37), 69 (18), 57 (100), 41 (33), 39 (18). No NMR and MS reference data were available for this compound.



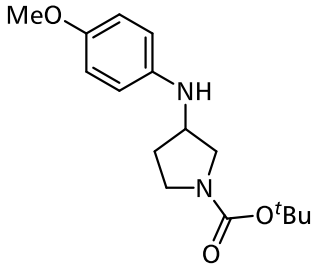
***tert*-Butyl *rac*-3-(benzylamino)pyrrolidine-1-carboxylate (c16-a6) [CAS 862906-31-8].** Prepared from *tert*-butyl 3-oxopyrrolidine-1-carboxylate (**c16**, 185 mg, 1.0 mmol) and benzylamine (**a6**, 328 μL, 321 mg, 3.0 mmol) in MeOH according to *General procedure A* (one-third of the usual batch size, 3 eq. of amine and AcOH). Purification by column chromatography (silica gel 60, cyclohexane/EtOAc = 2:1) gave 217 mg (0.79 mmol, 79%) of a pale-yellowish liquid. The product is a mixture of carbamate rotamers in nearly equal amounts. TLC (silica gel 60, cyclohexane/EtOAc = 2:1, $KMnO_4$ staining): R_f = 0.20. ^{1}H NMR (300 MHz, $CDCl_3$): δ [ppm] = 7.38–7.20 (5H, m), 3.80 (2H, s), 3.63–3.40 (2H, m), 3.39–3.25 (2H, m), 3.14 (1H, ddd, J = 24.0, 10.6, 5.3 Hz), 2.11–1.92 (2H, m), 1.74 (1H, tt, J = 13.0, 6.3 Hz), 1.45 (9H, s). ^{13}C NMR (75 MHz, $CDCl_3$): δ [ppm] = 154.7, 139.7, 128.6, 128.3, 127.3, 79.3, 57.1, 56.2, 52.2, 51.9, 51.4, 44.5, 44.2, 32.1, 31.3, 28.6. GC–MS (EI, 70 eV): m/z = 276 (M^+, <1), 219 (69), 203 (20), 175 (12), 146 (36), 132 (20), 106 (88), 91 (100), 85 (16), 57 (50), 41 (16), 39 (5). The characterisation data are in agreement with literature values.[91]



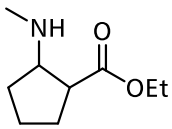
***tert*-Butyl *rac*-3-(phenethylamino)pyrrolidine-1-carboxylate (c16-a15) [CAS 1506851-92-8].** Prepared from *tert*-butyl 3-oxopyrrolidine-1-carboxylate (**c16**, 185 mg, 1.0 mmol) and 2-phenylethylamine (**a15**, 375 μL, 364 mg, 3.0 mmol) in MeOH according to *General procedure A* (one-third of the usual batch size, 3 eq. of amine and AcOH). Purification by column chromatography (silica gel 60, MTBE/MeOH/NH_4OH = 95:4:1) gave 175 mg (0.60 mmol, 60%) of a pale-yellowish liquid. The product is a mixture of carbamate rotamers in nearly equal amounts. TLC (silica gel 60, MTBE/MeOH/NH_4OH = 90:9:1, $KMnO_4$ staining): R_f = 0.73. ^{1}H NMR (300 MHz, $CDCl_3$): δ [ppm] = 7.35–7.08 (5H, m), 3.64–3.39 (2H, m), 3.38–3.22 (2H, m), 3.16–2.99 (1H, m), 2.94–2.78 (4H, m), 2.04 (2H, ddt + br s overlap, J = 11.6, 7.5, 5.7 Hz), 1.79–1.58 (1H, m), 1.44 (9H, s). ^{13}C NMR (75 MHz, $CDCl_3$): δ [ppm] = 154.7, 139.6, 128.8, 128.7, 126.4, 79.3, 57.8, 57.0, 51.8, 51.4, 49.5, 44.5, 44.2, 36.4, 32.1, 31.3, 28.6. GC–MS (EI, 70 eV): m/z = 290 (M^+, <1), 217 (21), 199 (32), 143 (100), 125 (21), 105 (24), 99 (56), 82 (9), 68 (10), 57 (56), 41 (12). The ^{1}H NMR data are in agreement with literature values.[92]



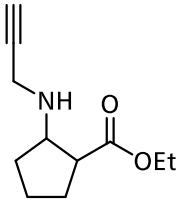
***tert*-Butyl *rac*-3-morpholinopyrrolidine-1-carboxylate (c16-a22) [CAS 1184914-30-4].** Prepared from *tert*-butyl 3-oxopyrrolidine-1-carboxylate (**c16**, 185 mg, 1.0 mmol) and morpholine (**a22**, 871 μL, 877 mg, 10.1 mmol) in MeOH according to *General procedure A* (one-third of the usual batch size). Purification by automated flash chromatography (silica gel 60, *Biotage* SFär Duo 25 g cartridge; gradient of cyclohexane/EtOAc = 75:25 to EtOAc) gave 42 mg (0.16 mmol, 16%) of a yellowish liquid. The product is a mixture of carbamate rotamers in nearly equal amounts. TLC (silica gel 60, EtOAc, ninhydrin staining): R_f = 0.60. ^{1}H NMR (300 MHz, $CDCl_3$): δ [ppm] = 3.70 (4H, t, J = 4.7 Hz), 3.67–3.42 (2H, m), 3.31–3.18 (1H, m), 3.06 (1H, td, J = 10.0, 5.6 Hz), 2.85–2.66 (1H, m), 2.56–2.37 (4H, m), 2.12–1.96 (1H, m), 1.72 (1H, dq, J = 19.0, 9.7 Hz), 1.43 (9H, s). ^{13}C NMR (75 MHz, $CDCl_3$): δ [ppm] = 154.6, 79.6, 66.9, 64.7, 64.1, 52.4, 49.9, 49.5, 45.0, 44.7, 29.6, 28.9, 28.6. GC–MS (EI, 70 eV): m/z = 256 (M^+, 6), 225 (8), 199 (73), 183 (54), 169 (30), 155 (52), 142 (8), 126 (92), 112 (100), 97 (9), 88 (28), 82 (8), 69 (20), 57 (84), 41 (40), 39 (11). No NMR and MS reference data were available for this compound.



***tert*-Butyl *rac*-3-((4-methoxyphenyl)amino)pyrrolidine-1-carboxylate (c16-a24) [CAS 816468-37-8].** Prepared from *tert*-butyl 3-oxopyrrolidine-1-carboxylate (**c16**, 185 mg, 1.0 mmol) and *p*-anisidine (**a24**, 1.23 g, 10.0 mmol) in MeOH according to *General procedure A* (one-third of the usual batch size). Purification by automated flash chromatography (silica gel 60, *Biotage* SFär Duo 25 g cartridge; gradient of cyclohexane/EtOAc = 88:12 to EtOAc) gave 78 mg (0.27 mmol, 27%) of a beige solid. The product is a mixture of carbamate rotamers in nearly equal amounts. TLC (silica gel 60, EtOAc, ninhydrin staining): R_f = 0.60. mp: 102–103 °C; ref.[93] 105 °C. ^{1}H NMR (300 MHz, $CDCl_3$): δ [ppm] = 6.82–6.74 (2H, m), 6.61–6.54 (2H, m), 4.01–3.91 (1H, m), 3.74 (3H, s), 3.73–3.59 (1H, m), 3.53–3.36 (3H, m), 3.29–3.10 (1H, m), 2.15 (1H, dtd, J = 13.1, 7.6, 5.6 Hz), 1.92–1.77 (1H, m), 1.46 (9H, s). ^{13}C NMR (75 MHz, $CDCl_3$): δ [ppm] = 154.7, 152.4, 141.1, 115.0, 114.7, 79.4, 55.8, 53.9, 53.2, 52.2, 51.9, 44.2, 43.9, 31.9, 31.2, 28.6. GC–MS (EI, 70 eV): m/z = 292 (M^+, 70), 236 (100), 219 (24), 192 (14), 161 (56), 149 (59), 134 (37), 123 (16), 108 (9), 77 (7), 57 (46), 41 (24), 39 (9). The characterisation data are in agreement with literature values.[93]

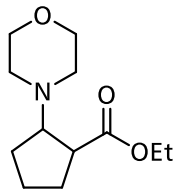


Ethyl *rac*-2-(methylamino)cyclopentane-1-carboxylate (c17-a2) [CAS 1378813-74-1]. Prepared from ethyl 2-oxocyclopentane-1-carboxylate (**c17**, 446 μL, 468 mg, 3.0 mmol) and methylamine (**a2**, 3.07 mL of a 40% w/w solution in MeOH; 0.93 g $MeNH_2$, 30.0 mmol) in MeOH according to *General procedure A*. Purification by automated flash chromatography (silica gel 60, *Biotage* SFär Duo 25 g cartridge; gradient of cyclohexane/EtOAc = 95:5 to EtOAc) gave 69 mg (0.40 mmol, 13%) of a pale-yellowish liquid. The product is a single diastereomer. TLC (silica gel 60, cyclohexane/EtOAc = 3:1, ninhydrin staining): R_f = 0.46. ^{1}H NMR (300 MHz, $CDCl_3$): δ [ppm] = 4.21 (2H, q, J = 7.1 Hz), 3.74 (1H, dt, J = 7.9, 6.8 Hz), 3.04 (1H, dt, J = 9.3, 7.0 Hz), 2.72 (3H, s), 2.29–2.15 (2H, m), 1.98–1.70 (3H, m), 1.29 (3H, t, J = 7.1 Hz). ^{13}C NMR (75 MHz, $CDCl_3$): δ [ppm] = 173.3, 63.1, 62.0, 47.4, 32.5, 29.7, 29.5, 23.7, 14.2. GC–MS (EI, 70 eV): m/z = 171 (M^+, 17), 156 (15), 142 (22), 126 (25), 96 (17), 83 (6), 70 (100), 56 (13), 42 (17). No NMR and MS reference data were available for this compound.



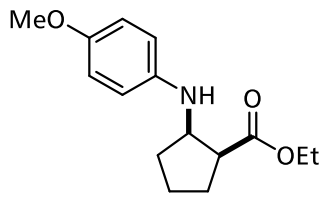
Ethyl *all-rac*-2-(prop-2-yn-1-ylamino)cyclopentane-1-carboxylate (c17-a4). Prepared from ethyl 2-oxocyclopentane-1-carboxylate (**c17**, 151 μL, 159 mg, 1.0 mmol) and propargylamine (**a4**, 640 μL, 550 mg, 10.0 mmol) in EtOH according to *General procedure A* (one-third of the usual batch size). Purification by column chromatography (silica gel 60, cyclohexane/EtOAc = 3:1) gave 14 mg (0.07 mmol, 7%) of a colourless liquid. The product is a mixture of diastereomers in a ratio of approx. 75:25. TLC (silica gel 60, cyclohexane/EtOAc = 3:1, ninhydrin staining): R_f = 0.30. ^{1}H NMR (300 MHz, $CDCl_3$): δ [ppm] = 4.26 (2H minor, qd, J = 7.2, 1.5 Hz), 4.15 (2H major, qd, J = 7.2, 2.5 Hz), 3.67 (1H minor, dt, J = 16.0, 3.6 Hz), 3.53–3.45 (1H minor, m), 3.47 (1H major, dd, J = 17.1, 2.4 Hz), 3.39 (1H major, dd, J = 17.1, 2.5 Hz), 2.97–2.86 (1H major, m), 2.73–2.61 (1H major + minor, m), 2.29 (1H minor, t, J = 2.5 Hz), 2.19 (1H major, t, J = 2.4 Hz), 2.18–2.11 (1H minor, m), 1.94–1.77 (4H major + minor, m), 1.74–1.54 (3H major + minor, m), 1.32 (3H minor, t, J = 7.1 Hz), 1.27 (3H, major, t, J = 7.1 Hz). ^{13}C NMR (75 MHz, $CDCl_3$): δ [ppm] = 174.7 (major), 171.4 (minor), 82.4 (major), 80.6 (minor), 72.4 (minor), 71.2 (major), 64.1 (minor), 61.7 (minor), 60.6 (major), 60.3 (major), 54.8 (minor), 47.7 (major), 38.2 (minor), 36.9 (major), 35.4 (minor), 31.5 (major), 27.5 (major), 25.8 (minor), 22.4 (major), 21.2 (minor), 14.4 (major), 14.3 (minor). GC–MS (EI, 70 eV): m/z = 195 (M^+, <1), 194 (6), 166 (19), 156 (56), 150 (35),

122 (31), 110 (10), 94 (100), 80 (63), 67 (28), 66 (9), 54 (44), 39 (21). HRMS calcd for $C_{11}H_{18}NO_2^+$ [M+H$^+$]: 196.1332, found: 196.1334. No NMR and MS reference data were available for this compound.

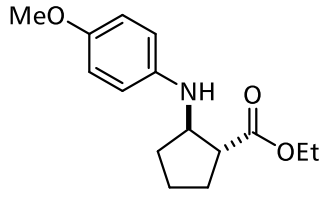


Ethyl *all-rac*-2-morpholinocyclopentane-1-carboxylate (c17-a22) [CAS 2671832-05-4]. Prepared from ethyl 2-oxocyclopentane-1-carboxylate (**c17**, 446 μL, 468 mg, 3.0 mmol) and morpholine (**a22**, 2.61 mL, 2.63 g, 30.2 mmol) in EtOH according to *General procedure A*. The crude product was used without purification. 745 mg (quant.) of a colourless, viscous liquid. TLC (silica gel 60, cyclohexane/EtOAc = 1:1, ninhydrin staining): R_f = 0.61. GC–MS (EI, 70 eV): *m/z* = 227 (M$^+$, 21), 198 (13), 182 (22), 169 (6), 154 (8), 126 (100), 112 (21), 96 (10), 86 (12), 82 (5), 67 (10), 55 (7), 41 (8). No NMR and MS reference data were available for this compound.

Ethyl *rac*-2-((4-methoxyphenyl)amino)cyclopentane-1-carboxylate (c17-a24). Prepared from ethyl 2-oxocyclopentane-1-carboxylate (**c17**, 446 μL, 468 mg, 3.0 mmol) and *p*-anisidine (**a24**, 1.11 g, 9.0 mmol) in EtOH according to *General procedure A* (3 eq. of amine and AcOH). Purification by automated flash chromatography (silica gel 60, *Biotage* SFär Duo 25 g cartridge; gradient of cyclohexane/EtOAc = 95:5 to cyclohexane/EtOAc = 65:35) gave the individual diastereomers, which could be identified by comparing their NMR spectra to literature values.[94]



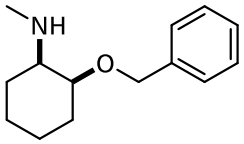
***rac-cis*-c17-a24 [CAS 2222725-08-6].** 30 mg (0.11 mmol, 4%) of an orange liquid. TLC (silica gel 60, cyclohexane/EtOAc = 5:1, ninhydrin staining): R_f = 0.36. ^{1}H NMR (500 MHz, $CDCl_3$): δ [ppm] = 6.77–6.73 (2H, m), 6.59–6.55 (2H, m), 4.05–3.91 (3H, m), 3.73 (3H, s), 3.05 (1H, q, J = 7.5 Hz), 2.12–1.91 (3H, m), 1.86 (1H, dtt, J = 13.1, 8.9, 4.6 Hz), 1.73 (1H, dq, J = 12.4, 7.6 Hz), 1.61 (1H, dquint, J = 12.6, 8.0 Hz), 1.09 (3H, t, J = 7.2 Hz). ^{13}C NMR (126 MHz, $CDCl_3$): δ [ppm] = 174.5, 152.1, 141.8, 114.8, 114.7, 60.4, 58.1, 55.9, 47.2, 32.9, 28.0, 22.5, 14.1. GC–MS (EI, 70 eV): *m/z* = 263 (M$^+$, 90), 248 (7), 234 (10), 218 (17), 188 (11), 175 (9), 162 (100), 149 (46), 134 (35), 122 (15), 108 (18), 95 (10), 77 (9), 67 (12), 41 (7). HRMS calcd for $C_{15}H_{22}NO_3^+$ [M+H$^+$]: 264.1594, found: 264.1596. The characterisation data are in agreement with literature values.[94]



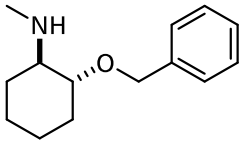
***rac-trans*-c17-a24 [CAS 2222725-09-7].** 234 mg (0.89 mmol, 30%) of a red liquid. TLC (silica gel 60, cyclohexane/EtOAc = 5:1, ninhydrin staining): R_f = 0.28. ^{1}H NMR (500 MHz, $CDCl_3$): δ [ppm] = 6.78–6.74 (2H, m), 6.62–6.58 (2H, m), 4.10 (2H, qd, J = 7.1, 1.7 Hz), 4.01 (1H, q, J = 6.3 Hz), 3.72 (3H, s), 3.38 (1H, br s), 2.63 (1H, ddd, J = 8.7, 7.4, 5.8 Hz), 2.16 (1H, dq, J = 14.4, 7.1 Hz), 2.00 (1H, dtd, J = 14.1, 8.3, 6.0 Hz), 1.91 (1H, dq, J = 13.0, 7.5 Hz), 1.82–1.72 (2H, m), 1.50 (1H, ddt, J = 13.1, 7.9, 6.3 Hz), 1.21 (3H, t, J = 7.2 Hz). ^{13}C NMR (126 MHz, $CDCl_3$): δ [ppm] = 175.4, 152.2, 141.6, 115.0, 114.8, 60.5, 59.6, 55.7, 51.2, 33.6, 28.6, 23.5, 14.2. GC–MS (EI, 70 eV): *m/z* = 263 (M$^+$, 100), 248 (8), 234 (11), 218 (21), 188 (13), 175 (9), 162 (98), 149 (44), 134 (32), 122 (15), 108 (18), 95 (5), 77 (8), 67 (11), 41 (6). The characterisation data are in agreement with literature values.[94]

***rac*-2-(Benzyloxy)-*N*-methylcyclohexan-1-amine (c18-a2).** Prepared from 2-(benzyloxy)-cyclohexan-1-one (**c18**, 190 μL, 209 mg, 1.0 mmol) and methylamine (**a2**, 1.02 mL of a 40% w/w solution in MeOH; 311 mg $MeNH_2$, 10.0 mmol) in MeOH according to *General procedure A* (one-third of the usual batch size). Purification by column chromatography (silica gel 60,

MTBE/MeOH/NH_4OH = 90:9:1) gave the individual diastereomers, which could be identified based on their NOESY NMR spectra. Since each of the two isolated diastereomers contains the other isomer as a minor contaminant, the ^{1}H NMR signal multiplicities given below are based on the number of contributing protons from the major isomer, as deduced from HSQC NMR spectra. The ^{13}C NMR listings are limited to the signals of the major isomer.

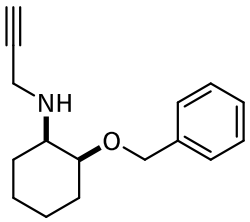


***rac-cis*-c18-a2.** 21 mg (0.10 mmol, 10%) of a pale-yellowish liquid. TLC (silica gel 60, MTBE/MeOH/NH_4OH = 90:9:1, $KMnO_4$ staining): R_f = 0.18. ^{1}H NMR (300 MHz, $CDCl_3$): δ [ppm] = 7.43–7.27 (5H, m), 6.71 (2H, br s), 4.66 (1H, d, J = 11.7 Hz), 4.48 (1H, d, J = 11.7 Hz), 3.90 (1H, quint, J = 2.4 Hz), 3.01 (1H, ddd, J = 11.3, 4.4, 2.9 Hz), 2.48 (3H, s), 2.21–2.06 (1H, m), 1.95–1.68 (3H, m), 1.58–1.41 (2H, m), 1.39–1.21 (2H, m). ^{13}C NMR (75 MHz, $CDCl_3$): δ [ppm] = 137.4, 128.8, 128.5, 128.2, 70.2, 70.2, 60.7, 30.7, 26.6, 24.2, 23.5, 19.0. GC–MS (EI, 70 eV): m/z = 219 (M^+, <1), 128 (100), 113 (61), 110 (8), 91 (46), 79 (14), 70 (33), 65 (11), 57 (8), 44 (11).



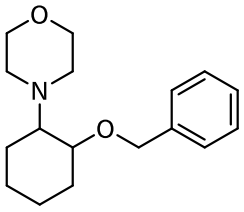
***rac-trans*-c18-a2.** 65 mg (0.30 mmol, 30%) of a pale-yellowish liquid. TLC (silica gel 60, MTBE/MeOH/NH_4OH = 90:9:1, $KMnO_4$ staining): R_f = 0.30. ^{1}H NMR (300 MHz, $CDCl_3$): δ [ppm] = 7.43–7.28 (5H, m), 4.63 (1H, d, J = 11.3 Hz), 4.57 (1H, d, J = 11.3 Hz), 3.54 (1H, td, J = 10.1, 4.4 Hz), 2.86 (1H, ddd, J = 12.3, 9.8, 4.2 Hz), 2.62 (3H, s), 2.29–2.21 (1H, m), 2.20–2.06 (1H, m), 1.87–1.70 (2H, m), 1.55–1.41 (1H, m), 1.39–1.12 (3H, m). ^{13}C NMR (75 MHz, $CDCl_3$): δ [ppm] = 137.4, 128.7, 128.5, 128.2, 77.3, 70.7, 63.3, 30.9, 30.0, 26.2, 23.9, 23.2. GC–MS (EI, 70 eV): m/z = 219 (M^+, <1), 128 (100), 113 (64), 110 (8), 91 (62), 82 (9), 79 (18), 70 (44), 65 (15), 57 (11), 44 (18), 41 (11). HRMS calcd for $C_{14}H_{22}NO^+$ [M+H$^+$]: 220.1696, found: 220.1696.

***rac*-2-(Benzyloxy)-*N*-(prop-2-yn-1-yl)cyclohexan-1-amine (c18-a4).** Prepared from 2-(benzyloxy)cyclohexan-1-one (**c18**, 190 μL, 209 mg, 1.0 mmol) and propargylamine (**a4**, 640 μL, 550 mg, 10.0 mmol) in MeOH according to *General procedure A* (one-third of the usual batch size). Purification by column chromatography (silica gel 60, cyclohexane/EtOAc = 3:1) gave the pure *cis*-diastereomer (70 mg, 0.29 mmol, 29%; identified based on NOESY NMR) along with a mixture of both diastereomers (60 mg, 0.25 mmol, 25%) in a ratio of approx. 40:60 (*cis/trans*).

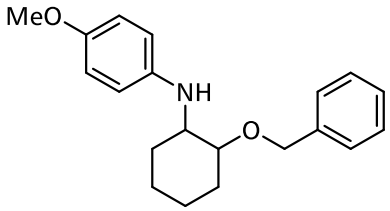


***rac-cis*-c18-a4.** 70 mg (0.29 mmol, 29%) of a yellowish liquid. TLC (silica gel 60, cyclohexane/EtOAc = 1:1, $KMnO_4$ staining): R_f = 0.40. ^{1}H NMR (300 MHz, $CDCl_3$): δ [ppm] = 7.38–7.27 (5H, m), 4.59 (1H, d, J = 11.8 Hz), 4.51 (1H, d, J = 11.8 Hz), 3.64 (1H, dt, J = 7.3, 3.1 Hz), 3.46 (1H, dd, J = 17.0, 2.5 Hz), 3.34 (1H, dd, J = 17.0, 2.4 Hz), 2.98 (1H, dt, J = 7.7, 3.4 Hz), 2.18 (1H, t, J = 2.4 Hz), 2.02–1.88 (1H, m), 1.77 (1H, br s), 1.72–1.14 (7H, m). ^{13}C NMR (75 MHz, $CDCl_3$): δ [ppm] = 139.1, 128.5, 127.7, 127.6, 82.9, 76.4, 71.0, 70.0, 55.4, 35.3, 27.5, 27.5, 22.5, 22.1. GC–MS (EI, 70 eV): m/z = 243 (M^+, <1), 152 (91), 136 (11), 120 (12), 108 (15), 94 (57), 91 (100), 80 (25), 65 (23), 56 (49), 54 (15), 39 (22). HRMS calcd for $C_{16}H_{22}NO^+$ [M+H$^+$]: 244.1696, found: 244.1697. No NMR and MS reference data were available for this compound.

***rac-trans*-c18-a4.** TLC (silica gel 60, cyclohexane/EtOAc = 1:1, $KMnO_4$ staining): R_f = 0.30. GC–MS (EI, 70 eV): m/z = 243 (M^+, <1), 152 (100), 136 (12), 120 (12), 108 (15), 94 (53), 91 (96), 80 (26), 65 (24), 56 (44), 54 (14), 39 (20). No NMR and MS reference data were available for this compound.

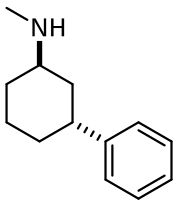


***rac*-4-(2-(Benzyloxy)cyclohexyl)morpholine (c18-a22).** Prepared from 2-(benzyloxy)cyclohexan-1-one (**c18**, 190 μL, 209 mg, 1.0 mmol) and morpholine (**a22**, 871 μL, 877 mg, 10.1 mmol) in MeOH according to *General procedure A* (one-third of the usual batch size). Purification by automated flash chromatography (silica gel 60, *Biotage* SFär Duo 5 g cartridge; gradient of cyclohexane/EtOAc = 95:5 to cyclohexane/EtOAc = 50:50) gave 37 mg (0.13 mmol, 13%) of an orange liquid. The product is a single diastereomer. TLC (silica gel 60, cyclohexane/EtOAc = 3:1, $KMnO_4$ staining): R_f = 0.57. ^{1}H NMR (300 MHz, $CDCl_3$): δ [ppm] = 7.43–7.22 (5H, m), 4.67 (1H, d, J = 11.7 Hz), 4.61 (1H, d, J = 11.7 Hz), 3.75–3.62 (4H, m), 3.34 (1H, td, J = 9.7, 4.2 Hz), 2.70–2.55 (4H, m), 2.45 (1H, td, J = 10.1, 3.6 Hz), 2.23–2.10 (1H, m), 1.93–1.57 (3H, m), 1.36–1.03 (4H, m). ^{13}C NMR (75 MHz, $CDCl_3$): δ [ppm] = 139.2, 128.4, 128.0, 127.6, 77.3, 70.8, 68.0, 67.9, 49.7, 31.5, 25.7, 25.1, 24.5. GC–MS (EI, 70 eV): m/z = 275 (M^+, <1), 184 (100), 126 (22), 91 (30), 87 (63), 65 (6), 55 (7), 41 (7). HRMS calcd for $C_{17}H_{26}NO_2^+$ [M+H$^+$]: 276.1958, found: 276.1959. No NMR and MS reference data were available for this compound.



***all-rac-N*-(2-(Benzyloxy)cyclohexyl)-4-methoxyaniline (c18-a24).** Prepared from 2-(benzyloxy)cyclohexan-1-one (**c18**, 190 μL, 209 mg, 1.0 mmol) and *p*-anisidine (**a24**, 1.23 g, 10.0 mmol) in MeOH according to *General procedure A* (one-third of the usual batch size). Purification by automated flash chromatography (silica gel 60, *Biotage* SFär Duo 25 g cartridge; gradient of cyclohexane/EtOAc = 95:5 to cyclohexane/EtOAc = 65:35) gave 245 mg (0.79 mmol, 79%) of a red liquid. The product is a mixture of diastereomers in a ratio of approx. 80:20. TLC (silica gel 60, cyclohexane/EtOAc = 5:1, ninhydrin staining): R_f = 0.42. ^{1}H NMR (300 MHz, $CDCl_3$): δ [ppm] = 7.37–7.17 (5H major + minor, m), 6.79–6.69 (2H major + minor, m), 6.65–6.49 (2H major + minor, m), 4.64 (1H minor, d, J = 11.9 Hz), 4.58 (1H major, d, J = 11.7 Hz), 4.47 (1H minor, d, J = 11.8 Hz), 4.35 (1H major, d, J = 11.7 Hz), 3.79–3.66 (1H major + minor, m), 3.72 (3H major + minor, s), 3.30 (1H major, dt, J = 10.4, 3.0 Hz), 3.16 (1H minor, td, J = 9.0, 3.9 Hz), 2.22–1.97 (1H major + minor, m), 1.83–1.10 (7H major + minor, m). ^{13}C NMR (75 MHz, $CDCl_3$): δ [ppm] = 152.3 (minor), 152.1 (major), 142.3 (minor), 141.6 (major), 139.0 (major), 138.9 (minor), 128.4 (minor), 128.4 (major), 127.8 (minor), 127.6 (major + minor), 127.5 (major), 115.7 (minor), 115.5 (major), 114.9 (major), 114.8 (minor), 80.7 (minor), 75.6 (major), 70.7 (minor), 70.5 (major), 57.9 (minor), 55.8 (minor), 55.8 (major), 55.2 (major), 31.5 (minor), 30.0 (minor), 28.2 (major), 27.7 (major), 24.5 (major), 23.9 (minor), 20.4 (major + minor). GC–MS (EI, 70 eV): m/z = 311 (M^+, 56), 220 (76), 162 (30), 149 (17), 134 (25), 123 (100), 108 (13), 91 (45), 77 (10), 65 (10). HRMS calcd for $C_{20}H_{26}NO_2^+$ [M+H]$^+$: 312.1958, found: 312.1960. No NMR and MS reference data were available for this compound.

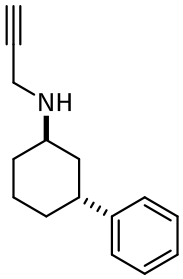
***rac-N*-Methyl-3-phenylcyclohexan-1-amine (c19-a2) [CAS 26400-08-8].** Prepared from 3-phenylcyclohexan-1-one (**c19**, 181 μL, 174 mg, 1.0 mmol) and methylamine (**a2**, 1.02 mL of a 40% w/w solution in MeOH; 311 mg $MeNH_2$, 10.0 mmol) in MeOH according to *General procedure A* (one-third of the usual batch size). Purification by column chromatography (silica gel 60, gradient of MTBE/MeOH/NH_4OH = 90:9:1 to MTBE/MeOH = 50:50) gave the pure *trans*-diastereomer (27 mg, 0.14 mmol, 14%; identified based on NOESY NMR) along with a mixture of both diastereomers (36 mg, 0.19 mmol, 19%) in a ratio of approx. 47:53 (*cis/trans*).



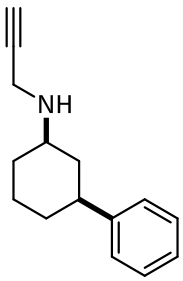
***rac-trans*-c19-a2.** 27 mg (0.14 mmol, 14%) of a colourless solid. TLC (silica gel 60, MTBE/MeOH/NH_4OH = 80:19:1, $KMnO_4$ staining): R_f = 0.07. mp: 122–124 °C. ^{1}H NMR (300 MHz, $CDCl_3$): δ [ppm] = 7.27–7.06 (5H, m), 6.16 (1H, br s), 3.06 (1H, t, J = 3.7 Hz), 3.02 (tt, J = 11.4, 3.8 Hz), 2.50 (3H, s), 2.03 (1H, dtt, J = 14.0, 3.7, 1.8 Hz), 1.94–1.69 (4H, m), 1.64–1.43 (3H, m). ^{13}C NMR (75 MHz, $CDCl_3$): δ [ppm] = 146.1, 128.6, 127.0, 126.2, 55.5, 37.2, 35.8, 33.2, 32.8, 28.5, 20.6. GC–MS (EI, 70 eV): m/z = 281 (M^+, 100), 238 (71), 162 (42), 149 (28), 134 (20), 123 (54), 117 (11), 108 (21), 91 (42), 77 (10). No NMR and MS reference data were available for this compound.

***rac-cis*-c19-a2.** TLC (silica gel 60, MTBE/MeOH/NH_4OH = 80:19:1, $KMnO_4$ staining): R_f = 0.04. GC–MS (EI, 70 eV): m/z = 189 (M^+, 25), 158 (61), 146 (100), 143 (14), 130 (14), 115 (17), 104 (14), 91 (30), 84 (9), 77 (10), 70 (80), 57 (41), 42 (14). No NMR and MS reference data were available for this compound.

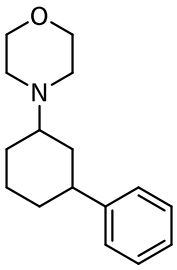
***rac*-3-Phenyl-*N*-(prop-2-yn-1-yl)cyclohexan-1-amine (c19-a4) [CAS 1870592-12-3].** Prepared from 3-phenylcyclohexan-1-one (**c19**, 181 μL, 174 mg, 1.0 mmol) and propargylamine (**a4**, 640 μL, 550 mg, 10.0 mmol) in MeOH according to *General procedure A* (one-third of the usual batch size). Purification by automated flash chromatography (silica gel 60, *Biotage* SFär Duo 25 g cartridge; gradient of cyclohexane/EtOAc = 88:12 to EtOAc) gave the individual diastereomers, which could be identified based on their NOESY NMR spectra.



***rac-trans*-c19-a4.** 22 mg (0.10 mmol, 10%) of a yellowish liquid. TLC (silica gel 60, cyclohexane/EtOAc = 3:1, ninhydrin staining): R_f = 0.47. ^{1}H NMR (300 MHz, $CDCl_3$): δ [ppm] = 7.34–7.11 (5H, m), 3.46 (2H, d, J = 2.4 Hz), 3.25 (1H, quint, J = 3.6 Hz), 2.96 (1H, ddt, J = 11.9, 6.9, 3.4 Hz), 2.20 (1H, t, J = 2.4 Hz), 1.94–1.38 (8H, m), 1.26 (1H, br s). ^{13}C NMR (75 MHz, $CDCl_3$): δ [ppm] = 147.5, 128.4, 127.1, 126.0, 82.7, 71.2, 51.2, 37.7, 37.7, 35.9, 34.2, 30.0, 20.9. GC–MS (EI, 70 eV): m/z = 213 (M^+, 7), 170 (76), 158 (100), 143 (17), 130 (17), 115 (17), 104 (14), 94 (45), 91 (30), 80 (51), 77 (11), 68 (8), 53 (6), 39 (13). No NMR and MS reference data were available for this compound.

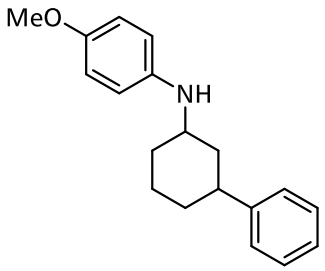


***rac-cis*-c19-a4.** 12 mg (0.06 mmol, 6%) of a yellowish liquid. TLC (silica gel 60, cyclohexane/EtOAc = 3:1, ninhydrin staining): R_f = 0.51. ^{1}H NMR (300 MHz, $CDCl_3$): δ [ppm] = 7.34–7.14 (5H, m), 3.48 (2H, d, J = 2.4 Hz), 2.84 (1H, tt, J = 11.1, 3.7 Hz), 2.60 (1H, tt, J = 12.0, 3.2 Hz), 2.21 (1H, t, J = 2.4 Hz), 2.13–1.76 (4H, m), 1.57–1.03 (5H, m). ^{13}C NMR (75 MHz, $CDCl_3$): δ [ppm] = 146.9, 128.5, 127.0, 126.2, 82.5, 71.3, 55.4, 43.2, 40.7, 35.3, 34.2, 32.8, 25.1. GC–MS (EI, 70 eV): m/z = 213 (M^+, 10), 170 (100), 158 (61), 143 (10), 130 (9), 115 (15), 104 (12), 94 (46), 91 (29), 80 (52), 77 (9), 68 (8), 53 (6), 39 (12). HRMS calcd for $C_{15}H_{20}N^+$ [M+H$^+$]: 214.1590, found: 214.1591. No NMR and MS reference data were available for this compound.

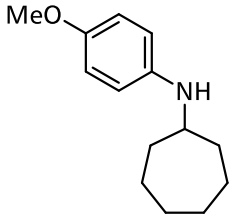


***all-rac*-4-(3-Phenylcyclohexyl)morpholine (c19-a22).** Prepared from 3-phenylcyclohexan-1-one (**c19**, 181 μL, 174 mg, 1.0 mmol) and morpholine (**a22**, 871 μL, 877 mg, 10.1 mmol) in MeOH according to *General procedure A* (one-third of the usual batch size). Purification by automated flash chromatography (silica gel 60, *Biotage* SFär Duo 5 g cartridge; gradient of cyclohexane/EtOAc = 88:12 to EtOAc) gave 33 mg (0.13 mmol, 13%) of a yellow liquid. The product is a mixture of diastereomers in a ratio of approx. 82:18. TLC (silica gel 60, cyclohexane/EtOAc = 1:1, $KMnO_4$ staining): R_f = 0.57. ^{1}H NMR (300 MHz, $CDCl_3$): δ [ppm] = 7.35–7.12 (5H major + minor, m), 4.23 (1H

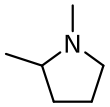
minor, quint, J = 3.1 Hz), 3.78–3.69 (4H major + minor, m), 3.02 (1H major, tt, J = 11.6, 3.4 Hz), 2.58 (1H minor, tt, J = 12.2, 3.4 Hz), 2.53–2.42 (4H major, m), 2.39–2.28 (4H minor, m), 2.20–1.16 (9H major + minor, m). ^{13}C NMR (75 MHz, $CDCl_3$): δ [ppm] = 147.4 (major), 147.2 (minor), 128.5 (minor), 128.4 (major), 127.1 (minor), 127.0 (major), 126.1 (minor), 125.9 (major), 67.5 (major + minor), 66.9 (minor), 59.4 (major), 50.7 (major + minor), 40.6 (minor), 37.6 (minor), 37.4 (major), 35.5 (major), 34.4 (major), 33.9 (minor), 32.5 (minor), 28.1 (major), 20.9 (major), 20.5 (minor). GC–MS (EI, 70 eV): *m/z* = 245 (M^+, 29), 202 (100), 158 (17), 143 (5), 126 (50), 115 (8), 100 (9), 91 (20), 55 (9). HRMS calcd for $C_{16}H_{24}NO^+$ [M+H$^+$]: 246.1852, found: 246.1854. No NMR and MS reference data were available for this compound.



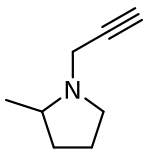
***rac*-4-Methoxy-*N*-(3-phenylcyclohexyl)aniline (c19-a24).** Prepared from 3-phenylcyclohexan-1-one (**c19**, 181 μL, 174 mg, 1.0 mmol) and *p*-anisidine (**a24**, 1.23 g, 10.0 mmol) in MeOH according to *General procedure A* (one-third of the usual batch size). Purification by automated flash chromatography (silica gel 60, *Biotage* SFär Duo 25 g cartridge; gradient of cyclohexane/EtOAc = 95:5 to cyclohexane/EtOAc = 50:50) gave 69 mg (0.25 mmol, 25%) of an orange solid. The product is a single diastereomer. TLC (silica gel 60, cyclohexane/EtOAc = 3:1, ninhydrin staining): R_f = 0.49. mp: 87–89 °C. ^{1}H NMR (300 MHz, $CDCl_3$): δ [ppm] = 7.32–7.12 (5H, m), 6.81–6.72 (2H, m), 6.64–6.56 (2H, m), 3.79–3.69 (1H, m), 3.73 (3H, s), 3.62 (1H, br s), 2.83 (1H, tt, J = 11.9, 3.3 Hz), 2.06 (1H, dtt, J = 13.2, 3.6, 1.9 Hz), 1.96–1.85 (2H, m), 1.80–1.44 (5H, m). ^{13}C NMR (75 MHz, $CDCl_3$): δ [ppm] = 152.0, 146.9, 141.7, 128.5, 127.0, 126.1, 115.1, 114.8, 55.9, 48.9, 38.2, 37.7, 33.7, 29.9, 21.1. GC–MS (EI, 70 eV): *m/z* = 281 (M^+, 100), 238 (71), 162 (42), 149 (28), 134 (20), 123 (54), 117 (11), 108 (21), 91 (42), 77 (10). HRMS calcd for $C_{19}H_{24}NO^+$ [M+H$^+$]: 282.1852, found: 282.1853. No NMR and MS reference data were available for this compound.



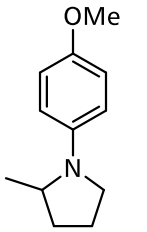
***N*-(4-Methoxyphenyl)cycloheptanamine (c20-a24) [CAS 227017-92-7].** Prepared from cycloheptanone (**c20**, 354 μL, 337 mg, 3.0 mmol) and *p*-anisidine (**a24**, 3.69 g, 30.0 mmol) in MeOH according to *General procedure A*. Purification by automated flash chromatography (silica gel 60, *Biotage* SFär Duo 25 g cartridge; gradient of cyclohexane/EtOAc = 92:8 to EtOAc) gave 611 mg (2.79 mmol, 93%) of a red liquid. TLC (silica gel 60, cyclohexane/EtOAc = 2:1, ninhydrin staining): R_f = 0.75. ^{1}H NMR (300 MHz, $CDCl_3$): δ [ppm] = 6.80–6.71 (2H, m), 6.56–6.49 (2H, m), 3.73 (3H, s), 3.37 (1H, dquint, J = 8.4, 4.1 Hz), 3.22 (1H, br s), 2.05–1.92 (2H, m), 1.73–1.32 (10H, m). ^{13}C NMR (75 MHz, $CDCl_3$): δ [ppm] = 151.8, 141.7, 115.0, 114.9, 55.9, 54.7, 35.0, 28.5, 24.6. GC–MS (EI, 70 eV): *m/z* = 219 (M^+, 60), 176 (12), 162 (100), 149 (23), 134 (15), 123 (9), 108 (19), 55 (7), 41 (6). No NMR and MS reference data were available for this compound.



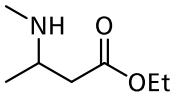
***rac*-1,2-Dimethylpyrrolidine (c21-a2) [CAS 802822-49-7].** Prepared from 5-chloropentan-2-one (**c21**, 402 μL of a preparation with 85% purity; 362 mg compound, 3.0 mmol) and methylamine (**a2**, 3.07 mL of a 40% w/w solution in MeOH; 0.93 g $MeNH_2$, 30.0 mmol) in MeOH according to *General procedure A*. To avoid loss of the volatile substance (bp 84–87 °C),[95] the crude product was used as GC reference material without purification. 317 mg (quant.) of an orange liquid. TLC (silica gel 60, MTBE/MeOH/NH_4OH = 90:9:1, $KMnO_4$ staining): R_f = 0.15. GC–MS (EI, 70 eV): *m/z* = 99 (M^+, 14), 84 (100), 71 (10), 56 (16), 42 (24). The MS spectrum is in agreement with literature values.[95]



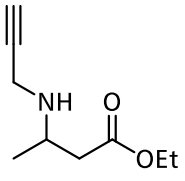
***rac*-2-Methyl-1-(prop-2-yn-1-yl)pyrrolidine (c21-a4) [CAS 1219931-38-0].** Prepared from 5-chloropentan-2-one (**c21**, 402 μL of a preparation with 85% purity; 362 mg compound, 3.0 mmol) and propargylamine (**a4**, 961 μL, 826 mg, 15.0 mmol) in MeOH according to *General procedure A* (5 eq. of amine and AcOH). Purification by column chromatography (silica gel 60, Et_2O) gave 43 mg (0.35 mmol, 12%) of an orange-brownish liquid. TLC (silica gel 60, EtOAc, ninhydrin staining): R_f = 0.25. ^{1}H NMR (300 MHz, $CDCl_3$): δ [ppm] = 3.55 (1H, dd, J = 17.1, 2.4 Hz), 3.37 (1H, dd, J = 17.1, 2.4 Hz), 3.03 (1H, ddd, J = 9.2, 8.0, 2.8 Hz), 2.62–2.47 (2H, m), 2.17 (1H, t, J = 2.4 Hz), 1.94 (1H, dddd, J = 12.0, 9.5, 7.1, 5.0 Hz), 1.85–1.63 (2H, m), 1.43 (1H, dddd, J = 12.0, 10.3, 8.8, 6.0 Hz), 1.08 (3H, d, J = 6.1 Hz). ^{13}C NMR (75 MHz, $CDCl_3$): δ [ppm] = 78.9, 72.6, 57.0, 52.8, 40.2, 32.9, 21.6, 18.6. GC–MS (EI, 70 eV): m/z = 123 (M^+, 8), 122 (9), 108 (100), 80 (5), 68 (9), 56 (9), 39 (13). No NMR and MS reference data were available for this compound.



***rac*-1-(4-Methoxyphenyl)-2-methylpyrrolidine (c21-a24) [CAS 105972-02-9].** Prepared from 5-chloropentan-2-one (**c21**, 402 μL of a preparation with 85% purity; 362 mg compound, 3.0 mmol) and *p*-anisidine (**a24**, 3.69 g, 30.0 mmol) in MeOH according to *General procedure A*. Purification by automated flash chromatography (silica gel 60, *Biotage* SFär Duo 25 g cartridge; gradient of cyclohexane/EtOAc = 88:12 to EtOAc) gave 421 mg (2.20 mmol, 73%) of a brownish liquid. TLC (silica gel 60, cyclohexane/EtOAc = 1:1, ninhydrin staining): R_f = 0.89. ^{1}H NMR (300 MHz, $CDCl_3$): δ [ppm] = 6.91–6.82 (2H, m), 6.58 (2H, d, J = 8.5 Hz), 3.86–3.75 (1H, m), 3.78 (3H, s), 3.47–3.36 (1H, m), 3.18–3.07 (1H, m), 2.16–1.92 (3H, m), 1.78–1.62 (1H, m), 1.18 (3H, d, J = 6.2 Hz). ^{13}C NMR (75 MHz, $CDCl_3$): δ [ppm] = 150.7, 142.5, 115.2, 112.8, 56.1, 54.2, 49.1, 33.3, 23.5, 19.7. GC–MS (EI, 70 eV): m/z = 191 (M^+, 26), 176 (100), 161 (6), 134 (7), 77 (5). The characterisation data are in agreement with literature values.[96]

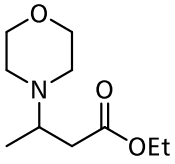


Ethyl *rac*-3-(methylamino)butanoate (c22-a2) [CAS 68384-70-3]. Prepared from ethyl acetoacetate (**c22**, 127 μL, 130 mg, 1.0 mmol) and methylamine (**a2**, 866 μL of a 40% w/w solution in water; 312 mg $MeNH_2$, 10.0 mmol) in EtOH according to *General procedure A* (one-third of the usual batch size). The crude product, which contains approx. 10% enamine, was used as GC reference material without purification. 14 mg (0.07 mmol, 7%) of a colourless liquid. TLC (silica gel 60, MTBE/MeOH/ NH_4OH = 90:9:1, $KMnO_4$ staining): R_f = 0.22. ^{1}H NMR (300 MHz, $CDCl_3$): δ [ppm] = 4.16 (2H, q, J = 7.2 Hz), 3.08 (1H, q, J = 6.4 Hz), 3.02 (1H, br s), 2.51 (1H, dd, J = 15.6, 6.7 Hz), 2.46 (3H, s), 2.38 (1H, dd, J = 15.6, 6.0 Hz), 1.27 (3H, t, J = 7.1 Hz), 1.16 (3H, d, J = 6.4 Hz). ^{13}C NMR (75 MHz, $CDCl_3$): δ [ppm] = 172.3, 60.7, 52.0, 40.7, 33.3, 19.6, 14.3. GC–MS (EI, 70 eV): m/z = 145 (M^+, 2), 130 (20), 84 (15), 58 (100), 42 (13). The characterisation data are in agreement with literature values.[97]

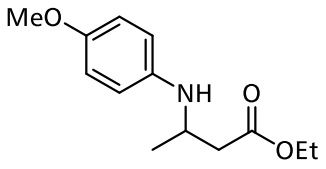


Ethyl *rac*-3-(prop-2-yn-1-ylamino)butanoate (c22-a4). Prepared from ethyl acetoacetate (**c22**, 127 μL, 130 mg, 1.0 mmol) and propargylamine (**a4**, 640 μL, 550 mg, 10.0 mmol) in EtOH according to *General procedure A* (one-third of the usual batch size). The crude product, which contains approx. 9% enamine, was used without purification. 157 mg (0.93 mmol, 93%) of a yellow liquid. TLC (silica gel 60, EtOAc, $KMnO_4$ staining): R_f = 0.48. ^{1}H NMR (300 MHz, $CDCl_3$): δ [ppm] = 4.15 (2H, q, J = 7.1 Hz), 3.46 (1H, d, J = 2.5 Hz), 3.44 (1H, d, J = 2.4 Hz), 3.31 (1H, q, J = 6.4 Hz), 2.45 (1H, dd, J = 15.4, 6.8 Hz), 2.36 (1H, dd, J = 15.4, 5.9 Hz), 2.22 (1H, t, J = 2.5 Hz), 1.27 (3H, t, J = 7.1 Hz), 1.13 (3H, d, J = 6.4 Hz). ^{13}C NMR (75 MHz, $CDCl_3$): δ [ppm] = 172.3, 82.0, 71.5, 60.5, 48.7, 41.5, 35.6, 20.0, 14.3. GC–MS (EI, 70 eV): m/z = 154

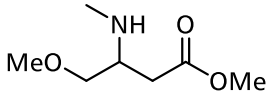
(M^+–CH_3, 10), 130 (9), 108 (11), 96 (8), 82 (100), 66 (8), 54 (19), 42 (10). HRMS calcd for $C_9H_{16}NO_2^+$ [M+H$^+$]: 170.1176, found: 170.1175. No NMR and MS reference data were available for this compound.



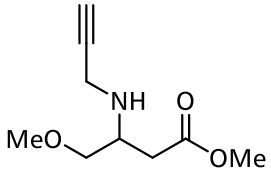
Ethyl *rac*-3-morpholinobutanoate (c22-a22) [CAS 42980-69-8]. Prepared from ethyl acetoacetate (**c22**, 127 μL, 130 mg, 1.0 mmol) and morpholine (**a22**, 871 μL, 877 mg, 10.1 mmol) in EtOH according to *General procedure A* (one-third of the usual batch size). Purification by column chromatography (silica gel 60, cyclohexane/EtOAc = 1:2) gave 105 mg (0.52 mmol, 52%) of a colourless liquid. TLC (silica gel 60, cyclohexane/EtOAc = 3:1, $KMnO_4$ staining): R_f = 0.24. ^{1}H NMR (300 MHz, $CDCl_3$): δ [ppm] = 4.15 (2H, q, J = 7.1 Hz), 3.68 (4H, t, J = 4.7 Hz), 3.12 (1H, dquint, J = 7.8, 6.7 Hz), 2.64–2.43 (5H, m), 2.25 (1H, dd, J = 14.3, 7.8 Hz), 1.26 (3H, t, J = 7.1 Hz), 1.06 (3H, d, J = 6.7 Hz). ^{13}C NMR (75 MHz, $CDCl_3$): δ [ppm] = 172.6, 67.5, 60.4, 56.8, 48.8, 38.6, 14.8, 14.4. GC–MS (EI, 70 eV): m/z = 201 (M^+, 7), 186 (16), 114 (100), 70 (8), 56 (10), 42 (7). No NMR and MS reference data were available for this compound.



Ethyl *rac*-3-((4-methoxyphenyl)amino)butanoate (c22-a24) [CAS 870654-46-9]. Prepared from ethyl acetoacetate (**c22**, 383 μL, 391 mg, 3.0 mmol) and *p*-anisidine (**a24**, 3.69 g, 30.0 mmol) in EtOH according to *General procedure A*. Purification by automated flash chromatography (silica gel 60, *Biotage* SFär Duo 25 g cartridge; gradient of cyclohexane/EtOAc = 92:8 to EtOAc) gave 687 mg (2.90 mmol, 96%) of a brownish liquid. TLC (silica gel 60, cyclohexane/EtOAc = 3:1, $KMnO_4$ staining): R_f = 0.44. ^{1}H NMR (300 MHz, $CDCl_3$): δ [ppm] = 6.81–6.75 (2H, m), 6.64–6.57 (2H, m), 4.13 (2H, q, J = 7.1 Hz), 3.91–3.78 (1H, m), 3.74 (3H, s), 3.45 (1H, br s), 2.59 (1H, dd, J = 15.0, 5.3 Hz), 2.39 (1H, dd, J = 15.0, 6.8 Hz), 1.25 (3H, t, J = 7.1 Hz), 1.25 (3H, d, J = 6.4 Hz). ^{13}C NMR (75 MHz, $CDCl_3$): δ [ppm] = 172.1, 152.6, 141.1, 115.6, 115.1, 60.5, 55.9, 47.4, 41.1, 20.8, 14.4. GC–MS (EI, 70 eV): m/z = 237 (M^+, 33), 222 (9), 150 (100), 134 (13). The characterisation data are in agreement with literature values.[97]

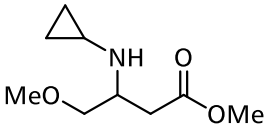


Methyl *rac*-4-methoxy-3-(methylamino)butanoate (c23-a2) [CAS 1780236-95-4]. Prepared from methyl 4-methoxy-3-oxobutanoate (**c23**, 388 μL, 438 mg, 3.0 mmol) and methylamine (**a2**, 1.53 mL of a 40% w/w solution in MeOH; 466 mg $MeNH_2$, 15.0 mmol) in MeOH according to *General procedure A* (5 eq. of amine and AcOH). Purification by column chromatography (silica gel 60, MTBE/MeOH/NH_4OH = 90:9:1) gave 136 mg (0.84 mmol, 28%) of a pale-yellowish liquid. TLC (silica gel 60, MTBE/MeOH/NH_4OH = 90:9:1, $KMnO_4$ staining): R_f = 0.09. ^{1}H NMR (300 MHz, $CDCl_3$): δ [ppm] = 3.76 (3H, s), 3.74–3.57 (3H, m), 3.42 (3H, s), 2.84 (2H, dd, J = 5.9, 3.1 Hz), 2.81 (3H, s). ^{13}C NMR (75 MHz, $CDCl_3$): δ [ppm] = 170.9, 69.6, 59.5, 56.2, 52.9, 32.4, 31.9. GC–MS (EI, 70 eV): m/z = 116 (M^+–$MeOCH_2$, 100), 88 (34), 84 (47), 74 (13), 56 (13), 42 (31). No NMR and MS reference data were available for this compound.

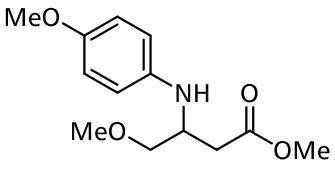


Methyl *rac*-4-methoxy-3-(prop-2-yn-1-ylamino)butanoate (c23-a4). Prepared from methyl 4-methoxy-3-oxobutanoate (**c23**, 133 μL, 150 mg, 1.0 mmol) and propargylamine (**a4**, 640 μL, 550 mg, 10.0 mmol) in MeOH according to *General procedure A* (one-third of the usual batch size). Purification by column chromatography (silica gel 60, gradient of cyclohexane/CH_2Cl_2 = 1:1 to methanol) gave 97 mg (0.52 mmol, 52%) of a brownish liquid. TLC (silica gel 60, EtOAc, $KMnO_4$ staining): R_f = 0.52. ^{1}H NMR (300 MHz, $CDCl_3$): δ [ppm] = 3.69 (3H, s), 3.48 (1H, d, J = 2.4 Hz), 3.48 (1H, d, J = 2.5 Hz), 3.46–3.37

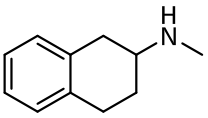
(3H, m), 3.36 (3H, s), 2.49 (2H, d, J = 5.6 Hz), 2.23 (1H, t, J = 2.4 Hz), 1.94 (1H, br s). ^{13}C NMR (75 MHz, $CDCl_3$): δ [ppm] = 172.5, 82.0, 74.4, 71.7, 59.1, 53.0, 51.8, 36.5, 36.0. GC–MS (EI, 70 eV): m/z = 140 (M^+–$MeOCH_2$, 100), 112 (14), 108 (31), 98 (9), 80 (15), 66 (27), 53 (7), 39 (9). HRMS calcd for $C_9H_{16}NO_3^+$ [M+H$^+$]: 186.1125, found: 186.1129. No NMR and MS reference data were available for this compound.



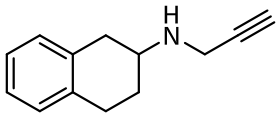
Methyl *rac*-3-(cyclopropylamino)-4-methoxybutanoate (c23-a10) [CAS 2106293-91-6]. Prepared from methyl 4-methoxy-3-oxobutanoate (**c23**, 133 μL, 150 mg, 1.0 mmol) and cyclopropanamine (**a10**, 348 μL, 286 mg, 5.0 mmol) in MeOH according to *General procedure A* (one-third of the usual batch size, 5 eq. of amine and AcOH). Purification by column chromatography (silica gel 60, cyclohexane/EtOAc = 1:1) gave 140 mg (0.75 mmol, 75%) of a yellowish liquid. TLC (silica gel 60, cyclohexane/EtOAc = 2:1, $KMnO_4$ staining): R_f = 0.18. ^{1}H NMR (300 MHz, $CDCl_3$): δ [ppm] = 3.66 (3H, s), 3.46–3.34 (2H, m), 3.33 (3H, s), 3.31–3.25 (1H, m), 2.55 (1H, dd, J = 15.6, 6.5 Hz), 2.44 (1H, dd, J = 15.6, 6.3 Hz), 2.36 (1H, br s), 2.10 (1H, tt, J = 6.6, 3.7 Hz), 0.46–0.37 (2H, m), 0.35–0.27 (2H, m). ^{13}C NMR (75 MHz, $CDCl_3$): δ [ppm] = 172.9, 74.3, 59.1, 55.0, 51.6, 36.9, 28.4, 6.9, 6.3. GC–MS (EI, 70 eV): m/z = 187 (M^+, 1), 155 (13), 142 (100), 114 (25), 110 (32), 100 (18), 82 (19), 71 (18), 68 (49), 41 (21). No NMR and MS reference data were available for this compound.



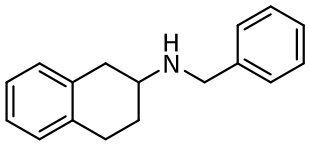
Methyl *rac*-4-methoxy-3-((4-methoxyphenyl)amino)-butanoate (c23-a24). Prepared from methyl 4-methoxy-3-oxobutanoate (**c23**, 133 μL, 150 mg, 1.0 mmol) and *p*-anisidine (**a24**, 1.23 g, 10.0 mmol) in MeOH according to *General procedure A* (one-third of the usual batch size). Purification by automated flash chromatography (silica gel 60, *Biotage* SFär Duo 50 g cartridge; gradient of cyclohexane/EtOAc = 92:8 to EtOAc) gave 48 mg (0.19 mmol, 19%) of a brownish liquid. TLC (silica gel 60, cyclohexane/EtOAc = 2:1, $KMnO_4$ staining): R_f = 0.52. ^{1}H NMR (300 MHz, CD_3OD): δ [ppm] = 6.78–6.72 (2H, m), 6.69–6.63 (2H, m), 3.94–3.81 (1H, m), 3.70 (3H, s), 3.63 (3H, s), 3.47 (1H, dd, J = 9.4, 4.2 Hz), 3.38 (1H, dd, J = 9.5, 5.9 Hz), 3.32 (3H, s), 2.58 (1H, dd, J = 15.3, 6.5 Hz), 2.51 (1H, dd, J = 15.2, 6.7 Hz). ^{13}C NMR (75 MHz, CD_3OD): δ [ppm] = 174.3, 154.1, 142.5, 117.1, 115.8, 74.9, 59.3, 56.1, 53.0, 52.1, 37.7. GC–MS (EI, 70 eV): m/z = 253 (M^+, 21), 208 (100), 180 (10), 148 (47), 134 (49), 107 (8), 77 (6), 45 (6). HRMS calcd for $C_{13}H_{20}NO_4^+$ [M+H$^+$]: 254.1387, found: 254.1390. No NMR and MS reference data were available for this compound.



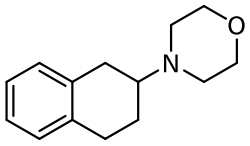
***rac*-*N*-Methyl-1,2,3,4-tetrahydronaphthalen-2-amine (c24-a2) [CAS 19485-85-9].** Prepared from 2-tetralone (**c24**, 403 μL, 447 mg, 3.1 mmol) and methylamine (**a2**, 3.07 mL of a 40% w/w solution in MeOH; 0.93 g $MeNH_2$, 30.0 mmol) in MeOH according to *General procedure A*. The crude product was used without purification. 708 mg (quant.) of a purple liquid. TLC (silica gel 60, MTBE/MeOH/NH_4OH = 90:9:1, $KMnO_4$ staining): R_f = 0.15. ^{1}H NMR (300 MHz, $CDCl_3$): δ [ppm] = 7.17–7.03 (4H, m), 6.10 (1H, br s), 3.18–3.05 (2H, m), 2.92–2.71 (3H, m), 2.62 (3H, s), 2.26–2.11 (1H, m), 1.85–1.67 (1H, m). ^{13}C NMR (75 MHz, $CDCl_3$): δ [ppm] = 135.1, 132.9, 129.4, 128.8, 126.5, 126.2, 55.8, 33.6, 31.8, 27.6, 27.1. GC–MS (EI, 70 eV): m/z = 161 (M^+, 100), 146 (30), 130 (56), 115 (21), 104 (37), 91 (11), 78 (12), 70 (11), 57 (11), 42 (11). No NMR and MS reference data were available for this compound.



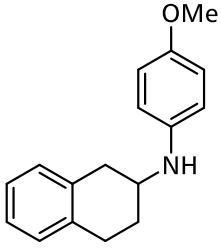
***rac-N*-(Prop-2-yn-1-yl)-1,2,3,4-tetrahydronaphthalen-2-amine (c24-a4) [CAS 134467-58-6].** Prepared from 2-tetralone (**c24**, 403 μL, 447 mg, 3.1 mmol) and propargylamine (**a4**, 1.92 mL, 1.65 g, 30.0 mmol) in MeOH according to *General procedure A*. The crude product was used without purification. 650 mg (quant.) of a brown liquid. TLC (silica gel 60, EtOAc, $KMnO_4$ staining): R_f = 0.62. ^{1}H NMR (300 MHz, $CDCl_3$): δ [ppm] = 7.17–7.03 (4H, m), 3.56 (2H, d, J = 2.4 Hz), 3.23 (1H, tdd, J = 9.6, 5.0, 3.0 Hz), 3.02 (1H, ddd, J = 16.0, 5.0, 1.7 Hz), 2.95–2.77 (2H, m), 2.61 (1H, dd, J = 16.0, 9.3 Hz), 2.22 (1H, t, J = 2.4 Hz), 2.10–1.97 (1H, m), 1.64 (1H, dtd, J = 12.8, 9.8, 6.4 Hz). ^{13}C NMR (75 MHz, $CDCl_3$): δ [ppm] = 136.2, 135.0, 129.5, 128.8, 126.0, 125.9, 82.1, 71.6, 51.8, 36.2, 35.5, 29.2, 27.9. GC–MS (EI, 70 eV): m/z = 185 (M^+, 24), 184 (84), 170 (61), 155 (19), 144 (44), 130 (100), 115 (63), 104 (88), 91 (41), 80 (86), 65 (12), 51 (12), 39 (26). The characterisation data are in agreement with literature values.[98]



***rac-N*-Benzyl-1,2,3,4-tetrahydronaphthalen-2-amine (c24-a6) [CAS 101583-59-9].** Prepared from 2-tetralone (**c24**, 132 μL, 146 mg, 1.0 mmol) and benzylamine (**a6**, 328 μL, 321 mg, 3.0 mmol) in MeOH according to *General procedure A* (one-third of the usual batch size, 3 eq. of amine and AcOH). Purification by column chromatography (silica gel 60, cyclohexane/EtOAc = 1:1) gave 125 mg (0.53 mmol, 53%) of a greenish liquid. TLC (silica gel 60, cyclohexane/EtOAc = 3:1, $KMnO_4$ staining): R_f = 0.35. ^{1}H NMR (300 MHz, $CDCl_3$): δ [ppm] = 7.31–7.10 (5H, m), 7.06–6.94 (4H, m), 3.82 (2H, s), 3.03–2.88 (2H, m), 2.87–2.65 (2H, m), 2.64–2.51 (1H, m), 2.11–1.90 (1H, m), 1.83 (1H, br s), 1.69–1.48 (1H, m). ^{13}C NMR (75 MHz, $CDCl_3$): δ [ppm] = 140.3, 136.3, 135.3, 129.5, 128.8, 128.6, 128.3, 127.2, 125.9, 125.8, 52.9, 51.2, 36.7, 29.5, 28.0. GC–MS (EI, 70 eV): m/z = 237 (M^+, 100), 146 (36), 91 (89), 65 (12). The characterisation data are in agreement with literature values.[99]

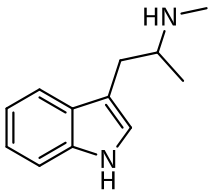


***rac*-4-(1,2,3,4-Tetrahydronaphthalen-2-yl)morpholine (c24-a22) [CAS 23853-56-7].** Prepared from 2-tetralone (**c24**, 403 μL, 447 mg, 3.1 mmol) and morpholine (**a22**, 2.61 mL, 2.63 g, 30.2 mmol) in MeOH according to *General procedure A*. Purification by automated flash chromatography (silica gel 60, *Biotage* SFär Duo 25 g cartridge; gradient of cyclohexane/EtOAc = 75:25 to EtOAc) gave 224 mg (1.03 mmol, 34%) of an off-white solid. TLC (silica gel 60, cyclohexane/EtOAc = 1:1, $KMnO_4$ staining): R_f = 0.22. mp: 49–50 °C. ^{1}H NMR (300 MHz, $CDCl_3$): δ [ppm] = 7.15–7.05 (4H, m), 3.79 (4H, t, J = 4.7 Hz), 3.04–2.62 (9H, m), 2.21–2.09 (1H, m), 1.65 (1H, dtd, J = 12.3, 11.1, 5.6 Hz). ^{13}C NMR (75 MHz, $CDCl_3$): δ [ppm] = 136.3, 135.5, 129.5, 128.6, 126.0, 125.8, 67.3, 60.9, 49.9, 32.0, 29.2, 25.9. GC–MS (EI, 70 eV): m/z = 217 (M^+, 100), 202 (5), 172 (7), 158 (12), 144 (15), 130 (54), 115 (20), 112 (32), 104 (8), 91 (14), 86 (6), 77 (6), 55 (7). No NMR and MS reference data were available for this compound.

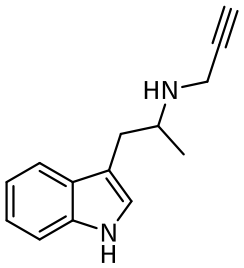


***rac-N*-(4-Methoxyphenyl)-1,2,3,4-tetrahydronaphthalen-2-amine (c24-a24) [CAS 59648-44-1].** Prepared from 2-tetralone (**c24**, 403 μL, 447 mg, 3.1 mmol) and *p*-anisidine (**a24**, 3.69 g, 30.0 mmol) in MeOH according to *General procedure A*. Purification by automated flash chromatography (silica gel 60, *Biotage* SFär Duo 50 g cartridge; gradient of cyclohexane/EtOAc = 92:8 to cyclohexane/EtOAc = 45:65) gave 178 mg (0.70 mmol, 23%) of a red solid. TLC (silica gel 60, cyclohexane/EtOAc = 2:1, $KMnO_4$ staining): R_f = 0.76. mp: 65–66 °C. ^{1}H NMR (300 MHz, $CDCl_3$): δ [ppm] = 7.43–7.27 (4H, m), 7.08–7.01 (2H, m), 6.87–6.79 (2H, m), 3.95 (3H, s), 3.99–3.86 (1H, m), 3.61 (1H, br s), 3.40 (1H, dd, J = 16.2, 4.9 Hz), 3.21–3.01 (2H, m), 2.86 (1H, dd, J = 16.2, 8.5 Hz),

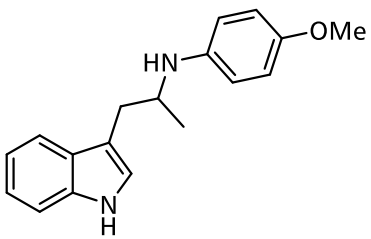
2.45–2.31 (1H, m), 1.92 (1H, dtd, J = 12.7, 8.5, 6.8 Hz). ^{13}C NMR (75 MHz, $CDCl_3$): δ [ppm] = 151.8, 141.1, 135.7, 134.7, 129.3, 128.6, 125.8, 125.6, 114.7, 55.4, 49.1, 36.3, 28.7, 27.4. GC–MS (EI, 70 eV): m/z = 253 (M^+, 100), 238 (8), 149 (18), 134 (22), 131 (25), 123 (23), 115 (9), 108 (13), 91 (10), 77 (6). The characterisation data are in agreement with literature values.[100]



***rac*-1-(1*H*-Indol-3-yl)-*N*-methylpropan-2-amine (c25-a2) [CAS 299-24-1].** Prepared from 1-(1*H*-indol-3-yl)propan-2-one (**c25**, 520 mg, 3.0 mmol) and methylamine (**a2**, 3.07 mL of a 40% w/w solution in MeOH; 0.93 g $MeNH_2$, 30.0 mmol) in MeOH according to *General procedure A*. Purification by automated flash chromatography (silica gel 60, *Biotage* SFär Duo 25 g cartridge; gradient of cyclohexane/EtOAc = 94:6 to cyclohexane/EtOAc = 30:70) gave 449 mg (2.38 mmol, 79%) of a brown, viscous liquid. TLC (silica gel 60, cyclohexane/EtOAc = 1:1, ninhydrin staining): R_f = 0.42. ^{1}H NMR (300 MHz, $CDCl_3$): δ [ppm] = 8.45 (1H, br s), 7.61 (1H, dt, J = 7.5, 1.0 Hz), 7.36 (1H, dt, J = 8.2, 1.0 Hz), 7.19 (1H, ddd, J = 8.1, 7.0, 1.3 Hz), 7.12 (1H, ddd, J = 8.1, 7.1, 1.2 Hz), 7.03 (1H, s), 3.14 (1H, br s), 3.03–2.96 (1H, m), 2.88 (2H, dd, J = 6.6, 2.1 Hz), 2.39 (3H, s), 1.16 (3H, d, J = 6.2 Hz). ^{13}C NMR (75 MHz, $CDCl_3$): δ [ppm] = 136.5, 127.6, 123.2, 122.1, 119.4, 119.0, 112.3, 111.4, 55.4, 33.3, 32.4, 19.3. GC–MS (EI, 70 eV): m/z = 188 (M^+, 2), 131 (63), 103 (8), 77 (12), 58 (100). No NMR and MS reference data were available for this compound.

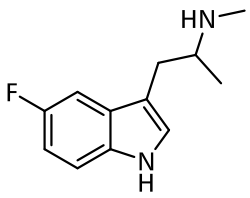


***rac*-*N*-(1-(1*H*-Indol-3-yl)propan-2-yl)prop-2-yn-1-amine (c25-a4).** Prepared from 1-(1*H*-indol-3-yl)propan-2-one (**c25**, 520 mg, 3.0 mmol) and propargylamine (**a4**, 1.92 mL, 1.65 g, 30.0 mmol) in MeOH according to *General procedure A*. Purification by automated flash chromatography (silica gel 60, *Biotage* SFär Duo 10 g cartridge; gradient of cyclohexane/EtOAc = 88:12 to EtOAc) gave 60 mg (0.28 mmol, 9%) of a yellow liquid. TLC (silica gel 60, cyclohexane/EtOAc = 1:1, ninhydrin staining): R_f = 0.19. ^{1}H NMR (300 MHz, $CDCl_3$): δ [ppm] = 8.44 (1H, br s), 7.64 (1H, d, J = 7.7 Hz), 7.37 (1H, d, J = 8.0 Hz), 7.21 (1H, ddd, J = 8.1, 7.0, 1.2 Hz), 7.13 (1H, ddd, J = 7.9, 6.9, 1.0 Hz), 7.05 (1H, d, J = 2.0 Hz), 3.52 (1H, dd, J = 17.1, 2.4 Hz), 3.43 (1H, dd, J = 17.0, 2.5 Hz), 3.35 (1H, q, J = 6.6 Hz), 2.96–2.84 (3H, m), 2.20 (1H, t, J = 2.4 Hz), 1.17 (3H, d, J = 6.2 Hz). ^{13}C NMR (75 MHz, $CDCl_3$): δ [ppm] = 136.5, 127.6, 123.0, 122.1, 119.4, 119.0, 112.3, 111.4, 80.9, 72.4, 51.8, 35.5, 32.6, 19.5. GC–MS (EI, 70 eV): m/z = 212 (M^+, 2), 131 (70), 103 (11), 82 (100), 77 (14), 39 (9). HRMS calcd for $C_{14}H_{17}N_2^+$ [M+H$^+$]: 213.1386, found: 213.1388. No NMR and MS reference data were available for this compound.

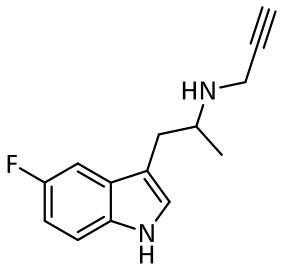


***rac*-*N*-(1-(1*H*-Indol-3-yl)propan-2-yl)-4-methoxyaniline (c25-a24).** Prepared from 1-(1*H*-indol-3-yl)propan-2-one (**c25**, 520 mg, 3.0 mmol) and *p*-anisidine (**a24**, 3.69 g, 30.0 mmol) in MeOH according to *General procedure A*. Purification by automated flash chromatography (silica gel 60, *Biotage* SFär Duo 50 g cartridge; gradient of cyclohexane/EtOAc = 94:6 to cyclohexane/EtOAc = 50:50) gave 594 mg (2.12 mmol, 71%) of a red liquid. TLC (silica gel 60, cyclohexane/EtOAc = 3:1, ninhydrin staining): R_f = 0.36. ^{1}H NMR (300 MHz, $CDCl_3$): δ [ppm] = 8.07 (1H, br s), 7.62 (1H, d, J = 7.8 Hz), 7.36 (1H, dt, J = 8.0, 1.0 Hz), 7.22 (1H, ddd, J = 8.2, 7.0, 1.3 Hz), 7.14 (1H, ddd, J = 8.0, 7.1, 1.2 Hz), 7.00 (1H, d, J = 2.3 Hz), 6.87–6.79 (2H, m), 6.71–6.61 (2H, m), 3.91–3.72 (1H, m), 3.78 (3H, s), 3.42 (1H, br s), 3.08 (1H, dd, J = 14.4, 4.9 Hz), 2.92 (1H, dd, J = 14.4, 6.8 Hz), 1.22 (3H, d, J = 6.3 Hz). ^{13}C NMR (75 MHz, $CDCl_3$): δ [ppm] = 152.2, 141.5,

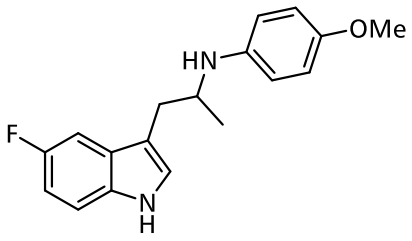
136.3, 128.1, 122.8, 122.1, 119.5, 119.2, 115.4, 115.1, 112.7, 111.2, 55.9, 50.0, 31.9, 20.8. GC–MS (EI, 70 eV): *m/z* = 280 (M^+, 280), 150 (100), 130 (11), 77 (5). HRMS calcd for $C_{18}H_{21}N_2O^+$ [M+H$^+$]: 281.1648, found: 281.1648. No NMR and MS reference data were available for this compound.



***rac*-1-(5-Fluoro-1*H*-indol-3-yl)-*N*-methylpropan-2-amine (c26-a2) [CAS 1893221-28-7].** Prepared from 1-(5-fluoro-1*H*-indol-3-yl)propan-2-one (**c26**, 191 mg, 1.0 mmol) and methylamine (**a2**, 1.02 mL of a 40% w/w solution in MeOH; 311 mg $MeNH_2$, 10.0 mmol) in MeOH according to *General procedure A* (one-third of the usual batch size). The crude product was used without purification. 290 mg (quant.) of a brown liquid. TLC (silica gel 60, cyclohexane/EtOAc = 1:1, ninhydrin staining): R_f = 0.40. ^{1}H NMR (300 MHz, $CDCl_3$): δ [ppm] = 9.17 (1H, br s), 7.28–7.18 (2H, m), 7.04 (1H, s), 6.92 (1H, td, J = 9.1, 2.5 Hz), 2.94 (1H, q, J = 6.4 Hz), 2.89–2.72 (3H, m), 2.40 (3H, s), 1.13 (3H, d, J = 6.2 Hz). ^{13}C NMR (75 MHz, $CDCl_3$): δ [ppm] = 157.7 (d, J_{CF} = 234.0 Hz), 133.0, 127.9 (d, J_{CF} = 9.6 Hz), 124.9, 112.4 (d, J_{CF} = 4.7 Hz), 112.0 (d, J_{CF} = 9.7 Hz), 110.2 (d, J_{CF} = 26.4 Hz), 103.7 (d, J = 23.3 Hz), 55.2, 33.4, 32.5, 19.5. GC–MS (EI, 70 eV): *m/z* = 206 (M^+, 2), 148 (31), 101 (12), 58 (100). No NMR and MS reference data were available for this compound.

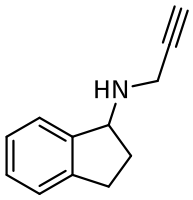


***rac*-*N*-(1-(5-Fluoro-1*H*-indol-3-yl)propan-2-yl)prop-2-yn-1-amine (c26-a4).** Prepared from 1-(5-fluoro-1*H*-indol-3-yl)propan-2-one (**c26**, 191 mg, 1.0 mmol) and propargylamine (**a4**, 640 μL, 550 mg, 10.0 mmol) in MeOH according to *General procedure A* (one-third of the usual batch size). Purification by automated flash chromatography (silica gel 60, *Biotage* SFär Duo 25 g cartridge; gradient of cyclohexane/EtOAc = 88:12 to EtOAc) gave 192 mg (0.65 mmol, 65%) of a brown liquid. TLC (silica gel 60, cyclohexane/EtOAc = 1:1, ninhydrin staining): R_f = 0.20. ^{1}H NMR (300 MHz, $CDCl_3$): δ [ppm] = 8.39 (1H, br s), 7.34–7.25 (2H, m), 7.12 (1H, d, J = 2.3 Hz), 6.95 (1H, td, J = 9.1, 2.5 Hz), 3.54 (1H, dd, J = 17.2, 2.5 Hz), 3.44 (1H, dd, J = 17.2, 2.4 Hz), 3.31 (1H, sext, J = 6.4 Hz), 2.90–2.76 (2H, m), 2.53 (1H, br s), 2.20 (1H, t, J = 2.4 Hz), 1.15 (3H, d, J = 6.2 Hz). ^{13}C NMR (75 MHz, $CDCl_3$): δ [ppm] = 157.8 (d, J_{CF} = 234.3 Hz), 133.0, 128.1 (d, J_{CF} = 9.6 Hz), 124.7, 113.0 (d, J = 4.8 Hz), 111.9 (d, J = 9.7 Hz), 110.5 (d, J_{CF} = 26.4 Hz), 104.1 (d, J_{CF} = 23.4 Hz), 81.6, 71.9, 51.4, 35.6, 32.9, 19.8. GC–MS (EI, 70 eV): *m/z* = 230 (M^+, <1), 149 (34), 146 (5), 101 (11), 82 (100), 39 (7). No NMR and MS reference data were available for this compound.

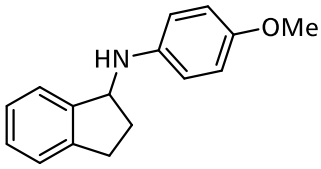


***rac*-*N*-(1-(5-Fluoro-1*H*-indol-3-yl)propan-2-yl)-4-methoxyaniline (c26-a24).** Prepared from 1-(5-fluoro-1*H*-indol-3-yl)propan-2-one (**c26**, 191 mg, 1.0 mmol) and *p*-anisidine (**a24**, 1.23 g, 10.0 mmol) in MeOH according to *General procedure A* (one-third of the usual batch size). Purification by automated flash chromatography (silica gel 60, *Biotage* SFär Duo 25 g cartridge; gradient of cyclohexane/EtOAc = 92:8 to cyclohexane/EtOAc = 45:65) gave 56 mg (0.19 mmol, 19%) of a brown liquid. TLC (silica gel 60, cyclohexane/EtOAc = 2:1, ninhydrin staining): R_f = 0.49. ^{1}H NMR (300 MHz, $CDCl_3$): δ [ppm] = 8.20 (1H, br s), 7.30–7.20 (2H, m), 7.05 (1H, d, J = 2.2 Hz), 6.96 (1H, td, J = 9.0, 2.5 Hz), 6.88–6.81 (2H, m), 6.75–6.66 (2H, m), 4.02 (1H, br s), 3.79 (3H, s), 3.82–3.75 (1H, m), 3.04 (1H, dd, J = 14.4, 5.0 Hz), 2.90 (1H, dd, J = 14.4, 6.8 Hz), 1.23 (3H, d, J = 6.3 Hz). ^{13}C NMR (75 MHz, $CDCl_3$): δ [ppm] = 157.9 (d, J_{CF} = 234.2 Hz), 152.7, 140.6, 132.8, 128.5 (d, J_{CF} = 9.6 Hz), 124.7, 116.0, 115.1, 112.7 (d, J_{CF} = 4.7 Hz), 111.9 (d, J_{CF} = 9.6 Hz), 110.4 (d, J_{CF} = 26.4 Hz), 104.0 (d, J_{CF} = 23.4 Hz), 55.9, 50.5,

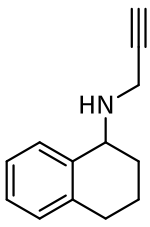
31.6, 20.6. GC–MS (EI, 70 eV): *m/z* = 298 (M^+, 7), 150 (100), 148 (11), 135 (6). No NMR and MS reference data were available for this compound.



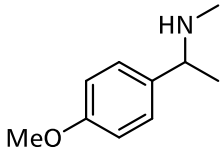
***rac-N*-(Prop-2-yn-1-yl)-2,3-dihydro-1*H*-inden-1-amine (c27-a4) [CAS 1875-50-9].** Prepared from 1-indanone (**c27**, 396 mg, 3.0 mmol) and propargylamine (**a4**, 1.92 mL, 1.65 g, 30.0 mmol) in MeOH according to *General procedure A*. Purification by column chromatography (silica gel 60, cyclohexane/EtOAc = 3:1) gave 402 mg (2.35 mmol, 78%) of a yellowish liquid. TLC (silica gel 60, cyclohexane/EtOAc = 2:1, $KMnO_4$ staining): R_f = 0.29. ^{1}H NMR (300 MHz, $CDCl_3$): δ [ppm] = 7.39–7.32 (1H, m), 7.28–7.16 (3H, m), 4.44 (1H, dd, *J* = 6.9, 5.1 Hz), 3.56 (1H, dd, *J* = 17.0, 2.5 Hz), 3.50 (1H, dd, *J* = 16.9, 2.5 Hz), 3.06 (1H, ddd, *J* = 15.9, 8.3, 5.8 Hz), 2.83 (1H, ddd, *J* = 15.8, 8.3, 6.0 Hz), 2.41 (2H, dddd + br s overlap, *J* = 12.8, 8.3, 6.9, 5.9 Hz), 2.28 (1H, t, *J* = 2.5 Hz), 1.88 (1H, dddd, *J* = 13.2, 8.3, 6.0, 5.1 Hz). ^{13}C NMR (75 MHz, CD_3OD): δ [ppm] = 144.2, 144.0, 127.9, 126.4, 125.0, 124.4, 82.2, 71.8, 61.9, 36.2, 33.2, 30.6. GC–MS (EI, 70 eV): *m/z* = 170 (M^+, 100), 156 (10), 132 (60), 117 (92), 115 (58), 103 (8), 91 (18), 77 (10), 63 (6), 51 (6), 39 (9). The characterisation data are in agreement with literature values.[70]



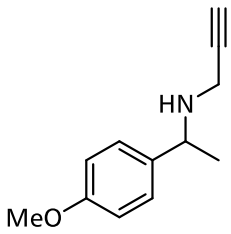
***rac-N*-(4-Methoxyphenyl)-2,3-dihydro-1*H*-inden-1-amine (c27-a24) [CAS 960009-54-5].** Prepared from 1-indanone (**c27**, 396 mg, 3.0 mmol) and *p*-anisidine (**a24**, 1.11 g, 9.0 mmol) in MeOH according to *General procedure A* (3 eq. amine and AcOH). Purification by automated flash chromatography (silica gel 60, *Biotage* SFär Duo 25 g cartridge; gradient of cyclohexane/EtOAc = 92:8 to cyclohexane/EtOAc = 45:65) gave 588 mg (2.46 mmol, 82%) of a yellow liquid. TLC (silica gel 60, cyclohexane/EtOAc = 2:1, ninhydrin staining): R_f = 0.27. ^{1}H NMR (500 MHz, $CDCl_3$): δ [ppm] = 7.40 (1H, d, *J* = 7.4 Hz), 7.31–7.21 (3H, m), 6.87–6.82 (2H, m), 6.74–6.70 (2H, m), 4.98 (1H, t, *J* = 6.8 Hz), 3.79 (3H, s), 3.04 (1H, ddd, *J* = 15.9, 8.7, 4.3 Hz), 2.91 (1H, dt, *J* = 15.9, 7.9 Hz), 2.60 (1H, dddd, *J* = 12.6, 8.2, 7.0, 4.3 Hz), 1.92 (1H, dddd, *J* = 12.8, 8.6, 7.6, 6.6 Hz). ^{13}C NMR (126 MHz, $CDCl_3$): δ [ppm] = 152.3, 144.9, 143.7, 142.0, 127.9, 126.7, 125.0, 124.4, 115.1, 114.8, 59.7, 55.9, 34.0, 30.3. GC–MS (EI, 70 eV): *m/z* = 239 (M^+, 34), 123 (95), 117 (100), 115 (65), 108 (60), 91 (16), 63 (7). The characterisation data are in agreement with literature values.[101]



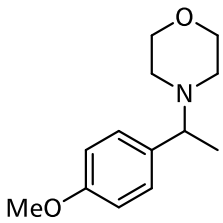
***rac-N*-(Prop-2-yn-1-yl)-1,2,3,4-tetrahydronaphthalen-1-amine (c28-a4) [CAS 1019560-85-0].** Prepared from 1-tetralone (**c28**, 138 μL, 150 mg, 1.0 mmol) and propargylamine (**a4**, 330 μL, 283 mg, 5.2 mmol) in MeOH according to *General procedure A* (one-third of the usual batch size, 5 eq. of amine and AcOH). Purification by automated flash chromatography (silica gel 60, *Biotage* SFär Duo 25 g cartridge; gradient of cyclohexane/EtOAc = 94:6 to EtOAc) gave 50 mg (0.27 mmol, 27%) of a yellowish liquid. TLC (silica gel 60, cyclohexane/EtOAc = 2:1, $KMnO_4$ staining): R_f = 0.55. ^{1}H NMR (300 MHz, $CDCl_3$): δ [ppm] = 7.34–7.27 (1H, m), 7.19–7.05 (3H, m), 3.99 (1H, t, *J* = 4.2 Hz), 3.53 (1H, dd, *J* = 17.2, 2.4 Hz), 3.46 (1H, dd, *J* = 17.2, 2.4 Hz), 2.82–2.63 (2H, m), 2.27 (1H, t, *J* = 2.4 Hz), 2.03–1.67 (4H, m), 1.47 (1H, br s). ^{13}C NMR (75 MHz, $CDCl_3$): δ [ppm] = 138.5, 137.7, 129.3, 129.2, 127.0, 125.9, 82.9, 71.5, 53.6, 36.0, 29.3, 27.9, 18.5. GC–MS (EI, 70 eV): *m/z* = 146 (M^+–C_3H_3), 131 (16), 118 (100), 90 (65), 63 (11), 51 (7), 39 (6). No NMR and MS reference data were available for this compound.



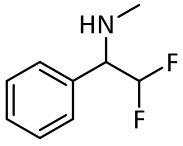
***rac*-1-(4-Methoxyphenyl)-*N*-methylethan-1-amine (c30-a2) [CAS 41684-13-3].** Prepared from 4-methoxyacetophenone (**c30**, 451 mg, 3.0 mmol) and methylamine (**a2**, 3.07 mL of a 40% w/w solution in MeOH; 0.93 g $MeNH_2$, 30.0 mmol) in MeOH according to *General procedure A*. Purification by automated flash chromatography (silica gel 60, *Biotage* SFär Duo 25 g cartridge; gradient of cyclohexane/EtOAc = 50:50 to EtOAc) gave 144 mg (0.87 mmol, 29%) of a colourless liquid. TLC (silica gel 60, cyclohexane/EtOAc = 1:8, $KMnO_4$ staining): R_f = 0.44. ^{1}H NMR (300 MHz, $CDCl_3$): δ [ppm] = 7.32–7.27 (2H, m), 6.95–6.89 (2H, m), 3.88 (1H, q, J = 6.7 Hz), 3.81 (3H, s), 2.38 (3H, s), 1.56 (3H, d, J = 6.8 Hz). ^{13}C NMR (75 MHz, $CDCl_3$): δ [ppm] = 159.9, 131.1, 128.6, 114.6, 59.8, 55.5, 32.4, 21.3. GC–MS (EI, 70 eV): m/z = 165 (M^+, 3), 150 (100), 135 (17), 91 (6), 42 (10). The characterisation data are in agreement with literature values.[102]



***rac*-*N*-(1-(4-Methoxyphenyl)ethyl)prop-2-yn-1-amine (c30-a4) [CAS 1019582-42-3].** Prepared from 4-methoxyacetophenone (**c30**, 451 mg, 3.0 mmol) and propargylamine (**a4**, 1.92 mL, 1.65 g, 30.0 mmol) in MeOH according to *General procedure A*. Purification by automated flash chromatography (silica gel 60, *Biotage* SFär Duo 25 g cartridge; gradient of cyclohexane/EtOAc = 94:6 to cyclohexane/EtOAc = 50:50) gave 227 mg (1.20 mmol, 40%) of a colourless liquid. TLC (silica gel 60, cyclohexane/EtOAc = 3:1, $KMnO_4$ staining): R_f = 0.24. ^{1}H NMR (300 MHz, $CDCl_3$): δ [ppm] = 7.29–7.22 (2H, m), 6.90–6.83 (2H, m), 3.97 (1H, q, J = 6.5 Hz), 3.79 (3H, s), 3.34 (1H, dd, J = 17.1, 2.5 Hz), 3.14 (1H, dd, J = 17.1, 2.4 Hz), 2.21 (1H, t, J = 2.4 Hz), 1.55 (1H, br s), 1.34 (3H, d, J = 6.6 Hz). ^{13}C NMR (75 MHz, $CDCl_3$): δ [ppm] = 158.8, 136.5, 128.0, 113.9, 82.4, 71.3, 55.7, 55.3, 35.9, 24.0. GC–MS (EI, 70 eV): m/z = 189 (M^+, 2), 174 (100), 135 (17), 91 (8), 77 (5). The characterisation data are in agreement with literature values.[70]

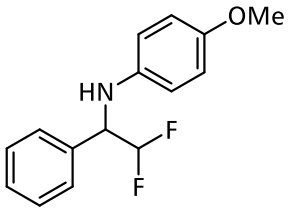


***rac*-4-(1-(4-Methoxyphenyl)ethyl)morpholine (c30-a22) [CAS 96921-36-7].** Prepared from 4-methoxyacetophenone (**c30**, 451 mg, 3.0 mmol) and morpholine (**a22**, 2.61 mL, 2.63 g, 30.2 mmol) in MeOH according to *General procedure A*. Purification by automated flash chromatography (silica gel 60, *Biotage* SFär Duo 25 g cartridge; gradient of cyclohexane/EtOAc = 94:6 to EtOAc) gave 114 mg (0.52 mmol, 17%) of a colourless liquid. TLC (silica gel 60, cyclohexane/EtOAc = 1:1, $KMnO_4$ staining): R_f = 0.77. ^{1}H NMR (300 MHz, $CDCl_3$): δ [ppm] = 7.25–7.19 (2H, m), 6.88–6.82 (2H, m), 3.80 (3H, s), 3.68 (4H, t, J = 4.7 Hz), 3.26 (1H, q, J = 6.7 Hz), 2.52–2.42 (2H, m), 2.39–2.30 (2H, m), 1.33 (3H, d, J = 6.7 Hz). ^{13}C NMR (75 MHz, $CDCl_3$): δ [ppm] = 158.7, 136.0, 128.8, 113.7, 67.4, 64.8, 55.4, 51.4, 19.9. GC–MS (EI, 70 eV): m/z = 221 (M^+, 11), 206 (71), 135 (100), 105 (10), 91 (10), 77 (6). The characterisation data are in agreement with literature values.[103]

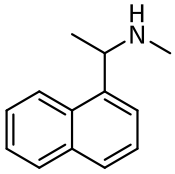


***rac*-2,2-Difluoro-*N*-methyl-1-phenylethan-1-amine (c31-a2) [CAS 1528654-50-3].** Prepared from α,α-difluoroacetophenone (**c31**, 468 mg, 3.0 mmol) and methylamine (**a2**, 920 μL of a 40% w/w solution in MeOH; 280 mg $MeNH_2$, 9.0 mmol) according to *General procedure B*. Purification by automated flash chromatography (silica gel 60, *Biotage* SFär Duo 25 g cartridge; gradient of cyclohexane/EtOAc = 98:2 to EtOAc) gave 20 mg (0.12 mmol, 4%) of a colourless liquid. TLC (silica gel 60, cyclohexane/EtOAc = 3:1, $KMnO_4$ staining): R_f = 0.36. ^{1}H NMR (300 MHz, CD_3OD): δ [ppm] = 7.41–7.32 (5H, m), 5.90 (1H, td, J_{FH} = 56.1 Hz, J_{HH} = 4.4 Hz), 3.83 (1H, td, J_{FH} = 12.3 Hz, J_{HH} = 4.4 Hz), 2.27 (3H, s). ^{13}C NMR (75 MHz, CD_3OD): δ [ppm] = 135.4 (t, J_{CF} = 3.2 Hz), 128.4, 128.3, 128.1, 116.6 (t, J_{CF} = 243.7 Hz), 66.3 (t, J_{CF} =

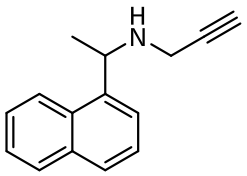
21.9 Hz), 32.7. GC–MS (EI, 70 eV): *m/z* = 171 (M^+, <1%), 120 (100), 91 (10), 77 (7), 51 (5), 42 (22). No NMR and MS reference data were available for this compound.



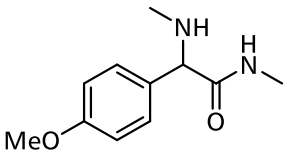
***rac-N*-(2,2-Difluoro-1-phenylethyl)-4-methoxyaniline (c31-a24) [CAS 908603-29-2].** Prepared from α,α-difluoroacetophenone (**c31**, 468 mg, 3.0 mmol) and *p*-anisidine (**a24**, 1.11 g, 9.0 mmol) according to *General procedure B*. Purification by automated flash chromatography (silica gel 60, *Biotage* SFär Duo 10 g cartridge; gradient of cyclohexane/EtOAc = 95:5 to EtOAc) gave 120 mg (0.46 mmol, 15%) of a yellow liquid. TLC (silica gel 60, cyclohexane/EtOAc = 9:1, $KMnO_4$ staining): R_f = 0.22. ^{1}H NMR (300 MHz, $CDCl_3$): δ [ppm] = 7.48–7.30 (5H, m), 6.80–6.68 (2H, m), 6.65–6.54 (2H, m), 6.01 (1H, td, J_{FH} = 55.9 Hz, J_{HH} = 3.2 Hz), 4.63 (1H, td, J_{FH} = 13.1 Hz, J_{HH} = 3.2 Hz), 3.71 (3H, s). ^{13}C NMR (75 MHz, $CDCl_3$): δ [ppm] = 153.2, 139.7, 135.5 (t, J_{CF} = 2.0 Hz), 129.0, 128.7, 128.0, 116.0 (t, J_{CF} = 246.9 Hz), 115.9, 114.9, 61.5 (t, J_{CF} = 21.9 Hz), 55.8. GC–MS (EI, 70 eV): *m/z* = 263 (M^+, 51), 212 (100), 134 (9), 122 (12), 91 (6), 77 (5). The characterisation data are in agreement with literature values.[104]



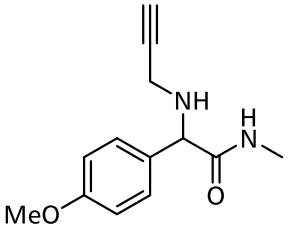
***rac-N*-Methyl-1-(naphthalen-1-yl)ethan-1-amine (c33-a2) [CAS 98978-55-3].** Prepared from 1-acetonaphthone (**c33**, 152 μL, 170 mg, 1.0 mmol) and methylamine (**a2**, 1.02 mL of a 40% w/w solution in MeOH; 311 mg $MeNH_2$, 10.0 mmol) in MeOH according to *General procedure A* (one-third of the usual batch size). Purification by automated flash chromatography (silica gel 60, *Biotage* SFär Duo 25 g cartridge; gradient of cyclohexane/EtOAc = 95:5 to cyclohexane/EtOAc = 25:75) gave 80 mg (0.43 mmol, 43%) of an orange liquid. TLC (silica gel 60, cyclohexane/EtOAc = 1:5, ninhydrin staining): R_f = 0.28. ^{1}H NMR (300 MHz, $CDCl_3$): δ [ppm] = 8.13 (1H, d, *J* = 8.3 Hz), 7.89 (1H, dd, *J* = 7.5, 2.0 Hz), 7.79 (1H, d, *J* = 8.2 Hz), 7.68 (1H, dd, *J* = 7.3, 1.3 Hz), 7.58–7.46 (3H, m), 4.63 (1H, q, *J* = 6.6 Hz), 4.57 (1H, br), 2.42 (3H, s), 1.58 (3H, d, *J* = 6.6 Hz). ^{13}C NMR (75 MHz, $CDCl_3$): δ [ppm] = 139.0, 134.0, 131.3, 129.2, 127.8, 126.2, 125.8, 125.6, 123.0, 122.7, 55.1, 33.9, 22.6. GC–MS (EI, 70 eV): *m/z* = 185 (M^+, 10), 170 (100), 153 (14), 127 (12), 58 (12), 42 (18). The characterisation data are in agreement with literature values.[105]



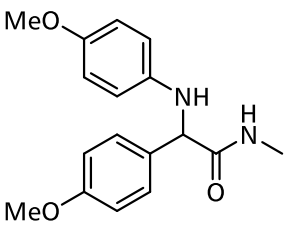
***rac-N*-(1-(Naphthalen-1-yl)ethyl)prop-2-yn-1-amine (c33-a4) [CAS 1019632-11-1].** Prepared from 1-acetonaphthone (**c33**, 152 μL, 170 mg, 1.0 mmol) and propargylamine (**a4**, 320 μL, 275 mg, 5.0 mmol) in MeOH according to *General procedure A* (one-third of the usual batch size, 5 eq. of amine and AcOH). Purification by column chromatography (silica gel 60, cyclohexane/EtOAc = 4:1) gave 181 mg (0.86 mmol, 86%) of a colourless liquid. TLC (silica gel 60, cyclohexane/EtOAc = 3:1, $KMnO_4$ staining): R_f = 0.30. ^{1}H NMR (300 MHz, $CDCl_3$): δ [ppm] = 8.27 (1H, dd, *J* = 8.2, 1.5 Hz), 7.87 (1H, dd, *J* = 7.9, 1.7 Hz), 7.75 (1H, dt, *J* = 8.1, 1.1 Hz), 7.68 (1H, dd, *J* = 7.1, 0.7 Hz), 7.56–7.43 (3H, m), 4.89 (1H, q, *J* = 6.5 Hz), 3.47 (1H, dd, *J* = 17.2, 2.4 Hz), 3.29 (1H, dd, *J* = 17.2, 2.4 Hz), 2.24 (1H, t, *J* = 2.4 Hz), 1.68 (1H, br s), 1.50 (3H, d, *J* = 6.6 Hz). ^{13}C NMR (75 MHz, $CDCl_3$): δ [ppm] = 140.2, 134.1, 131.5, 129.1, 127.6, 125.9, 125.8, 125.5, 123.3, 123.1, 82.5, 71.5, 51.9, 36.2, 23.3. GC–MS (EI, 70 eV): *m/z* = 209 (M^+, 10), 194 (100), 165 (7), 154 (21), 127 (14), 82 (8), 66 (5). HRMS calcd for $C_{15}H_{16}N^+$ [M+H^+]: 210.1277, found: 210.1276. No NMR and MS reference data were available for this compound.



***rac*-2-(4-Methoxyphenyl)-*N*-methyl-2-(methylamino)acetamide (c36-a2) [CAS 1367729-92-7].** Prepared from 2-(4-methoxyphenyl)-*N*-methyl-2-oxoacetamide (**c36**, 193 mg, 1.0 mmol) and methylamine (**a2**, 297 μL of a 40% w/w solution in MeOH; 93 mg $MeNH_2$, 3.0 mmol) according to *General procedure B*. The crude product was used without purification. 193 mg (0.93 mmol, 93%) of a colourless solid. TLC (silica gel 60, cyclohexane/EtOAc = 1:3, $KMnO_4$ staining): R_f = 0.10. mp: 162–164 °C. ^{1}H NMR (300 MHz, $CDCl_3$): δ [ppm] = 7.32–7.26 (2H, m), 7.09 (1H, br s), 6.88–6.82 (2H, m), 4.06 (1H, s), 3.77 (3H, s), 2.81 (3H, d, J = 5.0 Hz), 2.52 (1H, br s), 2.41 (3H, s). ^{13}C NMR (75 MHz, $CDCl_3$): δ [ppm] = 172.8, 159.6, 131.1, 128.6, 114.3, 68.9, 55.4, 35.2, 26.1. GC–MS (EI, 70 eV): m/z = 150 (M^+–C_2H_4NO, 100), 135 (5), 42 (12). No NMR and MS reference data were available for this compound.

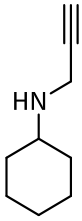


***rac*-2-(4-Methoxyphenyl)-*N*-methyl-2-(prop-2-yn-1-ylamino)-acetamide (c36-a4).** Prepared from 2-(4-methoxyphenyl)-*N*-methyl-2-oxoacetamide (**c36**, 193 mg, 1.0 mmol) and propargylamine (**a4**, 320 μL, 275 mg, 5.0 mmol) in MeOH according to *General procedure A* (one-third of the usual batch size, 5 eq. of amine and AcOH). Purification by automated flash chromatography (silica gel 60, *Biotage* SFär Duo 10 g cartridge; gradient of cyclohexane/EtOAc = 75:25 to EtOAc) gave 64 mg (0.28 mmol, 28%) of a pale-yellowish, viscous liquid. The product contains the corresponding alcohol, 2-hydroxy-2-(4-methoxyphenyl)-*N*-methylacetamide, as residual impurity and was used as GC reference material without further purification. TLC (silica gel 60, EtOAc, $KMnO_4$ staining): R_f = 0.33. ^{1}H NMR (300 MHz, $CDCl_3$): δ [ppm] = 7.32–7.24 (2H, m), 6.90–6.82 (2H, m), 4.38 (1H, s), 3.78 (3H, s), 3.37 (1H, dd, J = 17.2, 2.4 Hz), 3.29 (1H, dd, J = 17.2, 2.4 Hz), 2.79 (3H, d, J = 5.0 Hz), 2.25 (1H, t, J = 2.4 Hz). ^{13}C NMR (75 MHz, $CDCl_3$): δ [ppm] = 172.7, 159.7, 130.5, 129.0, 114.4, 81.2, 72.3, 65.1, 55.4, 36.6, 26.2. GC–MS (EI, 70 eV): m/z = 232 (M^+, <1), 174 (100), 134 (19).

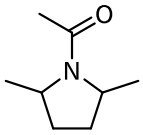


***rac*-2-(4-Methoxyphenyl)-2-((4-methoxyphenyl)amino)-*N*-methylacetamide (c36-a24) [CAS 1154423-53-6].** Prepared from 2-(4-methoxyphenyl)-*N*-methyl-2-oxoacetamide (**c36**, 193 mg, 1.0 mmol) and *p*-anisidine (**a24**, 370 mg, 3.0 mmol) in MeOH according to *General procedure A* (one-third of the usual batch size, 3 eq. of amine and AcOH). Purification by automated flash chromatography (silica gel 60, *Biotage* SFär Duo 25 g cartridge; gradient of cyclohexane/EtOAc = 95:5 to EtOAc) gave 60 mg (0.20 mmol, 20%) of an off-white solid. TLC (silica gel 60, cyclohexane/EtOAc = 3:1, $KMnO_4$ staining): R_f = 0.46. mp: 133–134 °C. ^{1}H NMR (300 MHz, $CDCl_3$): δ [ppm] = 7.37–7.30 (2H, m), 6.92–6.87 (2H, m), 6.86–6.82 (1H, br m), 6.81–6.74 (2H, m), 6.61–6.54 (2H, m), 4.61 (1H, s), 3.79 (3H, s), 3.74 (3H, s), 2.83 (3H, d, J = 4.9 Hz). ^{13}C NMR (75 MHz, $CDCl_3$): δ [ppm] = 172.5, 159.8, 153.2, 141.0, 131.2, 128.7, 115.1, 115.0, 114.6, 64.5, 55.8, 55.5, 26.4. GC–MS (EI, 70 eV): m/z = 300 (M^+, 4), 242 (100), 227 (5), 207 (19), 134 (15), 121 (6), 77 (6). HRMS calcd for $C_{17}H_{21}N_2O_3^+$ [M+H$^+$]: 301.1547, found: 301.1550. No NMR and MS reference data were available for this compound.

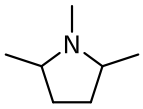
One achiral and three racemic product reference compounds were synthesized by methods other than reductive amination, *e.g.*, through catalytic hydrogenation of aromatic or *N*-protected precursors, or by *N*-alkylation of the corresponding primary amines.



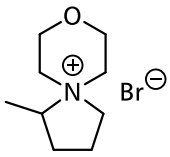
***N*-(Prop-2-yn-1-yl)cyclohexanamine (c1-a4) [CAS 18292-76-7].**[106] An oven-dried round-bottom flask (100 mL) with magnetic stirring bar and reflux condenser was flushed with argon, charged with a solution of cyclohexylamine (4.58 mL, 3.97 g, 40 mmol) in anhydrous methanol (20 mL) and cooled to 0 °C on an ice bath. Propargyl bromide (700 μL of an 80% w/w solution in toluene; 778 mg C_3H_3Br, 6.5 mmol) was added dropwise *via* syringe at 0 °C, the reaction mixture was heated to 50 °C and stirred overnight. After cooling to room temperature, saturated aqueous NH_4Cl solution (50 mL) was added and the product was extracted into CH_2Cl_2 (3 × 40 mL). The combined organic phases were dried over Na_2SO_4, filtered, and the solvent was carefully removed under reduced pressure (600 mbar, 40 °C) to give 589 mg of a brownish liquid. Purification by column chromatography (silica gel 60, cyclohexane/EtOAc = 1:1) afforded the title compound (256 mg, 1.87 mmol, 29%) as a brownish liquid. TLC (silica gel 60, cyclohexane/EtOAc = 1:1, ninhydrin staining): R_f = 0.28. ^{1}H NMR (300 MHz, $CDCl_3$): δ [ppm] = 3.41 (2H, d, J = 2.5 Hz), 2.61 (1H, tt, J = 10.3, 3.8 Hz), 2.15 (1H, t, J = 2.5 Hz), 1.87–1.52 (5H, m), 1.43 (1H, br s), 1.32–0.93 (5H, m). ^{13}C NMR (75 MHz, $CDCl_3$): δ [ppm] = 82.6, 71.1, 55.0, 35.1, 33.1, 26.1, 24.9. GC–MS (EI, 70 eV): m/z = 137 (M^+, 13), 108 (6), 94 (100), 80 (53), 67 (7), 54 (9), 9 (18). The characterisation data are in agreement with literature values.[107]



***all-rac*-1-(2,5-Dimethylpyrrolidin-1-yl)ethan-1-one (c4-a1-Ac) [CAS 228099-02-3].**[108] In a round-bottom flask (100 mL) equipped with a magnetic stirring bar, 1-benzyl-2,5-dimethylpyrrolidine (**c4-a6**; 370 mg, 1.95 mmol) was dissolved in AcOH (15 mL). Palladium on activated charcoal (214 mg; 10% w/w Pd) was added, and the reaction mixture was stirred overnight at room temperature under a hydrogen atmosphere (balloon). The catalyst was removed by paper filtration and the filtrate was basified with aqueous NaOH solution (10 M, pH >12). The product was extracted into EtOAc (3 × 50 mL), and the combined organic phases were stirred with saturated aqueous Na_2CO_3 solution (10 mL) and acetic anhydride (1 mL) for 2 h. Then, the organic phase was separated and the aqueous phase was extracted with EtOAc (3 × 20 mL). The combined organic phases were washed with brine (20 mL), dried over Na_2SO_4, filtered, and the solvent was removed under reduced pressure to give the title compound (97 mg, 0.69 mmol, 35%) as a yellowish liquid. The product is a mixture of diastereomers in a ratio of approx. 55:45 (*trans/cis*). In ^{13}C NMR, peak splitting due to amide rotamers is also observed, but split peaks belonging to the same diastereomer are reported as a single chemical shift followed by (2) for clarity. TLC (silica gel 60, EtOAc, $KMnO_4$ staining): R_f = 0.21. ^{1}H NMR (300 MHz, $CDCl_3$): δ [ppm] = 4.21 (1H minor, quint, J = 6.6 Hz), 4.09 (1H major, sext, J = 6.3 Hz), 4.03–3.86 (1H major + minor, m), 2.30–2.09 (2H minor, m), 2.08 (3H minor, s), 2.07 (3H major, s), 2.08–1.89 (2H major, m), 1.74–1.48 (2H major + minor, m), 1.29 (3H major, d, J = 6.3 Hz), 1.25 (3H major, d, J = 6.5 Hz), 1.18 (6H minor, d, J = 6.4 Hz). ^{13}C NMR (75 MHz, $CDCl_3$): δ [ppm] = 168.9 (major), 168.9 (minor), 55.0 (2, major), 54.4 (2, minor), 53.7 (2, major), 53.0 (2, minor), 32.1 (minor), 31.2 (major), 30.9 (minor), 29.3 (major), 22.8 (2, minor), 22.5 (2, major), 22.3 (major), 21.8 (minor), 21.5 (minor), 19.2 (major). GC–MS (EI, 70 eV): m/z = 141 (M^+, 25), 126 (17), 99 (6), 84 (100), 67 (6), 43 (12). The characterisation data are in agreement with literature values.[109]



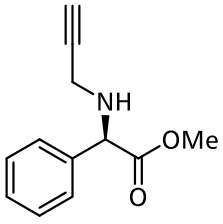
***all-rac*-1,2,5-Trimethylpyrrolidine (c4-a2) [CAS 54884-61-6].** In a round-bottom flask (250 mL) equipped with a magnetic stirring bar, 1,2,5-trimethylpyrrole (541 μL, 437 mg, 4.0 mmol) was dissolved in AcOH (45 mL). Palladium on activated charcoal (670 mg; 10% w/w Pd) was added, and the reaction mixture was stirred overnight at room temperature under a hydrogen atmosphere (balloon). The catalyst was removed by paper filtration and the filtrate was basified with aqueous NaOH solution (10 M, pH >12). The product was extracted into Et_2O (3 × 50 mL), and the combined organic phases were dried over Na_2SO_4, filtered, and carefully concentrated under reduced pressure (600 mbar, 30 °C) to give the title compound (686 mg, quant.) as a brownish liquid. The product is a mixture of diastereomers in a ratio of approx. 85:15 (*cis/trans*). TLC (silica gel 60, MTBE/MeOH/NH_4OH = 90:9:1, $KMnO_4$ staining): R_f = 0.64. ^{1}H NMR (300 MHz, $CDCl_3$): δ [ppm] = 3.05–2.90 (2H minor, m), 2.31 (3H minor, s), 2.22 (3H major, s), 2.20–2.09 (2H major, m), 2.06–1.95 (2H minor, m), 1.89–1.75 (2H major, m), 1.44–1.29 (2H major + minor, m), 1.11 (6H major, d, J = 6.1 Hz), 0.99 (6H minor, d, J = 6.3 Hz). ^{13}C NMR (75 MHz, $CDCl_3$): δ [ppm] = 62.7 (major), 57.6 (minor), 38.2 (major), 34.8 (minor), 31.2 (minor), 31.0 (major), 19.4 (major), 16.6 (minor). GC–MS (EI, 70 eV): m/z = 113 (M^+, 10), 98 (100), 70 (8), 56 (9), 42 (15). The characterisation data are in agreement with literature values.[110]



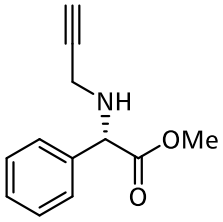
***rac*-1-Methyl-8-oxa-5-azaspiro[4.5]decan-5-ium bromide (c21-a22).** An oven-dried Schlenk flask (25 mL) was equipped with a magnetic stirring bar and flushed with argon. Under constant argon flow, the flask was charged with *rac*-2-methylpyrrolidine (306 μL, 255 mg, 3.0 mmol), bis(2-bromoethyl) ether (377 μL, 701 mg, 3.0 mmol) and MeCN (15 mL). The flask was closed with a rubber septum and the reaction mixture was allowed to stir at room temperature for 48 h. Afterwards, the solvent was evaporated under reduced pressure and the residue was taken up in H_2O (20 mL). The aqueous solution was acidified with conc. hydrobromic acid and lyophilized overnight to give the title compound (570 mg, 2.41 mmol, 80%) as a brown oil. ^{1}H NMR (500 MHz, CD_3OD): δ [ppm] = 4.12 (1H, ddd, J = 12.2, 8.0, 6.2 Hz), 4.07–3.96 (4H, m), 3.86 (1H, dquint, J = 9.5, 6.8 Hz), 3.69–3.55 (2H, m), 3.40 (1H, dddd, J = 12.9, 9.7, 5.2, 1.4 Hz), 3.28 (1H, dq, J = 13.0, 2.4 Hz), 3.22 (1H, dq, J = 12.9, 2.4 Hz), 2.47–2.37 (1H, m), 2.24–2.14 (2H, m), 1.97–1.87 (1H, m), 1.47 (3H, dt, J = 6.7, 1.7 Hz). ^{13}C NMR (75 MHz, $CDCl_3$): δ [ppm] = 74.8, 63.3, 62.5, 59.4, 52.5, 29.3, 20.2, 13.7. HPLC–MS (ESI, pos.): m/z = 156 (M^+). HRMS calcd for $C_9H_{18}NO^+$ [M^+]: 156.1383, found: 156.1385. No NMR and MS reference data were available for this compound.

Non-racemic product reference compounds:
Non-racemic chiral reference compounds were generally synthesized by *N*-alkylation or *N*-arylation of the corresponding primary or secondary amines. In the case of compound **c5-a4**, both enantiomers were prepared on a 5 mmol scale and purified. For the remaining compounds, the alkylation reactions were carried out on a smaller scale (0.05 mmol) to generate samples of the enantioenriched amines for analytical chromatography. *N*-Arylation reactions were performed on a 1-mmol scale according to a literature procedure.[111] The required non-racemic primary amines were either obtained from commercial suppliers or prepared from the corresponding ketones by literature-known biocatalytic transamination reactions.[112,113]

Methyl 2-phenyl-2-(prop-2-ynylamino)acetate (c5-a4).[114,115] An oven-dried, three-neck round-bottom flask (100 mL) equipped with a reflux condenser and a magnetic stirring bar was flushed with argon and charged with anhydrous DMF (40 mL), powdered 4 Å molecular sieves (5.0 g) and LiOH (263 mg, 11 mmol). After stirring at room temperature for 1 h, methyl 2-amino-2-phenylacetate hydrochloride (1.0 g, 5.0 mmol) was added and the reaction mixture was stirred for another 45 min. Then, propargyl bromide (520 μL of an 80% w/w solution in toluene; 578 mg C_3H_3Br, 4.9 mmol) was added dropwise at room temperature and the reaction mixture was stirred overnight. The resulting suspension was filtered to remove solids, and the filter was washed with EtOAc (100 mL). The combined filtrate was washed with brine (3 × 30 mL), dried over Na_2SO_4, filtered, and the solvent was evaporated under reduced pressure to give the crude product as a brown liquid. Purification by column chromatography (silica gel 60, cyclohexane/EtOAc = 4:1) afforded the desired monoalkylation product.



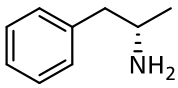
(*R*)-c5-a4 [CAS 451492-33-4]. 104 mg (0.51 mmol, 11%) of a yellow liquid. TLC (silica gel 60, cyclohexane/EtOAc = 4:1, ninhydrin staining): R_f = 0.38. ^{1}H NMR (300 MHz, $CDCl_3$): δ [ppm] = 7.44–7.30 (5H, m), 4.65 (1H, s), 3.70 (3H, s), 3.49 (1H, dd, J = 17.1, 2.4 Hz), 3.28 (1H, dd, J = 17.1, 2.4 H), 2.44 (1H, br s), 2.26 (1H, t, J = 2.4 Hz). ^{13}C NMR (75 MHz, $CDCl_3$): δ [ppm] = 172.8, 137.1, 128.9, 128.5, 128.1, 81.0, 72.4, 63.6, 52.6, 35.9. GC–MS (EI, 70 eV): m/z = 203 (M^+, <1), 144 (100), 115 (16), 104 (12), 91 (8), 77 (9), 39 (7). The characterisation data are in agreement with literature values.[115]



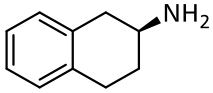
(*S*)-c5-a4 [CAS 1041425-37-9]. 113 mg (0.56 mmol, 11%) of a yellow liquid. TLC (silica gel 60, cyclohexane/EtOAc = 4:1, ninhydrin staining): R_f = 0.38. ^{1}H NMR (300 MHz, $CDCl_3$): δ [ppm] = 7.43–7.30 (5H, m), 4.65 (1H, s), 3.69 (3H, s), 3.47 (1H, dd, J = 17.2, 2.4 Hz), 3.28 (1H, dd, J = 17.2, 2.5 Hz), 2.28 (1H, br s), 2.26 (1H, t, J = 2.5 Hz). ^{13}C NMR (75 MHz, $CDCl_3$): δ [ppm] = 172.9, 137.3, 128.8, 128.4, 127.9, 81.1, 72.2, 63.5, 52.4, 35.8. GC–MS (EI, 70 eV): m/z = 203 (M^+, <1), 144 (100), 115 (21), 104 (15), 91 (9), 77 (11), 39 (7). The characterisation data are in agreement with literature values.[115]

General procedure for transamination reactions: An Erlenmeyer flask with glass joint (100 mL) was charged with transaminase preparation (1.0 g lyophilised cells, final concentration: 20 mg/mL) and 2-$PrNH_2$–phosphate buffer (50 mL; 500 mM 2-$PrNH_2$, pH 8.0) containing pyridoxal 5'-phosphate (PLP; 1 mM), and the flask was closed with a rubber septum and placed in an incubator shaker at 30 °C and 120 rpm for 30 min to rehydrate and resuspend the cells. Afterwards, the substrate (**c8** or **c24**, see below; 2.5 mmol; final concentration: 50 mM) was added by pipette and incubation was continued at 30 °C and 120 rpm for 24 h. The reaction mixture was basified (pH ≥12) by addition of half-saturated Na_2CO_3 solution (20 mL), transferred to polypropylene tubes (2 × 50 mL), and extracted with EtOAc (5 × 10 mL per tube), whereby phase separation was accelerated by centrifugation (4,500 rpm, 5 min). The

combined organic phases were dried over Na_2SO_4, filtered, and the solvent was removed under reduced pressure to give the crude amine products, which were purified by column chromatography.



(*S*)-1-Phenylpropan-2-amine (c8-a1) [CAS 51-64-9].[112] Biotransformation using phenylacetone (**c8**; 335 mg, 332 μL, 2.5 mmol) and transaminase from *Chromobacterium violaceum* (*Cv*-TA) gave 278 mg of a yellow liquid. Purification by column chromatography (silica gel 60, MTBE/MeOH/NH_4OH = 90:9:1) afforded the title compound (52 mg, 0.38 mmol, 15%) as a pale-yellowish liquid. TLC (silica gel 60, MTBE/MeOH/NH_4OH = 90:9:1, $KMnO_4$ staining): R_f = 0.37. $[\alpha]_D^{20}$ = +32.4 (*c* 0.97, $CHCl_3$); lit.[112] $[\alpha]_D^{20}$ = +45.0 (*c* = 0.20, $CHCl_3$). ^{1}H NMR (300 MHz, $CDCl_3$): δ [ppm] = 7.34–7.15 (5H, m), 3.20 (1H, dp, *J* = 7.7, 6.2 Hz), 2.72 (1H, dd, *J* = 13.2, 5.8 Hz), 2.59 (1H, dd, *J* = 13.3, 7.7 Hz), 2.52 (2H, br s), 1.14 (3H, d, *J* = 6.3 Hz). ^{13}C NMR (75 MHz, $CDCl_3$): δ [ppm] = 139.4, 129.4, 128.5, 126.4, 48.7, 46.2, 23.1. GC–MS (EI, 70 eV): *m/z* = 134 (M^+–H, 1), 120 (4), 91 (15), 65 (7), 44 (100). The characterisation data are in agreement with literature values.[112]

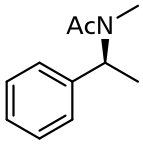


(*S*)-1,2,3,4-Tetrahydronaphthalen-2-amine (c24-a1) [CAS 21880-87-5].[113] Biotransformation using 2-tetralone (**c24**; 365 mg, 329 μL, 2.5 mmol) and transaminase from *Arthrobacter citreus* (*ArS*-TA) gave 347 mg of a brown, viscous liquid. Purification by column chromatography (silica gel 60, MTBE/MeOH/NH_4OH = 90:9:1) afforded the title compound (133 mg, 0.90 mmol, 36%) as a purple liquid. TLC (silica gel 60, MTBE/MeOH/NH_4OH = 90:9:1, $KMnO_4$ staining): R_f = 0.41. $[\alpha]_D^{20}$ = –91.4 (*c* 1.13, $CHCl_3$); lit.[116] $[\alpha]_D^{22}$ = –84.5 (*c* = 0.54, $CHCl_3$). ^{1}H NMR (300 MHz, $CDCl_3$): δ [ppm] = 7.14–7.03 (4H, m), 3.19 (1H, tdd, *J* = 9.8, 5.0, 3.1 Hz), 3.00 (1H, ddd, *J* = 16.2, 5.1, 1.8 Hz), 2.95–2.78 (2H, m), 2.57 (1H, dd, *J* = 16.1, 9.4 Hz), 2.07–1.95 (1H, m), 1.68–1.52 (3H, m). ^{13}C NMR (75 MHz, $CDCl_3$): δ [ppm] = 135.9, 135.3, 129.3, 128.7, 125.8, 125.7, 47.3, 39.5, 32.9, 28.1. GC–MS (EI, 70 eV): *m/z* = 147 (M^+, 31), 130 (100), 115 (20), 104 (60), 91 (8), 78 (15). The characterisation data are in agreement with literature values.[117]

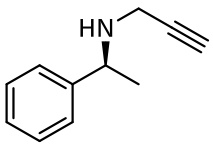
General procedure for small-scale N-alkylation of primary amines: In a microcentrifuge tube (2 mL), anhydrous K_2CO_3 (10.3 mg, 75 μmol) was suspended in acetonitrile (300 μL), and the primary amine (50 μmol) as well as the haloalkane (50 μmol) were added by pipette. The tube was closed and incubated at 35 °C and 600 rpm in a benchtop thermoshaker for 16 h. Afterwards, water (500 μL) and saturated aqueous Na_2CO_3 solution (200 μL) were added, and the mixture was extracted with EtOAc (2 × 500 μL), whereby phase separation was accelerated by centrifugation (13,000 rpm, 1 min). The organic phases were combined in another micro-centrifuge tube (1.5 mL), dried over Na_2SO_4, and centrifuged again to pellet the solid. The supernatant was transferred to a crimp-cap glass vial for GC–MS, GC–FID, or HPLC analysis.

Samples prepared in this way typically contained a mixture of primary amine (unreacted starting material), secondary amine (monoalkylation product) and tertiary amine (bisalkylation product). In most cases, they could be used for determining the elution order of enantiomers on chiral-phase GC or HPLC without purification. If co-elution of impurities with the analyte of interest was observed, the samples were further purified by small-scale column chromatography (*ca*. 5 cm of silica gel 60 in a Pasteur pipette).

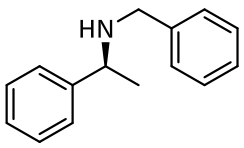
In cases where the acetamide derivative was required for GC or HPLC analysis, the samples were acetylated by treatment with saturated aqueous Na_2CO_3 solution (200 μL) and acetic anhydride (10 μL) for 2 min, followed by drying over Na_2SO_4 and K_2CO_3, and centrifugation to pellet the solids. The supernatant was transferred to a crimp-cap glass vial for analysis.



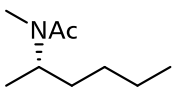
(*S*)-*N*-methyl-*N*-(1-phenylethyl)acetamide (c3-a2-Ac) [CAS 69048-31-3]. Prepared from (*S*)-1-phenylethan-1-amine (6.0 mg, 6.3 μL, 50 μmol) and iodomethane (7.1 mg, 3.1 μL, 50 μmol), followed by acetylation. GC–MS (EI, 70 eV; method GC-MS2): t_r = 8.9 min, *m/z* = 177 (M^+, 62), 162 (11), 134 (8), 120 (100), 105 (43), 77 (18), 58 (13), 43 (13); 60% unreacted, 28% monoalkylation, 12% bisalkylation.



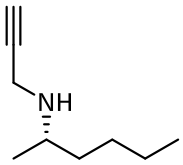
(*S*)-*N*-(1-Phenylethyl)prop-2-yn-1-amine (c3-a4) [CAS 441771-18-2]. Prepared from (*S*)-1-phenylethan-1-amine (6.0 mg, 6.3 μL, 50 μmol) and propargyl bromide (5.6 μL of an 80% w/w solution in toluene; 6.2 mg C_3H_3Br, 52 μmol). GC–MS (EI, 70 eV; method GC-MS2): t_r = 5.5 min, *m/z* = 159 (M^+, <1), 144 (100), 115 (11), 105 (11), 91 (6), 77 (12), 39 (6); 10% unreacted, 70% monoalkylation, 20% bisalkylation.



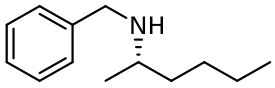
(*S*)-*N*-Benzyl-1-phenylethan-1-amine (c3-a6) [CAS 17480-69-2]. Prepared from (*S*)-1-phenylethan-1-amine (6.0 mg, 6.3 μL, 50 μmol) and benzyl bromide (8.6 mg, 6.0 μL, 50 μmol). GC–MS (EI, 70 eV; method GC-MS2): t_r = 11.1 min, *m/z* = 211 (M^+, 2), 196 (100), 134 (5), 105 (14), 91 (92), 77 (10); 6% unreacted, 80% monoalkylation, 14% bisalkylation.



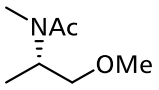
(*S*)-*N*-(Hexan-2-yl)-*N*-methylacetamide (c6-a2-Ac). Prepared from (*S*)-hexan-2-amine (5.0 mg, 7.6 μL, 50 μmol) and iodomethane (7.1 mg, 3.1 μL, 50 μmol), followed by acetylation. GC–MS (EI, 70 eV; method GC-MS1): t_r = 12.7 min, *m/z* = 157 (M^+, 4), 142 (10), 100 (63), 58 (100), 43 (13); 75% unreacted, 21% monoalkylation, 4% bisalkylation.



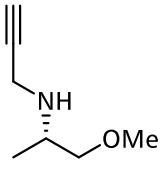
(*S*)-*N*-(Prop-2-yn-1-yl)hexan-2-amine (c6-a4) [CAS 215509-60-7]. Prepared from (*S*)-hexan-2-amine (5.0 mg, 7.6 μL, 50 μmol) and propargyl bromide (5.6 μL of an 80% w/w solution in toluene; 6.2 mg C_3H_3Br, 52 μmol). GC–MS (EI, 70 eV; method GC-MS1): t_r = 9.1 min, *m/z* = 139 (M^+, <1), 124 (9), 82 (100), 39 (7); 8% unreacted, 58% monoalkylation, 34% bisalkylation.



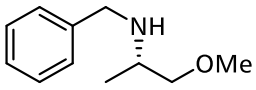
(*S*)-*N*-Benzylhexan-2-amine (c6-a6) [CAS 178033-74-4]. Prepared from (*S*)-hexan-2-amine (5.0 mg, 7.6 μL, 50 μmol) and benzyl bromide (8.6 mg, 6.0 μL, 50 μmol). GC–MS (EI, 70 eV; method GC-MS1): t_r = 15.4 min, *m/z* = 191 (M^+, <1), 176 (6), 134 (81), 91 (100), 65 (7); 6% unreacted, 94% monoalkylation.



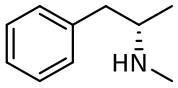
(*S*)-*N*-(1-Methoxypropan-2-yl)-*N*-methylacetamide (c7-a2-Ac). Prepared from (*S*)-1-methoxypropan-2-amine (4.5 mg, 5.3 μL, 50 μmol) and iodomethane (7.1 mg, 3.1 μL, 50 μmol), followed by acetylation. GC–MS (EI, 70 eV; method GC-MS1): t_r = 11.5 min, *m/z* = 130 (M^+–CH_3, <1), 113 (14), 100 (42), 58 (100), 43 (15); 57% unreacted, 37% monoalkylation, 6% bisalkylation.



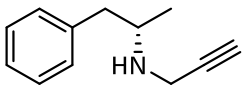
(*S*)-*N*-(1-Methoxypropan-2-yl)prop-2-yn-1-amine (c7-a4). Prepared from (*S*)-1-methoxypropan-2-amine (4.5 mg, 5.3 μL, 50 μmol) and propargyl bromide (5.6 μL of an 80% w/w solution in toluene; 6.2 mg C_3H_3Br, 52 μmol). GC–MS (EI, 70 eV; method GC-MS1): t_r = 7.4 min, *m/z* = 126 (M^+–H, <1), 82 (100), 42 (11), 39 (9); 63% monoalkylation, 37% bisalkylation.



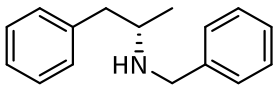
(*S*)-*N*-Benzyl-1-methoxypropan-2-amine (c7-a6). Prepared from (*S*)-1-methoxypropan-2-amine (4.5 mg, 5.3 μL, 50 μmol) and benzyl bromide (8.6 mg, 6.0 μL, 50 μmol). GC–MS (EI, 70 eV; method GC-MS1): t_r = 14.2 min, *m/z* = 178 (M^+–H, <1), 134 (62), 91 (100), 65 (8); quantitative monoalkylation.



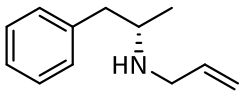
(*S*)-*N*-Methyl-1-phenylpropan-2-amine (c8-a2) [CAS 537-46-2]. Prepared from (*S*)-1-phenylpropan-2-amine (6.8 mg, 7.0 μL, 50 μmol) and iodomethane (7.1 mg, 3.1 μL, 50 μmol). GC–MS (EI, 70 eV; method GC-MS1): t_r = 11.6 min, *m/z* = 148 (M^+–H, 1), 134 (3), 91 (10), 58 (100); 43% unreacted, 31% monoalkylation, 26% bisalkylation.



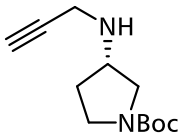
(*S*)-*N*-(1-Phenylpropan-2-yl)prop-2-yn-1-amine (c8-a4) [CAS 56862-30-7]. Prepared from (*S*)-1-phenylpropan-2-amine (6.8 mg, 7.0 μL, 50 μmol) and propargyl bromide (5.6 μL of an 80% w/w solution in toluene; 6.2 mg C_3H_3Br, 52 μmol). GC–MS (EI, 70 eV; method GC-MS1): t_r = 14.1 min, *m/z* = 172 (M^+–H, <1), 91 (13), 82 (100); 1% unreacted, 99% monoalkylation.



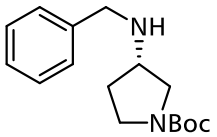
(*S*)-*N*-Benzyl-1-phenylpropan-2-amine (c8-a6) [CAS 15062-72-3]. Prepared from (*S*)-1-phenylpropan-2-amine (6.8 mg, 7.0 μL, 50 μmol) and benzyl bromide (8.6 mg, 6.0 μL, 50 μmol). GC–MS (EI, 70 eV; method GC-MS2): t_r = 12.1 min, *m/z* = 224 (M^+–H, <1), 134 (79), 91 (100), 65 (10); 21% monoalkylation, 79% bisalkylation.



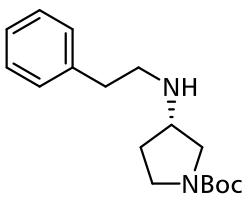
(*S*)-*N*-(1-Phenylpropan-2-yl)prop-2-en-1-amine (c8-a9). Prepared from (*S*)-1-phenylpropan-2-amine (6.8 mg, 7.0 μL, 50 μmol) and allyl bromide (6.0 mg, 4.3 μL, 50 μmol). GC–MS (EI, 70 eV; method GC-MS1): t_r = 13.7 min, *m/z* = 174 (M^+–H, <1), 91 (14), 84 (100), 41 (18); 5% unreacted, 55% monoalkylation, 40% bisalkylation.



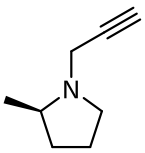
***tert*-Butyl (*S*)-3-(prop-2-yn-1-ylamino)pyrrolidine-1-carboxylate (c16-a4) [CAS 2829419-19-2].** Prepared from *tert*-butyl (*S*)-3-amino-pyrrolidine-1-carboxylate (9.3 mg, 8.7 μL, 50 μmol) and propargyl bromide (5.6 μL of an 80% w/w solution in toluene; 6.2 mg C_3H_3Br, 52 μmol). GC–MS (EI, 70 eV; method GC-MS2): t_r = 10.1 min, *m/z* = 224 (M^+, <1), 167 (13), 151 (20), 123 (53), 113 (38), 94 (80), 80 (31), 69 (18), 57 (100), 41 (31); 2% unreacted, 64% monoalkylation, 34% bisalkylation.



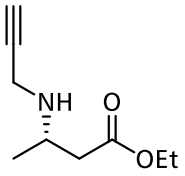
***tert*-Butyl (*S*)-3-(benzylamino)pyrrolidine-1-carboxylate (c16-a6) [CAS 2423707-46-2].** Prepared from *tert*-butyl (*S*)-3-aminopyrrolidine-1-carboxylate (9.3 mg, 8.7 μL, 50 μmol) and benzyl bromide (8.6 mg, 6.0 μL, 50 μmol). GC–MS (EI, 70 eV; method GC-MS2): t_r = 15.0 min, *m/z* = 276 (M^+, <1), 219 (66), 203 (20), 175 (12), 146 (34), 132 (20), 106 (84), 91 (100), 57 (48), 41 (16); 95% monoalkylation, 5% bisalkylation.



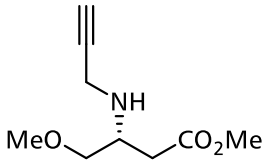
***tert*-Butyl (*S*)-3-(phenethylamino)pyrrolidine-1-carboxylate (c16-a15).** Prepared from *tert*-butyl (*S*)-3-aminopyrrolidine-1-carboxylate (9.3 mg, 8.7 μL, 50 μmol) and (2-bromoethyl)benzene (9.3 mg, 6.8 μL, 50 μmol). GC–MS (EI, 70 eV; method GC-MS2): t_r = 15.8 min, *m/z* = 217 (M^+–O^{t}Bu, 16), 199 (26), 160 (9), 143 (100), 125 (22), 99 (51), 57 (34), 41 (17); 89% unreacted, 11% monoalkylation.



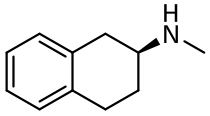
(*R*)-2-Methyl-1-(prop-2-yn-1-yl)pyrrolidine (c21-a4). Prepared from (*R*)-2-methylpyrrolidine (4.3 mg, 5.1 μL, 50 μmol) and propargyl bromide (5.6 μL of an 80% w/w solution in toluene; 6.2 mg C_3H_3Br, 52 μmol). GC–MS (EI, 70 eV; method GC-MS1): t_r = 7.2 min, *m/z* = 123 (M^+, 10), 122 (10), 108 (100), 68 (9), 56 (8), 39 (12); quantitative monoalkylation.



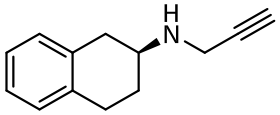
Ethyl (*S*)-3-(prop-2-yn-1-ylamino)butanoate (c22-a4). Prepared from ethyl (*S*)-3-aminobutanoate hydrochloride (8.4 mg, 50 μmol), propargyl bromide (5.6 μL of an 80% w/w solution in toluene; 6.2 mg C_3H_3Br, 52 μmol), and the double amount of K_2CO_3 (20.6 mg, 150 μmol). GC–MS (EI, 70 eV; method GC-MS1): t_r = 11.7 min, *m/z* = 224 (M^+–H, 1), 154 (11), 130 (9), 108 (10), 96 (8), 82 (100), 66 (8), 54 (18), 42 (10), 39 (10); 3% unreacted, 78% monoalkylation, 19% bisalkylation.



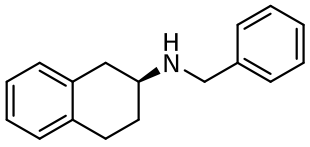
Methyl (*R*)-4-methoxy-3-(prop-2-yn-1-ylamino)butanoate (c23-a4). Prepared from methyl (*R*)-3-amino-4-methoxybutanoate hydrochloride (9.2 mg, 50 μmol), propargyl bromide (5.6 μL of an 80% w/w solution in toluene; 6.2 mg C_3H_3Br, 52 μmol), and the double amount of K_2CO_3 (20.6 mg, 150 μmol). GC–MS (EI, 70 eV; method GC-MS1): t_r = 13.1 min, *m/z* = 184 (M^+–H, <1), 140 (100), 108 (28), 98 (7), 80 (12), 66 (23); 15% unreacted, 57% monoalkylation, 28% bisalkylation.



(*S*)-*N*-Methyl-1,2,3,4-tetrahydronaphthalen-2-amine (c24-a2) [CAS 142697-64-1]. Prepared from (*S*)-1,2,3,4-tetrahydronaphthalen-2-amine (7.4 mg, 7.2 μL, 50 μmol) and iodomethane (7.1 mg, 3.1 μL, 50 μmol). GC–MS (EI, 70 eV; method GC-MS2): t_r = 7.7 min, *m/z* = 161 (M^+, 100), 146 (26), 130 (60), 115 (20), 104 (39), 91 (11), 57 (14); 68% unreacted, 23% monoalkylation, 9% bisalkylation.

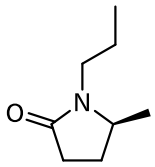


(*S*)-*N*-(Prop-2-yn-1-yl)-1,2,3,4-tetrahydronaphthalen-2-amine (c24-a4) [CAS 2104033-98-7]. Prepared from (*S*)-1,2,3,4-tetrahydronaphthalen-2-amine (7.4 mg, 7.2 μL, 50 μmol) and propargyl bromide (5.6 μL of an 80% w/w solution in toluene; 6.2 mg C_3H_3Br, 52 μmol). GC–MS (EI, 70 eV; method GC-MS2): t_r = 9.9 min, *m/z* = 185 (M^+, 26), 184 (92), 170 (65), 155 (22), 144 (38), 130 (100), 115 (62), 104 (91), 91 (40), 80 (95), 65 (13), 39 (27); 15% unreacted, 63% monoalkylation, 22% bisalkylation.

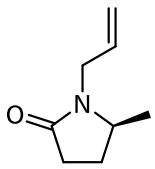


(*S*)-*N*-Benzyl-1,2,3,4-tetrahydronaphthalen-2-amine (c24-a6) [CAS 1246472-55-8]. Prepared from (*S*)-1,2,3,4-tetrahydronaphthalen-2-amine (7.4 mg, 7.2 μL, 50 μmol) and benzyl bromide (8.6 mg, 6.0 μL, 50 μmol). GC–MS (EI, 70 eV; method GC-MS2): t_r = 15.1 min, *m/z* = 237 (M^+, 96), 146 (36), 130 (34), 117 (14), 106 (15), 91 (100), 65 (13); 8% unreacted, 55% monoalkylation, 37% bisalkylation.

General procedure for small-scale N-alkylation of 5-methylpyrrolidin-2-one: In a screw-top glass vial (1.5 mL), powdered KOH (4.2 mg, 75 μmol) was suspended in acetonitrile (300 μL), and (*S*)-5-methylpyrrolidin-2-one (5.0 mg, 4.8 μL, 50 μmol) as well as the haloalkane (50 μmol) were added by pipette. The vial was closed tightly with a screw cap and incubated at 65 °C and 600 rpm in a benchtop thermoshaker for 4 h. Afterwards, water (500 μL) and saturated aqueous Na_2CO_3 solution (200 μL) were added, and the mixture was transferred to a microcentrifuge tube (2 mL) and extracted with EtOAc (2 × 500 μL), whereby phase separation was accelerated by centrifugation (13,000 rpm, 1 min). The organic phases were combined in another microcentrifuge tube (1.5 mL), dried over Na_2SO_4, and centrifuged again to pellet the solid. The supernatant was transferred to a crimp-cap glass vial for GC–MS and GC–FID analysis.

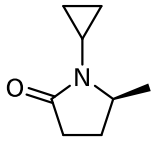


(*S*)-5-Methyl-1-propylpyrrolidin-2-one (c10-a8). Prepared from (*S*)-5-methylpyrrolidin-2-one (5.0 mg, 4.8 μL, 50 μmol) and 1-bromopropane (6.1 mg, 4.5 μL, 50 μmol). GC–MS (EI, 70 eV; method GC-MS2): t_r = 5.4 min, *m/z* = 141 (M^+, 48), 126 (39), 112 (100), 98 (8), 84 (52), 55 (17), 41 (16); 14% unreacted, 86% alkylated.



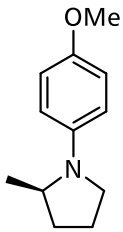
(*S*)-1-Allyl-5-methylpyrrolidin-2-one (c10-a9) [CAS 126265-74-5]. Prepared from (*S*)-5-methylpyrrolidin-2-one (5.0 mg, 4.8 μL, 50 μmol) and allyl bromide (6.0 mg, 4.3 μL, 50 μmol). GC–MS (EI, 70 eV; method GC-MS2): t_r = 5.2 min, *m/z* = 139 (M^+, 47), 124 (100), 112 (6), 96 (8), 84 (14), 68 (7), 55 (13), 41 (33); 6% unreacted, 94% alkylated.

Due to the lower reactivity of bromocyclopropane compared to 1-bromopropane and allyl bromide, the cyclopropyl derivative **c10-a10** could not be prepared in the above-described way. Moreover, co-elution of **c10-a10** with the starting material, 5-methylpyrrolidin-2-one, on chiral-phase GC made purification of the sample necessary. Therefore, the reaction was carried out with 5 equiv. of bromocyclopropane and 2 equiv. of KOH in DMSO at 90 °C and 600 rpm for 16 h. After the usual work-up, the sample was evaporated under a stream of air, re-dissolved in EtOAc (50 μL), and purified by small-scale column chromatography (*ca*. 5 cm of silica gel 60 in a Pasteur pipette, cyclohexane/EtOAc = 1:1).

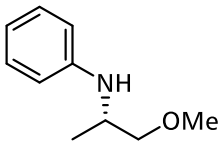


(*S*)-1-Cyclopropyl-5-methylpyrrolidin-2-one (c10-a10). Prepared from (*S*)-5-methylpyrrolidin-2-one (5.0 mg, 4.8 μL, 50 μmol), bromocyclopropane (30.2 mg, 20 μL, 250 μmol), and KOH (5.6 mg, 100 μmol) in DMSO (300 μL). GC–MS (EI, 70 eV; method GC-MS1): t_r = 12.9 min, *m/z* = 139 (M^+, 49), 124 (100), 96 (13), 84 (45), 68 (22), 55 (28), 41 (35); 43% unreacted, 57% alkylated.

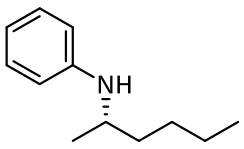
General procedure for copper(I)-catalysed N-arylation:[111] An oven-dried Schlenk tube (10 mL) equipped with a magnetic stir bar was charged with copper(I) iodide (19 mg, 0.1 mmol), 2-(2,6-dimethylphenylamino)-2-oxoacetic acid (DMPAO; 38 mg, 0.2 mmol), and potassium phosphate (K_3PO_4; 425 mg, 2.0 mmol). The bromoarene (1.0 mmol) was added, the tube was closed with a rubber septum, and evacuated and refilled with nitrogen three times. Anhydrous DMSO (1 mL) and the primary or secondary amine (1.5 mmol) were added by syringe, and the tube was heated to 90 °C in an oil bath under magnetic stirring for 18–24 h. Afterwards, the reaction mixture was allowed to cool to room temperature, diluted with water (15 mL), and extracted with EtOAc (3 × 20 mL). The combined organic phases were dried over Na_2SO_4, filtered, and the solvent was removed under reduced pressure to give the crude *N*-arylation products, which were purified by column chromatography.



(*R*)-1-(4-Methoxyphenyl)-2-methylpyrrolidine (c21-a24). Prepared from (*R*)-2-methylpyrrolidine (128 mg, 152 μL, 1.5 mmol) and 4-bromoanisole (187 mg, 125 μL, 1.0 mmol). Purification by column chromatography (silica gel 60, cyclohexane/EtOAc = 15:1) gave 145 mg (0.76 mmol, 76%) of a yellowish liquid. TLC (silica gel 60, cyclohexane/EtOAc = 9:1, UV visualisation): R_f = 0.49. ^{1}H NMR (300 MHz, $CDCl_3$): δ [ppm] = 6.93–6.84 (2H, m), 6.60 (2H, d, J = 8.4 Hz), 3.88–3.74 (1H, m), 3.80 (3H, s), 3.52–3.36 (1H, m), 3.15 (1H, q, J = 8.2 Hz), 2.18–1.89 (3H, m), 1.79–1.64 (1H, m), 1.21 (3H, d, J = 6.2 Hz). ^{13}C NMR (75 MHz, $CDCl_3$): δ [ppm] = 150.6, 142.4, 115.1, 112.8, 56.0, 54.1, 49.0, 33.2, 23.4, 19.6. GC–MS (EI, 70 eV): m/z = 191 (M^+, 28), 176 (100), 161 (6), 134 (7). The characterisation data are in agreement with those of the racemic compound.



(*S*)-*N*-(1-Methoxypropan-2-yl)aniline (c7-a7) [CAS 137769-88-1]. Prepared from (*S*)-1-methoxypropan-2-amine (134 mg, 159 μL, 1.5 mmol) and bromobenzene (157 mg, 105 μL, 1.0 mmol). Purification by column chromatography (silica gel 60, cyclohexane/EtOAc = 9:1) gave 76 mg (0.46 mmol, 46%) of a pale-yellowish liquid. TLC (silica gel 60, cyclohexane/EtOAc = 3:1, UV visualisation): R_f = 0.71. ^{1}H NMR (300 MHz, $CDCl_3$): δ [ppm] = 7.23–7.12 (2H, m), 6.72 (1H, tt, J = 7.3, 1.1 Hz), 6.68–6.60 (2H, m), 3.90 (1H, br s), 3.68 (1H, dtd, J = 11.3, 6.4, 4.8 Hz), 3.47 (1H, dd, J = 9.3, 4.6 Hz), 3.40 (1H, dd, J = 9.3, 5.1 Hz), 3.39 (3H, s), 1.25 (3H, d, J = 6.5 Hz). ^{13}C NMR (75 MHz, $CDCl_3$): δ [ppm] = 147.3, 129.4, 117.6, 113.7, 76.1, 59.2, 48.4, 17.9. GC–MS (EI, 70 eV): m/z = 165 (M^+, 13), 120 (100), 77 (9). The characterisation data are in agreement with those of the racemic compound.



(*S*)-*N*-(Hexan-2-yl)aniline (c6-a7) [CAS 1596378-65-2]. Prepared from (*S*)-hexan-2-amine (152 mg, 203 μL, 1.5 mmol) and bromobenzene (157 mg, 105 μL, 1.0 mmol). Purification by column chromatography (silica gel 60, cyclohexane/EtOAc = 24:1) gave 94 mg (0.53 mmol, 53%) of a pale-yellowish liquid. TLC (silica gel 60, cyclohexane/EtOAc = 9:1, UV visualisation): R_f = 0.77. ^{1}H NMR (300 MHz, $CDCl_3$): δ [ppm] = 7.24–7.14 (2H, m), 6.69 (1H, tt, J = 7.3, 1.1 Hz), 6.64–6.58 (2H, m), 3.65 (1H, br s), 3.47 (1H, sext, J = 6.2 Hz), 1.67–1.55 (1H, m), 1.51–1.28 (5H, m), 1.20 (3H, d, J = 6.3 Hz), 0.93 (3H, t, J = 6.9 Hz). ^{13}C NMR (75 MHz, $CDCl_3$): δ [ppm] = 147.6, 129.4, 117.0, 113.4, 48.7, 37.0, 28.5, 22.9, 20.8, 14.2. GC–MS (EI, 70 eV): m/z = 177 (M^+, 19), 162 (8), 120 (100), 106 (5), 77 (6). The characterisation data are in agreement with those of the racemic compound.

Analytical Methods

Gas chromatography with mass-selective detection (achiral stationary phase): GC–MS analyses were carried out on an *Agilent* 7890A GC system equipped with an *Agilent J&W* HP-5ms capillary column (dimensions: 30 m × 0.25 mm × 0.25 μm; stationary phase: bonded & cross-linked 5%-phenyl-methylpolysiloxane) and coupled to an Agilent 5975C mass-selective detector (electron impact ionisation, 70 eV; quadrupole mass selection), using helium (0.7 mL/min flow rate) as carrier gas.

Method GC-MS1	
Column:	HP-5ms (30 m × 0.25 mm × 0.25 μm)
Carrier gas:	Helium
Flow rate:	0.7 mL/min
Inlet temperature:	250 °C
MS transfer line temperature:	300 °C
MS ion source temperature:	230 °C
MS quadrupole temperature:	150 °C
MS scan range:	m/z = 33–400
Split ratio:	90:1
Oven temperature program:	40 °C, 2 min; 10 °C/min to 180 °C; 180 °C, 1 min
Total run time:	17 min

Method GC-MS2	
Column:	HP-5ms (30 m × 0.25 mm × 0.25 μm)
Carrier gas:	Helium
Flow rate:	0.7 mL/min
Inlet temperature:	250 °C
MS transfer line temperature:	300 °C
MS ion source temperature:	230 °C
MS quadrupole temperature:	150 °C
MS scan range:	m/z = 33–400
Split ratio:	90:1
Oven temperature program:	100 °C, 0.5 min; 10 °C/min to 300 °C
Total run time:	20.5 min

Method GC-MS3	
Column:	HP-5ms (30 m × 0.25 mm × 0.25 μm)
Carrier gas:	Helium
Flow rate:	0.7 mL/min
Inlet temperature:	250 °C
MS transfer line temperature:	300 °C
MS ion source temperature:	230 °C
MS quadrupole temperature:	150 °C
MS scan range:	m/z = 33–400
Split ratio:	90:1
Oven temperature program:	40 °C, 2 min; 10 °C/min to 300 °C; 300 °C, 2 min
Total run time:	30 min

Exemplary chromatograms are shown on the following pages.

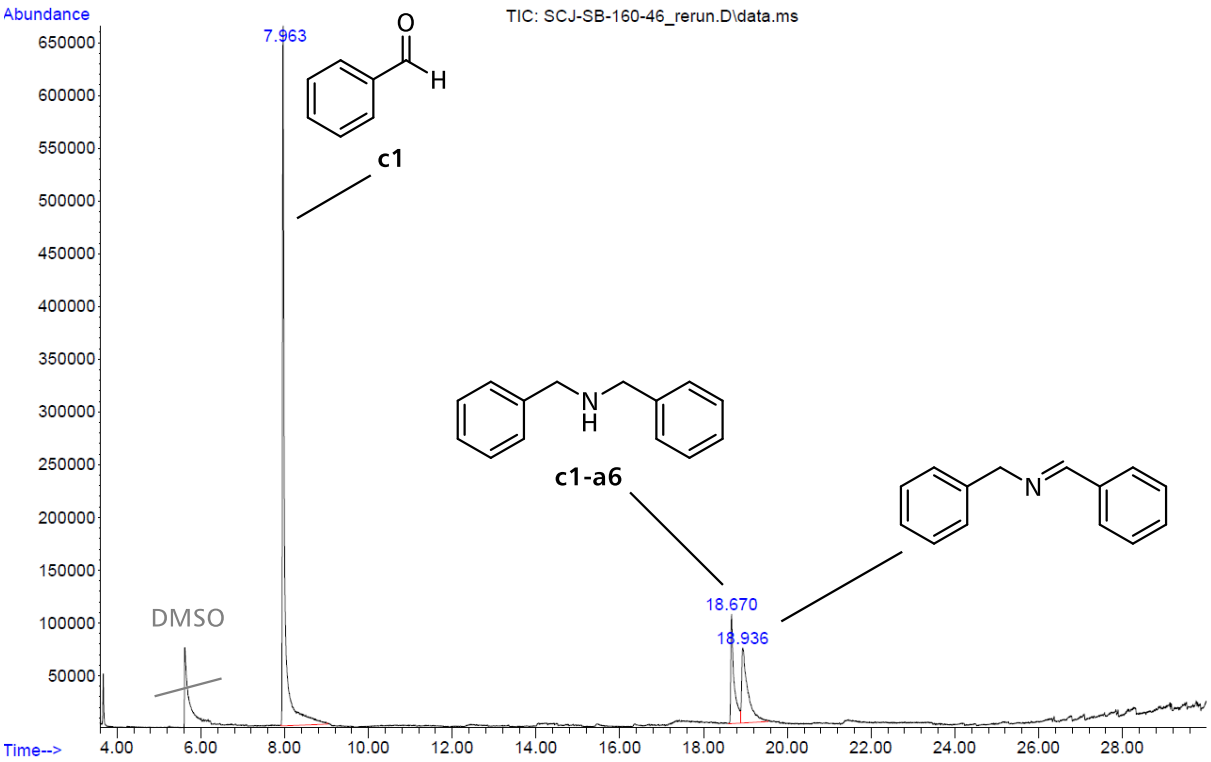


Figure S35. Chromatographic separation of benzaldehyde (**c1**, t_r 8.0 min), dibenzylamine (**c1-a6**, t_r 18.7 min), and *N*-benzyl-1-phenylmethanimine (t_r 18.9 min) using GC–MS method GC-MS3. Sample generated by biotransformation of **c1** and ammonium acetate (**a1**) using IR0021.

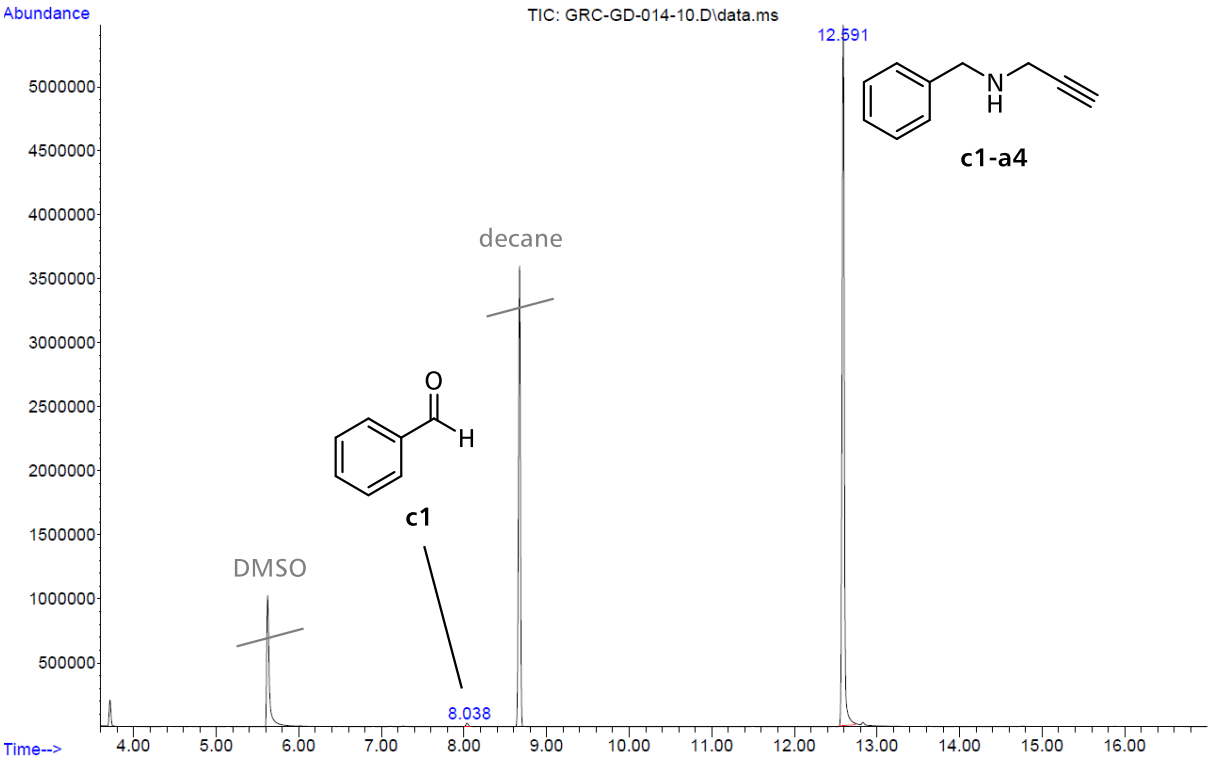


Figure S36. Chromatographic separation of benzaldehyde (**c1**, t_r 8.0 min) and *N*-benzylprop-2-yn-1-amine (**c1-a4**, t_r 12.6 min) using GC–MS method GC-MS1. Sample generated by biotransformation of **c1** and propargylamine (**a4**) using IR0032.

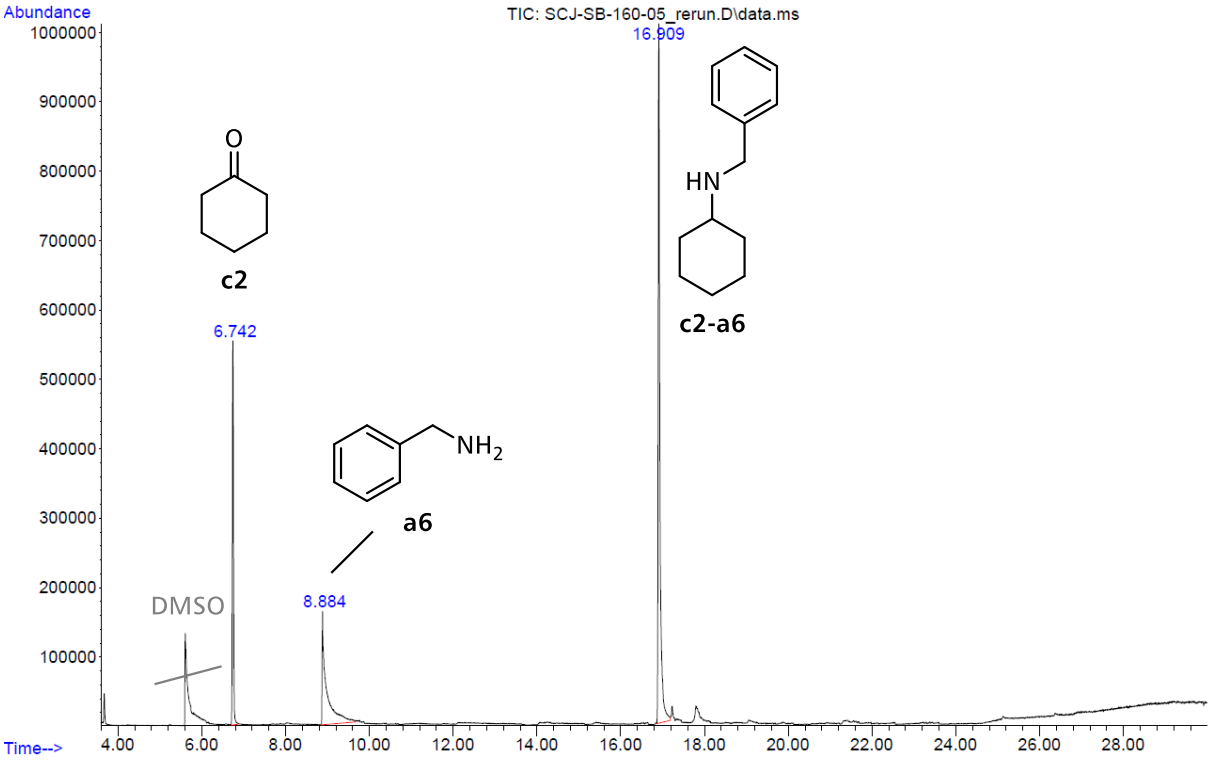


Figure S37. Chromatographic separation of cyclohexanone (**c2**, t_r 6.7 min), benzylamine (**a6**, t_r 8.9 min), and *N*-benzylcyclohexanamine (**c2-a6**, t_r 16.9 min) using GC–MS method GC-MS3. Sample generated by biotransformation of **c2** and **a6** using IR0070.

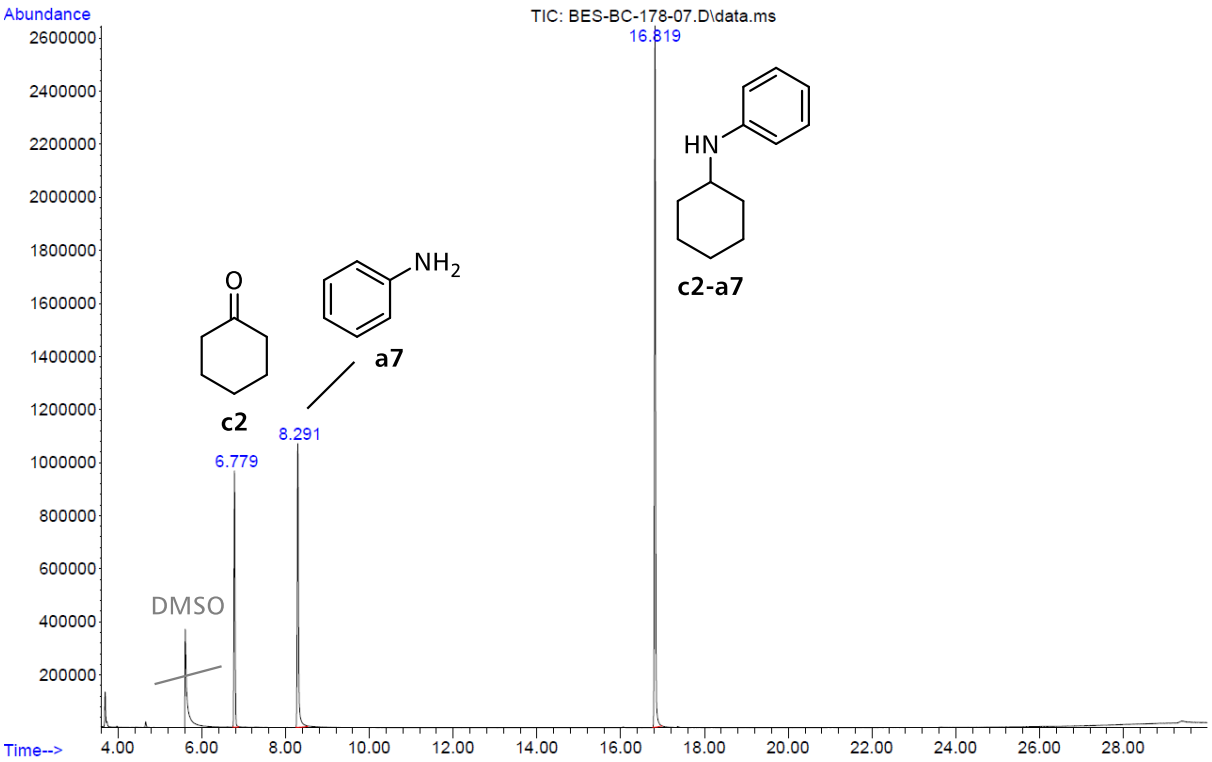


Figure S38. Chromatographic separation of cyclohexanone (**c2**, t_r 6.8 min), aniline (**a7**, t_r 8.3 min), and *N*-cyclohexylaniline (**c2-a7**, t_r 16.8 min) using GC–MS method GC-MS3. Sample generated by biotransformation of **c2** and **a7** using IR1105.

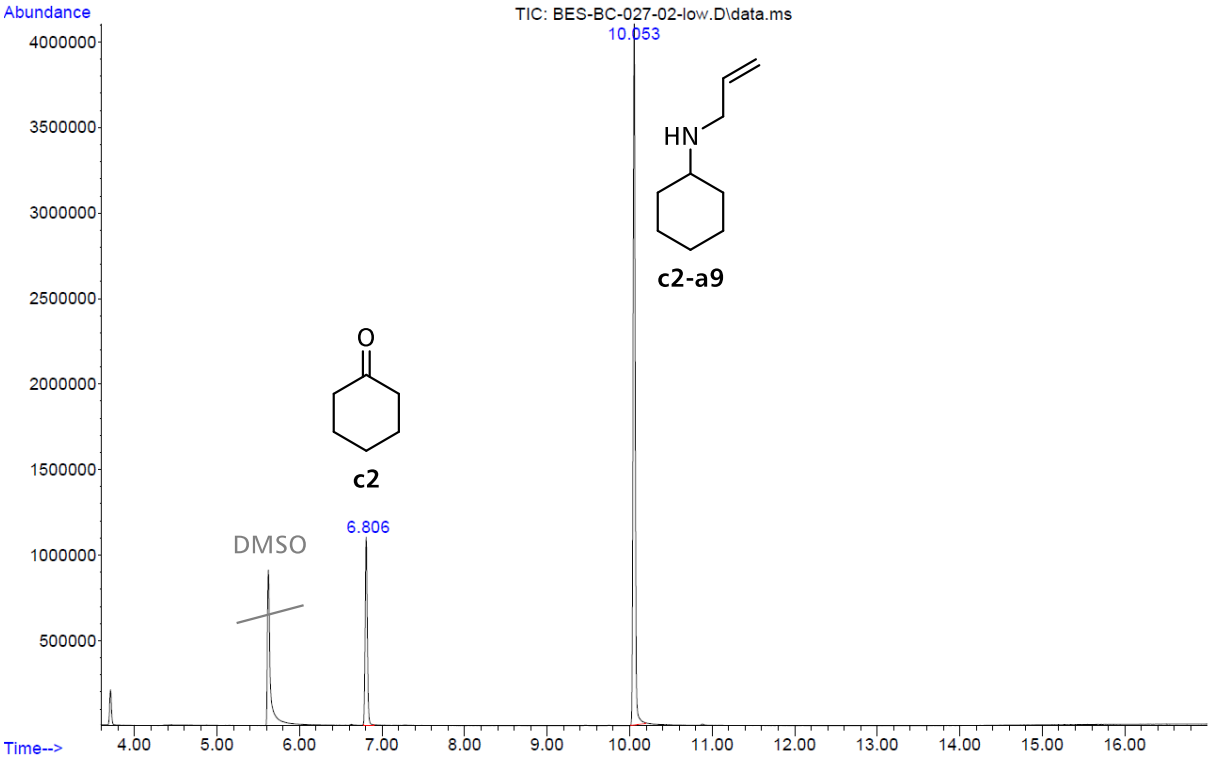


Figure S39. Chromatographic separation of cyclohexanone (**c2**, t_r 6.8 min) and *N*-allylcyclohexanamine (**c2-a9**, t_r 10.1 min) using GC–MS method GC-MS1. Sample generated by biotransformation of **c2** and **a9** using IR0020.

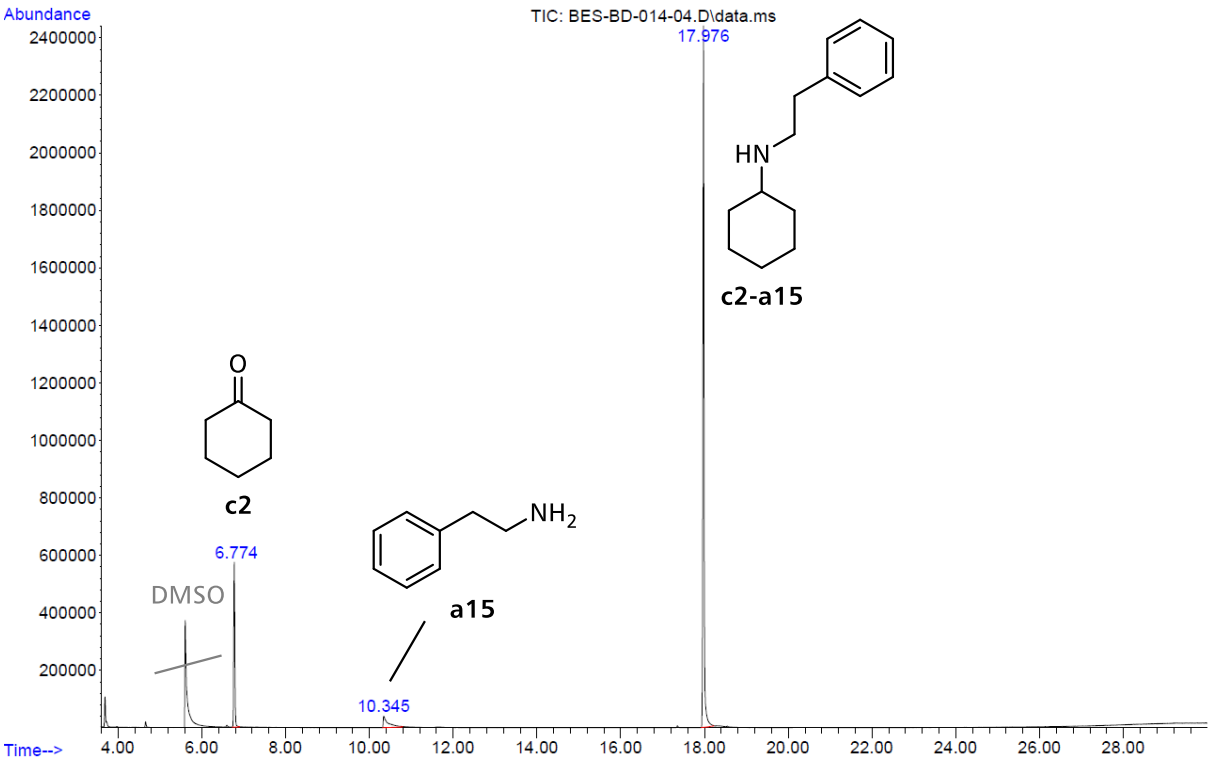


Figure S40. Chromatographic separation of cyclohexanone (**c2**, t_r 6.8 min), 2-phenylethylamine (**a15**, t_r 10.3 min), and *N*-phenethylcyclohexanamine (**c2-a15**, t_r 18.0 min) using GC–MS method GC-MS3. Sample generated by biotransformation of **c2** and **a15** using IR0468.

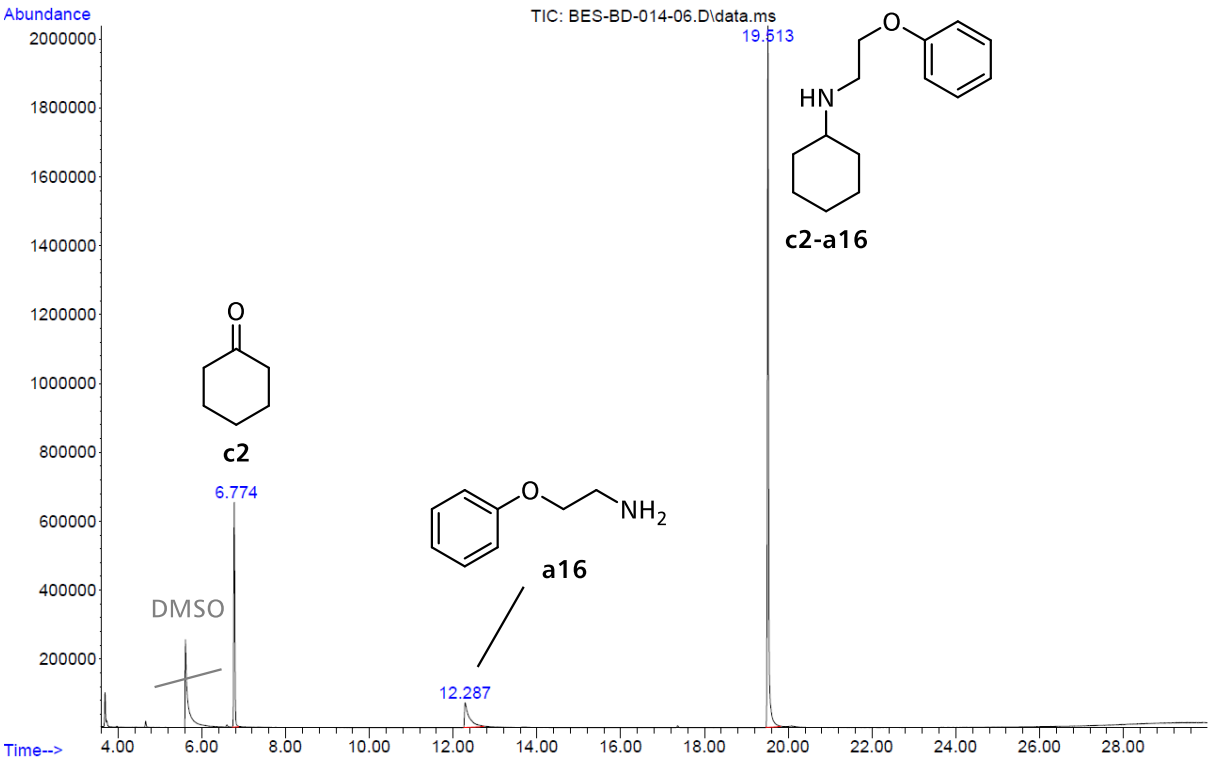


Figure S41. Chromatographic separation of cyclohexanone (**c2**, t_r 6.8 min), 2-phenoxyethan-1-amine (**a16**, t_r 12.3 min), and *N*-(2-phenoxyethyl)cyclohexanamine (**c2-a16**, t_r 19.5 min) using GC–MS method GC-MS3. Sample generated by biotransformation of **c2** and **a16** using IR1738.

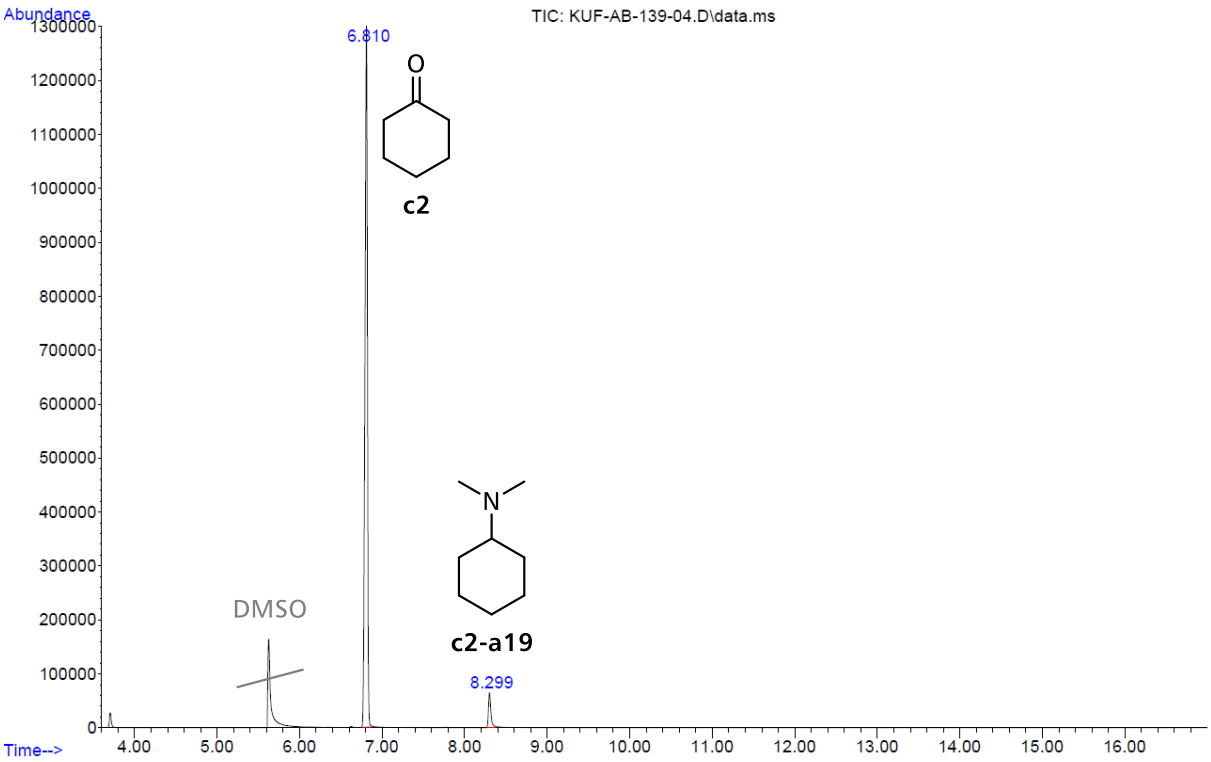


Figure S42. Chromatographic separation of cyclohexanone (**c2**, t_r 6.8 min) and *N*,*N*-dimethylcyclohexanamine (**c2-a19**, t_r 8.3 min) using GC–MS method GC-MS1. Sample generated by biotransformation of **c2** and dimethylamine (**a19**) using IR0052.

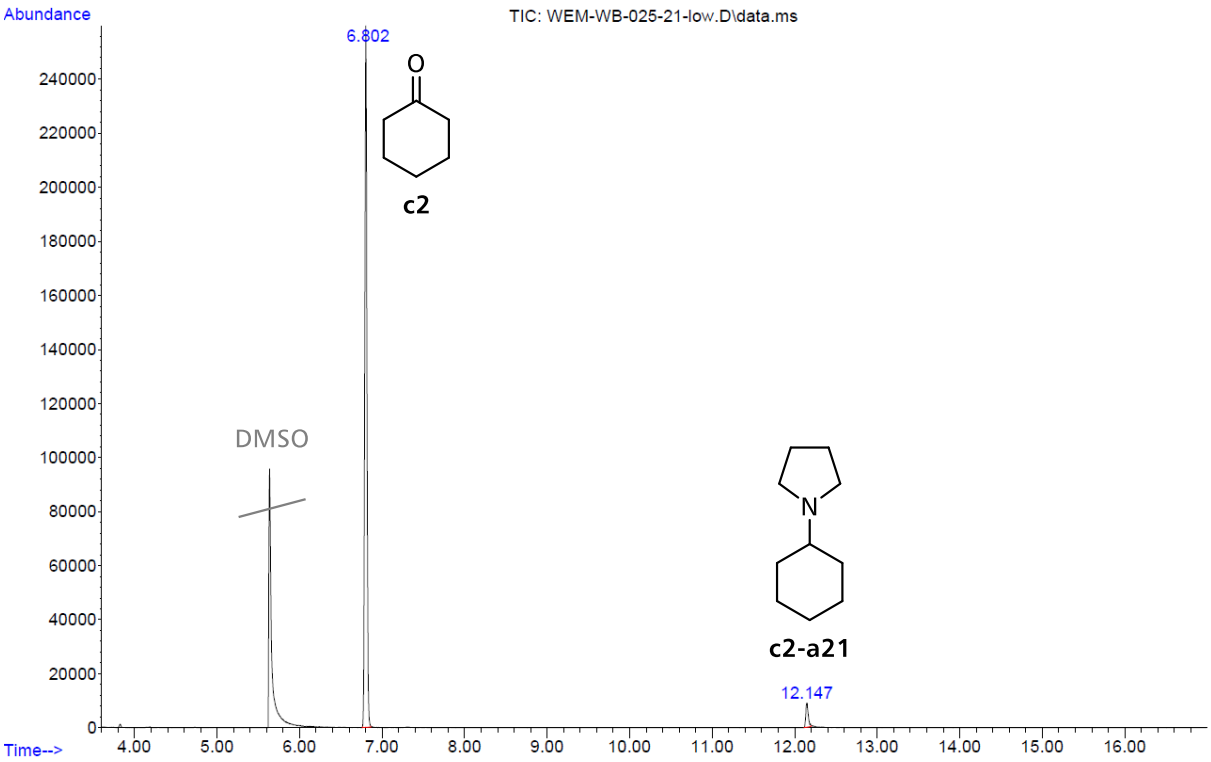


Figure S43. Chromatographic separation of cyclohexanone (**c2**, t_r 6.8 min) and 1-cyclohexylpyrrolidine (**c2-a21**, t_r 12.1 min) using GC–MS method GC-MS1. Sample generated by biotransformation of **c2** and pyrrolidine (**a21**) using IR0001.

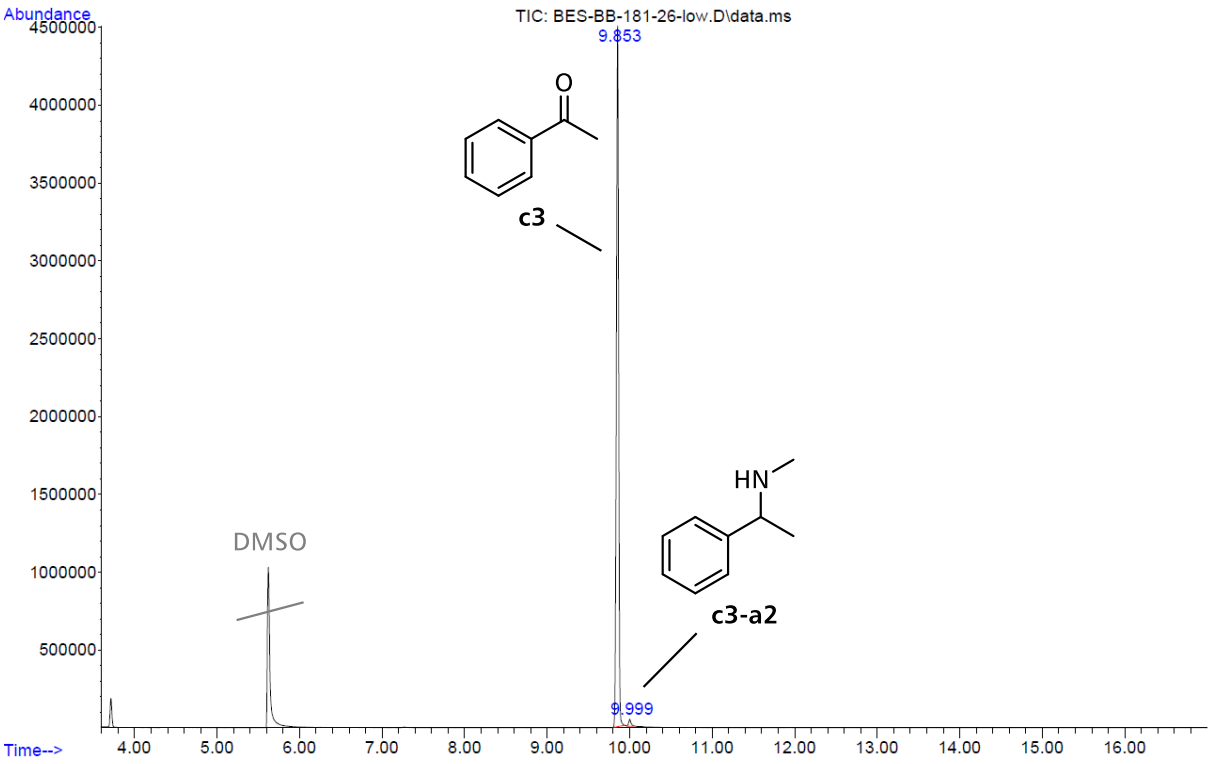


Figure S44. Chromatographic separation of acetophenone (**c3**, t_r 9.9 min) and *N*-methyl-1-phenylethan-1-amine (**c3-a2**, t_r 10.0 min) using GC–MS method GC-MS1. Sample generated by biotransformation of **c3** and methylamine (**a2**) using IR0041.

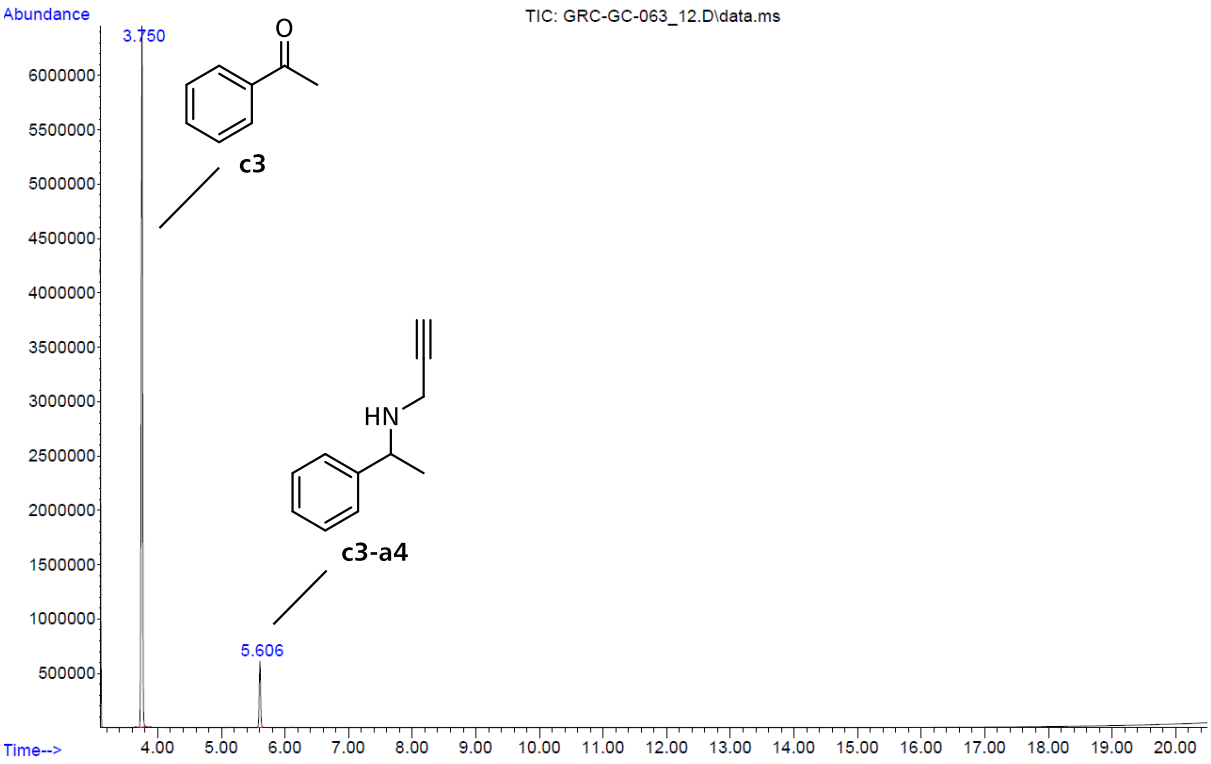


Figure S45. Chromatographic separation of acetophenone (**c3**, t_r 3.8 min) and *N*-(1-phenylethyl)-prop-2-yn-1-amine (**c3-a4**, t_r 5.6 min) using GC–MS method GC-MS2. Sample generated by biotransformation of **c3** and propargylamine (**a4**) using IR0035.

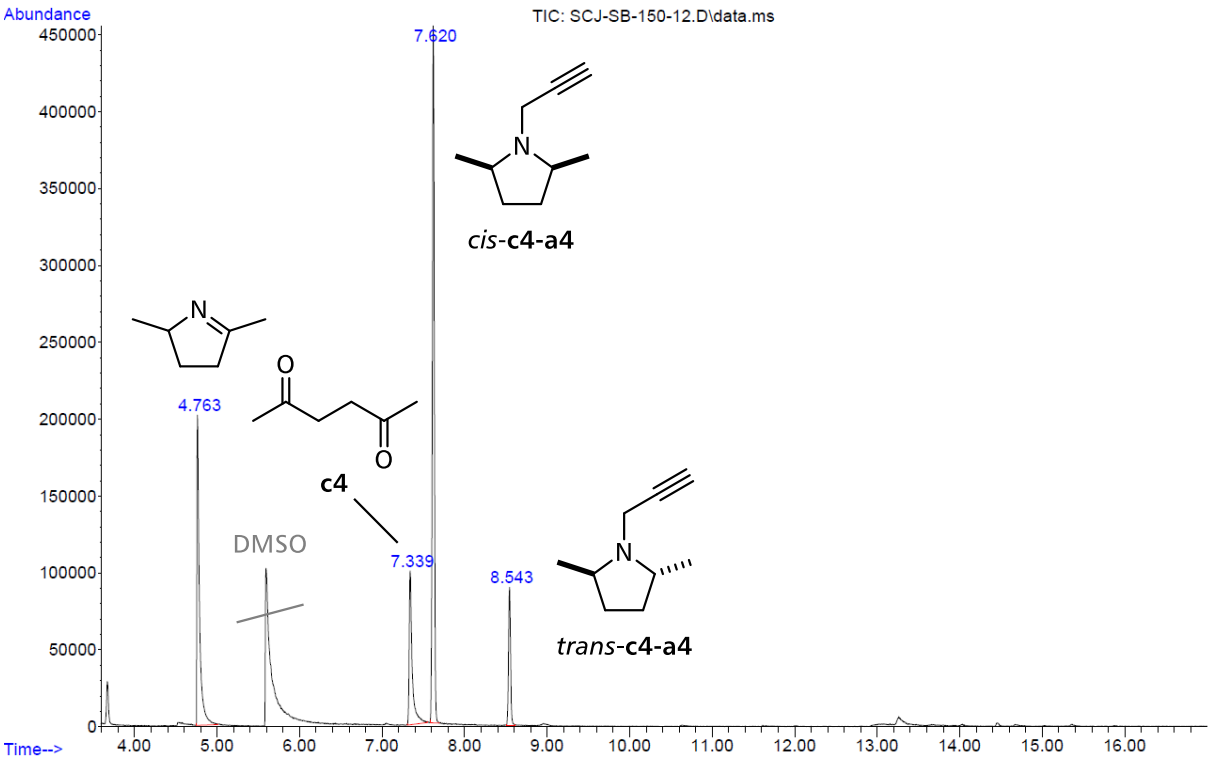


Figure S46. Chromatographic separation of 2,5-dimethyl-3,4-dihydro-2*H*-pyrrole (t_r 4.8 min), hexane-2,5-dione (**c4**, t_r 7.3 min), *cis*-2,5-dimethyl-1-(prop-2-yn-1-yl)pyrrolidine (*cis*-**c4-a4**, t_r 7.6 min), and *trans*-2,5-dimethyl-1-(prop-2-yn-1-yl)pyrrolidine (*trans*-**c4-a4**, t_r 8.5 min) using GC–MS method GC-MS1. Sample generated by biotransformation of **c4** and propargylamine (**a4**) using IR0035.

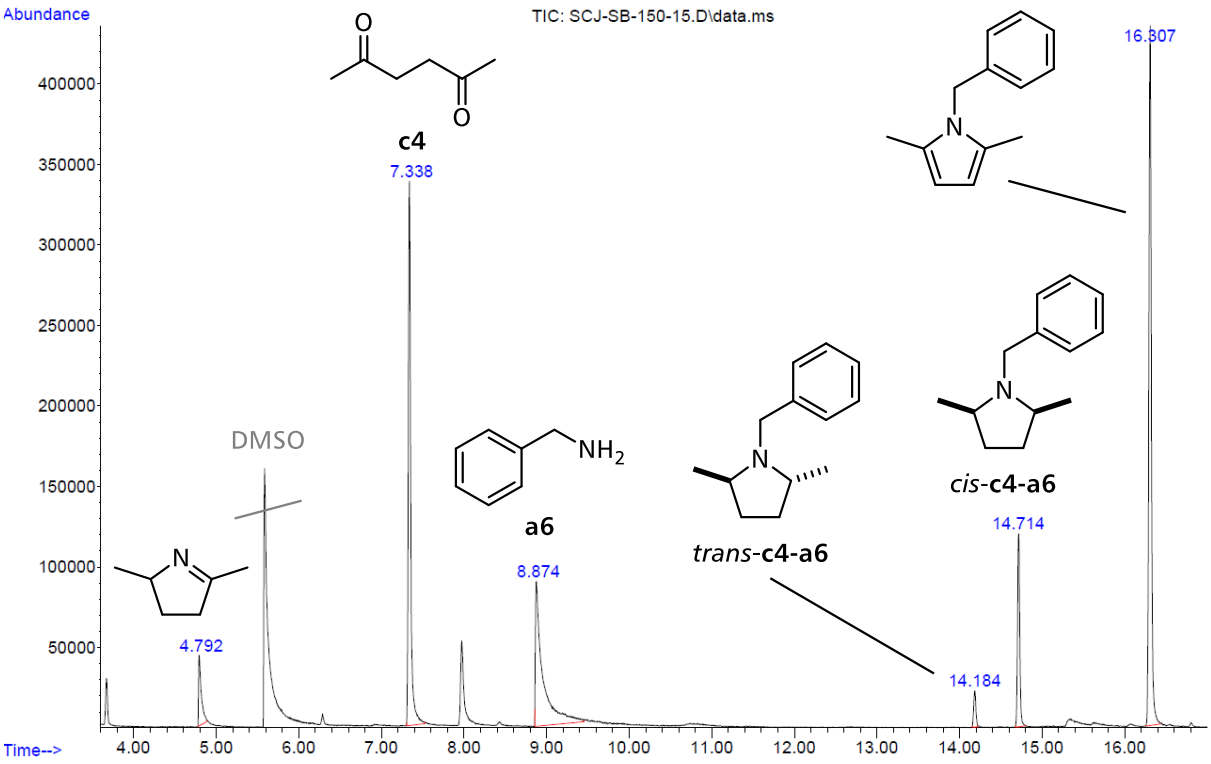


Figure S47. Chromatographic separation of 2,5-dimethyl-3,4-dihydro-2*H*-pyrrole (t_r 4.8 min), hexane-2,5-dione (**c4**, t_r 7.3 min), benzylamine (**a6**, t_r 8.9 min), *trans*-1-benzyl-2,5-dimethylpyrrolidine (*trans*-**c4-a6**, t_r 14.2 min), *cis*-1-benzyl-2,5-dimethylpyrrolidine (*cis*-**c4-a6**, t_r 14.7 min), and 1-benzyl-2,5-dimethyl-1*H*-pyrrole (t_r 16.3 min) using GC–MS method GC-MS1. Sample generated by biotransformation of **c4** and **a6** using IR2128.

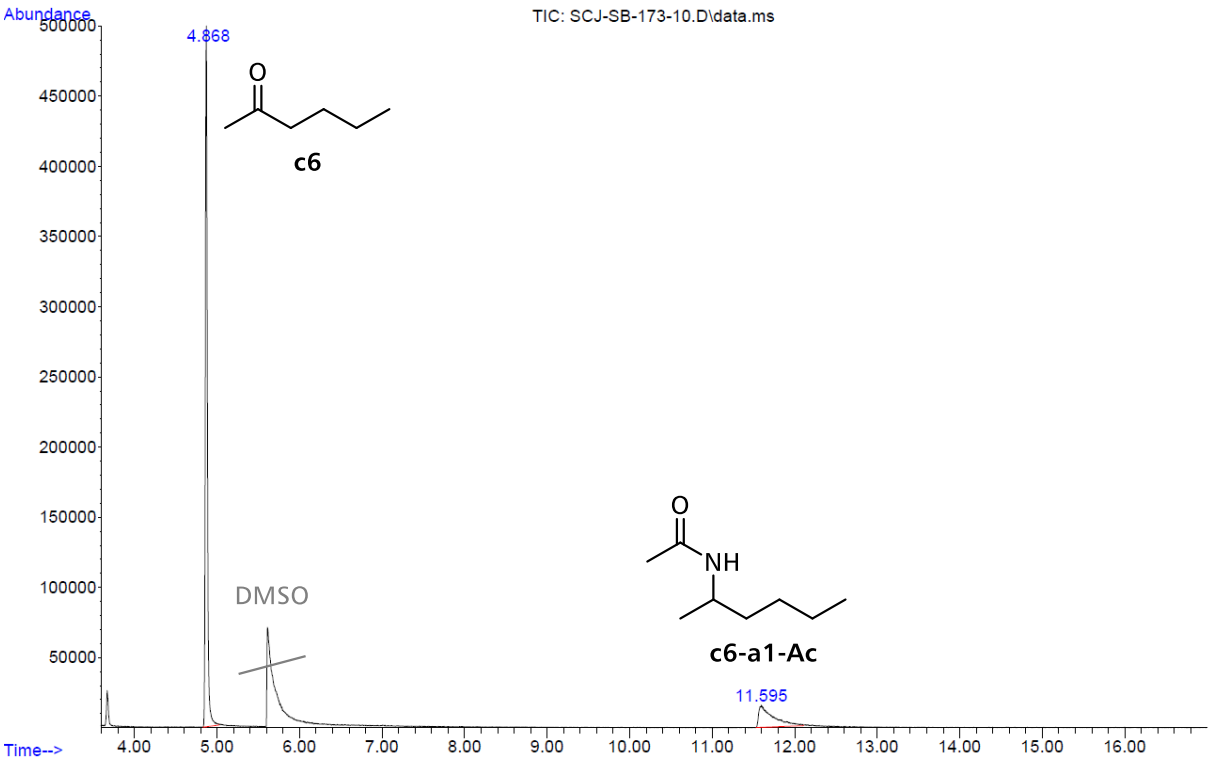


Figure S48. Chromatographic separation of hexan-2-one (**c6**, t_r 4.9 min) and *N*-(hexan-2-yl)acetamide (**c6-a1-Ac**, t_r 11.6 min) using GC–MS method GC-MS1. Sample generated by biotransformation of **c6** and ammonium acetate (**a1**) using IR2010, followed by acetylation.

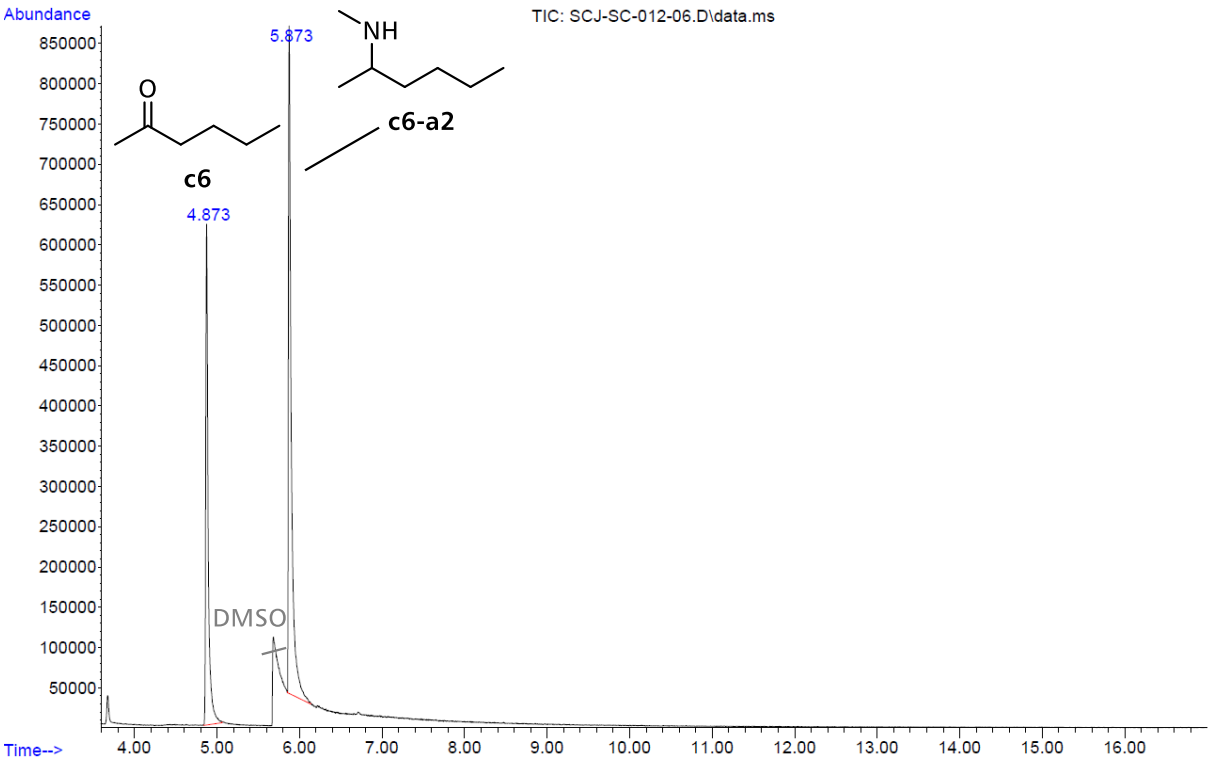


Figure S49. Chromatographic separation of hexan-2-one (**c6**, t_r 4.9 min) and *N*-methylhexan-2-amine (**c6-a2**, t_r 5.9 min) using GC–MS method GC-MS1. Sample generated by biotransformation of **c6** and methylamine (**a2**) using IR2021.

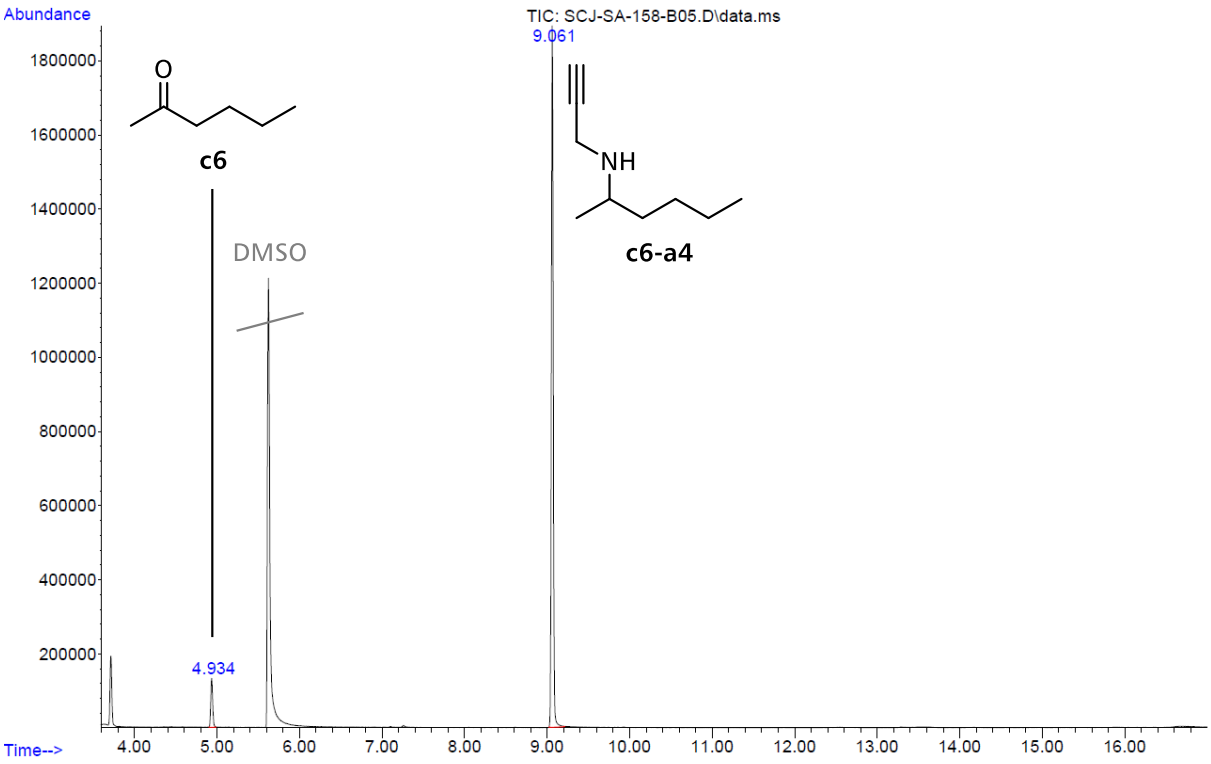


Figure S50. Chromatographic separation of hexan-2-one (**c6**, t_r 4.9 min) and *N*-(prop-2-yn-1-yl)hexan-2-amine (**c6-a4**, t_r 9.1 min) using GC–MS method GC-MS1. Sample generated by biotransformation of **c6** and propargylamine (**a4**) using IR0023.

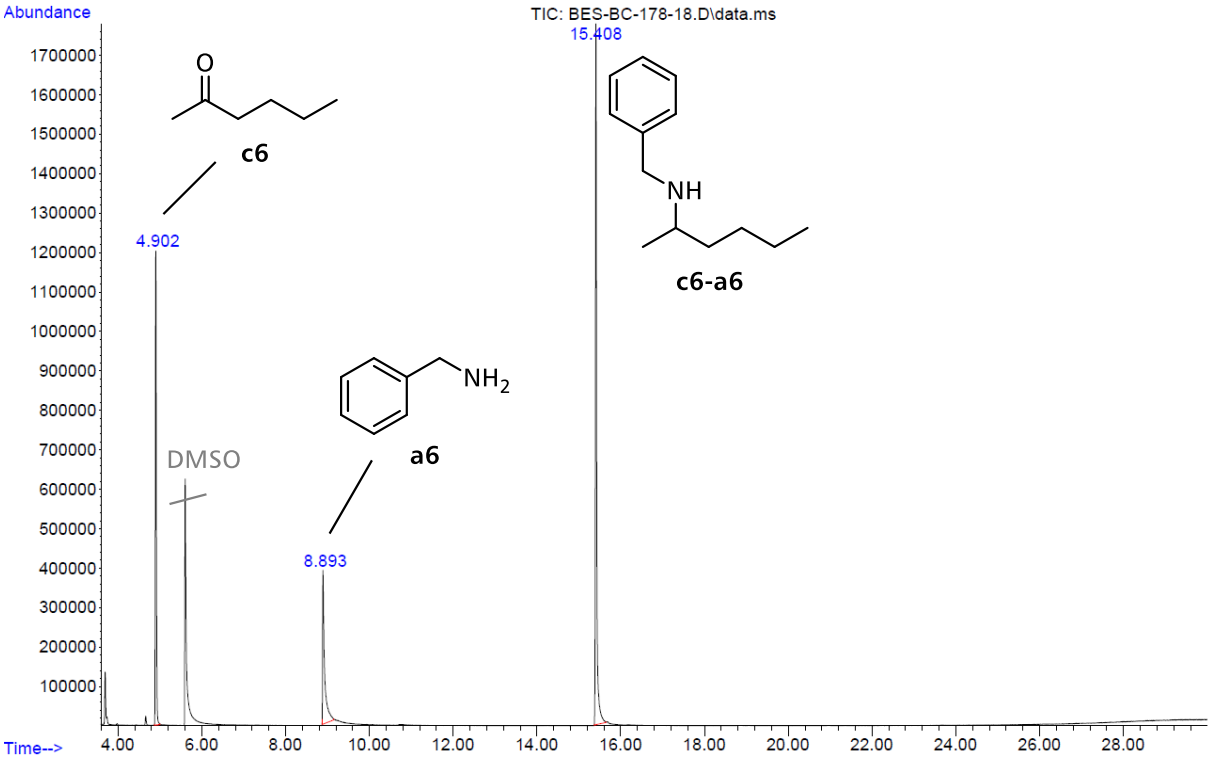


Figure S51. Chromatographic separation of hexan-2-one (**c6**, t_r 4.9 min), benzylamine (**a6**, t_r 8.9 min), and *N*-benzylhexan-2-amine (**c6-a6**, t_r 15.4 min) using GC–MS method GC-MS3. Sample generated by biotransformation of **c6** and **a6** using IR1589.

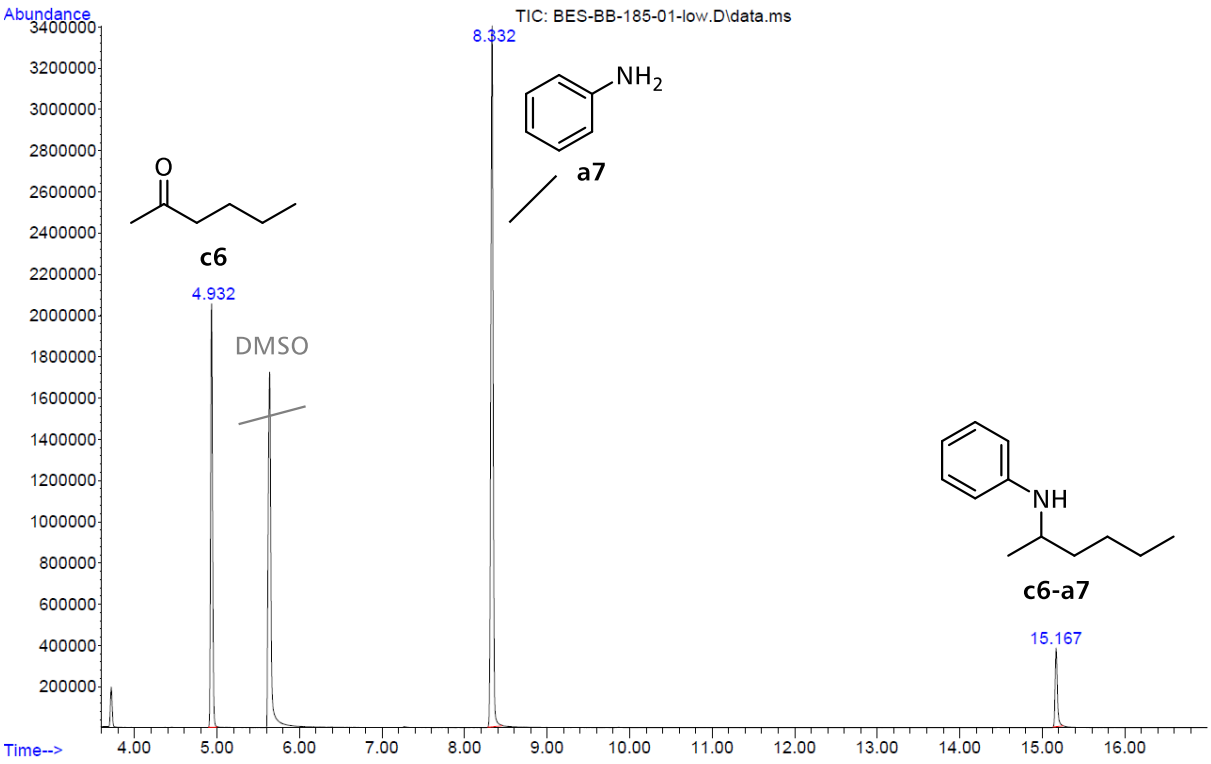


Figure S52. Chromatographic separation of hexan-2-one (**c6**, t_r 4.9 min), aniline (**a7**, t_r 8.3 min), and *N*-(hexan-2-yl)aniline (**c6-a7**, t_r 15.2 min) using GC–MS method GC-MS1. Sample generated by biotransformation of **c6** and **a7** using IR0032.

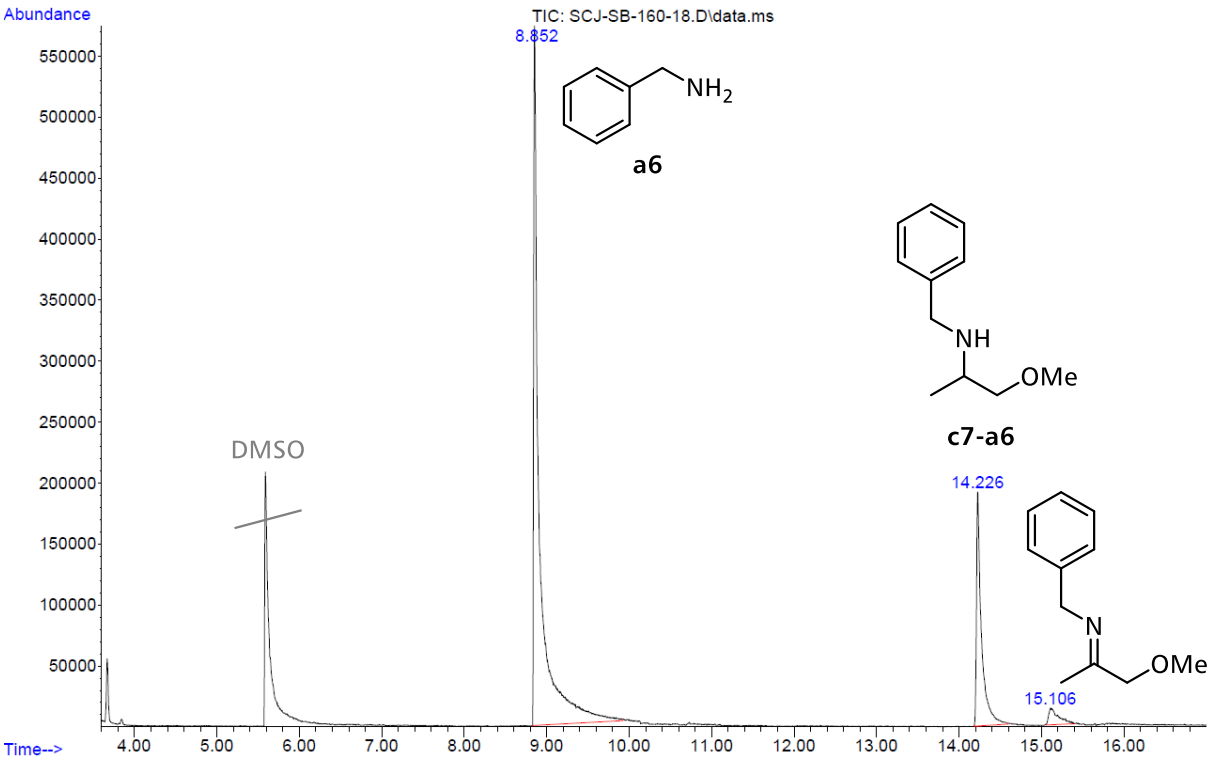


Figure S53. Chromatographic separation of benzylamine (**a6**, t_r 8.9 min), *N*-benzyl-1-methoxypropan-2-amine (**c7-a6**, t_r 14.2 min), and *N*-benzyl-1-methoxypropan-2-imine (t_r 15.1 min) using GC–MS method GC-MS1. Sample generated by biotransformation of methoxyacetone (**c7**) and **a6** using IR1392.

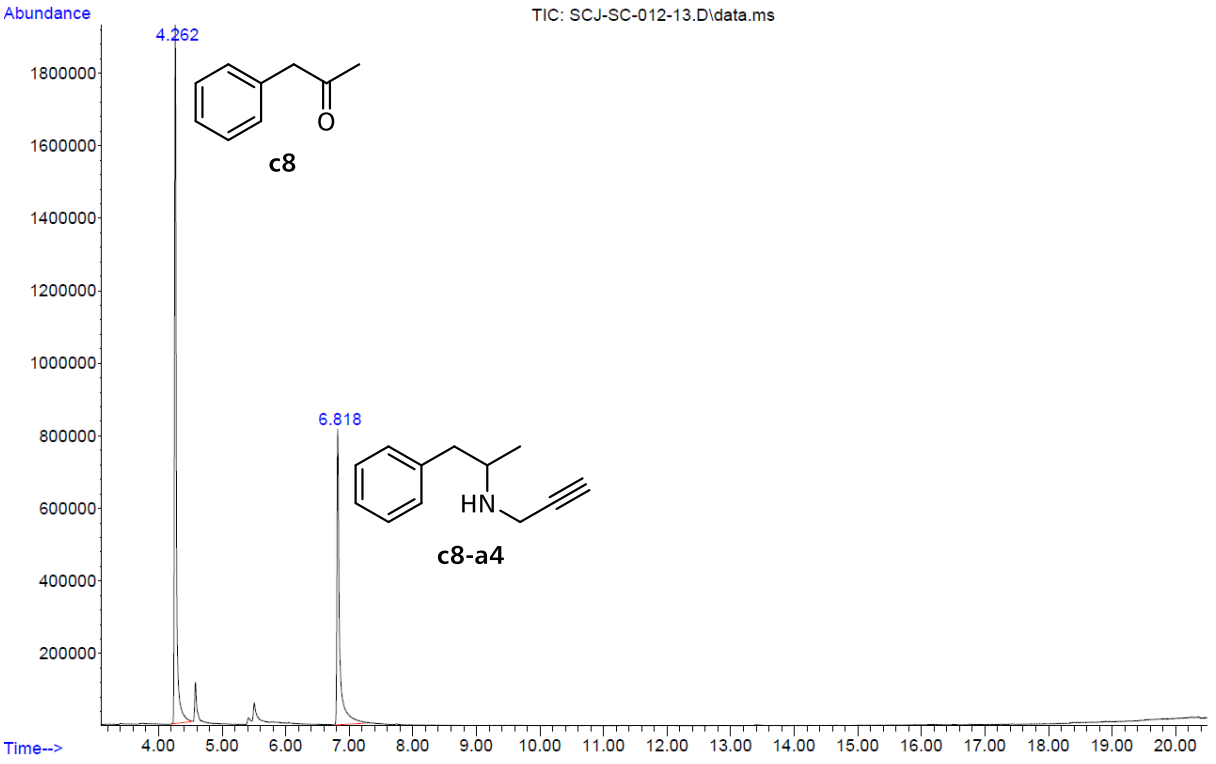


Figure S54. Chromatographic separation of phenylacetone (**c8**, t_r 4.3 min) and *N*-(1-phenylpropan-2-yl)prop-2-yn-1-amine (**c8-a4**, t_r 6.8 min) using GC–MS method GC-MS2. Sample generated by biotransformation of **c8** and propargylamine (**a4**) using IR2021.

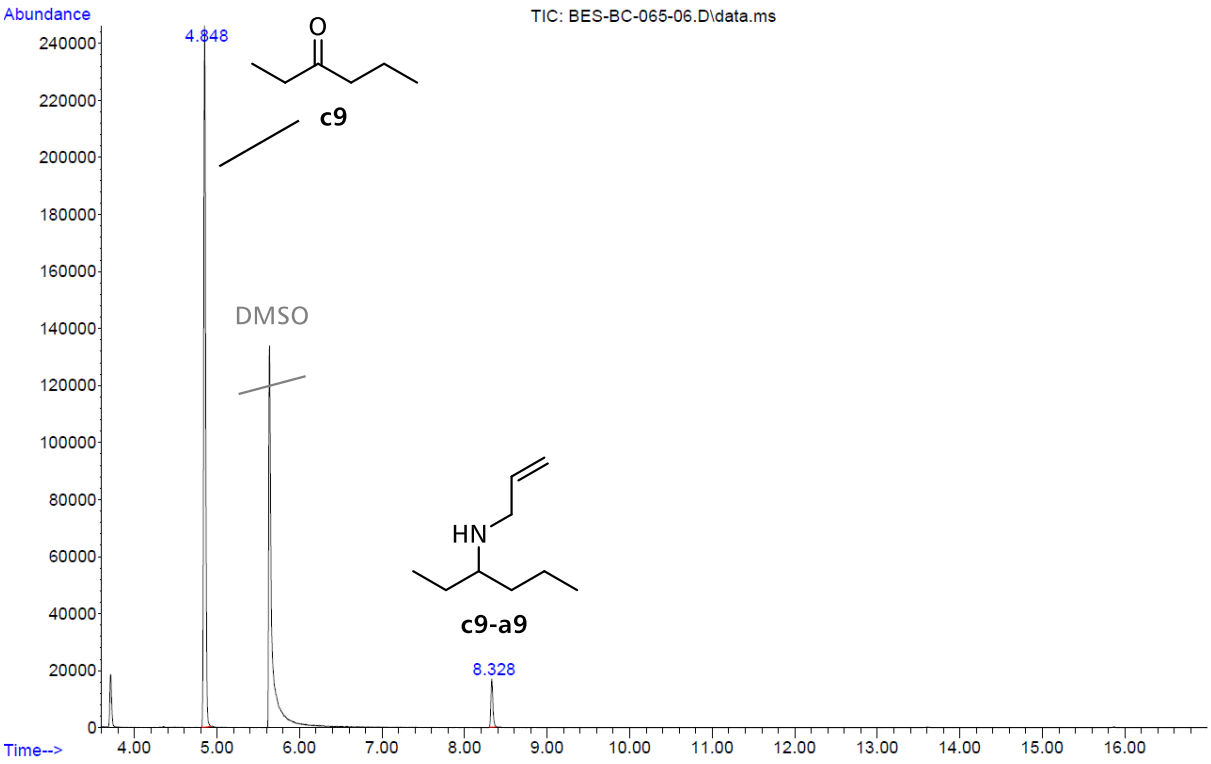


Figure S55. Chromatographic separation of hexan-3-one (**c9**, t_r 4.8 min) and *N*-allylhexan-3-amine (**c9-a9**, t_r 8.3 min) using GC–MS method GC-MS1. Sample generated by biotransformation of **c9** and allylamine (**a9**) using IR0071.

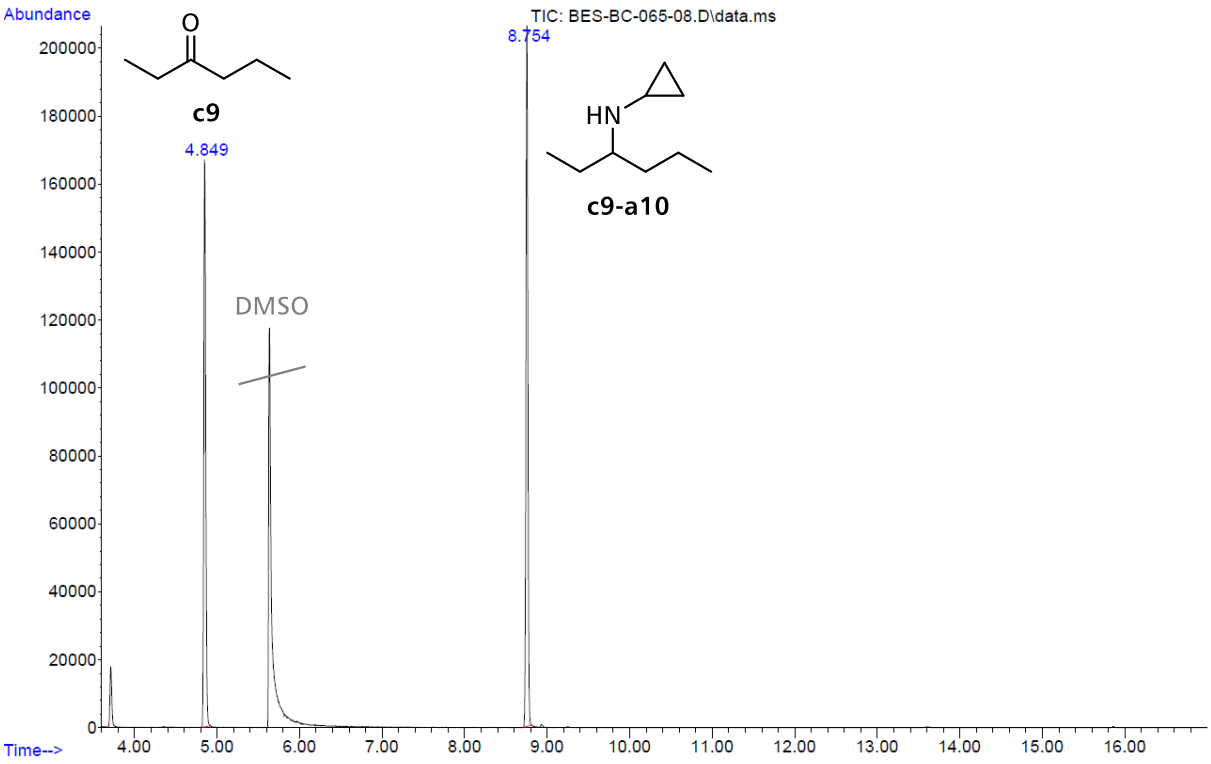


Figure S56. Chromatographic separation of hexan-3-one (**c9**, t_r 4.8 min) and *N*-(hexan-3-yl)-cyclopropanamine (**c9-a10**, t_r 8.8 min) using GC–MS method GC-MS1. Sample generated by biotransformation of **c9** and cyclopropanamine (**a10**) using IR0376.

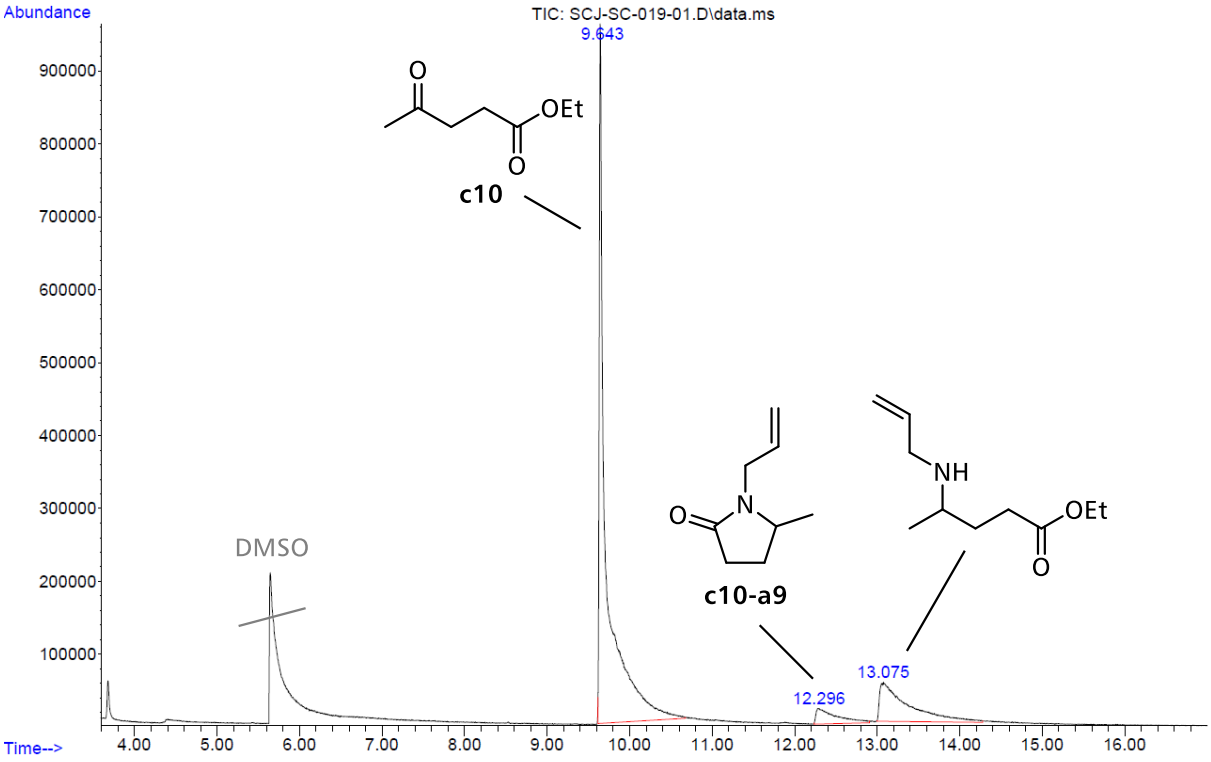


Figure S57. Chromatographic separation of ethyl levulinate (**c10**, t_r 9.6 min), 1-allyl-5-methyl-pyrrolidin-2-one (**c10-a9**, t_r 12.3 min), and ethyl 4-(allylamino)pentanoate (t_r 13.1 min) using GC–MS method GC-MS1. Sample generated by biotransformation of **c10** and allylamine (**a9**) using IR0043.

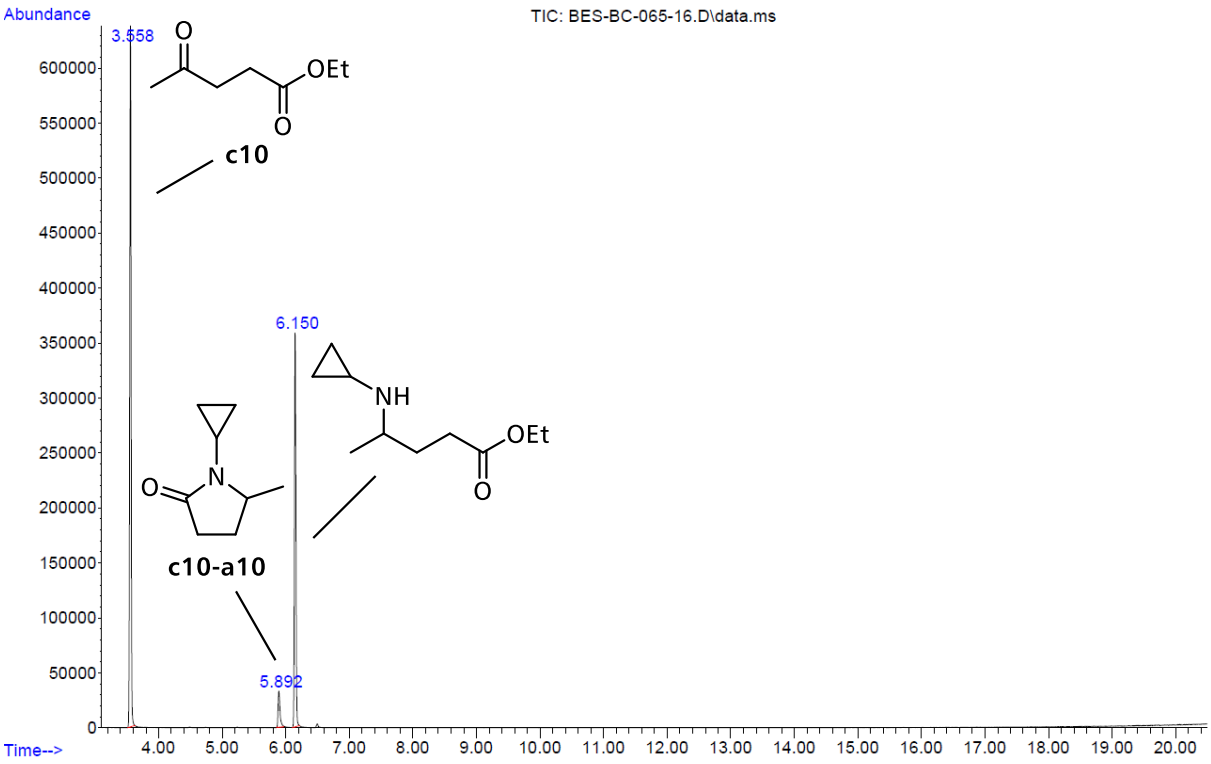


Figure S58. Chromatographic separation of ethyl levulinate (**c10**, t_r 3.6 min), 1-cyclopropyl-5-methyl-pyrrolidin-2-one (**c10-a10**, t_r 5.9 min), and ethyl 4-(cyclopropylamino)pentanoate (t_r 6.2 min) using GC–MS method GC-MS2. Sample generated by biotransformation of **c10** and cyclopropanamine (**a10**) using IR0041.

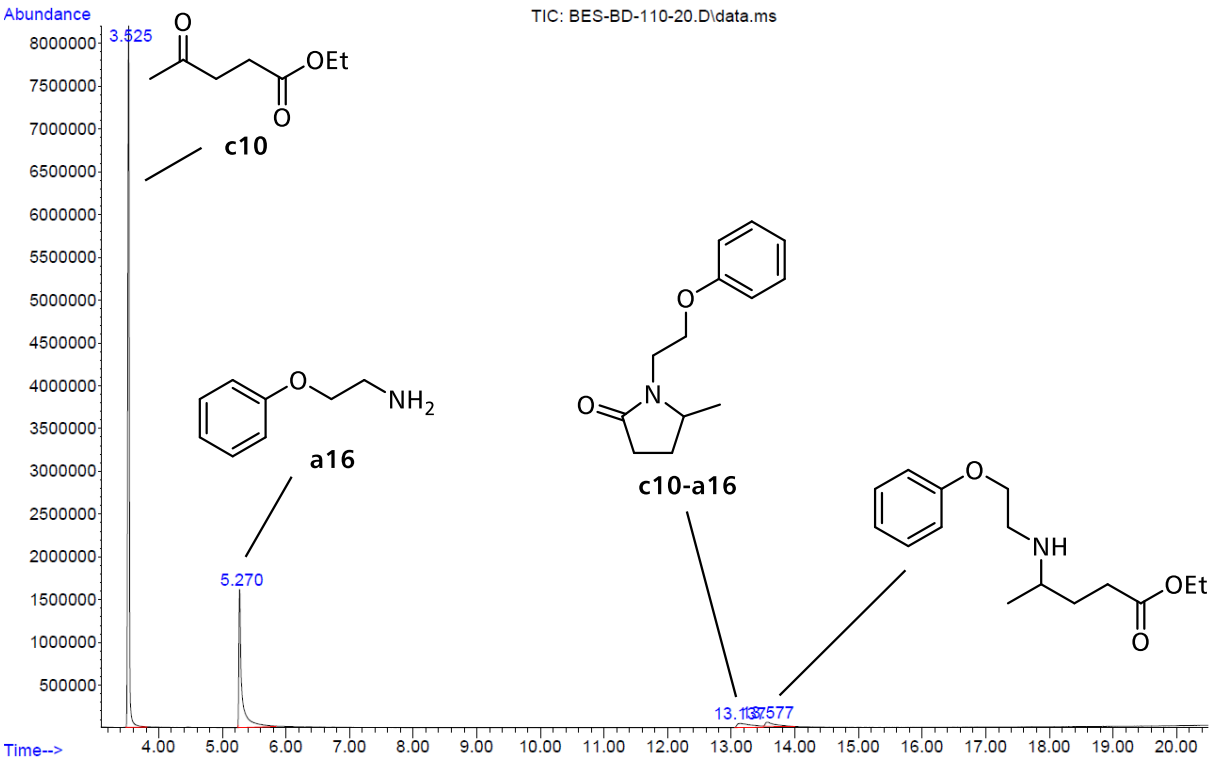


Figure S59. Chromatographic separation of ethyl levulinate (**c10**, t_r 3.5 min), 2-phenoxyethan-1-amine (**a16**, t_r 5.3 min), 5-methyl-1-(2-phenoxyethyl)pyrrolidin-2-one (**c10-a16**, t_r 13.1 min), and ethyl 4-((2-phenoxyethyl)amino)pentanoate (t_r 13.6 min) using GC–MS method GC-MS2. Sample generated by biotransformation of **c10** and **a16** using IR1460.

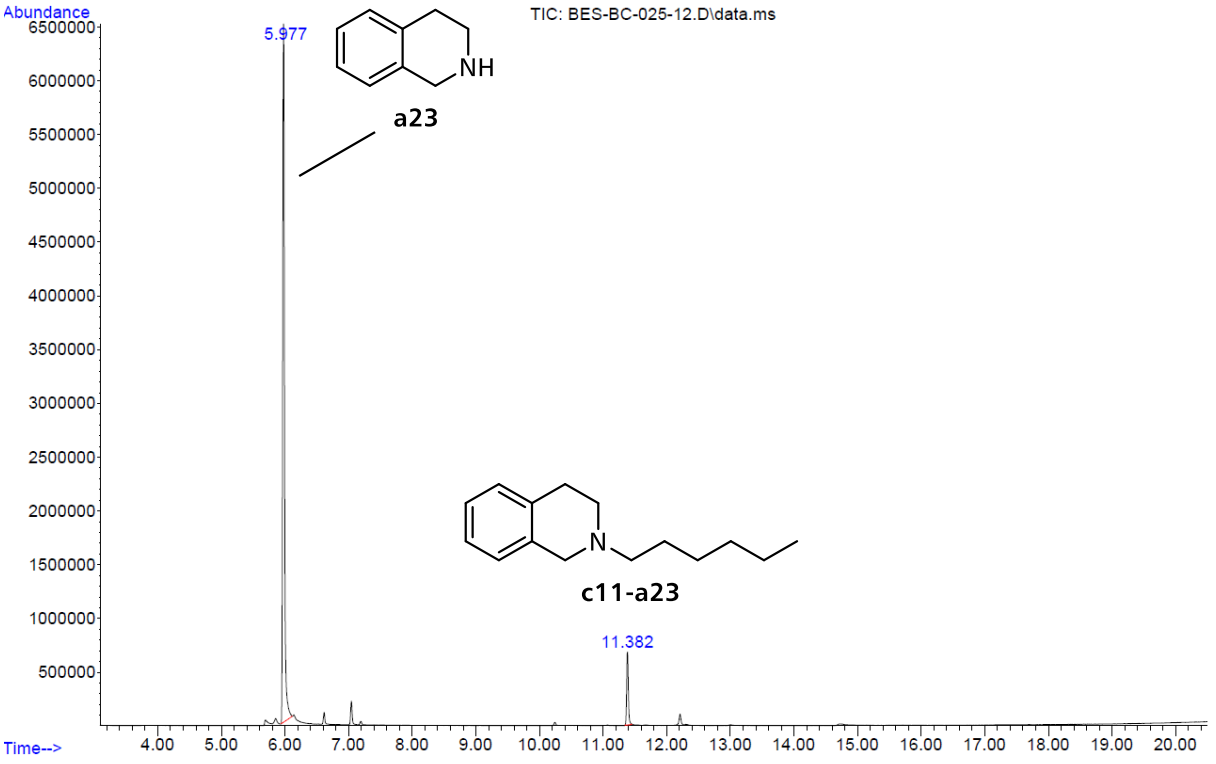


Figure S60. Chromatographic separation of 1,2,3,4-tetrahydroisoquinoline (**a23**, t_r 6.0 min) and 2-hexyl-1,2,3,4-tetrahydroisoquinoline (**c11-a23**, t_r 11.4 min) using GC–MS method GC-MS2. Sample generated by biotransformation of hexanal (**c11**) and **a23** using IR0027.

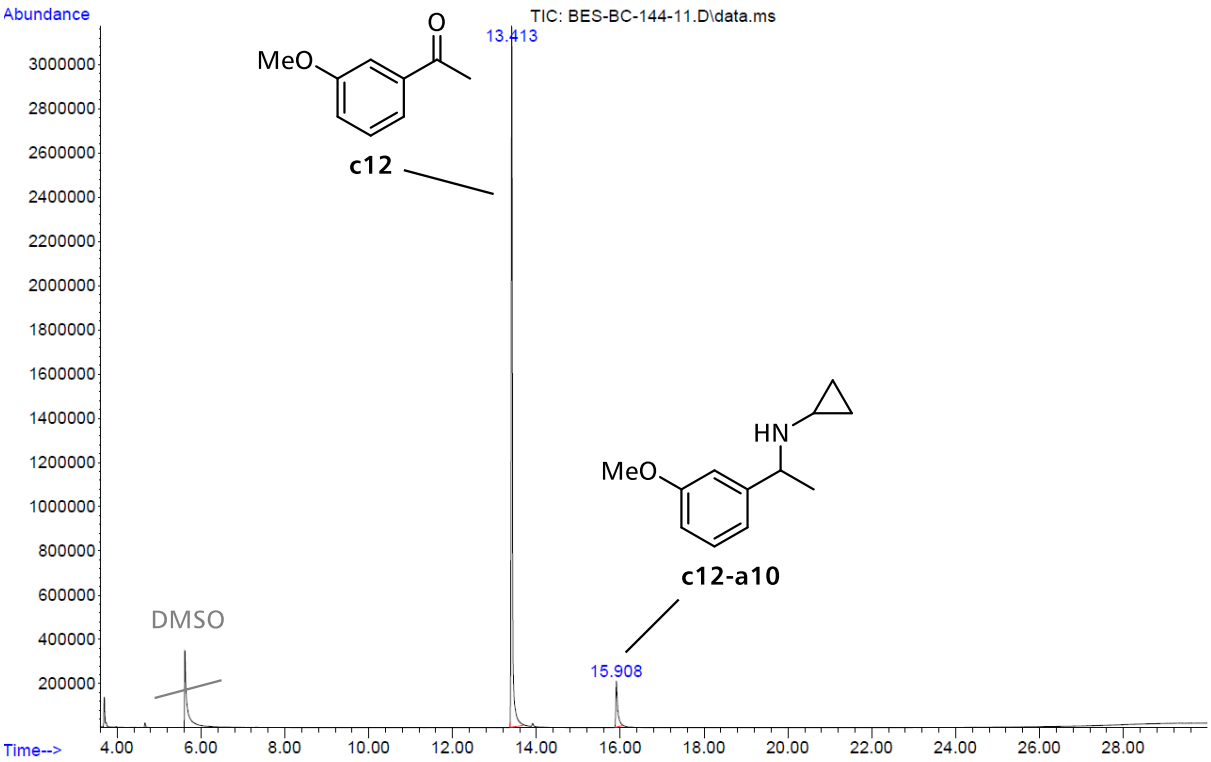


Figure S61. Chromatographic separation of 3-methoxyacetophenone (**c12**, t_r 13.4 min) and *N*-(1-(3-methoxyphenyl)ethyl)cyclopropanamine (**c12-a10**, t_r 15.9 min) using GC–MS method GC-MS3. Sample generated by biotransformation of **c12** and cyclopropanamine (**a10**) using IR2173.

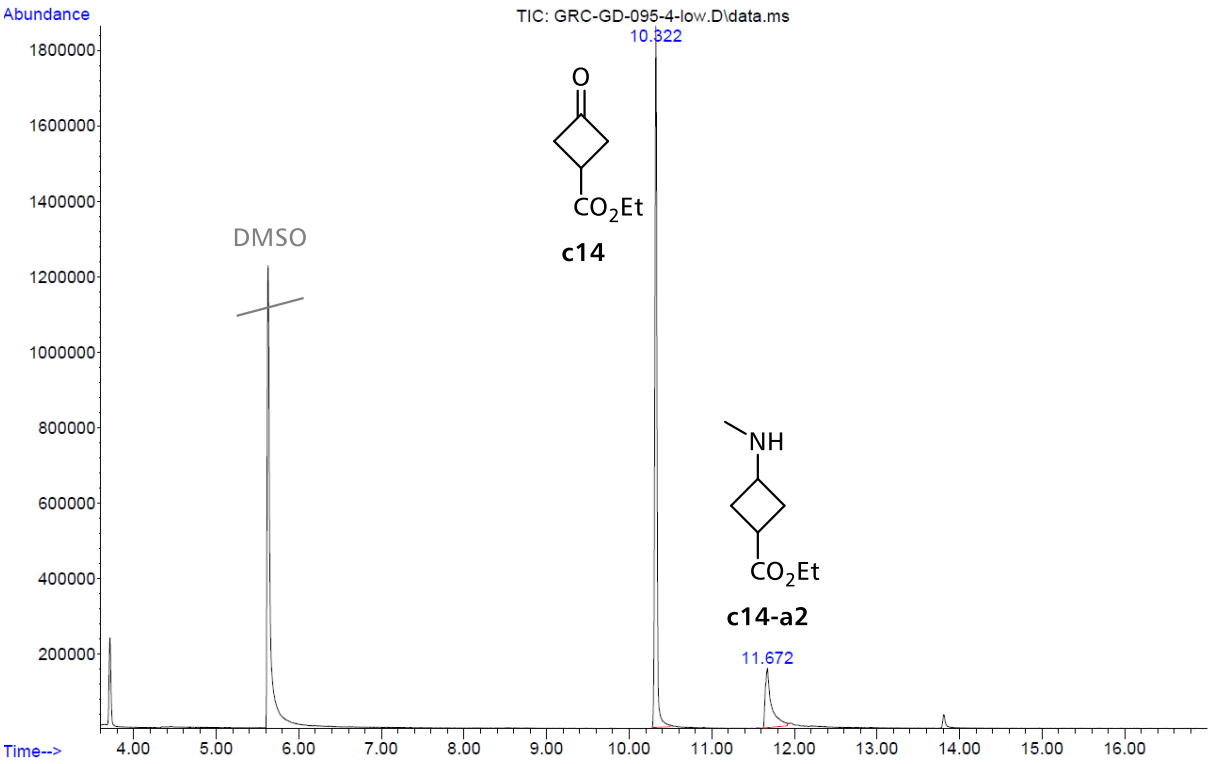


Figure S62. Chromatographic separation of ethyl 3-oxocyclobutane-1-carboxylate (**c14**, t_r 10.3 min) and ethyl 3-(methylamino)cyclobutane-1-carboxylate (**c14-a2**, t_r 11.7 min) using GC–MS method GC-MS1. Sample generated by biotransformation of **c14** and methylamine (**a2**) using IR2021.

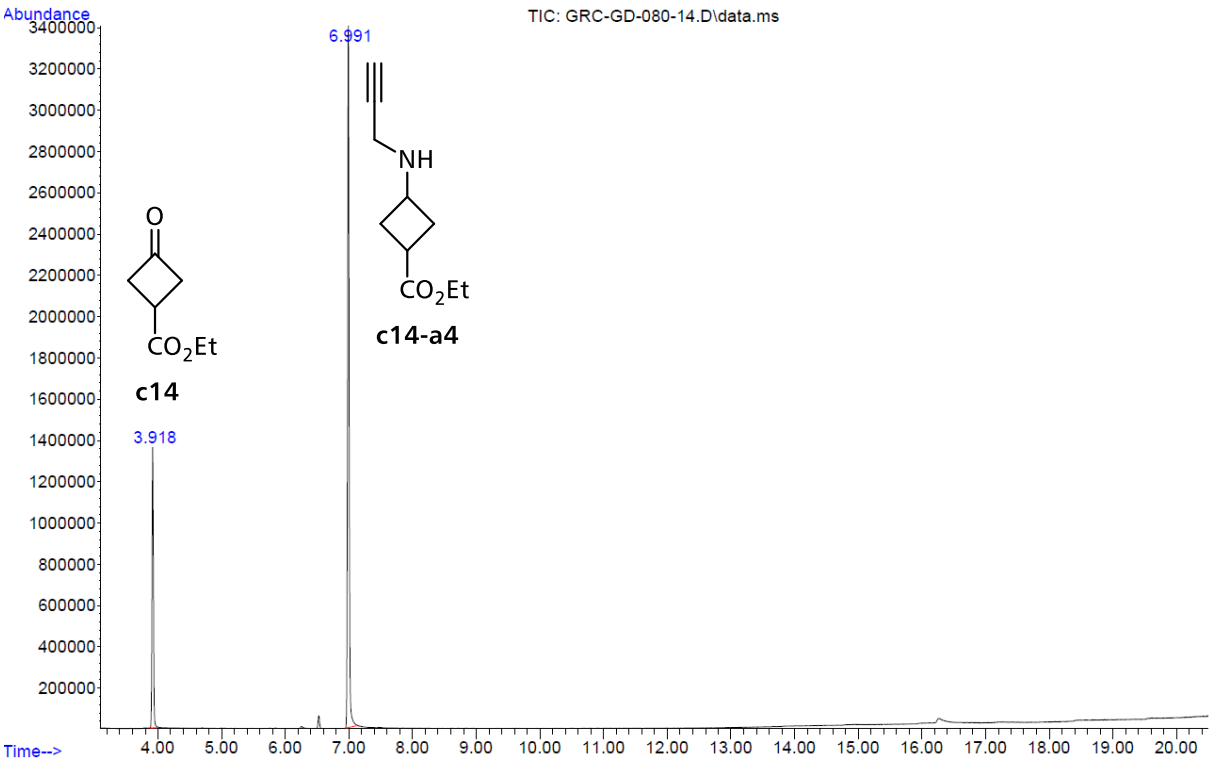


Figure S63. Chromatographic separation of ethyl 3-oxocyclobutane-1-carboxylate (**c14**, t_r 3.9 min) and ethyl 3-(prop-2-yn-1-ylamino)cyclobutane-1-carboxylate (**c14-a4**, t_r 7.0 min) using GC–MS method GC-MS2. Sample generated by biotransformation of **c14** and propargylamine (**a4**) using IR2021.

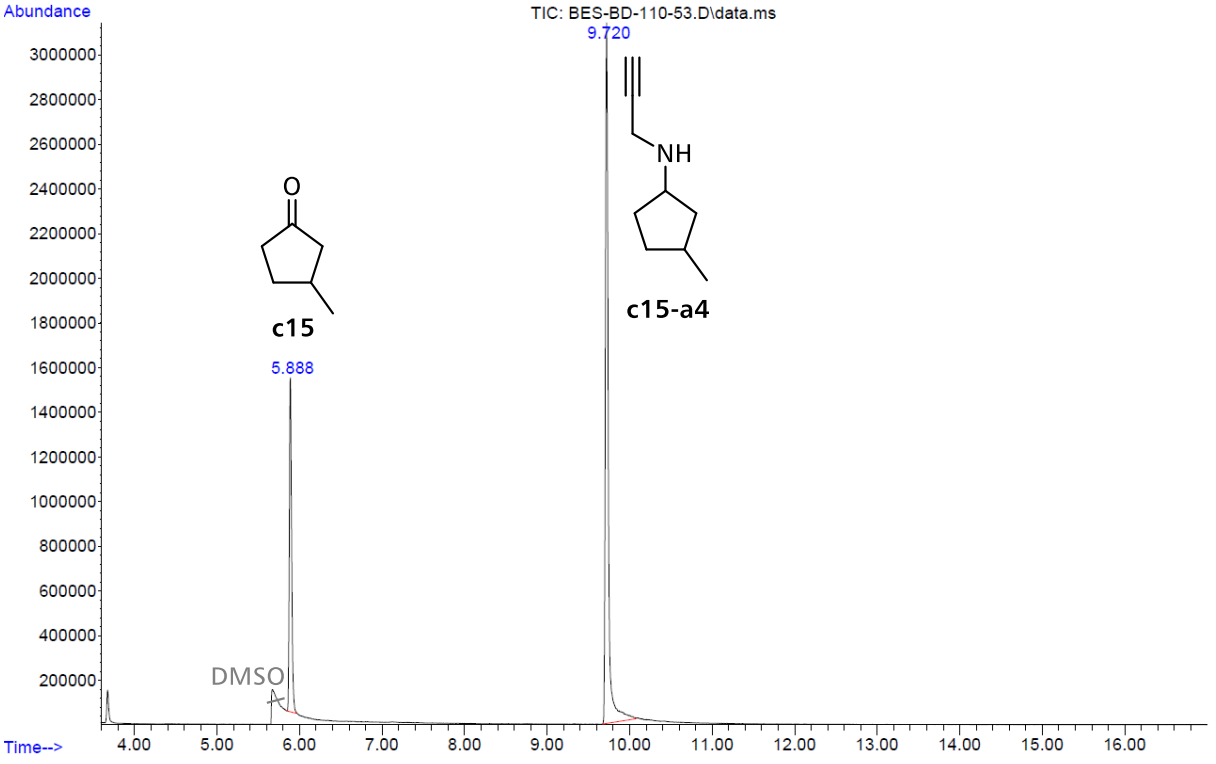


Figure S64. Chromatographic separation of 3-methylcyclopentan-1-one (**c15**, t_r 5.9 min) and 3-methyl-*N*-(prop-2-yn-1-yl)cyclopentan-1-amine (**c15-a4**, t_r 9.7 min) using GC–MS method GC-MS1. Sample generated by biotransformation of **c15** and propargylamine (**a4**) using IR0009.

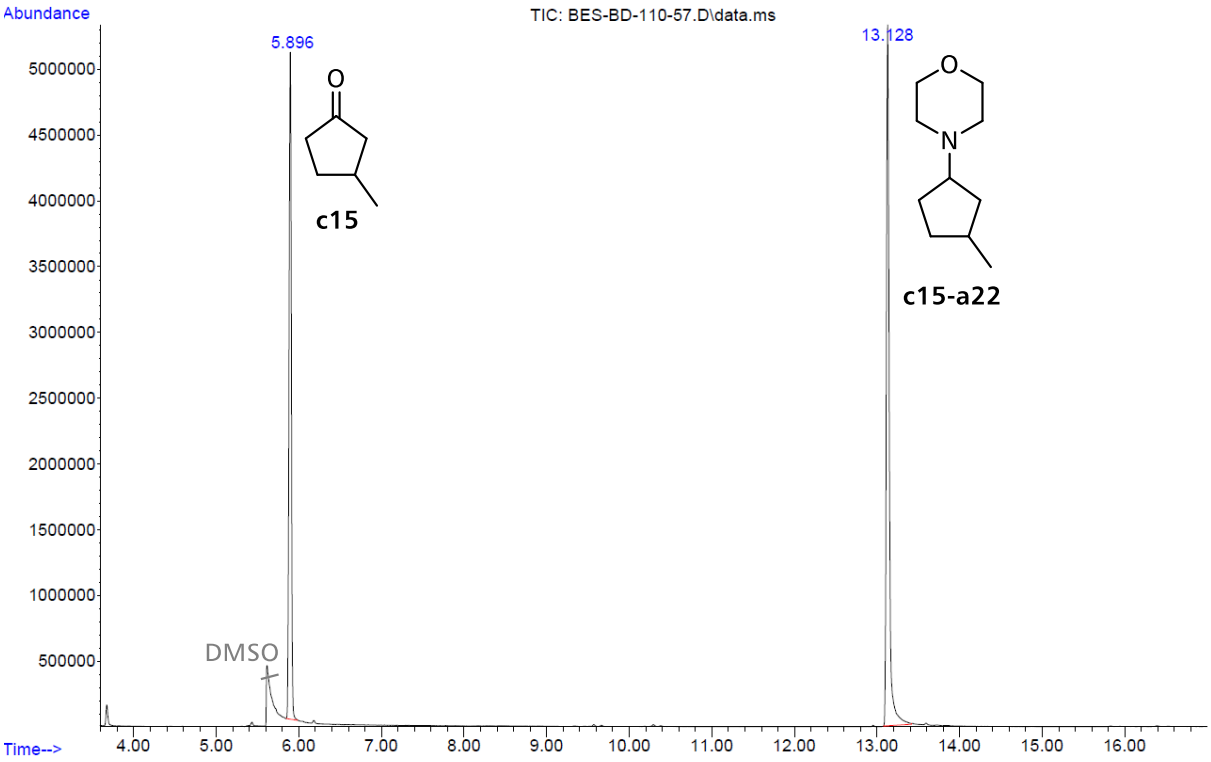


Figure S65. Chromatographic separation of 3-methylcyclopentan-1-one (**c15**, t_r 5.9 min) and 4-(3-methylcyclopentyl)morpholine (**c15-a22**, t_r 13.1 min) using GC–MS method GC-MS1. Sample generated by biotransformation of **c15** and morpholine (**a22**) using IR0064.

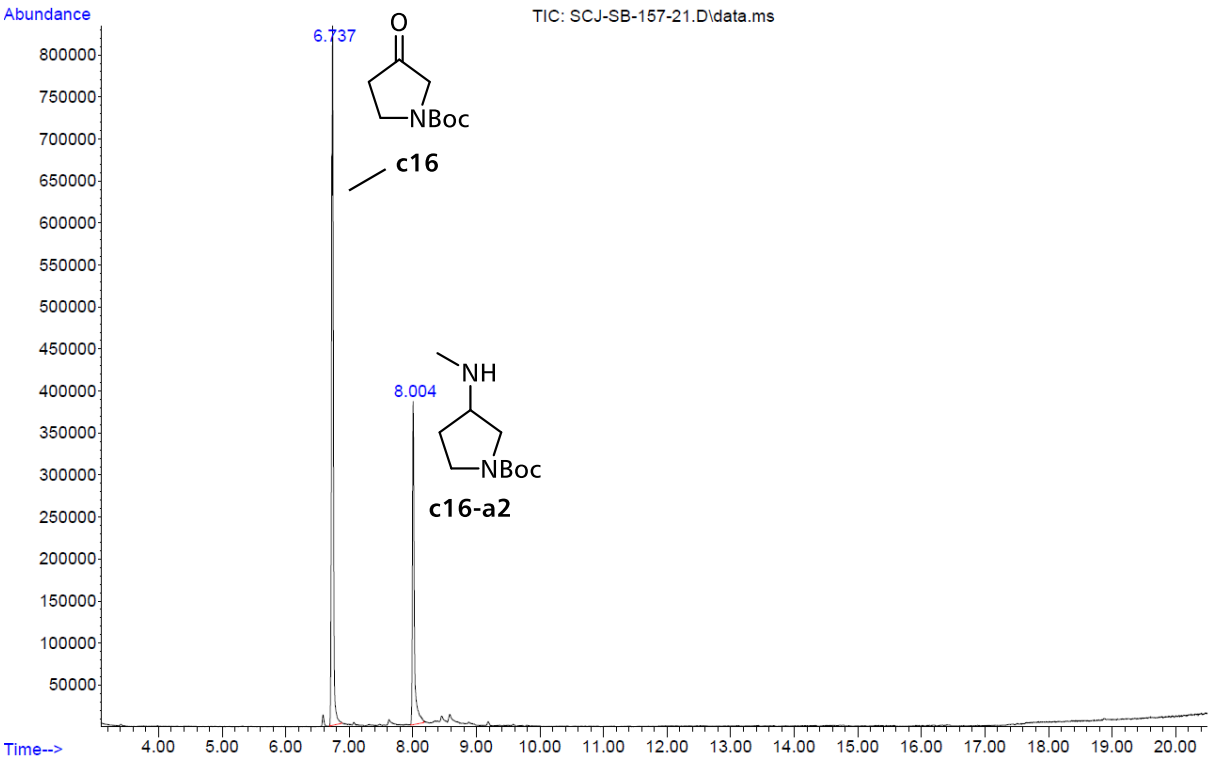


Figure S66. Chromatographic separation of *tert*-butyl 3-oxo-pyrrolidine-1-carboxylate (**c16**, t_r 6.7 min) and *tert*-butyl 3-(methylamino)pyrrolidine-1-carboxylate (**c16-a2**, t_r 8.0 min) using GC–MS method GC-MS2. Sample generated by biotransformation of **c16** and methylamine (**a2**) using IR0069.

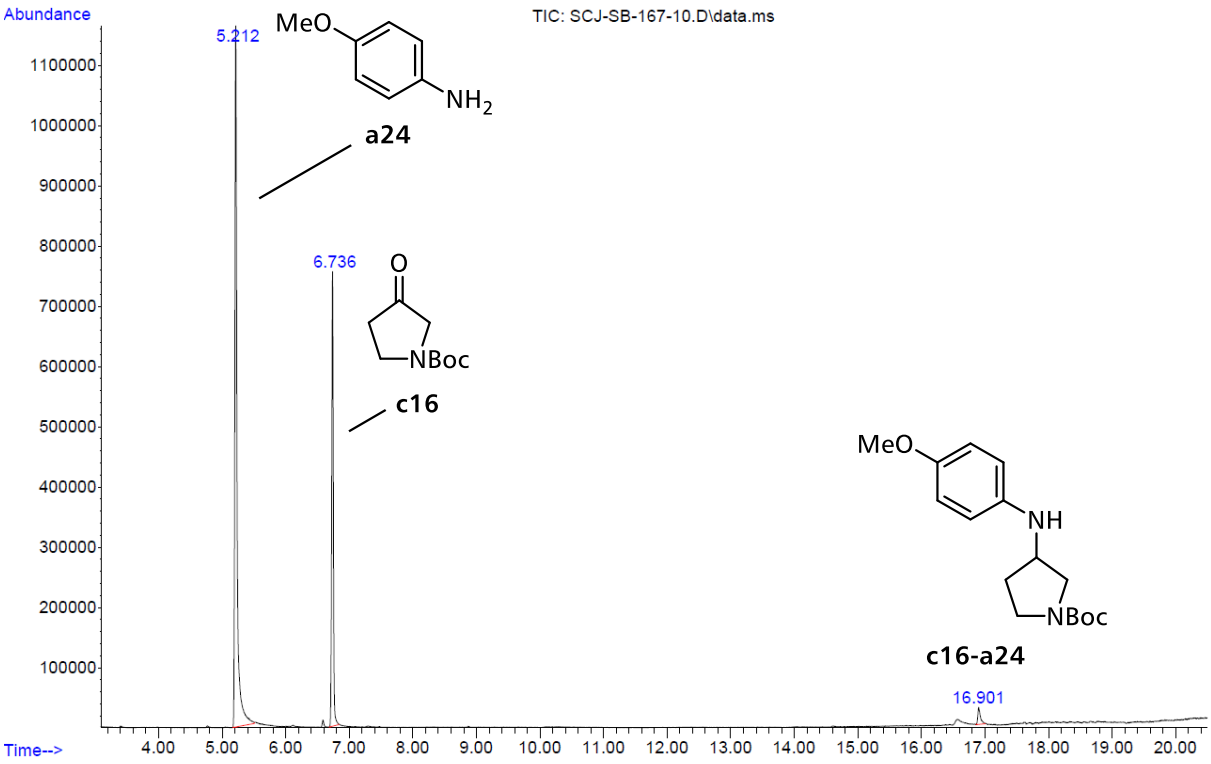


Figure S67. Chromatographic separation of *para*-anisidine (**a24**, t_r 5.2 min), *tert*-butyl 3-oxo-pyrrolidine-1-carboxylate (**c16**, t_r 6.7 min) and *tert*-butyl 3-((4-methoxyphenyl)amino)pyrrolidine-1-carboxylate (**c16-a24**, t_r 16.9 min) using GC–MS method GC-MS2. Sample generated by biotransformation of **c16** and **a24** using IR0040.

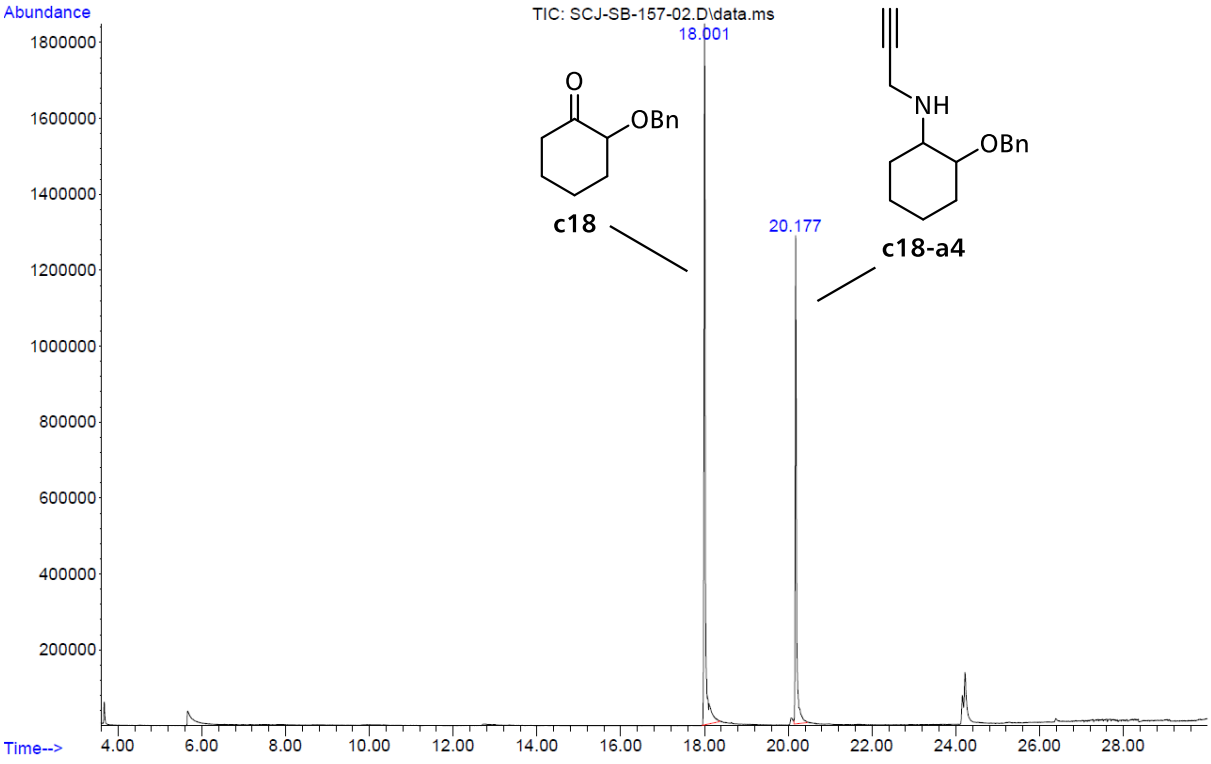


Figure S68. Chromatographic separation of 2-(benzyloxy)cyclohexan-1-one (**c18**, t_r 18.0 min) and 2-(benzyloxy)-*N*-(prop-2-yn-1-yl)cyclohexan-1-amine (**c18-a4**, t_r 20.2 min) using GC–MS method GC-MS3. Sample generated by biotransformation of **c18** and propargylamine (**a4**) using IR1105.

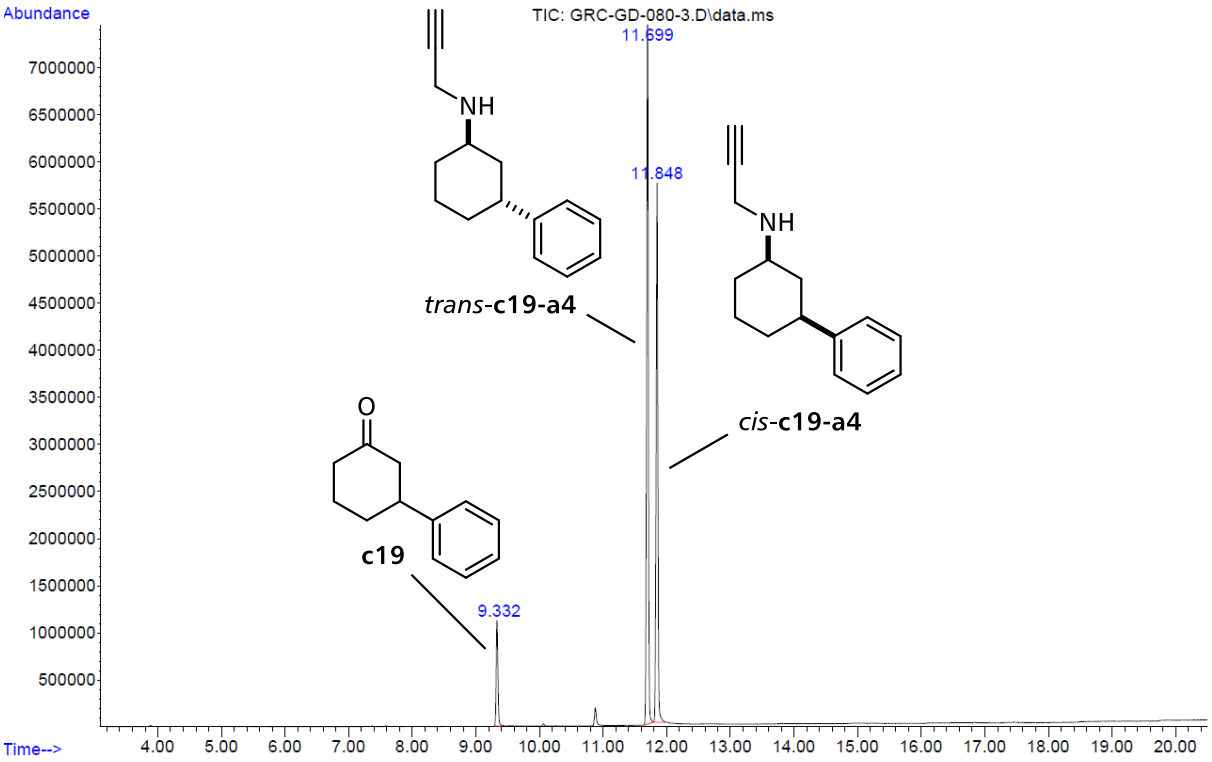


Figure S69. Chromatographic separation of 3-phenylcyclohexan-1-one (**c19**, t_r 9.3 min), *trans*-3-phenyl-*N*-(prop-2-yn-1-yl)cyclohexan-1-amine (*trans*-**c19-a4**, t_r 11.7 min), and *cis*-3-phenyl-*N*-(prop-2-yn-1-yl)cyclohexan-1-amine (*cis*-**c19-a4**, t_r 11.8 min) using GC–MS method GC-MS2. Sample generated by biotransformation of **c18** and propargylamine (**a4**) using IR2021.

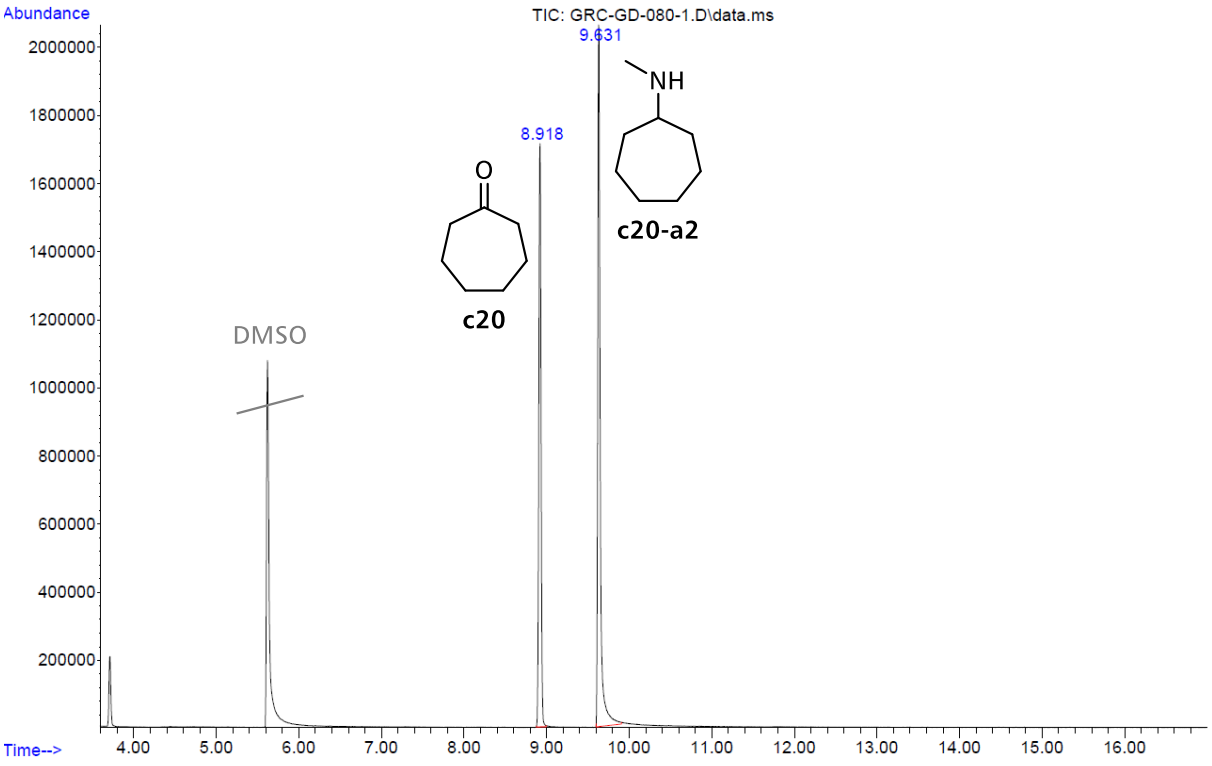


Figure S70. Chromatographic separation of cycloheptanone (**c20**, t_r 8.9 min) and *N*-methylcycloheptanamine (**c20-a2**, t_r 9.6 min) using GC–MS method GC-MS1. Sample generated by biotransformation of **c20** and methylamine (**a2**) using IR2021.

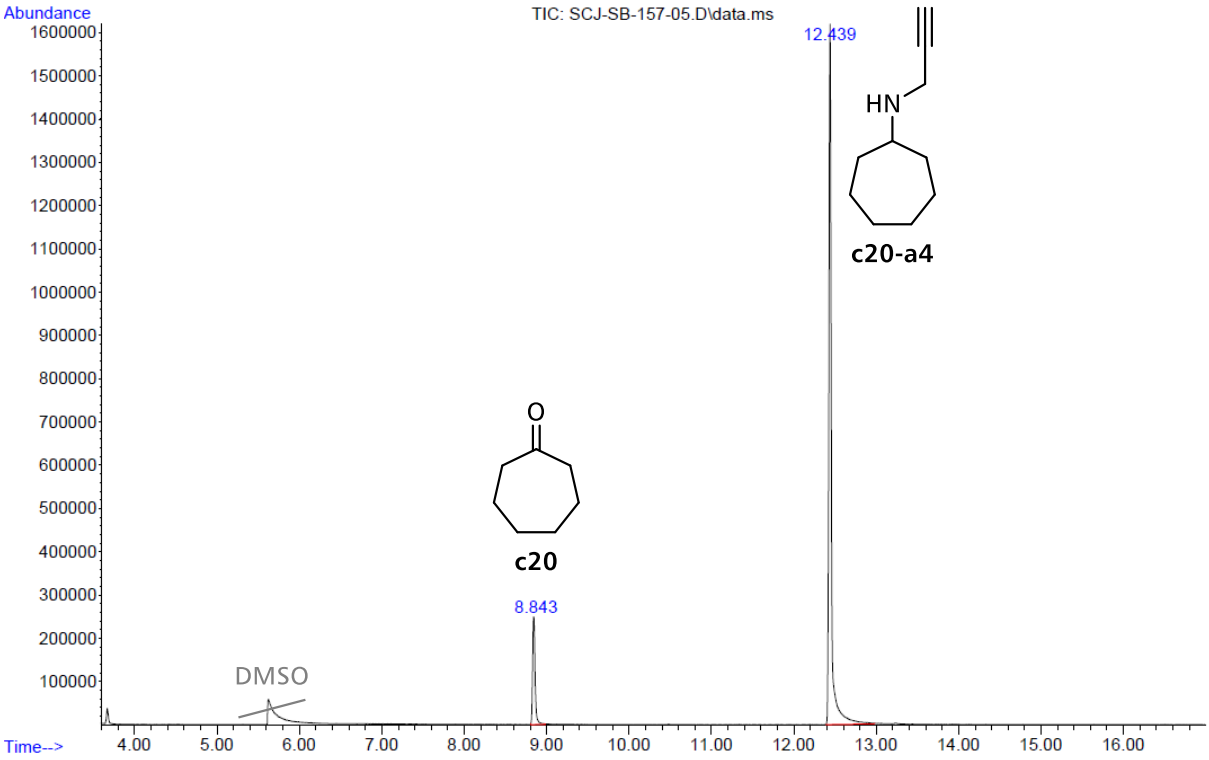


Figure S71. Chromatographic separation of cycloheptanone (**c20**, t_r 8.8 min) and *N*-(prop-2-yn-1-yl)-cycloheptanamine (**c20-a4**, t_r 12.4 min) using GC–MS method GC-MS1. Sample generated by biotransformation of **c20** and propargylamine (**a4**) using IR1460.

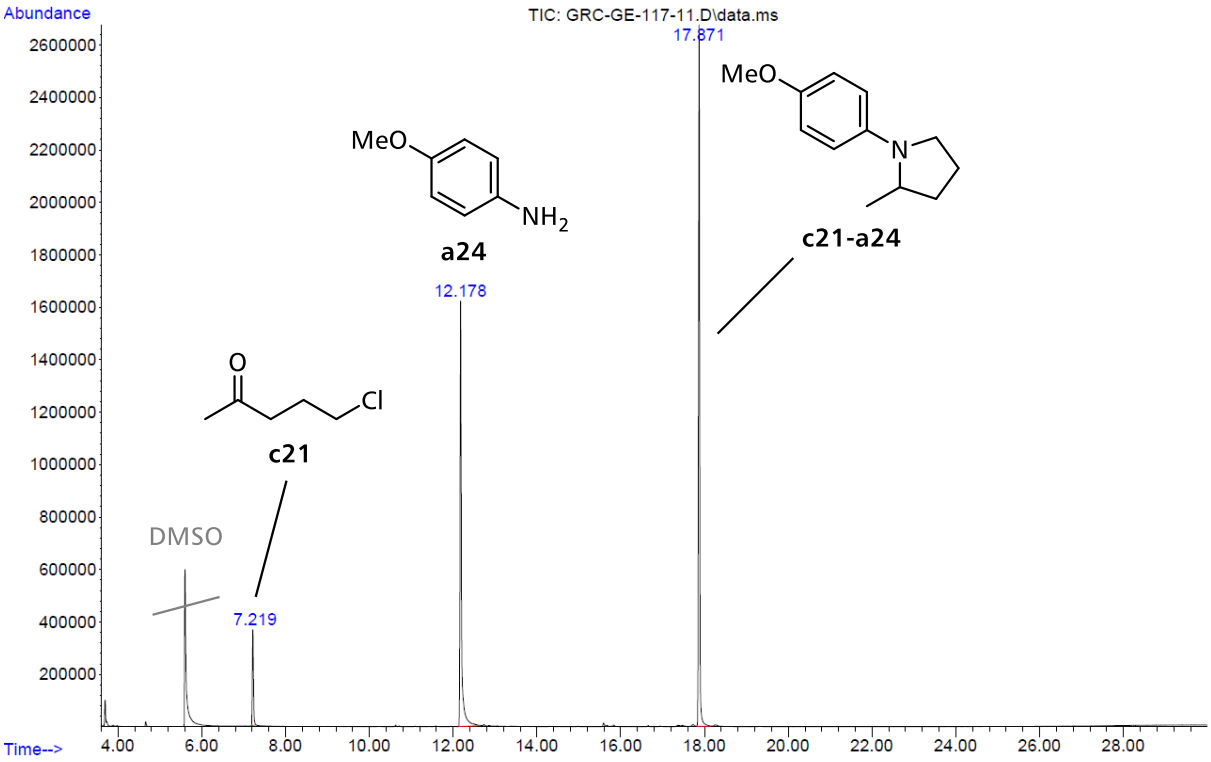


Figure S72. Chromatographic separation of 5-chloropentan-2-one (**c21**, t_r 7.2 min), *para*-anisidine (**a24**, t_r 12.2 min), and 1-(4-methoxyphenyl)-2-methylpyrrolidine (**c21-a24**, t_r 17.9 min) using GC–MS method GC-MS3. Sample generated by biotransformation of **c21** and **a24** using IR0010.

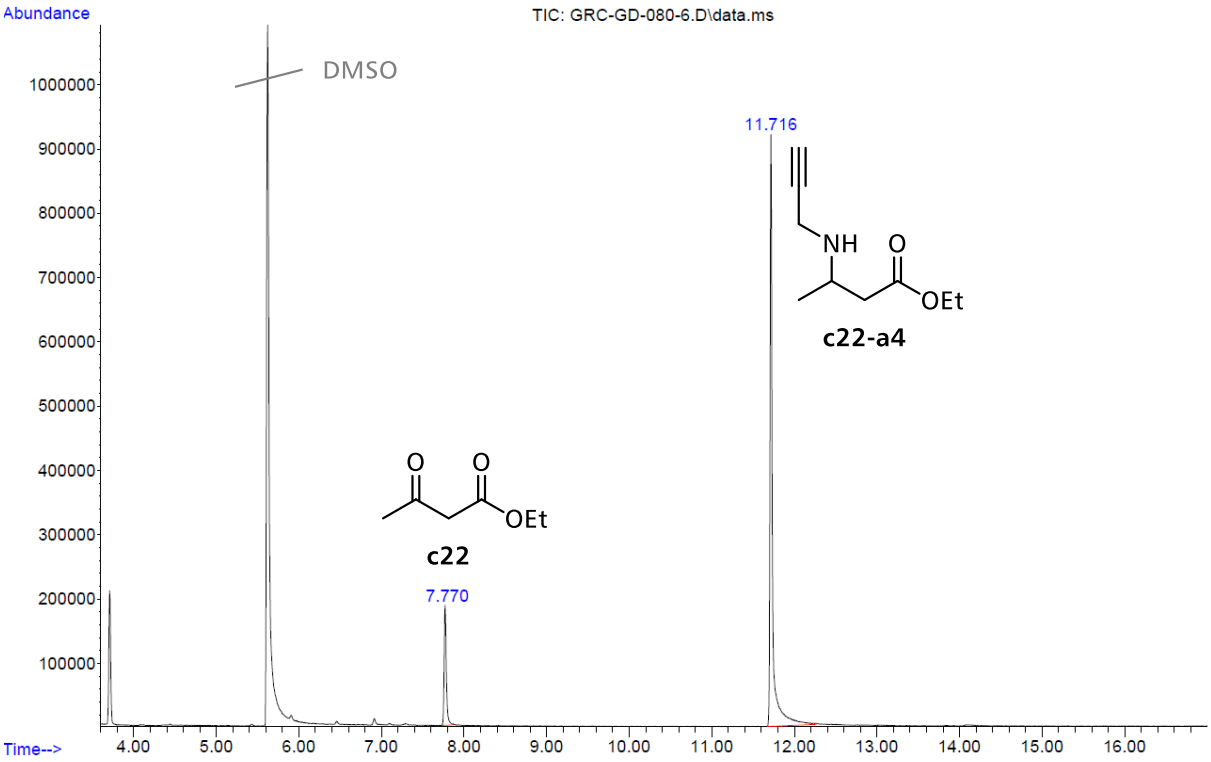


Figure S73. Chromatographic separation of ethyl acetoacetate (**c22**, t_r 7.8 min) and ethyl 3-(prop-2-yn-1-ylamino)butanoate (**c22-a4**, t_r 11.7 min) using GC–MS method GC-MS1. Sample generated by biotransformation of **c22** and propargylamine (**a4**) using IR2021.

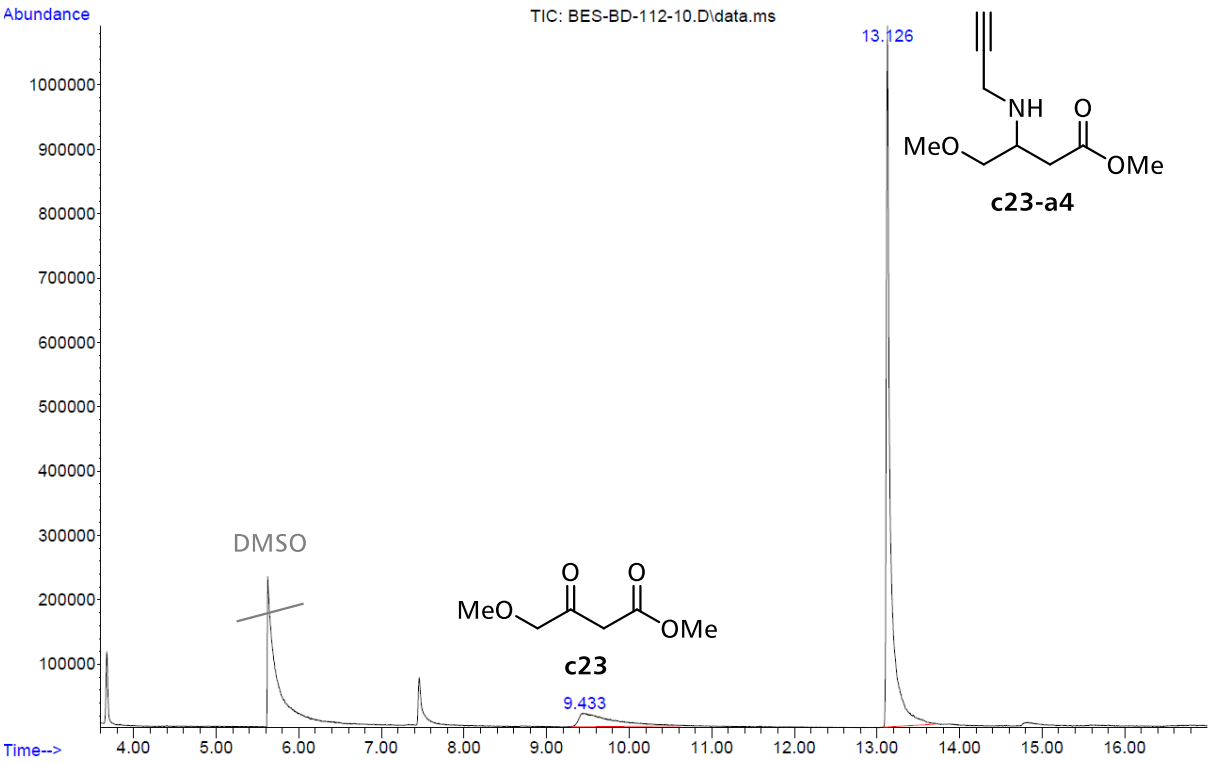


Figure S74. Chromatographic separation of methyl 4-methoxy-3-oxobutanoate (**c23**, t_r 9.4 min) and methyl 4-methoxy-3-(prop-2-yn-1-ylamino)butanoate (**c23-a4**, t_r 13.1 min) using GC–MS method GC-MS1. Sample generated by biotransformation of **c23** and propargylamine (**a4**) using IR0030.

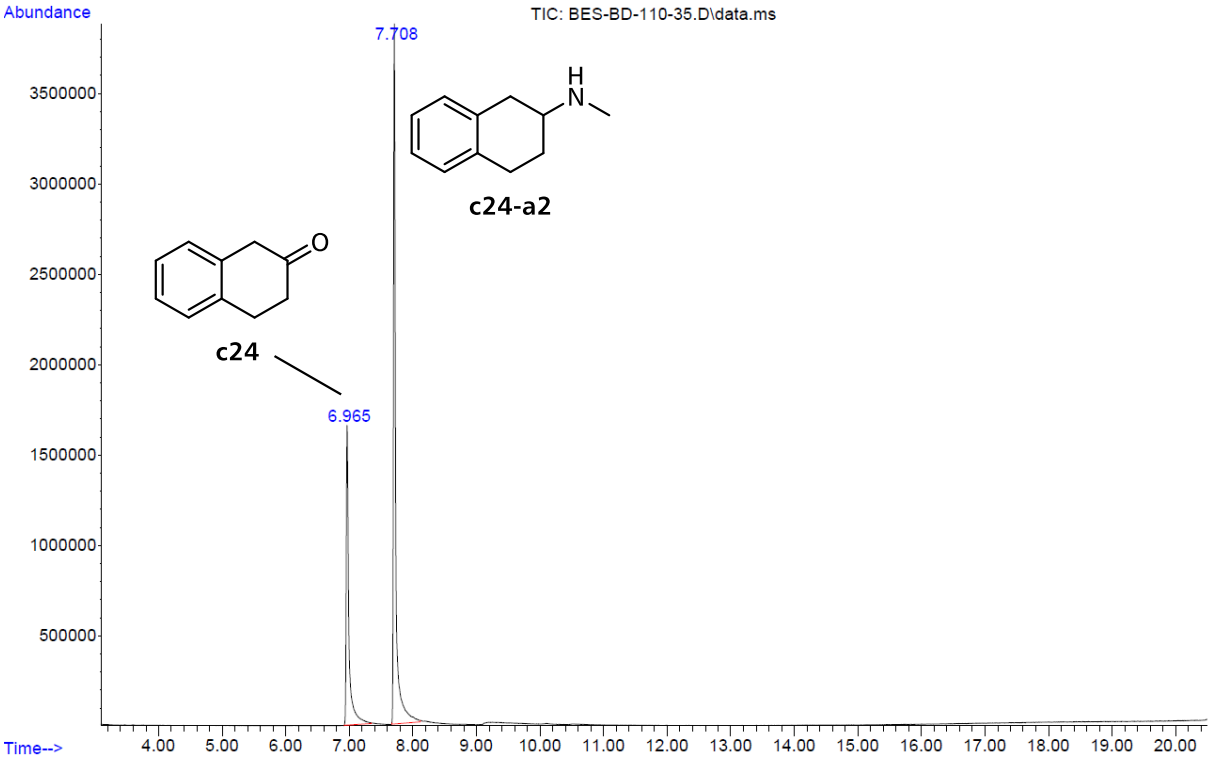


Figure S75. Chromatographic separation of 2-tetralone (**c24**, t_r 7.0 min) and *N*-methyl-1,2,3,4-tetrahydronaphthalen-2-amine (**c24-a2**, t_r 7.7 min) using GC–MS method GC-MS2. Sample generated by biotransformation of **c24** and methylamine (**a2**) using IR0035.

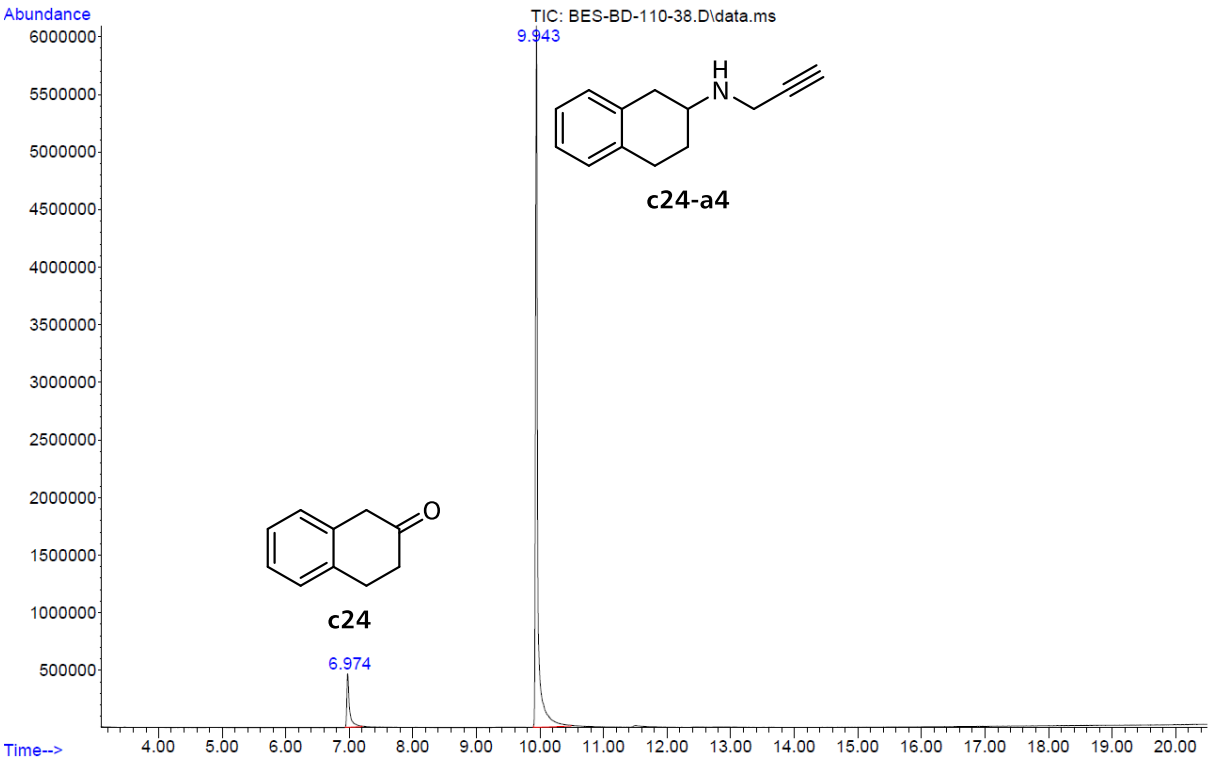


Figure S76. Chromatographic separation of 2-tetralone (**c24**, t_r 7.0 min) and *N*-(prop-2-yn-1-yl)-1,2,3,4-tetrahydronaphthalen-2-amine (**c24-a4**, t_r 9.9 min) using GC–MS method GC-MS2. Sample generated by biotransformation of **c24** and propargylamine (**a4**) using IR1589.

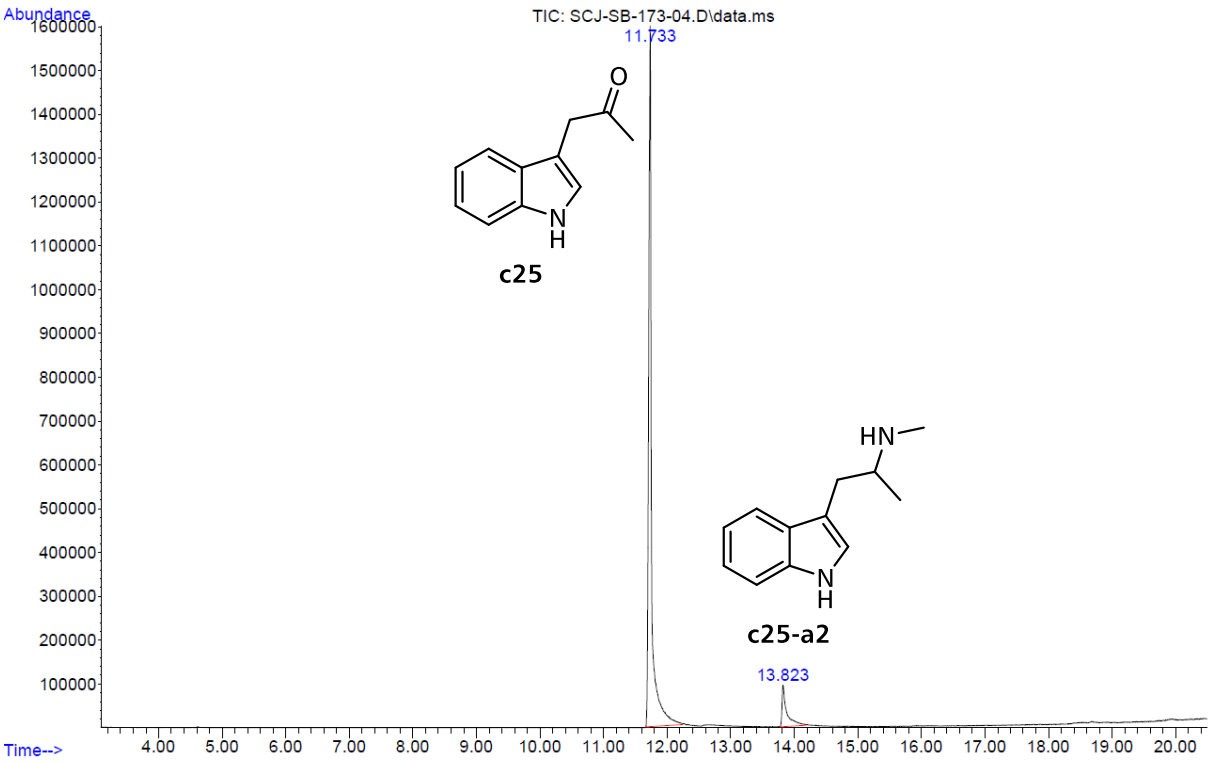


Figure S77. Chromatographic separation of 1-(1*H*-indol-3-yl)propan-2-one (**c25**, t_r 11.7 min) and 1-(1*H*-indol-3-yl)-*N*-methylpropan-2-amine (**c25-a2**, t_r 13.8 min) using GC–MS method GC-MS2. Sample generated by biotransformation of **c25** and methylamine (**a2**) using IR2021.

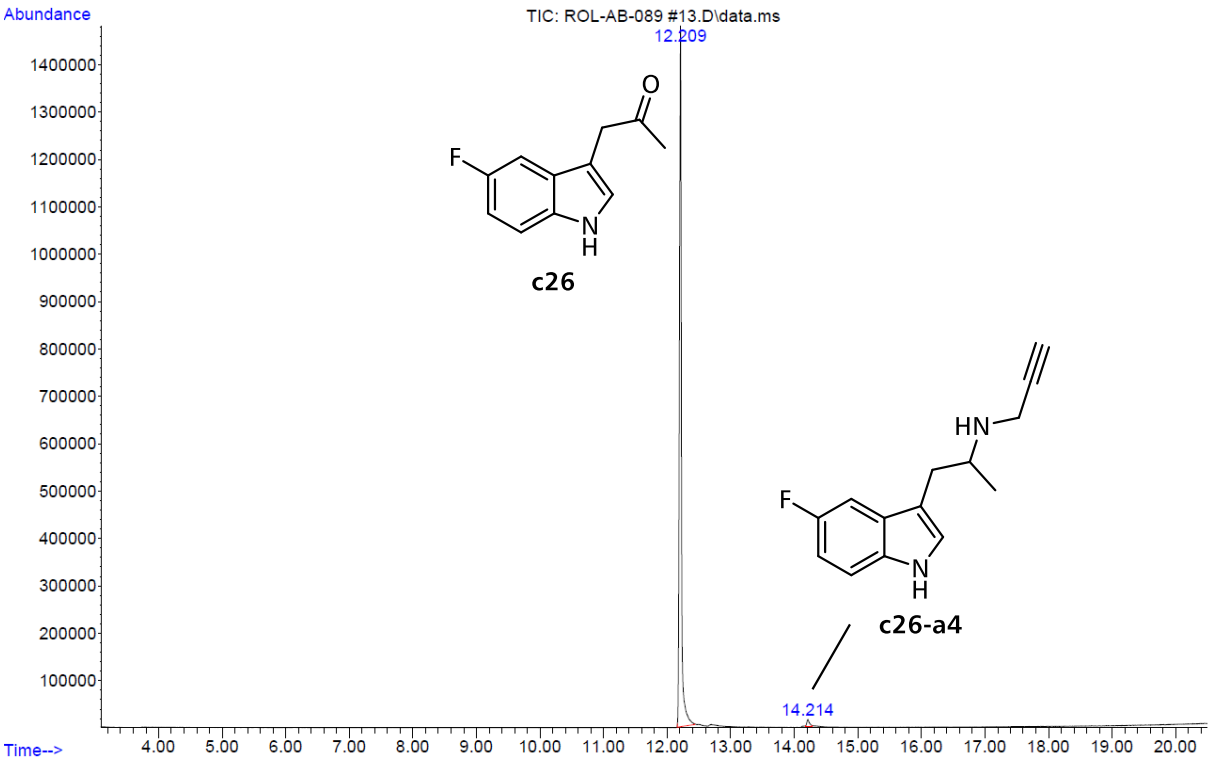


Figure S78. Chromatographic separation of 1-(5-fluoro-1*H*-indol-3-yl)propan-2-one (**c26**, t_r 12.2 min) and *N*-(1-(5-fluoro-1*H*-indol-3-yl)propan-2-yl)prop-2-yn-1-amine (**c26-a4**, t_r 14.2 min) using GC–MS method GC-MS2. Sample generated by biotransformation of **c26** and propargylamine (**a4**) using IR0041.

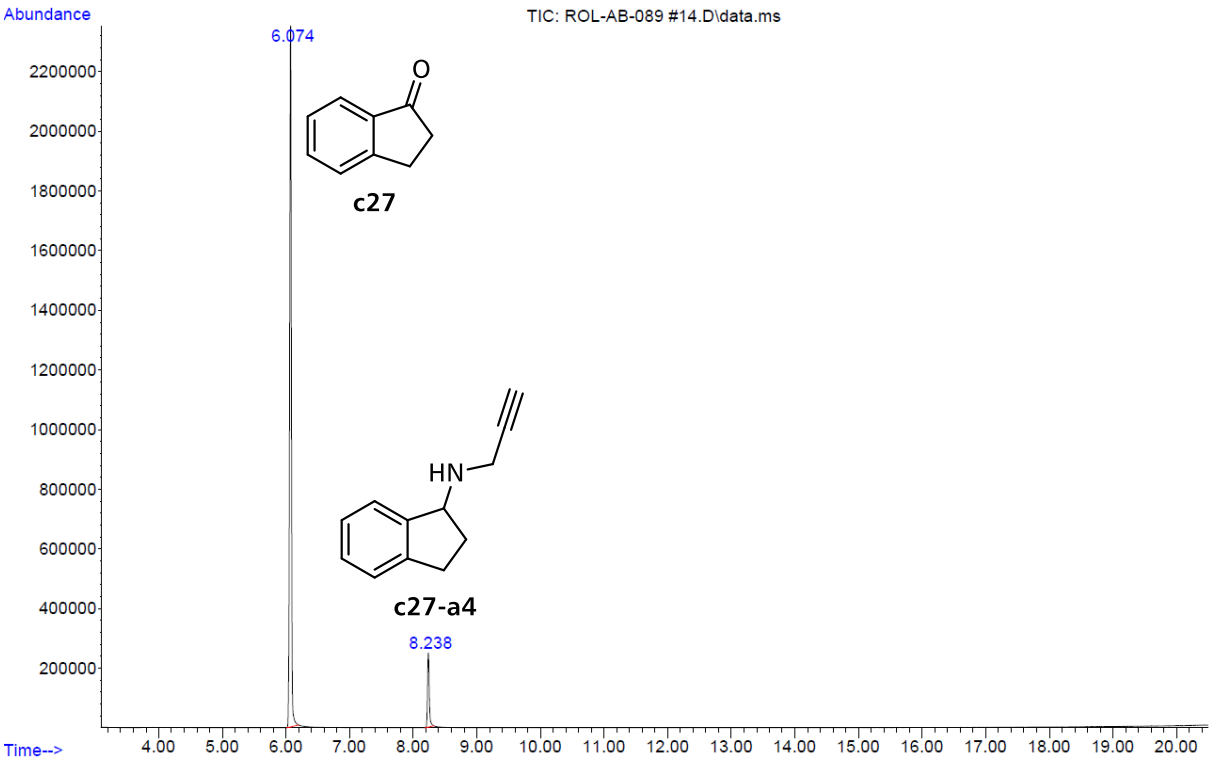


Figure S79. Chromatographic separation of 1-indanone (**c27**, t_r 6.1 min) and *N*-(prop-2-yn-1-yl)-2,3-dihydro-1*H*-inden-1-amine (**c27-a4**, rasagiline; t_r 8.2 min) using GC–MS method GC-MS2. Sample generated by biotransformation of **c27** and propargylamine (**a4**) using IR0041.

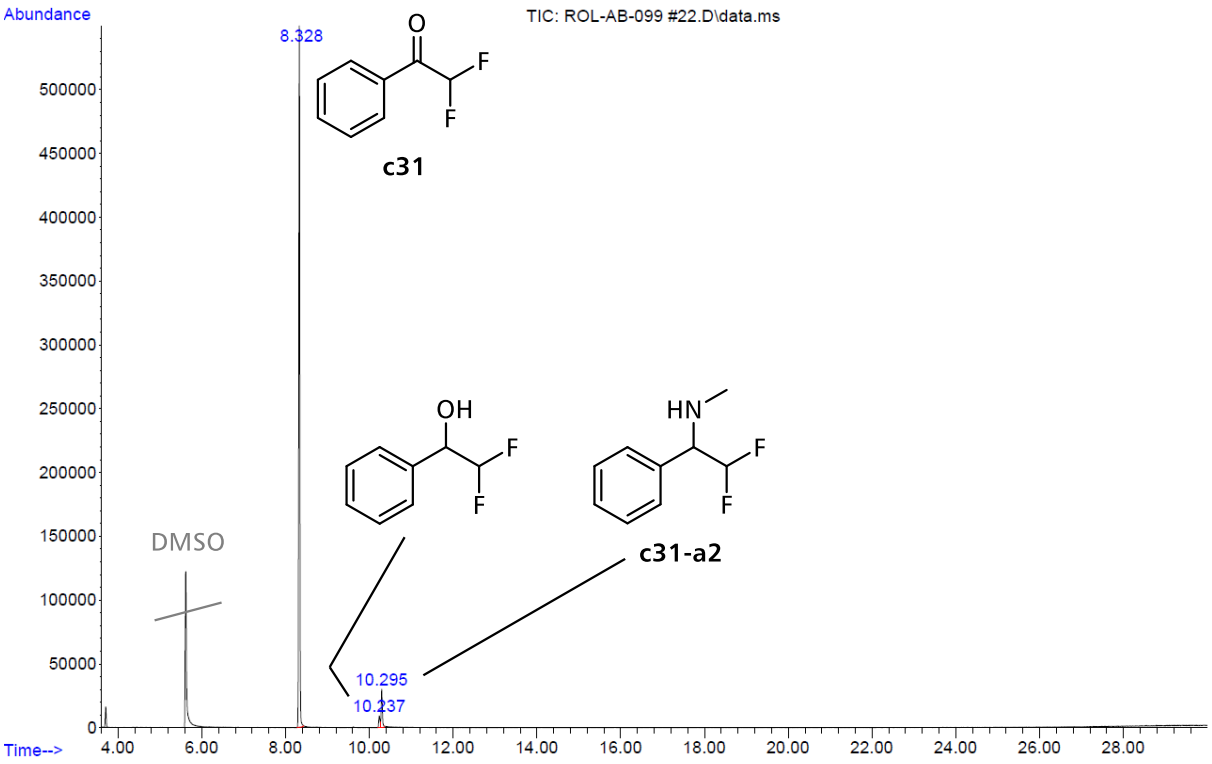


Figure S80. Chromatographic separation of 2,2-difluoro-1-phenylethan-1-one (**c31**, t_r 8.3 min), 2,2-difluoro-1-phenylethan-1-ol (t_r 10.2 min), and 2,2-difluoro-*N*-methyl-1-phenylethan-1-amine (**c31-a2**, t_r 10.3 min) using GC–MS method GC-MS3. Sample generated by biotransformation of **c31** and methylamine (**a2**) using IR0041.

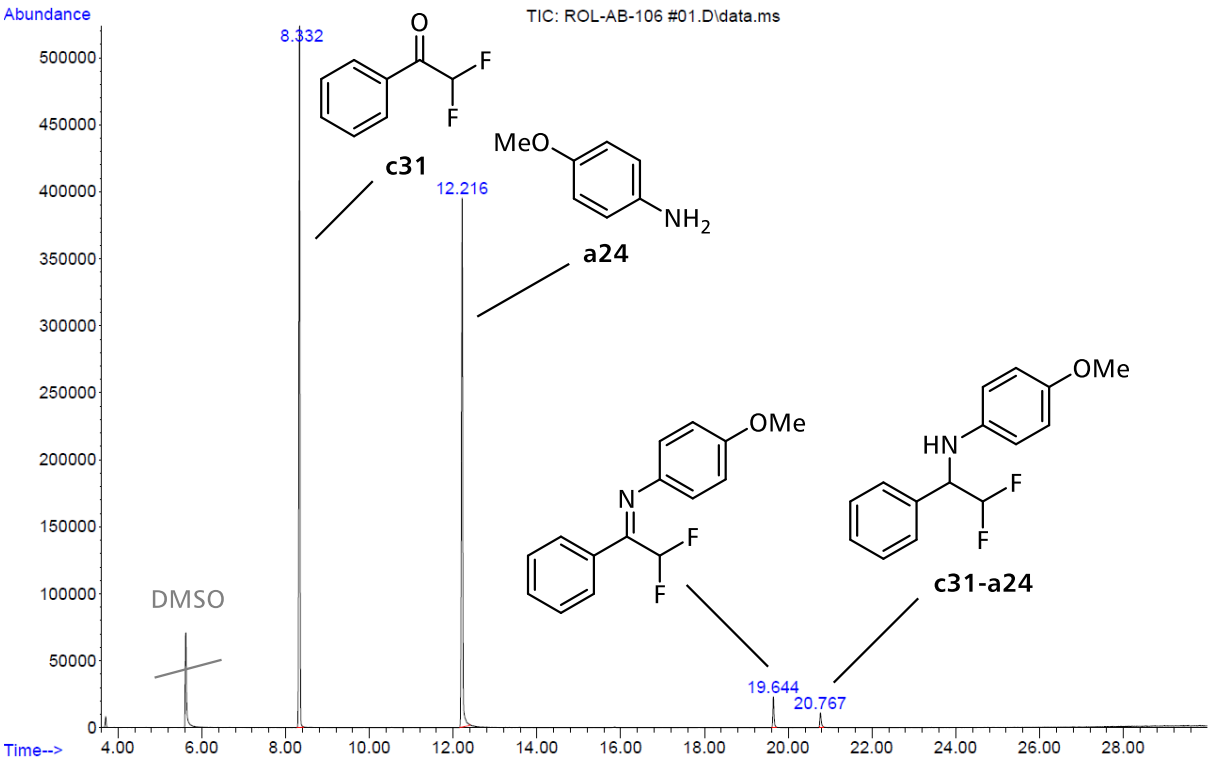


Figure S81. Chromatographic separation of 2,2-difluoro-1-phenylethan-1-one (**c31**, t_r 8.3 min), *para*-anisidine (**a24**, t_r 12.2 min), 2,2-difluoro-*N*-(4-methoxyphenyl)-1-phenylethan-1-imine (t_r 19.6 min), and *N*-(2,2-difluoro-1-phenylethyl)-4-methoxyaniline (**c31-a24**, t_r 20.8 min) using GC–MS method GC-MS3. Sample generated by biotransformation of **c31** and **a24** using IR0049.

Gas chromatography (achiral stationary phase):
Achiral-phase GC analyses were carried out on an *Agilent* 7890A GC system equipped with a flame-ionisation detector (FID) and an *Agilent J&W* HP-5 capillary column (dimensions: 30 m × 0.25 mm × 0.25 μm; stationary phase: bonded & cross-linked 5%-phenyl-methylpolysiloxane) or an *Agilent J&W* DB-1701 capillary column (dimensions: 30 m × 0.25 mm × 0.25 μm; stationary phase: bonded & cross-linked 14% cyanopropylphenyl-methylpolysiloxane), using helium as carrier gas.

Method GC-A1	
Column:	HP-5 (30 m × 0.25 mm × 0.25 μm)
Carrier gas:	Helium
Flow rate:	1.3 mL/min
Inlet temperature:	250 °C
Split ratio:	90:1
Detector temperature:	300 °C
Oven temperature program:	40 °C, 2 min; 10 °C/min to 200 °C; 200 °C, 2 min
Total run time:	20 min

Method GC-A2	
Column:	DB-1701 (30 m × 0.25 mm × 0.25 μm)
Carrier gas:	Helium
Flow rate:	1.0 mL/min
Inlet temperature:	250 °C
Split ratio:	50:1
Detector temperature:	270 °C
Oven temperature program:	50 °C, 1 min; 10 °C/min to 220 °C; 220 °C, 2 min
Total run time:	20 min

Method GC-A3	
Column:	DB-1701 (30 m × 0.25 mm × 0.25 μm)
Carrier gas:	Helium
Flow rate:	1.0 mL/min
Inlet temperature:	250 °C
Split ratio:	50:1
Detector temperature:	270 °C
Oven temperature program:	80 °C, 1 min; 10 °C/min to 250 °C; 250 °C, 2 min
Total run time:	20 min

Method GC-A4	
Column:	DB-1701 (30 m × 0.25 mm × 0.25 μm)
Carrier gas:	Helium
Flow rate:	1.0 mL/min
Inlet temperature:	250 °C
Split ratio:	50:1
Detector temperature:	280 °C
Oven temperature program:	120 °C, 1 min; 10 °C/min to 270 °C; 270 °C, 4 min
Total run time:	20 min

Product formation was quantified through response factors determined by linear calibration of the product amine (five levels: 50 mM, 20 mM, 5 mM, 2 mM, blank) against a constant level of internal standard (*n*-decane or *n*-dodecane, 10 mM) contained in the solvent (EtOAc) used for liquid–liquid extraction.

For most substrate combinations, the concentration of at least one of the substrates could be quantified in the same way. In these cases, conversion was calculated as the concentration of reductive amination product relative to the total analyte concentration (product + substrate, if one of the substrates was quantified; product + average of substrates, if both substrates were quantified). Mass balances of 80–110% (total analyte concentrations of 40–55 mM) were typically observed in these biotransformations, with a tendency towards lower values when volatile substrates (*e.g.*, **c2**, **c7**, **c21**) were used. However, if neither of the two substrates produced a sufficient detector response (*e.g.*, **c23** and **a11**) or if side reactions were observed, conversion was calculated as the concentration of reductive amination product relative to the initial substrate concentration (c_0, 50 mM).

Internal standards and response factors used for quantification as well as the methods used for calculating conversion are summarised in Table S34:

Table S34. Internal standards (ISTD) and response factors used for quantification of amine products by GC–FID analysis and methods used for conversion calculation.

Product	ISTD	Response[a]	Conv. calc.[b]	Product	ISTD	Response[a]	Conv. calc.[b]
c1-a2	decane	2.8074	total anal.	**c8-a9**	decane	2.0339	total anal.
c1-a3	decane	2.0508	total anal.	**c8-a10**	decane	2.5705	total anal.
c1-a4	decane	2.3786	total anal.	**c9-a9**	dodecane	4.8539	total anal.
c1-a5	decane	2.8440	total anal.	**c9-a10**	dodecane	5.5145	total anal.
c2-a1	decane	8.9089	total anal.	**c10-a9**	decane	3.7428	total anal.
c2-a2	decane	3.5975	total anal.	**c10-a10**	decane	3.7404	total anal.
c2-a3	decane	2.4731	total anal.	**c12-a10**	decane	2.3534	total anal.
c2-a4	decane	2.7912	total anal.	**c15-a4-Ac**	decane	2.7736	total anal.
c2-a5	decane	3.0517	total anal.	**c15-a22**	decane	2.3830	total anal.
c2-a6	dodecane	2.2073	total anal.	**c16-a2**	dodecane	3.2853	total anal.
c2-a7	dodecane	2.1779	total anal.	**c16-a4**	dodecane	4.2596	total anal.
c3-a2	decane	2.5286	total anal.	**c16-a6**	dodecane	3.7467	c_0 (50 mM)
c3-a4	decane	4.0155	total anal.	**c16-a15**	dodecane	3.2753	c_0 (50 mM)
c3-a6	decane	1.3754	total anal.	**c18-a2**	dodecane	2.5071	total anal.
c4-a4	dodecane	3.0202	total anal.	**c18-a4**	dodecane	3.1791	total anal.
c4-a6	dodecane	2.6676	total anal.	**c19-a2**	dodecane	2.3052	total anal.
c6-a2	decane	3.4686	total anal.	**c19-a4**	dodecane	2.9679	total anal.
c6-a4	decane	2.8125	total anal.	**c21-a4**	dodecane	5.9175	total anal.
c6-a6	dodecane	2.3053	total anal.	**c21-a24**	dodecane	2.6791	total anal.
c6-a7	dodecane	2.2758	total anal.	**c22-a4**	decane	3.5190	c_0 (50 mM)
c7-a2-Ac	decane	15.465	total anal.	**c23-a2**	decane	10.563	c_0 (50 mM)
c7-a4-Ac	decane	4.1090	total anal.	**c23-a4**	decane	4.2125	c_0 (50 mM)
c7-a6	dodecane	2.8800	total anal.	**c23-a10**	decane	3.2414	c_0 (50 mM)
c7-a7	dodecane	2.9004	total anal.	**c24-a2**	dodecane	2.4904	total anal.
c8-a2	decane	4.8103	total anal.	**c24-a4**	dodecane	3.7824	total anal.
c8-a4	decane	2.5844	total anal.	**c24-a6**	decane	1.3291	c_0 (50 mM)

[a] Response factor determined by linear regression of: area(prod)/area(ISTD) *vs*. conc(prod)/conc(ISTD). Higher values indicate a lower detector response. [b] Method of conversion calculation. total anal.: conv. [%] = *c*(product) / *c*(total analytes) · 100%, c_0 (50 mM): conv. [%] = *c*(product) / c_0(substrates) · 100%

Exemplary chromatograms are shown on the following pages.

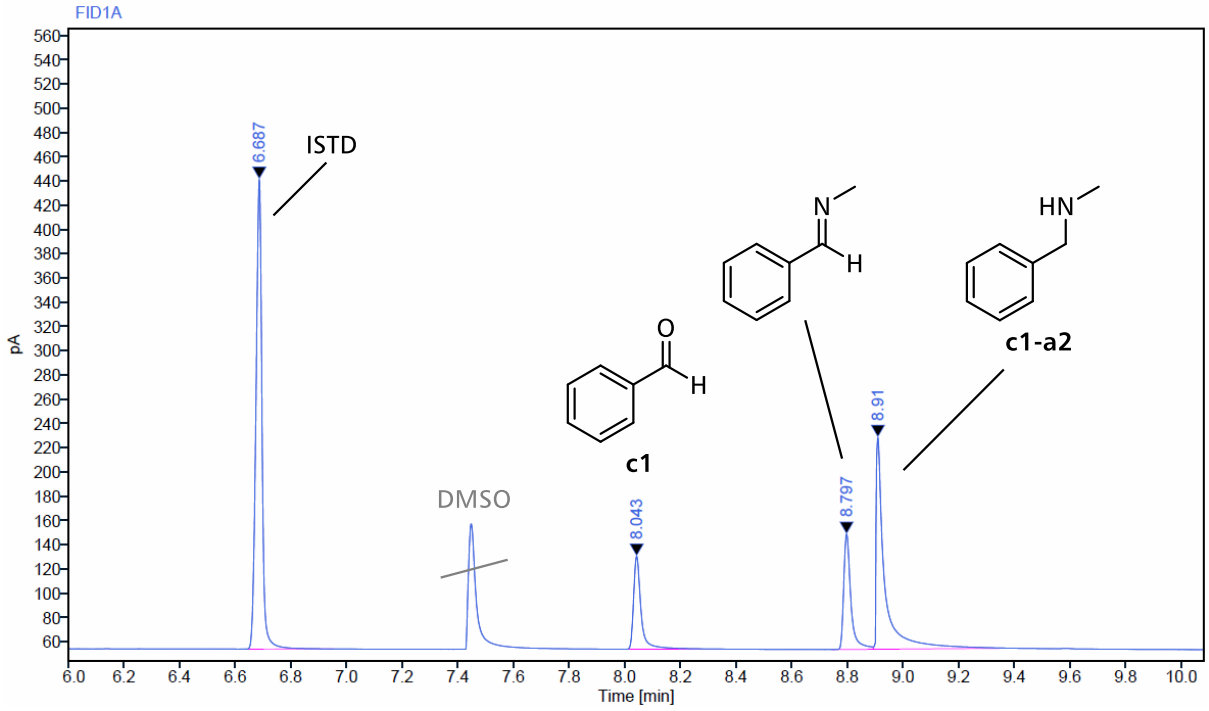


Figure S82. Chromatographic separation of *n*-decane (ISTD, t_r 6.7 min), benzaldehyde (**c1**, t_r 8.0 min), *N*-methyl-1-phenylmethanimine (t_r 8.8 min), and *N*-methylbenzylamine (**c1-a2**, t_r 8.9 min) using GC–FID method GC-A2. Calibration standard containing 10 mM of ISTD and 20 mM of each analyte. The observed imine forms spontaneously through condensation of **c1** and **a2**.

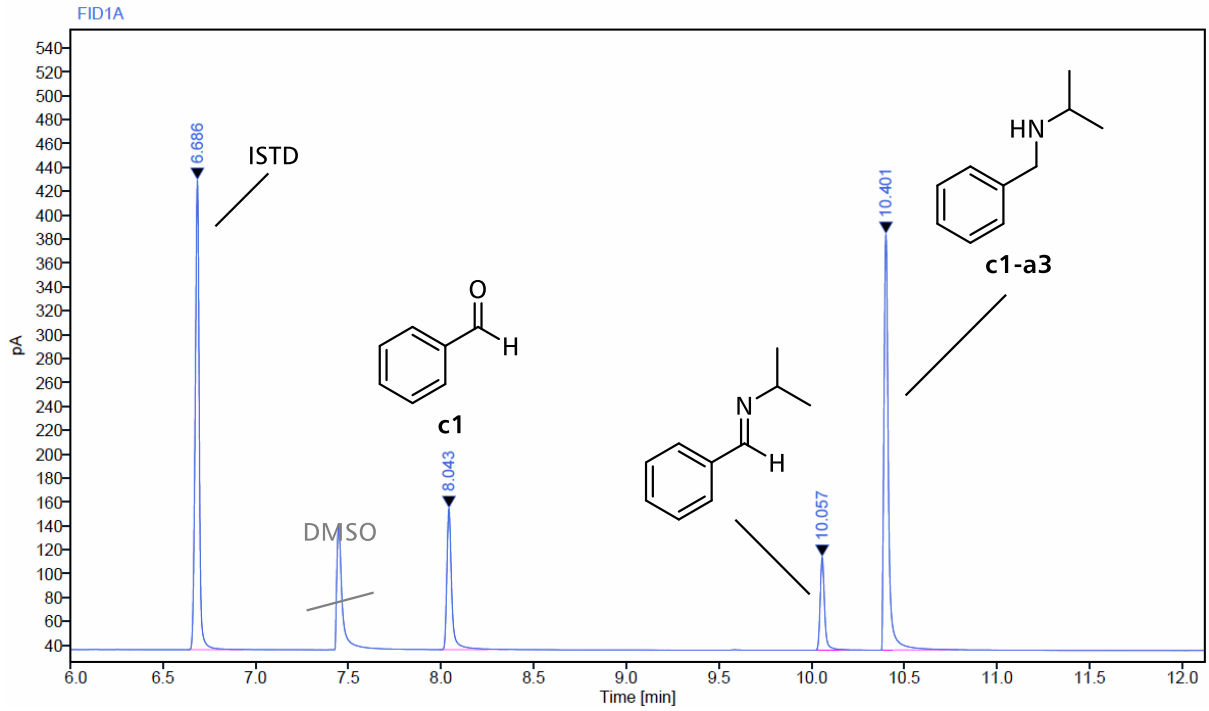


Figure S83. Chromatographic separation of *n*-decane (ISTD, t_r 6.7 min), benzaldehyde (**c1**, t_r 8.0 min), *N*-isopropyl-1-phenylmethanimine (t_r 10.1 min), and *N*-isopropylbenzylamine (**c1-a3**, t_r 10.4 min) using GC–FID method GC-A2. Calibration standard containing 10 mM of ISTD and 20 mM of each analyte. The observed imine forms spontaneously through condensation of **c1** and **a3**.

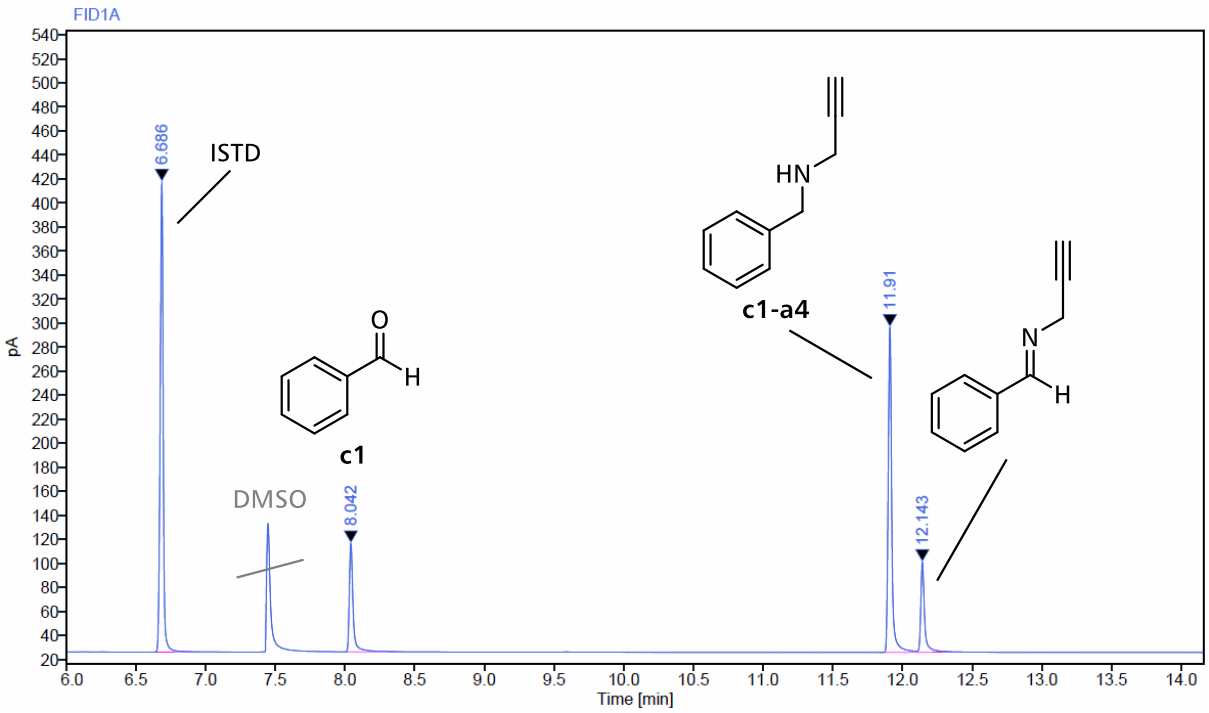


Figure S84. Chromatographic separation of *n*-decane (ISTD, t_r 6.7 min), benzaldehyde (**c1**, t_r 8.0 min), *N*-propargylbenzylamine (**c1-a4**, t_r 11.9 min), and *N*-propargyl-1-phenylmethanimine (t_r 12.1 min) using GC–FID method GC-A2. Calibration standard containing 10 mM of ISTD and 20 mM of each analyte. The observed imine forms spontaneously through condensation of **c1** and **a4**.

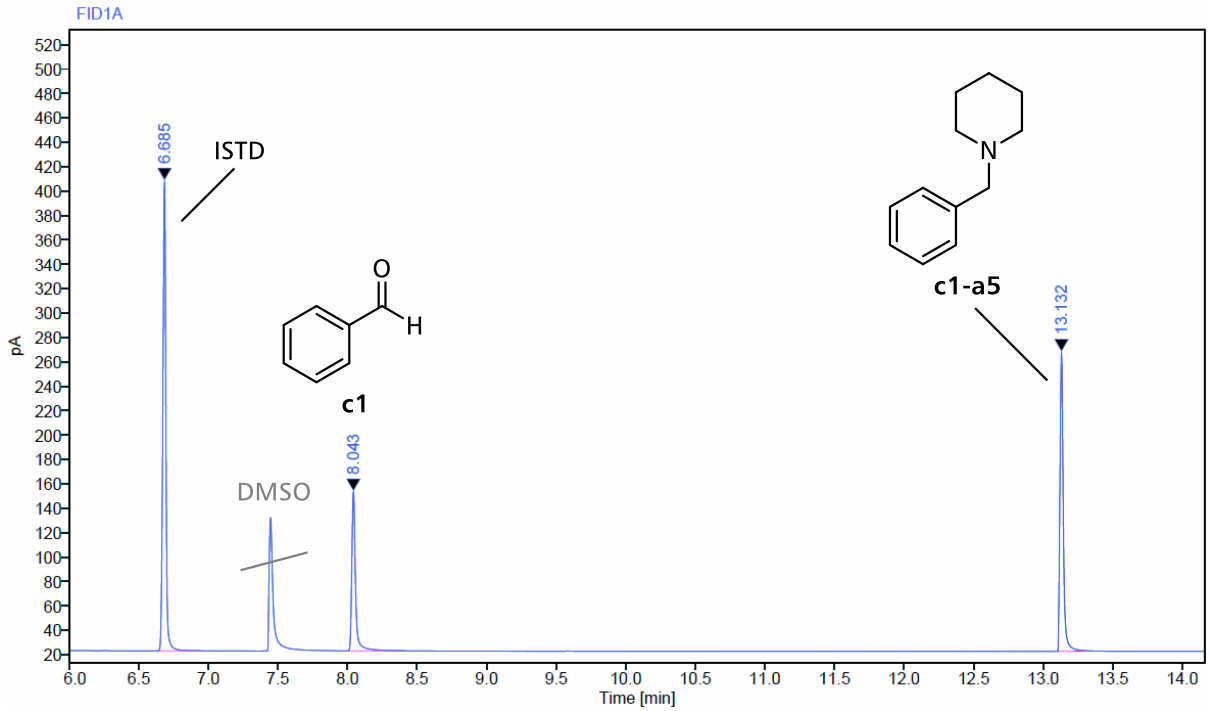


Figure S85. Chromatographic separation of *n*-decane (ISTD, t_r 6.7 min), benzaldehyde (**c1**, t_r 8.0 min), and 1-benzylpiperidine (**c1-a5**, t_r 13.1 min) using GC–FID method GC-A2. Calibration standard containing 10 mM of ISTD and 20 mM of each analyte.

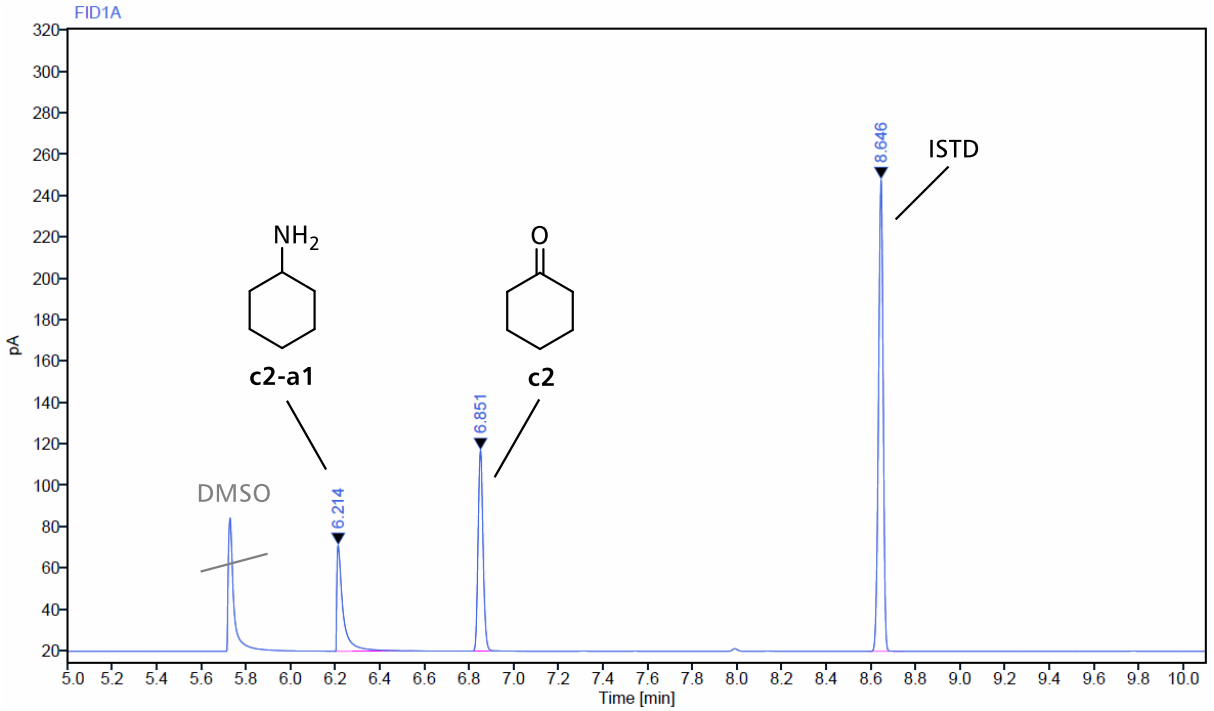


Figure S86. Chromatographic separation of cyclohexanamine (**c2-a1**, t_r 6.2 min), cyclohexanone (**c2**, t_r 6.9 min), and *n*-decane (ISTD, t_r 8.6 min) using GC–FID method GC-A1. Calibration standard containing 10 mM of ISTD and 20 mM of each analyte.

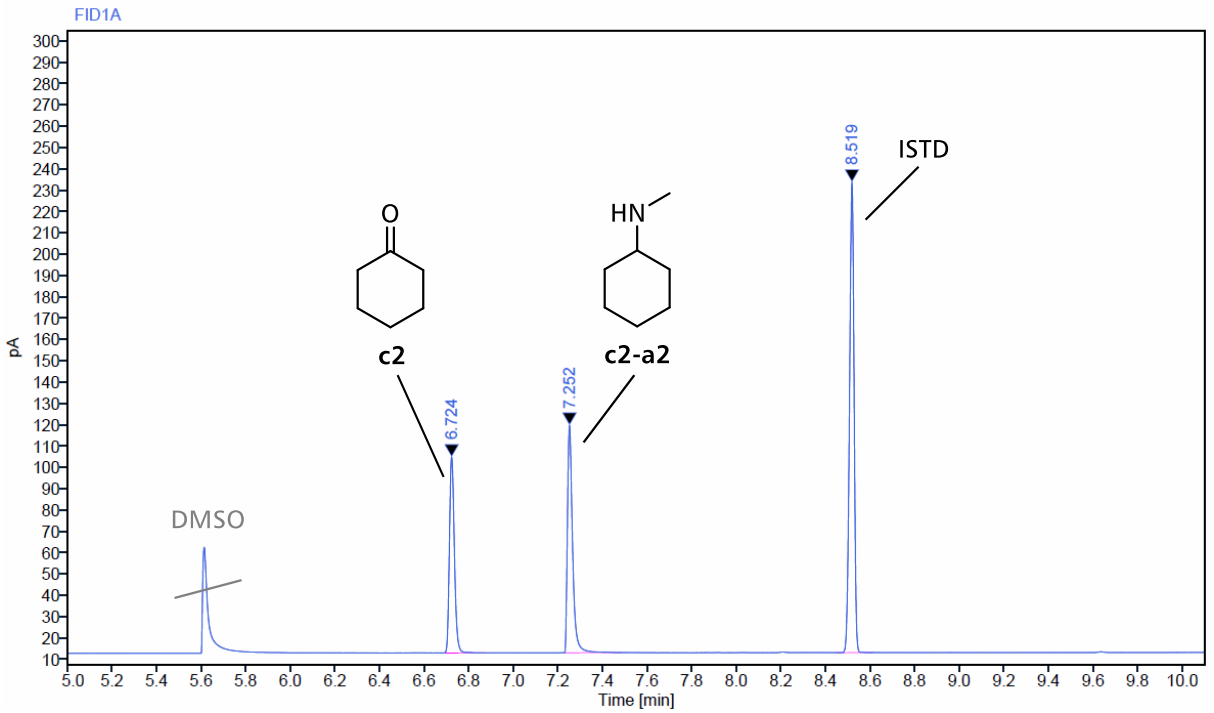


Figure S87. Chromatographic separation of cyclohexanone (**c2**, t_r 6.7 min), *N*-methylcyclohexanamine (**c2-a2**, t_r 7.3 min), and *n*-decane (ISTD, t_r 8.5 min) using GC–FID method GC-A1. Calibration standard containing 10 mM of ISTD and 20 mM of each analyte.

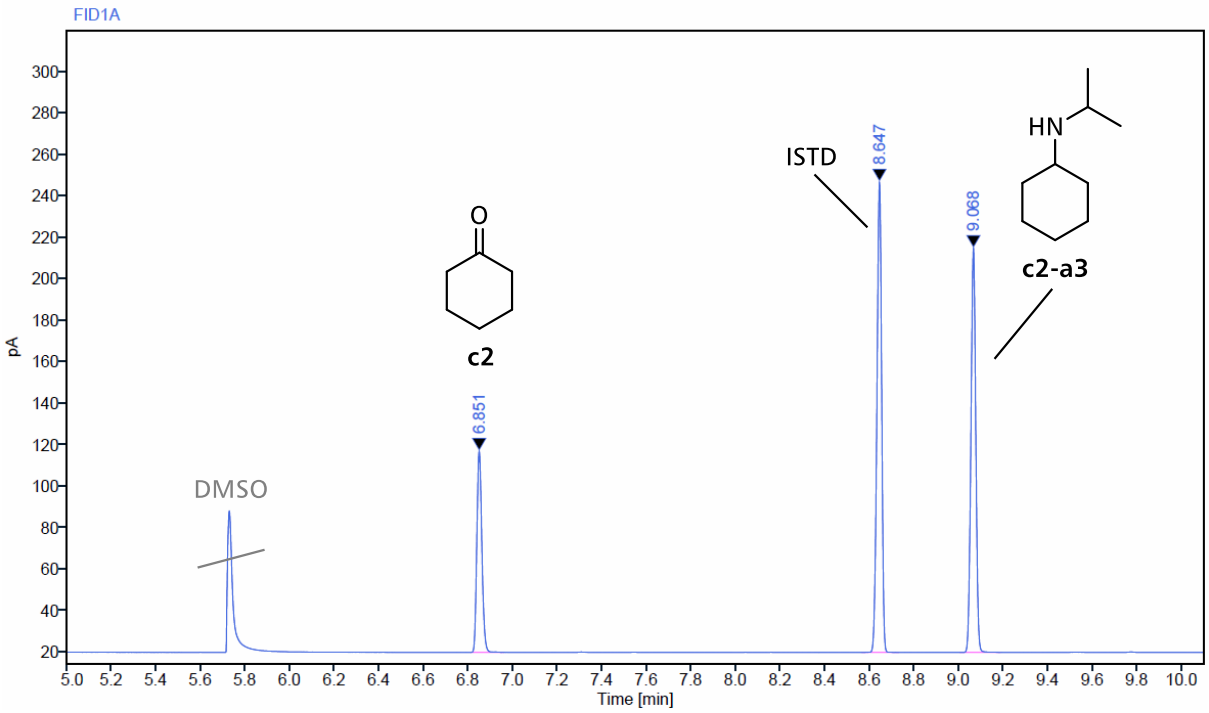


Figure S88. Chromatographic separation of cyclohexanone (**c2**, t_r 6.9 min), *n*-decane (ISTD, t_r 8.6 min), and *N*-isopropylcyclohexanamine (**c2-a3**, t_r 9.1 min) using GC–FID method GC-A1. Calibration standard containing 10 mM of ISTD and 20 mM of each analyte.

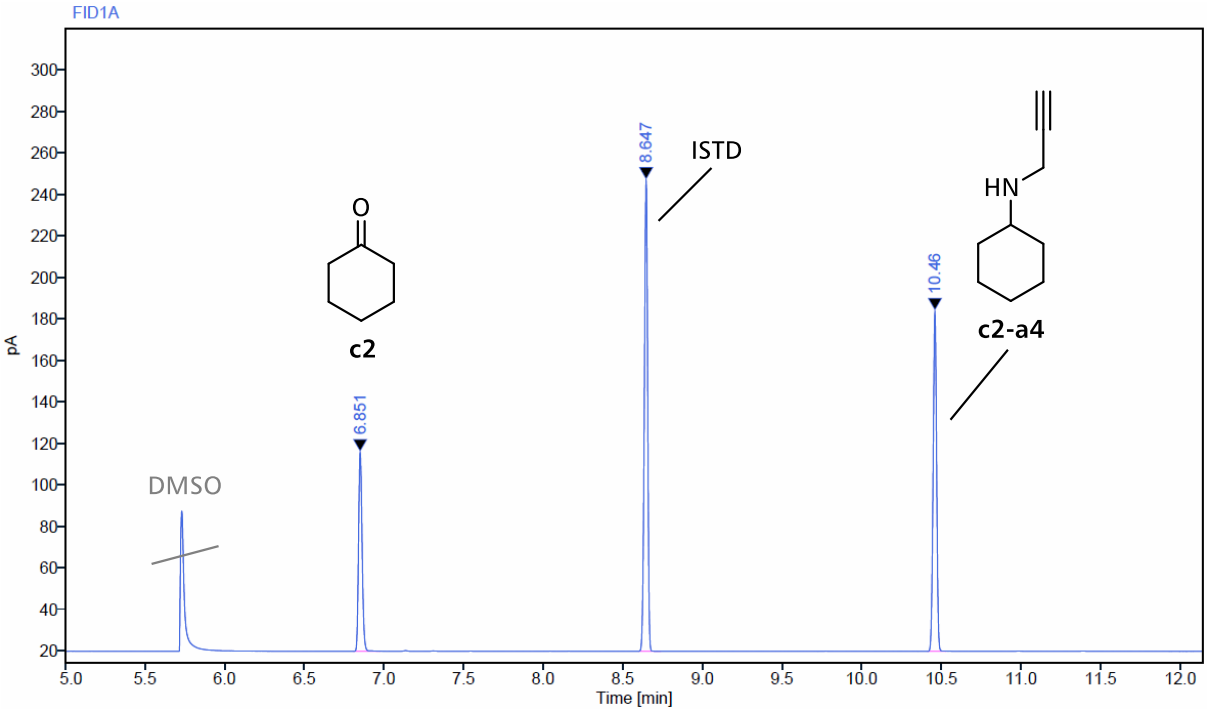


Figure S89. Chromatographic separation of cyclohexanone (**c2**, t_r 6.9 min), *n*-decane (ISTD, t_r 8.6 min), and *N*-propargylcyclohexanamine (**c2-a4**, t_r 10.5 min) using GC–FID method GC-A1. Calibration standard containing 10 mM of ISTD and 20 mM of each analyte.

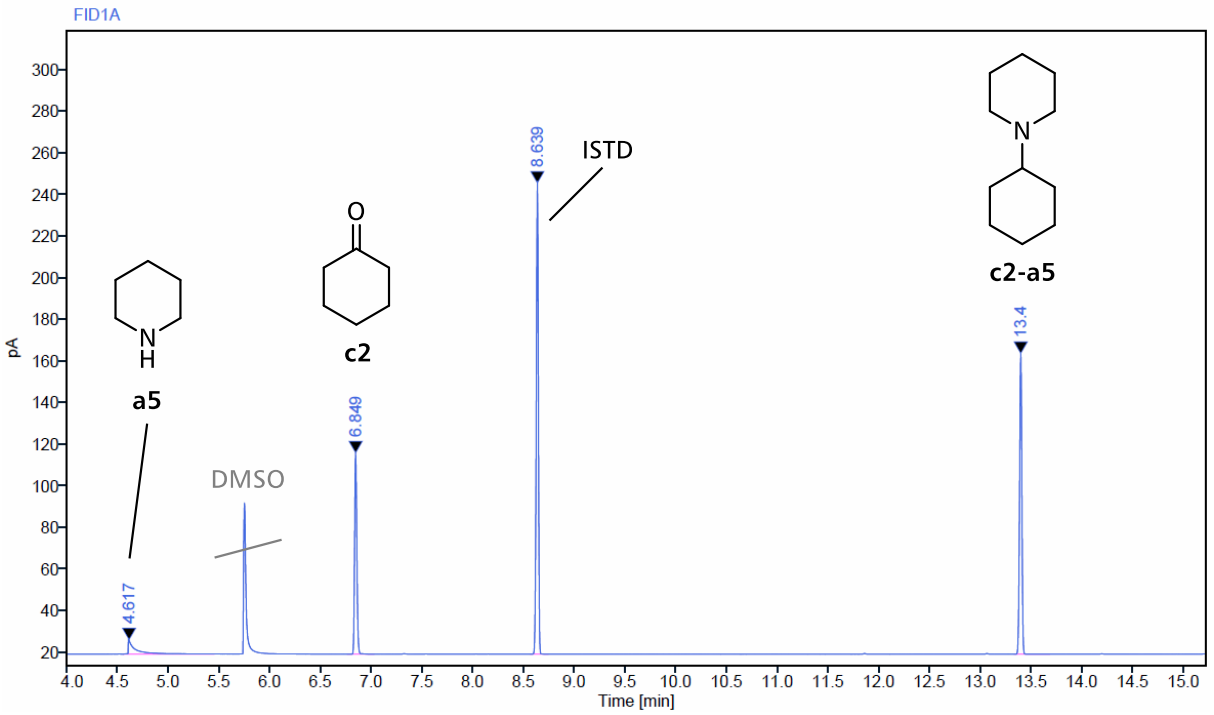


Figure S90. Chromatographic separation of piperidine (**a5**, t_r 4.6 min), cyclohexanone (**c2**, t_r 6.8 min), *n*-decane (ISTD, t_r 8.6 min), and 1-cyclohexylpiperidine (**c2-a5**, t_r 13.4 min) using GC–FID method GC-A1. Calibration standard containing 10 mM of ISTD and 20 mM of each analyte.

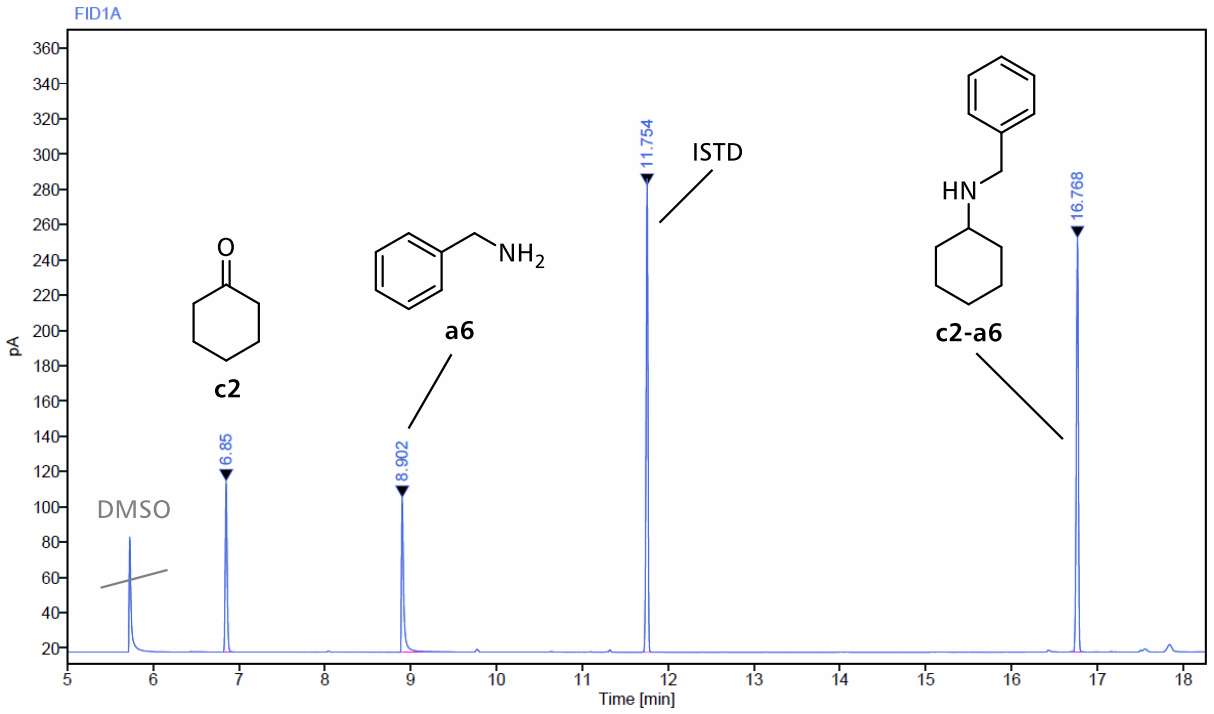


Figure S91. Chromatographic separation of cyclohexanone (**c2**, t_r 6.9 min), benzylamine (**a6**, t_r 8.9 min), *n*-dodecane (ISTD, t_r 11.8 min), and *N*-benzylcyclohexanamine (**c2-a6**, t_r 16.8 min) using GC–FID method GC-A1. Calibration standard containing 10 mM of ISTD and 20 mM of each analyte.

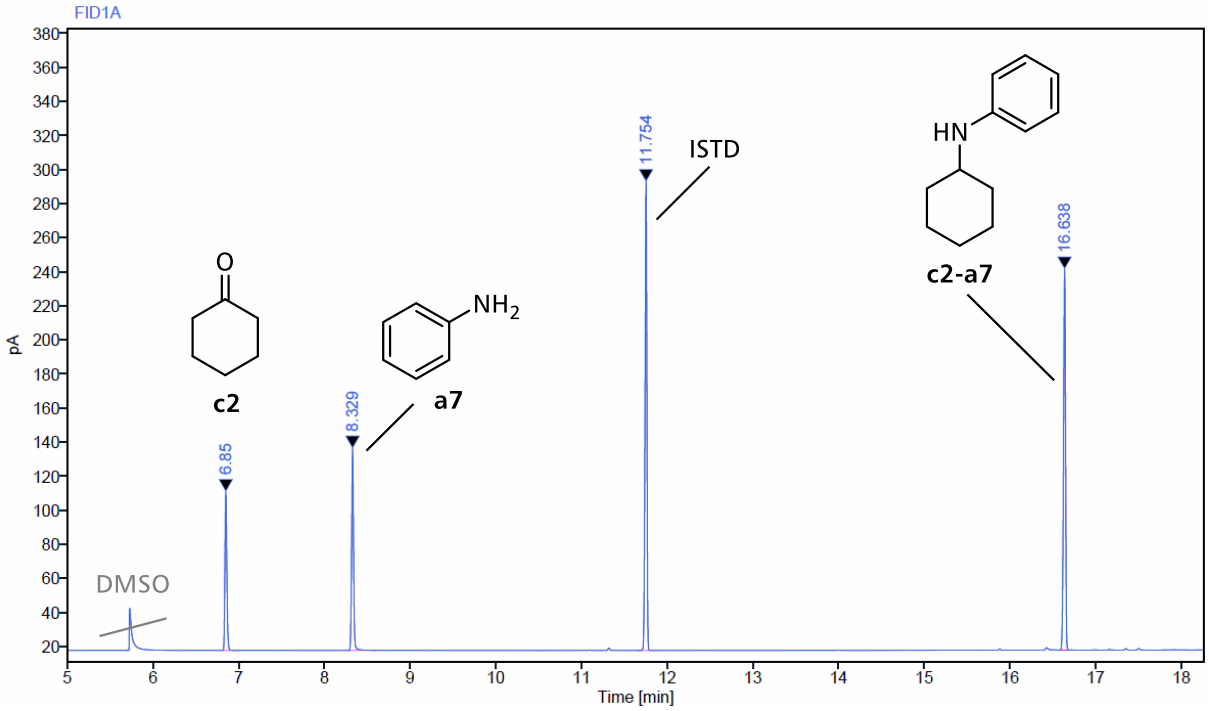


Figure S92. Chromatographic separation of cyclohexanone (**c2**, t_r 6.9 min), aniline (**a7**, t_r 8.3 min), *n*-dodecane (ISTD, t_r 11.8 min), and *N*-cyclohexylaniline (**c2-a7**, t_r 16.6 min) using GC–FID method GC-A1. Calibration standard containing 10 mM of ISTD and 20 mM of each analyte.

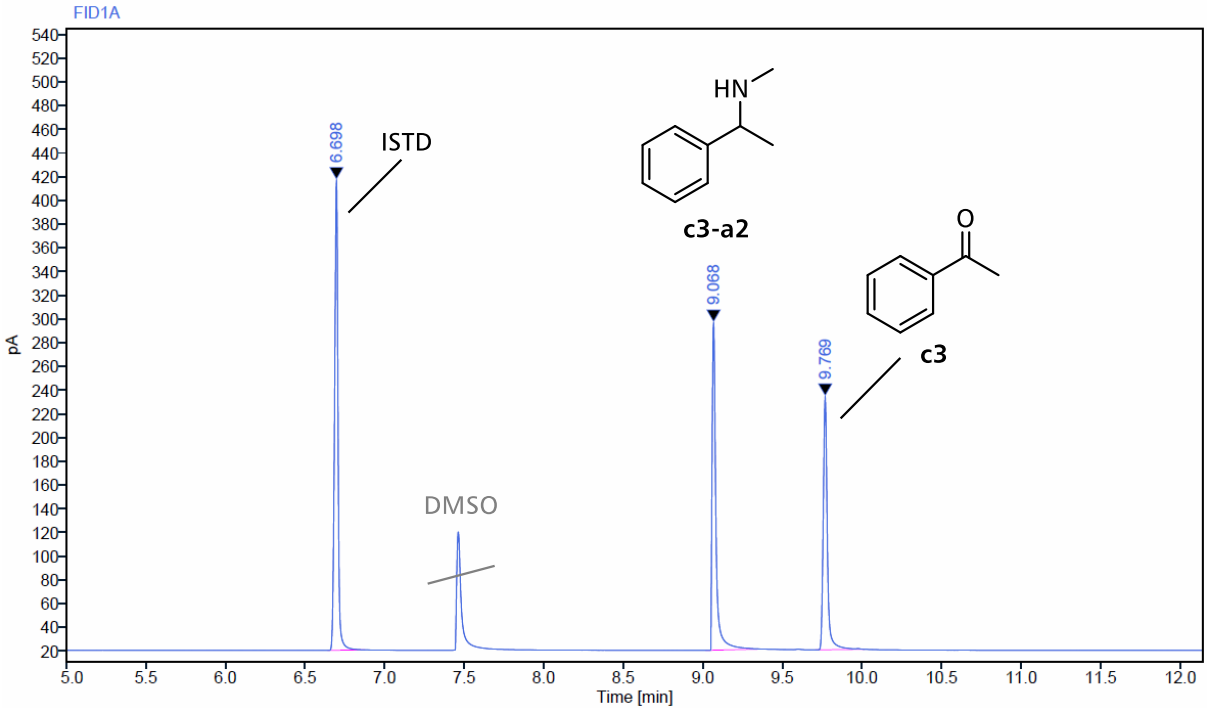


Figure S93. Chromatographic separation of *n*-decane (ISTD, t_r 6.7 min), *N*-methyl-1-phenylethan-1-amine (**c3-a2**, t_r 9.1 min), and acetophenone (**c3**, t_r 9.8 min) using GC–FID method GC-A2. Calibration standard containing 10 mM of ISTD and 20 mM of each analyte.

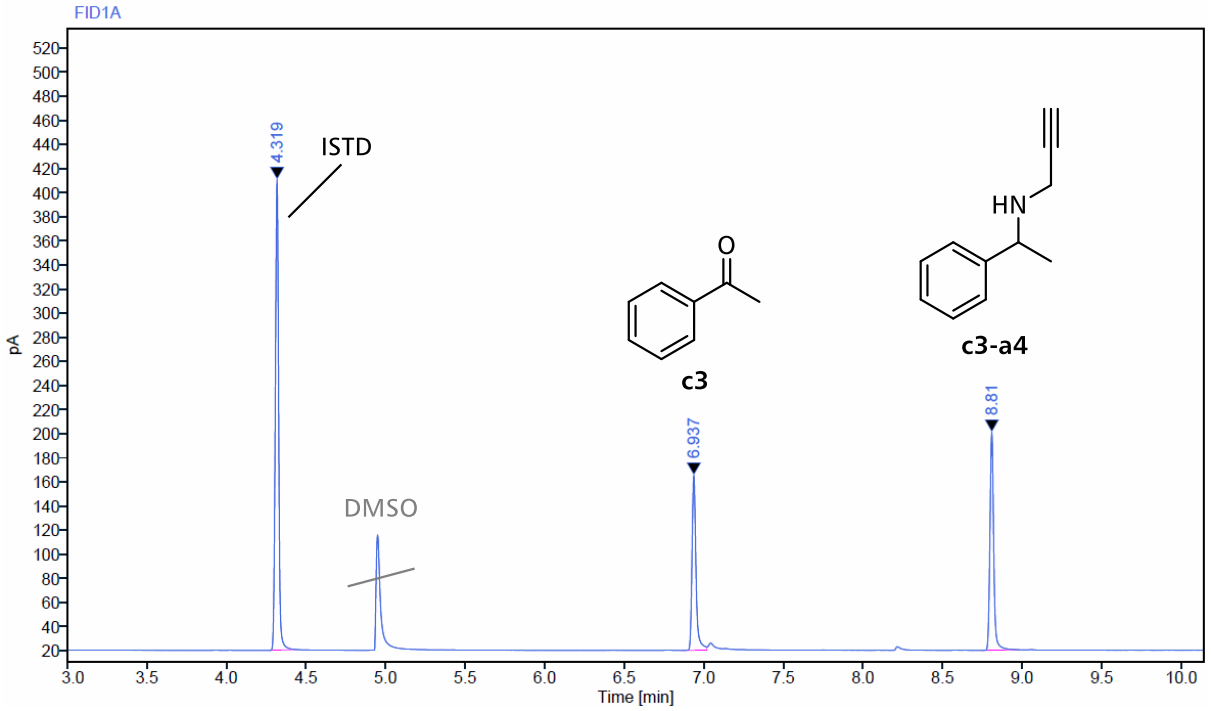


Figure S94. Chromatographic separation of *n*-decane (ISTD, t_r 4.3 min), acetophenone (**c3**, t_r 6.9 min), and *N*-propargyl-1-phenylethan-1-amine (**c3-a4**, t_r 8.8 min) using GC–FID method GC-A3. Calibration standard containing 10 mM of ISTD and 20 mM of each analyte.

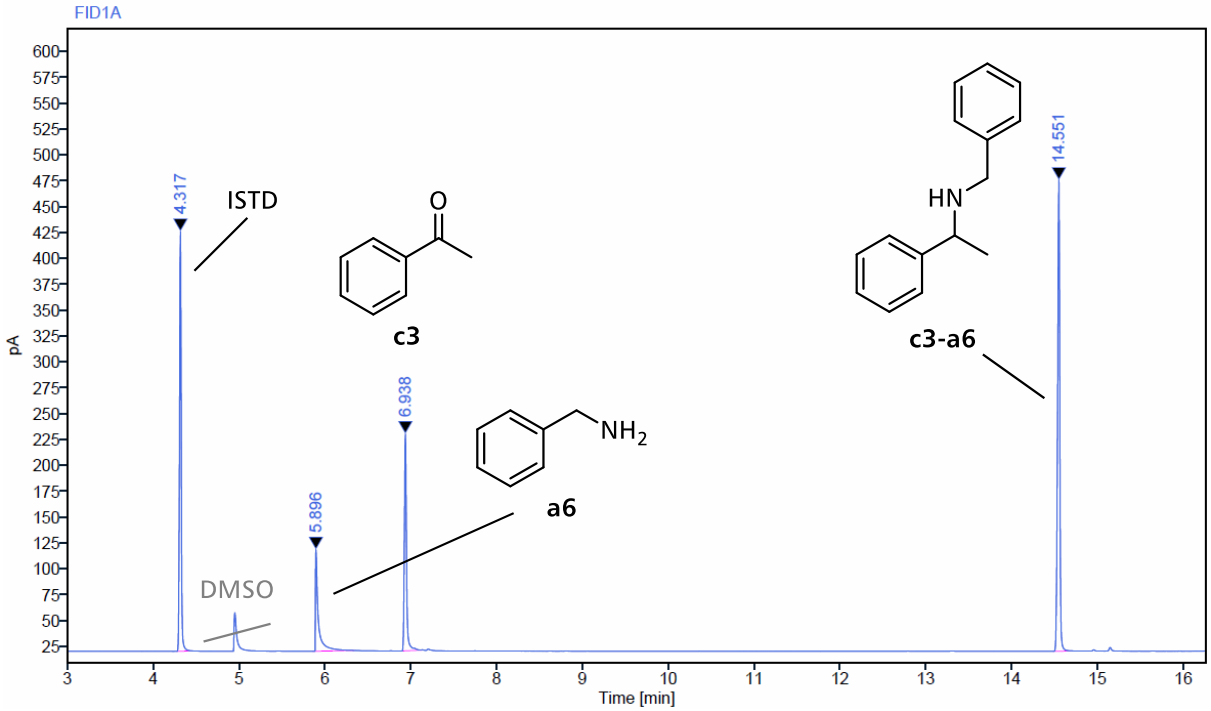


Figure S95. Chromatographic separation of *n*-decane (ISTD, t_r 4.3 min), benzylamine (**a6**, t_r 5.9 min), acetophenone (**c3**, t_r 6.9 min), and *N*-benzyl-1-phenylethan-1-amine (**c3-a6**, t_r 14.6 min) using GC–FID method GC-A3. Calibration standard containing 10 mM of ISTD and 20 mM of each analyte.

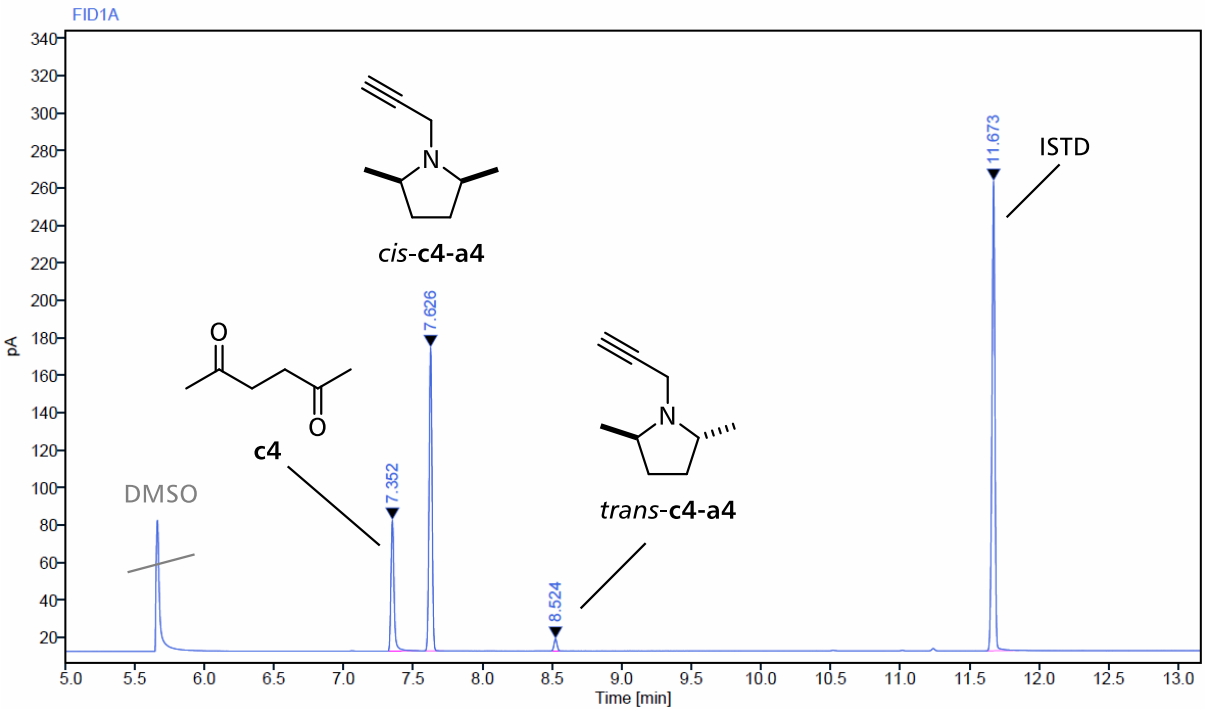


Figure S96. Chromatographic separation of hexane-2,5-dione (**c4**, t_r 7.4 min), *cis*-2,5-dimethyl-1-propargylpyrrolidine (*cis*-**c4-a4**, t_r 7.6 min), *trans*-2,5-dimethyl-1-propargylpyrrolidine (*trans*-**c4-a4**, t_r 8.5 min), and *n*-dodecane (ISTD, t_r 11.7 min) using GC–FID method GC-A1. Calibration standard containing 10 mM of ISTD and 20 mM of each analyte.

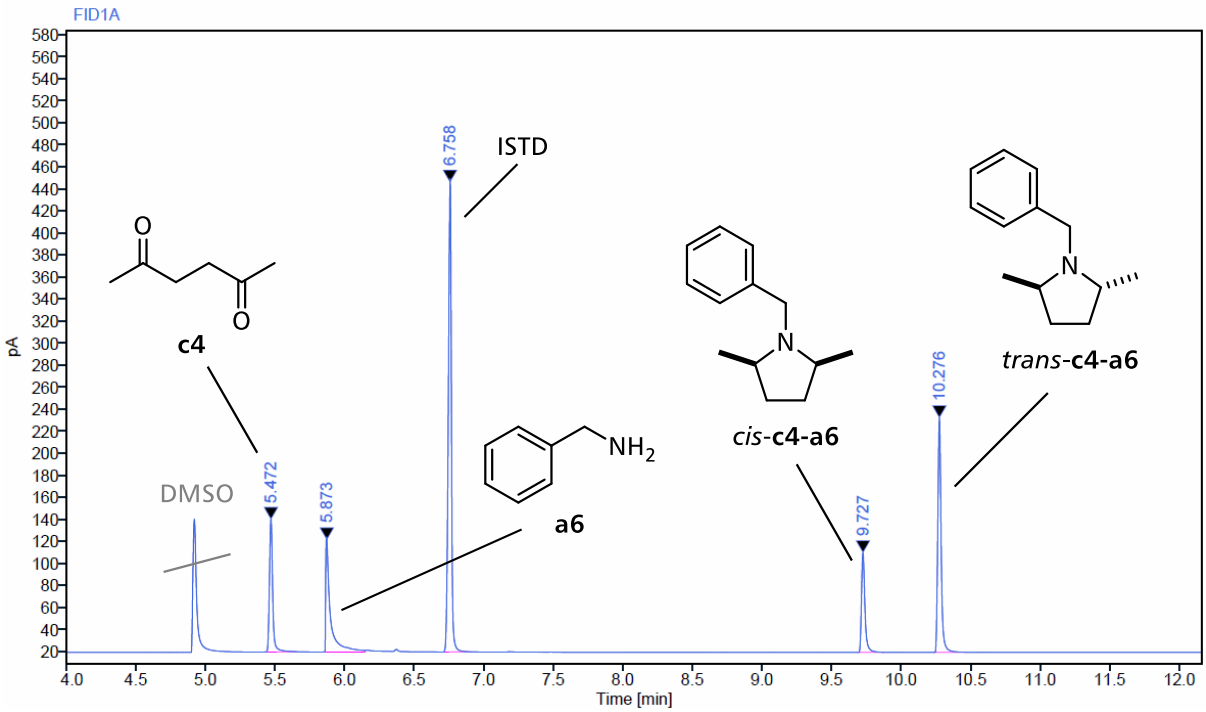


Figure S97. Chromatographic separation of hexane-2,5-dione (**c4**, t_r 5.5 min), benzylamine (**a6**, t_r 5.9 min), *n*-dodecane (ISTD, t_r 6.8 min), *cis*-1-benzyl-2,5-dimethylpyrrolidine (*cis*-**c4-a6**, t_r 9.7 min), and *trans*-1-benzyl-2,5-dimethylpyrrolidine (*trans*-**c4-a6**, t_r 10.3 min) using GC–FID method GC-A3. Calibration standard containing 10 mM of ISTD and 20 mM of each analyte.

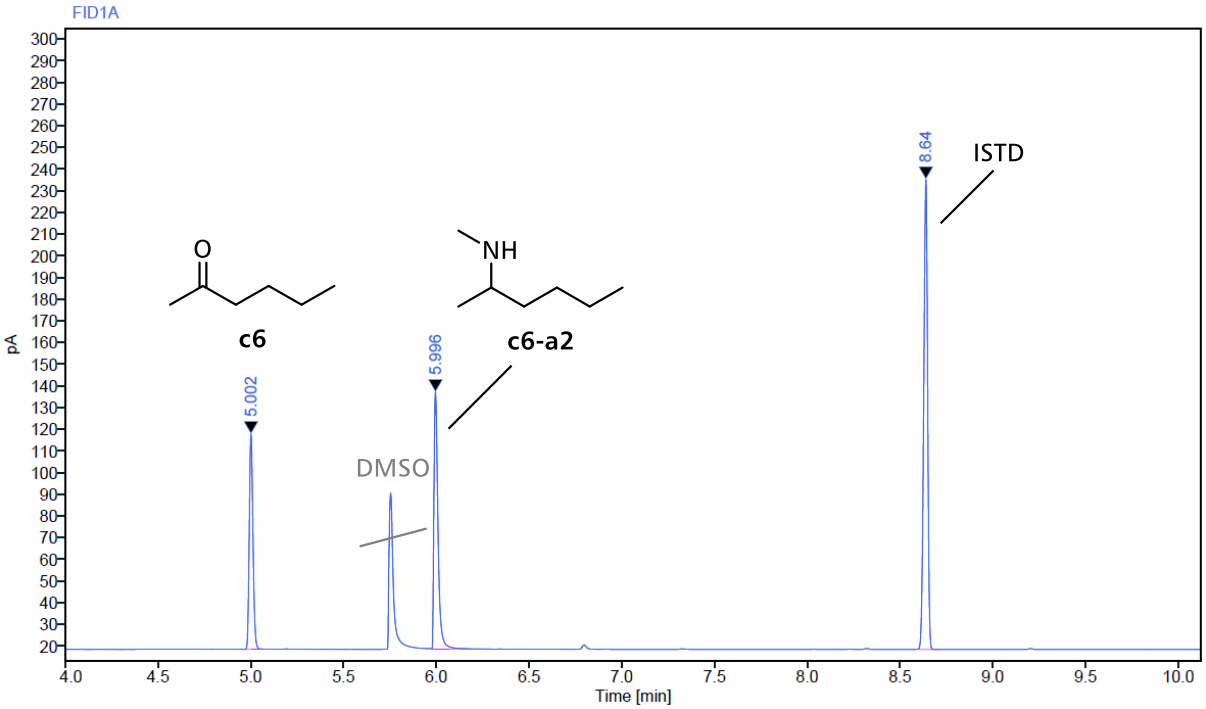


Figure S98. Chromatographic separation of hexan-2-one (**c6**, t_r 5.0 min), *N*-methylhexan-2-amine (**c6-a2**, t_r 6.0 min), and *n*-decane (ISTD, t_r 8.6 min) using GC–FID method GC-A1. Calibration standard containing 10 mM of ISTD and 20 mM of each analyte.

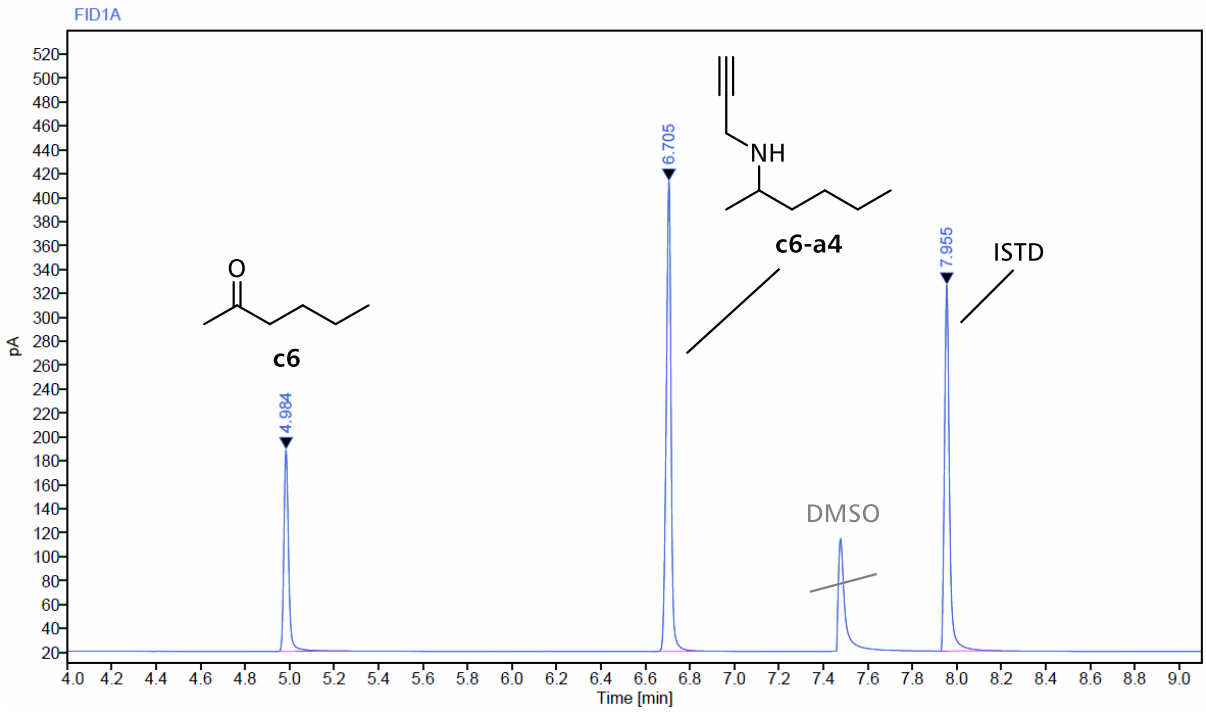


Figure S99. Chromatographic separation of hexan-2-one (**c6**, t_r 5.0 min), *N*-propargylhexan-2-amine (**c6-a4**, t_r 6.7 min), and *n*-decane (ISTD, t_r 8.0 min) using GC–FID method GC-A2. Calibration standard containing 10 mM of ISTD and 20 mM of each analyte.

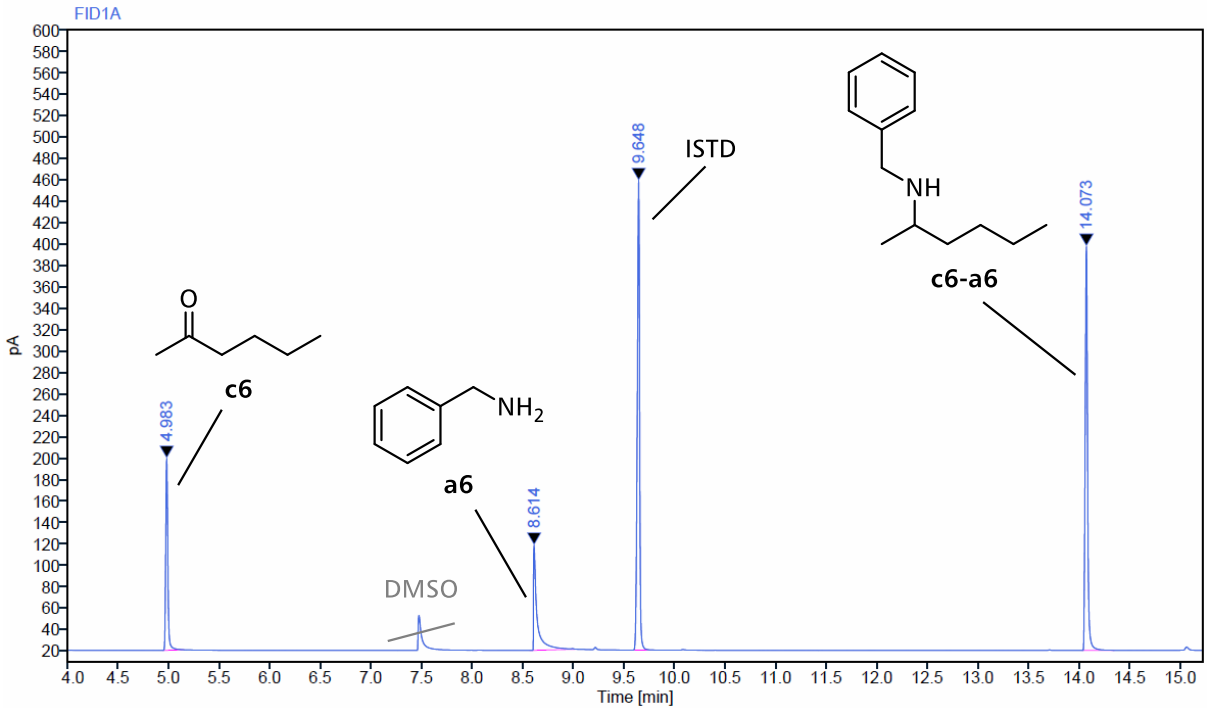


Figure S100. Chromatographic separation of hexan-2-one (**c6**, t_r 5.0 min), benzylamine (**a6**, t_r 8.6 min), *n*-dodecane (ISTD, t_r 9.6 min), and *N*-benzylhexan-2-amine (**c6-a6**, t_r 14.1 min) using GC–FID method GC-A2. Calibration standard containing 10 mM of ISTD and 20 mM of each analyte.

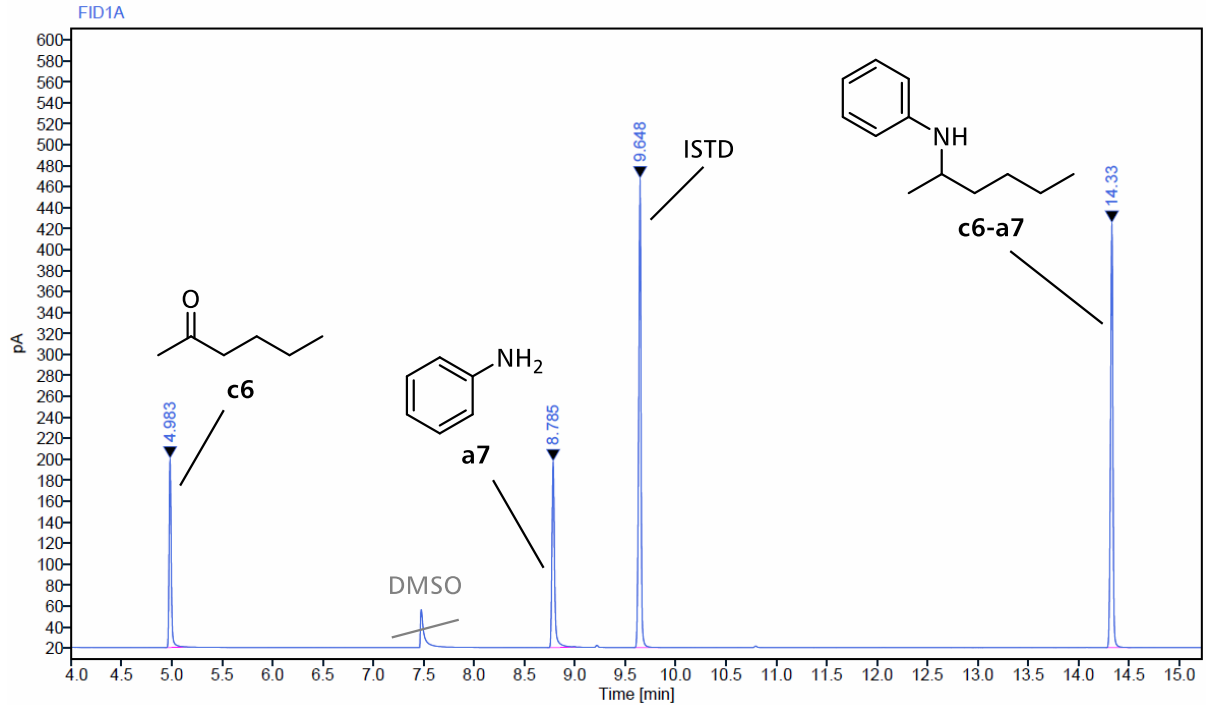


Figure S101. Chromatographic separation of hexan-2-one (**c6**, t_r 5.0 min), aniline (**a7**, t_r 8.8 min), *n*-dodecane (ISTD, t_r 9.6 min), and *N*-(hexan-2-yl)aniline (**c6-a7**, t_r 14.3 min) using GC–FID method GC-A2. Calibration standard containing 10 mM of ISTD and 20 mM of each analyte.

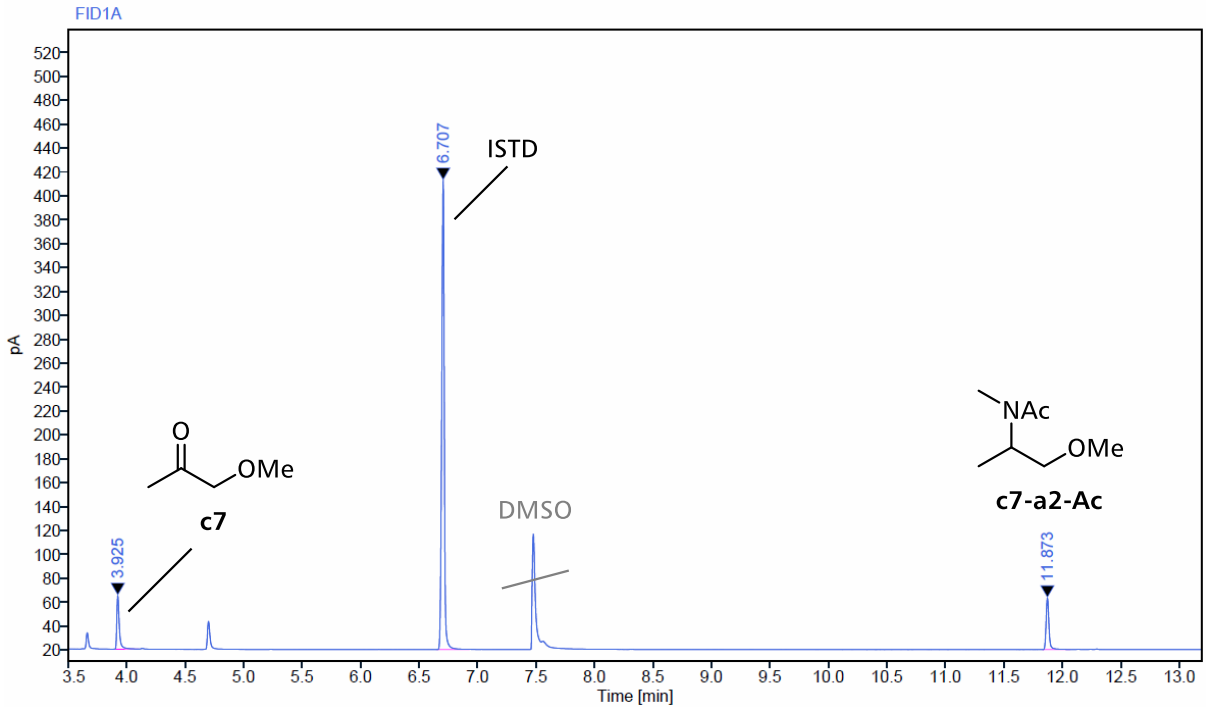


Figure S102. Chromatographic separation of methoxyacetone (**c7**, t_r 3.9 min), *n*-decane (ISTD, t_r 6.7 min), and *N*-(1-methoxypropan-2-yl)-*N*-methylacetamide (**c7-a2-Ac**, t_r 11.9 min) using GC–FID method GC-A2. Calibration standard containing 10 mM of ISTD and 20 mM of each analyte.

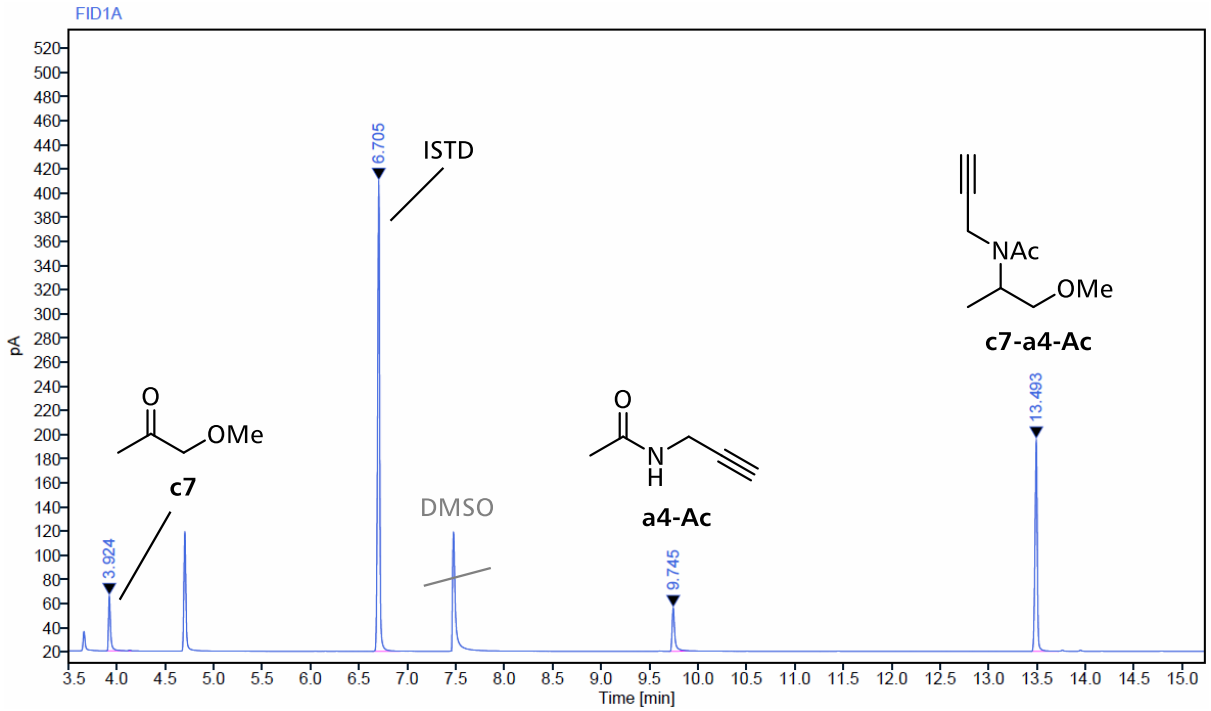


Figure S103. Chromatographic separation of methoxyacetone (**c7**, t_r 3.9 min), *n*-decane (ISTD, t_r 6.7 min), *N*-propargylacetamide (**a4-Ac**, t_r 9.7 min), and *N*-(1-methoxypropan-2-yl)-*N*-propargyl-acetamide (**c7-a4-Ac**, t_r 13.5 min) using GC–FID method GC-A2. Calibration standard containing 10 mM of ISTD and 20 mM of each analyte.

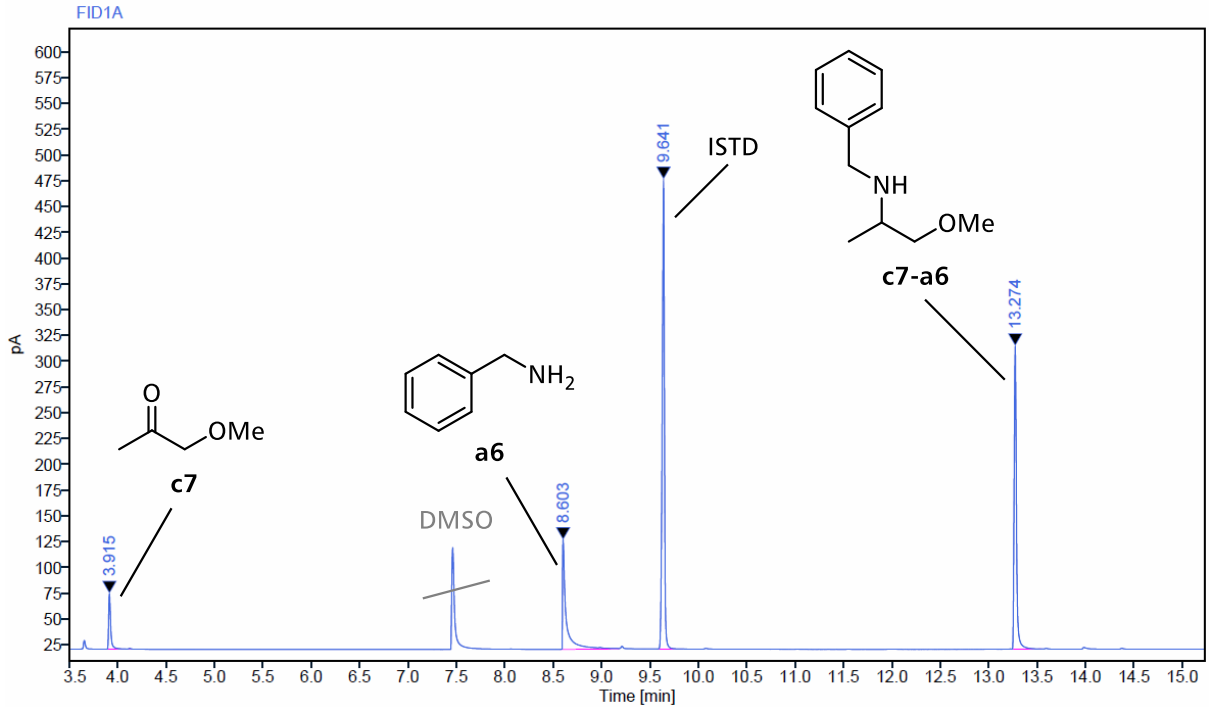


Figure S104. Chromatographic separation of methoxyacetone (**c7**, t_r 3.9 min), benzylamine (**a6**, t_r 8.6 min), *n*-dodecane (ISTD, t_r 9.6 min), and *N*-benzyl-1-methoxypropan-2-amine (**c7-a6**, t_r 13.3 min) using GC–FID method GC-A2. Calibration standard containing 10 mM of ISTD and 20 mM of each analyte.

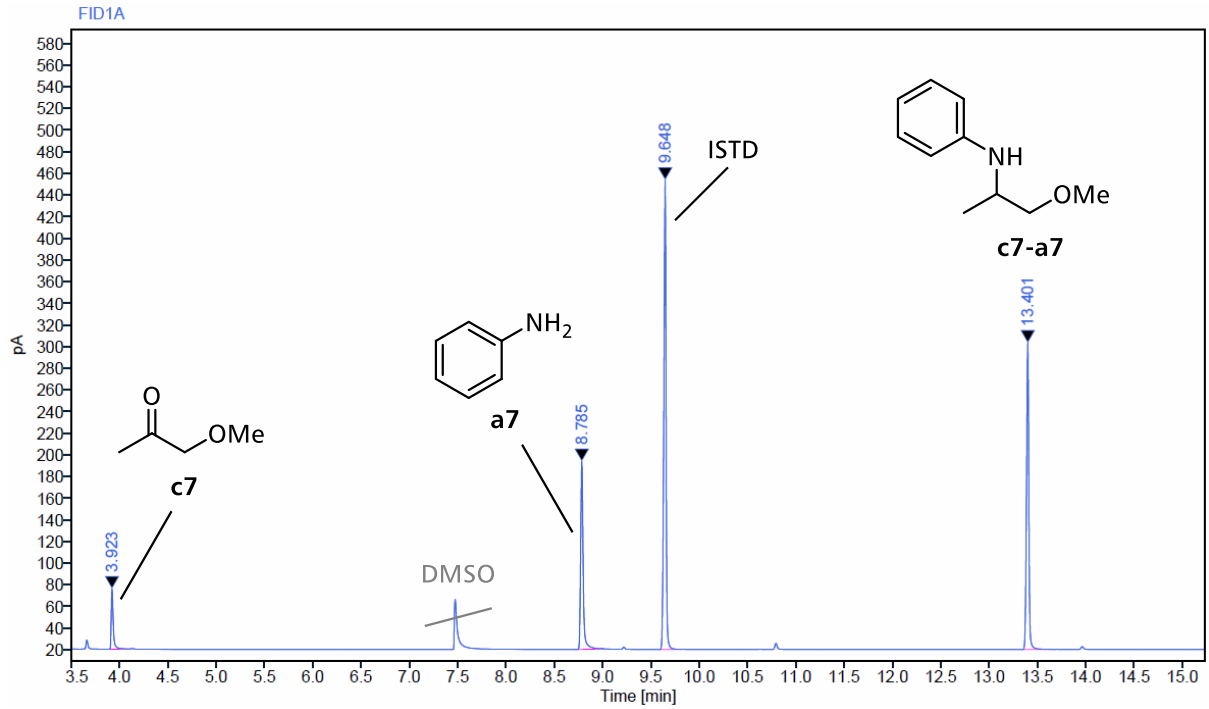


Figure S105. Chromatographic separation of methoxyacetone (**c7**, t_r 3.9 min), aniline (**a7**, t_r 8.8 min), *n*-dodecane (ISTD, t_r 9.6 min), and *N*-(1-methoxypropan-2-yl)aniline (**c7-a7**, t_r 13.4 min) using GC–FID method GC-A2. Calibration standard containing 10 mM of ISTD and 20 mM of each analyte.

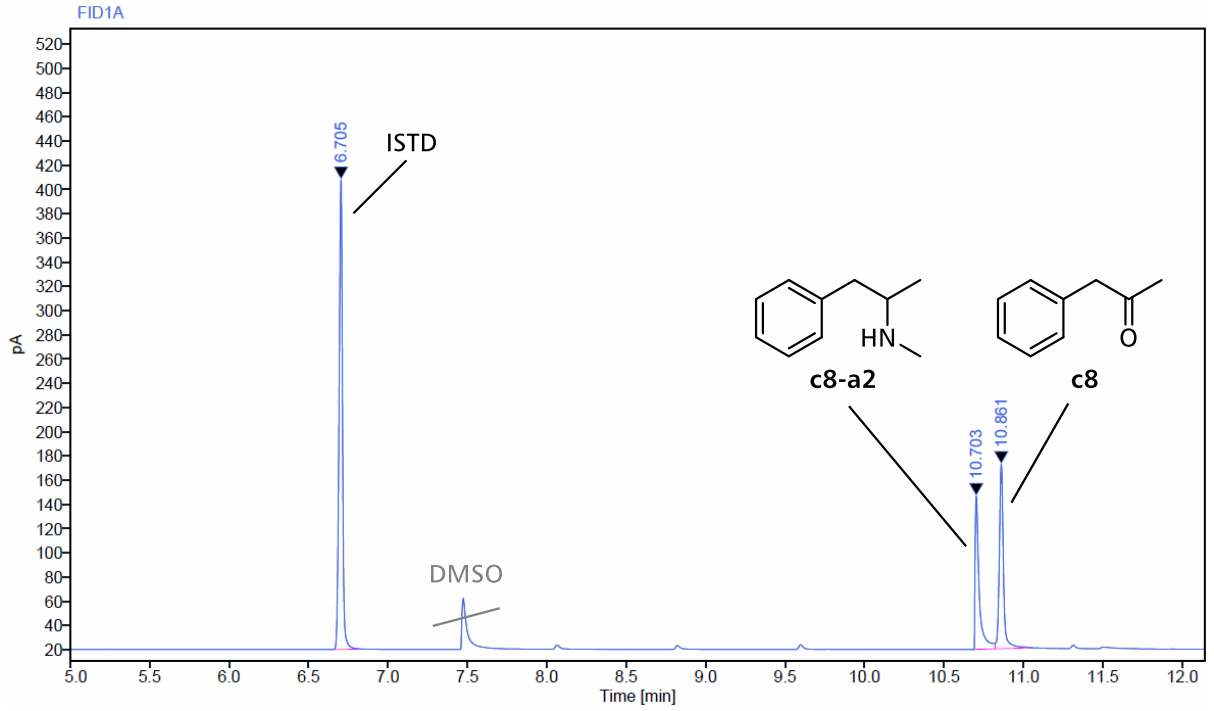


Figure S106. Chromatographic separation of *n*-decane (ISTD, t_r 6.7 min), *N*-methyl-1-phenylpropan-2-amine (**c8-a2**, t_r 10.7 min), and phenylacetone (**c8**, t_r 10.9 min) using GC–FID method GC-A2. Calibration standard containing 10 mM of ISTD and 20 mM of each analyte.

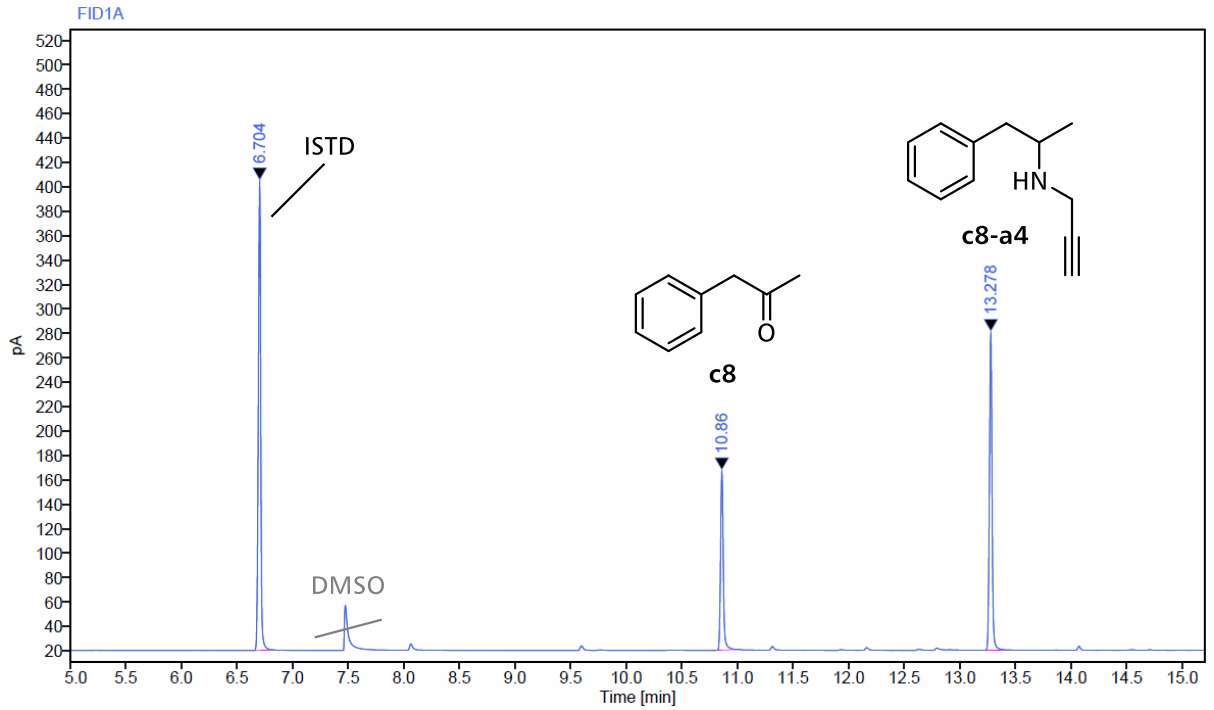


Figure S107. Chromatographic separation of *n*-decane (ISTD, t_r 6.7 min), phenylacetone (**c8**, t_r 10.9 min), and *N*-(1-phenylpropan-2-yl)prop-2-yn-1-amine (**c8-a4**, t_r 13.3 min) using GC–FID method GC-A2. Calibration standard containing 10 mM of ISTD and 20 mM of each analyte.

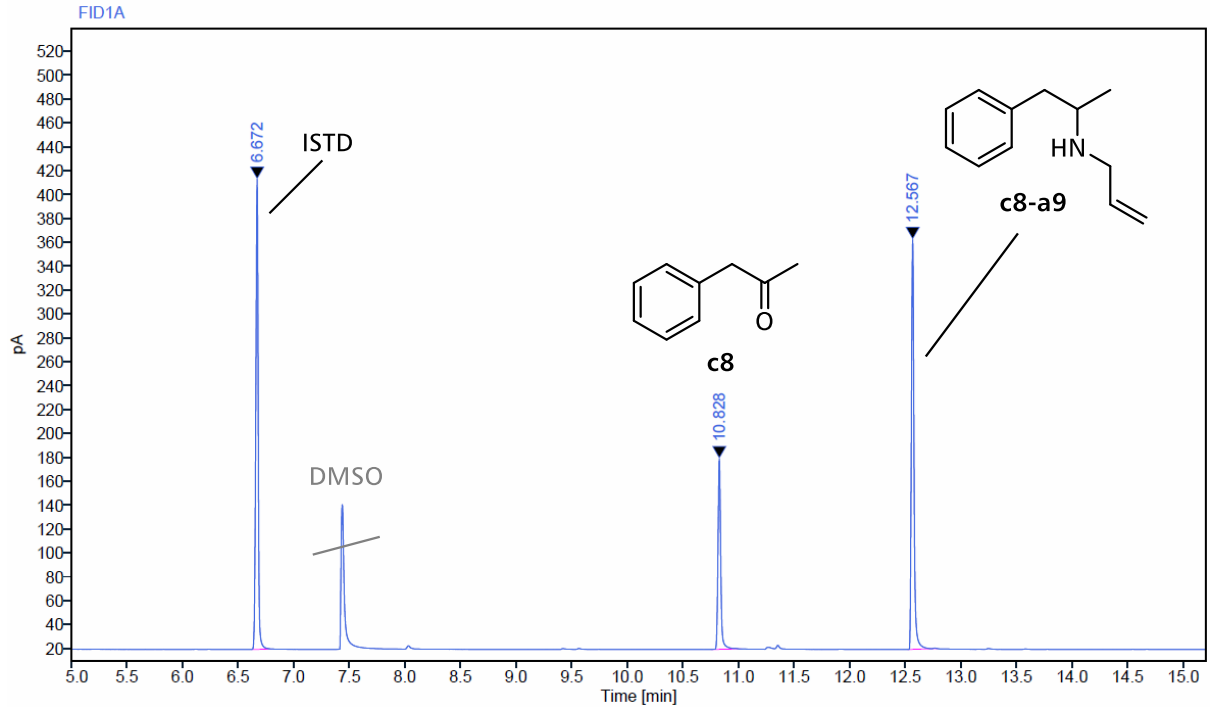


Figure S108. Chromatographic separation of *n*-decane (ISTD, t_r 6.7 min), phenylacetone (**c8**, t_r 10.8 min), and *N*-(1-phenylpropan-2-yl)prop-2-en-1-amine (**c8-a9**, t_r 12.6 min) using GC–FID method GC-A2. Calibration standard containing 10 mM of ISTD and 20 mM of each analyte.

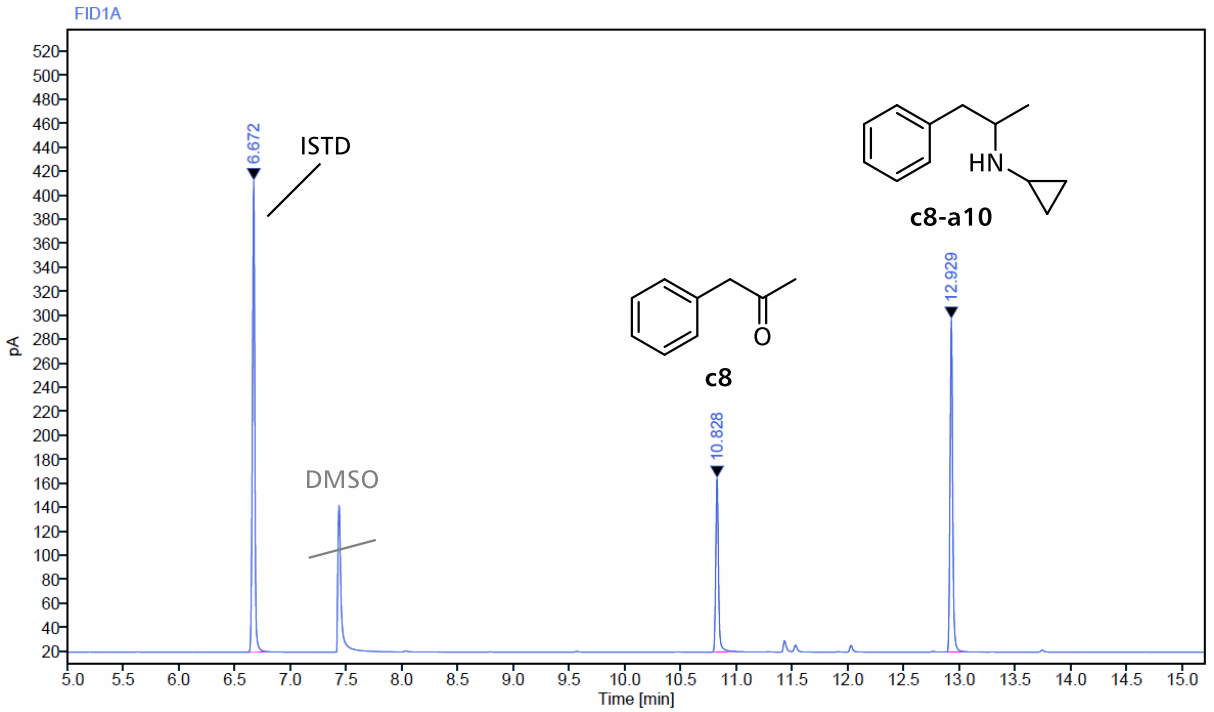


Figure S109. Chromatographic separation of *n*-decane (ISTD, t_r 6.7 min), phenylacetone (**c8**, t_r 10.8 min), and *N*-(1-phenylpropan-2-yl)cyclopropanamine (**c8-a10**, t_r 12.9 min) using GC–FID method GC-A2. Calibration standard containing 10 mM of ISTD and 20 mM of each analyte.

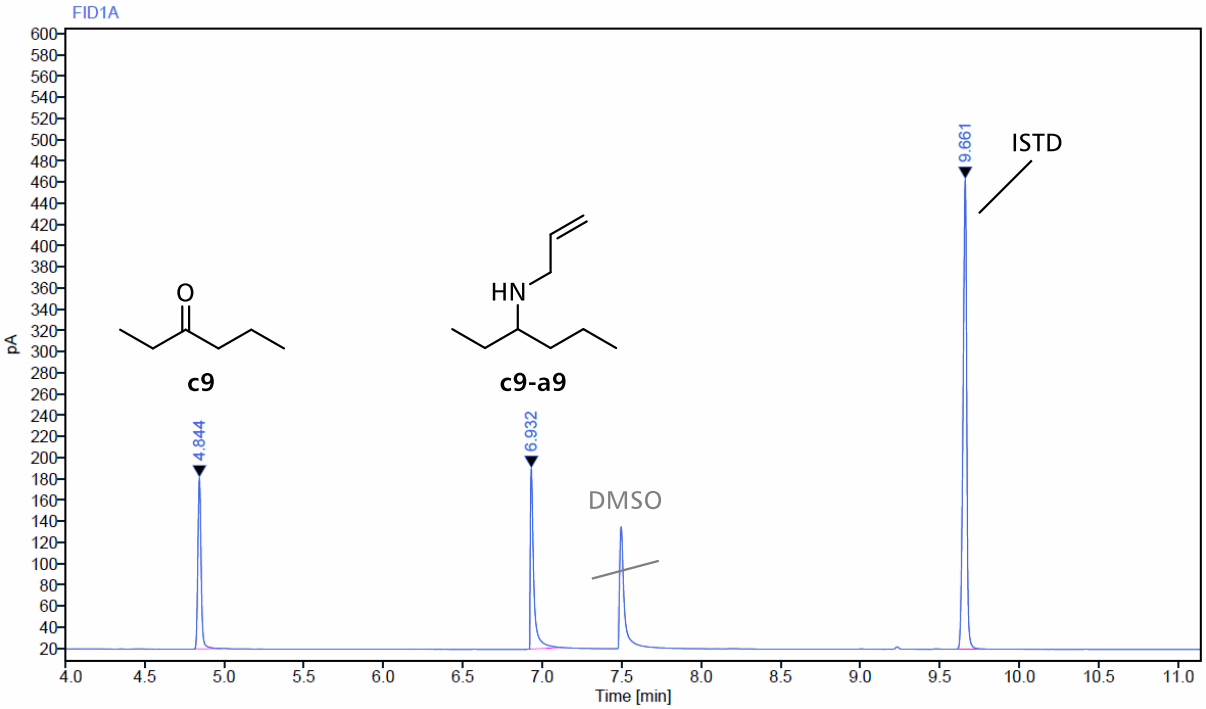


Figure S110. Chromatographic separation of hexan-3-one (**c9**, t_r 4.8 min), *N*-allylhexan-3-amine (**c9-a9**, t_r 6.9 min), and *n*-dodecane (ISTD, t_r 9.7 min) using GC–FID method GC-A2. Calibration standard containing 10 mM of ISTD and 20 mM of each analyte.

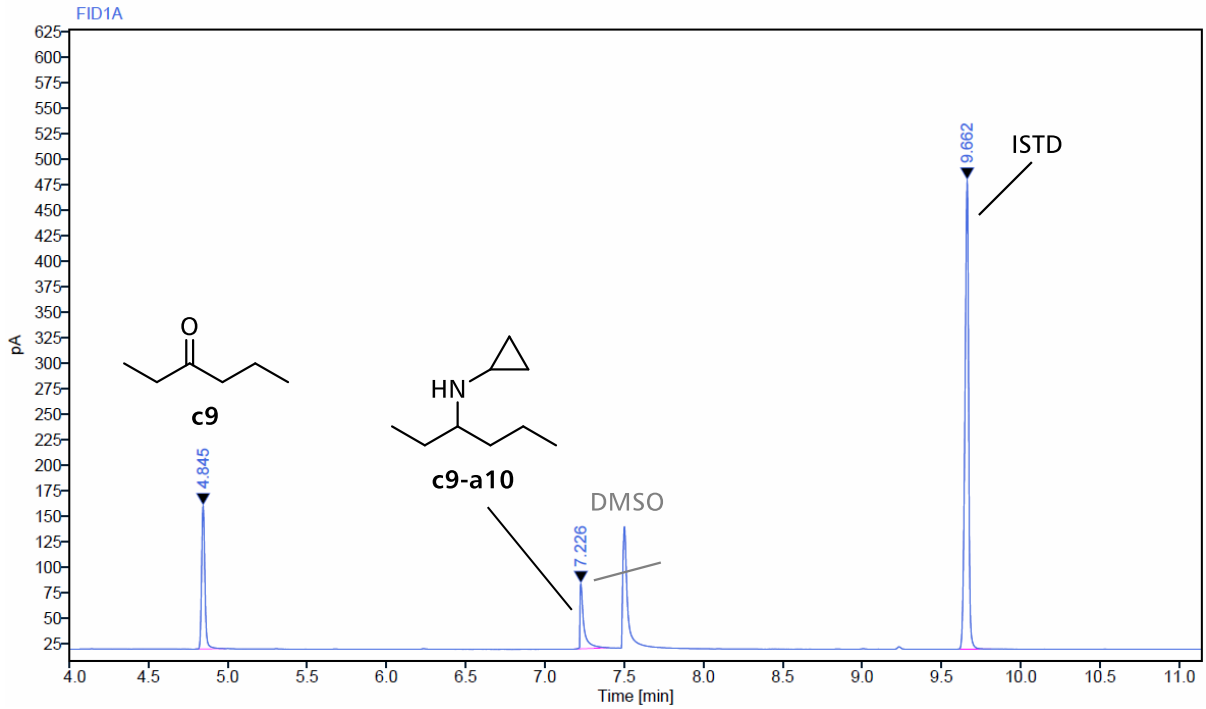


Figure S111. Chromatographic separation of hexan-3-one (**c9**, t_r 4.8 min), *N*-(hexan-3-yl)cyclopropanamine (**c9-a10**, t_r 7.2 min), and *n*-dodecane (ISTD, t_r 9.7 min) using GC–FID method GC-A2. Calibration standard containing 10 mM of ISTD, 20 mM of ketone, and 10 mM of amine product.

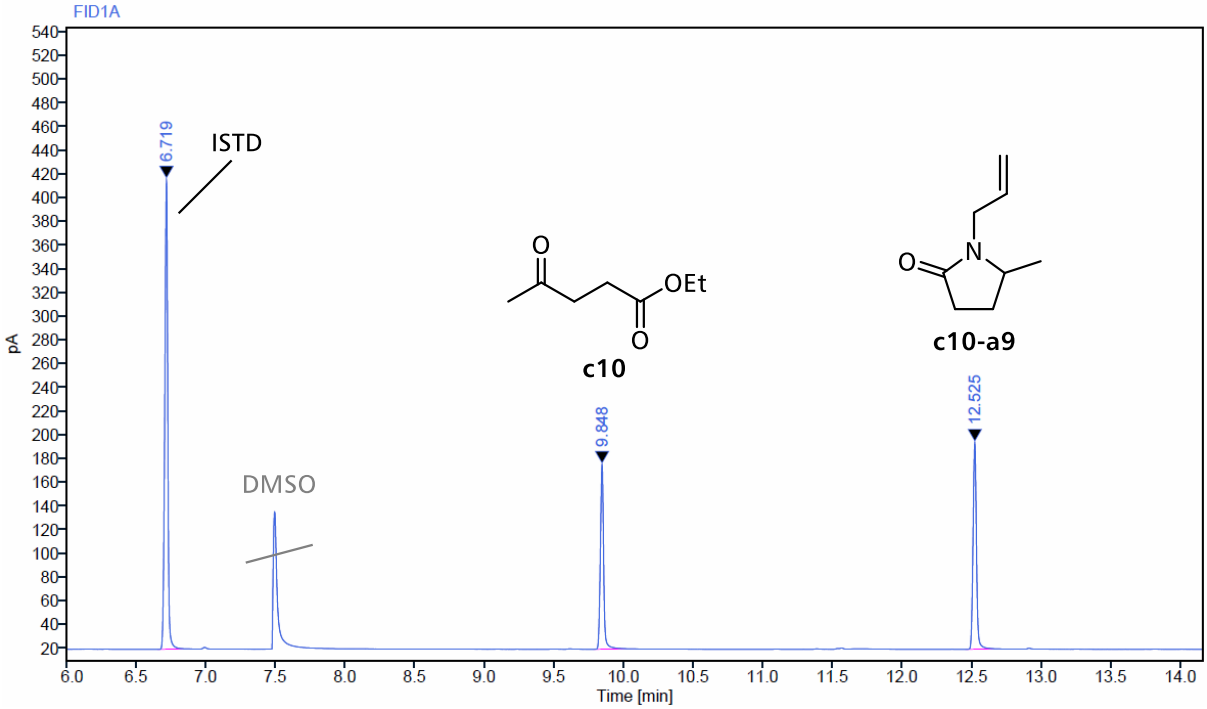


Figure S112. Chromatographic separation of *n*-decane (ISTD, t_r 6.7 min), ethyl levulinate (**c10**, t_r 9.8 min), and 1-allyl-5-methylpyrrolidin-2-one (**c10-a9**, t_r 12.5 min) using GC–FID method GC-A2. Calibration standard containing 10 mM of ISTD and 20 mM of each analyte.

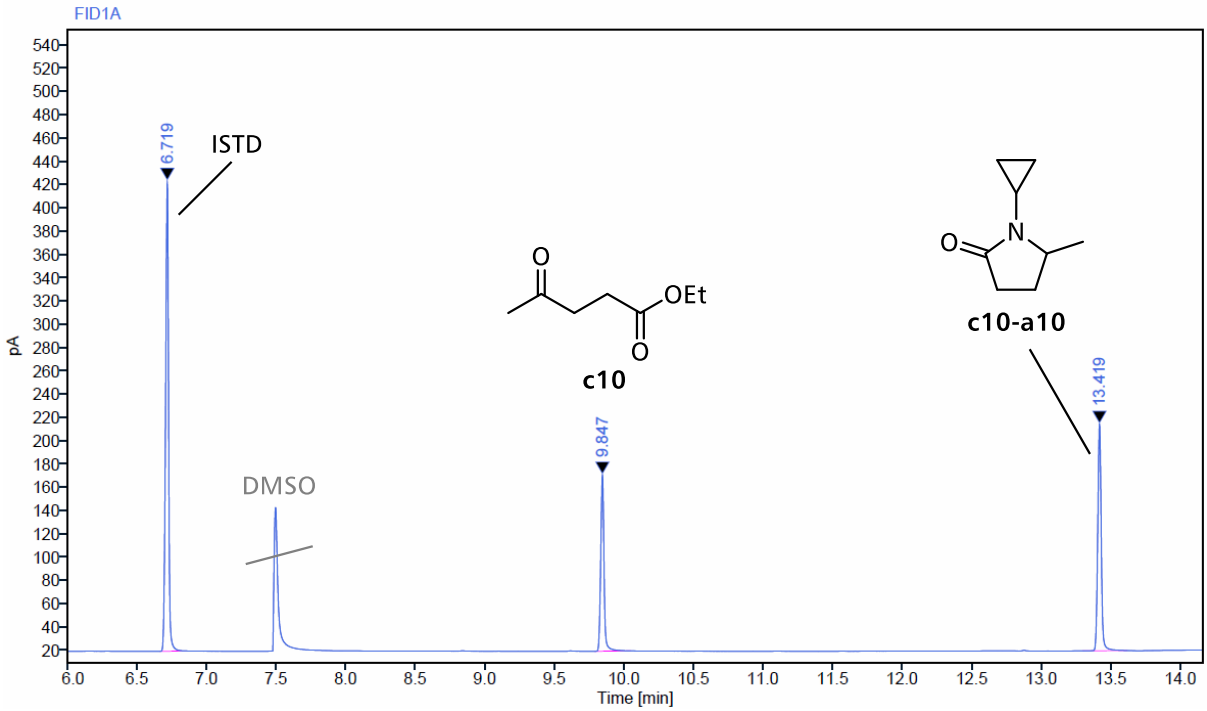


Figure S113. Chromatographic separation of *n*-decane (ISTD, t_r 6.7 min), ethyl levulinate (**c10**, t_r 9.8 min), and 1-cyclopropyl-5-methylpyrrolidin-2-one (**c10-a10**, t_r 13.4 min) using GC–FID method GC-A2. Calibration standard containing 10 mM of ISTD and 20 mM of each analyte.

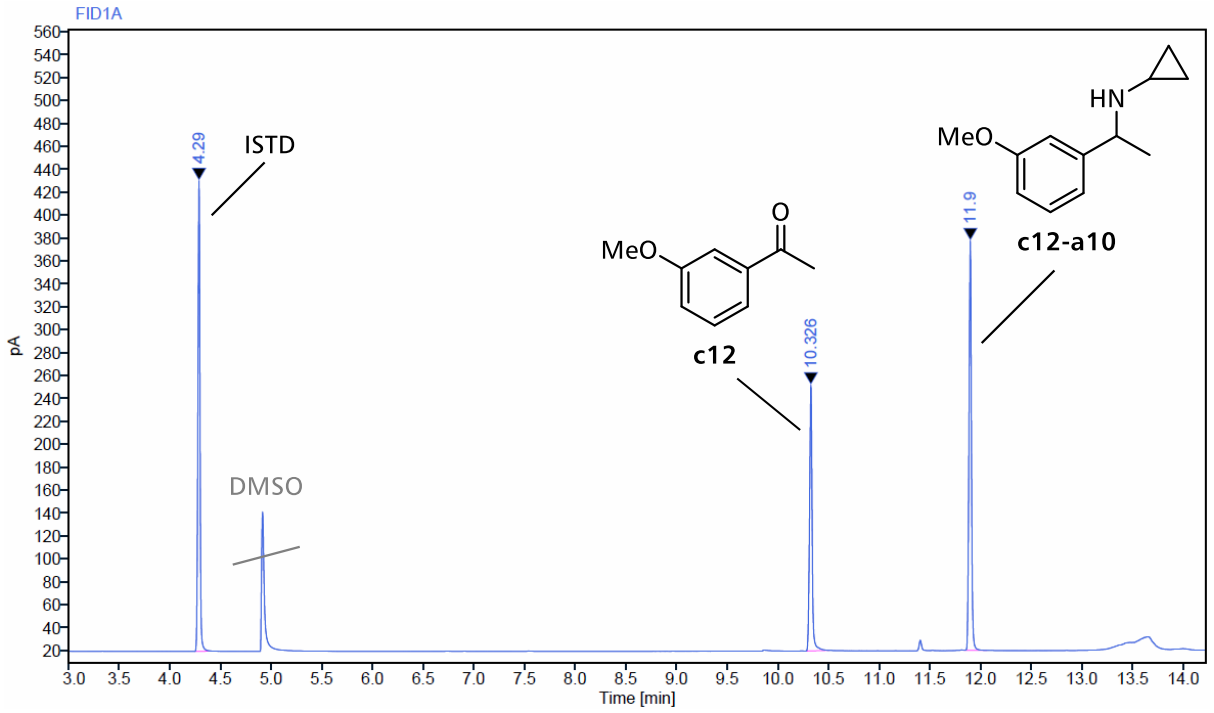


Figure S114. Chromatographic separation of *n*-decane (ISTD, t_r 4.3 min), 3-methoxyacetophenone (**c12**, t_r 10.3 min), and *N*-(1-(3-methoxyphenyl)ethyl)cyclopropanamine (**c12-a10**, t_r 11.9 min) using GC–FID method GC-A3. Calibration standard containing 10 mM of ISTD and 20 mM of each analyte.

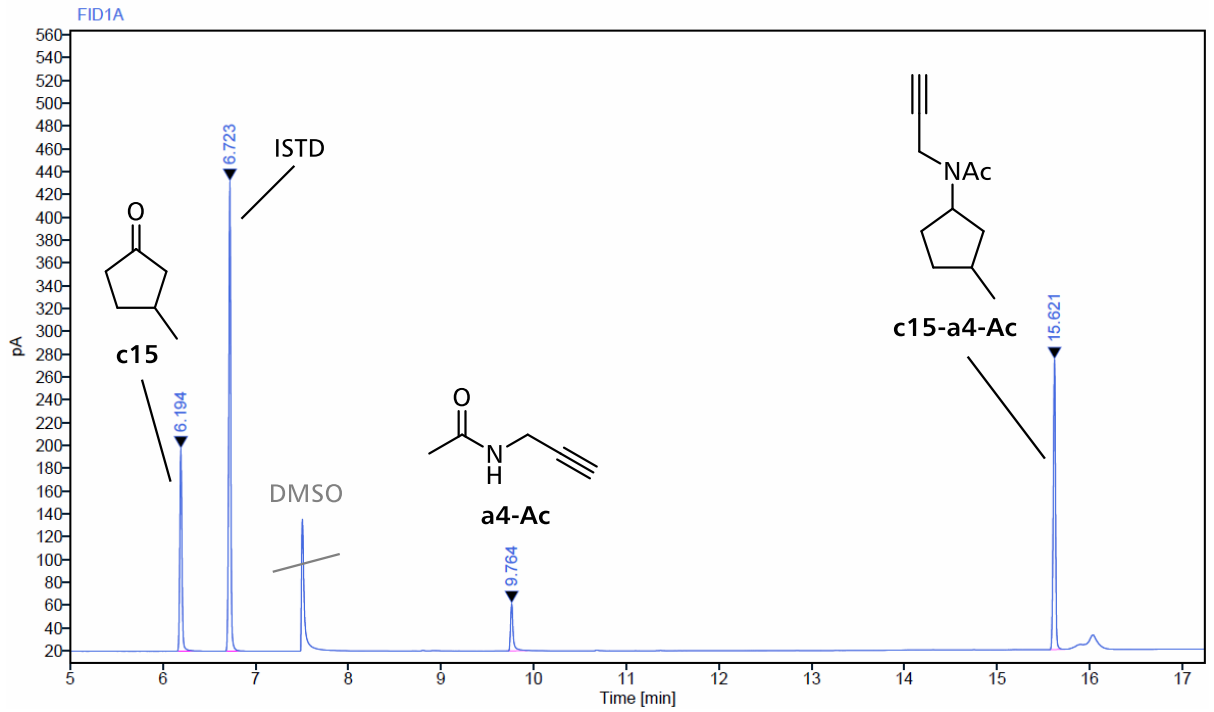


Figure S115. Chromatographic separation of 3-methylcyclopentan-1-one (**c15**, t_r 6.2 min), *n*-decane (ISTD, t_r 6.7 min), *N*-propargylacetamide (**a4-Ac**, t_r 9.8 min), and *N*-(3-methylcyclopentyl)-*N*-propargylacetamide (**c15-a4-Ac**, t_r 15.6 min) using GC–FID method GC-A2. Calibration standard containing 10 mM of ISTD and 20 mM of each analyte. The chromatographic method does not achieve separation of the product diastereomers.

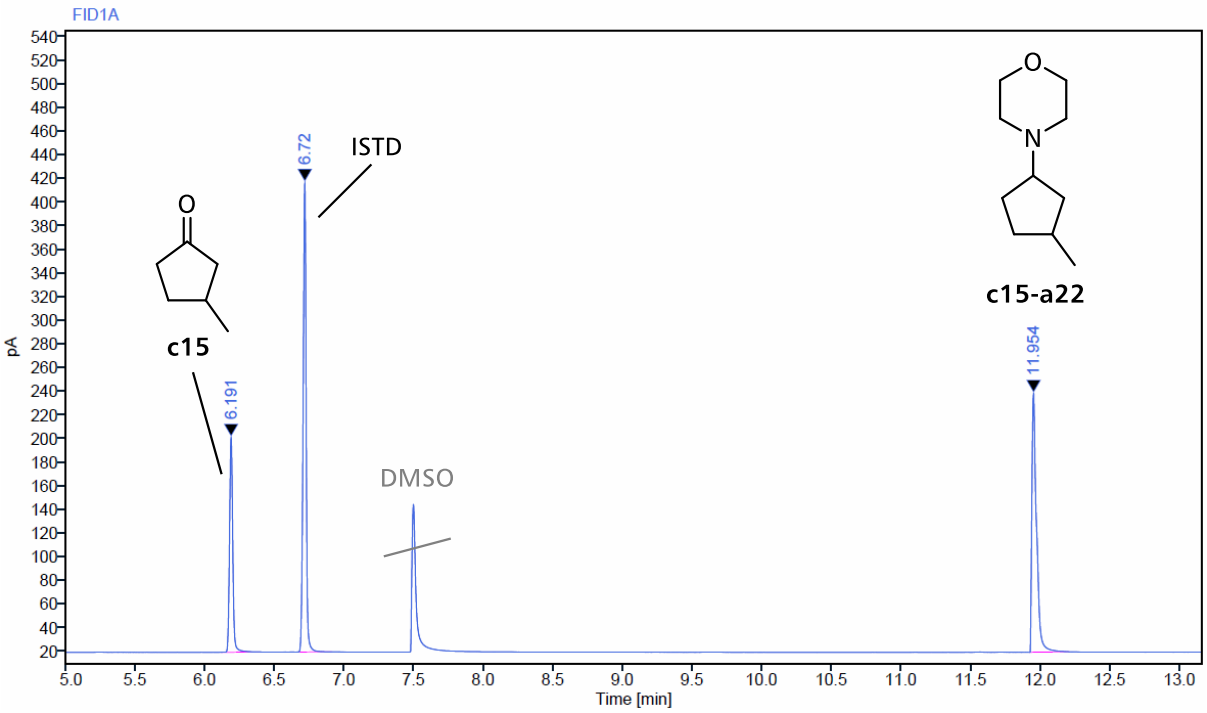


Figure S116. Chromatographic separation of 3-methylcyclopentan-1-one (**c15**, t_r 6.2 min), *n*-decane (ISTD, t_r 6.7 min), and 4-(3-methylcyclopentyl)morpholine (**c15-a22**, t_r 12.0 min) using GC–FID method GC-A2. Calibration standard containing 10 mM of ISTD and 20 mM of each analyte. The chromatographic method does not achieve separation of the product diastereomers.

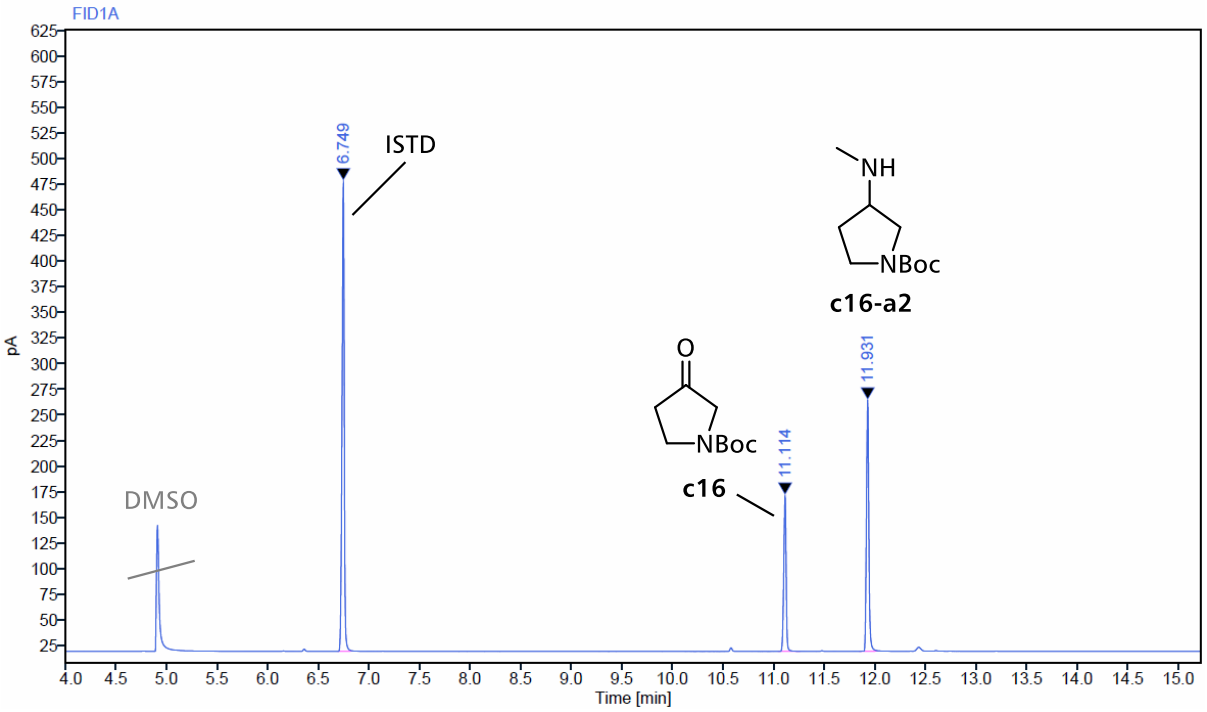


Figure S117. Chromatographic separation of *n*-dodecane (ISTD, t_r 6.7 min), *tert*-butyl 3-oxo-pyrrolidine-1-carboxylate (**c16**, t_r 11.1 min), and *tert*-butyl 3-(methylamino)pyrrolidine-1-carboxylate (**c16-a2**, t_r 11.9 min) using GC–FID method GC-A3. Calibration standard containing 10 mM of ISTD and 20 mM of each analyte.

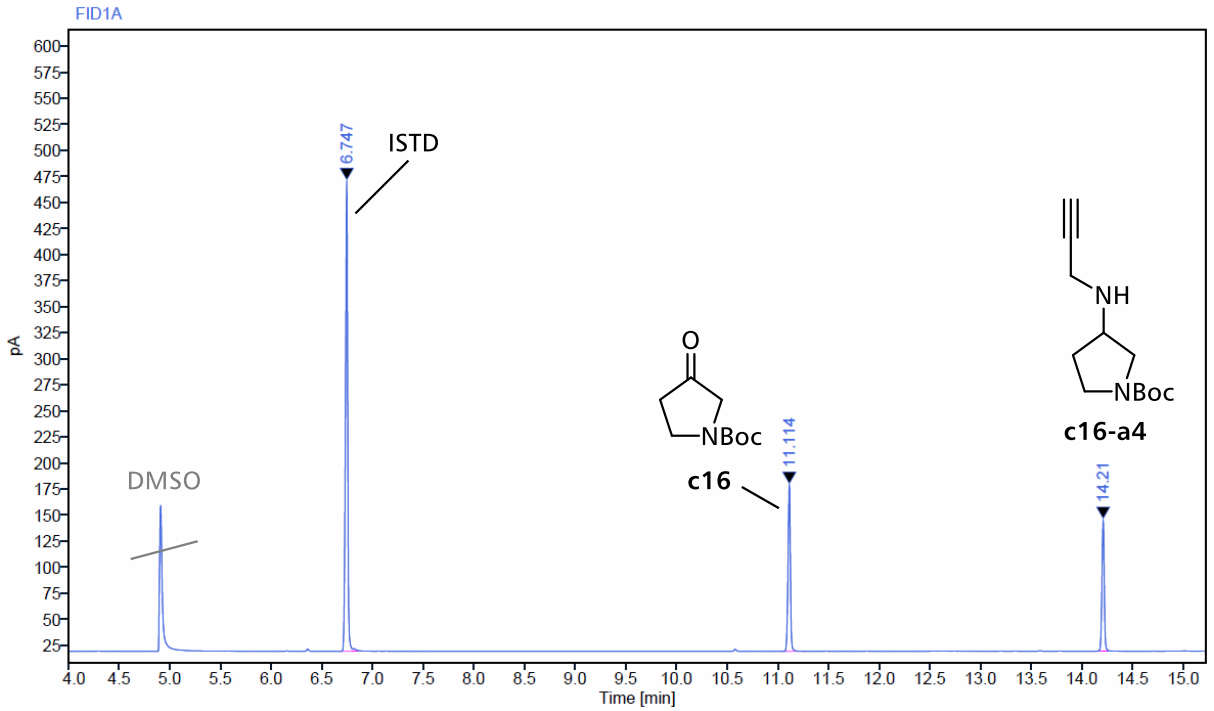


Figure S118. Chromatographic separation of *n*-dodecane (ISTD, t_r 6.7 min), *tert*-butyl 3-oxo-pyrrolidine-1-carboxylate (**c16**, t_r 11.1 min), and *tert*-butyl 3-(propargylamino)pyrrolidine-1-carboxylate (**c16-a4**, t_r 14.2 min) using GC–FID method GC-A3. Calibration standard containing 10 mM of ISTD and 20 mM of each analyte.

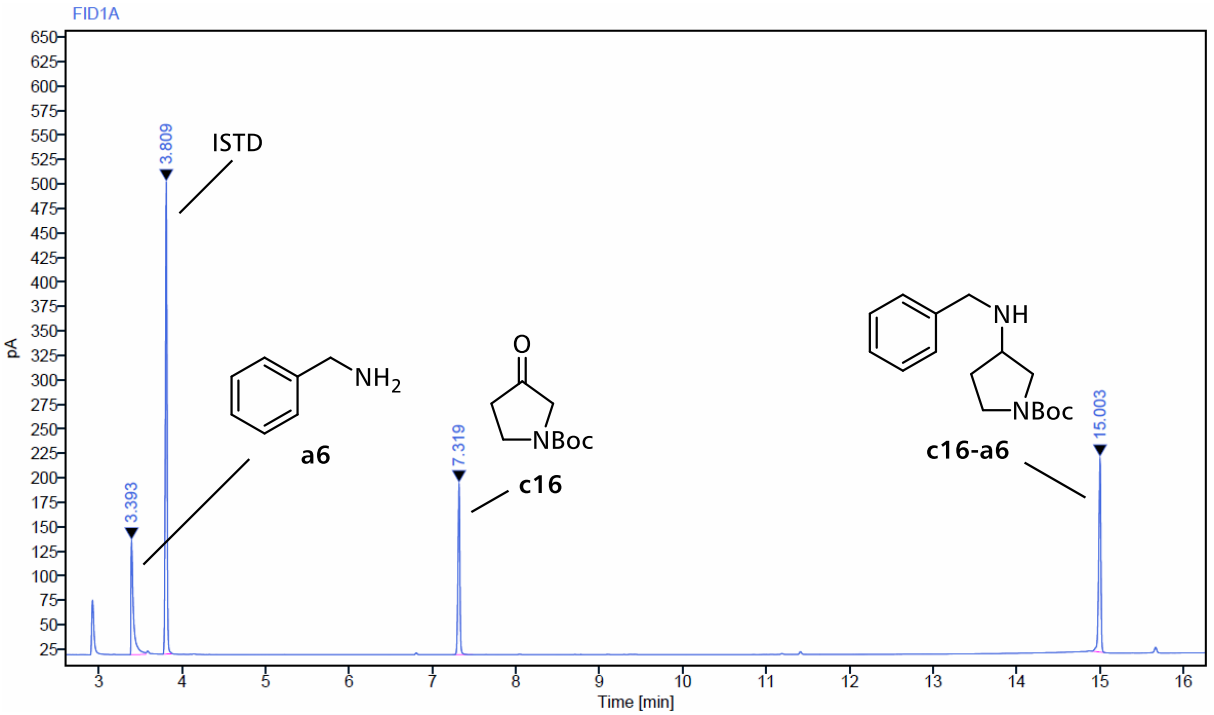


Figure S119. Chromatographic separation of benzylamine (**a6**, t_r 3.4 min), *n*-dodecane (ISTD, t_r 3.8 min), *tert*-butyl 3-oxopyrrolidine-1-carboxylate (**c16**, t_r 7.3 min), and *tert*-butyl 3-(benzylamino)-pyrrolidine-1-carboxylate (**c16-a6**, t_r 15.0 min) using GC–FID method GC-A4. Calibration standard containing 10 mM of ISTD and 20 mM of each analyte.

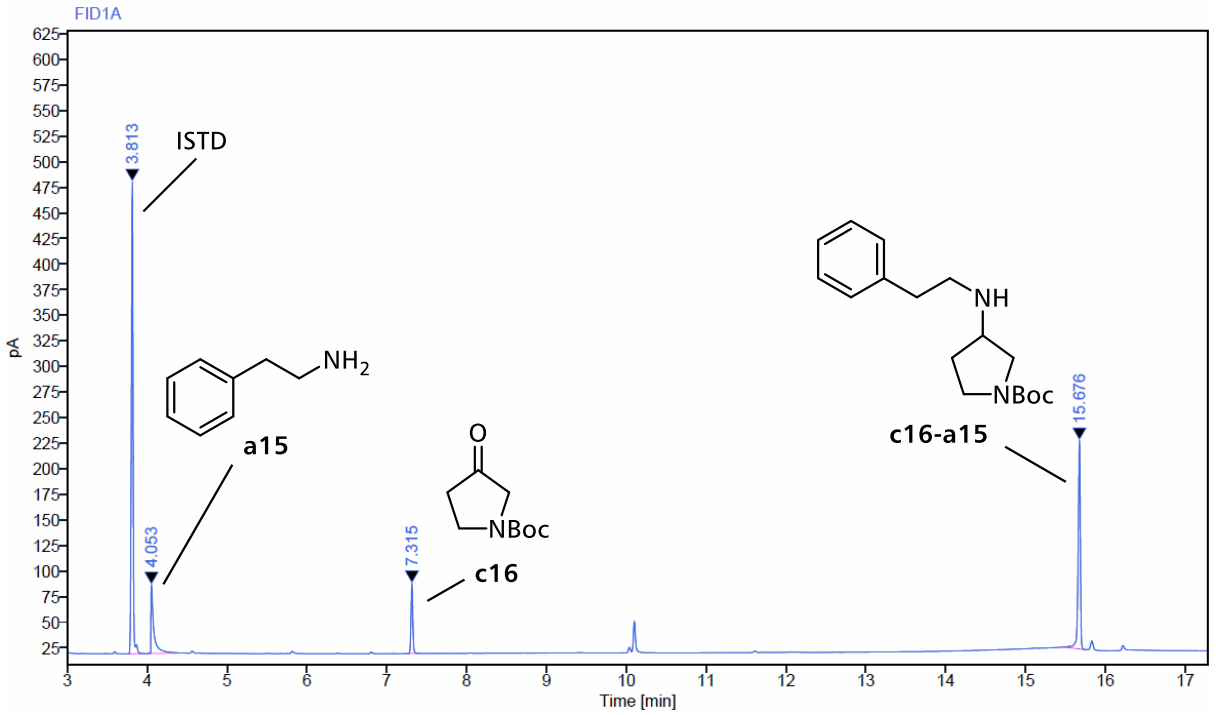


Figure S120. Chromatographic separation of *n*-dodecane (ISTD, t_r 3.8 min), phenethylamine (**a15**, t_r 4.1 min), *tert*-butyl 3-oxopyrrolidine-1-carboxylate (**c16**, t_r 7.3 min), and *tert*-butyl 3-(phenethylamino)pyrrolidine-1-carboxylate (**c16-a15**, t_r 15.7 min) using GC–FID method GC-A4. Calibration standard containing 10 mM of ISTD and 20 mM of each analyte.

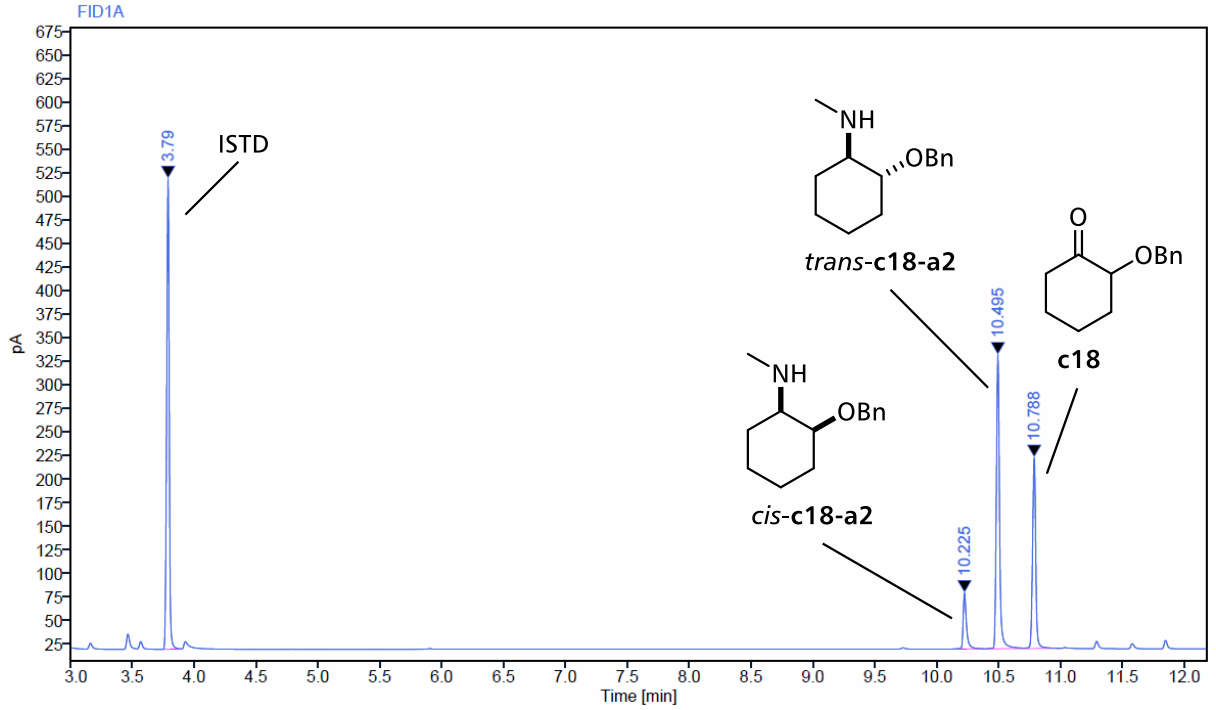


Figure S121. Chromatographic separation of *n*-dodecane (ISTD, t_r 3.8 min), *cis*-2-(benzyloxy)-*N*-methylcyclohexan-1-amine (*cis*-**c18-a2**, t_r 10.2 min), *trans*-2-(benzyloxy)-*N*-methylcyclohexan-1-amine (*trans*-**c18-a2**, t_r 10.5 min), and 2-(benzyloxy)cyclohexan-1-one (**c18**, t_r 10.8 min) using GC–FID method GC-A4. Calibration standard containing 10 mM of ISTD and 20 mM of each analyte.

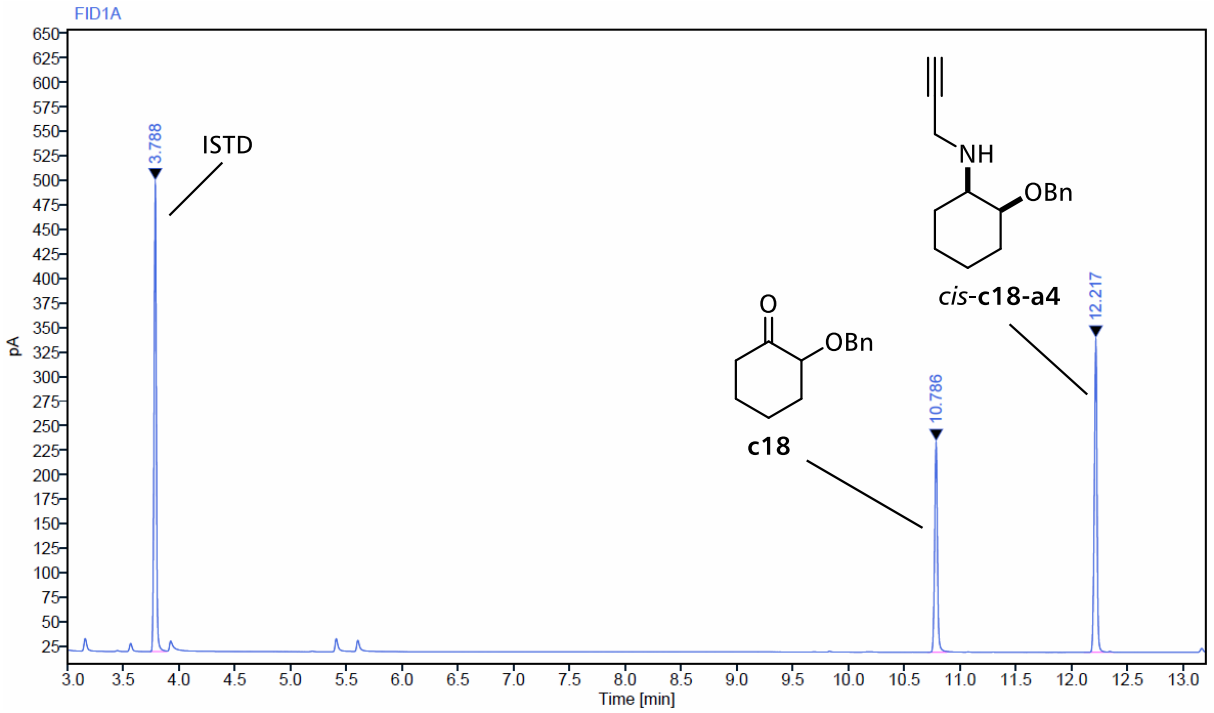


Figure S122. Chromatographic separation of *n*-dodecane (ISTD, t_r 3.8 min), 2-(benzyloxy)cyclohexan-1-one (**c18**, t_r 10.8 min), and *cis*-2-(benzyloxy)-*N*-propargylcyclohexan-1-amine (*cis*-**c18-a4**, t_r 12.2 min) using GC–FID method GC-A4. Calibration standard containing 10 mM of ISTD and 20 mM of each analyte. The other product diastereomer (*trans*-**c18-a4**, t_r 12.4 min) is not visible in the chromatogram because pure *cis*-**c18-a4** was used as the product reference compound.

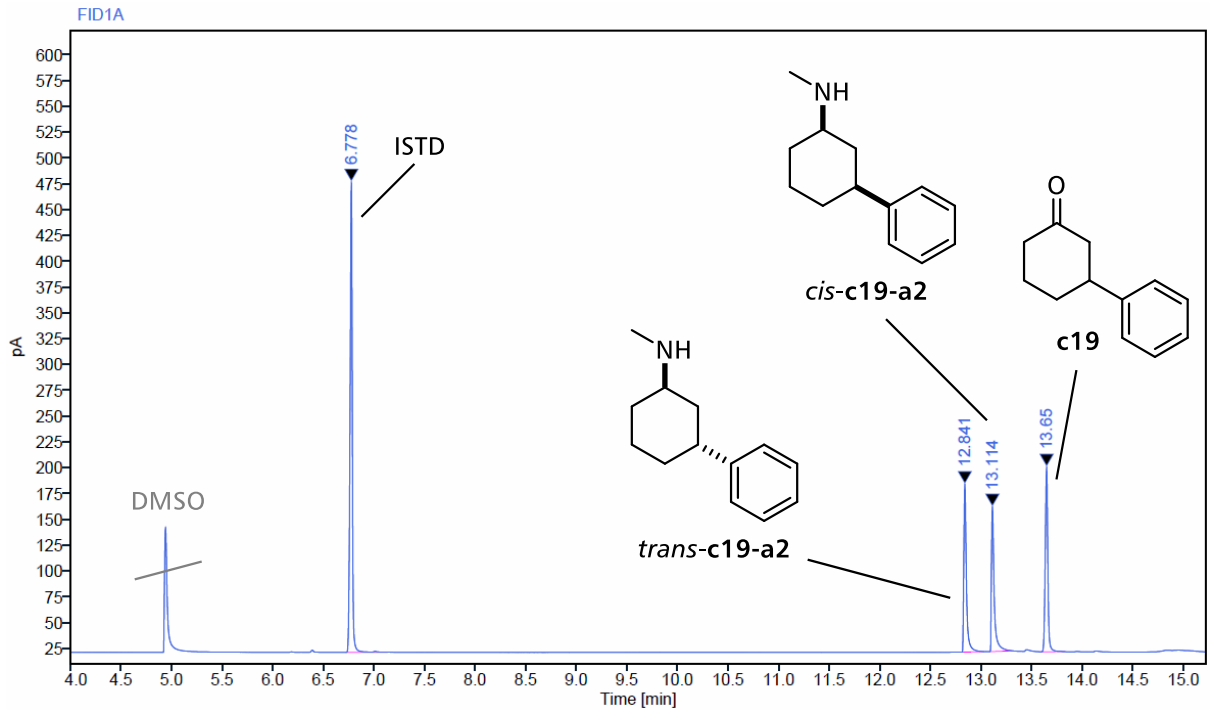


Figure S123. Chromatographic separation of *n*-dodecane (ISTD, t_r 6.8 min), *trans*-*N*-methyl-3-phenylcyclohexan-1-amine (*trans*-**c19-a2**, t_r 12.8 min), *cis*-*N*-methyl-3-phenylcyclohexan-1-amine (*cis*-**c19-a2**, t_r 13.1 min), and 3-phenylcyclohexan-1-one (**c19**, t_r 13.7 min) using GC–FID method GC-A3. Calibration standard containing 10 mM of ISTD and 20 mM of each analyte.

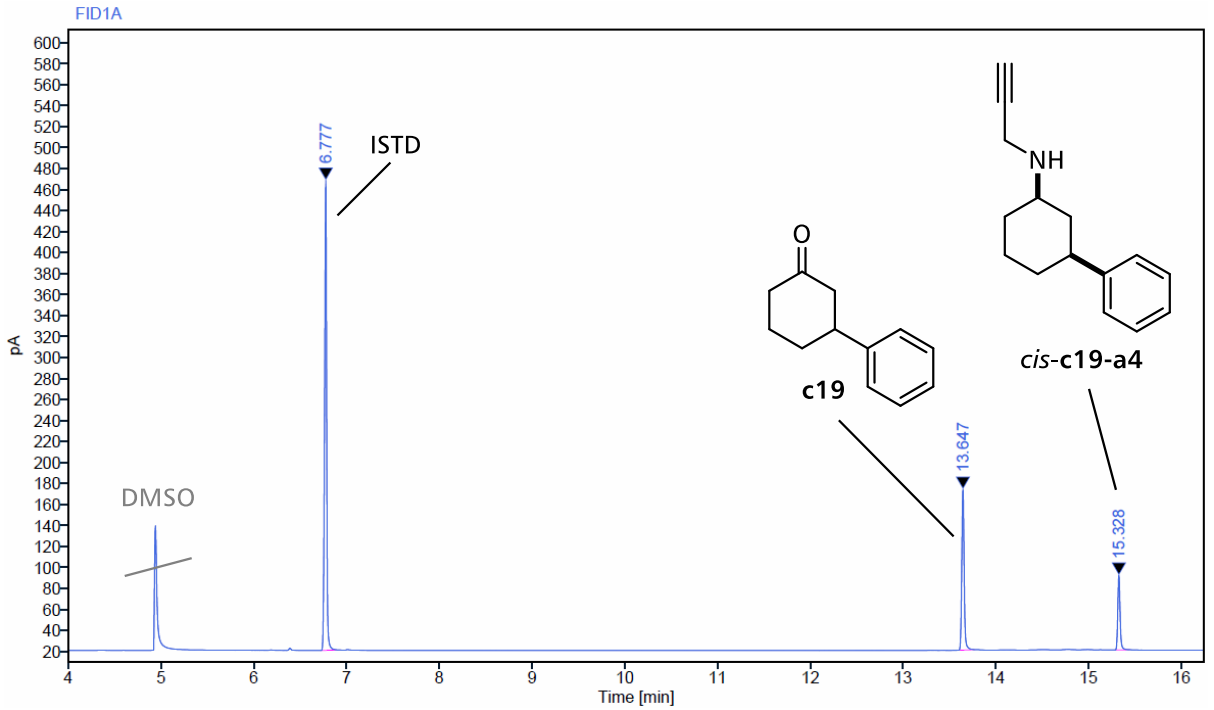


Figure S124. Chromatographic separation of *n*-dodecane (ISTD, t_r 6.8 min), 3-phenylcyclohexan-1-one (**c19**, t_r 13.6 min), and *cis*-3-phenyl-*N*-propargylcyclohexan-1-amine (*cis*-**c19-a4**, t_r 15.3 min) using GC–FID method GC-A3. Calibration standard containing 10 mM of ISTD, 20 mM of ketone, and 10 mM of amine product. The other product diastereomer (*trans*-**c19-a4**, t_r 15.1 min) is not visible in the chromatogram because pure *cis*-**c19-a4** was used as the product reference compound.

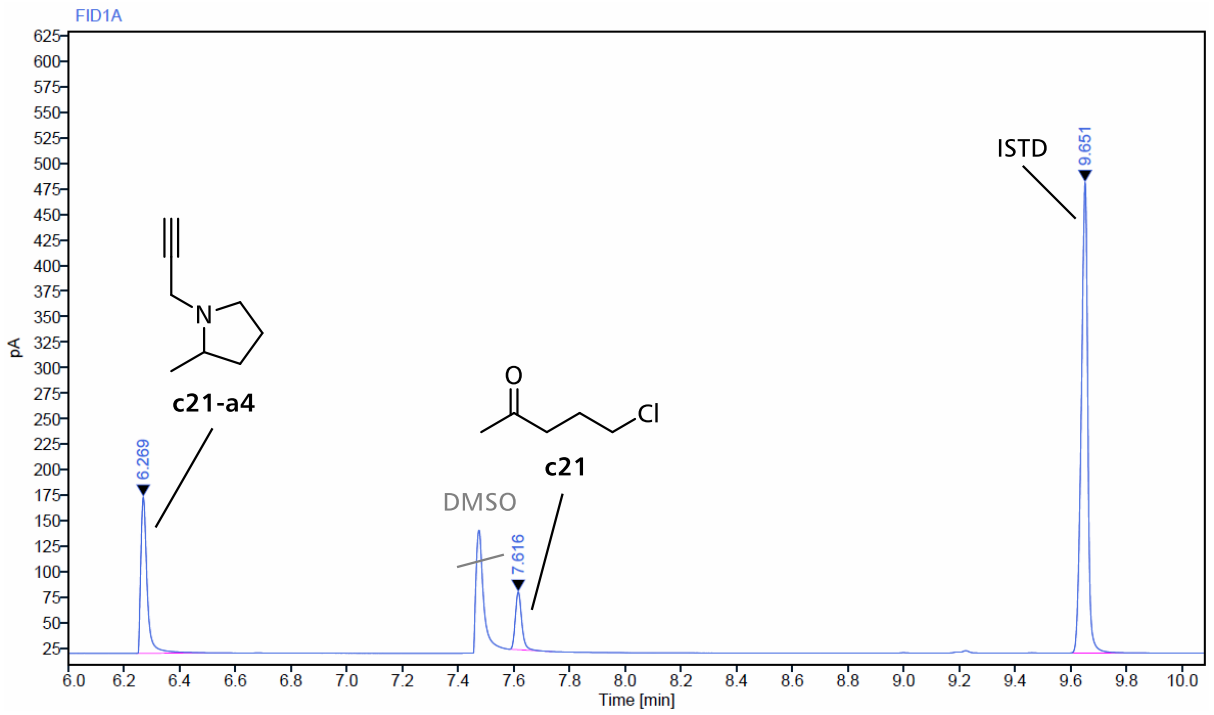


Figure S125. Chromatographic separation of 2-methyl-1-(prop-2-yn-1-yl)pyrrolidine (**c21-a4**, t_r 6.3 min), 5-chloropentan-2-one (**c21**, t_r 7.6 min), and *n*-dodecane (ISTD, t_r 9.7 min) using GC–FID method GC-A2. Calibration standard containing 10 mM of ISTD and 20 mM of each analyte.

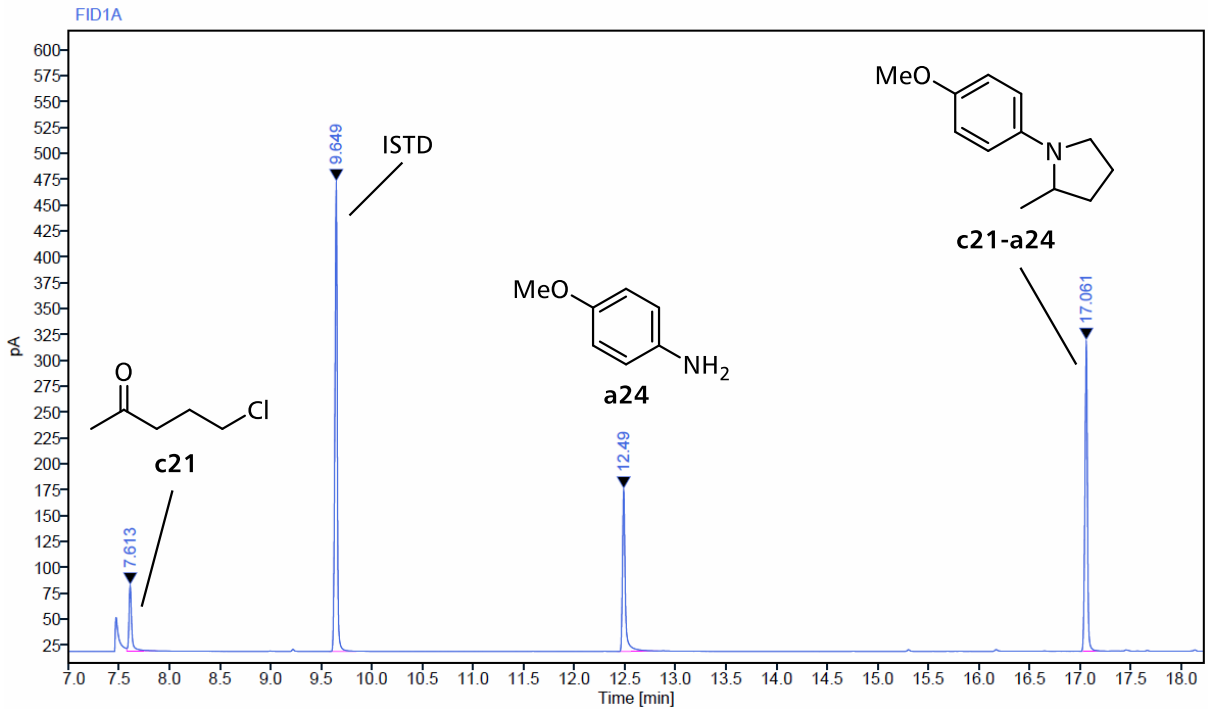


Figure S126. Chromatographic separation of 5-chloropentan-2-one (**c21**, t_r 7.6 min), *n*-dodecane (ISTD, t_r 9.6 min), *para*-anisidine (**a24**, t_r 12.5 min), and 1-(4-methoxyphenyl)-2-methylpyrrolidine (**c21-a24**, t_r 17.1 min) using GC–FID method GC-A2. Calibration standard containing 10 mM of ISTD and 20 mM of each analyte.

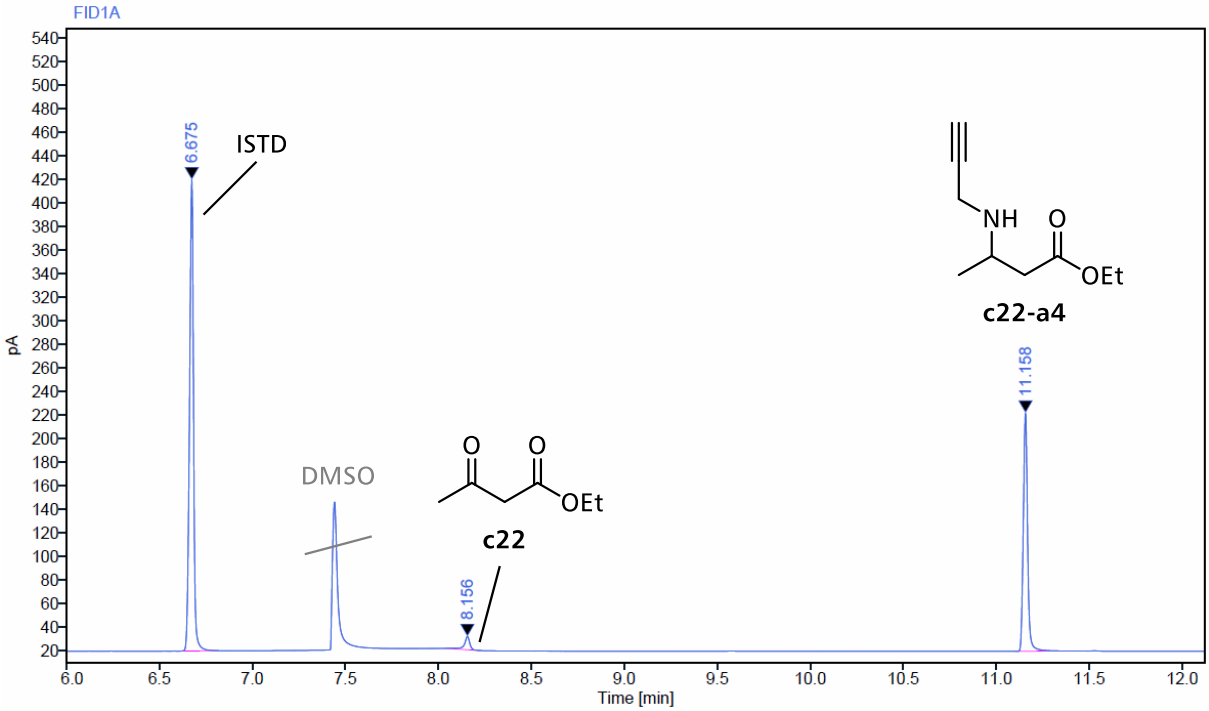


Figure S127. Chromatographic separation of *n*-decane (ISTD, t_r 6.7 min), ethyl acetoacetate (**c22**, t_r 8.2 min), and ethyl 3-(propargylamino)butanoate (**c22-a4**, t_r 11.2 min) using GC–FID method GC-A2. Calibration standard containing 10 mM of ISTD and 20 mM of each analyte.

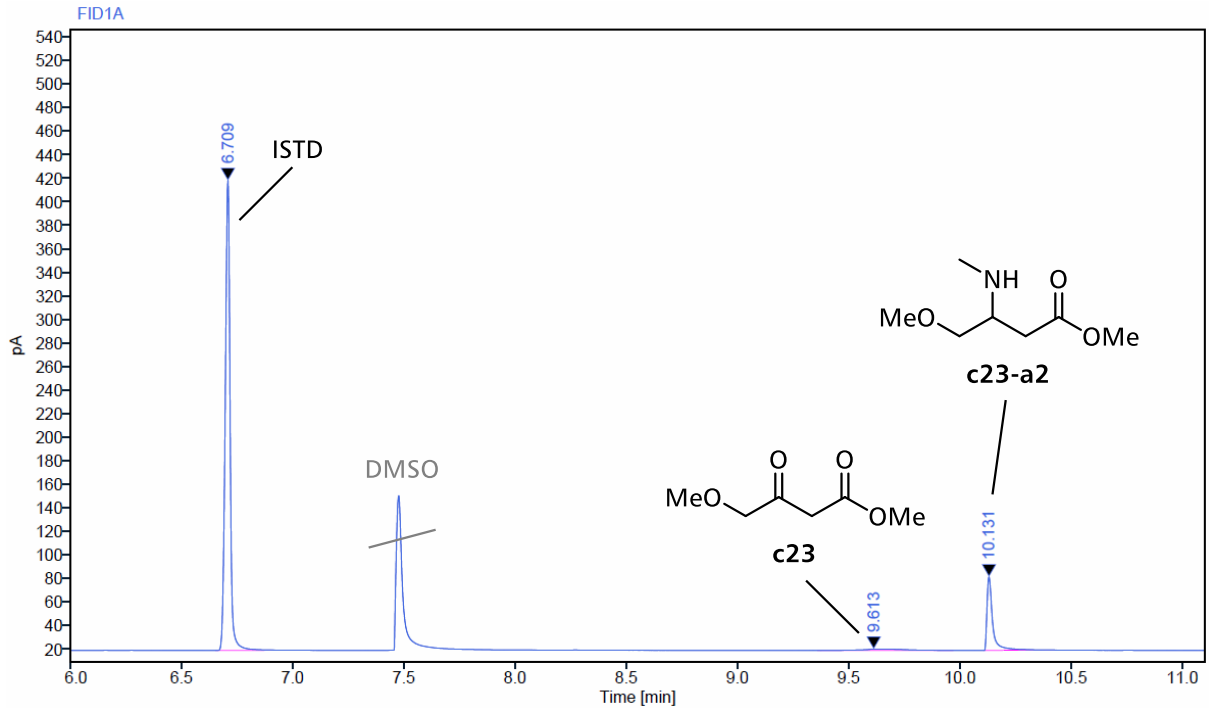


Figure S128. Chromatographic separation of *n*-decane (ISTD, t_r 6.7 min), methyl 4-methoxy-3-oxo-butanoate (**c23**, t_r 9.6 min), and methyl 4-methoxy-3-(methylamino)butanoate (**c23-a2**, t_r 10.1 min) using GC–FID method GC-A2. Calibration standard containing 10 mM of ISTD and 20 mM of each analyte.

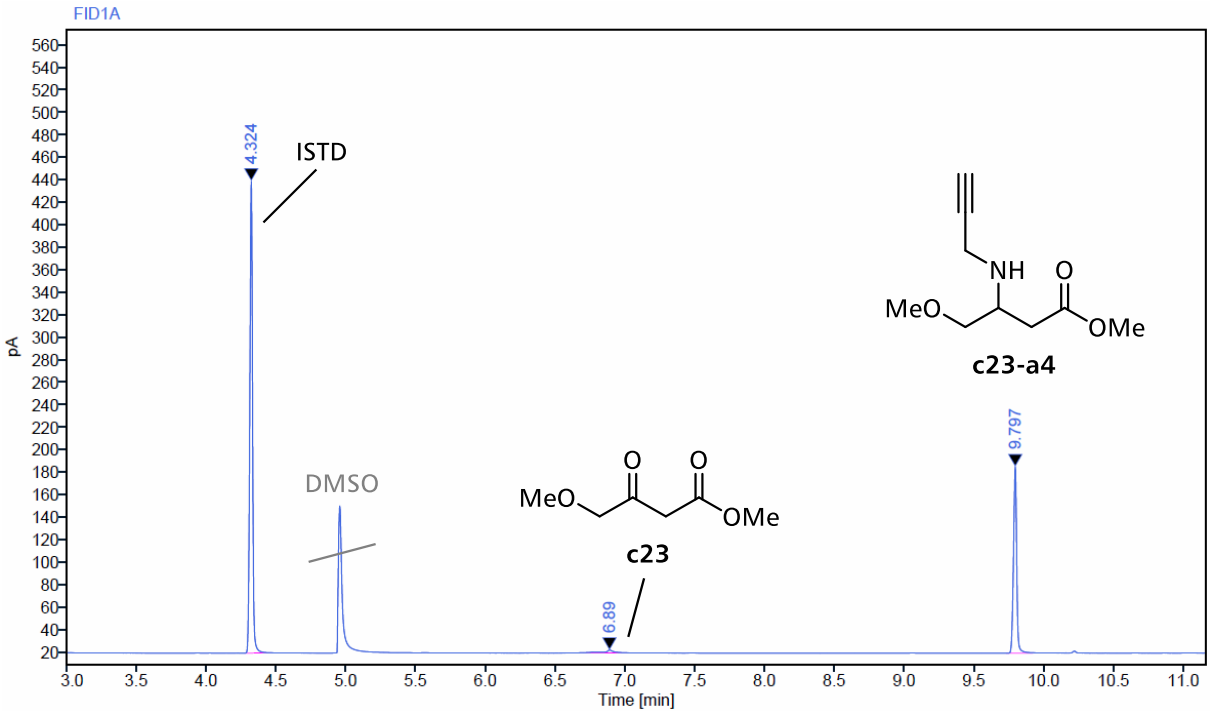


Figure S129. Chromatographic separation of *n*-decane (ISTD, t_r 4.3 min), methyl 4-methoxy-3-oxo-butanoate (**c23**, t_r 6.9 min), and methyl 4-methoxy-3-(propargylamino)butanoate (**c23-a4**, t_r 9.8 min) using GC–FID method GC-A3. Calibration standard containing 10 mM of ISTD and 20 mM of each analyte.

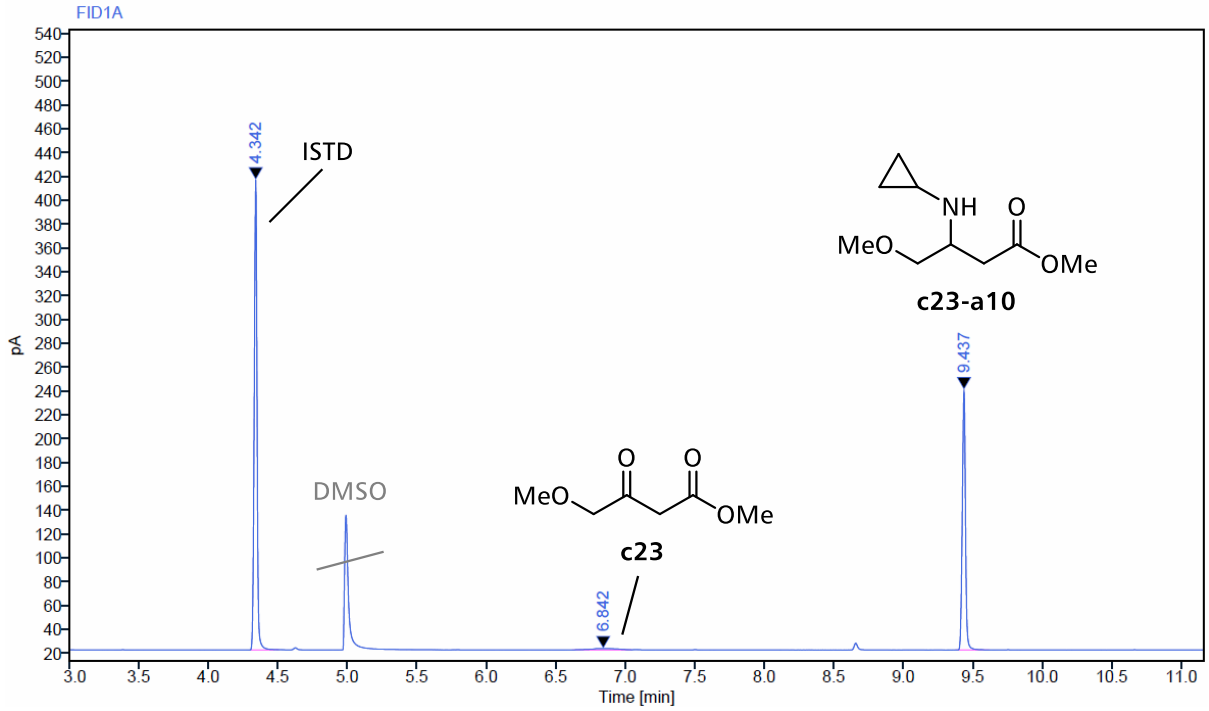


Figure S130. Chromatographic separation of *n*-decane (ISTD, t_r 4.3 min), methyl 4-methoxy-3-oxobutanoate (**c23**, t_r 6.8 min), and methyl 3-(cyclopropylamino)-4-methoxybutanoate (**c23-a10**, t_r 9.4 min) using GC–FID method GC-A3. Calibration standard containing 10 mM of ISTD and 20 mM of each analyte.

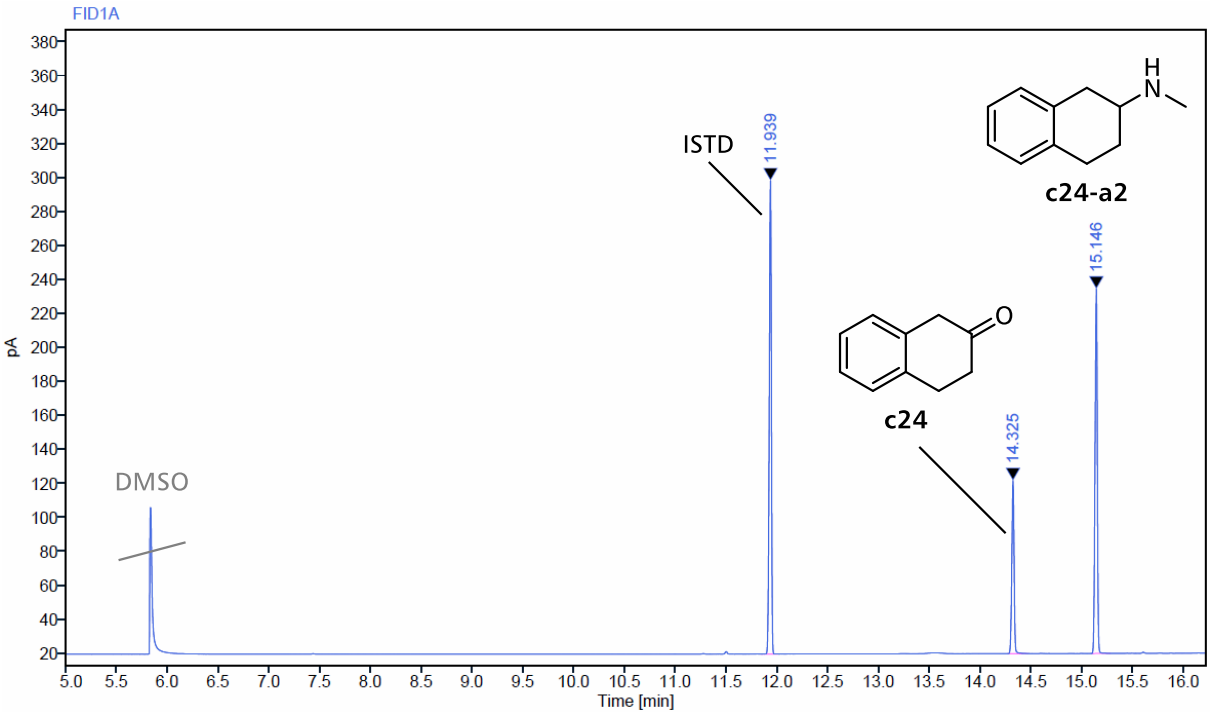


Figure S131. Chromatographic separation of *n*-dodecane (ISTD, t_r 11.9 min), 2-tetralone (**c24**, t_r 14.3 min), and *N*-methyl-1,2,3,4-tetrahydronaphthalen-2-amine (**c24-a2**, t_r 15.1 min) using GC–FID method GC-A1. Calibration standard containing 10 mM of ISTD and 20 mM of each analyte.

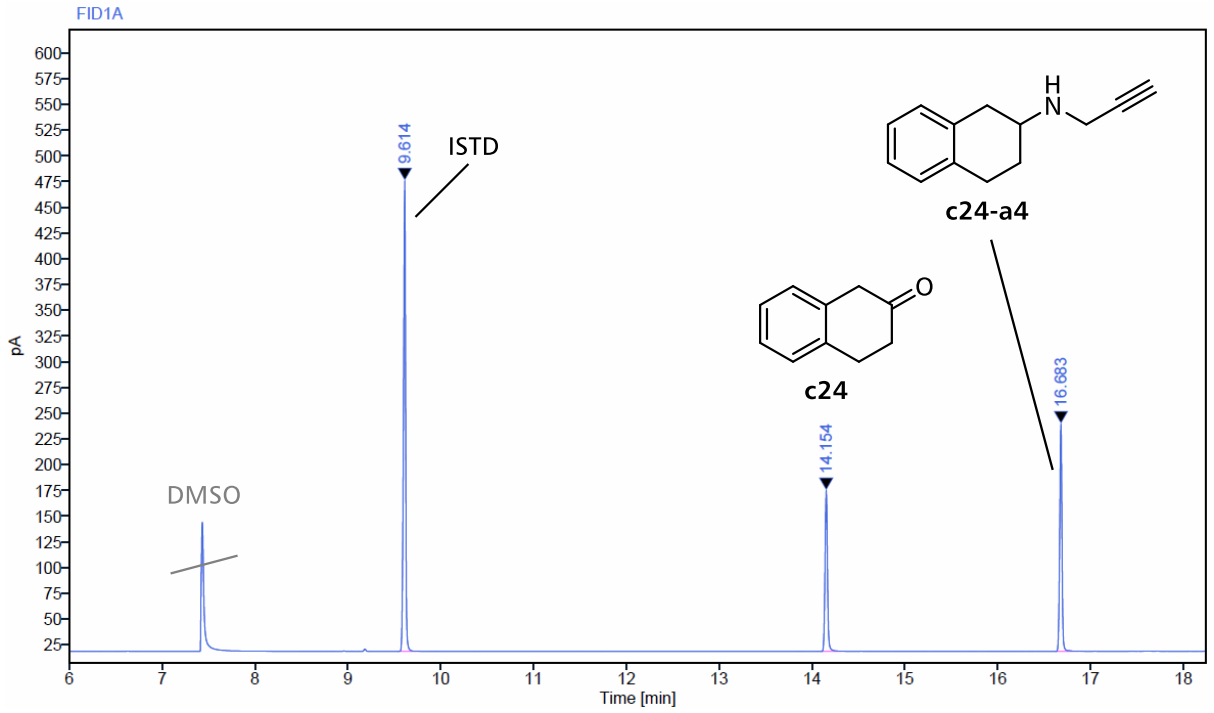


Figure S132. Chromatographic separation of *n*-dodecane (ISTD, t_r 9.6 min), 2-tetralone (**c24**, t_r 14.2 min), and *N*-propargyl-1,2,3,4-tetrahydronaphthalen-2-amine (**c24-a4**, t_r 16.7 min) using GC–FID method GC-A2. Calibration standard containing 10 mM of ISTD and 20 mM of each analyte.

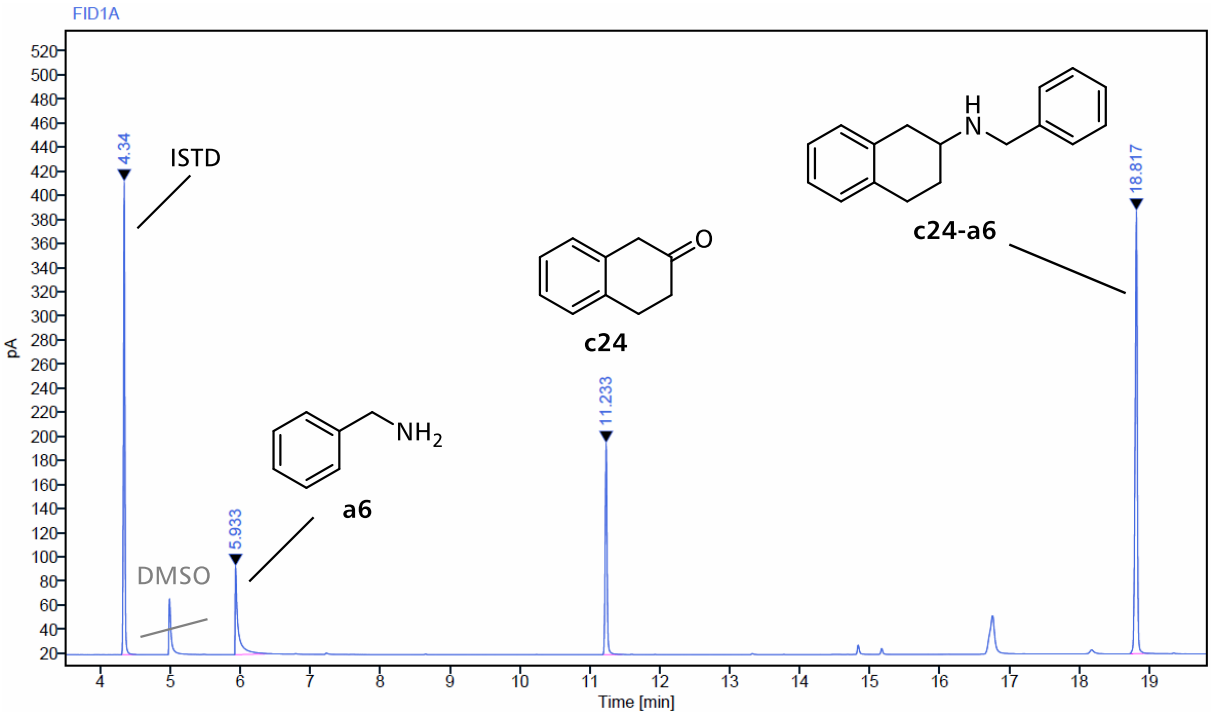


Figure S133. Chromatographic separation of *n*-decane (ISTD, t_r 4.3 min), benzylamine (**a6**, t_r 5.9 min), 2-tetralone (**c24**, t_r 11.2 min), and *N*-benzyl-1,2,3,4-tetrahydronaphthalen-2-amine (**c24-a6**, t_r 18.8 min) using GC–FID method GC-A3. Calibration standard containing 10 mM of ISTD and 20 mM of each analyte.

Gas chromatography (chiral stationary phase):
Chiral-phase GC analyses were carried out on an *Agilent* 7890A GC system equipped with a flame-ionisation detector (FID) and a *Macherey–Nagel* Hydrodex β-6TBDAc capillary column (50 m × 0.25 mm × 0.12 μm; stationary phase: 2,3-di-*O*-acetyl-6-*O*-*tert*-butyldimethylsilyl-β-cyclodextrin in polysiloxane) or a *Restek* Rt-βDEXse capillary column (30 m × 0.32 mm × 0.25 μm; stationary phase: 2,3-di-*O*-ethyl-6-*O*-*tert*-butyldimethylsilyl-β-cyclodextrin added into 14% cyanopropylphenyl / 86% dimethyl polysiloxane), using hydrogen as carrier gas.

Method GC-C1 (compounds **c6-a4-Ac**, **c7-a4-Ac**, **c15-a4-Ac**)

Column:	Hydrodex β-6TBDAc (50 m × 0.25 mm × 0.12 μm)
Carrier gas:	Hydrogen
Flow rate:	1.5 mL/min
Inlet temperature:	230 °C
Detector temperature:	250 °C
Split ratio:	50:1
Oven temperature program:	60 °C, 1 min; 5 °C/min to 220 °C; 220 °C, 2 min
Total run time:	35 min

Method GC-C2 (compound **c7-a2-Ac**)

Column:	Hydrodex β-6TBDAc (50 m × 0.25 mm × 0.12 μm)
Carrier gas:	Hydrogen
Flow rate:	1.0 mL/min
Inlet temperature:	230 °C
Detector temperature:	250 °C
Split ratio:	50:1
Oven temperature program:	80 °C, 1 min; 20 °C/min to 120 °C; 120 °C, 23 min; 20 °C/min to 180 °C, 180 °C, 1 min
Total run time:	30 min

Method GC-C3 (compound **c8-a2-Ac**)

Column:	Hydrodex β-6TBDAc (50 m × 0.25 mm × 0.12 μm)
Carrier gas:	Hydrogen
Flow rate:	1.5 mL/min
Inlet temperature:	230 °C
Detector temperature:	250 °C
Split ratio:	50:1
Oven temperature program:	120 °C, 1 min; 2 °C/min to 180 °C; 180 °C, 2 min; 10 °C/min to 220 °C; 220 °C, 1 min
Total run time:	38 min

Method GC-C4 (compounds **c16-a2-Ac**, **c16-a4-Ac**)

Column:	Hydrodex β-6TBDAc (50 m × 0.25 mm × 0.12 μm)
Carrier gas:	Hydrogen
Flow rate:	1.5 mL/min
Inlet temperature:	230 °C
Detector temperature:	250 °C
Split ratio:	50:1
Oven temperature program:	100 °C, 1 min; 20 °C/min to 200 °C; 200 °C, 23 min; 20 °C/min to 220 °C; 220 °C, 2 min
Total run time:	32 min

Method GC-C5 (compound **c6-a7**)

Column:	Hydrodex β-6TBDAc (50 m × 0.25 mm × 0.12 μm)
Carrier gas:	Hydrogen
Flow rate:	1.5 mL/min
Inlet temperature:	230 °C
Detector temperature:	250 °C
Split ratio:	50:1
Oven temperature program:	100 °C, 1 min; 2 °C/min to 160 °C; 160 °C, 2 min; 10 °C/min to 220 °C; 220 °C, 1 min
Total run time:	40 min

Method GC-C6 (compound **c22-a4-Ac**)

Column:	Hydrodex β-6TBDAc (50 m × 0.25 mm × 0.12 μm)
Carrier gas:	Hydrogen
Flow rate:	1.5 mL/min
Inlet temperature:	230 °C
Detector temperature:	250 °C
Split ratio:	90:1
Oven temperature program:	60 °C, 1 min; 20 °C/min to 160 °C; 160 °C, 30 min; 20 °C/min to 200 °C; 200 °C, 2 min
Total run time:	40 min

Method GC-C7 (compounds **c3-a4**, **c7-a7**, **c10-a10**)

Column:	Rt-βDEXse (30 m × 0.32 mm × 0.25 μm)
Carrier gas:	Hydrogen
Flow rate:	2.0 mL/min
Inlet temperature:	220 °C
Detector temperature:	250 °C
Split ratio:	30:1
Oven temperature program:	80 °C, 1 min; 2 °C/min to 140 °C; 140 °C, 1 min; 10 °C/min to 180 °C; 180 °C, 1 min
Total run time:	37 min

Method GC-C8 (compound **c4-a4**)

Column:	Rt-βDEXse (30 m × 0.32 mm × 0.25 μm)
Carrier gas:	Hydrogen
Flow rate:	1.5 mL/min
Inlet temperature:	220 °C
Detector temperature:	250 °C
Split ratio:	30:1
Oven temperature program:	60 °C, 1 min; 2 °C/min to 100 °C; 100 °C, 1 min; 10 °C/min to 180 °C; 180 °C, 1 min
Total run time:	31 min

Method GC-C9 (compounds **c6-a2-Ac**, **c10-a9**)

Column:	Rt-βDEXse (30 m × 0.32 mm × 0.25 μm)
Carrier gas:	Hydrogen
Flow rate:	2.0 mL/min
Inlet temperature:	220 °C
Detector temperature:	250 °C
Split ratio:	30:1
Oven temperature program:	60 °C, 1 min; 5 °C/min to 180 °C; 180 °C, 2 min
Total run time:	27 min

Method GC-C10 (compound **c15-a22**)

Column:	Rt-βDEXse (30 m × 0.32 mm × 0.25 μm)
Carrier gas:	Hydrogen
Flow rate:	2.0 mL/min
Inlet temperature:	220 °C
Detector temperature:	250 °C
Split ratio:	30:1
Oven temperature program:	60 °C, 1 min; 2 °C/min to 140 °C; 140 °C, 1 min; 10 °C/min to 180 °C; 180 °C, 1 min
Total run time:	47 min

Method GC-C11 (compound **c21-a4**)

Column:	Rt-βDEXse (30 m × 0.32 mm × 0.25 μm)
Carrier gas:	Hydrogen
Flow rate:	2.0 mL/min
Inlet temperature:	220 °C
Detector temperature:	250 °C
Split ratio:	30:1
Oven temperature program:	40 °C, 1 min; 20 °C/min to 65 °C; 65 °C, 20 min; 20 °C/min to 200 °C; 200 °C, 1 min
Total run time:	30 min

Method GC-C12 (compound **c8-a4**)

Column:	Rt-βDEXse (30 m × 0.32 mm × 0.25 μm)
Carrier gas:	Hydrogen
Flow rate:	2.0 mL/min
Inlet temperature:	220 °C
Detector temperature:	250 °C
Split ratio:	30:1
Oven temperature program:	60 °C, 1 min; 20 °C/min to 105 °C; 105 °C, 31 min; 20 °C/min to 200 °C; 200 °C, 1 min
Total run time:	40 min

Method GC-C13 (compounds **c3-a2-Ac**, **c19-a2**)

Column:	Rt-βDEXse (30 m × 0.32 mm × 0.25 μm)
Carrier gas:	Hydrogen
Flow rate:	2.0 mL/min
Inlet temperature:	220 °C
Detector temperature:	250 °C
Split ratio:	30:1
Oven temperature program:	100 °C, 1 min; 2 °C/min to 160 °C; 20 °C/min to 200 °C; 200 °C, 2 min
Total run time:	35 min

Method GC-C14 (compound **c24-a2**)

Column:	Rt-βDEXse (30 m × 0.32 mm × 0.25 μm)
Carrier gas:	Hydrogen
Flow rate:	2.0 mL/min
Inlet temperature:	220 °C
Detector temperature:	250 °C
Split ratio:	30:1
Oven temperature program:	60 °C, 1 min; 2 °C/min to 110 °C; 1 °C/min to 140 °C; 10 °C/min to 180 °C
Total run time:	60 min

Exemplary chromatograms are shown on the following pages.

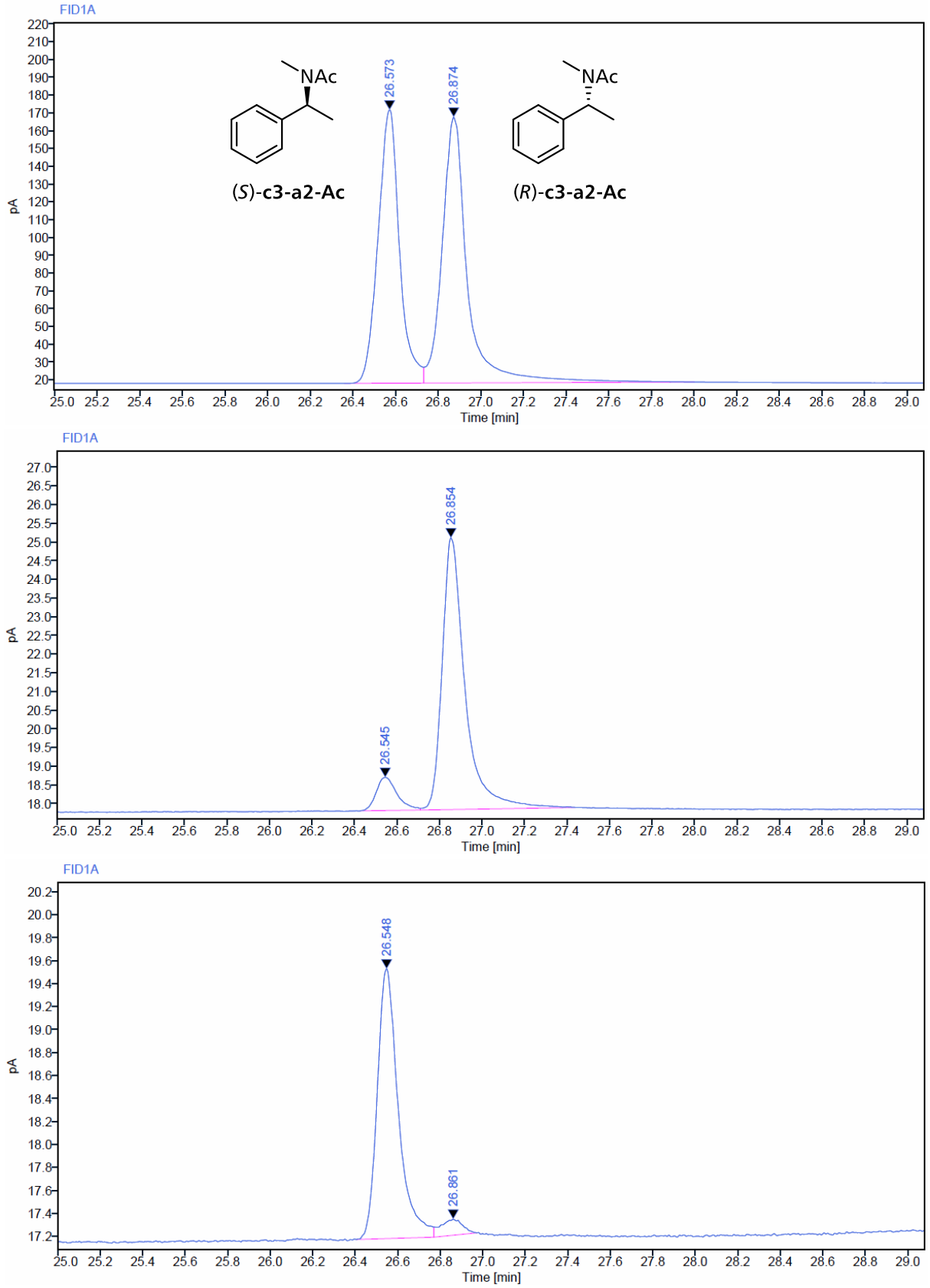


Figure S134. Chromatographic separation of the enantiomers of *N*-acetylated amine **c3-a2-Ac** using GC method GC-C13. Elution order: (*S*)-**c3-a2-Ac** (t_r 26.6 min), (*R*)-**c3-a2-Ac** (t_r 26.9 min). Racemic reference (top), (*R*)-selective biotransformation using IR0041 (middle), (*S*)-selective biotransformation using IR2253 (bottom).

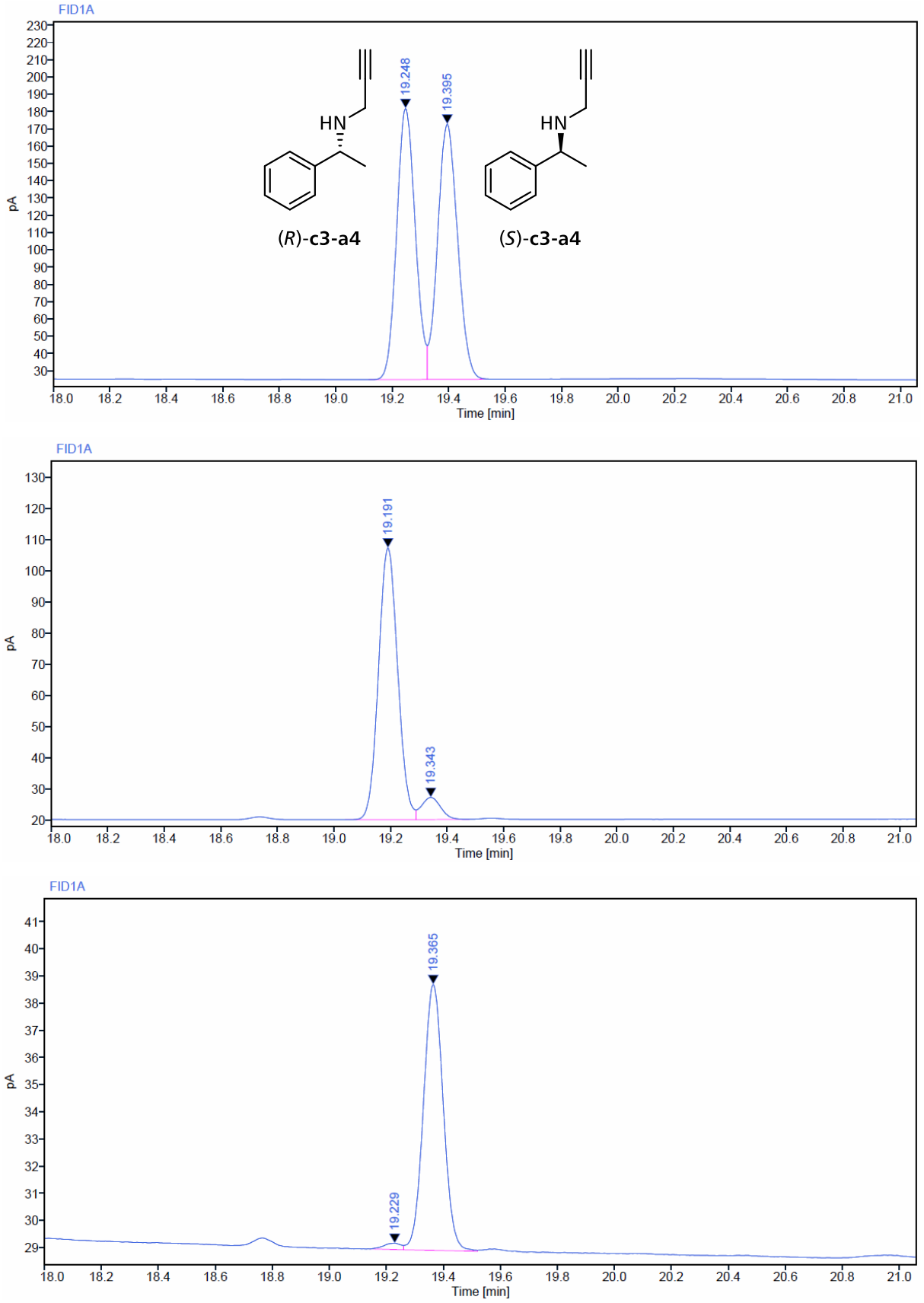


Figure S135. Chromatographic separation of the enantiomers of amine **c3-a4** using GC method GC-C7. Elution order: (*R*)-**c3-a4** (t_r 19.2 min), (*S*)-**c3-a4** (t_r 19.4 min). Racemic reference (top), (*R*)-selective biotransformation using IR0041 (middle), (*S*)-selective biotransformation using IR0059 (bottom).

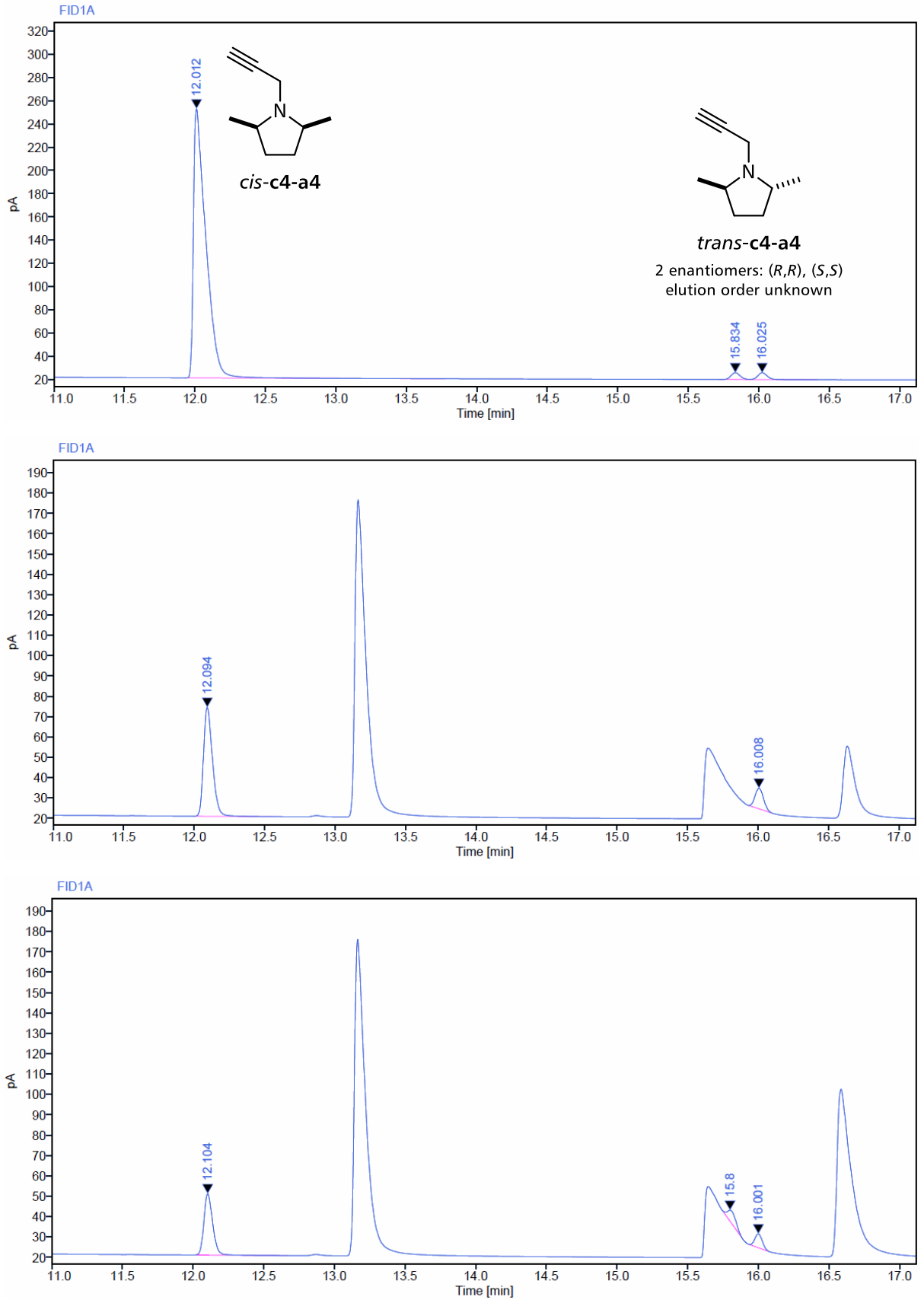


Figure S136. Chromatographic separation of the stereoisomers of amine **c4-a4** using GC method GC-C8. Elution order: *cis*-**c4-a4** (t_r 12.0 min), *trans*-**c4-a4** (t_r 15.8 min, 16.0 min). Racemic reference (top), enantio- and diastereoselective biotransformation using IR0035 (middle), poorly enantio- and diastereoselective biotransformation using IR0015 (bottom).

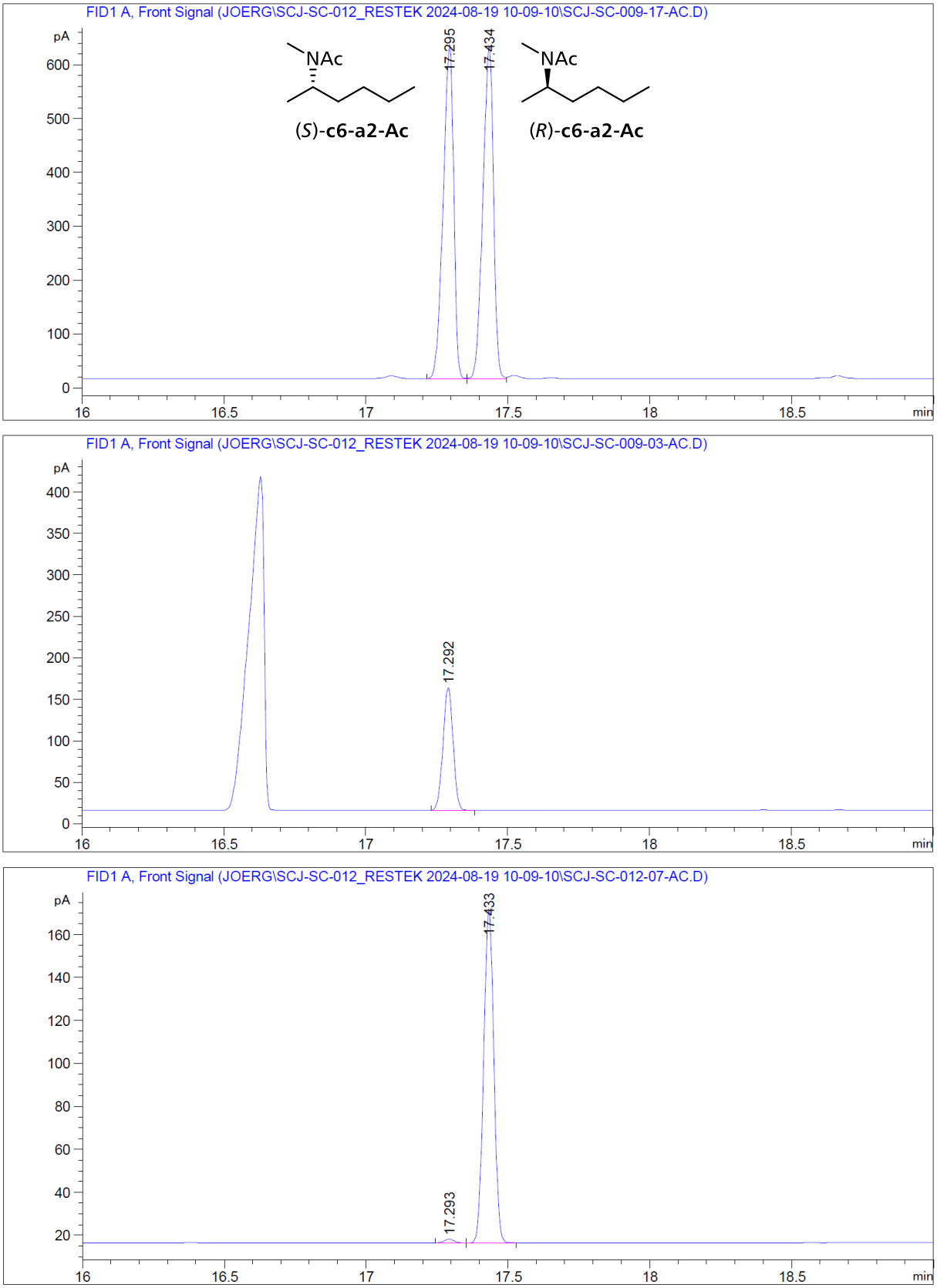


Figure S137. Chromatographic separation of the enantiomers of *N*-acetylated amine **c6-a2-Ac** using GC method GC-C9. Elution order: (*S*)-**c6-a2-Ac** (t_r 17.3 min), (*R*)-**c6-a2-Ac** (t_r 17.4 min). Racemic reference (top), independently synthesised (*S*)-enantiomer (middle), (*R*)-selective biotransformation using IR1674 (bottom).

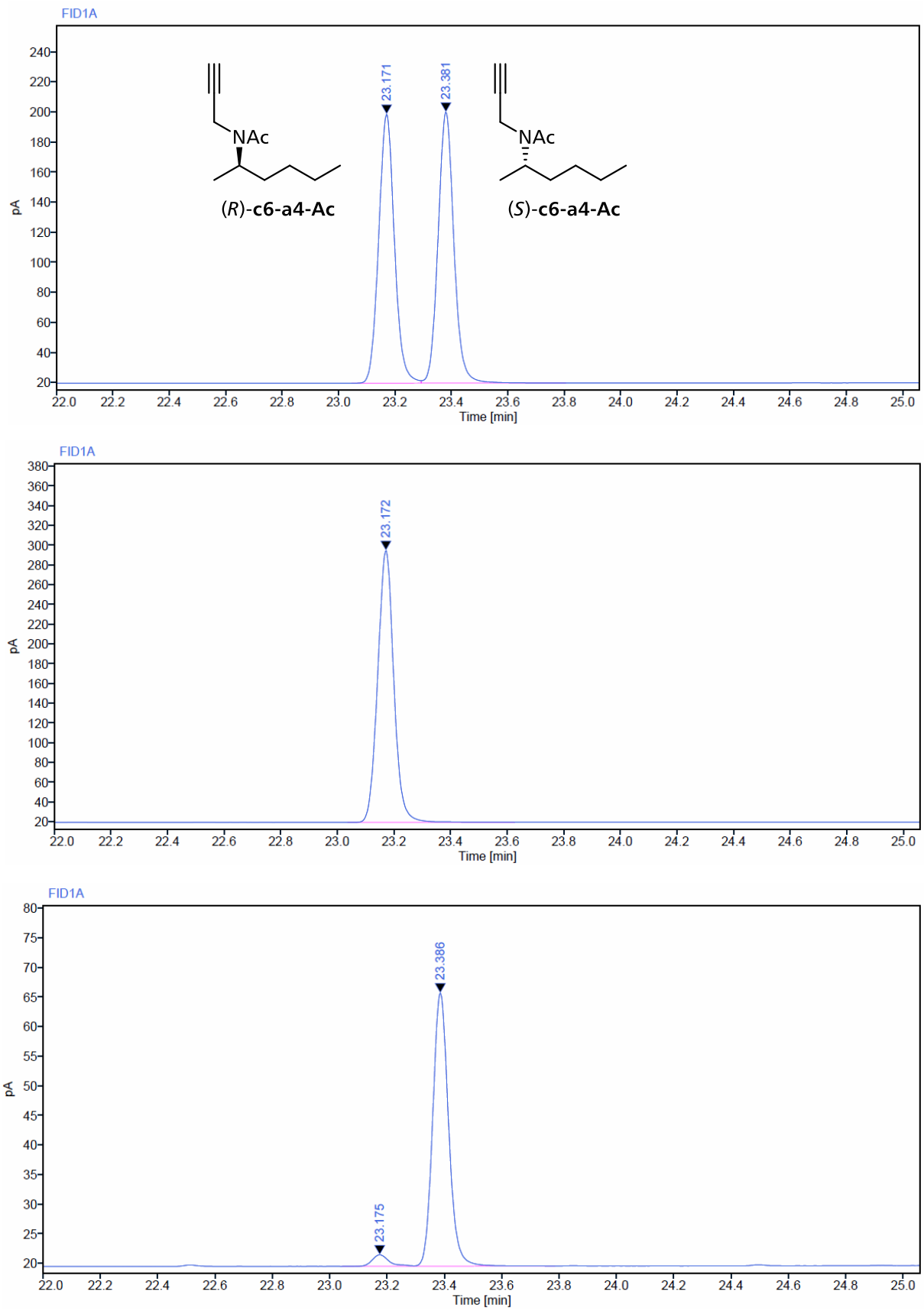


Figure S138. Chromatographic separation of the enantiomers of *N*-acetylated amine **c6-a4-Ac** using GC method GC-C1. Elution order: (*R*)-**c6-a4-Ac** (t_r 23.2 min), (*S*)-**c6-a4-Ac** (t_r 23.4 min). Racemic reference (top), (*R*)-selective biotransformation using IR0068 (middle), (*S*)-selective biotransformation using IR0015 (bottom).

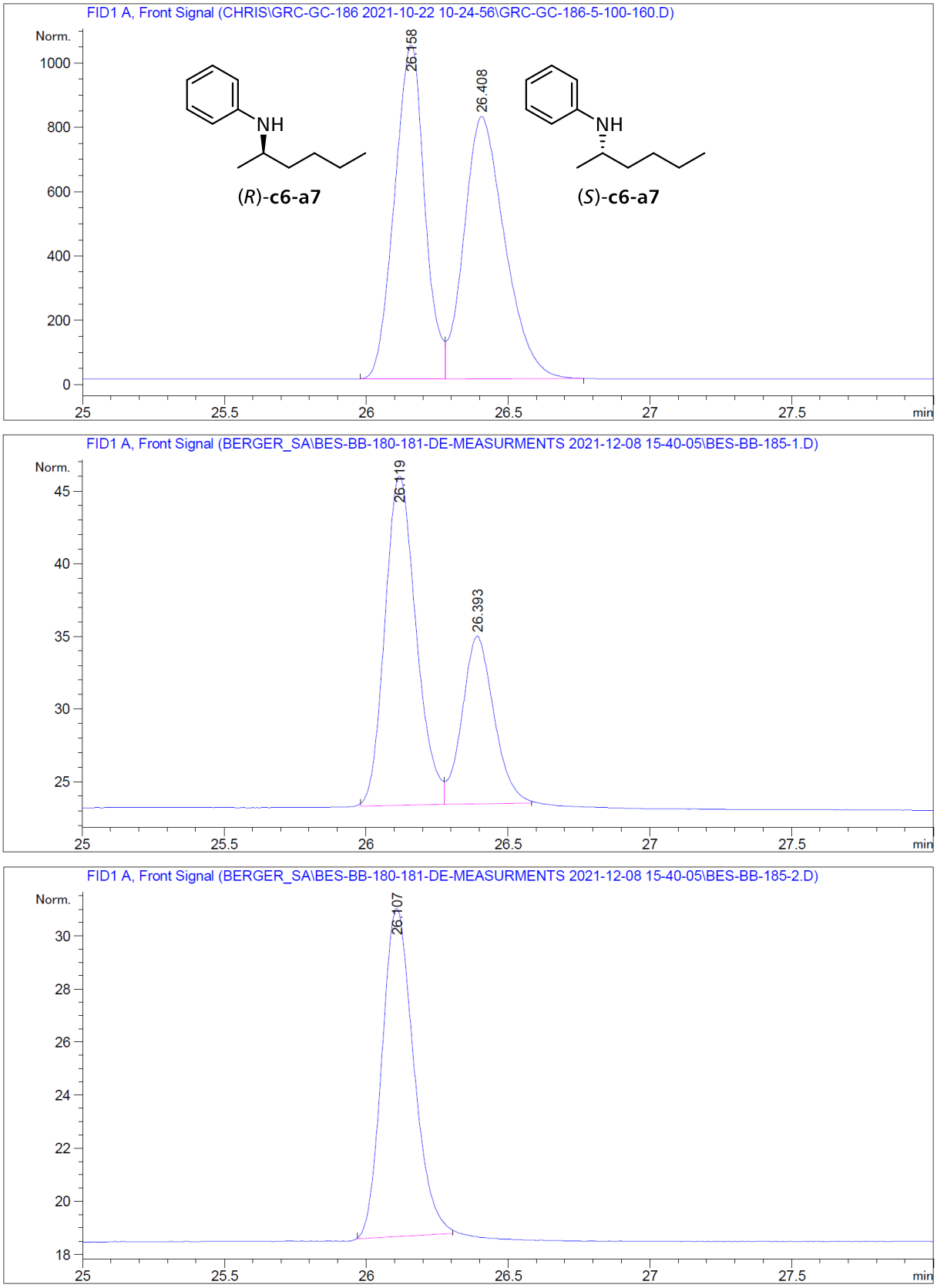


Figure S139. Chromatographic separation of the enantiomers of amine **c6-a7** using GC method GC-C5. Elution order: (*R*)-**c6-a7** (t_r 26.2 min), (*S*)-**c6-a7** (t_r 26.4 min). Racemic reference (top), moderately (*R*)-selective biotransformation using IR0032 (middle), highly (*R*)-selective biotrans-formation using IR0041 (bottom).

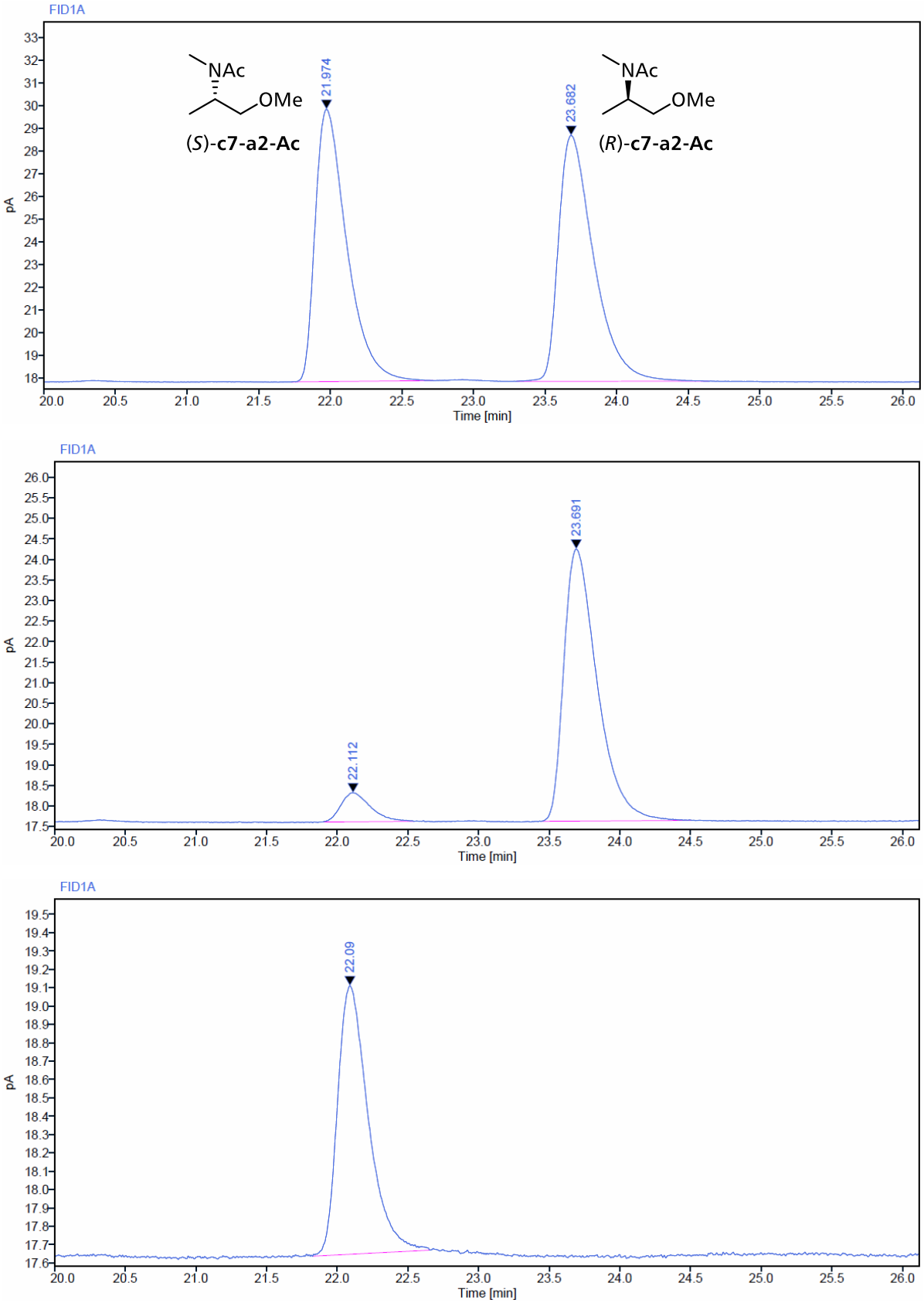


Figure S140. Chromatographic separation of the enantiomers of *N*-acetylated amine **c7-a2-Ac** using GC method GC-C2. Elution order: (*S*)-**c7-a2-Ac** (t_r 22.0 min), (*R*)-**c7-a2-Ac** (t_r 23.7 min). Racemic reference (top), (*R*)-selective biotransformation using IR0020 (middle), (*S*)-selective biotransformation using IR0032 (bottom).

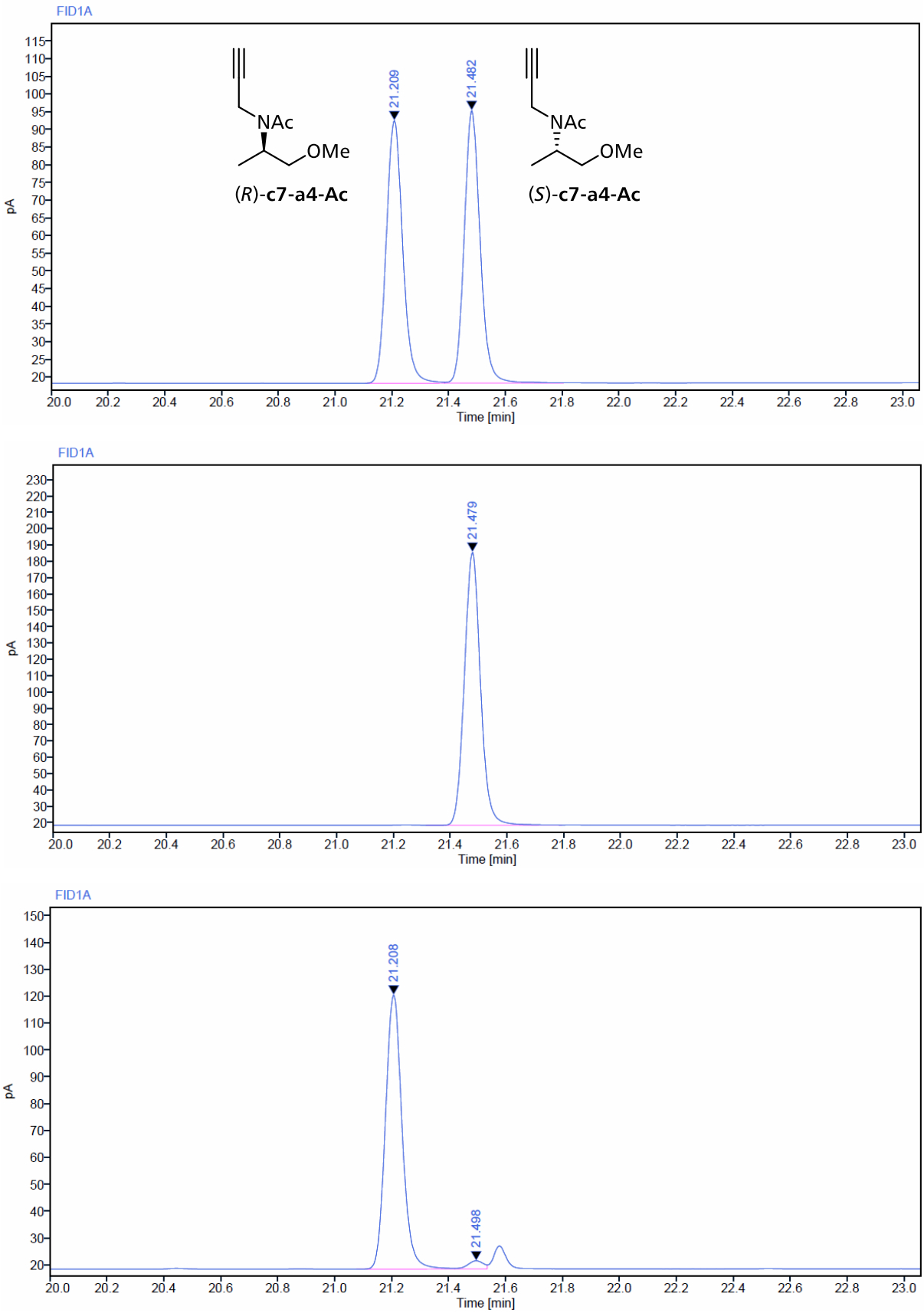


Figure S141. Chromatographic separation of the enantiomers of *N*-acetylated amine **c7-a4-Ac** using GC method GC-C1. Elution order: (*R*)-**c7-a4-Ac** (t_r 21.2 min), (*S*)-**c7-a4-Ac** (t_r 21.5 min). Racemic reference (top), independently synthesised (*S*)-enantiomer (middle), (*R*)-selective biotransformation using IR2010 (bottom).

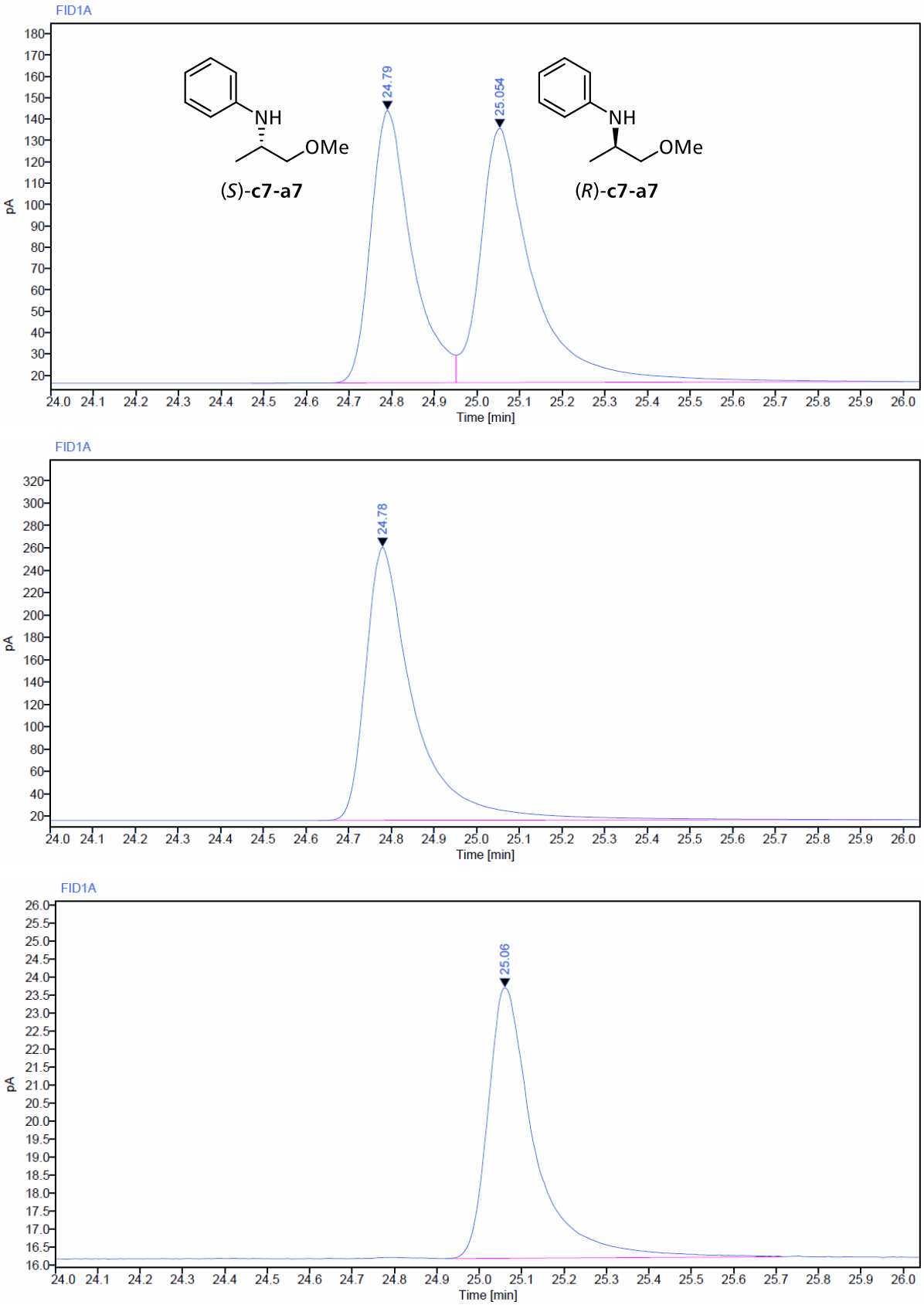


Figure S142. Chromatographic separation of the enantiomers of amine **c7-a7** using GC method GC-C7. Elution order: (*S*)-**c7-a7** (t_r 24.8 min), (*R*)-**c7-a7** (t_r 25.1 min). Racemic reference (top), independently synthesised (*S*)-enantiomer (middle), (*R*)-selective biotransformation using IR0041 (bottom).

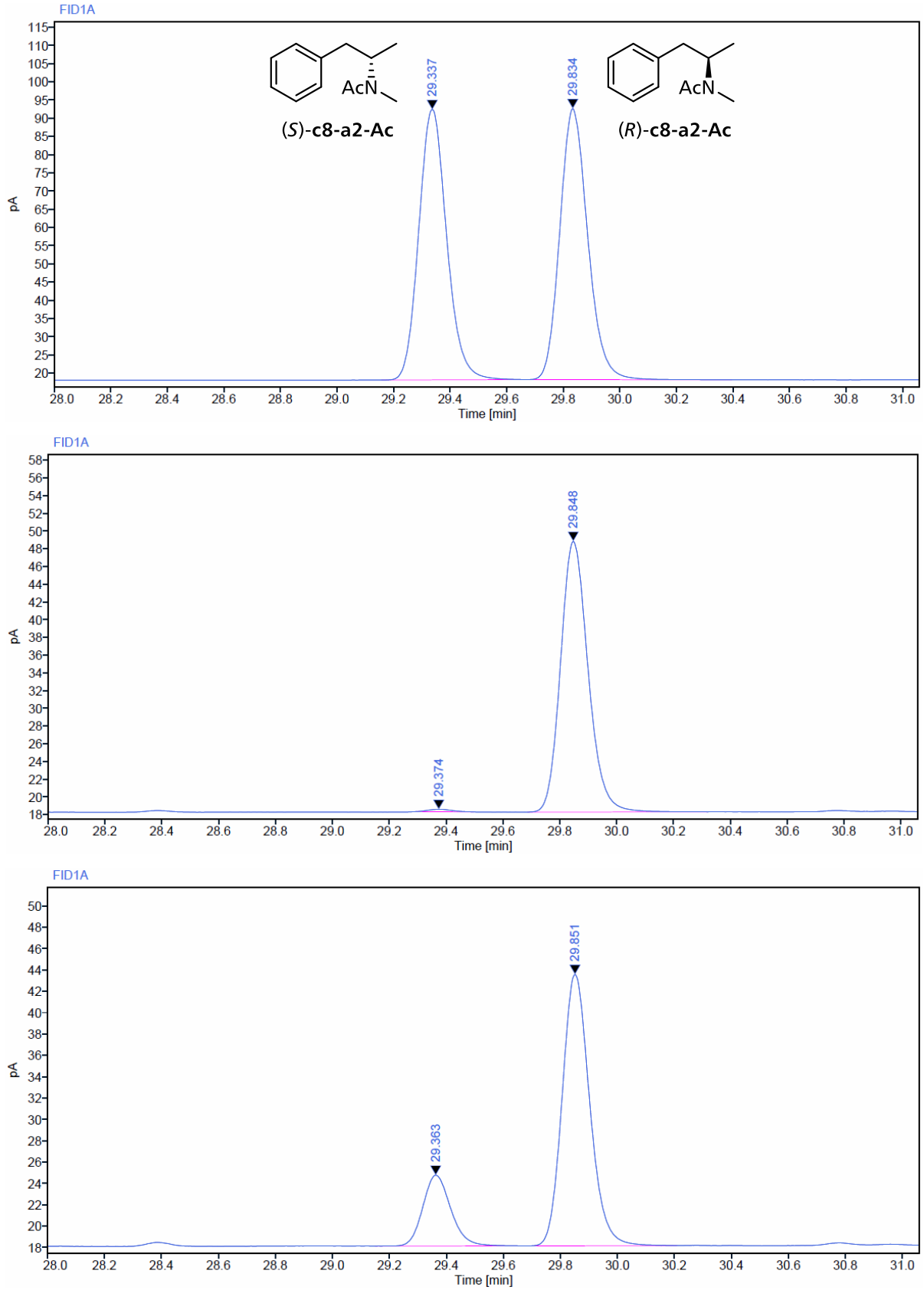


Figure S143. Chromatographic separation of the enantiomers of *N*-acetylated amine **c8-a2-Ac** using GC method GC-C3. Elution order: (*S*)-**c8-a2-Ac** (t_r 29.3 min), (*R*)-**c8-a2-Ac** (t_r 29.8 min). Racemic reference (top), highly (*R*)-selective biotransformation using IR0035 (middle), moderately (*R*)-selective biotransformation using IR1134 (bottom).

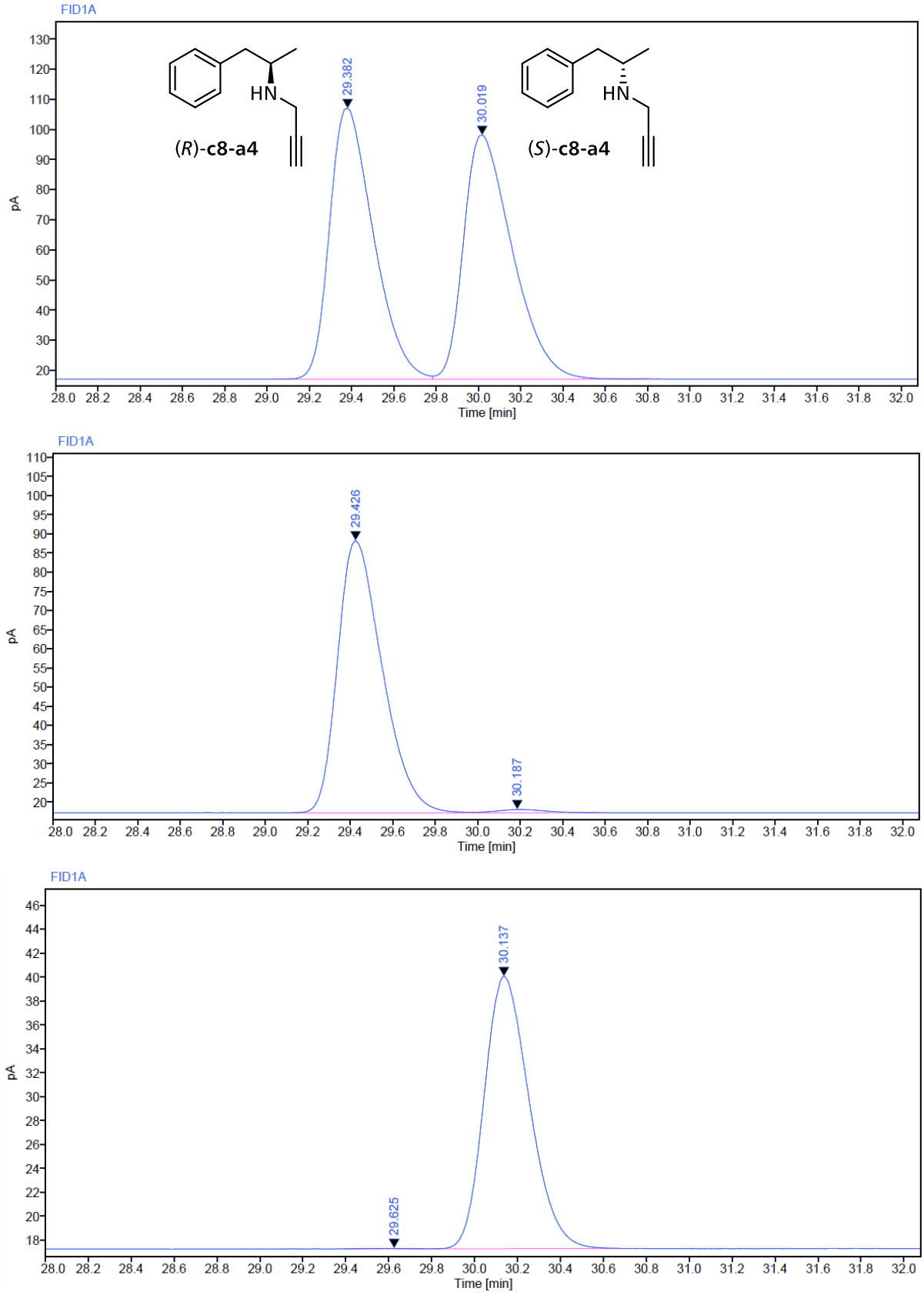


Figure S144. Chromatographic separation of the enantiomers of amine **c8-a4** using GC method GC-C12. Elution order: (*R*)-**c8-a4** (t_r 29.4 min), (*S*)-**c8-a4** (t_r 30.0 min). Racemic reference (top), (*R*)-selective biotransformation using IR0035 (middle), (*S*)-selective biotransformation using IR1855 (bottom).

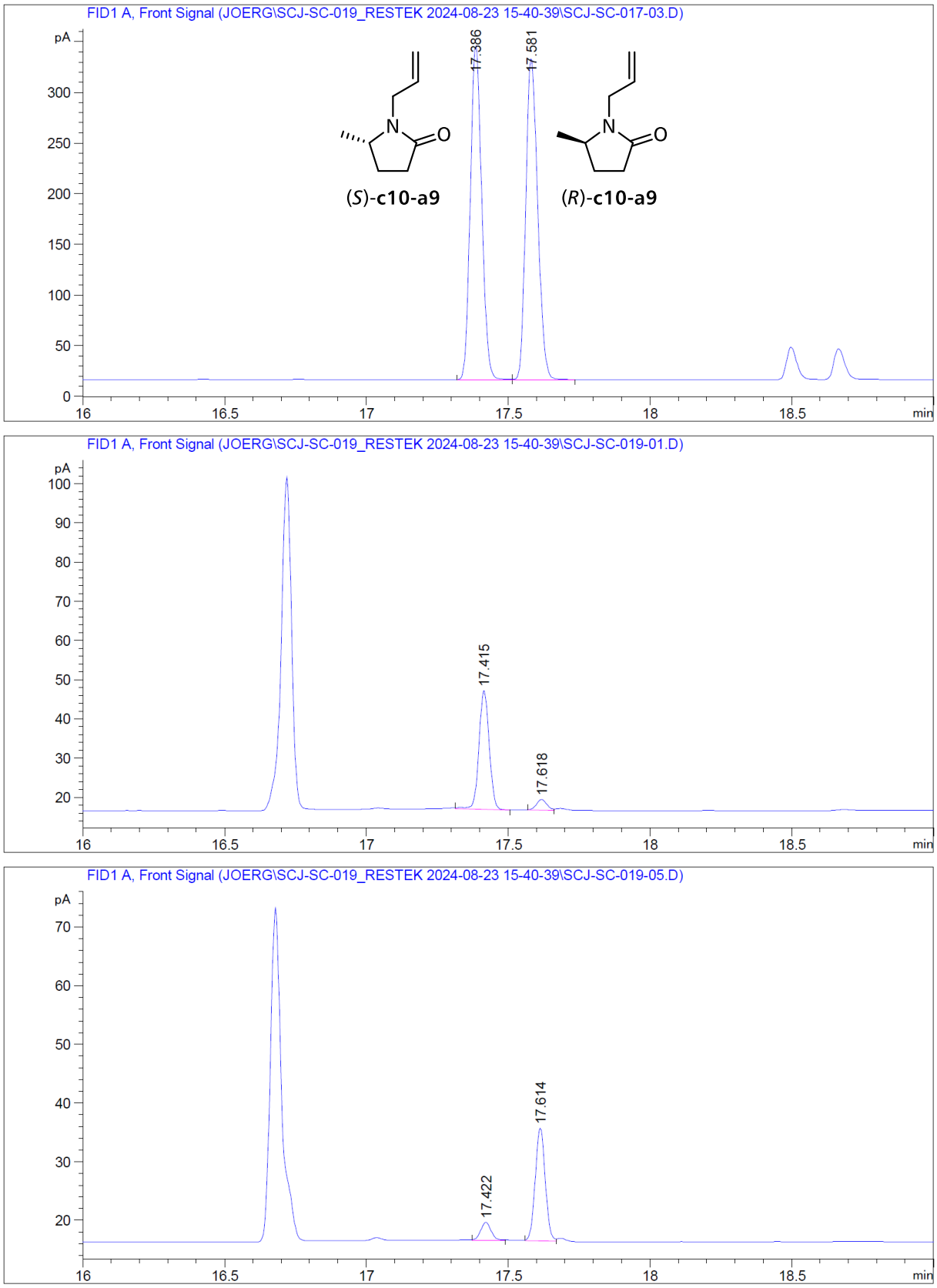


Figure S145. Chromatographic separation of the enantiomers of lactam **c10-a9** using GC method GC-C9. Elution order: (*S*)-**c10-a9** (t_r 17.4 min), (*R*)-**c10-a9** (t_r 17.6 min). Racemic reference (top), (*S*)-selective biotransformation using IR0043 (middle), (*R*)-selective biotransformation using IR0068 (bottom).

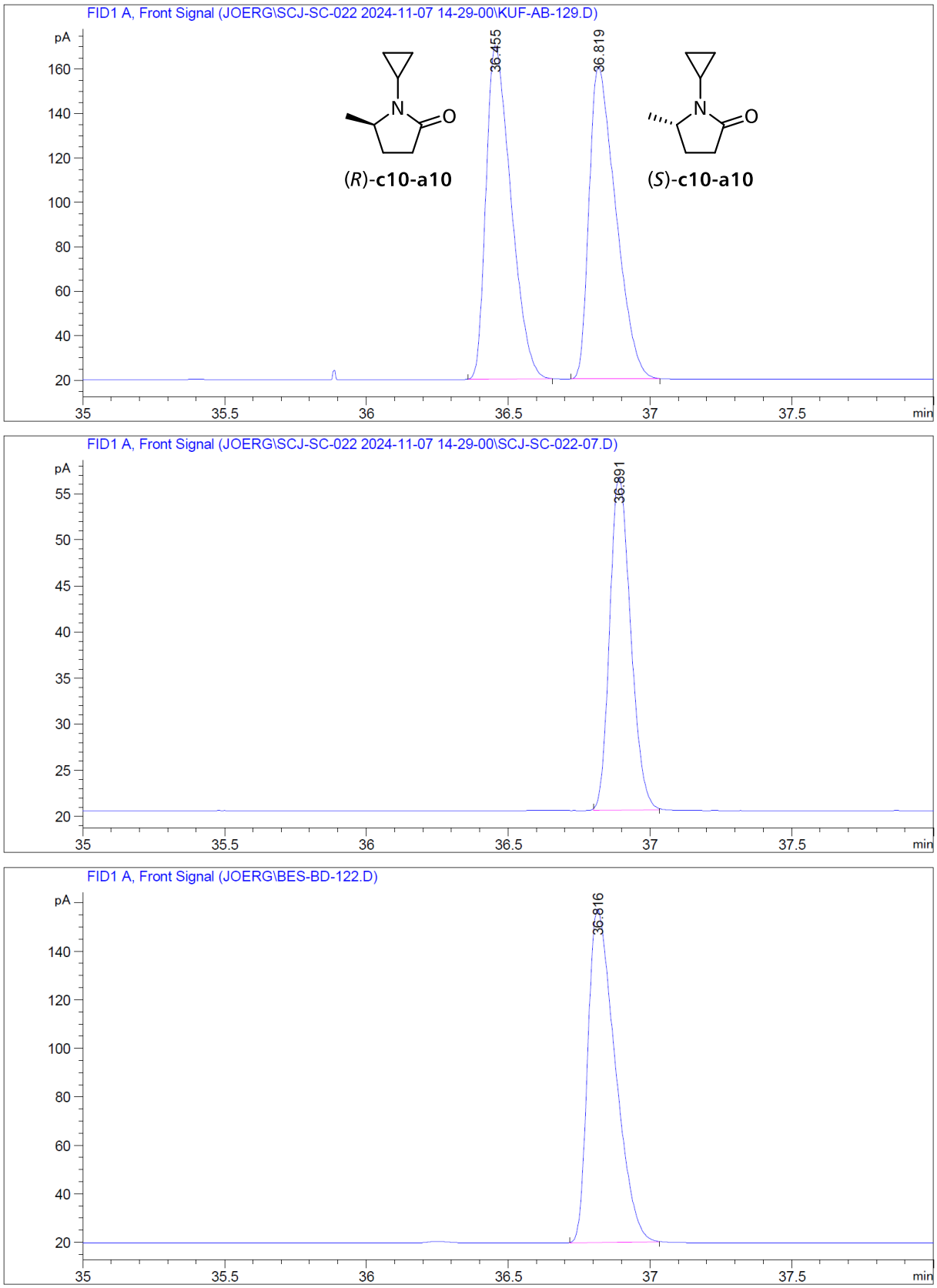


Figure S146. Chromatographic separation of the enantiomers of lactam **c10-a10** using GC method GC-C7. Elution order: (*R*)-**c10-a10** (t_r 36.5 min), (*S*)-**c10-a10** (t_r 36.8 min). Racemic reference (top), independently synthesised (*S*)-enantiomer (middle), (*S*)-selective biotransformation using IR1855 (bottom).

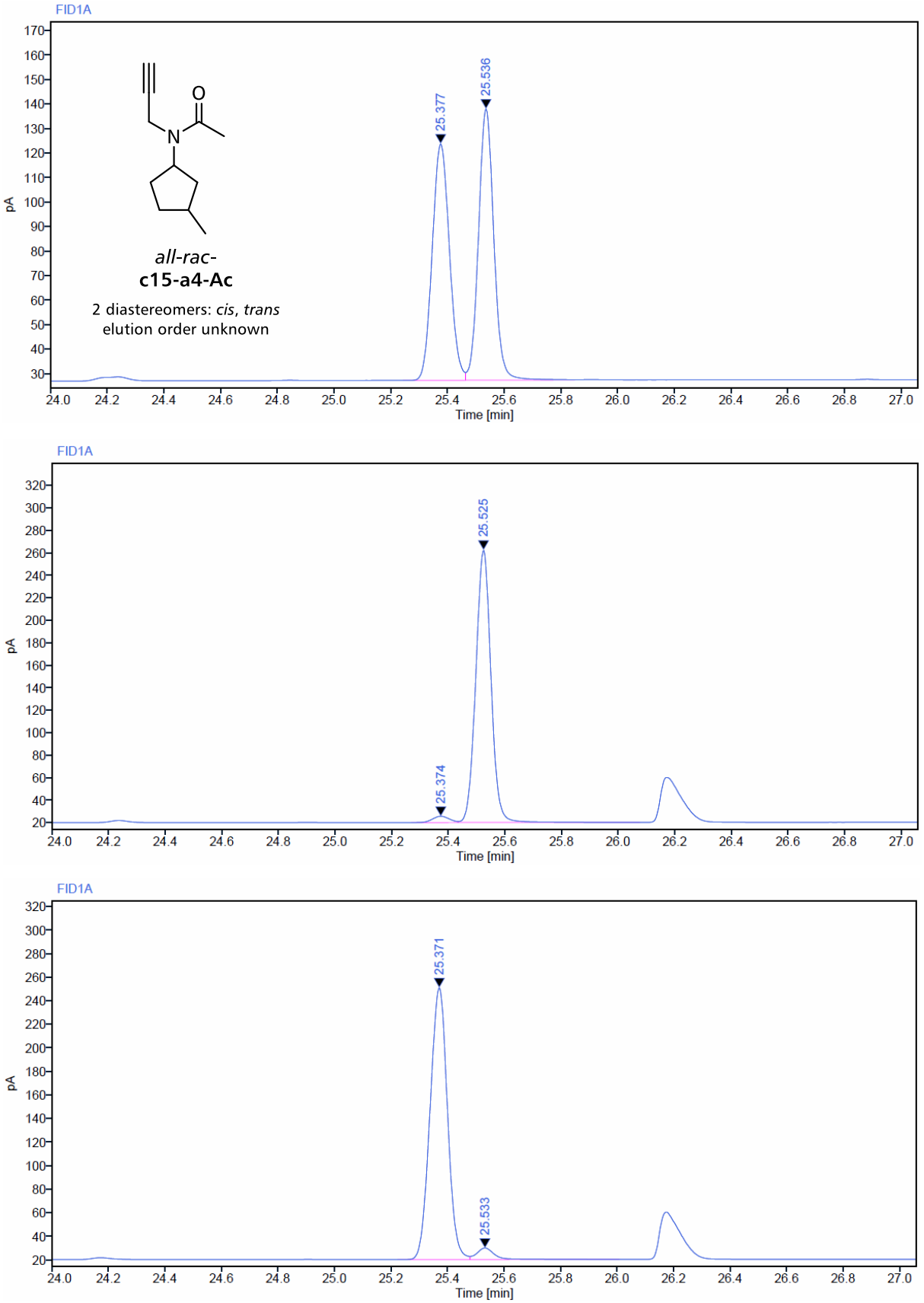


Figure S147. Chromatographic separation of the diastereomers of amine **c15-a4-Ac** using GC method GC-C1. The elution order of diastereomers is unknown, and the method does not achieve separation of enantiomers. Racemic reference (top), biotransformation using IR0015 (middle), biotransformation using IR0039 (bottom).

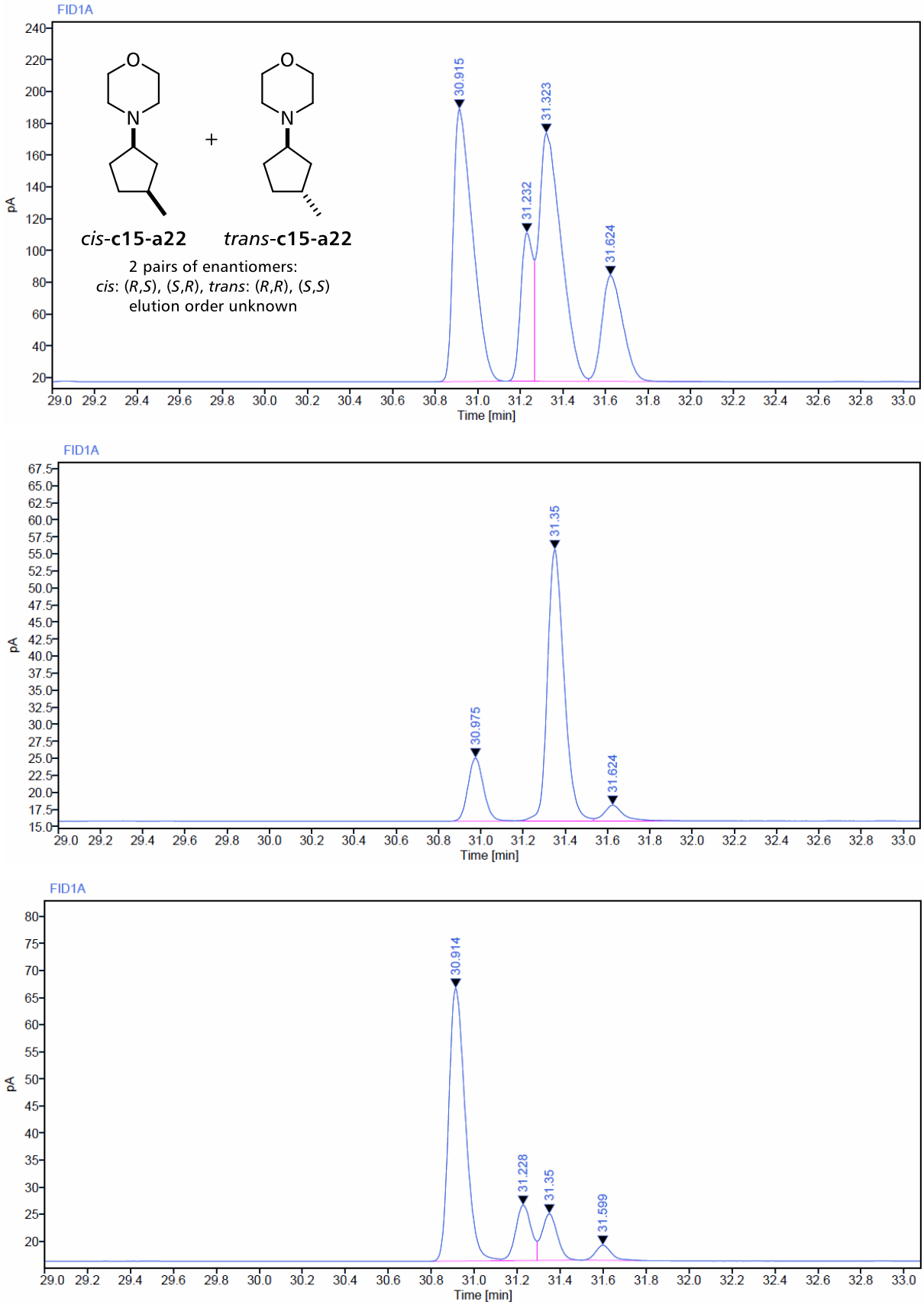


Figure S148. Chromatographic separation of the stereoisomers of amine **c15-a22** using GC method GC-C10. The isomers eluting first (t_r 30.9 min) and third (t_r 31.3 min) and those eluting second (t_r 31.2 min) and fourth (t_r 31.6 min) are pairs of enantiomers. Racemic reference (top), biotransformation using IR0015 (middle), biotransformation using IR0065 (bottom).

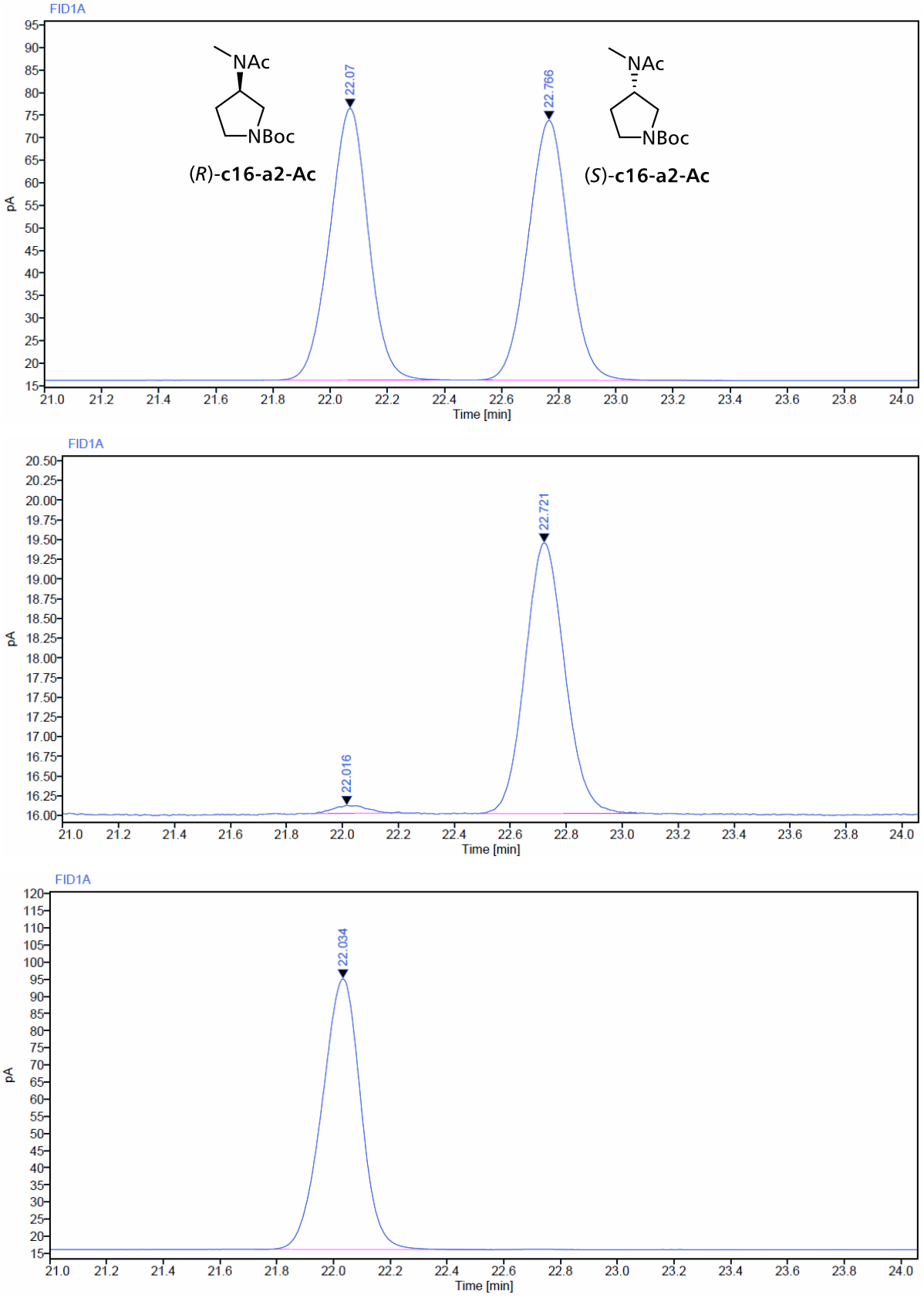


Figure S149. Chromatographic separation of the enantiomers of *N*-acetylated amine **c16-a2-Ac** using GC method GC-C4. Elution order: (*R*)-**c16-a2-Ac** (t_r 22.0 min), (*S*)-**c16-a2-Ac** (t_r 22.8 min). Racemic reference (top), independently synthesised (*S*)-enantiomer (middle), (*R*)-selective biotransformation using IR0035 (bottom).

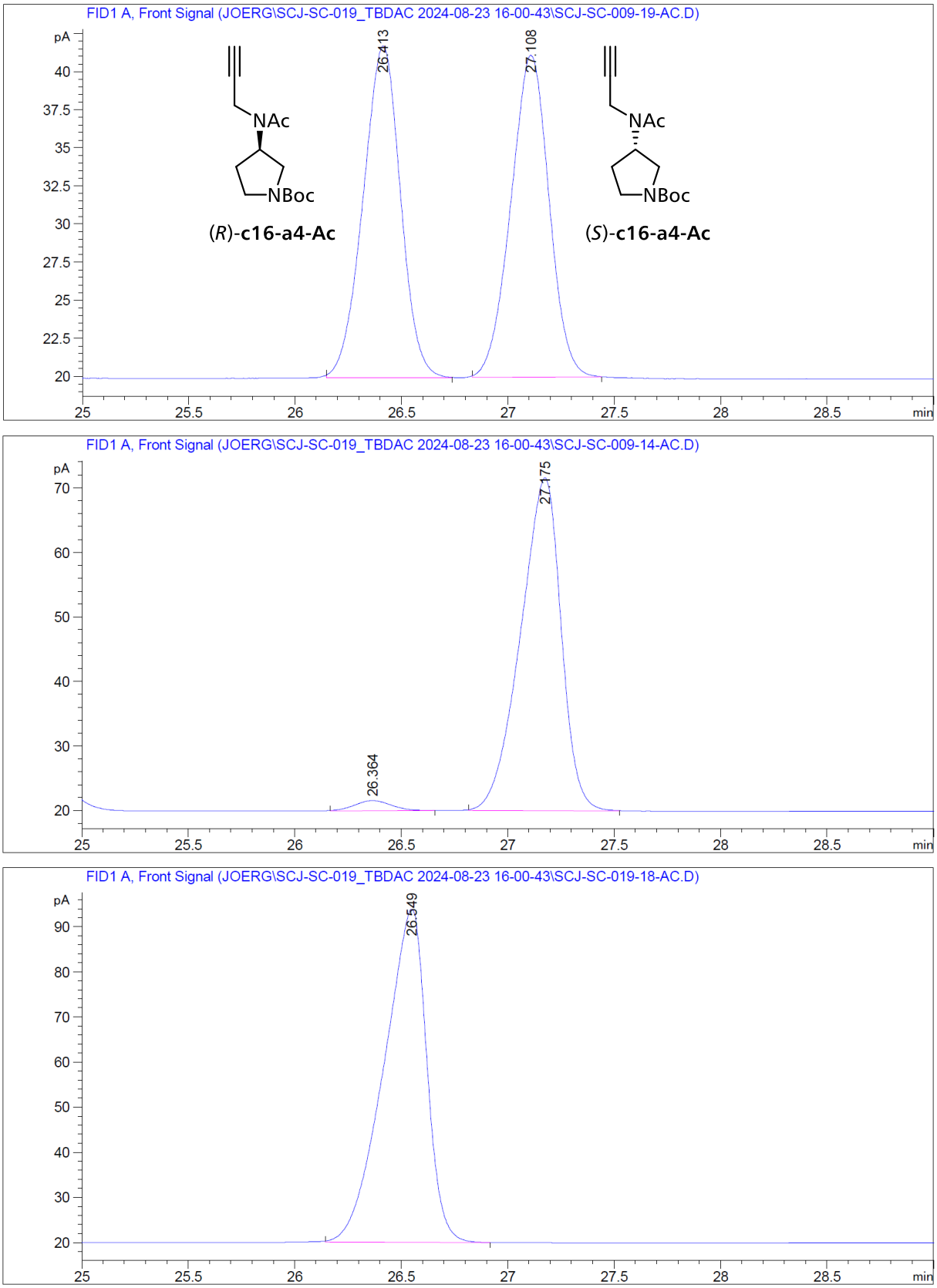


Figure S150. Chromatographic separation of the enantiomers of *N*-acetylated amine **c16-a4-Ac** using GC method GC-C4. Elution order: (*R*)-**c16-a4-Ac** (t_r 26.4 min), (*S*)-**c16-a4-Ac** (t_r 27.1 min). Racemic reference (top), independently synthesised (*S*)-enantiomer (middle), (*R*)-selective biotransformation using IR0041 (bottom).

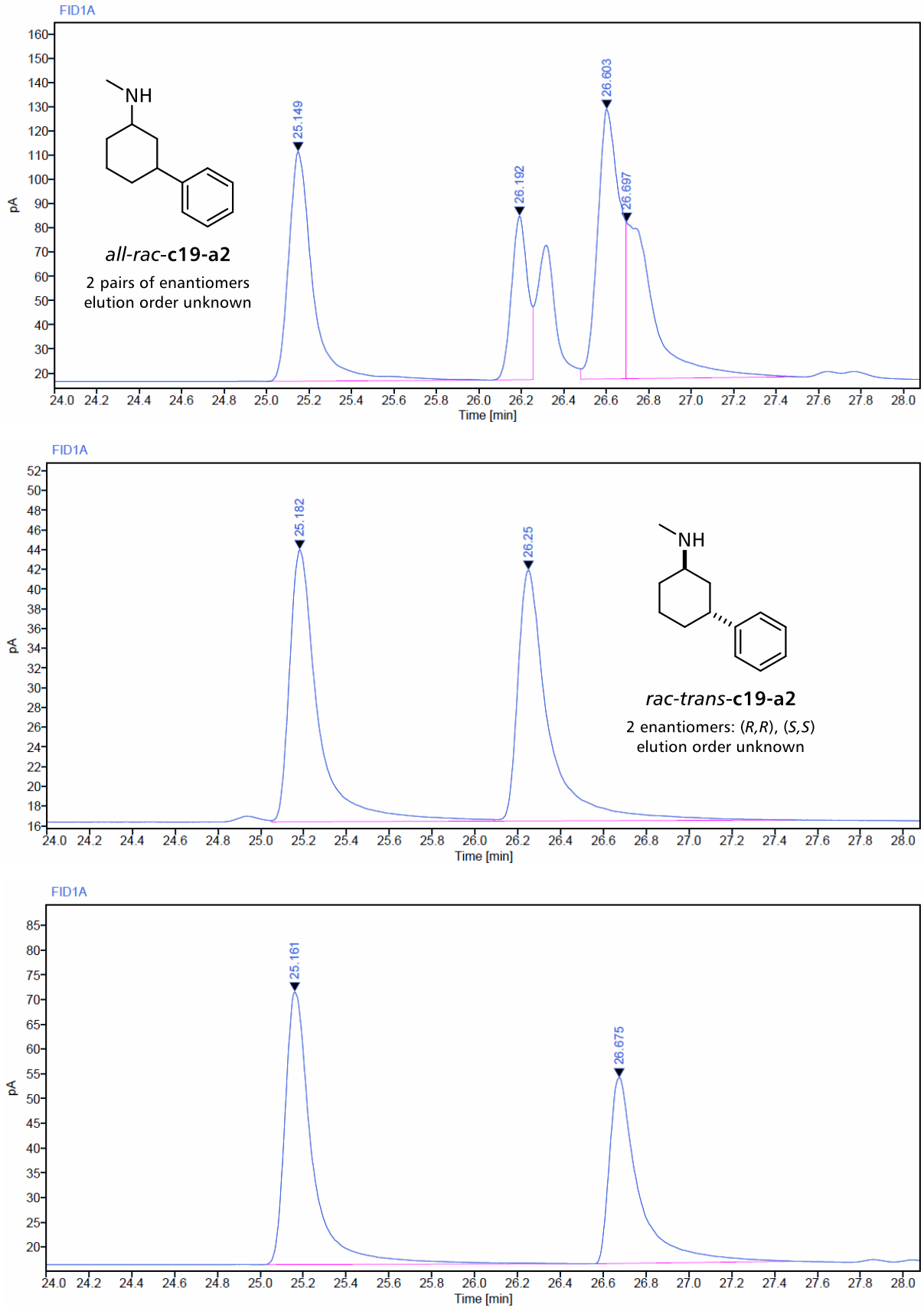


Figure S151. Chromatographic separation of the enantiomers of *N*-acetylated amine **c19-a2** using GC method GC-C13. Elution order of enantiomers unknown. Racemic reference of both diastereomers (top), racemic reference of *trans*-diastereomer (middle), biotransformation using IR1855 (bottom).

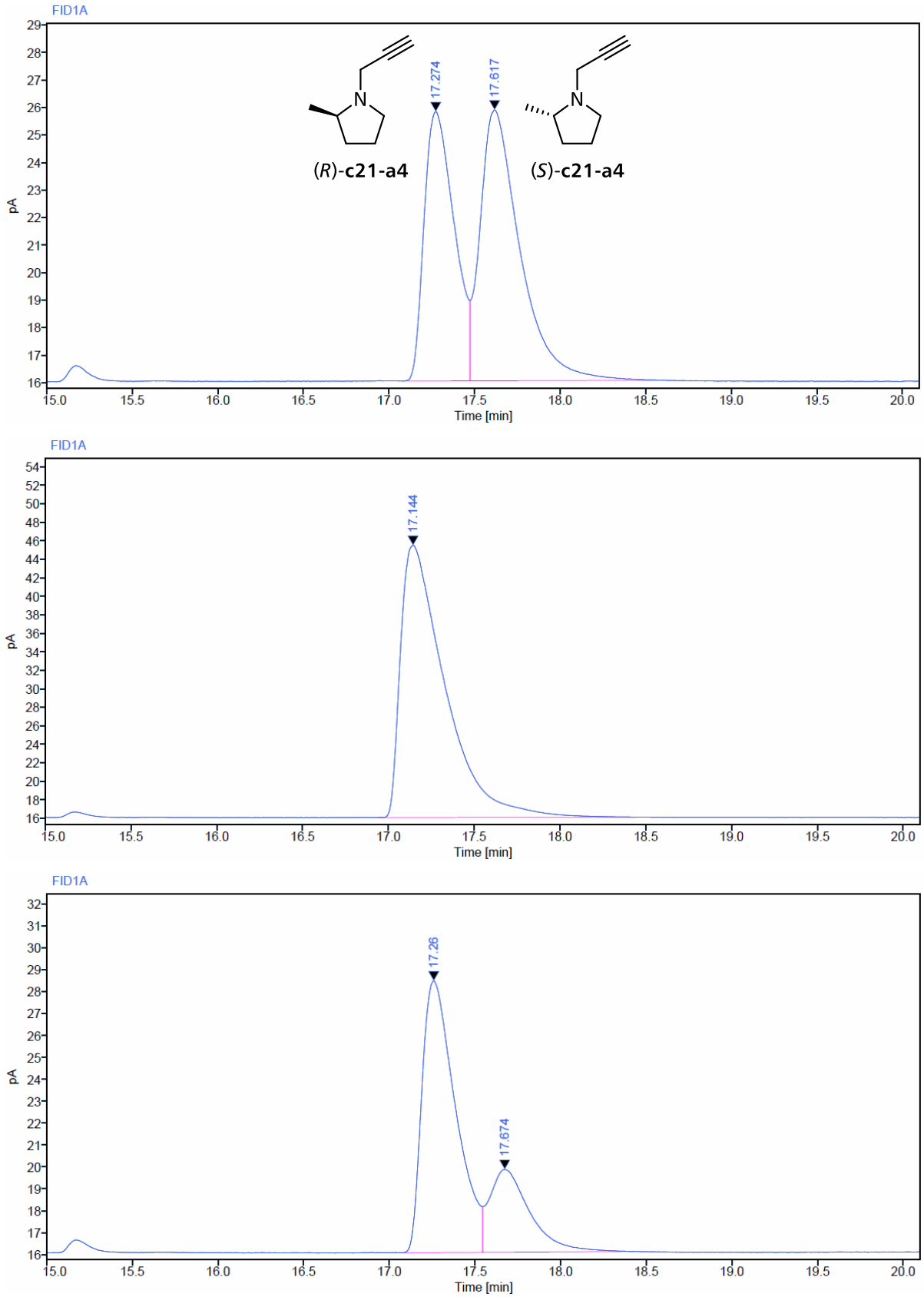


Figure S152. Chromatographic separation of the enantiomers of amine **c21-a4** using GC method GC-C11. Elution order: (*R*)-**c21-a4** (t_r 17.3 min), (*S*)-**c21-a4** (t_r 17.6 min). Racemic reference (top), highly (*R*)-selective biotransformation using IR0039 (middle), moderately (*R*)-selective biotransformation using IR0015 (bottom).

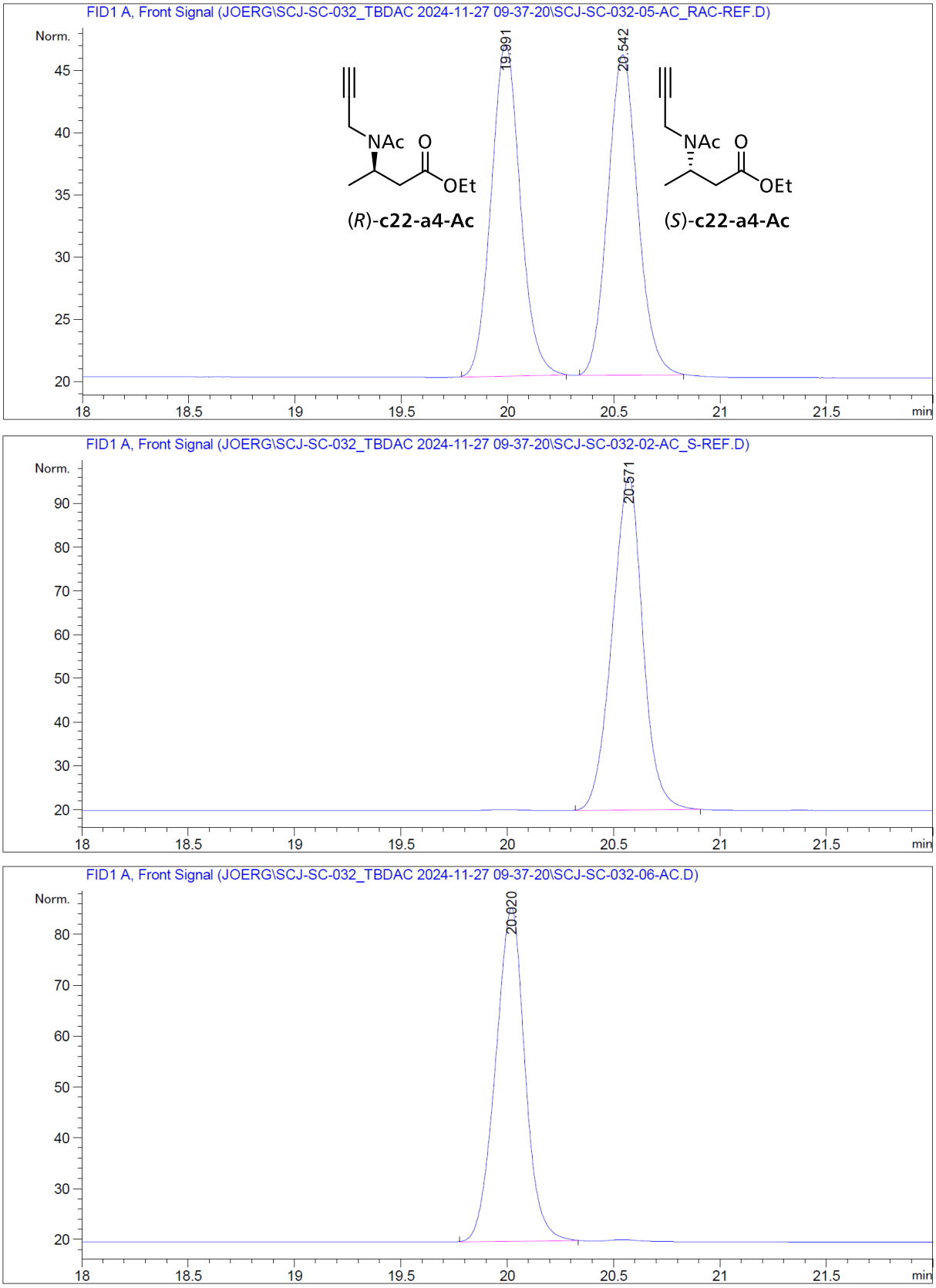


Figure S153. Chromatographic separation of the enantiomers of *N*-acetylated amine **c22-a4-Ac** using GC method GC-C6. Elution order: (*R*)-**c22-a4-Ac** (t_r 20.0 min), (*S*)-**c22-a4-Ac** (t_r 20.5 min). Racemic reference (top), independently synthesised (*S*)-enantiomer (middle), (*R*)-selective biotransformation using IR0068 (bottom).

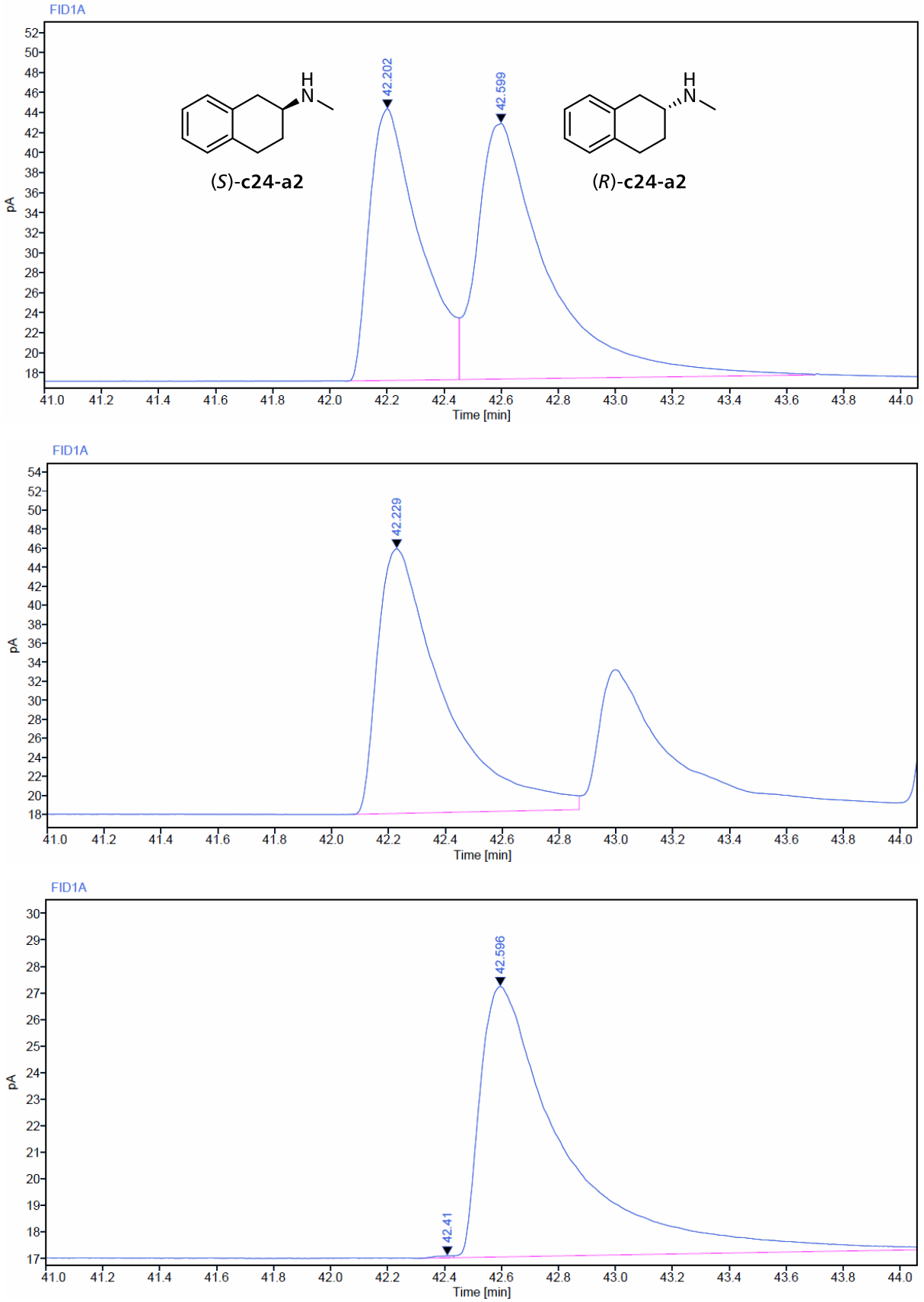


Figure S154. Chromatographic separation of the enantiomers of *N*-acetylated amine **c24-a2** using GC method GC-C14. Elution order: (*S*)-**c24-a2** (t_r 42.2 min), (*R*)-**c24-a2** (t_r 42.6 min). Racemic reference (top), independently synthesised (*S*)-enantiomer (middle), (*R*)-selective biotransformation using IR0041 (bottom).

High performance liquid chromatography with mass-selective detection (achiral stationary phase):
HPLC–MS analyses were carried out on an *Agilent* 1260 Infinity HPLC system (G1311B quaternary pump, G1329B autosampler, G1316A thermostatted column compartment, G1314F variable wavelength detector) equipped with a *Phenomenex* Kinetex C18 column (dimensions: 50 mm × 4.6 mm, stationary phase: core–shell silica, C18 derivative with TMS endcapping, particle size: 2.6 μm) or a *Phenomenex* Luna C18(2) column (dimensions: 250 mm × 4.6 mm, stationary phase: fully porous silica, C18 derivative with TMS endcapping, particle size: 5 μm) and coupled to an *Agilent* 6120 single-quadrupole MS detector, using water and acetonitrile, each containing 0.1% (v/v) formic acid, as eluents.

Formation of the expected reductive amination products was surveyed in selected ion monitoring (SIM) mode and confirmed by comparison of the observed retention times with those of independently synthesised reference compounds.

Method HPLC-MS1

Column:	Kinetex C18 (50 mm × 4.6 mm)
Column temperature:	40 °C

Eluent gradient:	start at H_2O/MeCN = 90:10 (+ 0.1% FA);
	linear gradient to H_2O/MeCN = 0:100 (+ 0.1% FA), 10 min;
	linear gradient to H_2O/MeCN = 90:10 (+ 0.1% FA), 1 min;
	H_2O/MeCN = 90:10 (+ 0.1% FA), 2 min

Eluent flow rate:	1.0 mL/min
Run time:	13 min
Injection volume:	5 μL
Ionisation mode:	API-ES, positive polarity
Drying gas temperature:	350 °C
Drying gas flow:	10.0 L/min
Nebuliser pressure:	35 psig (2.4 bar)
Capillary voltage:	3000 V
Signal 1 (scan):	50% cycle time mass range 40–250 fragmentor 40 V
Signal 2 (SIM):	50% cycle time SIM on target mass fragmentor 40 V

Method HPLC-MS2

Column:	Luna C18(2) (250 mm × 4.6 mm)
Column temperature:	40 °C

Eluent gradient:	start at H_2O/MeCN = 90:10 (+ 0.1% FA);
	linear gradient to H_2O/MeCN = 30:70 (+ 0.1% FA), 10 min;
	linear gradient to H_2O/MeCN = 90:10 (+ 0.1% FA), 2 min;
	H_2O/MeCN = 90:10 (+ 0.1% FA), 1 min

Eluent flow rate:	1.0 mL/min
Run time:	13 min
Injection volume:	5 μL

Ionisation mode:	API-ES, positive polarity
Drying gas temperature:	350 °C
Drying gas flow:	10.0 L/min
Nebuliser pressure:	35 psig (2.4 bar)
Capillary voltage:	3000 V
Signal 1 (scan):	50% cycle time mass range 50–400 fragmentor 40 V
Signal 2 (SIM):	50% cycle time SIM on target mass fragmentor 40 V

Exemplary chromatograms are shown below.

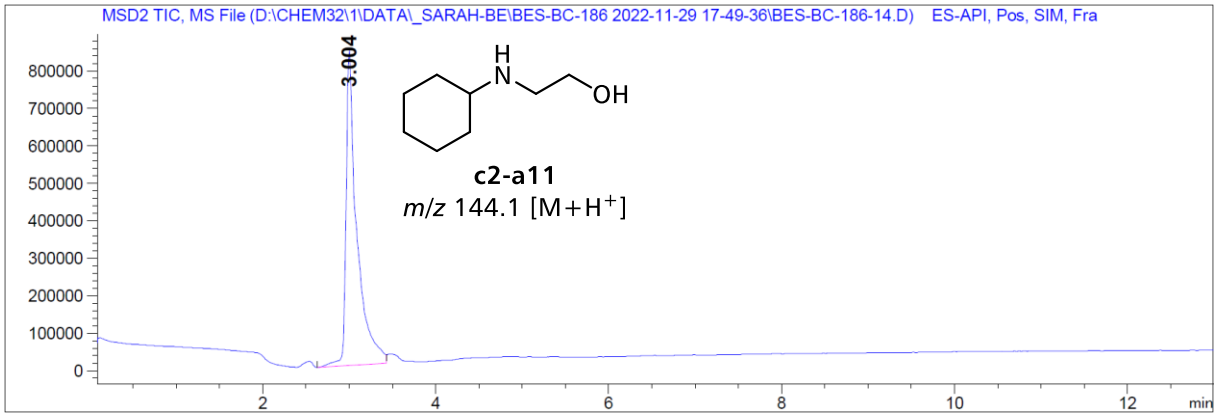


Figure S155. HPLC–MS chromatogram (method HPLC-MS2; selected ion monitoring, *m/z* = 144) confirming formation of 2-(cyclohexylamino)ethan-1-ol (**c2-a11**). Sample generated by biotransformation of cyclohexanone (**c2**) and ethanolamine (**a11**) using IR1662.

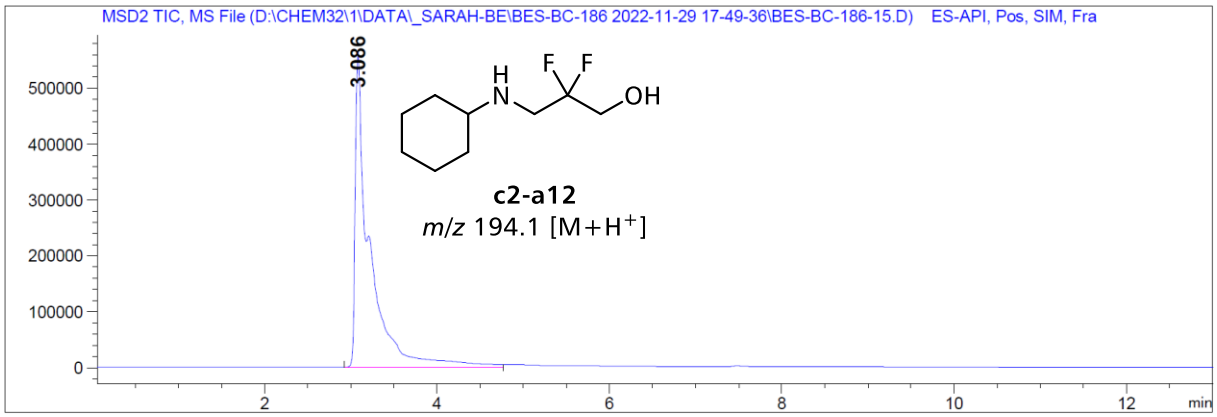


Figure S156. HPLC–MS chromatogram (method HPLC-MS2; selected ion monitoring, *m/z* = 194) confirming formation of 3-(cyclohexylamino)-2,2-difluoropropan-1-ol (**c2-a11**). Sample generated by biotransformation of cyclohexanone (**c2**) and 3-amino-2,2-difluoropropan-1-ol (**a11**) using IR2257.

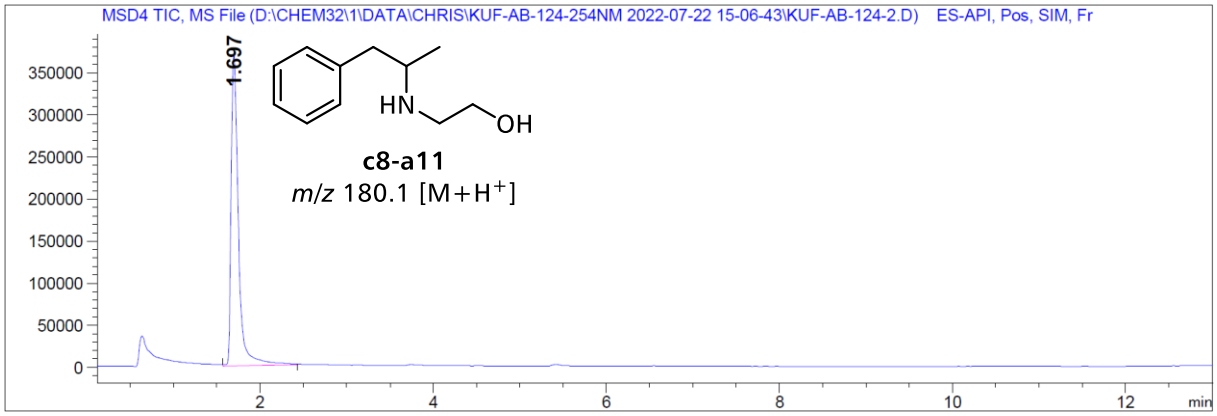


Figure S157. HPLC–MS chromatogram (method HPLC-MS1; selected ion monitoring, *m/z* = 180) confirming formation of 2-((1-phenylpropan-2-yl)amino)ethan-1-ol (**c8-a11**). Sample generated by biotransformation of phenylacetone (**c8**) and ethanolamine (**a11**) using IR1855.

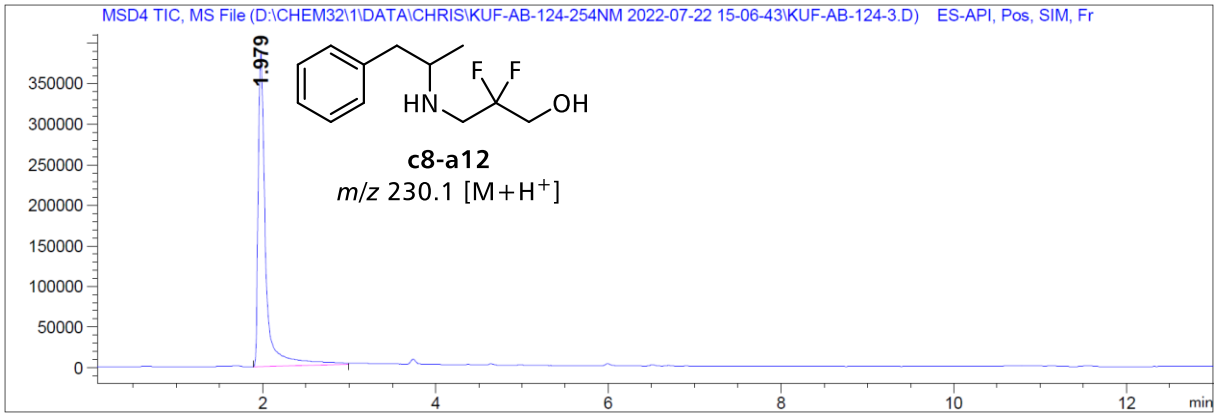


Figure S158. HPLC–MS chromatogram (method HPLC-MS1; selected ion monitoring, *m/z* = 230) confirming formation of 2,2-difluoro-3-((1-phenylpropan-2-yl)amino)propan-1-ol (**c8-a12**). Sample generated by biotransformation of phenylacetone (**c8**) and 3-amino-2,2-difluoropropan-1-ol (**a12**) using IR0063.

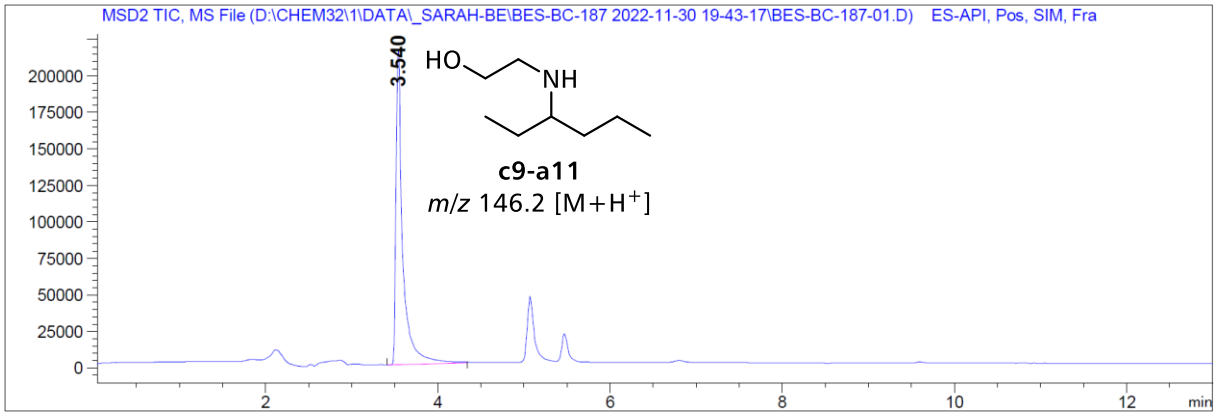


Figure S159. HPLC–MS chromatogram (method HPLC-MS2; selected ion monitoring, *m/z* = 146) confirming formation of 2-(hexan-3-ylamino)ethan-1-ol (**c9-a11**). Sample generated by biotransformation of hexan-3-one (**c9**) and ethanolamine (**a11**) using IR1855.

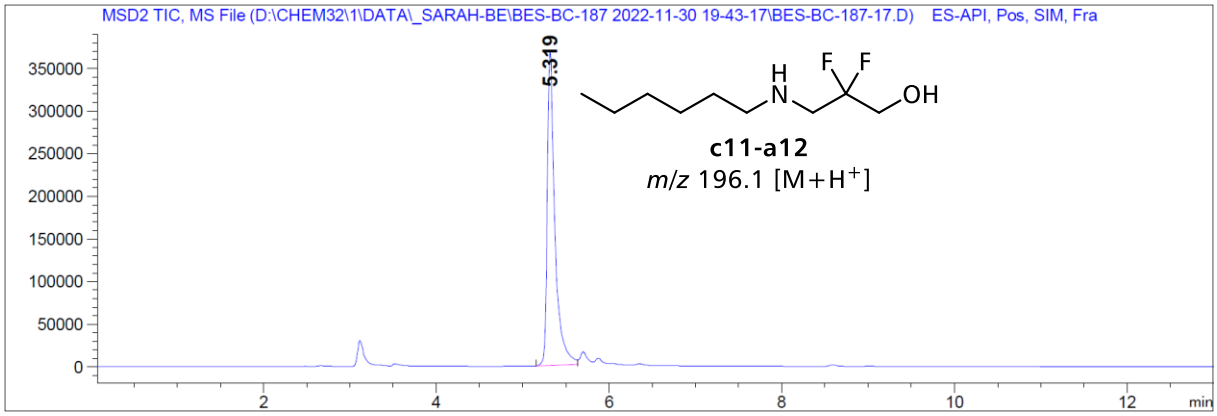


Figure S160. HPLC–MS chromatogram (method HPLC-MS2; selected ion monitoring, *m/z* = 196) confirming formation of 2,2-difluoro-3-(hexylamino)propan-1-ol (**c11-a12**). Sample generated by biotransformation of hexanal (**c11**) and 3-amino-2,2-difluoropropan-1-ol (**a12**) using IR0887.

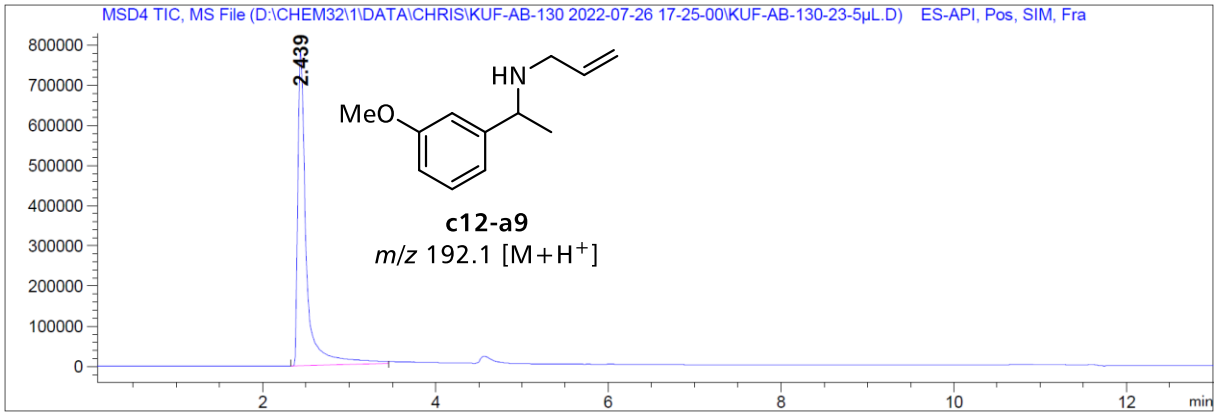


Figure S161. HPLC–MS chromatogram (method HPLC-MS1; selected ion monitoring, *m/z* = 192) confirming formation of *N*-(1-(3-methoxyphenyl)ethyl)prop-2-en-1-amine (**c12-a9**). Sample generated by biotransformation of 3-methoxyacetophenone (**c12**) and allylamine (**a9**) using IR1855.

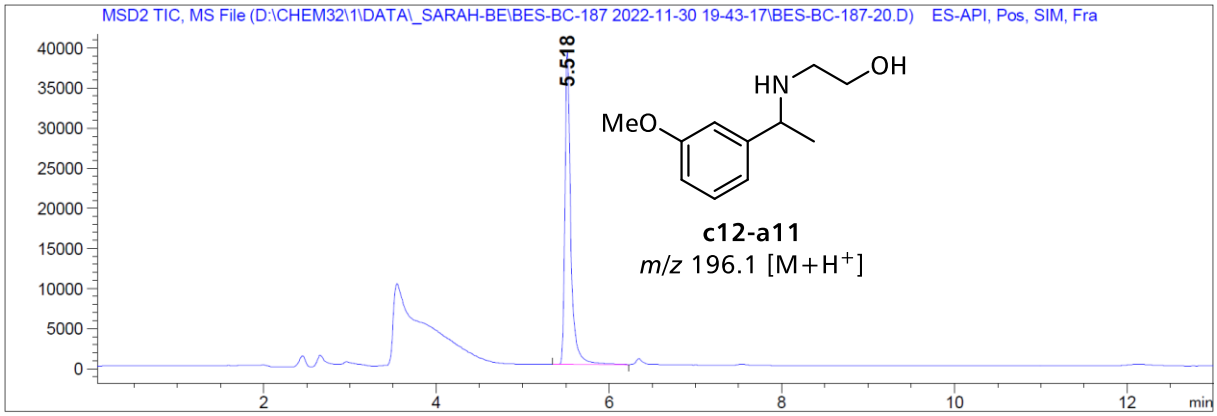


Figure S162. HPLC–MS chromatogram (method HPLC-MS2; selected ion monitoring, *m/z* = 196) confirming formation of 2-((1-(3-methoxyphenyl)ethyl)amino)ethan-1-ol (**c12-a11**). Sample generated by biotransformation of 3-methoxyacetophenone (**c12**) and ethanolamine (**a11**) using IR1855.

High-performance liquid chromatography (chiral stationary phase):
Chiral-phase HPLC analyses were carried out on a *Shimadzu* Prominence HPLC system (Degasser DGU-20A5, Liquid Chromatograph LC-20AD, Autosampler SIL-20AC, Column Oven CTO-20AC, Diode Array Detector SPD-M20A, Communication Bus Module CBM-20A) equipped with a *Daicel* Chiralcel OD-H column (dimensions: 250 mm × 4.6 mm, stationary phase: cellulose tris(3,5-dimethylphenylcarbamate) coated on silica gel, particle size: 5 μm), a *Daicel* Chiralpak IA column (dimensions: 250 mm × 4.6 mm, stationary phase: amylose tris(3,5-dimethylphenylcarbamate) immobilised on silica gel, particle size: 5 μm), a *Daicel* Chiralpak IB column (dimensions: 250 mm × 4.6 mm, stationary phase: cellulose tris(3,5-dimethylphenylcarbamate)) immobilised on silica gel, particle size: 5 μm), or a *Daicel* Chiralpak IC column (dimensions: 250 mm × 4.6 mm, stationary phase: cellulose tris(3,5-dichlorophenylcarbamate) immobilised on silica gel, particle size: 5 μm), using *n*-heptane and 2-propanol, each containing 0.1% (v/v) of diethylamine, as eluents.

Method HPLC-C1 (compound **c4-a6**)	
Column:	Chiralcel OD-H (250 mm × 4.6 mm)
Column temperature:	18 °C
Eluent:	*n*-heptane (+ 0.1% DEA)
Eluent flow rate:	0.4 mL/min
Run time:	40 min
Integration wavelength:	254 nm

Method HPLC-C2 (compounds **c3-a6**, **c6-a6**, **c12-a10**)	
Column:	Chiralcel OD-H (250 mm × 4.6 mm)
Column temperature:	25 °C
Eluent:	*n*-heptane/2-propanol = 99:1 (+ 0.1% DEA)
Eluent flow rate:	0.5 mL/min
Run time:	40 min
Integration wavelength:	258 nm (**c3-a6**), 258 (**c6-a6**), 273 nm (**c12-a10**)

Method HPLC-C3 (compound **c21-a24**)	
Column:	Chiralcel OD-H (250 mm × 4.6 mm)
Column temperature:	20 °C
Eluent:	*n*-heptane/2-propanol = 99.5:0.5 (+ 0.1% DEA)
Eluent flow rate:	0.5 mL/min
Run time:	60 min
Integration wavelength:	254 nm

Method HPLC-C4 (compound **c7-a6**)	
Column:	Chiralcel OD-H (250 mm × 4.6 mm)
Column temperature:	25 °C
Eluent:	*n*-heptane/2-propanol = 95:5 (+ 0.1% DEA)
Eluent flow rate:	0.5 mL/min
Run time:	30 min
Integration wavelength:	258 nm

Method HPLC-C5 (compound **c24-a6**)

Column:	Chiralpak IA (250 mm × 4.6 mm)
Column temperature:	30 °C
Eluent:	*n*-heptane/2-propanol = 90:10 (+ 0.1% DEA)
Eluent flow rate:	0.5 mL/min
Run time:	30 min
Integration wavelength:	265 nm

Method HPLC-C6 (compound **c16-a15**)

Column:	Chiralpak IA (250 mm × 4.6 mm)
Column temperature:	30 °C
Eluent:	*n*-heptane/2-propanol = 95:5 (+ 0.1% DEA)
Eluent flow rate:	0.5 mL/min
Run time:	40 min
Integration wavelength:	258 nm

Method HPLC-C7 (compounds **c9-a9-Fmoc**, **c9-a10-Fmoc**, **c18-a2**)

Column:	Chiralpak IA (250 mm × 4.6 mm)
Column temperature:	25 °C
Eluent:	*n*-heptane/2-propanol = 99:1 (+ 0.1% DEA)
Eluent flow rate:	0.5 mL/min
Run time:	60 min
Integration wavelength:	301 nm (**c9-a9-Fmoc**, **c9-a10-Fmoc**), 258 nm (**c18-a2**)

Method HPLC-C8 (compound **c18-a4**)

Column:	Chiralpak IA (250 mm × 4.6 mm)
Column temperature:	25 °C
Eluent:	*n*-heptane/2-propanol = 98:2 (+ 0.1% DEA)
Eluent flow rate:	0.5 mL/min
Run time:	60 min
Integration wavelength:	258 nm

Method HPLC-C9 (compound **c16-a6**)

Column:	Chiralpak IB (250 mm × 4.6 mm)
Column temperature:	30 °C
Eluent:	*n*-heptane/2-propanol = 95:5 (+ 0.1% DEA)
Eluent flow rate:	0.5 mL/min
Run time:	40 min
Integration wavelength:	258 nm

Method HPLC-C10 (compounds **c8-a10-Ac**, **c24-a4**)

Column:	Chiralpak IC (250 mm × 4.6 mm)
Column temperature:	25 °C
Eluent:	*n*-heptane/2-propanol = 98:2 (+ 0.1% DEA)
Eluent flow rate:	1.0 mL/min
Run time:	90 min
Integration wavelength:	258 nm (**c8-a10-Ac**), 265 nm (**c24-a4**)

Method HPLC-C11 (compound **c24-a2**)

Column:	Chiralpak IC (250 mm × 4.6 mm)
Column temperature:	20 °C
Eluent:	*n*-heptane/2-propanol = 90:10 (+ 0.1% DEA)
Eluent flow rate:	1.0 mL/min
Run time:	30 min
Integration wavelength:	266 nm

Method HPLC-C12 (compound **c23-a4-Fmoc**, **c23-a10-Fmoc**)

Column:	Chiralpak IC (250 mm × 4.6 mm)
Column temperature:	30 °C
Eluent:	*n*-heptane/2-propanol = 85:15 (+ 0.1% DEA)
Eluent flow rate:	0.5 mL/min
Run time:	60 min
Integration wavelength:	300 nm (**c23-a4-Fmoc**), 265 nm (**c23-a10-Fmoc**)

Method HPLC-C13 (compound **c8-a9-Ac**, **c8-a10-Ac**)

Column:	Chiralpak IC (250 mm × 4.6 mm)
Column temperature:	25 °C
Eluent:	*n*-heptane/2-propanol = 95:5 (+ 0.1% DEA)
Eluent flow rate:	1.0 mL/min
Run time:	60 min
Integration wavelength:	222 nm

Method HPLC-C14 (compound **c23-a2-Fmoc**)

Column:	Chiralpak IC (250 mm × 4.6 mm)
Column temperature:	30 °C
Eluent:	*n*-heptane/2-propanol = 80:20 (+ 0.1% DEA)
Eluent flow rate:	0.5 mL/min
Run time:	60 min
Integration wavelength:	301 nm

Method HPLC-C15 (compound **c19-a4**)

Column:	Chiralpak IC (250 mm × 4.6 mm)
Column temperature:	25 °C
Eluent:	*n*-heptane/2-propanol = 98:2 (+ 0.1% DEA)
Eluent flow rate:	0.5 mL/min
Run time:	60 min
Integration wavelength:	259 nm

Exemplary chromatograms are shown on the following pages.

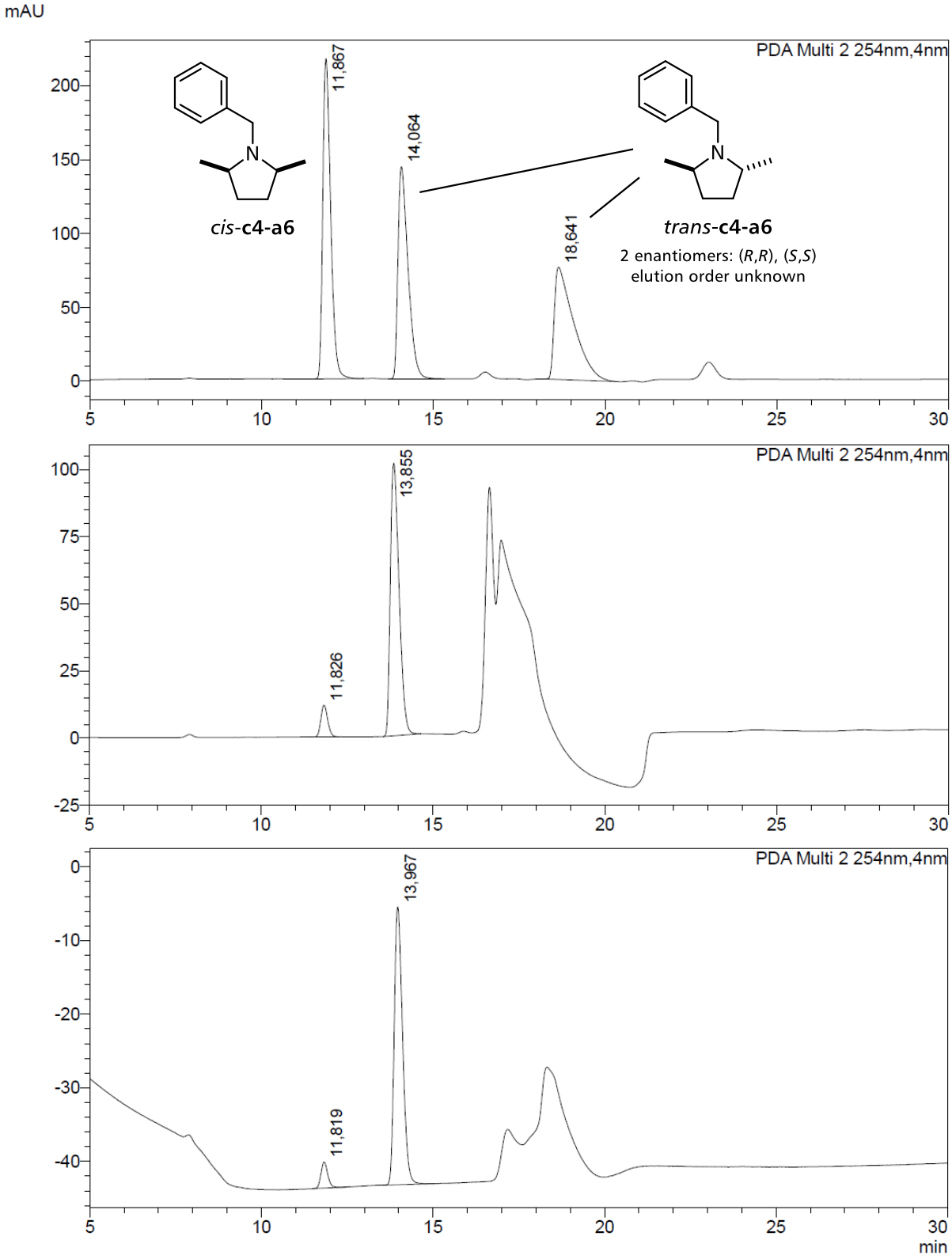


Figure S163. Chromatographic separation of the stereoisomers of amine **c4-a6** using HPLC method HPLC-C1. Elution order: *cis*-**c4-a6** (t_r 11.9 min), (*A*,*A*)-*trans*-**c4-a6** (t_r 14.1 min), (*B*,*B*)-*trans*-**c4-a6** (t_r 18.6 min). Racemic reference (top), biotransformation using IR2147 (middle), biotransformation using IR0499 (bottom).

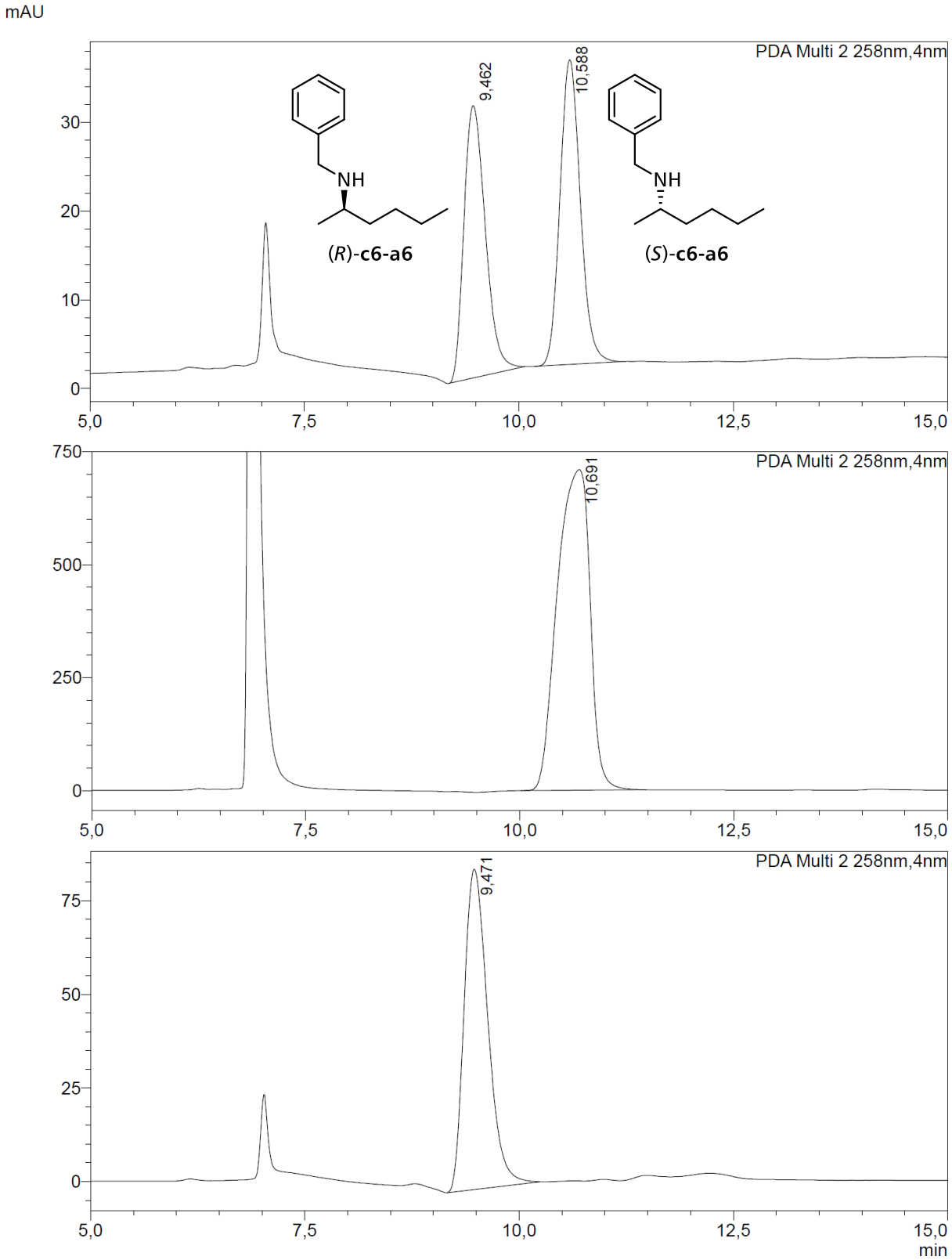


Figure S164. Chromatographic separation of the enantiomers of amine **c6-a6** using HPLC method HPLC-C2. Elution order: (*R*)-**c6-a6** (t_r 9.5 min), (*S*)-**c6-a6** (t_r 10.6 min). Racemic reference (top), independently synthesised (*S*)-enantiomer (middle), (*R*)-selective biotransformation using IR1460 (bottom).

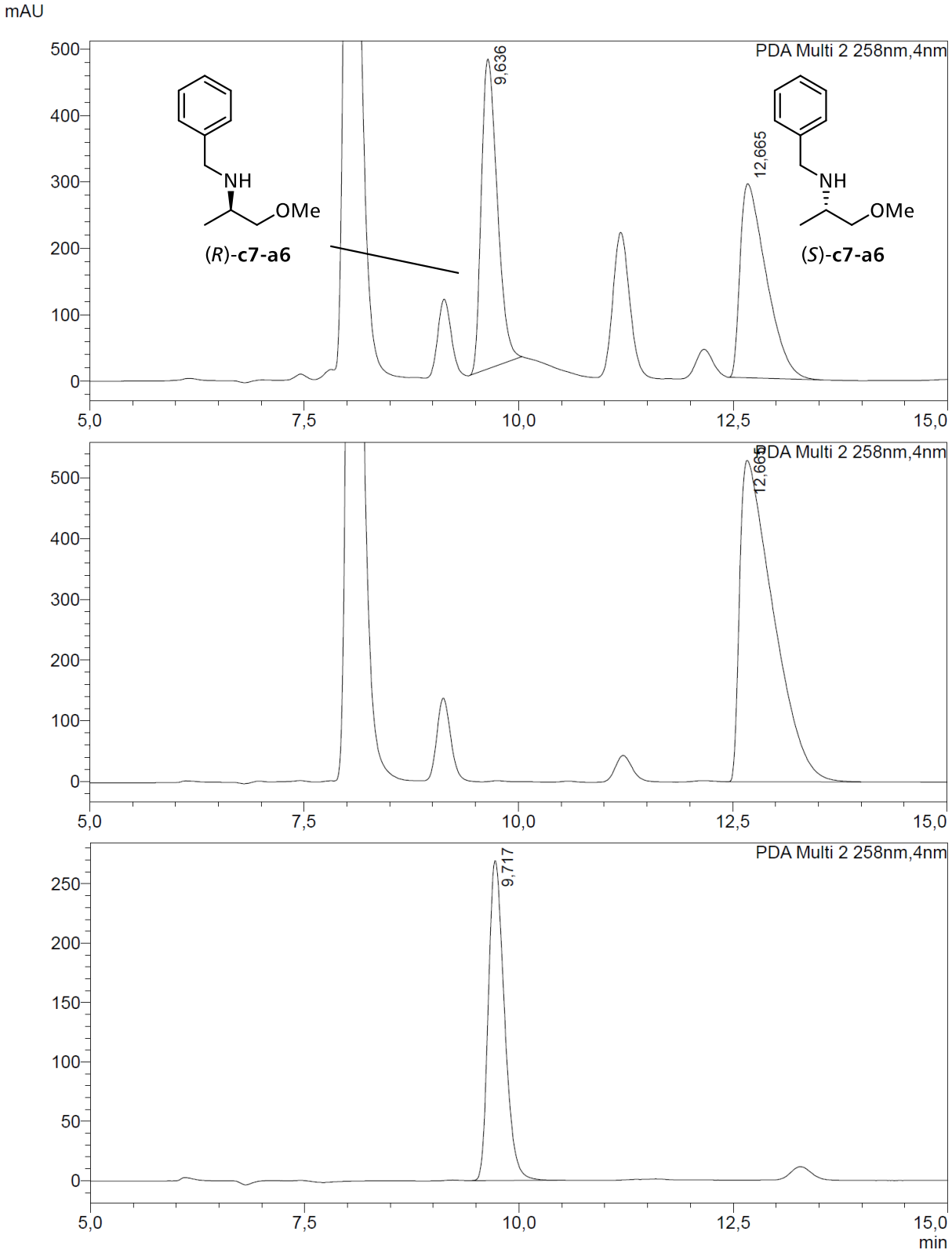


Figure S165. Chromatographic separation of the enantiomers of amine **c7-a6** using HPLC method HPLC-C4. Elution order: (*R*)-**c7-a6** (t_r 9.6 min), (*S*)-**c7-a6** (t_r 12.7 min). Racemic reference (top), independently synthesised (*S*)-enantiomer (middle), (*R*)-selective biotransformation using IR2147 (bottom). *Note:* The small peak at t_r 13.3 min in the bottom chromatogram is also present in negative controls and hence does not indicate formation of the (*S*)-enantiomer.

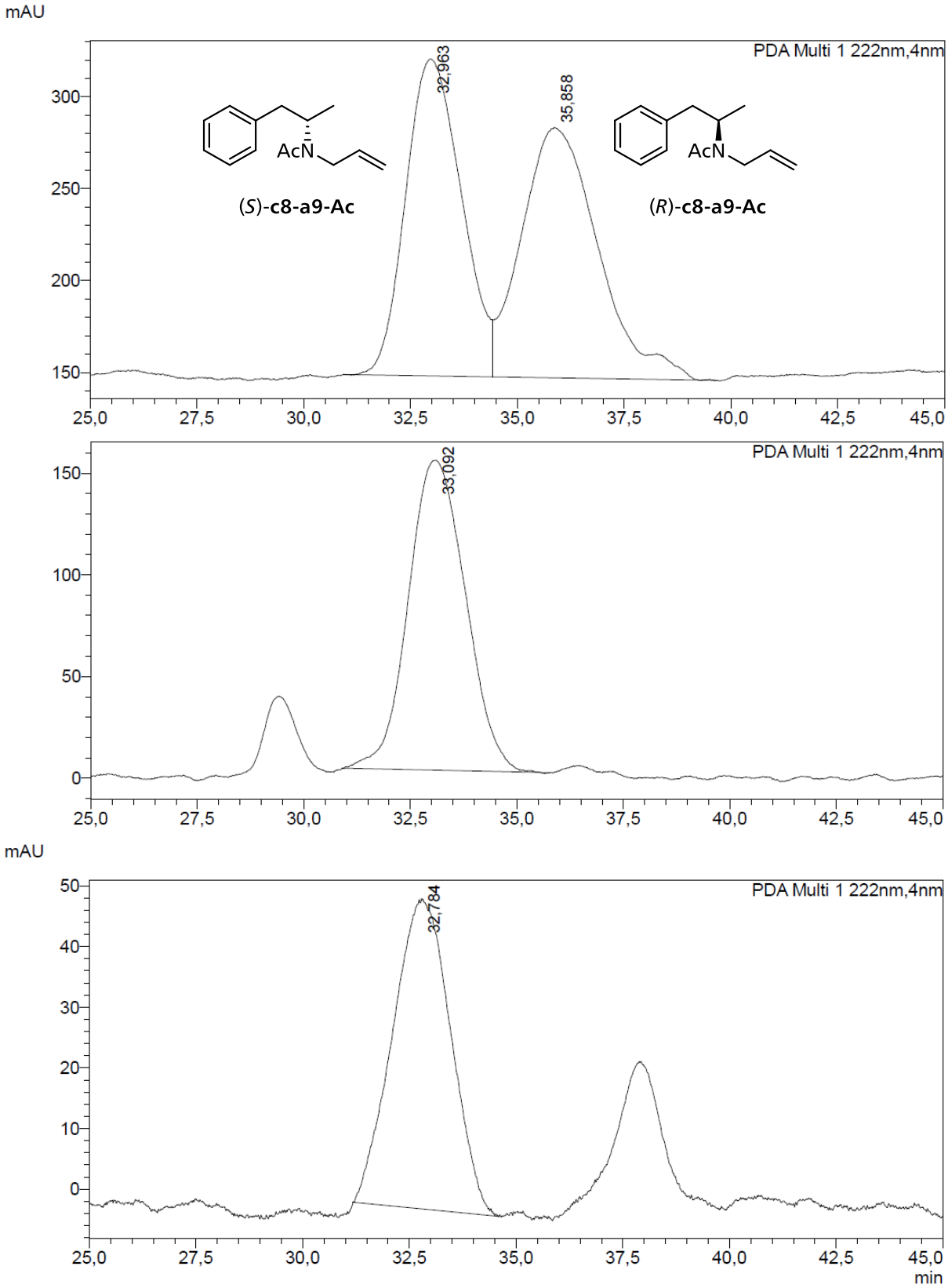


Figure S166. Chromatographic separation of the enantiomers of *N*-acetylated amine **c8-a9-Ac** using HPLC method HPLC-C13. Elution order: (*S*)-**c8-a9-Ac** (t_r 33.0 min), (*R*)-**c8-a9-Ac** (t_r 35.9 min). Racemic reference (top), independently synthesised (*S*)-enantiomer (middle), (*S*)-selective biotransformation using IR1855 (bottom). *Note:* The peak at t_r 37.6 min in the bottom chromatogram is also present in negative controls and hence does not indicate formation of the (*R*)-enantiomer.

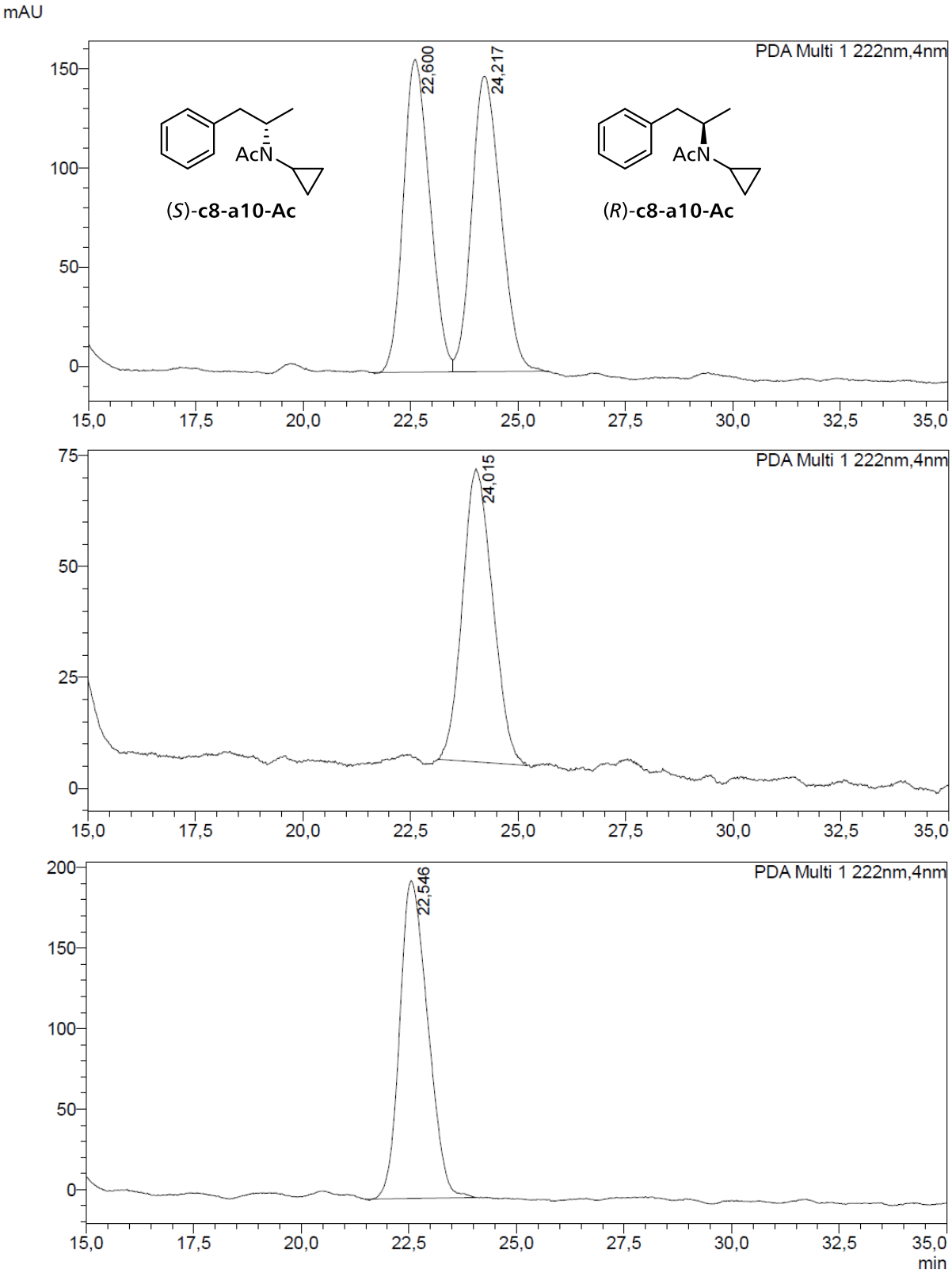


Figure S167. Chromatographic separation of the enantiomers of *N*-acetylated amine **c8-a10-Ac** using HPLC method HPLC-C13. Elution order: (*S*)-**c8-a10-Ac** (t_r 22.6 min), (*R*)-**c8-a10-Ac** (t_r 24.2 min). Racemic reference (top), (*R*)-selective biotransformation using IR0068 (middle), (*S*)-selective biotransformation using IR1855 (bottom).

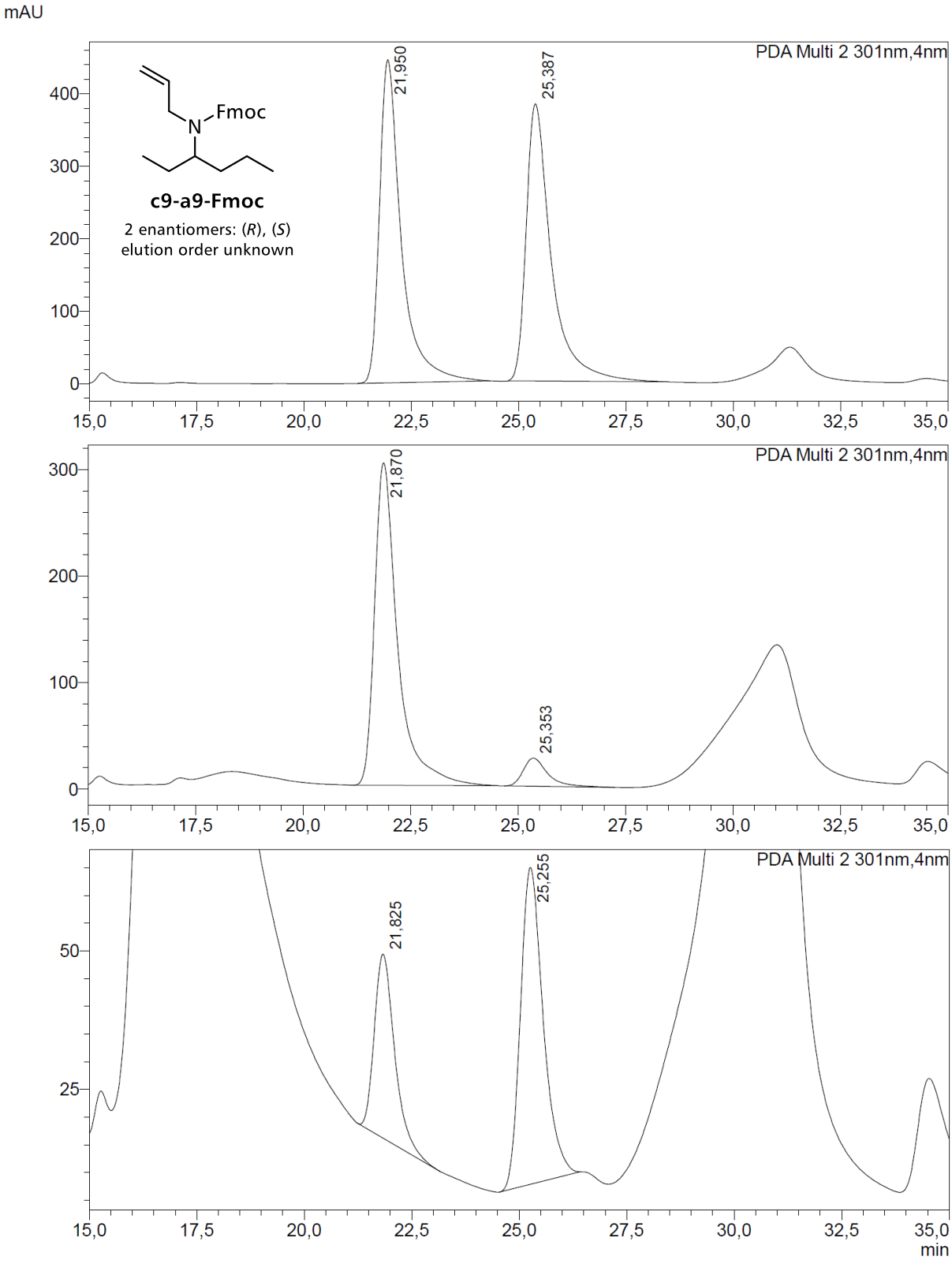


Figure S168. Chromatographic separation of the enantiomers of Fmoc-derivatised amine **c9-a9-Fmoc** using HPLC method HPLC-C7. Elution order of enantiomers unknown. Racemic reference (top), biotransformation using IR0043 (middle), biotransformation using IR1855 (bottom).

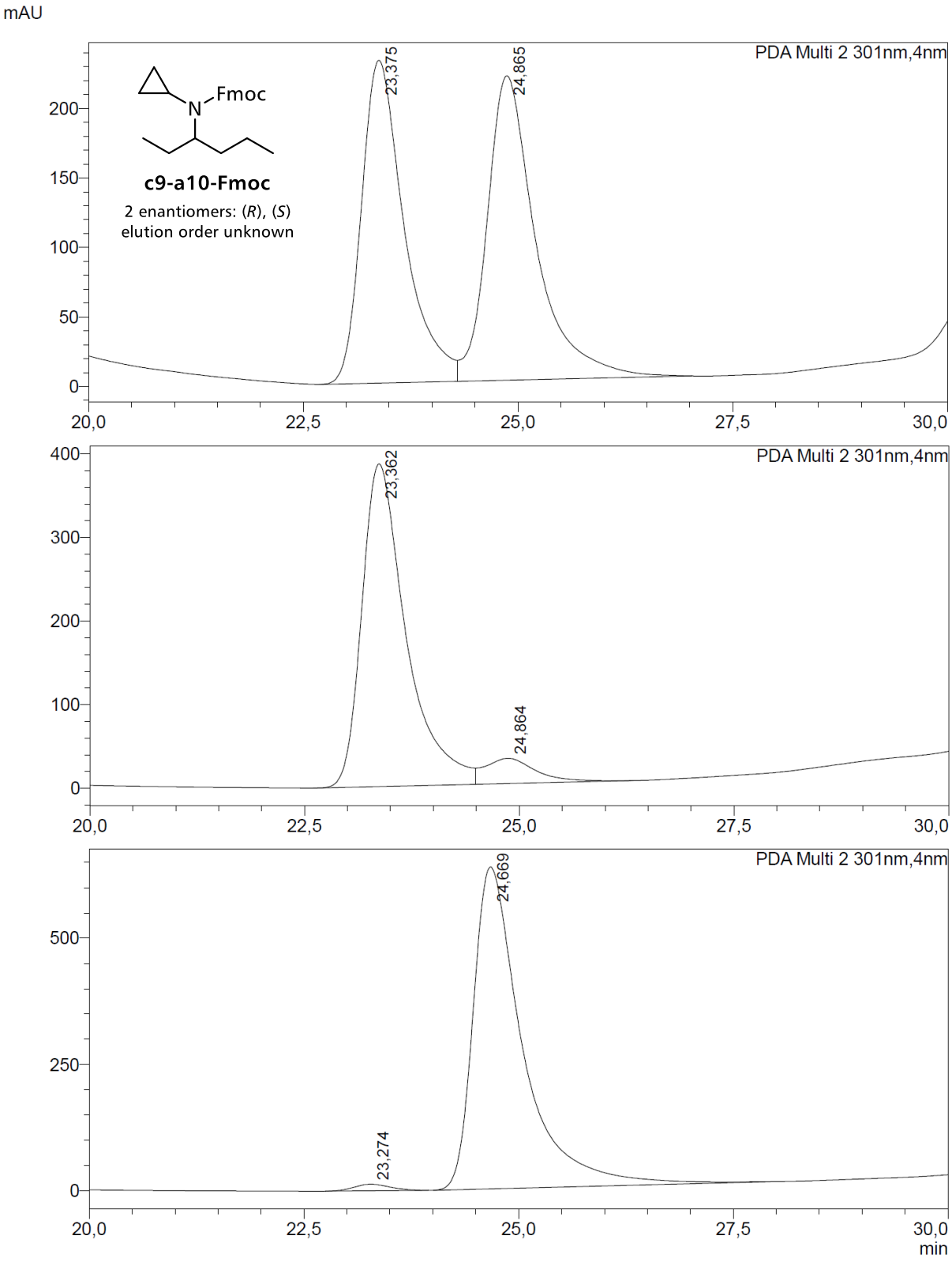


Figure S169. Chromatographic separation of the enantiomers of Fmoc-derivatised amine **c9-a10-Fmoc** using HPLC method HPLC-C7. Elution order of enantiomers unknown. Racemic reference (top), biotransformation using IR0393(middle), biotransformation using IR1855 (bottom).

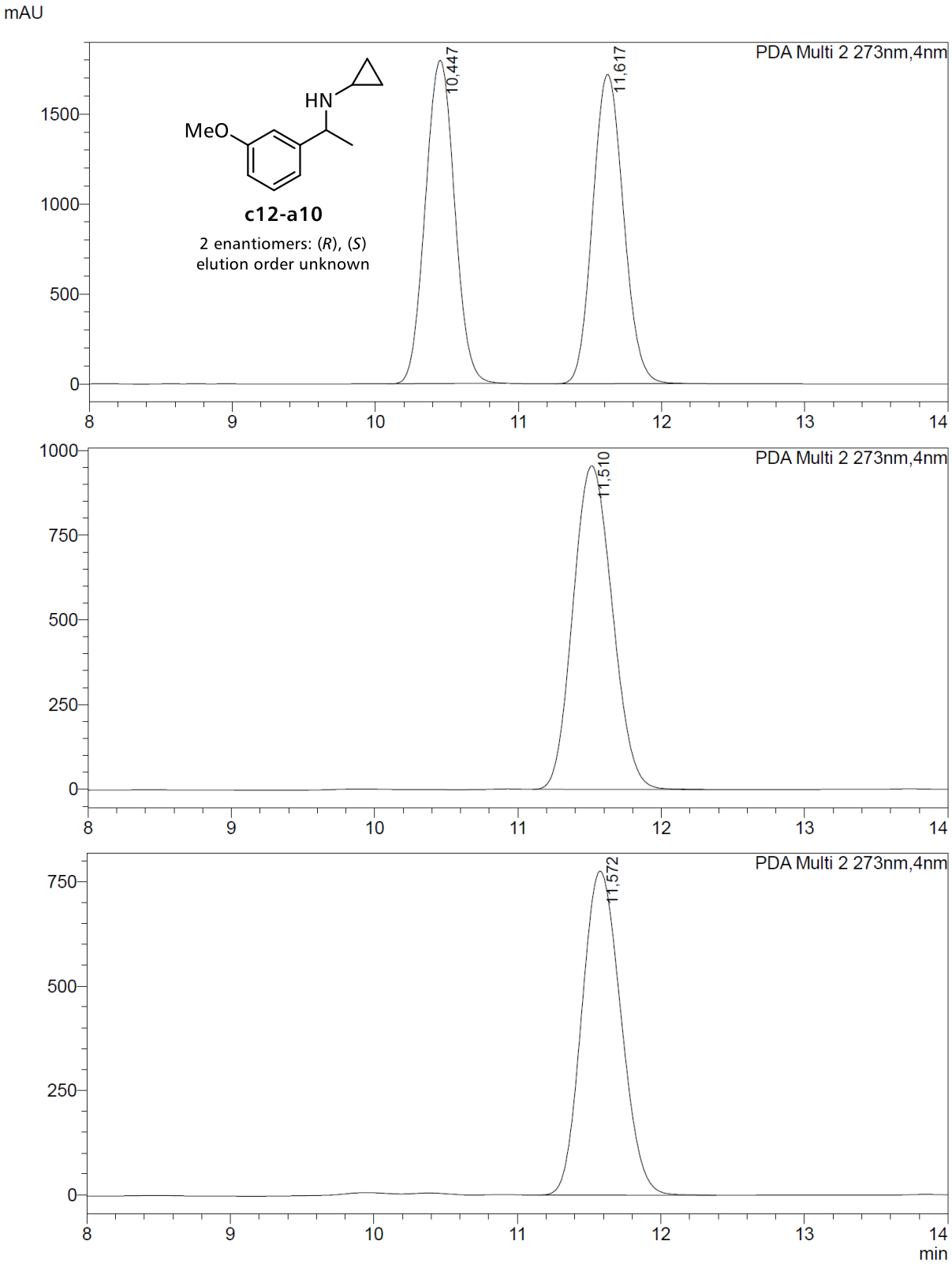


Figure S170. Chromatographic separation of the enantiomers of amine **c12-a10** using HPLC method HPLC-C2. Elution order of enantiomers unknown. Racemic reference (top), biotransformation using IR1855 (middle), biotransformation using IR2253 (bottom).

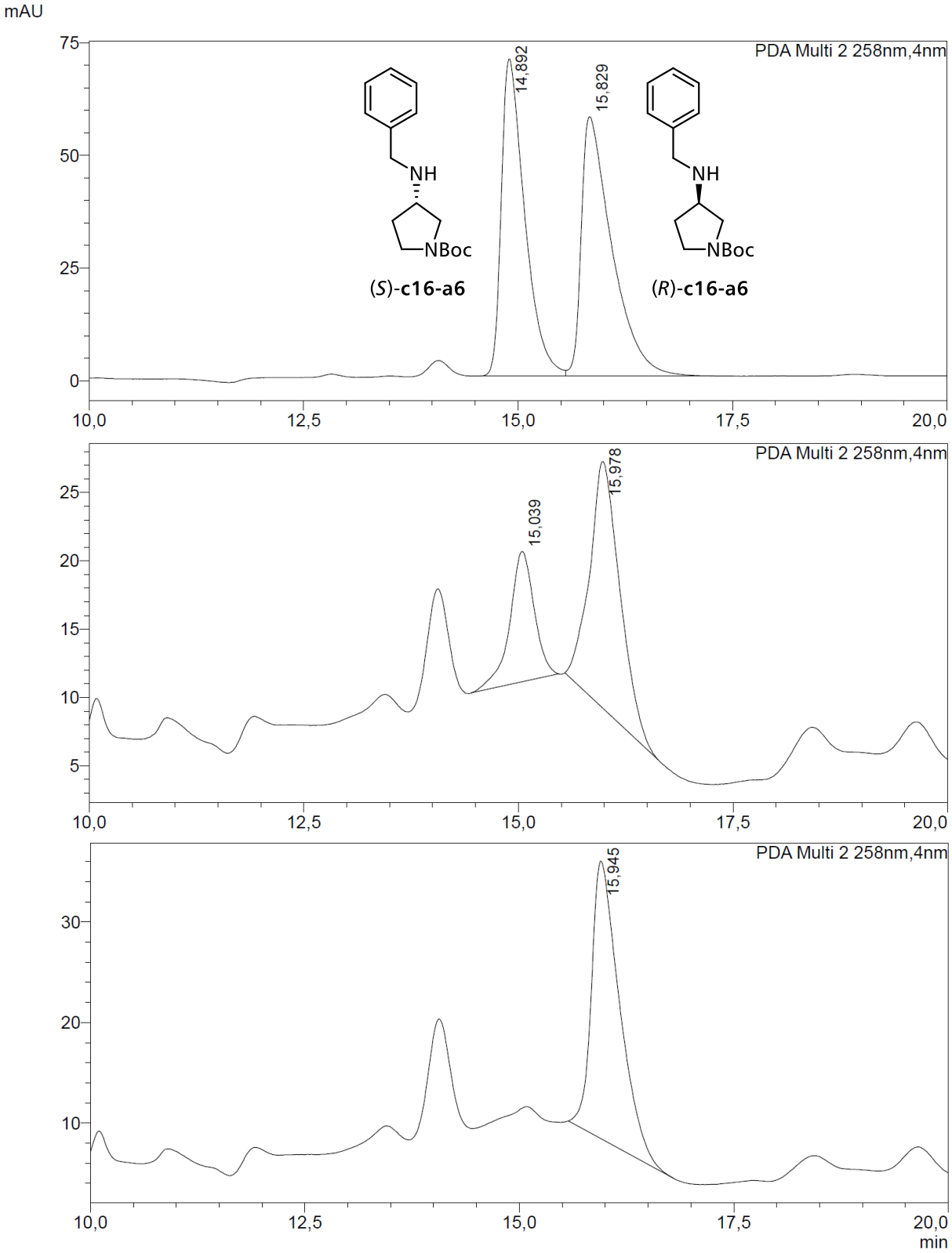


Figure S171. Chromatographic separation of the enantiomers of amine **c16-a6** using HPLC method HPLC-C9. Elution order: (*S*)-**c16-a6** (t_r 14.9 min), (*R*)-**c16-a6** (t_r 15.8 min). Racemic reference (top), moderately (*R*)-selective biotransformation using IR2128 (middle), (*R*)-selective biotransformation using IR1437 (bottom).

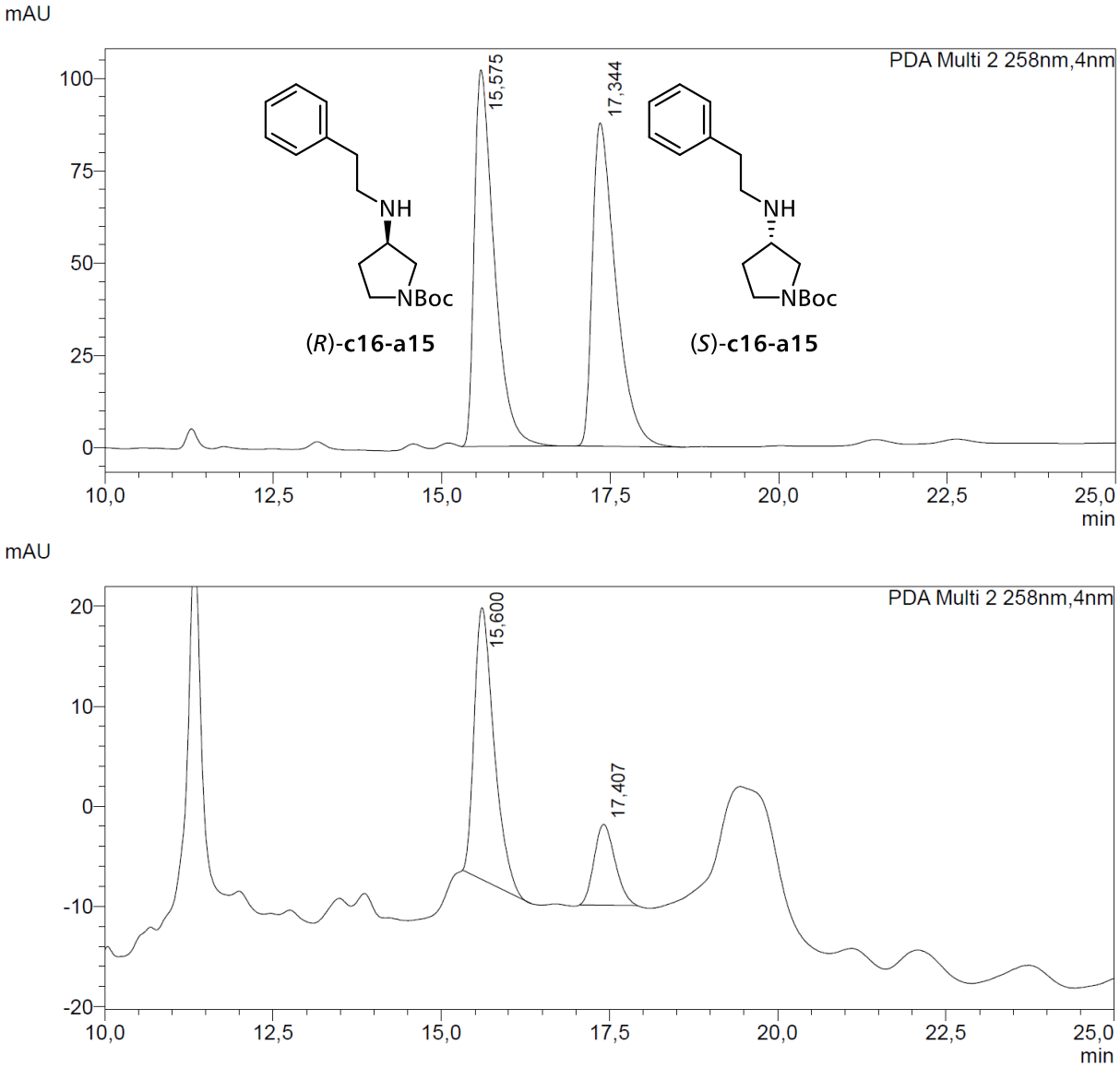


Figure S172. Chromatographic separation of the enantiomers of amine **c16-a15** using HPLC method HPLC-C6. Elution order: (*R*)-**c16-a15** (t_r 15.6 min), (*S*)-**c16-a15** (t_r 17.3 min). Racemic reference (upper), moderately (*R*)-selective biotransformation using IR0464 (lower).

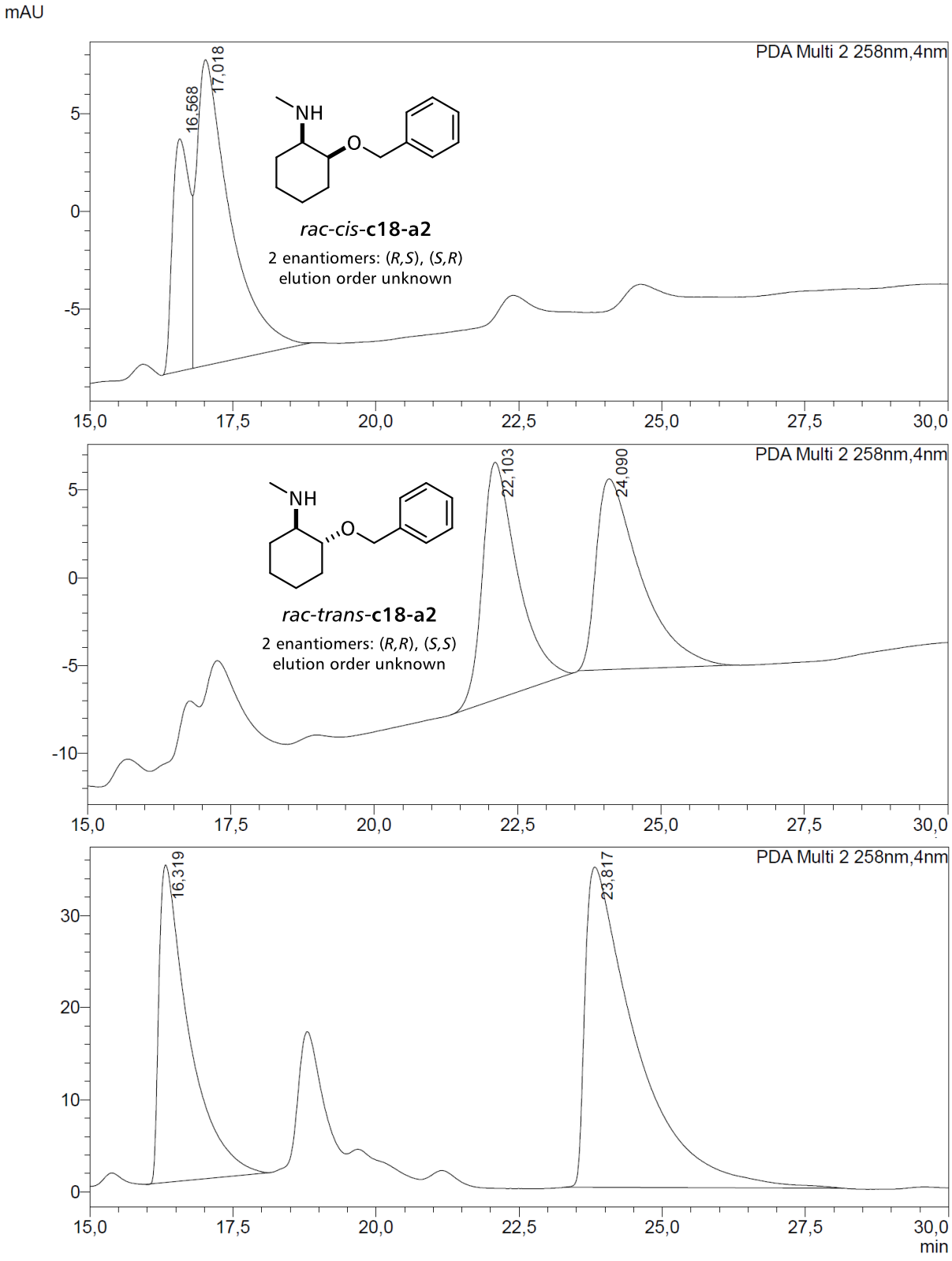


Figure S173. Chromatographic separation of the enantiomers of amine **c18-a2** using HPLC method HPLC-C7. Elution order of enantiomers unknown. Racemic reference of *cis*-diastereomer (top), racemic reference of *trans*-diastereomer (middle), biotransformation using IR1855 (bottom).

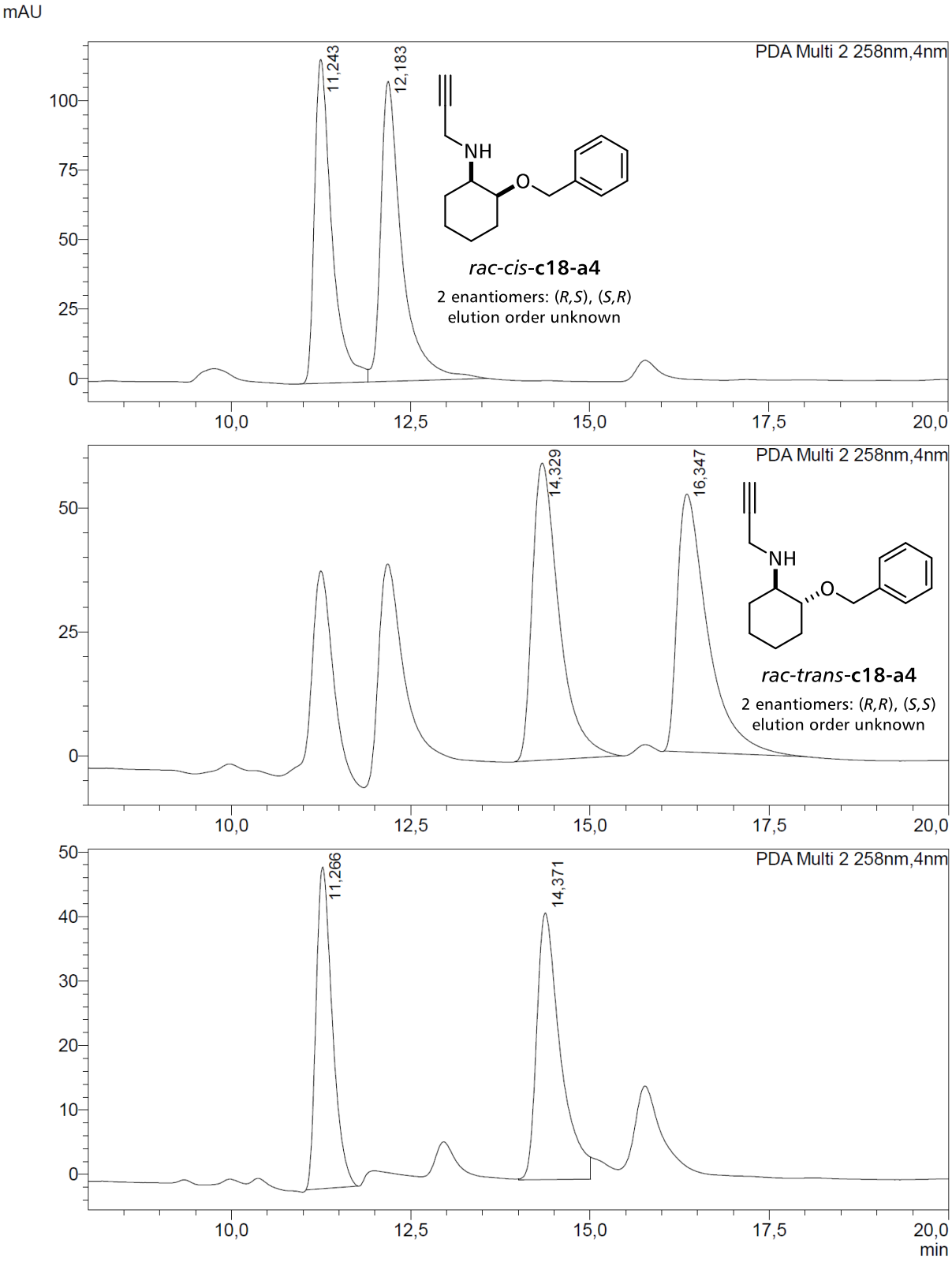


Figure S174. Chromatographic separation of the enantiomers of amine **c18-a4** using HPLC method HPLC-C8. Elution order of enantiomers unknown. Racemic reference of *cis*-diastereomer (top), racemic reference of *trans*-diastereomer (middle), biotransformation using IR0064 (bottom).

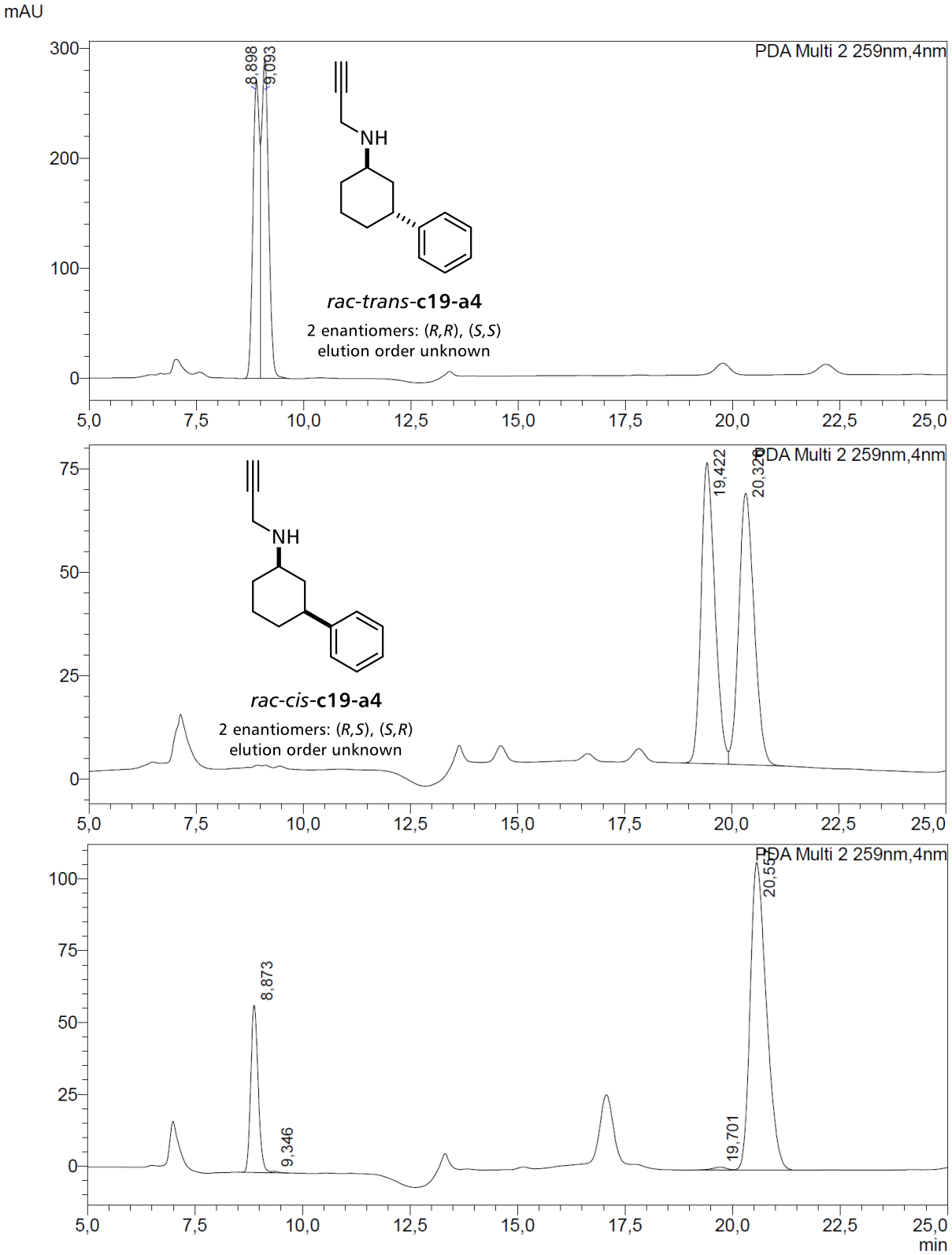


Figure S175. Chromatographic separation of the enantiomers of amine **c19-a4** using HPLC method HPLC-C15. Elution order of enantiomers unknown. Racemic reference of *trans*-diastereomer (top), racemic reference of *cis*-diastereomer (middle), biotransformation using IR0233 (bottom).

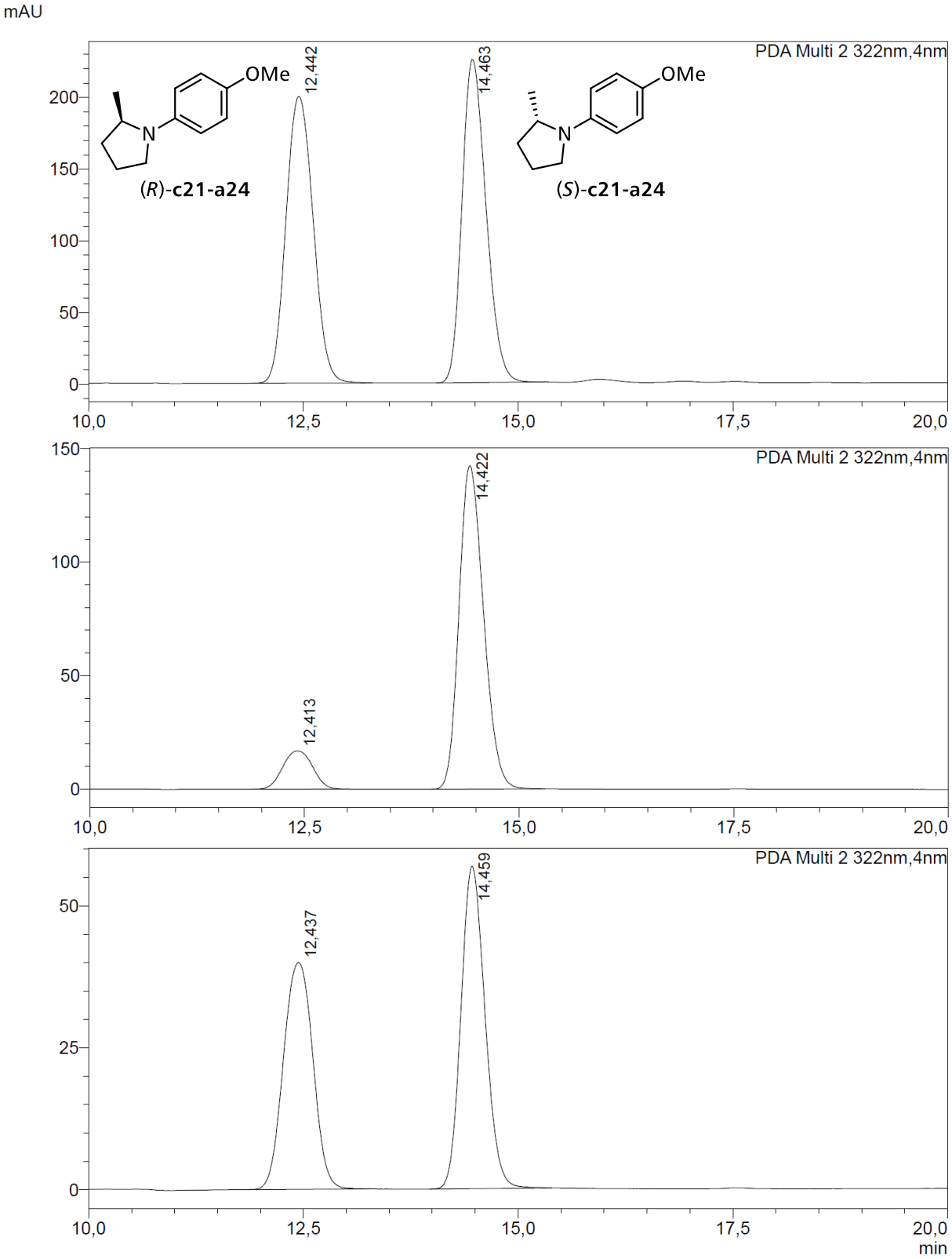


Figure S176. Chromatographic separation of the enantiomers of amine **c21-a24** using HPLC method HPLC-C3. Elution order: (*R*)-**c21-a24** (t_r 12.4 min), (*S*)-**c21-a24** (t_r 14.5 min). Racemic reference (top), moderately (*S*)-selective biotransformation using IR0035 (middle), moderately (*S*)-selective biotransformation using IR0052 (bottom).

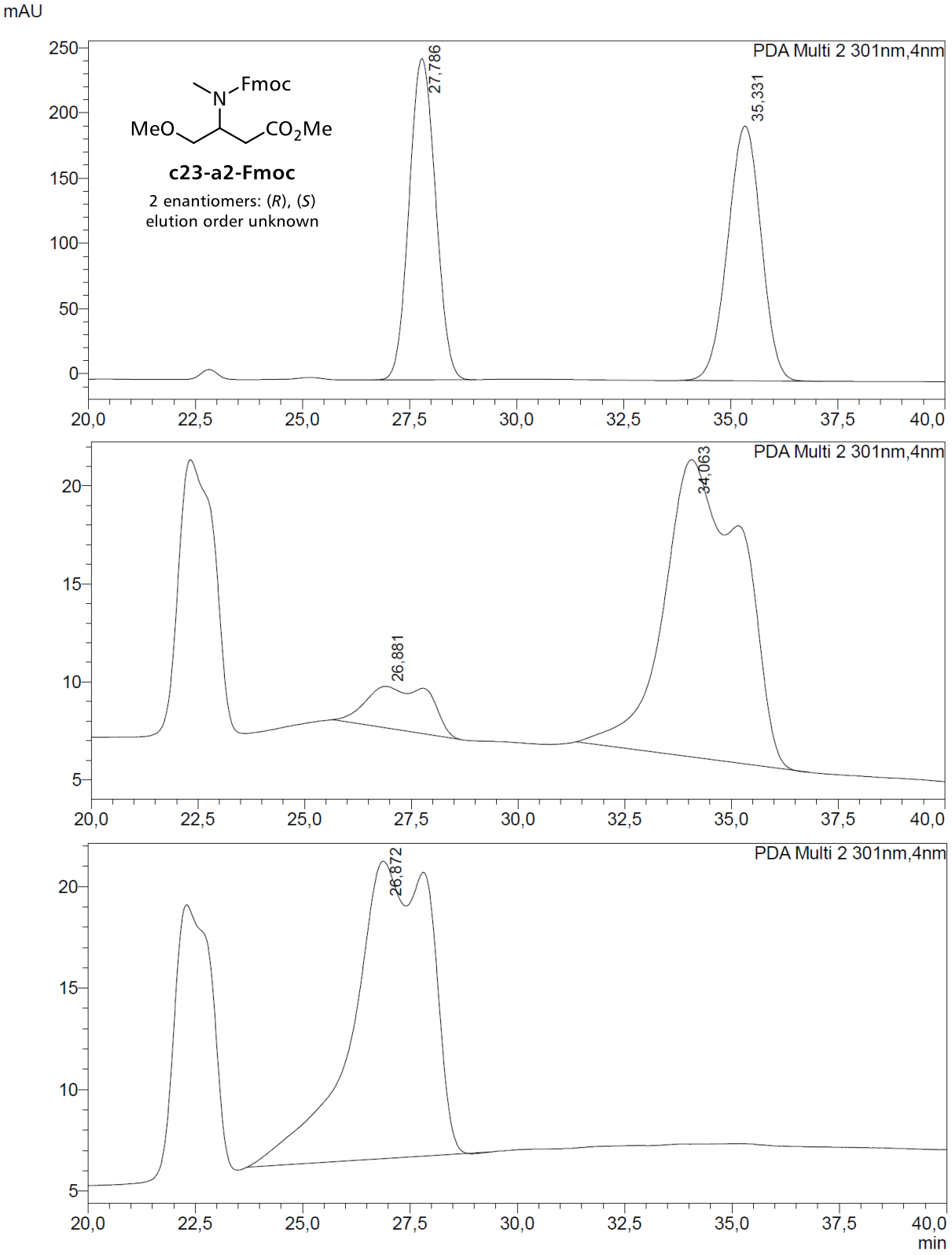


Figure S177. Chromatographic separation of the enantiomers of Fmoc-derivatised amine **c23-a2-Fmoc** using HPLC method HPLC-C14. Elution order of enantiomers unknown. Racemic reference (top), biotransformation using IR0063 (middle), biotransformation using IR0035 (bottom). *Note:* The peak splitting evident in the lower two chromatograms was only observed in biotransformation samples and could not be prevented by purifying the sample (using small-scale column chromatography) before Fmoc derivatisation.

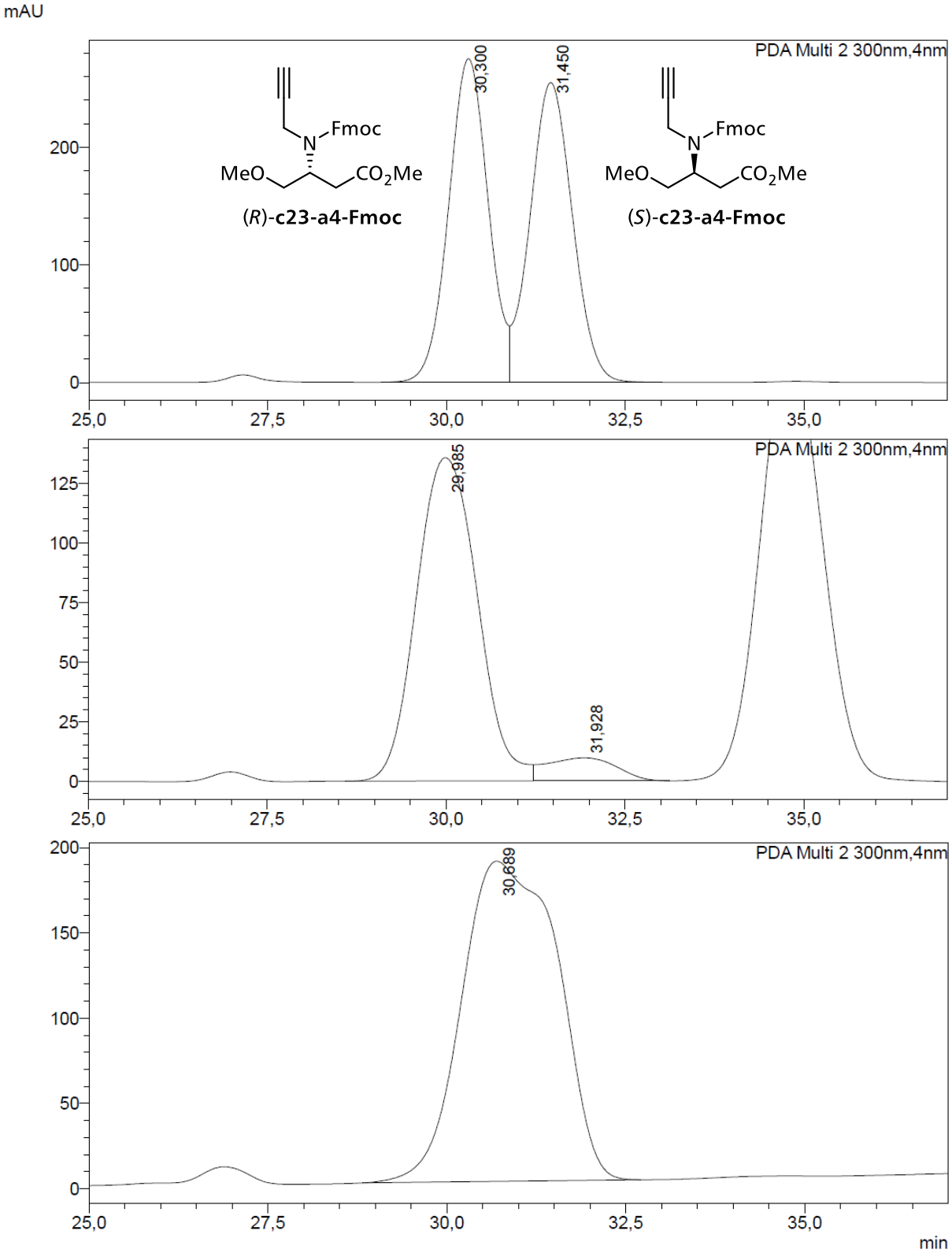


Figure S178. Chromatographic separation of the enantiomers of Fmoc-derivatised amine **c23-a4-Fmoc** using HPLC method HPLC-C12. Elution order: (*R*)-**c23-a4-Fmoc** (t_r 30.3 min), (*S*)-**c23-a4-Fmoc** (t_r 31.5 min). Racemic reference (top), independently synthesised (*R*)-enantiomer (middle), biotransformation using IR0041 (bottom). *Note:* The peak splitting evident in the lower chromatogram was only observed in biotransformation samples and could not be prevented by purifying the sample (using small-scale column chromatography) before Fmoc derivatisation.

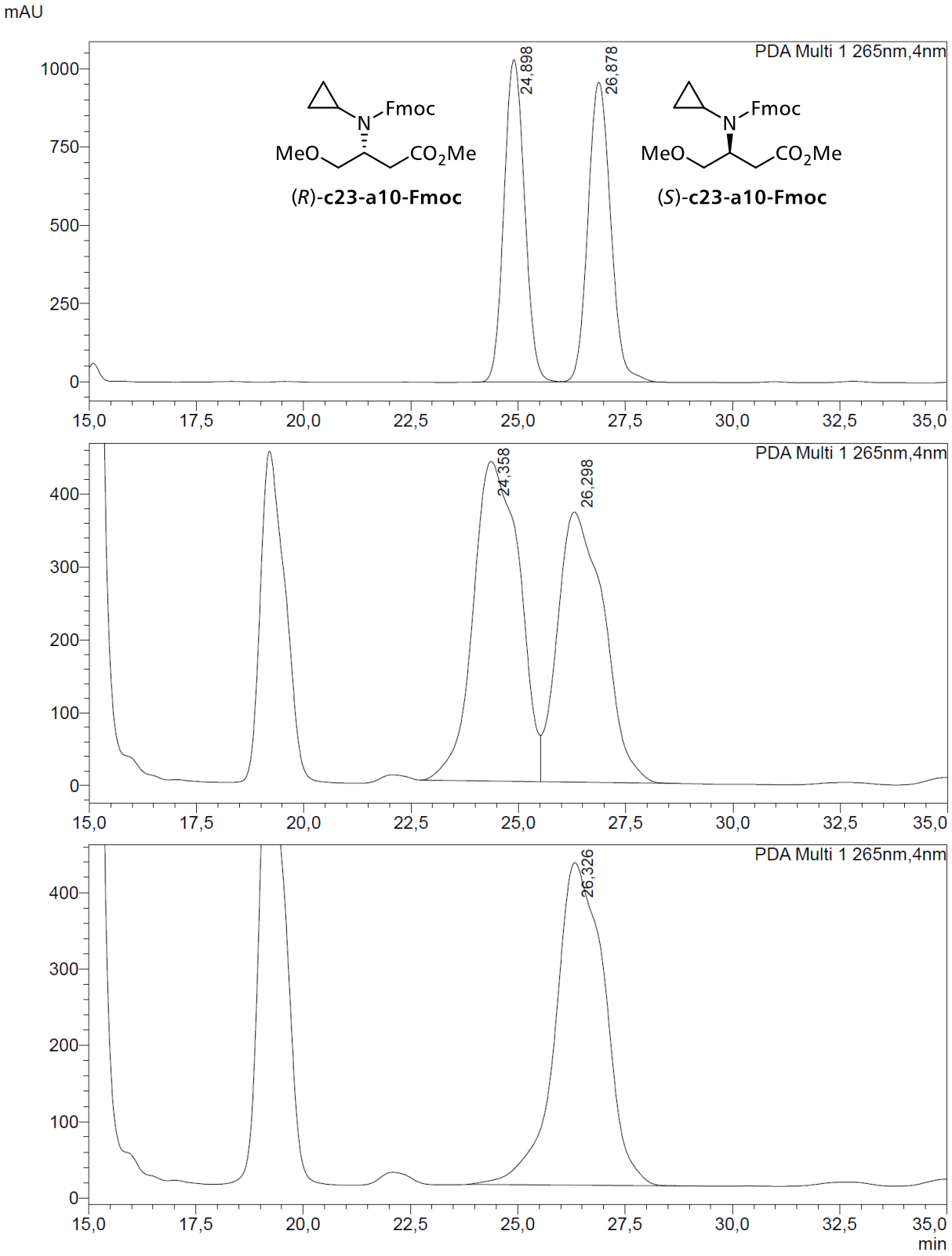


Figure S179. Chromatographic separation of the enantiomers of Fmoc-derivatised amine **c23-a10-Fmoc** using HPLC method HPLC-C12. Elution order of enantiomers unknown. Racemic reference (top), biotransformation using IR0063 (middle), biotransformation using IR0035 (bottom). *Note:* The peak splitting evident in the lower two chromatograms was only observed in biotransformation samples and could not be prevented by purifying the sample (using small-scale column chromatography) before Fmoc derivatisation.

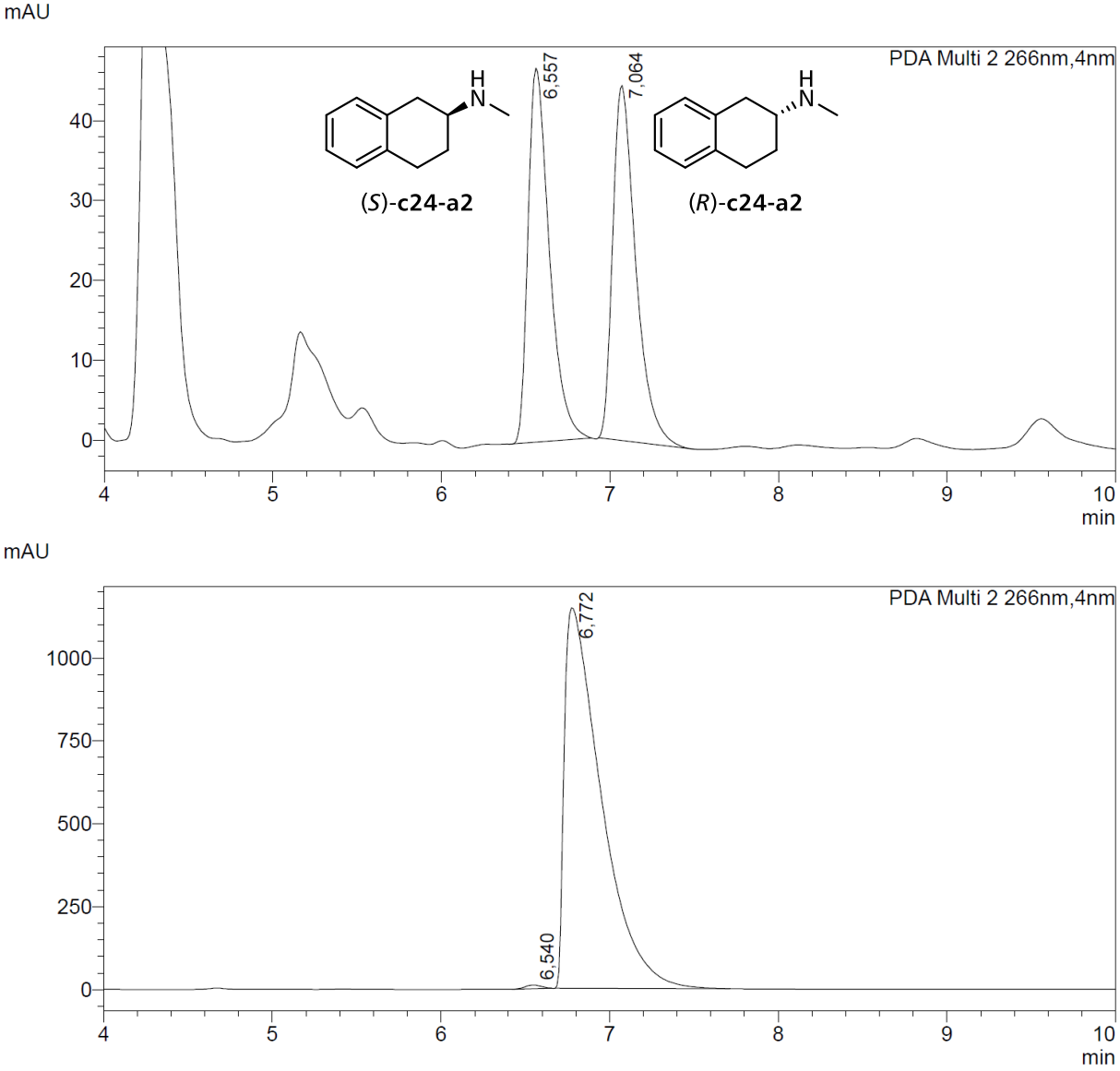


Figure S180. Chromatographic separation of the enantiomers of amine **c24-a2** using HPLC method HPLC-C11. Elution order: (*S*)-**c24-a2** (t_r 6.6 min), (*R*)-**c24-a2** (t_r 7.1 min). Racemic reference (upper), (*R*)-selective biotransformation using IR0035 (lower).

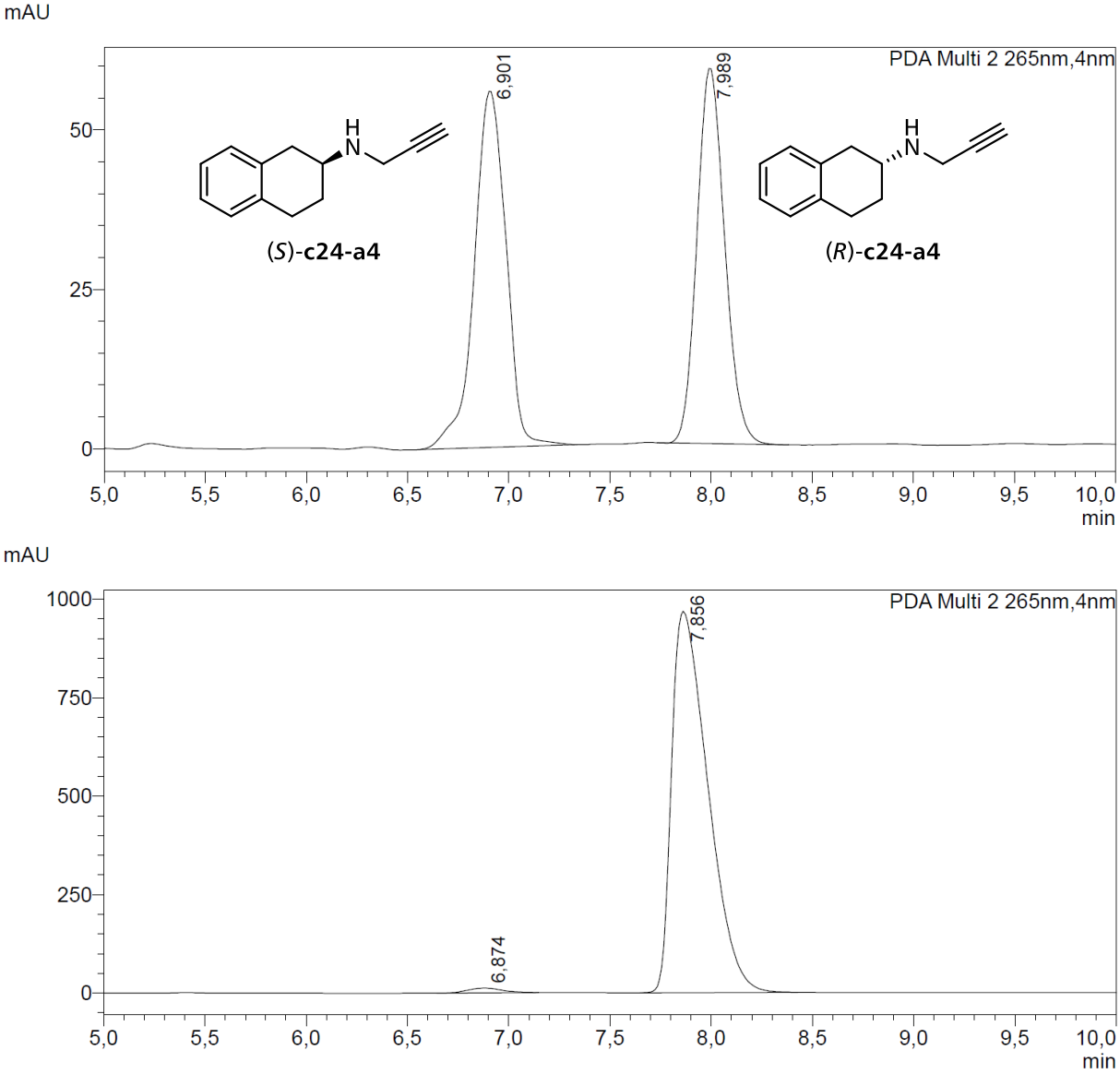


Figure S181. Chromatographic separation of the enantiomers of amine **c24-a4** using HPLC method HPLC-C10. Elution order: (*S*)-**c24-a4** (t_r 6.9 min), (*R*)-**c24-a4** (t_r 8.0 min). Racemic reference (upper), (*R*)-selective biotransformation using IR2021 (lower).

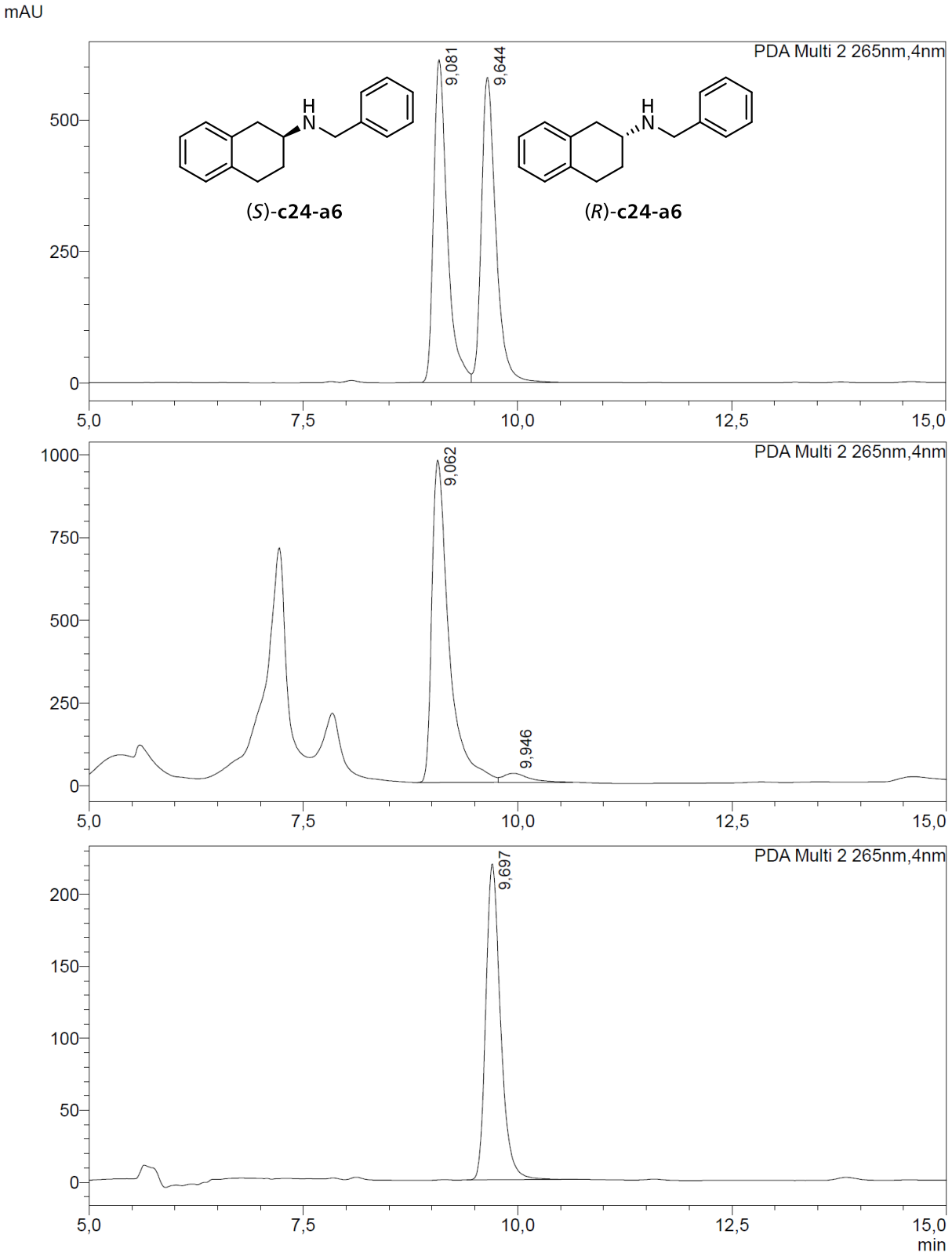


Figure S182. Chromatographic separation of the enantiomers of amine **c24-a6** using HPLC method HPLC-C5. Elution order: (*S*)-**c24-a6** (t_r 9.1 min), (*R*)-**c24-a6** (t_r 9.6 min). Racemic reference (top), independently synthesised (*S*)-enantiomer (middle), (*R*)-selective biotransformation using IR2147 (bottom).

Determination of absolute configurations:
Where absolute configurations are reported for reductive amination products, these were determined by one or more of the following methods: (*i*) Comparison of GC or HPLC retention time with a commercially available or independently synthesised, enantiomerically pure reference compound, (*ii*) comparison of the sign of optical rotation of the isolated compound with values reported in the literature, (*iii*) comparison of GC or HPLC elution order of enantiomers with the elution order reported in the literature for identical chromatographic conditions, and (*iv*) analogy of GC or HPLC elution order of enantiomers with a closely related compound from our own data set. Table S35 shows the methods used for each chiral amine product and lists relevant literature references, where applicable.

Table S35. Summary of methods used for determining absolute configurations.

	Method			
Product	*Ref. compound*	*Optical rotation*	*Elution comparison*	*Elution analogy*
c3-a2	●			
c3-a4	●			
c6-a2	●			
c6-a4	●			
c6-a6	●			
c6-a7	●			
c7-a2	●			
c7-a4	●			
c7-a6	●			
c7-a7	●			
c8-a2	●			
c8-a4	●			
c8-a9	●			
c8-a10		● (ref. 118)	● (ref. 118)	
c10-a9	●			
c10-a10	●			
c16-a2	●			
c16-a4	●			
c16-a6	●			
c16-a15	●			
c21-a4	●			
c21-a24	●			
c22-a4	●			
c23-a4	●			
c23-a10				● (**c23-a4**)
c24-a2	●		● (ref. 119)	
c24-a4	●		● (ref. 119)	
c24-a6	●			

NMR and MS Spectra

Reference Compounds

Provided Spectra:

- **c1-a4:** ^{1}H NMR, ^{13}C NMR
- **c2-a4:** ^{1}H NMR, ^{13}C NMR
- **c2-a10:** ^{1}H NMR, ^{13}C NMR
- *rac*-**c3-a4:** ^{1}H NMR, ^{13}C NMR
- *rac*-**c3-a6:** ^{1}H NMR, ^{13}C NMR
- *rac*-**c3-a7:** ^{1}H NMR, ^{13}C NMR
- *all-rac*-**c4-a1-Ac:** ^{1}H NMR, ^{13}C NMR
- *all-rac*-**c4-a2:** ^{1}H NMR, ^{13}C NMR
- *all-rac*-**c4-a6:** ^{1}H NMR, ^{13}C NMR
- *all-rac*-**c4-a7:** ^{1}H NMR, ^{13}C NMR
- (*R*)-**c5-a4:** ^{1}H NMR, ^{13}C NMR
- (*S*)-**c5-a4:** ^{1}H NMR, ^{13}C NMR
- *rac*-**c6-a2:** ^{1}H NMR, ^{13}C NMR
- *rac*-**c6-a4:** ^{1}H NMR, ^{13}C NMR
- *rac*-**c6-a6:** ^{1}H NMR, ^{13}C NMR
- *rac*-**c6-a7:** ^{1}H NMR, ^{13}C NMR
- *rac*-**c7-a2-Ac:** ^{1}H NMR, ^{13}C NMR
- *rac*-**c7-a4-Ac:** ^{1}H NMR, ^{13}C NMR
- *rac*-**c7-a6:** ^{1}H NMR, ^{13}C NMR
- *rac*-**c7-a7:** ^{1}H NMR, ^{13}C NMR
- *rac*-**c8-a1:** ^{1}H NMR, ^{13}C NMR
- (*S*)-**c8-a1:** ^{1}H NMR, ^{13}C NMR
- *rac*-**c8-a2:** ^{1}H NMR, ^{13}C NMR
- *rac*-**c8-a4:** ^{1}H NMR, ^{13}C NMR
- *rac*-**c8-a6:** ^{1}H NMR, ^{13}C NMR
- *rac*-**c8-a7:** ^{1}H NMR, ^{13}C NMR
- *rac*-**c8-a8:** ^{1}H NMR, ^{13}C NMR
- *rac*-**c8-a9:** ^{1}H NMR, ^{13}C NMR
- *rac*-**c8-a10:** ^{1}H NMR, ^{13}C NMR
- *rac*-**c8-a11:** ^{1}H NMR, ^{13}C NMR
- *rac*-**c8-a12:** ^{1}H NMR, ^{13}C NMR
- *rac*-**c8-a15:** ^{1}H NMR, ^{13}C NMR
- *rac*-**c8-a22:** ^{1}H NMR, ^{13}C NMR
- *rac*-**c8-a23:** ^{1}H NMR, ^{13}C NMR
- *rac*-**c9-a8:** ^{1}H NMR, ^{13}C NMR
- *rac*-**c9-a9:** ^{1}H NMR, ^{13}C NMR
- *rac*-**c9-a10:** ^{1}H NMR, ^{13}C NMR
- *rac*-**c9-a11:** ^{1}H NMR, ^{13}C NMR
- *rac*-**c9-a12:** ^{1}H NMR, ^{13}C NMR
- *rac*-**c9-a15:** ^{1}H NMR, ^{13}C NMR
- *rac*-**c9-a16:** ^{1}H NMR, ^{13}C NMR
- *rac*-**c9-a21:** ^{1}H NMR, ^{13}C NMR
- *rac*-**c9-a22:** ^{1}H NMR, ^{13}C NMR
- *rac*-**c9-a23:** ^{1}H NMR, ^{13}C NMR
- *rac*-**c10-a8:** ^{1}H NMR, ^{13}C NMR
- *rac*-**c10-a9:** ^{1}H NMR, ^{13}C NMR
- *rac*-**c10-a10:** ^{1}H NMR, ^{13}C NMR
- *rac*-**c10-a11:** ^{1}H NMR, ^{13}C NMR
- *rac*-**c10-a12:** ^{1}H NMR, ^{13}C NMR
- *rac*-**c10-a15:** ^{1}H NMR, ^{13}C NMR
- *rac*-**c10-a16:** ^{1}H NMR, ^{13}C NMR
- *rac*-**c10-a20:** ^{1}H NMR, ^{13}C NMR
- *rac*-**c10-a21:** ^{1}H NMR, ^{13}C NMR
- *rac*-**c10-a22:** ^{1}H NMR, ^{13}C NMR
- *rac*-**c10-a23:** ^{1}H NMR, ^{13}C NMR
- **c11-a8:** ^{1}H NMR, ^{13}C NMR
- *rac*-**c12-a8:** ^{1}H NMR, ^{13}C NMR
- *rac*-**c12-a9:** ^{1}H NMR, ^{13}C NMR
- *rac*-**c12-a10:** ^{1}H NMR, ^{13}C NMR
- *rac*-**c12-a11:** ^{1}H NMR, ^{13}C NMR
- *rac*-**c12-a22:** ^{1}H NMR, ^{13}C NMR
- *rac*-**c12-a23:** ^{1}H NMR, ^{13}C NMR
- **c13-a22:** ^{1}H NMR, ^{13}C NMR
- **c11-a24:** ^{1}H NMR, ^{13}C NMR
- **c14-a4:** ^{1}H NMR, ^{13}C NMR
- **c14-a22:** ^{1}H NMR, ^{13}C NMR
- **c14-a24:** ^{1}H NMR, ^{13}C NMR
- *all-rac*-**c15-a2-Ac:** ^{1}H NMR, ^{13}C NMR
- *all-rac*-**c15-a4-Ac:** ^{1}H NMR, ^{13}C NMR
- *all-rac*-**c15-a22:** ^{1}H NMR, ^{13}C NMR
- *all-rac*-**c15-a24:** ^{1}H NMR, ^{13}C NMR
- *rac*-**c16-a4:** ^{1}H NMR, ^{13}C NMR
- *rac*-**c16-a6:** ^{1}H NMR, ^{13}C NMR
- *rac*-**c16-a15:** ^{1}H NMR, ^{13}C NMR
- *rac*-**c16-a22:** ^{1}H NMR, ^{13}C NMR
- *rac*-**c16-a24:** ^{1}H NMR, ^{13}C NMR
- *rac*-**c17-a2:** ^{1}H NMR, ^{13}C NMR
- *all-rac*-**c17-a4:** ^{1}H NMR, ^{13}C NMR
- *rac-cis*-**c17-a24:** ^{1}H NMR, ^{13}C NMR
- *rac-trans*-**c17-a24:** ^{1}H NMR, ^{13}C NMR
- *rac-cis*-**c18-a2:** ^{1}H NMR, ^{13}C NMR, NOESY
- *rac-trans*-**c18-a2:** ^{1}H NMR, ^{13}C NMR, NOESY
- *rac-cis*-**c18-a4:** ^{1}H NMR, ^{13}C NMR, NOESY
- *rac*-**c18-a22:** ^{1}H NMR, ^{13}C NMR
- *rac*-**c18-a24:** ^{1}H NMR, ^{13}C NMR
- *rac-trans*-**c19-a2:** ^{1}H NMR, ^{13}C NMR, NOESY
- *rac-trans*-**c19-a4:** ^{1}H NMR, ^{13}C NMR, NOESY
- *rac-cis*-**c19-a4:** ^{1}H NMR, ^{13}C NMR, NOESY
- *all-rac*-**c19-a22:** ^{1}H NMR, ^{13}C NMR
- *all-rac*-**c19-a24:** ^{1}H NMR, ^{13}C NMR
- **c20-a24:** ^{1}H NMR, ^{13}C NMR
- *rac*-**c21-a4:** ^{1}H NMR, ^{13}C NMR

Provided Spectra (continued):

- *rac*-**c21-a22:** ^{1}H NMR, ^{13}C NMR
- *rac*-**c21-a24:** ^{1}H NMR, ^{13}C NMR
- *rac*-**c22-a2:** ^{1}H NMR, ^{13}C NMR
- *rac*-**c22-a4:** ^{1}H NMR, ^{13}C NMR
- *rac*-**c22-a22:** ^{1}H NMR, ^{13}C NMR
- *rac*-**c22-a24:** ^{1}H NMR, ^{13}C NMR
- *rac*-**c23-a2:** ^{1}H NMR, ^{13}C NMR
- *rac*-**c23-a4:** ^{1}H NMR, ^{13}C NMR
- *rac*-**c23-a10:** ^{1}H NMR, ^{13}C NMR
- *rac*-**c23-a24:** ^{1}H NMR, ^{13}C NMR
- *rac*-**c24-a1:** ^{1}H NMR, ^{13}C NMR
- *rac*-**c24-a2:** ^{1}H NMR, ^{13}C NMR
- *rac*-**c24-a4:** ^{1}H NMR, ^{13}C NMR
- *rac*-**c24-a6:** ^{1}H NMR, ^{13}C NMR
- *rac*-**c24-a22:** ^{1}H NMR, ^{13}C NMR
- *rac*-**c24-a24:** ^{1}H NMR, ^{13}C NMR
- *rac*-**c25-a2:** ^{1}H NMR, ^{13}C NMR
- *rac*-**c25-a4:** ^{1}H NMR, ^{13}C NMR
- *rac*-**c25-a24:** ^{1}H NMR, ^{13}C NMR
- *rac*-**c26-a2:** ^{1}H NMR, ^{13}C NMR
- *rac*-**c26-a4:** ^{1}H NMR, ^{13}C NMR
- *rac*-**c26-a24:** ^{1}H NMR, ^{13}C NMR
- *rac*-**c27-a4:** ^{1}H NMR, ^{13}C NMR
- *rac*-**c27-a24:** ^{1}H NMR, ^{13}C NMR
- *rac*-**c28-a4:** ^{1}H NMR, ^{13}C NMR
- *rac*-**c30-a2:** ^{1}H NMR, ^{13}C NMR
- *rac*-**c30-a4:** ^{1}H NMR, ^{13}C NMR
- *rac*-**c30-a22:** ^{1}H NMR, ^{13}C NMR
- *rac*-**c31-a2:** ^{1}H NMR, ^{13}C NMR
- *rac*-**c31-a24:** ^{1}H NMR, ^{13}C NMR
- *rac*-**c33-a2:** ^{1}H NMR, ^{13}C NMR
- *rac*-**c33-a4:** ^{1}H NMR, ^{13}C NMR
- *rac*-**c36-a2:** ^{1}H NMR, ^{13}C NMR
- *rac*-**c36-a4:** ^{1}H NMR, ^{13}C NMR
- *rac*-**c36-a24:** ^{1}H NMR, ^{13}C NMR

All spectra are also openly available as raw data and MNOVA files in the Mendeley Data repository (https://data.mendeley.com/) at https://doi.org/10.17632/jn4sfsrz8x.2.

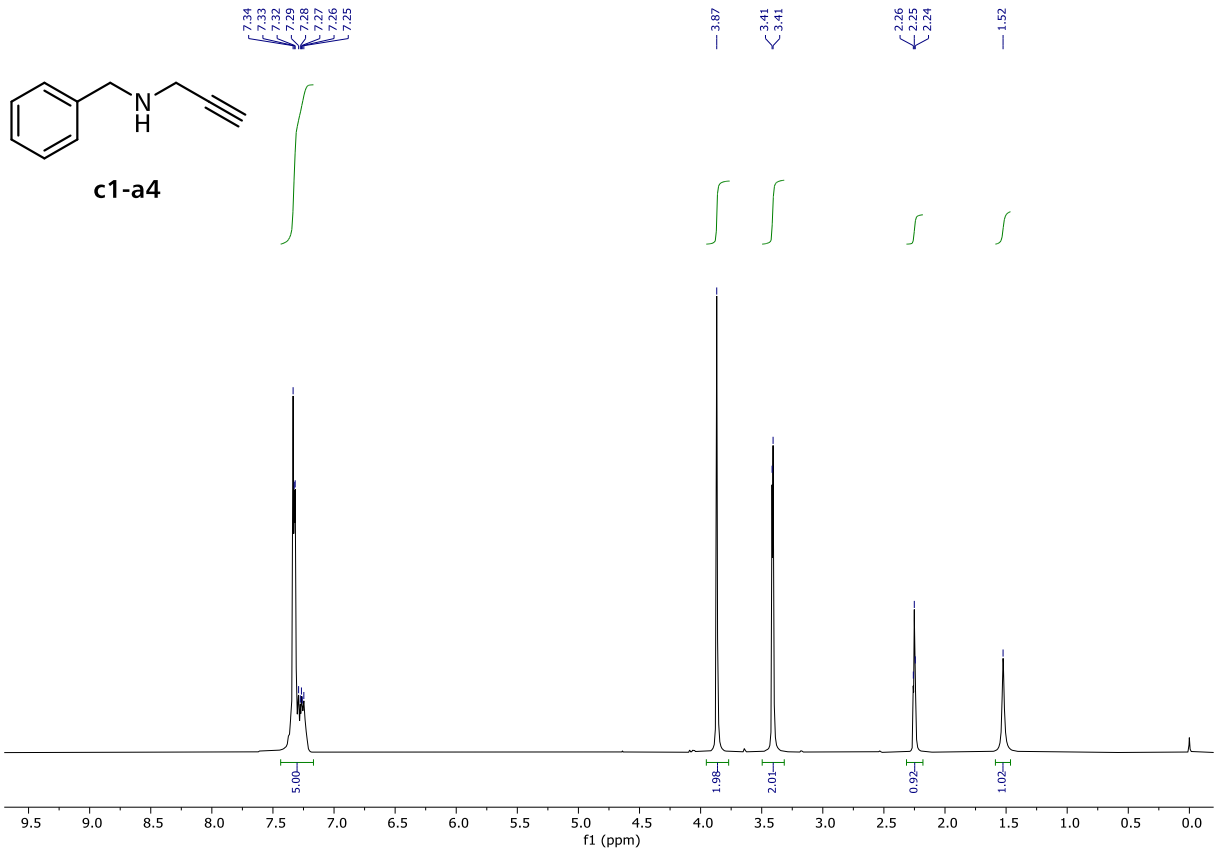


Figure S183. ^{1}H NMR spectrum of *N*-benzylprop-2-yn-1-amine (**c1-a4**).

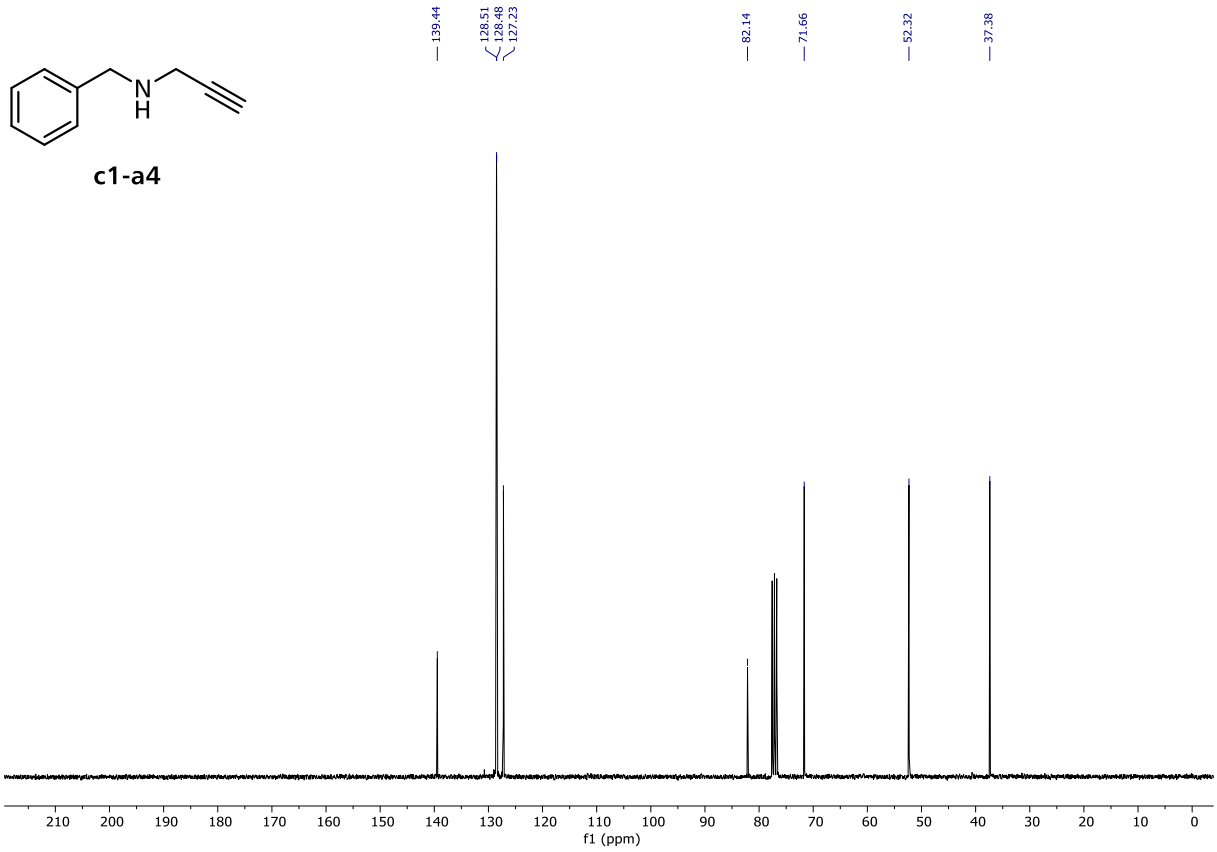


Figure S184. ^{13}C NMR spectrum of *N*-benzylprop-2-yn-1-amine (**c1-a4**).

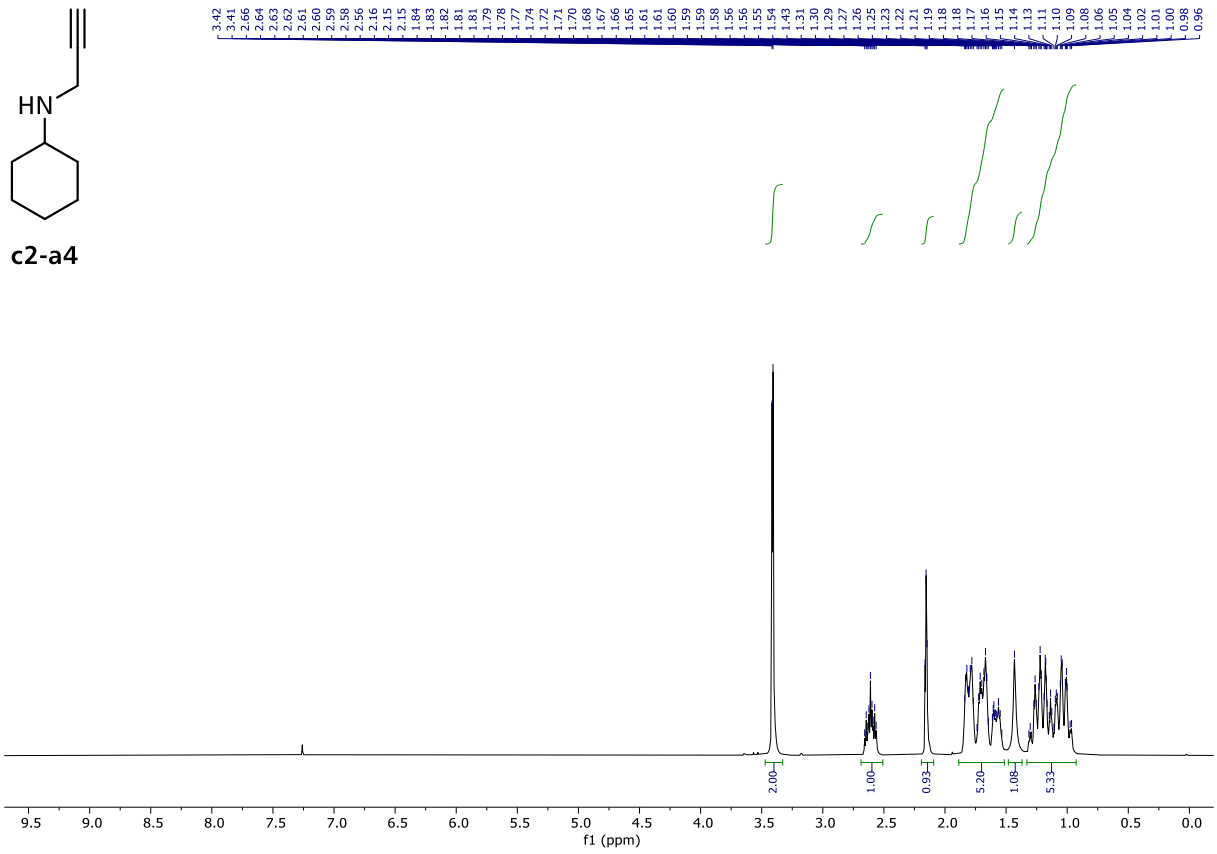


Figure S185. ^{1}H NMR spectrum of *N*-(prop-2-yn-1-yl)cyclohexanamine (**c2-a4**).

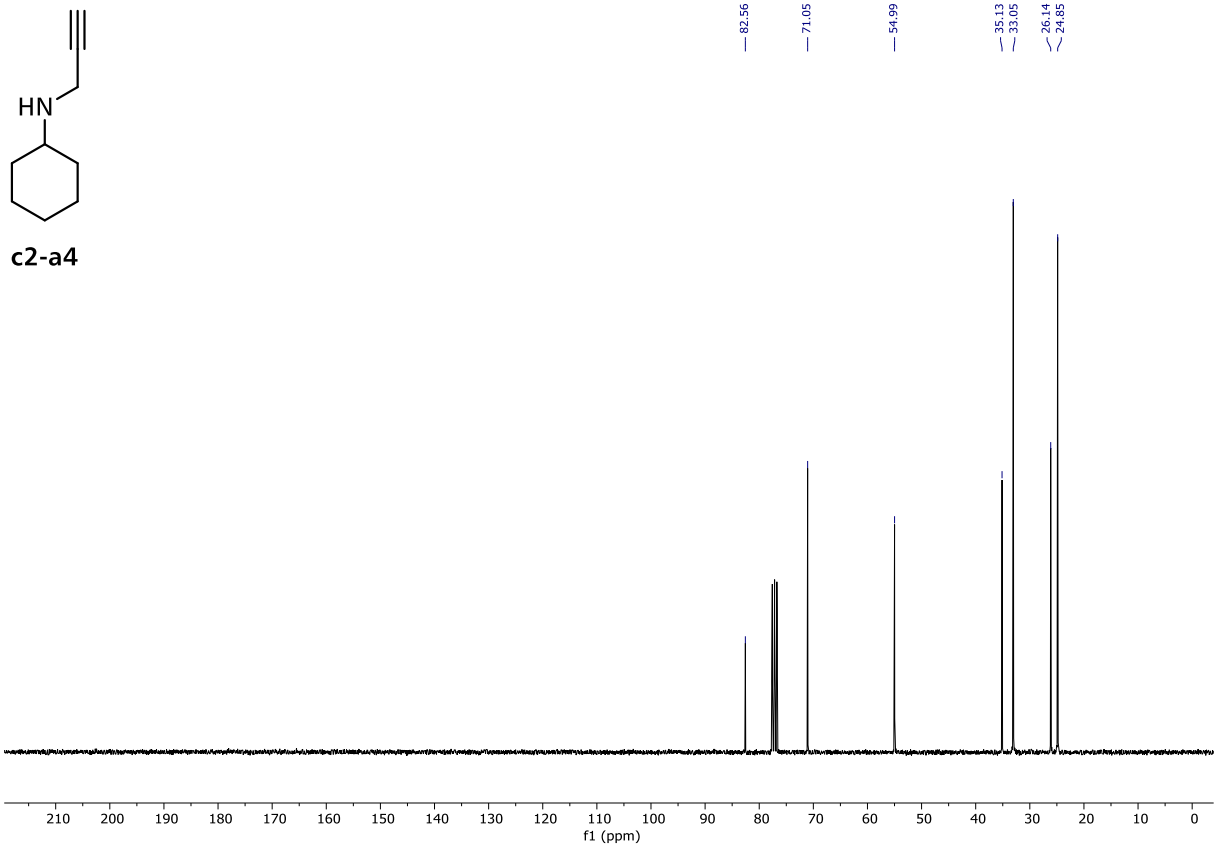


Figure S186. ^{13}C NMR spectrum of *N*-(prop-2-yn-1-yl)cyclohexanamine (**c2-a4**).

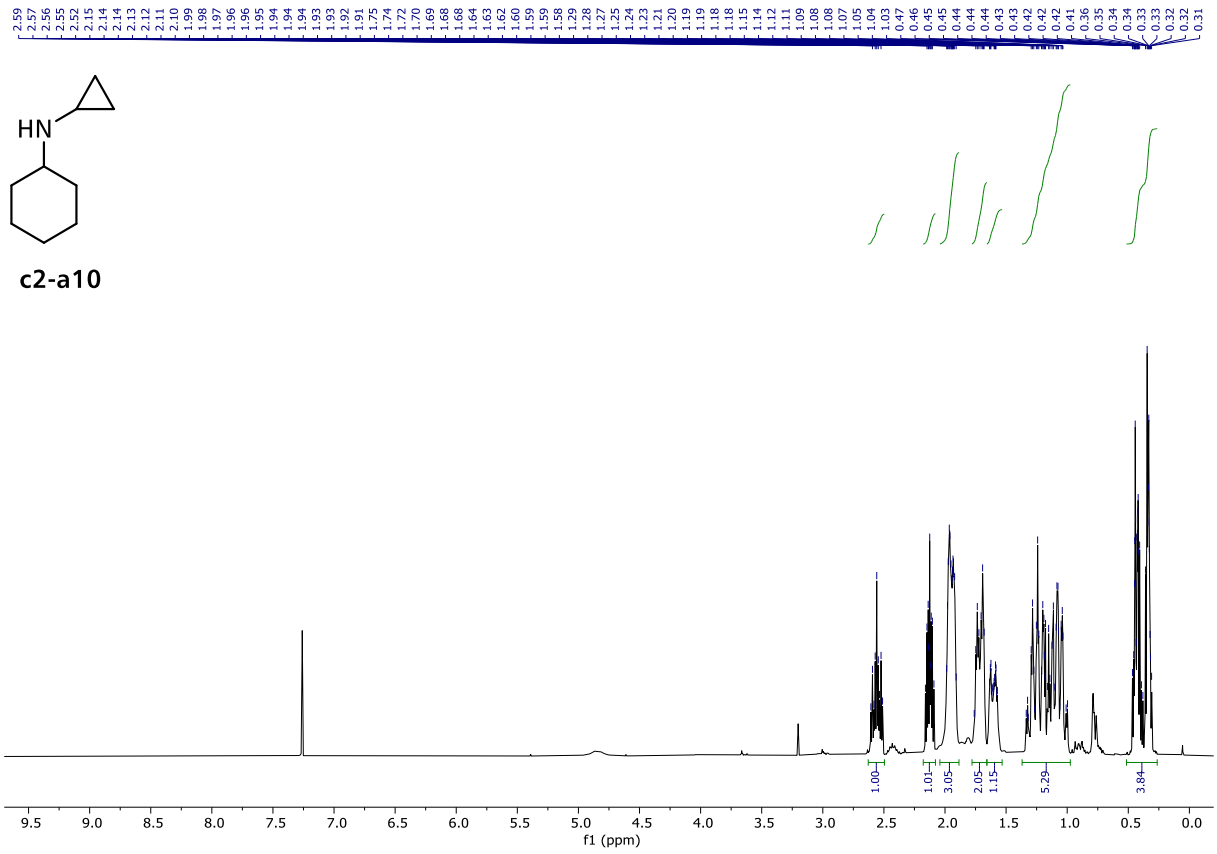


Figure S187. ^{1}H NMR spectrum of *N*-cyclopropylcyclohexanamine (**c2-a10**).

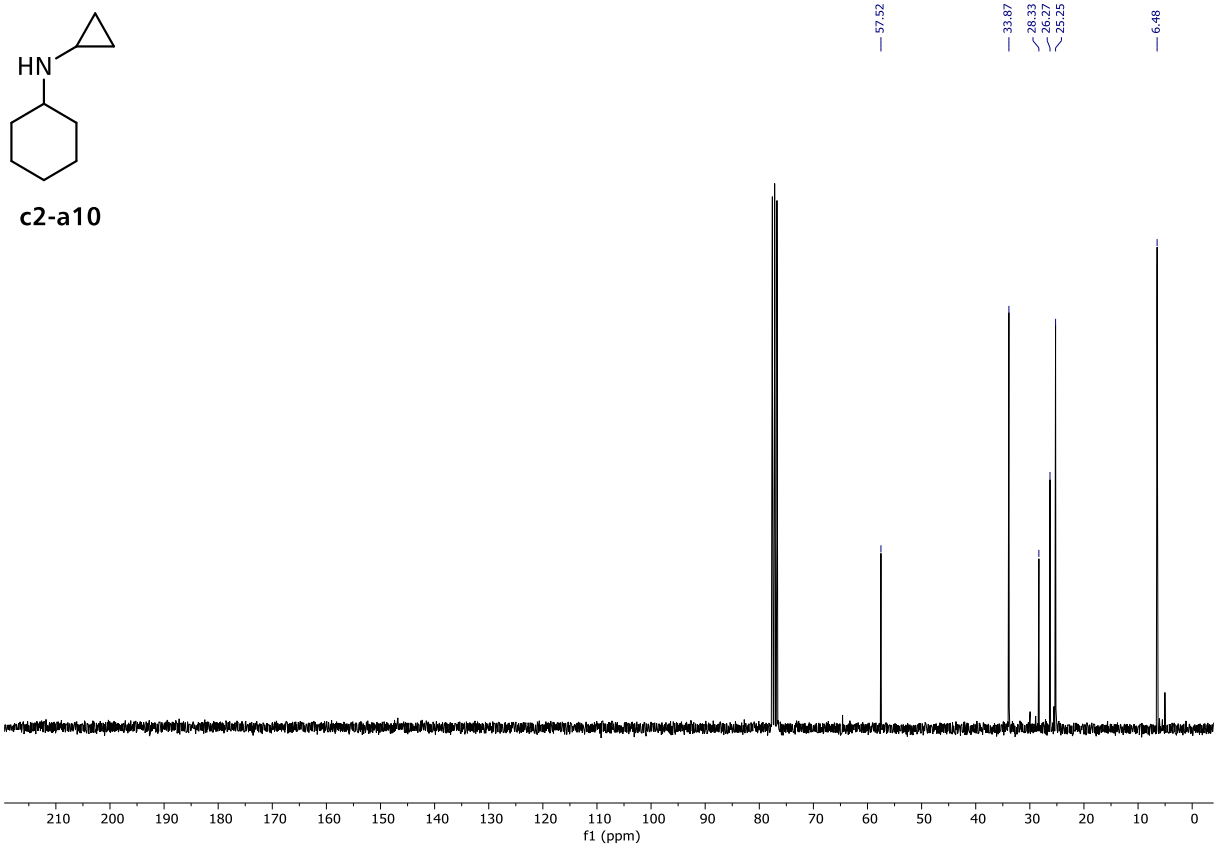


Figure S188. ^{13}C NMR spectrum of *N*-cyclopropylcyclohexanamine (**c2-a10**).

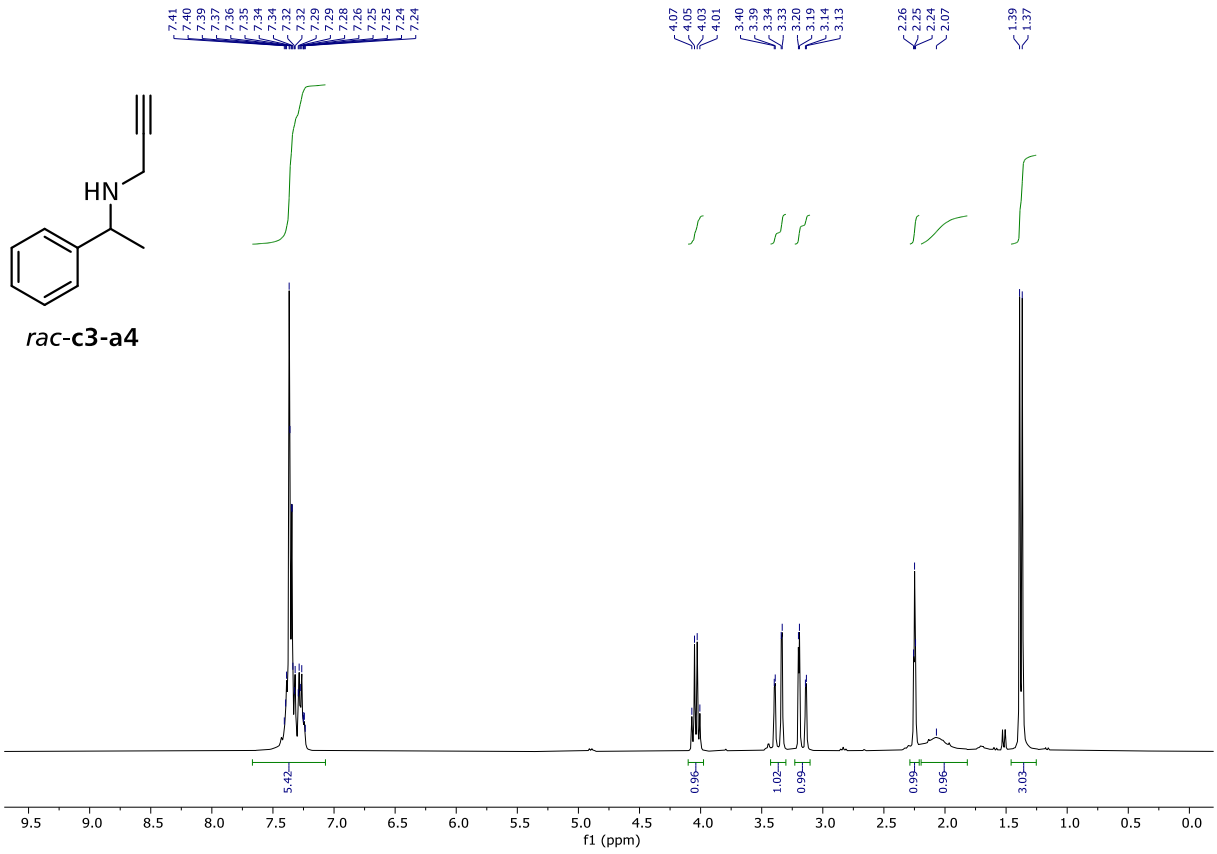


Figure S189. ^{1}H NMR spectrum of *rac*-*N*-(1-phenylethyl)prop-2-yn-1-amine (**c3-a4**).

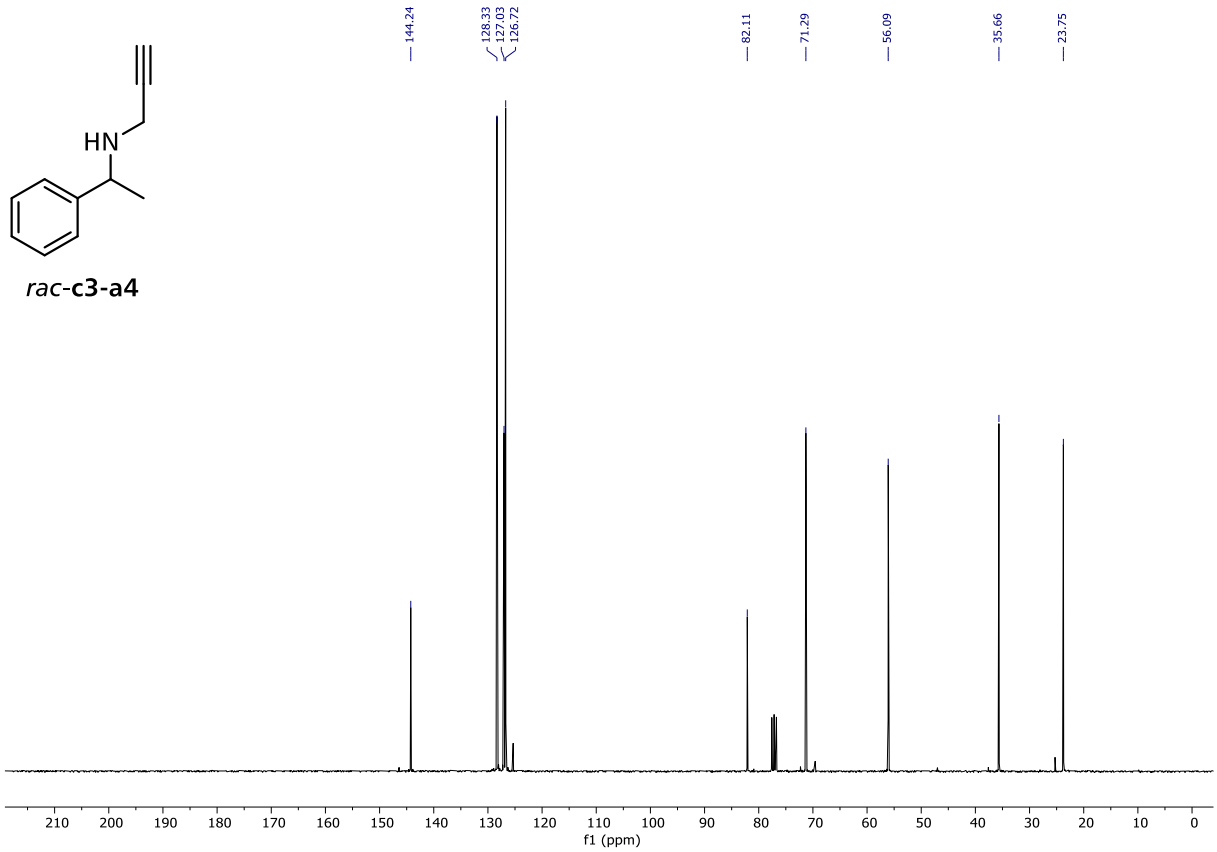


Figure S190. ^{13}C NMR spectrum of *rac*-*N*-(1-phenylethyl)prop-2-yn-1-amine (**c3-a4**).

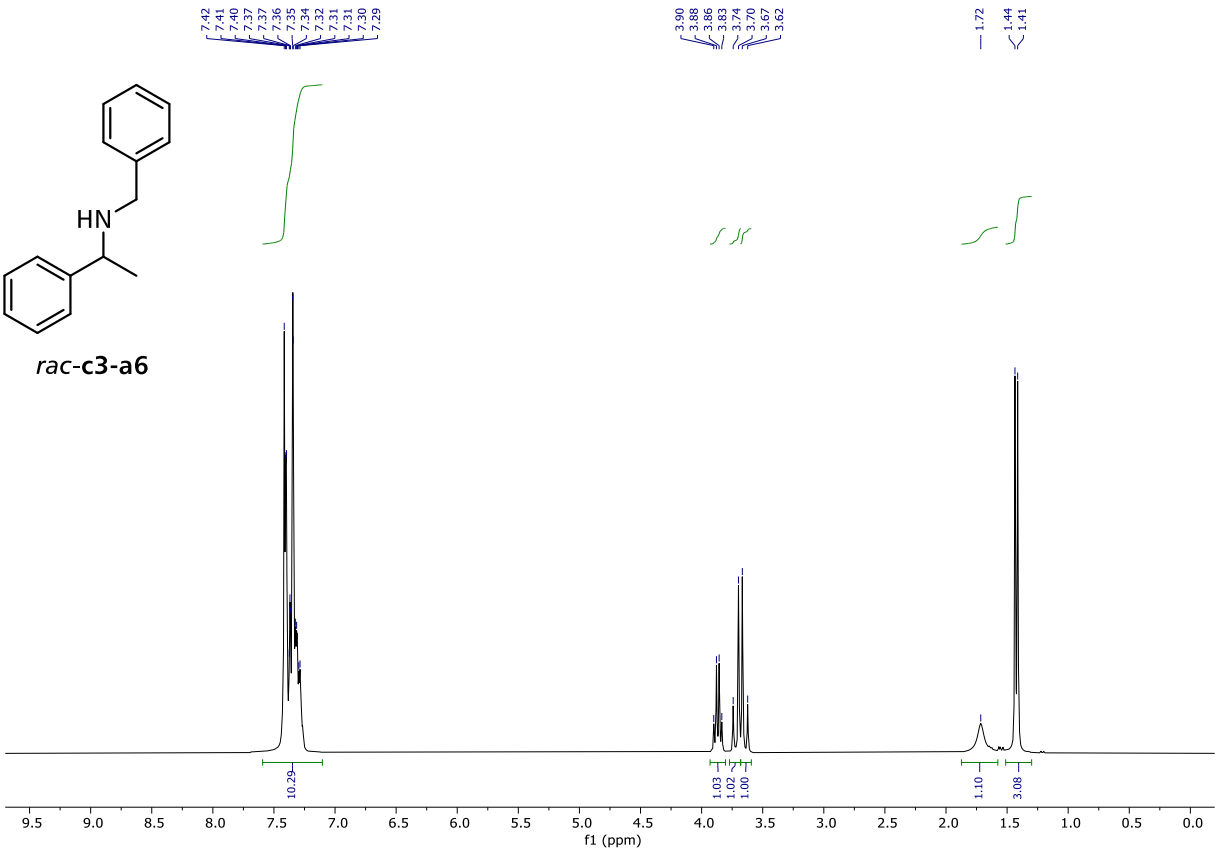


Figure S191. ^{1}H NMR spectrum of *rac*-*N*-benzyl-1-phenylethan-1-amine (**c3-a6**).

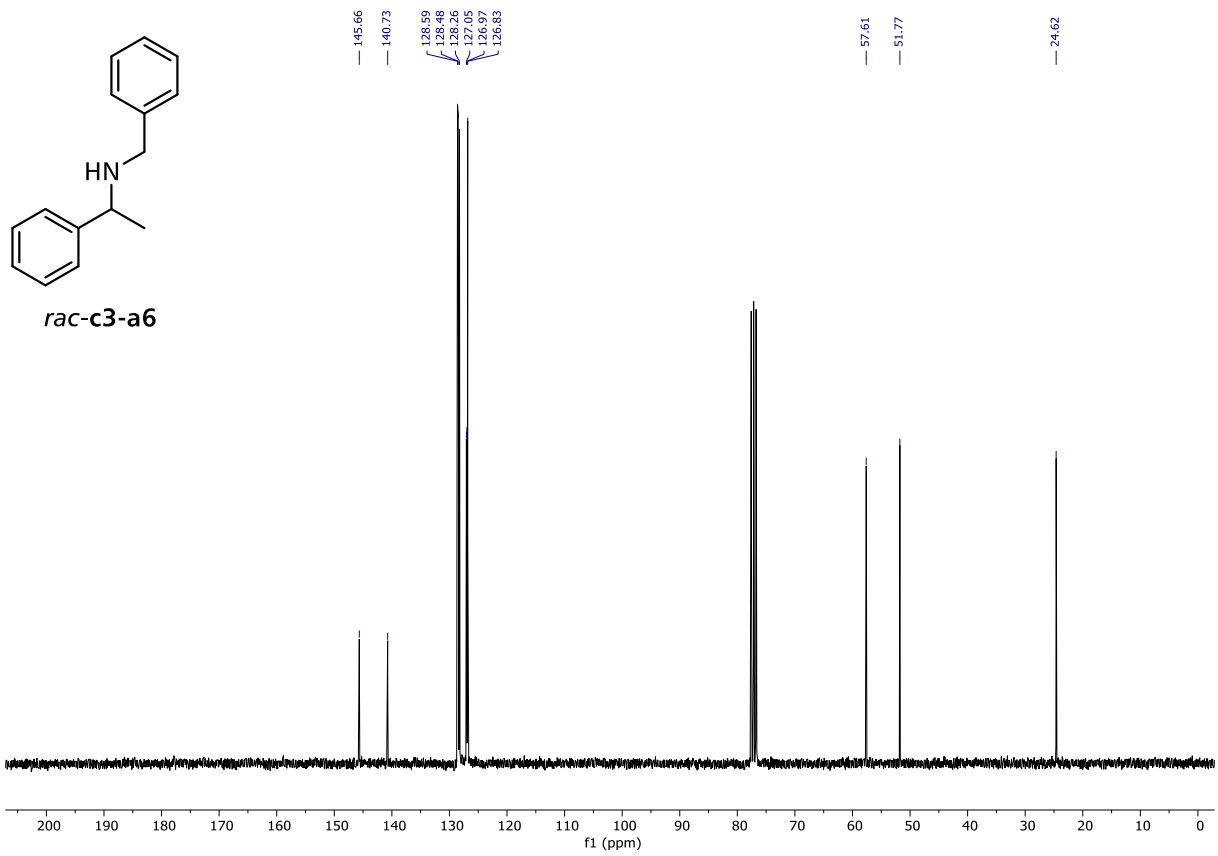


Figure S192. ^{13}C NMR spectrum of *rac*-*N*-benzyl-1-phenylethan-1-amine (**c3-a6**).

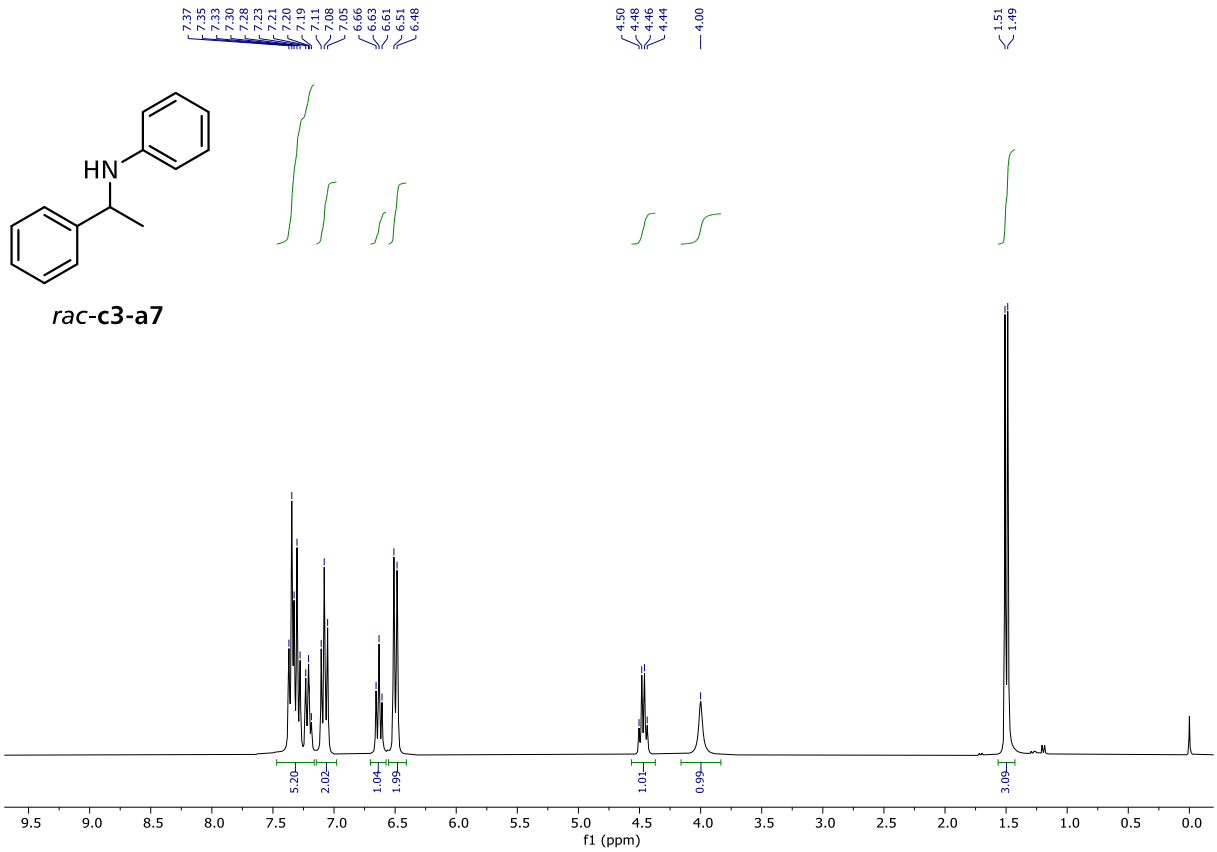


Figure S193. ^{1}H NMR spectrum of *rac*-*N*-(1-phenylethyl)aniline (**c3-a7**).

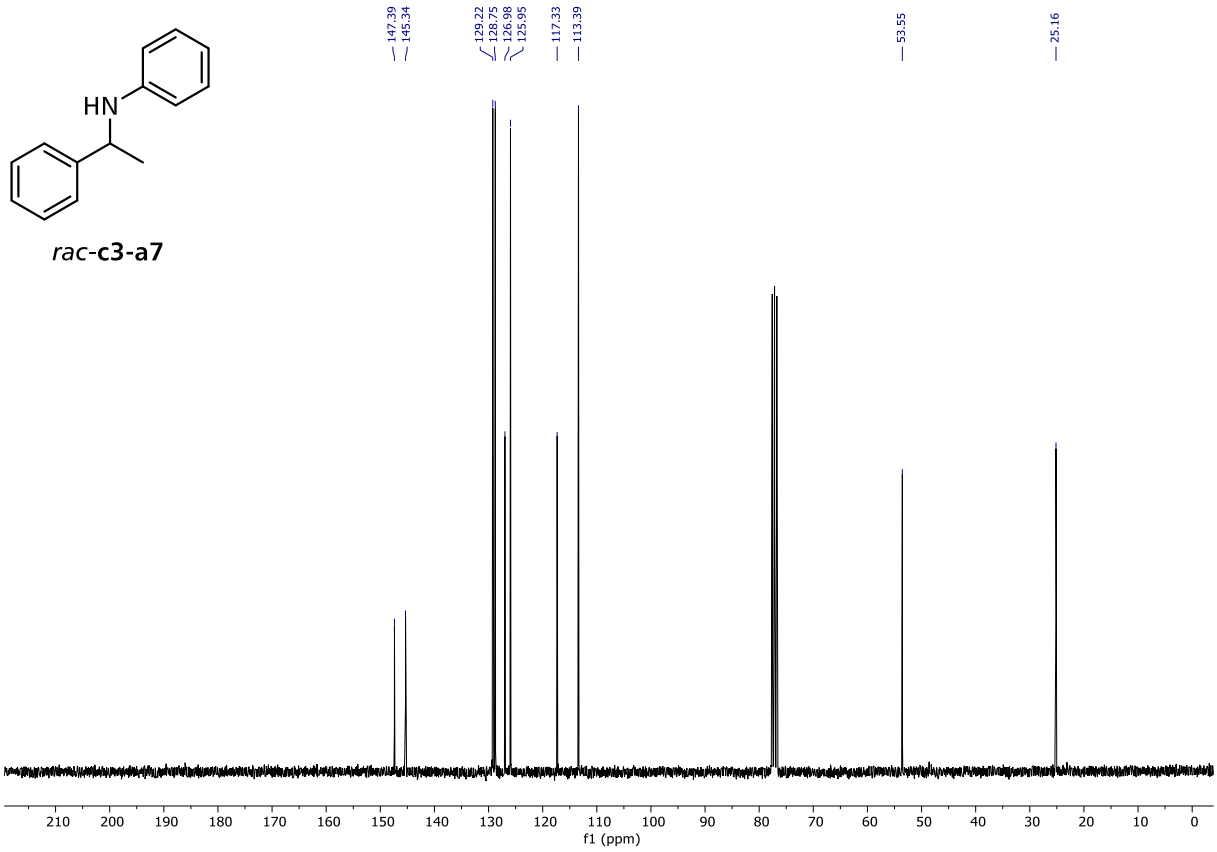
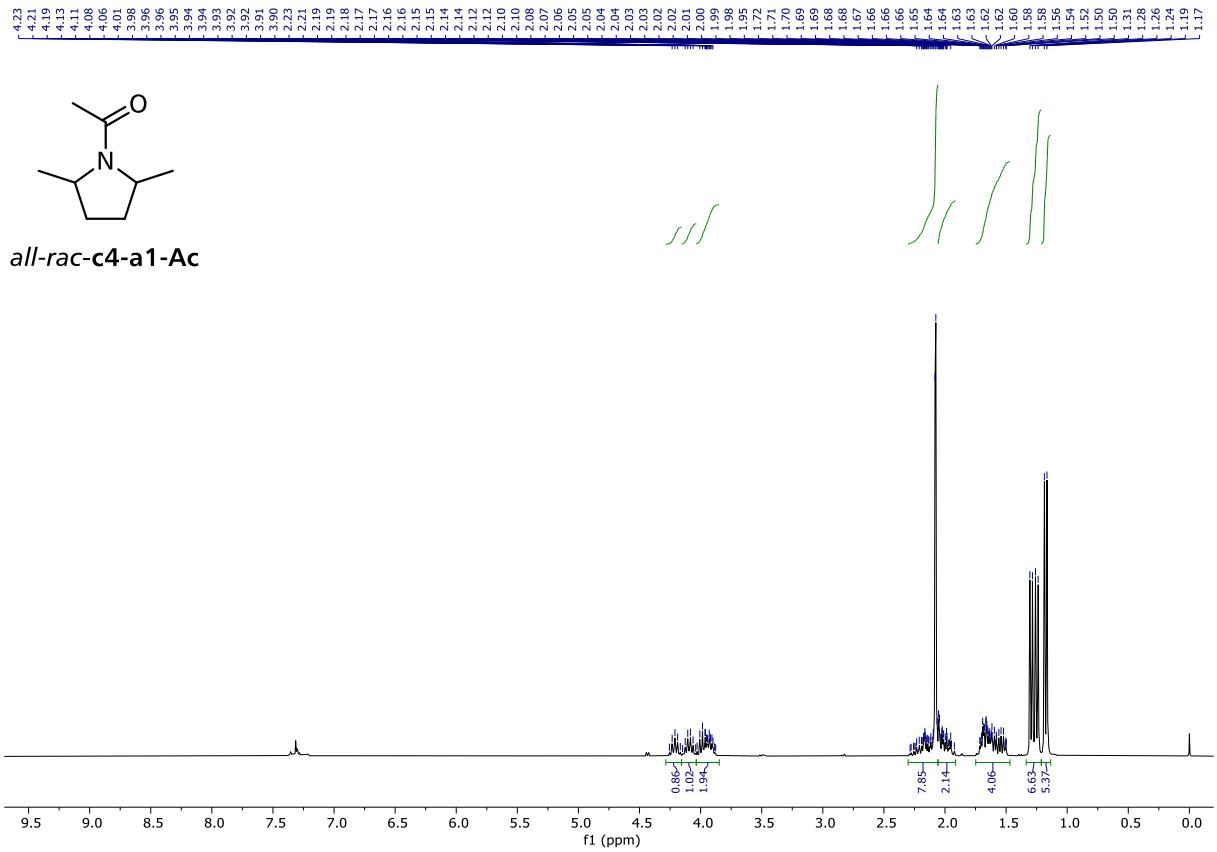
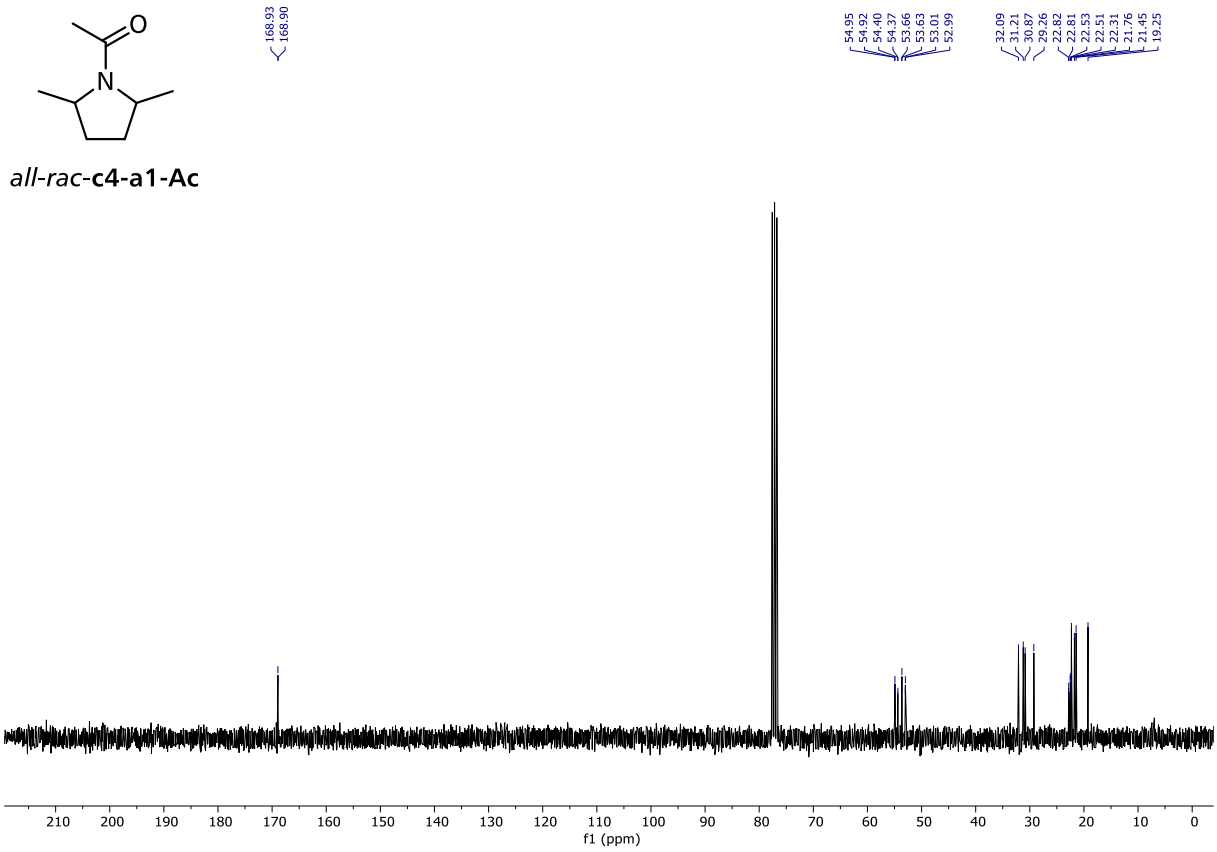


Figure S194. ^{13}C NMR spectrum of *rac*-*N*-(1-phenylethyl)aniline (**c3-a7**).



all-rac-**c4-a1-Ac**

Figure S195. ^{1}H NMR spectrum of *all-rac*-1-(2,5-dimethylpyrrolidin-1-yl)ethan-1-one (**c4-a1-Ac**).



all-rac-**c4-a1-Ac**

Figure S196. ^{13}C NMR spectrum of *all-rac*-1-(2,5-dimethylpyrrolidin-1-yl)ethan-1-one (**c4-a1-Ac**).

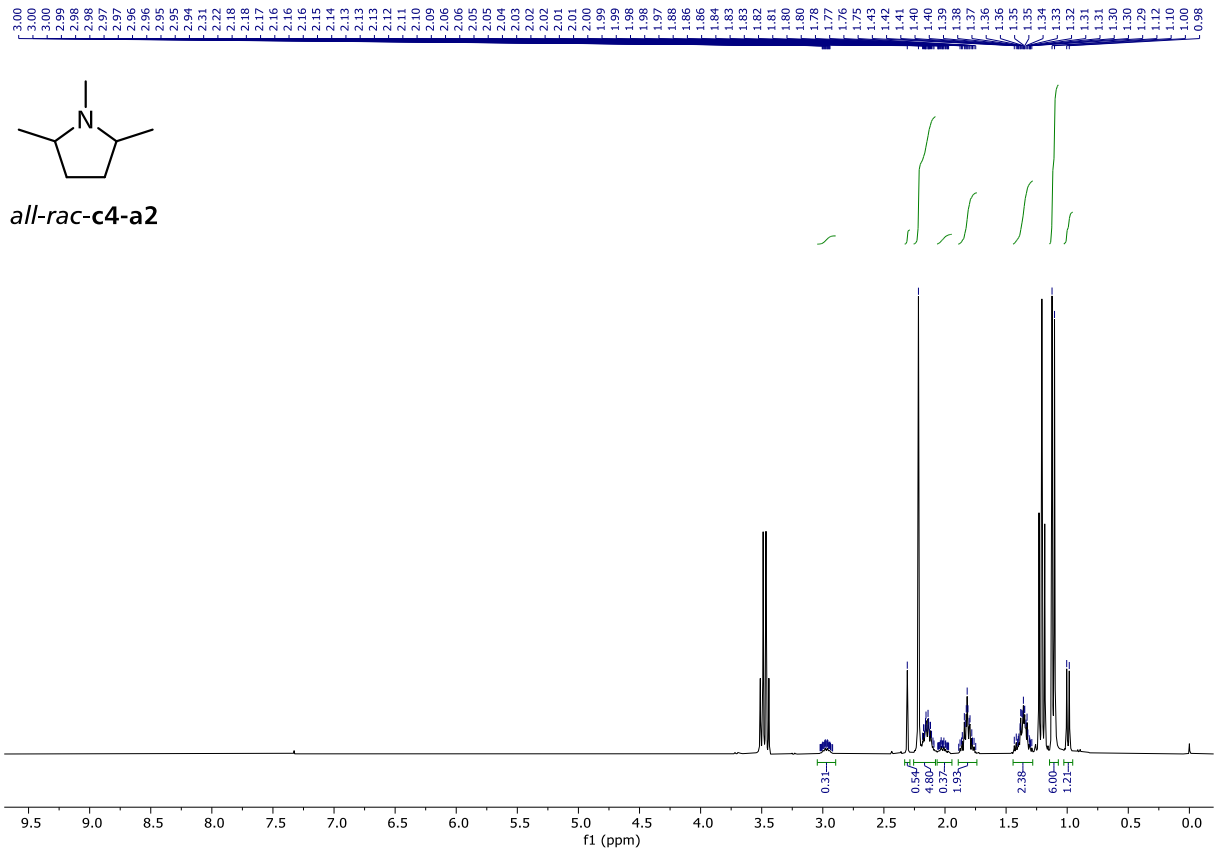


Figure S197. ^{1}H NMR spectrum of *all-rac*-1,2,5-trimethylpyrrolidine (**c4-a2**).

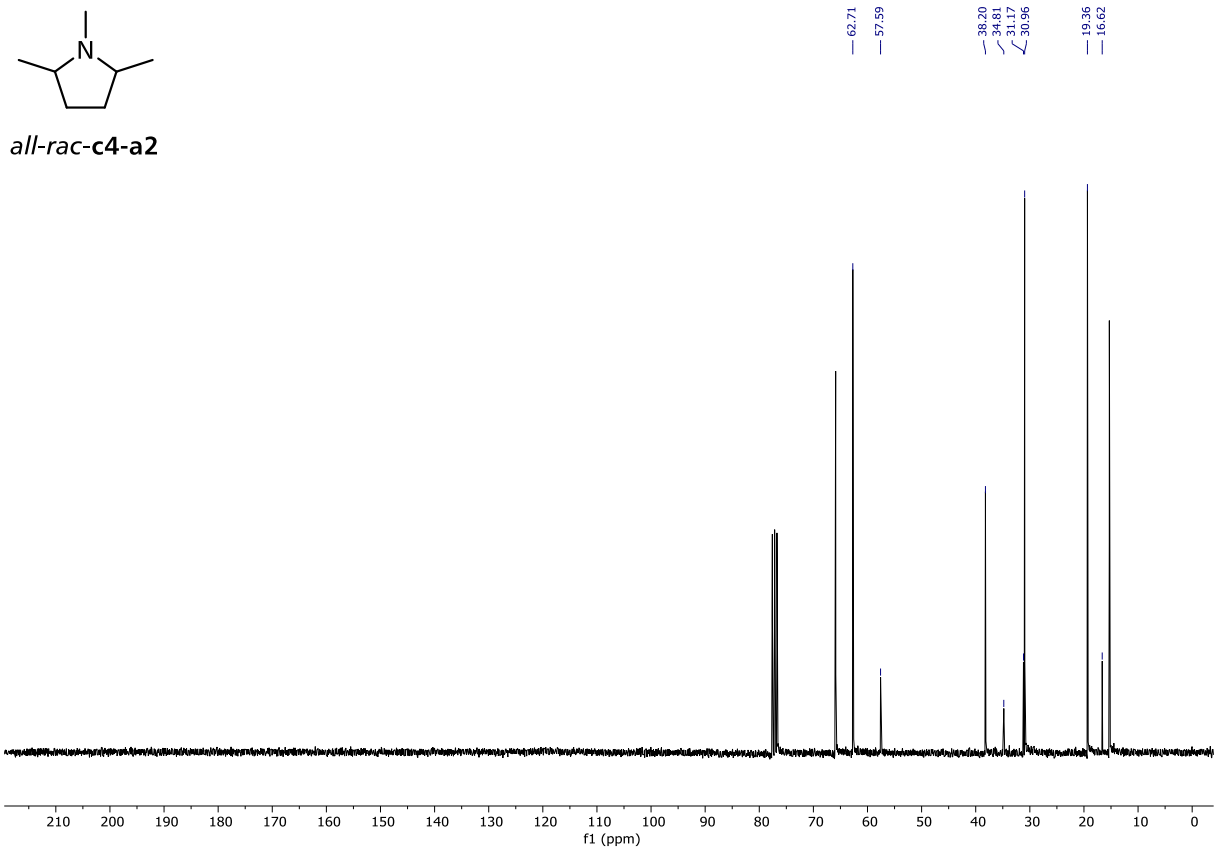


Figure S198. ^{13}C NMR spectrum of *all-rac*-1,2,5-trimethylpyrrolidine (**c4-a2**).

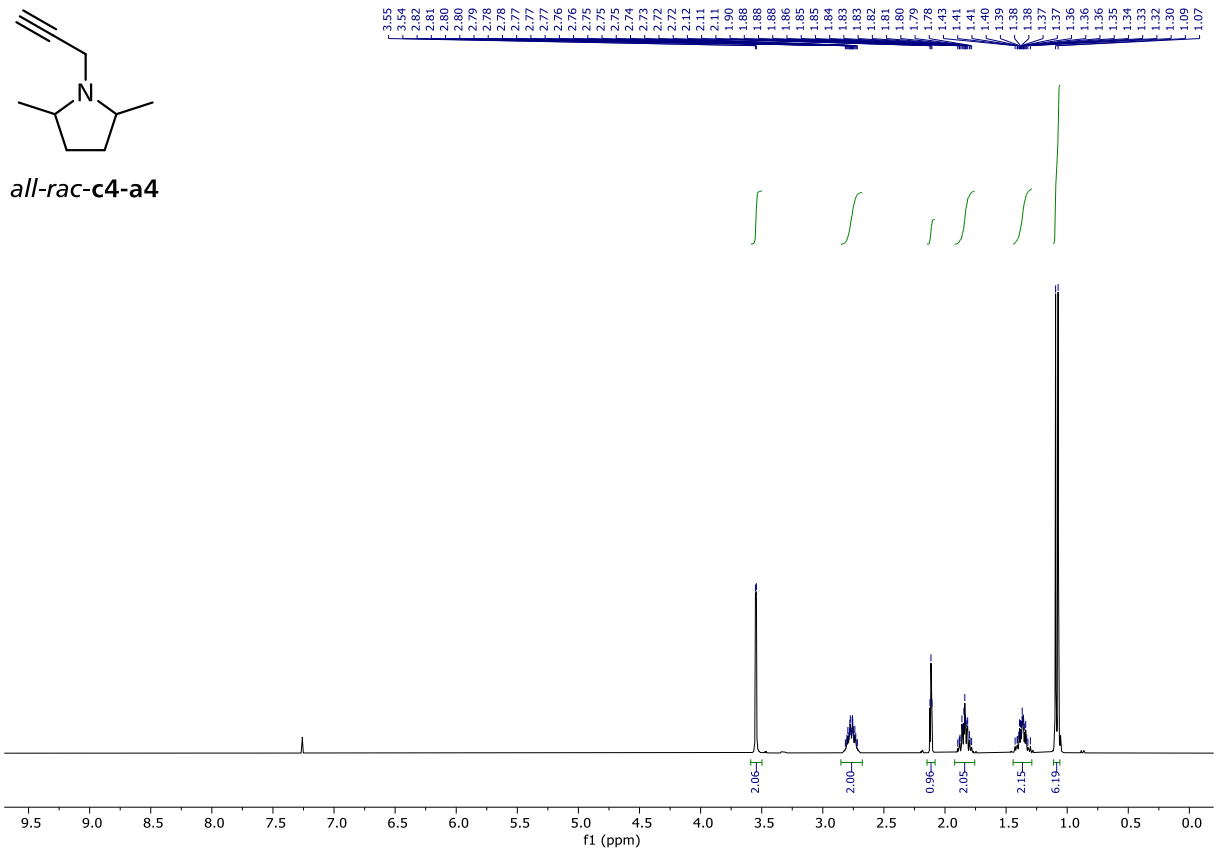


Figure S199. ^{1}H NMR spectrum of *all-rac*-2,5-dimethyl-1-(prop-2-yn-1-yl)pyrrolidine (**c4-a4**).

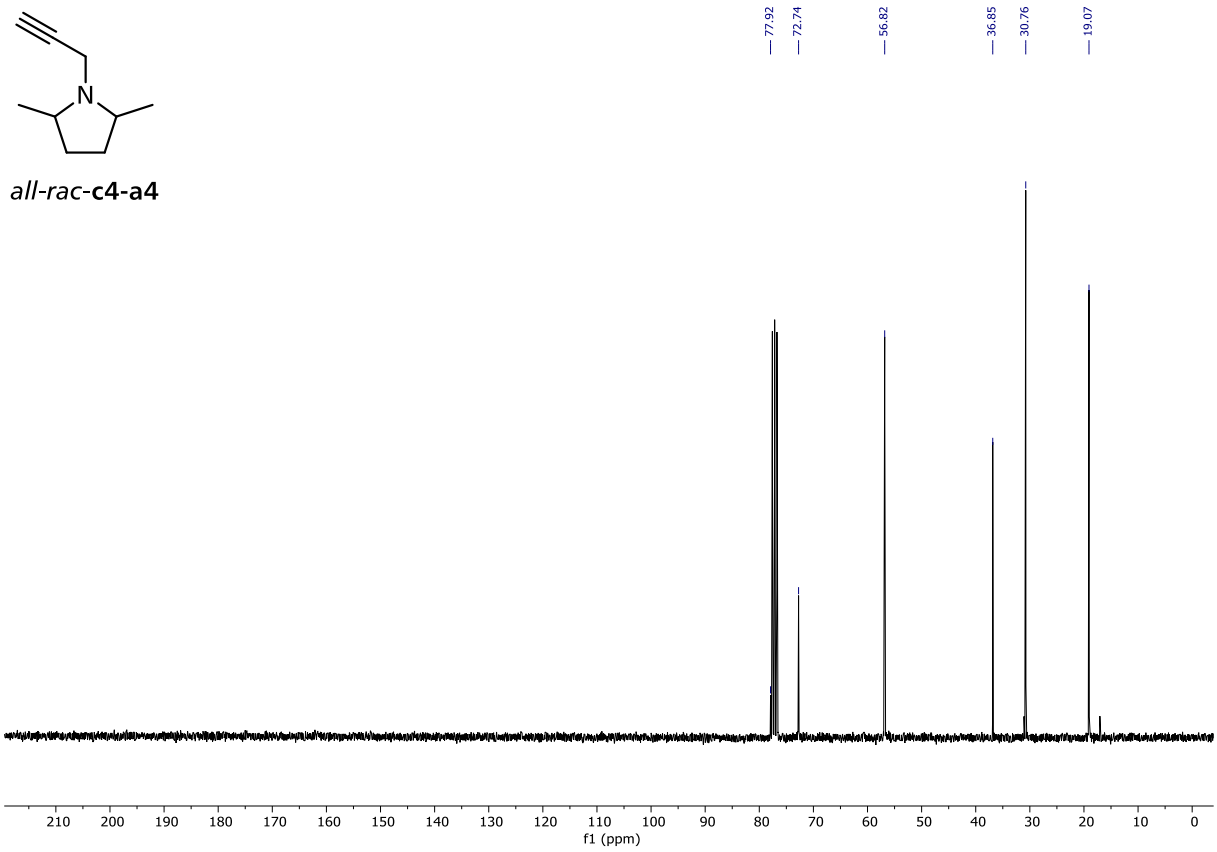


Figure S200. ^{13}C NMR spectrum of *all-rac*-2,5-dimethyl-1-(prop-2-yn-1-yl)pyrrolidine (**c4-a4**).

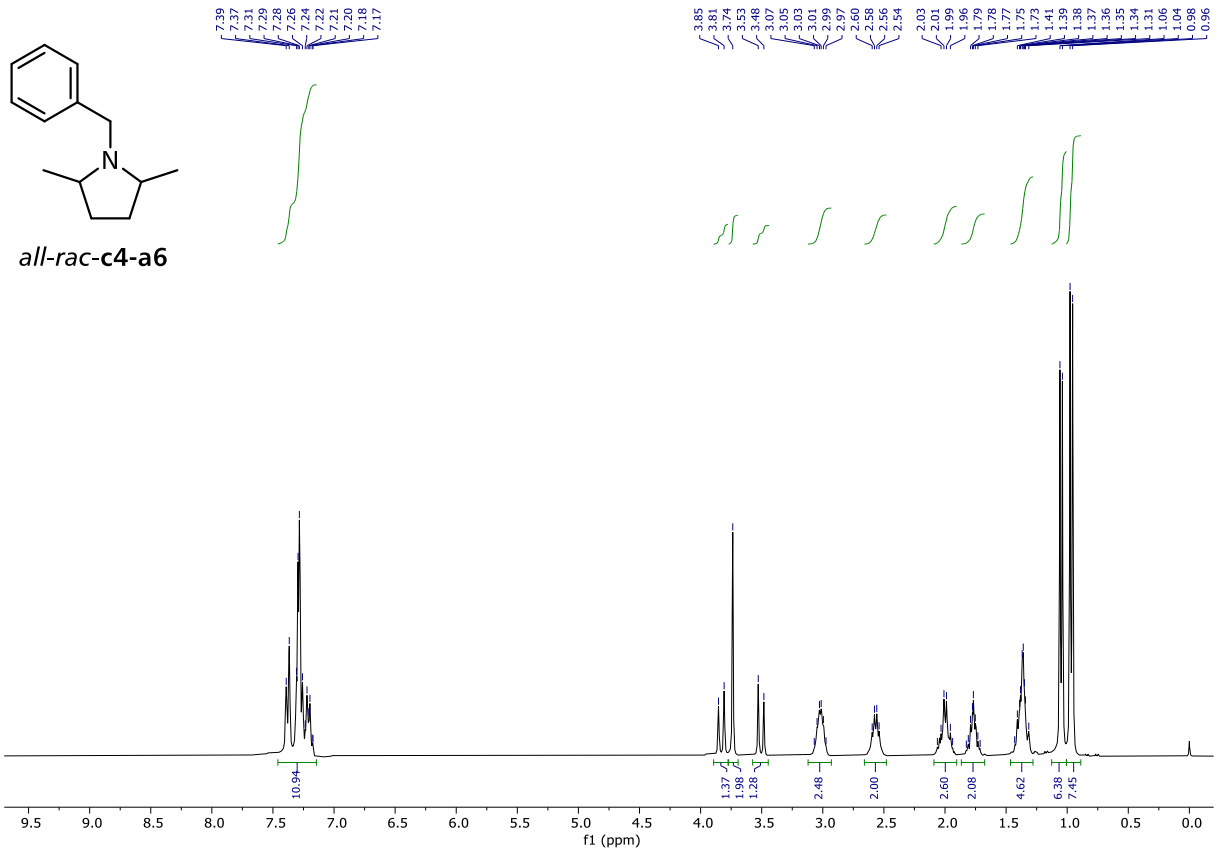


Figure S201. ^{1}H NMR spectrum of *all-rac*-1-benzyl-2,5-dimethylpyrrolidine (**c4-a6**).

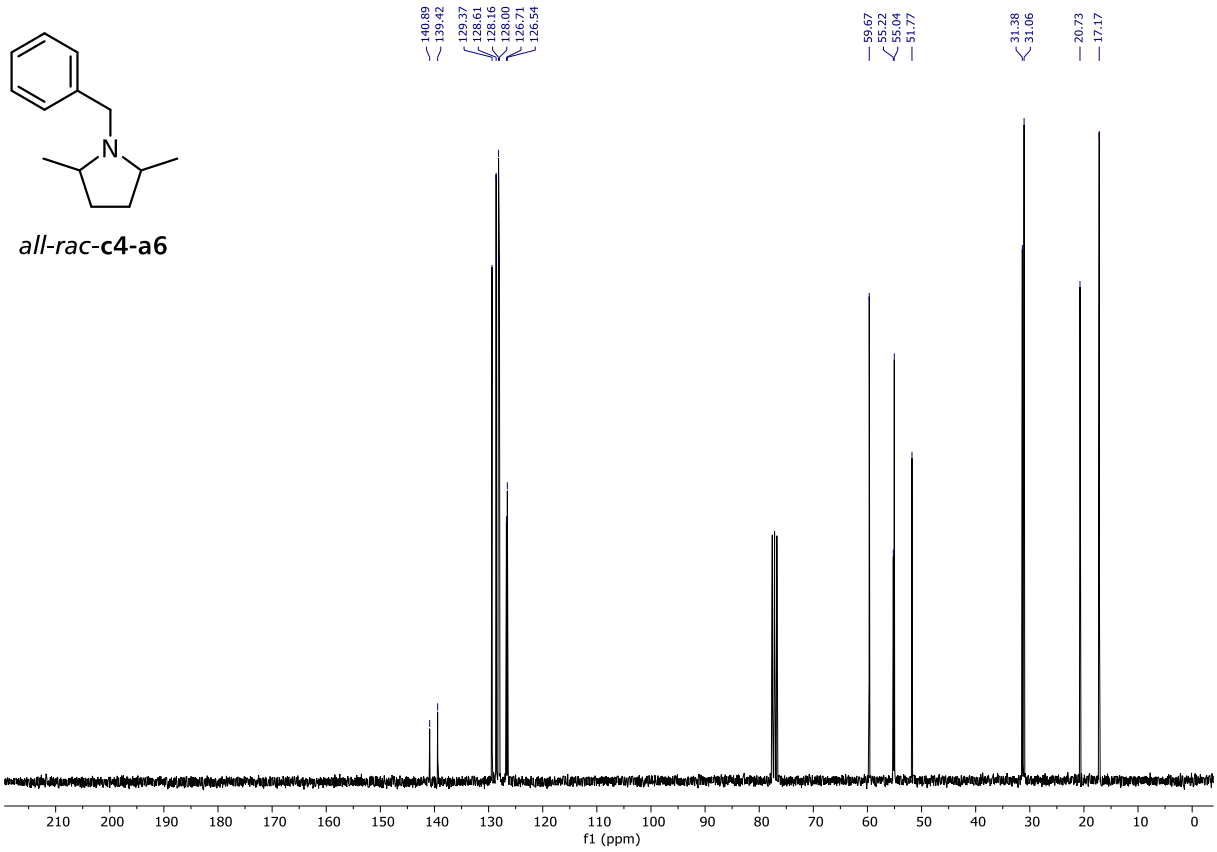


Figure S202. ^{13}C NMR spectrum of *all-rac*-1-benzyl-2,5-dimethylpyrrolidine (**c4-a6**).

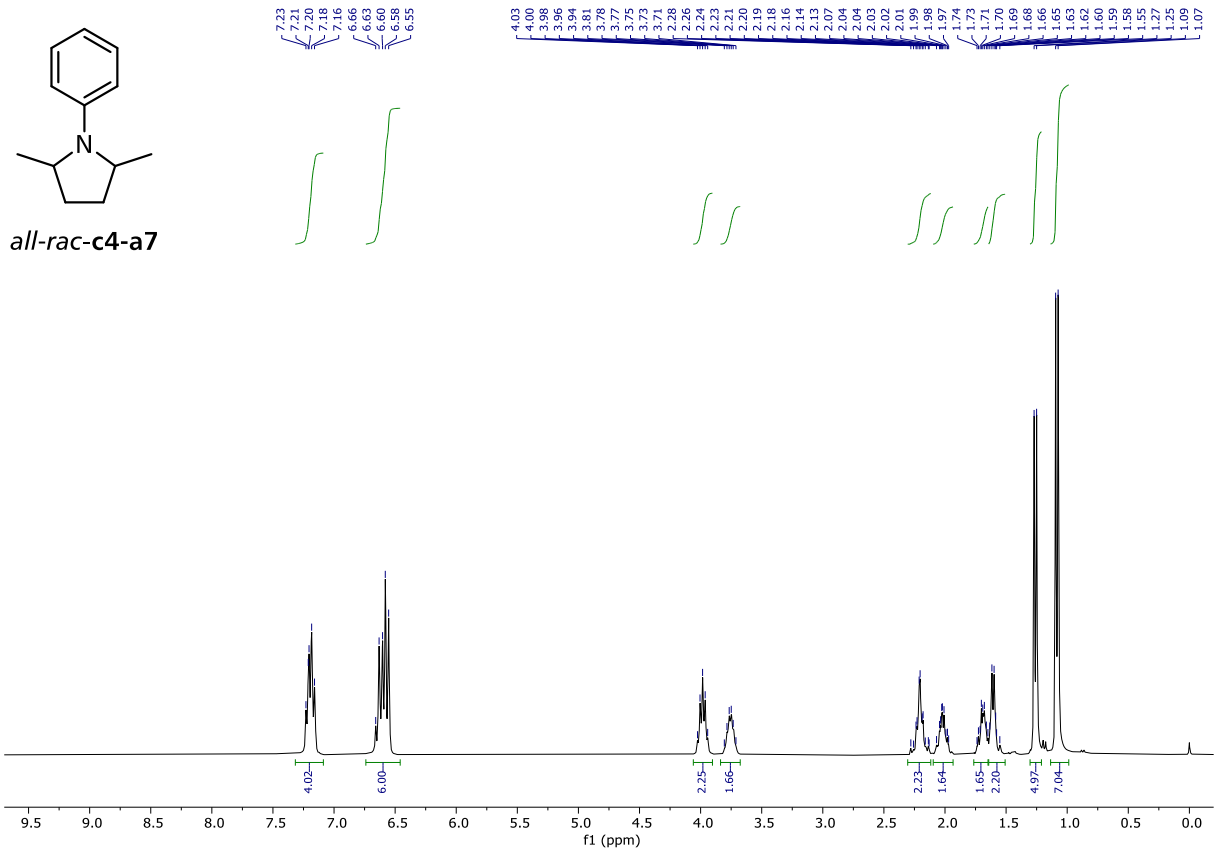


Figure S203. ^{1}H NMR spectrum of *all-rac*-2,5-dimethyl-1-phenylpyrrolidine (**c4-a7**).

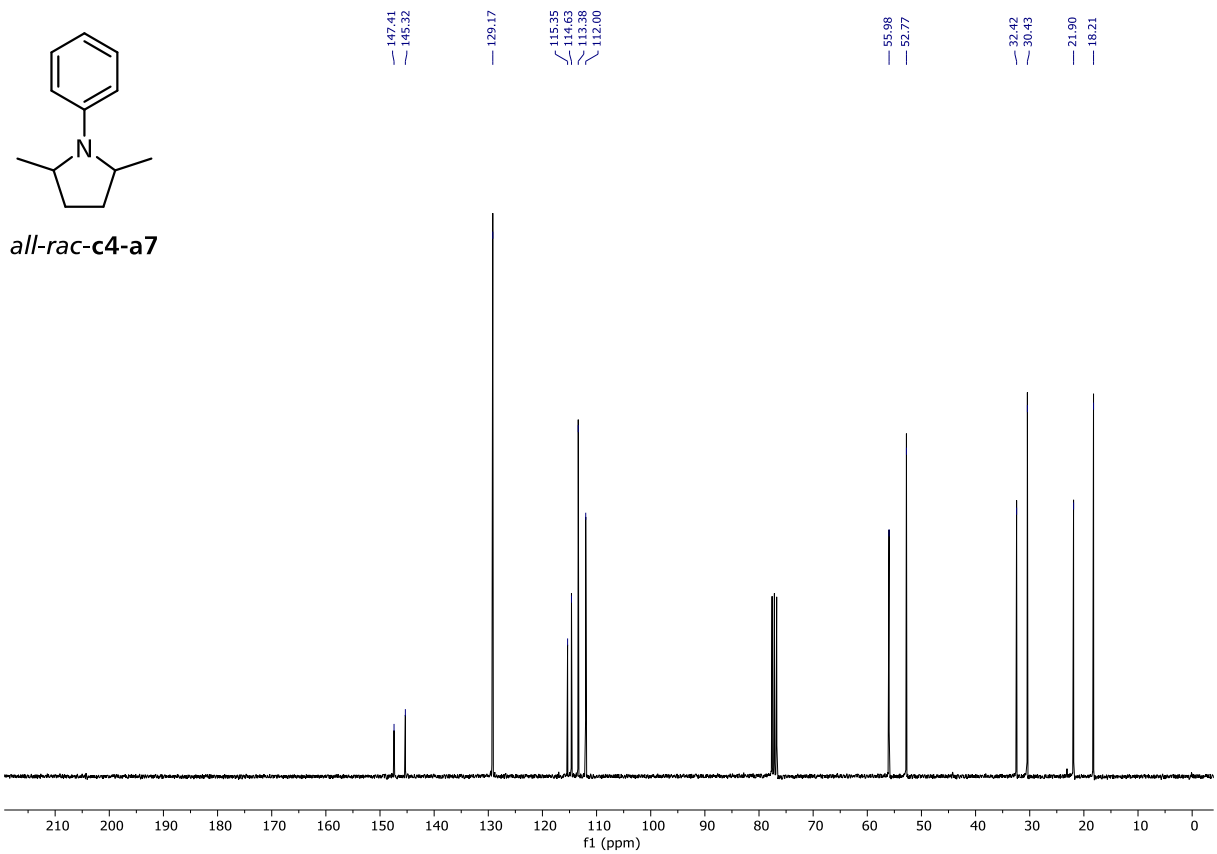


Figure S204. ^{13}C NMR spectrum of *all-rac*-2,5-dimethyl-1-phenylpyrrolidine (**c4-a7**).

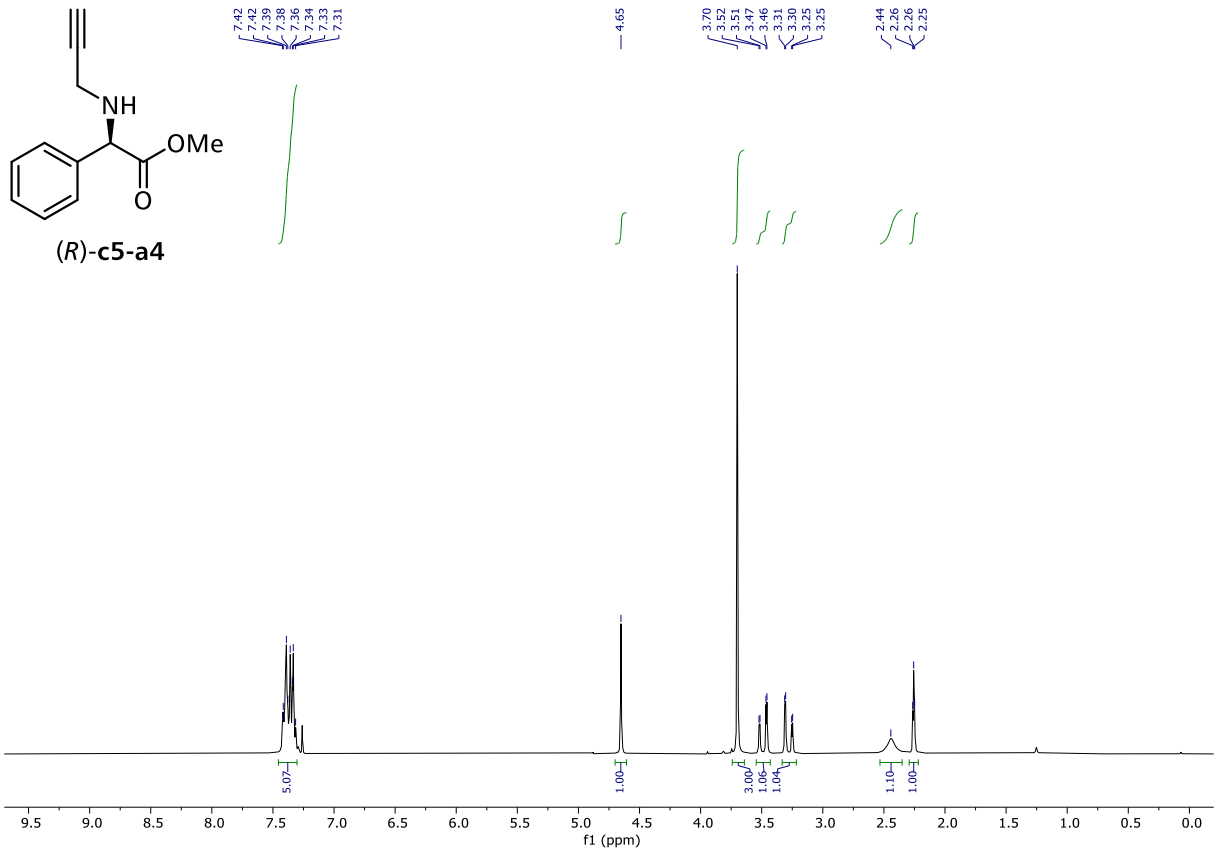


Figure S205. ^{1}H NMR spectrum of methyl (*R*)-2-phenyl-2-(prop-2-ynylamino)acetate (**c5-a4**).

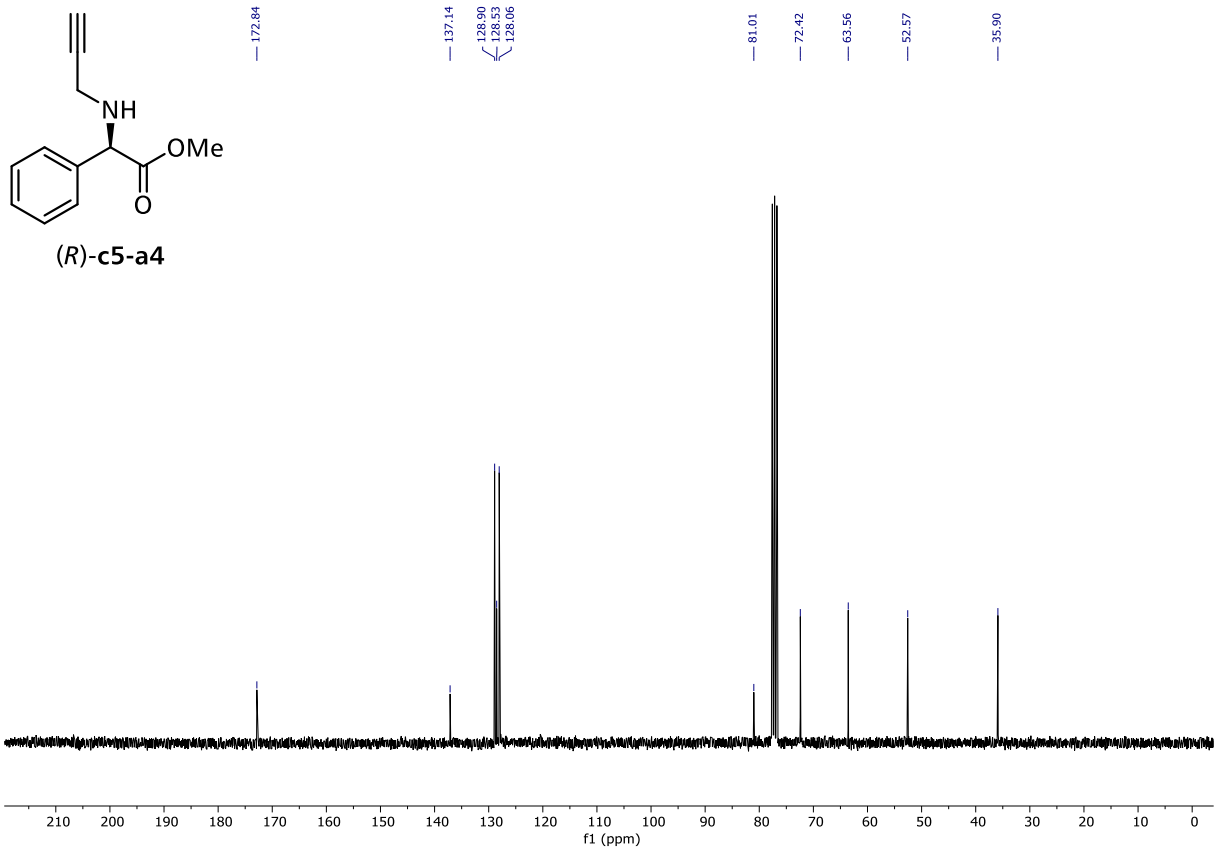


Figure S206. ^{13}C NMR spectrum of methyl (*R*)-2-phenyl-2-(prop-2-ynylamino)acetate (**c5-a4**).

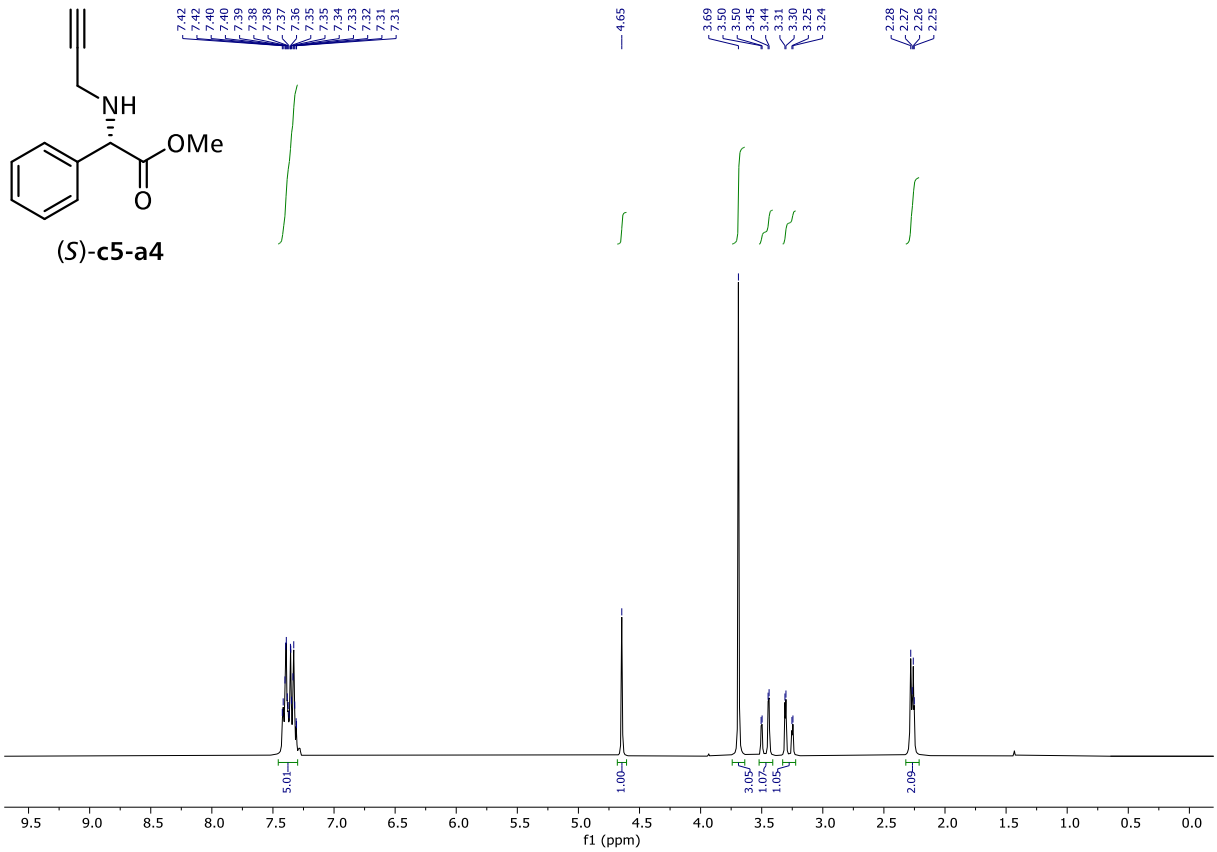


Figure S207. ^{1}H NMR spectrum of methyl (*S*)-2-phenyl-2-(prop-2-ynylamino)acetate (**c5-a4**).

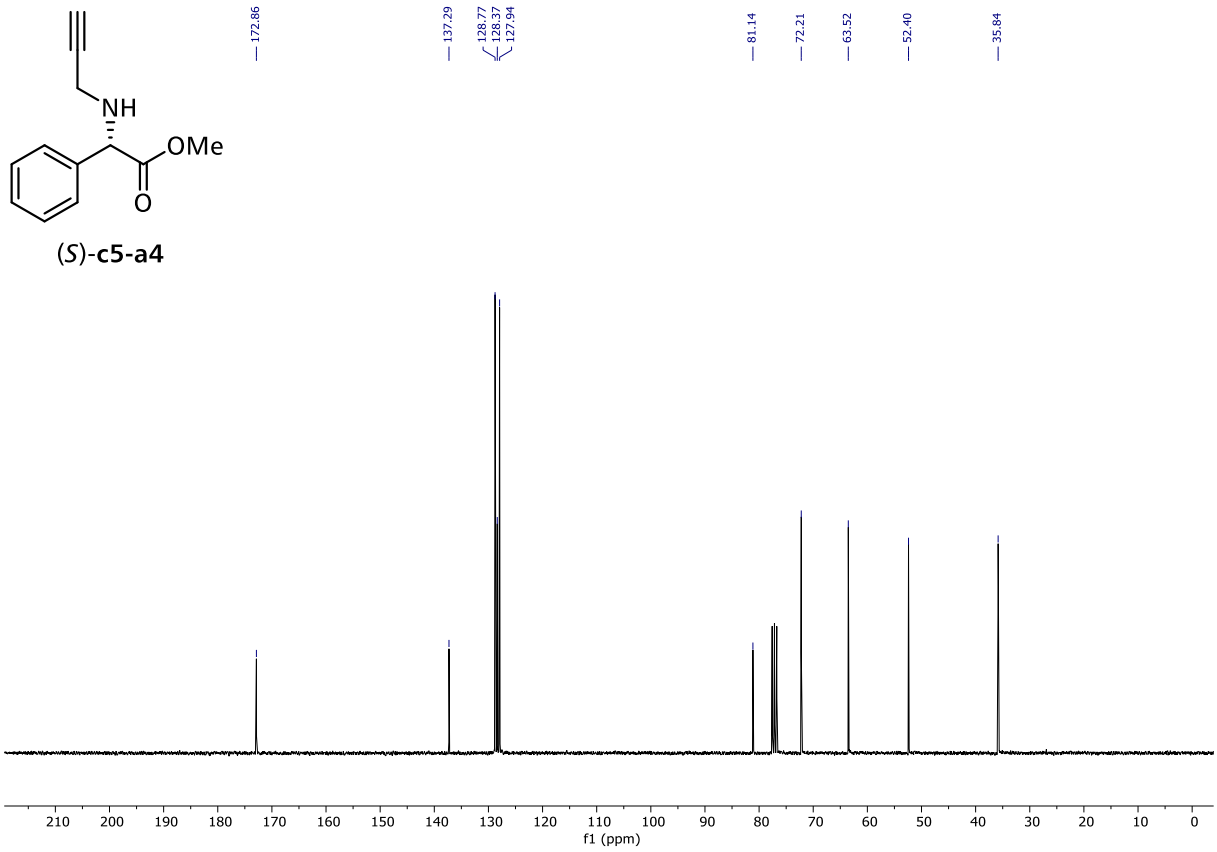


Figure S208. ^{13}C NMR spectrum of methyl (*S*)-2-phenyl-2-(prop-2-ynylamino)acetate (**c5-a4**).

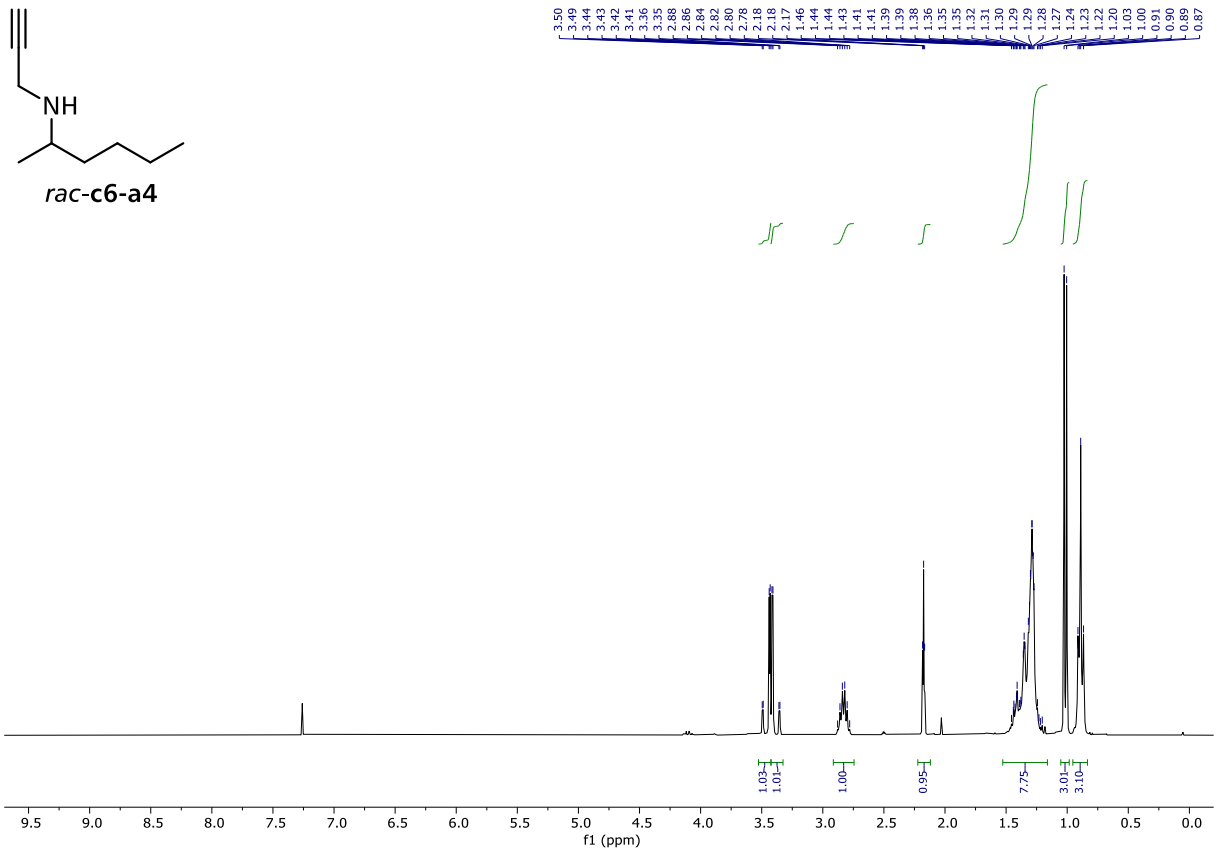


Figure S209. ^{1}H NMR spectrum of *rac*-*N*-(prop-2-yn-1-yl)hexan-2-amine (**c6-a4**).

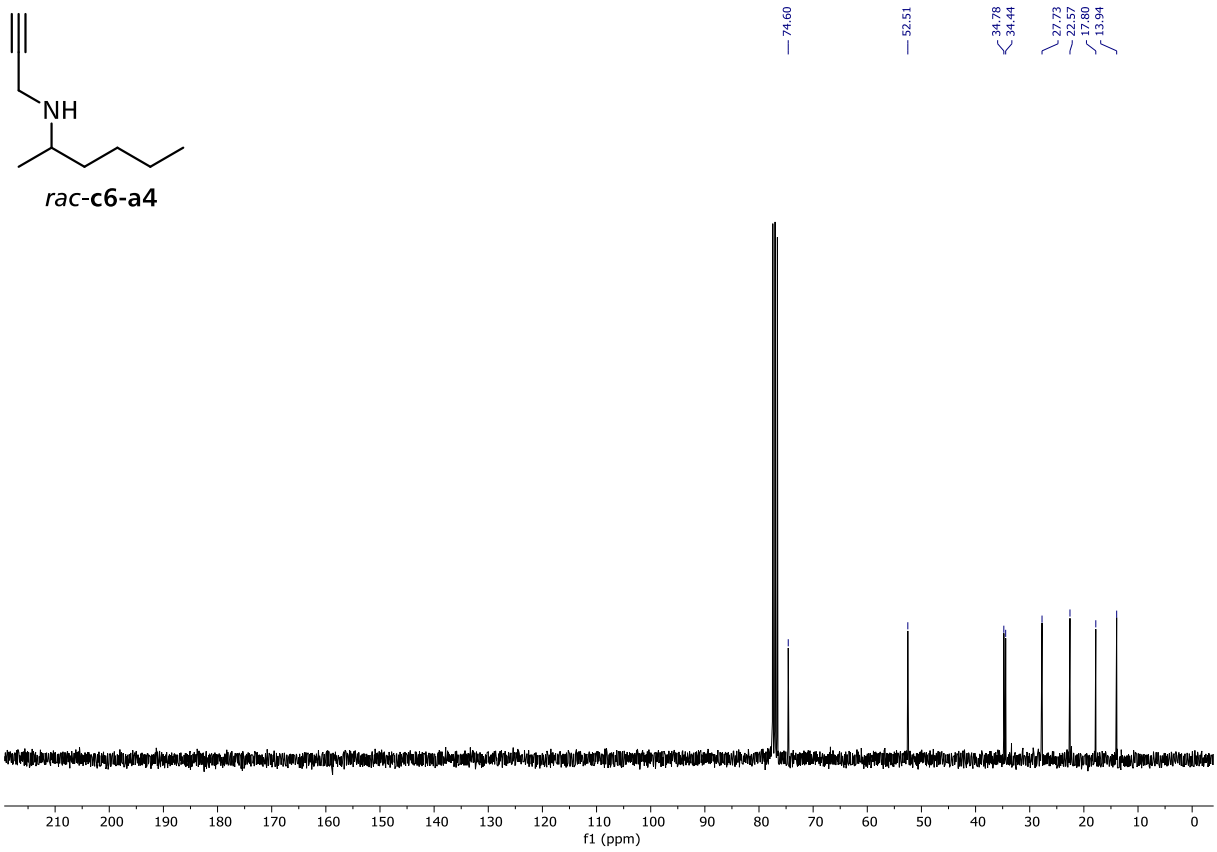


Figure S210. ^{13}C NMR spectrum of *rac*-*N*-(prop-2-yn-1-yl)hexan-2-amine (**c6-a4**).

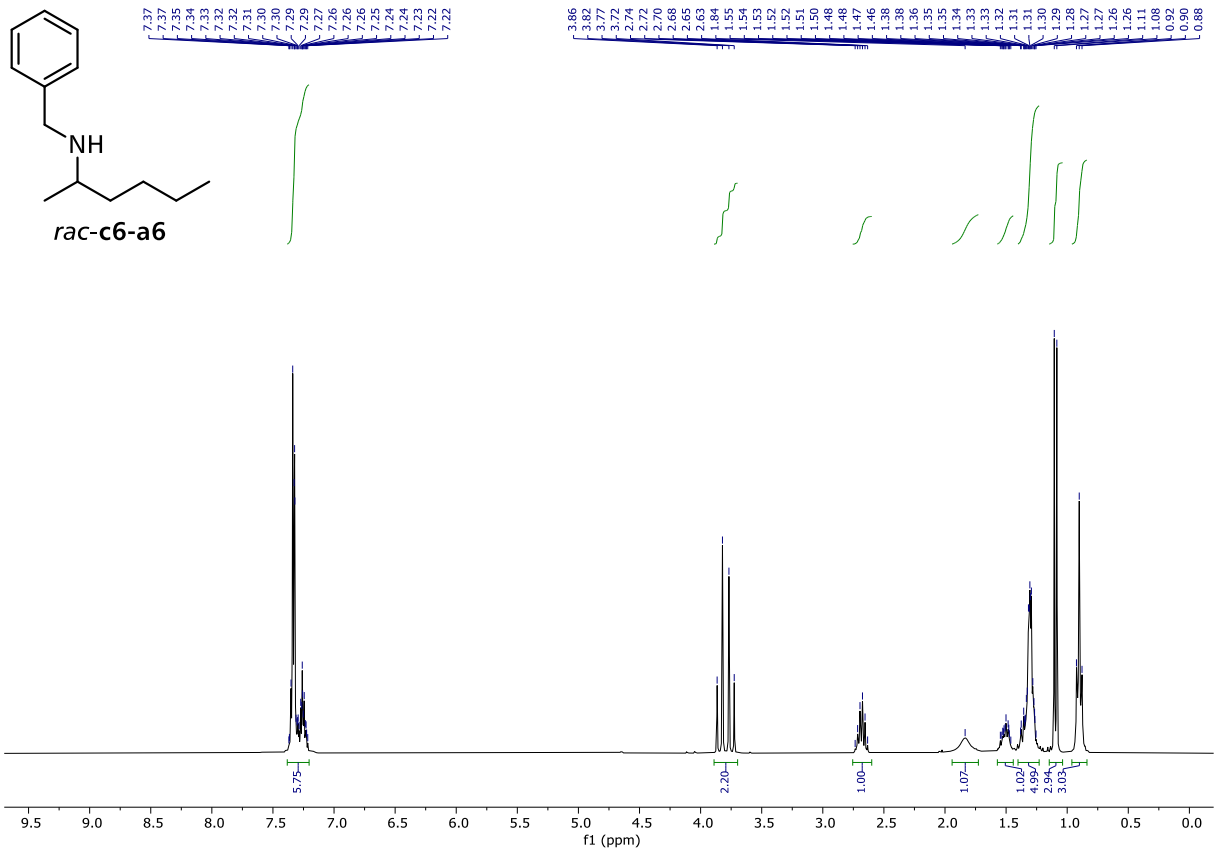


Figure S211. ^{1}H NMR spectrum of *rac*-*N*-benzylhexan-2-amine (**c6-a6**).

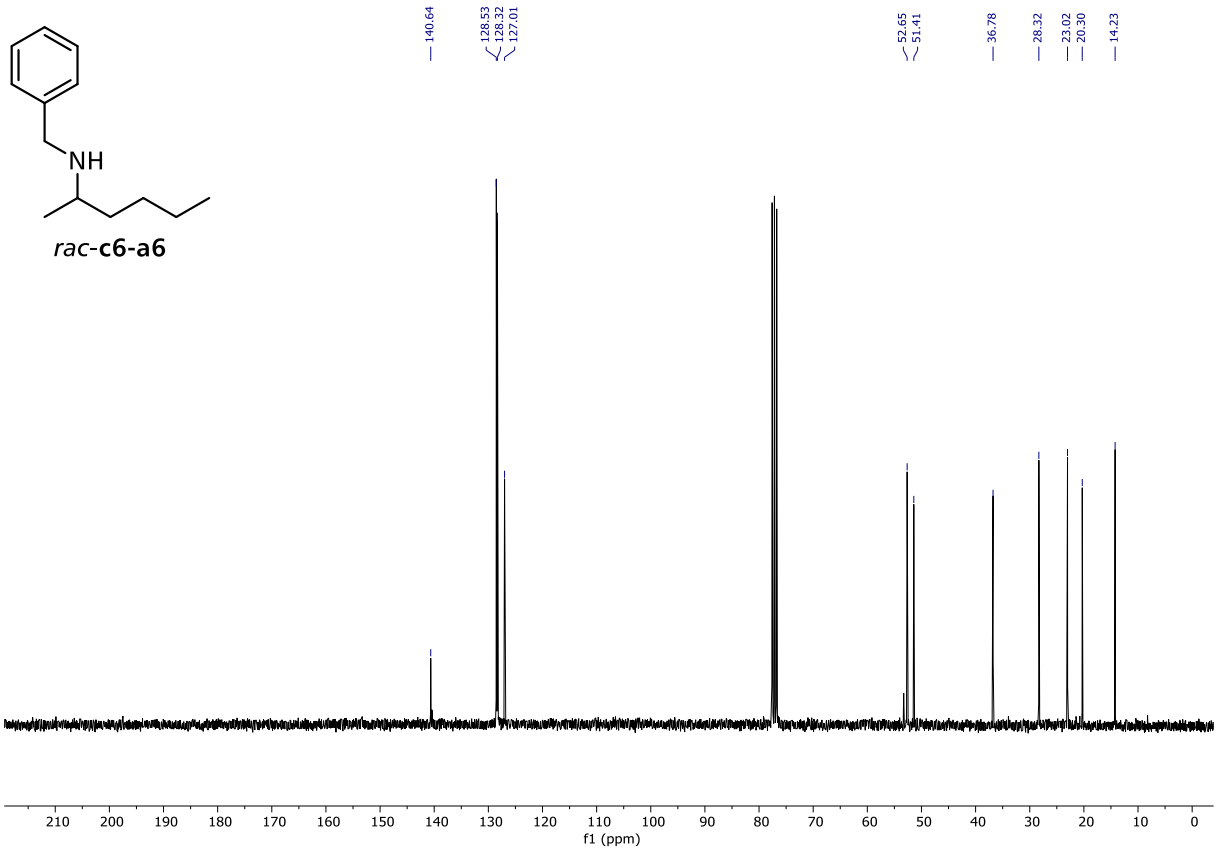


Figure S212. ^{13}C NMR spectrum of *rac*-*N*-benzylhexan-2-amine (**c6-a6**).

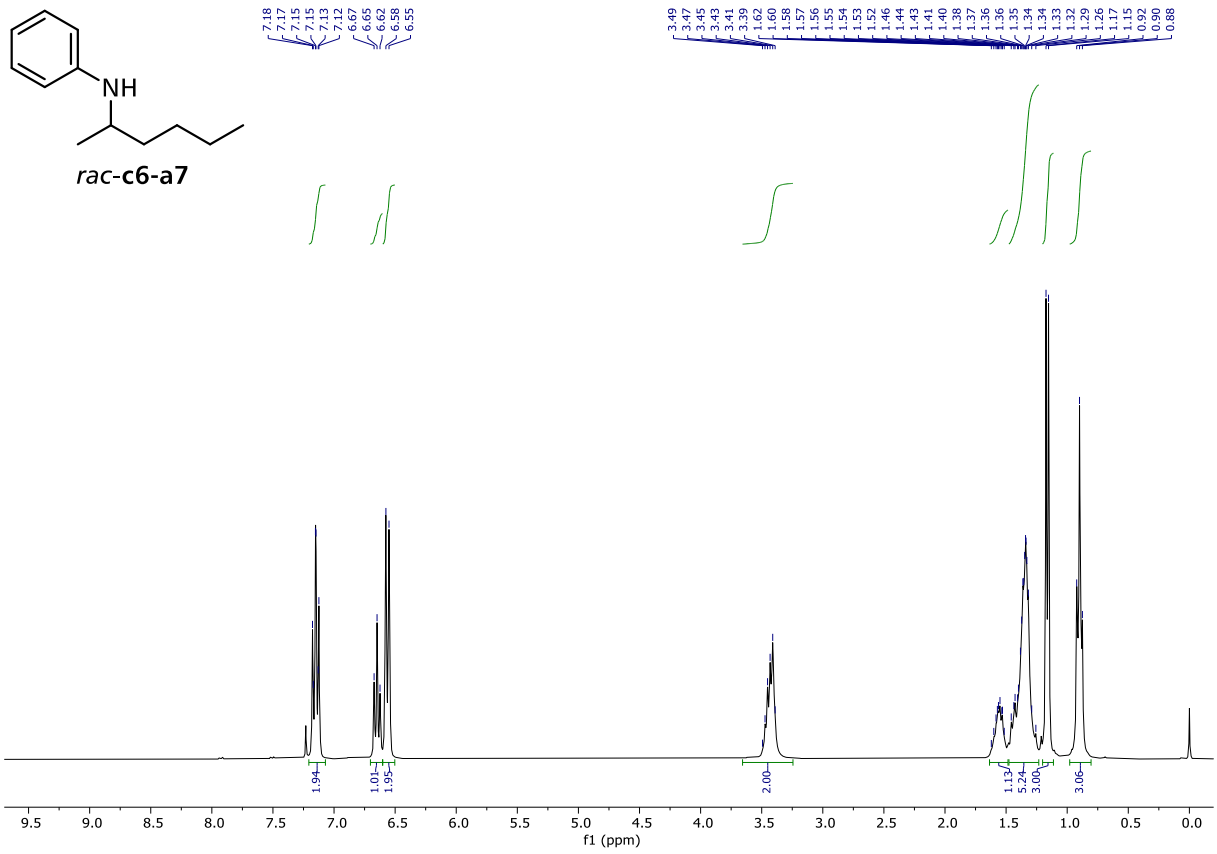


Figure S213. ^{1}H NMR spectrum of *rac*-*N*-(hexan-2-yl)aniline (**c6-a7**).

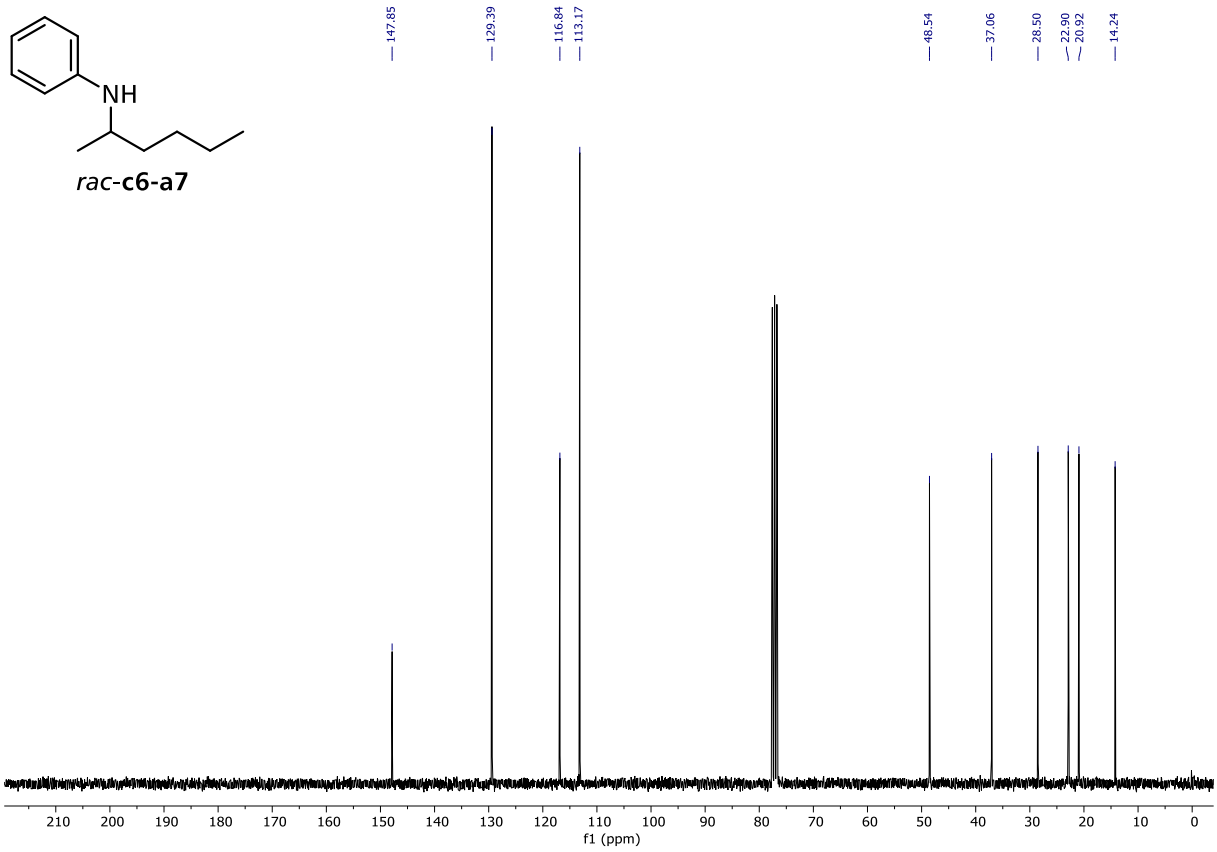


Figure S214. ^{13}C NMR spectrum of *rac*-*N*-(hexan-2-yl)aniline (**c6-a7**).

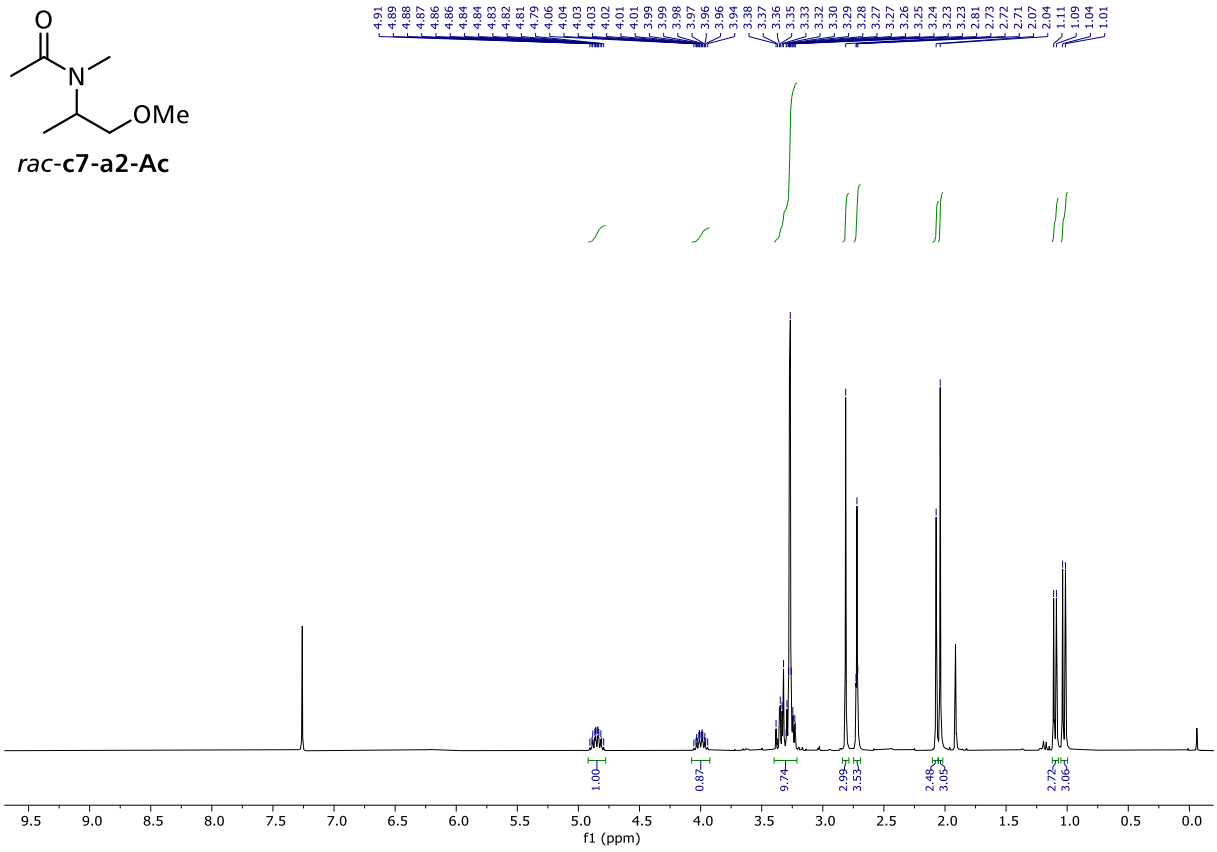


Figure S215. ^{1}H NMR spectrum of *rac*-*N*-(1-methoxypropan-2-yl)-*N*-methylacetamide (**c7-a2-Ac**).

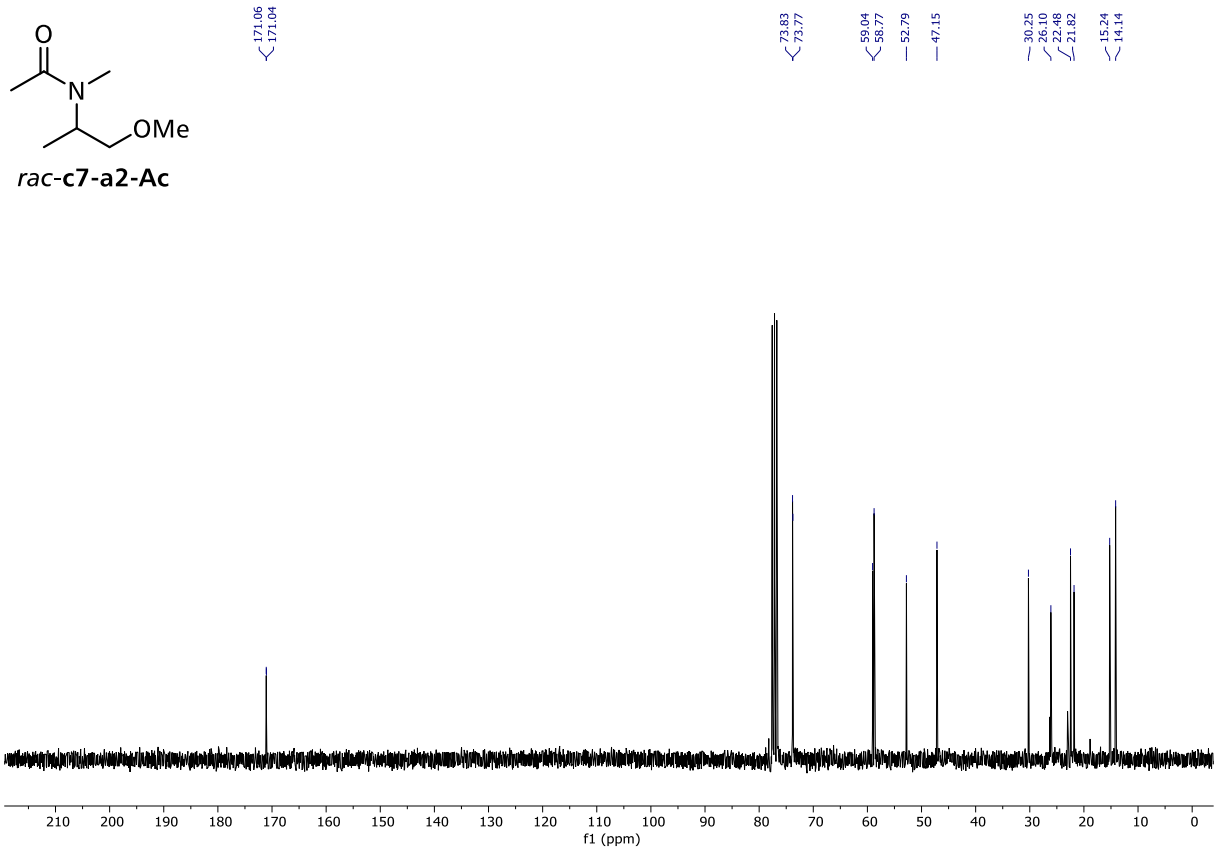


Figure S216. ^{13}C NMR spectrum of *rac*-*N*-(1-methoxypropan-2-yl)-*N*-methylacetamide (**c7-a2-Ac**).

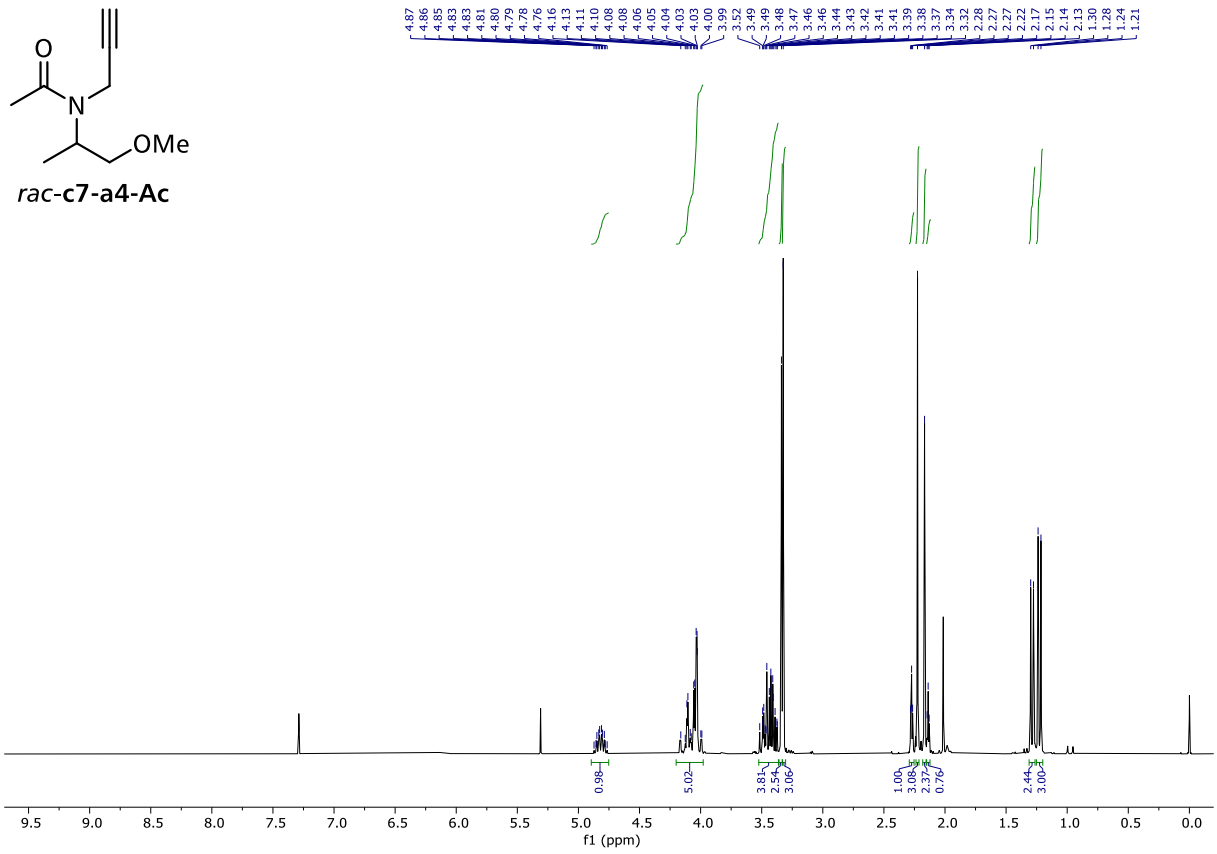


Figure S217. ^{1}H NMR spectrum of *rac*-*N*-(1-methoxypropan-2-yl)-*N*-(prop-2-yn-1-yl)acetamide (**c7-a4-Ac**).

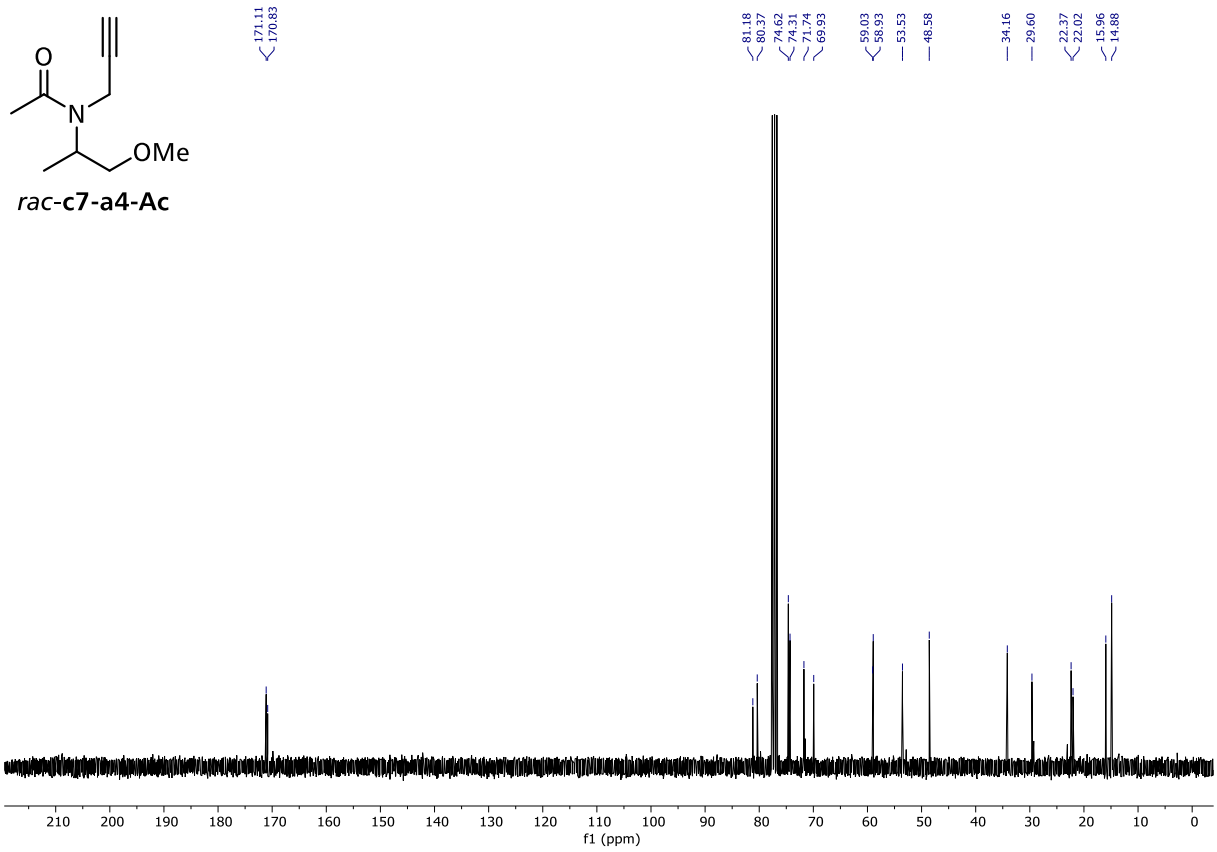


Figure S218. ^{13}C NMR spectrum of *rac*-*N*-(1-methoxypropan-2-yl)-*N*-(prop-2-yn-1-yl)acetamide (**c7-a4-Ac**).

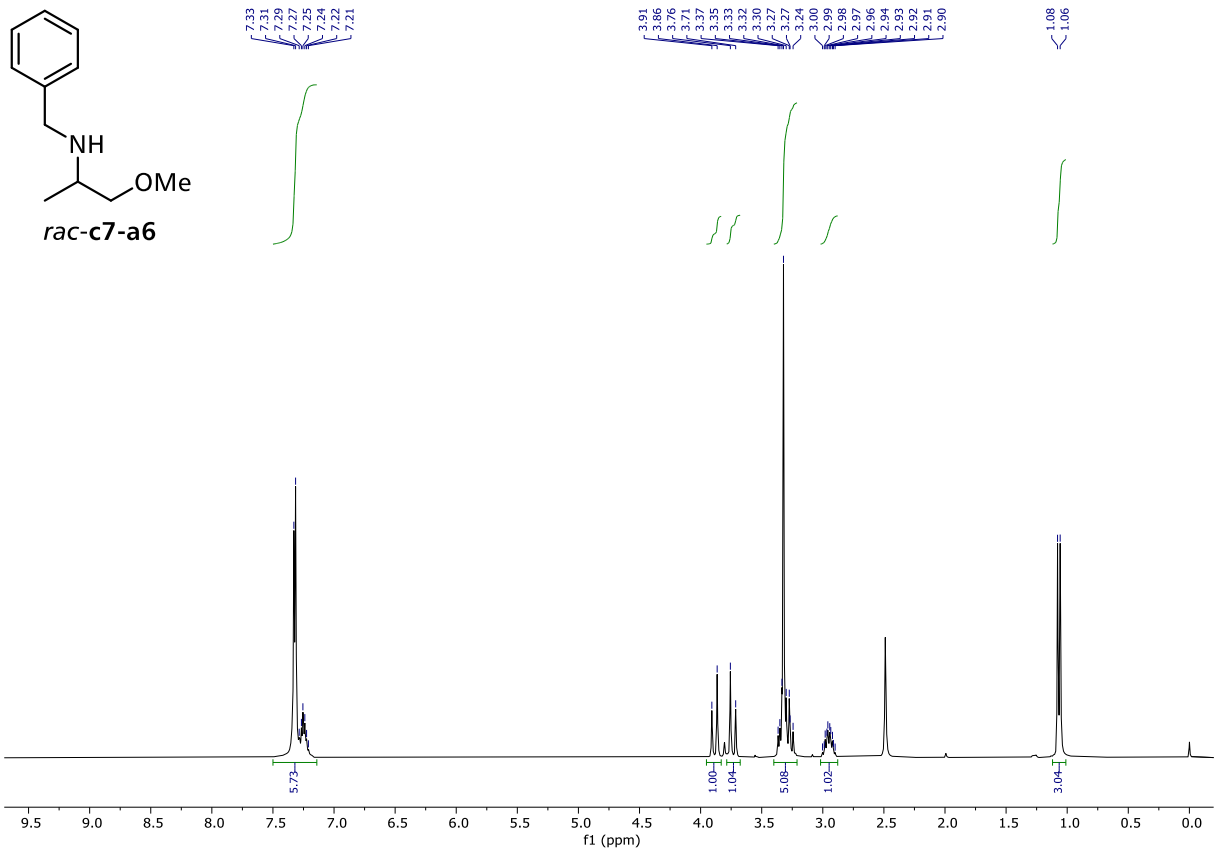


Figure S219. ^{1}H NMR spectrum of *rac*-*N*-benzyl-1-methoxypropan-2-amine (**c7-a6**).

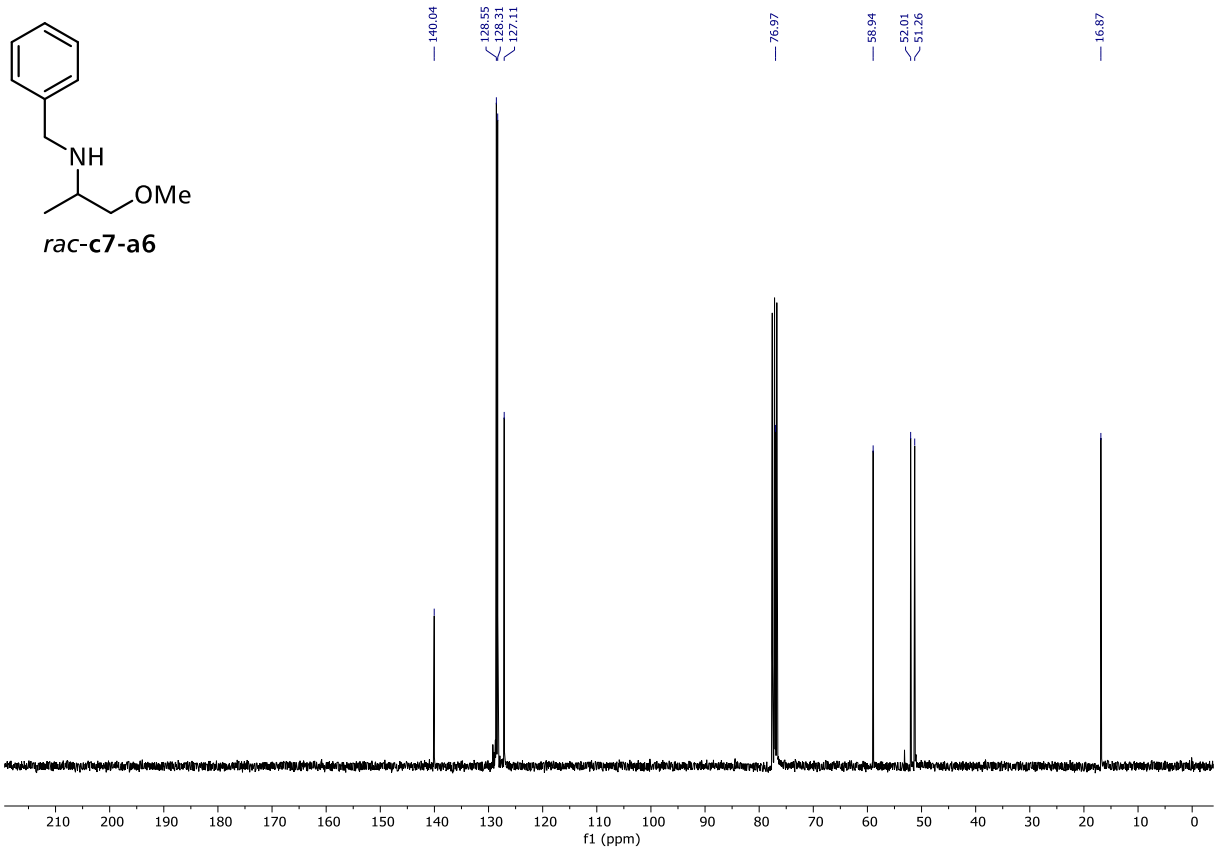


Figure S220. ^{13}C NMR spectrum of *rac*-*N*-benzyl-1-methoxypropan-2-amine (**c7-a6**).

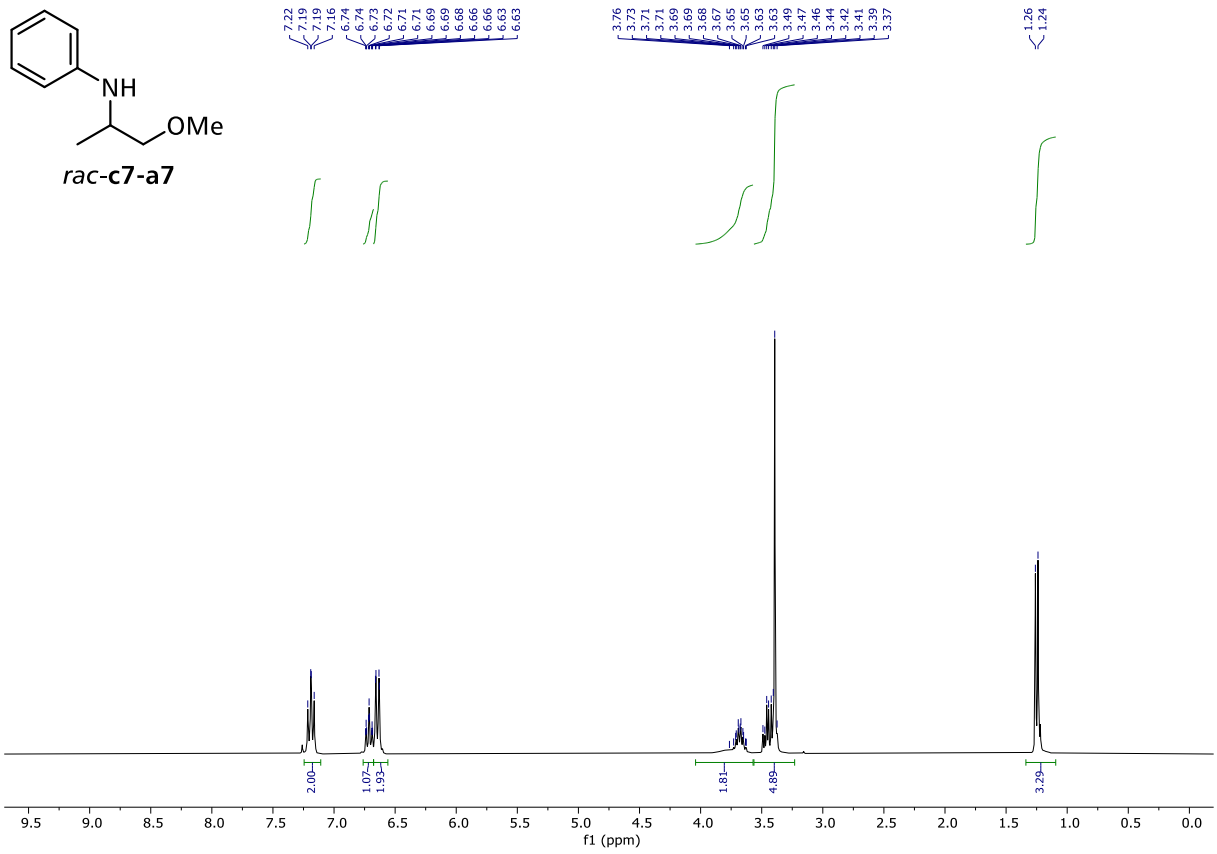


Figure S221. ^{1}H NMR spectrum of *rac*-*N*-(1-methoxypropan-2-yl)aniline (**c7-a7**).

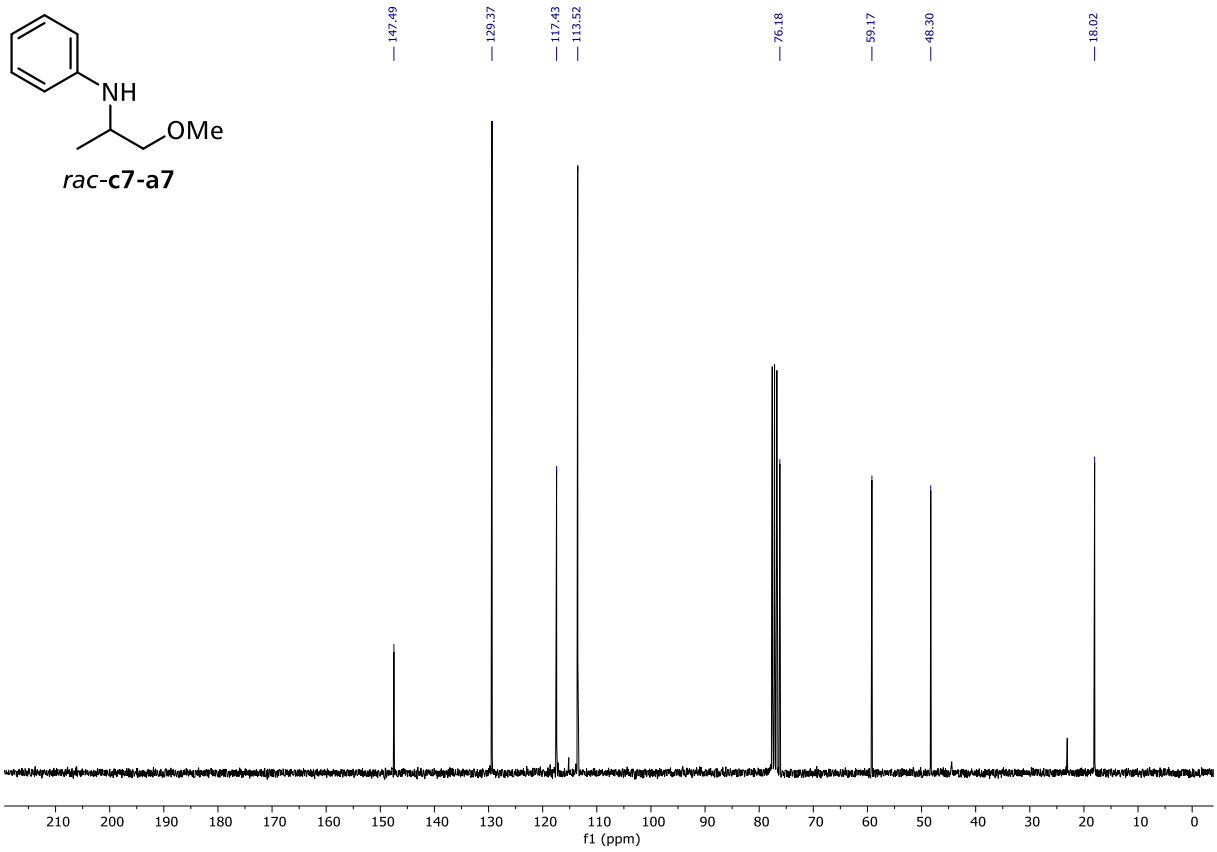


Figure S222. ^{13}C NMR spectrum of *rac*-*N*-(1-methoxypropan-2-yl)aniline (**c7-a7**).

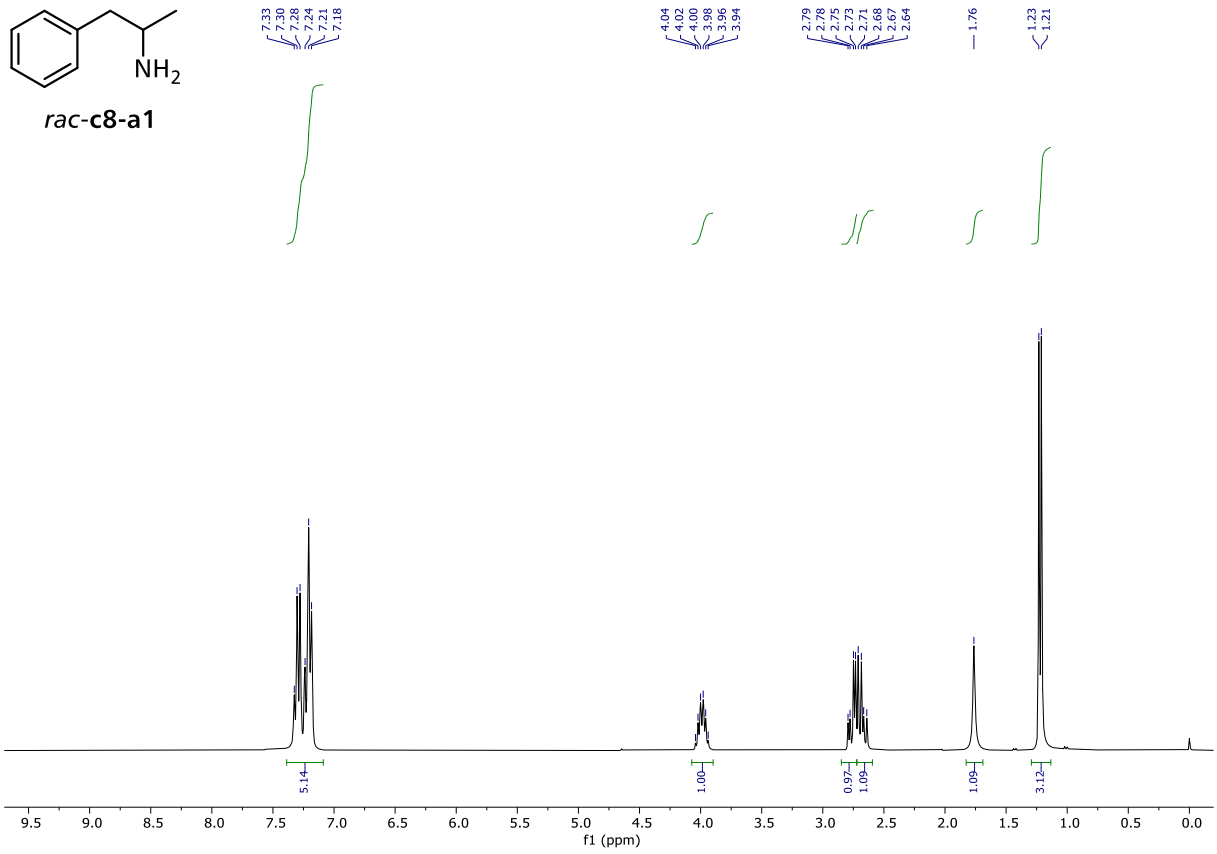


Figure S223. ^{1}H NMR spectrum of *rac*-1-phenylpropan-2-amine (**c8-a1**).

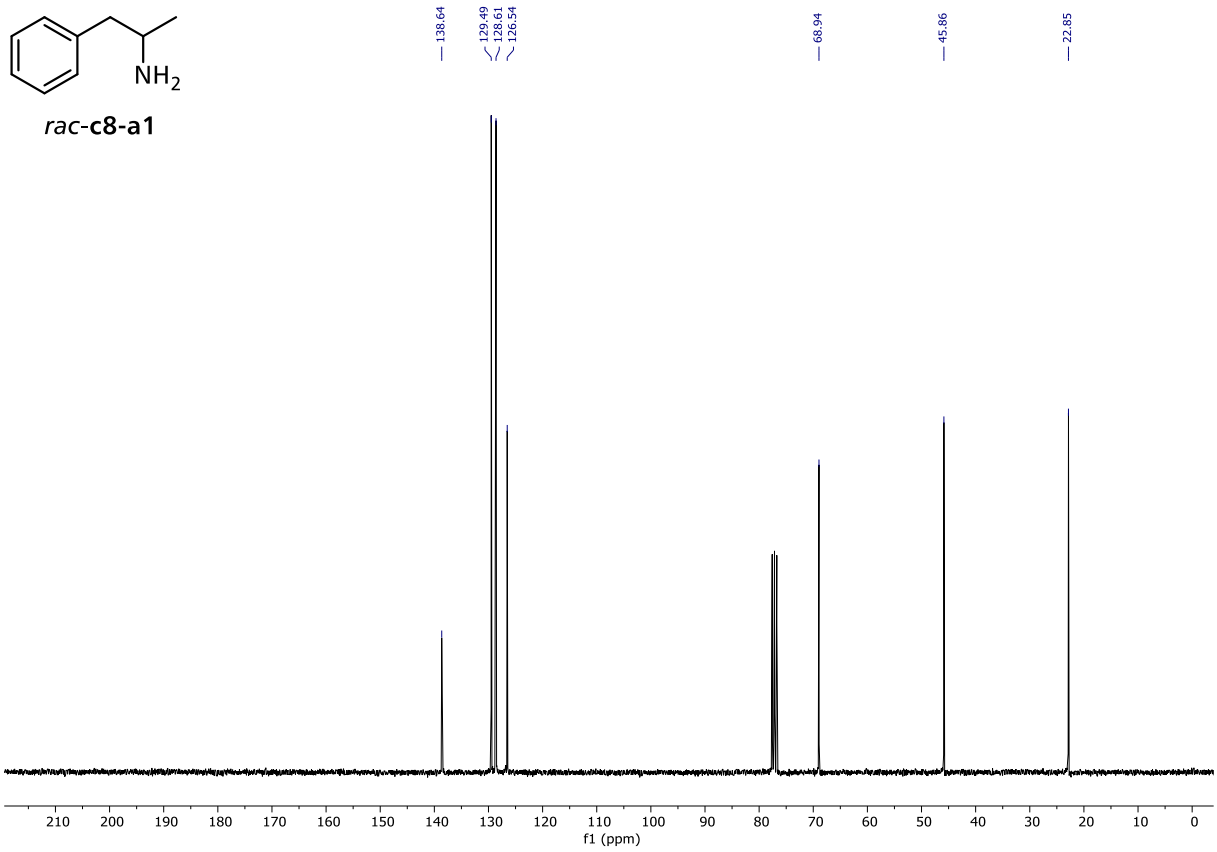


Figure S224. ^{13}C NMR spectrum of *rac*-1-phenylpropan-2-amine (**c8-a1**).

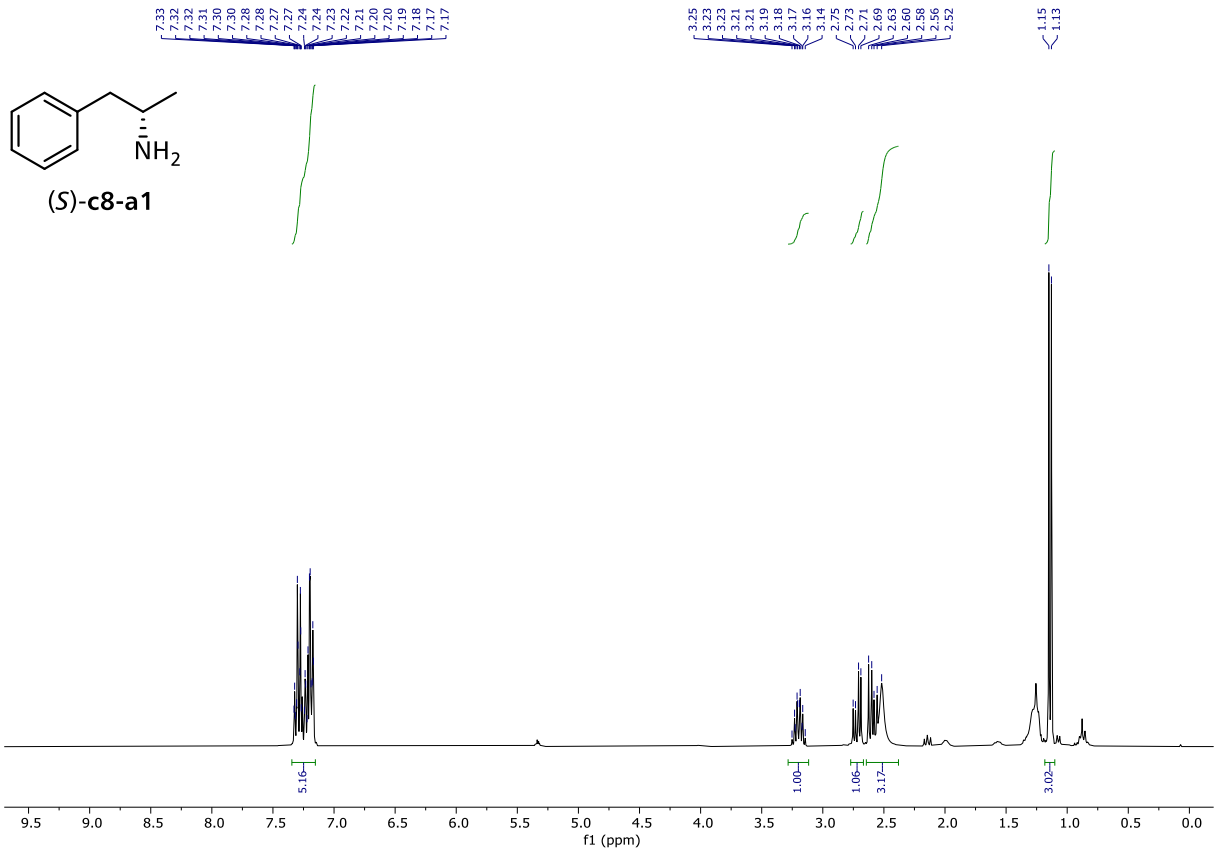


Figure S225. ^{1}H NMR spectrum of (*S*)-1-phenylpropan-2-amine (**c8-a1**).

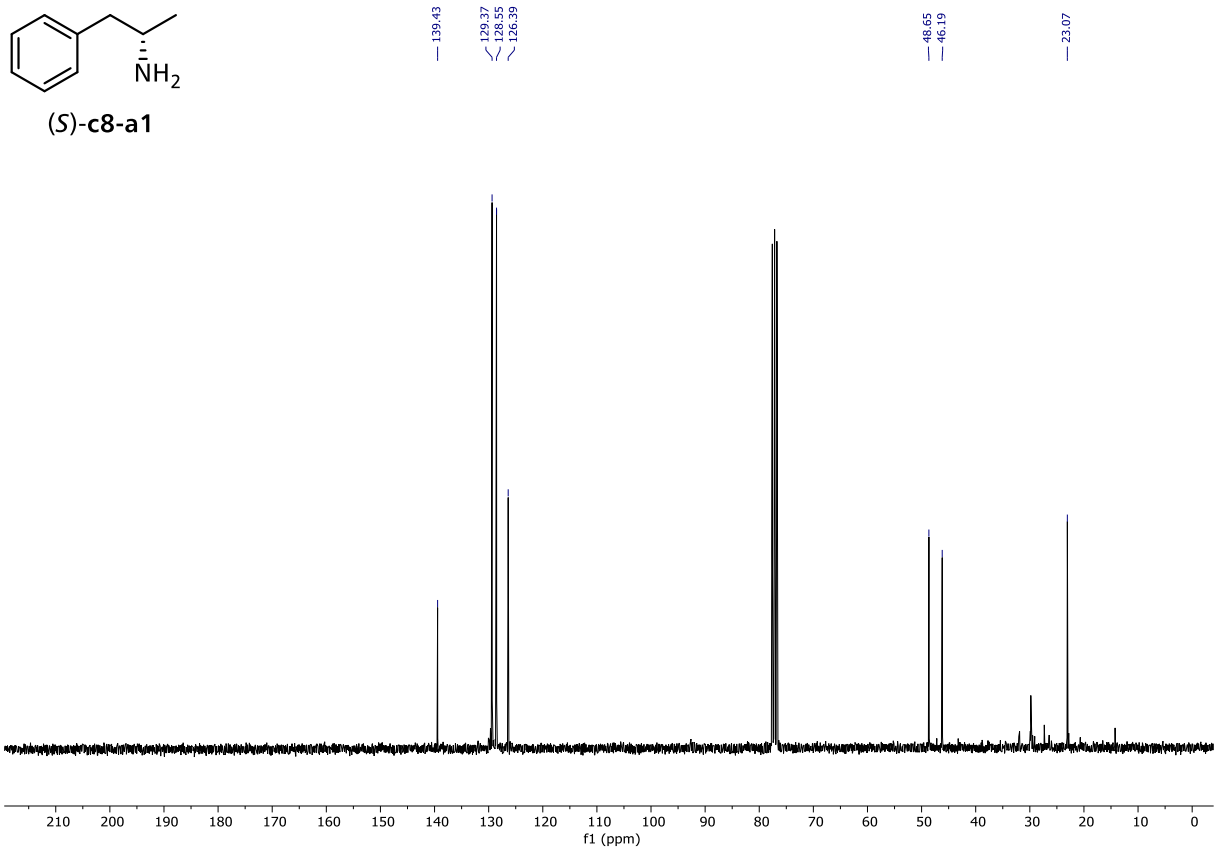


Figure S226. ^{13}C NMR spectrum of (*S*)-1-phenylpropan-2-amine (**c8-a1**).

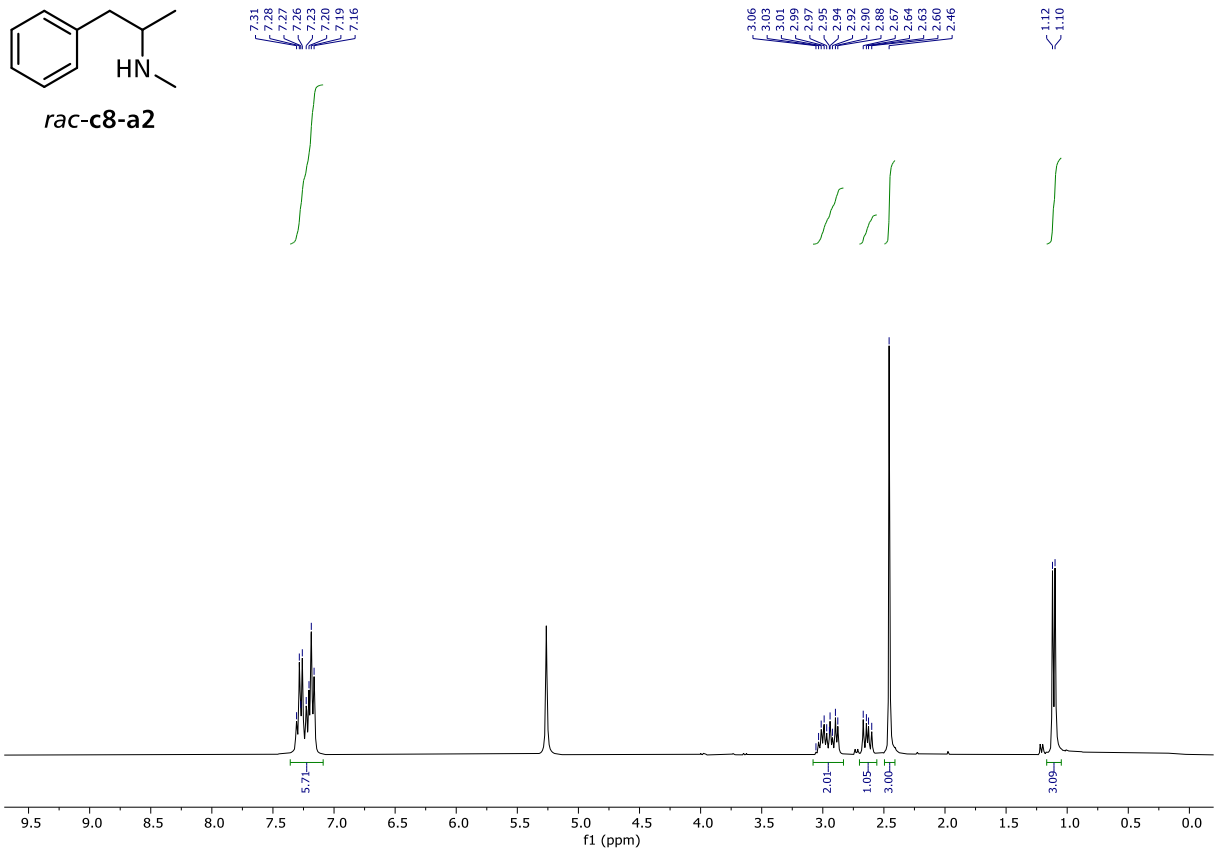


Figure S227. ^{1}H NMR spectrum of *rac*-*N*-methyl-1-phenylpropan-2-amine (**c8-a2**).

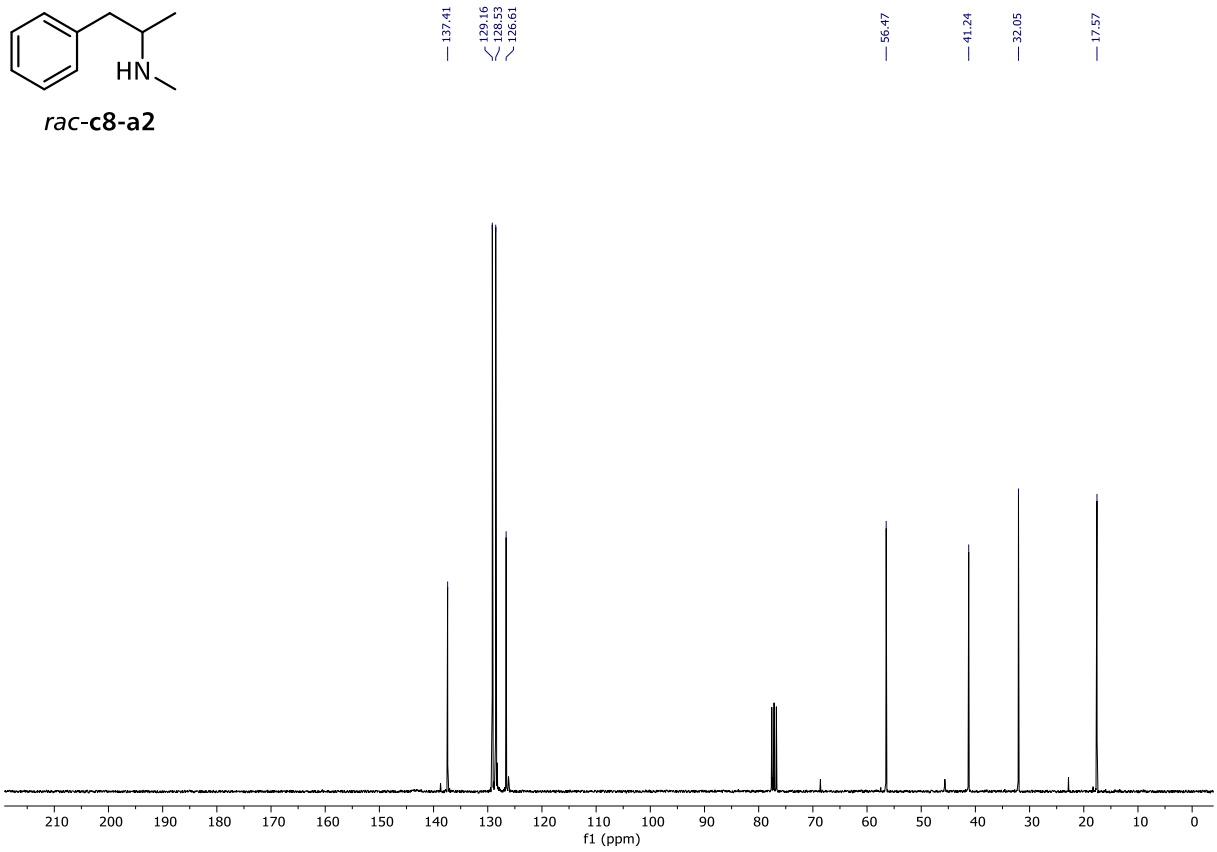


Figure S228. ^{13}C NMR spectrum of *rac*-*N*-methyl-1-phenylpropan-2-amine (**c8-a2**).

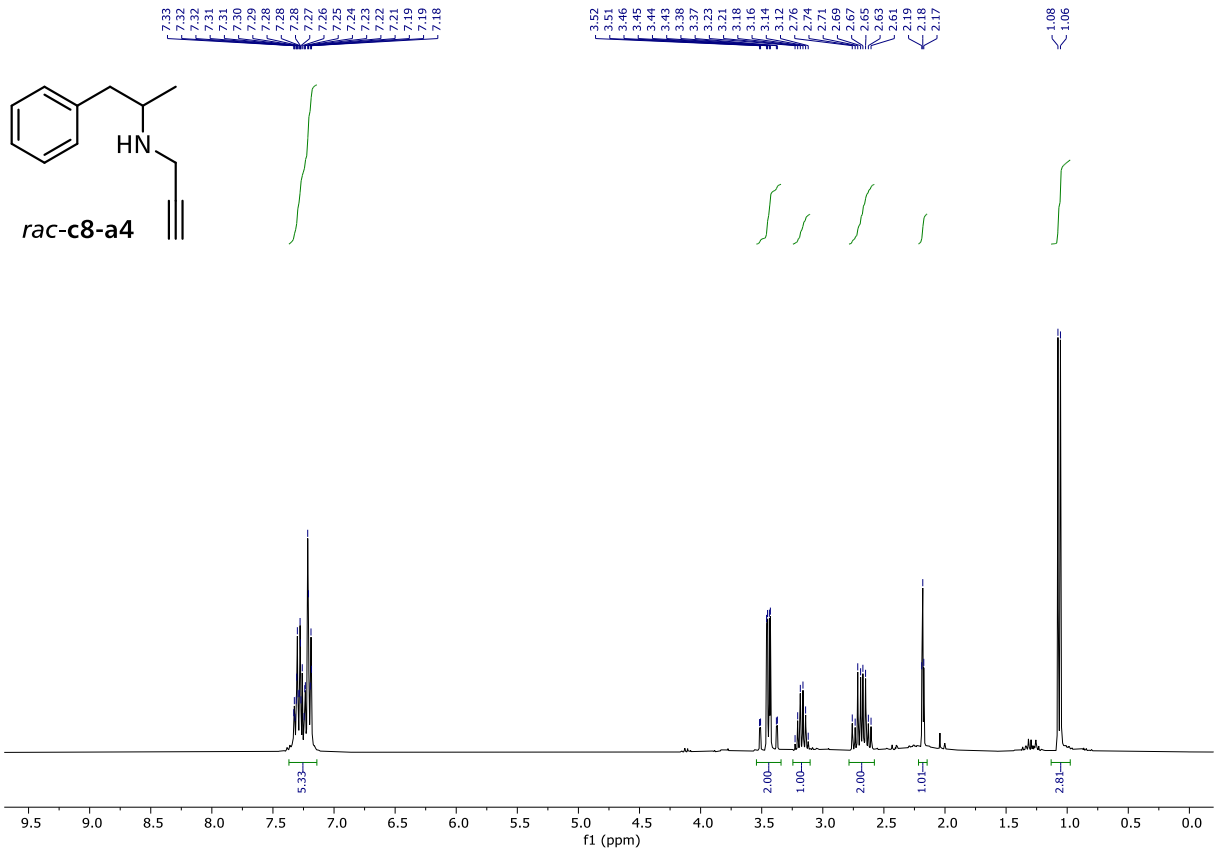


Figure S229. ^{1}H NMR spectrum of *rac*-*N*-(1-phenylpropan-2-yl)prop-2-yn-1-amine (**c8-a4**).

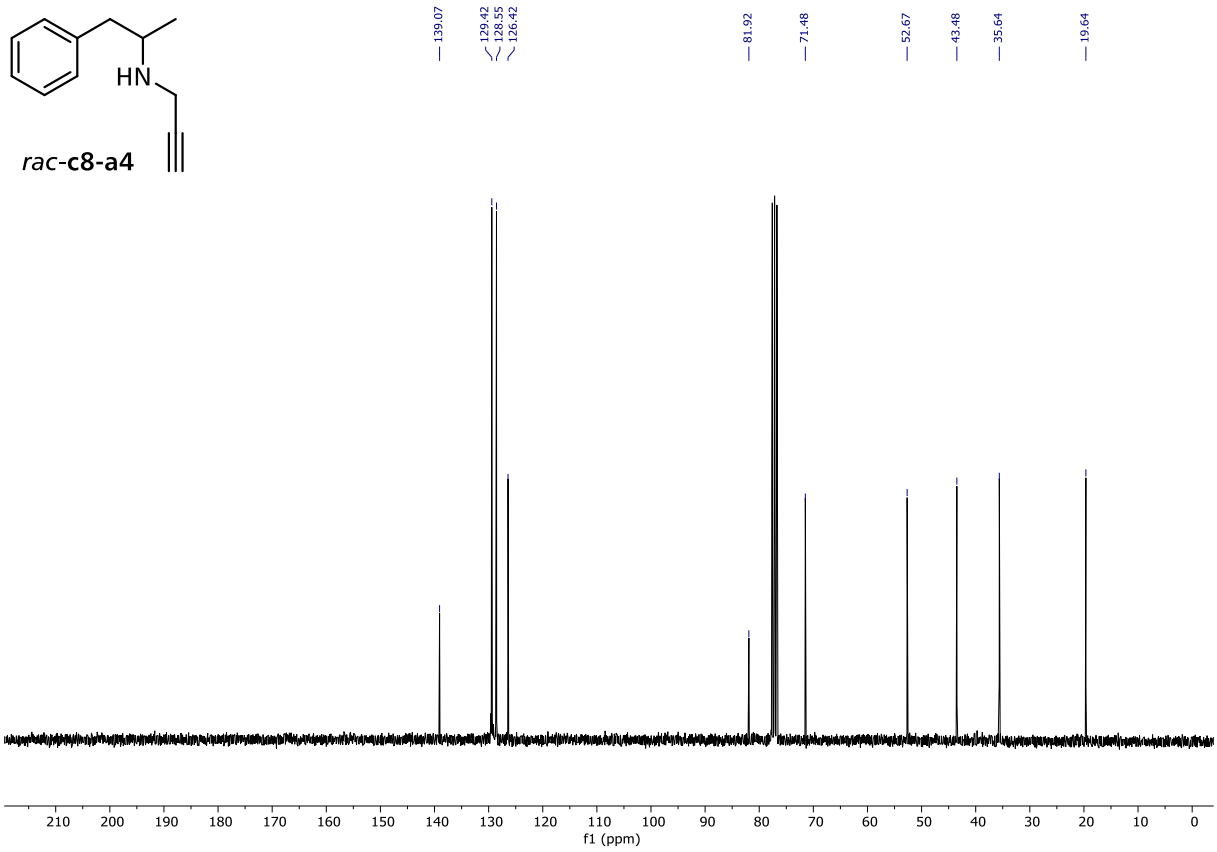


Figure S230. ^{13}C NMR spectrum of *rac*-*N*-(1-phenylpropan-2-yl)prop-2-yn-1-amine (**c8-a4**).

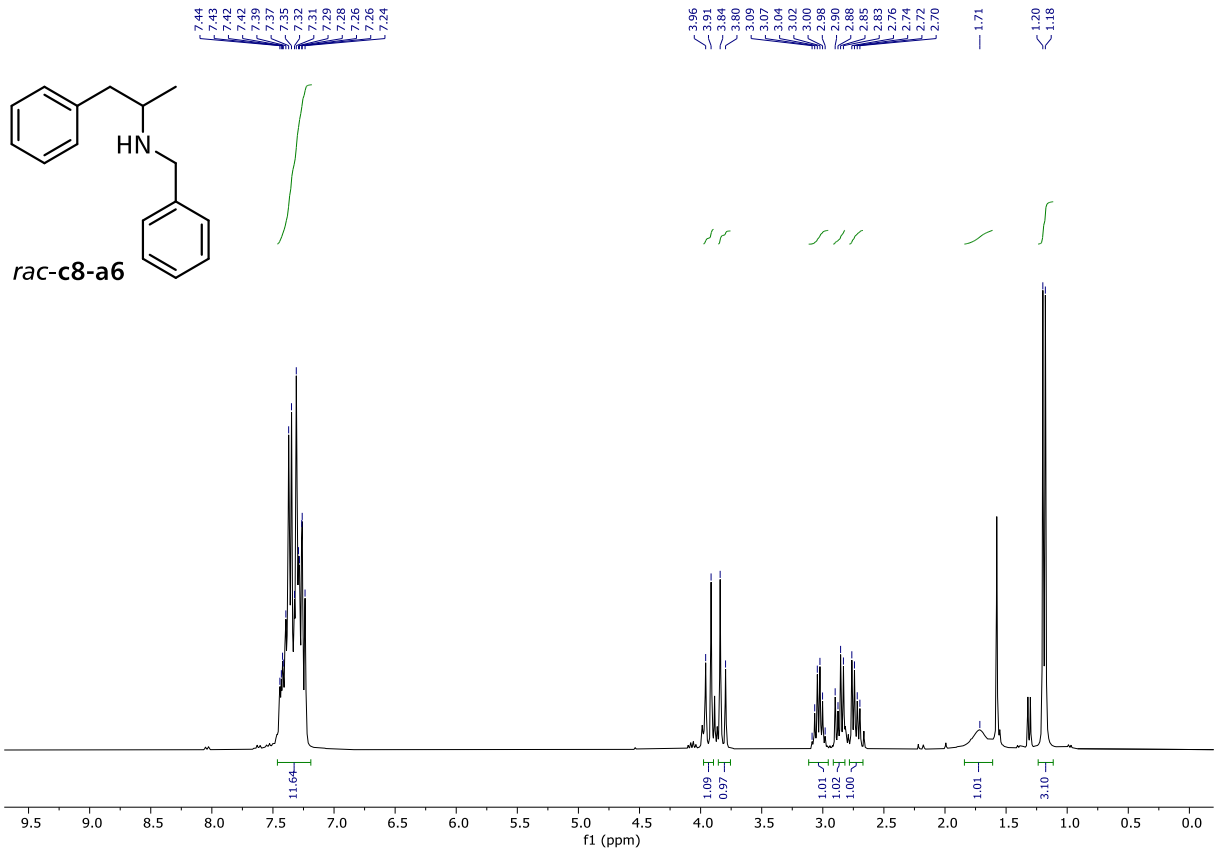


Figure S231. ^{1}H NMR spectrum of *rac*-*N*-benzyl-1-phenylpropan-2-amine (**c8-a6**).

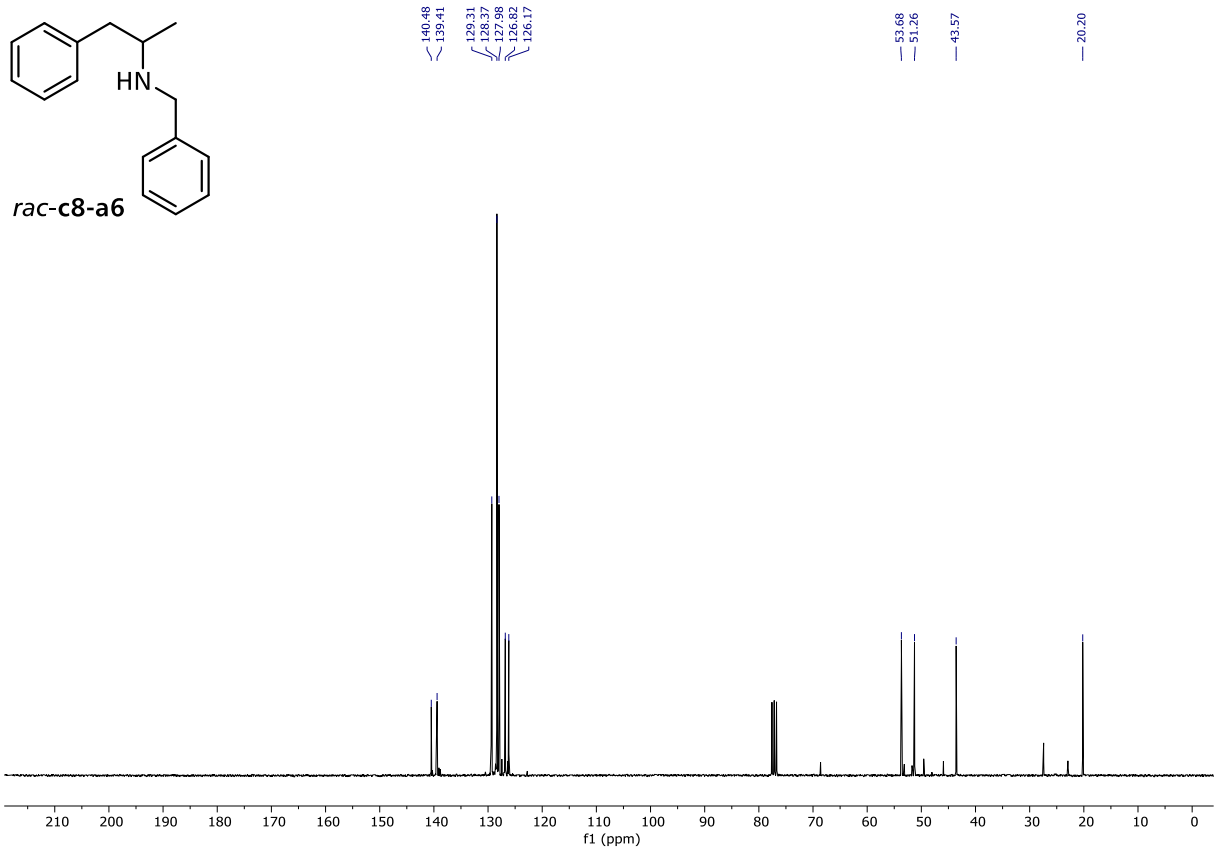


Figure S232. ^{13}C NMR spectrum of *rac*-*N*-benzyl-1-phenylpropan-2-amine (**c8-a6**).

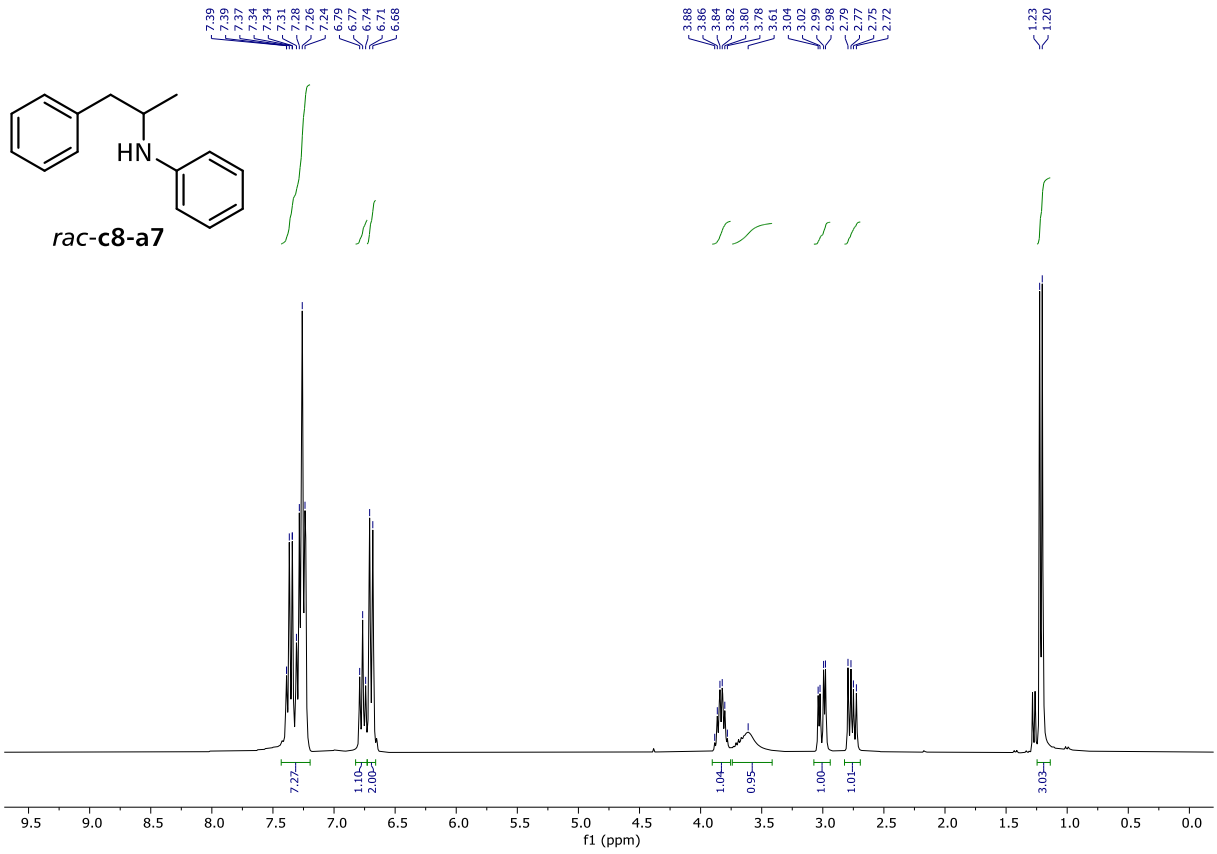


Figure S233. ^{1}H NMR spectrum of *rac*-*N*-(1-phenylpropan-2-yl)aniline (**c8-a7**).

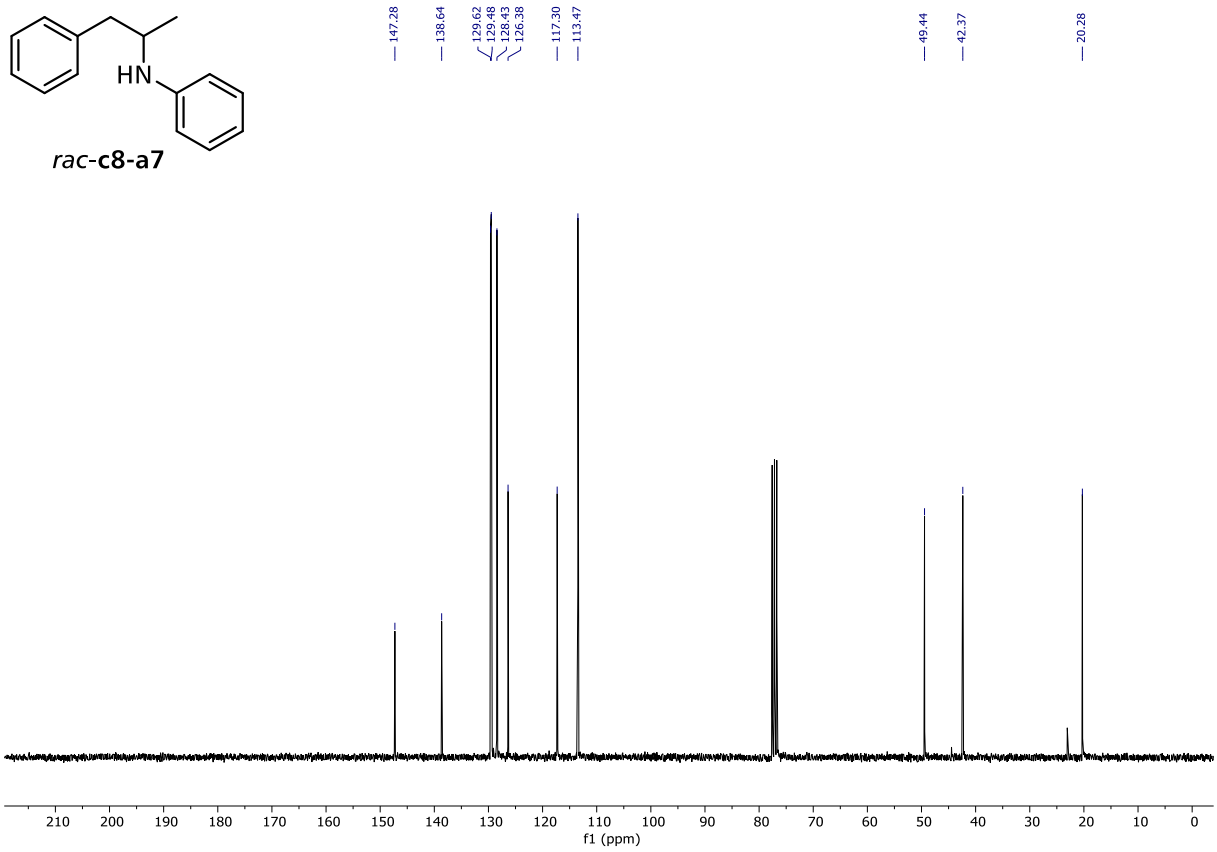


Figure S234. ^{13}C NMR spectrum of *rac*-*N*-(1-phenylpropan-2-yl)aniline (**c8-a7**).

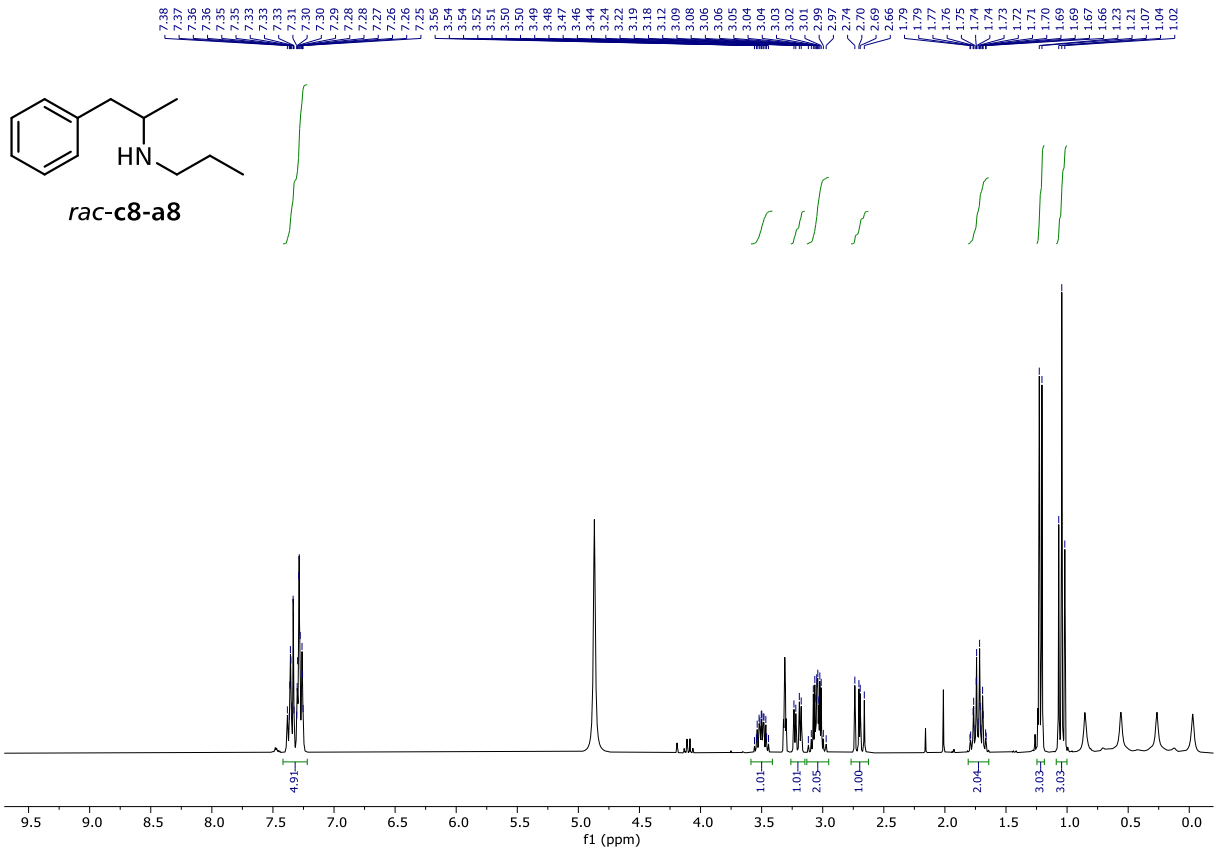


Figure S235. ^{1}H NMR spectrum of *rac*-*N*-(1-phenylpropan-2-yl)propan-1-amine (**c8-a8**).

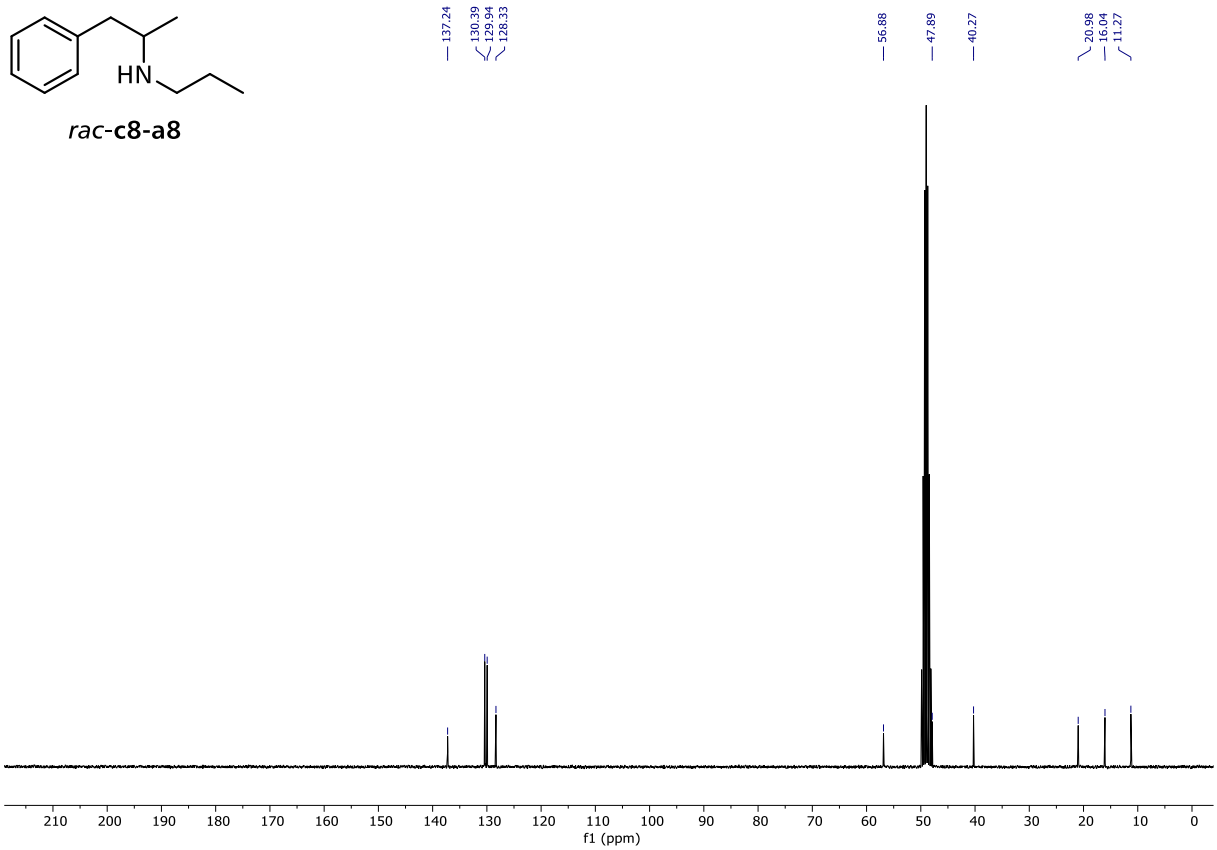


Figure S236. ^{13}C NMR spectrum of *rac*-*N*-(1-phenylpropan-2-yl)propan-1-amine (**c8-a8**).

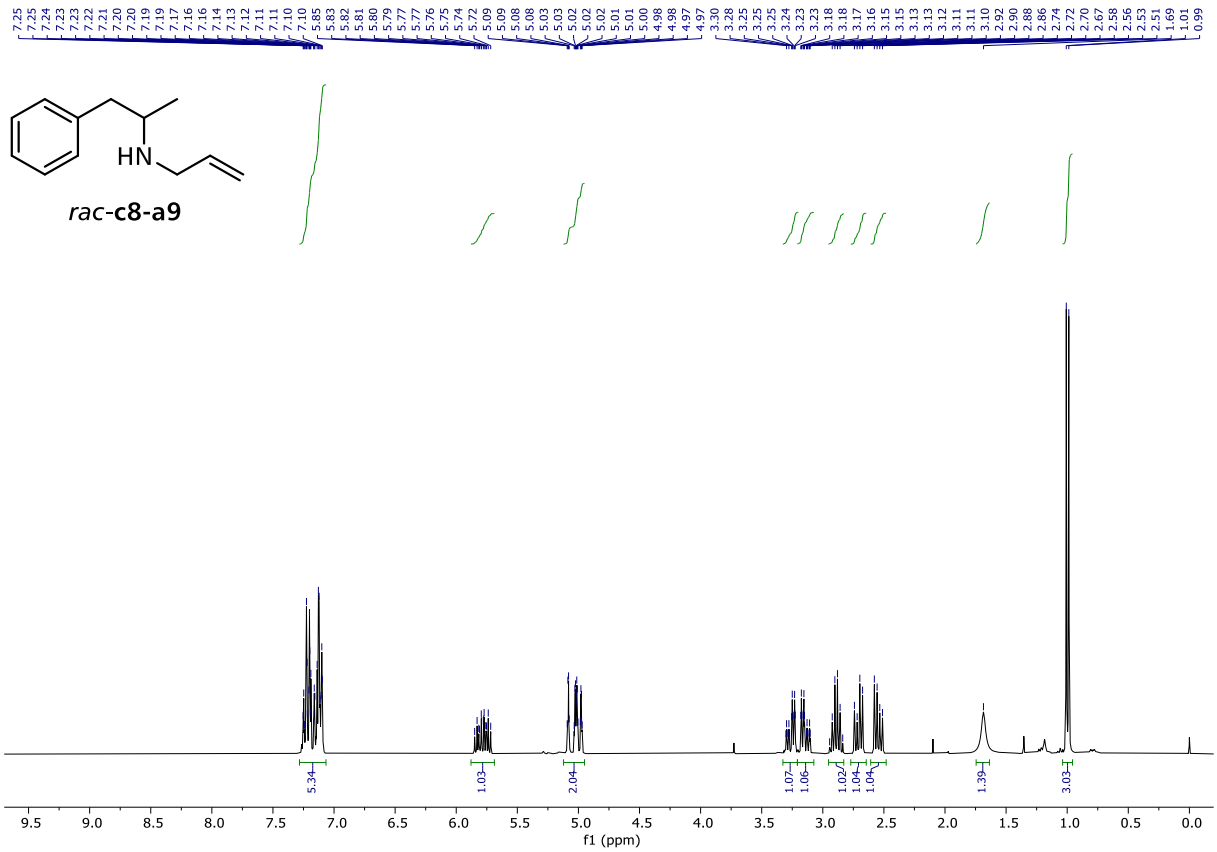


Figure S237. ^{1}H NMR spectrum of *rac*-*N*-(1-phenylpropan-2-yl)prop-2-en-1-amine (**c8-a9**).

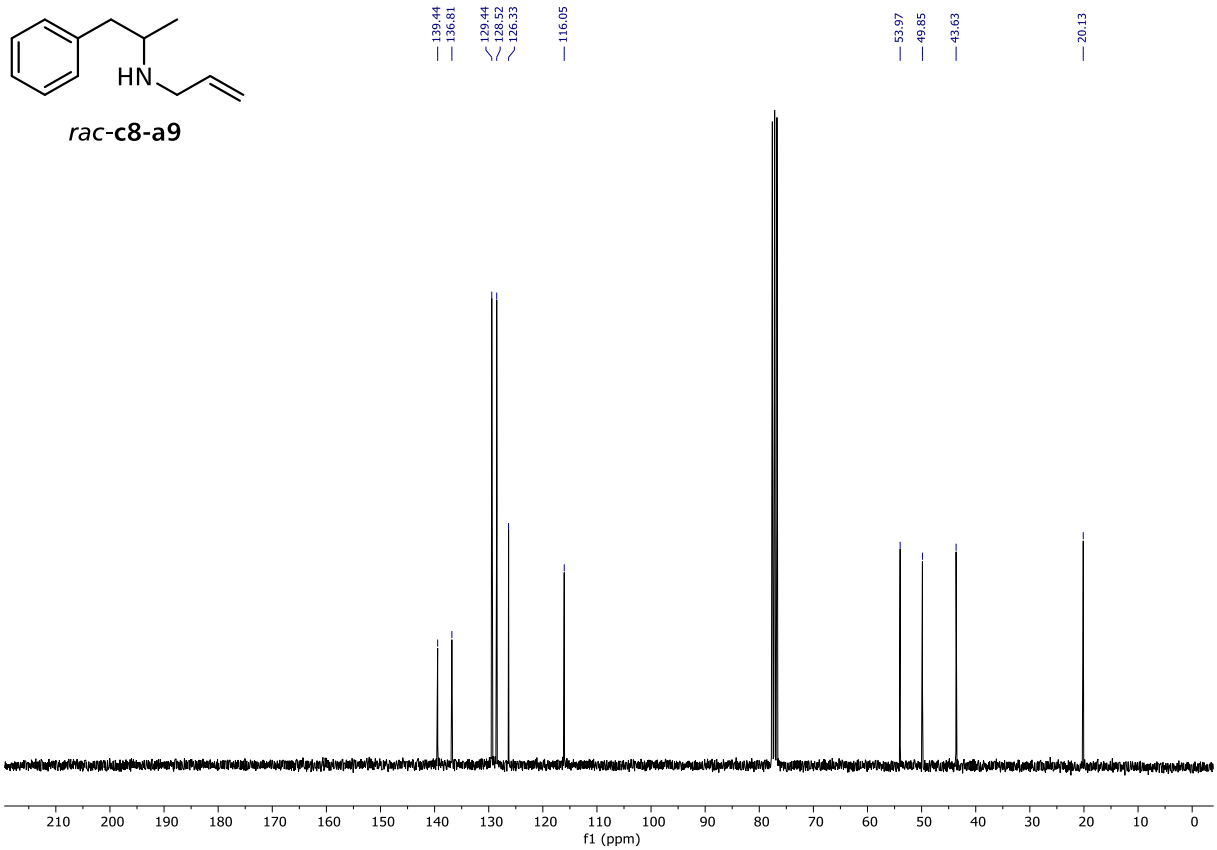


Figure S238. ^{13}C NMR spectrum of *rac*-*N*-(1-phenylpropan-2-yl)prop-2-en-1-amine (**c8-a9**).

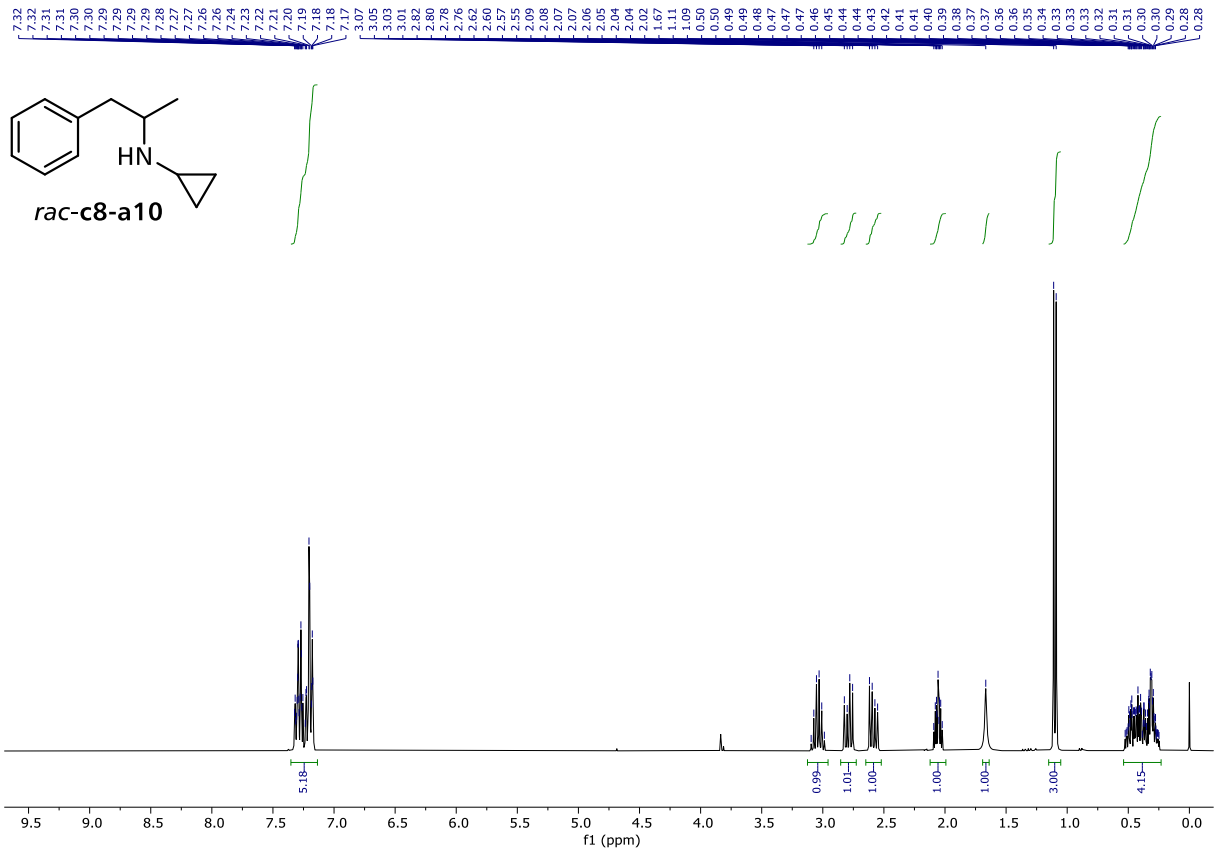


Figure S239. ^{1}H NMR spectrum of *rac*-*N*-(1-phenylpropan-2-yl)cyclopropanamine (**c8-a10**).

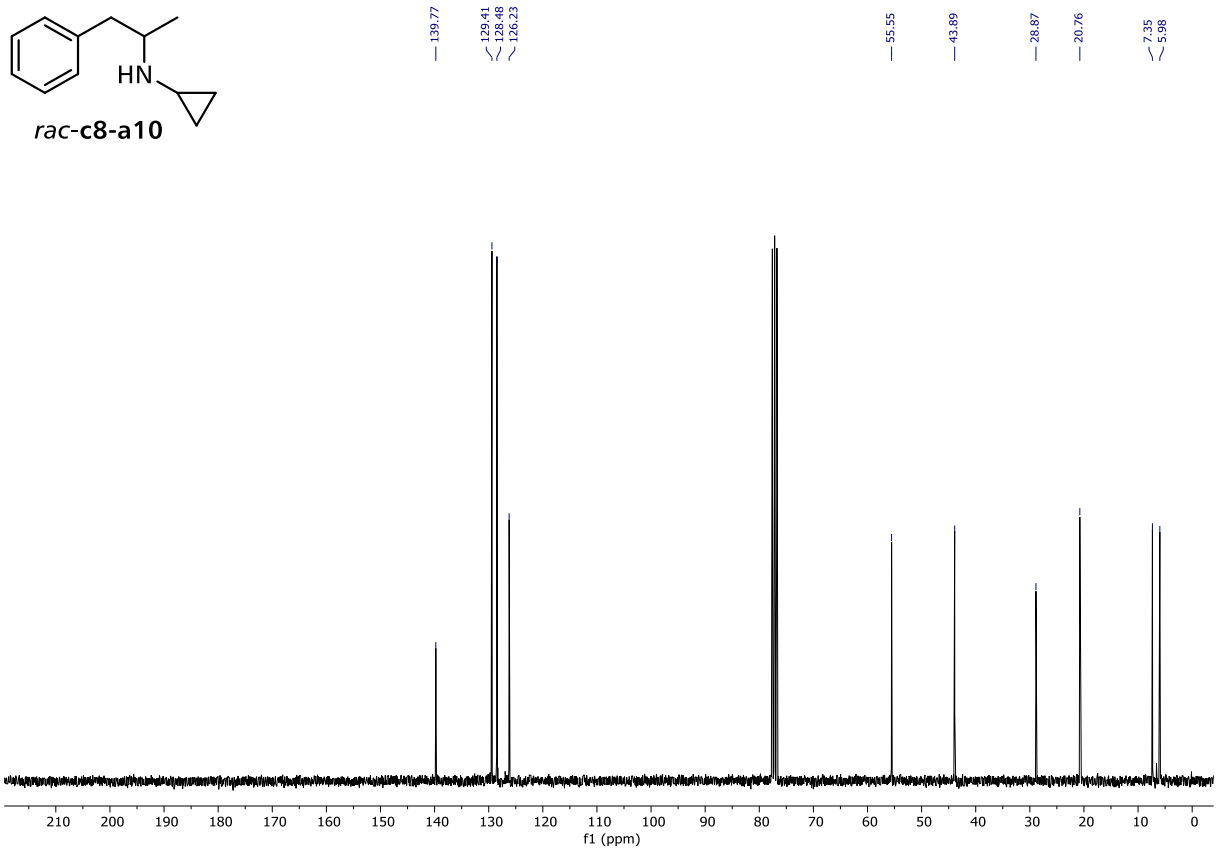


Figure S240. ^{13}C NMR spectrum of *rac*-*N*-(1-phenylpropan-2-yl)cyclopropanamine (**c8-a10**).

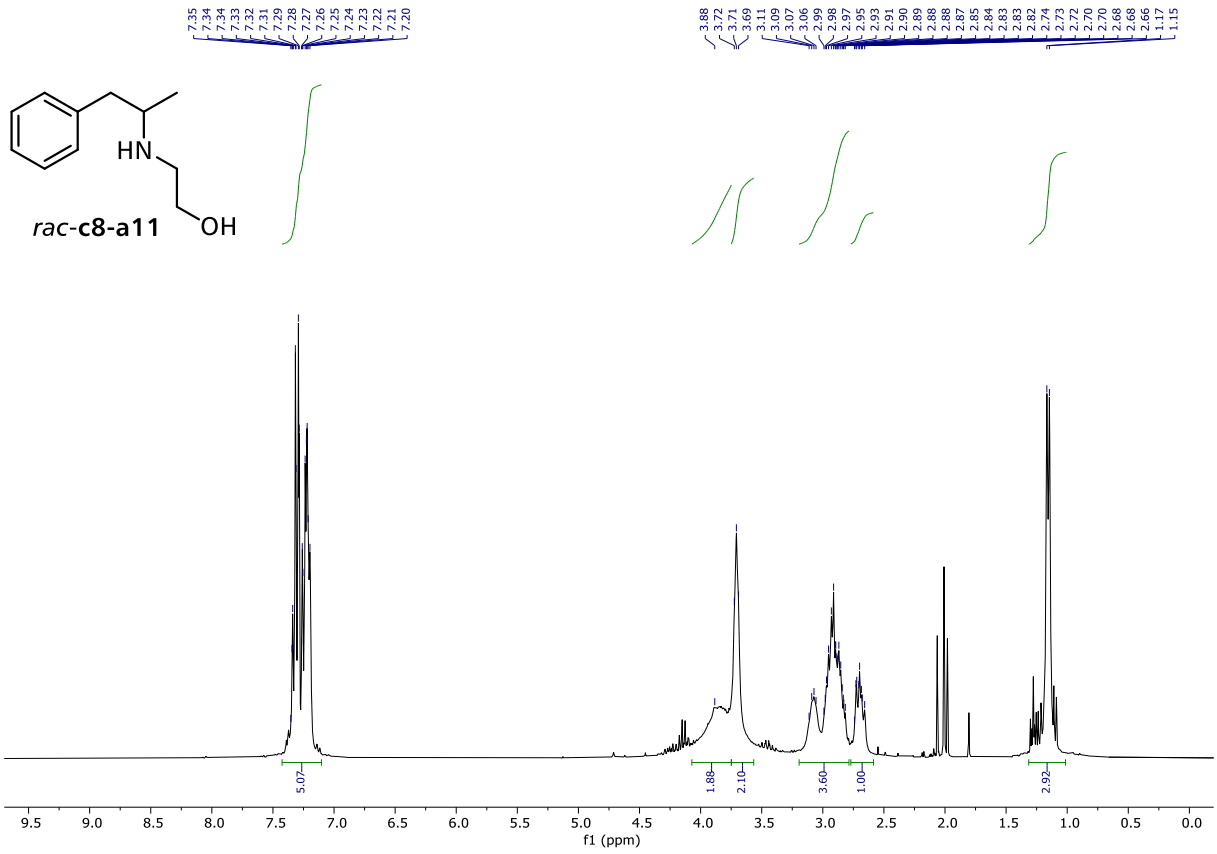


Figure S241. ^{1}H NMR spectrum of *rac*-2-((1-phenylpropan-2-yl)amino)ethan-1-ol (**c8-a11**).

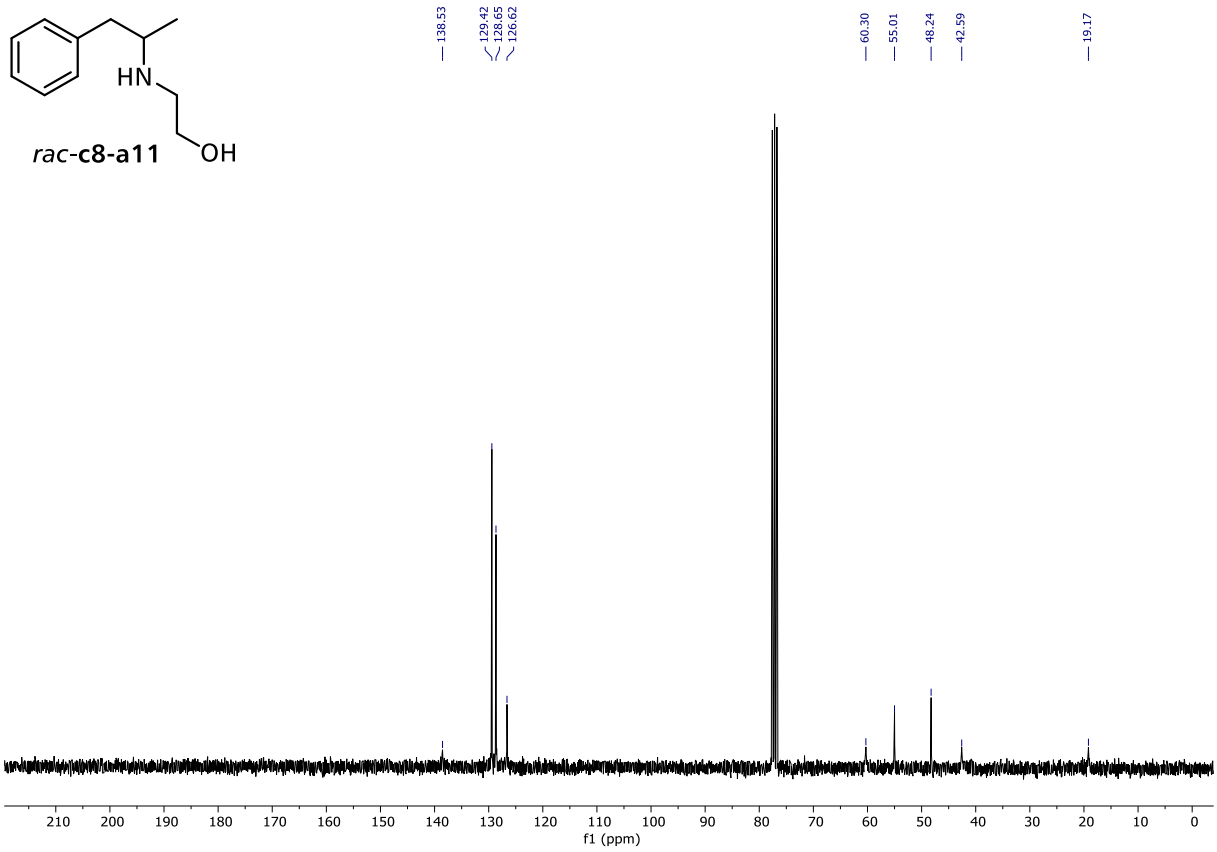


Figure S242. ^{13}C NMR spectrum of *rac*-2-((1-phenylpropan-2-yl)amino)ethan-1-ol (**c8-a11**).

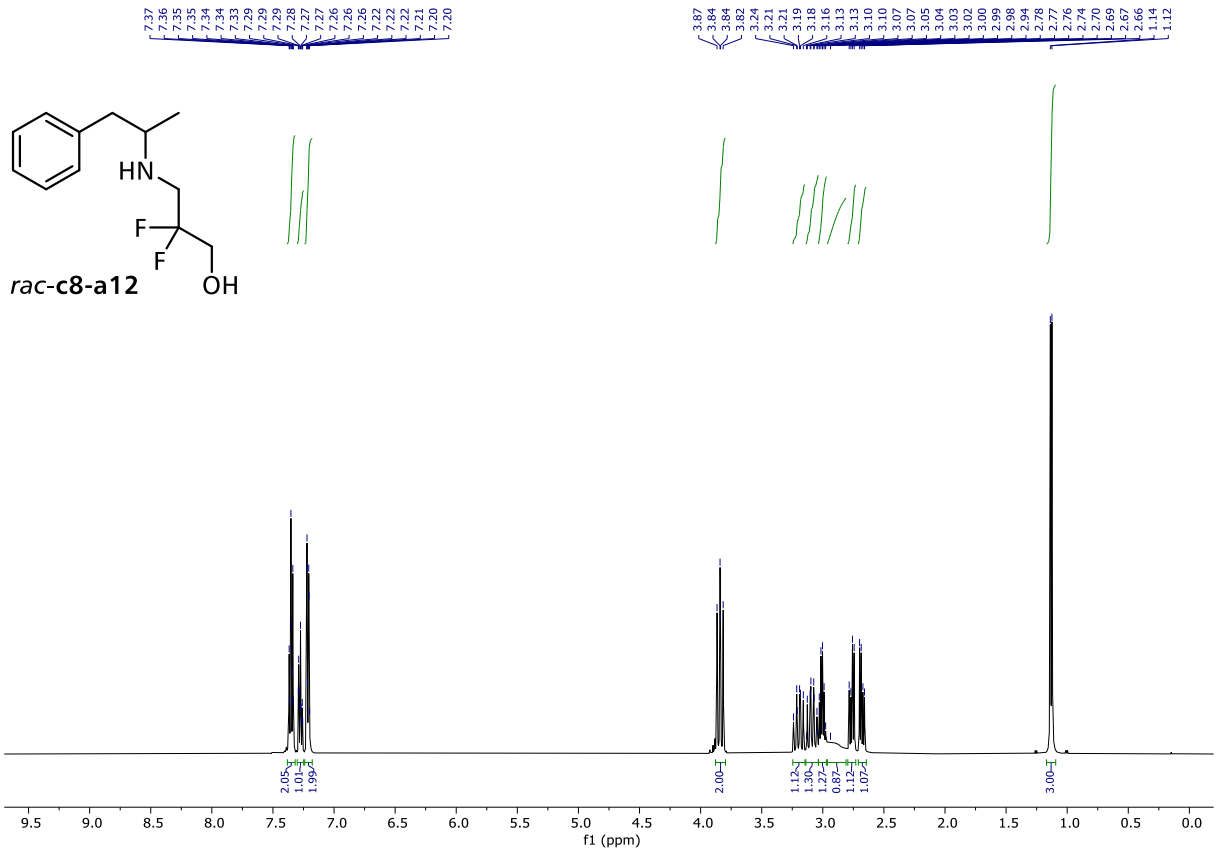


Figure S243. ^{1}H NMR spectrum of *rac*-2,2-difluoro-3-((1-phenylpropan-2-yl)amino)propan-1-ol (**c8-a12**).

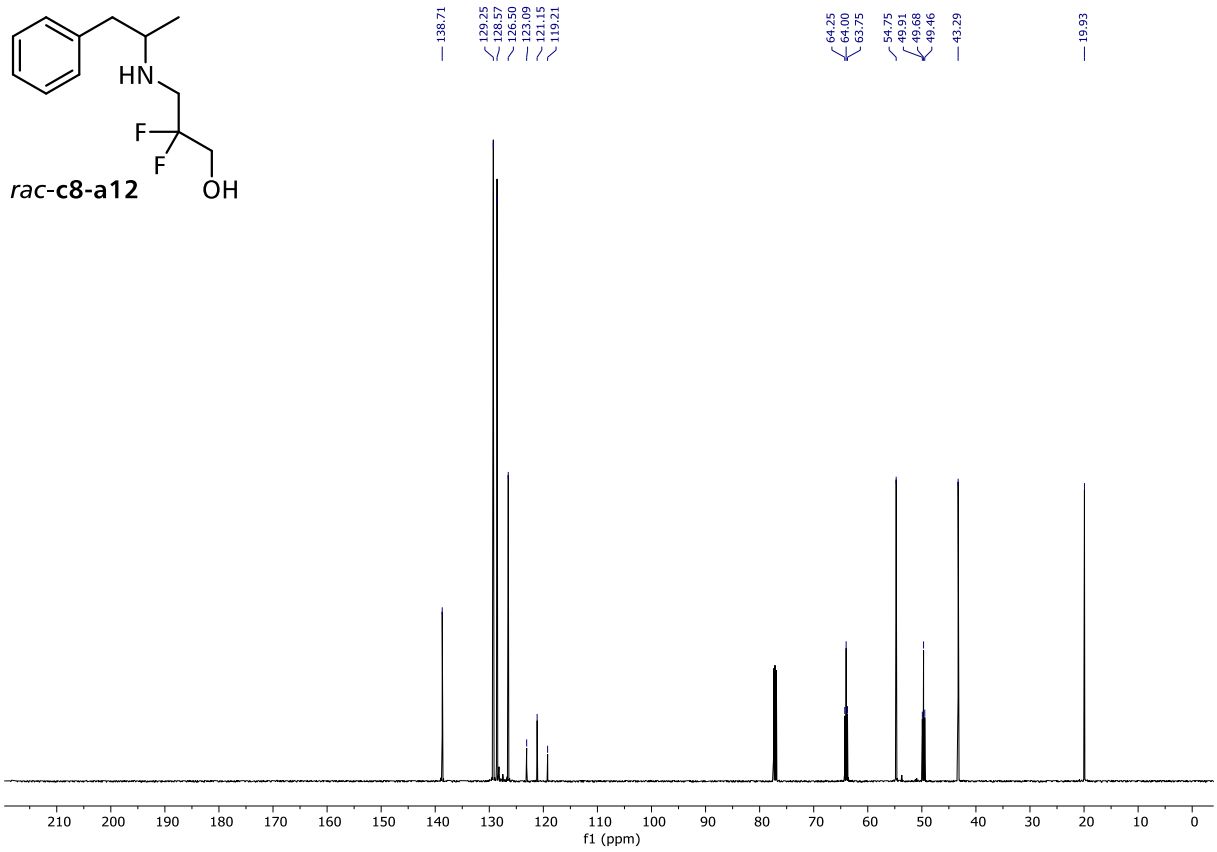


Figure S244. ^{13}C NMR spectrum of *rac*-2,2-difluoro-3-((1-phenylpropan-2-yl)amino)propan-1-ol (**c8-a12**).

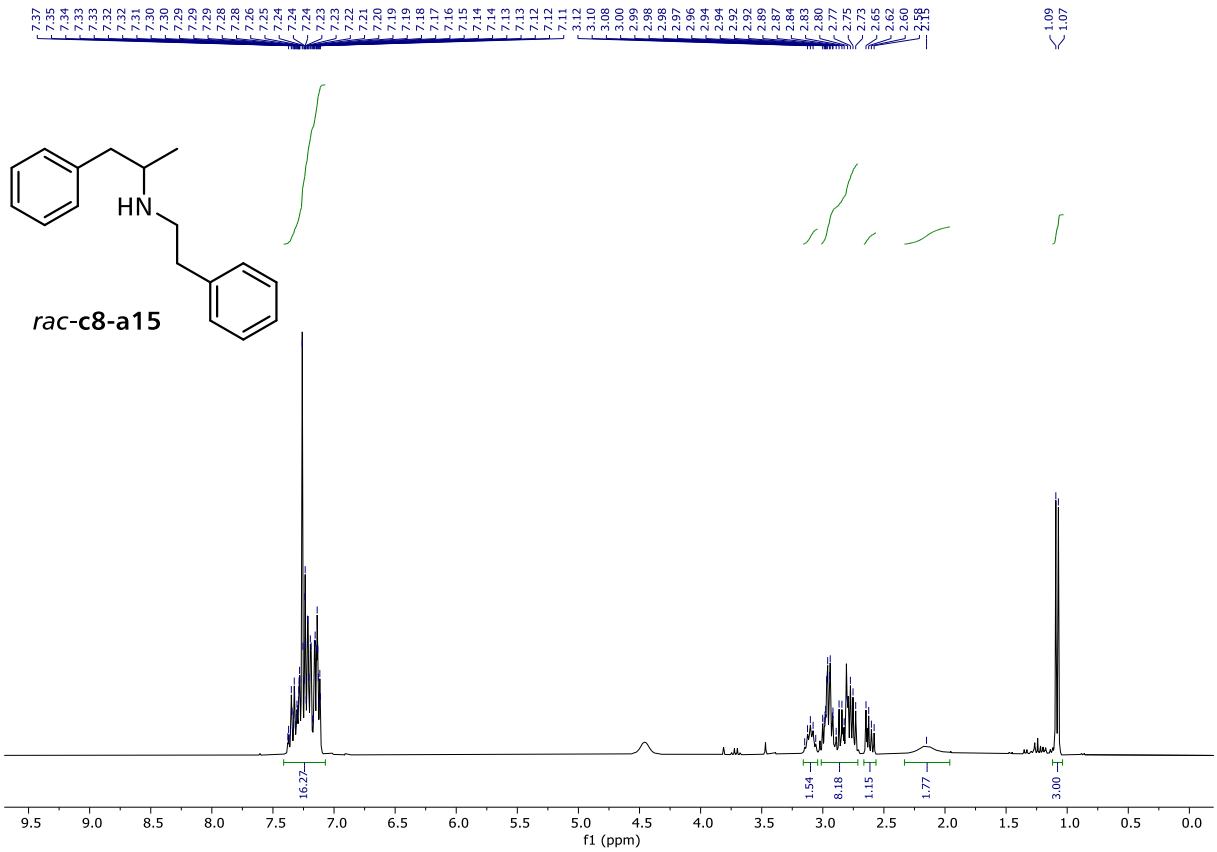


Figure S245. ^{1}H NMR spectrum of *rac*-*N*-phenethyl-1-phenylpropan-2-amine (**c8-a15**).

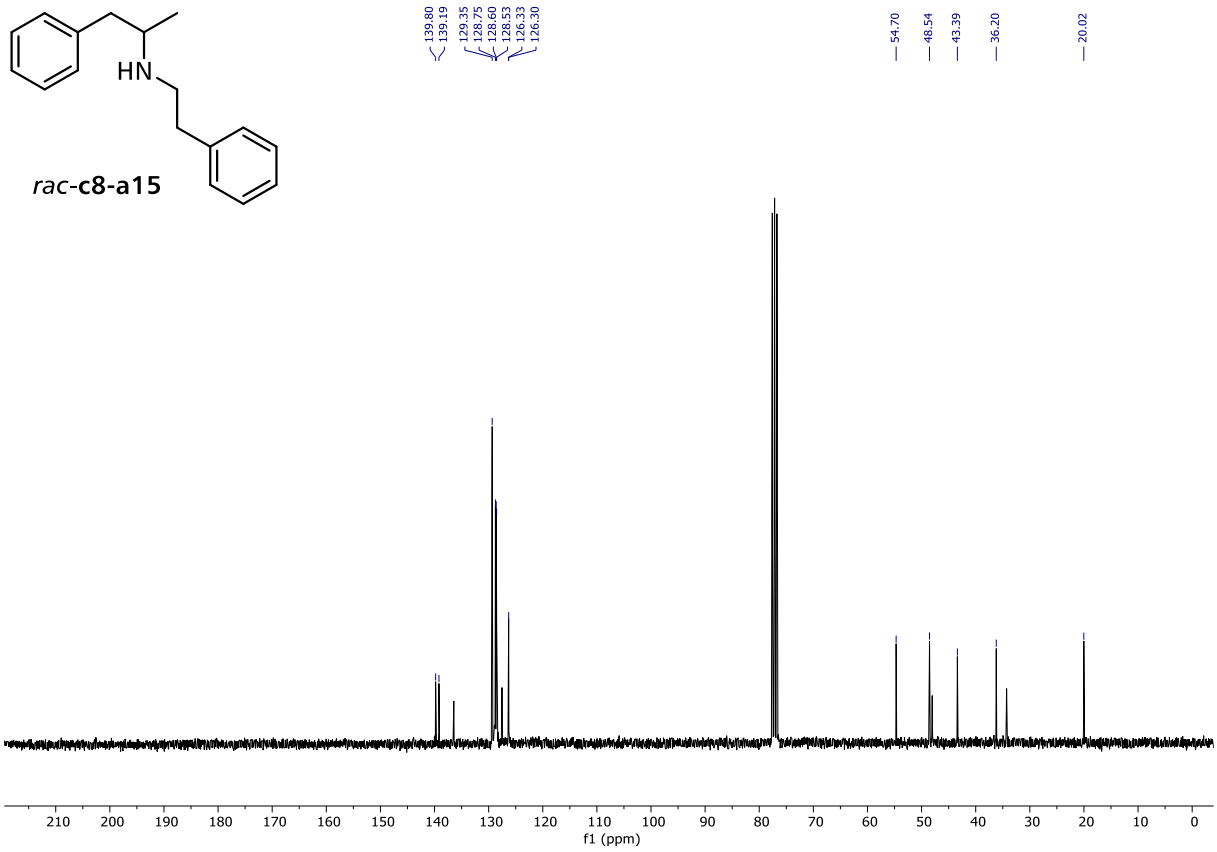


Figure S246. ^{13}C NMR spectrum of *rac*-*N*-phenethyl-1-phenylpropan-2-amine (**c8-a15**).

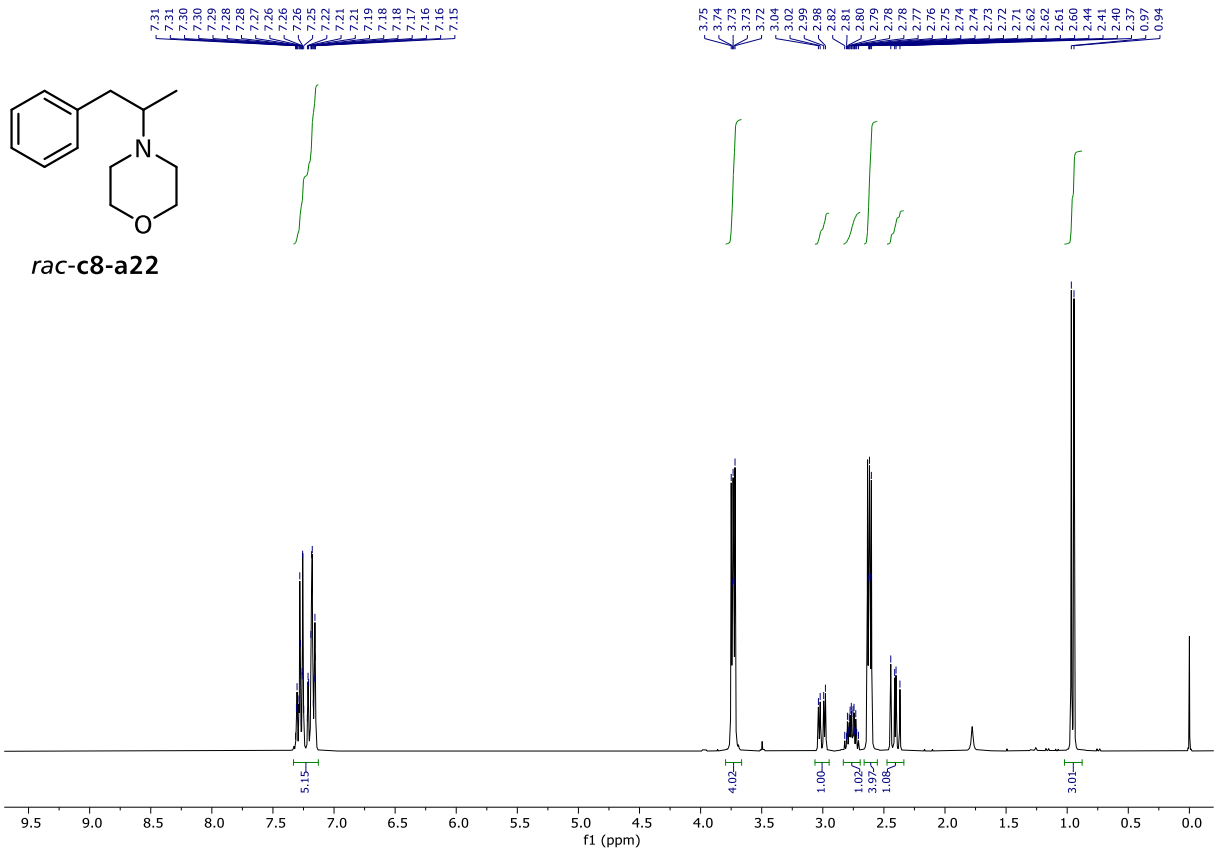


Figure S247. ^{1}H NMR spectrum of *rac*-4-(1-phenylpropan-2-yl)morpholine (**c8-a22**).

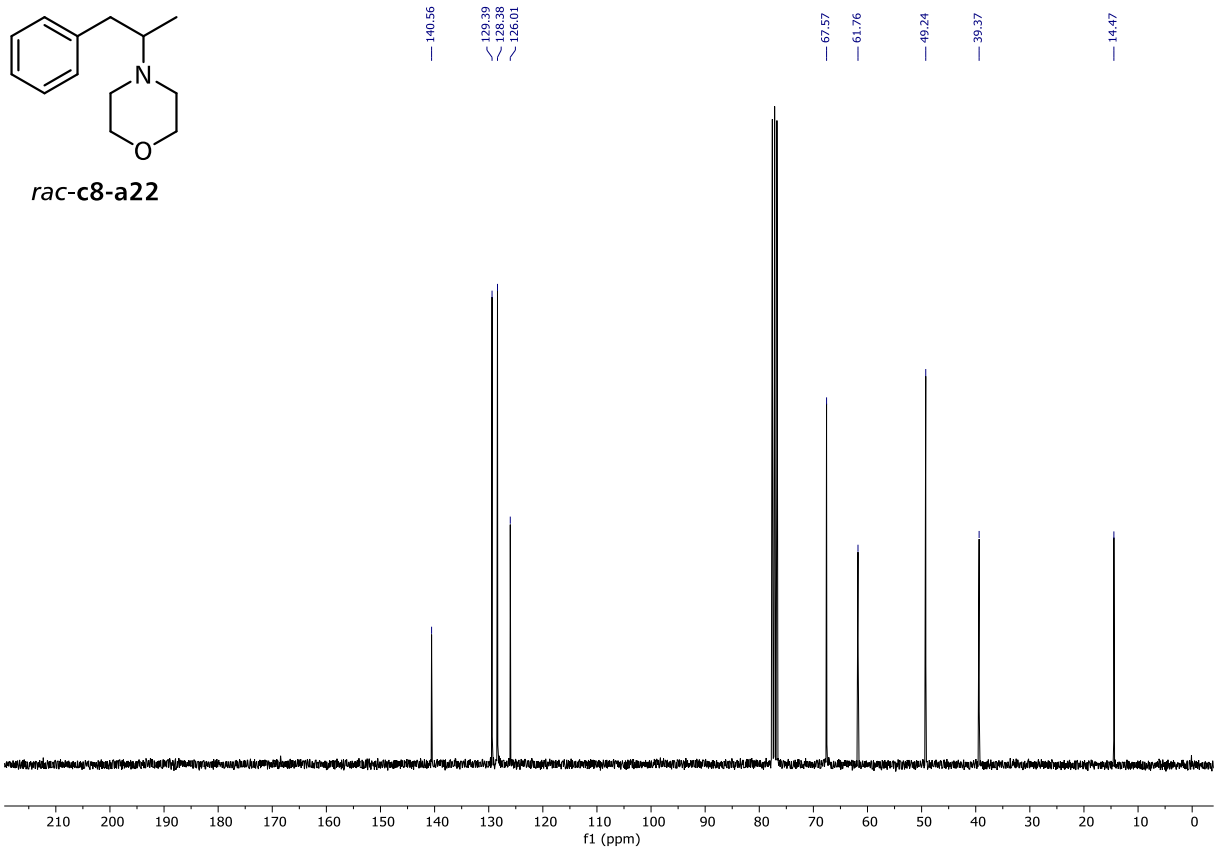


Figure S248. ^{13}C NMR spectrum of *rac*-4-(1-phenylpropan-2-yl)morpholine (**c8-a22**).

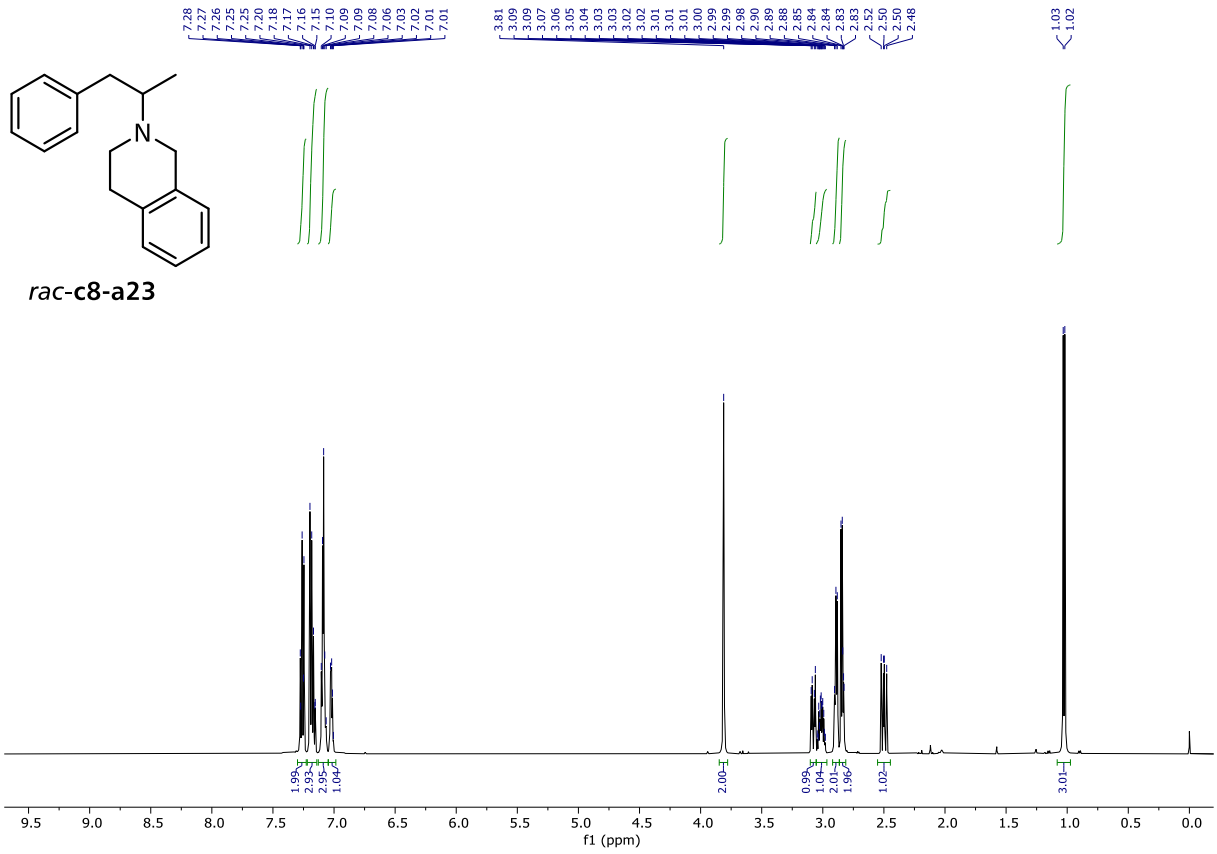


Figure S249. ^{1}H NMR spectrum of *rac*-2-(1-phenylpropan-2-yl)-1,2,3,4-tetrahydroisoquinoline (**c8-a23**).

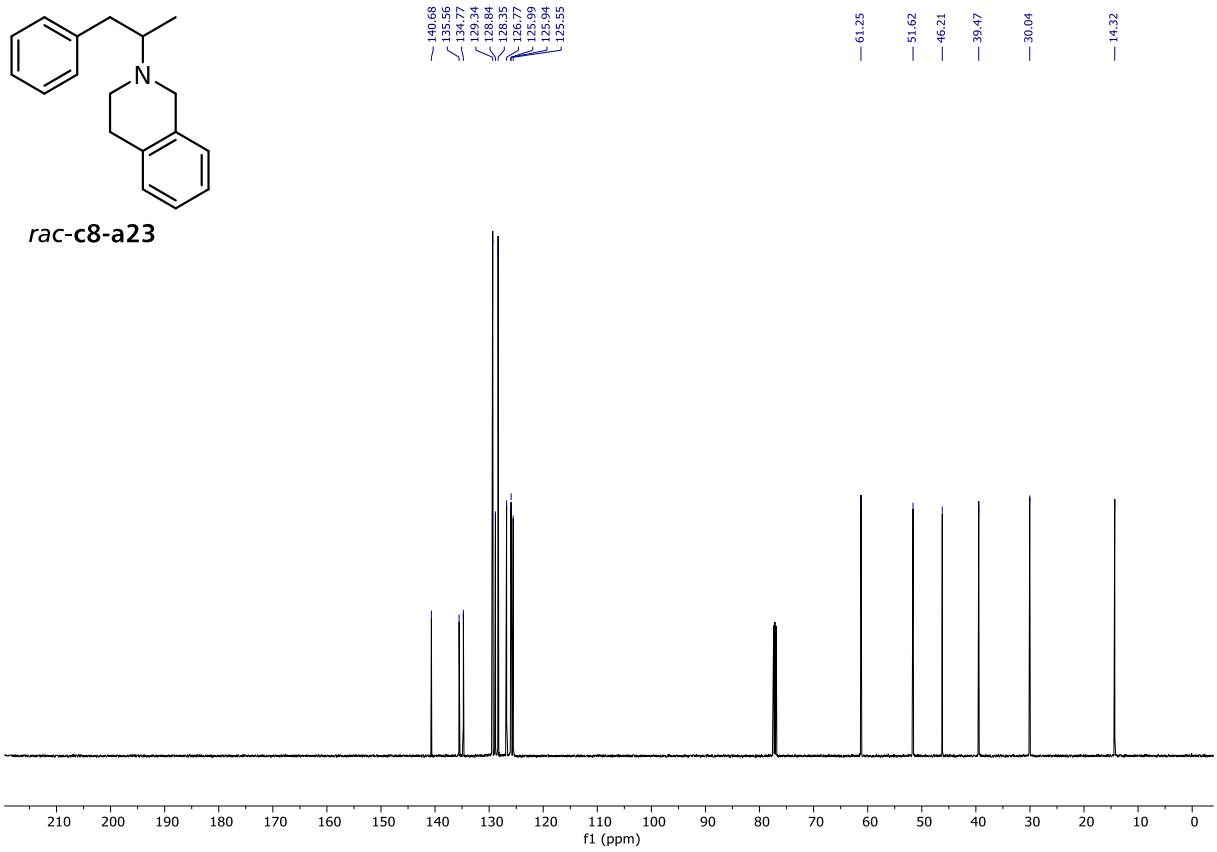


Figure S250. ^{13}C NMR spectrum of *rac*-2-(1-phenylpropan-2-yl)-1,2,3,4-tetrahydroisoquinoline (**c8-a23**).

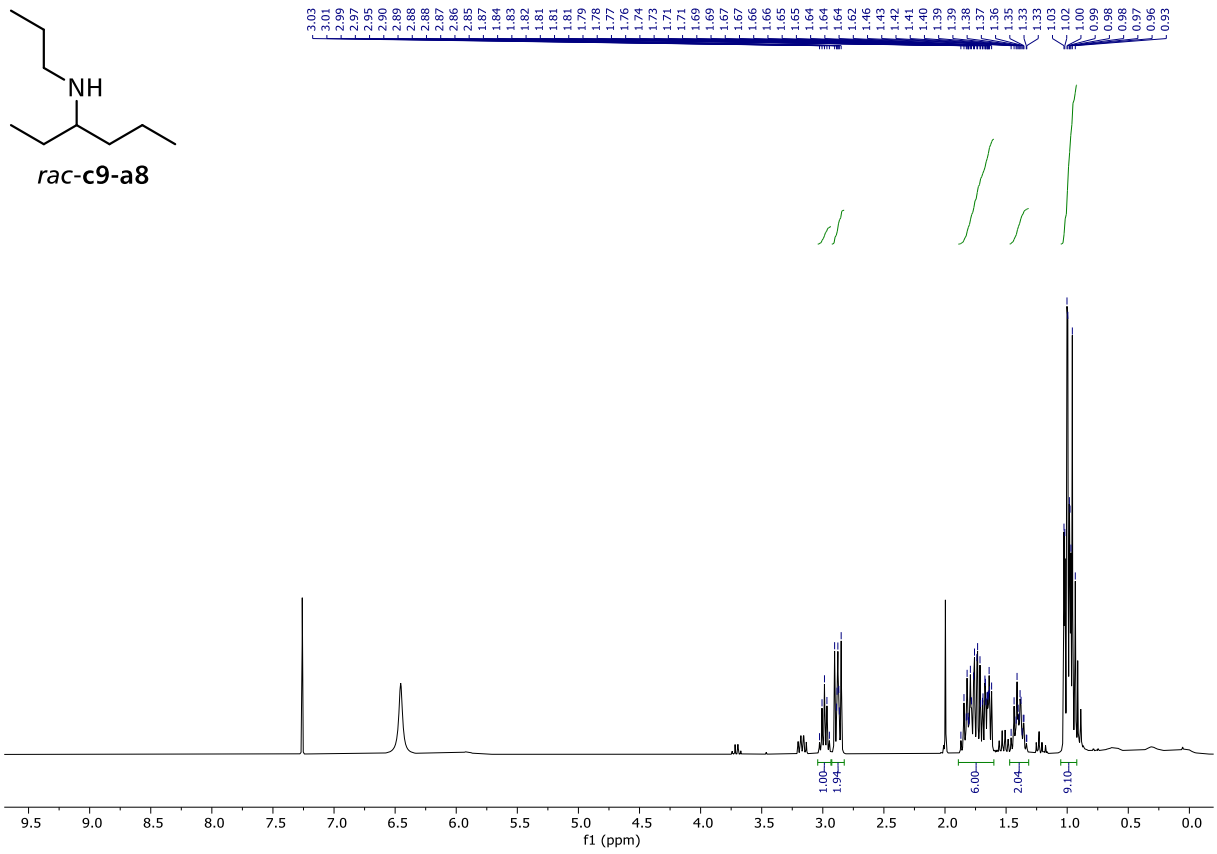


Figure S251. ^{1}H NMR spectrum of *rac*-*N*-propylhexan-3-amine (**c9-a8**).

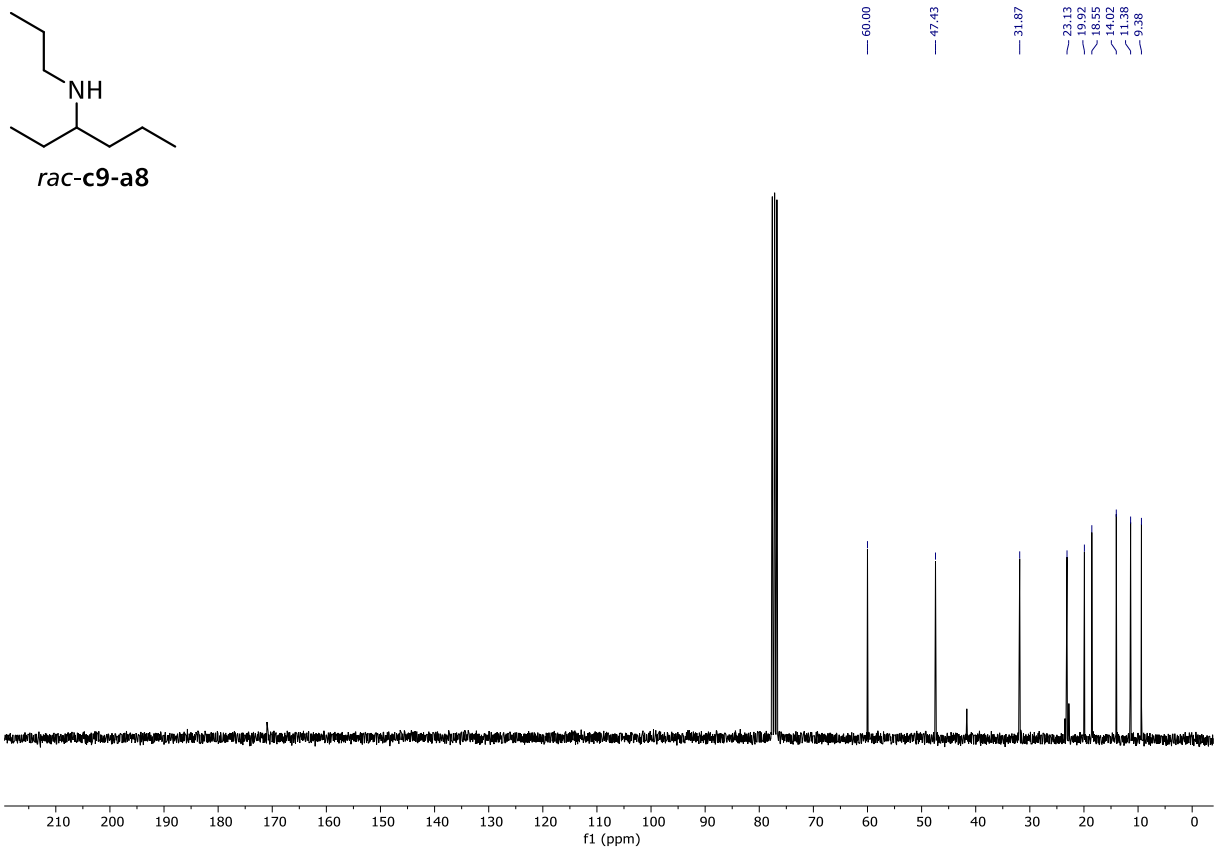


Figure S252. ^{13}C NMR spectrum of *rac*-*N*-propylhexan-3-amine (**c9-a8**).

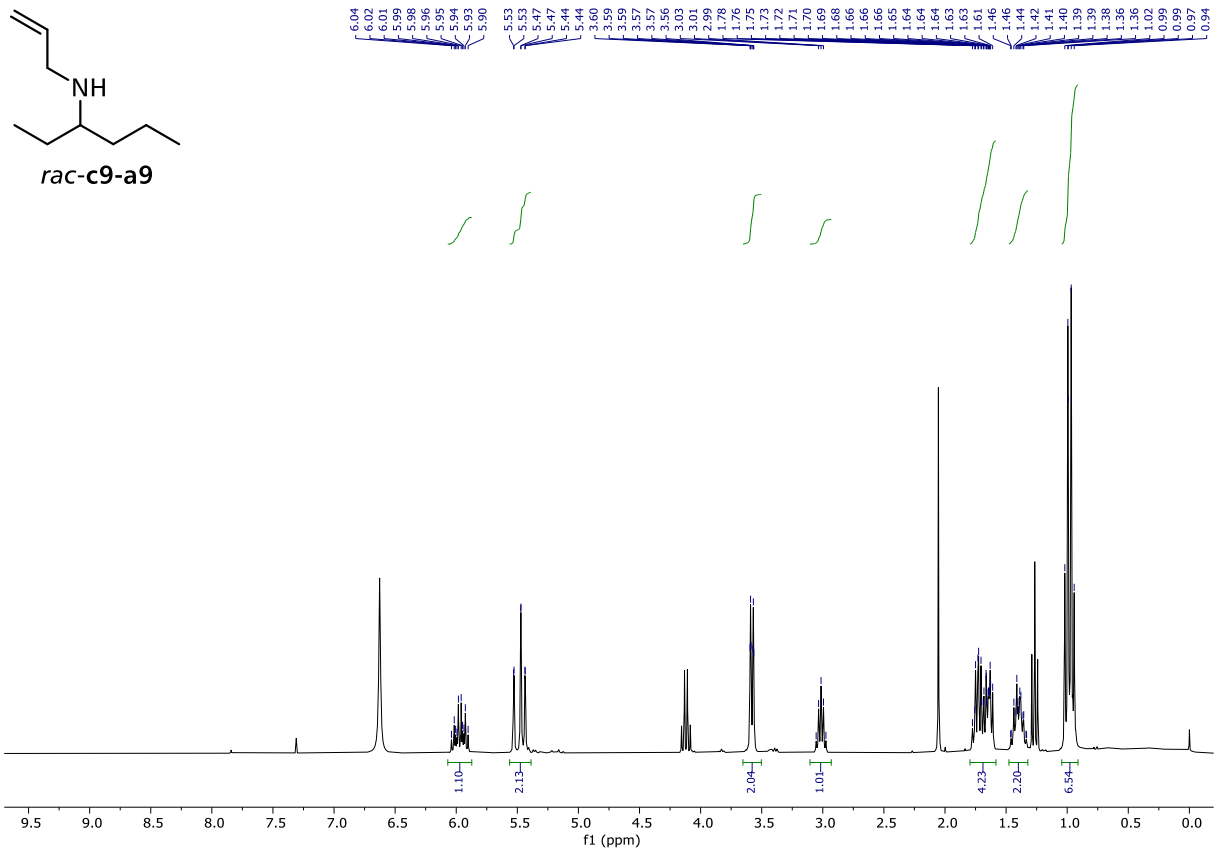


Figure S253. ^{1}H NMR spectrum of *rac*-*N*-allylhexan-3-amine (**c9-a9**).

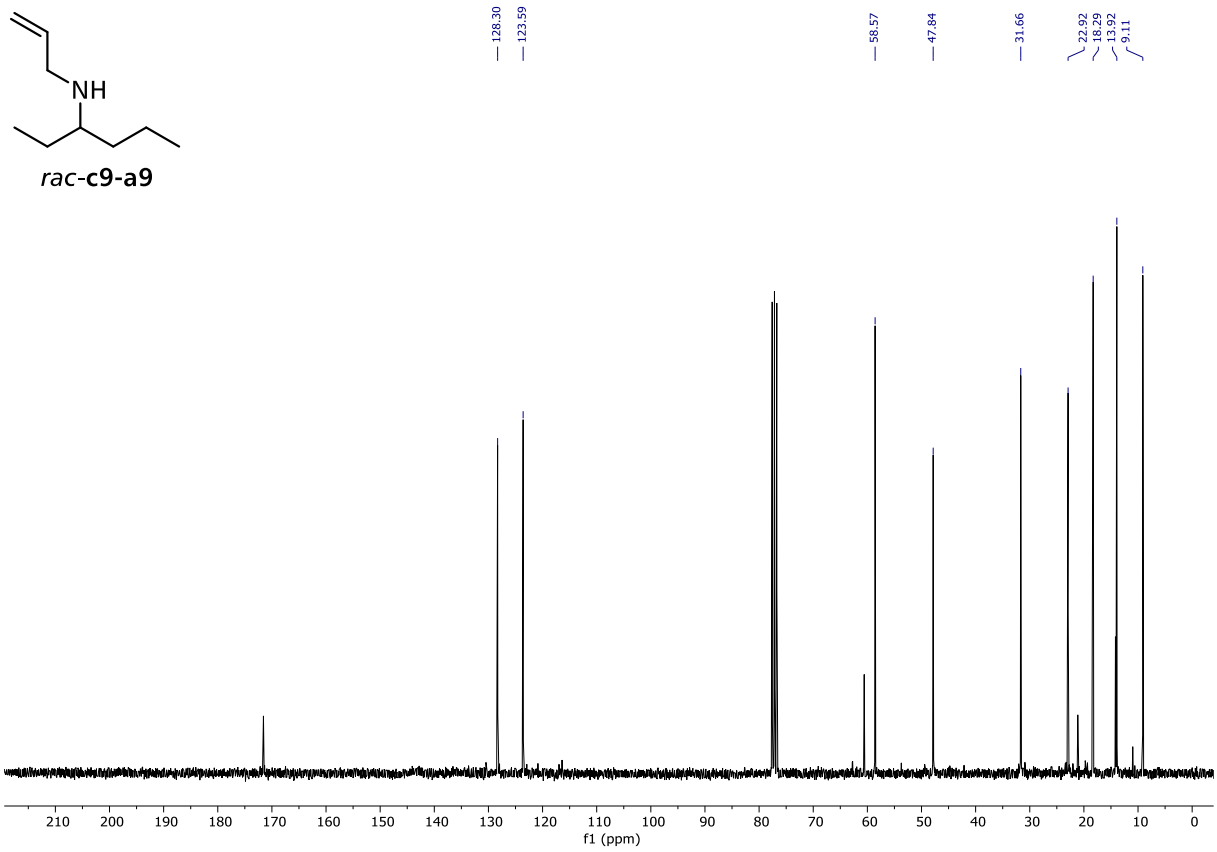


Figure S254. ^{13}C NMR spectrum of *rac*-*N*-allylhexan-3-amine (**c9-a9**).

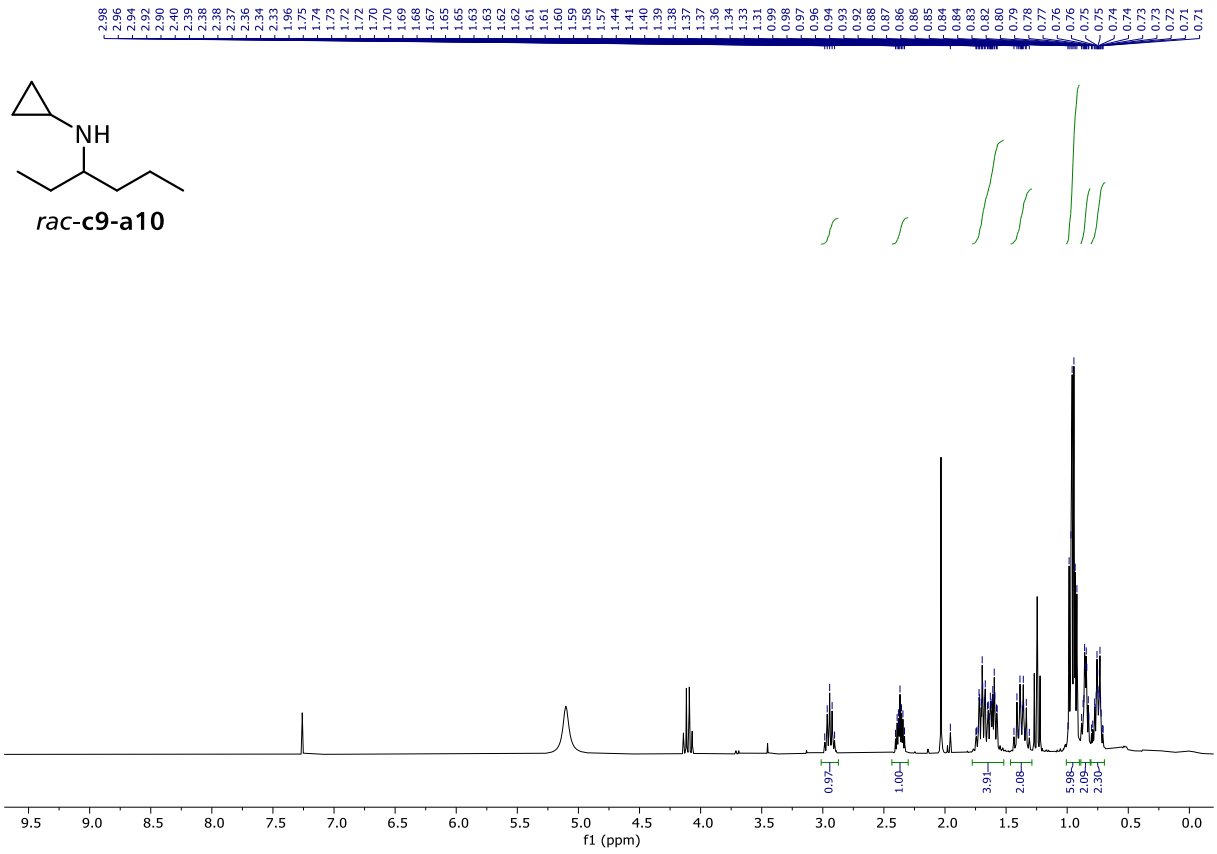


Figure S255. ^{1}H NMR spectrum of *rac*-*N*-(hexan-3-yl)cyclopropanamine (**c9-a10**).

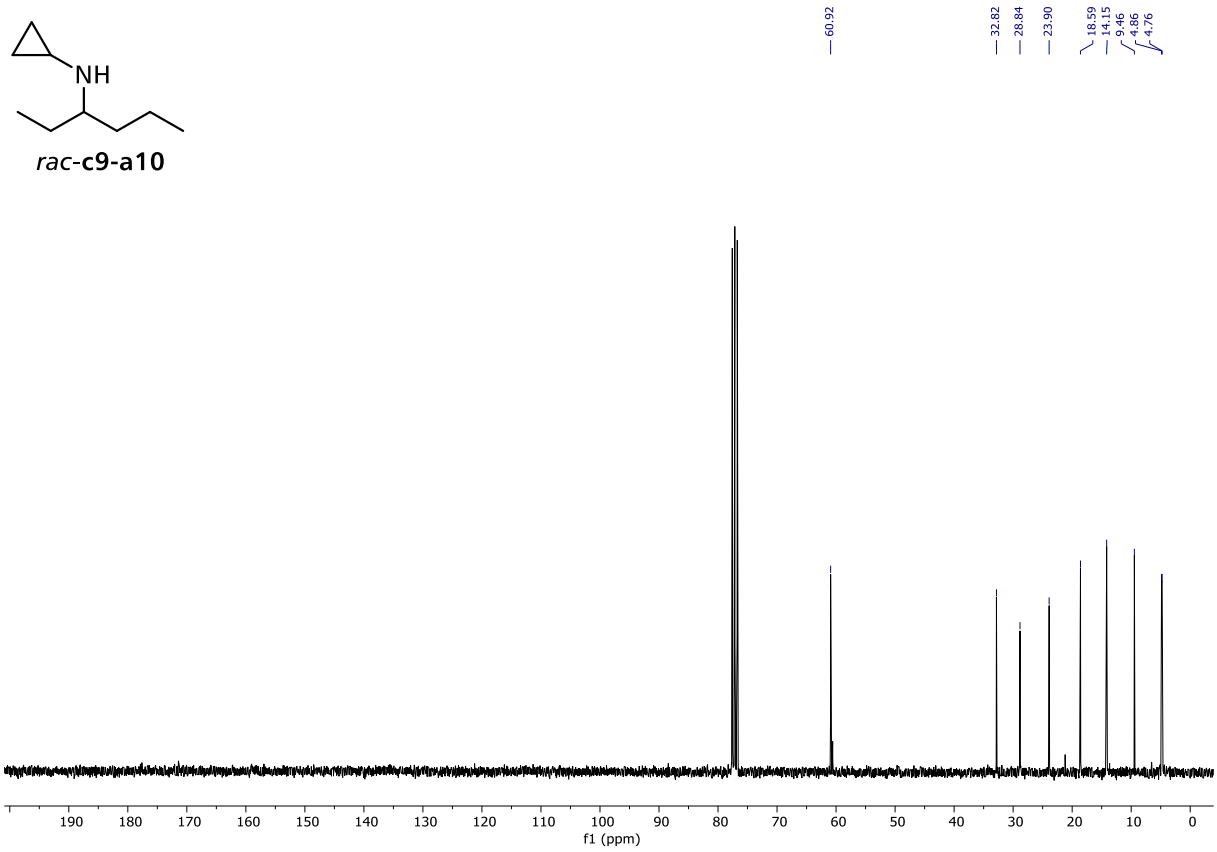


Figure S256. ^{13}C NMR spectrum of *rac*-*N*-(hexan-3-yl)cyclopropanamine (**c9-a10**).

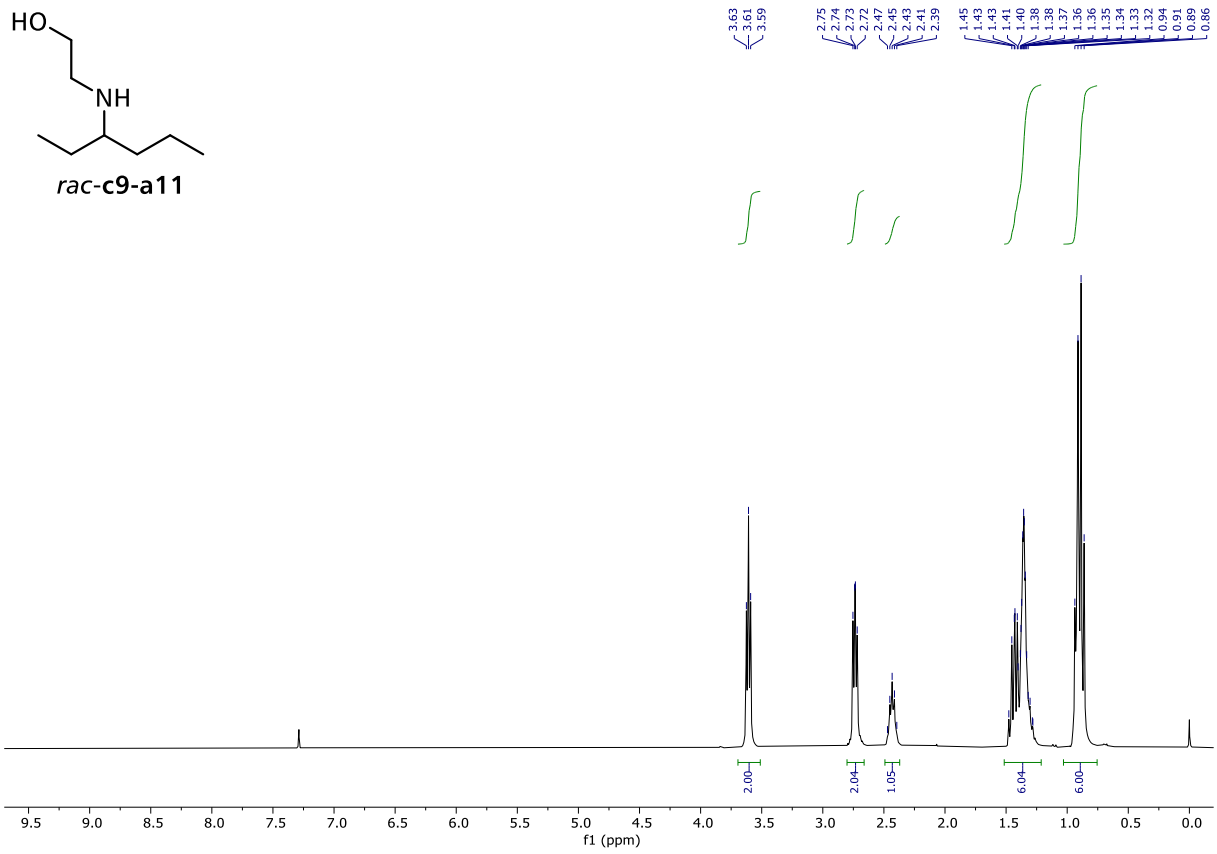


Figure S257. ^{1}H NMR spectrum of *rac*-2-(hexan-3-ylamino)ethan-1-ol (**c9-a11**).

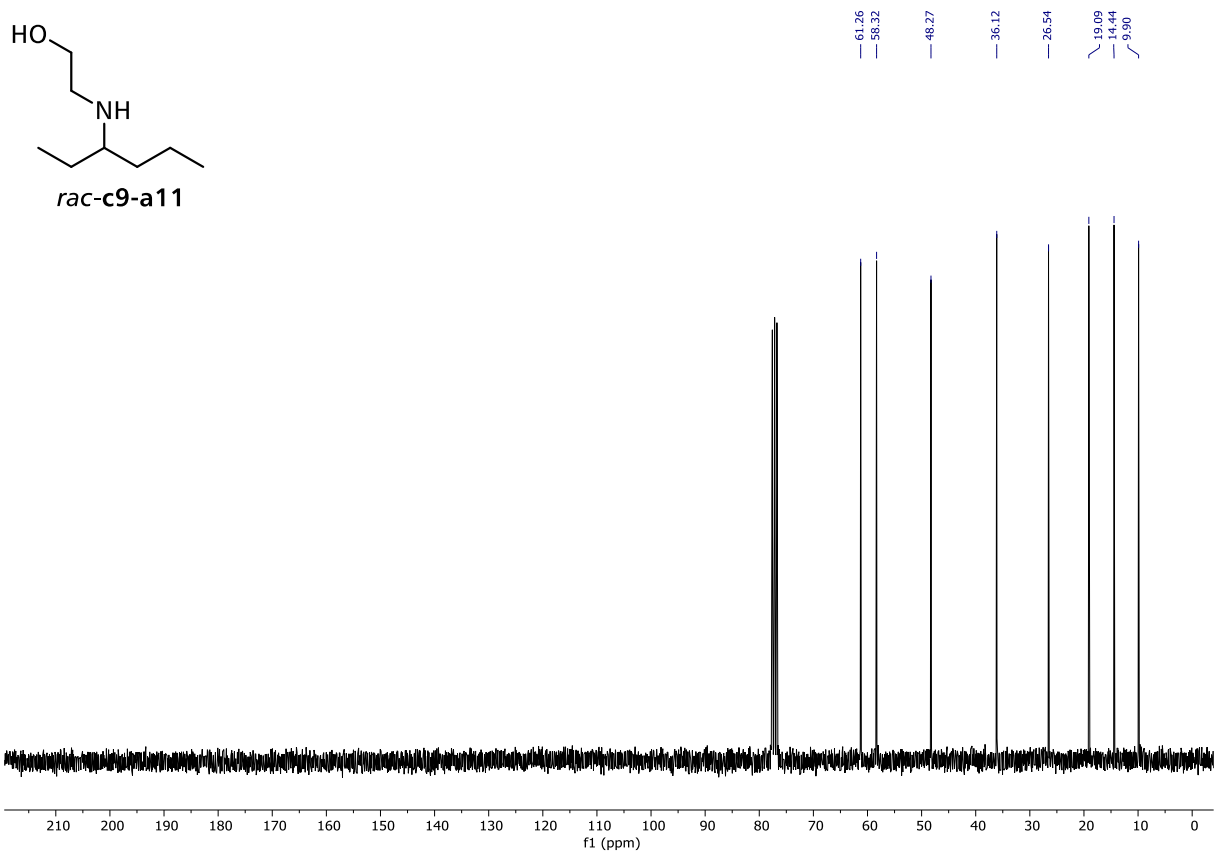


Figure S258. ^{13}C NMR spectrum of *rac*-2-(hexan-3-ylamino)ethan-1-ol (**c9-a11**).

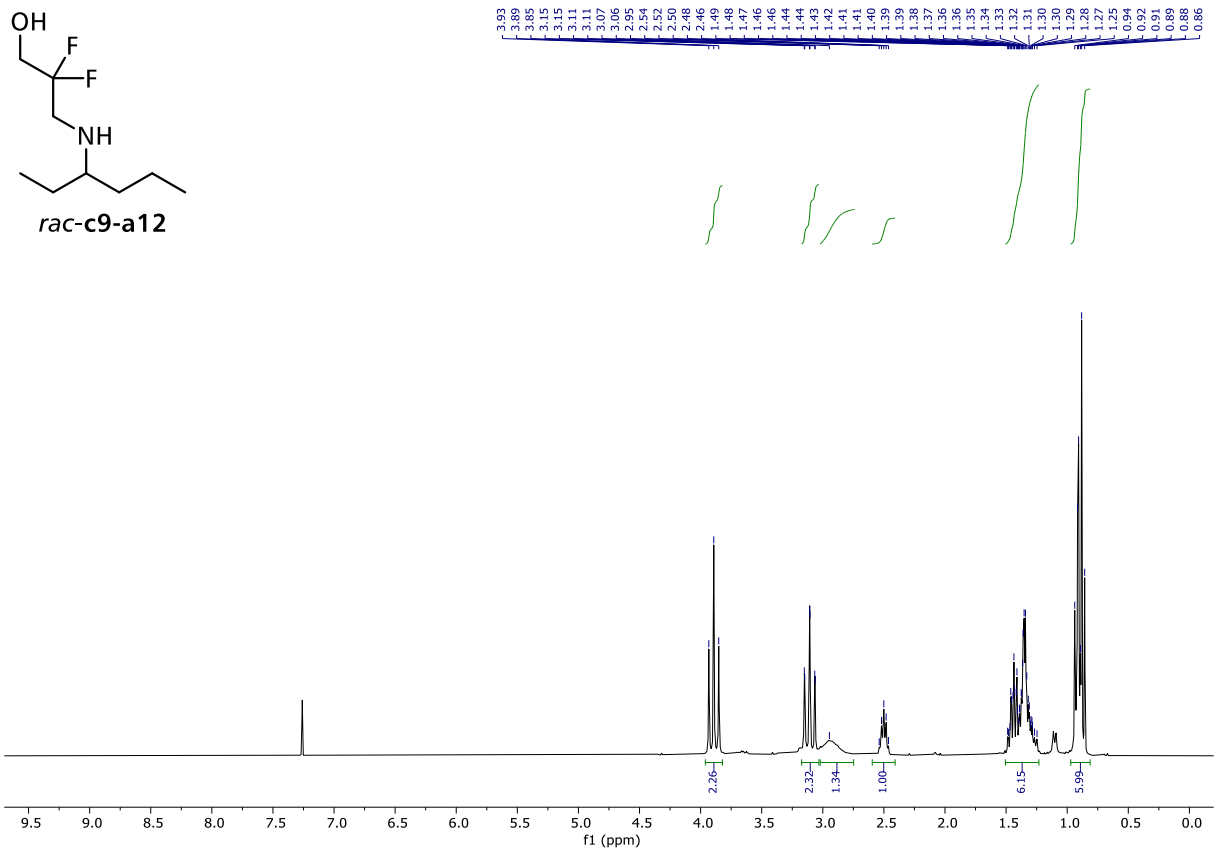


Figure S259. ^{1}H NMR spectrum of *rac*-2,2-difluoro-3-(hexan-3-ylamino)propan-1-ol (**c9-a12**).

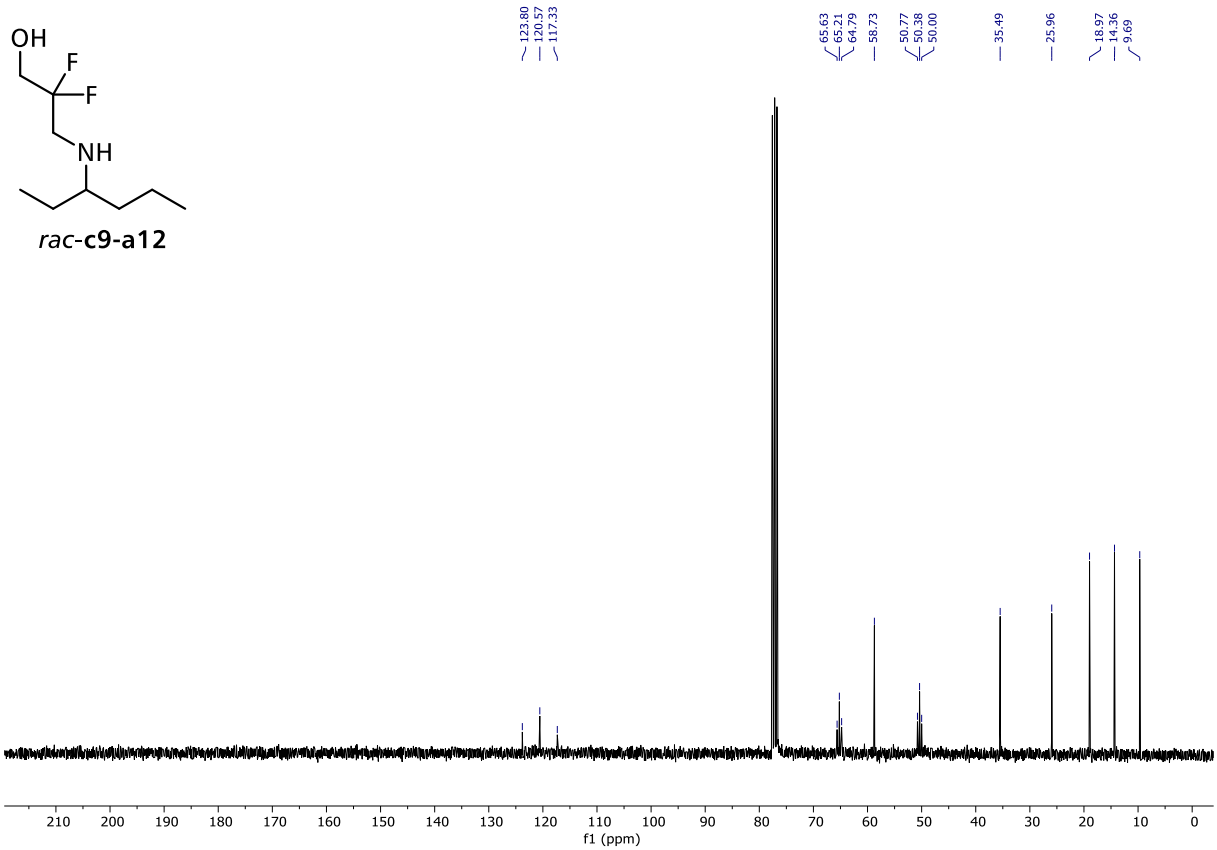


Figure S260. ^{13}C NMR spectrum of *rac*-2,2-difluoro-3-(hexan-3-ylamino)propan-1-ol (**c9-a12**).

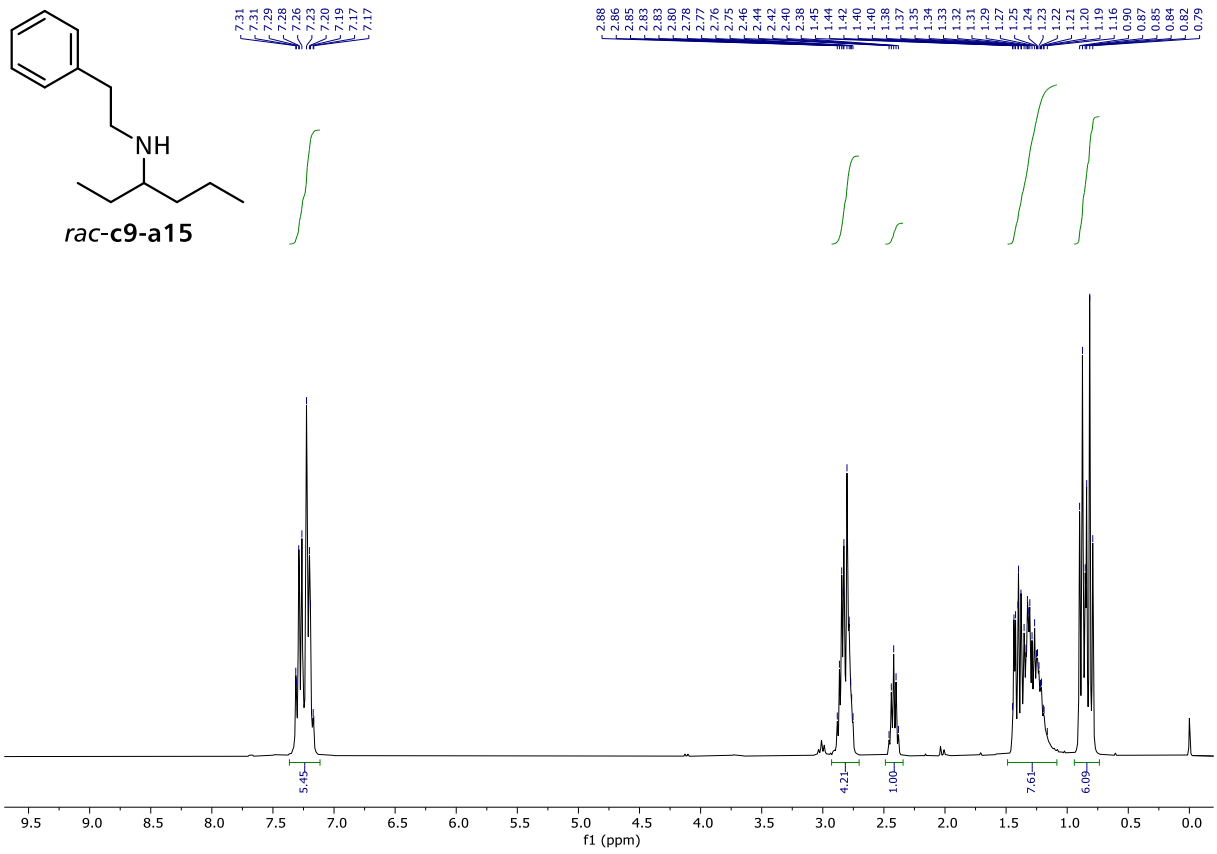


Figure S261. ^{1}H NMR spectrum of *rac*-*N*-phenethylhexan-3-amine (**c9-a15**).

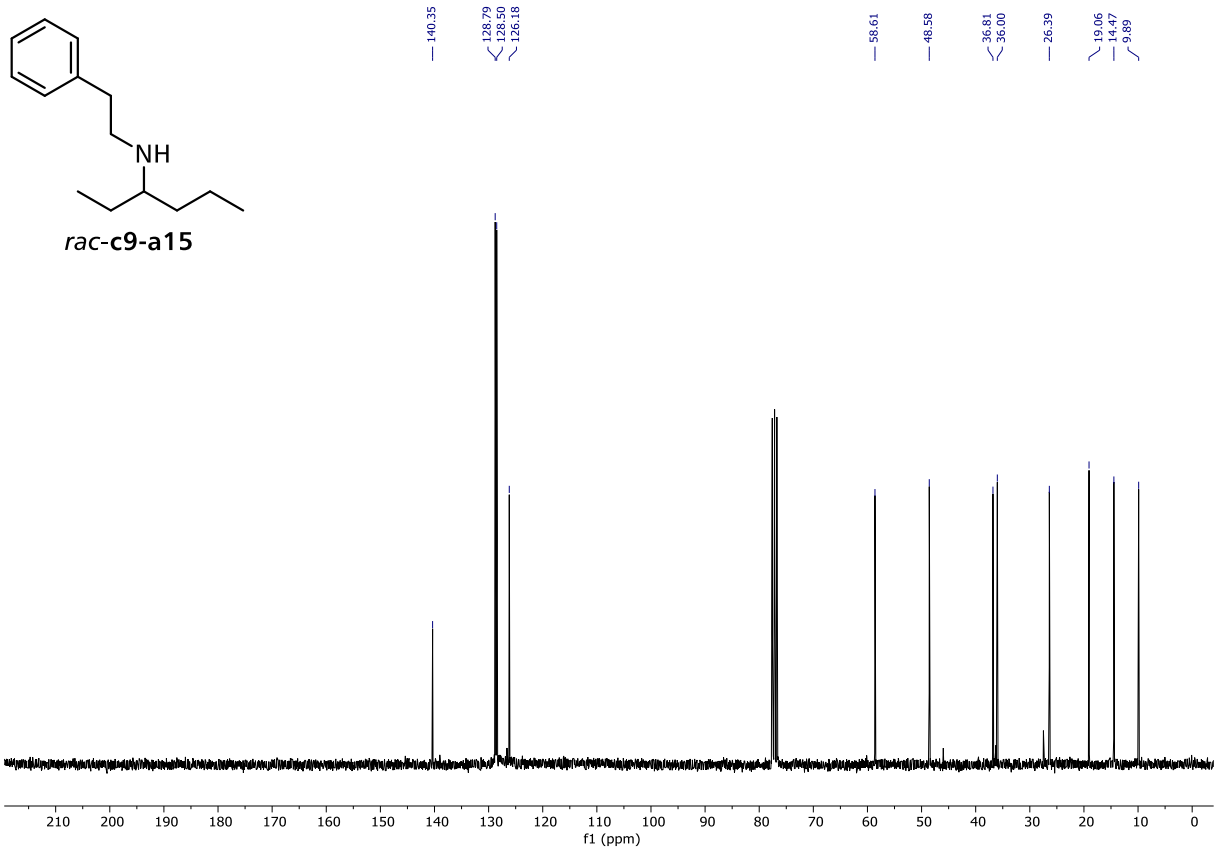


Figure S262. ^{13}C NMR spectrum of *rac*-*N*-phenethylhexan-3-amine (**c9-a15**).

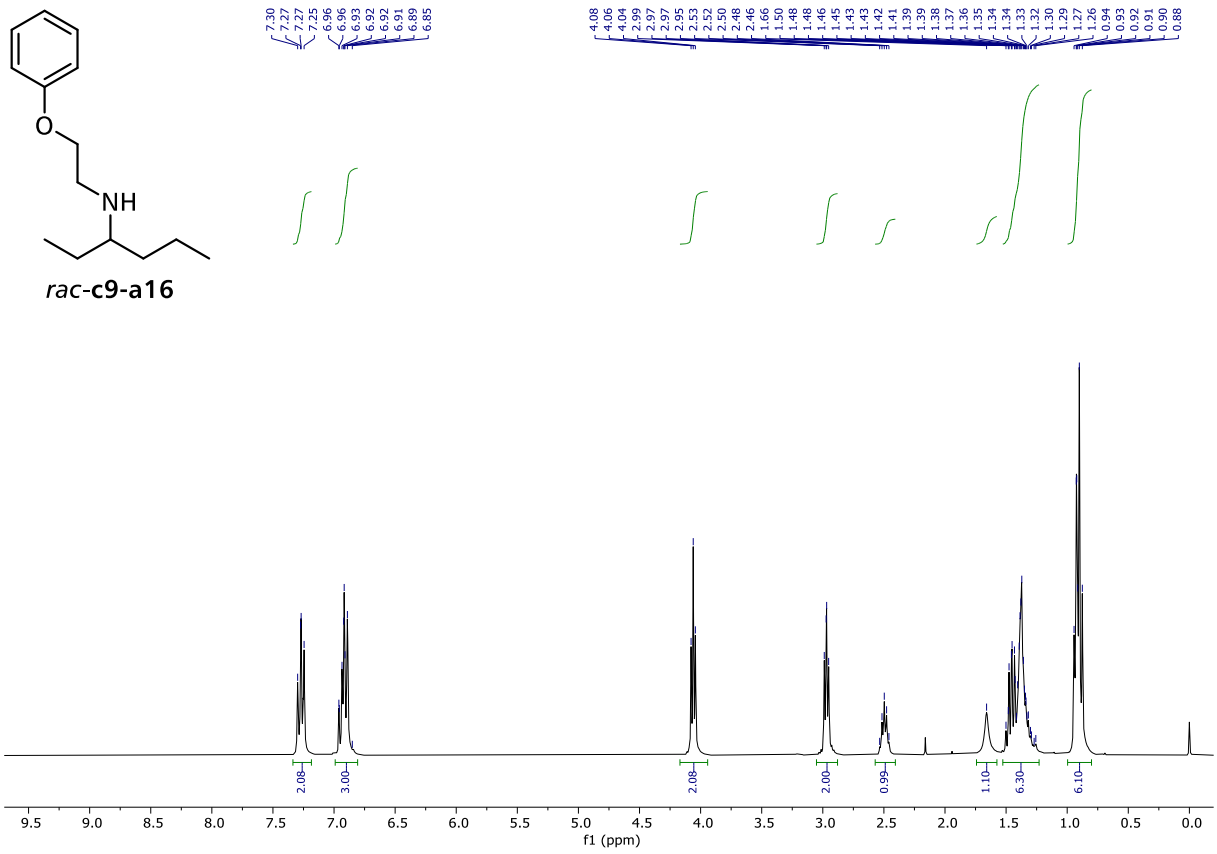


Figure S263. ^{1}H NMR spectrum of *rac*-*N*-(2-phenoxyethyl)hexan-3-amine (**c9-a16**).

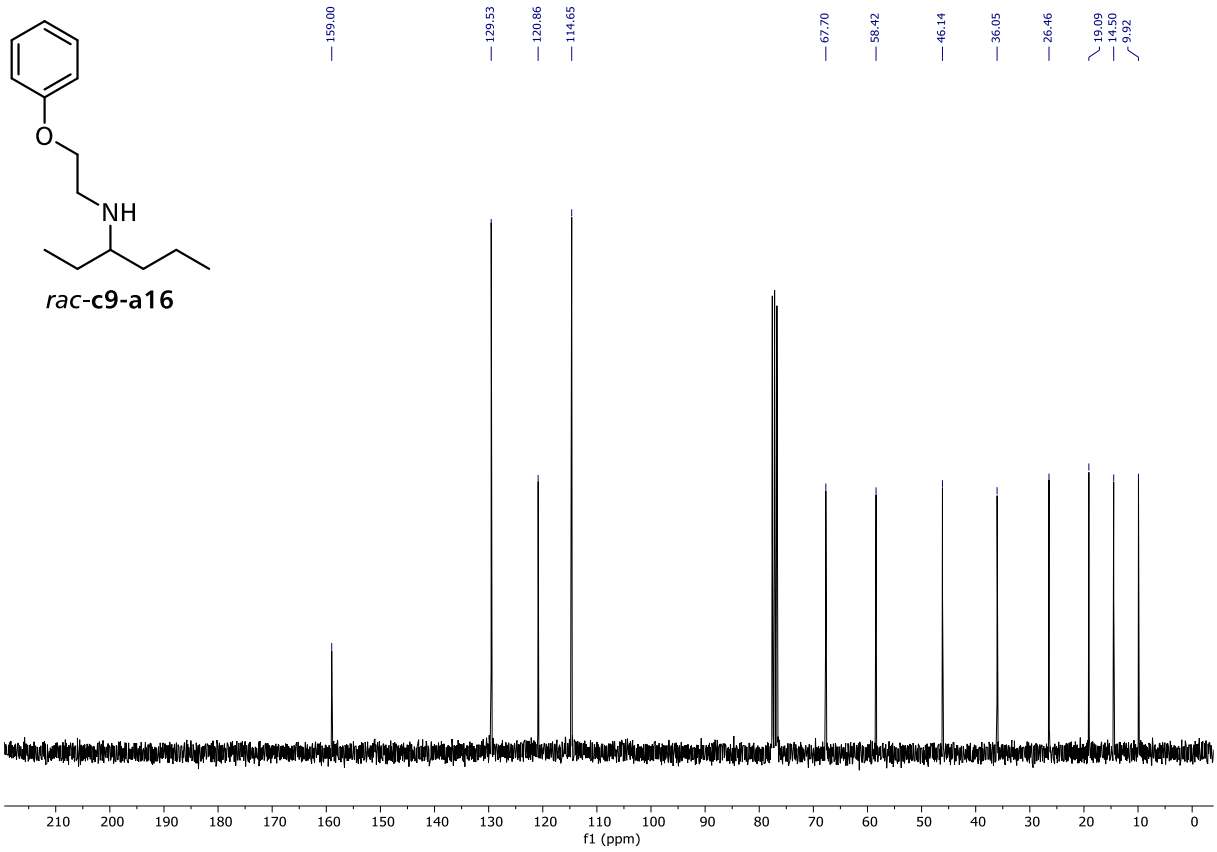


Figure S264. ^{13}C NMR spectrum of *rac*-*N*-(2-phenoxyethyl)hexan-3-amine (**c9-a16**).

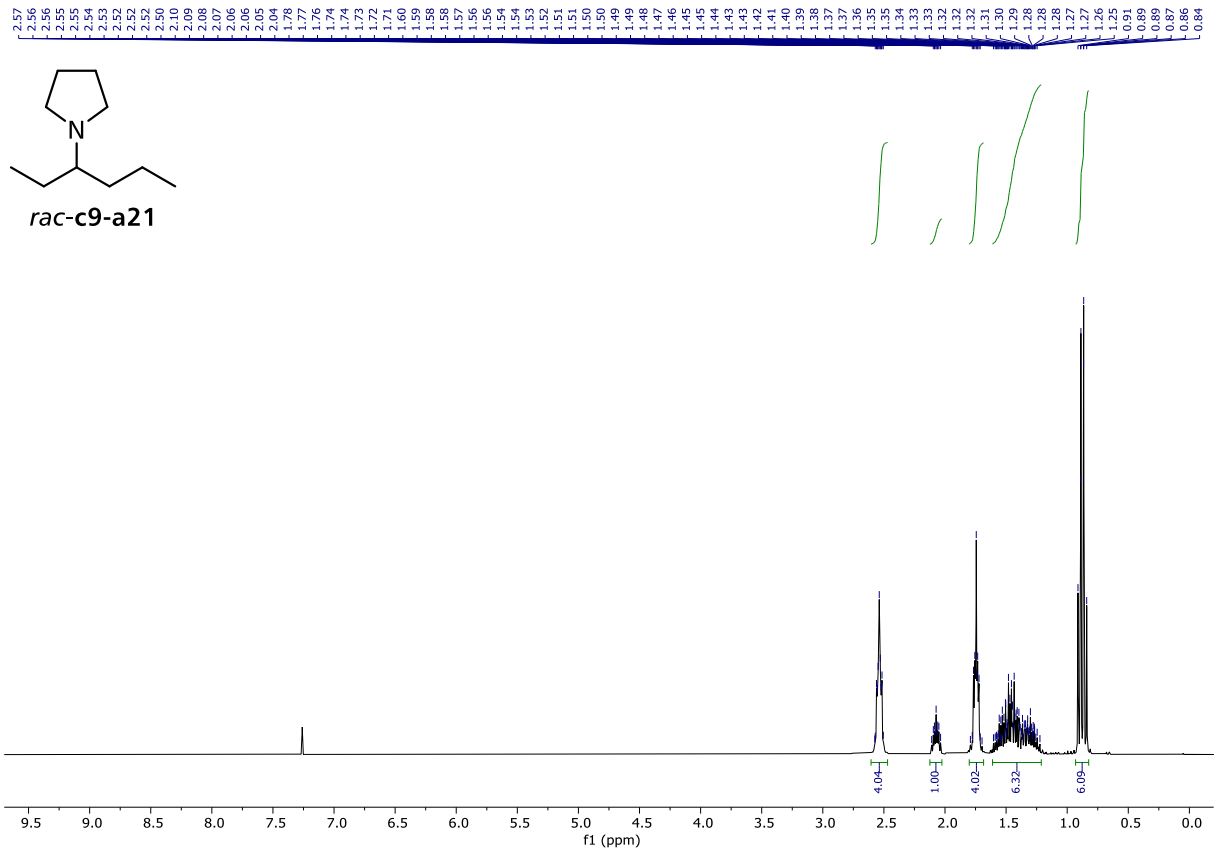


Figure S265. ^{1}H NMR spectrum of *rac*-1-(hexan-3-yl)pyrrolidine (**c9-a21**).

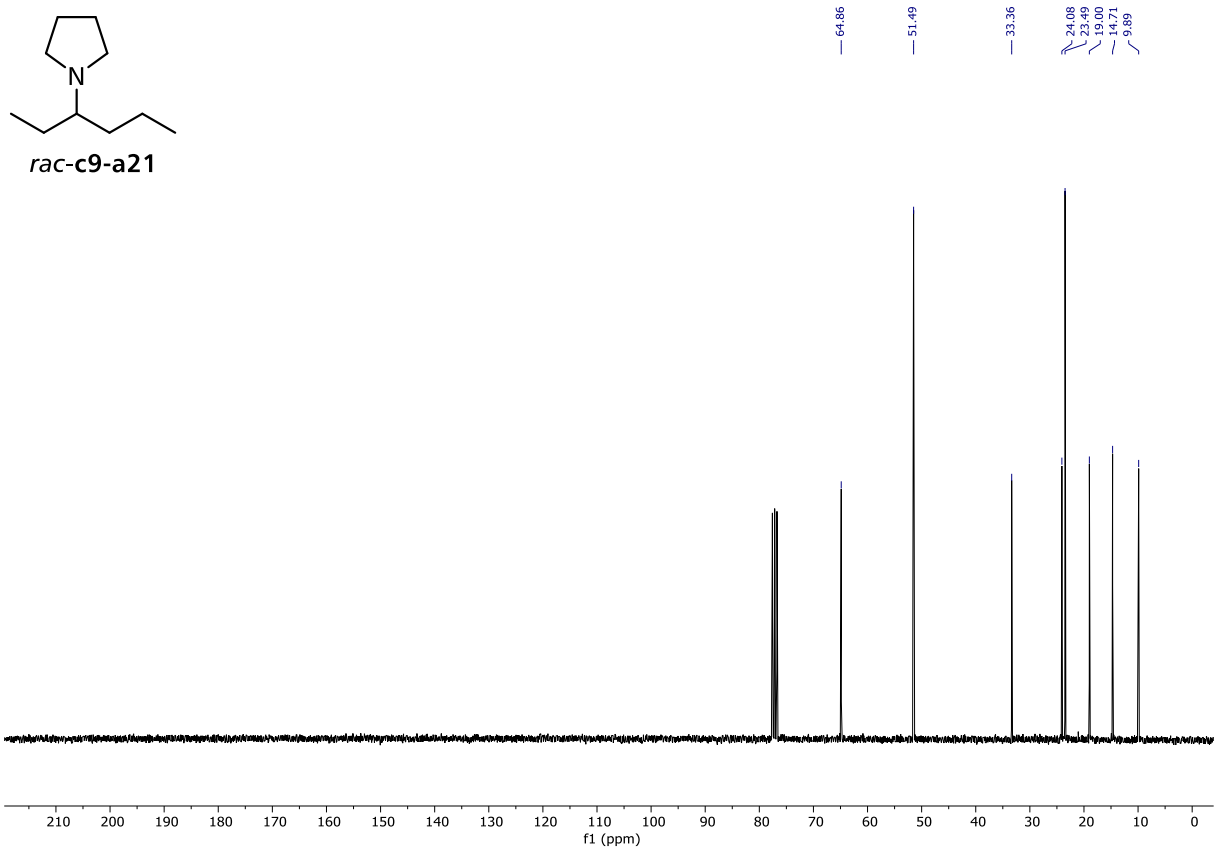


Figure S266. ^{13}C NMR spectrum of *rac*-1-(hexan-3-yl)pyrrolidine (**c9-a21**).

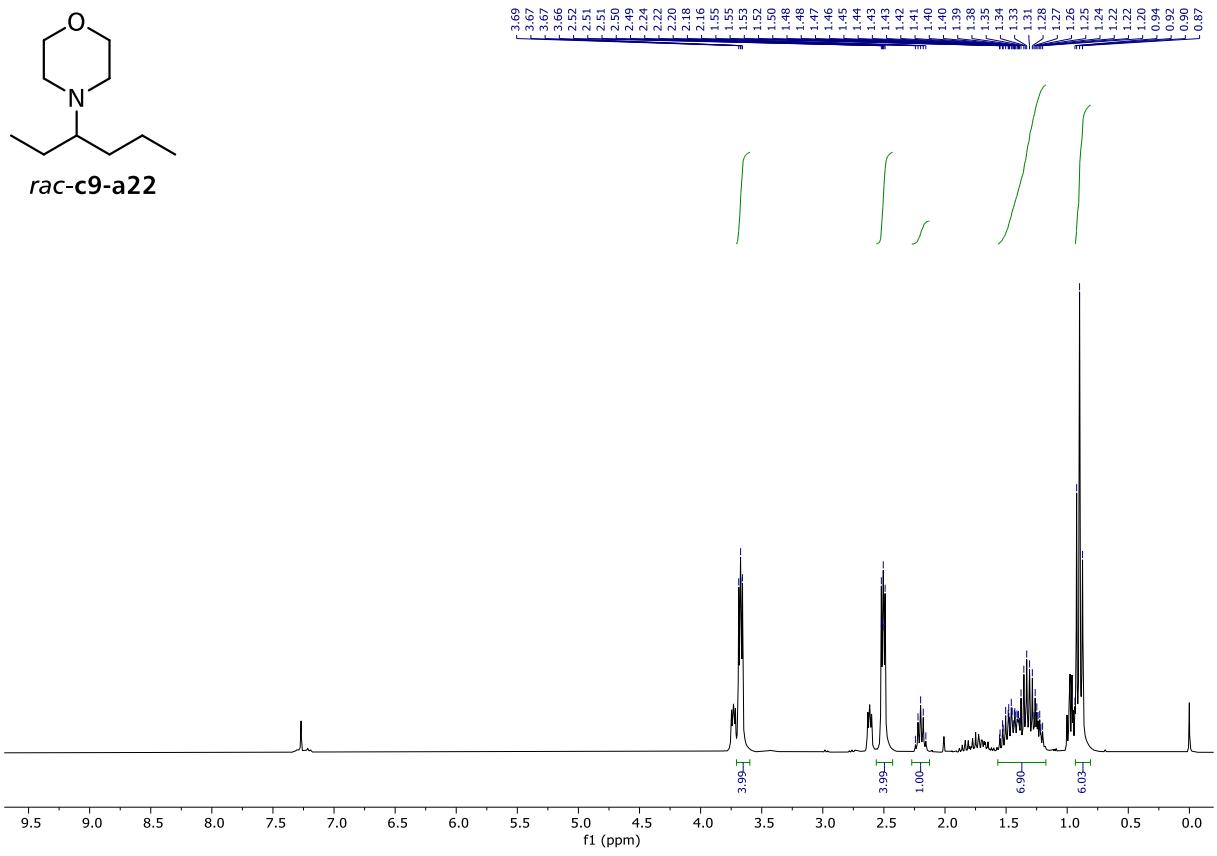


Figure S267. ^{1}H NMR spectrum of *rac*-4-(hexan-3-yl)morpholine (**c9-a22**).

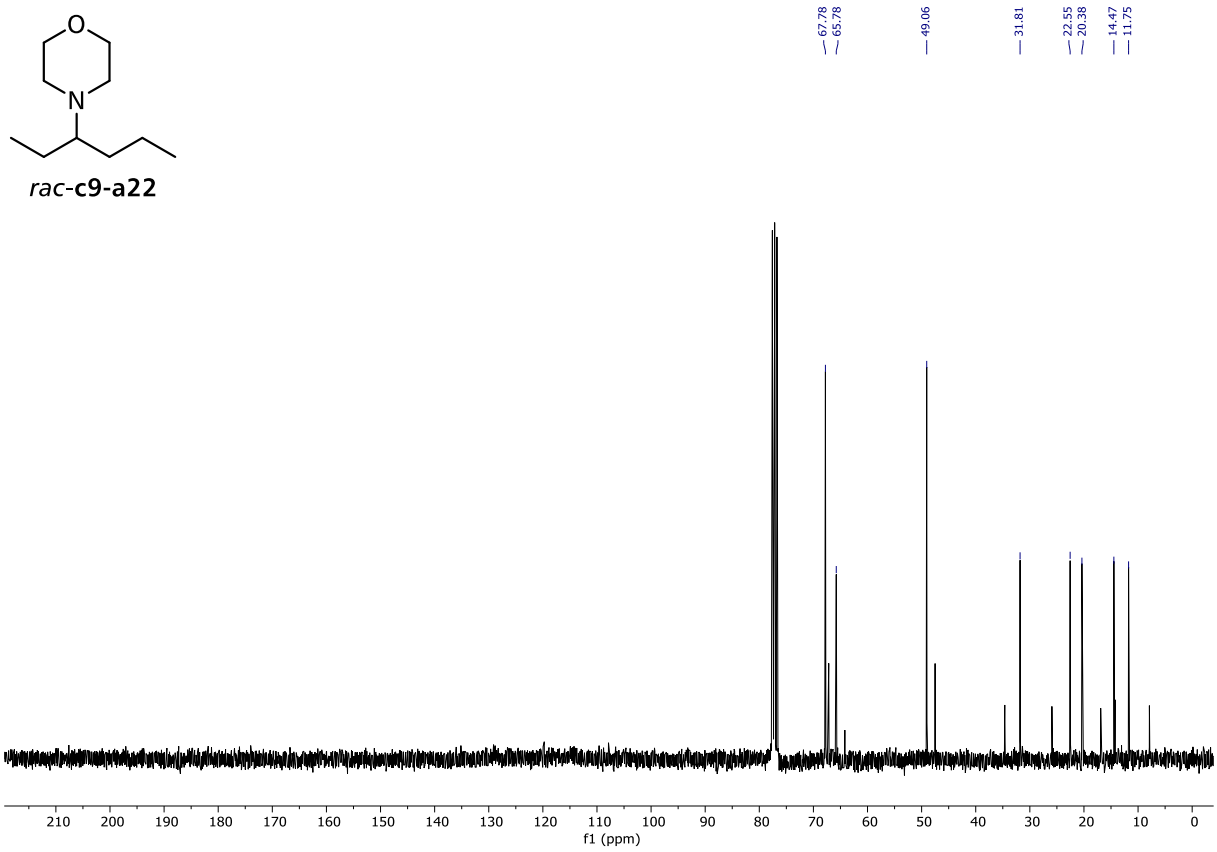


Figure S268. ^{13}C NMR spectrum of *rac*-4-(hexan-3-yl)morpholine (**c9-a22**).

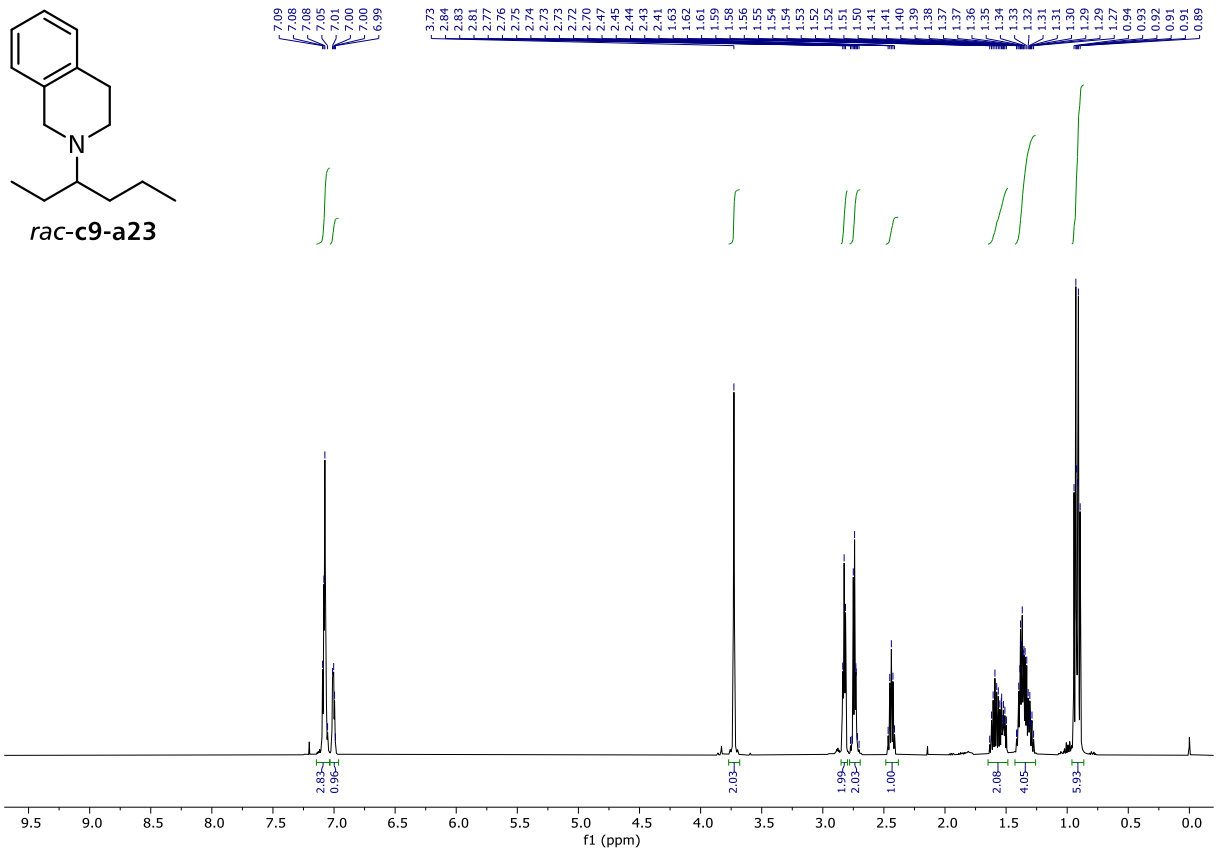


Figure S269. ^{1}H NMR spectrum of *rac*-2-(hexan-3-yl)-1,2,3,4-tetrahydroisoquinoline (**c9-a23**).

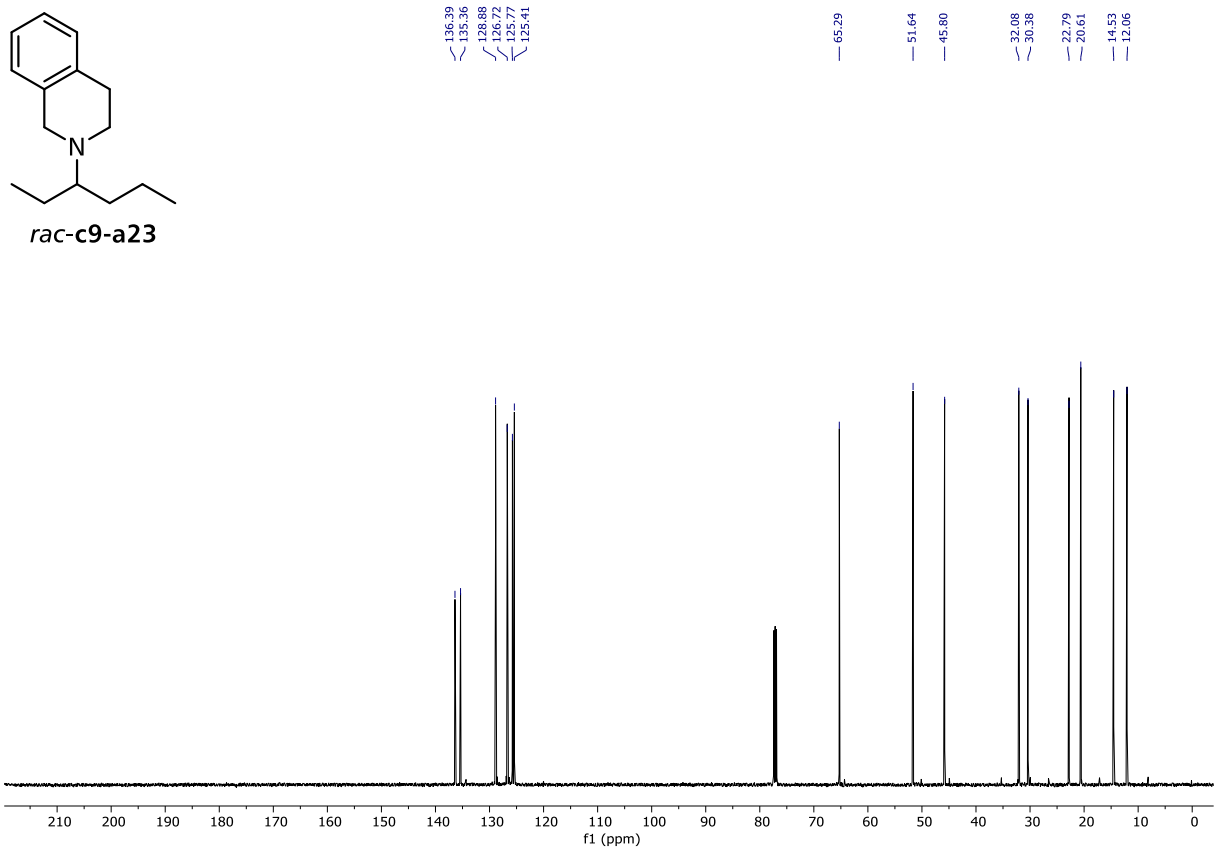


Figure S270. ^{13}C NMR spectrum of *rac*-2-(hexan-3-yl)-1,2,3,4-tetrahydroisoquinoline (**c9-a23**).

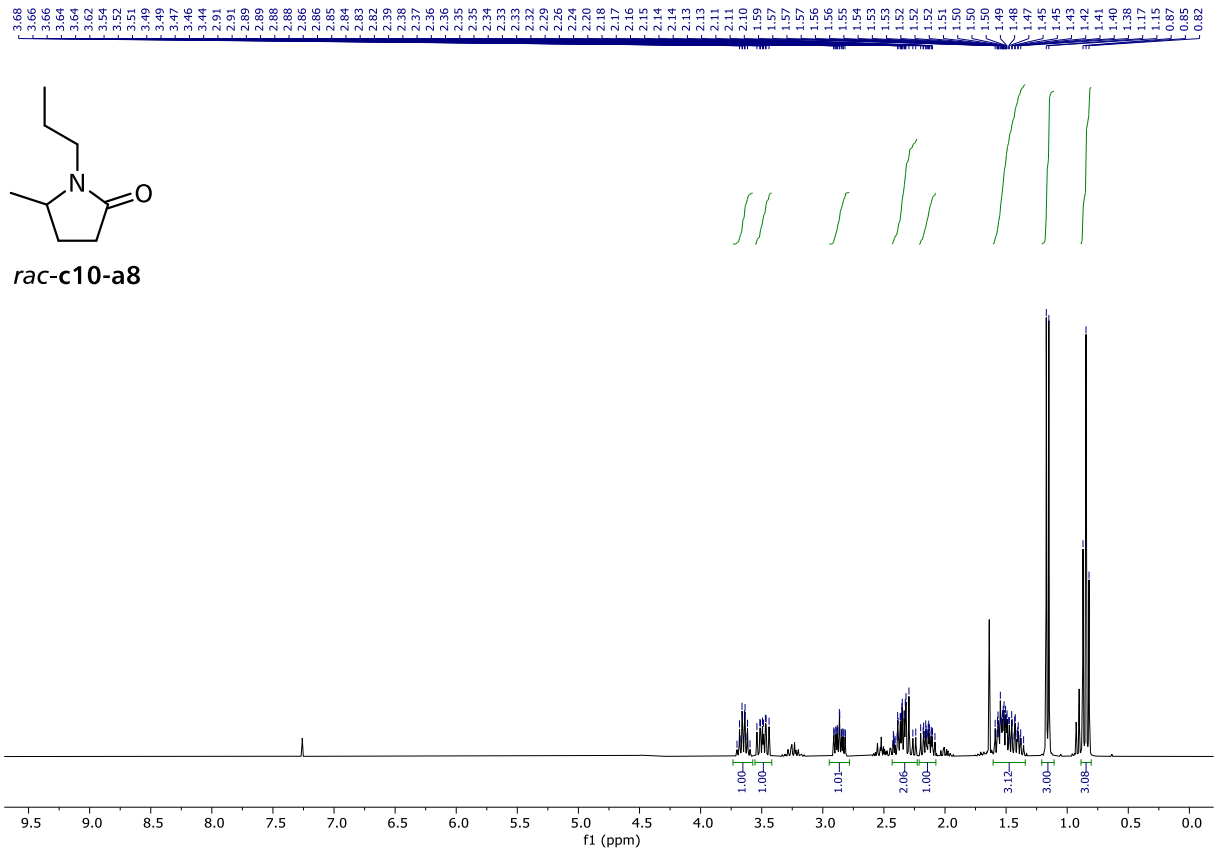


Figure S271. ^{1}H NMR spectrum of *rac*-5-methyl-1-propylpyrrolidin-2-one (**c10-a8**).

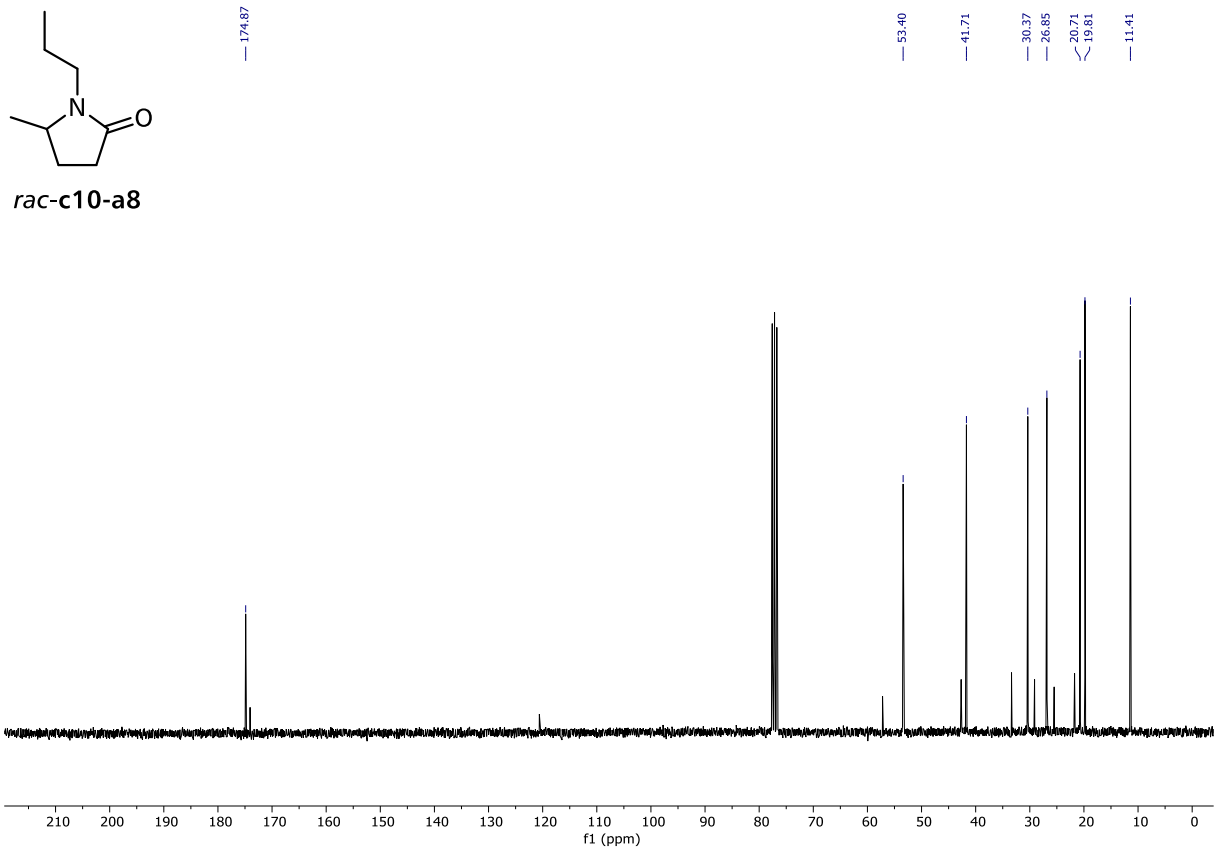


Figure S272. ^{13}C NMR spectrum of *rac*-5-methyl-1-propylpyrrolidin-2-one (**c10-a8**).

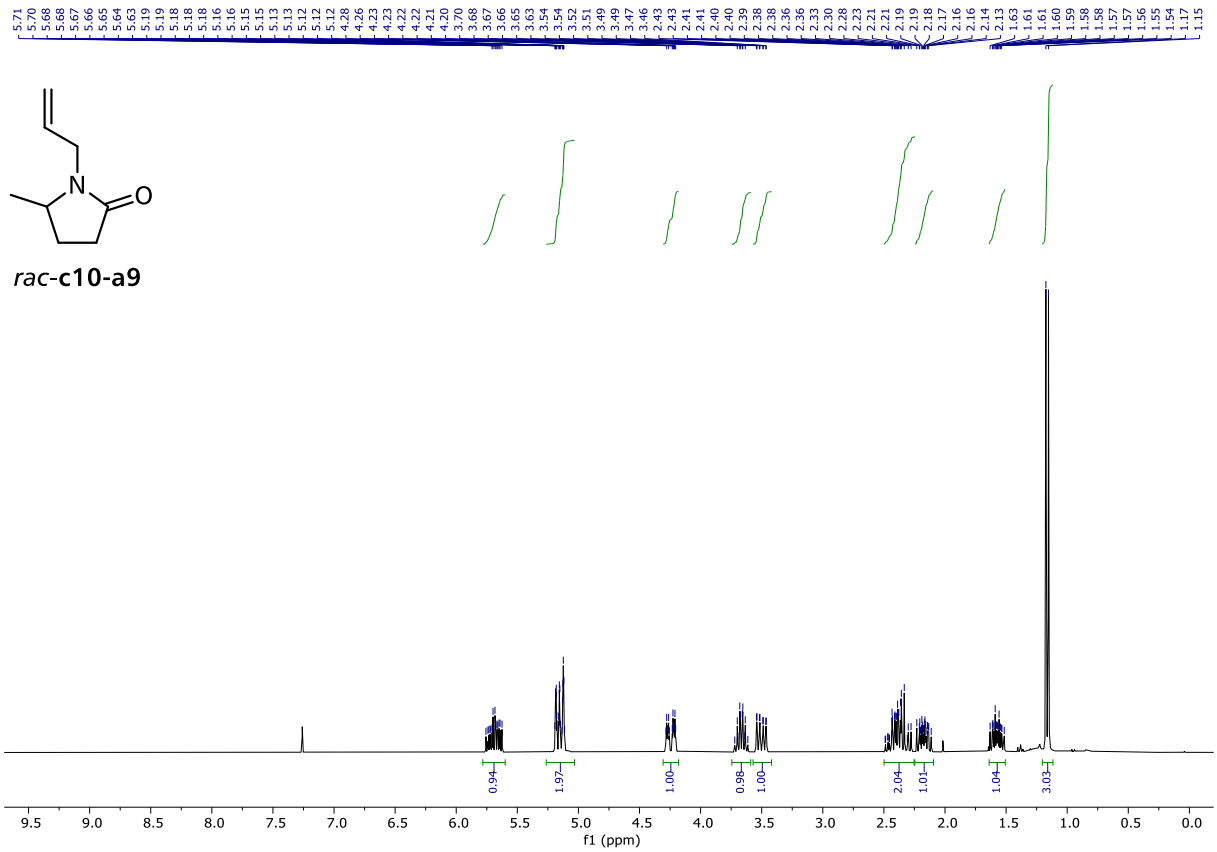


Figure S273. ^{1}H NMR spectrum of *rac*-1-allyl-5-methylpyrrolidin-2-one (**c10-a9**).

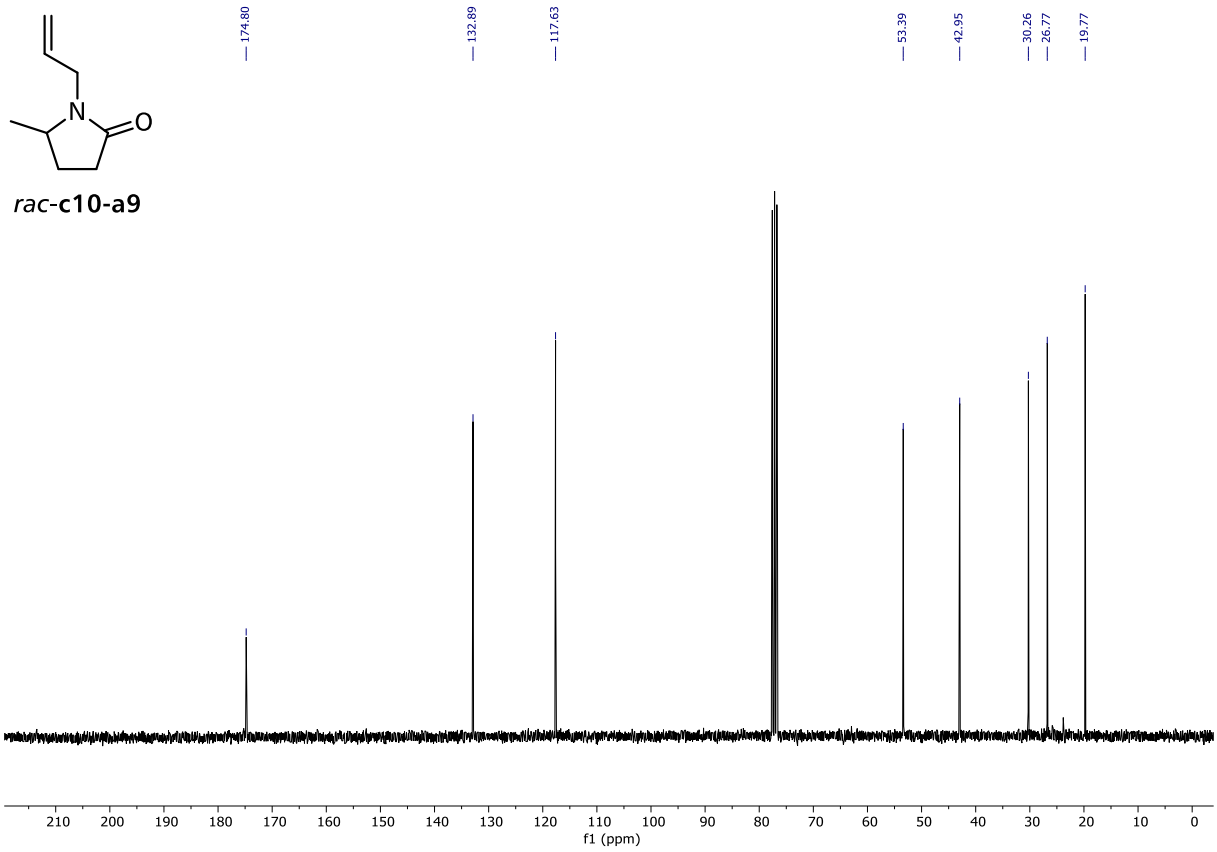


Figure S274. ^{13}C NMR spectrum of *rac*-1-allyl-5-methylpyrrolidin-2-one (**c10-a9**).

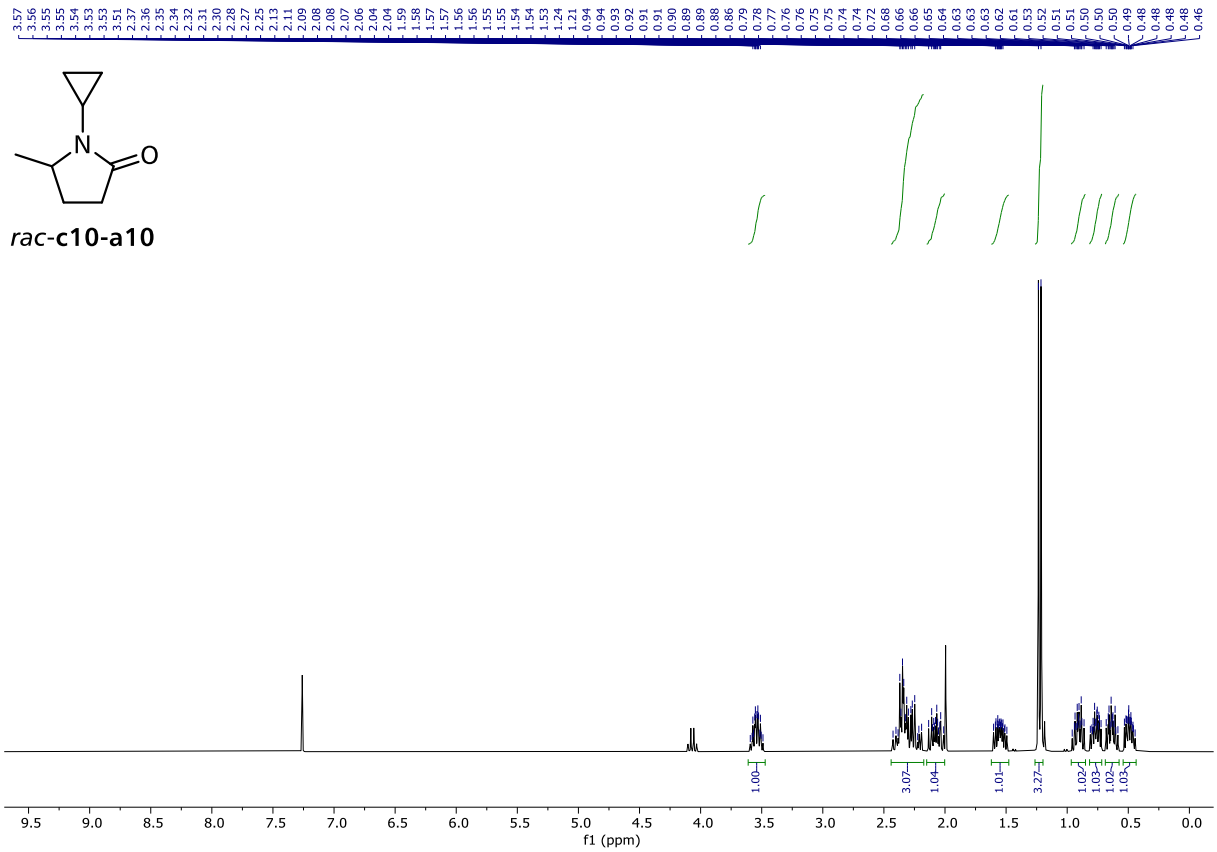


Figure S275. ^{1}H NMR spectrum of *rac*-1-cyclopropyl-5-methylpyrrolidin-2-one (**c10-a10**).

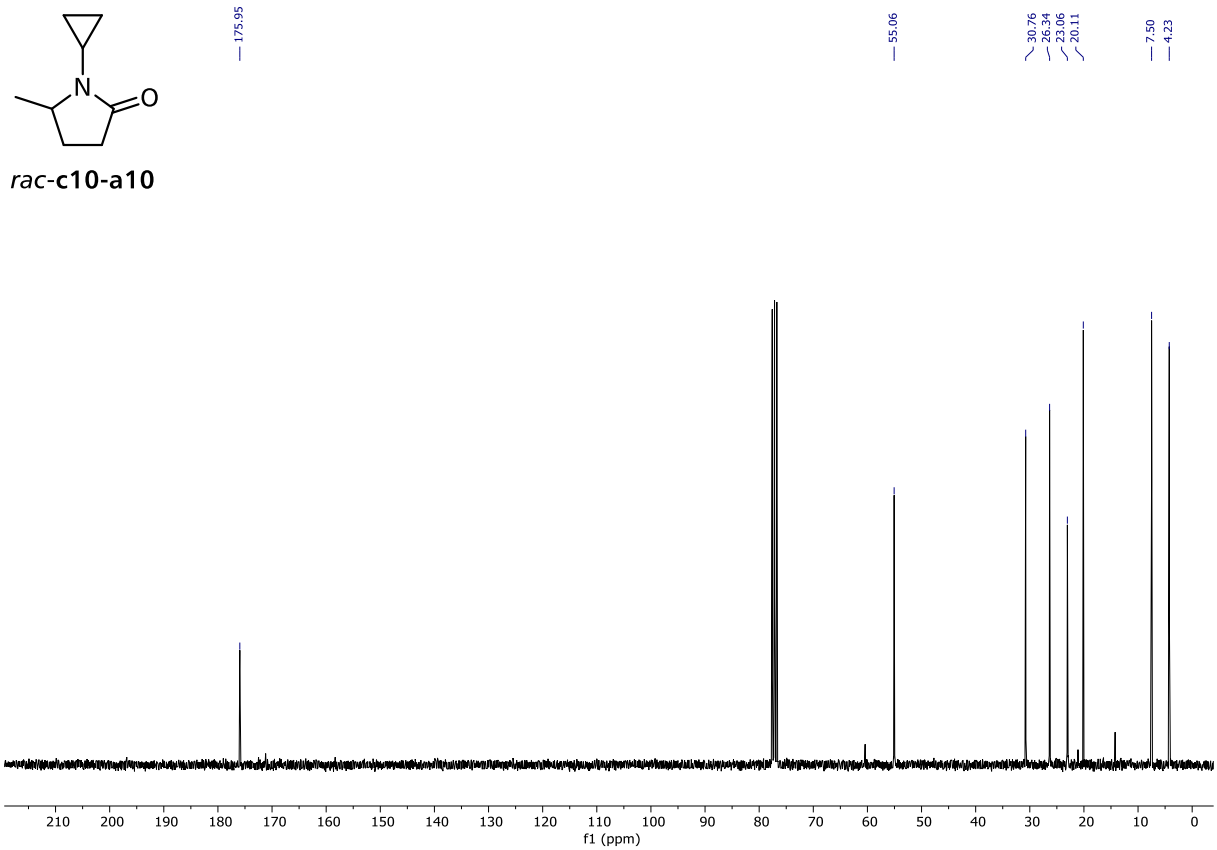


Figure S276. ^{13}C NMR spectrum of *rac*-1-cyclopropyl-5-methylpyrrolidin-2-one (**c10-a10**).

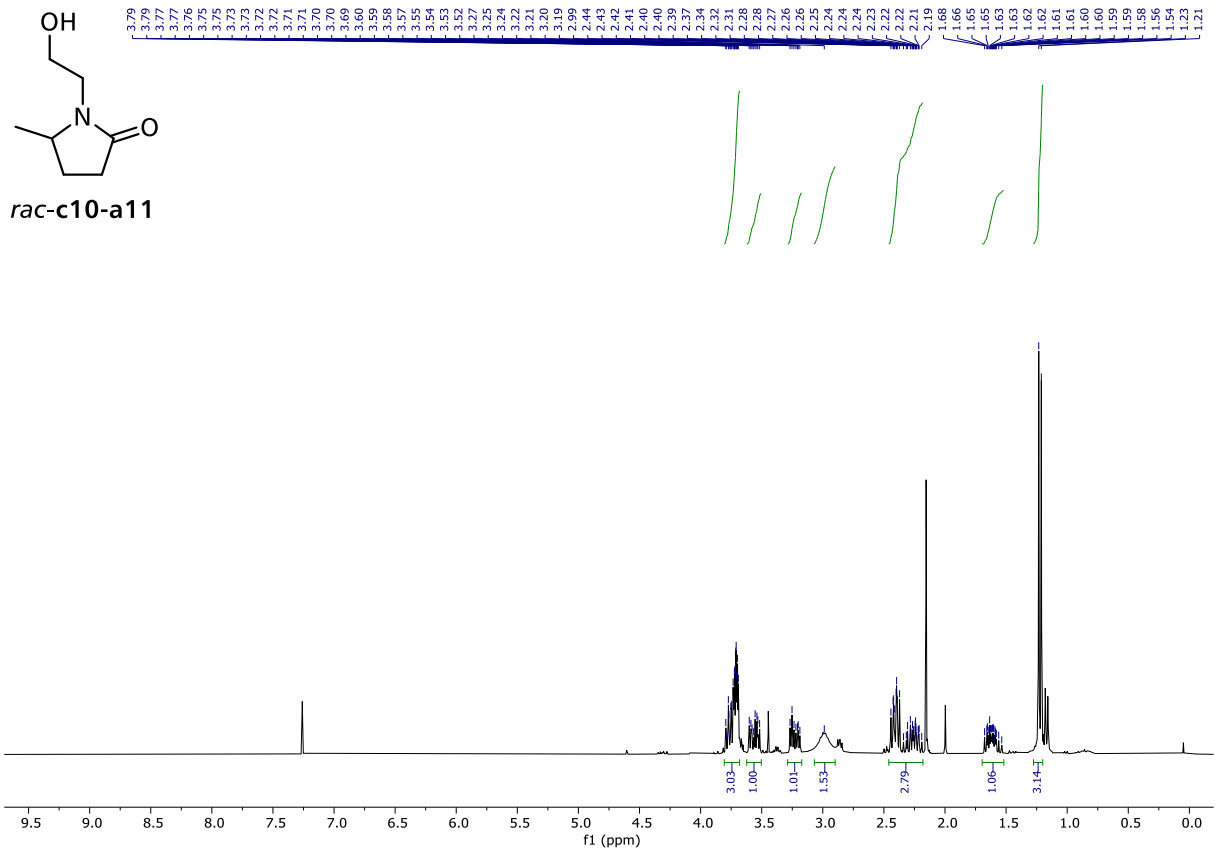


Figure S277. ^{1}H NMR spectrum of *rac*-1-(2-hydroxyethyl)-5-methylpyrrolidin-2-one (**c10-a11**).

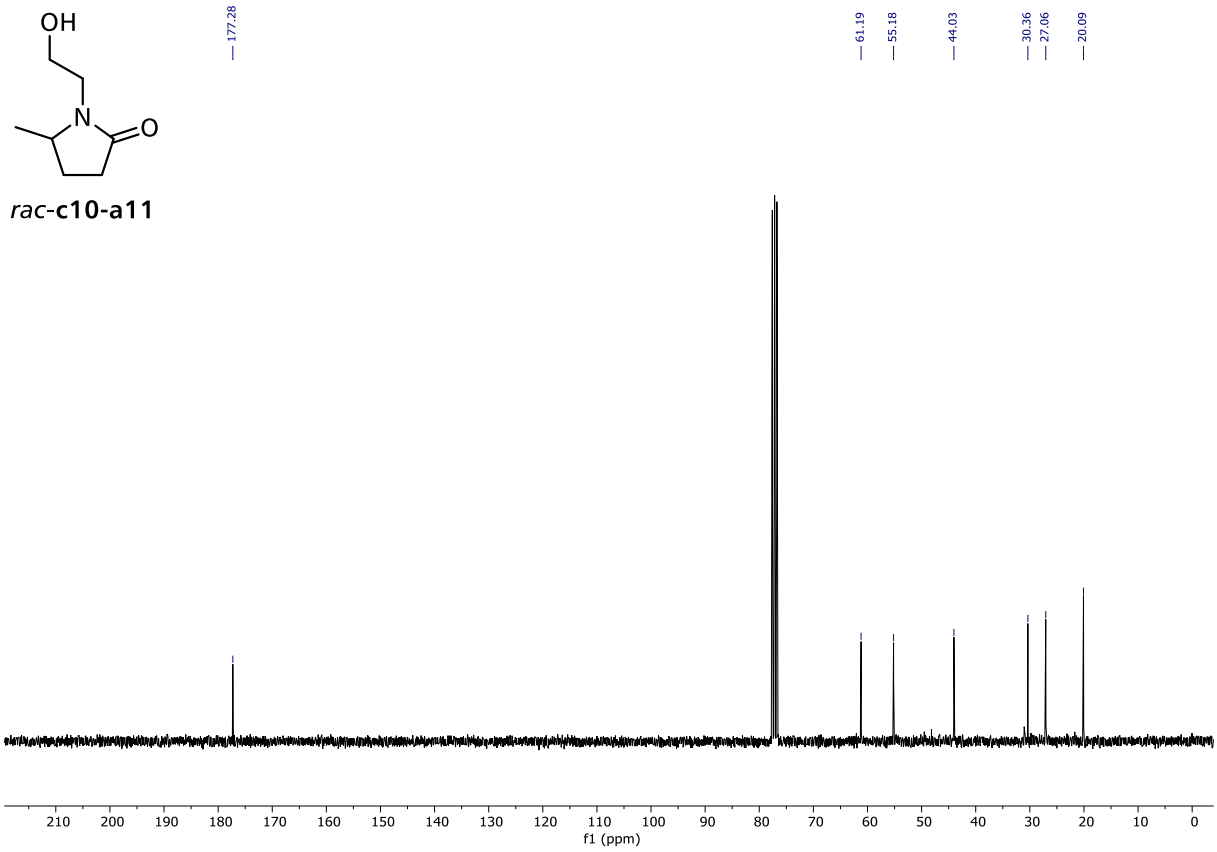


Figure S278. ^{13}C NMR spectrum of *rac*-1-(2-hydroxyethyl)-5-methylpyrrolidin-2-one (**c10-a11**).

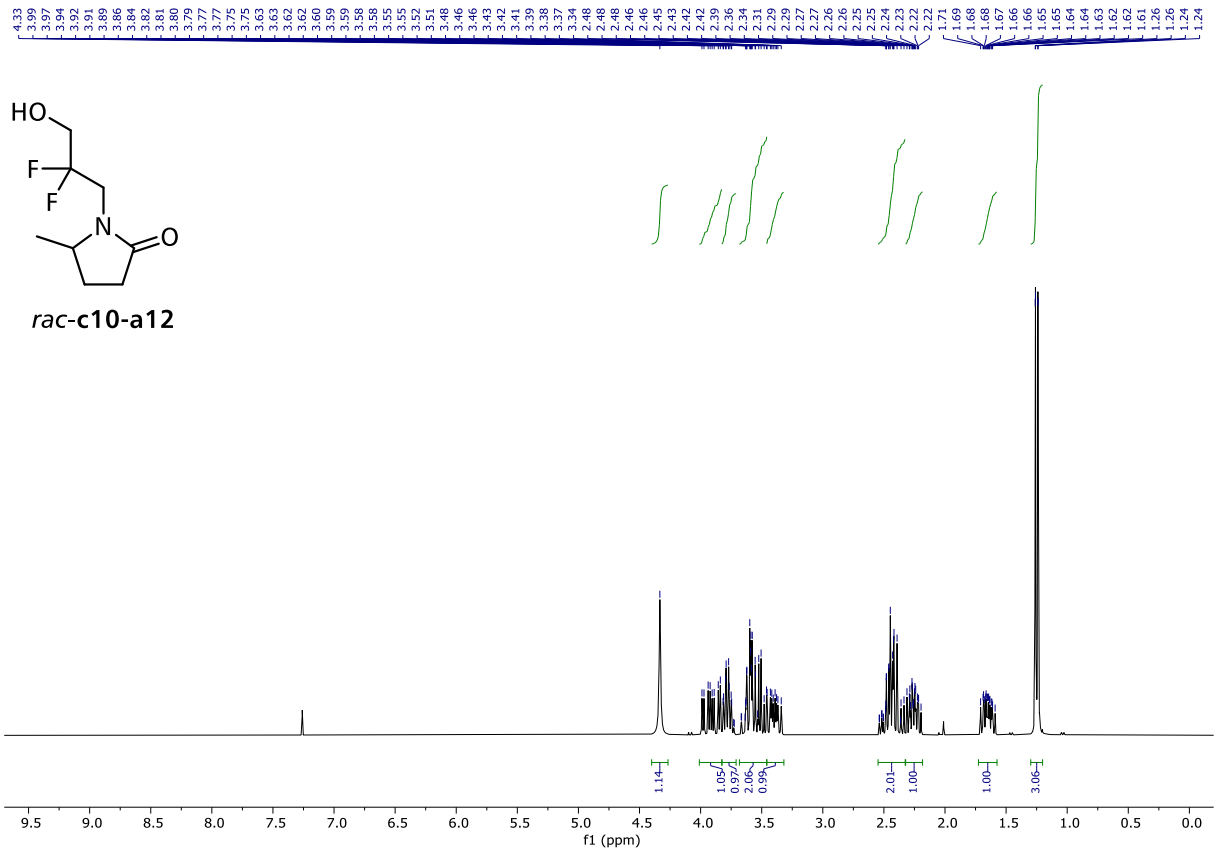


Figure S279. ^{1}H NMR spectrum of *rac*-1-(2,2-difluoro-3-hydroxypropyl)-5-methylpyrrolidin-2-one (**c10-a12**).

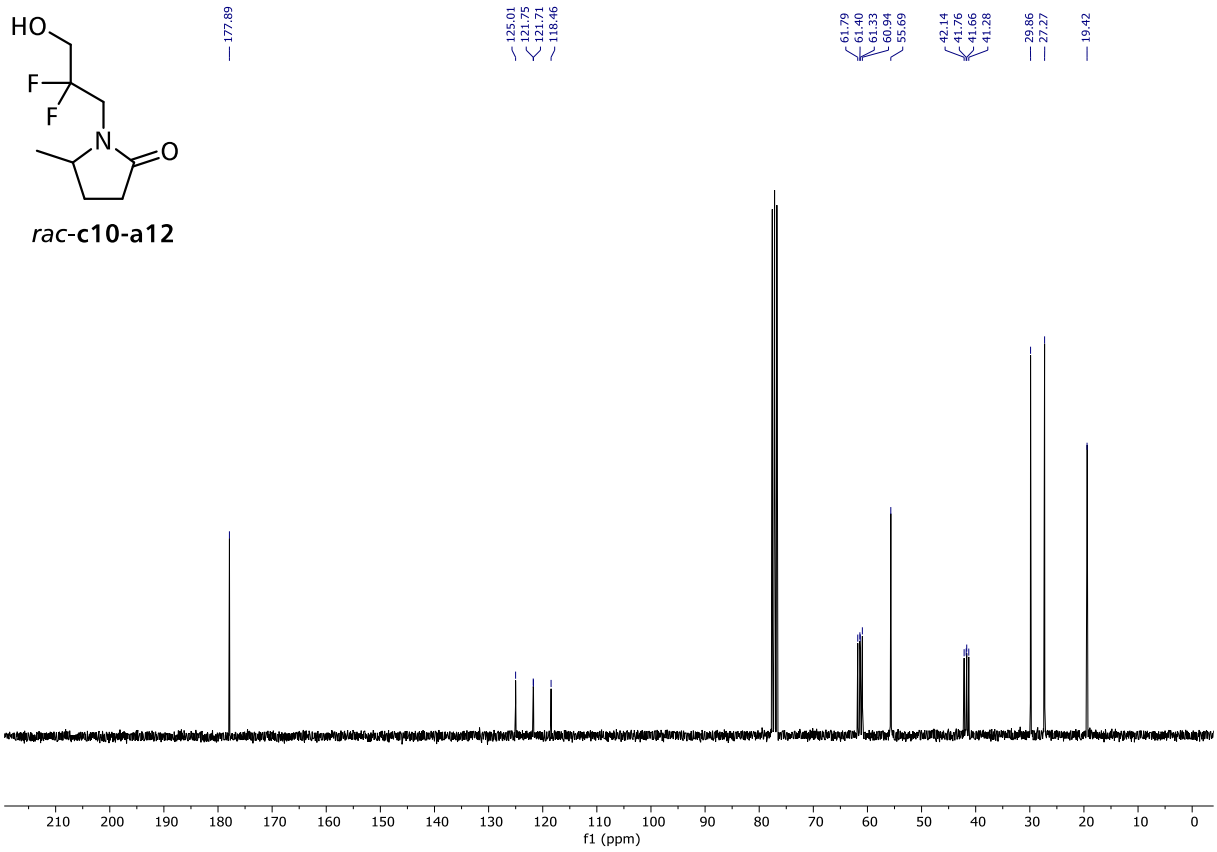


Figure S280. ^{13}C NMR spectrum of *rac*-1-(2,2-difluoro-3-hydroxypropyl)-5-methylpyrrolidin-2-one (**c10-a12**).

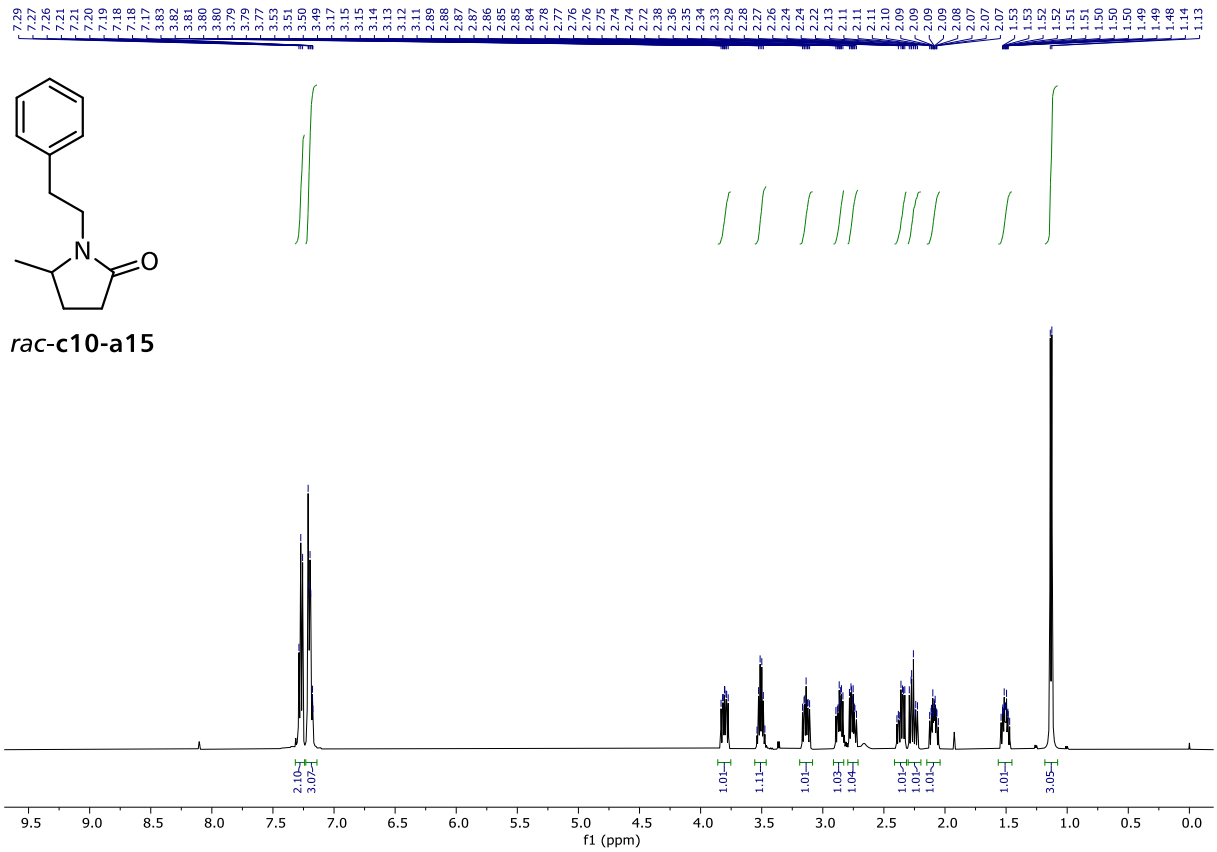


Figure S281. ^{1}H NMR spectrum of *rac*-5-methyl-1-phenethylpyrrolidin-2-one (**c10-a15**).

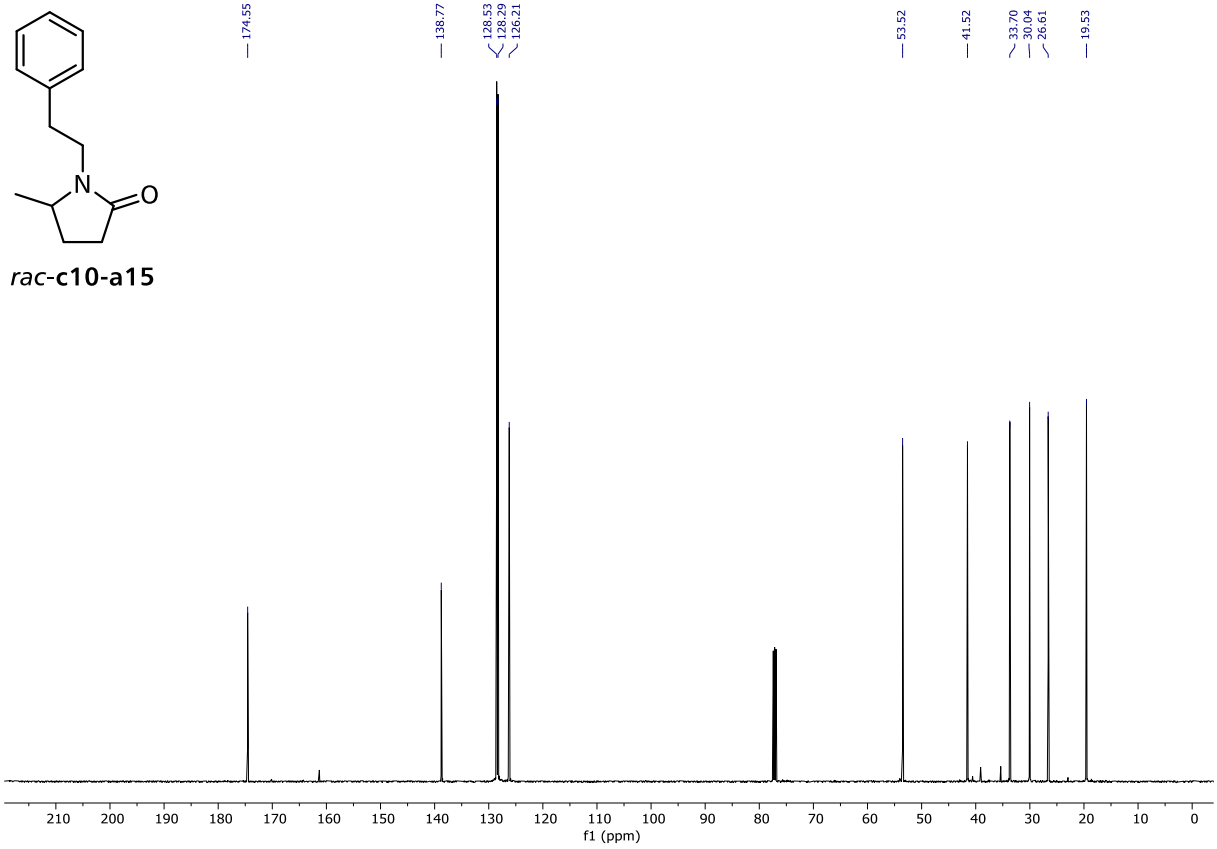


Figure S282. ^{13}C NMR spectrum of *rac*-5-methyl-1-phenethylpyrrolidin-2-one (**c10-a15**).

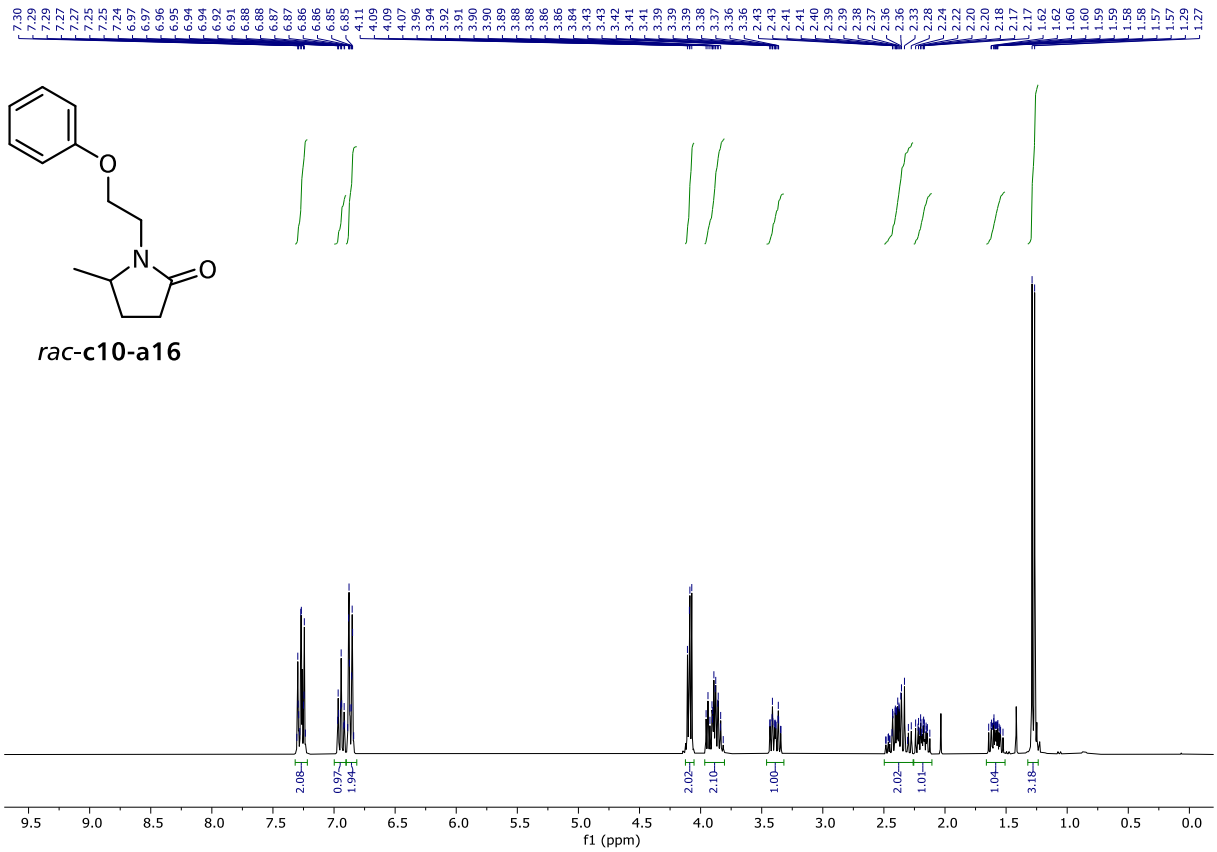


Figure S283. ^{1}H NMR spectrum of *rac*-5-methyl-1-(2-phenoxyethyl)pyrrolidin-2-one (**c10-a16**).

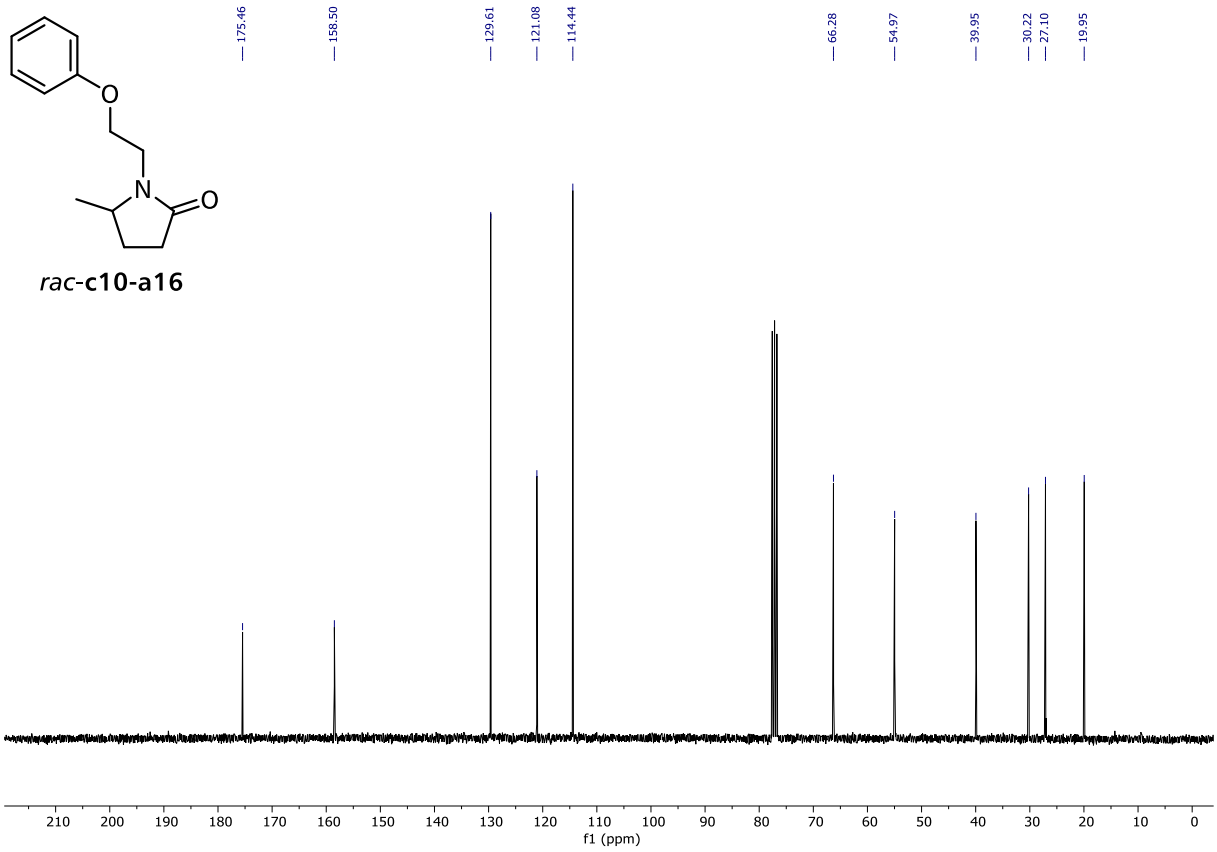


Figure S284. ^{13}C NMR spectrum of *rac*-5-methyl-1-(2-phenoxyethyl)pyrrolidin-2-one (**c10-a16**).

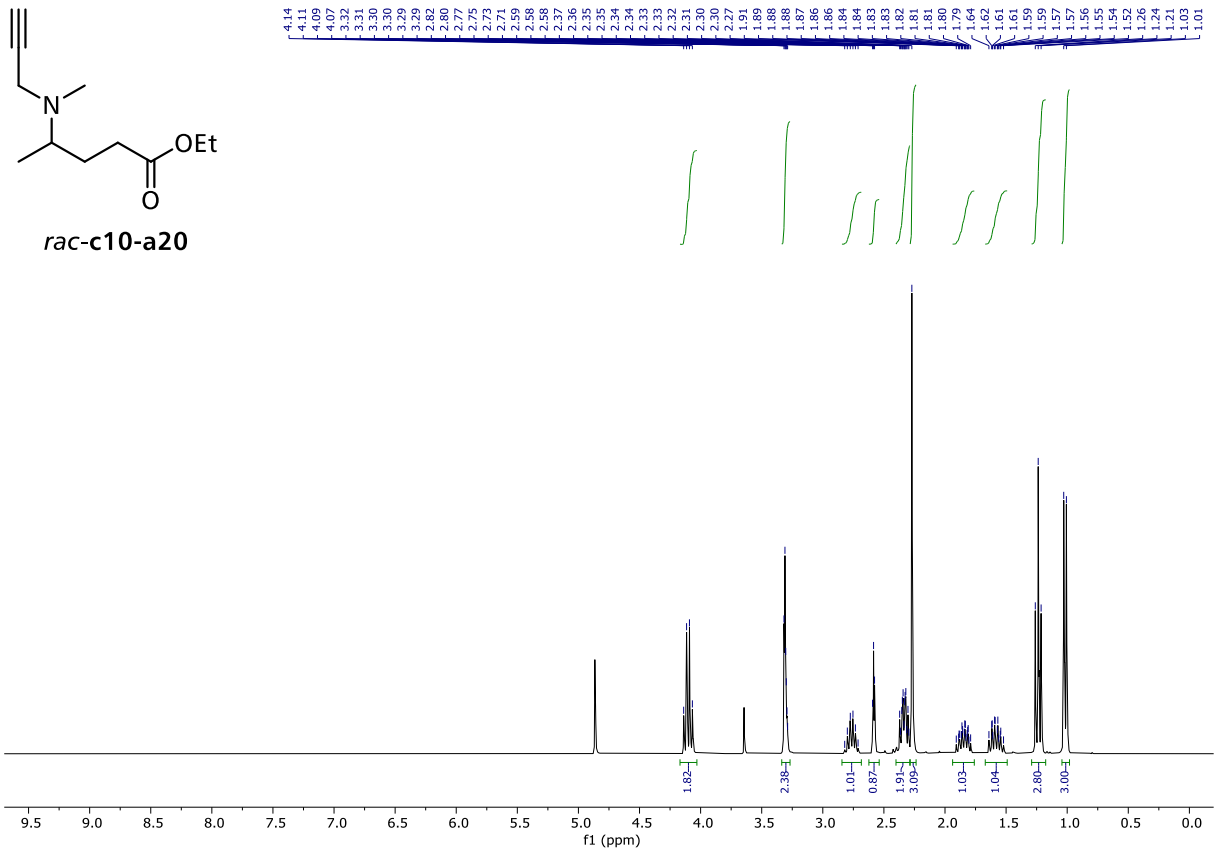


Figure S285. ^{1}H NMR spectrum of ethyl *rac*-4-(methyl(prop-2-yn-1-yl)amino)pentanoate (**c10-a20**).

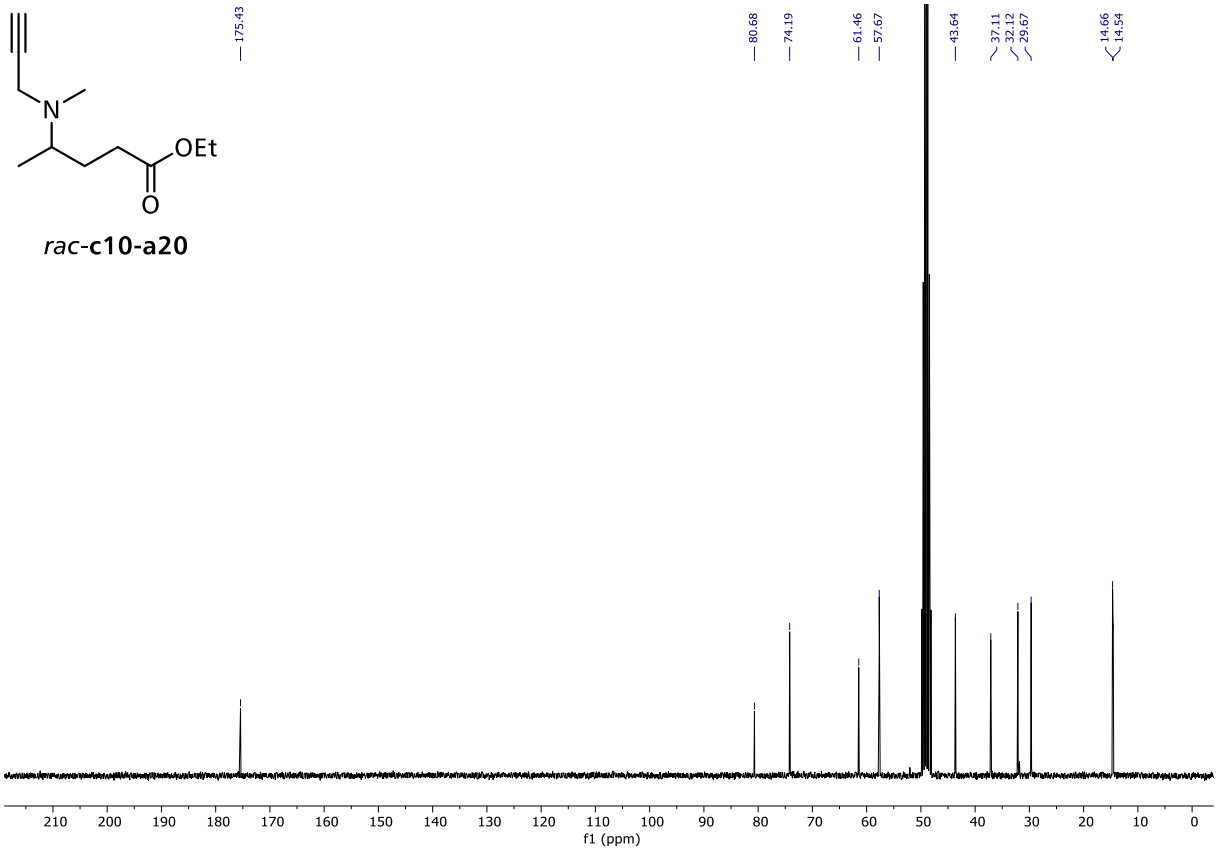


Figure S286. ^{13}C NMR spectrum of ethyl *rac*-4-(methyl(prop-2-yn-1-yl)amino)pentanoate (**c10-a20**).

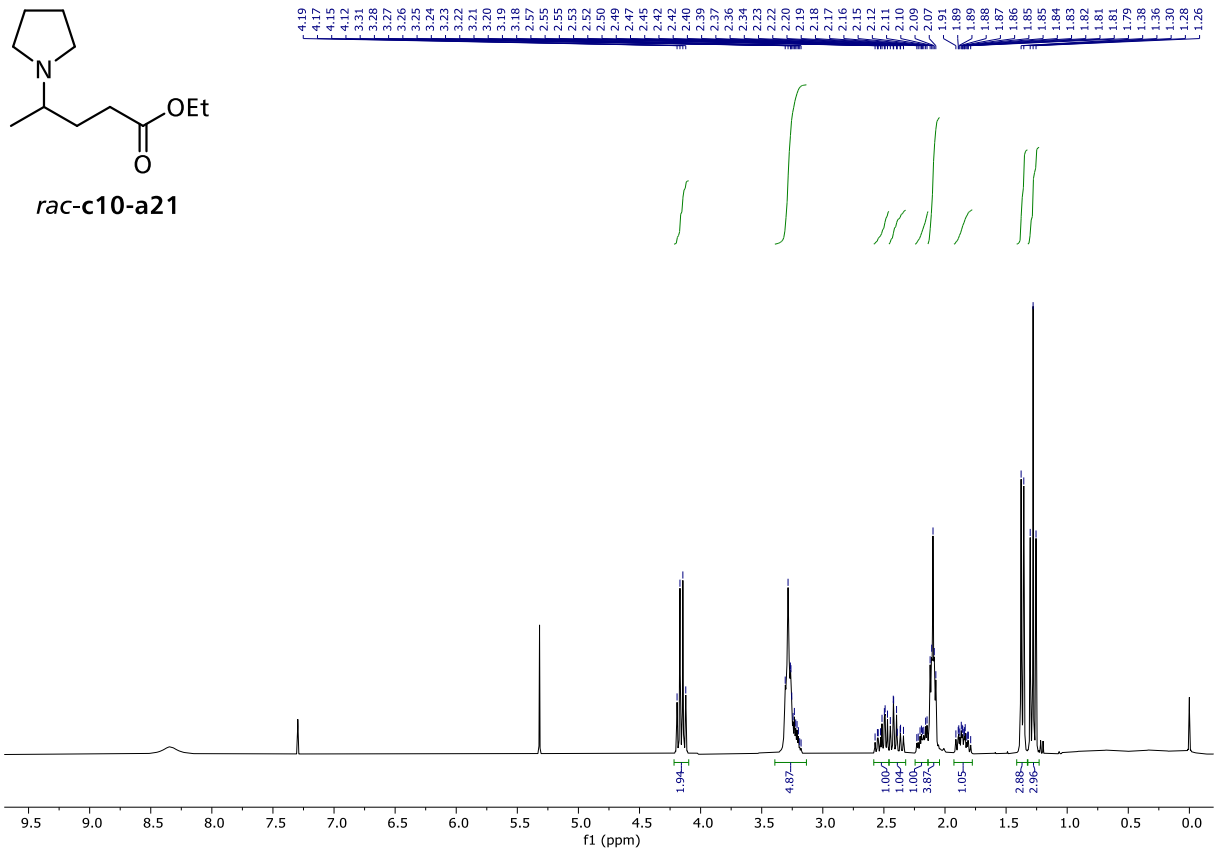


Figure S287. ^{1}H NMR spectrum of ethyl *rac*-4-(pyrrolidin-1-yl)pentanoate (**c10-a21**).

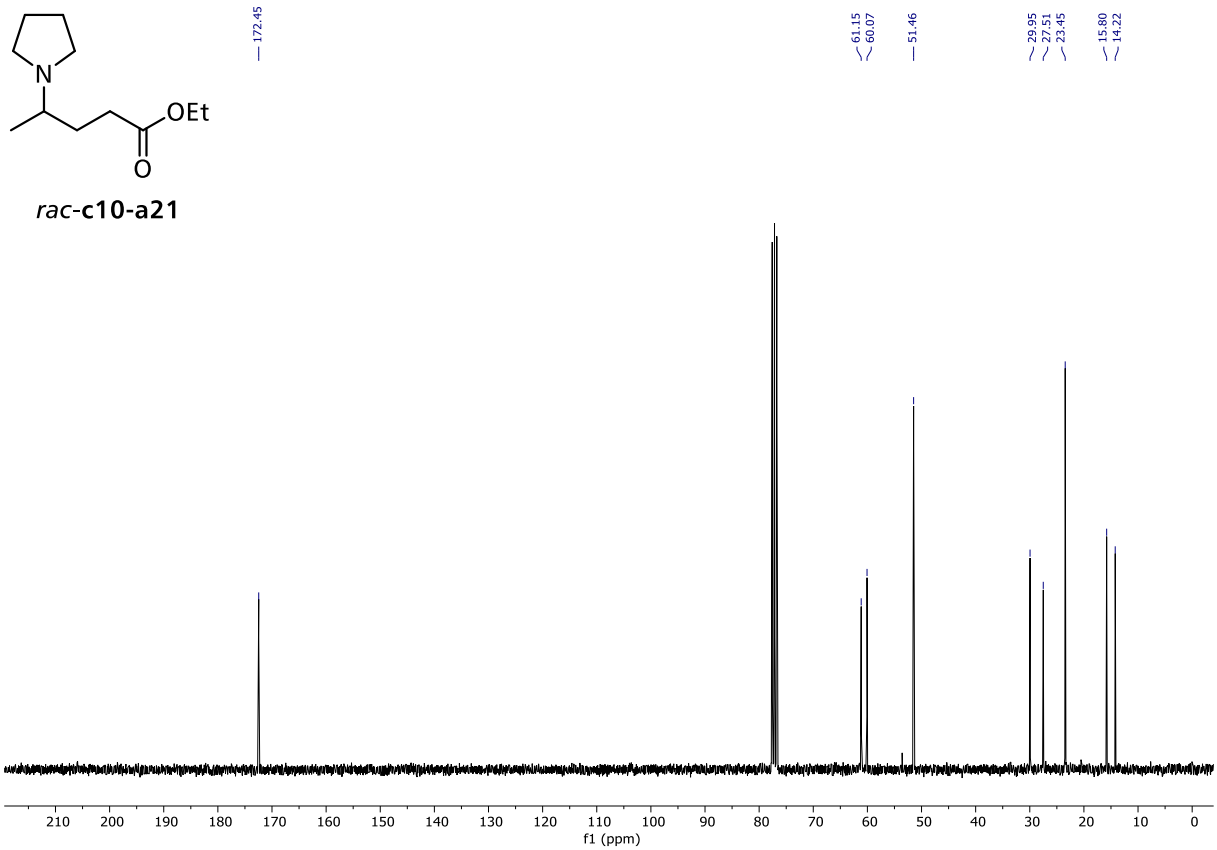


Figure S288. ^{13}C NMR spectrum of ethyl *rac*-4-(pyrrolidin-1-yl)pentanoate (**c10-a21**).

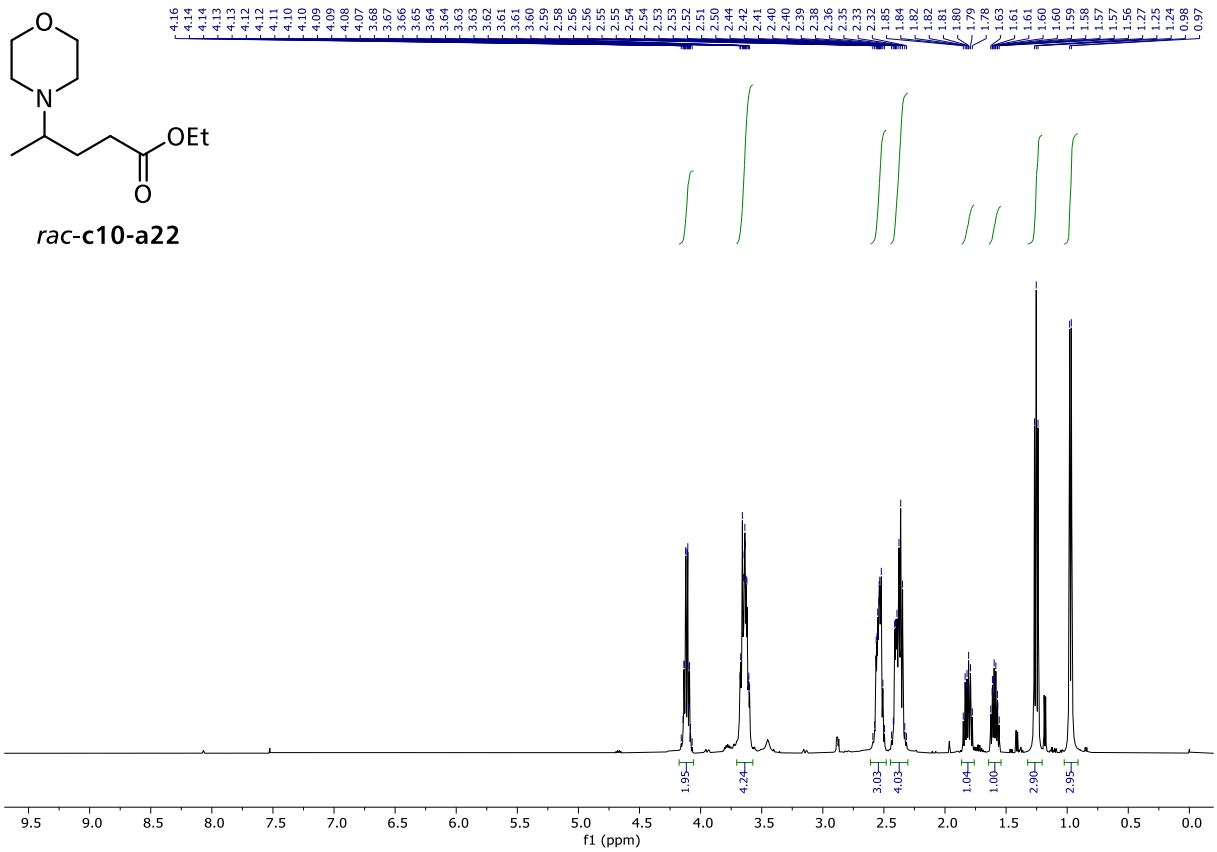


Figure S289. ^{1}H NMR spectrum of ethyl *rac*-4-morpholinopentanoate (**c10-a22**).

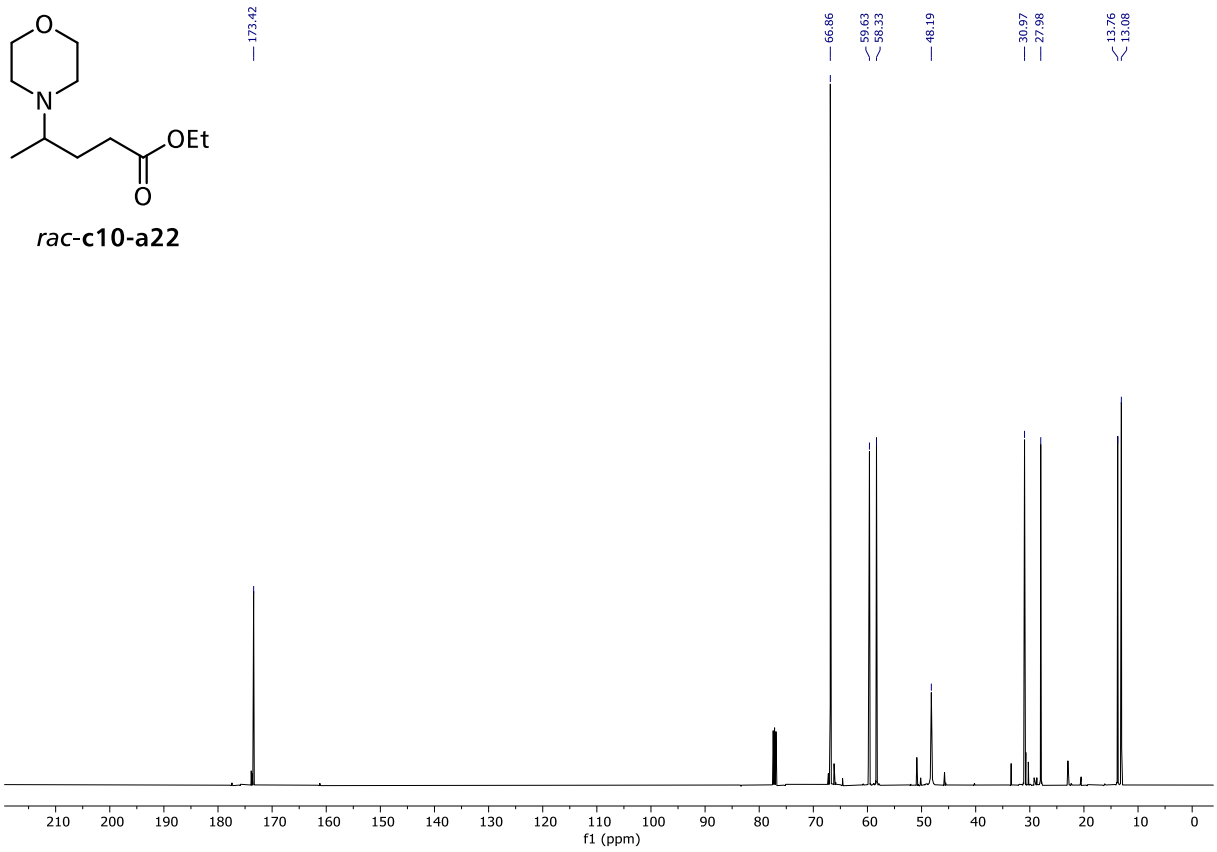


Figure S290. ^{13}C NMR spectrum of ethyl *rac*-4-morpholinopentanoate (**c10-a22**).

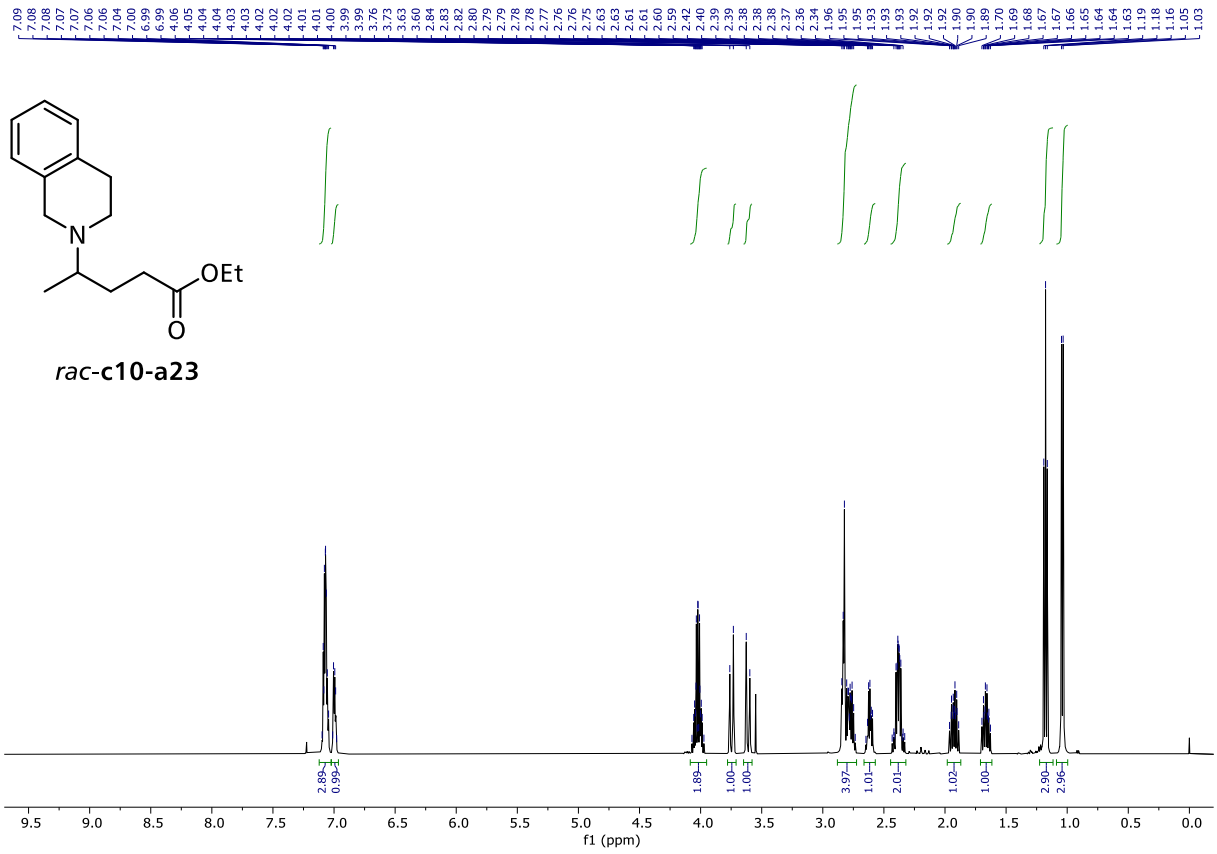


Figure S291. ^{1}H NMR spectrum of ethyl *rac*-4-(3,4-dihydroisoquinolin-2(1*H*)-yl)pentanoate (**c10-a23**).

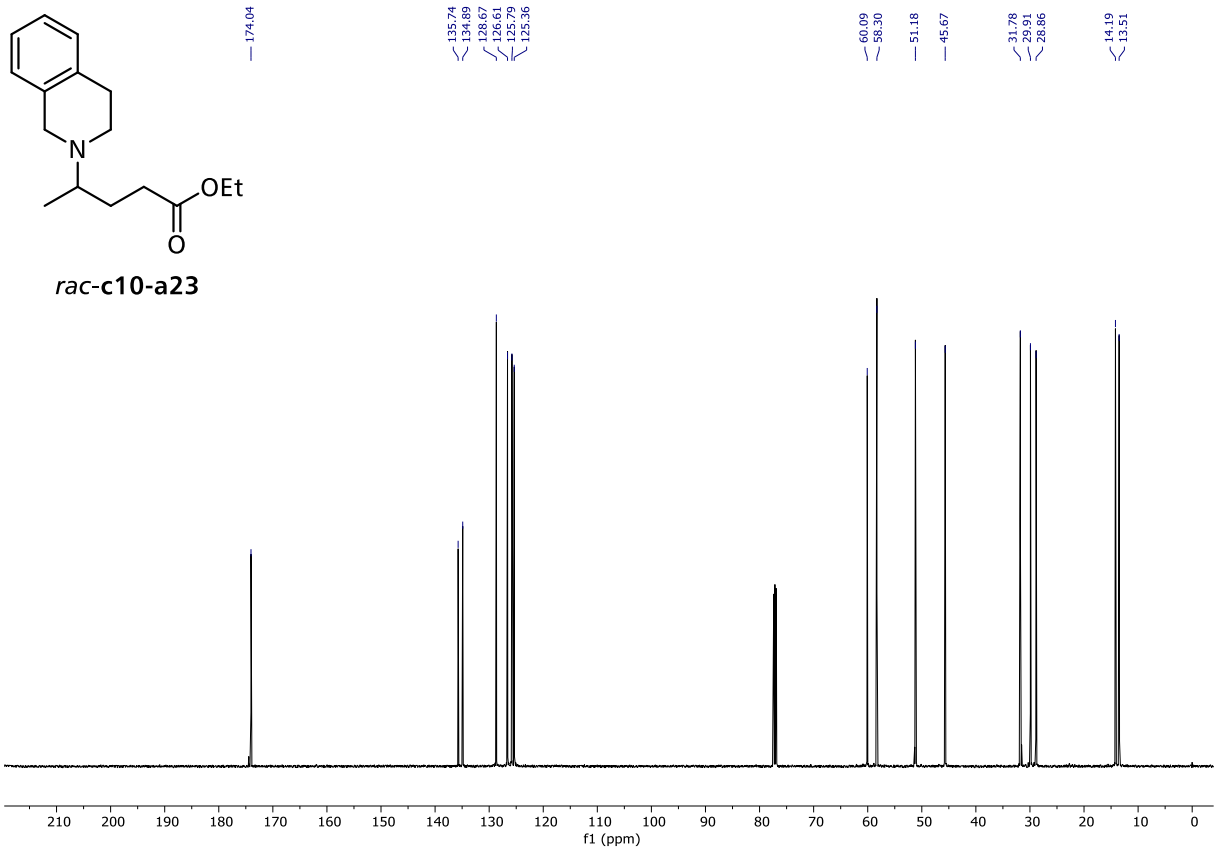


Figure S292. ^{13}C NMR spectrum of ethyl *rac*-4-(3,4-dihydroisoquinolin-2(1*H*)-yl)pentanoate (**c10-a23**).

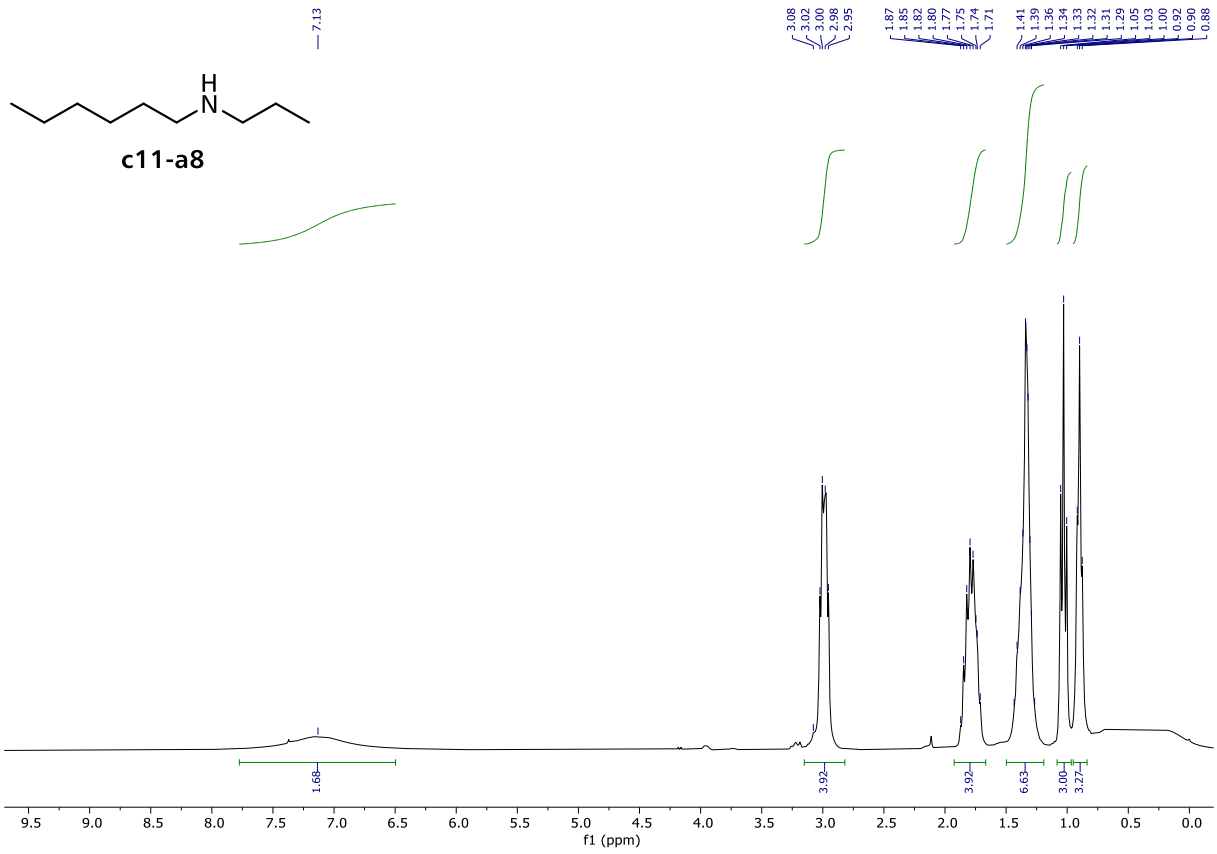


Figure S293. ^{1}H NMR spectrum of *N*-propylhexan-1-amine (**c11-a8**).

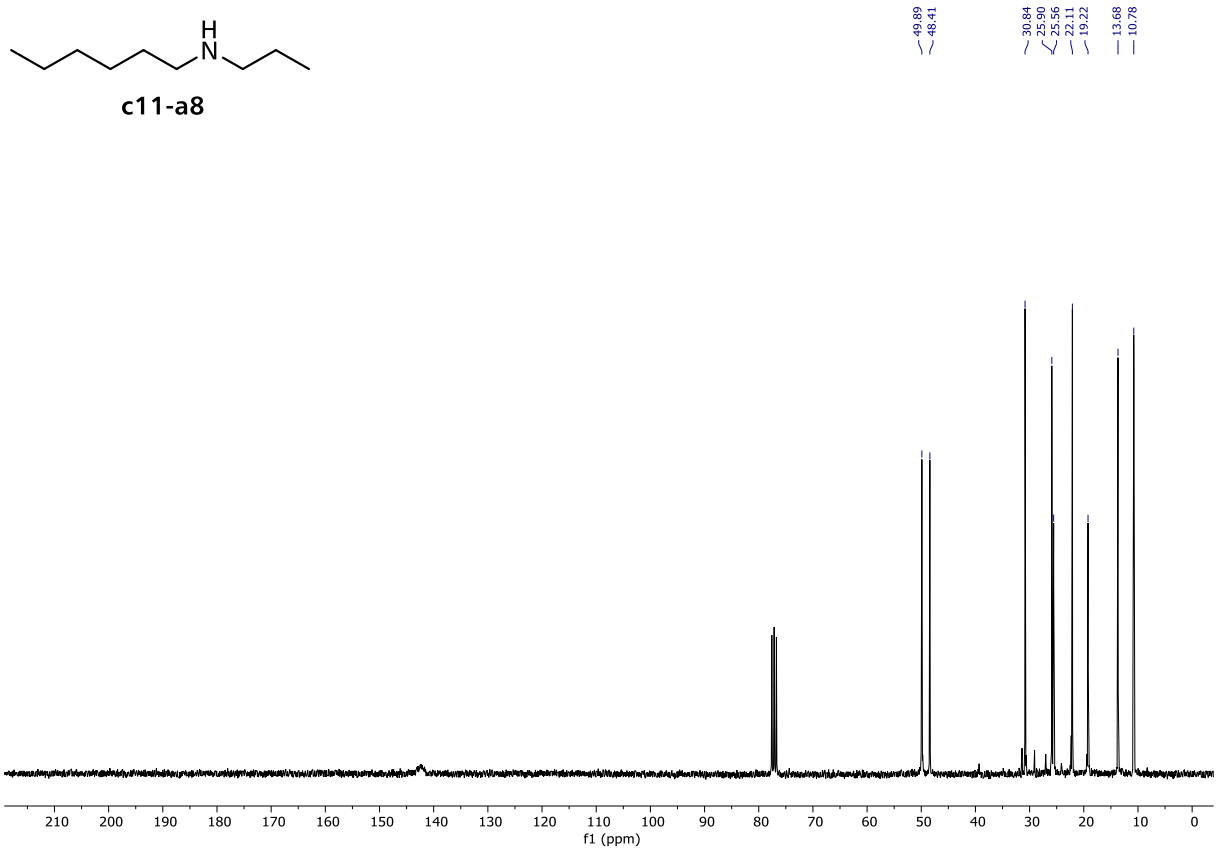


Figure S294. ^{13}C NMR spectrum of *N*-propylhexan-1-amine (**c11-a8**).

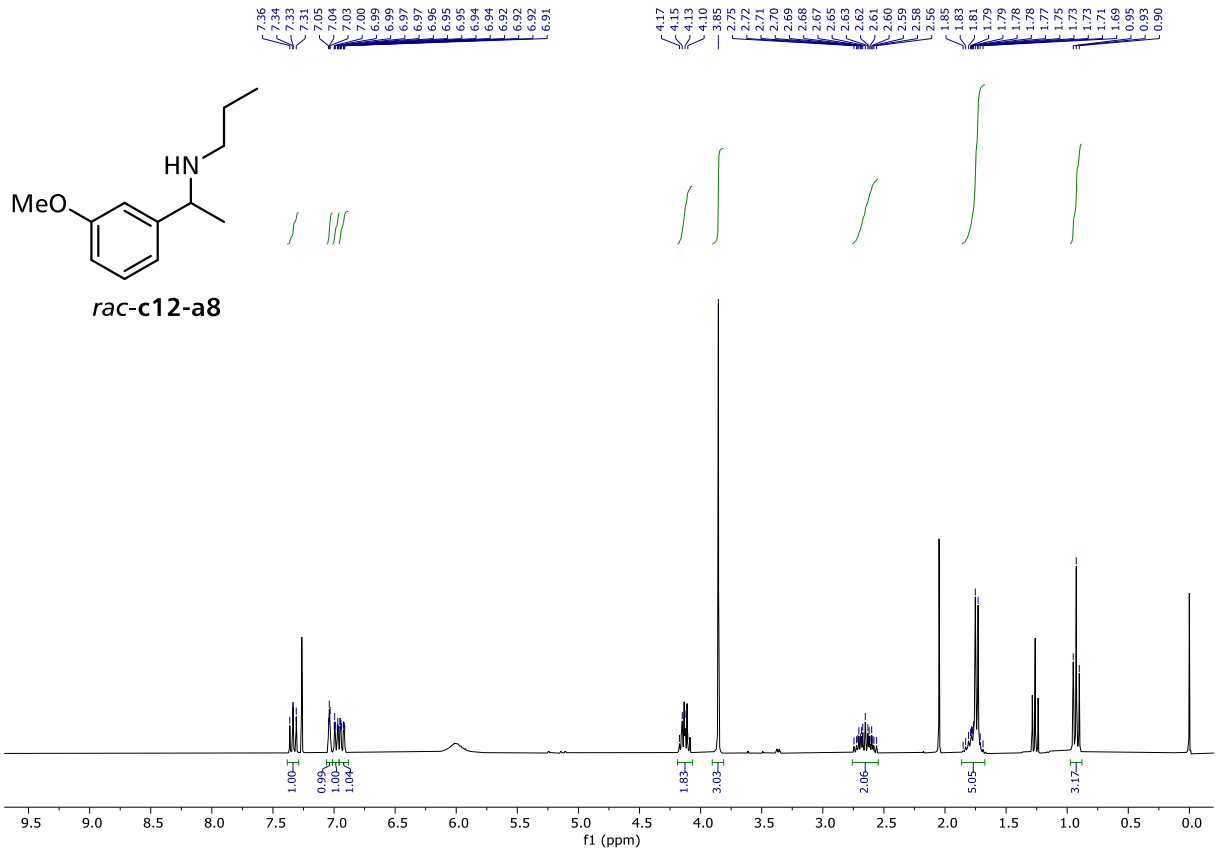


Figure S295. ^{1}H NMR spectrum of *rac-N*-(1-(3-methoxyphenyl)ethyl)propan-1-amine (**c12-a8**).

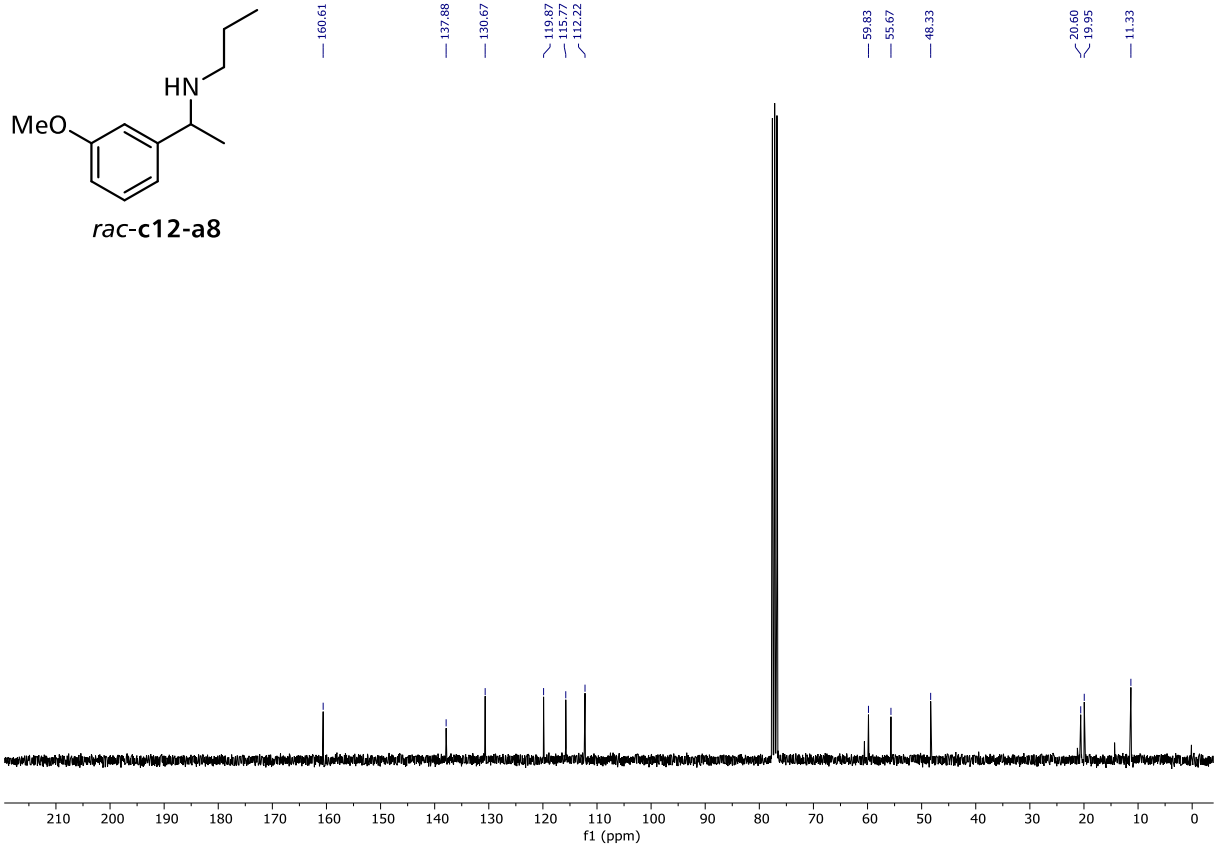


Figure S296. ^{13}C NMR spectrum of *rac-N*-(1-(3-methoxyphenyl)ethyl)propan-1-amine (**c12-a8**).

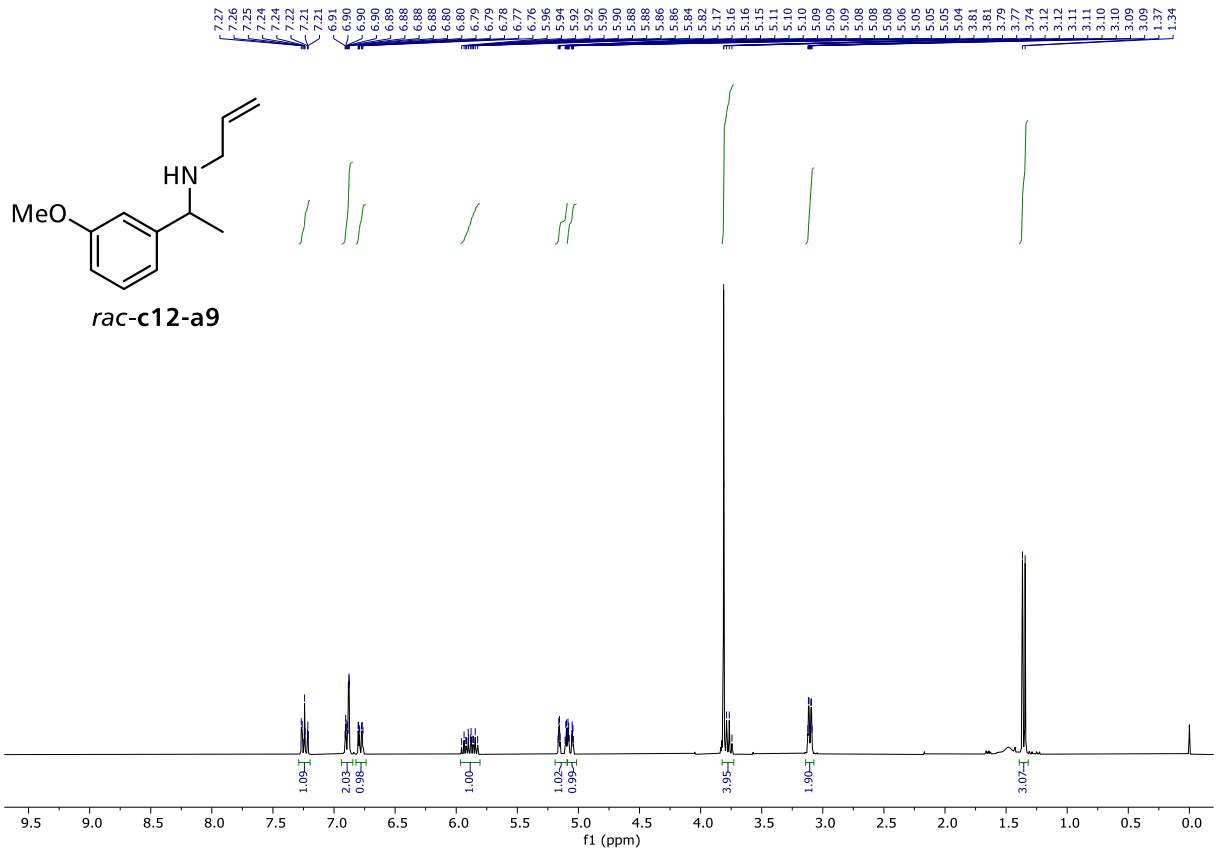


Figure S297. ^{1}H NMR spectrum of *rac*-*N*-(1-(3-methoxyphenyl)ethyl)prop-2-en-1-amine (**c12-a9**).

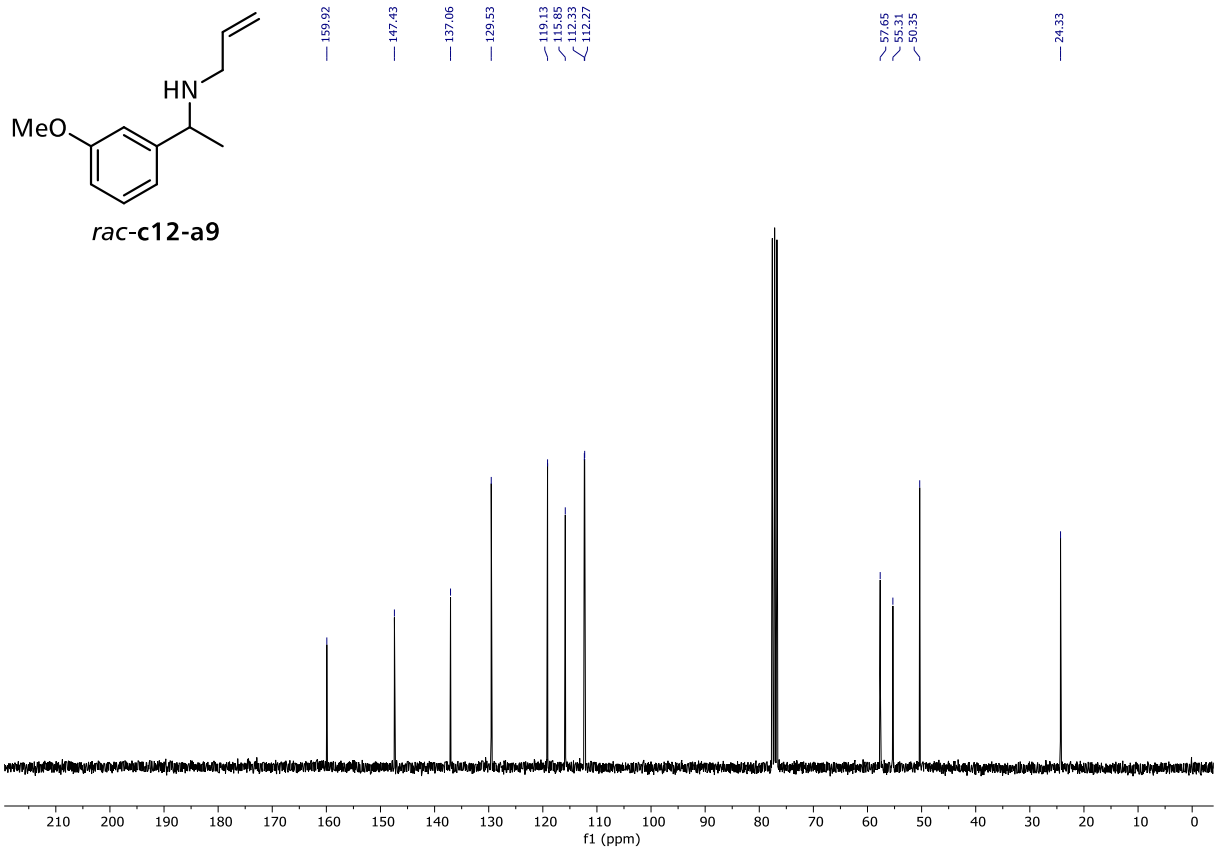


Figure S298. ^{13}C NMR spectrum of *rac*-*N*-(1-(3-methoxyphenyl)ethyl)prop-2-en-1-amine (**c12-a9**).

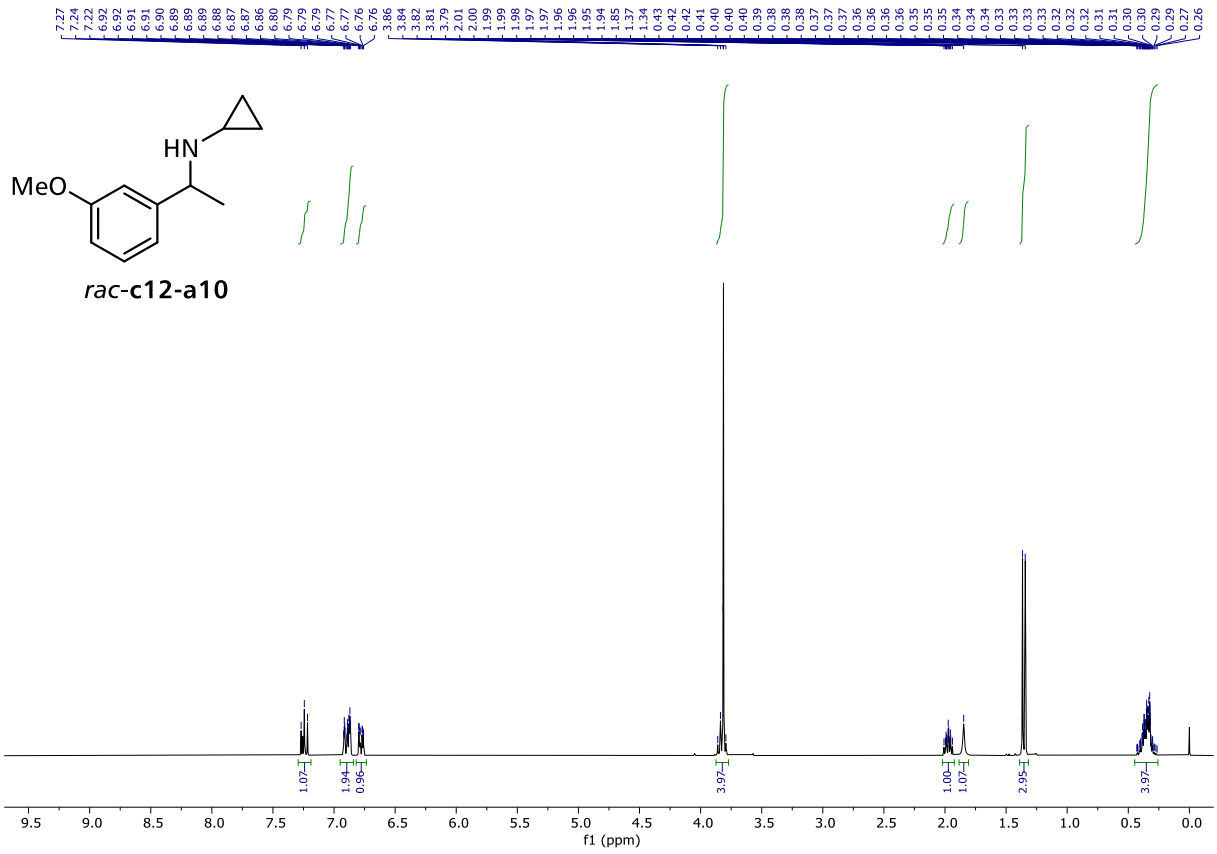


Figure S299. ^{1}H NMR spectrum of *rac*-*N*-(1-(3-methoxyphenyl)ethyl)cyclopropanamine (**c12-a10**).

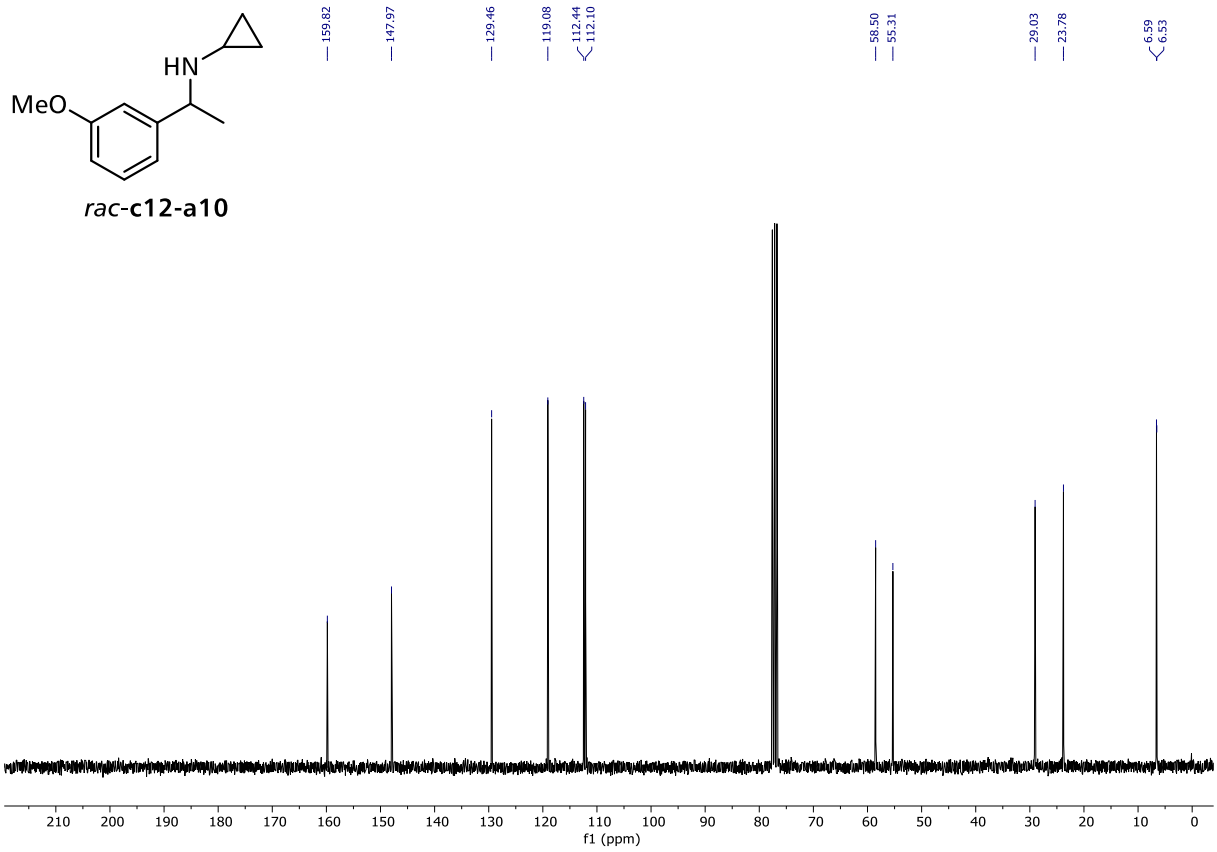


Figure S300. ^{13}C NMR spectrum of *rac*-*N*-(1-(3-methoxyphenyl)ethyl)cyclopropanamine (**c12-a10**).

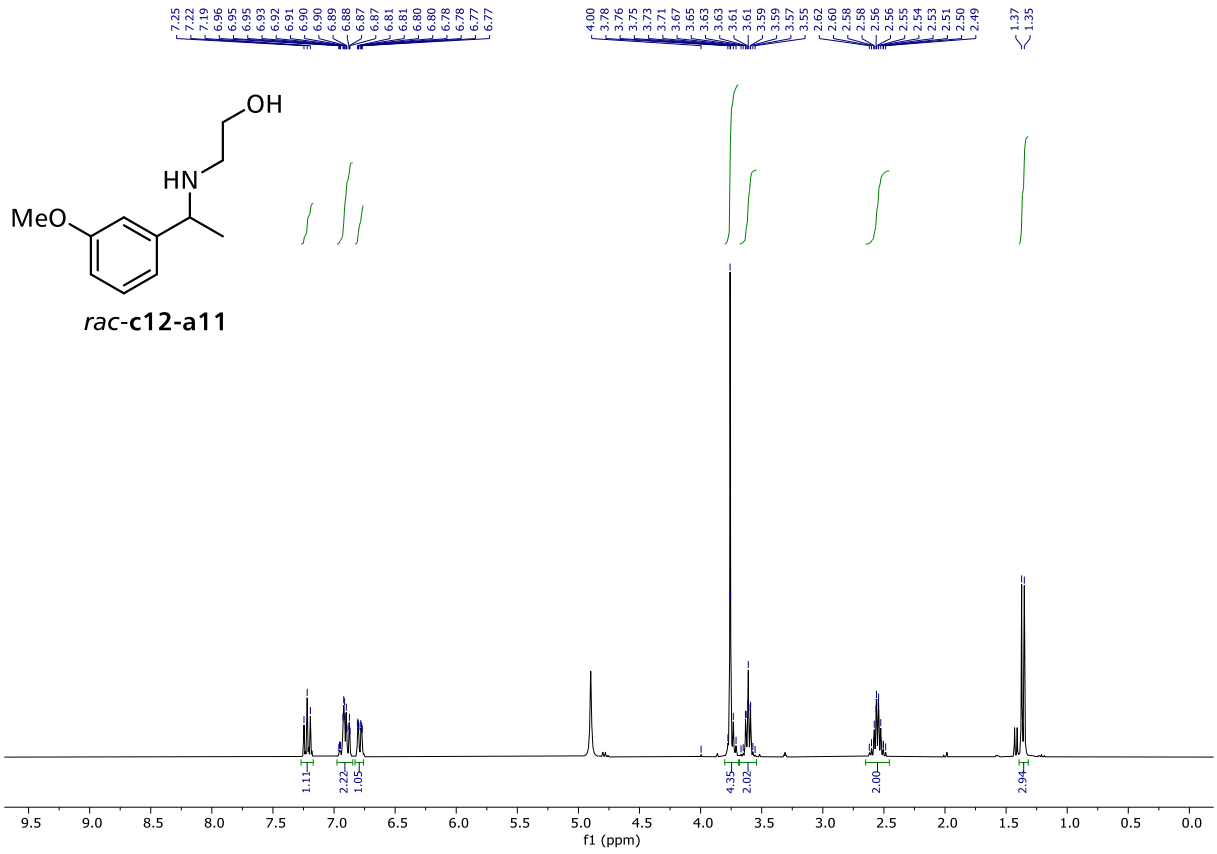


Figure S301. ^{1}H NMR spectrum of *rac*-2-((1-(3-methoxyphenyl)ethyl)amino)ethan-1-ol (**c12-a11**).

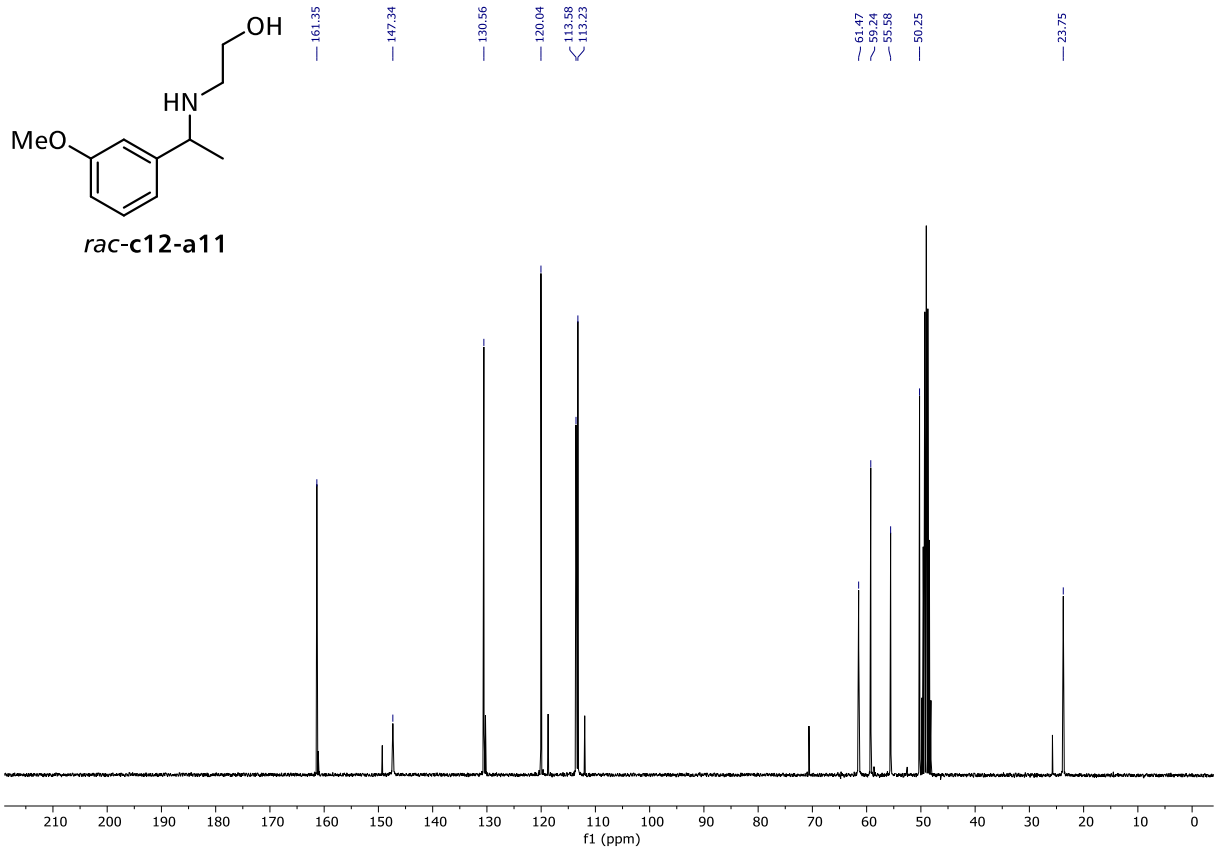


Figure S302. ^{13}C NMR spectrum of *rac*-2-((1-(3-methoxyphenyl)ethyl)amino)ethan-1-ol (**c12-a11**).

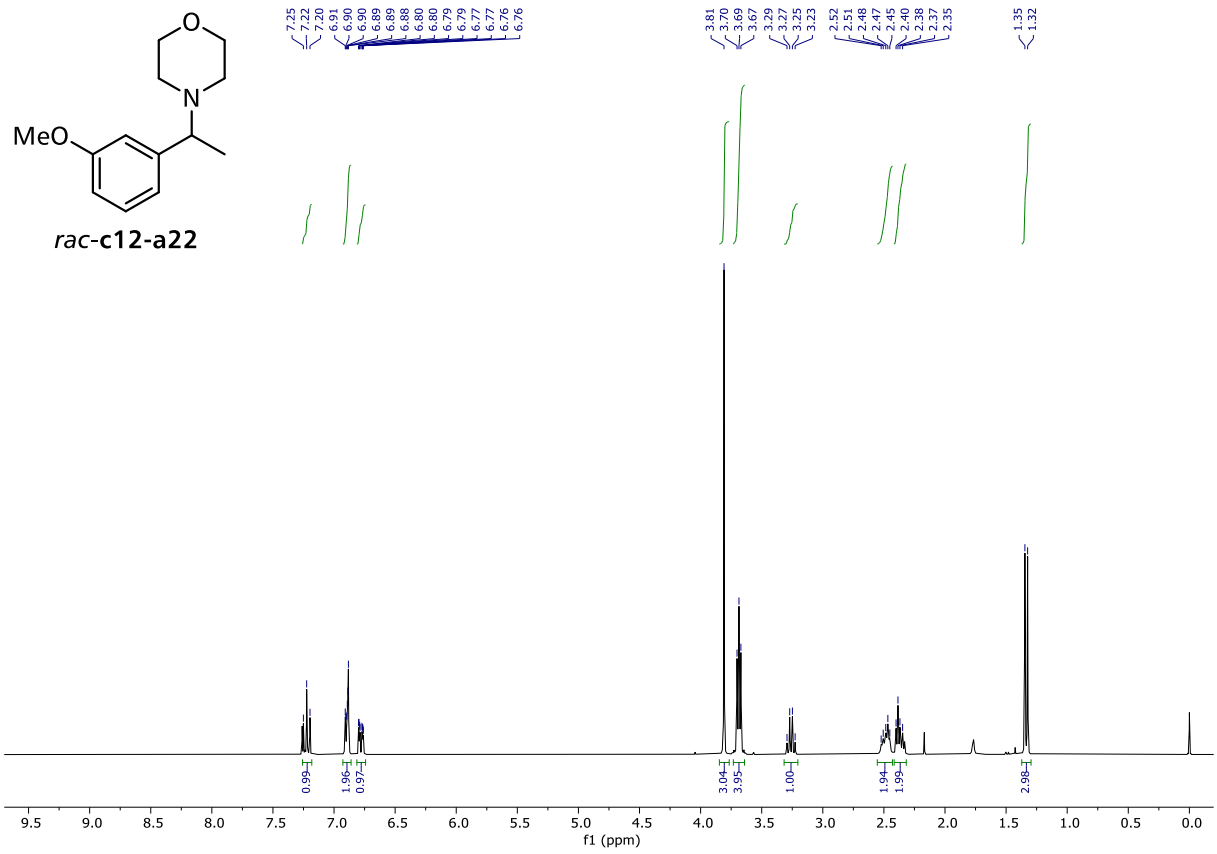


Figure S303. ^{1}H NMR spectrum of *rac*-4-(1-(3-methoxyphenyl)ethyl)morpholine (**c12-a22**).

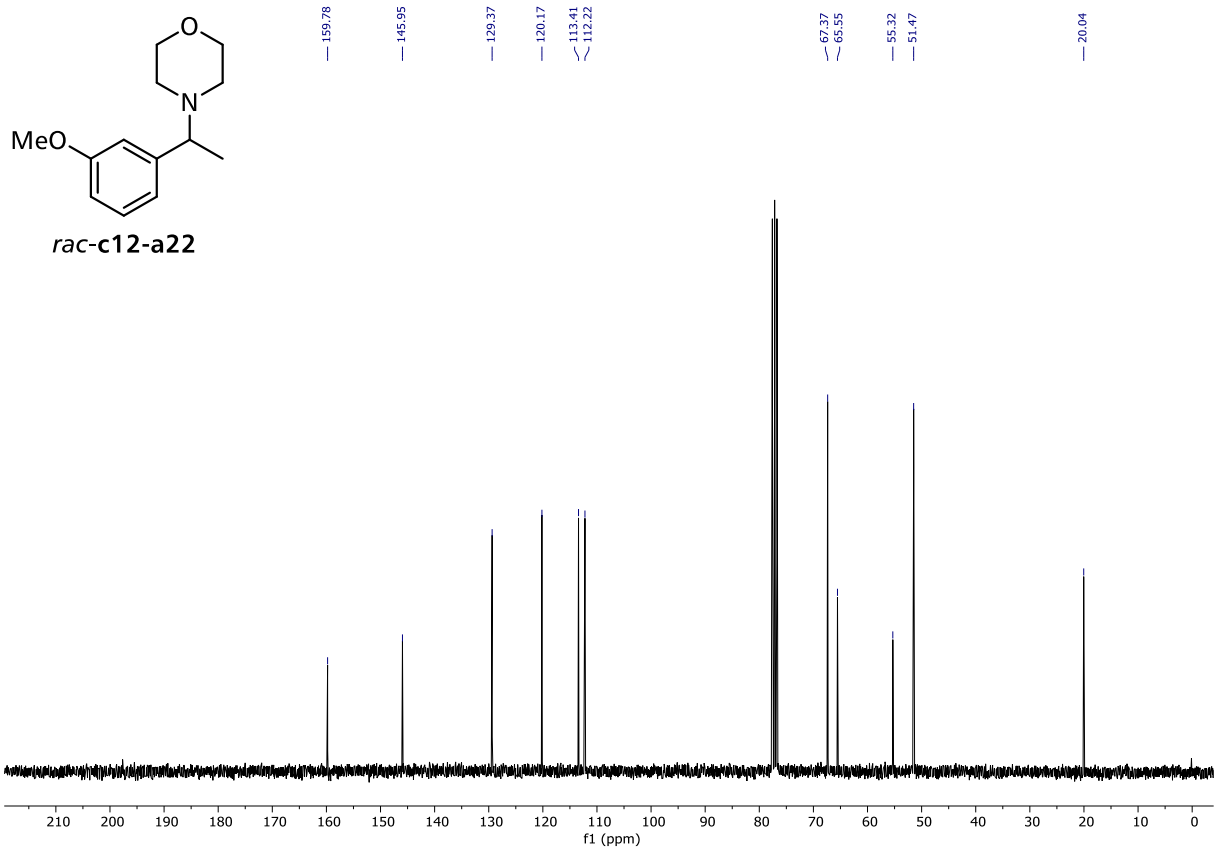


Figure S304. ^{13}C NMR spectrum of *rac*-4-(1-(3-methoxyphenyl)ethyl)morpholine (**c12-a22**).

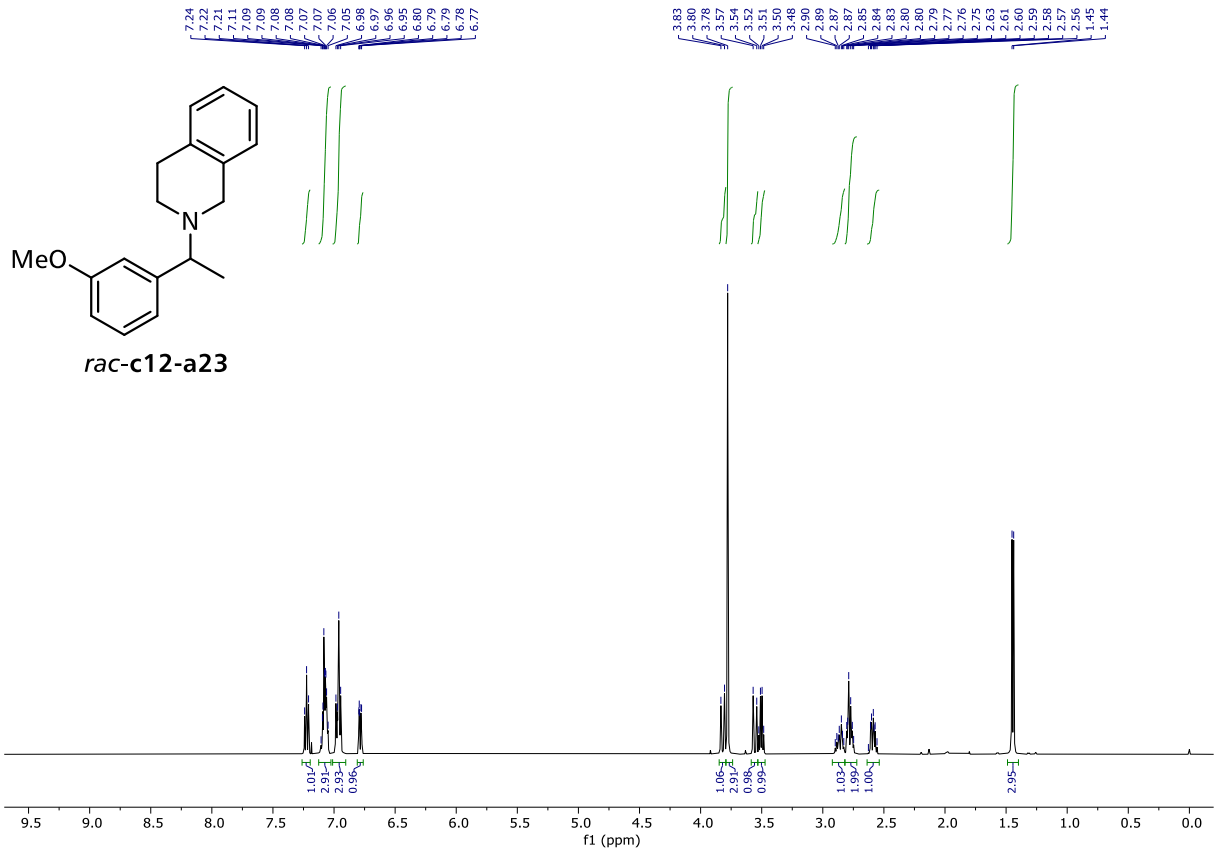


Figure S305. ^{1}H NMR spectrum of *rac*-2-(1-(3-methoxyphenyl)ethyl)-1,2,3,4-tetrahydroisoquinoline (**c12-a23**).

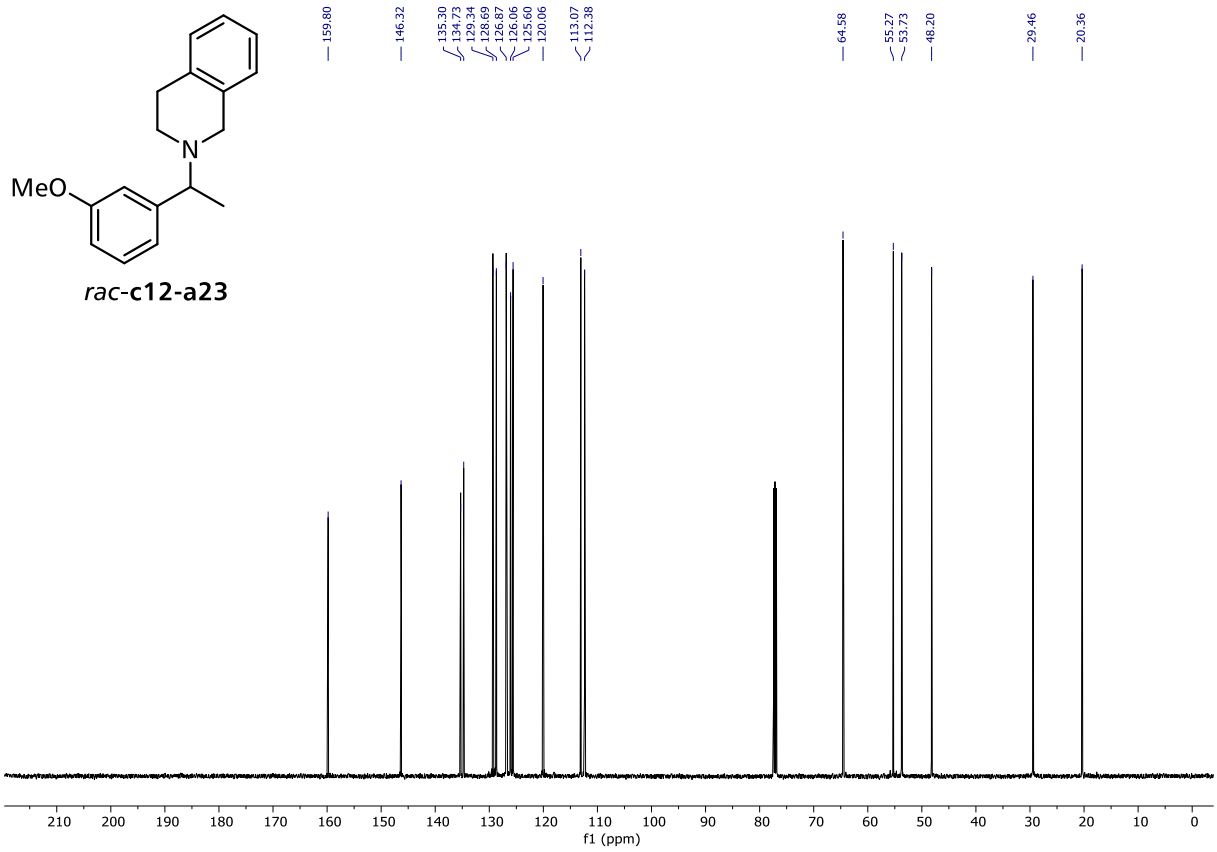


Figure S306. ^{13}C NMR spectrum of *rac*-2-(1-(3-methoxyphenyl)ethyl)-1,2,3,4-tetrahydroisoquinoline (**c12-a23**).

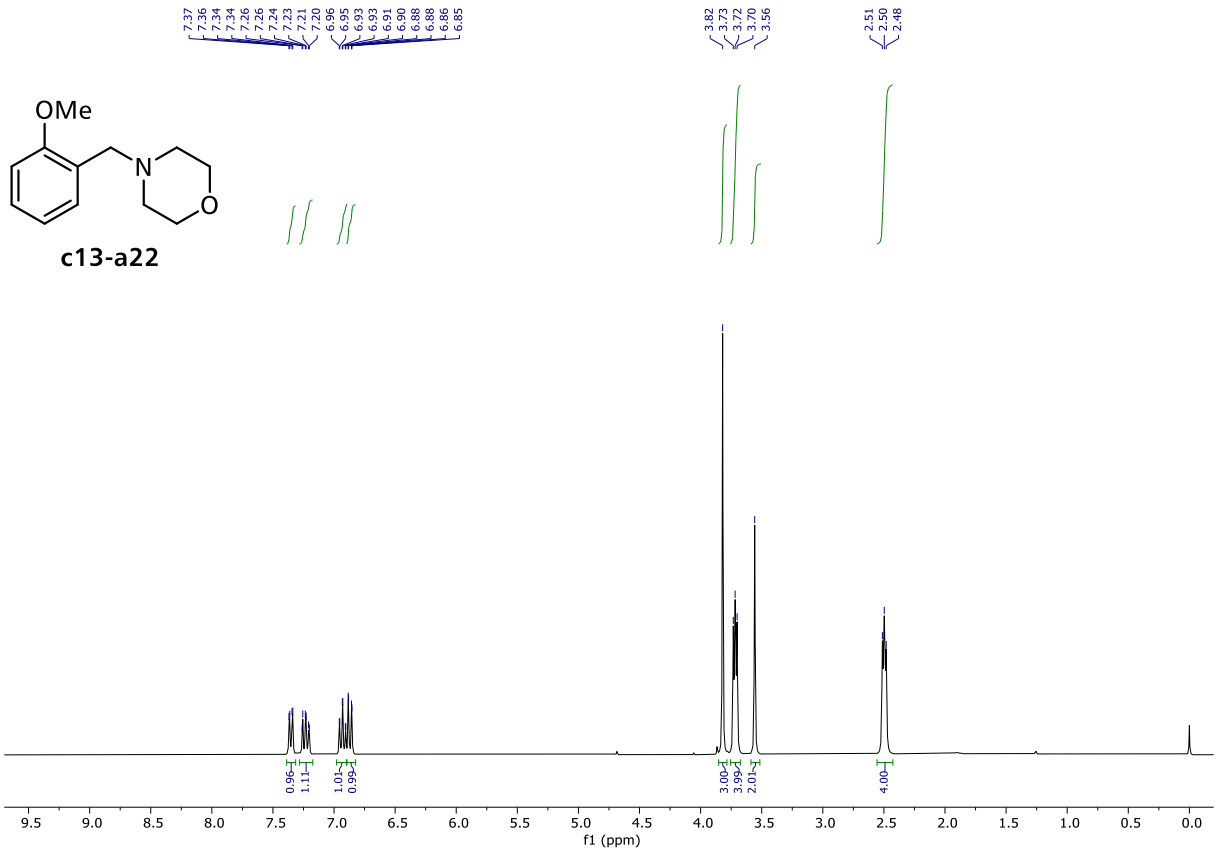


Figure S307. ^{1}H NMR spectrum of 4-(2-methoxybenzyl)morpholine (**c13-a22**).

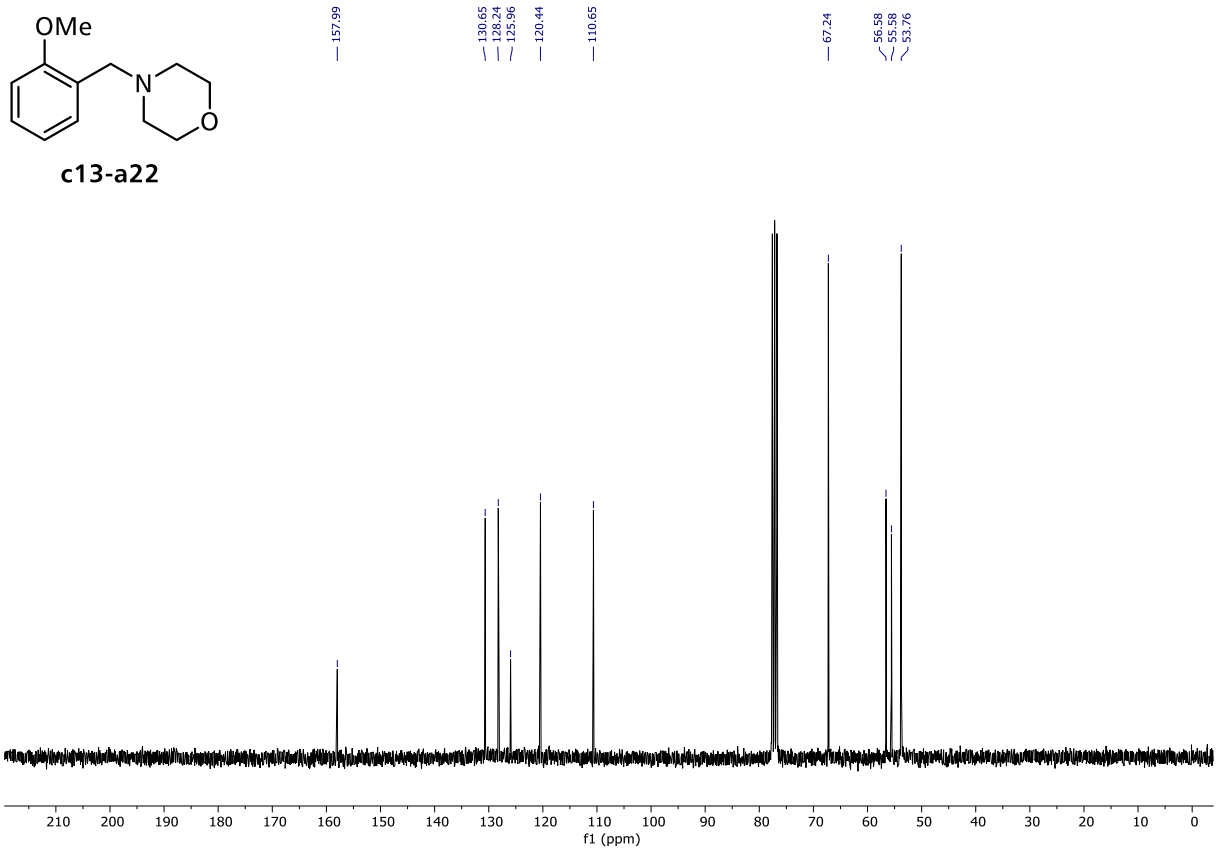


Figure S308. ^{13}C NMR spectrum of 4-(2-methoxybenzyl)morpholine (**c13-a22**).

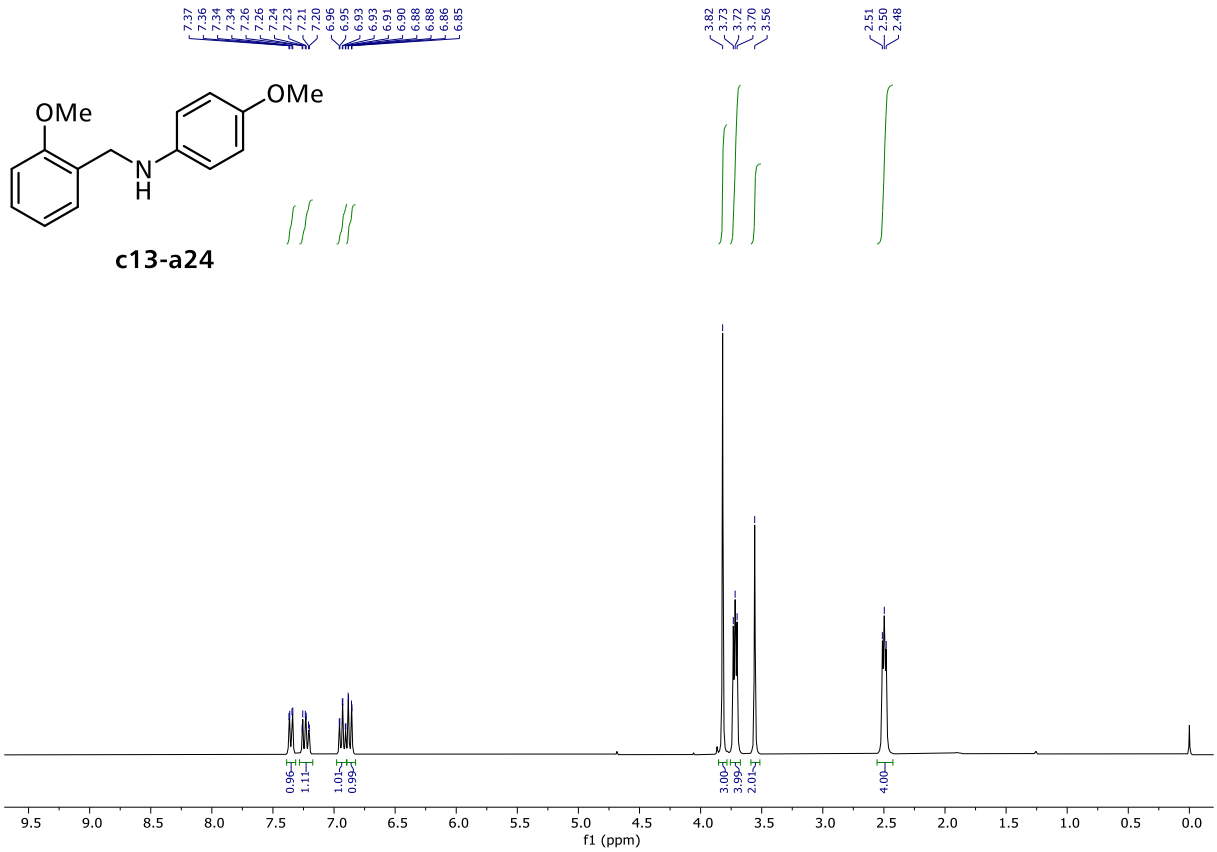


Figure S309. ^{1}H NMR spectrum of 4-methoxy-*N*-(2-methoxybenzyl)aniline (**c13-a24**).

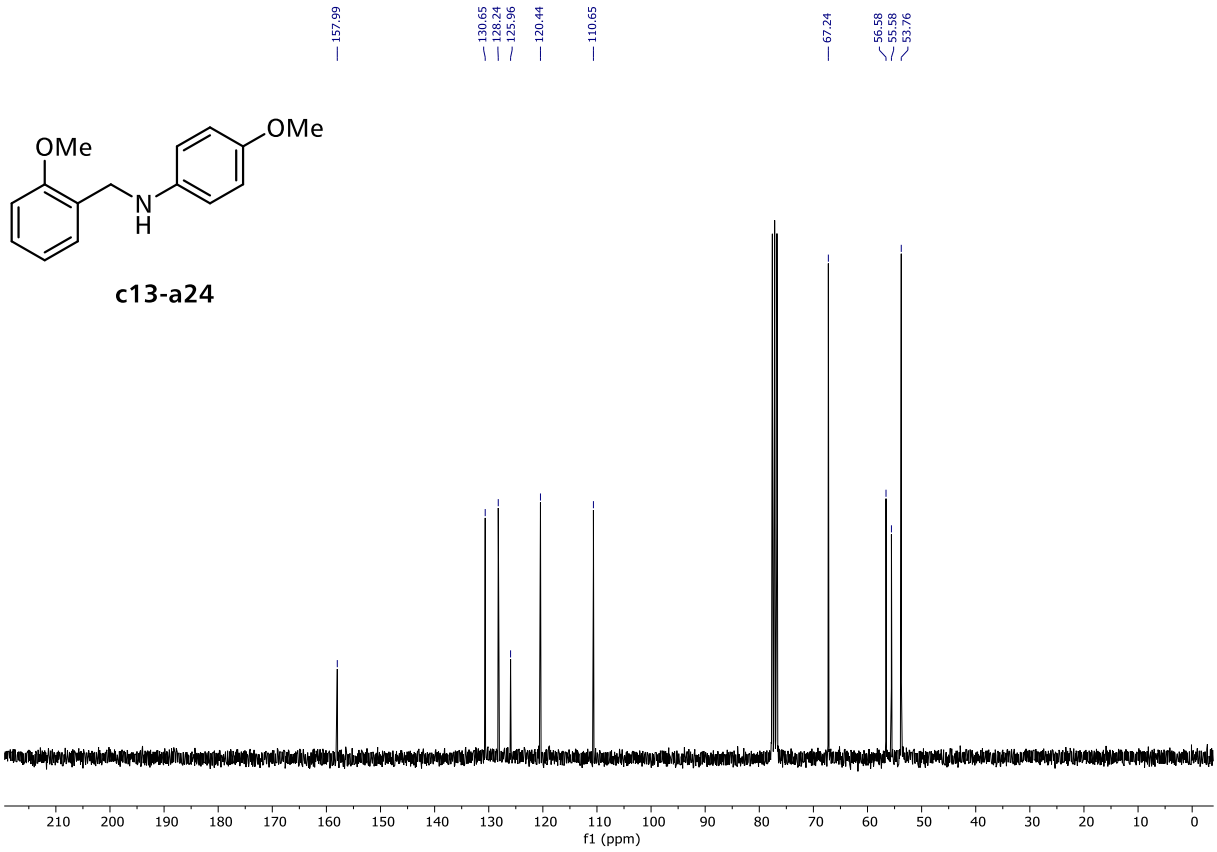


Figure S310. ^{13}C NMR spectrum of 4-methoxy-*N*-(2-methoxybenzyl)aniline (**c13-a24**).

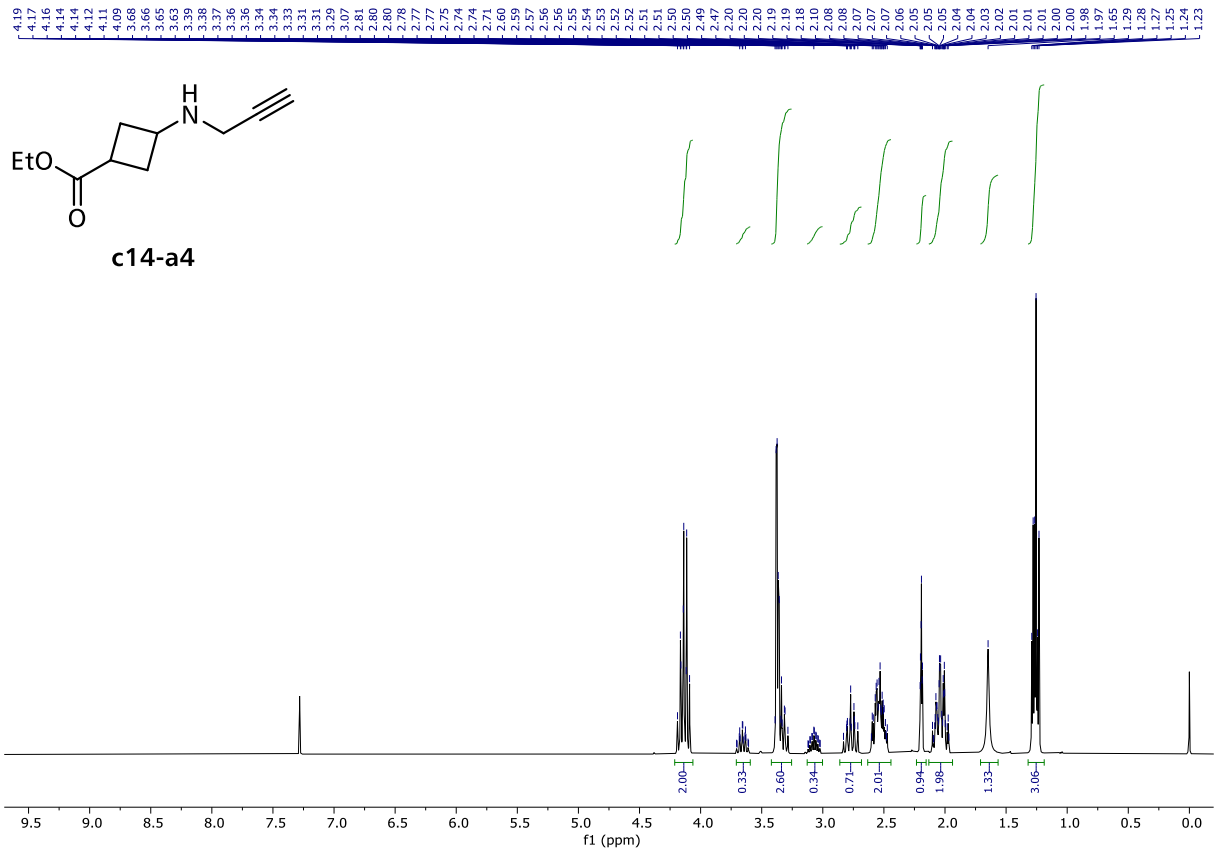


Figure S311. ^{1}H NMR spectrum of ethyl 3-(prop-2-yn-1-ylamino)cyclobutane-1-carboxylate (**c14-a4**).

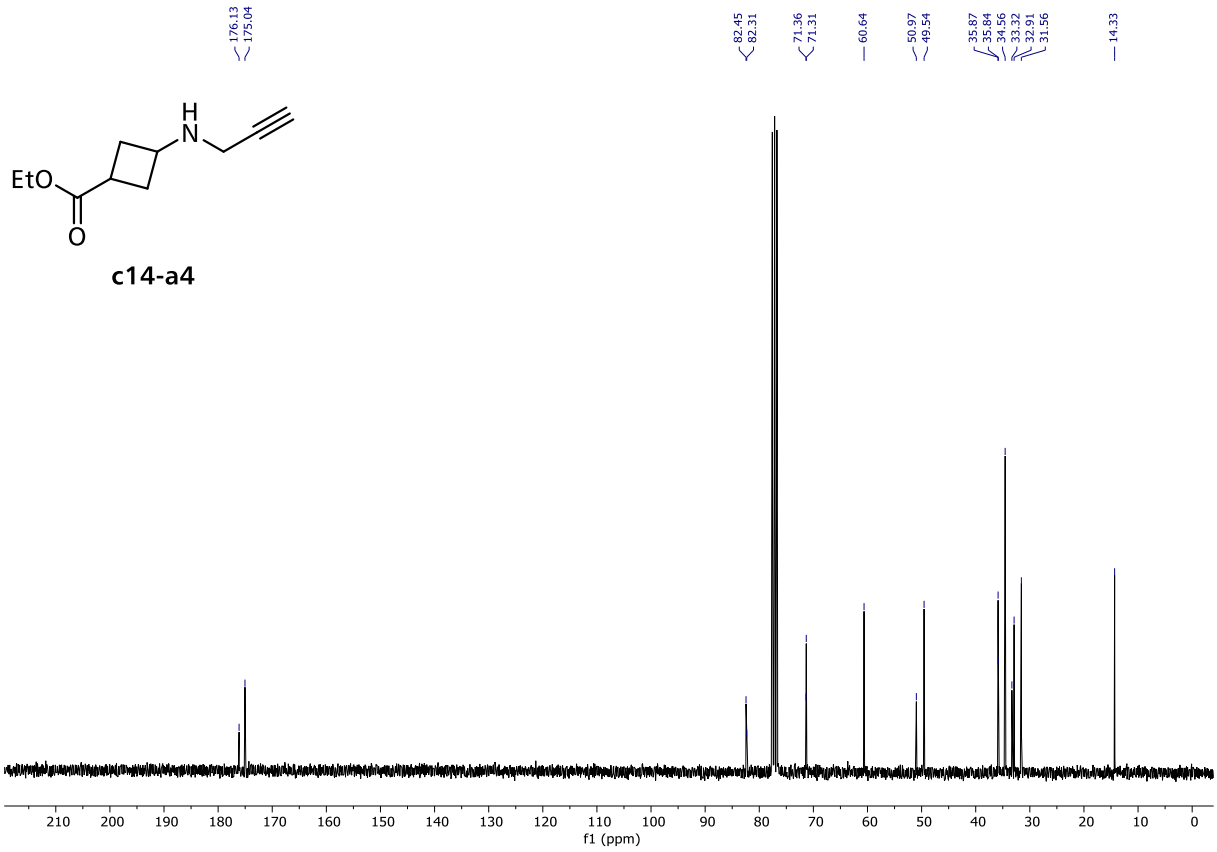


Figure S312. ^{13}C NMR spectrum of ethyl 3-(prop-2-yn-1-ylamino)cyclobutane-1-carboxylate (**c14-a4**).

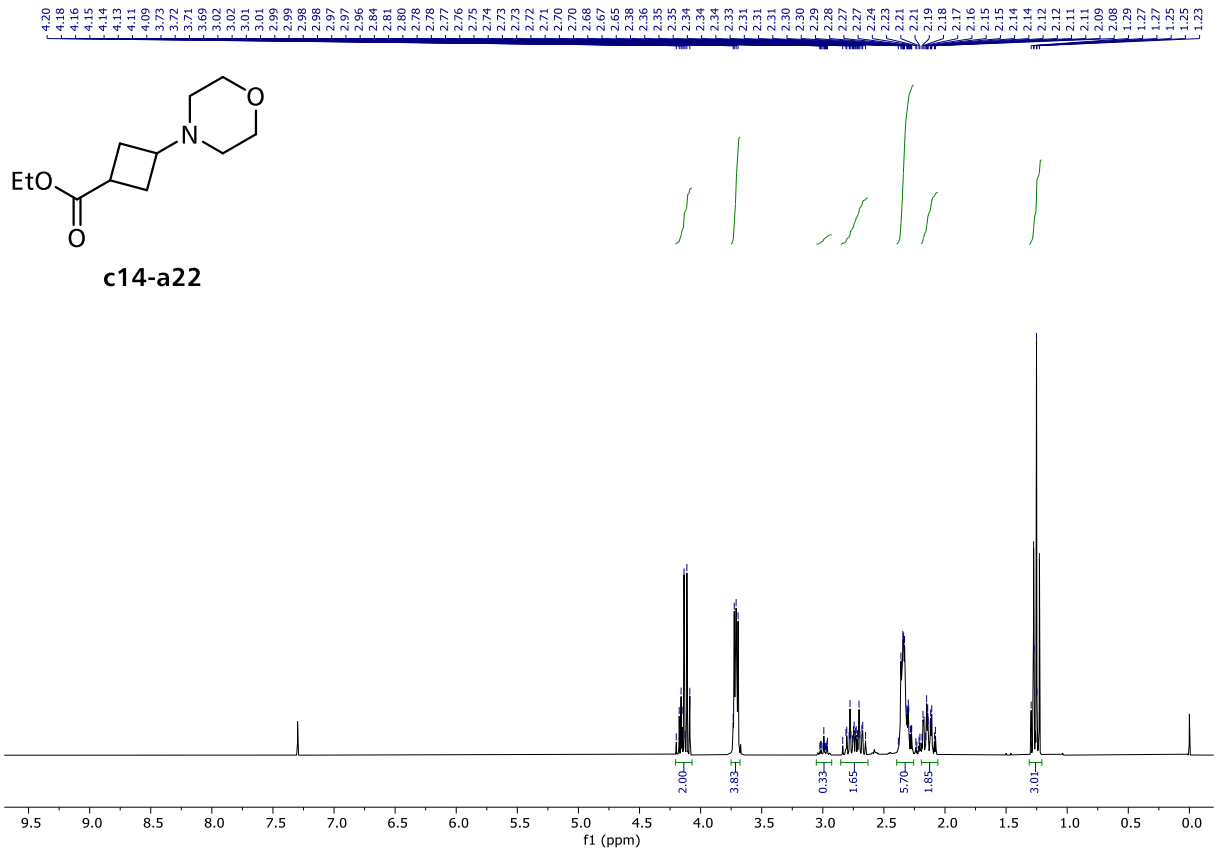


Figure S313. ^{1}H NMR spectrum of ethyl 3-morpholinocyclobutane-1-carboxylate (**c14-a22**).

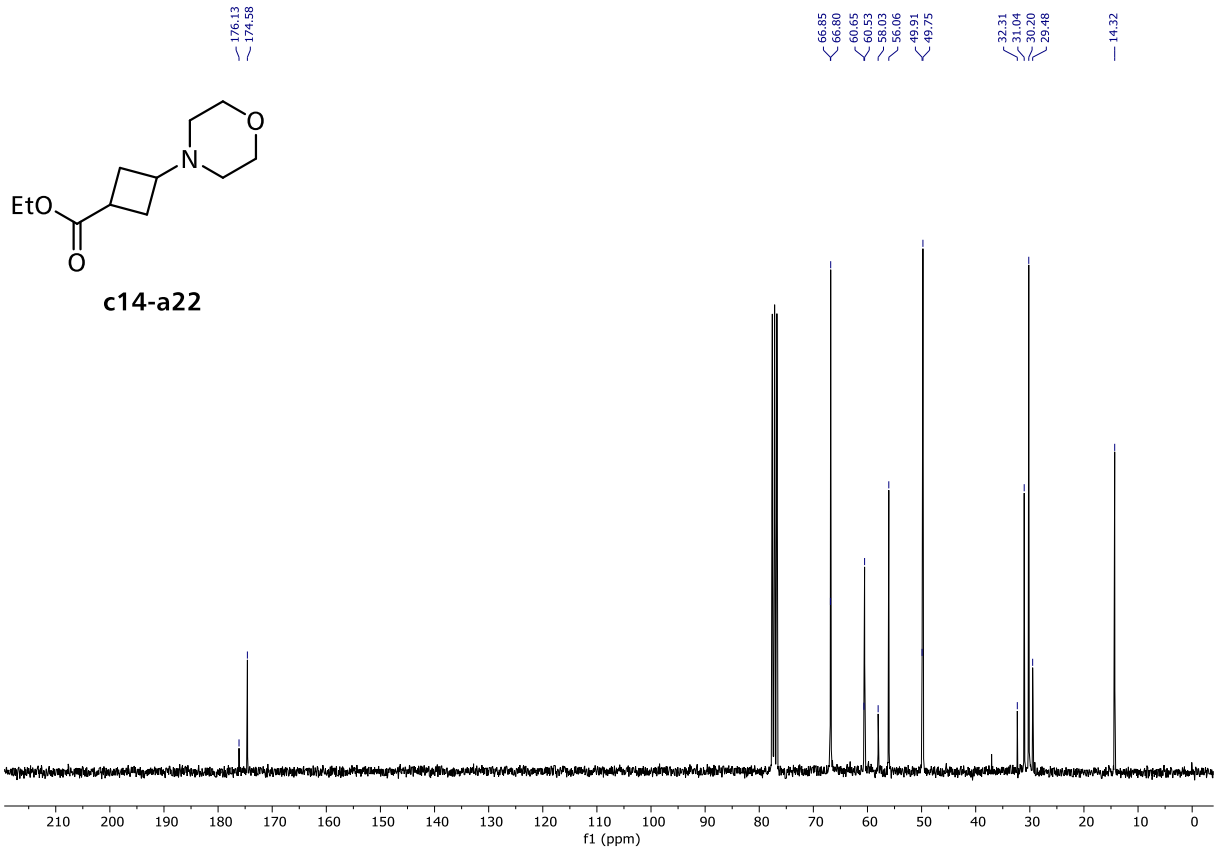


Figure S314. ^{13}C NMR spectrum of ethyl 3-morpholinocyclobutane-1-carboxylate (**c14-a22**).

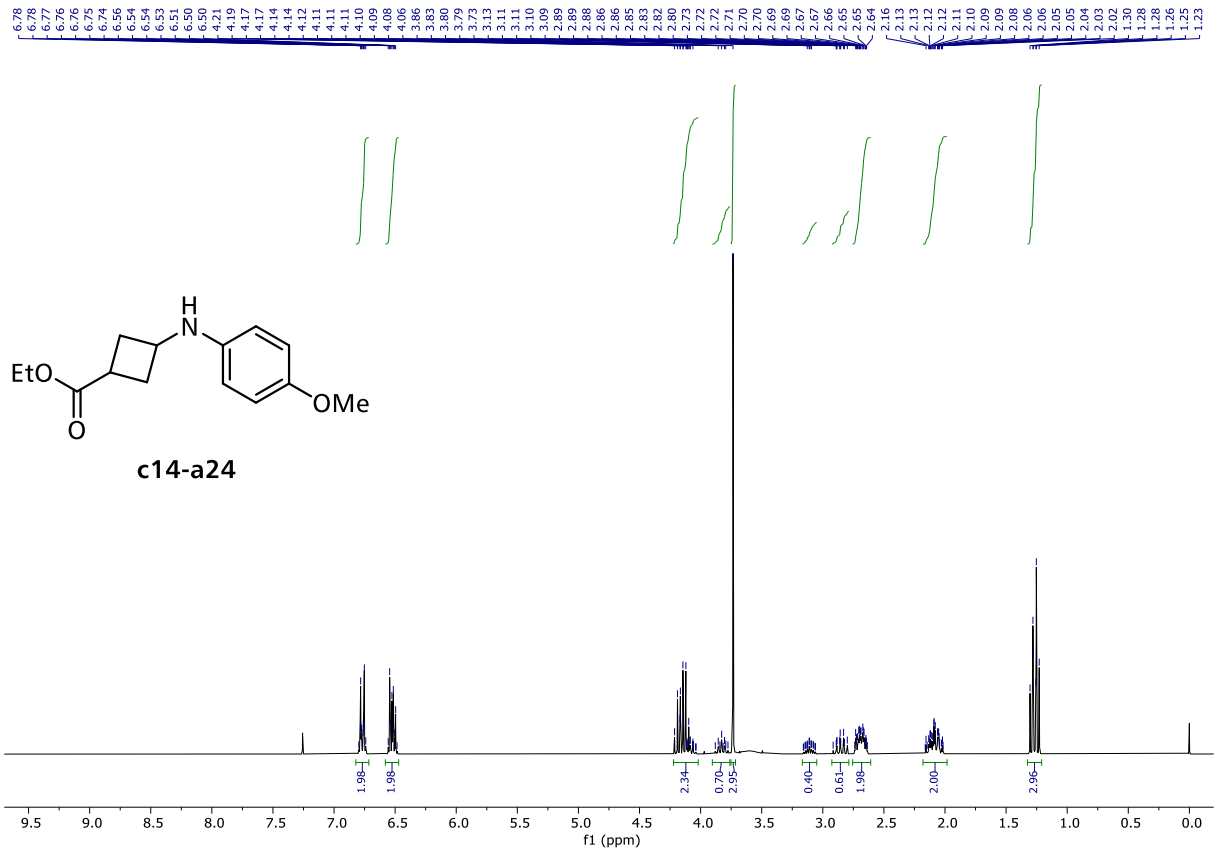


Figure S315. ^{1}H NMR spectrum of ethyl 3-((4-methoxyphenyl)amino)cyclobutane-1-carboxylate (**c14-a24**).

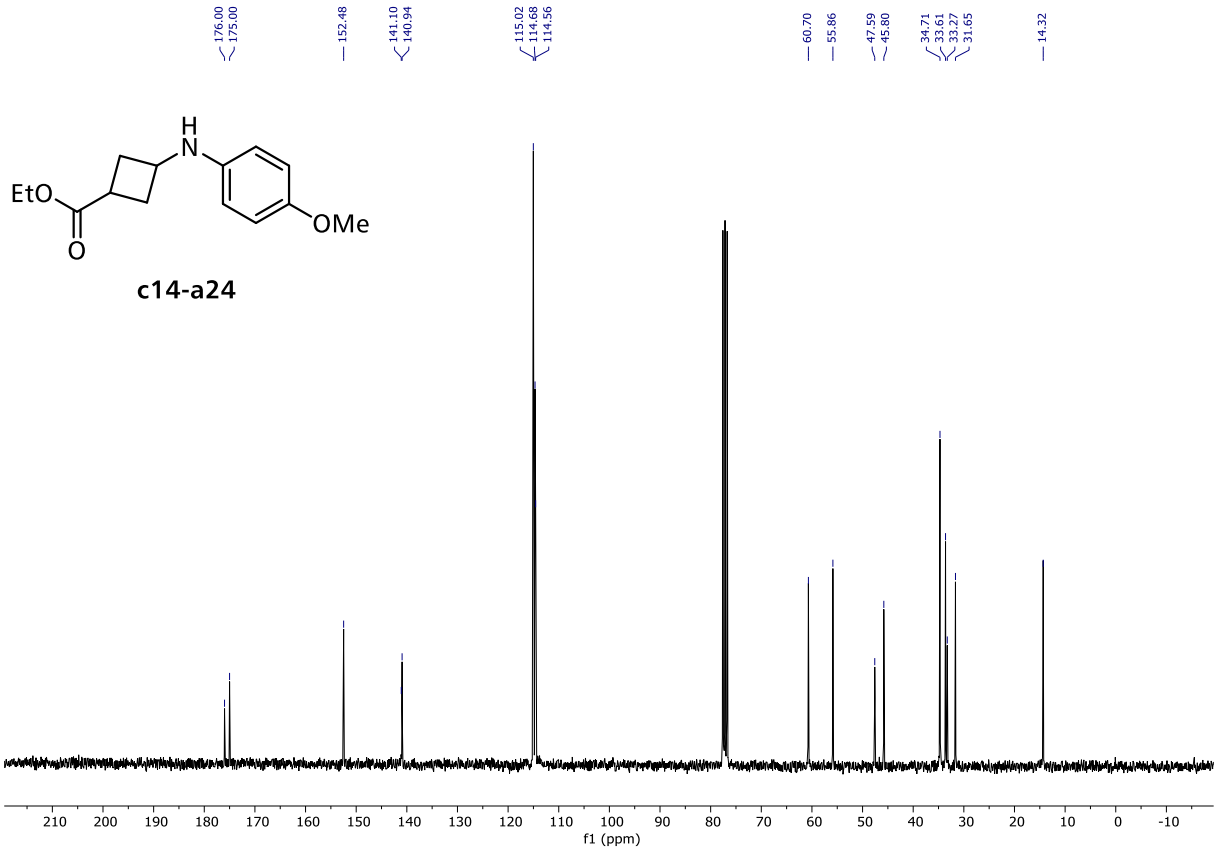


Figure S316. ^{13}C NMR spectrum of ethyl 3-((4-methoxyphenyl)amino)cyclobutane-1-carboxylate (**c14-a24**).

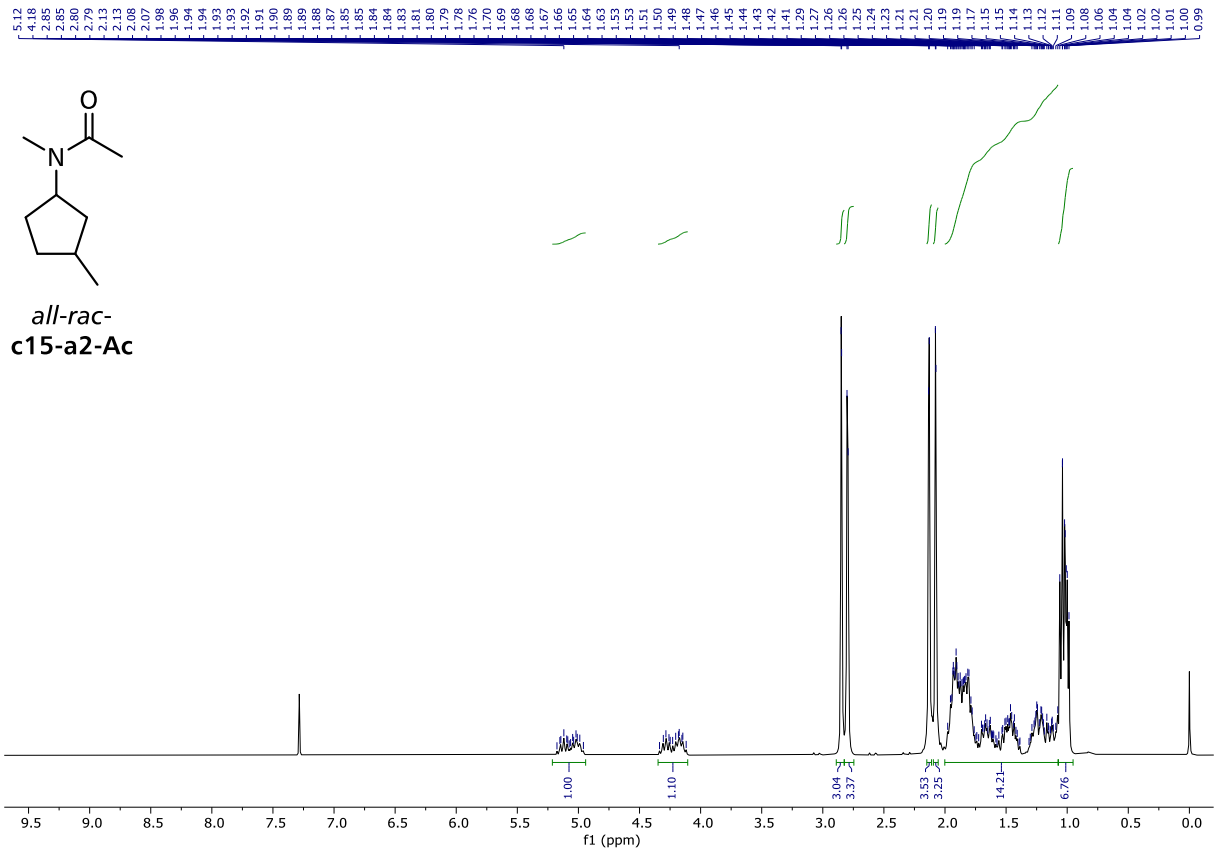


Figure S317. ^{1}H NMR spectrum of *all-rac-N*-methyl-*N*-(3-methylcyclopentyl)acetamide (**c15-a2-Ac**).

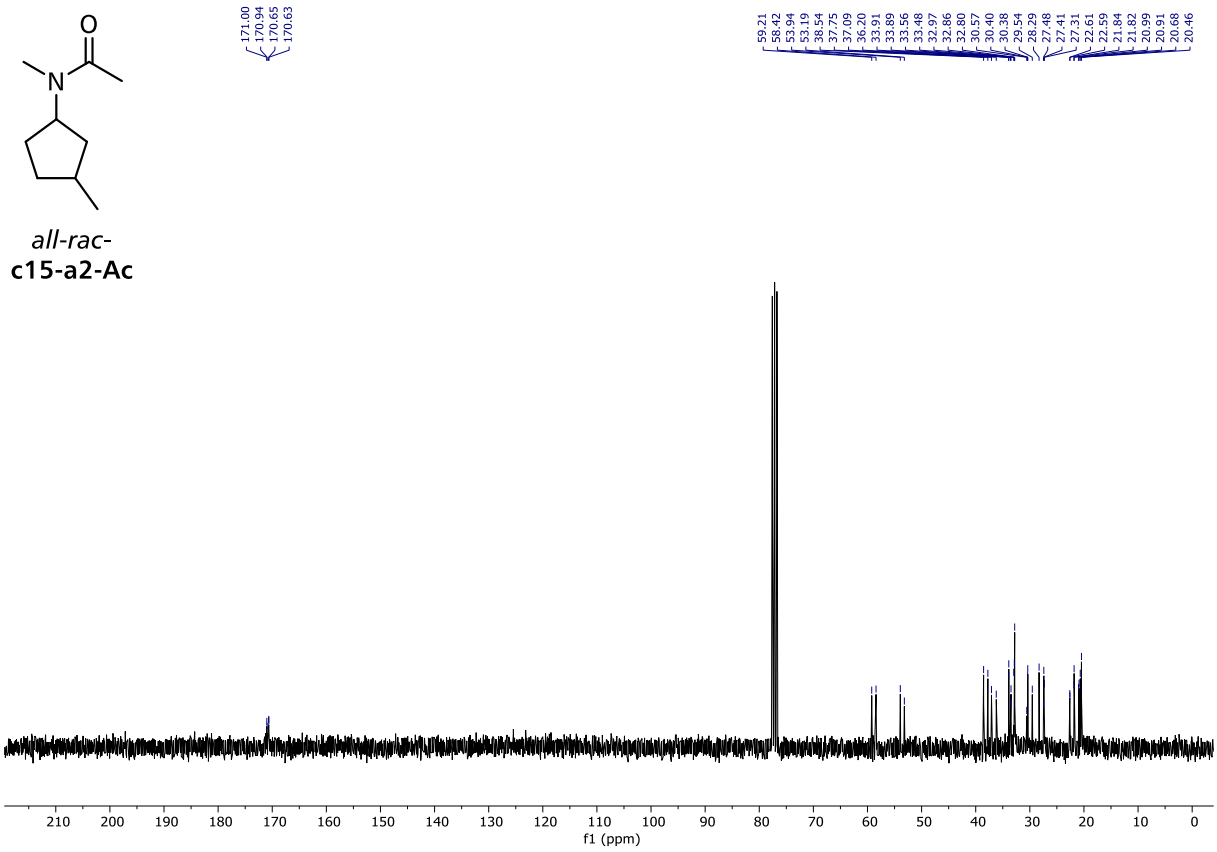


Figure S318. ^{13}C NMR spectrum of *all-rac-N*-methyl-*N*-(3-methylcyclopentyl)acetamide (**c15-a2-Ac**).

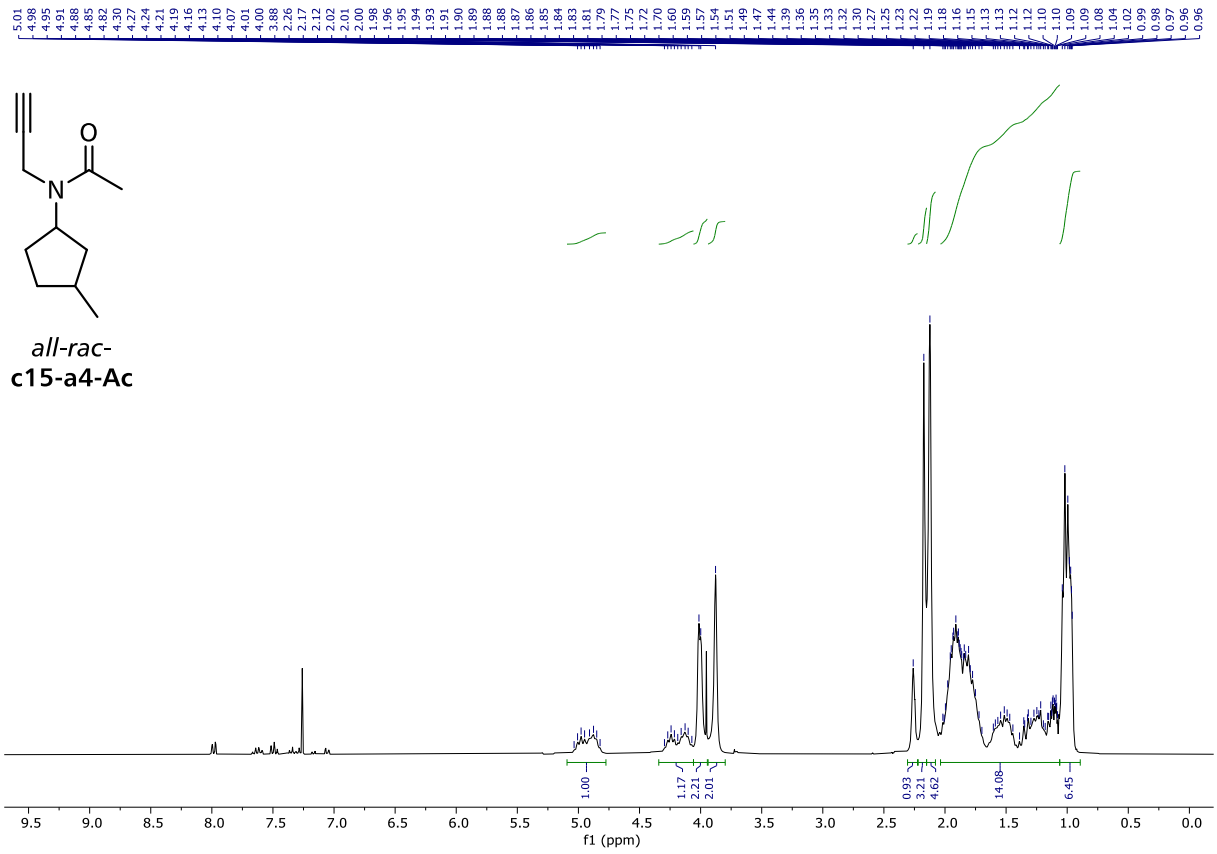


Figure S319. ^{1}H NMR spectrum of *all-rac-N*-(3-methylcyclopentyl)-*N*-(prop-2-yn-1-yl)acetamide (**c15-a4-Ac**).

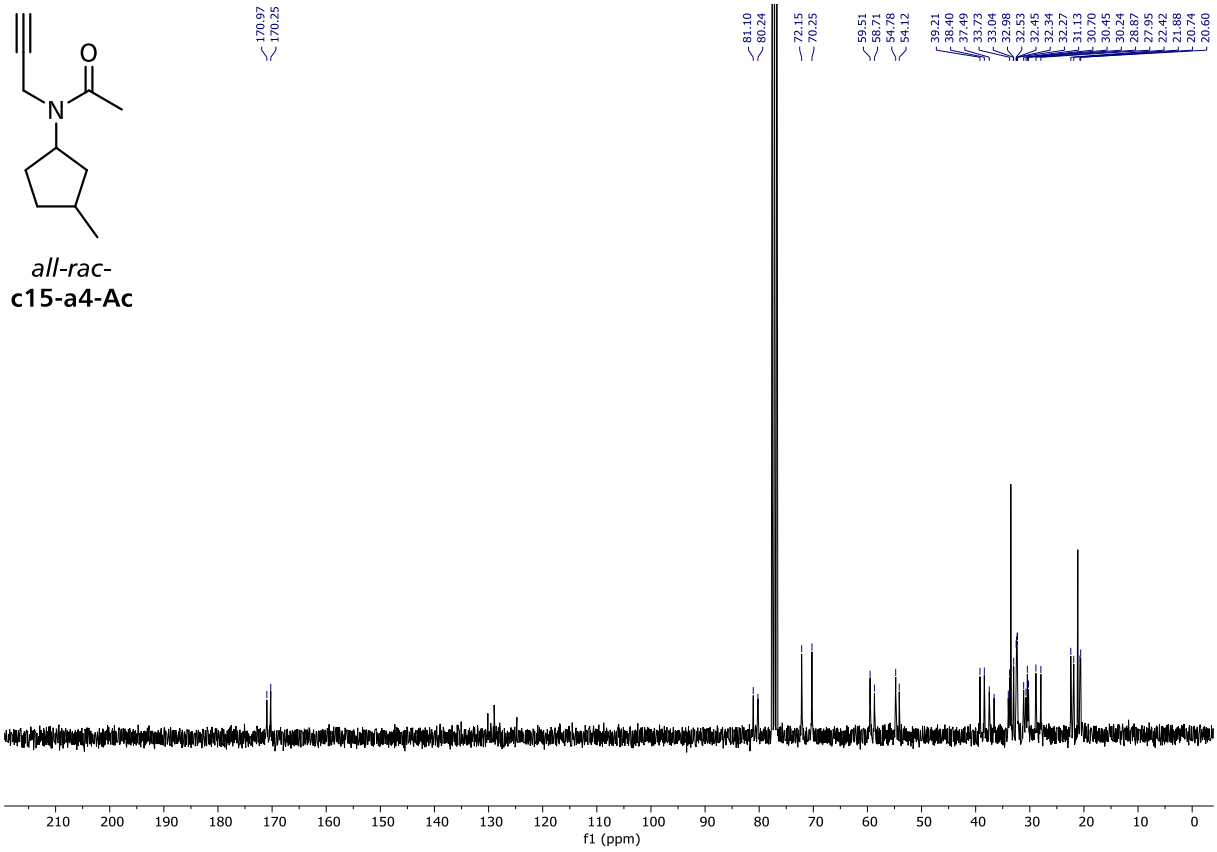


Figure S320. ^{13}C NMR spectrum of *all-rac-N*-(3-methylcyclopentyl)-*N*-(prop-2-yn-1-yl)acetamide (**c15-a4-Ac**).

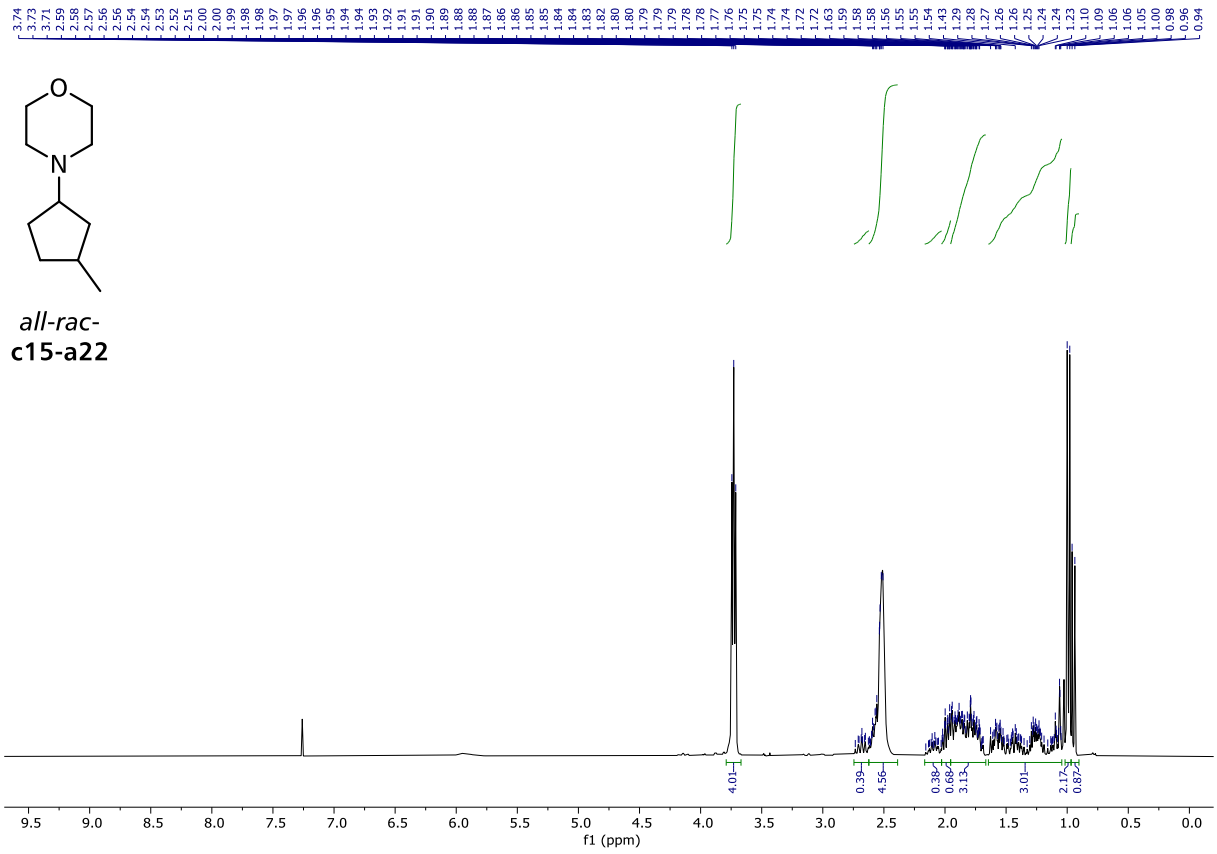


Figure S321. ^{1}H NMR spectrum of *all-rac*-4-(3-methylcyclopentyl)morpholine (**c15-a22**).

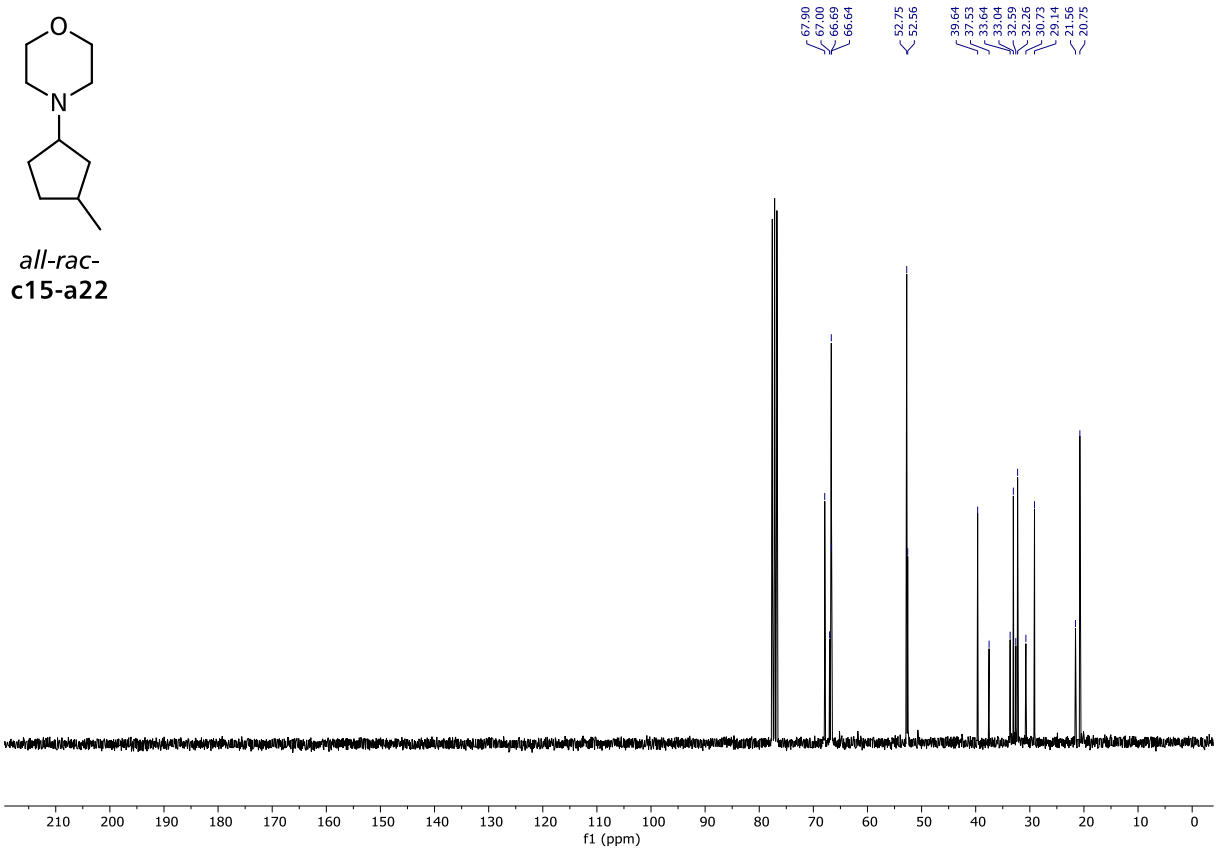


Figure S322. ^{13}C NMR spectrum of *all-rac*-4-(3-methylcyclopentyl)morpholine (**c15-a22**).

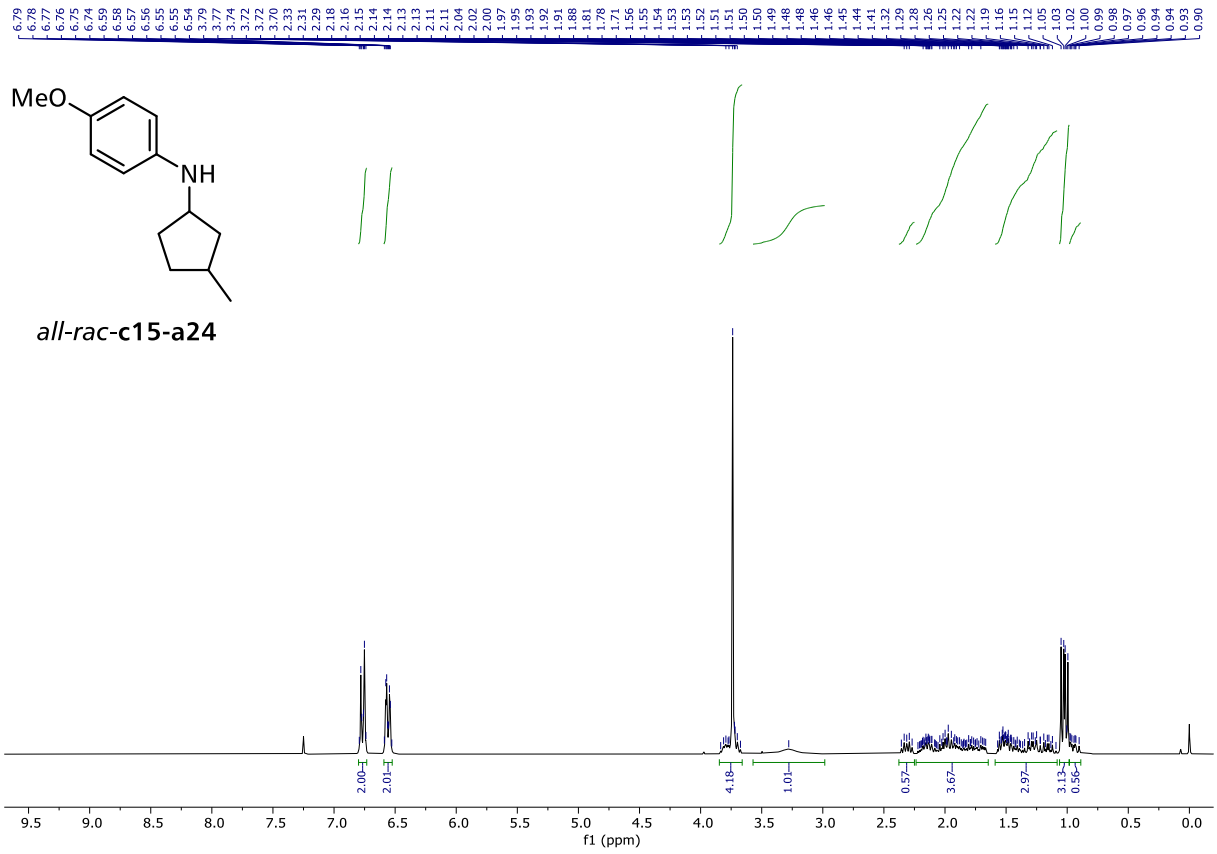


Figure S323. ^{1}H NMR spectrum of *all-rac*-4-methoxy-*N*-(3-methylcyclopentyl)aniline (**c15-a24**).

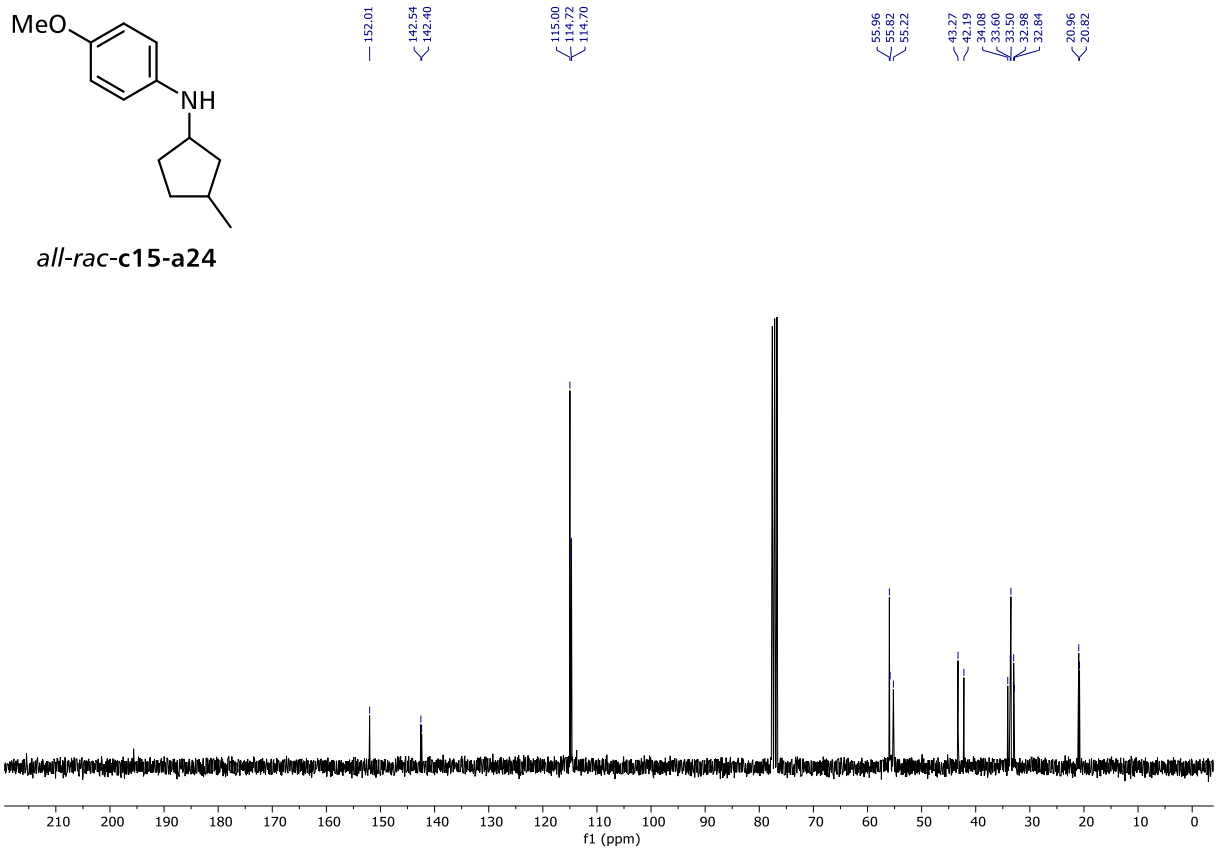


Figure S324. ^{13}C NMR spectrum of *all-rac*-4-methoxy-*N*-(3-methylcyclopentyl)aniline (**c15-a24**).

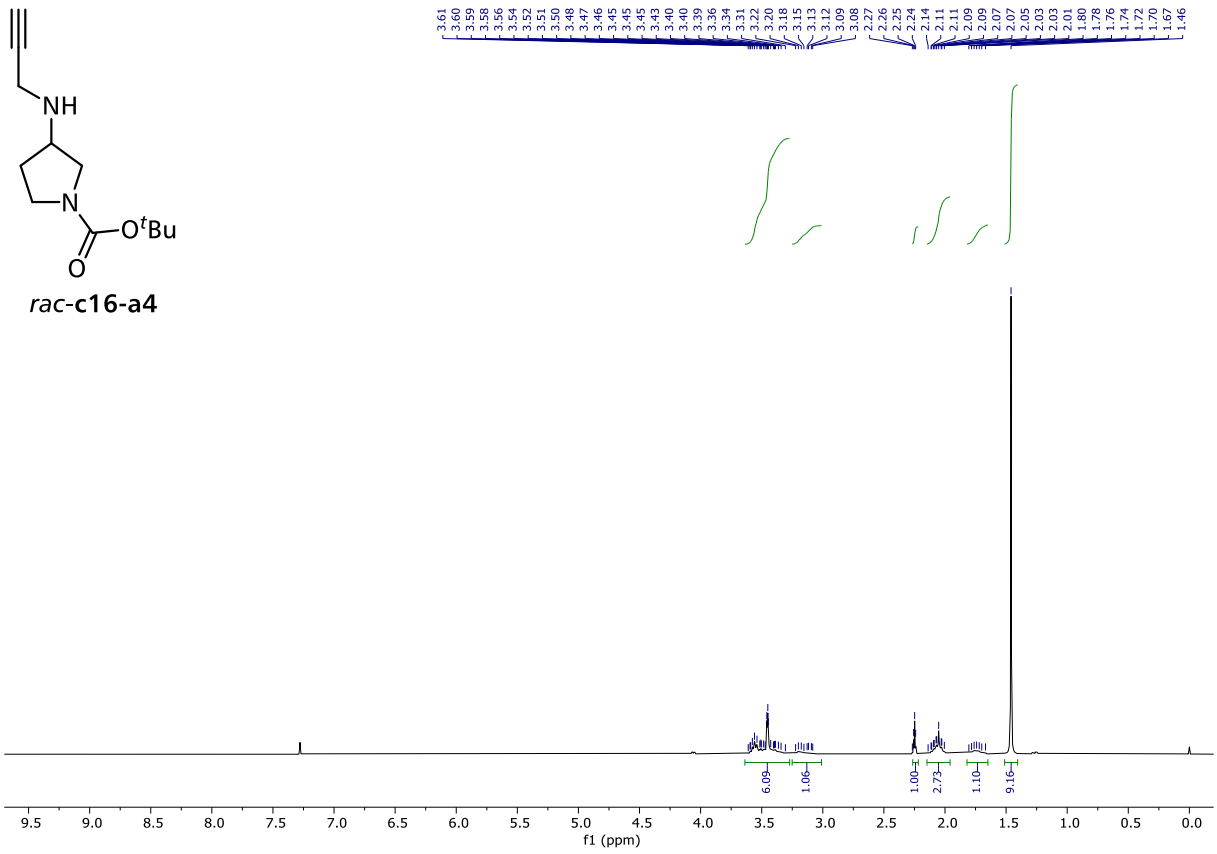


Figure S325. ^{1}H NMR spectrum of *tert*-butyl *rac*-3-(prop-2-yn-1-ylamino)pyrrolidine-1-carboxylate (**c16-a4**).

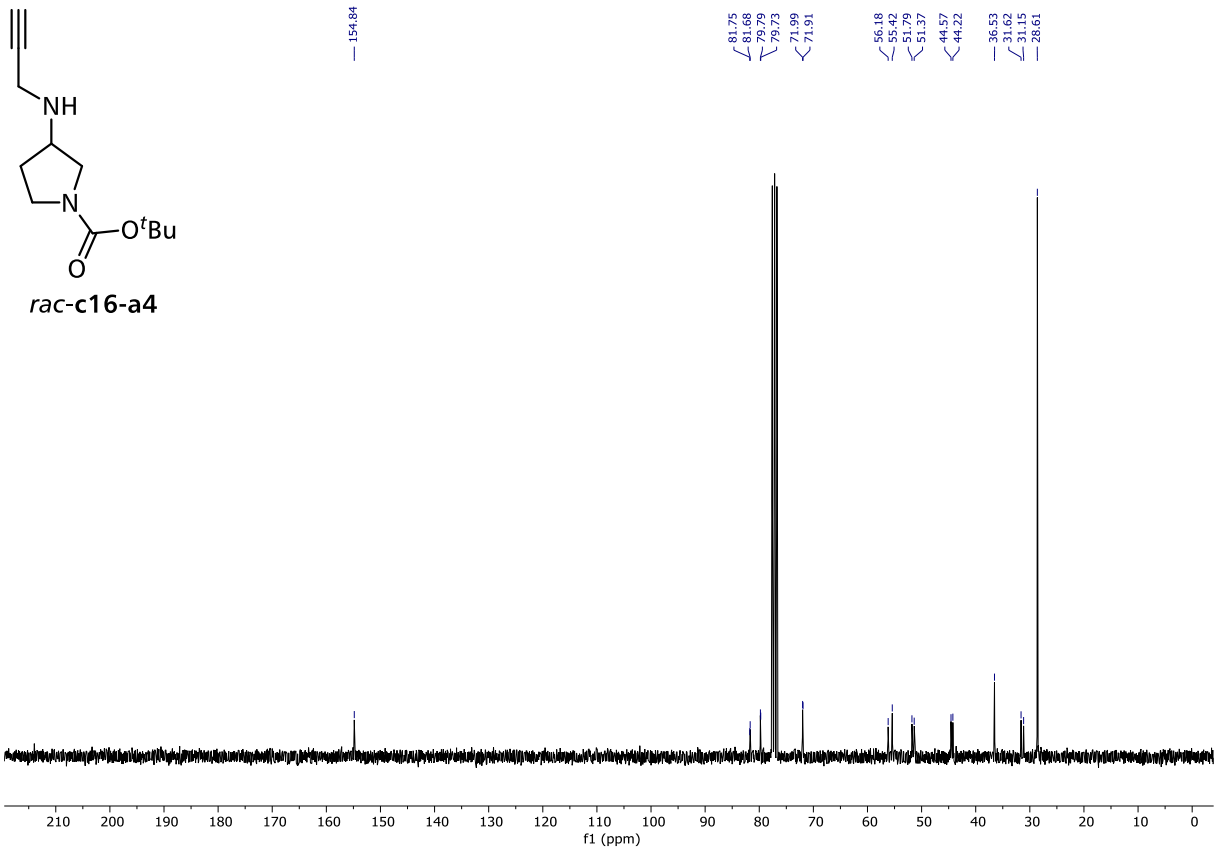


Figure S326. ^{13}C NMR spectrum of *tert*-butyl *rac*-3-(prop-2-yn-1-ylamino)pyrrolidine-1-carboxylate (**c16-a4**).

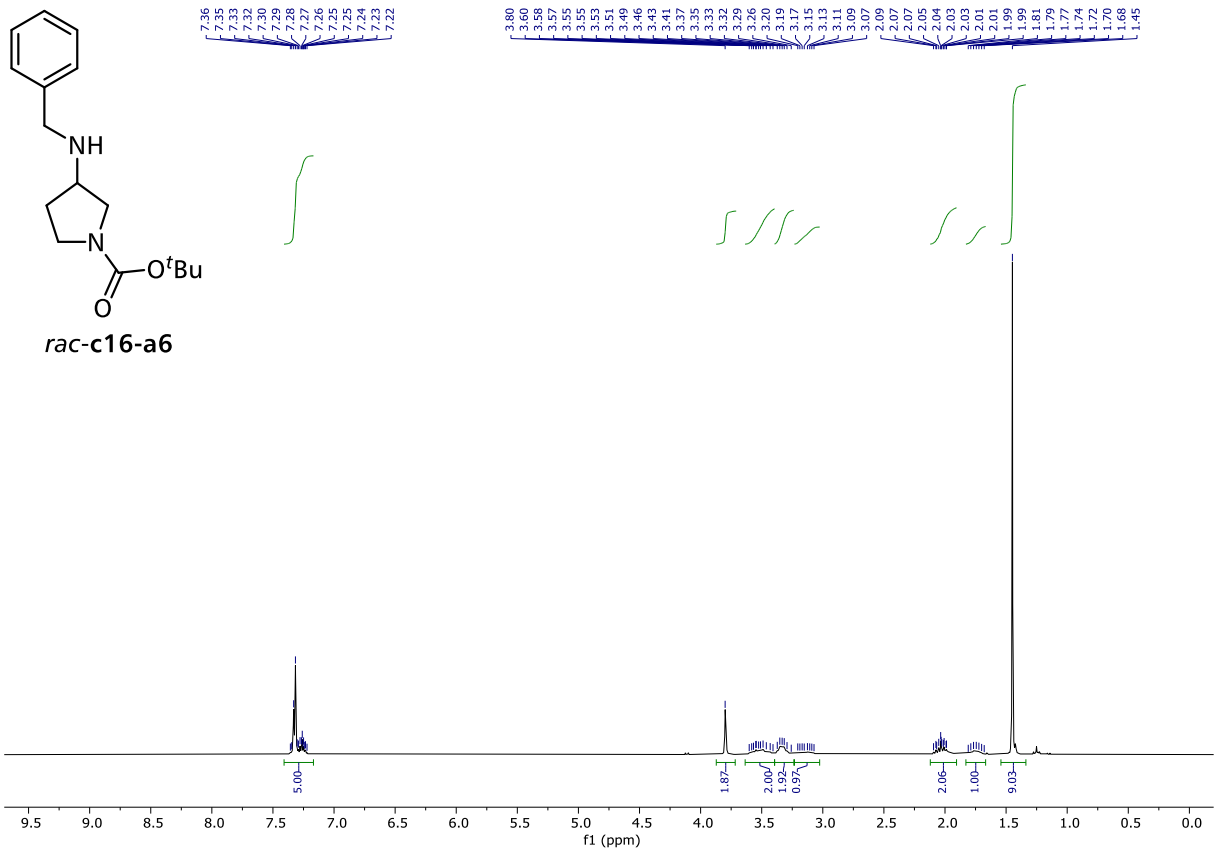


Figure S327. ^{1}H NMR spectrum of *tert*-butyl *rac*-3-(benzylamino)pyrrolidine-1-carboxylate (**c16-a6**).

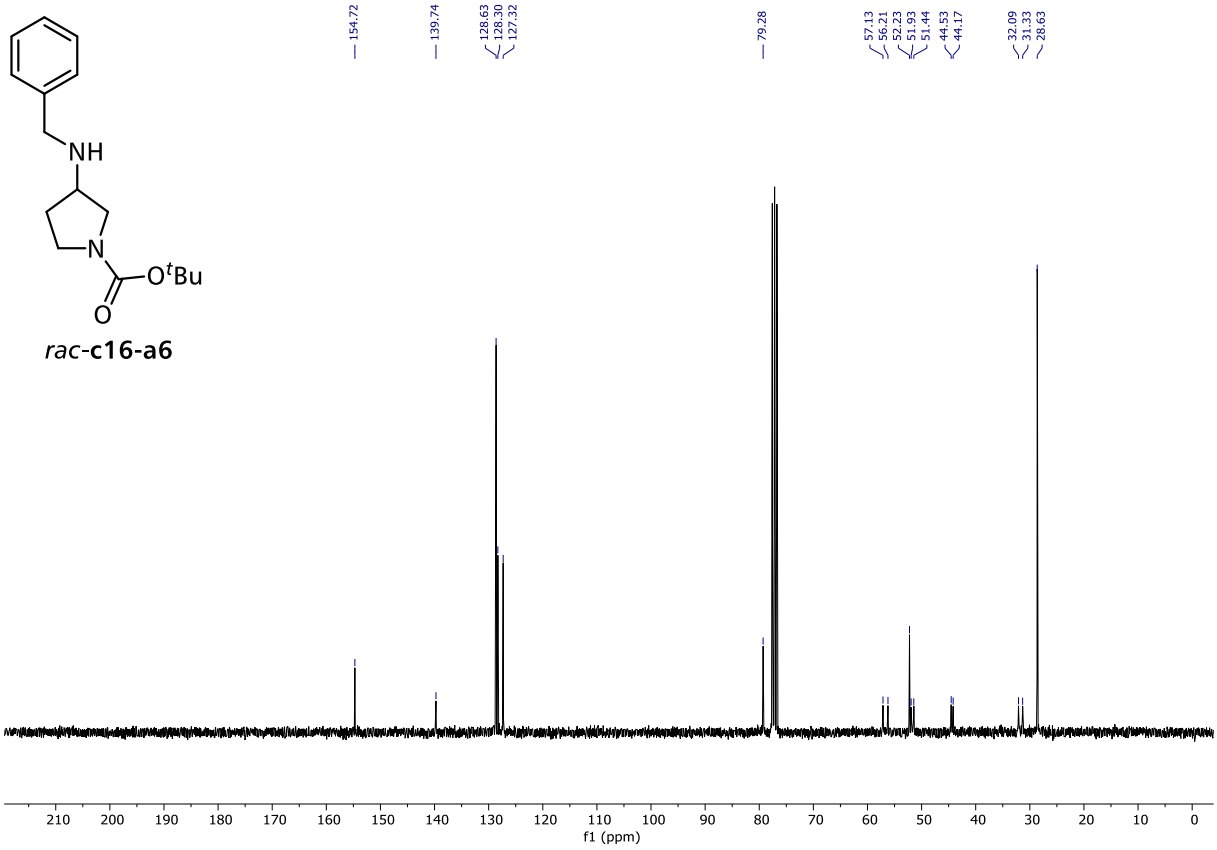


Figure S328. ^{13}C NMR spectrum of *tert*-butyl *rac*-3-(benzylamino)pyrrolidine-1-carboxylate (**c16-a6**).

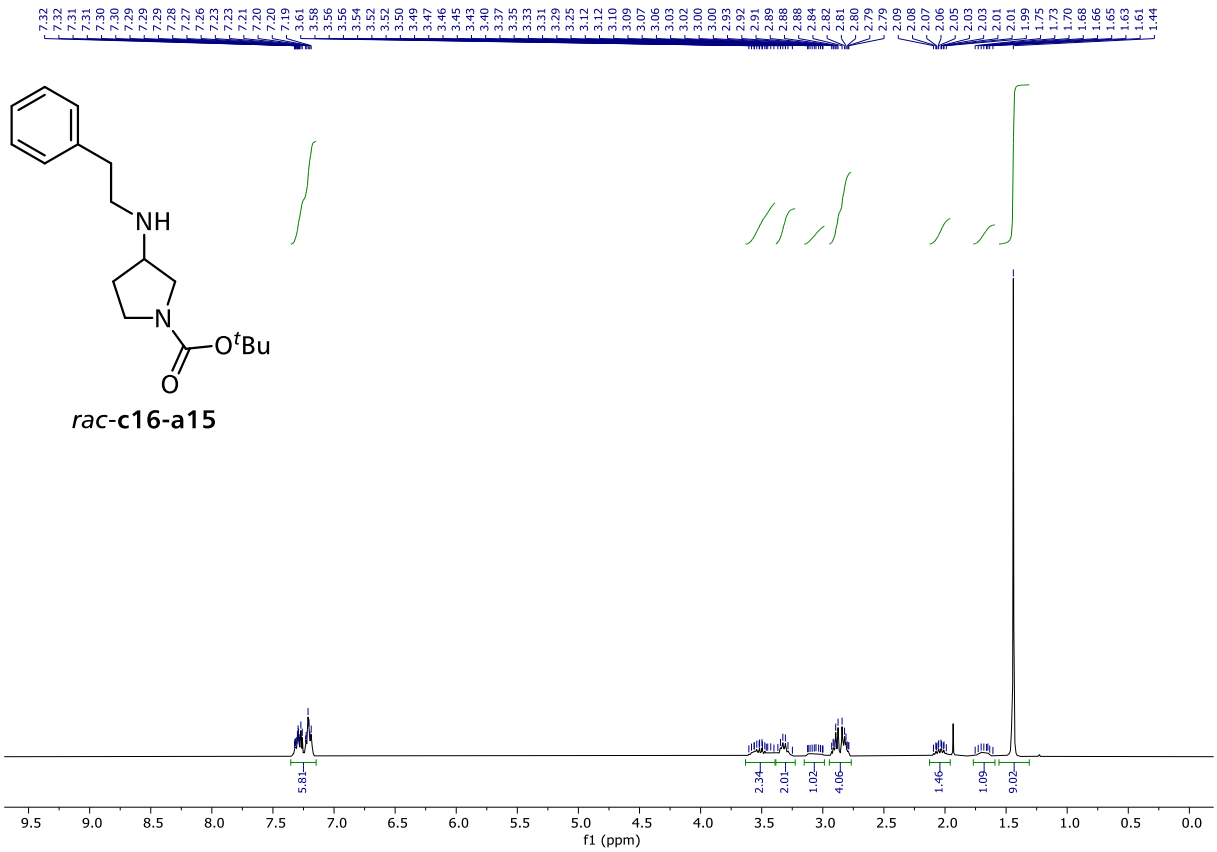


Figure S329. ^{1}H NMR spectrum of *tert*-butyl *rac*-3-(phenethylamino)pyrrolidine-1-carboxylate (**c16-a15**).

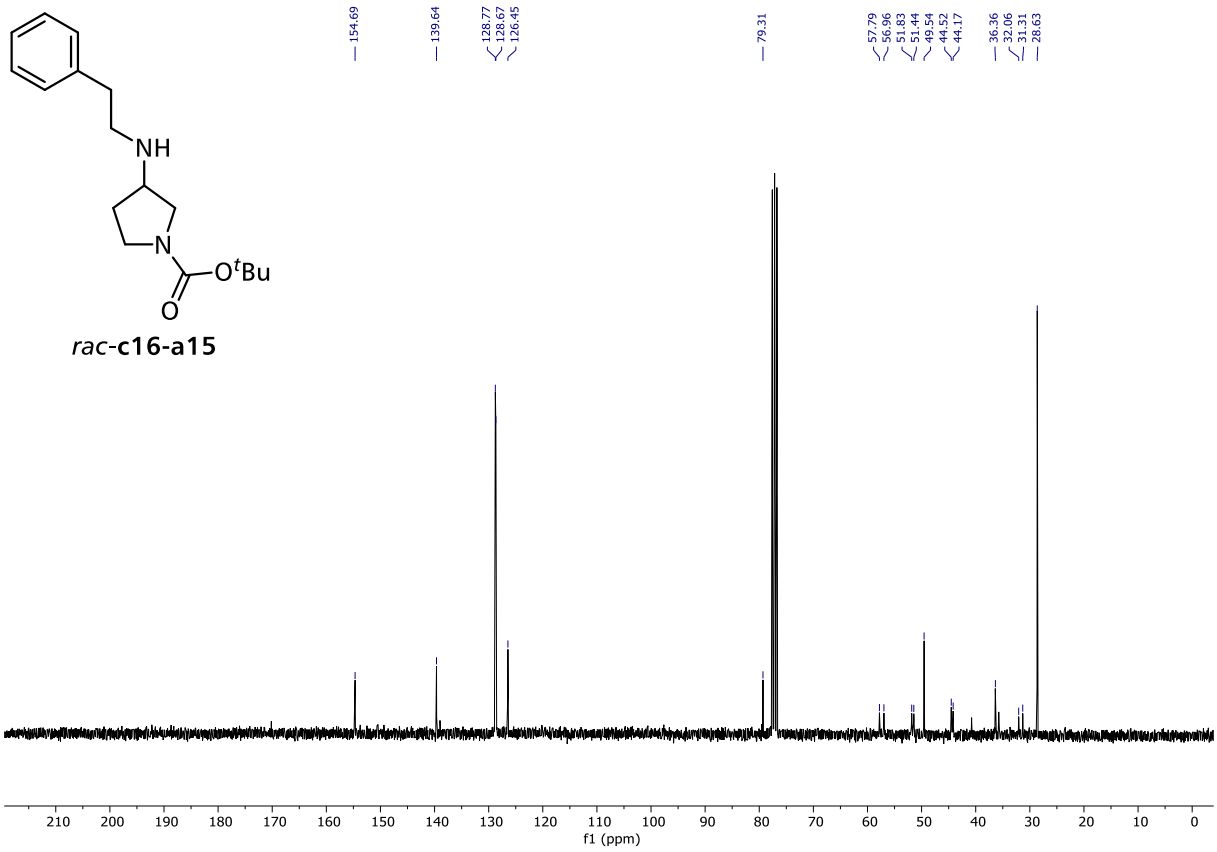


Figure S330. ^{13}C NMR spectrum of *tert*-butyl *rac*-3-(phenethylamino)pyrrolidine-1-carboxylate (**c16-a15**).

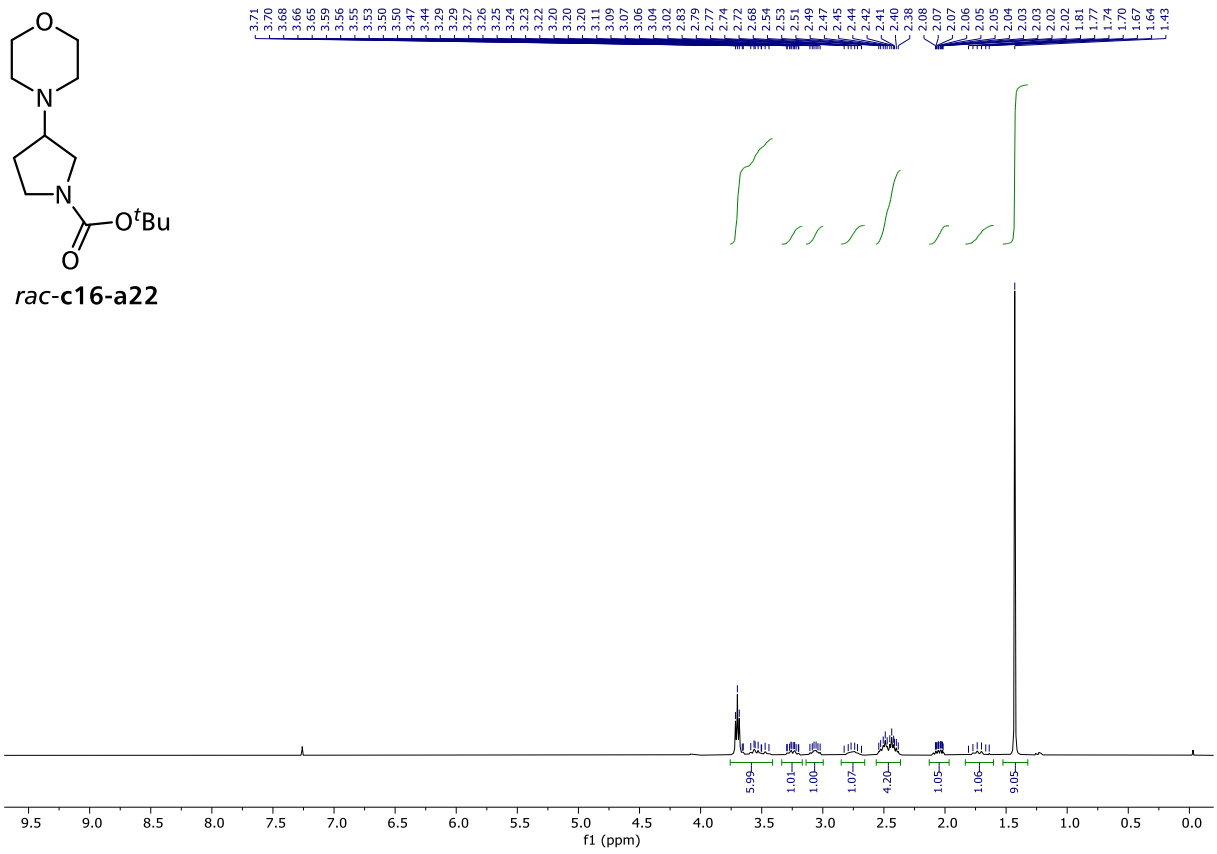


Figure S331. ^{1}H NMR spectrum of *tert*-butyl *rac*-3-morpholinopyrrolidine-1-carboxylate (**c16-a22**).

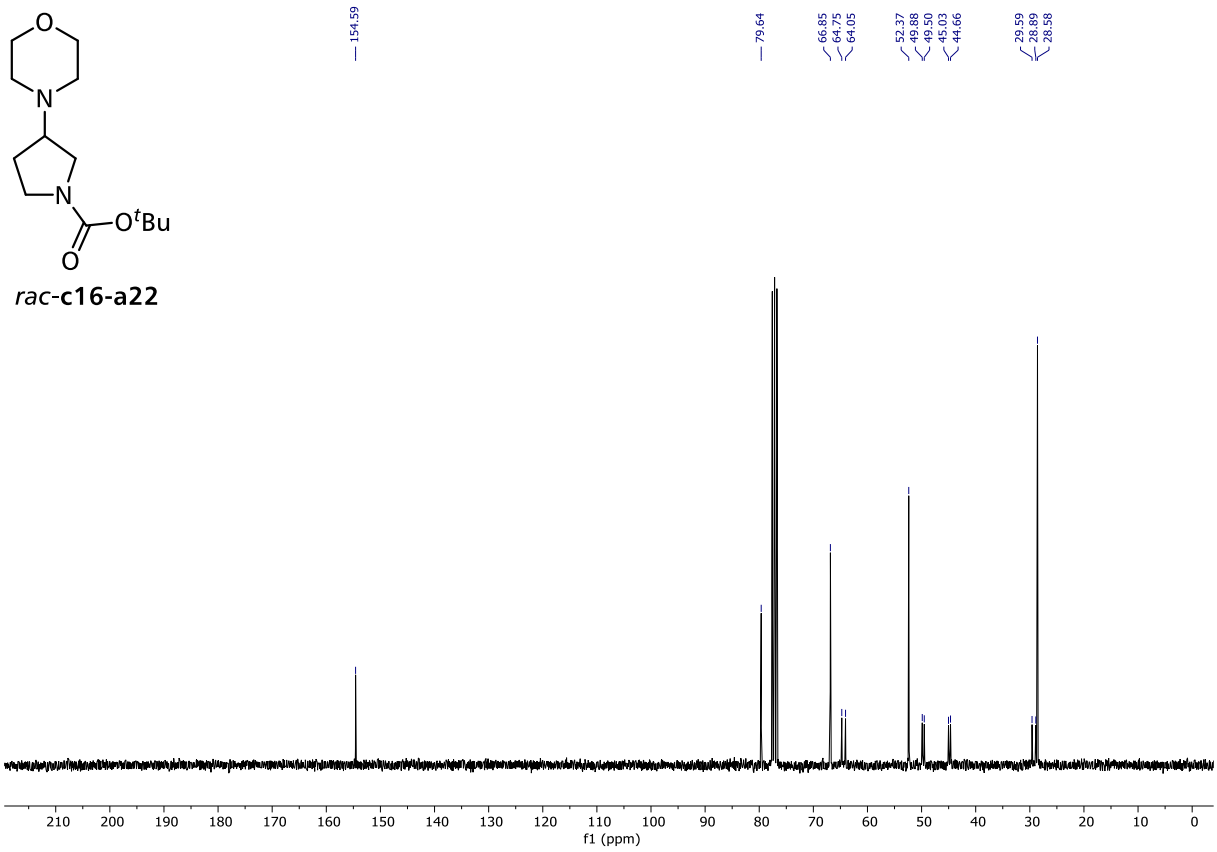


Figure S332. ^{13}C NMR spectrum of *tert*-butyl *rac*-3-morpholinopyrrolidine-1-carboxylate (**c16-a22**).

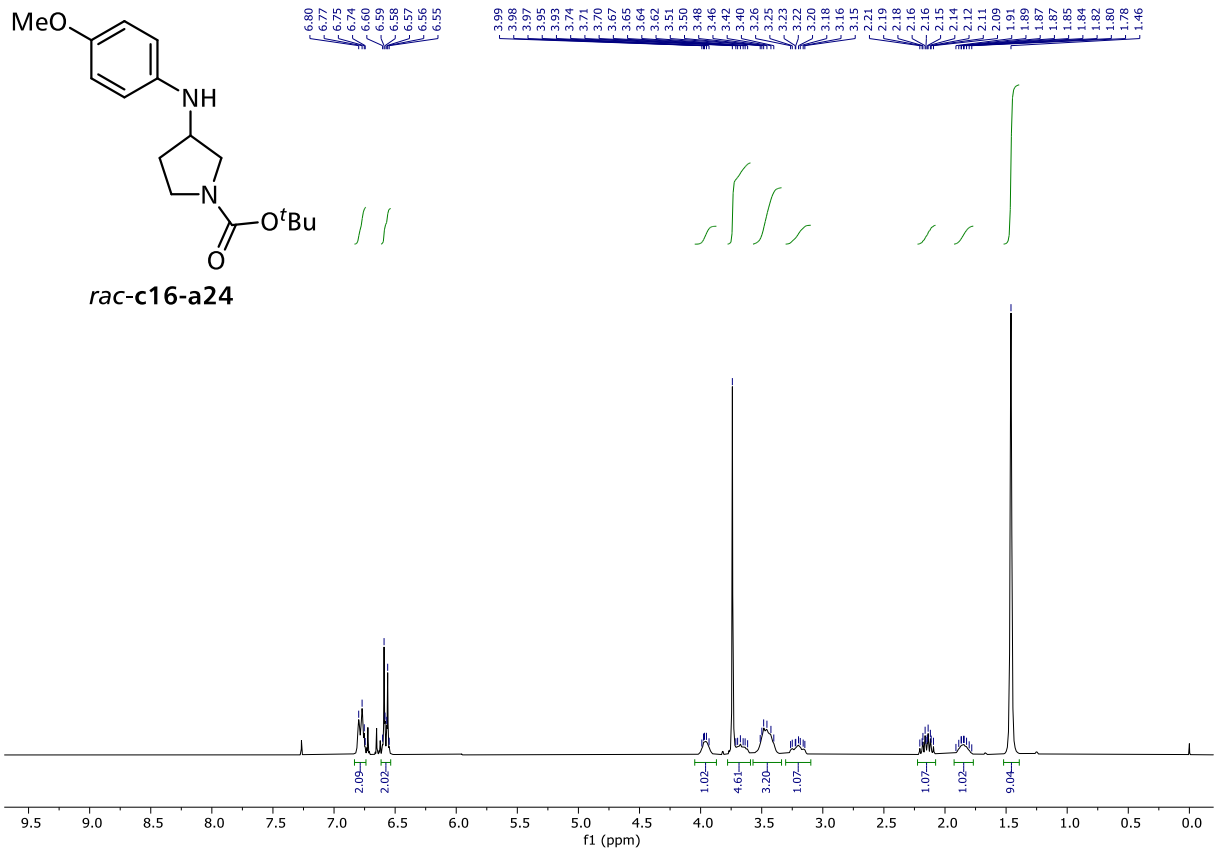


Figure S333. ^{1}H NMR spectrum of *tert*-butyl *rac*-3-((4-methoxyphenyl)amino)pyrrolidine-1-carboxylate (**c16-a24**).

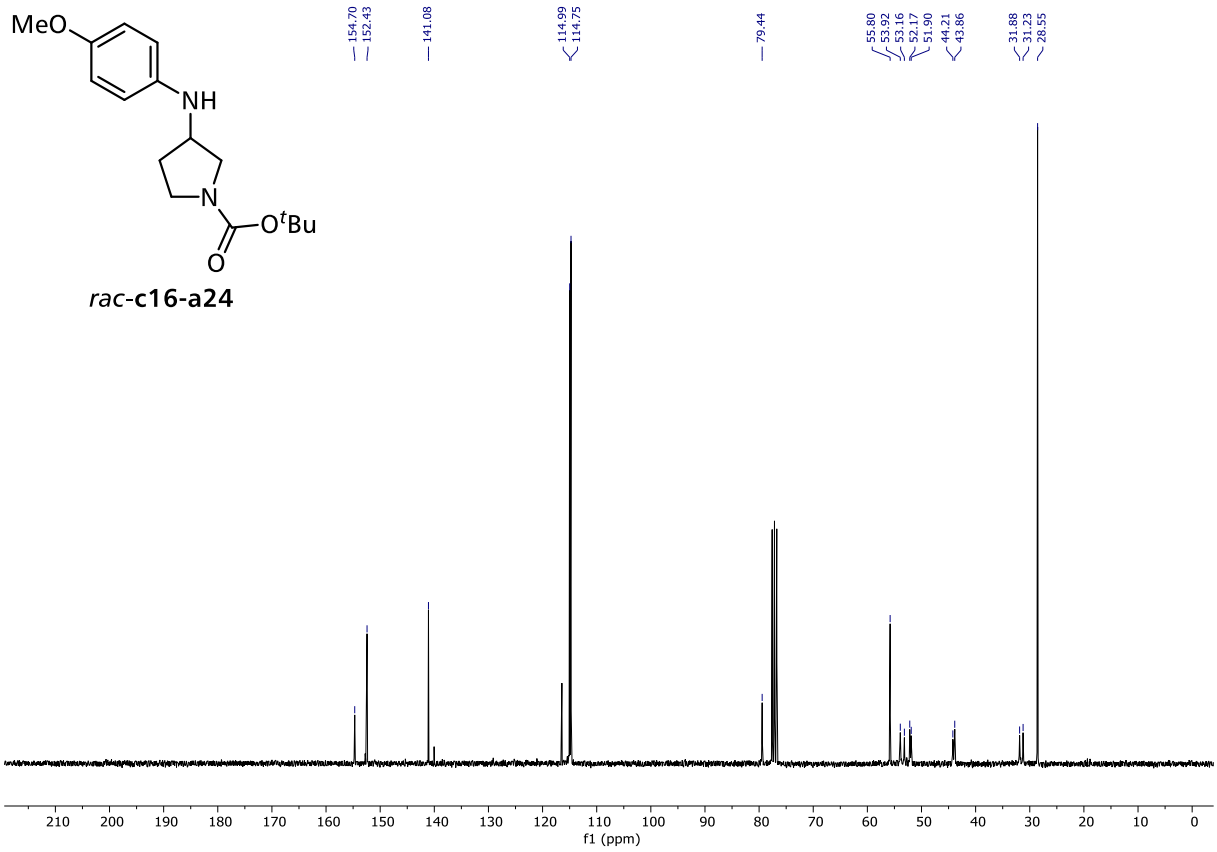


Figure S334. ^{13}C NMR spectrum of *tert*-butyl *rac*-3-((4-methoxyphenyl)amino)pyrrolidine-1-carboxylate (**c16-a24**).

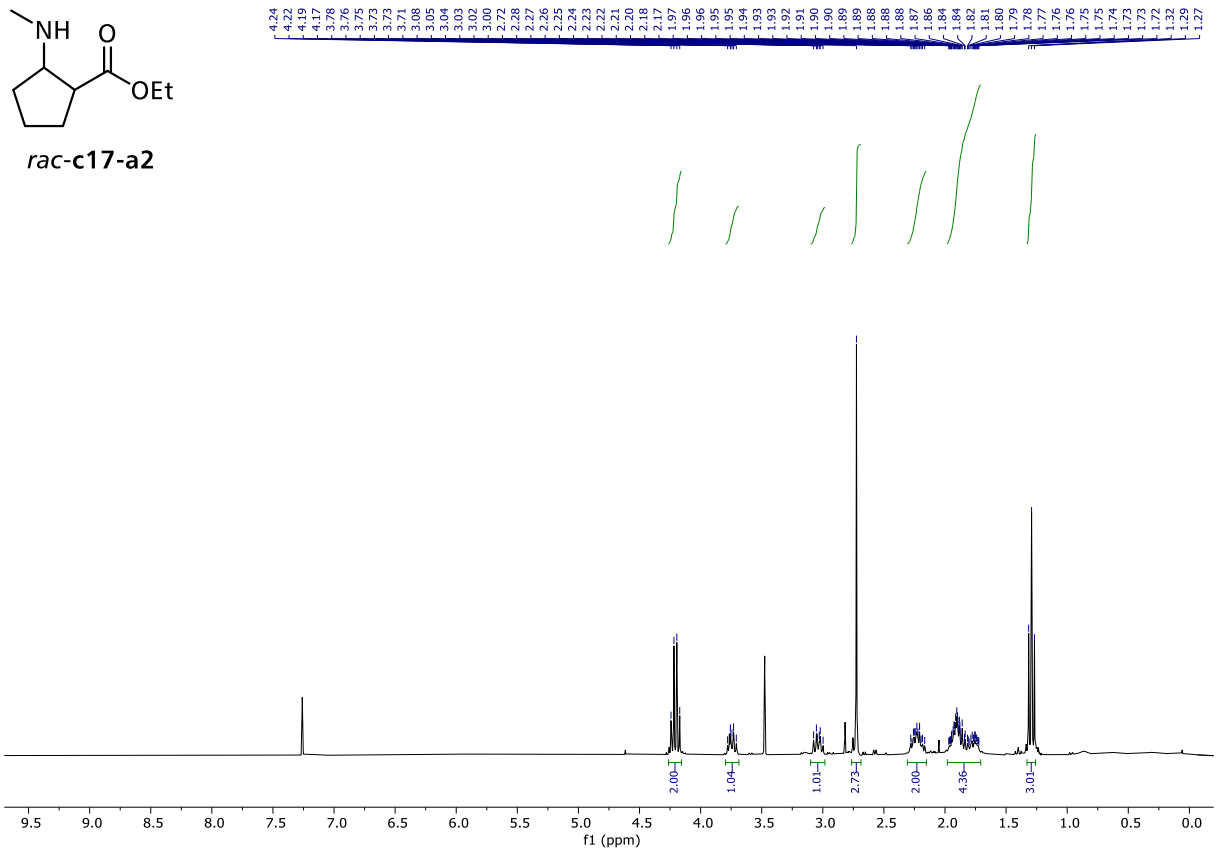


Figure S335. ^{1}H NMR spectrum of ethyl *rac*-2-(methylamino)cyclopentane-1-carboxylate (**c17-a2**).

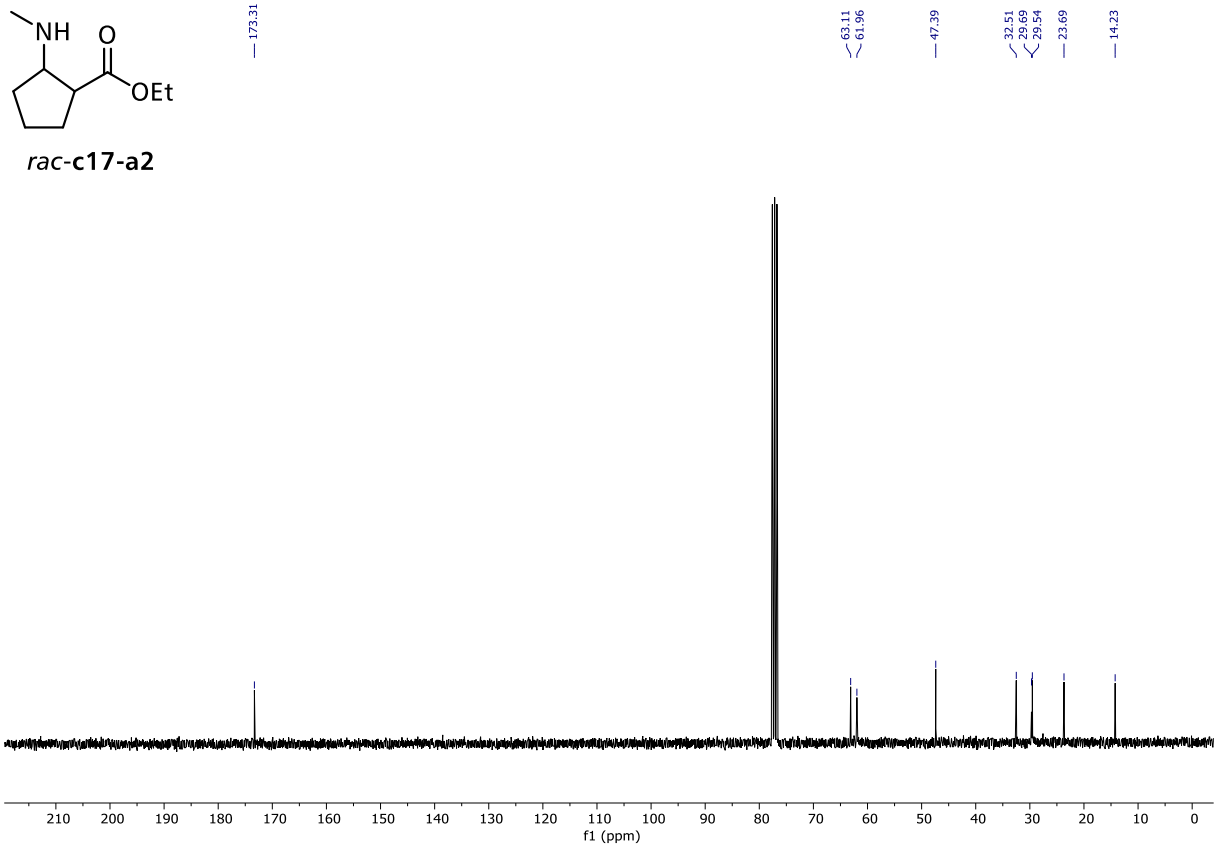


Figure S336. ^{13}C NMR spectrum of ethyl *rac*-2-(methylamino)cyclopentane-1-carboxylate (**c17-a2**).

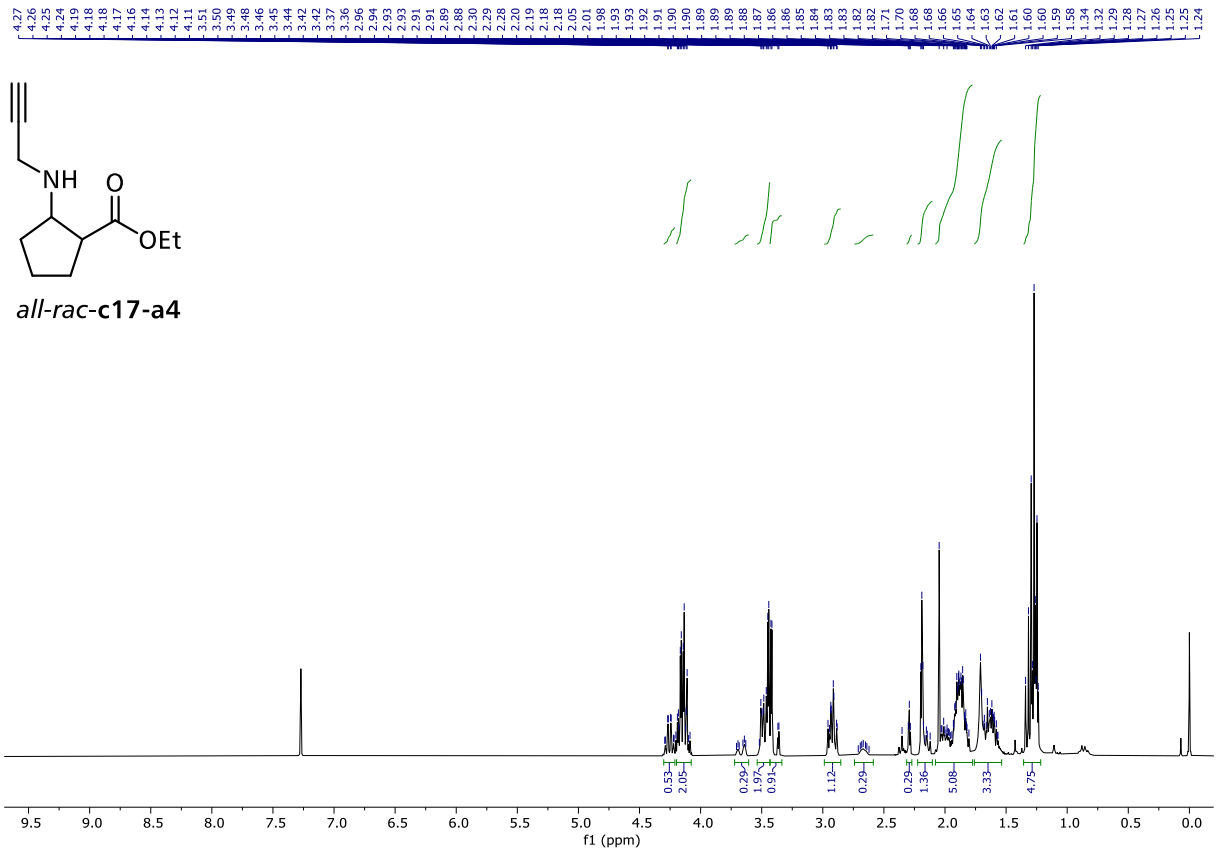


Figure S337. ^{1}H NMR spectrum of ethyl *all-rac*-2-(prop-2-yn-1-ylamino)cyclopentane-1-carboxylate (**c17-a4**).

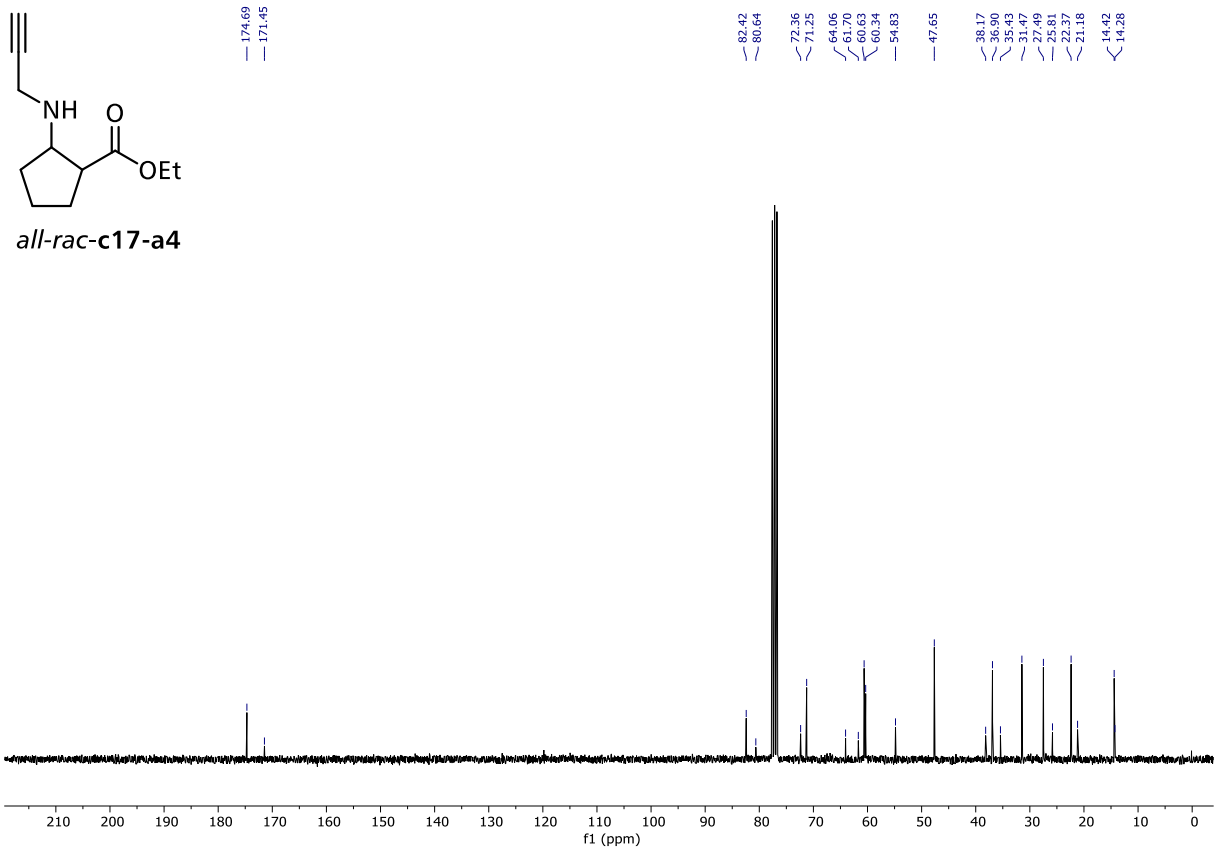


Figure S338. ^{13}C NMR spectrum of ethyl *all-rac*-2-(prop-2-yn-1-ylamino)cyclopentane-1-carboxylate (**c17-a4**).

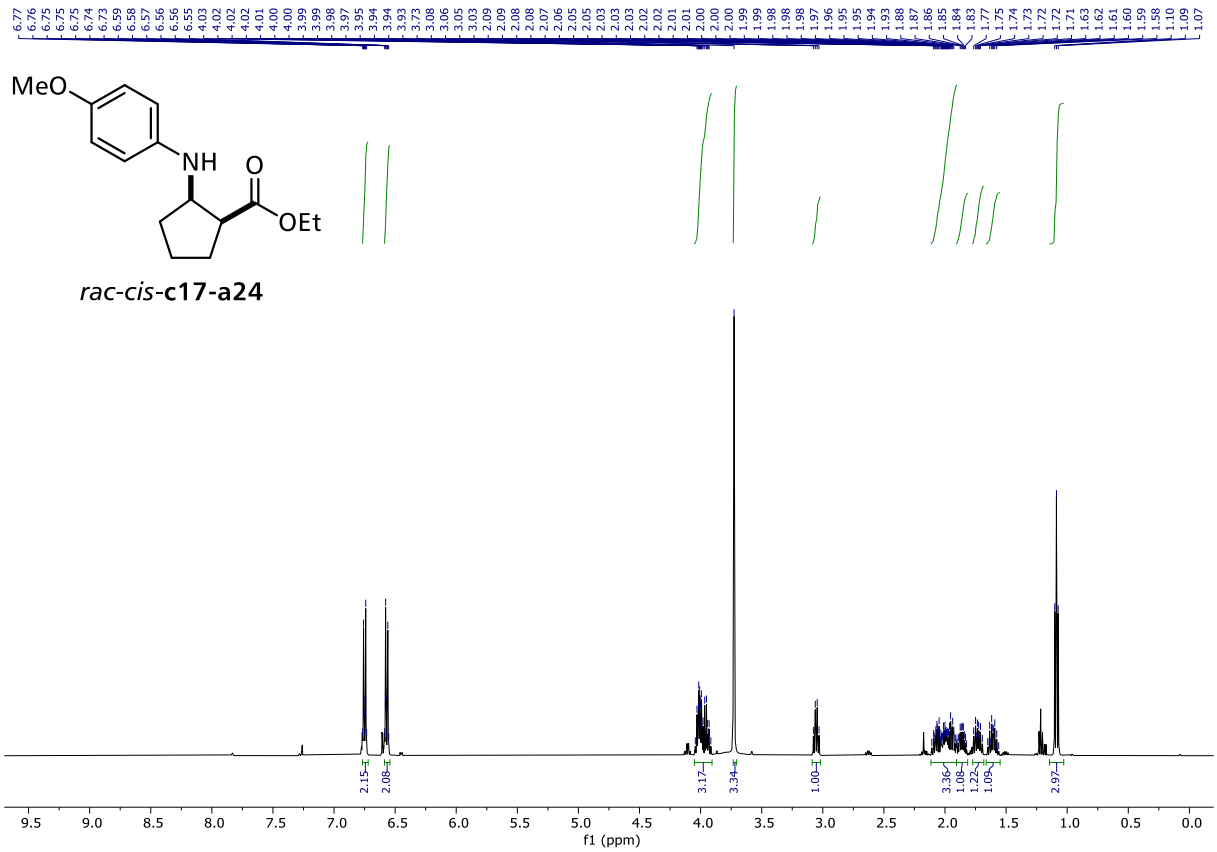


Figure S339. ^{1}H NMR spectrum of ethyl *rac-cis*-2-((4-methoxyphenyl)amino)cyclopentane-1-carboxylate (**c17-a24**).

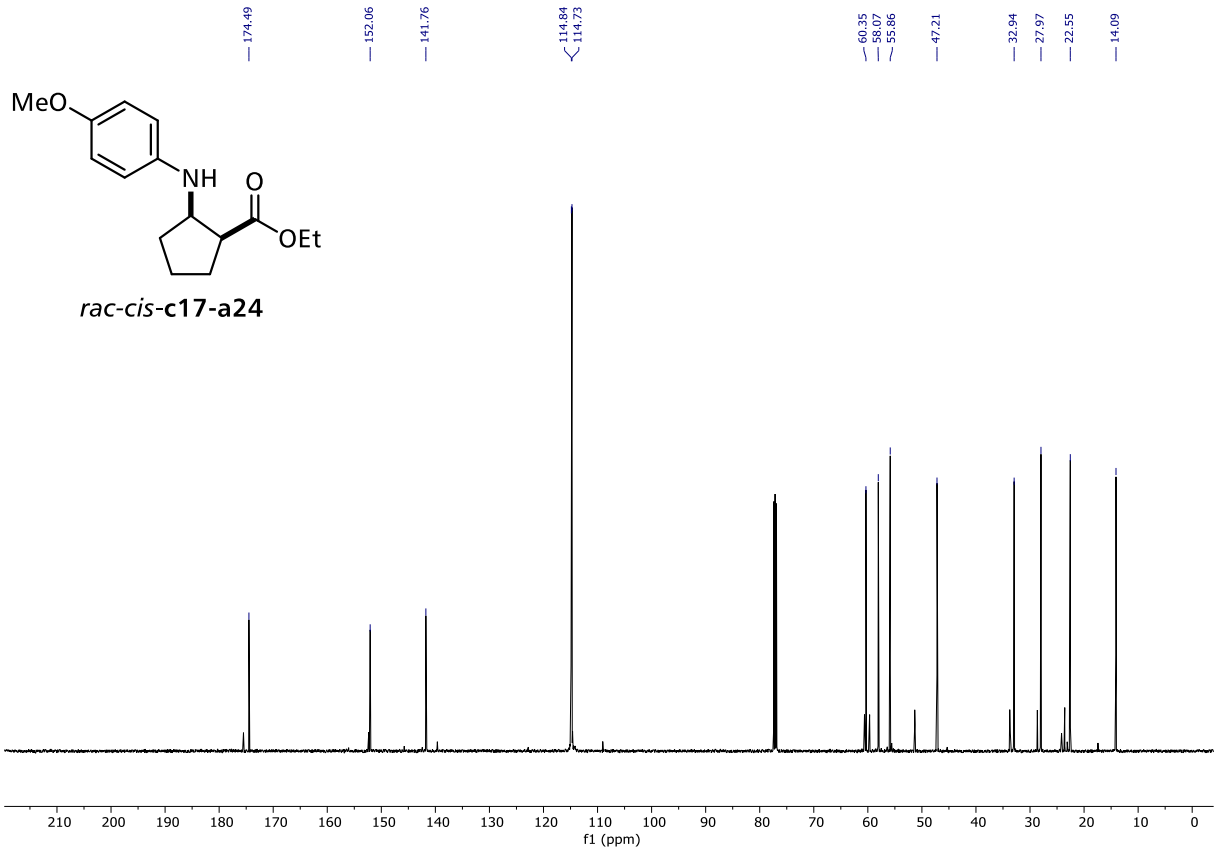


Figure S340. ^{13}C NMR spectrum of ethyl *rac-cis*-2-((4-methoxyphenyl)amino)cyclopentane-1-carboxylate (**c17-a24**).

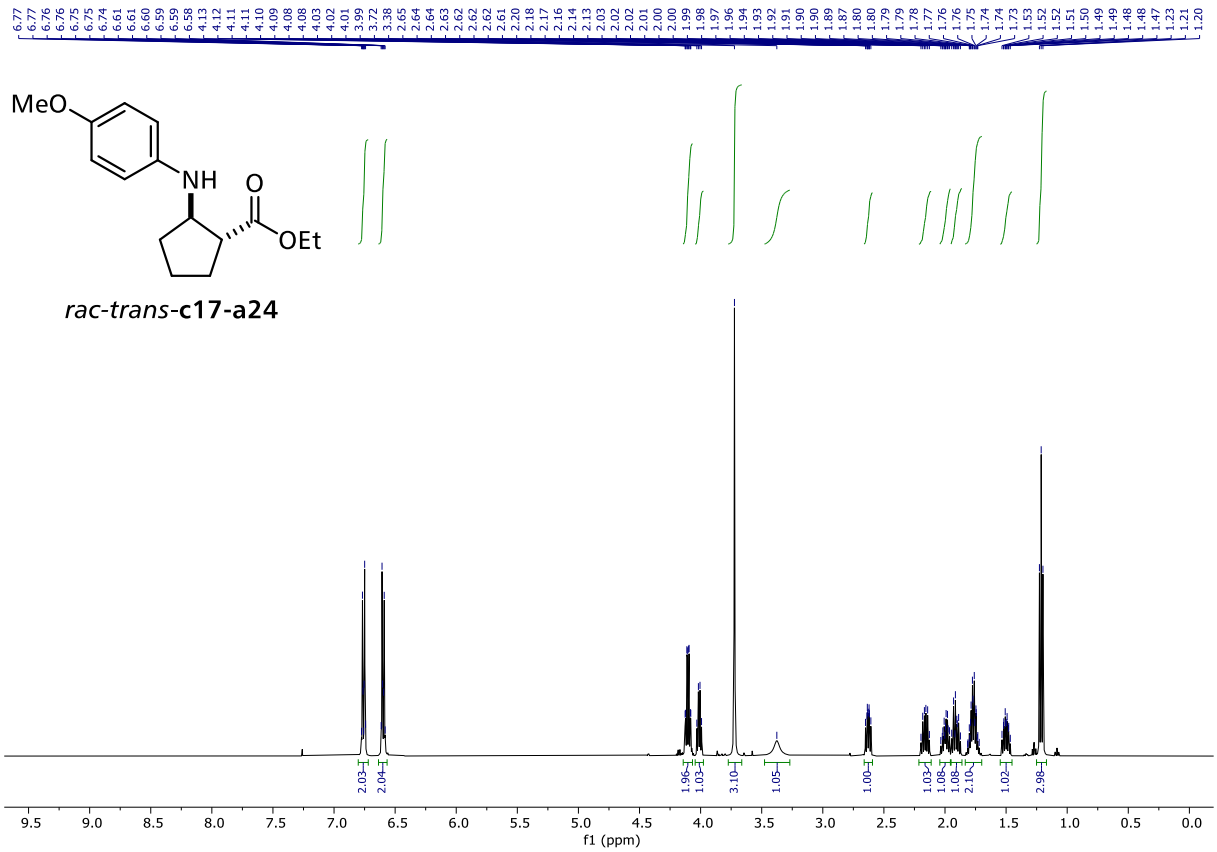


Figure S341. ^{1}H NMR spectrum of ethyl *rac-trans*-2-((4-methoxyphenyl)amino)cyclopentane-1-carboxylate (**c17-a24**).

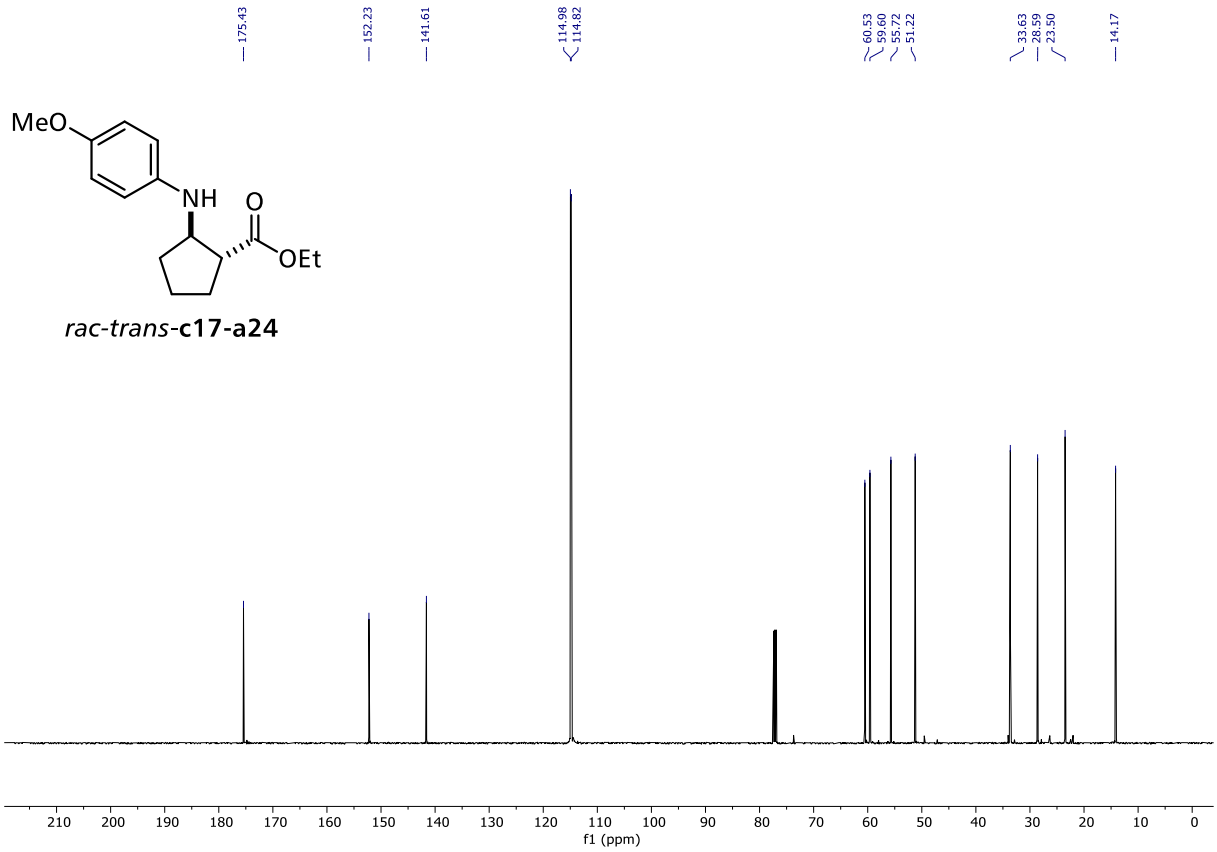


Figure S342. ^{13}C NMR spectrum of ethyl *rac-trans*-2-((4-methoxyphenyl)amino)cyclopentane-1-carboxylate (**c17-a24**).

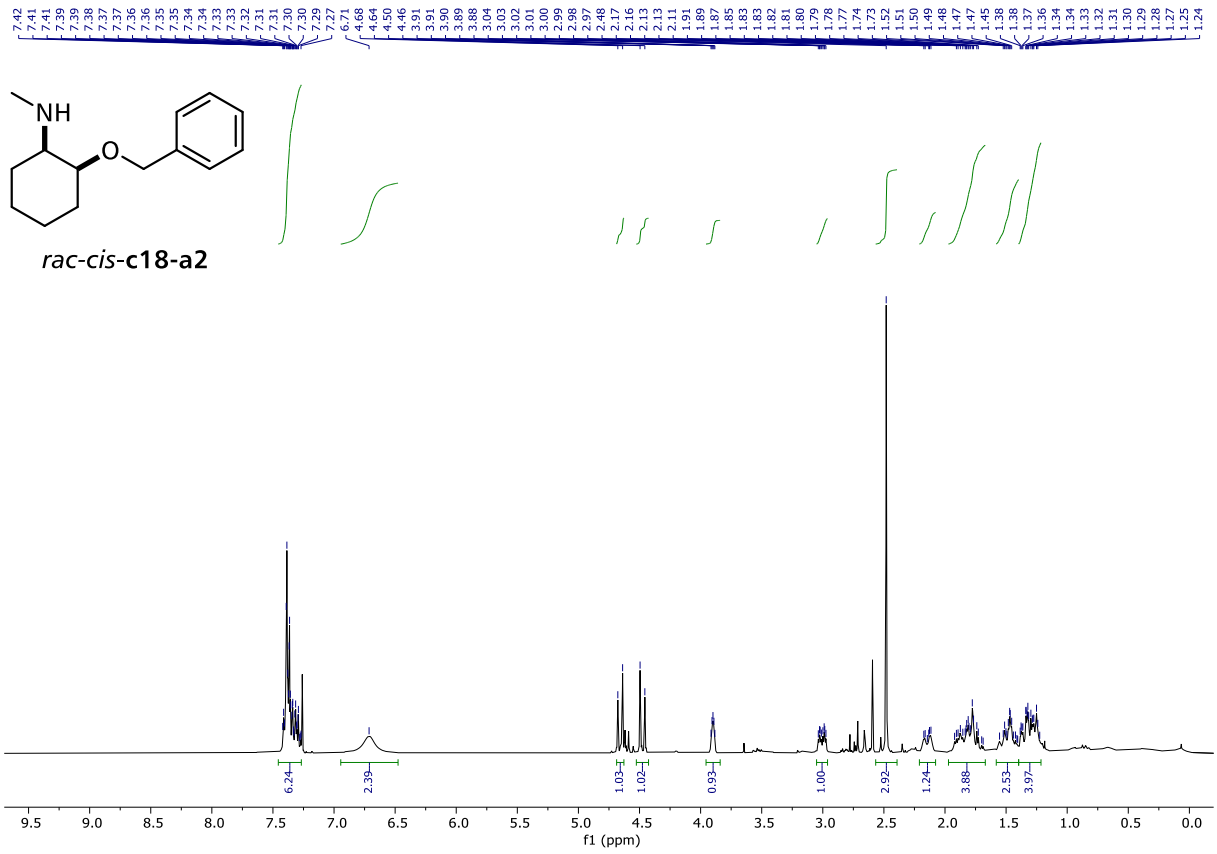


Figure S343. ^{1}H NMR spectrum of *rac-cis*-2-(benzyloxy)-*N*-methylcyclohexan-1-amine (**c18-a2**).

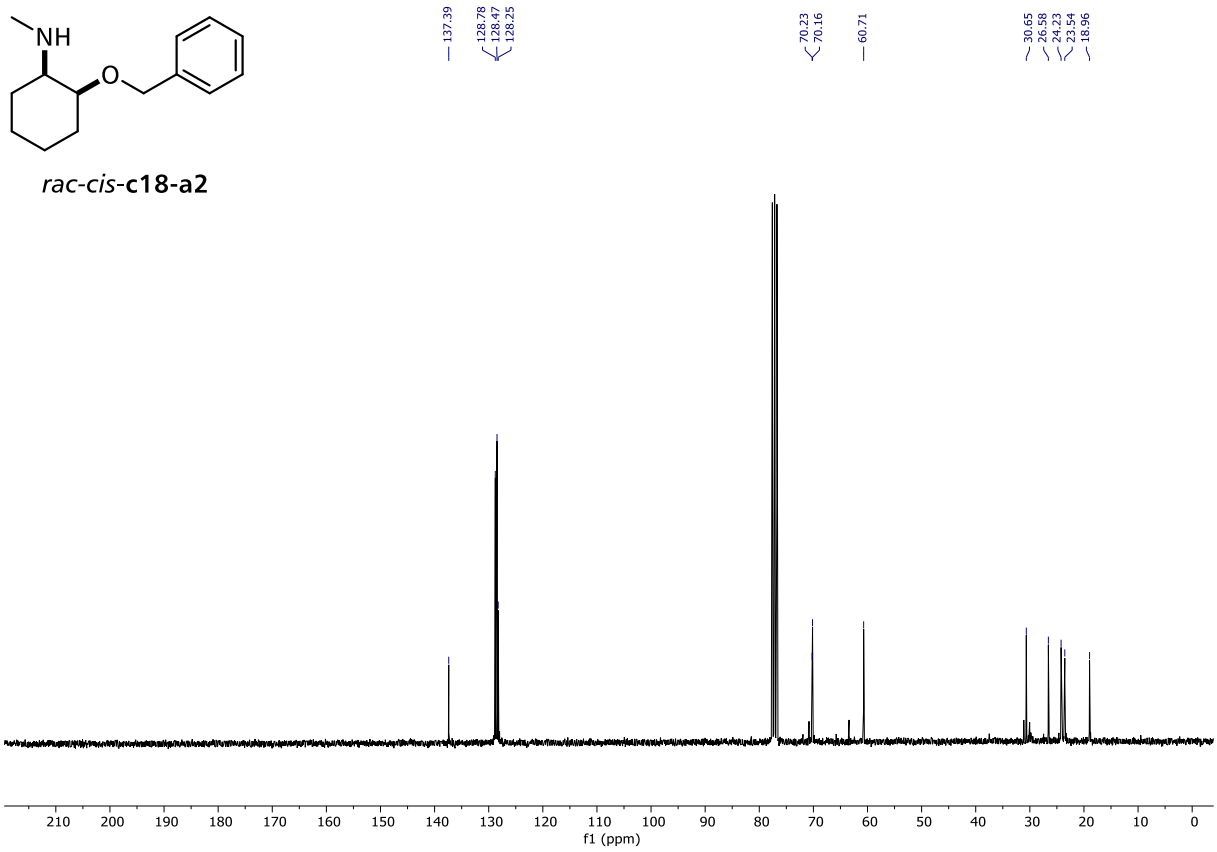


Figure S344. ^{13}C NMR spectrum of *rac-cis*-2-(benzyloxy)-*N*-methylcyclohexan-1-amine (**c18-a2**).

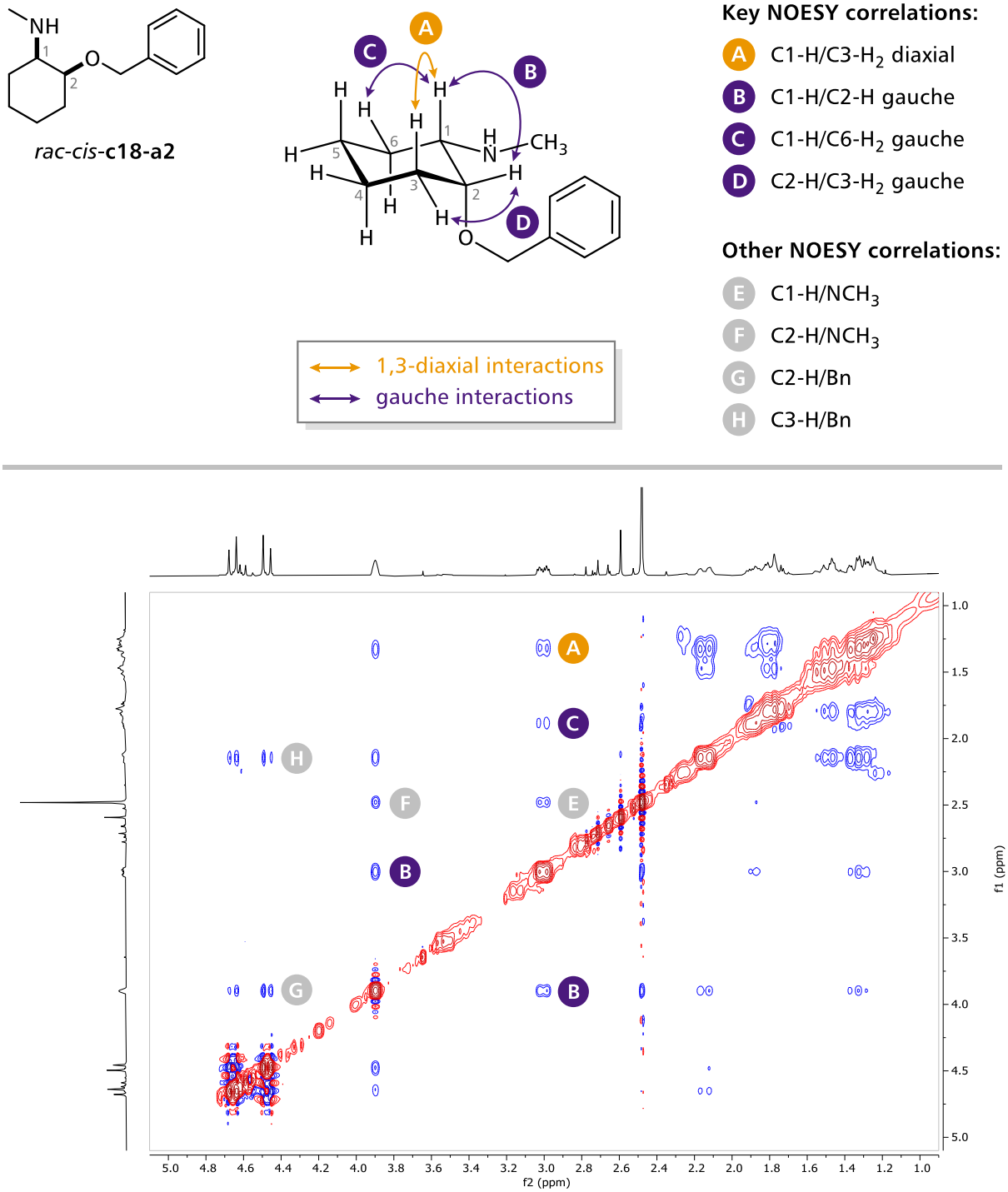


Figure S345. NOESY NMR spectrum of *rac-cis*-2-(benzyloxy)-*N*-methylcyclohexan-1-amine (**c18-a2**).

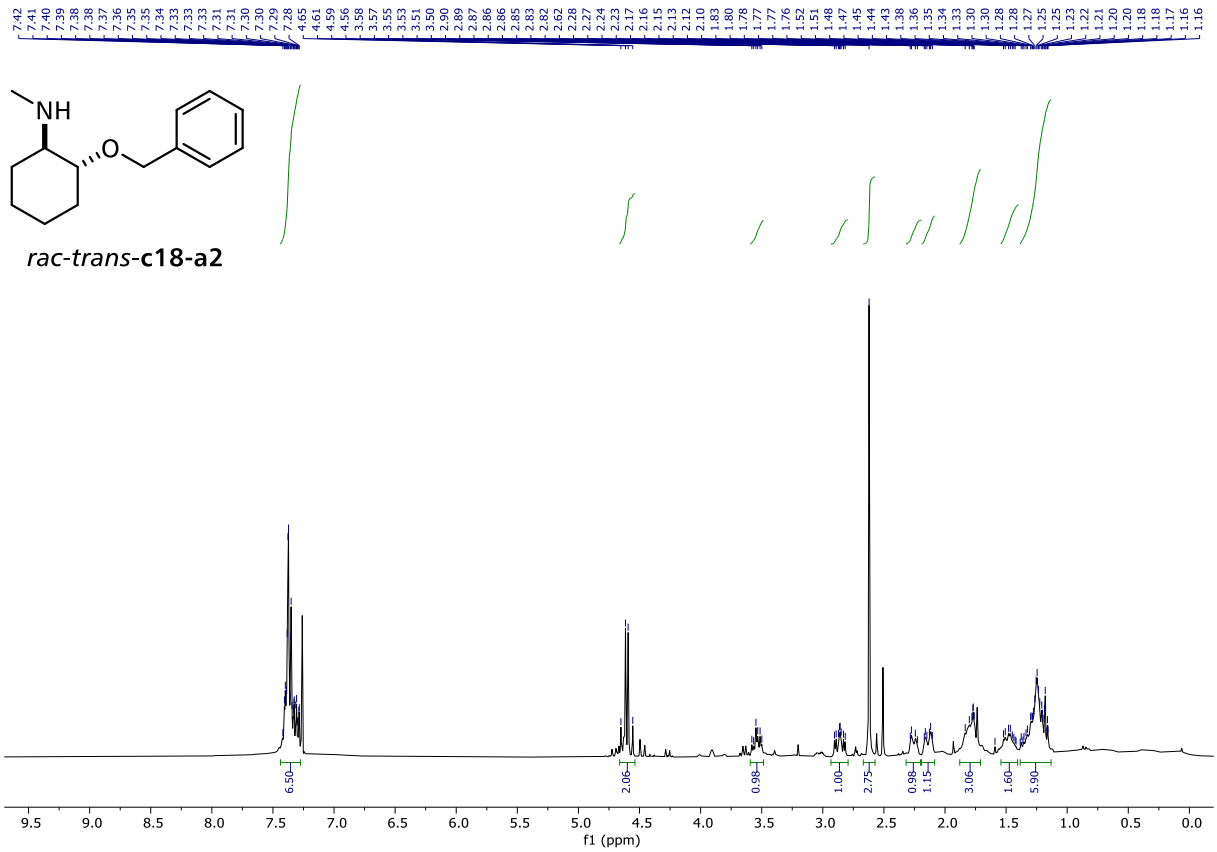


Figure S346. ^{1}H NMR spectrum of *rac-trans*-2-(benzyloxy)-*N*-methylcyclohexan-1-amine (**c18-a2**).

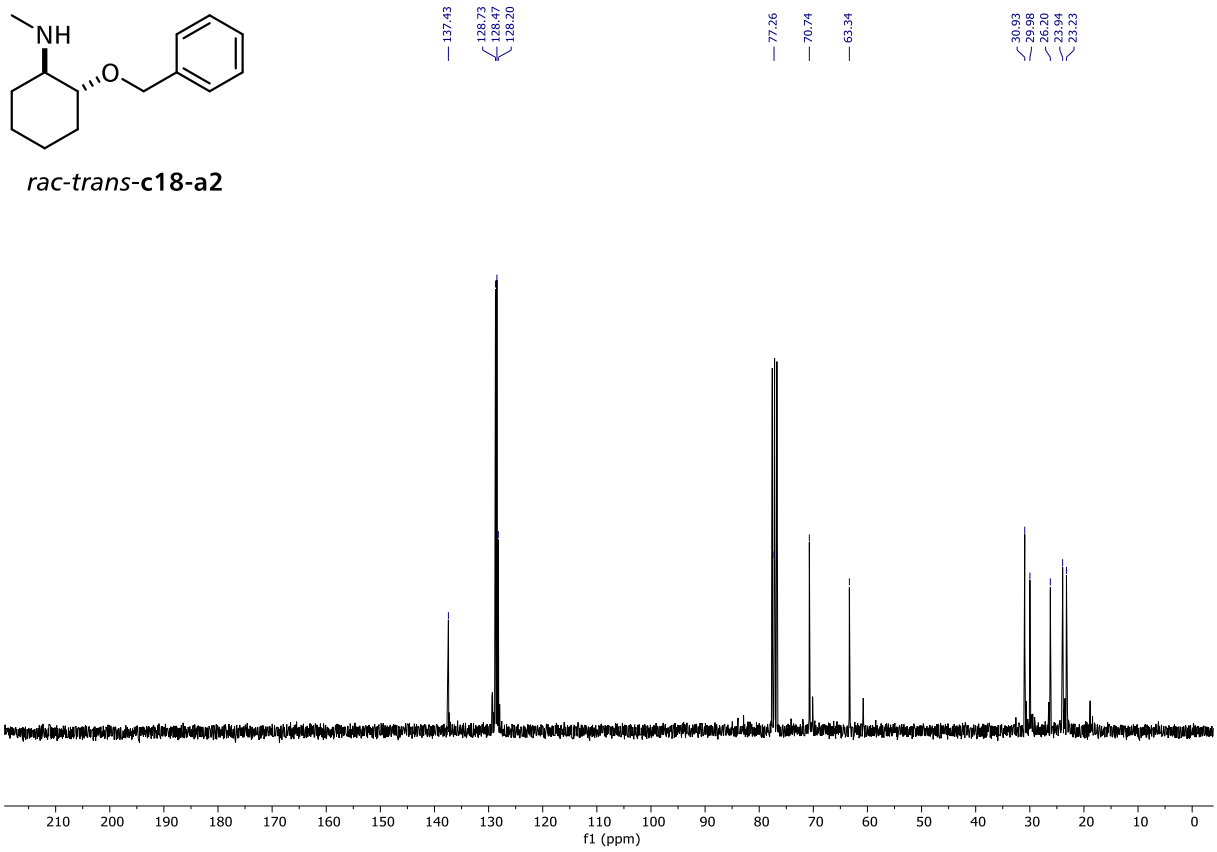
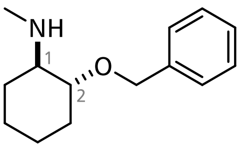
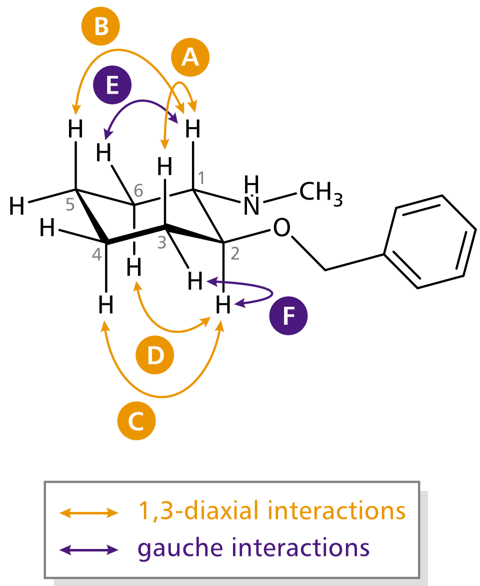


Figure S347. ^{13}C NMR spectrum of *rac-trans*-2-(benzyloxy)-*N*-methylcyclohexan-1-amine (**c18-a2**).



rac-trans-**c18-a2**



Key NOESY correlations:

- A C1-H/C3-H_2 diaxial
- B C1-H/C5-H_2 diaxial
- C C2-H/C4-H_2 diaxial
- D C2-H/C6-H_2 diaxial
- E C1-H/C6-H_2 gauche
- F C2-H/C3-H_2 gauche

Other NOESY correlations:

- G C1-H/NCH_3
- H C2-H/Bn
- I C3-H/Bn

NOESY correlation absent:

- J C1-H/C2-H

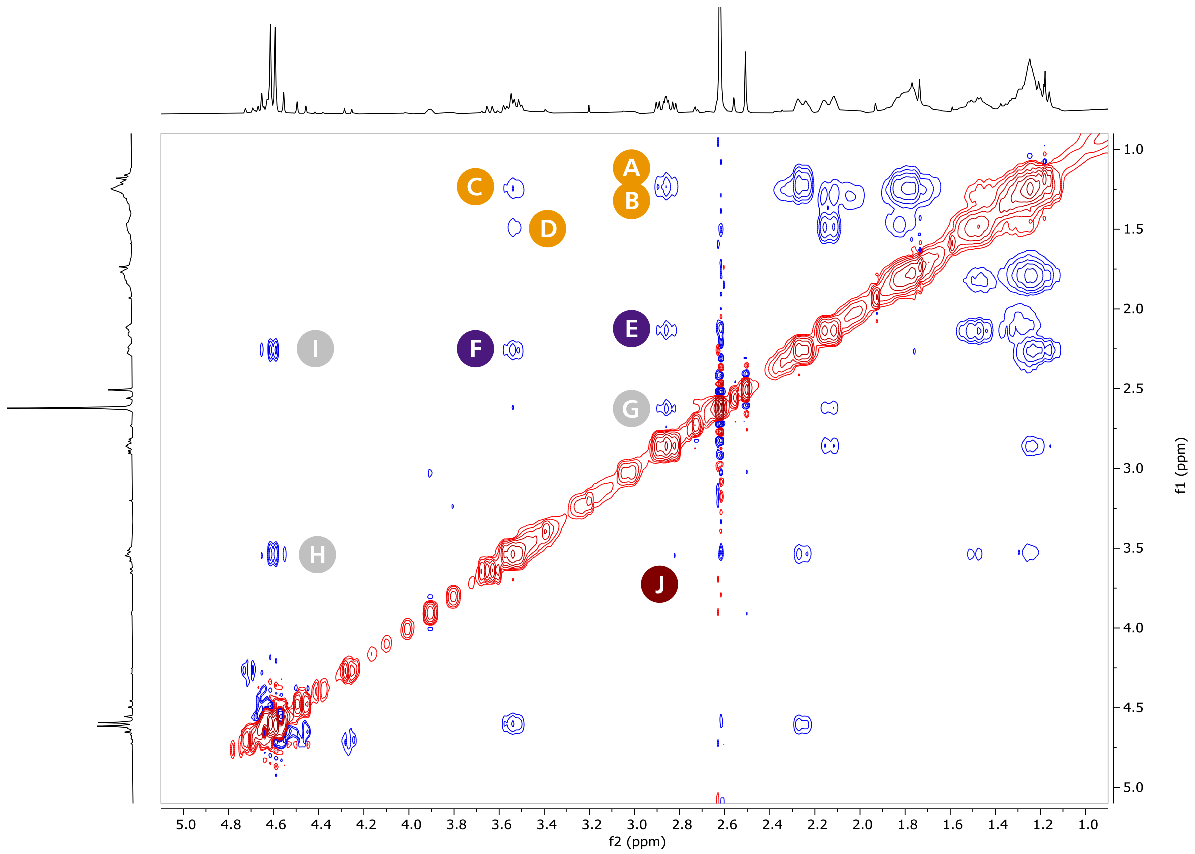


Figure S348. NOESY NMR spectrum of *rac-trans*-2-(benzyloxy)-*N*-methylcyclohexan-1-amine (**c18-a2**).

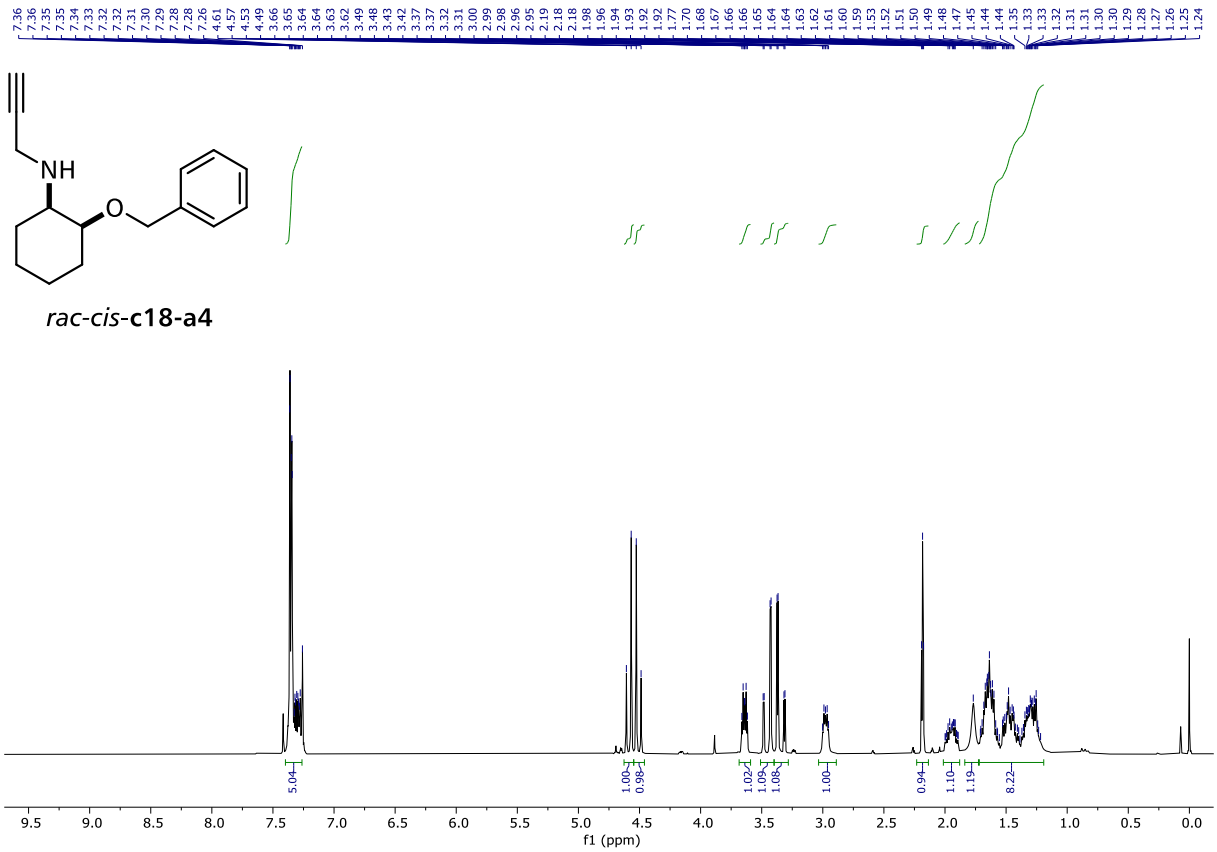


Figure S349. ^{1}H NMR spectrum of *rac-cis*-2-(benzyloxy)-*N*-(prop-2-yn-1-yl)cyclohexan-1-amine (**c18-a4**).

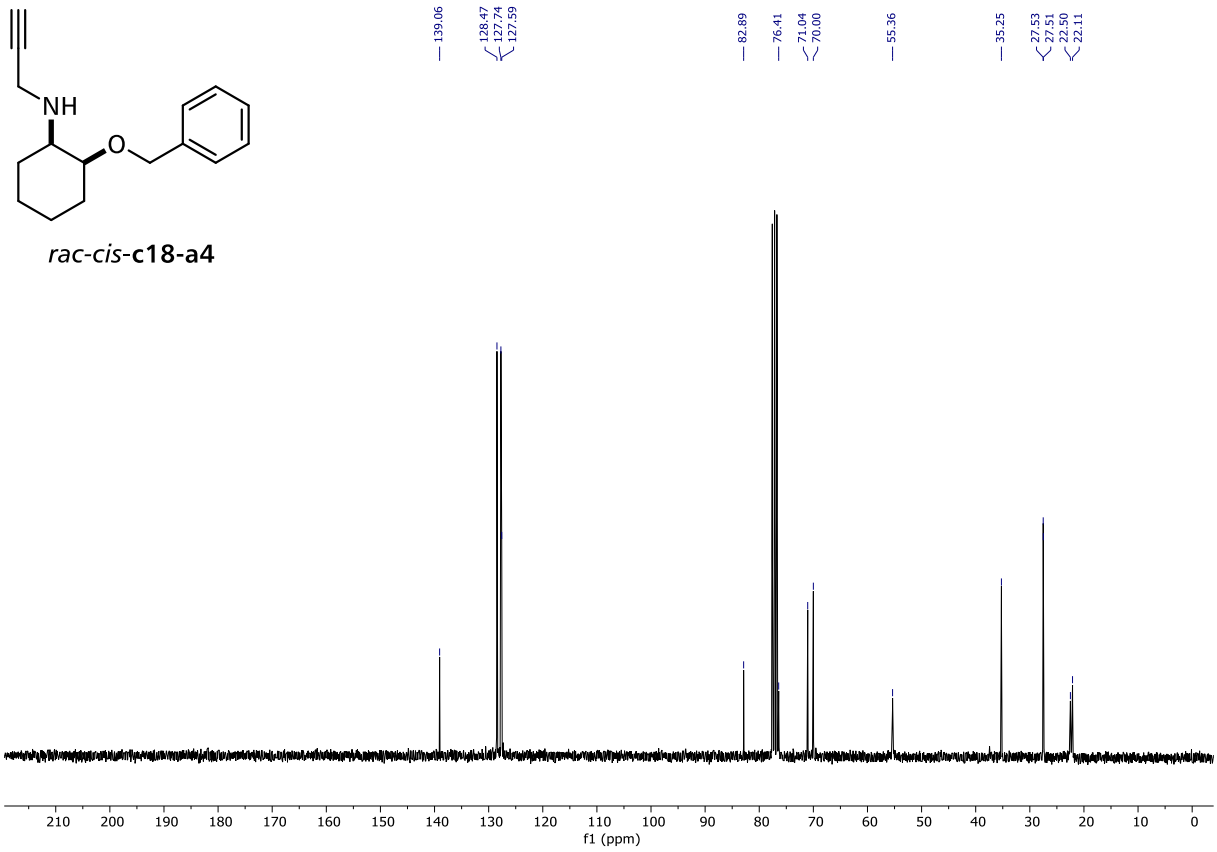


Figure S350. ^{13}C NMR spectrum of *rac-cis*-2-(benzyloxy)-*N*-(prop-2-yn-1-yl)cyclohexan-1-amine (**c18-a4**).

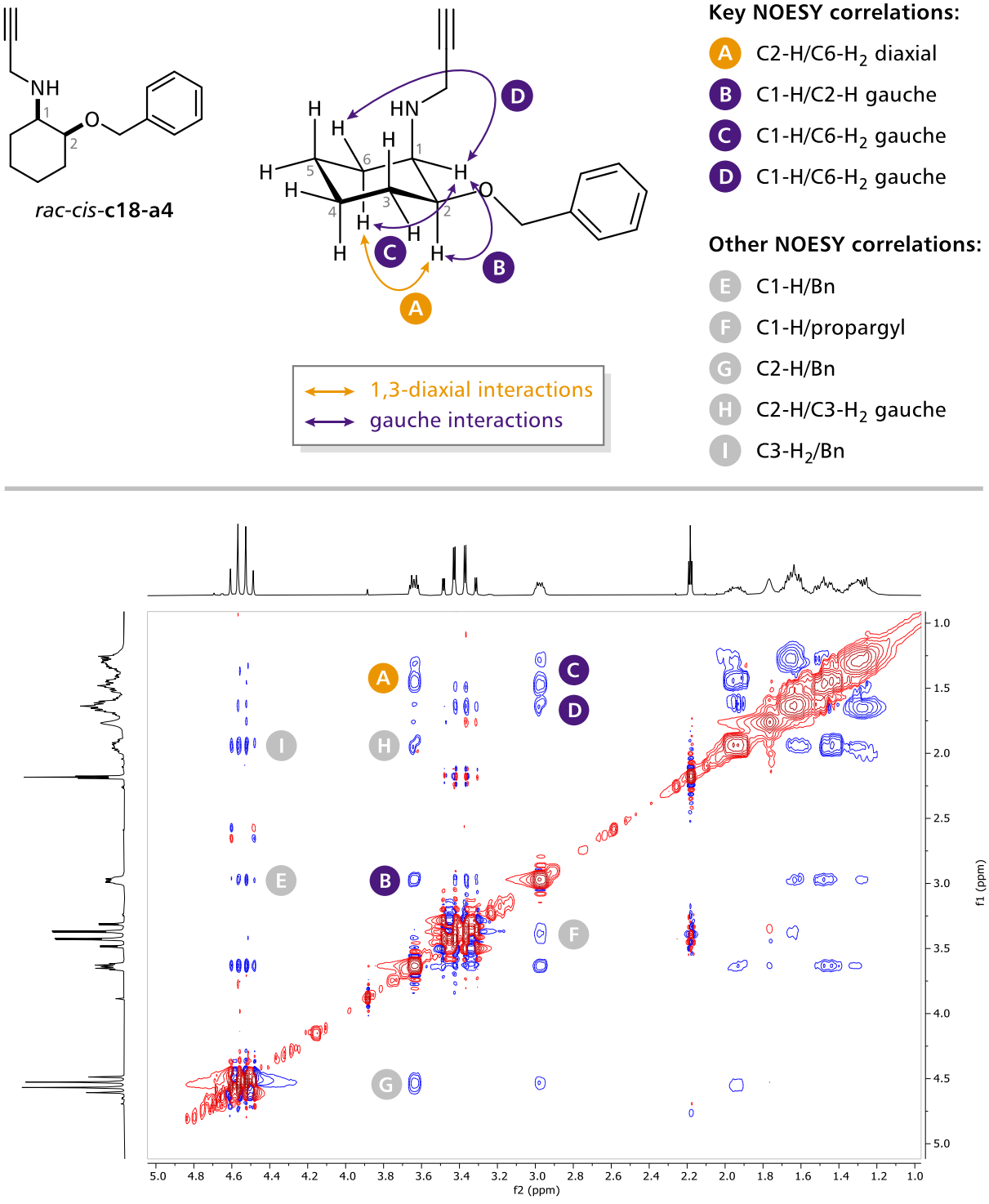


Figure S351. NOESY NMR spectrum of *rac-cis*-2-(benzyloxy)-*N*-(prop-2-yn-1-yl)cyclohexan-1-amine (**c18-a4**).

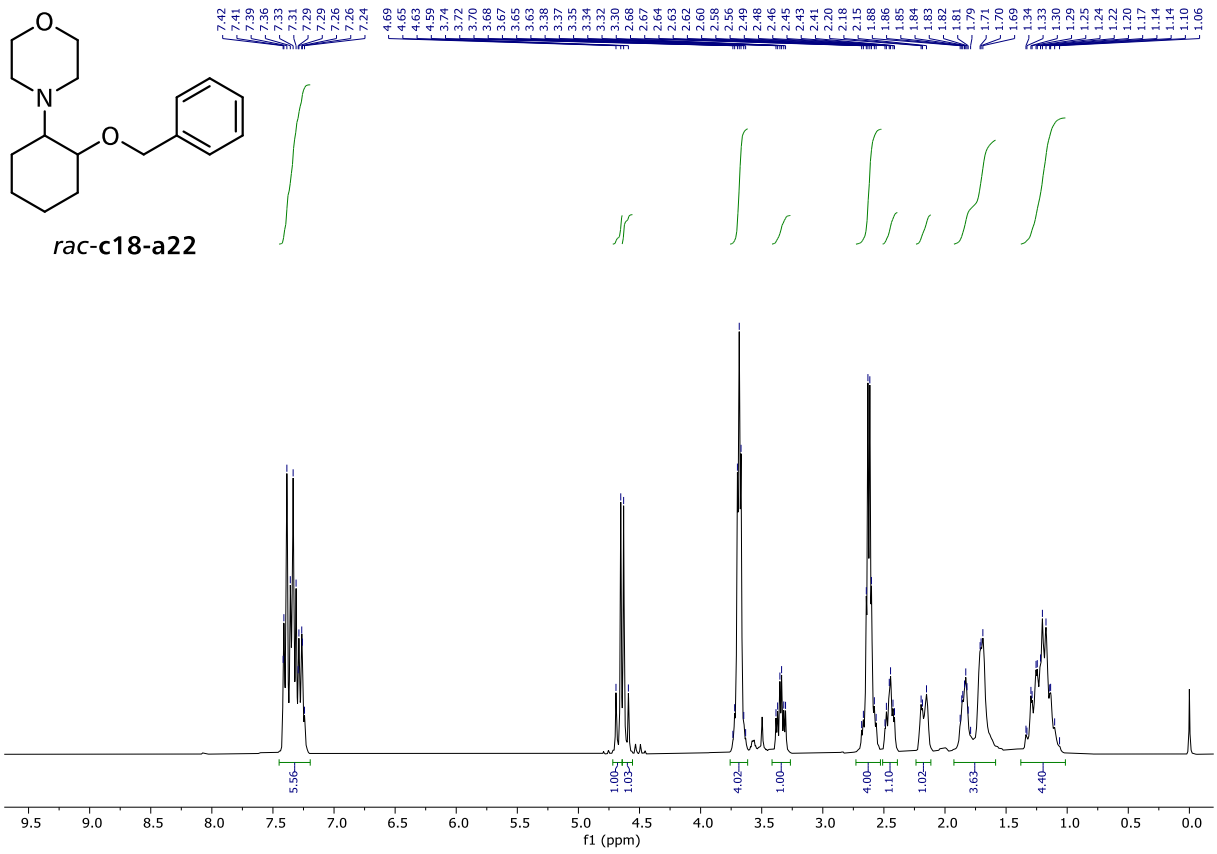


Figure S352. ^{1}H NMR spectrum of *rac*-4-(2-(benzyloxy)cyclohexyl)morpholine (**c18-a22**).

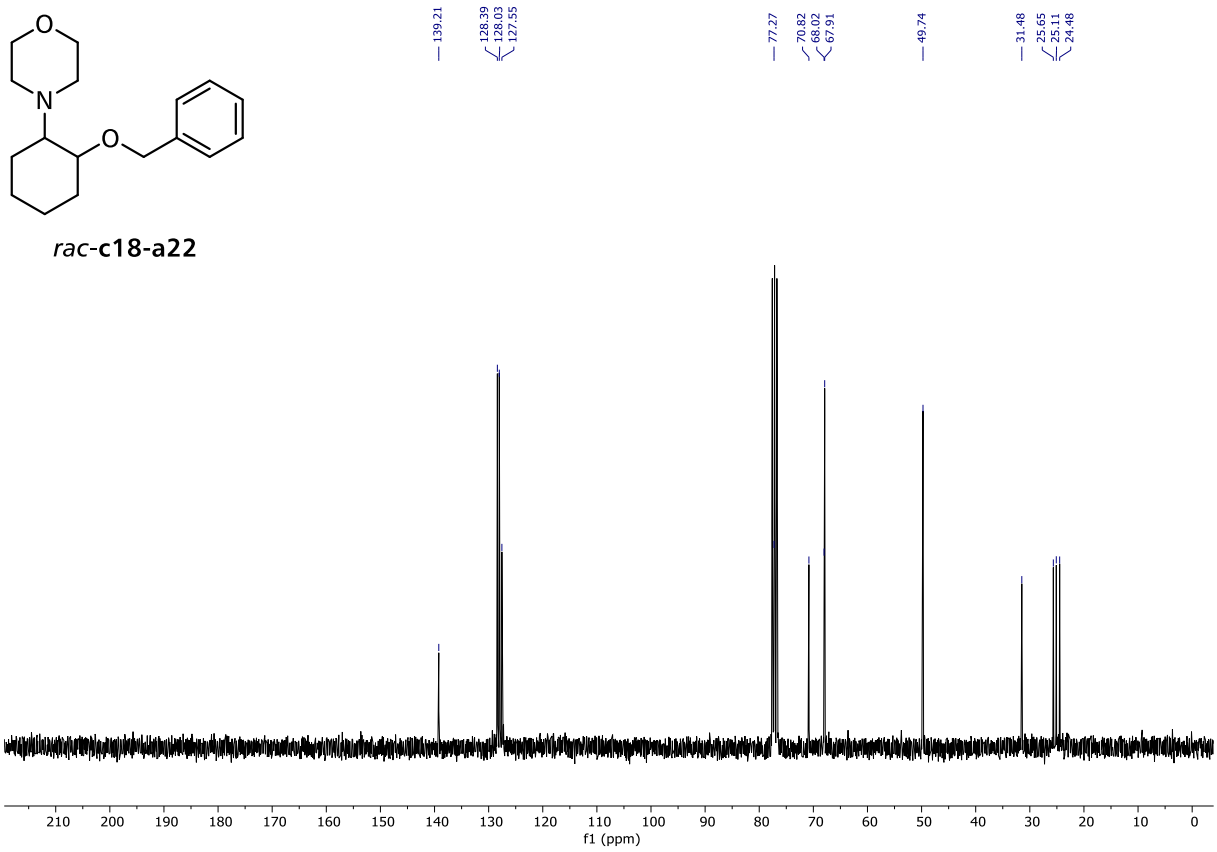


Figure S353. ^{13}C NMR spectrum of *rac*-4-(2-(benzyloxy)cyclohexyl)morpholine (**c18-a22**).

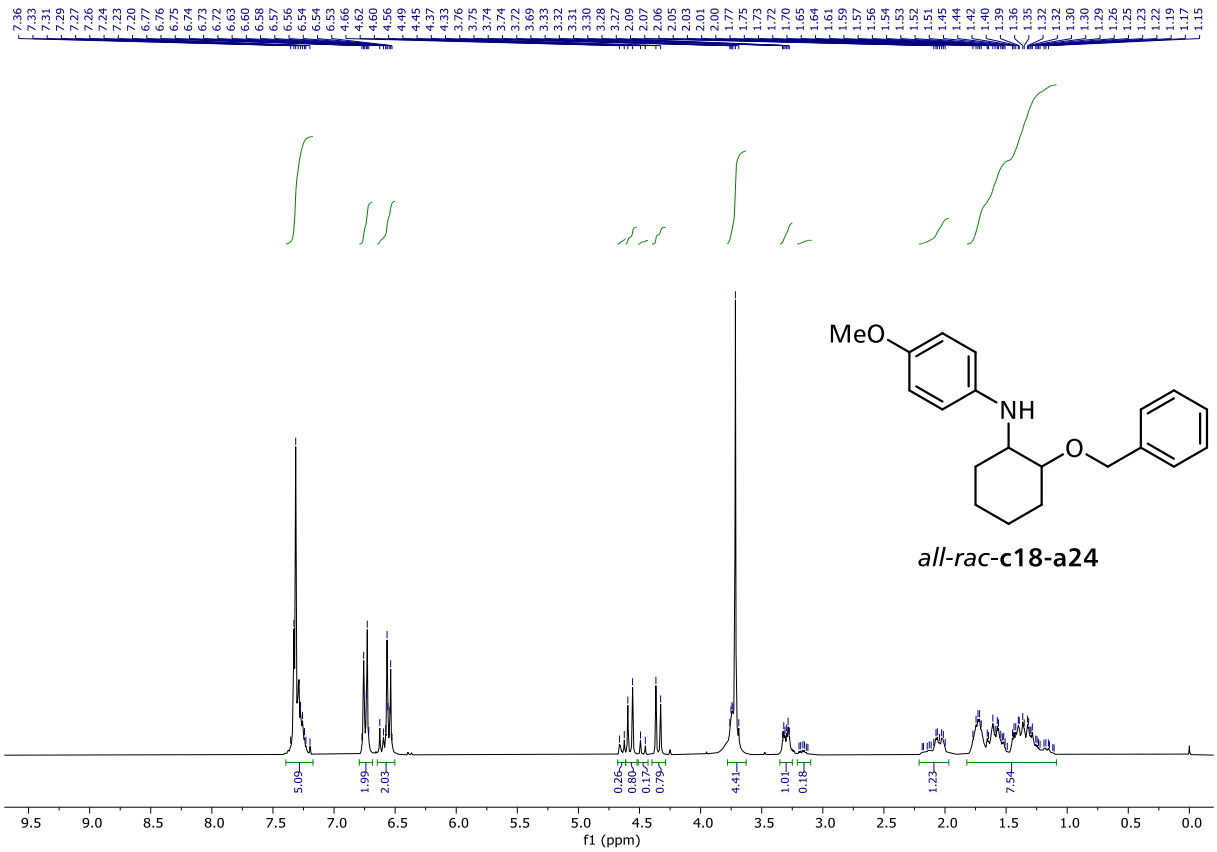


Figure S354. ^{1}H NMR spectrum of *rac-N*-(2-(benzyloxy)cyclohexyl)-4-methoxyaniline (**c18-a24**).

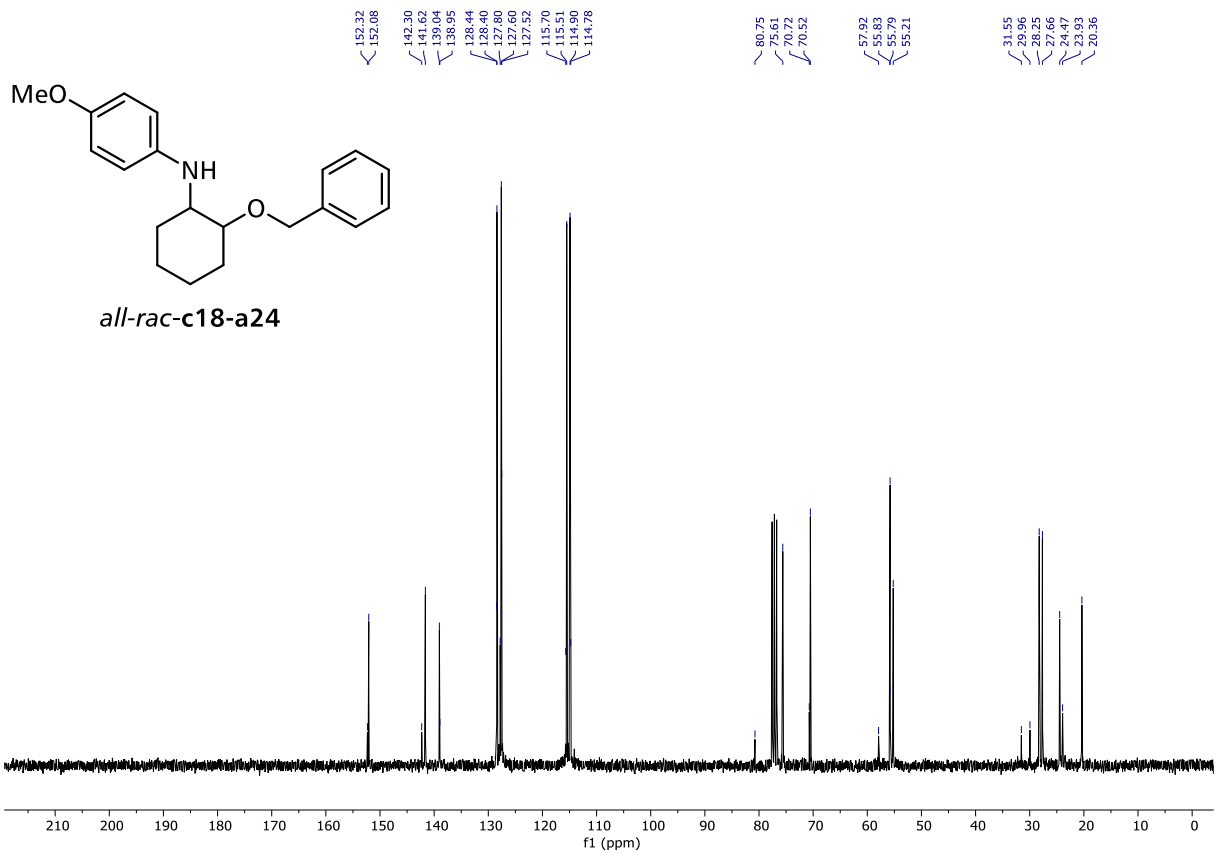


Figure S355. ^{13}C NMR spectrum of *rac-N*-(2-(benzyloxy)cyclohexyl)-4-methoxyaniline (**c18-a24**).

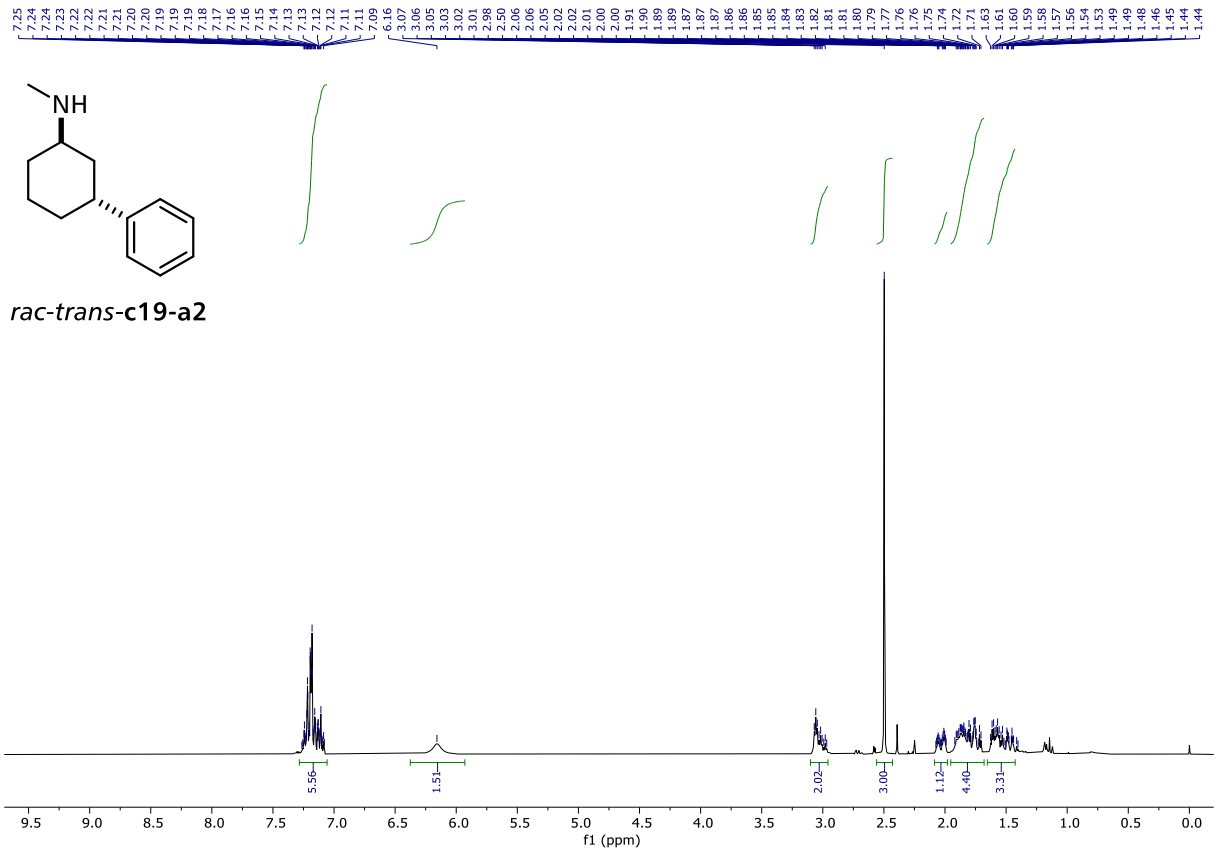


Figure S356. ^{1}H NMR spectrum of *rac-trans-N*-methyl-3-phenylcyclohexan-1-amine (**c19-a2**).

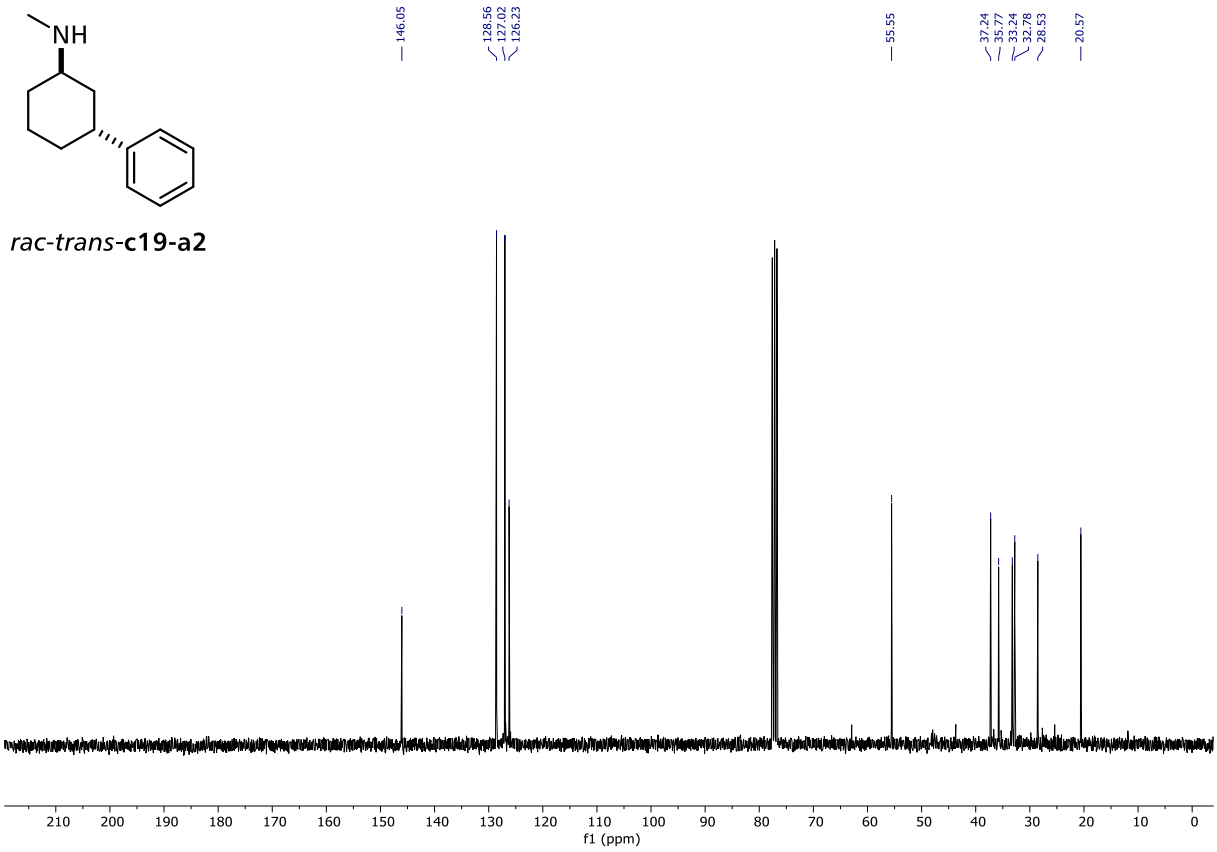


Figure S357. ^{13}C NMR spectrum of *rac-trans-N*-methyl-3-phenylcyclohexan-1-amine (**c19-a2**).

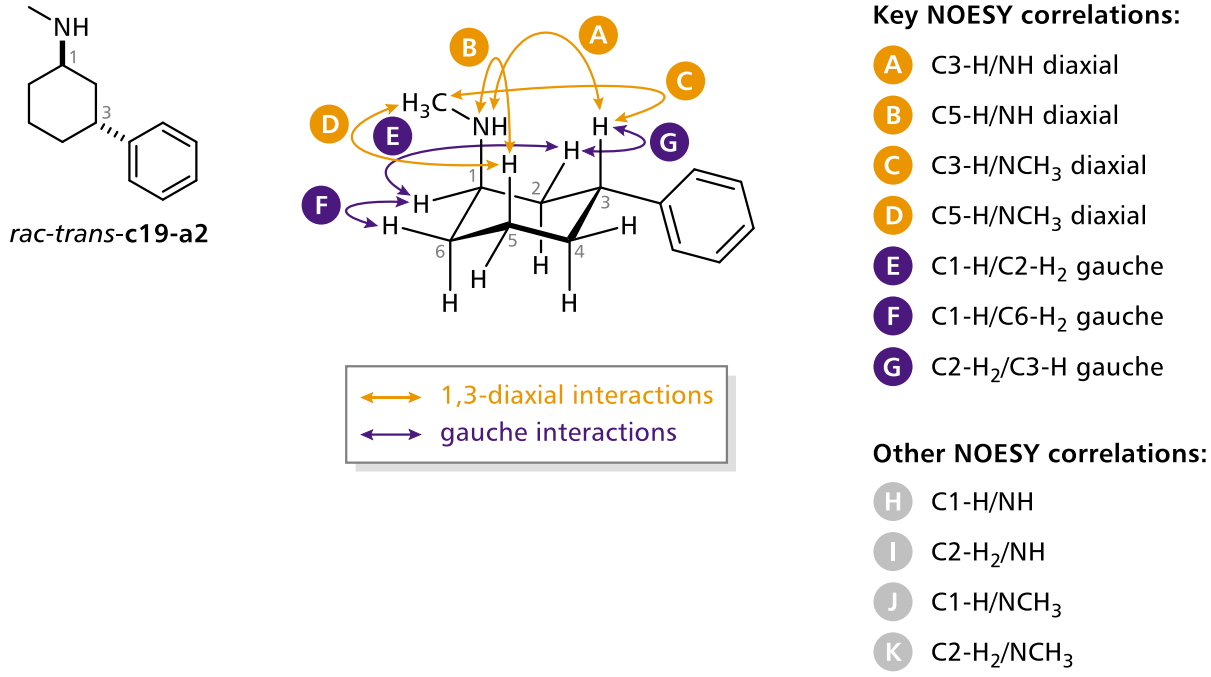


Figure S358. NOESY NMR spectrum of *rac-trans-N*-methyl-3-phenylcyclohexan-1-amine (**c19-a2**).

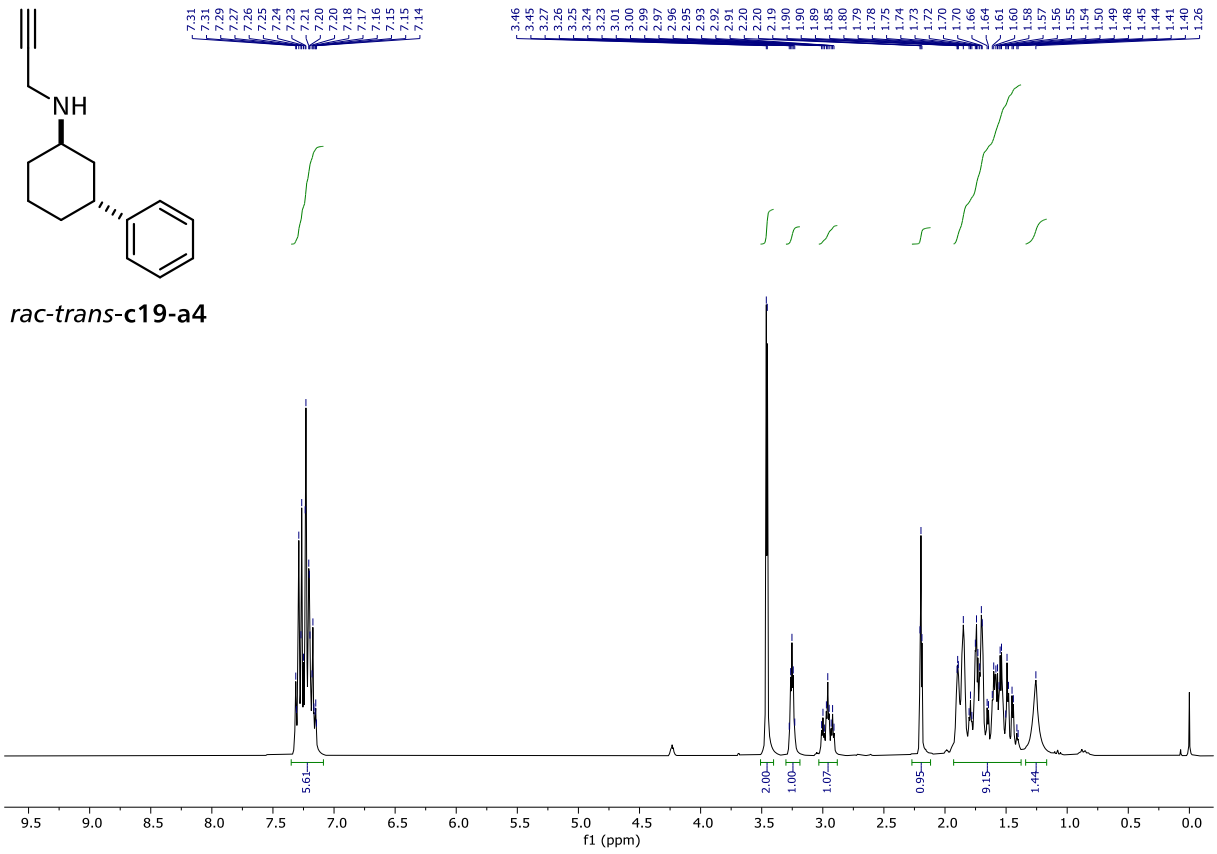


Figure S359. ^{1}H NMR spectrum of *rac-trans*-3-phenyl-*N*-(prop-2-yn-1-yl)cyclohexan-1-amine (**c19-a4**).

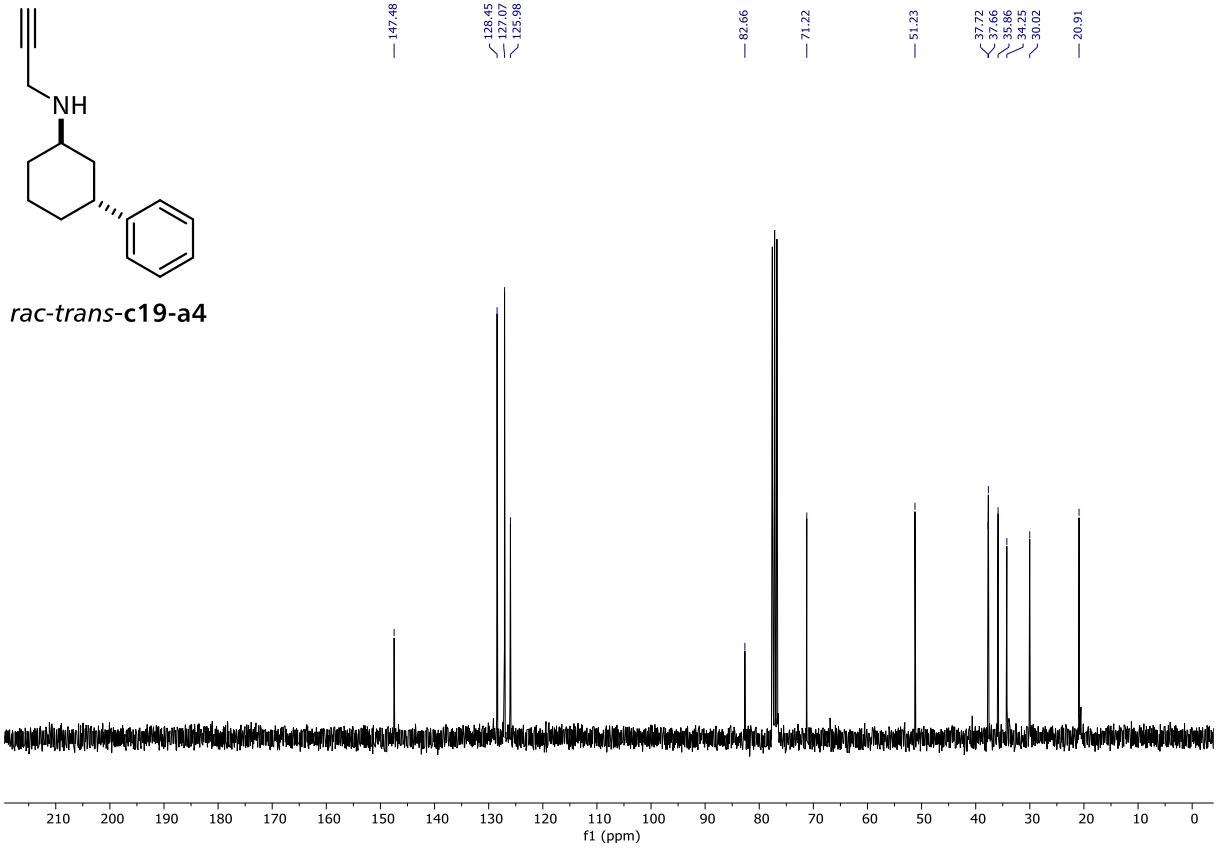
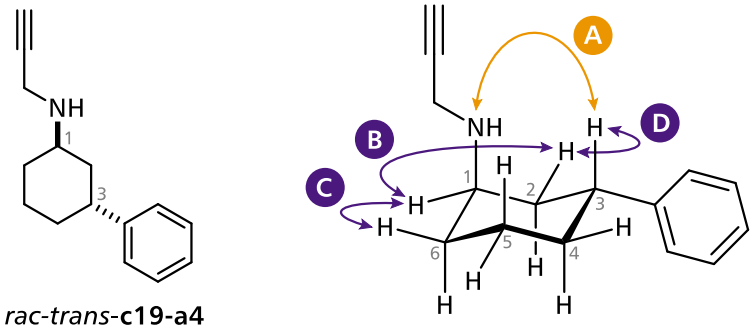


Figure S360. ^{13}C NMR spectrum of *rac-trans*-3-phenyl-*N*-(prop-2-yn-1-yl)cyclohexan-1-amine (**c19-a4**).



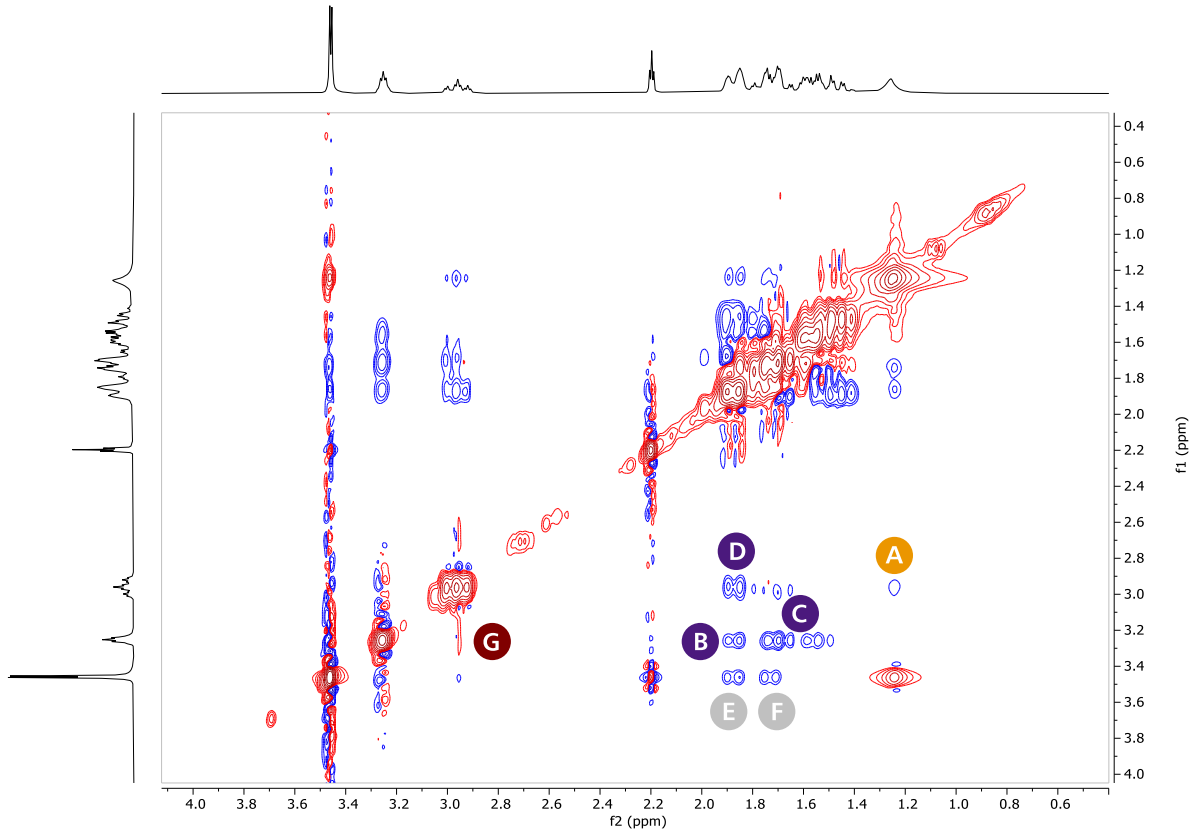


Figure S361. NOESY NMR spectrum of *rac-trans*-3-phenyl-*N*-(prop-2-yn-1-yl)cyclohexan-1-amine (**c19-a4**).

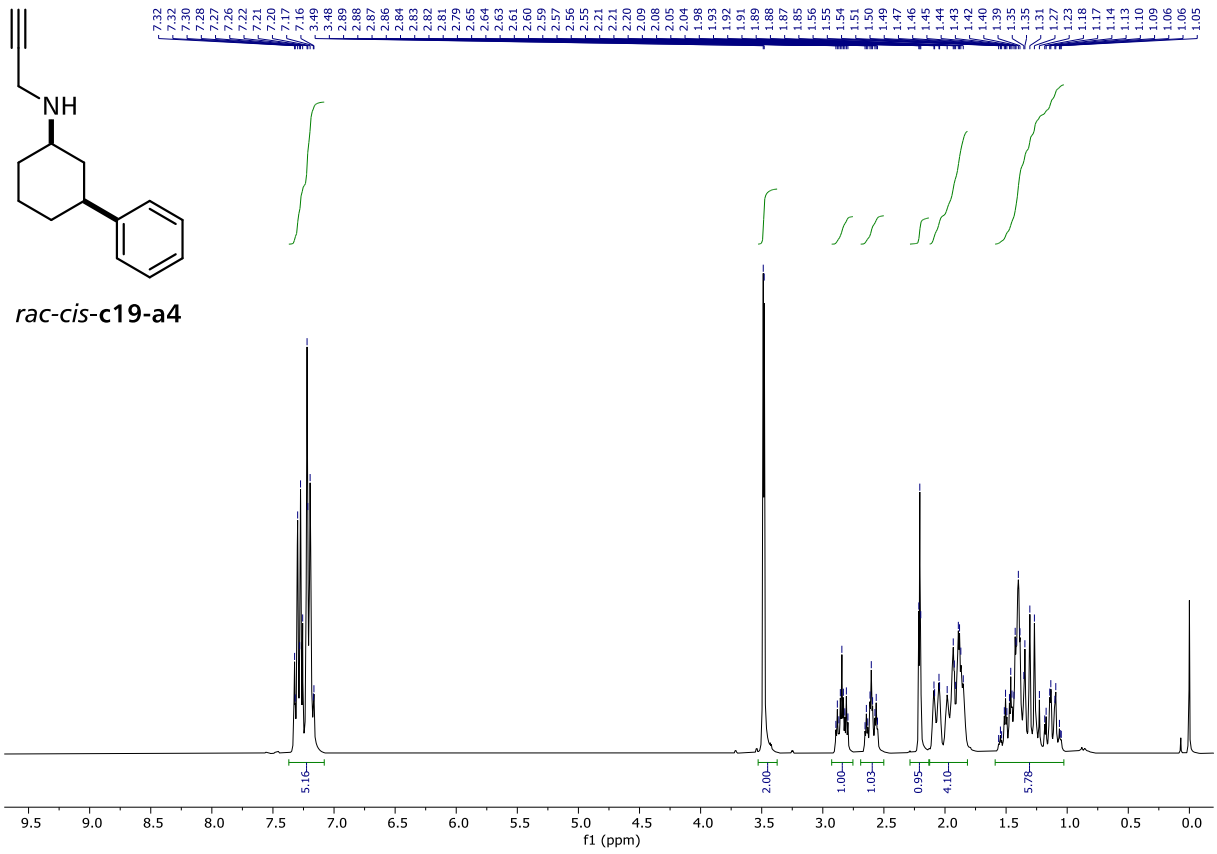


Figure S362. ^{1}H NMR spectrum of *rac-cis*-3-phenyl-*N*-(prop-2-yn-1-yl)cyclohexan-1-amine (**c19-a4**).

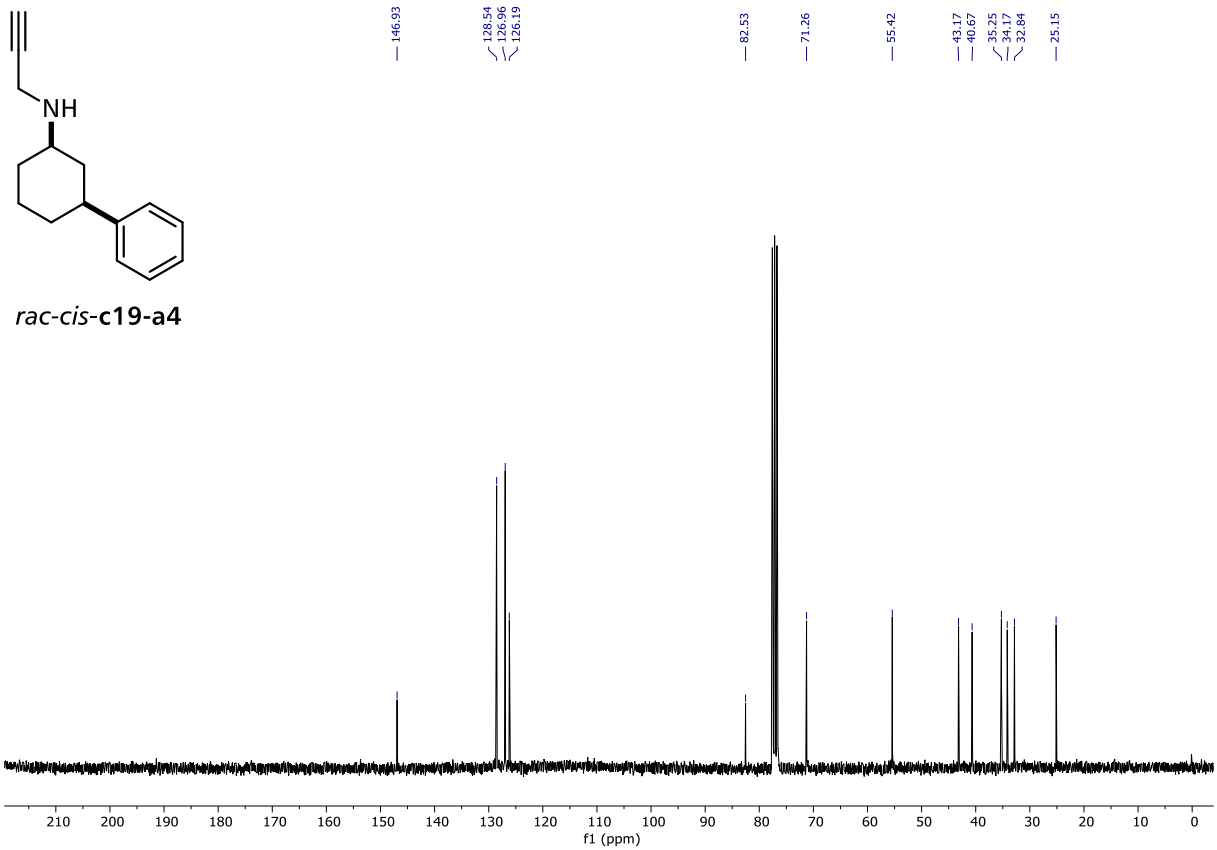
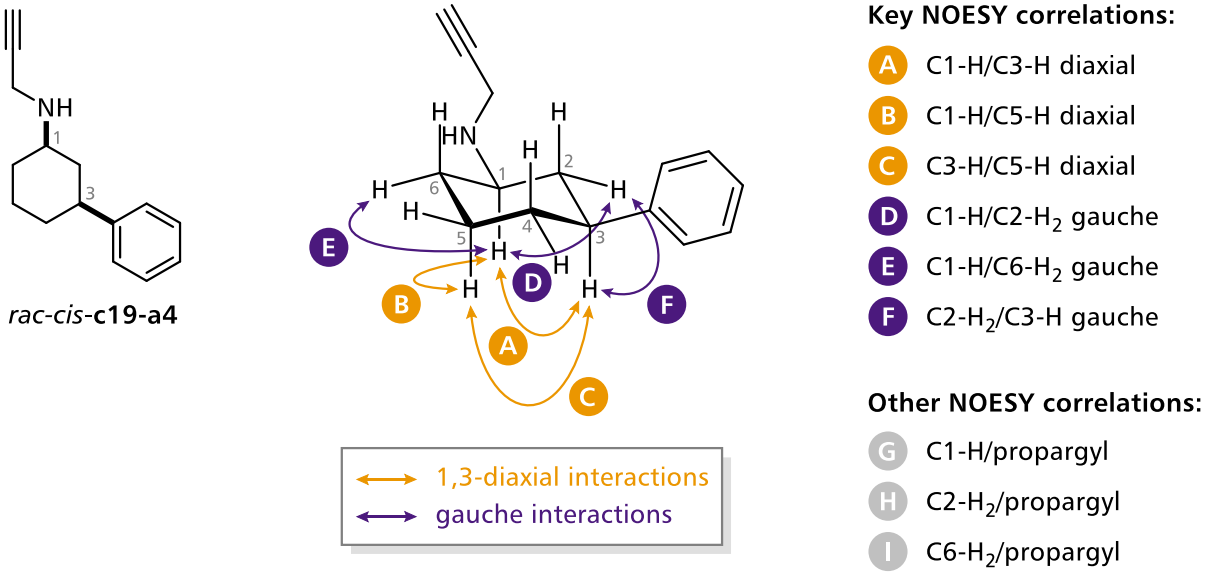


Figure S363. ^{13}C NMR spectrum of *rac-cis*-3-phenyl-*N*-(prop-2-yn-1-yl)cyclohexan-1-amine (**c19-a4**).



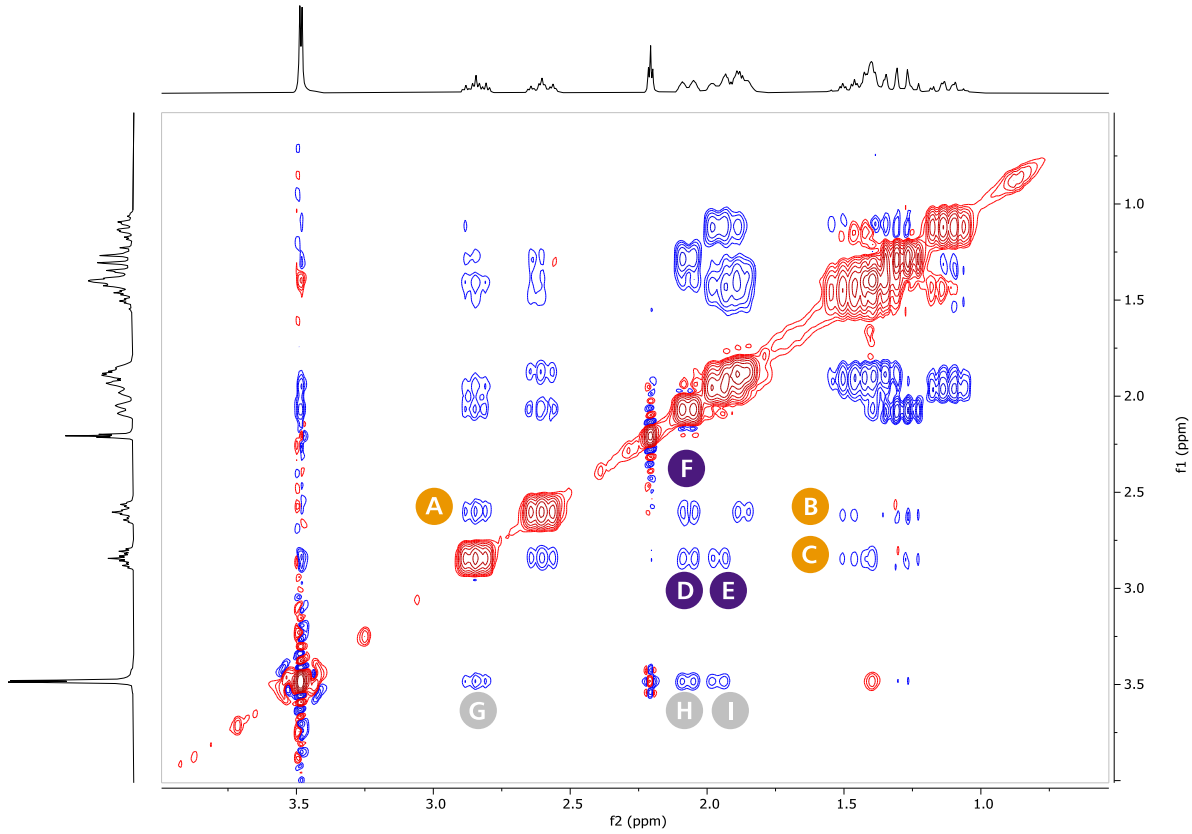


Figure S364. NOESY NMR spectrum of *rac-cis*-3-phenyl-*N*-(prop-2-yn-1-yl)cyclohexan-1-amine (**c19-a4**).

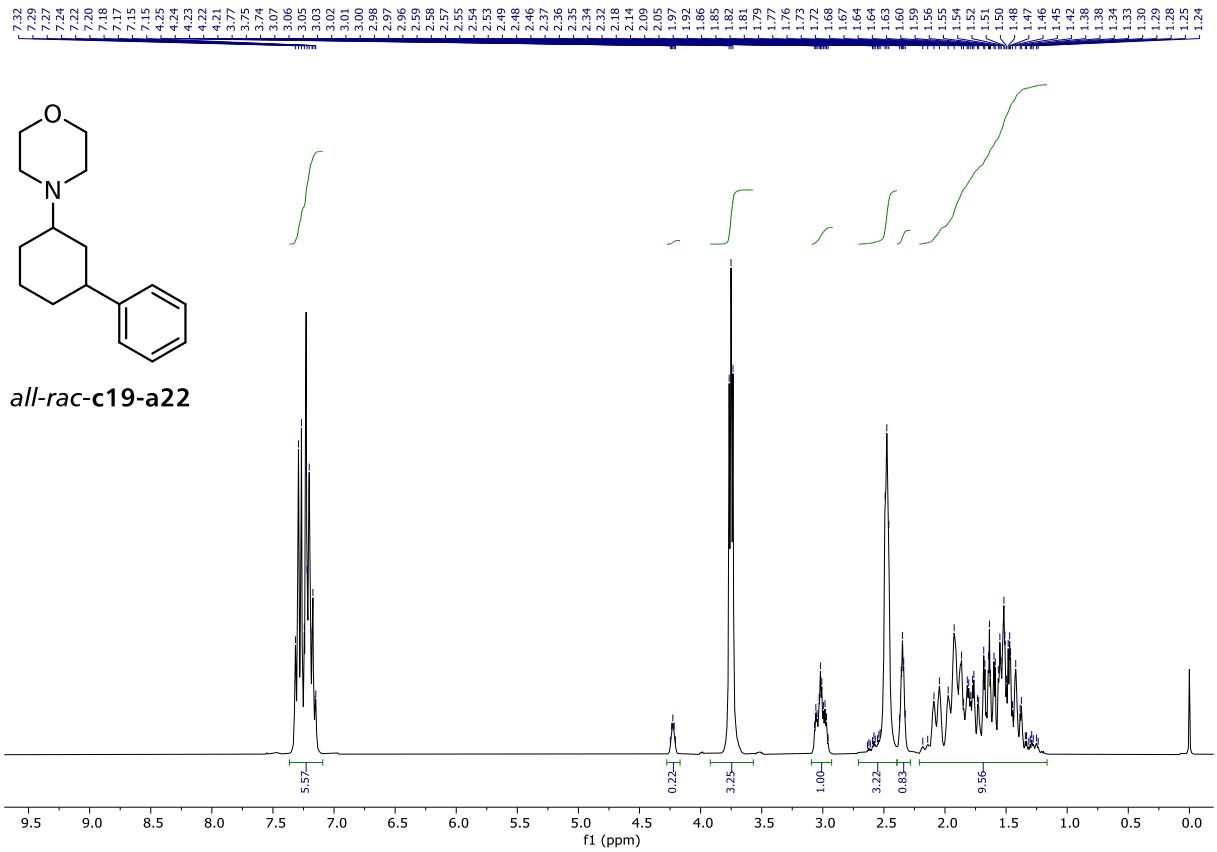


Figure S365. ^{1}H NMR spectrum of *all-rac*-4-(3-phenylcyclohexyl)morpholine (**c19-a22**).

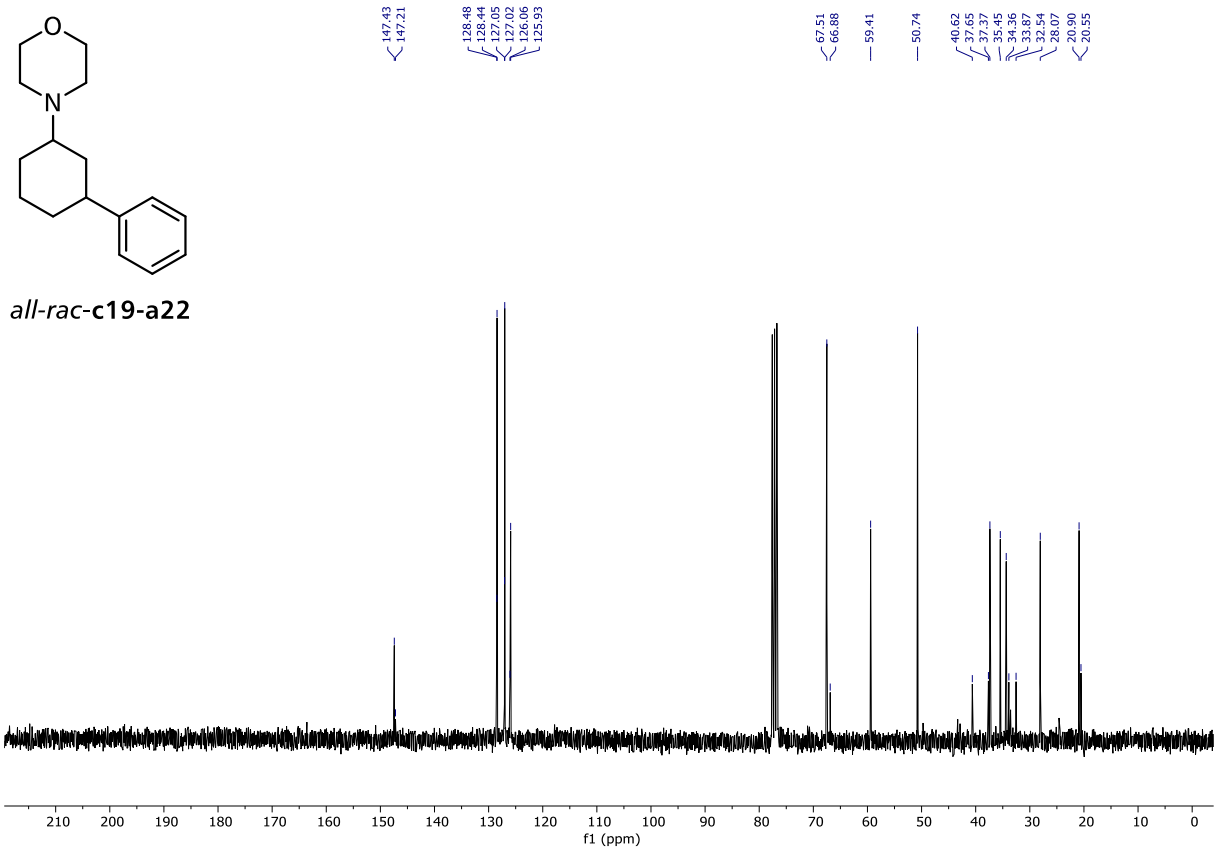


Figure S366. ^{13}C NMR spectrum of *all-rac*-4-(3-phenylcyclohexyl)morpholine (**c19-a22**).

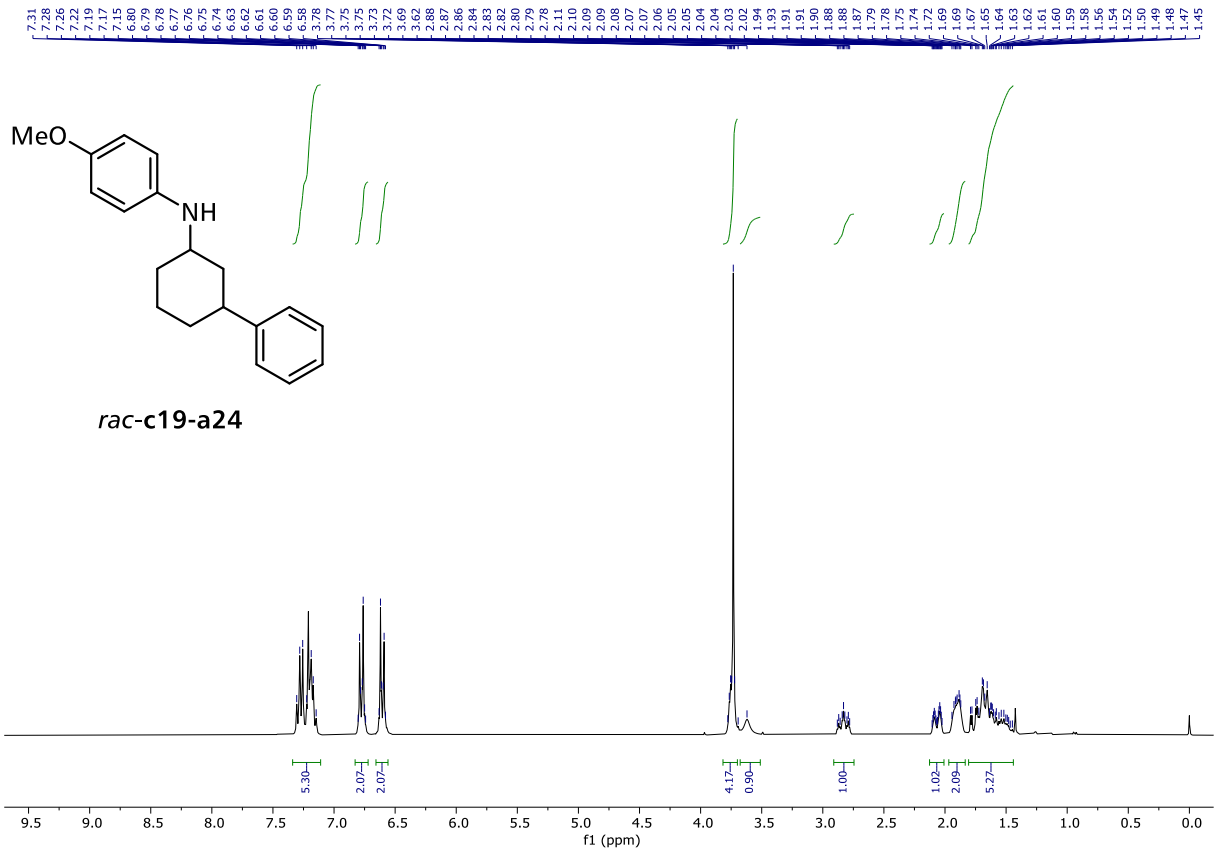


Figure S367. ^{1}H NMR spectrum of *rac*-4-methoxy-*N*-(3-phenylcyclohexyl)aniline (**c19-a24**).

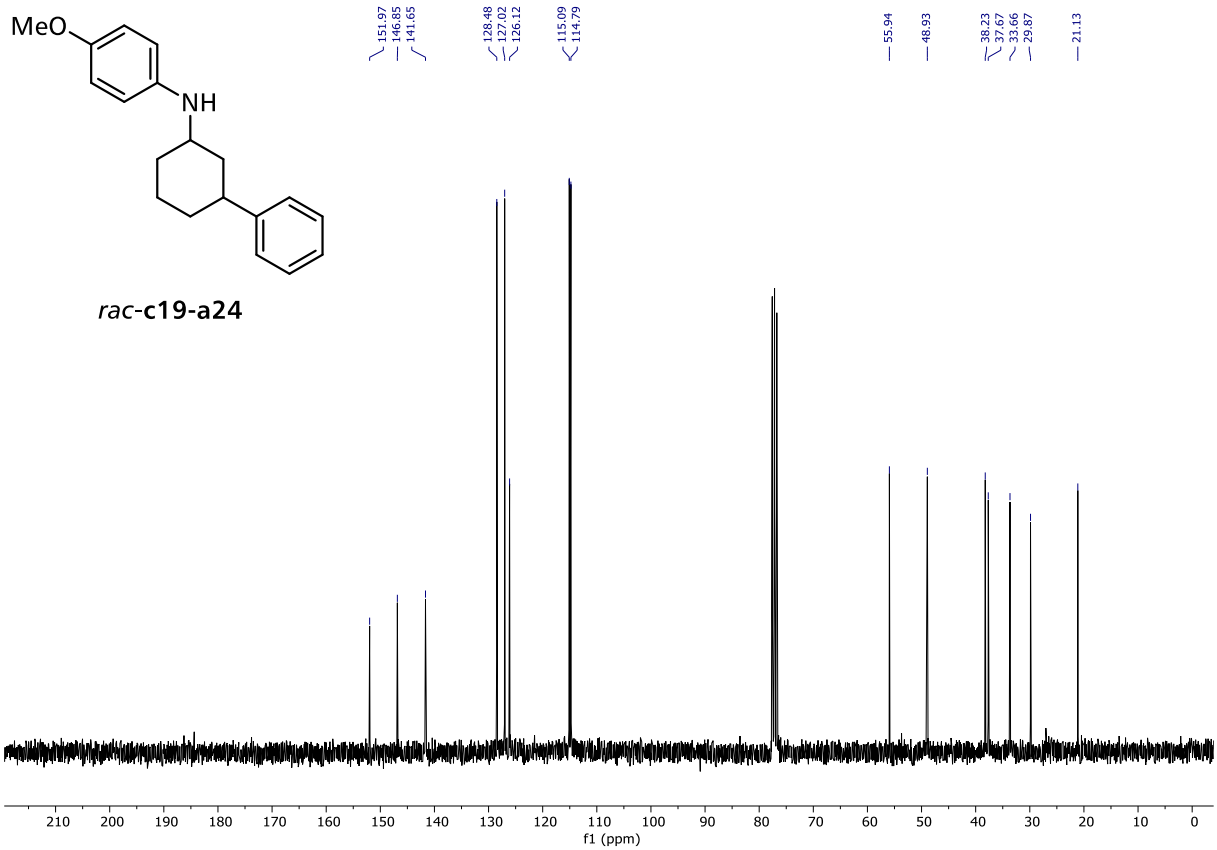


Figure S368. ^{13}C NMR spectrum of *rac*-4-methoxy-*N*-(3-phenylcyclohexyl)aniline (**c19-a24**).

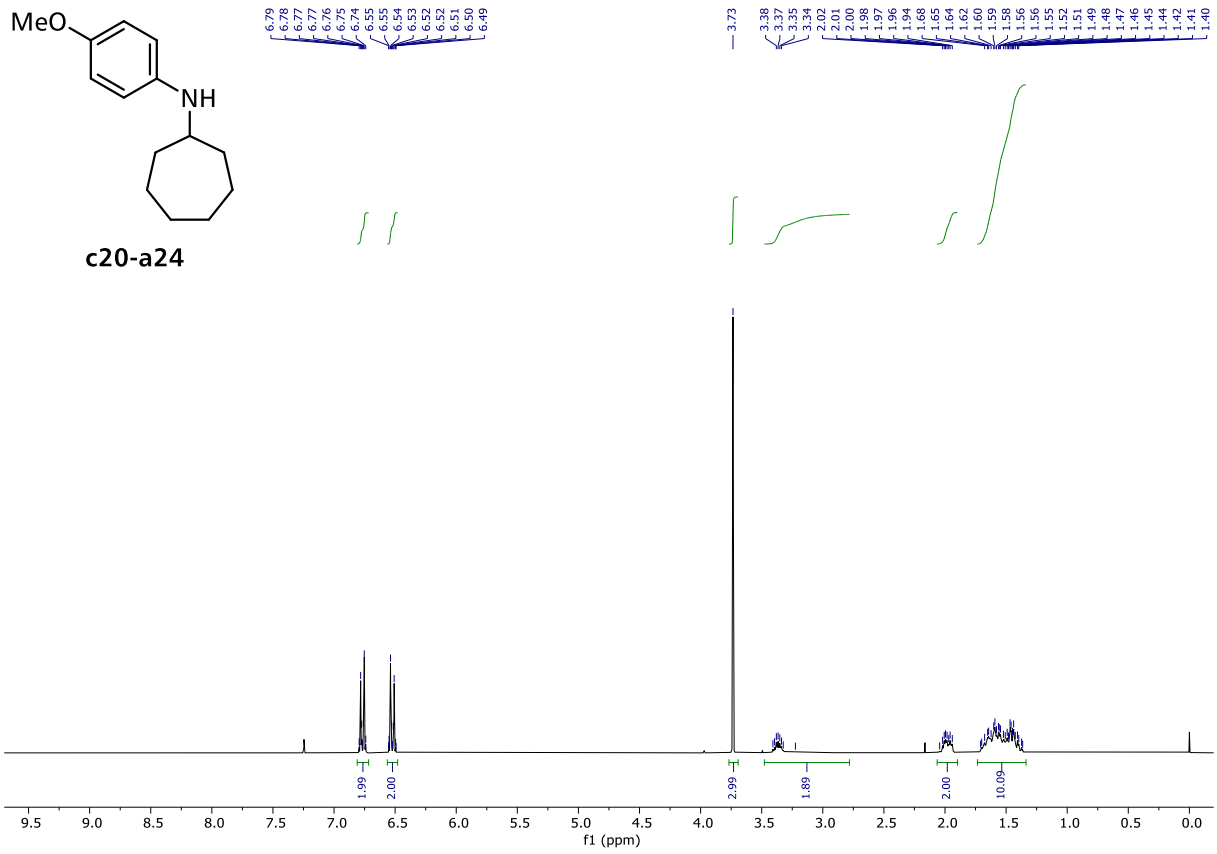


Figure S369. ^{1}H NMR spectrum of *N*-(4-methoxyphenyl)cycloheptanamine (**c20-a24**).

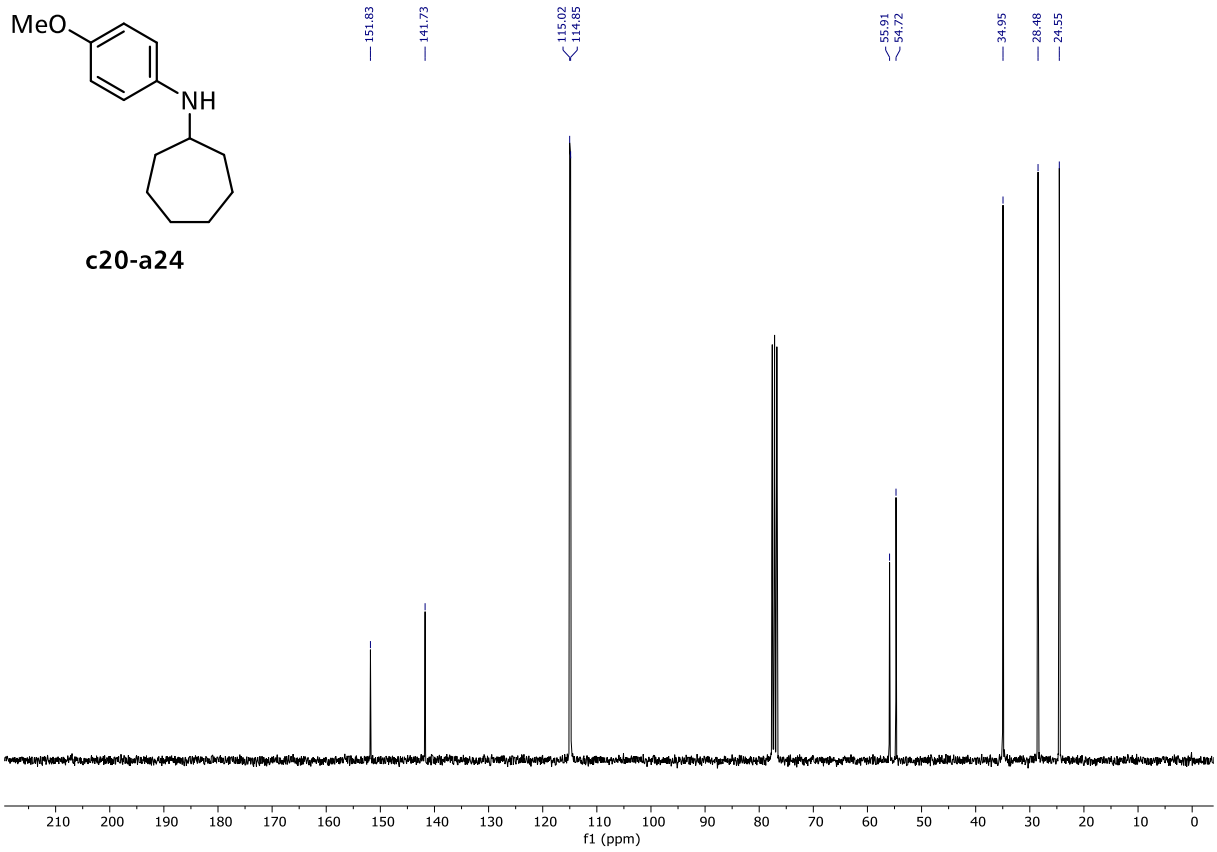


Figure S370. ^{13}C NMR spectrum of *N*-(4-methoxyphenyl)cycloheptanamine (**c20-a24**).

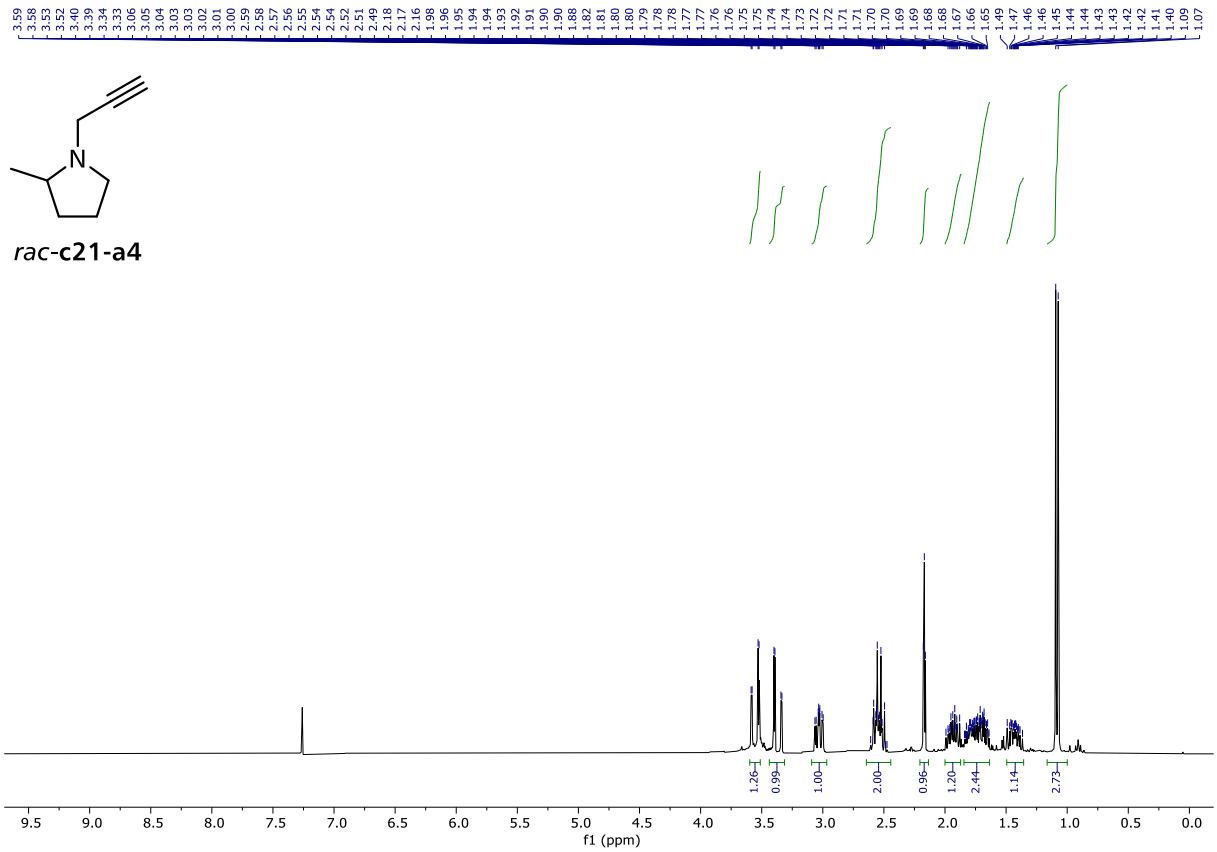


Figure S371. ^{1}H NMR spectrum of *rac*-2-methyl-1-(prop-2-yn-1-yl)pyrrolidine (**c21-a4**).

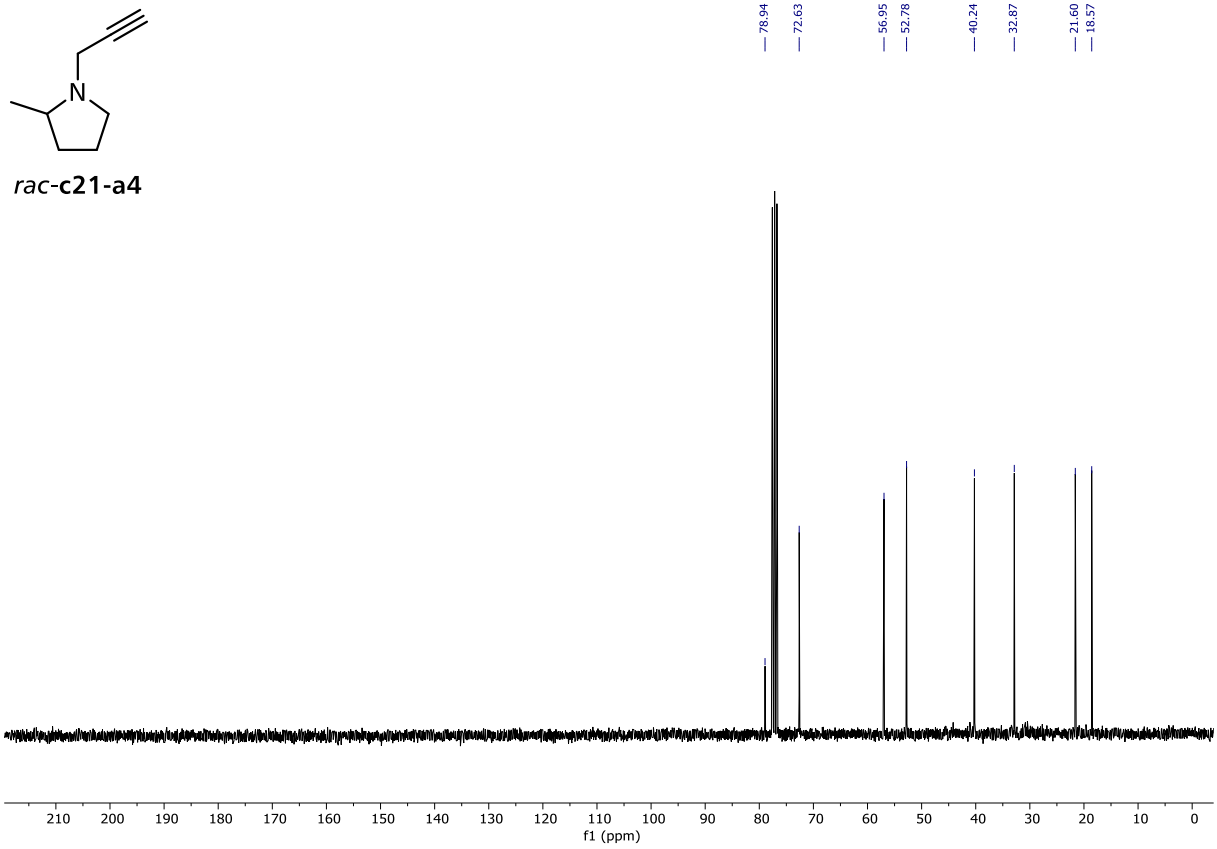


Figure S372. ^{13}C NMR spectrum of *rac*-2-methyl-1-(prop-2-yn-1-yl)pyrrolidine (**c21-a4**).

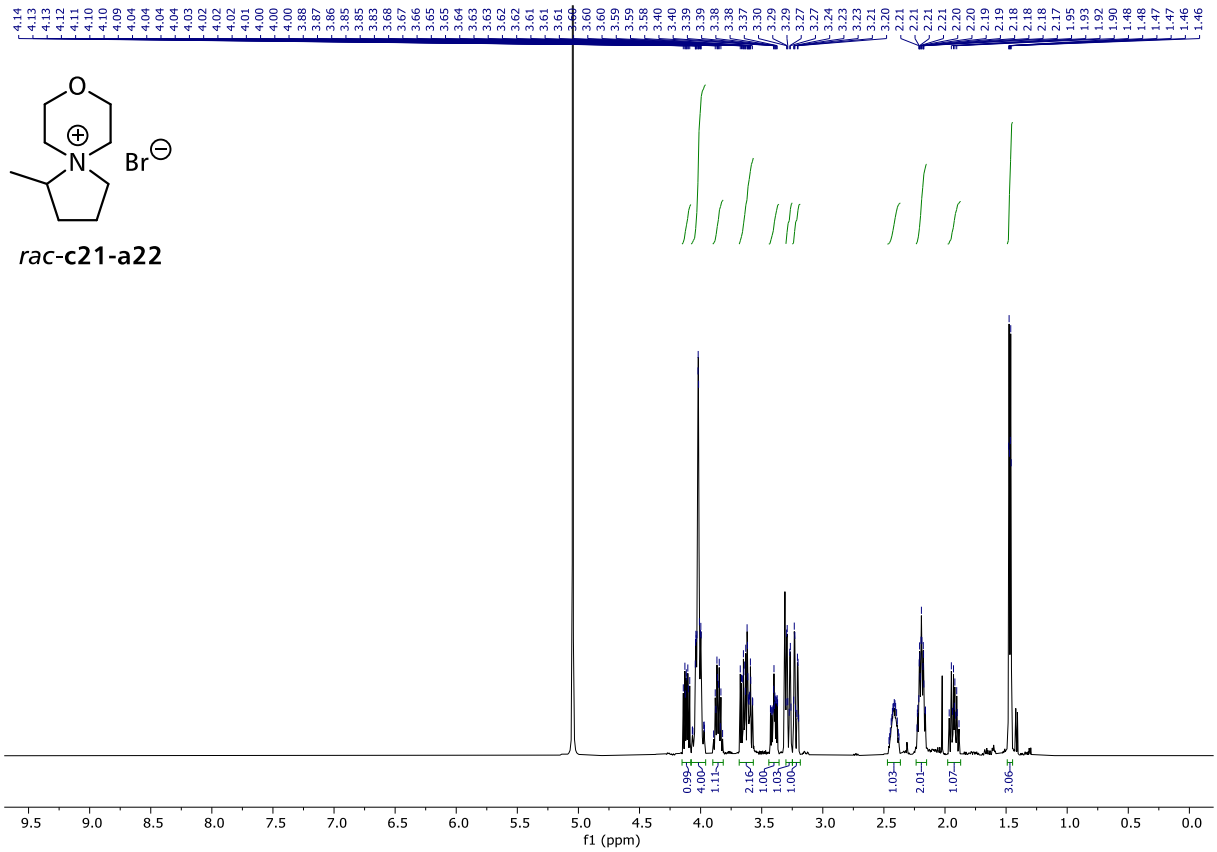


Figure S373. ^{1}H NMR spectrum of *rac*-1-methyl-8-oxa-5-azaspiro[4.5]decan-5-ium bromide (**c21-a22**).

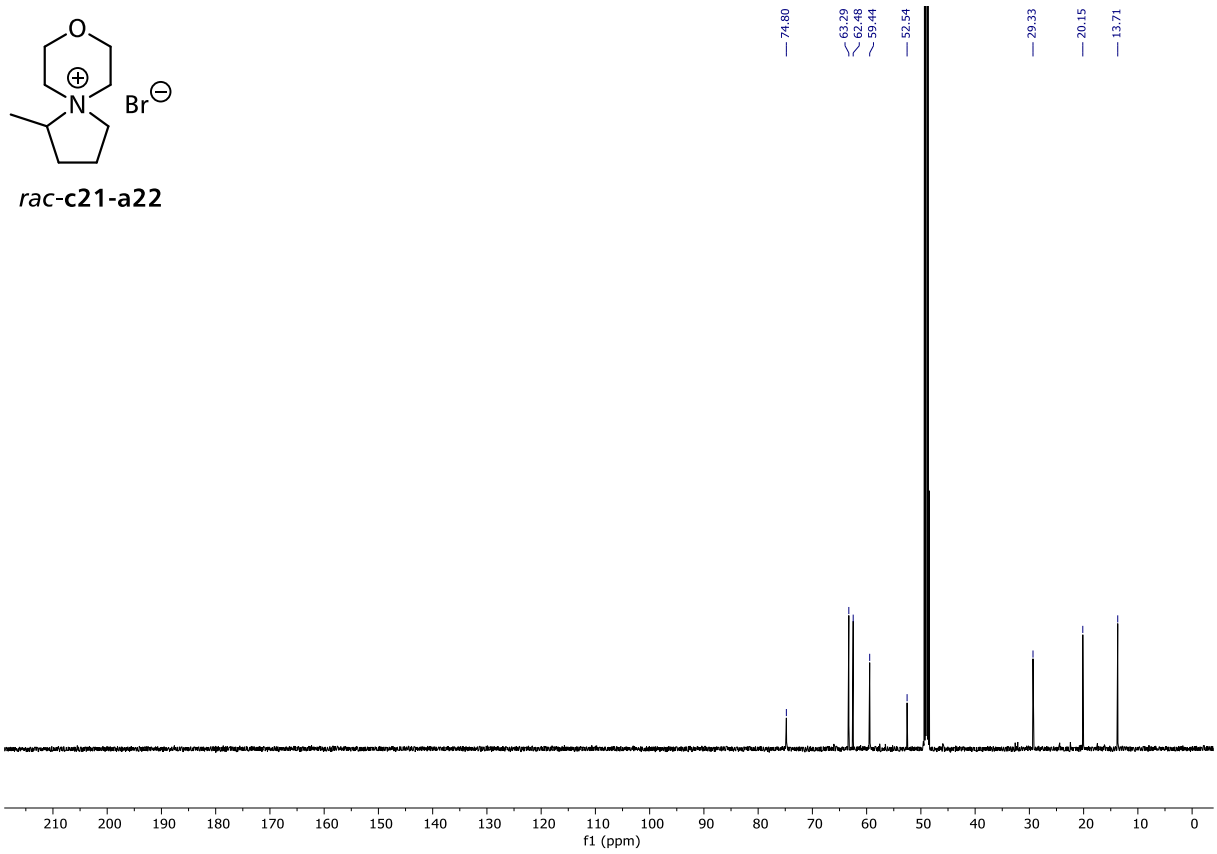


Figure S374. ^{13}C NMR spectrum of *rac*-1-methyl-8-oxa-5-azaspiro[4.5]decan-5-ium bromide (**c21-a22**).

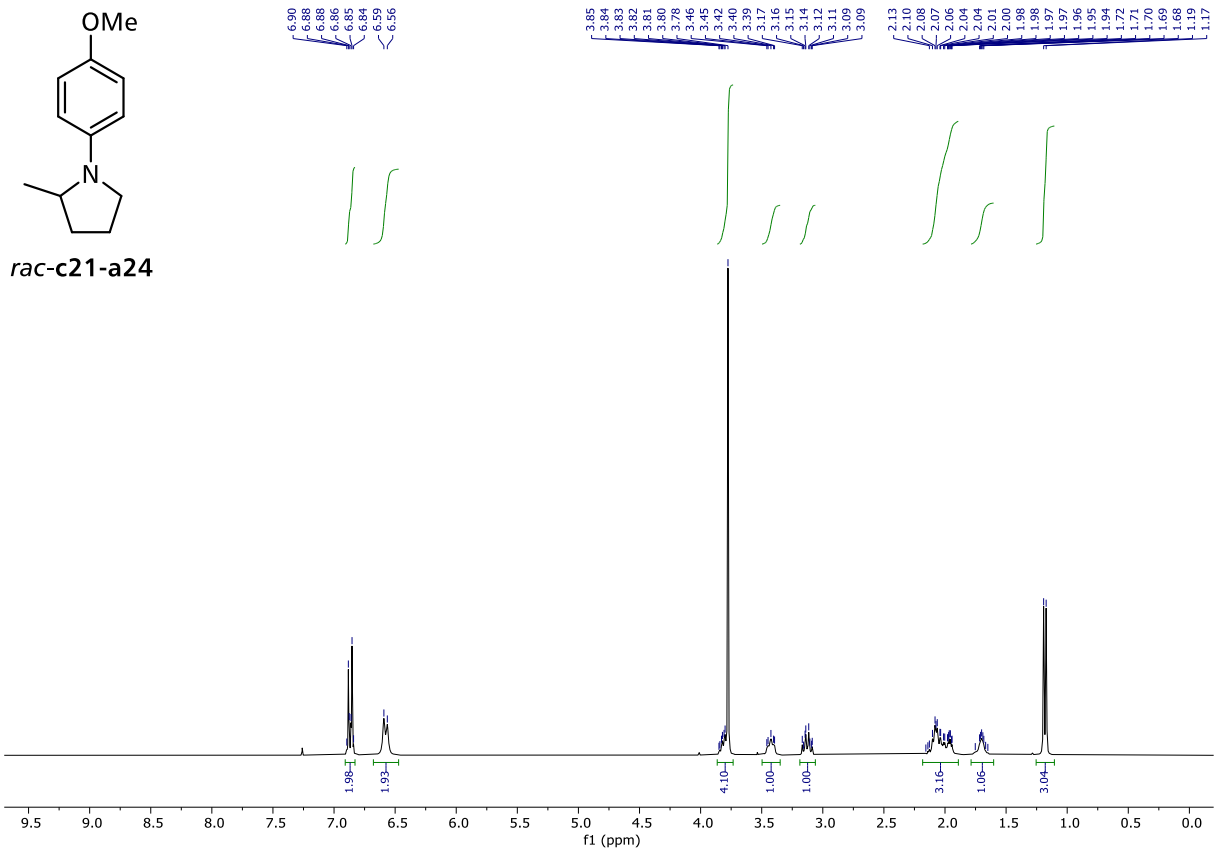


Figure S375. ^{1}H NMR spectrum of *rac*-1-(4-methoxyphenyl)-2-methylpyrrolidine (**c21-a24**).

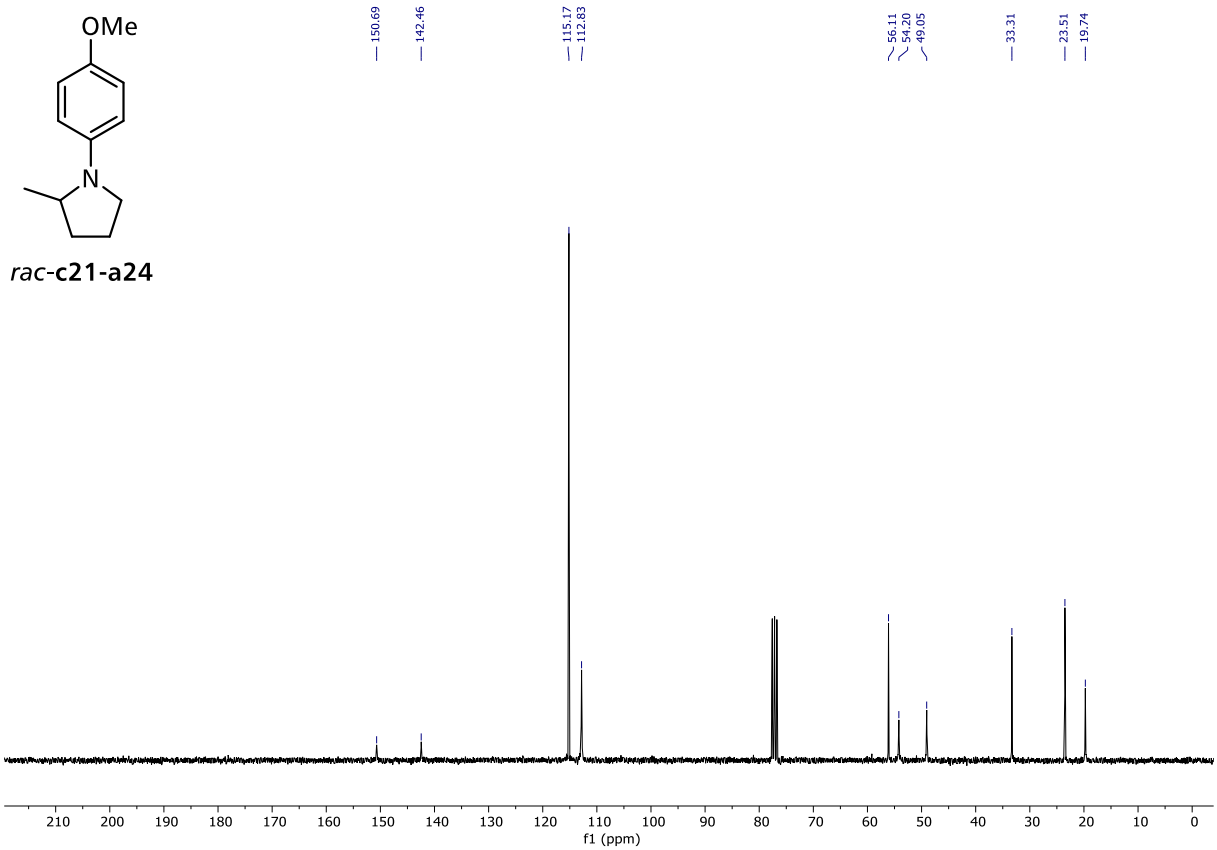


Figure S376. ^{13}C NMR spectrum of *rac*-1-(4-methoxyphenyl)-2-methylpyrrolidine (**c21-a24**).

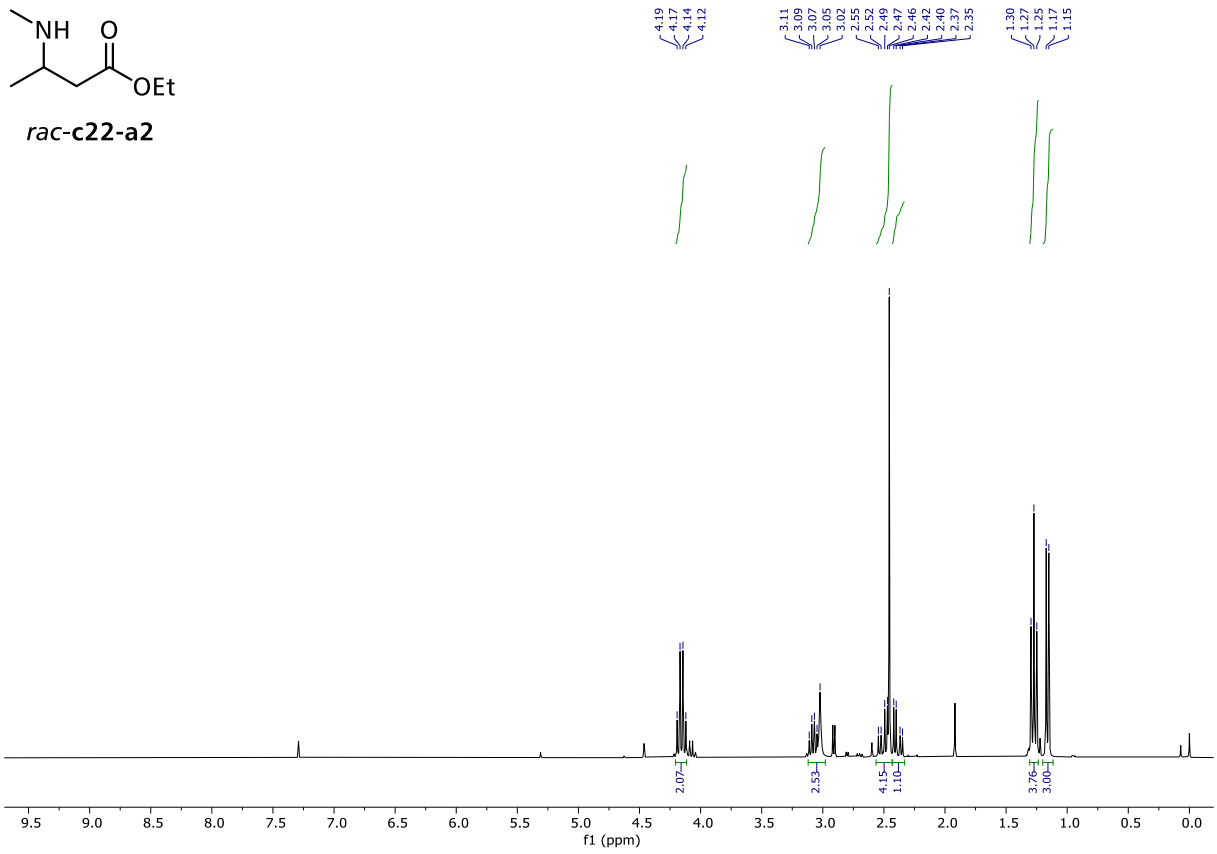


Figure S377. ^{1}H NMR spectrum of ethyl *rac*-3-(methylamino)butanoate (**c22-a2**).

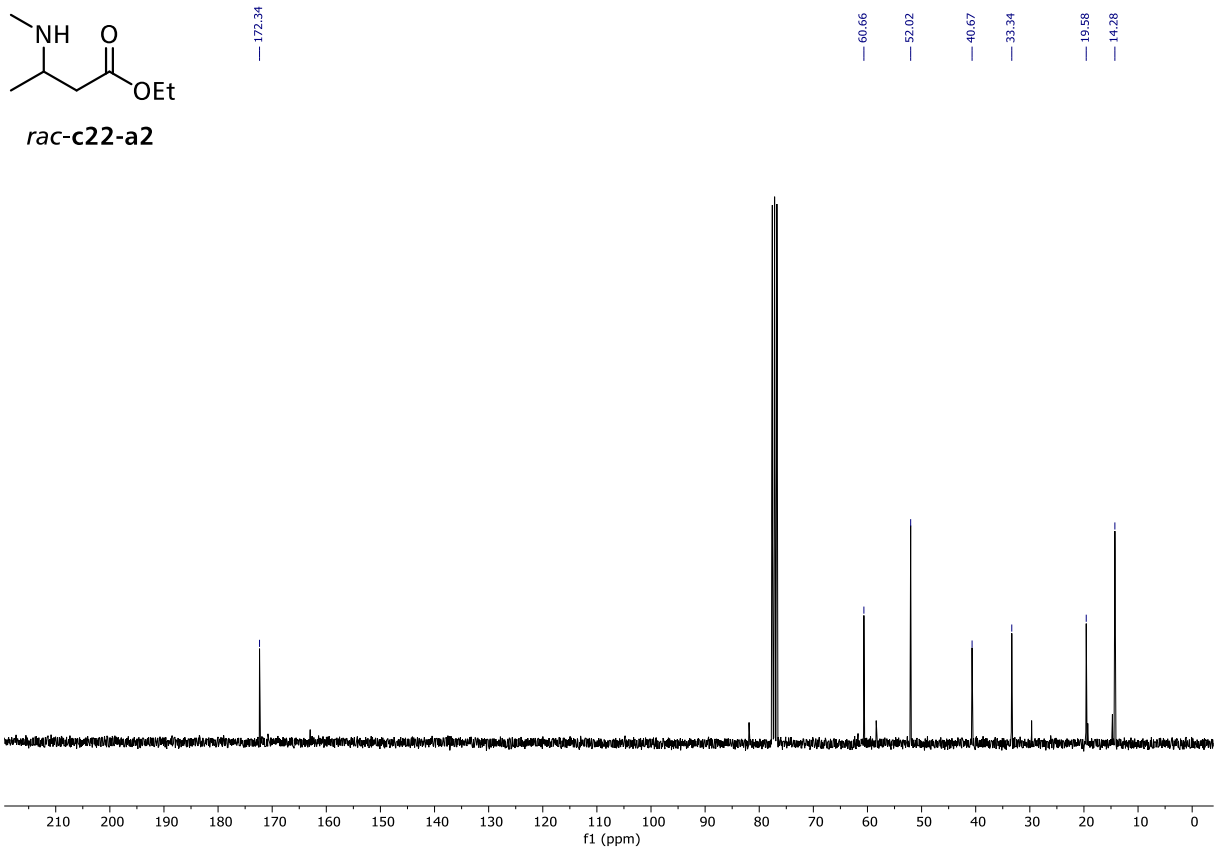


Figure S378. ^{13}C NMR spectrum of ethyl *rac*-3-(methylamino)butanoate (**c22-a2**).

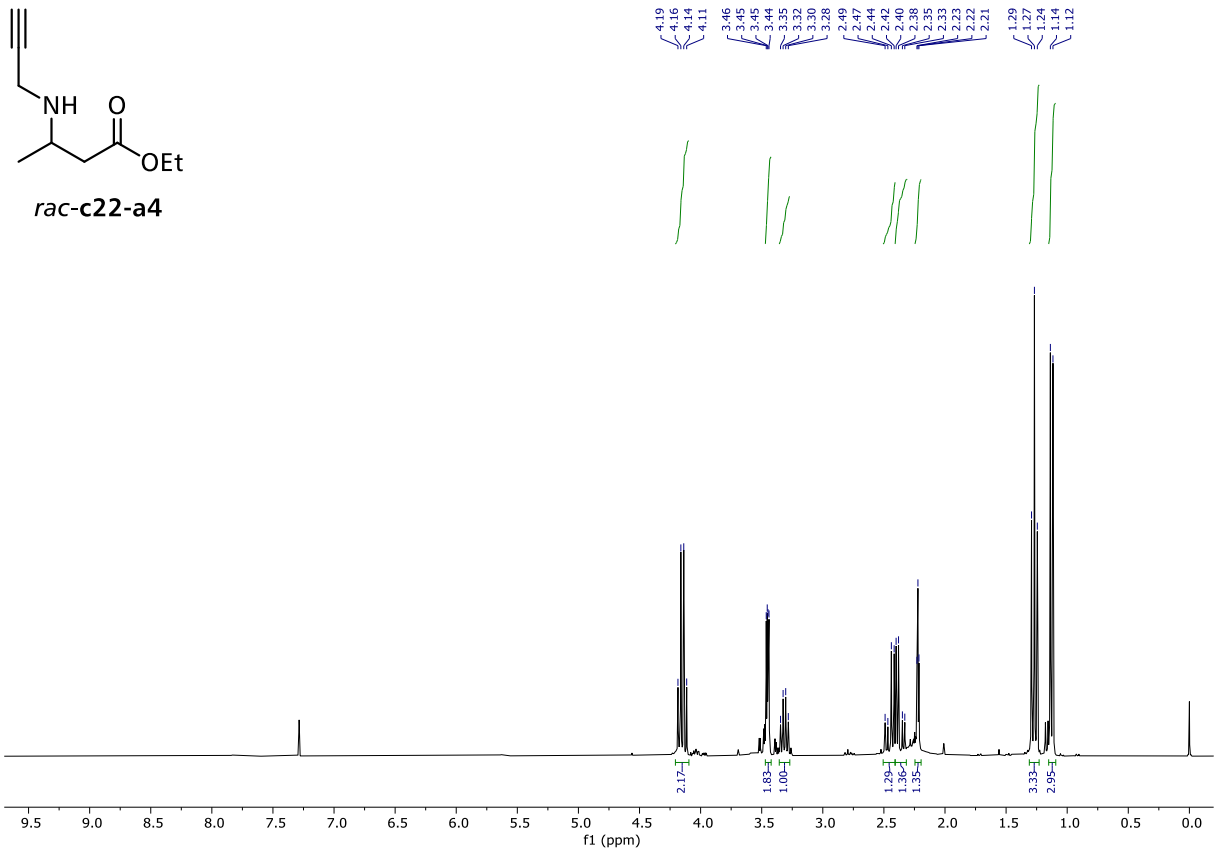


Figure S379. ^{1}H NMR spectrum of ethyl *rac*-3-(prop-2-yn-1-ylamino)butanoate (**c22-a4**).

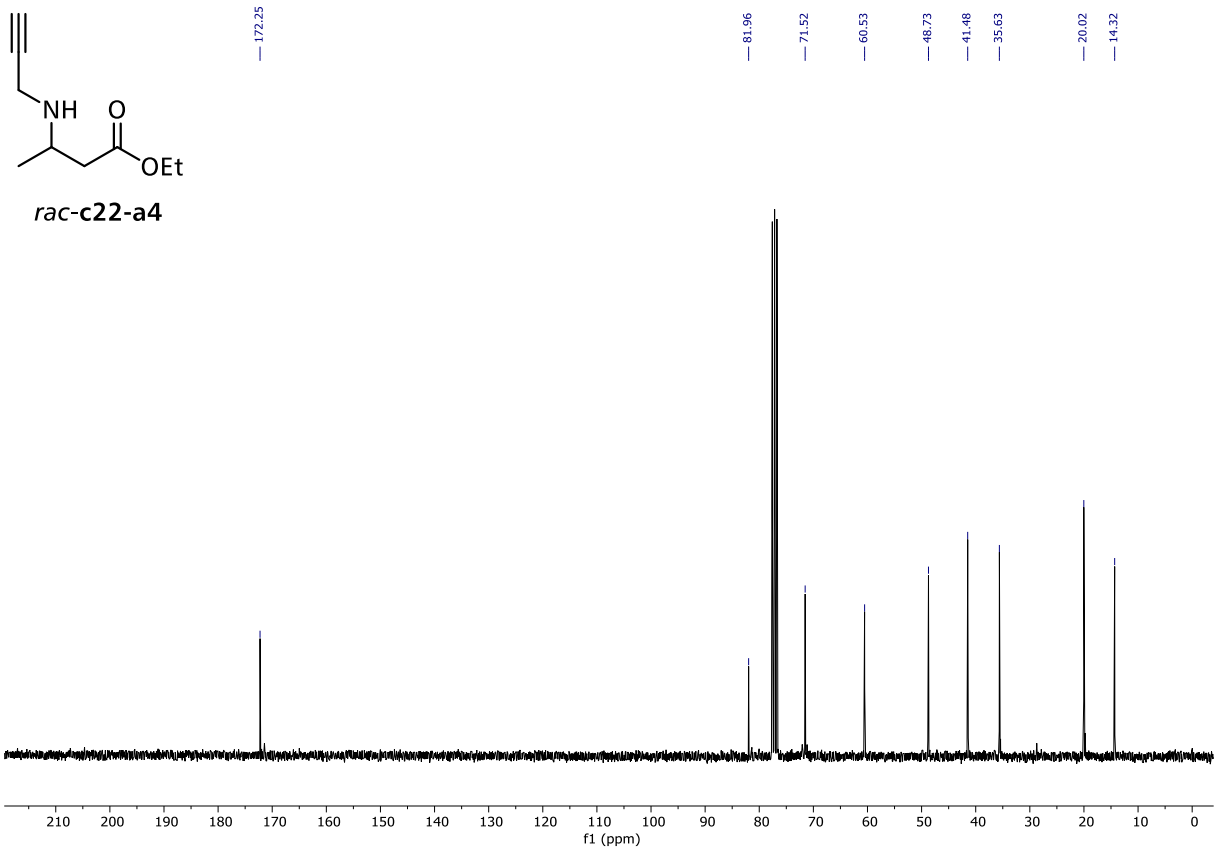
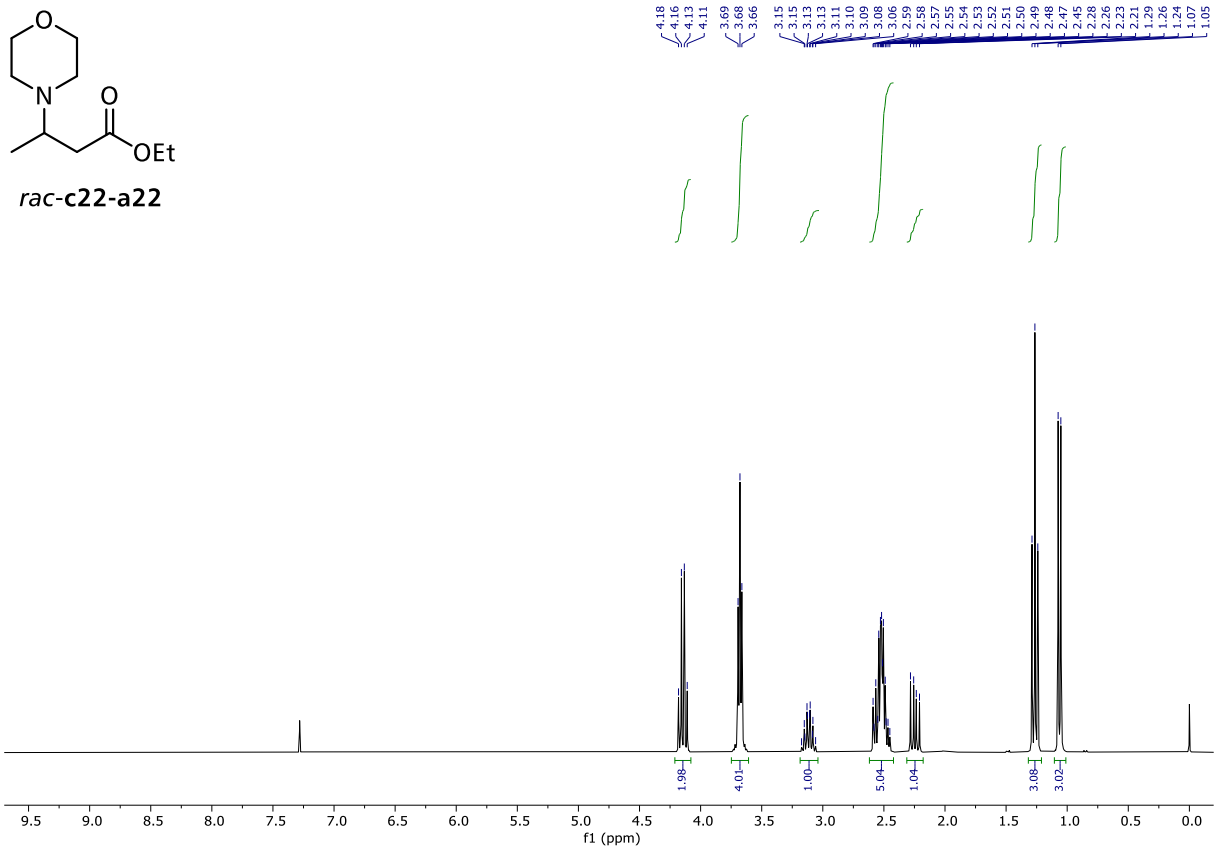
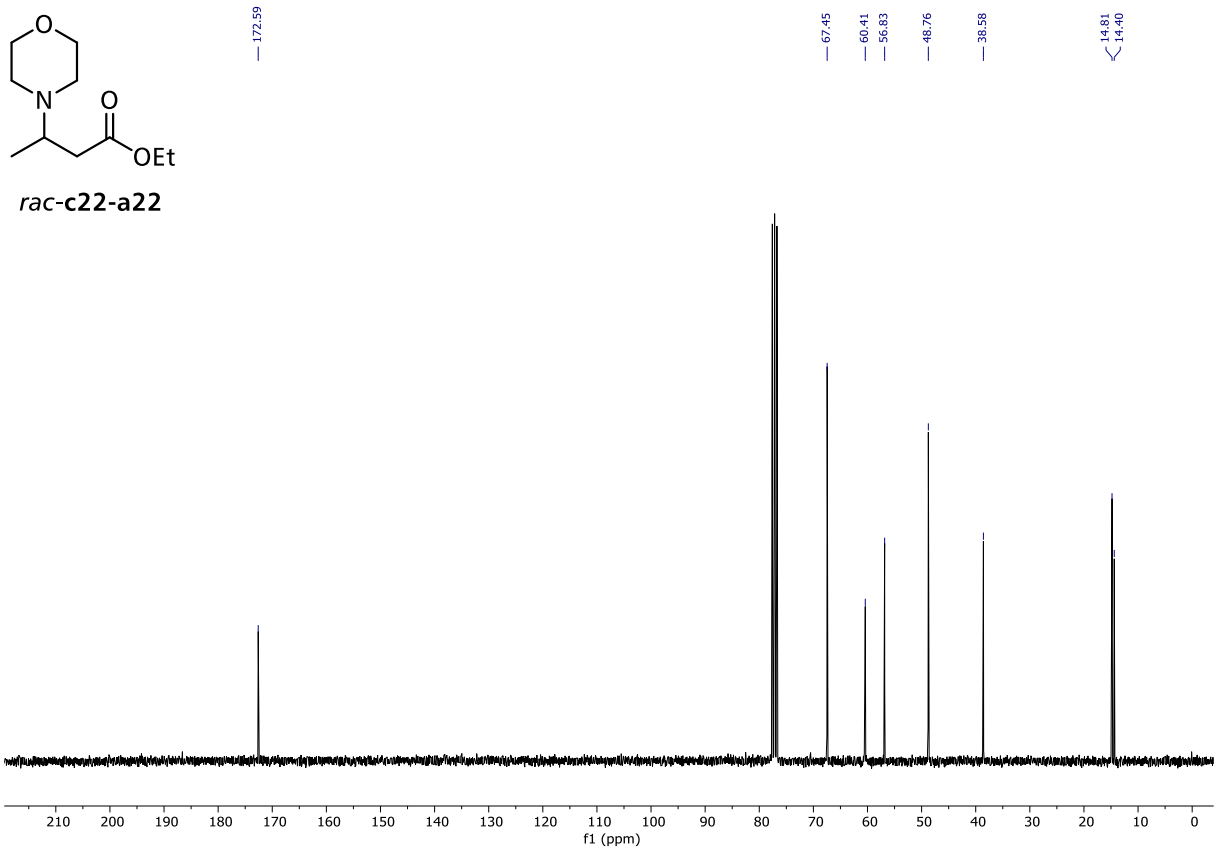


Figure S380. ^{13}C NMR spectrum of ethyl *rac*-3-(prop-2-yn-1-ylamino)butanoate (**c22-a4**).



rac-**c22-a22**

Figure S381. ^{1}H NMR spectrum of ethyl *rac*-3-morpholinobutanoate (**c22-a22**).



rac-**c22-a22**

Figure S382. ^{13}C NMR spectrum of ethyl *rac*-3-morpholinobutanoate (**c22-a22**).

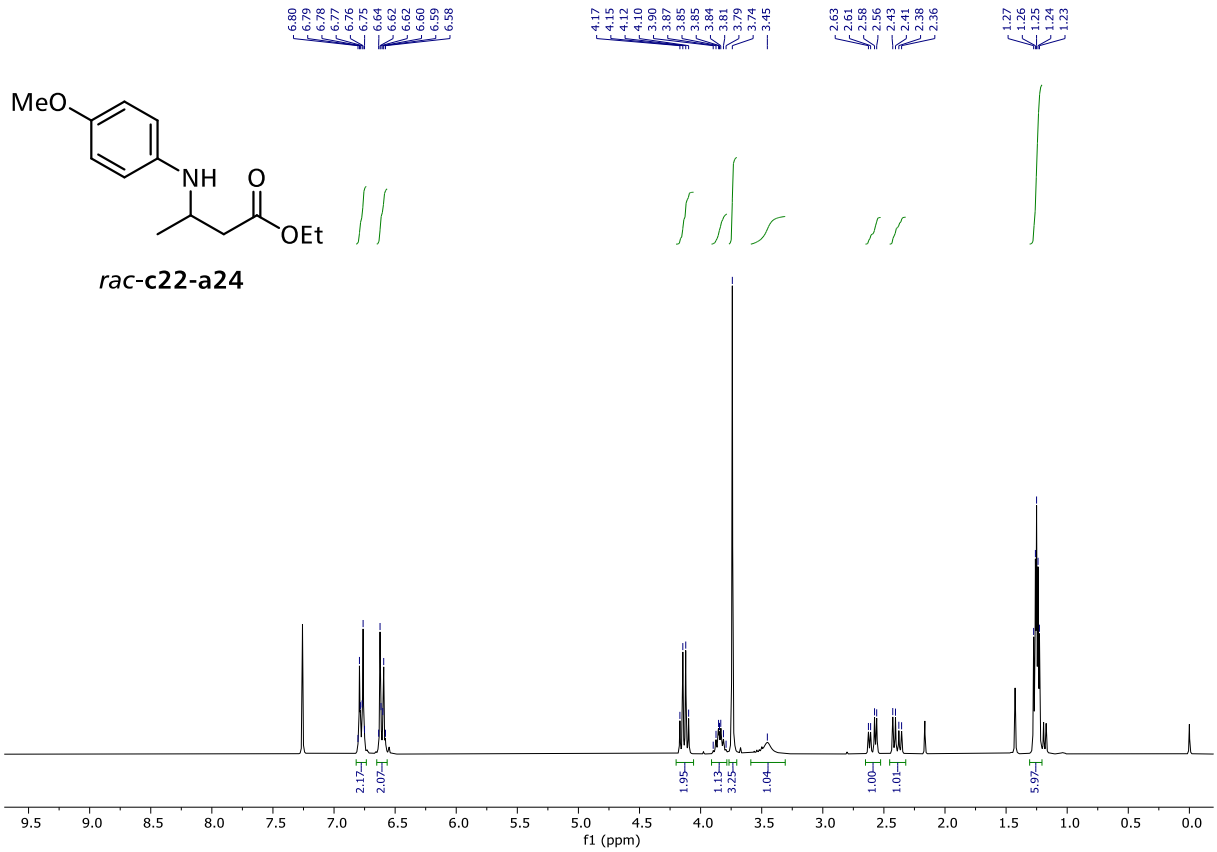


Figure S383. ^{1}H NMR spectrum of ethyl *rac*-3-((4-methoxyphenyl)amino)butanoate (**c22-a24**).

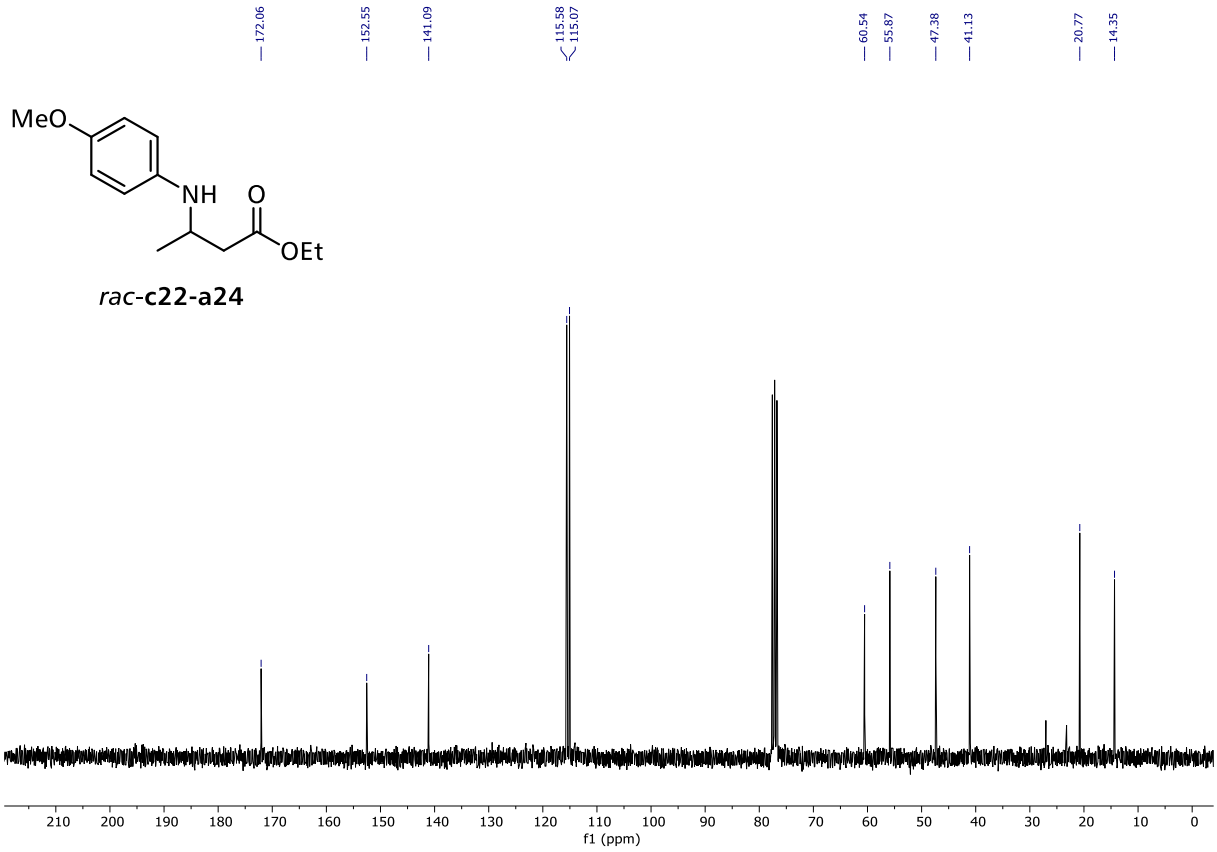


Figure S384. ^{13}C NMR spectrum of ethyl *rac*-3-((4-methoxyphenyl)amino)butanoate (**c22-a24**).

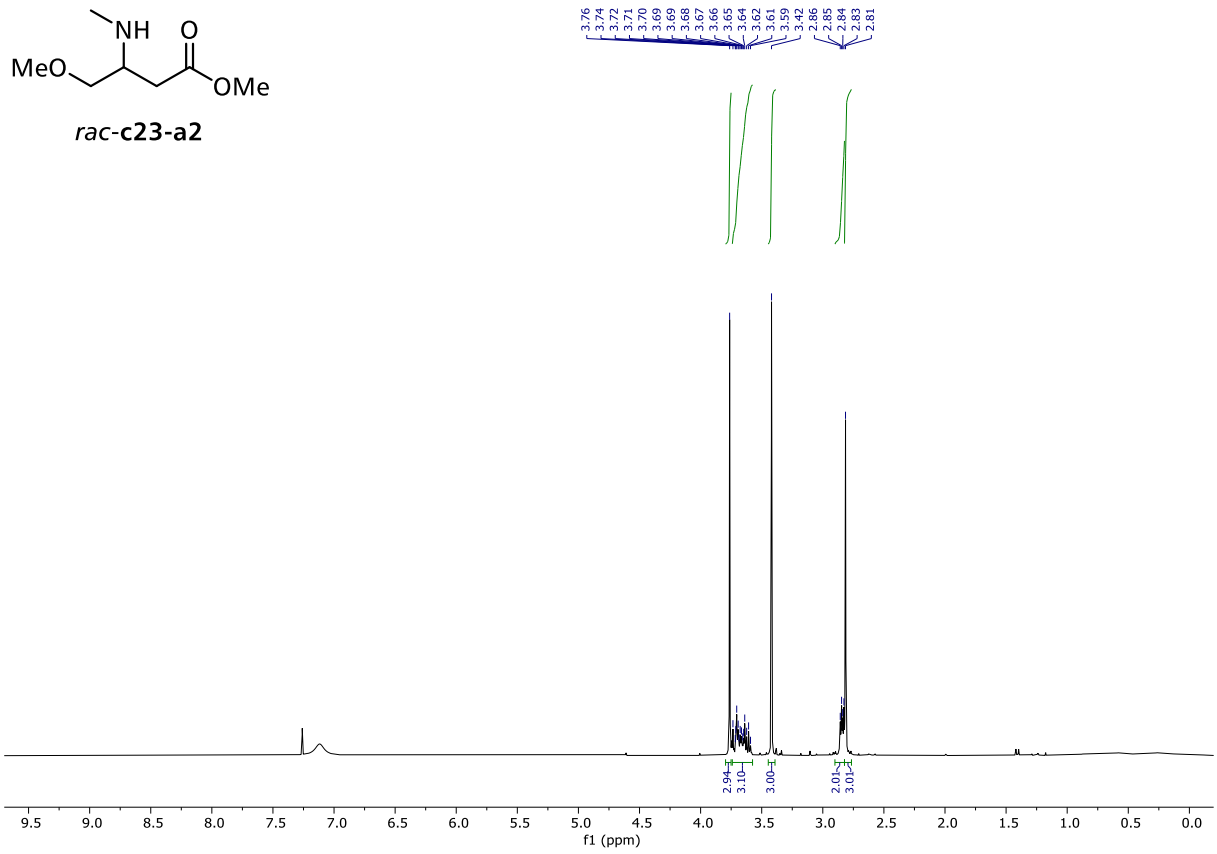


Figure S385. ^{1}H NMR spectrum of methyl *rac*-4-methoxy-3-(methylamino)butanoate (**c23-a2**).

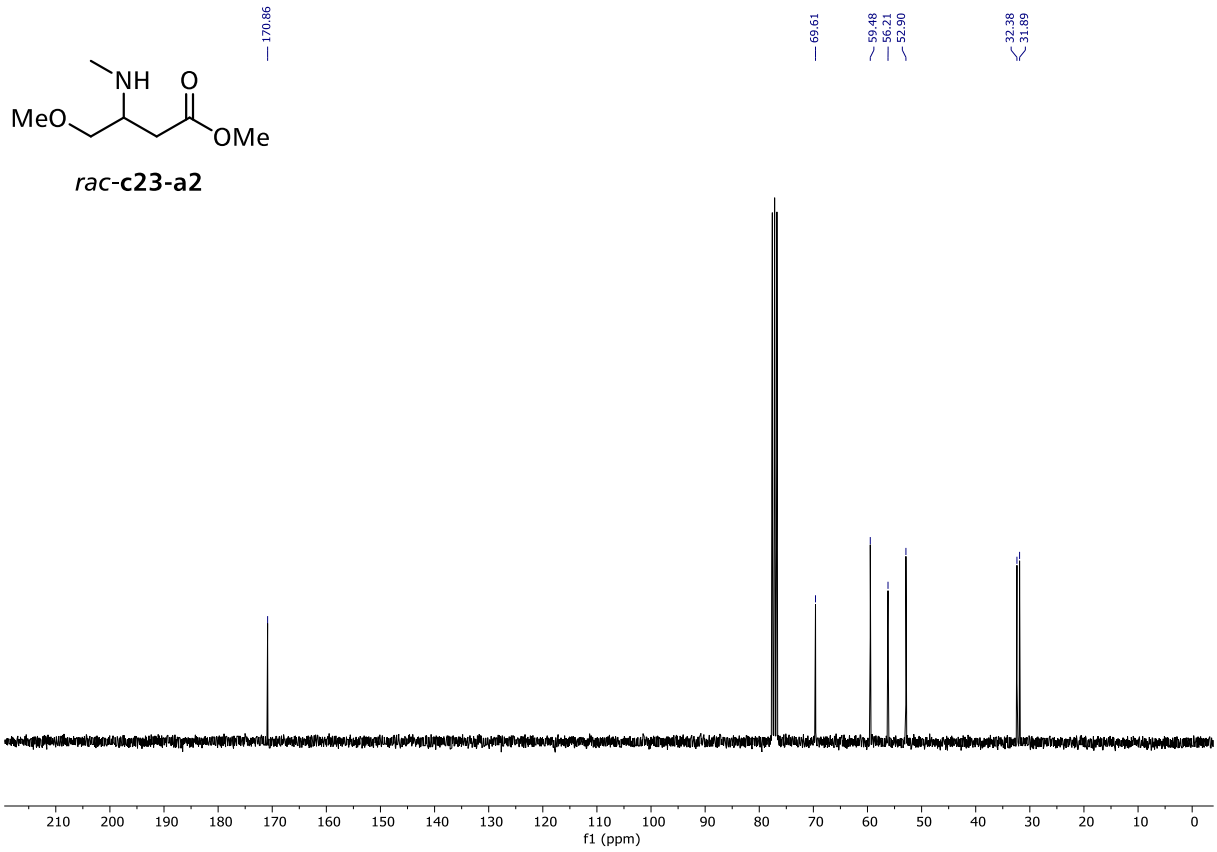


Figure S386. ^{13}C NMR spectrum of methyl *rac*-4-methoxy-3-(methylamino)butanoate (**c23-a2**).

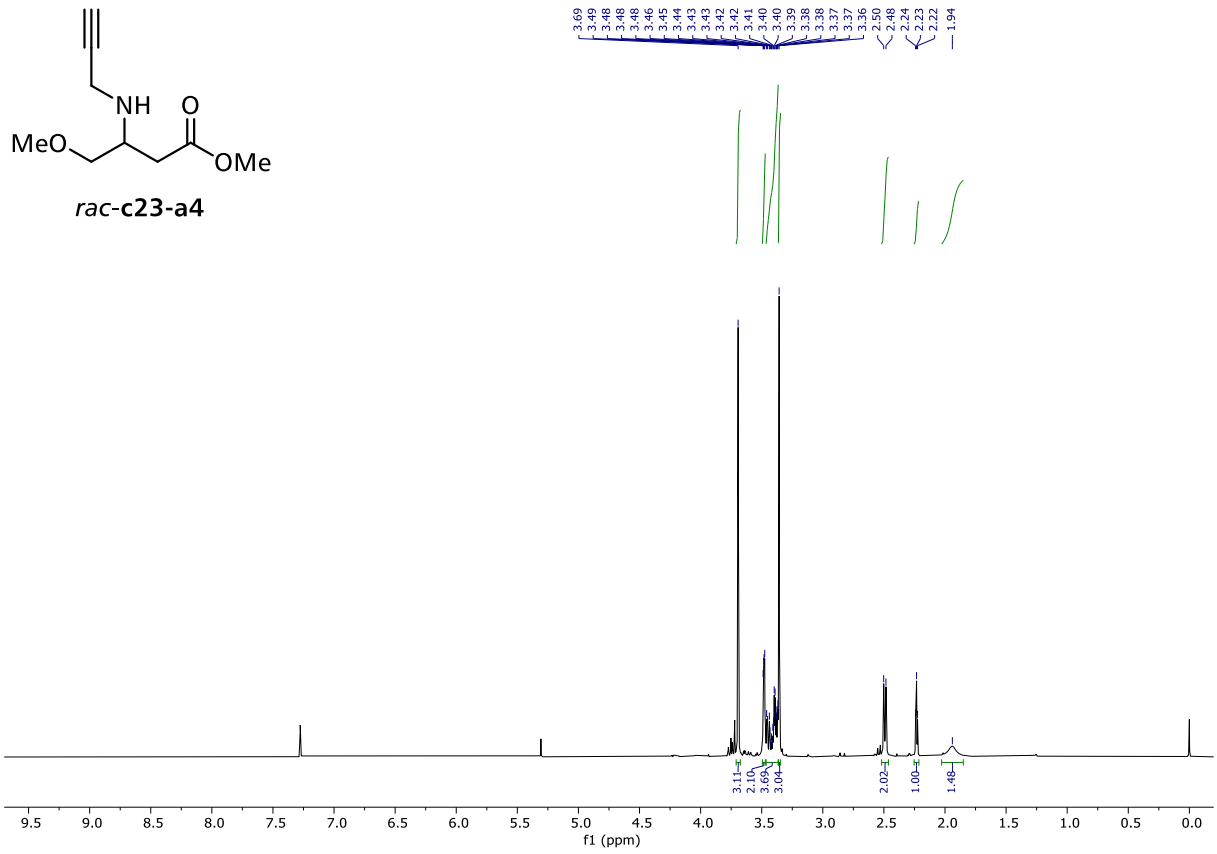


Figure S387. ^{1}H NMR spectrum of methyl *rac*-4-methoxy-3-(prop-2-yn-1-ylamino)butanoate (**c23-a4**).

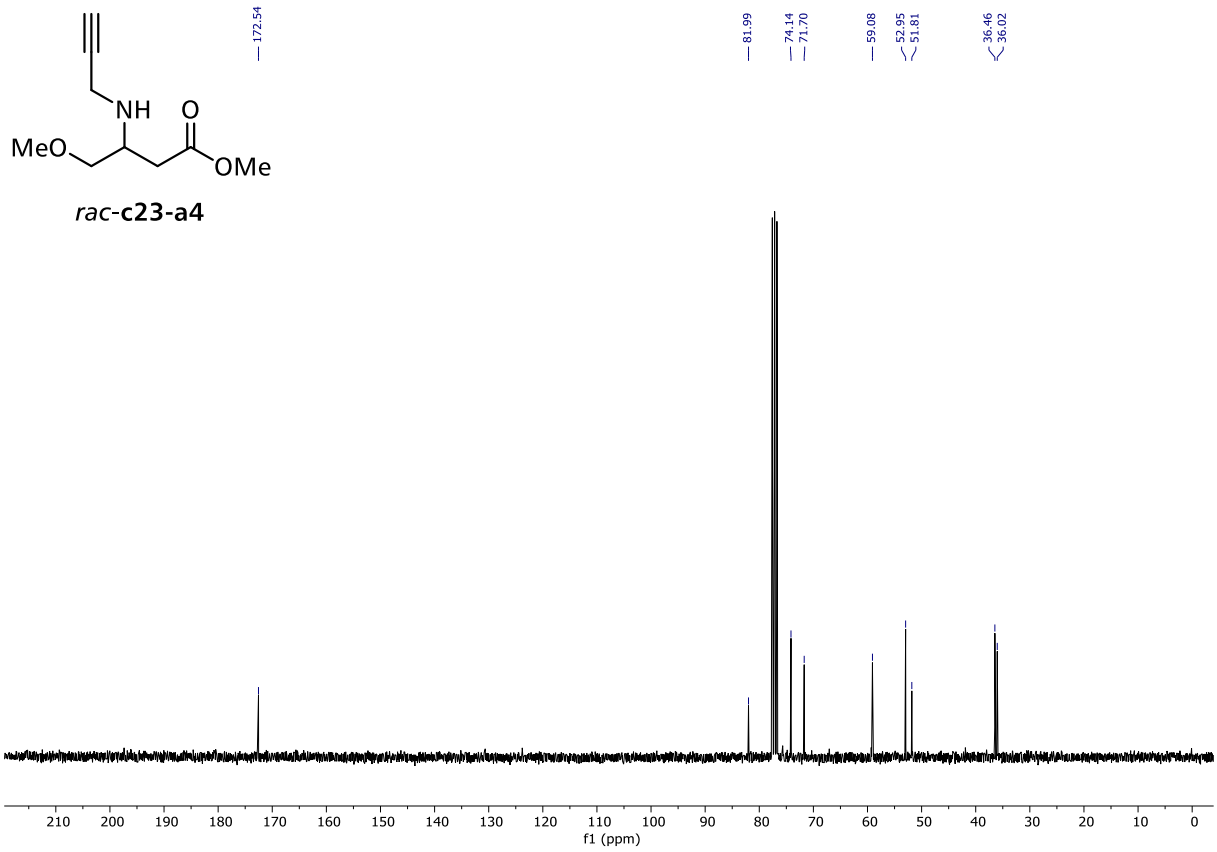


Figure S388. ^{13}C NMR spectrum of methyl *rac*-4-methoxy-3-(prop-2-yn-1-ylamino)butanoate (**c23-a4**).

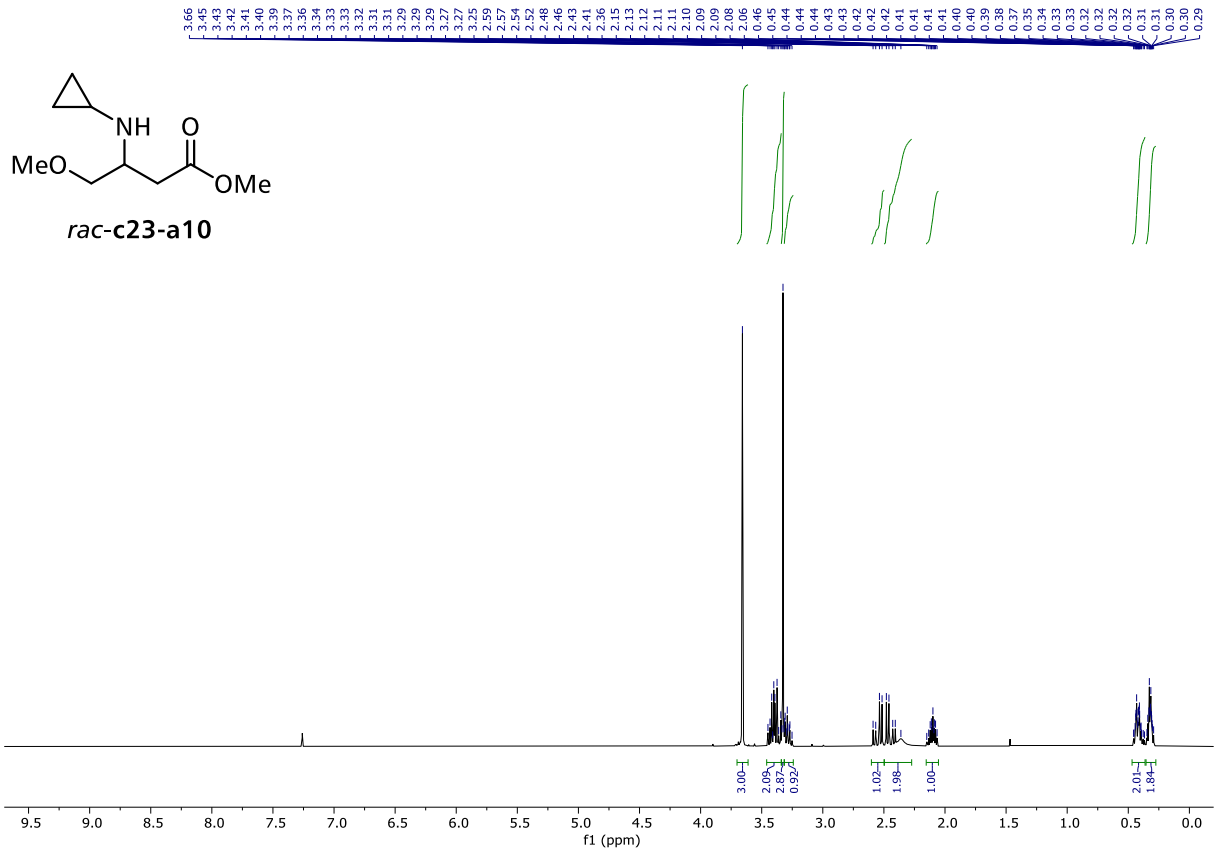


Figure S389. ^{1}H NMR spectrum of methyl *rac*-3-(cyclopropylamino)-4-methoxybutanoate (**c23-a10**).

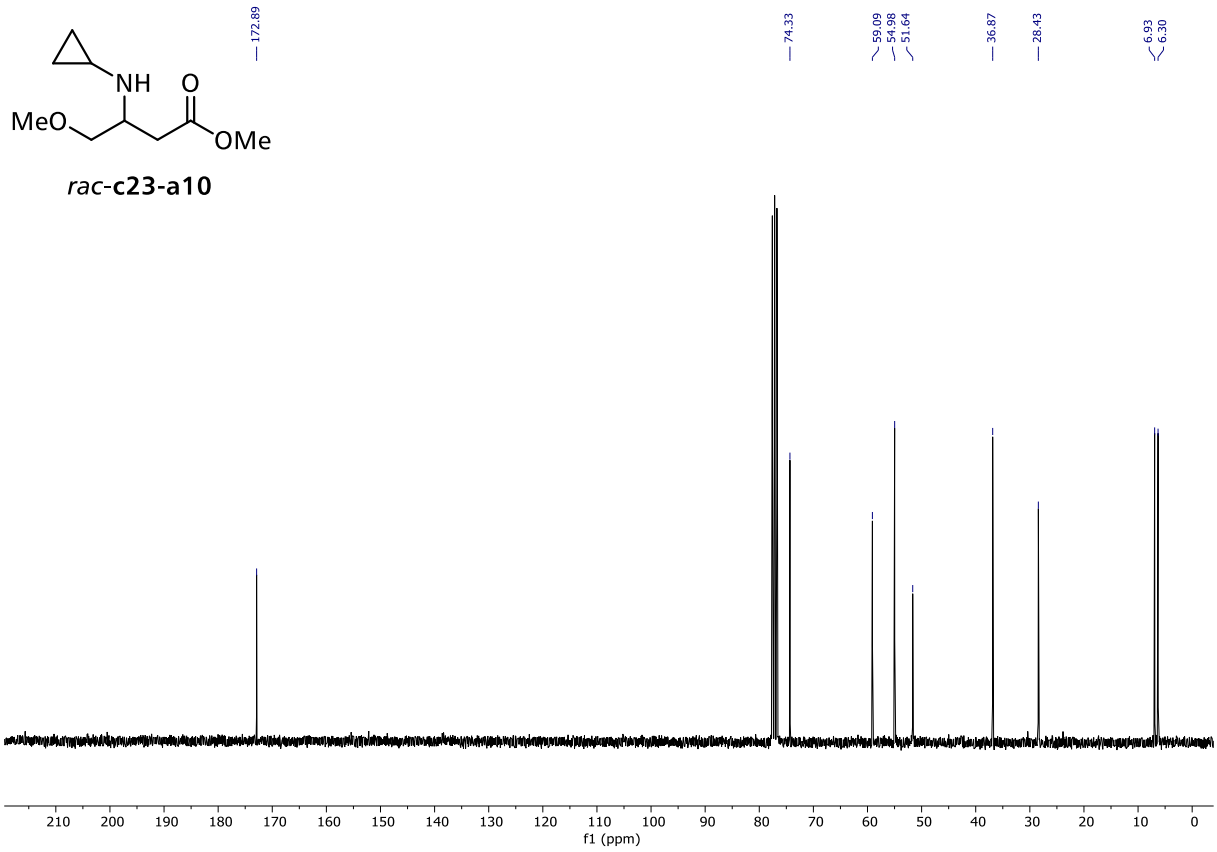


Figure S390. ^{13}C NMR spectrum of methyl *rac*-3-(cyclopropylamino)-4-methoxybutanoate (**c23-a10**).

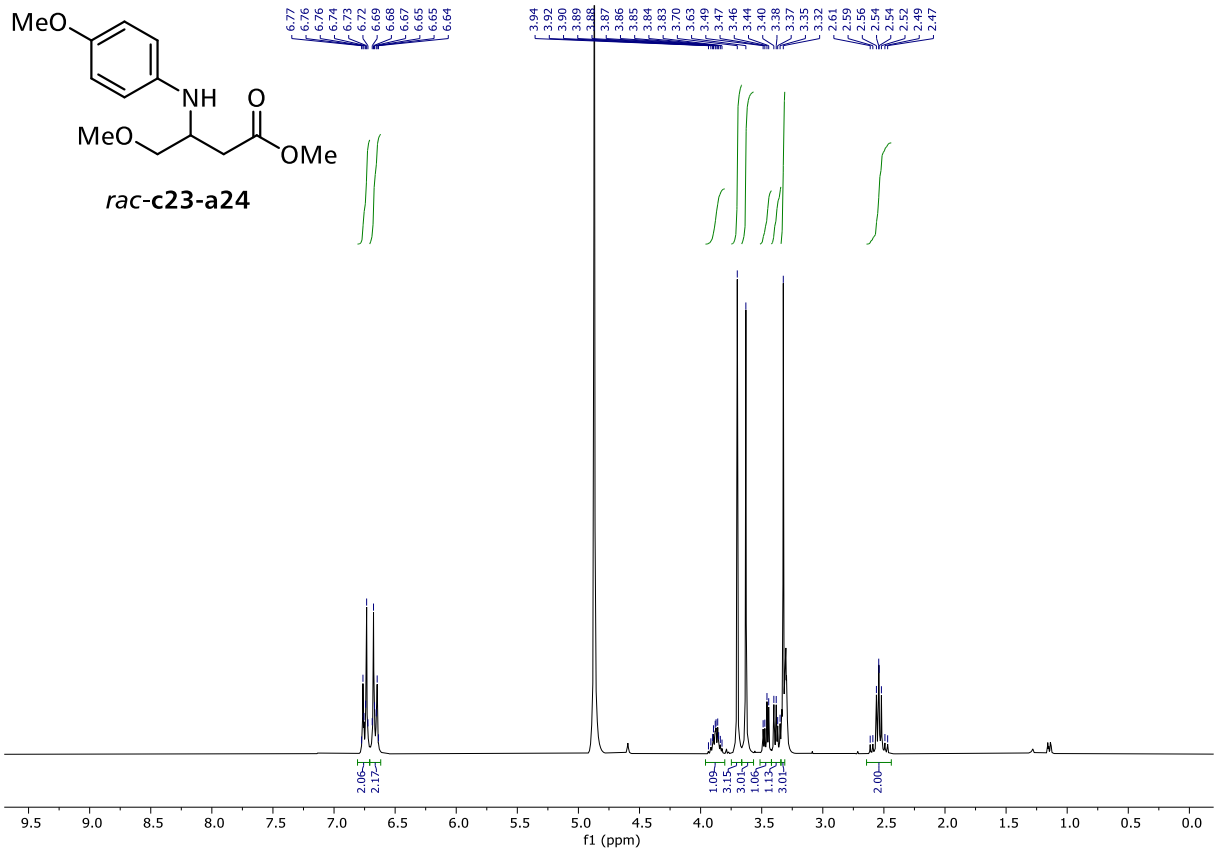


Figure S391. ^{1}H NMR spectrum of methyl *rac*-4-methoxy-3-((4-methoxyphenyl)amino)butanoate (**c23-a24**).

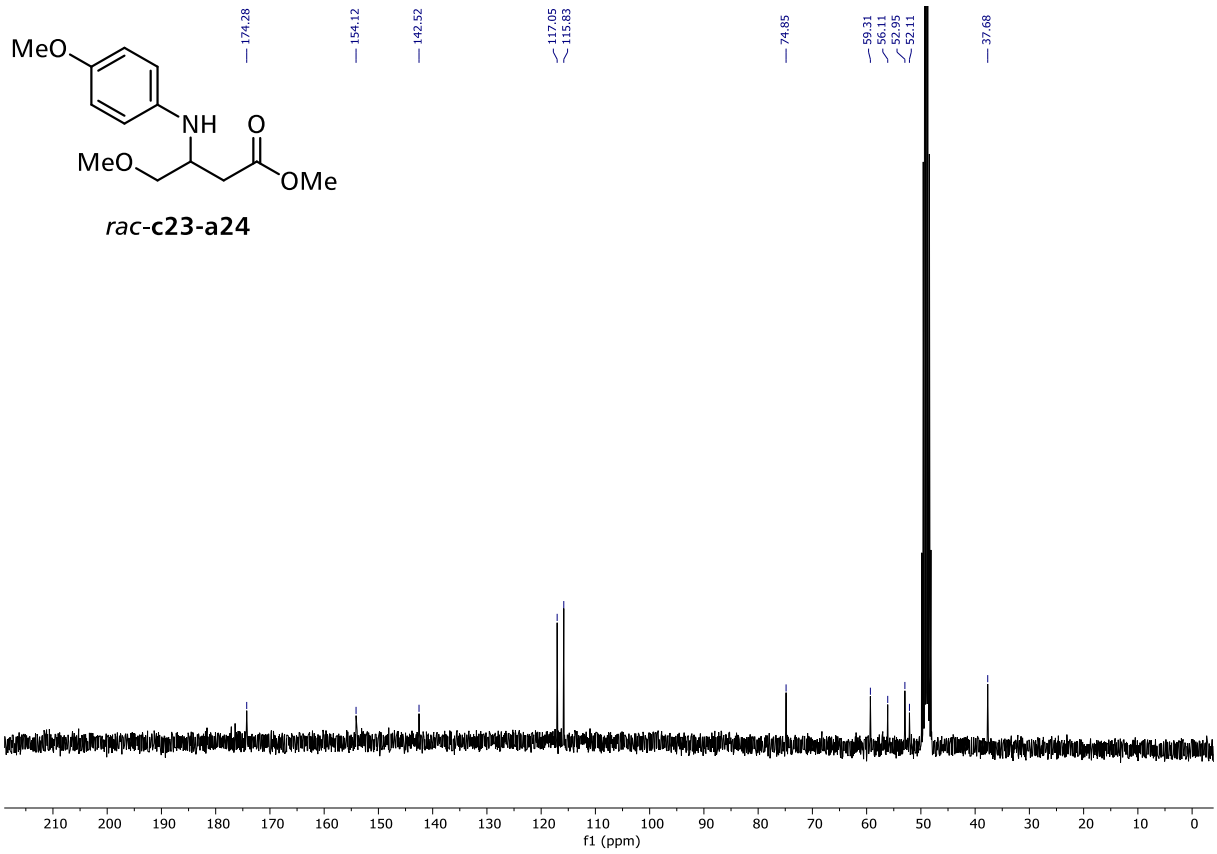


Figure S392. ^{13}C NMR spectrum of methyl *rac*-4-methoxy-3-((4-methoxyphenyl)amino)butanoate (**c23-a24**).

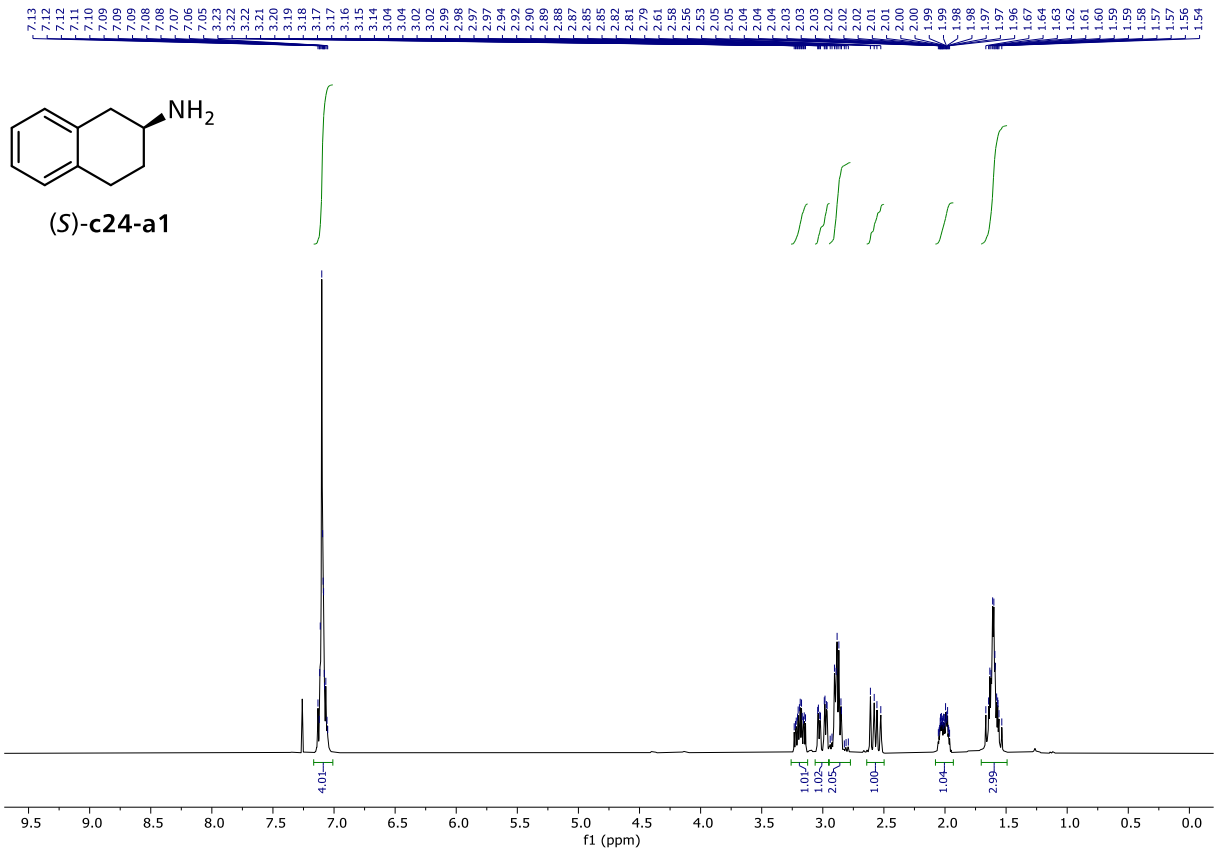


Figure S393. ^{1}H NMR spectrum of (*S*)-1,2,3,4-tetrahydronaphthalen-2-amine (**c24-a1**).

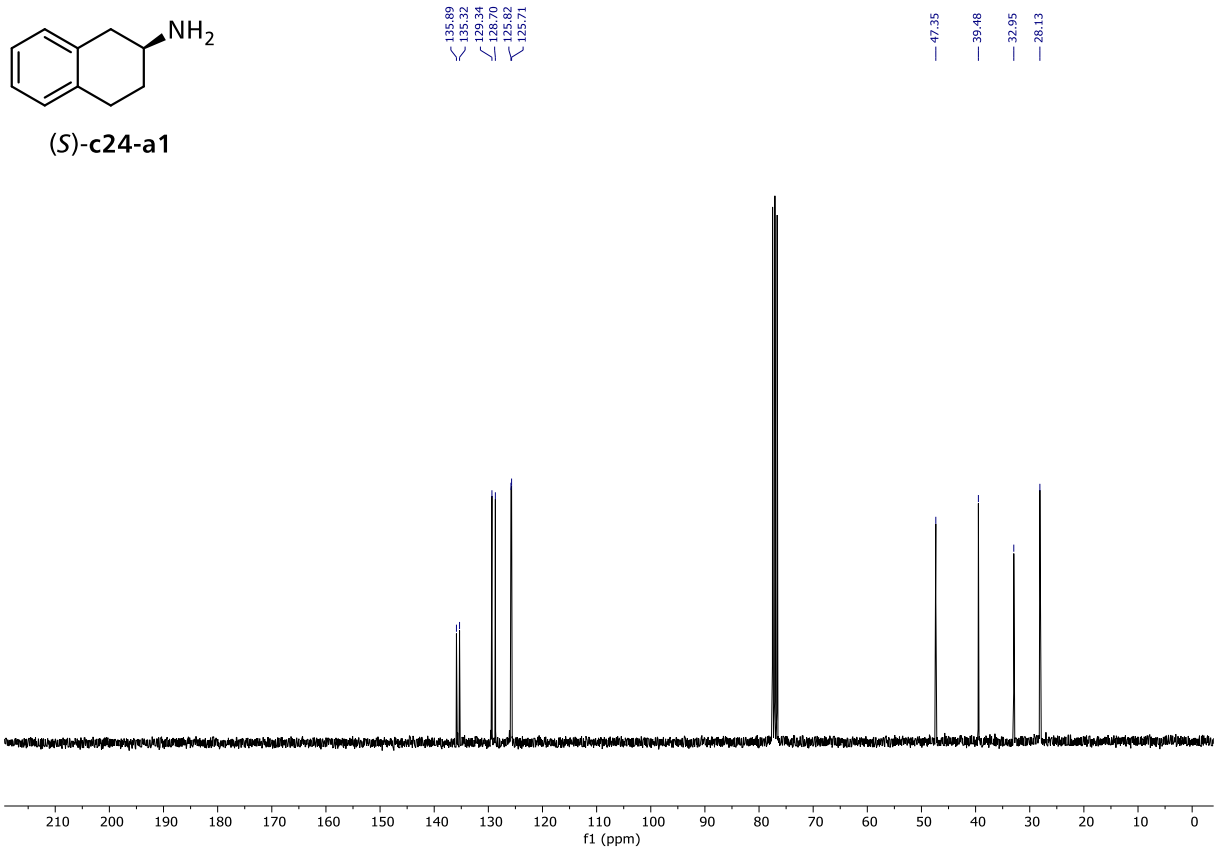


Figure S394. ^{13}C NMR spectrum of (*S*)-1,2,3,4-tetrahydronaphthalen-2-amine (**c24-a1**).

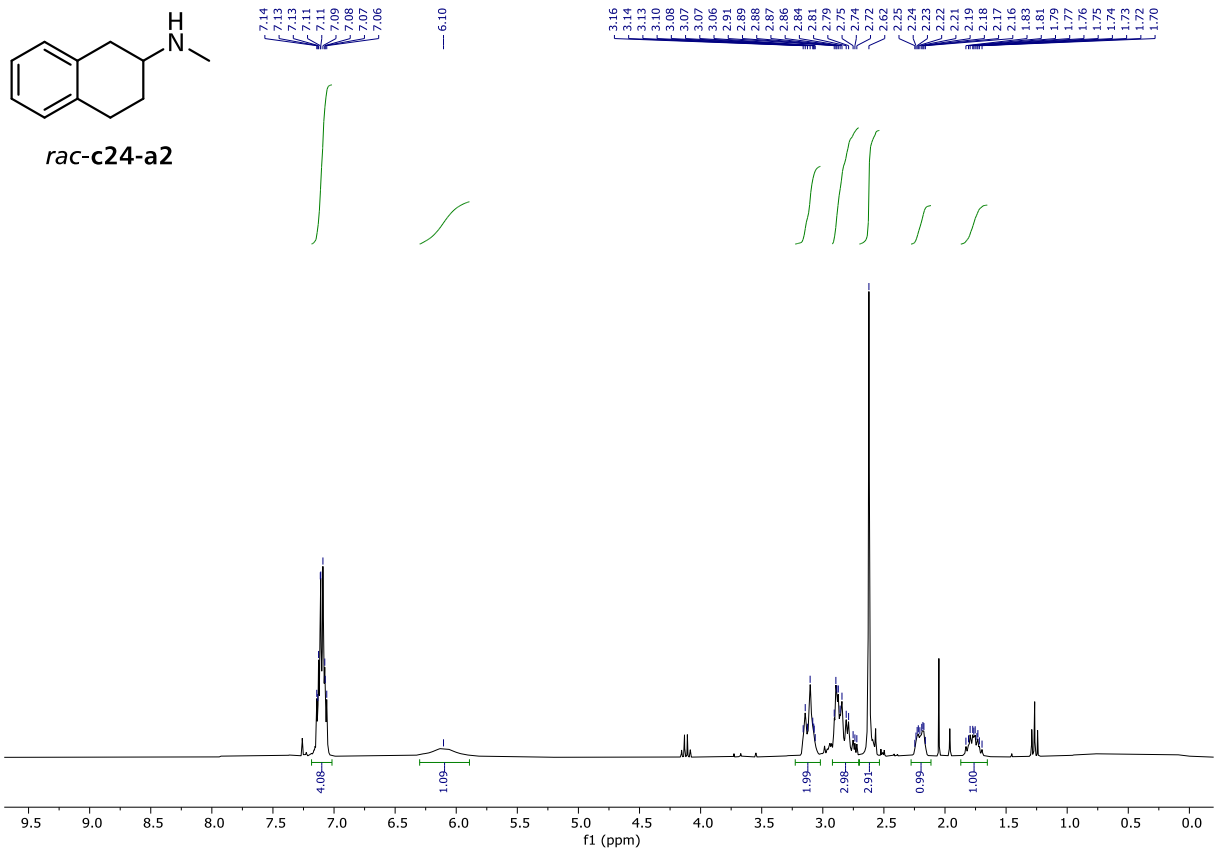


Figure S395. ^{1}H NMR spectrum of *rac*-*N*-methyl-1,2,3,4-tetrahydronaphthalen-2-amine (**c24-a2**).

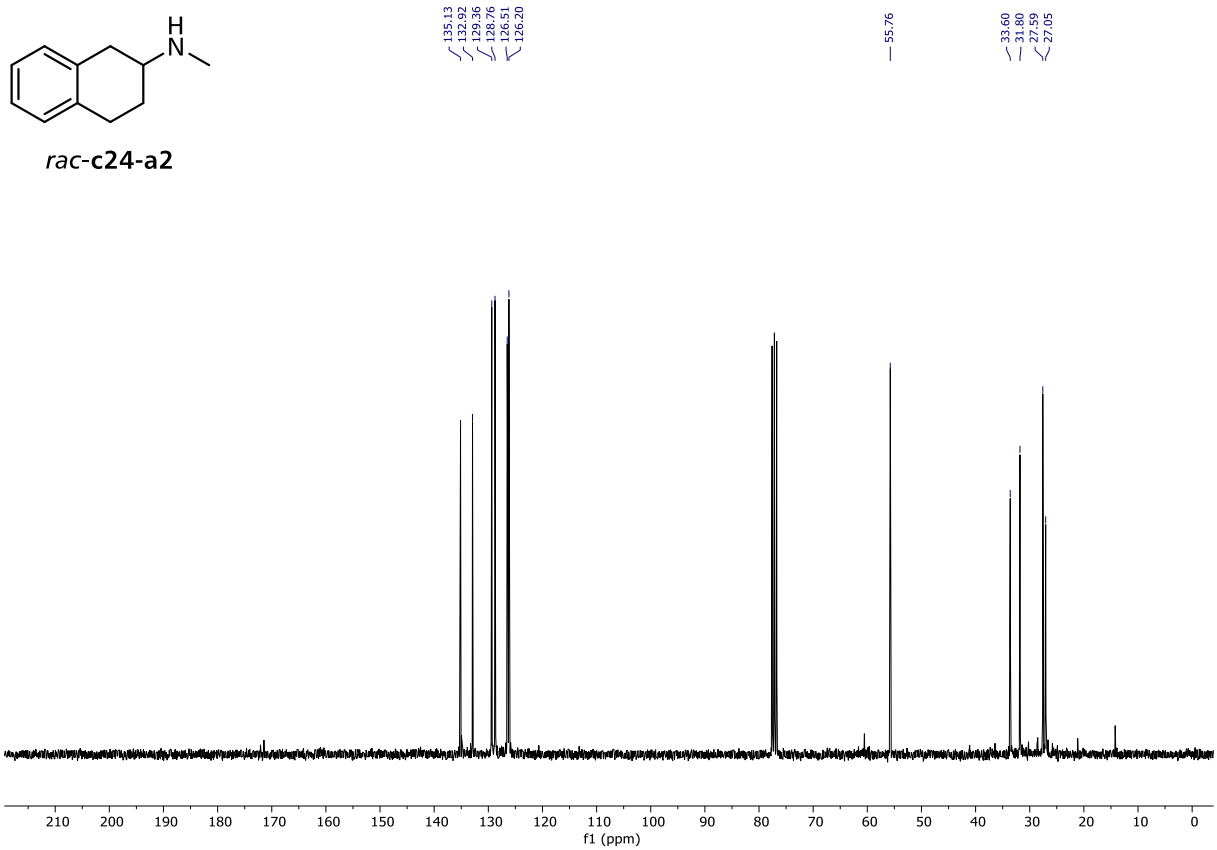


Figure S396. ^{13}C NMR spectrum of *rac*-*N*-methyl-1,2,3,4-tetrahydronaphthalen-2-amine (**c24-a2**).

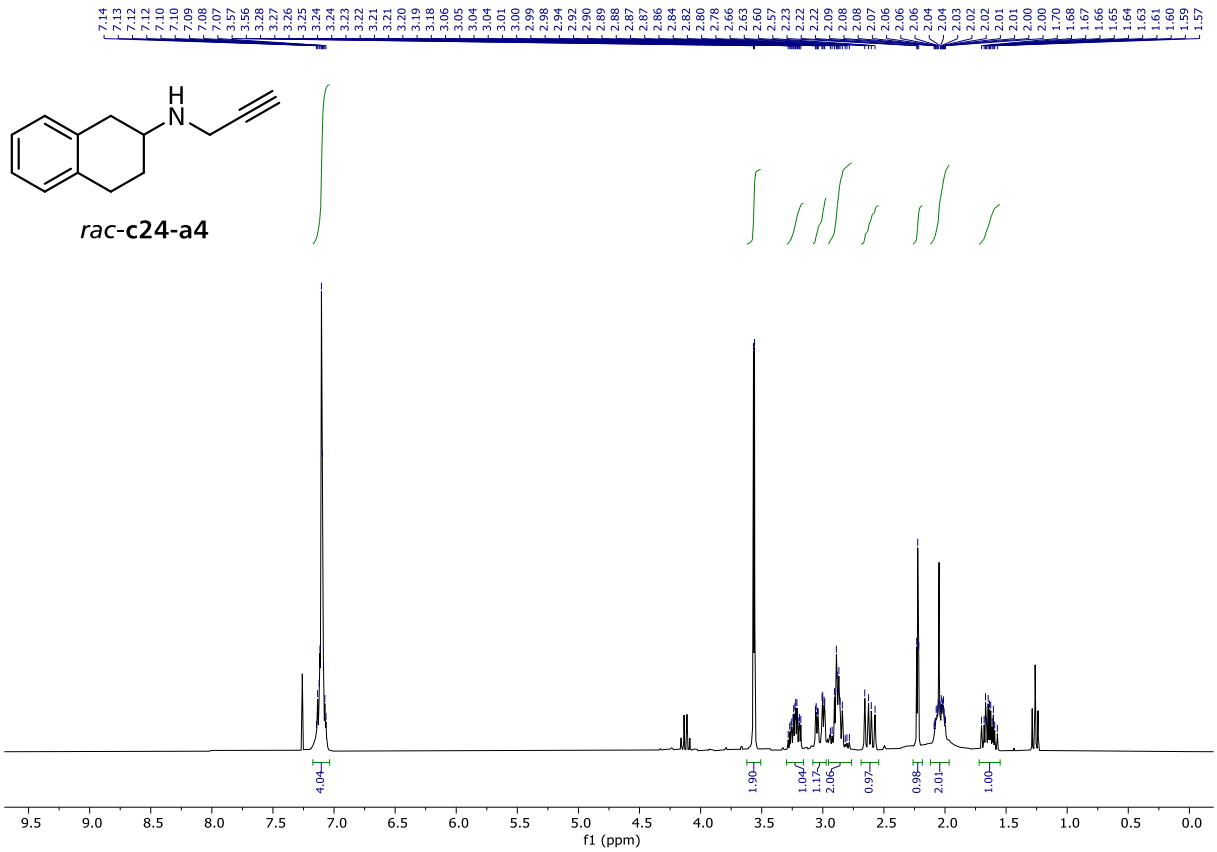


Figure S397. ^{1}H NMR spectrum of *rac*-*N*-(prop-2-yn-1-yl)-1,2,3,4-tetrahydronaphthalen-2-amine (**c24-a4**).

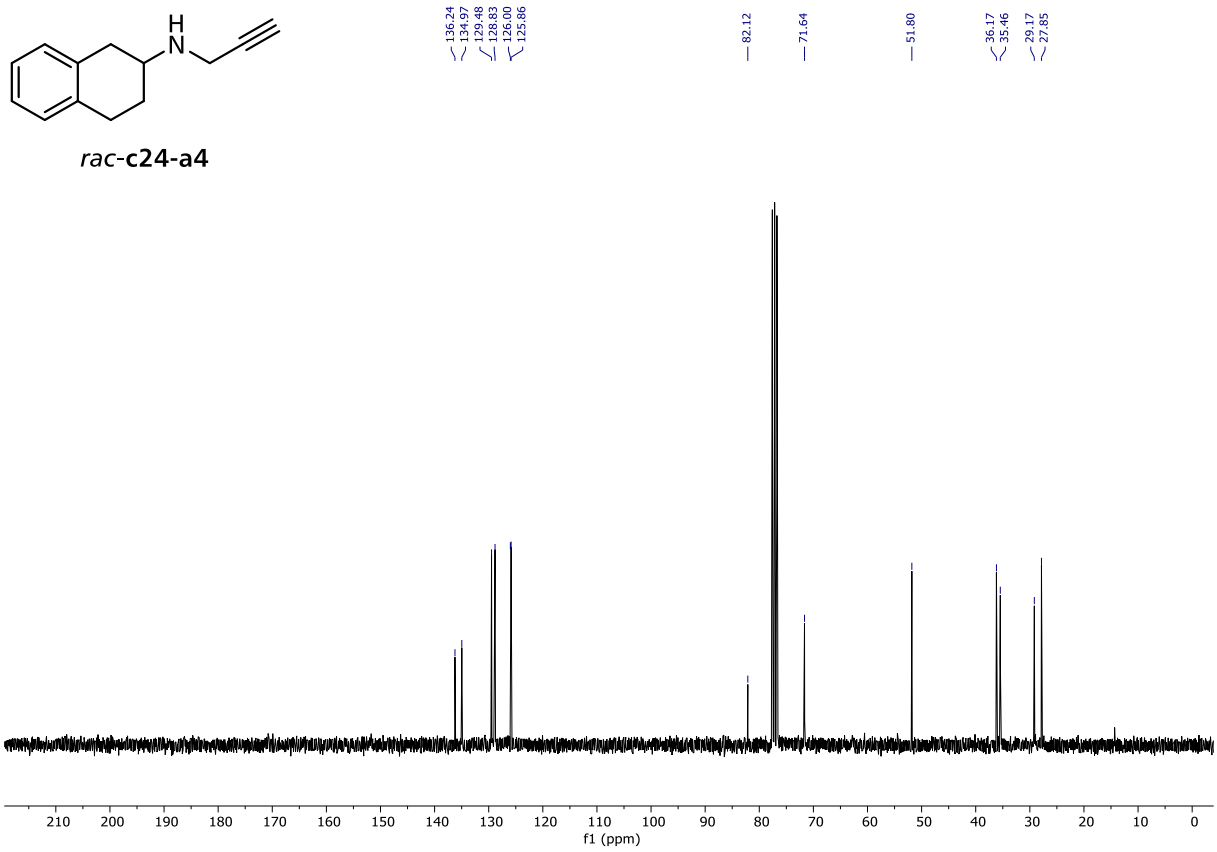


Figure S398. ^{13}C NMR spectrum of *rac*-*N*-(prop-2-yn-1-yl)-1,2,3,4-tetrahydronaphthalen-2-amine (**c24-a4**).

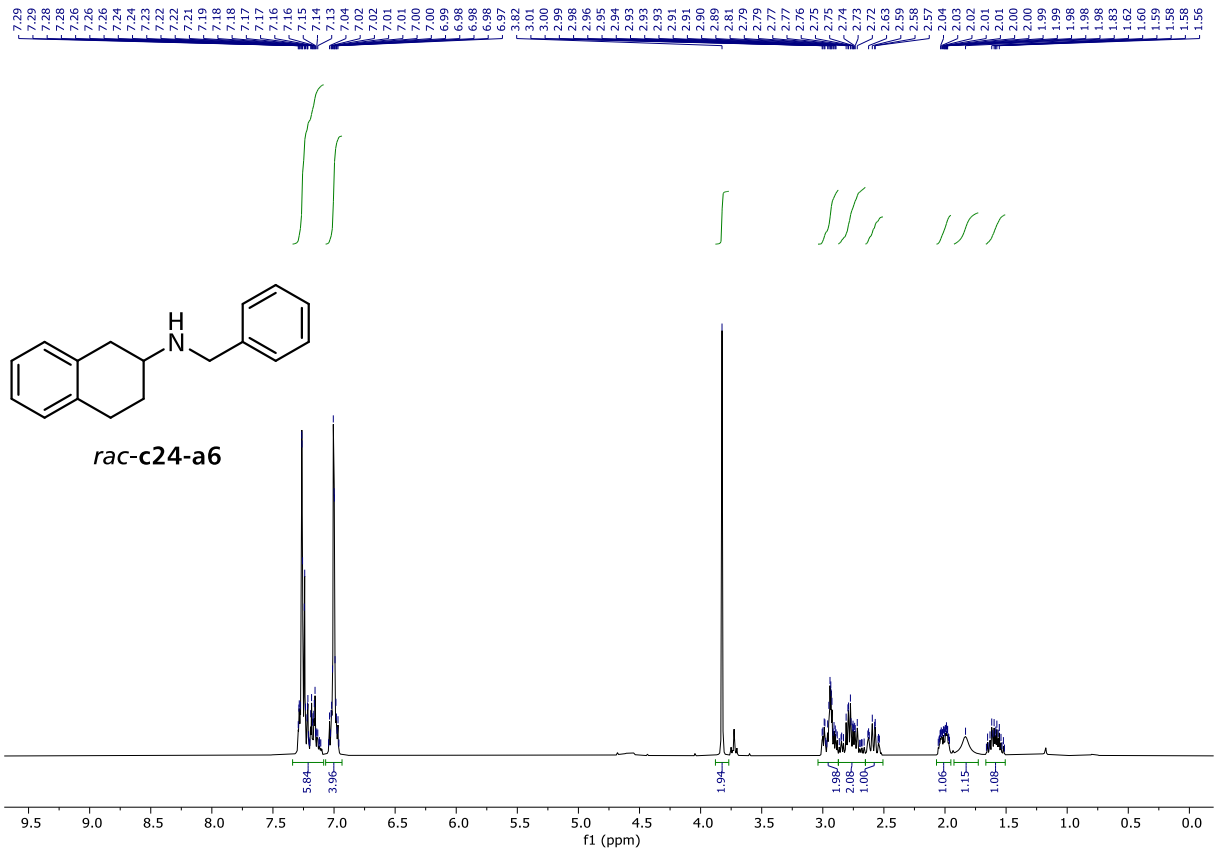


Figure S399. ^{1}H NMR spectrum of *rac*-*N*-benzyl-1,2,3,4-tetrahydronaphthalen-2-amine (**c24-a6**).

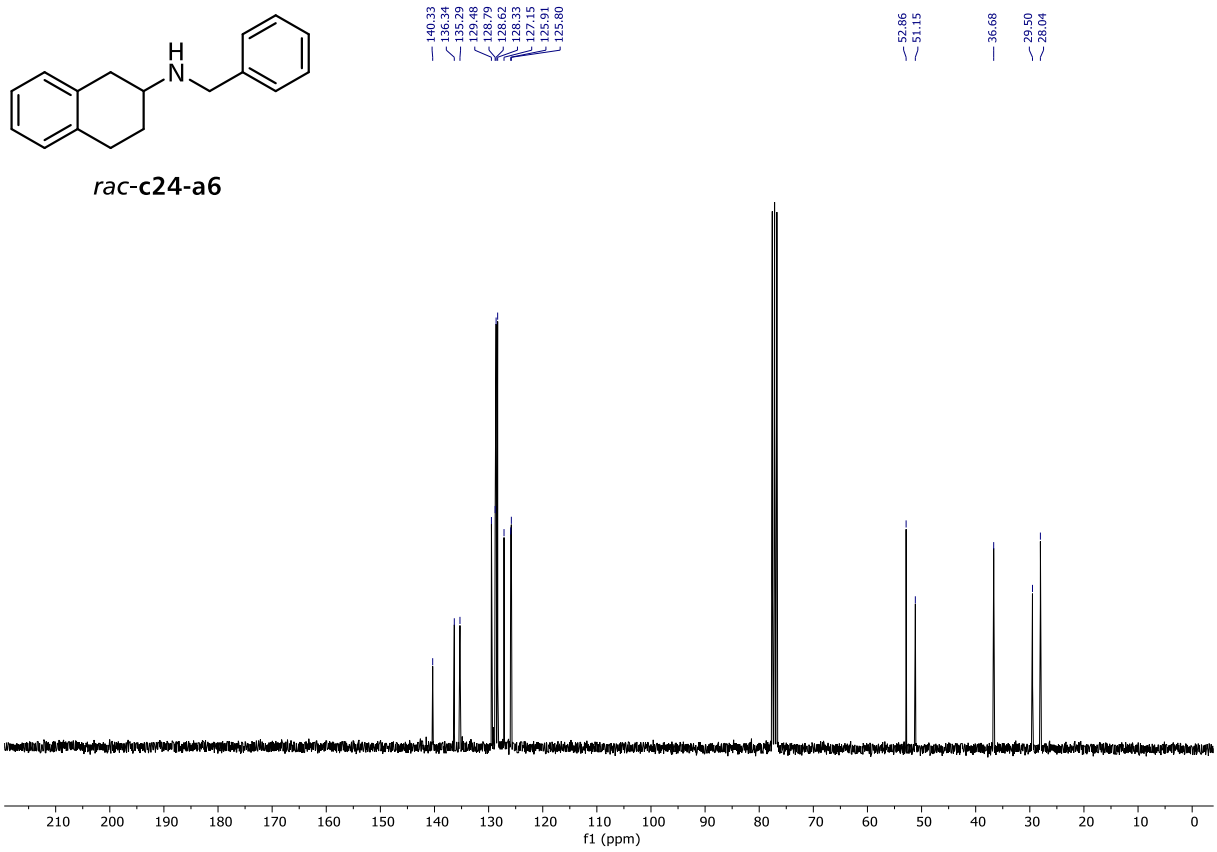


Figure S400. ^{13}C NMR spectrum of *rac*-*N*-benzyl-1,2,3,4-tetrahydronaphthalen-2-amine (**c24-a6**).

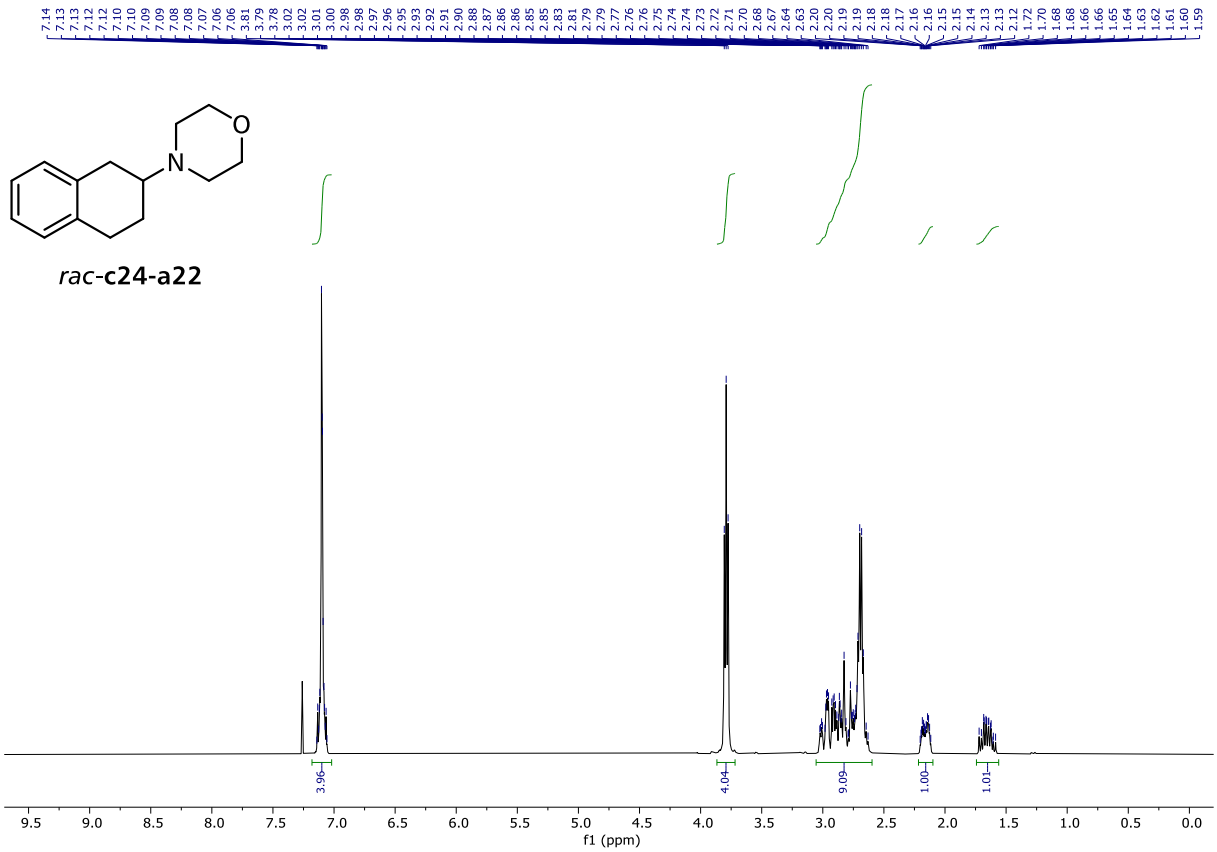


Figure S401. ^{1}H NMR spectrum of *rac*-4-(1,2,3,4-tetrahydronaphthalen-2-yl)morpholine (**c24-a22**).

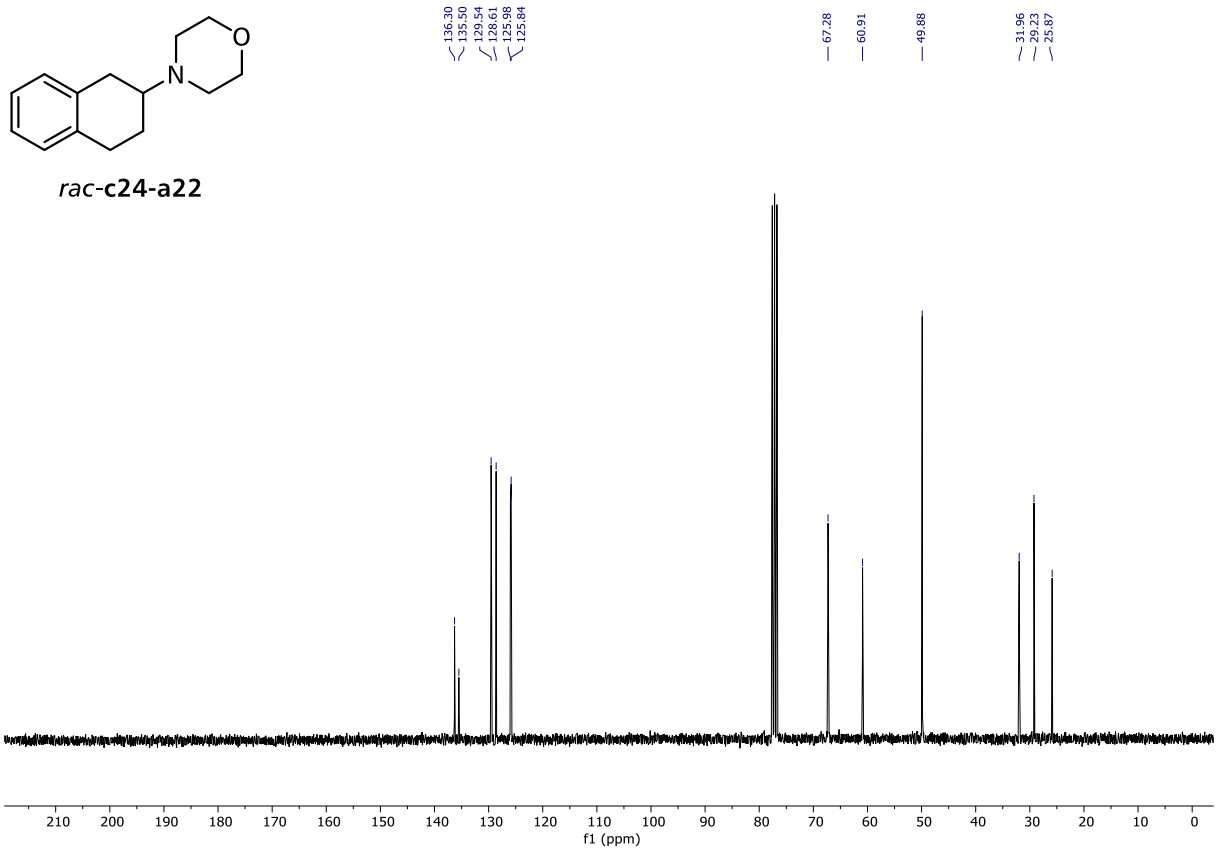


Figure S402. ^{13}C NMR spectrum of *rac*-4-(1,2,3,4-tetrahydronaphthalen-2-yl)morpholine (**c24-a22**).

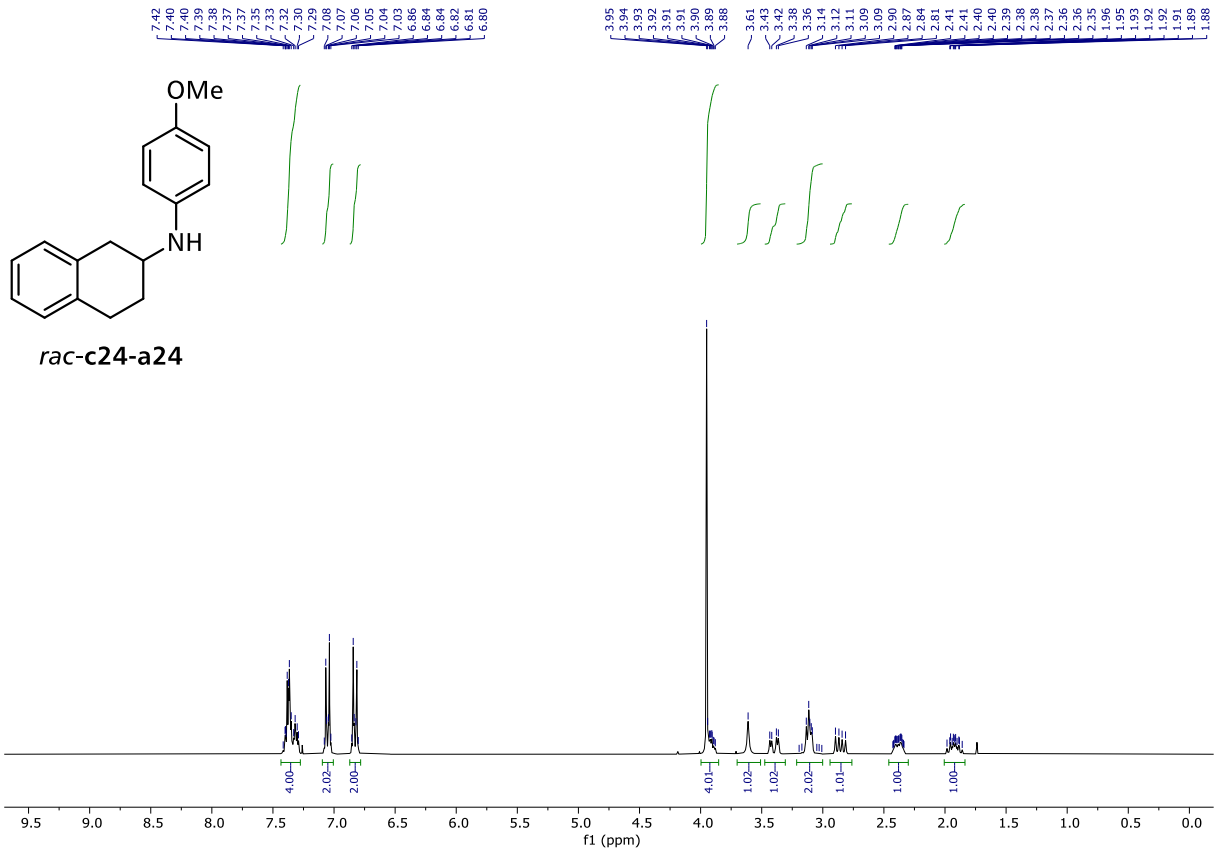


Figure S403. ^{1}H NMR spectrum of *rac*-*N*-(4-methoxyphenyl)-1,2,3,4-tetrahydronaphthalen-2-amine (**c24-a24**).

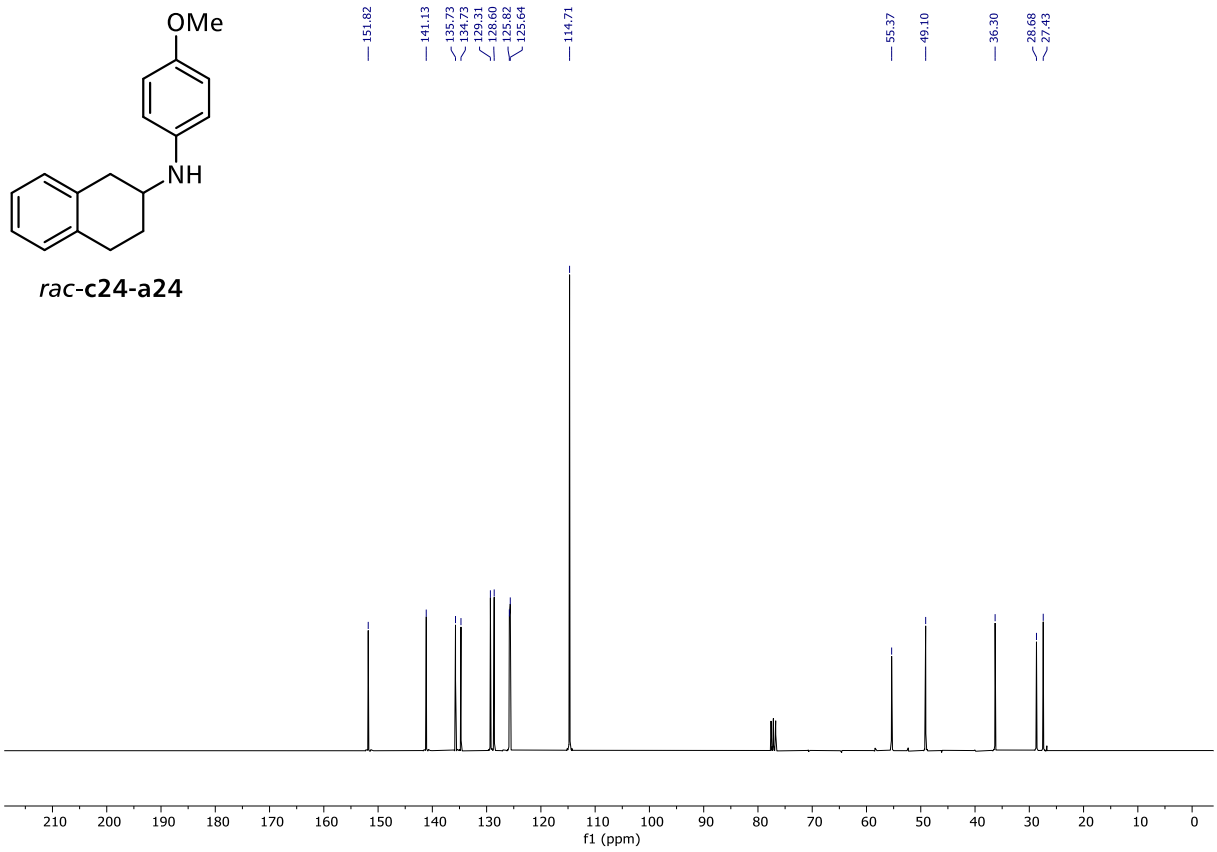


Figure S404. ^{13}C NMR spectrum of *rac*-*N*-(4-methoxyphenyl)-1,2,3,4-tetrahydronaphthalen-2-amine (**c24-a24**).

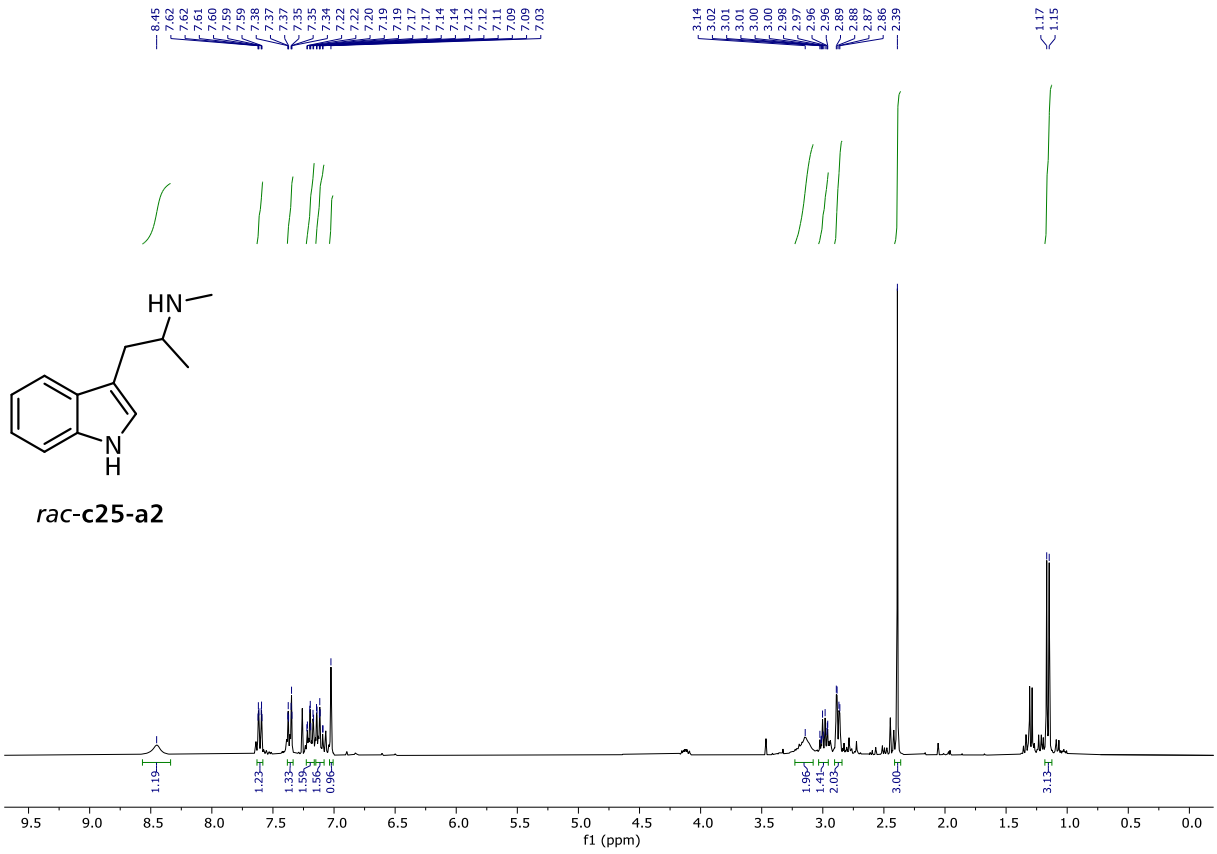


Figure S405. ^{1}H NMR spectrum of *rac*-1-(1*H*-indol-3-yl)-*N*-methylpropan-2-amine (**c25-a2**).

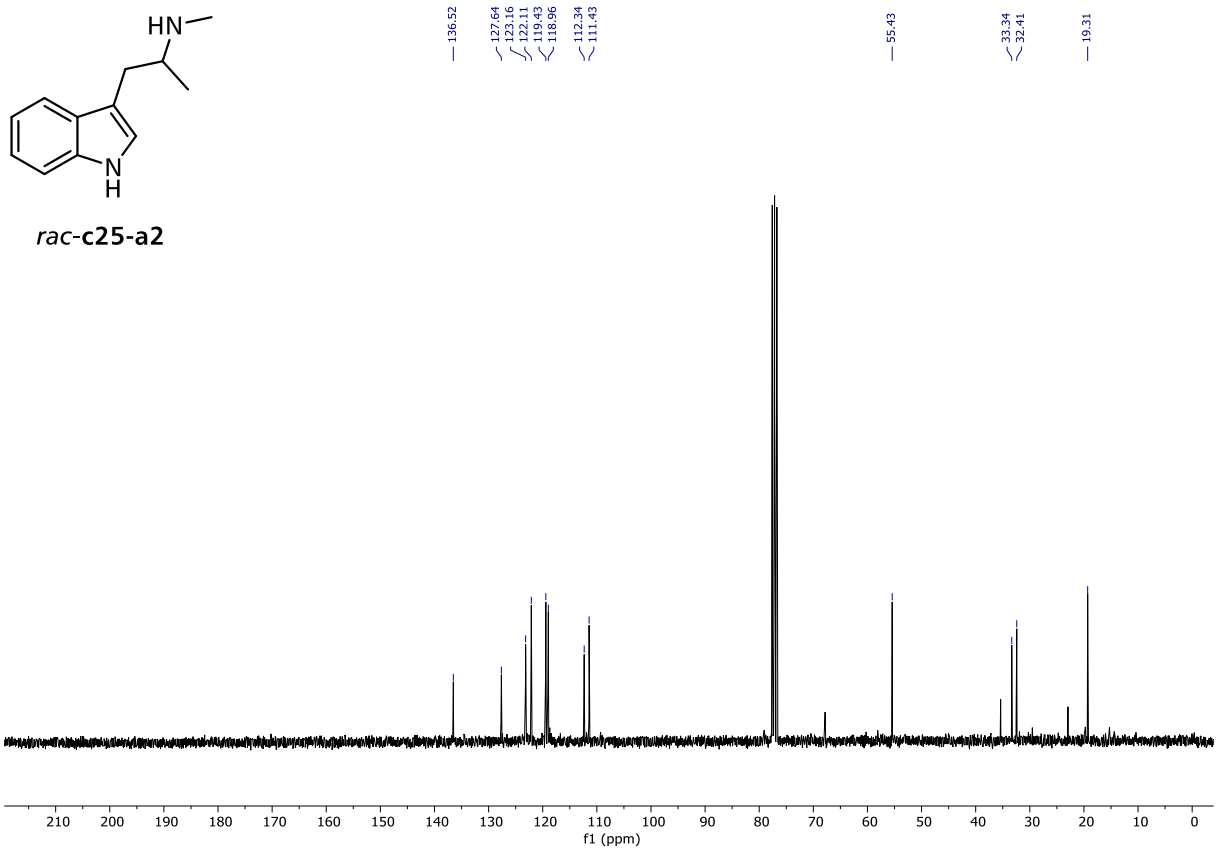


Figure S406. ^{13}C NMR spectrum of *rac*-1-(1*H*-indol-3-yl)-*N*-methylpropan-2-amine (**c25-a2**).

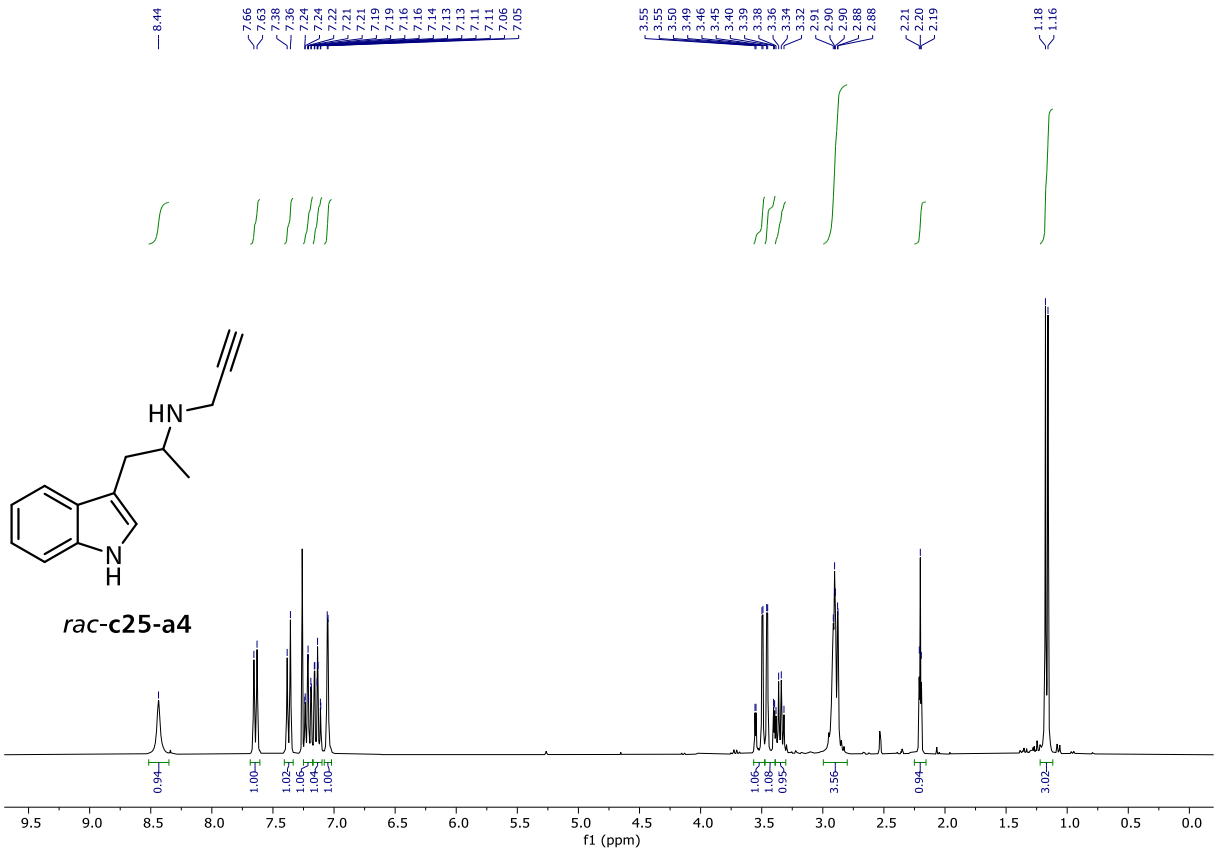


Figure S407. ^{1}H NMR spectrum of *rac*-*N*-(1-(1*H*-indol-3-yl)propan-2-yl)prop-2-yn-1-amine (**c25-a4**).

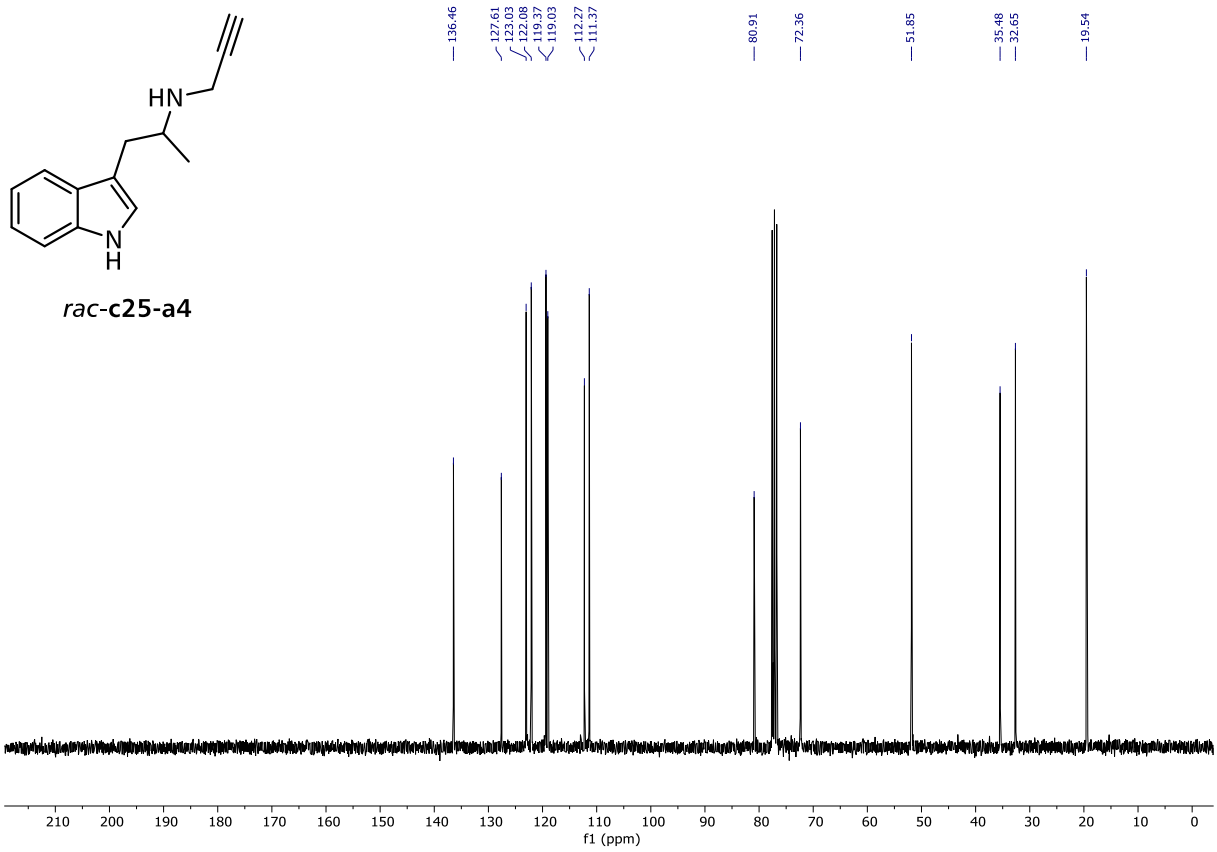


Figure S408. ^{13}C NMR spectrum of *rac*-*N*-(1-(1*H*-indol-3-yl)propan-2-yl)prop-2-yn-1-amine (**c25-a4**).

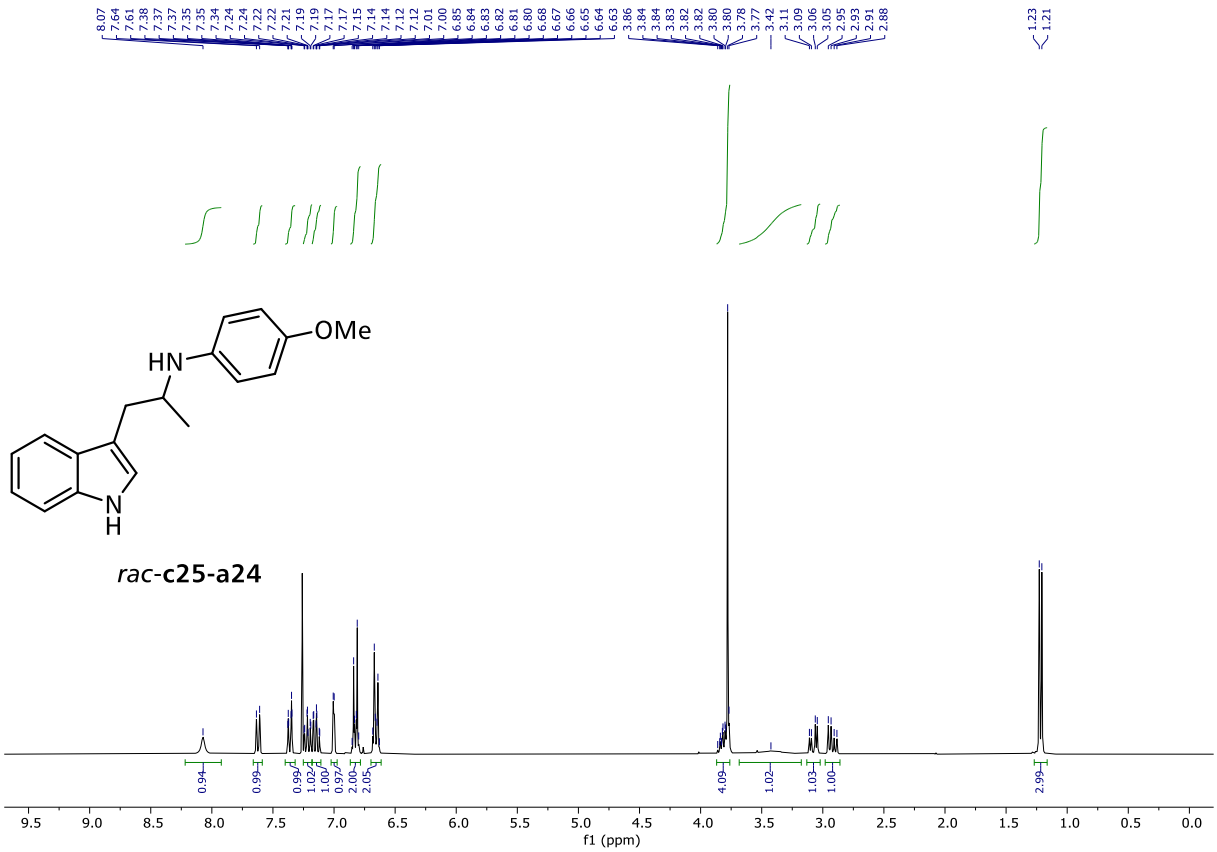


Figure S409. ^{1}H NMR spectrum of *rac*-*N*-(1-(1*H*-indol-3-yl)propan-2-yl)-4-methoxyaniline (**c25-a24**).

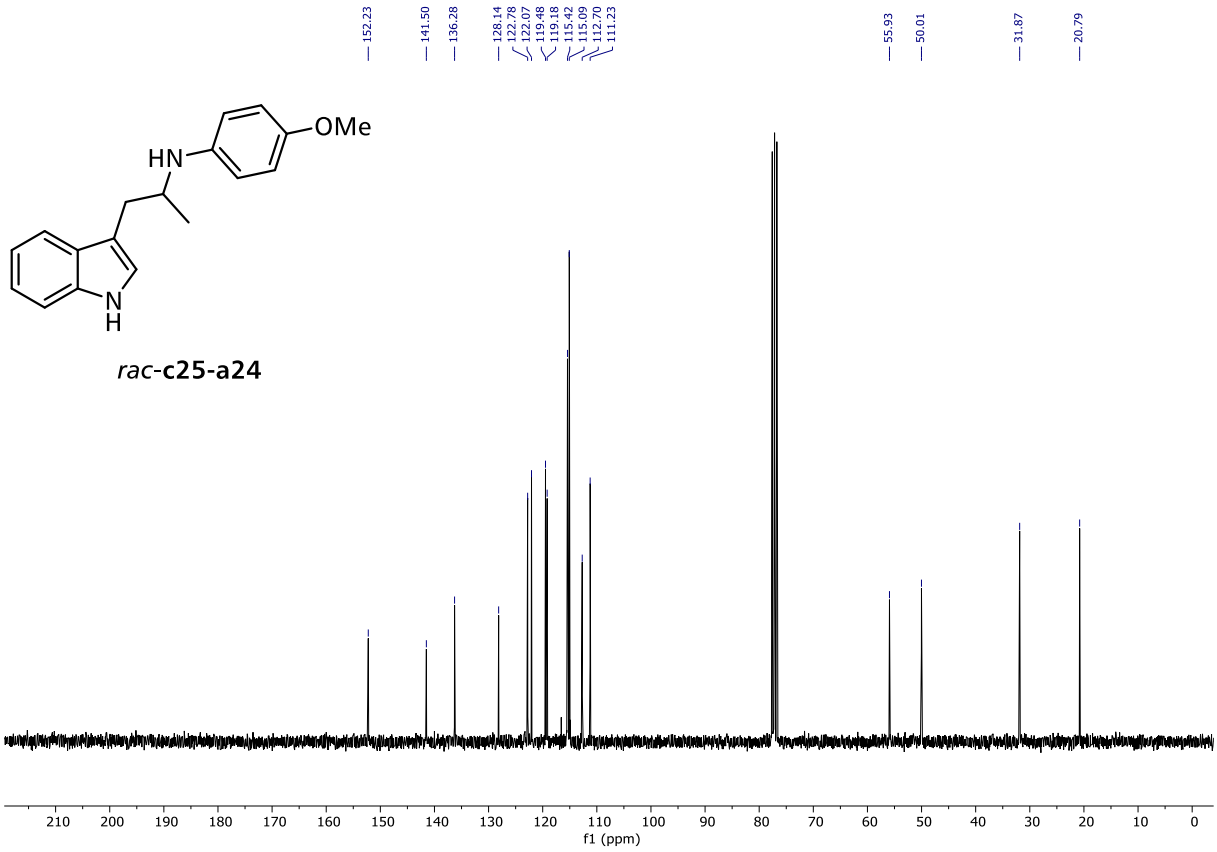


Figure S410. ^{13}C NMR spectrum of *rac*-*N*-(1-(1*H*-indol-3-yl)propan-2-yl)-4-methoxyaniline (**c25-a24**).

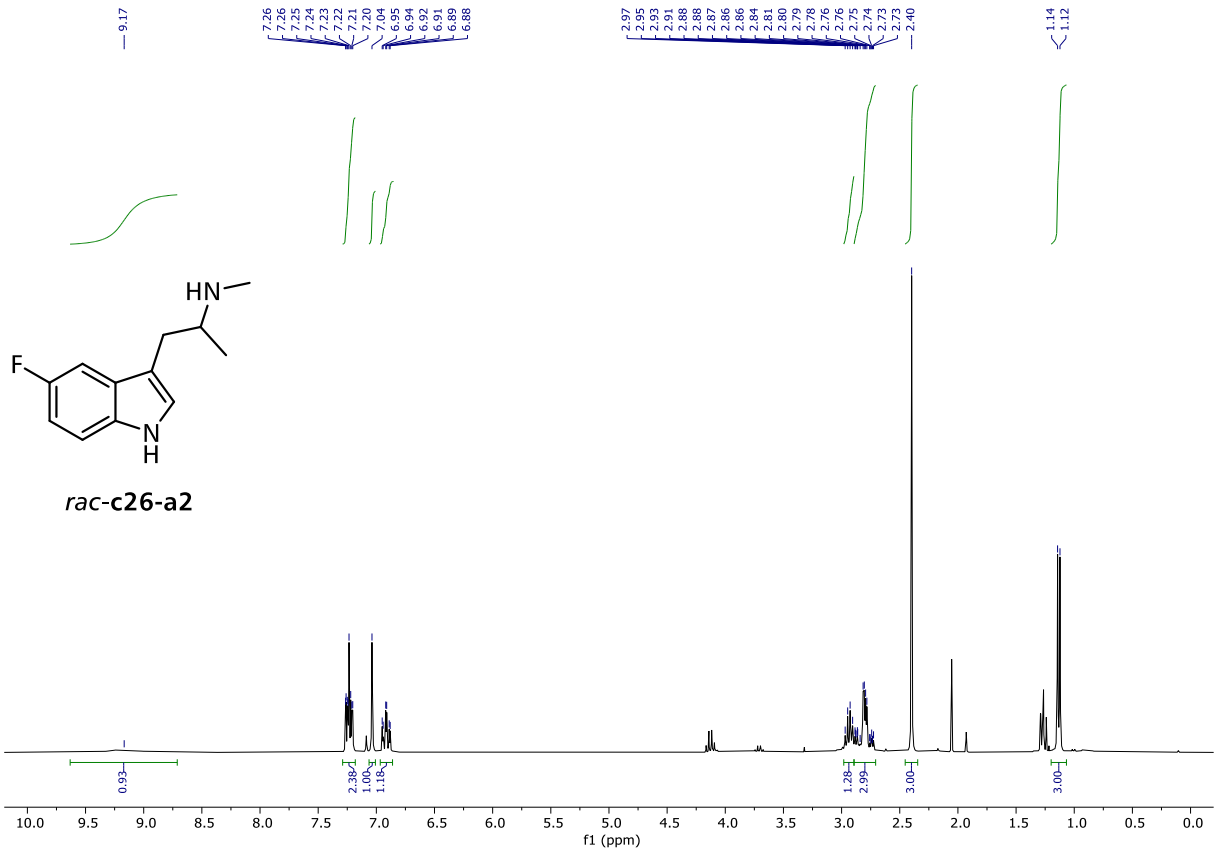


Figure S411. ^{1}H NMR spectrum of *rac*-1-(5-fluoro-1*H*-indol-3-yl)-*N*-methylpropan-2-amine (**c26-a2**).

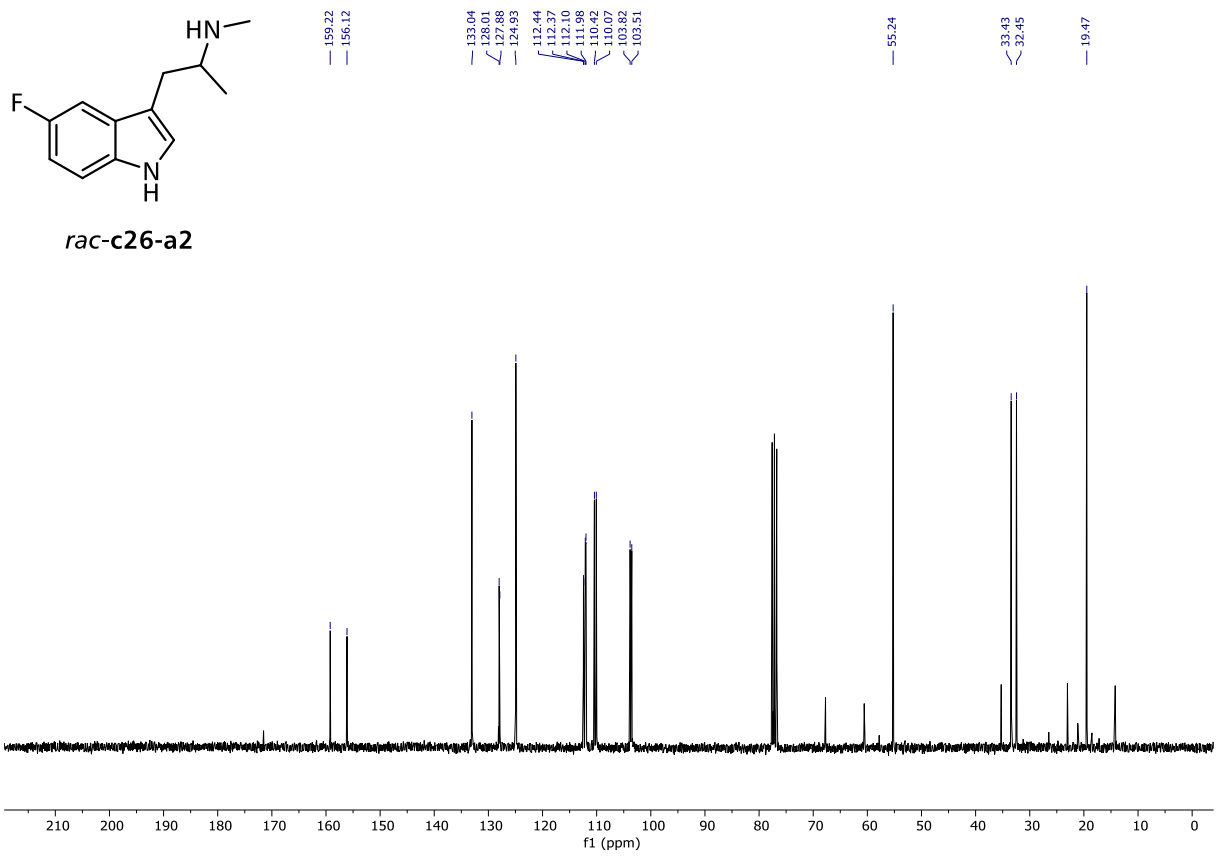


Figure S412. ^{13}C NMR spectrum of *rac*-1-(5-fluoro-1*H*-indol-3-yl)-*N*-methylpropan-2-amine (**c26-a2**).

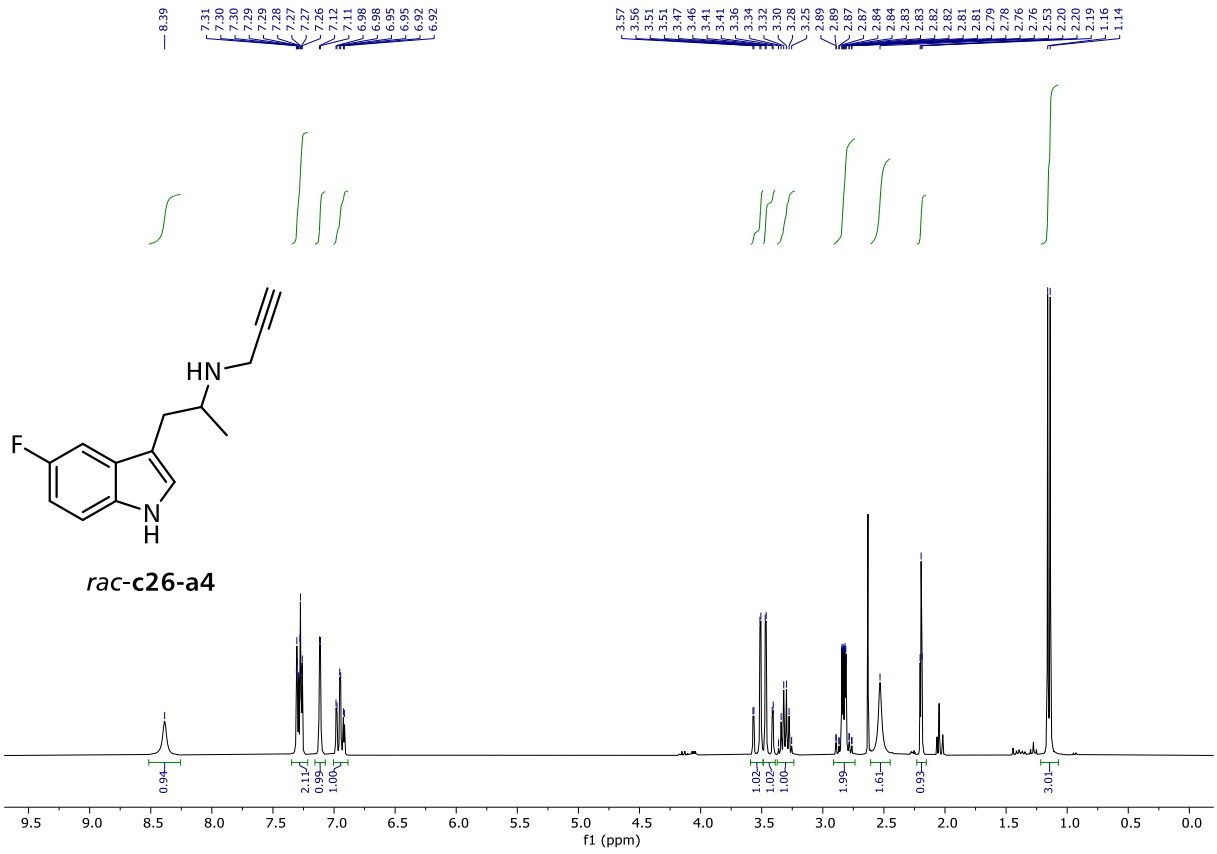


Figure S413. ^{1}H NMR spectrum of *rac*-*N*-(1-(5-fluoro-1*H*-indol-3-yl)propan-2-yl)prop-2-yn-1-amine (**c26-a4**).

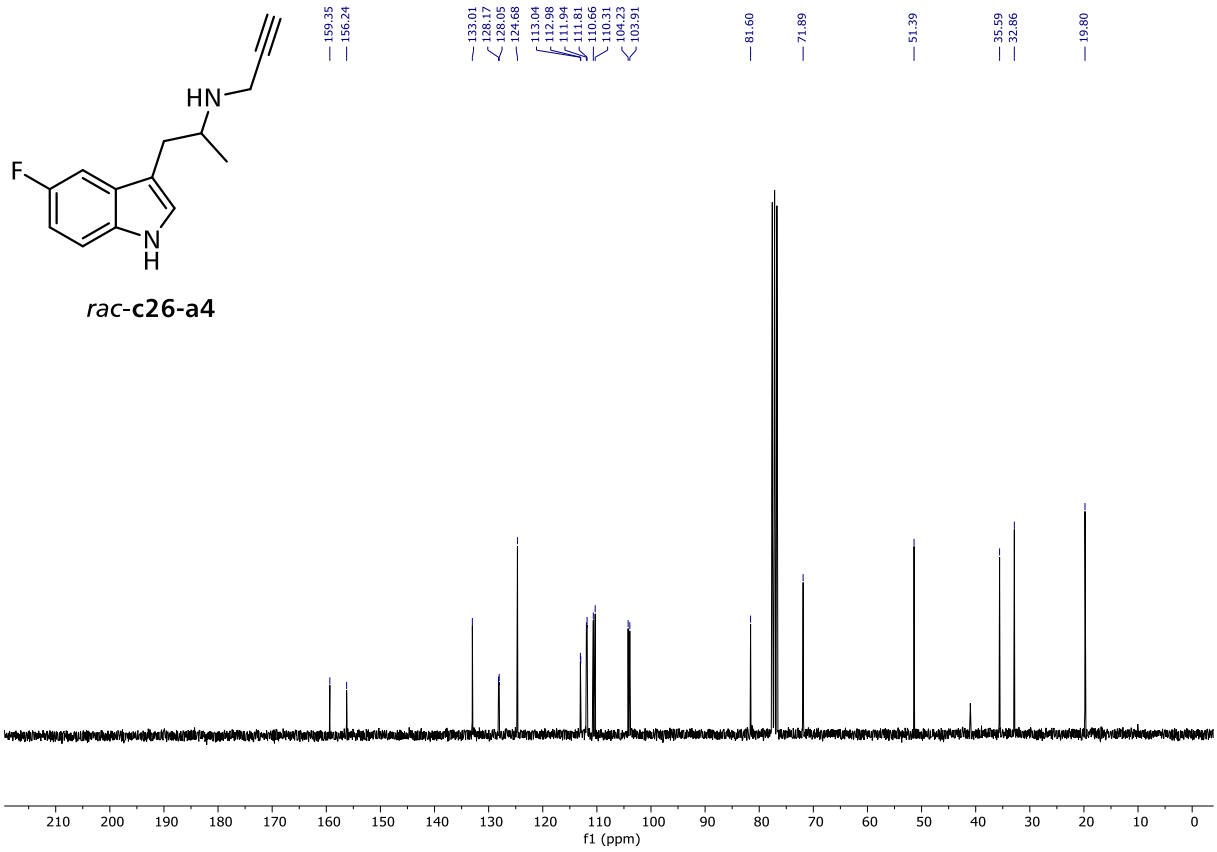


Figure S414. ^{13}C NMR spectrum of *rac*-*N*-(1-(5-fluoro-1*H*-indol-3-yl)propan-2-yl)prop-2-yn-1-amine (**c26-a4**).

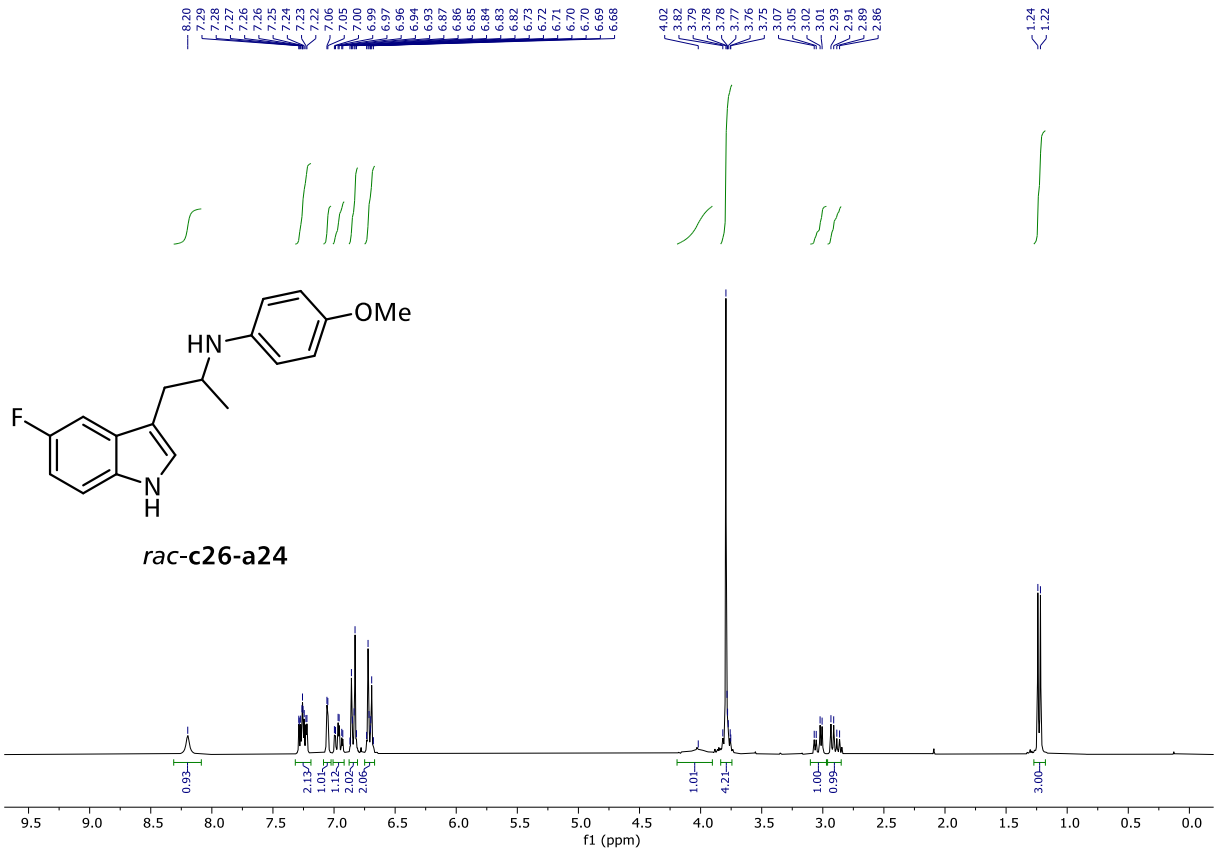


Figure S415. ^{1}H NMR spectrum of *rac*-*N*-(1-(5-fluoro-1*H*-indol-3-yl)propan-2-yl)-4-methoxyaniline (**c26-a24**).

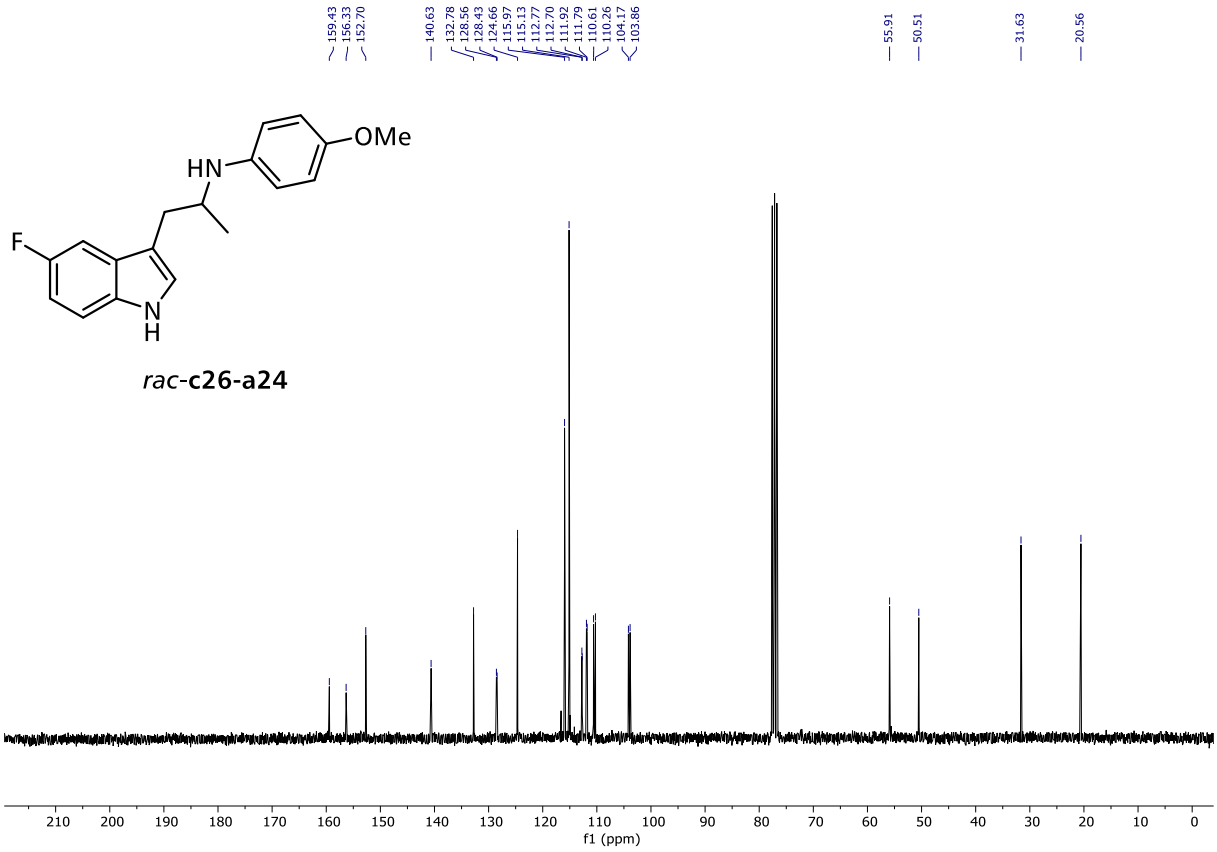


Figure S416. ^{13}C NMR spectrum of *rac*-*N*-(1-(5-fluoro-1*H*-indol-3-yl)propan-2-yl)-4-methoxyaniline (**c26-a24**).

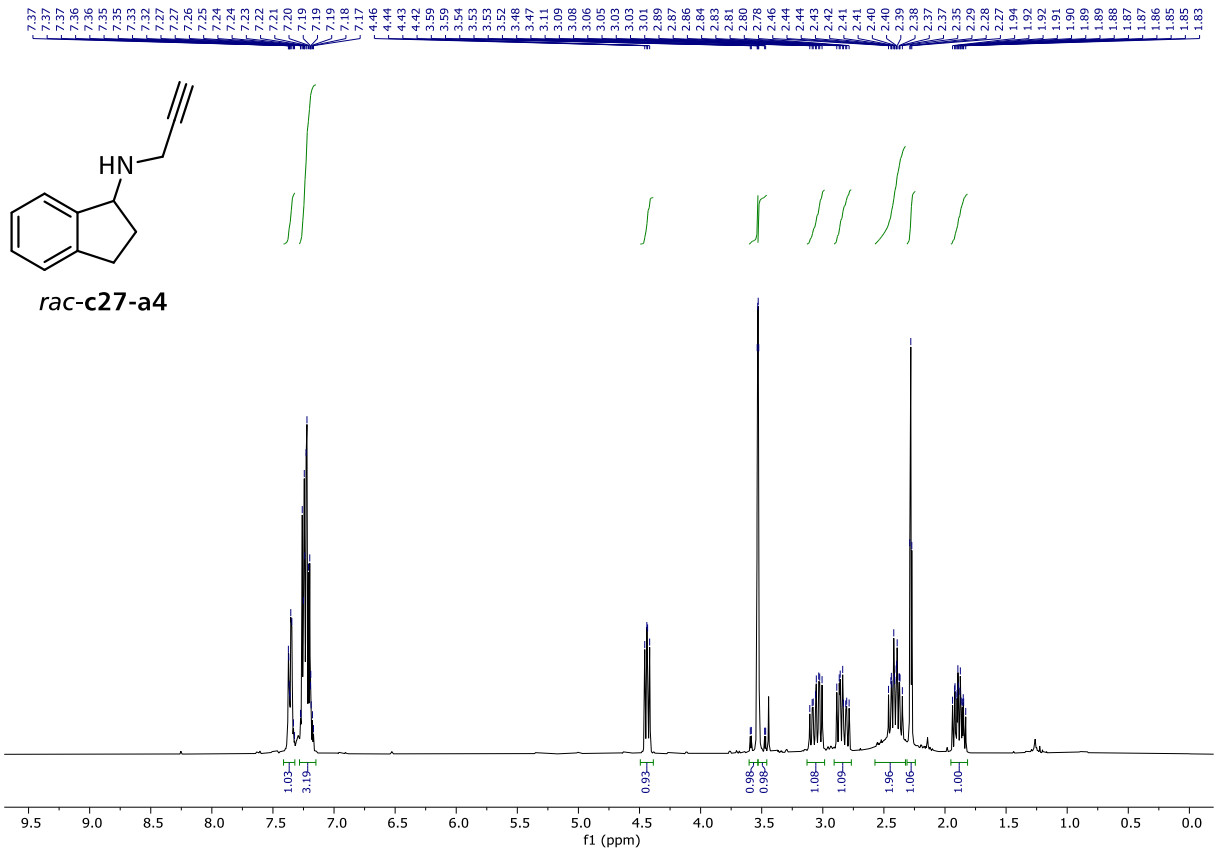


Figure S417. ^{1}H NMR spectrum of *rac*-*N*-(prop-2-yn-1-yl)-2,3-dihydro-1*H*-inden-1-amine (**c27-a4**).

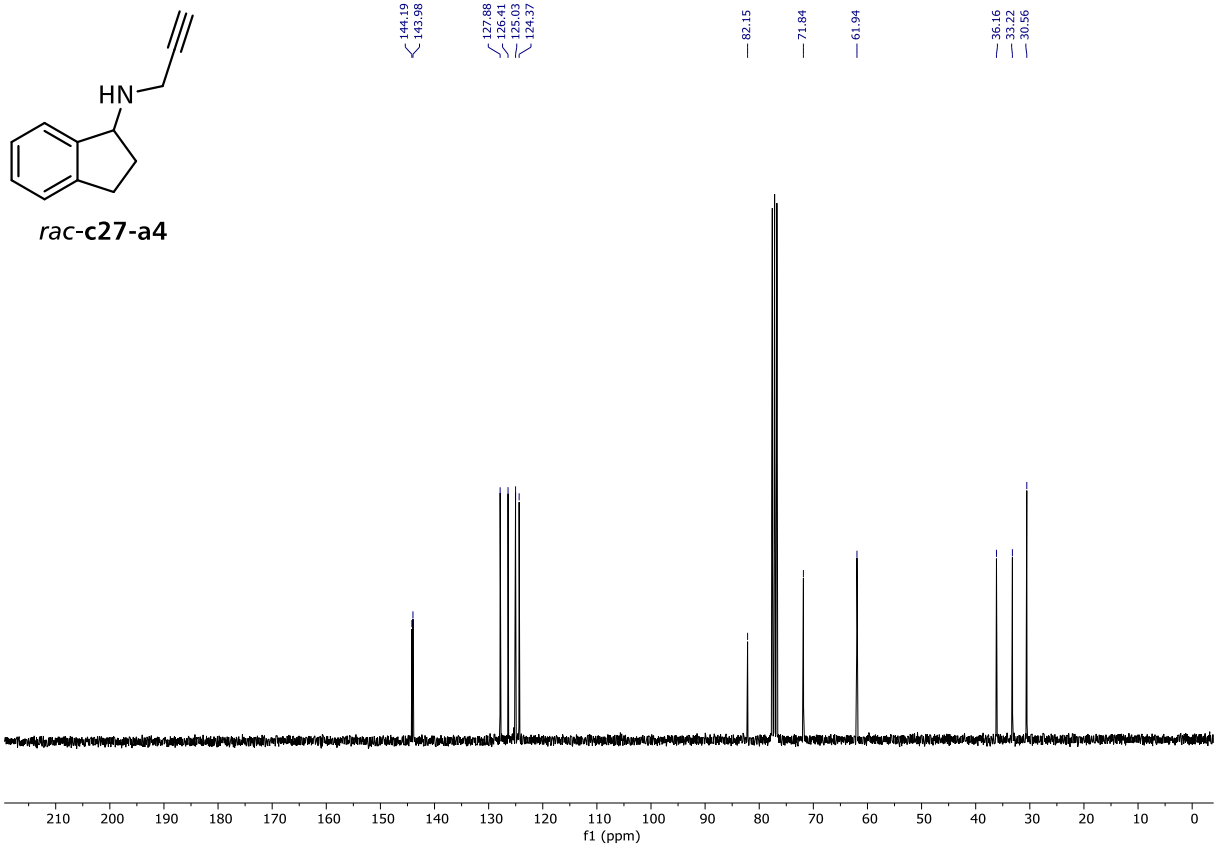


Figure S418. ^{13}C NMR spectrum of *rac*-*N*-(prop-2-yn-1-yl)-2,3-dihydro-1*H*-inden-1-amine (**c27-a4**).

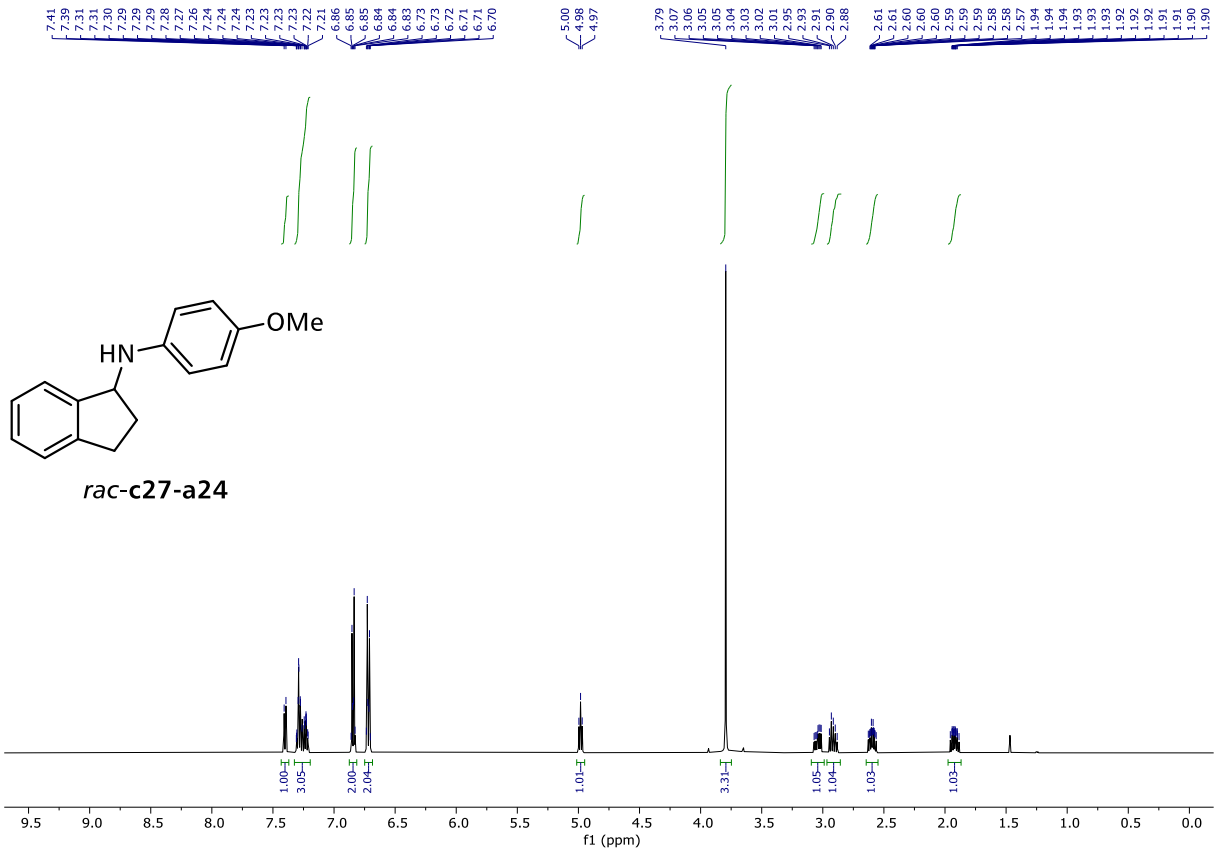


Figure S419. ^{1}H NMR spectrum of *rac*-*N*-(4-methoxyphenyl)-2,3-dihydro-1*H*-inden-1-amine (**c27-a24**).

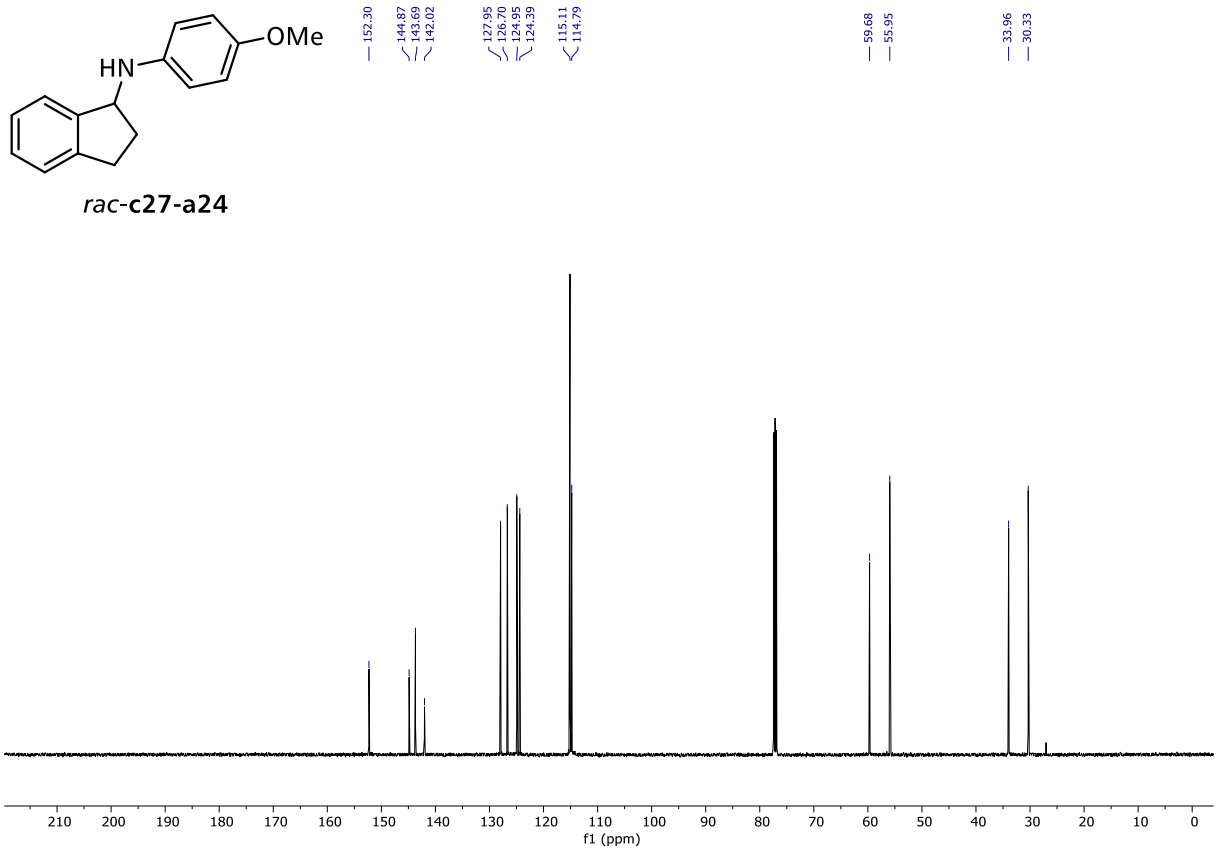


Figure S420. ^{13}C NMR spectrum of *rac*-*N*-(4-methoxyphenyl)-2,3-dihydro-1*H*-inden-1-amine (**c27-a24**).

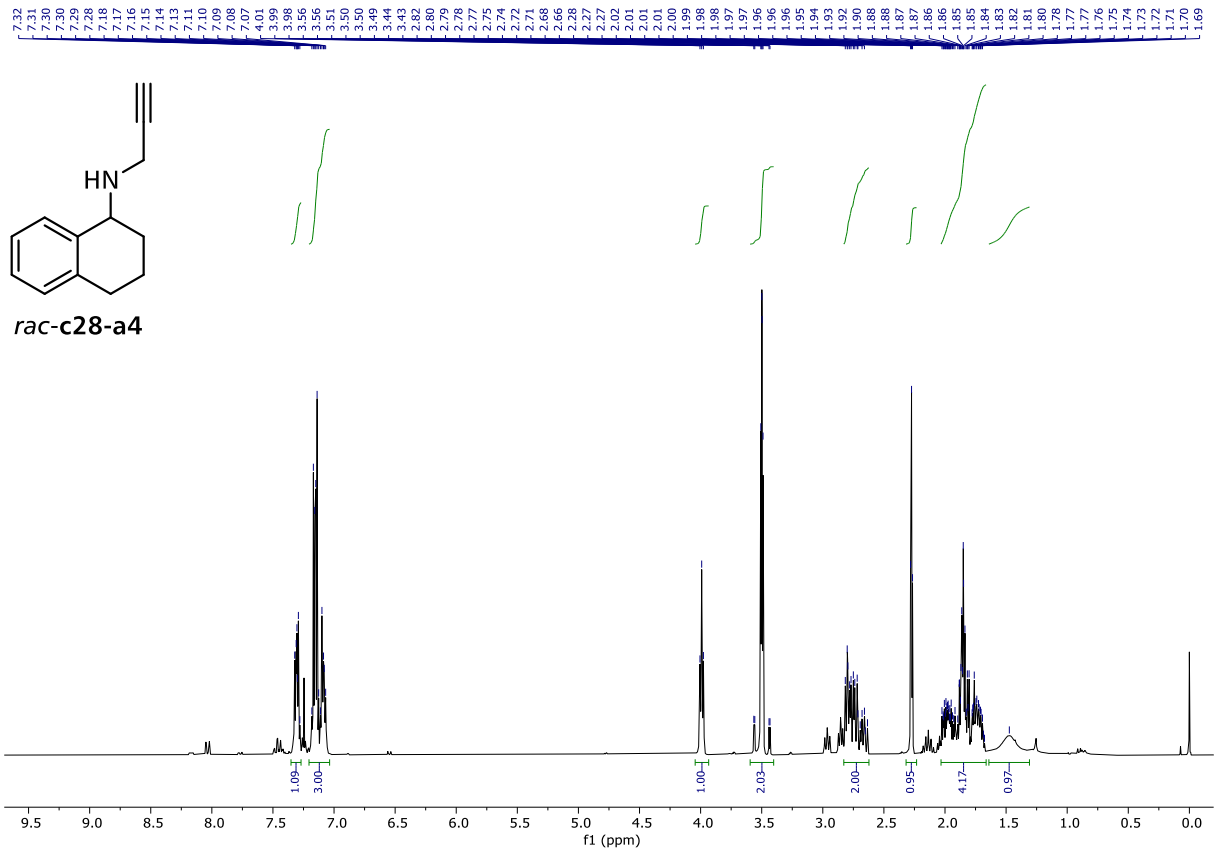


Figure S421. ^{1}H NMR spectrum of *rac*-*N*-(prop-2-yn-1-yl)-1,2,3,4-tetrahydronaphthalen-1-amine (**c28-a4**).

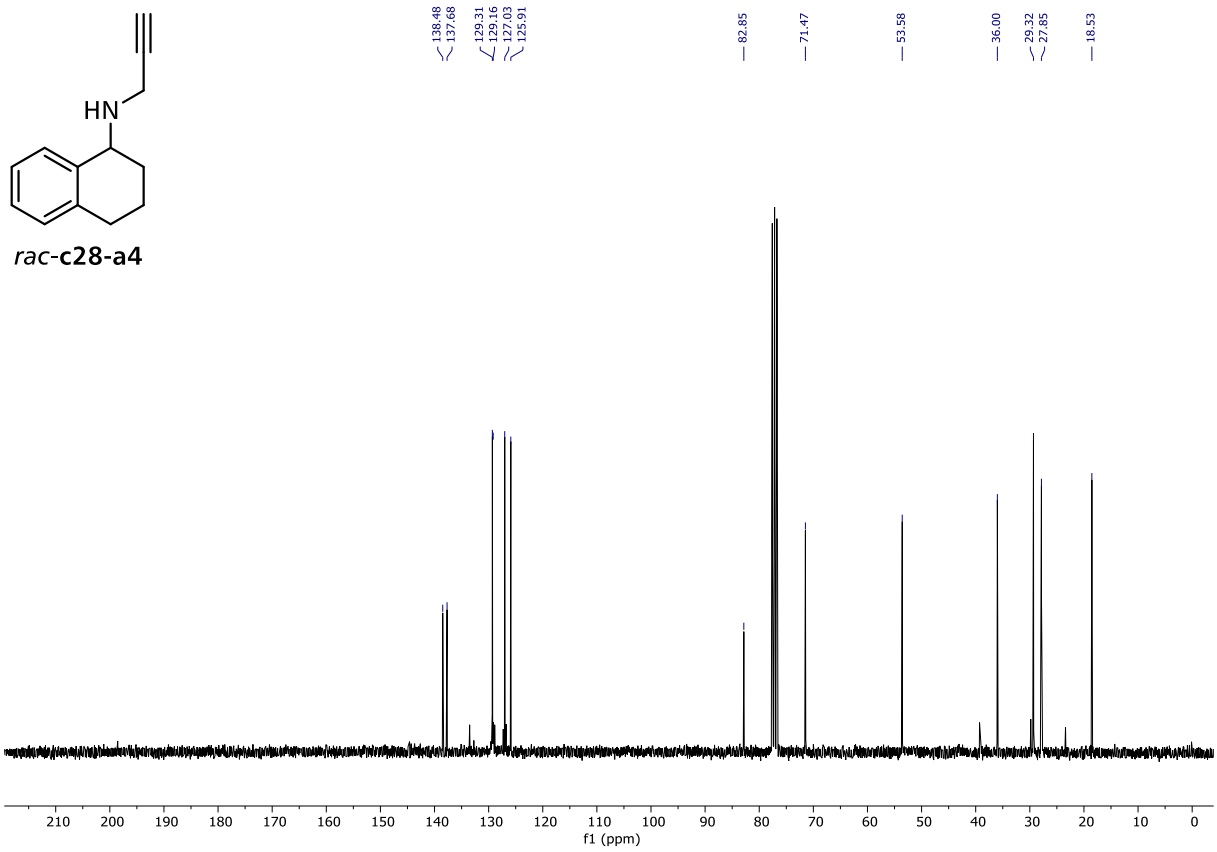


Figure S422. ^{13}C NMR spectrum of *rac*-*N*-(prop-2-yn-1-yl)-1,2,3,4-tetrahydronaphthalen-1-amine (**c28-a4**).

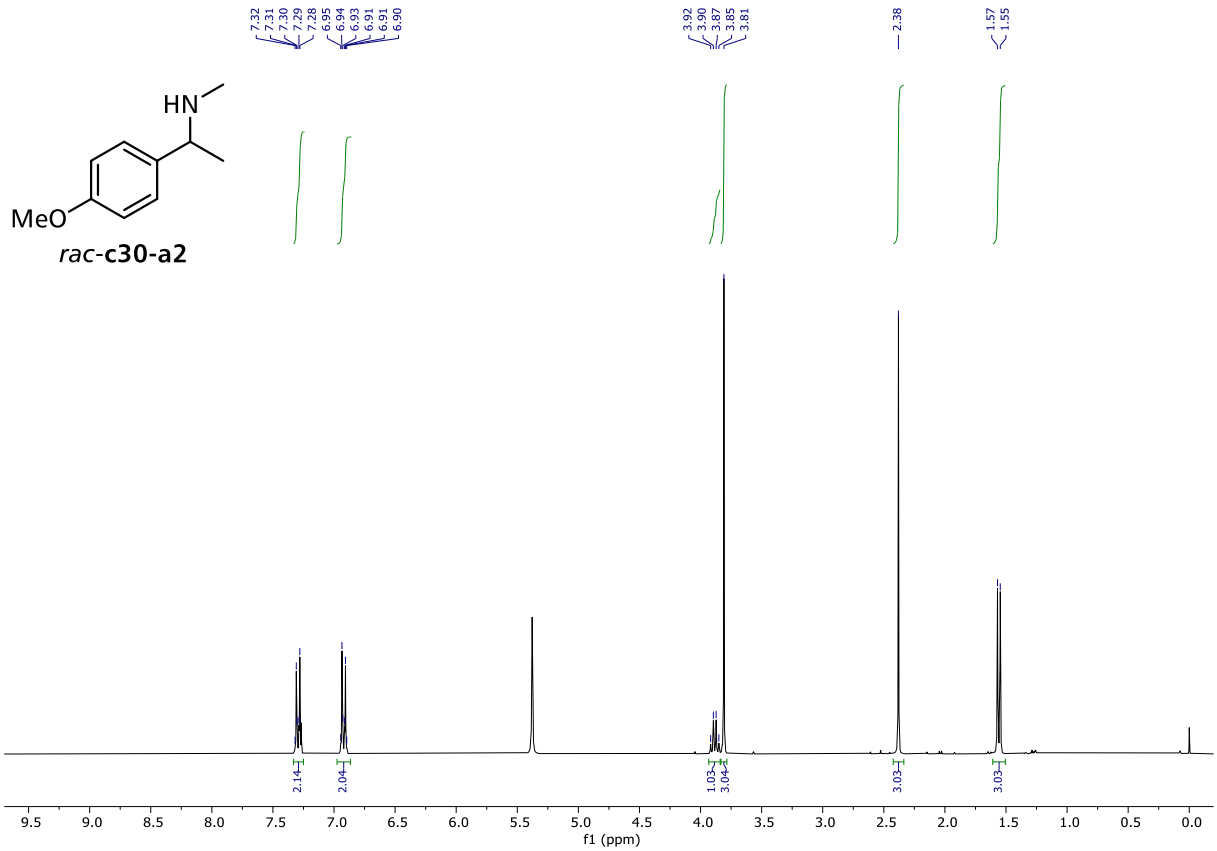


Figure S423. ^{1}H NMR spectrum of *rac*-1-(4-methoxyphenyl)-*N*-methylethan-1-amine (**c30-a2**).

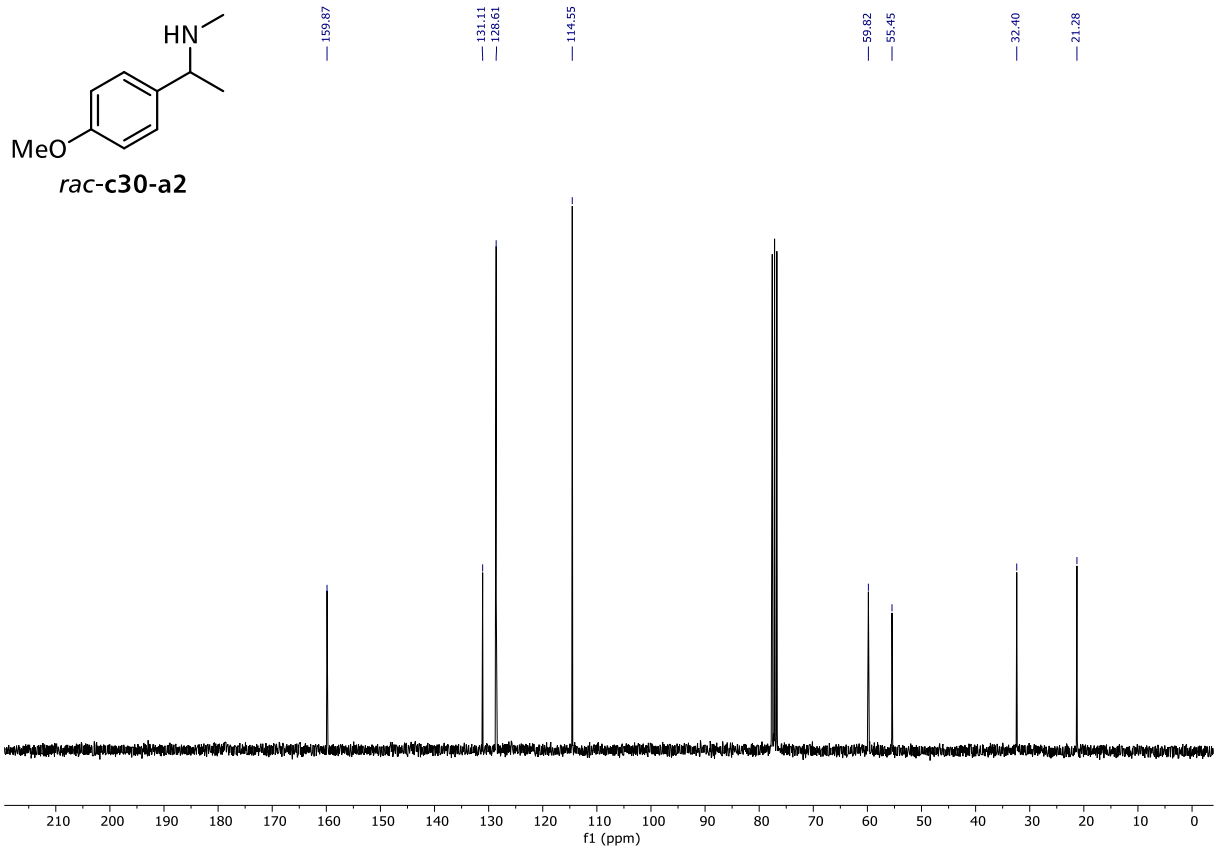


Figure S424. ^{13}C NMR spectrum of *rac*-1-(4-methoxyphenyl)-*N*-methylethan-1-amine (**c30-a2**).

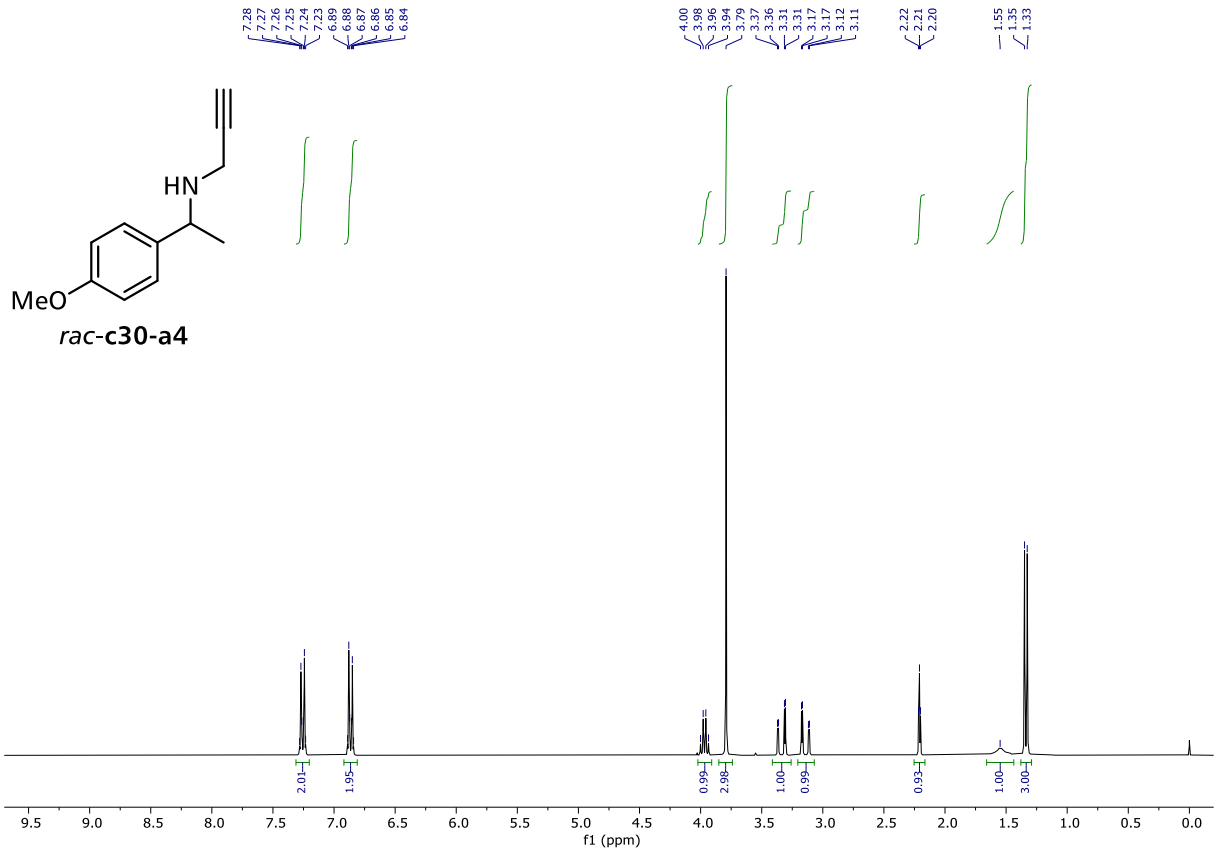


Figure S425. ^{1}H NMR spectrum of *rac*-*N*-(1-(4-methoxyphenyl)ethyl)prop-2-yn-1-amine (**c30-a4**).

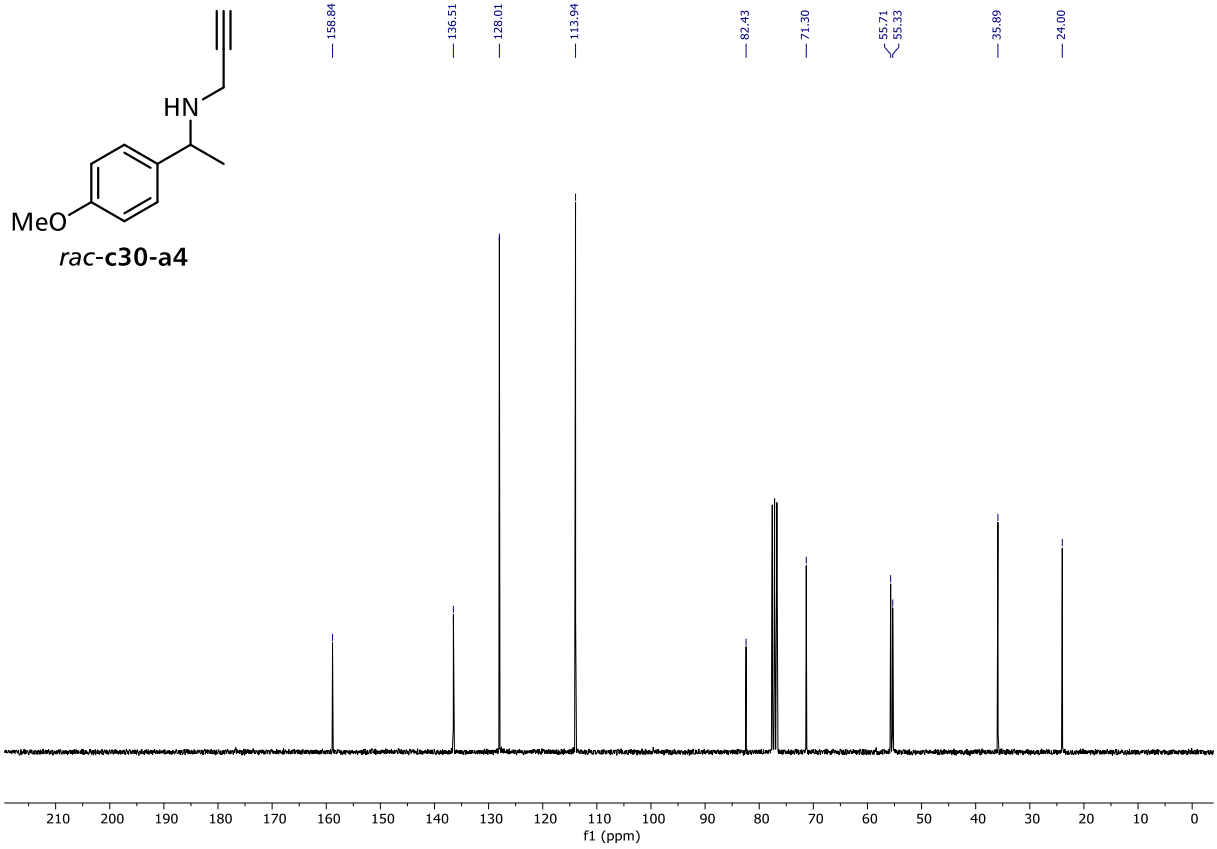


Figure S426. ^{13}C NMR spectrum of *rac*-*N*-(1-(4-methoxyphenyl)ethyl)prop-2-yn-1-amine (**c30-a4**).

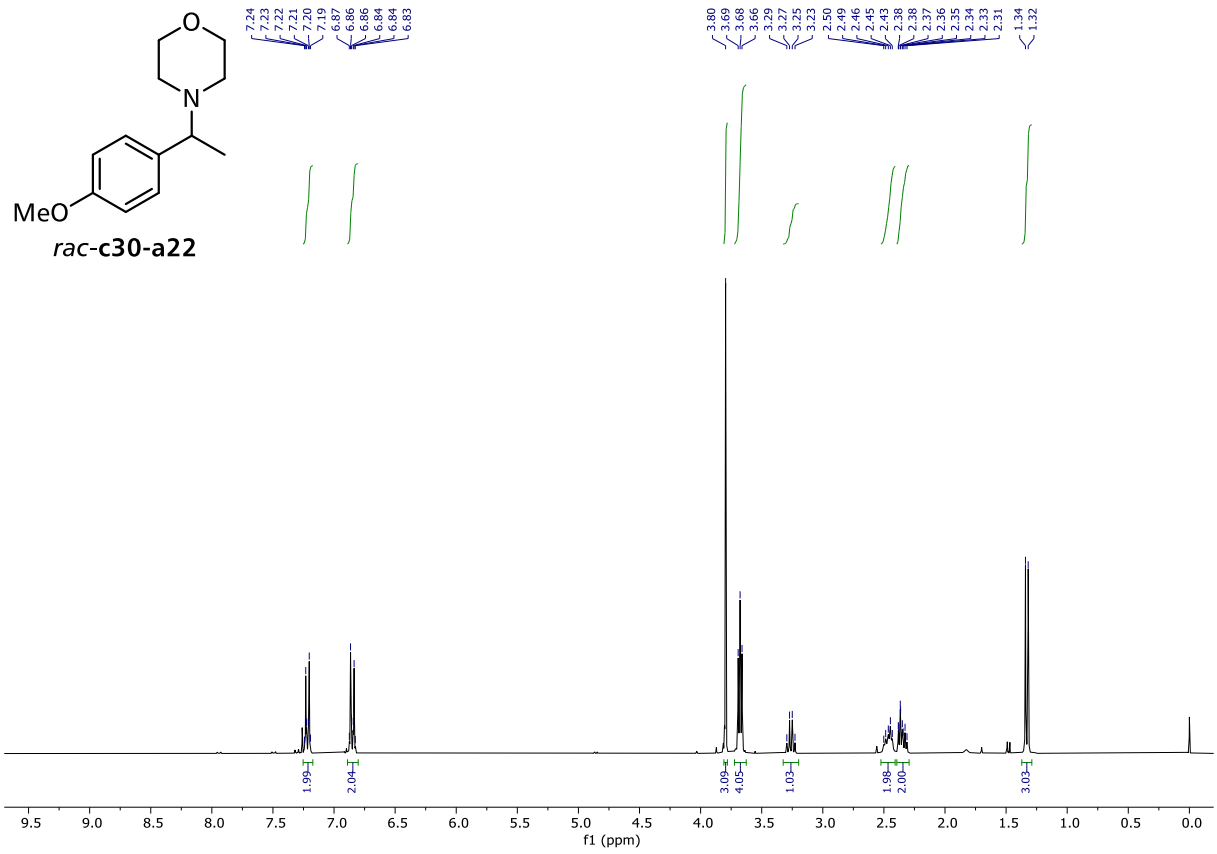


Figure S427. ^{1}H NMR spectrum of *rac*-4-(1-(4-methoxyphenyl)ethyl)morpholine (**c30-a22**).

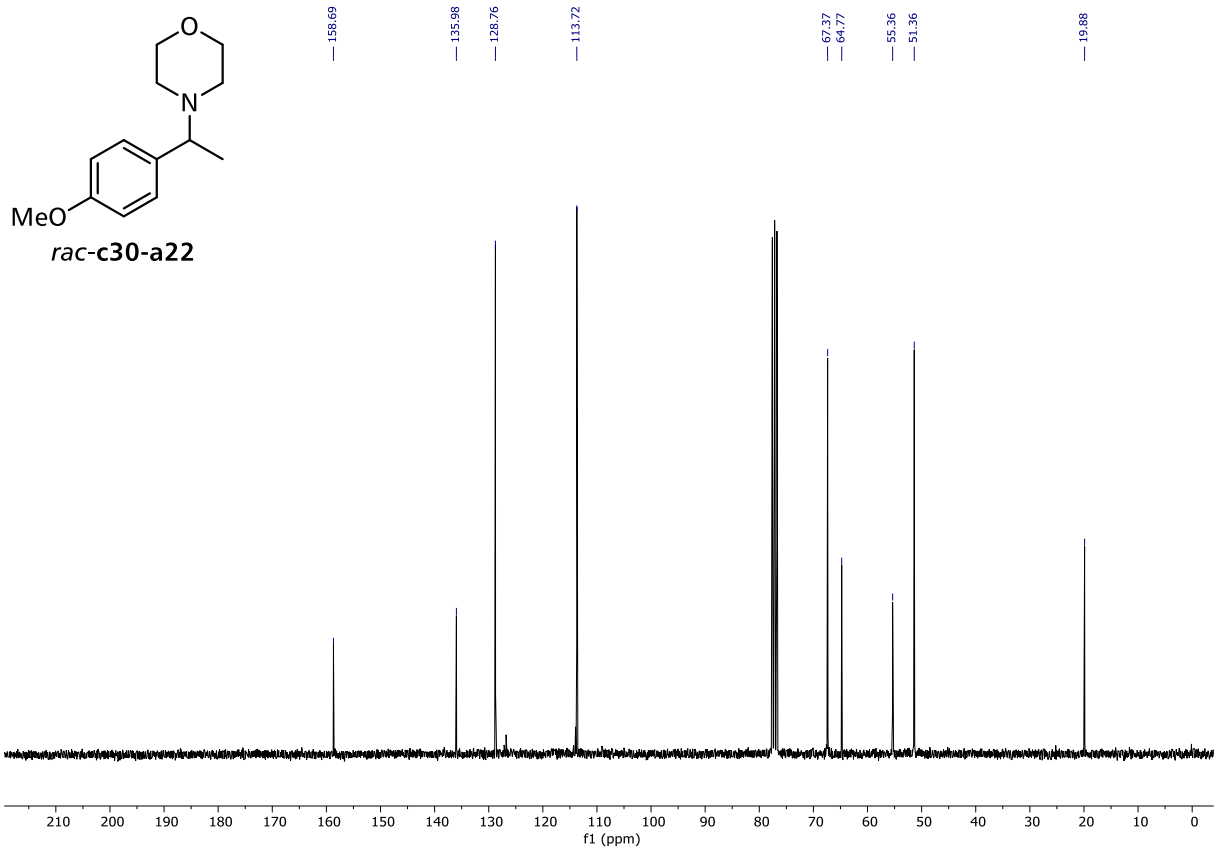


Figure S428. ^{13}C NMR spectrum of *rac*-4-(1-(4-methoxyphenyl)ethyl)morpholine (**c30-a22**).

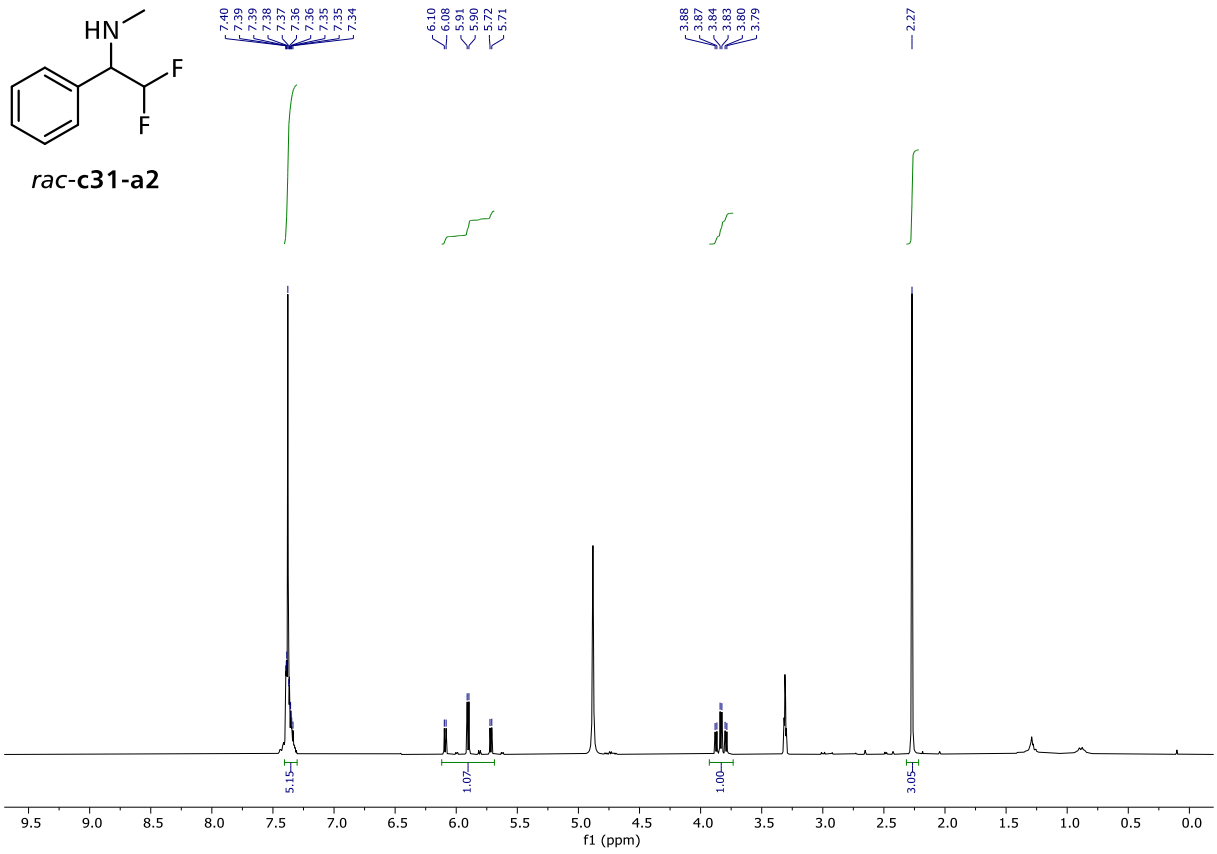


Figure S429. ^{1}H NMR spectrum of *rac*-2,2-difluoro-*N*-methyl-1-phenylethan-1-amine (**c31-a2**).

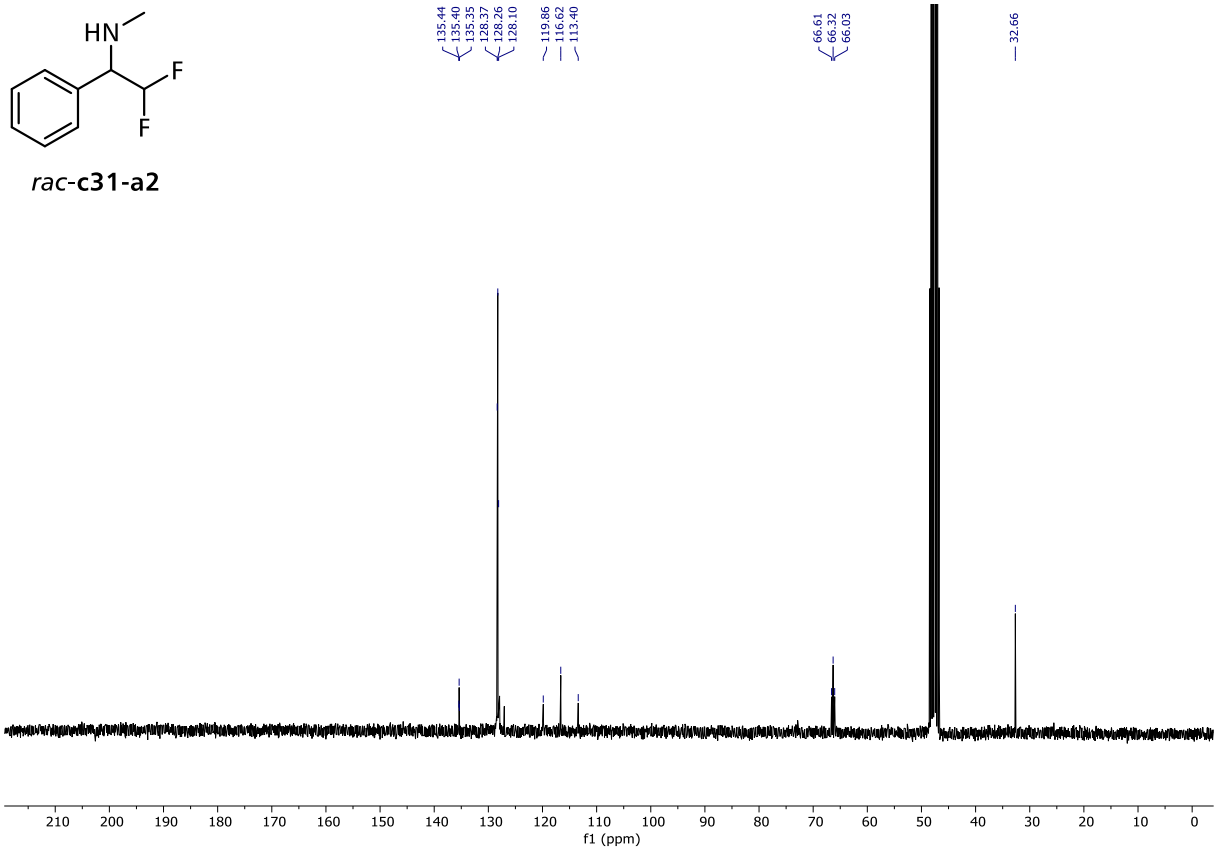


Figure S430. ^{13}C NMR spectrum of *rac*-2,2-difluoro-*N*-methyl-1-phenylethan-1-amine (**c31-a2**).

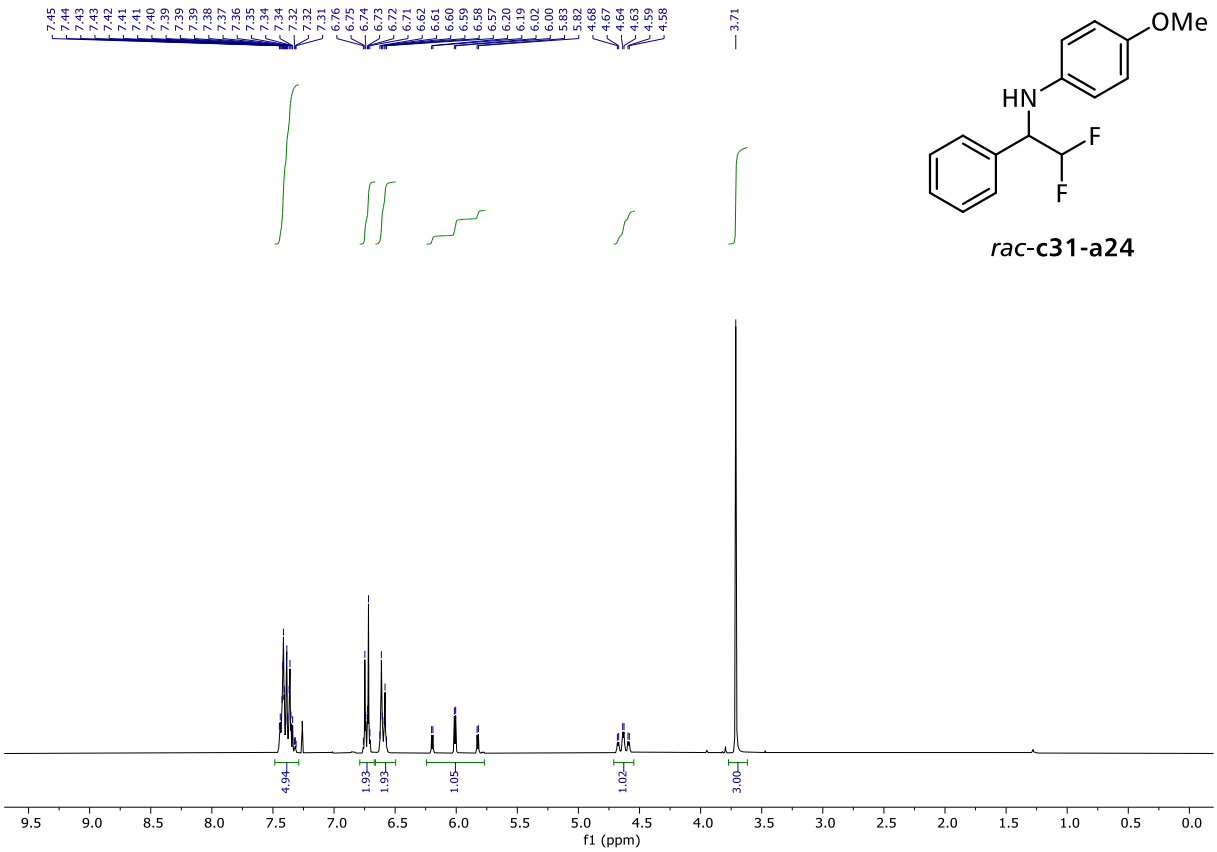


Figure S431. ^{1}H NMR spectrum of *rac*-*N*-(2,2-difluoro-1-phenylethyl)-4-methoxyaniline (**c31-a24**).

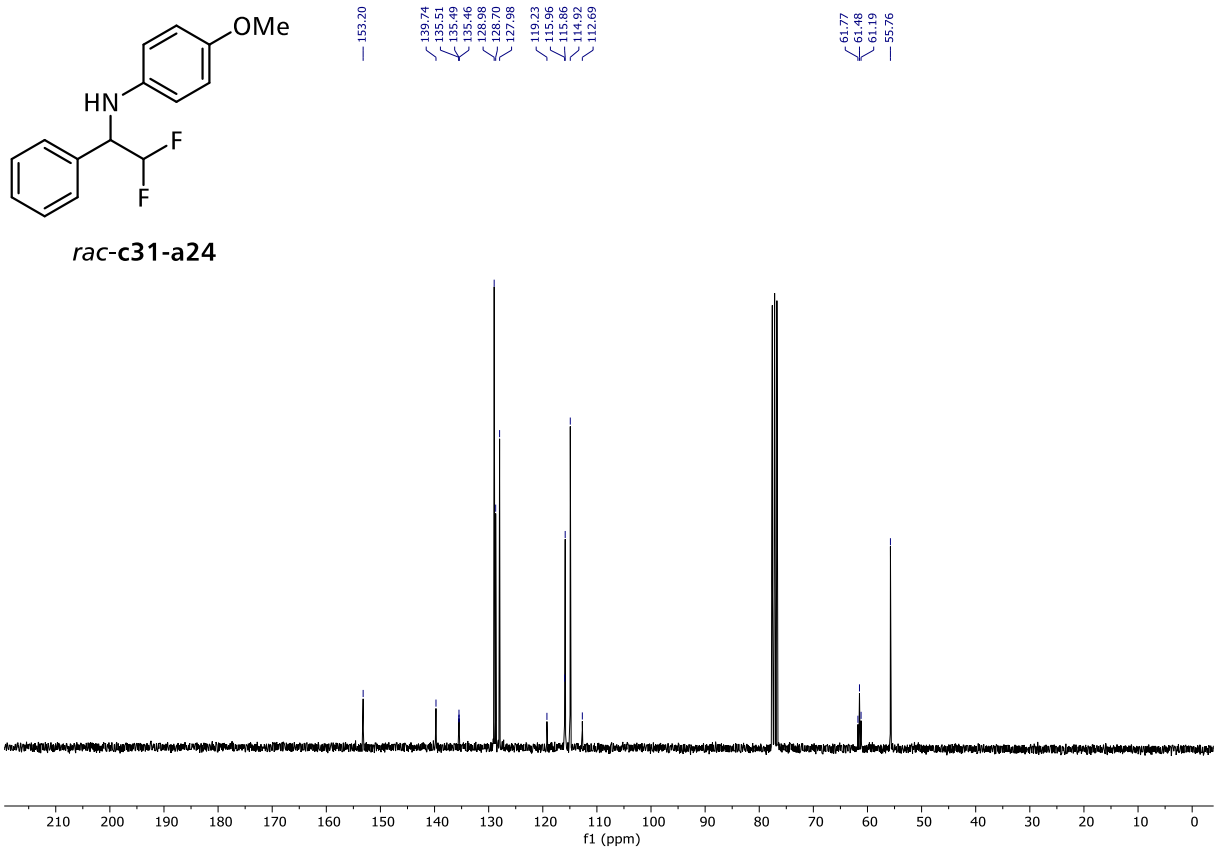


Figure S432. ^{13}C NMR spectrum of *rac*-*N*-(2,2-difluoro-1-phenylethyl)-4-methoxyaniline (**c31-a24**).

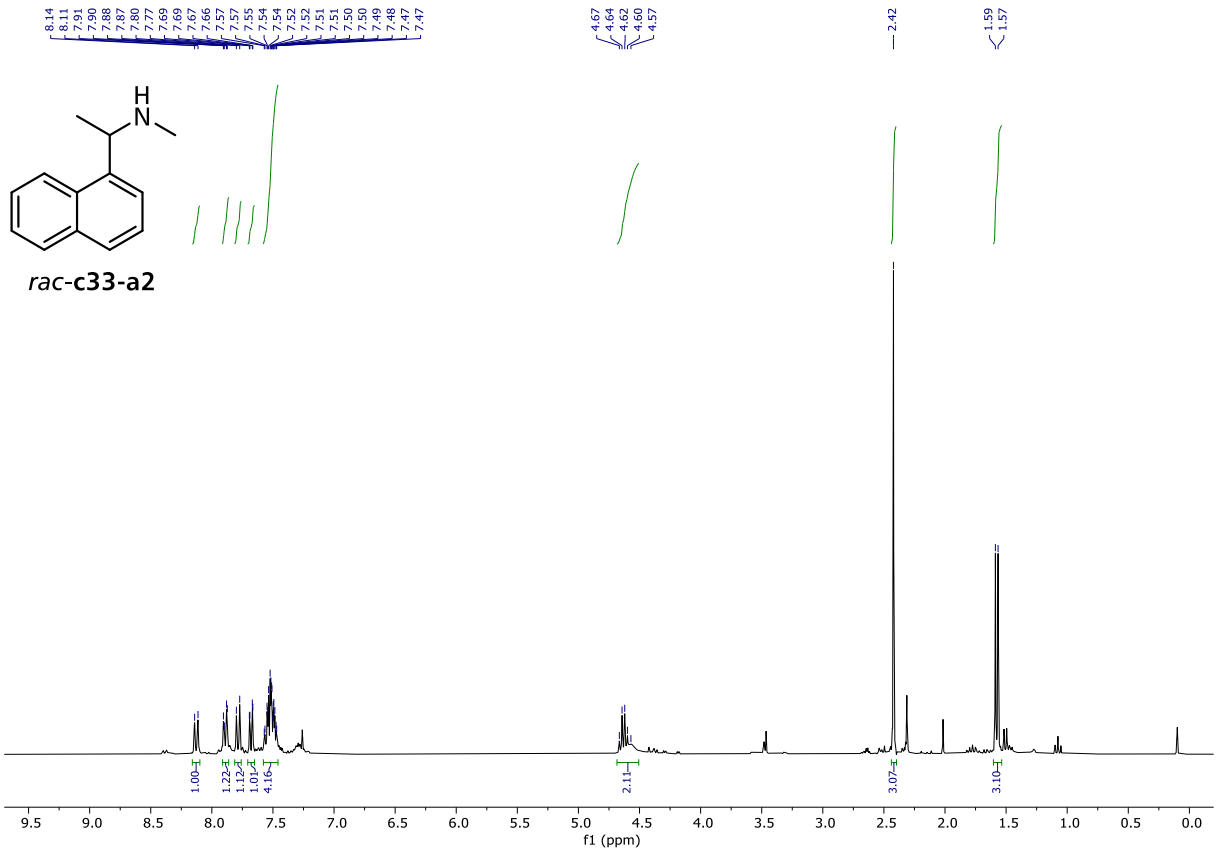


Figure S433. ^{1}H NMR spectrum of *rac*-*N*-methyl-1-(naphthalen-1-yl)ethan-1-amine (**c33-a2**).

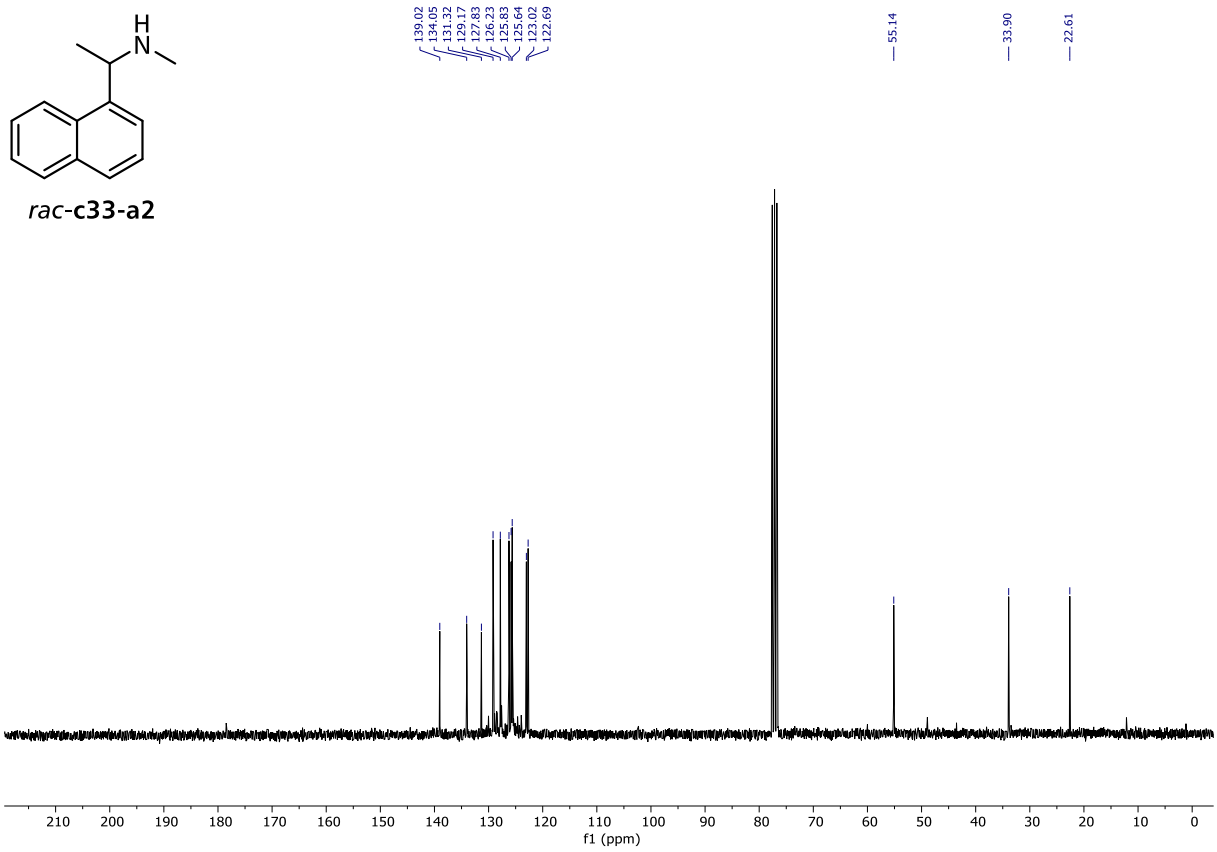


Figure S434. ^{13}C NMR spectrum of *rac*-*N*-methyl-1-(naphthalen-1-yl)ethan-1-amine (**c33-a2**).

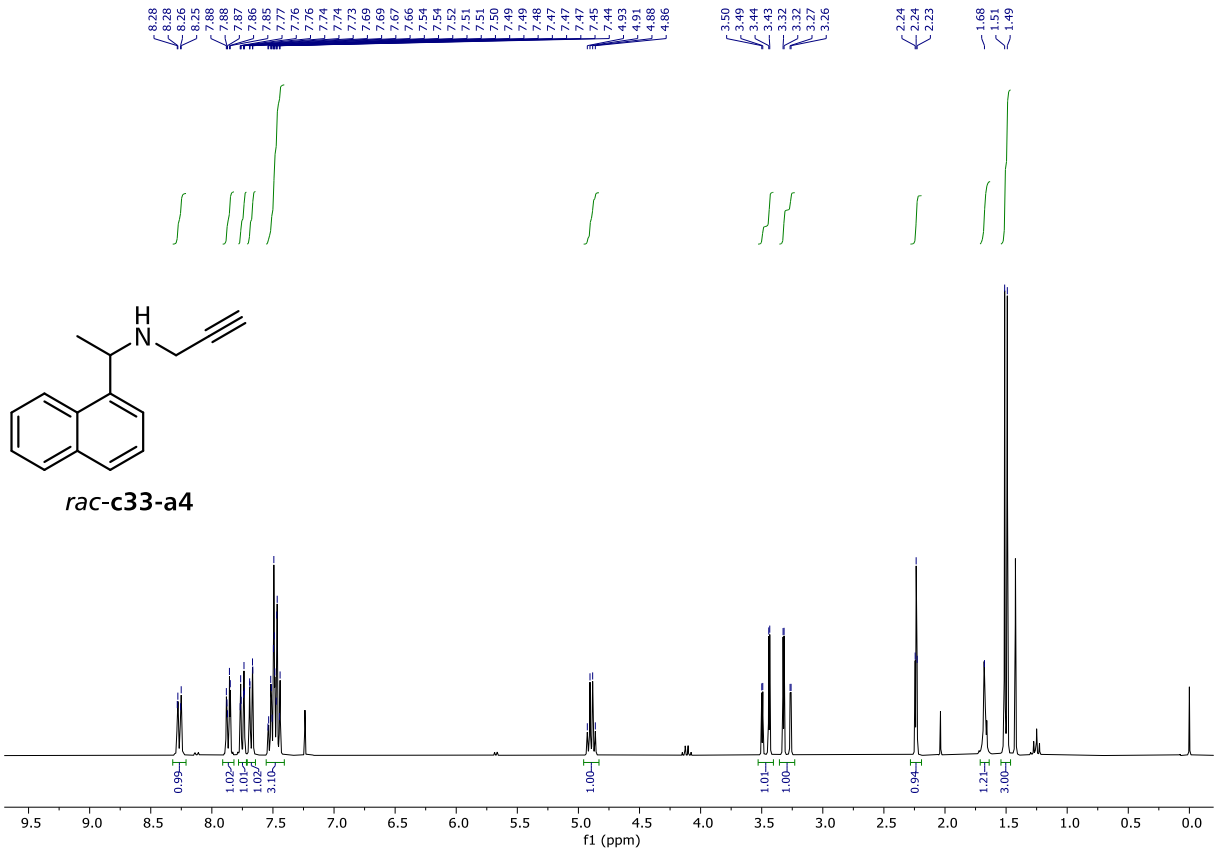


Figure S435. ^{1}H NMR spectrum of *rac*-*N*-(1-(naphthalen-1-yl)ethyl)prop-2-yn-1-amine (**c33-a4**).

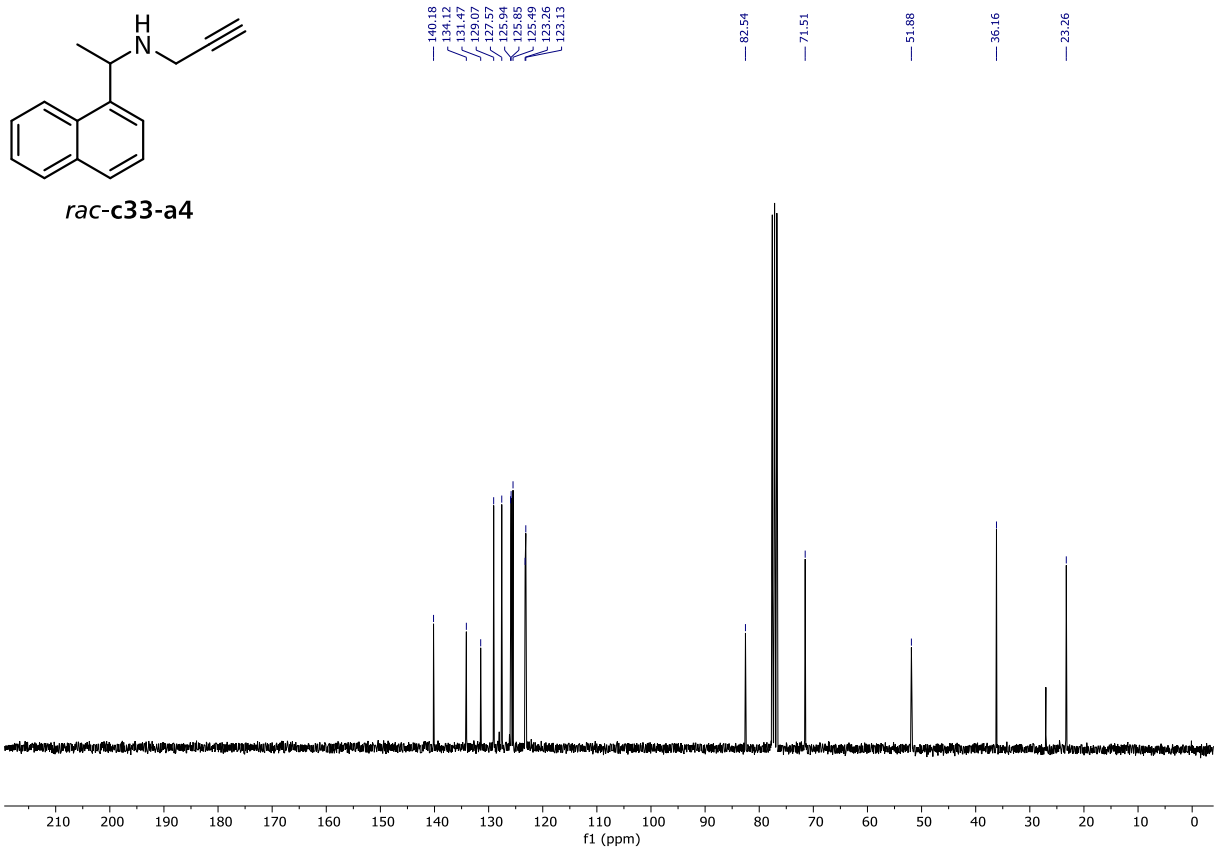


Figure S436. ^{13}C NMR spectrum of *rac*-*N*-(1-(naphthalen-1-yl)ethyl)prop-2-yn-1-amine (**c33-a4**).

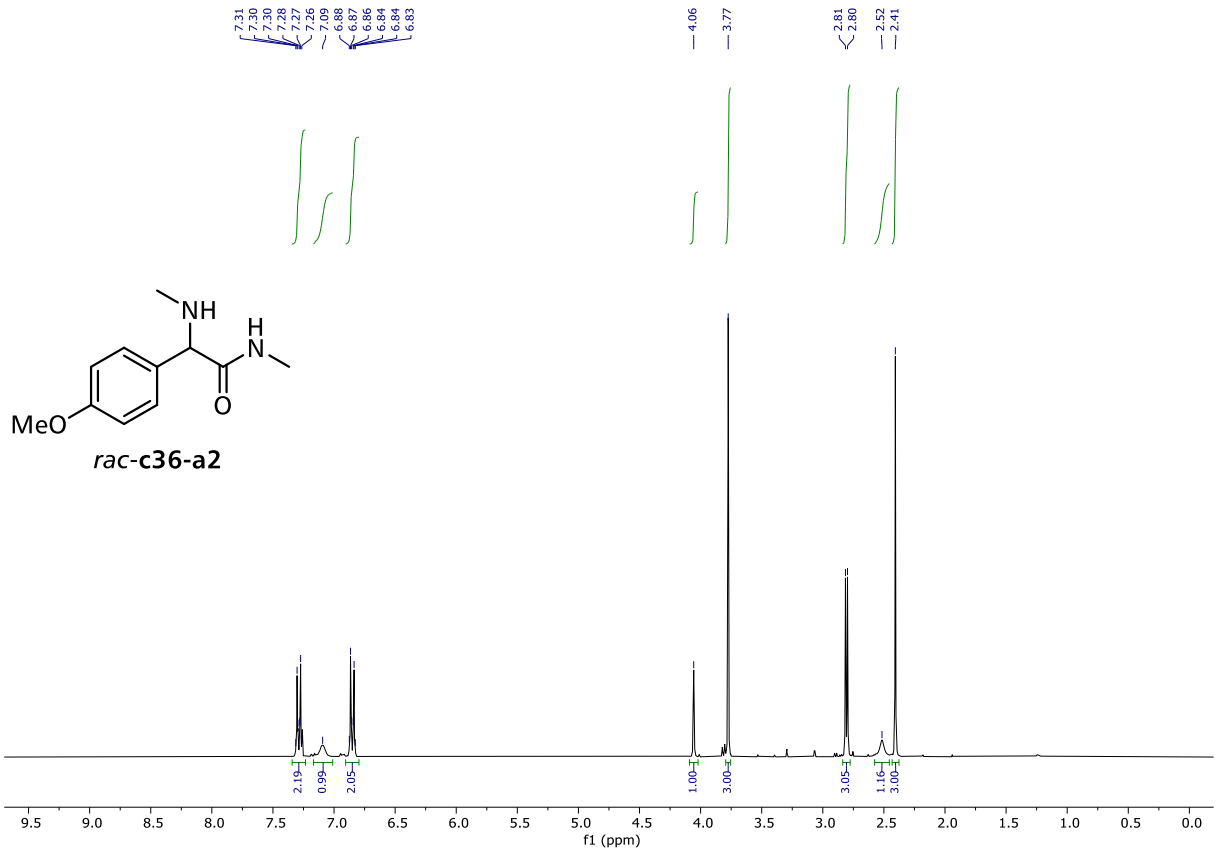


Figure S437. ^{1}H NMR spectrum of *rac*-2-(4-methoxyphenyl)-*N*-methyl-2-(methylamino)acetamide (**c36-a2**).

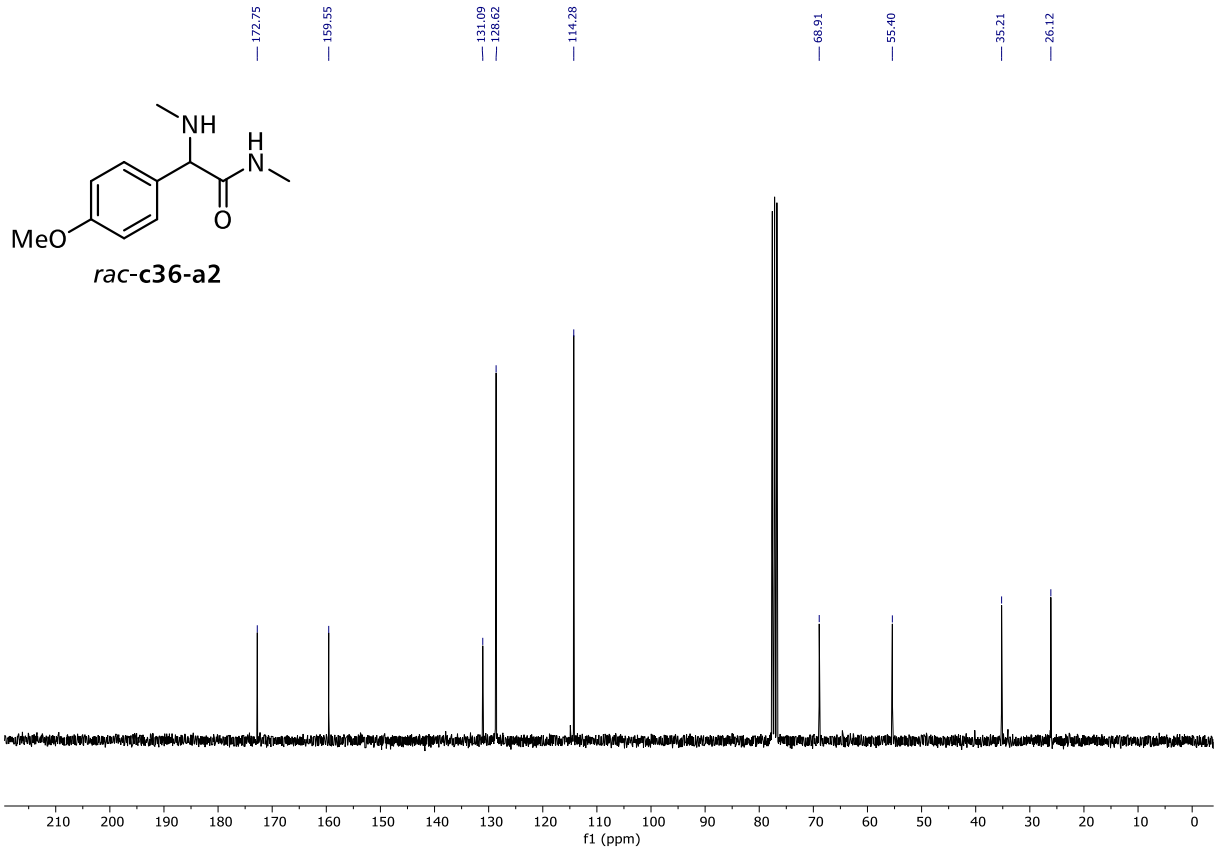


Figure S438. ^{13}C NMR spectrum of *rac*-2-(4-methoxyphenyl)-*N*-methyl-2-(methylamino)acetamide (**c36-a2**).

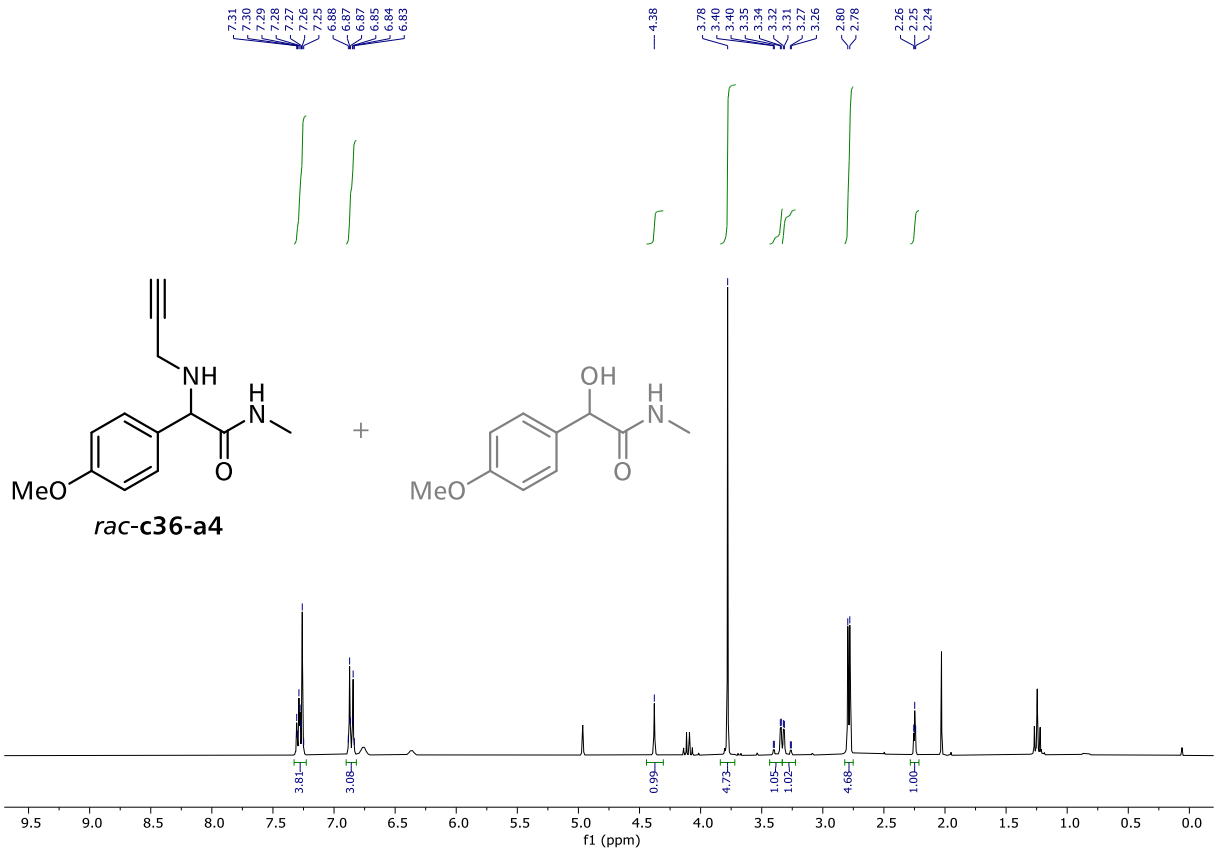


Figure S439. ^{1}H NMR spectrum of *rac*-2-(4-methoxyphenyl)-*N*-methyl-2-(prop-2-yn-1-ylamino)acetamide (**c36-a2**).

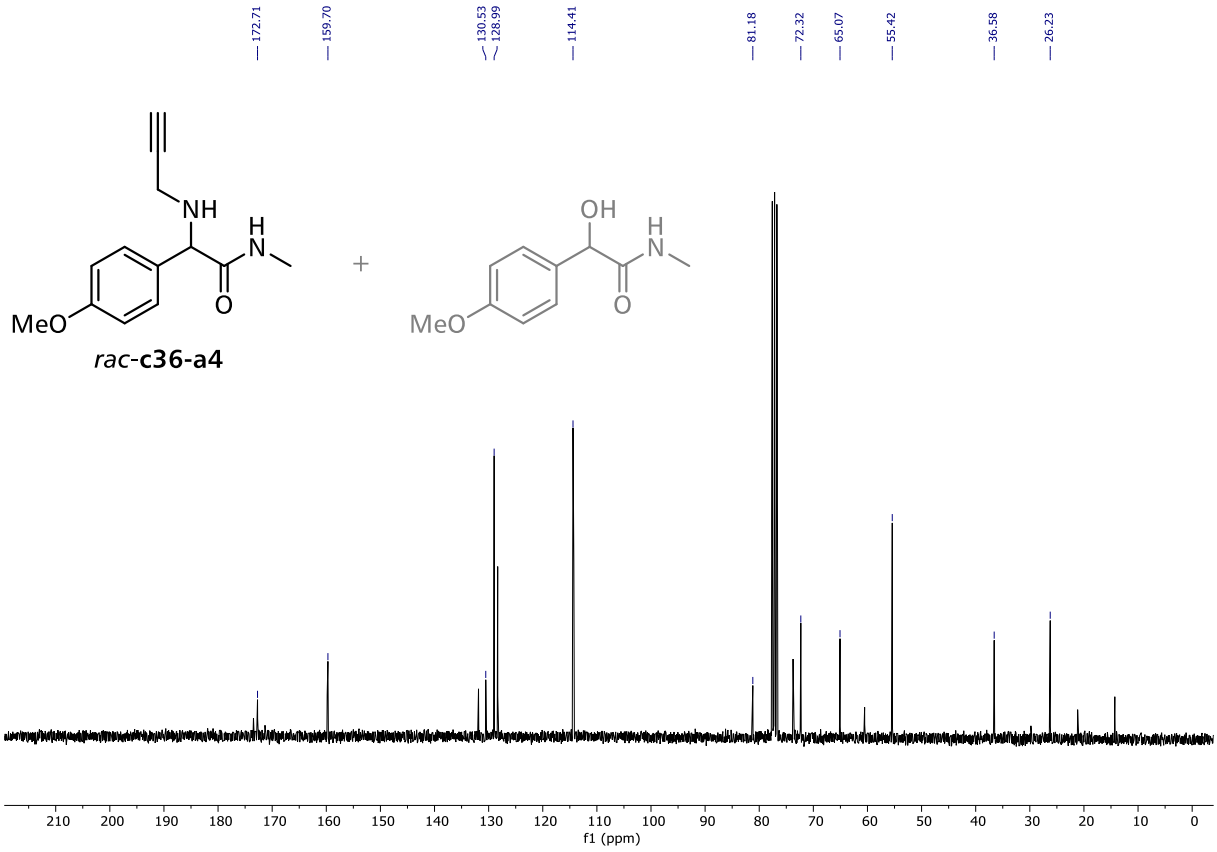


Figure S440. ^{13}C NMR spectrum of *rac*-2-(4-methoxyphenyl)-*N*-methyl-2-(prop-2-yn-1-ylamino)acetamide (**c36-a2**).

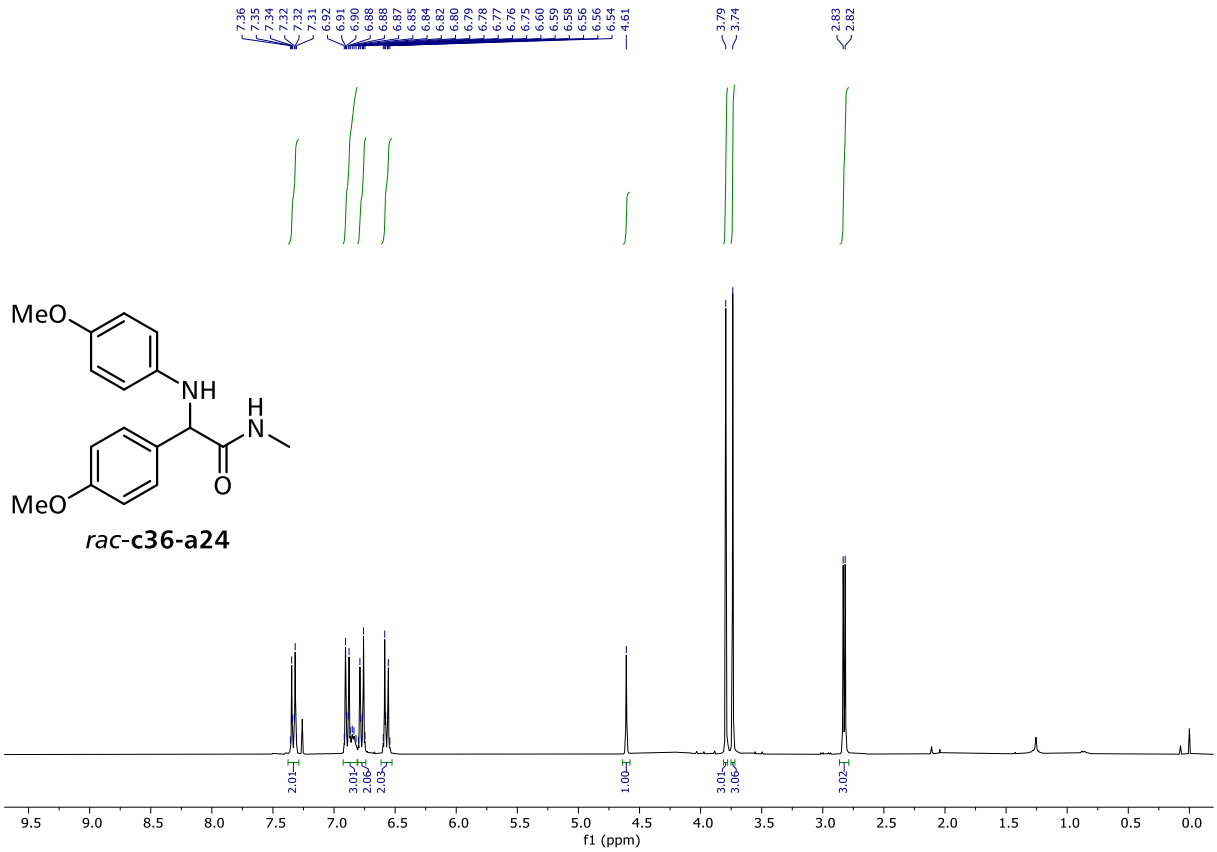


Figure S441. ^{1}H NMR spectrum of *rac*-2-(4-methoxyphenyl)-2-((4-methoxyphenyl)amino)-*N*-methyl-acetamide (**c36-a24**).

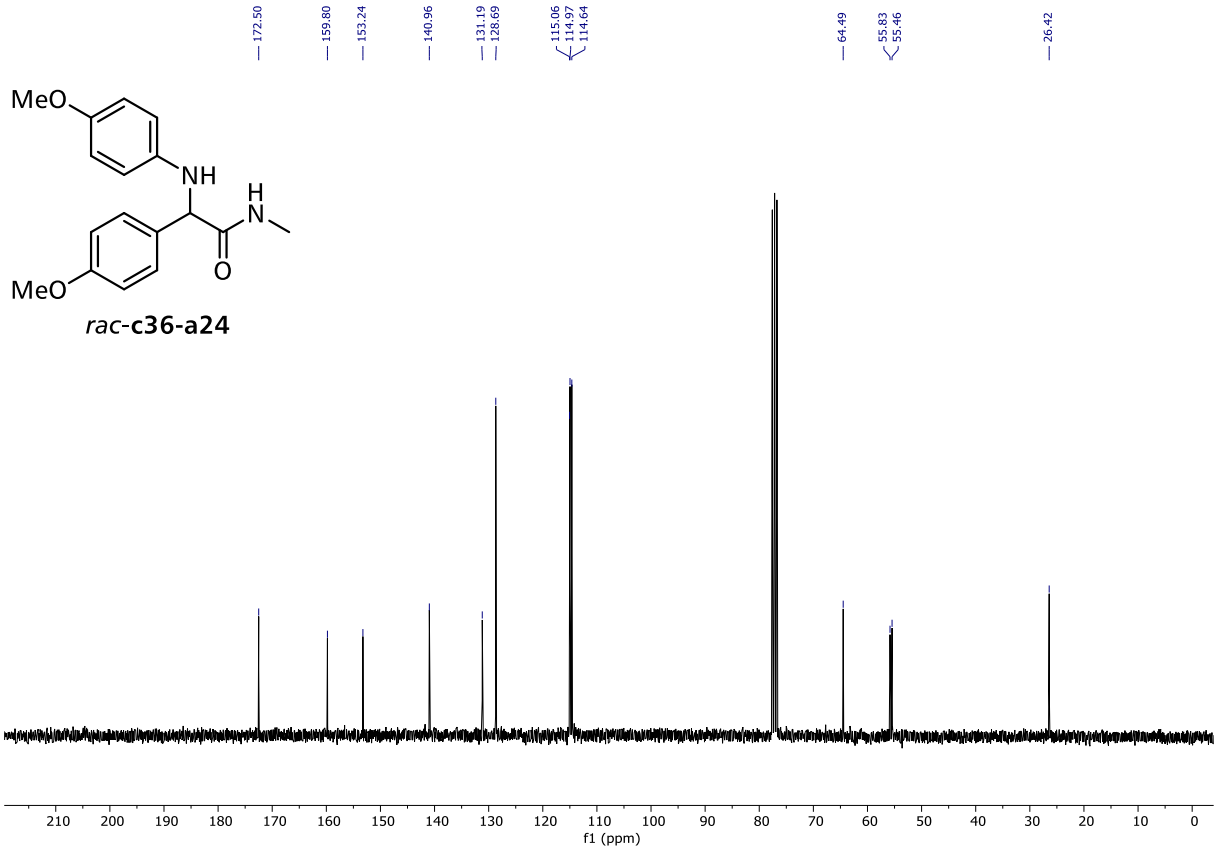


Figure S442. ^{13}C NMR spectrum of *rac*-2-(4-methoxyphenyl)-2-((4-methoxyphenyl)amino)-*N*-methyl-acetamide (**c36-a24**).

Products of Preparative-Scale Biotransformations

Provided Spectra and Chromatograms:

- (*S*)-**c8-a10:** ^{1}H NMR, ^{13}C NMR, GC–MS, HRMS, chiral-phase HPLC
- (*S*)-**c10-a10:** ^{1}H NMR, ^{13}C NMR, GC–MS, HRMS, chiral-phase GC
- (*R*)-**c22-a4:** ^{1}H NMR, ^{13}C NMR, GC–MS, HRMS, chiral-phase GC
- (*R*)-**c24-a2:** ^{1}H NMR, ^{13}C NMR, GC–MS, HRMS, chiral-phase HPLC
- (*R*)-**c24-a4:** ^{1}H NMR, ^{13}C NMR, GC–MS, HRMS, chiral-phase HPLC

All NMR spectra are also openly available as raw data and MNOVA files in the Mendeley Data repository (https://data.mendeley.com/) at https://doi.org/10.17632/jn4sfsrz8x.2.

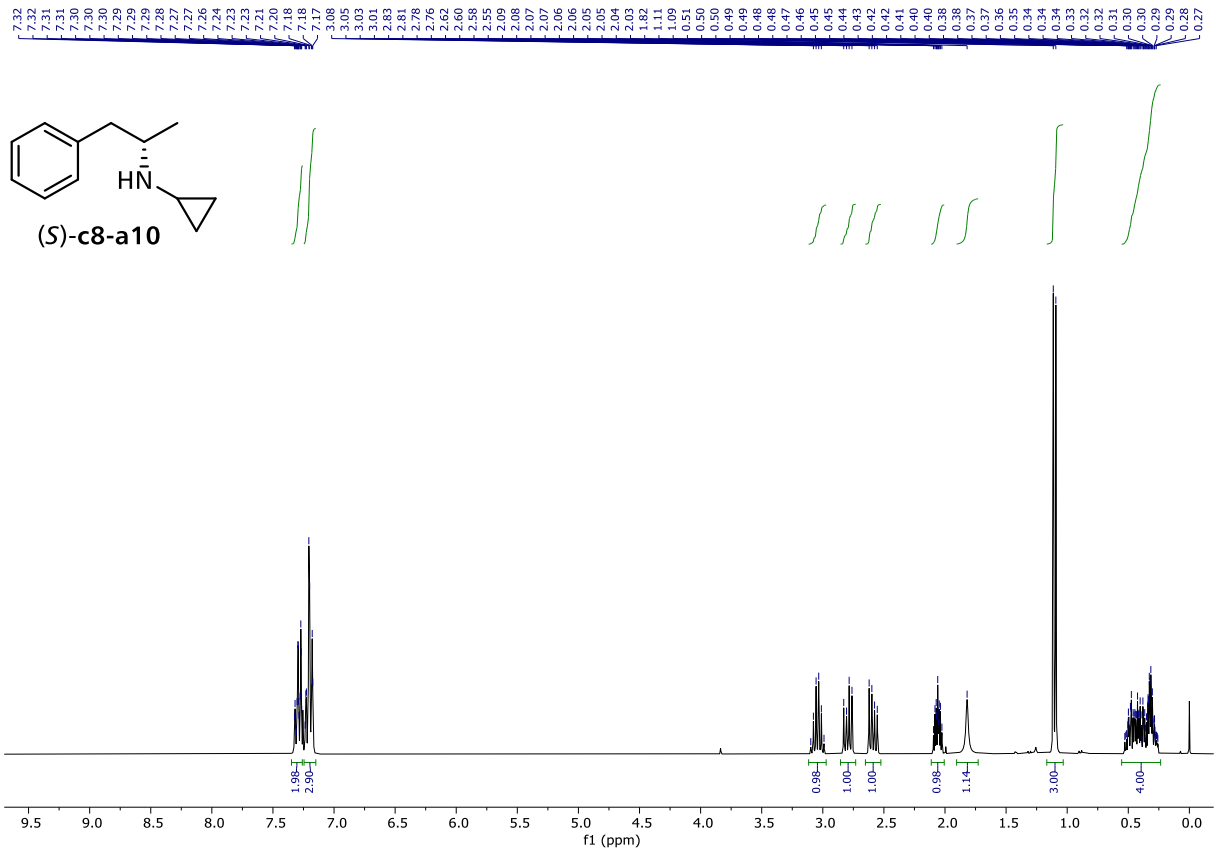


Figure S443. ^{1}H NMR spectrum of (*S*)-*N*-(1-phenylpropan-2-yl)cyclopropanamine (**c8-a10**).

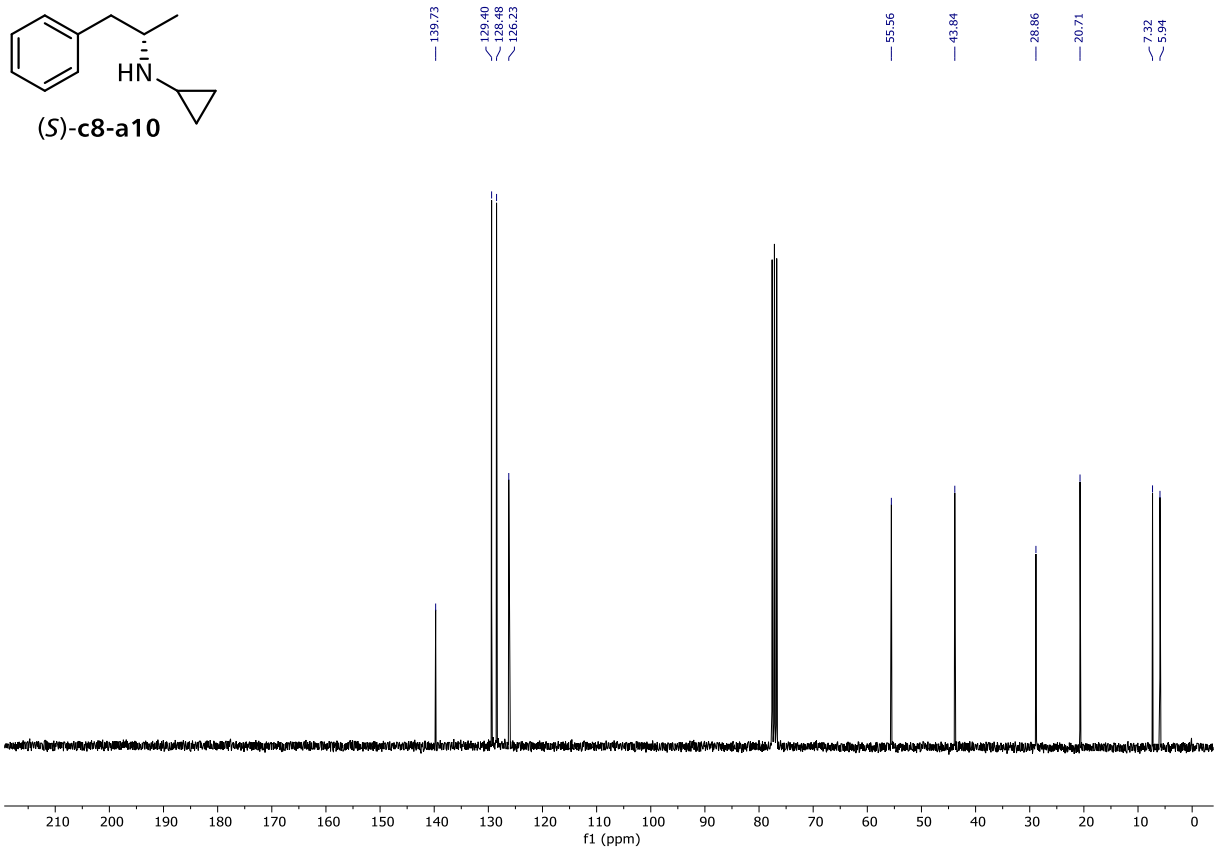


Figure S444. ^{13}C NMR spectrum of (*S*)-*N*-(1-phenylpropan-2-yl)cyclopropanamine (**c8-a10**).

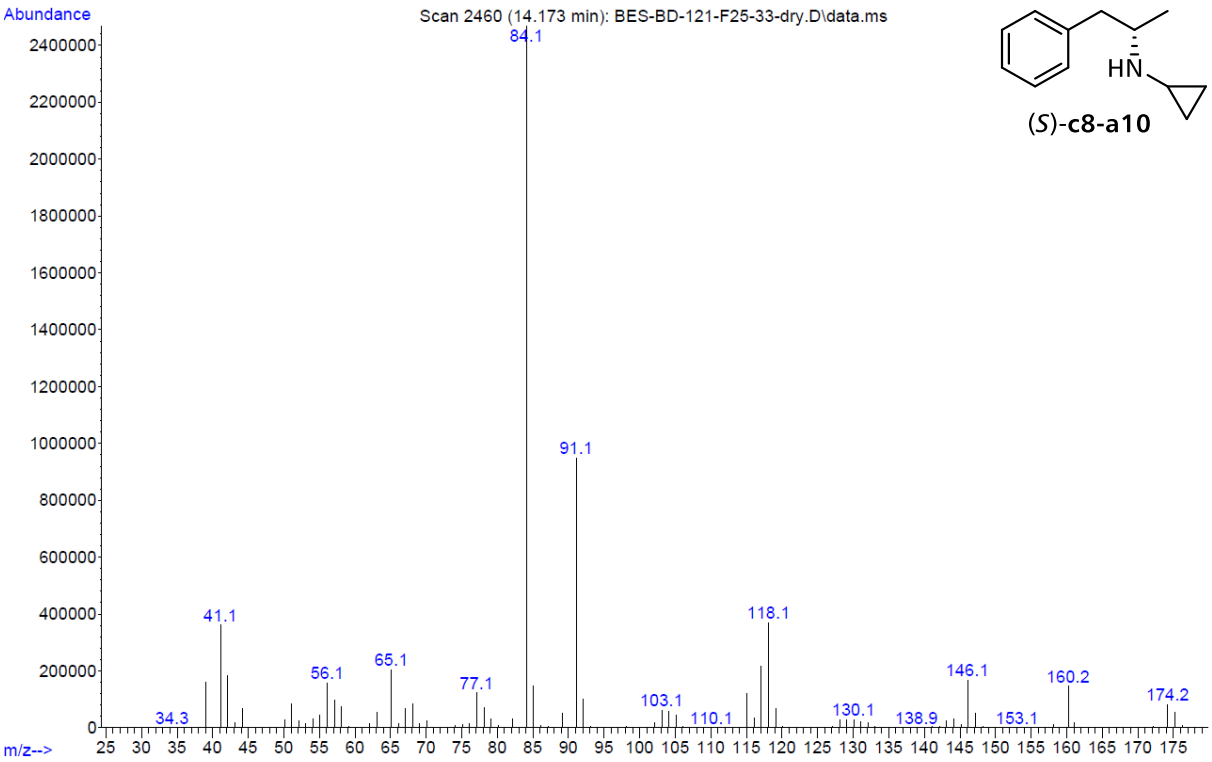


Figure S445. GC–MS spectrum of (*S*)-*N*-(1-phenylpropan-2-yl)cyclopropanamine (**c8-a10**).

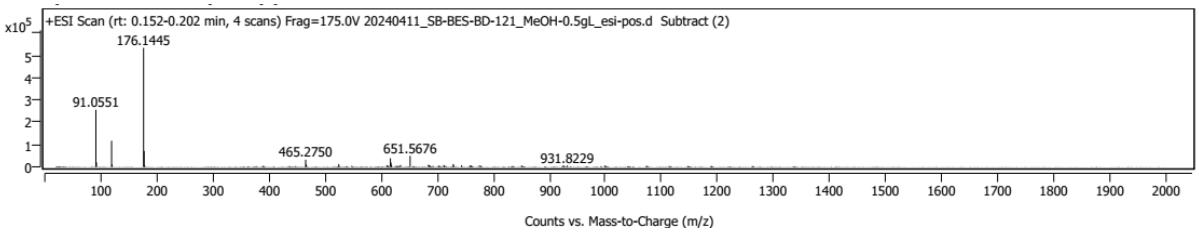


Figure S446. HRMS spectrum of (*S*)-*N*-(1-phenylpropan-2-yl)cyclopropanamine (**c8-a10**).

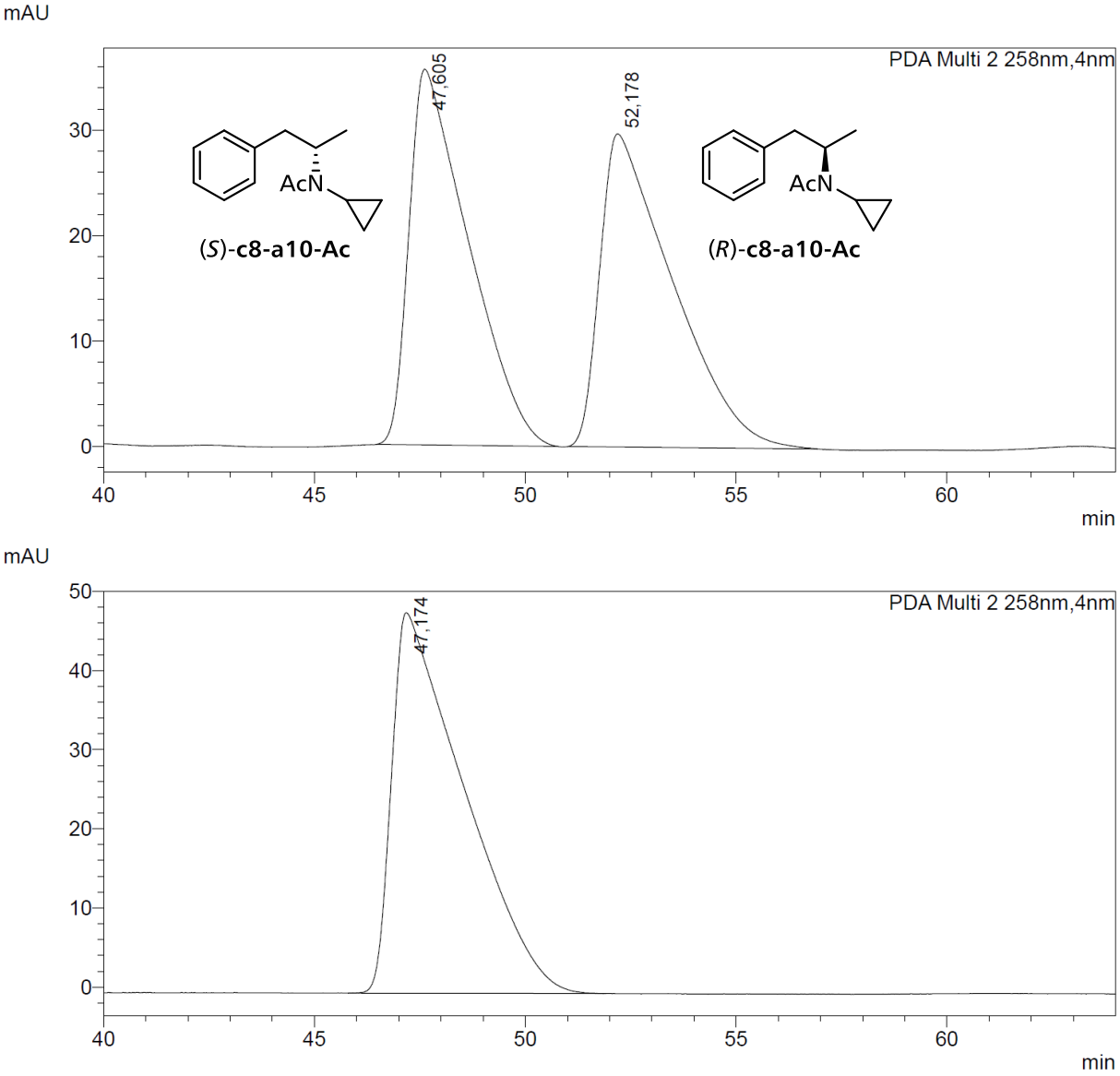


Figure S447. Determination of the enantiomeric excess and absolute configuration of (*S*)-**c8-a10-Ac** using HPLC method HPLC-C10. Racemic reference (top), biotransformation product (bottom). The peaks were assigned to the two enantiomers based on the elution order reported by Gergel *et al*. (2023).[118]

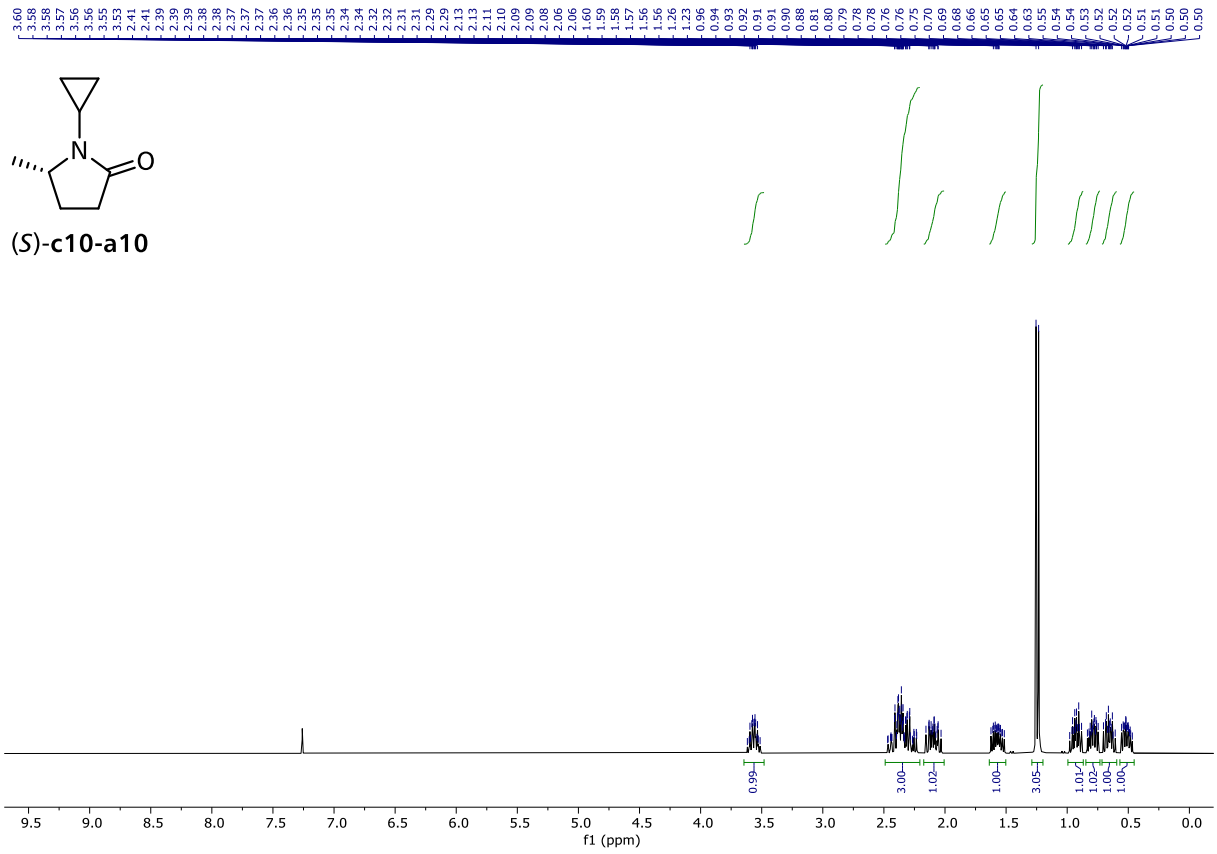


Figure S448. ^{1}H NMR spectrum of (*S*)-1-cyclopropyl-5-methylpyrrolidin-2-one (**c10-a10**).

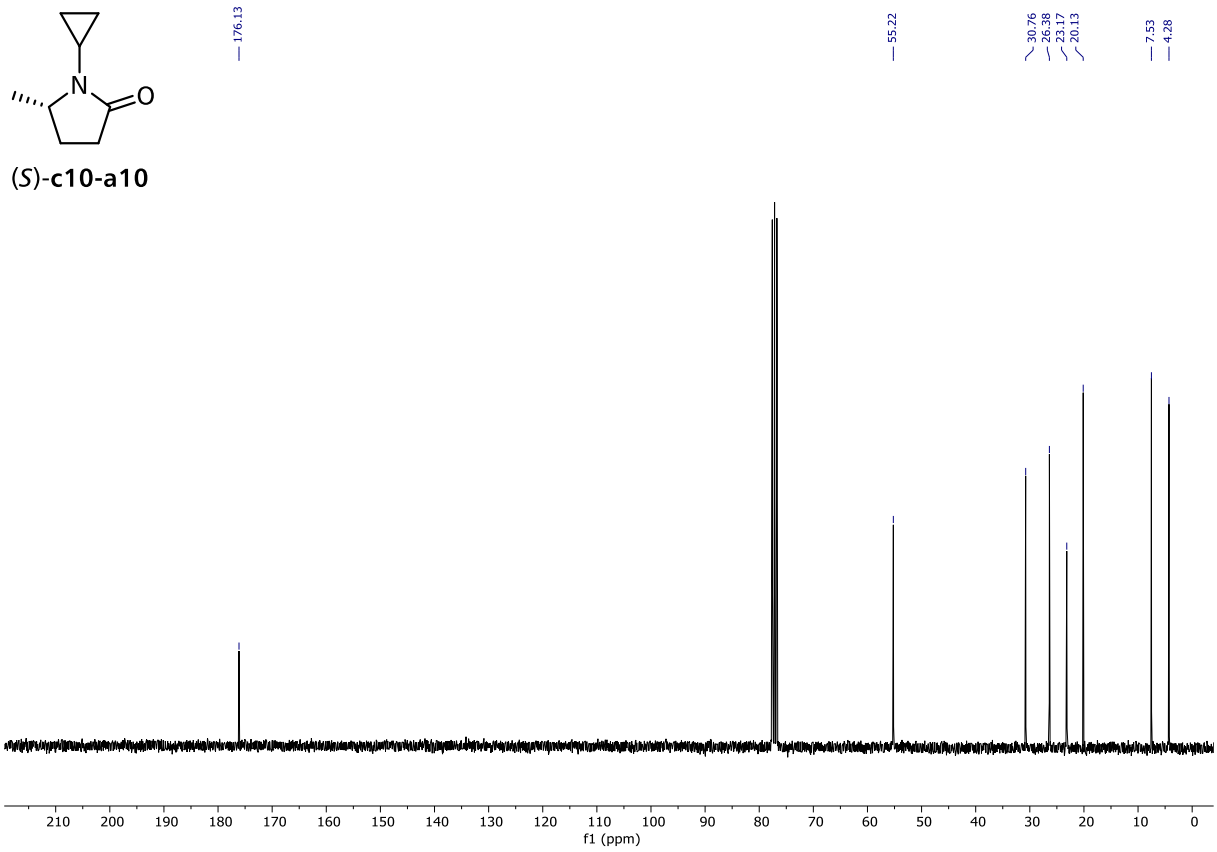


Figure S449. ^{13}C NMR spectrum of (*S*)-1-cyclopropyl-5-methylpyrrolidin-2-one (**c10-a10**).

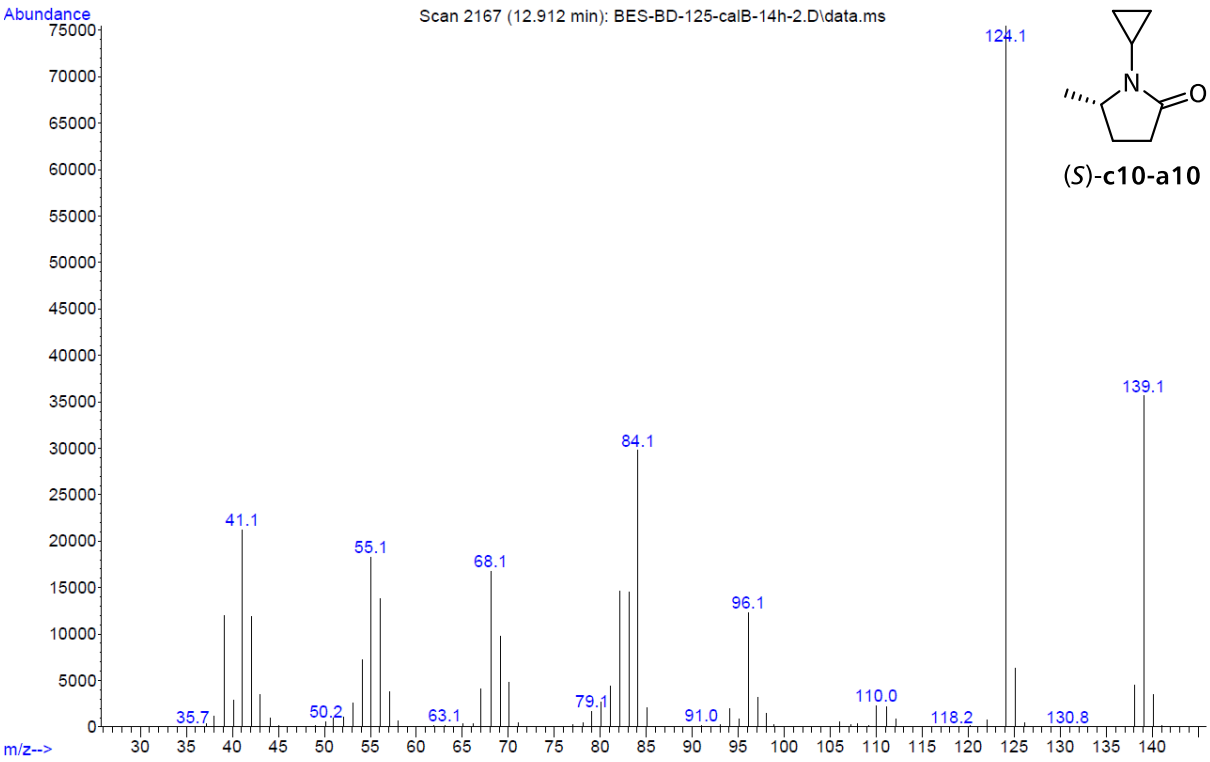


Figure S450. GC–MS spectrum of (*S*)-1-cyclopropyl-5-methylpyrrolidin-2-one (**c10-a10**).

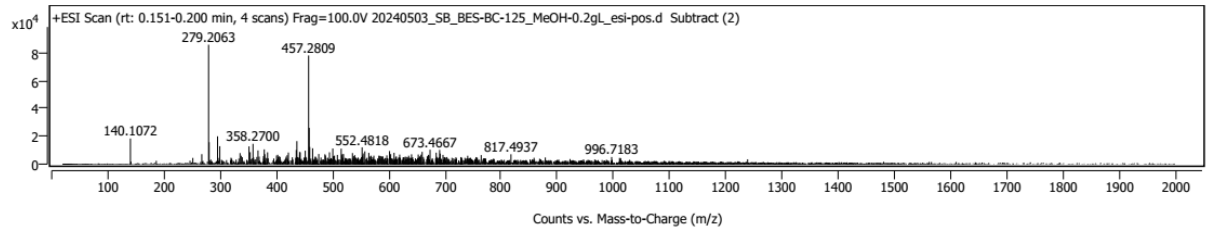


Figure S451. HRMS spectrum of (*S*)-1-cyclopropyl-5-methylpyrrolidin-2-one (**c10-a10**).

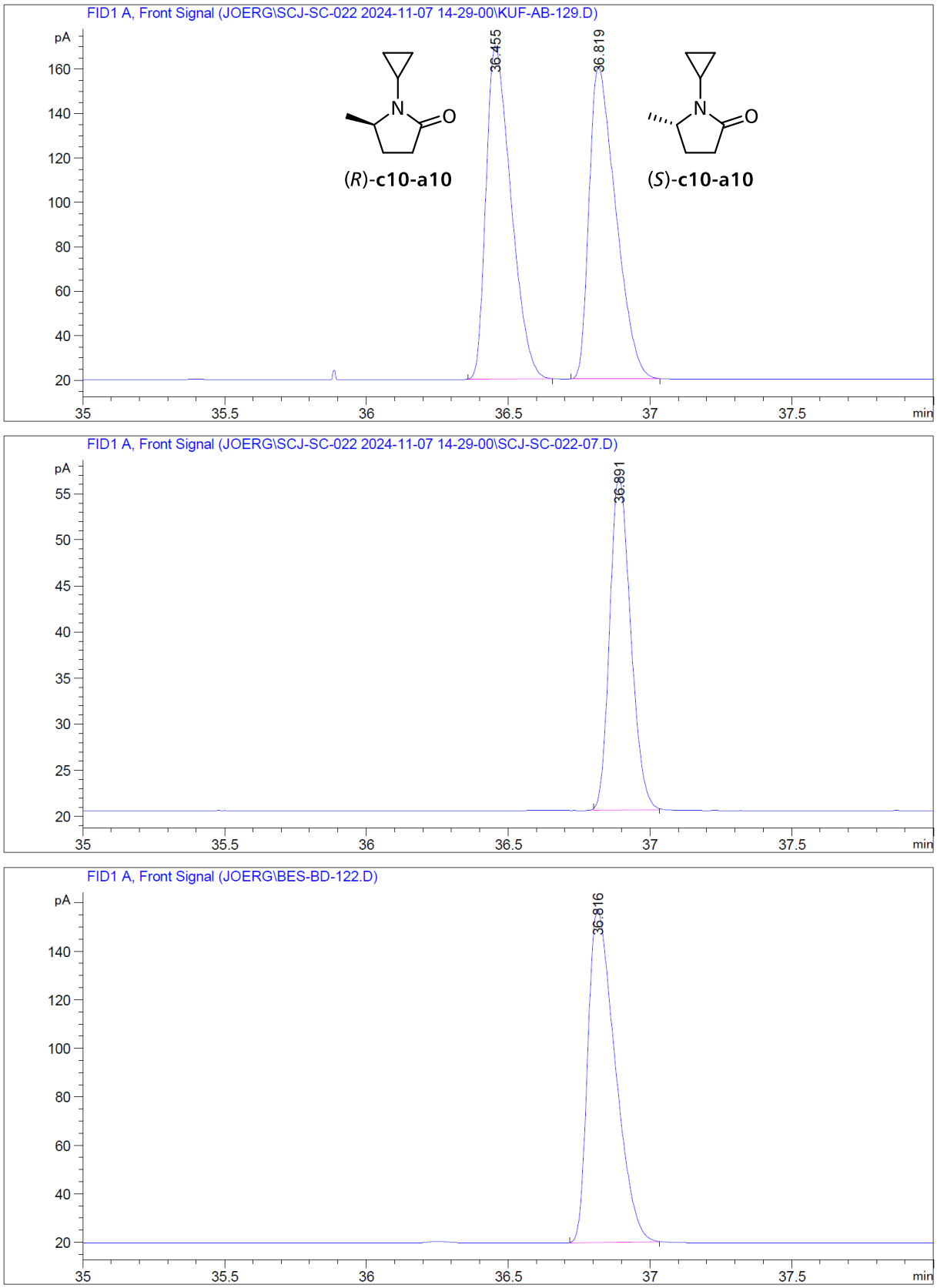


Figure S452. Determination of the enantiomeric excess and absolute configuration of (*S*)-**c10-a10** using GC method GC-C7. Racemic reference (top), independently synthesised (*S*)-enantiomer (middle), biotransformation product (bottom).

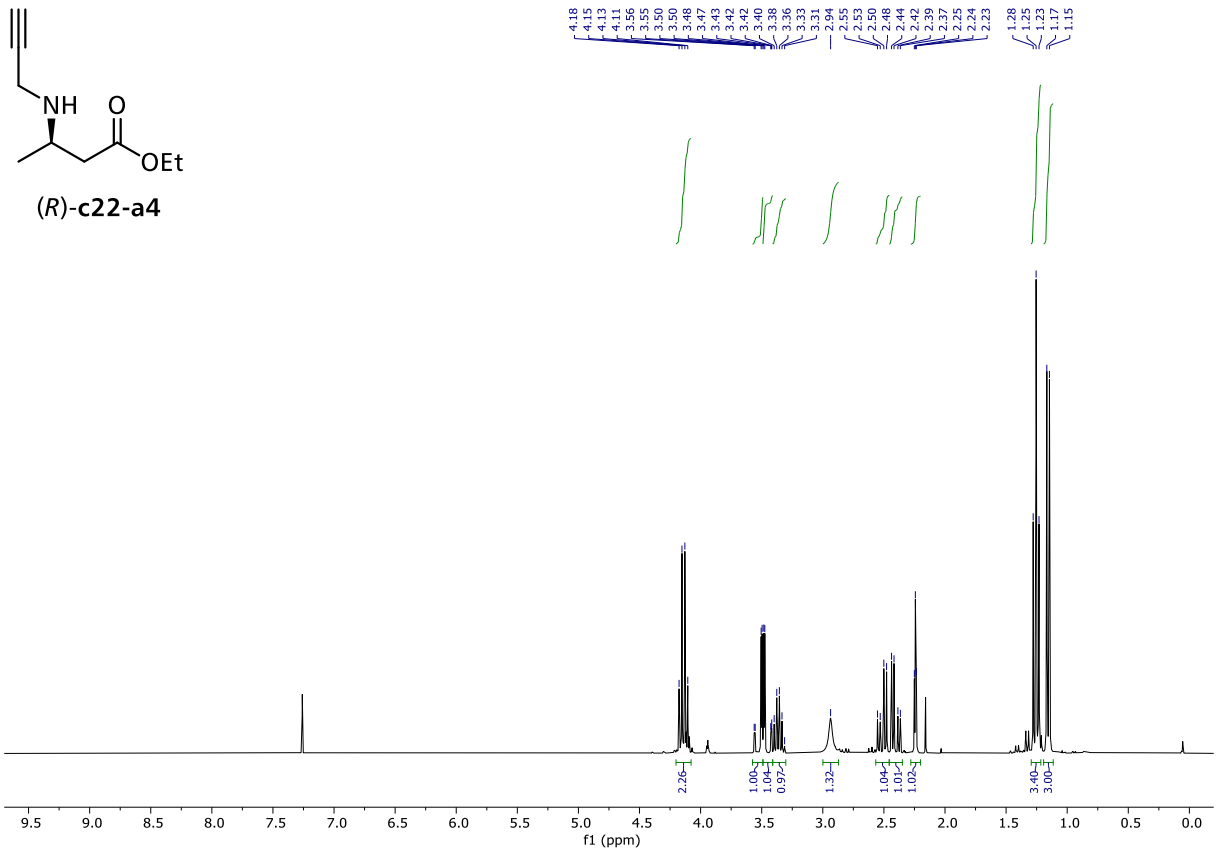


Figure S453. ^{1}H NMR spectrum of (*R*)-ethyl 3-(prop-2-yn-1-ylamino)butanoate (**c22-a4**).

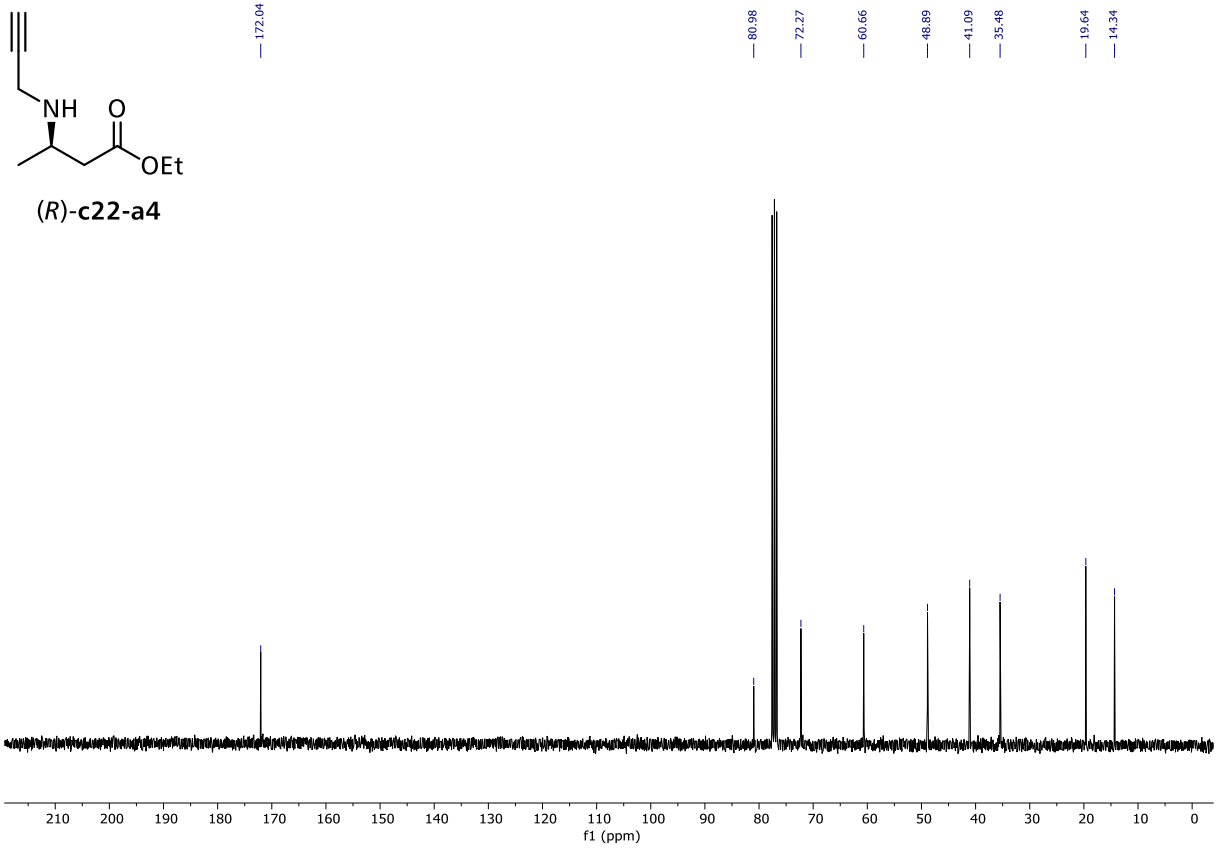


Figure S454. ^{13}C NMR spectrum of (*R*)-ethyl 3-(prop-2-yn-1-ylamino)butanoate (**c22-a4**).

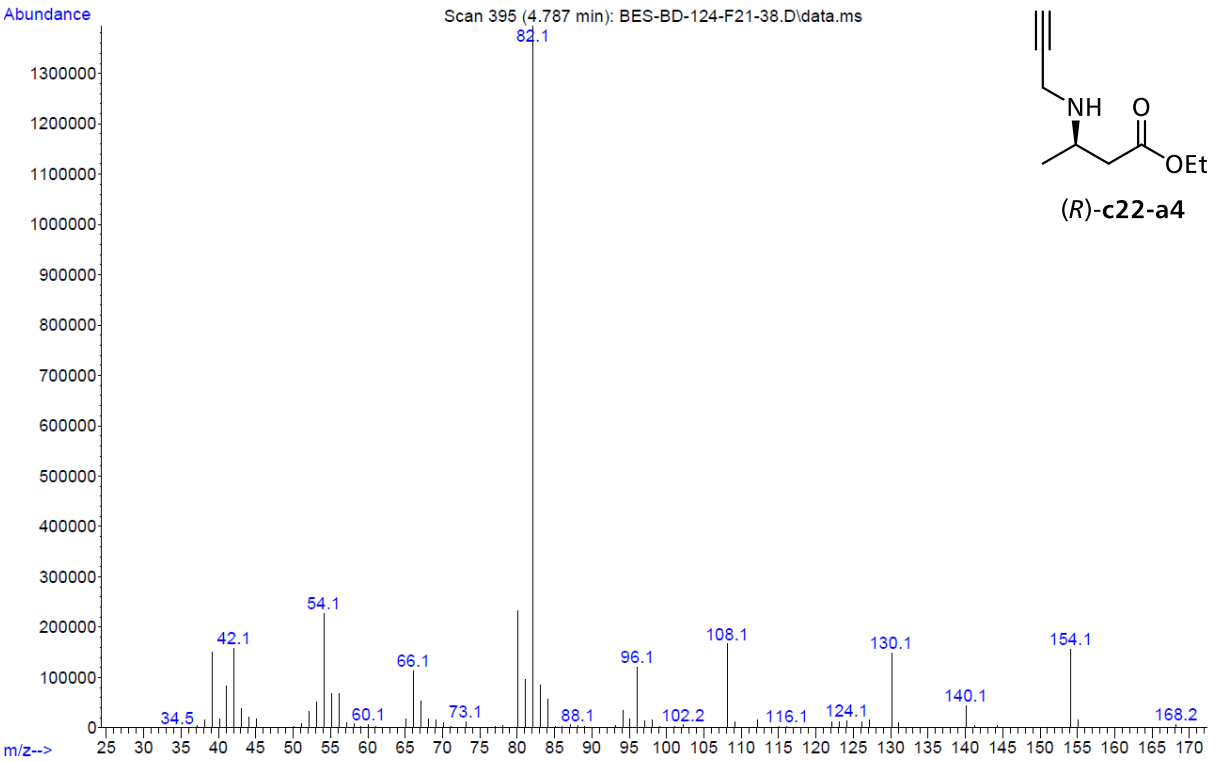


Figure S455. GC–MS spectrum of (*R*)-ethyl 3-(prop-2-yn-1-ylamino)butanoate (**c22-a4**).

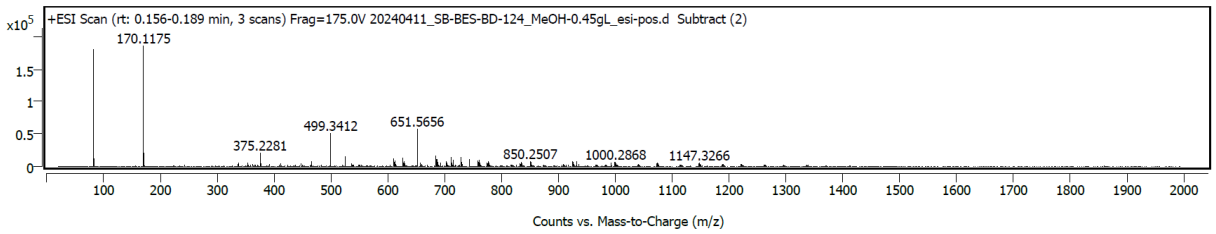


Figure S456. HRMS spectrum of (*R*)-ethyl 3-(prop-2-yn-1-ylamino)butanoate (**c22-a4**).

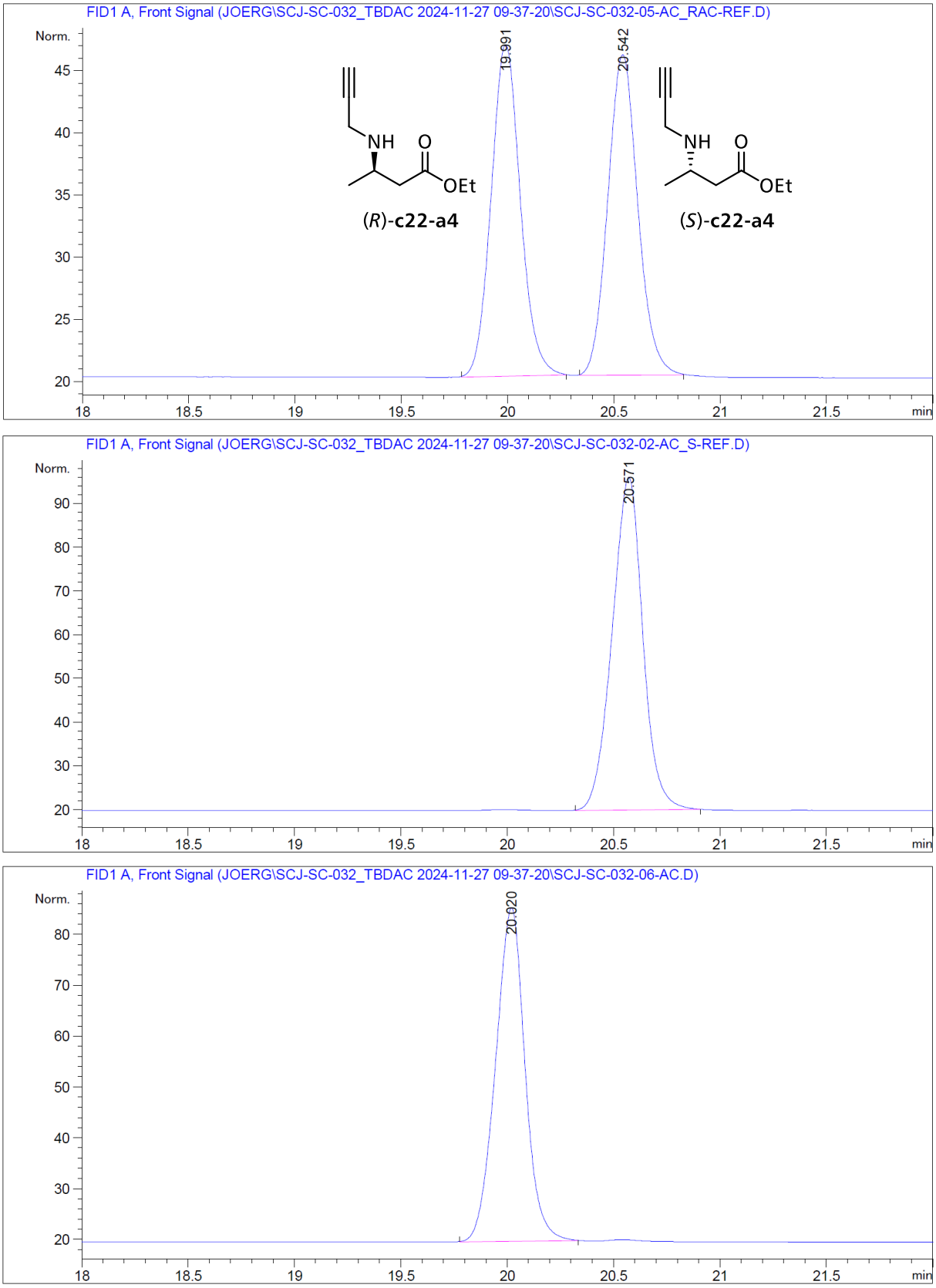


Figure S457. Determination of the enantiomeric excess of (*R*)-**c22-a4-Ac** using GC method GC-C6. Racemic reference (top), independently synthesised (*S*)-enantiomer (middle), biotransformation product (bottom).

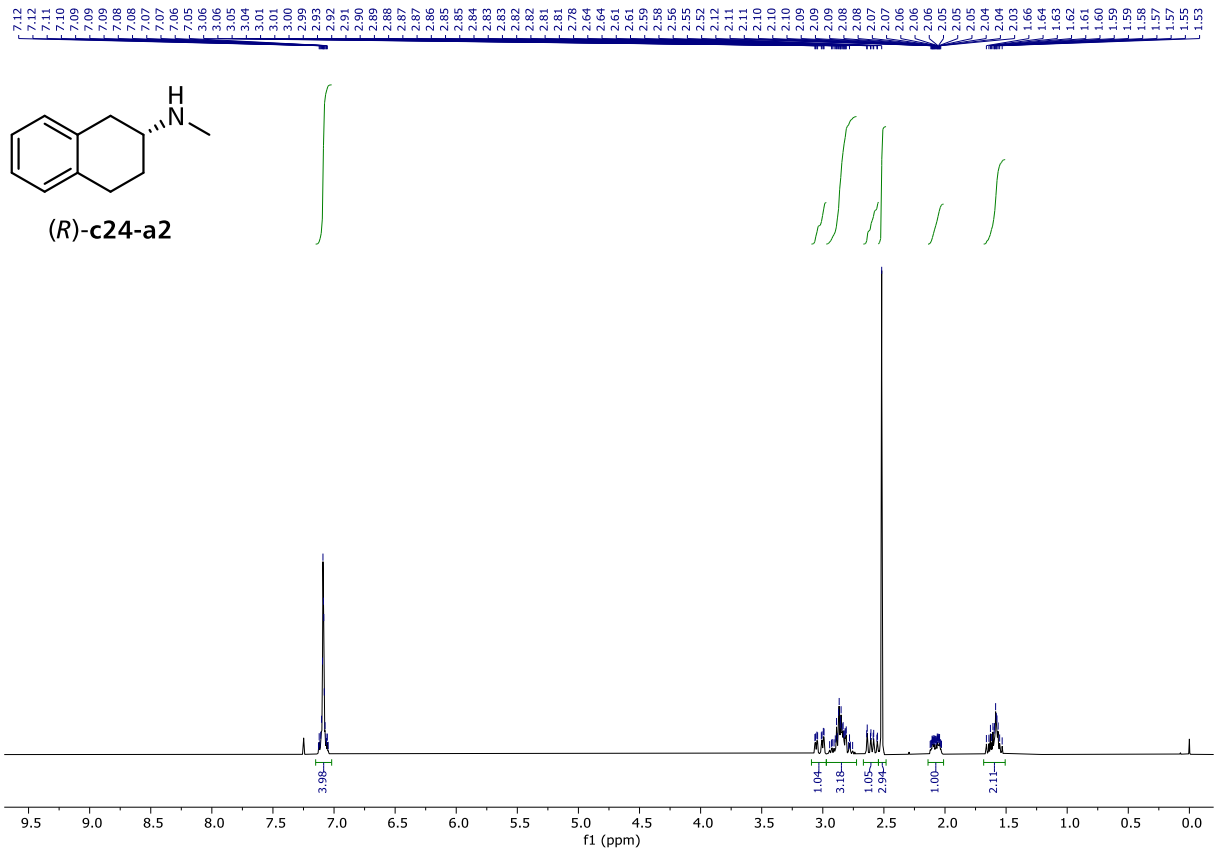


Figure S458. ^{1}H NMR spectrum of (*R*)-*N*-methyl-1,2,3,4-tetrahydronaphthalen-2-amine (**c24-a2**).

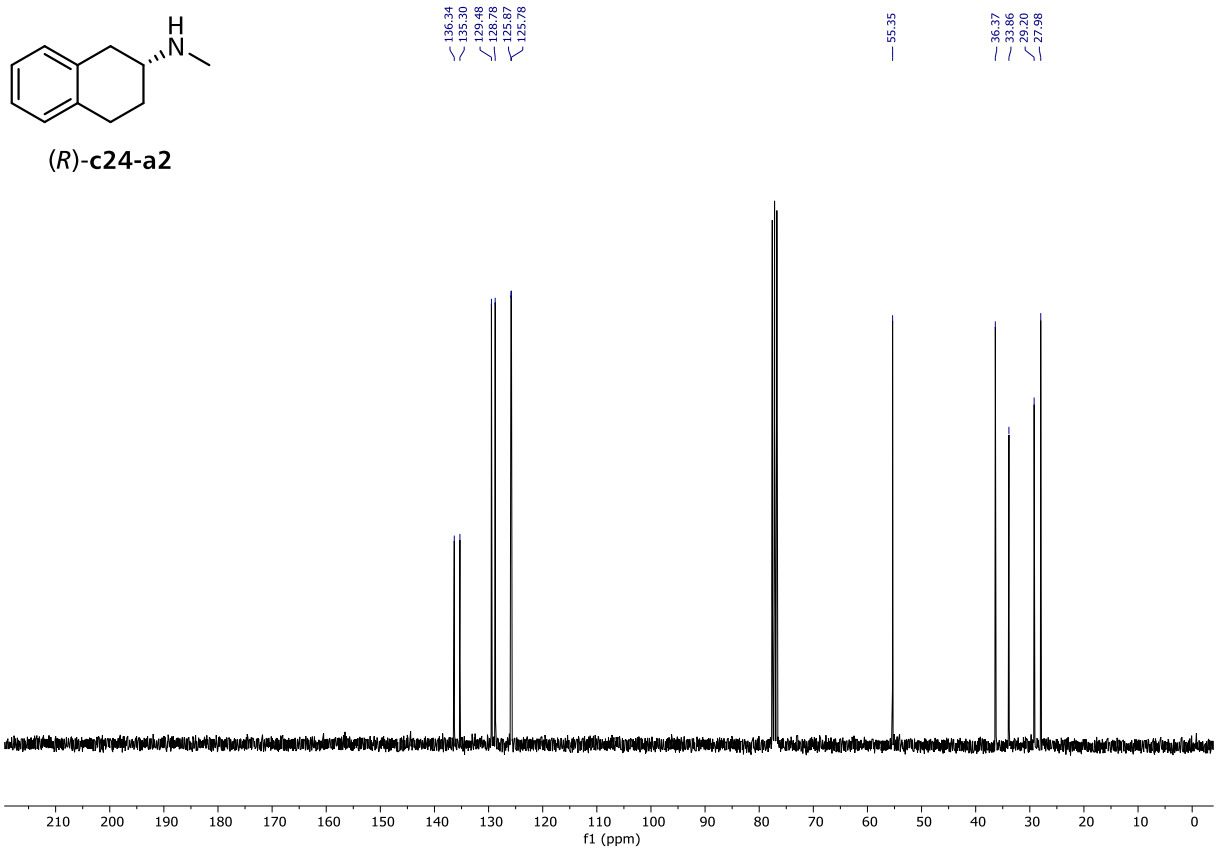


Figure S459. ^{13}C NMR spectrum of (*R*)-*N*-methyl-1,2,3,4-tetrahydronaphthalen-2-amine (**c24-a2**).

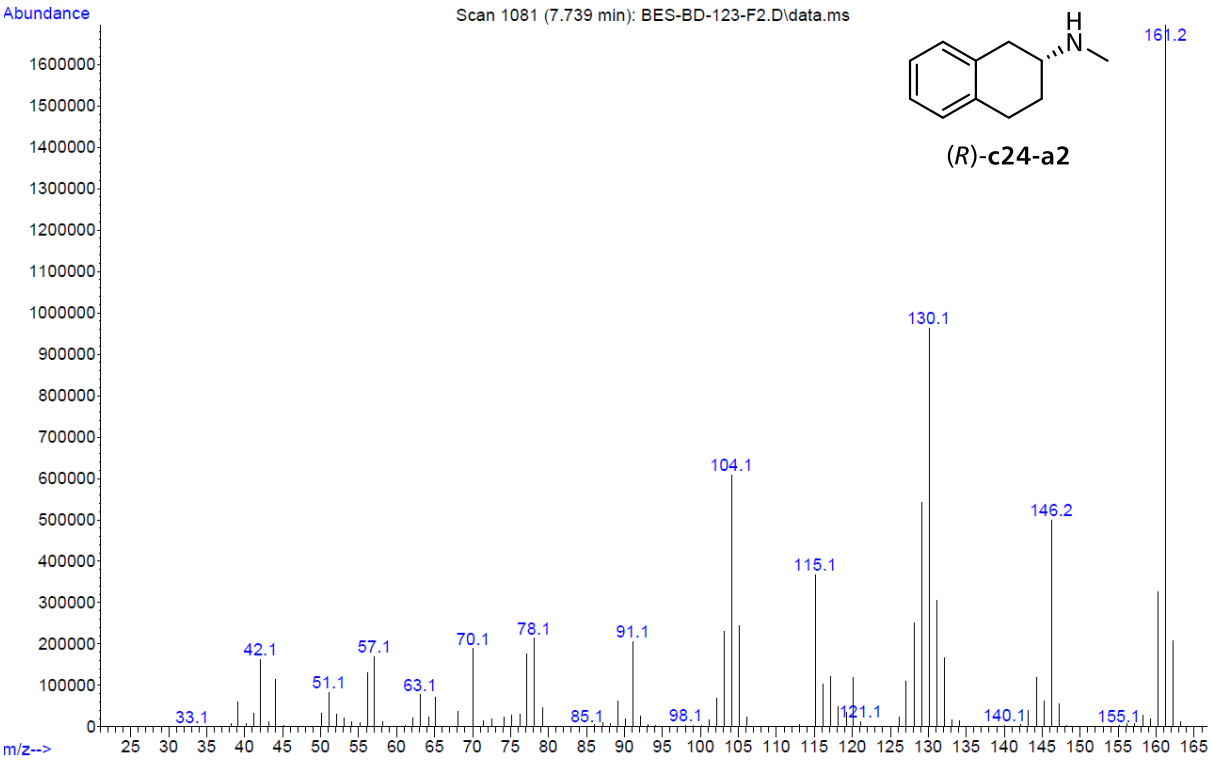


Figure S460. GC–MS spectrum of (*R*)-*N*-methyl-1,2,3,4-tetrahydronaphthalen-2-amine (**c24-a2**).

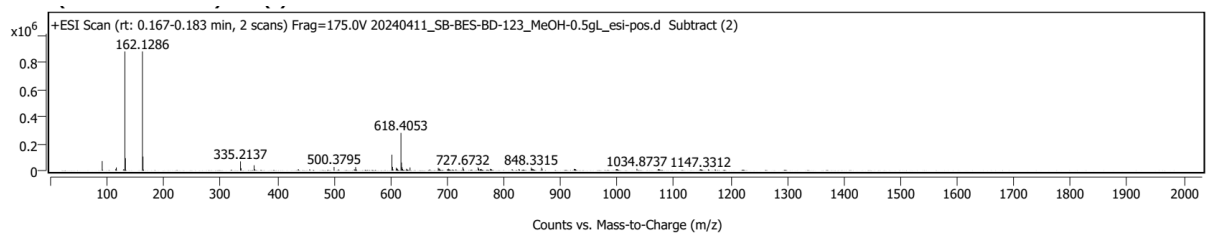


Figure S461. HRMS spectrum of (*R*)-*N*-methyl-1,2,3,4-tetrahydronaphthalen-2-amine (**c24-a2**).

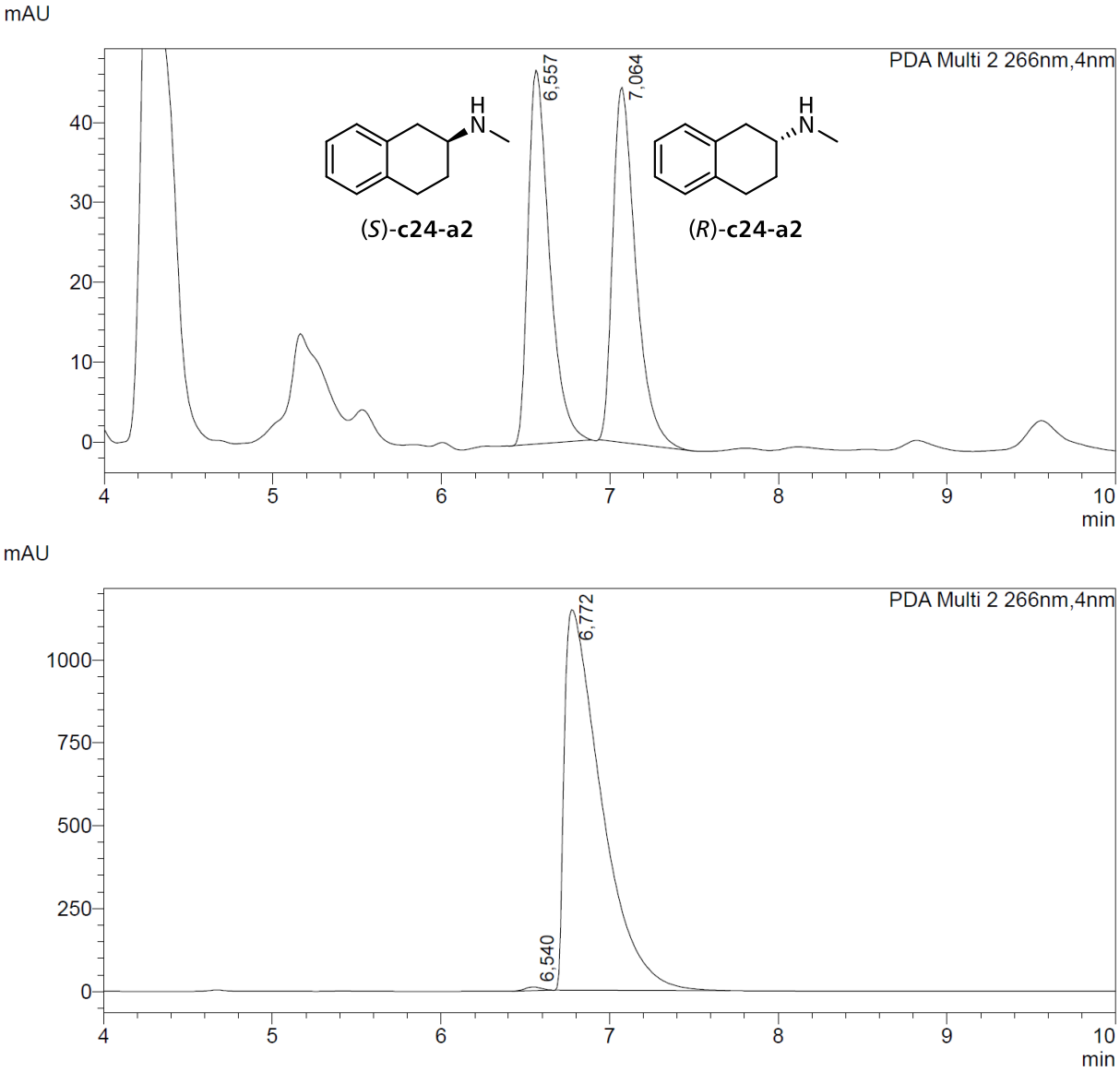


Figure S462. Determination of the enantiomeric excess and absolute configuration of (*R*)-**c24-a2** using HPLC method HPLC-C11. Racemic reference (top), biotransformation product (bottom). The peaks were assigned to the two enantiomers based on the elution order reported by Aleku *et al*. (2018).[119]

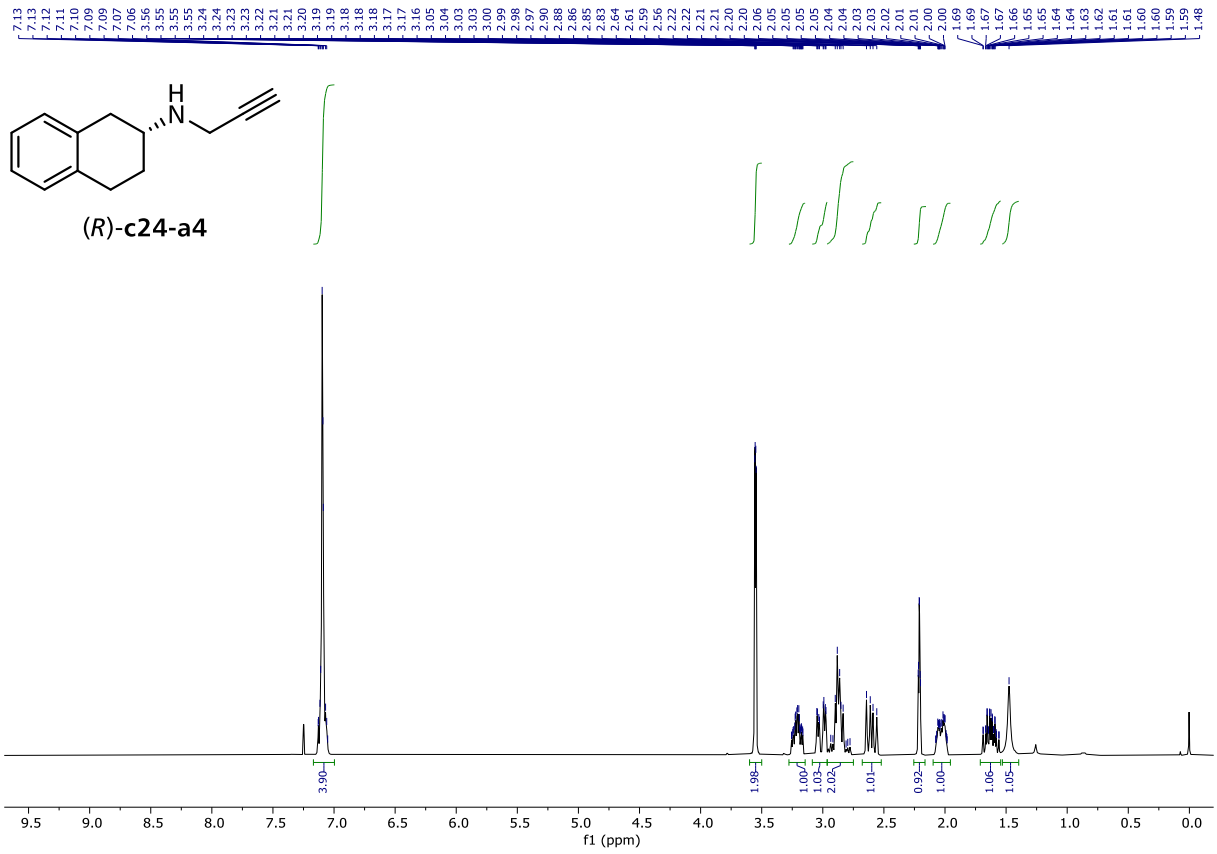


Figure S463. ^{1}H NMR spectrum of (*R*)-*N*-(prop-2-yn-1-yl)-1,2,3,4-tetrahydronaphthalen-2-amine (**c24-a4**).

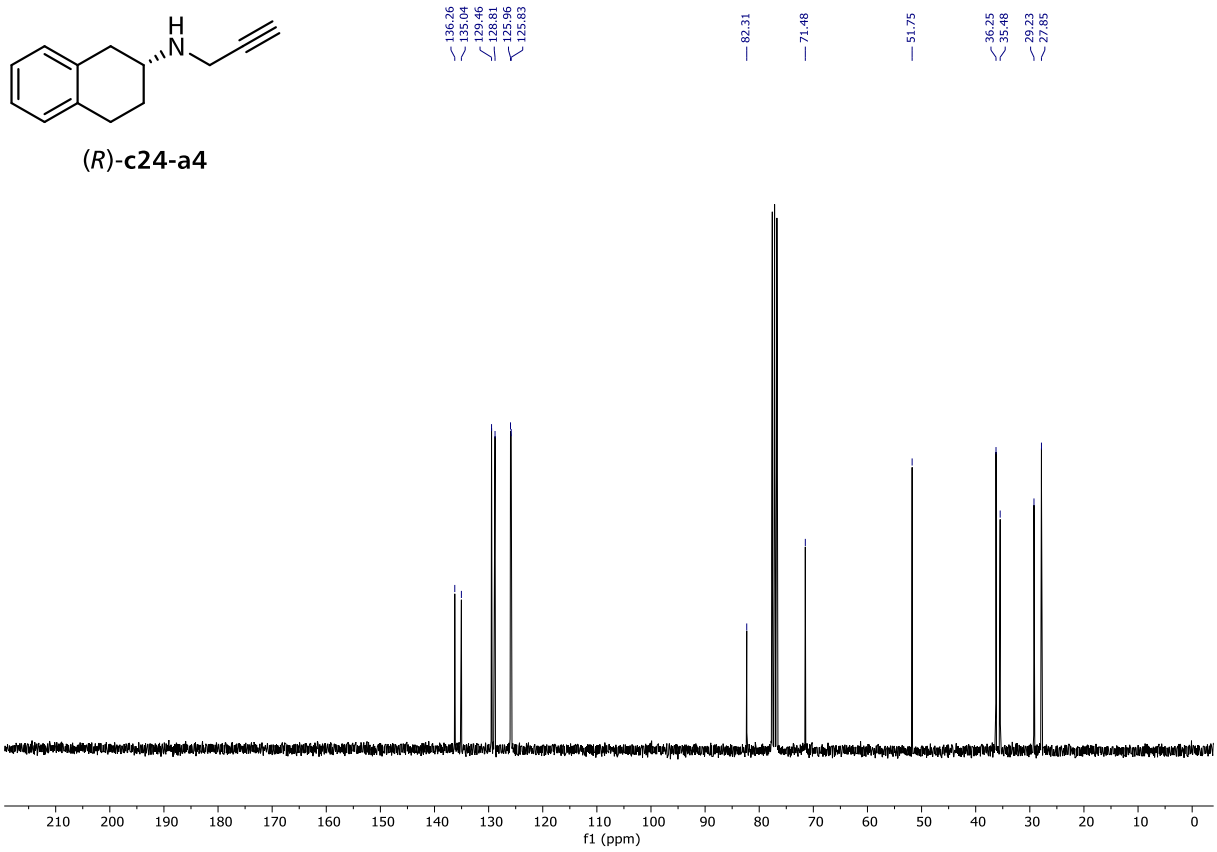


Figure S464. ^{13}C NMR spectrum of (*R*)-*N*-(prop-2-yn-1-yl)-1,2,3,4-tetrahydronaphthalen-2-amine (**c24-a4**).

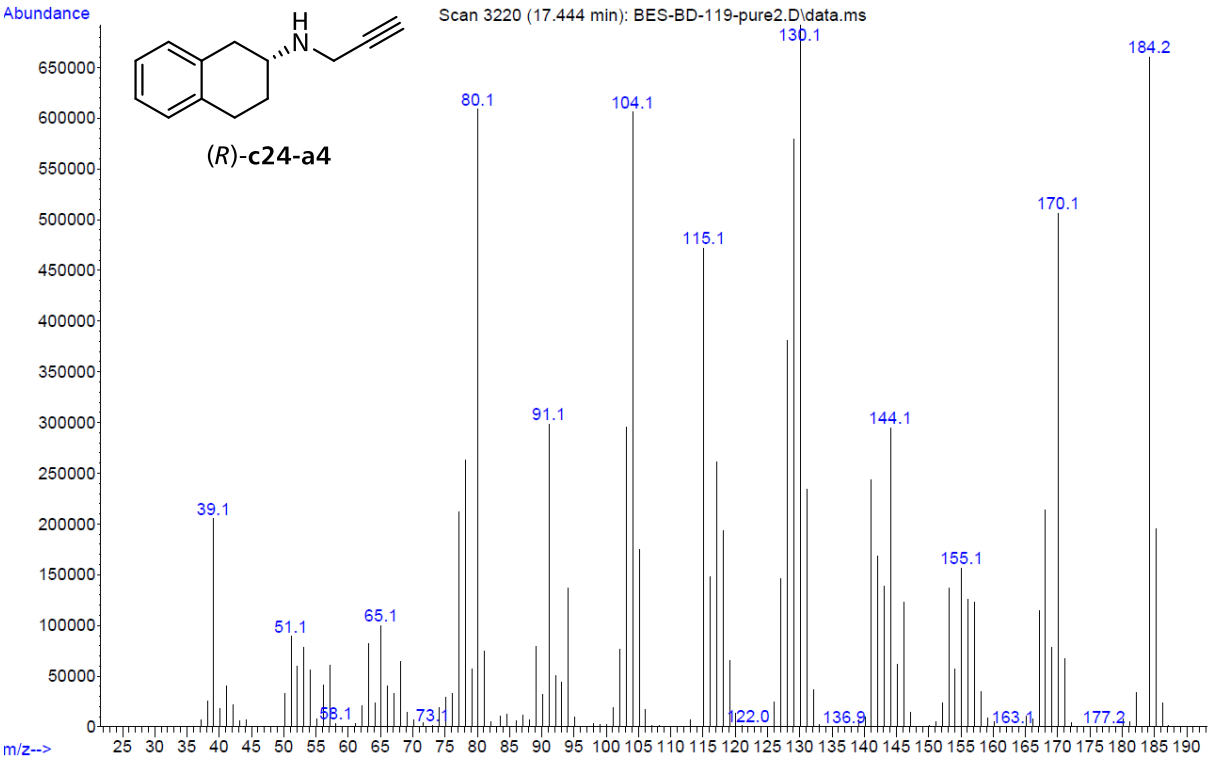


Figure S465. GC–MS spectrum of (*R*)-*N*-(prop-2-yn-1-yl)-1,2,3,4-tetrahydronaphthalen-2-amine (**c24-a4**).

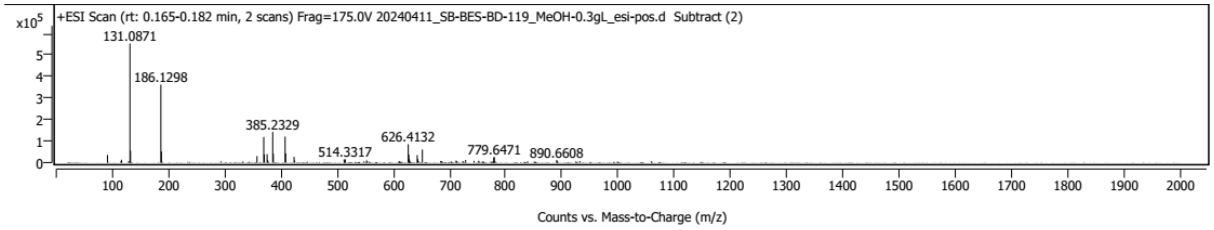


Figure S466. HRMS spectrum of (*R*)-*N*-(prop-2-yn-1-yl)-1,2,3,4-tetrahydronaphthalen-2-amine (**c24-a4**).

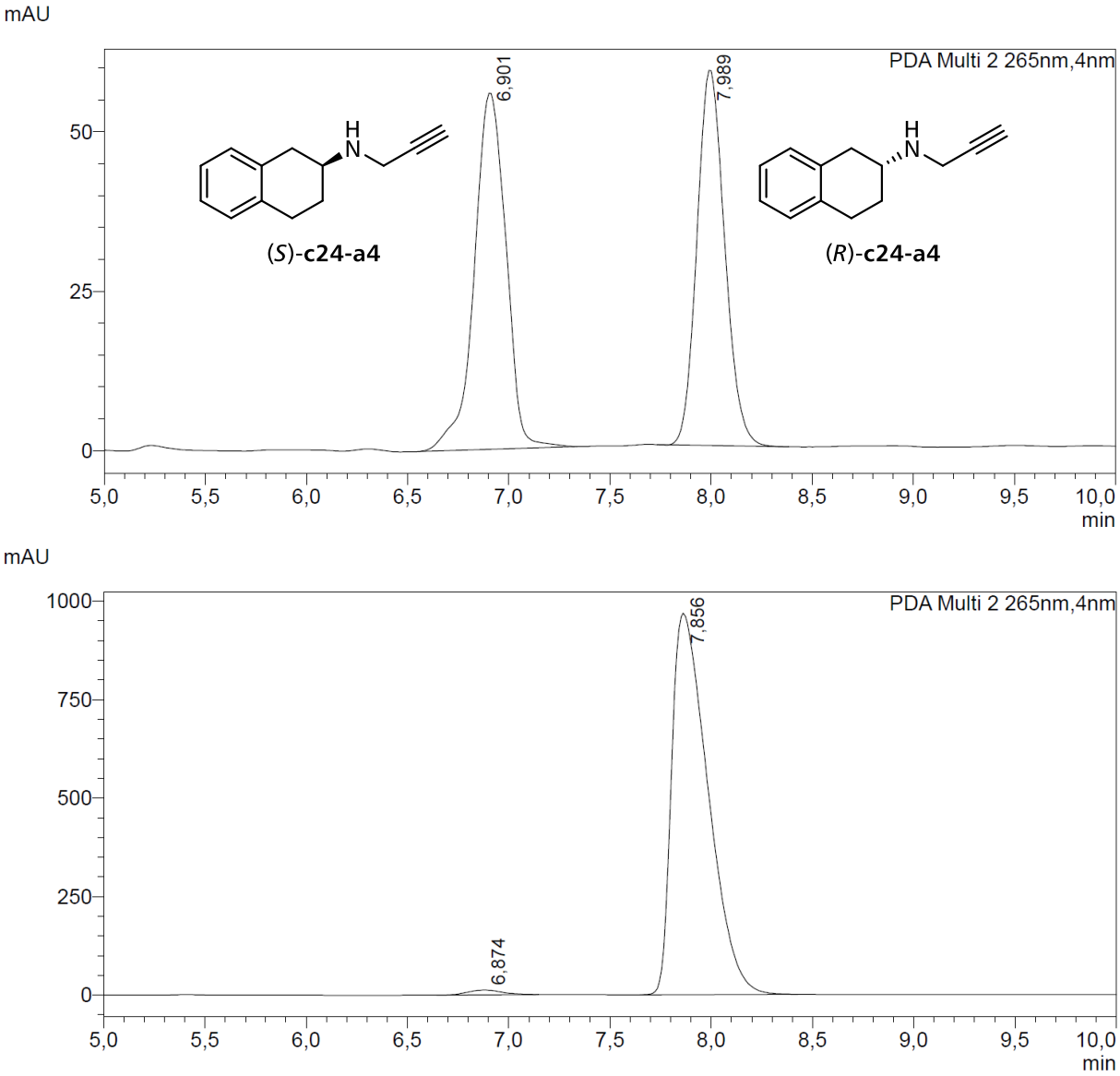


Figure S467. Determination of the enantiomeric excess and absolute configuration of (*R*)-**c24-a4** using HPLC method HPLC-C10. Racemic reference (top), biotransformation product (bottom). The peaks were assigned to the two enantiomers based on the elution order reported by Aleku *et al*. (2018).[119]

Supplementary References

1 R: A language and environment for statistical computing (R Foundation for Statistical Computing, Vienna, Austria, 2022).

2 Wetzl, D. *et al.* Expanding the Imine Reductase Toolbox by Exploring the Bacterial Protein-Sequence Space. *ChemBioChem* **16**, 1749–1756 (2015).

3 Wetzl, D. *et al.* Asymmetric Reductive Amination of Ketones Catalyzed by Imine Reductases. *ChemCatChem* **8**, 2023–2026 (2016).

4 Velikogne, S., Resch, V., Dertnig, C., Schrittwieser, J. H. & Kroutil, W. Sequence-Based *In-silico* Discovery, Characterisation, and Biocatalytic Application of a Set of Imine Reductases. *ChemCatChem* **10**, 3236–3246 (2018).

5 Gand, M., Müller, H., Wardenga, R. & Höhne, M. Characterization of three novel enzymes with imine reductase activity. *J. Mol. Catal. B: Enzym.* **110**, 126–132 (2014).

6 Man, H. *et al.* Structure, Activity and Stereoselectivity of NADPH-Dependent Oxidoreductases Catalysing the *S*-Selective Reduction of the Imine Substrate 2-Methylpyrroline. *ChemBioChem* **16**, 1052–1059 (2015).

7 Aleku, G. A. *et al.* A reductive aminase from *Aspergillus oryzae*. *Nat. Chem.* **9**, 961–969 (2017).

8 Roiban, G.-D. *et al.* Efficient Biocatalytic Reductive Aminations by Extending the Imine Reductase Toolbox. *ChemCatChem* **9**, 4475–4479 (2017).

9 Zhu, J. *et al.* Enantioselective Synthesis of 1-Aryl-Substituted Tetrahydroisoquinolines Employing Imine Reductase. *ACS Catal.* **7**, 7003–7007 (2017).

10 France, S. P. *et al.* Identification of Novel Bacterial Members of the Imine Reductase Enzyme Family that Perform Reductive Amination. *ChemCatChem* **10**, 510–514 (2018).

11 Mangas-Sanchez, J. *et al.* Asymmetric synthesis of primary amines catalyzed by thermotolerant fungal reductive aminases. *Chem. Sci.* **11**, 5052–5057 (2020).

12 Marshall, J. R. *et al.* Screening and characterization of a diverse panel of metagenomic imine reductases for biocatalytic reductive amination. *Nat. Chem.* **13**, 140–148 (2021).

13 Fademrecht, S., Scheller, P. N., Nestl, B. M., Hauer, B. & Pleiss, J. Identification of imine reductase-specific sequence motifs. *Proteins Struct. Funct. Bioinf.* **84**, 600–610 (2016).

14 Lenz, M. *et al.* New imine-reducing enzymes from β-hydroxyacid dehydrogenases by single amino acid substitutions. *Protein Eng. Des. Sel.* **31**, 109–120 (2018).

15 Stockinger, P., Roth, S., Müller, M. & Pleiss, J. Systematic Evaluation of Imine-Reducing Enzymes: Common Principles in Imine Reductases, β-Hydroxy Acid Dehydrogenases, and Short-Chain Dehydrogenases/ Reductases. *ChemBioChem* **21**, 2689–2695 (2020).

16 Stockinger, P. *et al.* Engineering of Thermostable β-Hydroxyacid Dehydrogenase for the Asymmetric Reduction of Imines. *ChemBioChem* **21**, 3511–3514 (2020).

17 Schober, M. *et al.* Chiral synthesis of LSD1 inhibitor GSK2879552 enabled by directed evolution of an imine reductase. *Nat. Catal.* **2**, 909–915 (2019).

18 Aleku, G. A. *et al.* Stereoselectivity and Structural Characterization of an Imine Reductase (IRED) from *Amycolatopsis orientalis*. *ACS Catal.* **6**, 3880–3889 (2016).

19 Sharma, M. *et al.* A Mechanism for Reductive Amination Catalyzed by Fungal Reductive Aminases. *ACS Catal.* **8**, 11534–11541 (2018).

20 Montgomery, S. L. *et al.* Characterization of imine reductases in reductive amination for the exploration of structure-activity relationships. *Sci. Adv.* **6**, eaay9320 (2020).

21 Ducrot, L., Bennett, M., Grogan, G. & Vergne-Vaxelaire, C. NAD(P)H-Dependent Enzymes for Reductive Amination: Active Site Description and Carbonyl-Containing Compound Spectrum. *Adv. Synth. Catal.* **363**, 328–351 (2021).

22 Gooderham, J. *et al.* Improved stereocontrol in reductive aminases through steric modification of residues around substrate and cofactor binding pockets. *Catal. Sci. Technol.* **15**, 3113–3121 (2025).

23 Xing, J. *et al.* Functional Mapping of Key Residues in Reductive Aminases Enabled by a High-Throughput *RedAm Detect* Assay. *JACS Au* **5**, 3468–3482 (2025).

24 Brennan, C. K. *et al.* Data Driven Discovery of Reductive Aminases for Arylamine Substrates. *Adv. Synth. Catal.* **368**, e70527 (2026).

25 Aleku, G. A. Imine Reductases and Reductive Aminases in Organic Synthesis. *ACS Catal.* **14**, 14308–14329 (2024).

26 Santos-Martins, D. *et al.* Meeko: Molecule Parametrization and Software Interoperability for Docking and Beyond. *J. Chem. Inf. Model.* **65**, 13045–13050 (2025).

27 Eberhardt, J., Santos-Martins, D., Tillack, A. F. & Forli, S. AutoDock Vina 1.2.0: New Docking Methods, Expanded Force Field, and Python Bindings. *J. Chem. Inf. Model.* **61**, 3891–3898 (2021).

28 Trott, O. & Olson, A. J. AutoDock Vina: Improving the speed and accuracy of docking with a new scoring function, efficient optimization, and multithreading. *J. Comput. Chem.* **31**, 455–461 (2010).

29 Berger, S. *et al.* Process for the reduction of aromatic imines with novel imine reductases (IREDs). International patent WO2025017089A1 (2025).

30 Passaro, S. *et al.* Boltz-2: Towards Accurate and Efficient Binding Affinity Prediction. *bioRxiv*, 2025.06.14.659707 (2025). https://doi.org/10.1101/2025.06.14.659707.

31 Casamajo, A. R. *et al.* Biocatalysis in Drug Design: Engineered Reductive Aminases (RedAms) Are Used to Access Chiral Building Blocks with Multiple Stereocenters. *J. Am. Chem. Soc.* **145**, 22041–22046 (2023).

32 González-Martínez, D. *et al.* Asymmetric Synthesis of Primary and Secondary β-Fluoroarylamines using Reductive Aminases from Fungi. *ChemCatChem* **12**, 2421–2425 (2020).

33 Burke, A. J. *et al.* Engineered Biocatalysts for Enantioselective Reductive Aminations of Cyclic Secondary Amines. *ChemCatChem* **15**, e202300256 (2023).

34 Molecular Operating Environment (MOE) v. 2022.02 (Chemical Computing Group ULC, Montreal, Canada, 2023).

35 Gerber, P. R. & Müller, K. MAB, a generally applicable molecular force field for structure modelling in medicinal chemistry. *J. Comput. Aided Mol. Des.* **9**, 251–268 (1995).

36 Milletti, F. *et al.* Extending pK_a prediction accuracy: High-throughput pK_a measurements to understand pK_a modulation of new chemical series. *Eur. J. Med. Chem.* **45**, 4270-4279 (2010).

37 Bochevarov, A. D. *et al.* Jaguar: A high-performance quantum chemistry software program with strengths in life and materials sciences. *Int. J. Quantum Chem* **113**, 2110–2142 (2013).

38 Schrödinger Release 2023-3: Jaguar (Schrödinger, LLC, New York, USA, 2023).

39 Broccatelli, F., Trager, R., Reutlinger, M., Karypis, G. & Li, M. Benchmarking Accuracy and Generalizability of Four Graph Neural Networks Using Large In Vitro ADME Datasets from Different Chemical Spaces. *Mol. Inform.* **41**, 2100321 (2022).

40 Waterhouse, A. M., Procter, J. B., Martin, D. M. A., Clamp, M. & Barton, G. J. Jalview Version 2—a multiple sequence alignment editor and analysis workbench. *Bioinformatics* **25**, 1189–1191 (2009).

41 Sievers, F. & Higgins, D. G. in *Multiple Sequence Alignment Methods*. (ed David J. Russell) 105–116 (Humana Press, 2014).

42 Letunic, I. & Bork, P. Interactive Tree Of Life (iTOL) v5: an online tool for phylogenetic tree display and annotation. *Nucleic Acids Res.* **49**, W293–W296 (2021).

43 Meyer, T., Zumbrägel, N., Geerds, C., Gröger, H. & Niemann, H. H. Structural Characterization of an S-enantioselective Imine Reductase from Mycobacterium Smegmatis. *Biomolecules* **10**, 1130 (2020).

44 Stockinger, P. *et al.* Inverting the Stereoselectivity of an NADH-Dependent Imine-Reductase Variant. *ChemCatChem* **13**, 5210–5215 (2021).

45 Lokanath, N. K. *et al.* Crystal Structure of Novel NADP-dependent 3-Hydroxyisobutyrate Dehydrogenase from Thermus thermophilus HB8. *J. Mol. Biol.* **352**, 905–917 (2005).

46 France, S. P. *et al.* Biocatalytic Routes to Enantiomerically Enriched Dibenz[*c*,*e*]azepines. *Angew. Chem. Int. Ed.* **56**, 15589–15593 (2017).

47 Cheng, Z., Sun, L., He, J. & Gong, W. Crystal structure of human μ-crystallin complexed with NADPH. *Protein Sci.* **16**, 329–335 (2007).

48 Huber, T. *et al.* Direct Reductive Amination of Ketones: Structure and Activity of *S*-Selective Imine Reductases from *Streptomyces*. *ChemCatChem* **6**, 2248–2252 (2014).

49 Borel, F., Hachi, I., Palencia, A., Gaillard, M.-C. & Ferrer, J.-L. Crystal structure of mouse mu-crystallin complexed with NADPH and the T3 thyroid hormone. *FEBS J.* **281**, 1598–1612 (2014).

50 Steinegger, M. & Söding, J. MMseqs2 enables sensitive protein sequence searching for the analysis of massive data sets. *Nat. Biotechnol.* **35**, 1026–1028 (2017).

51 Moriwaki, H., Tian, Y.-S., Kawashita, N. & Takagi, T. Mordred: a molecular descriptor calculator. *J. Cheminform.* **10**, 4 (2018).

52 Pedregosa, F. *et al.* Scikit-learn: Machine Learning in Python. *J. Mach. Learn. Res.* **12**, 2825−2830 (2011).

53 Chen, T. & Guestrin, C. in *Proceedings of the 22nd ACM SIGKDD International Conference on Knowledge Discovery and Data Mining*. 785–794 (Association for Computing Machinery).

54 Li, H., Tian, P., Xu, J.-H. & Zheng, G.-W. Identification of an Imine Reductase for Asymmetric Reduction of Bulky Dihydroisoquinolines. *Org. Lett.* **19**, 3151–3154 (2017).

55 Hoelsch, K., Sührer, I., Heusel, M. & Weuster-Botz, D. Engineering of formate dehydrogenase: synergistic effect of mutations affecting cofactor specificity and chemical stability. *Appl. Microbiol. Biotechnol.* **97**, 2473–2481 (2013).

56 Pometun, A. A. *et al.* Influence of His_6 Sequence on the Properties of Formate Dehydrogenase from Bacterium *Pseudomonas* sp. 101. *Moscow University Chemistry Bulletin* **75**, 250–257 (2020).

57 Calzadiaz-Ramirez, L. *et al. In Vivo* Selection for Formate Dehydrogenases with High Efficiency and Specificity toward $NADP^+$. *ACS Catal.* **10**, 7512–7525 (2020).

58 Makino, Y., Negoro, S., Urabe, I. & Okada, H. Stability-increasing Mutants of Glucose Dehydrogenase from *Bacillus megaterium* IWG3. *J. Biol. Chem.* **264**, 6381–6385 (1989).

59 Lampel, K. A., Uratani, B., Chaudhry, G. R., Ramaley, R. F. & Rudikoff, S. Characterization of the developmentally regulated *Bacillus subtilis* glucose dehydrogenase gene. *J. Bacteriol.* **166**, 238–243 (1986).

60 Johannes, T. W., Woodyer, R. D. & Zhao, H. Directed Evolution of a Thermostable Phosphite Dehydrogenase for NAD(P)H Regeneration. *Appl. Environ. Microbiol.* **71**, 5728–5734 (2005).

61 Bradford, M. M. A rapid and sensitive method for the quantitation of microgram quantities of protein utilizing the principle of protein-dye binding. *Anal. Biochem.* **72**, 248–254 (1976).

62 Schneider, C. A., Rasband, W. S. & Eliceiri, K. W. NIH Image to ImageJ: 25 years of image analysis. *Nat. Methods* **9**, 671–675 (2012).

63 Berger, S. A. *et al.* Rapid, Label-Free Screening of Diverse Biotransformations by Flow-Injection Mass Spectrometry. *ChemBioChem* **24**, e202300170 (2023).

64 Jarque, C. M. & Bera, A. K. A Test for Normality of Observations and Regression Residuals. *Int. Stat. Rev.* **55**, 163–172 (1987).

65 Shapiro, S. S. & Wilk, M. B. An analysis of variance test for normality (complete samples). *Biometrika* **52**, 591–611 (1965).

66 Dong, L., Aleem, S. & Fink, C. A. Microwave-accelerated reductive amination between ketones and ammonium acetate. *Tetrahedron Lett.* **51**, 5210–5212 (2010).

67 Salmi, C., Loncle, C., Letourneux, Y. & Brunel, J. M. Efficient preparation of secondary aminoalcohols through a Ti(IV) reductive amination procedure. Application to the synthesis and antibacterial evaluation of new 3β-*N*-[hydroxyalkyl]aminosteroid derivatives. *Tetrahedron* **64**, 4453–4459 (2008).

68 Montgomery, S. L. *et al.* Direct Alkylation of Amines with Primary and Secondary Alcohols through Biocatalytic Hydrogen Borrowing. *Angew. Chem. Int. Ed.* **56**, 10491–10494 (2017).

69 Cao, C.-S. *et al.* Highly Efficient Conversion of Propargylic Amines and CO_2 Catalyzed by Noble-Metal-Free [Zn_{116}] Nanocages. *Angew. Chem. Int. Ed.* **59**, 8586–8593 (2020).

70 Adams, M. R., Tien, C.-H., Huchenski, B. S. N., Ferguson, M. J. & Speed, A. W. H. Diazaphospholene Precatalysts for Imine and Conjugate Reductions. *Angew. Chem. Int. Ed.* **56**, 6268–6271 (2017).

71 Chatterjee, I. & Oestreich, M. $B(C_6F_5)_3$-Catalyzed Transfer Hydrogenation of Imines and Related Heteroarenes Using Cyclohexa-1,4-dienes as a Dihydrogen Source. *Angew. Chem. Int. Ed.* **54**, 1965–1968 (2015).

72 Quinet, C. *et al.* Highly efficient, base-catalysed, intramolecular hydroamination of non-activated olefins. *Tetrahedron* **64**, 1077–1087 (2008).

73 Boga, C., Manescalchi, F. & Savoia, D. Diastereoselective synthesis of 2,5-dimethylpyrrolidines and 2,6-dimethylpiperidines by reductive amination of 2,5-hexanedione and 2,6-heptanedione with hydride reagents. *Tetrahedron* **50**, 4709–4722 (1994).

74 Varjosaari, S. E. *et al.* Simple Metal-Free Direct Reductive Amination Using Hydrosilatrane to Form Secondary and Tertiary Amines. *Adv. Synth. Catal.* **359**, 1872–1878 (2017).

75 Wu, K., He, W., Sun, C. & Yu, Z. Scalable synthesis of secondary and tertiary amines by heterogeneous Pt-Sn/γ-Al2O3 catalyzed N-alkylation of amines with alcohols. *Tetrahedron* **72**, 8516–8521 (2016).

76 Arcelli, A., Cecchi, R., Porzi, G., Rinaldi, S. & Sandri, S. Mechanistic investigation of an anomalous anchimeric assistance in the acid hydrolysis of the ether linkage. Part 4. *Tetrahedron* **57**, 4039–4043 (2001).

77 Martínez-Montero, L., Díaz-Rodríguez, A., Gotor, V., Gotor-Fernández, V. & Lavandera, I. Broadening the chemical scope of laccases: selective deprotection of *N*-benzyl groups. *Green Chem.* **17**, 2794–2798 (2015).

78 Kunalan, V., Nic Daéid, N., Kerr, W. J., Buchanan, H. A. S. & McPherson, A. R. Characterization of Route Specific Impurities Found in Methamphetamine Synthesized by the Leuckart and Reductive Amination Methods. *Anal. Chem.* **81**, 7342–7348 (2009).

79 Albarrán-Velo, J., Gotor-Fernández, V. & Lavandera, I. Markovnikov Wacker-Tsuji Oxidation of Allyl(hetero)arenes and Application in a One-Pot Photo-Metal-Biocatalytic Approach to Enantioenriched Amines and Alcohols. *Adv. Synth. Catal.* **363**, 4096–4108 (2021).

80 Aldrich, K. E. & Odom, A. L. Titanium-Catalyzed Hydroamination and Multicomponent Coupling with a Simple Silica-Supported Catalyst. *Organometallics* **37**, 4341–4349 (2018).

81 Bach, M. V., Coutts, R. T. & Baker, G. B. Metabolism of *N*,*N*-dialkylated amphetamines, including deprenyl, by CYP2D6 expressed in a human cell line. *Xenobiotica* **30**, 297–306 (2000).

82 Guisado, C., Waterhouse, J. E., Price, W. S., Jorgensen, M. R. & Miller, A. D. The facile preparation of primary and secondary amines via an improved Fukuyama–Mitsunobu procedure. Application to the synthesis of a lung-targeted gene delivery agent. *Org. Biomol. Chem.* **3**, 1049–1057 (2005).

83 Hamid, M. H. S. A. *et al.* Ruthenium-Catalyzed *N*-Alkylation of Amines and Sulfonamides Using Borrowing Hydrogen Methodology. *J. Am. Chem. Soc.* **131**, 1766–1774 (2009).

84 Heutling, A. & Doye, S. $Cp^*_2TiMe_2$: An Improved Catalyst for the Intermolecular Addition of *n*-Alkyl- and Benzylamines to Alkynes. *J. Org. Chem.* **67**, 1961–1964 (2002).

85 Ledoux, A., Sandjong Kuigwa, L., Framery, E. & Andrioletti, B. A highly sustainable route to pyrrolidone derivatives – direct access to biosourced solvents. *Green Chem.* **17**, 3251–3254 (2015).

86 Sun, Z., Chen, J. & Tu, T. NHC-based coordination polymers as solid molecular catalysts for reductive amination of biomass levulinic acid. *Green Chem.* **19**, 789–794 (2017).

87 Muzzio, M. *et al.* Reductive amination of ethyl levulinate to pyrrolidones over AuPd nanoparticles at ambient hydrogen pressure. *Green Chem.* **21**, 1895–1899 (2019).

88 Nacario, R., Kotakonda, S., Fouchard, D. M. D., Tillekeratne, L. M. V. & Hudson, R. A. Reductive Monoalkylation of Aromatic and Aliphatic Nitro Compounds and the Corresponding Amines with Nitriles. *Org. Lett.* **7**, 471–474 (2005).

89 Kuchuk, E., Muratov, K., Perekalin, D. S. & Chusov, D. Anthracene–rhodium complexes with metal coordination at the central ring – a new class of catalysts for reductive amination. *Org. Biomol. Chem.* **17**, 83–87 (2019).

90 Kolesnikov, P. N., Yagafarov, N. Z., Usanov, D. L., Maleev, V. I. & Chusov, D. Ruthenium-Catalyzed Reductive Amination without an External Hydrogen Source. *Org. Lett.* **17**, 173–175 (2015).

91 Zhang, J. *et al.* Tuning an Imine Reductase for the Asymmetric Synthesis of Azacycloalkylamines by Concise Structure-Guided Engineering. *Angew. Chem. Int. Ed.* **61**, e202201908 (2022).

92 Xu, B. *et al.* 3-Amino nafoxidine-containing quinazoline ketone PARP (Poly Adenosine Diphosphate Ribose Polymerase)-1/2 inhibitor as well as preparation method, medicinal composition and application thereof. Chinese patent CN108727343A (2018).

93 Jean, L., Rouden, J., Maddaluno, J. & Lasne, M.-C. Palladium-Mediated Arylation of 3-Aminopiperidines and 3-Aminopyrrolidines. *J. Org. Chem.* **69**, 8893–8902 (2004).

94 Kuang, Y., Ning, Y., Zhu, J. & Wang, Y. Dirhodium(II)-Catalyzed (3 + 2) Cycloaddition of the *N*-Arylaminocyclopropane with Alkene Derivatives. *Org. Lett.* **20**, 2693–2697 (2018).

95 Tokuda, M., Yamada, Y., Takagi, T., Suginome, H. & Furusaki, A. Cyclization of aminyl radicals generated by anodic oxidation of lithium alkenylamides. Stereo- and regioselective synthesis of *cis*-1-alkyl-2,5-disubstituted pyrrolidines. *Tetrahedron* **43**, 281–296 (1987).

96 Wei, D., Netkaew, C. & Darcel, C. Iron-Catalysed Switchable Synthesis of Pyrrolidines vs Pyrrolidinones by Reductive Amination of Levulinic Acid Derivatives *via* Hydrosilylation. *Adv. Synth. Catal.* **361**, 1781–1786 (2019).

97 Bartoli, G., Cimarelli, C., Marcantoni, E., Palmieri, G. & Petrini, M. Chemo- and Diastereoselective Reduction of β-Enamino Esters: A Convenient Synthesis of Both *cis*- and *trans*-γ-Amino Alcohols and β-Amino Esters. *J. Org. Chem.* **59**, 5328–5335 (1994).

98 Meiring, L., Petzer, J. P., Legoabe, L. J. & Petzer, A. The evaluation of *N*-propargylamine-2-aminotetralin as an inhibitor of monoamine oxidase. *Bioorg. Med. Chem. Lett.* **67**, 128746 (2022).

99 Brinkmann, C., Barrett, A. G. M., Hill, M. S. & Procopiou, P. A. Heavier Alkaline Earth Catalysts for the Intermolecular Hydroamination of Vinylarenes, Dienes, and Alkynes. *J. Am. Chem. Soc.* **134**, 2193–2207 (2012).

100 Li, G., Liu, Y. & Du, H. $B(C_6F_5)_3$-catalyzed metal-free hydrogenation of naphthylamines. *Org. Biomol. Chem.* **13**, 2875–2878 (2015).

101 Bachu, P., Zhu, C. & Akiyama, T. Molecular iodine catalyzed transfer hydrogenation: reduction of aldimines, ketimines, and α-imino esters. *Tetrahedron Lett.* **54**, 3977–3981 (2013).

102 Kim, T. *et al.* Mechanistic investigation of electrocatalytic reductive amination at copper electrode. *Chem. Commun.* **59**, 4818–4821 (2023).

103 Miki, Y., Hirano, K., Satoh, T. & Miura, M. Copper-Catalyzed Intermolecular Regioselective Hydroamination of Styrenes with Polymethylhydrosiloxane and Hydroxylamines. *Angew. Chem. Int. Ed.* **52**, 10830–10834 (2013).

104 Zhang, S. *et al.* Visible-Light-Induced Multicomponent Reaction of Aromatic Aldehydes, Amines and Sodium Difluoromethanesulfinate: Synthesis of CF_2H-Substituted Secondary Amines. *Adv. Synth. Catal.* **365**, 4132–4137 (2023).

105 Chen, H. J., Hong Xiang Teo, R., Li, Y., Pullarkat, S. A. & Leung, P.-H. Stereogenic Lock in 1-Naphthylethanamine Complexes for Catalyst and Auxiliary Design: Structural and Reactivity Analysis for Cycloiridated Pseudotetrahedral Complexes. *Organometallics* **37**, 99–106 (2018).

106 Cervantes-Reyes, A. *et al.* Expanded Ring NHC Silver Carboxylate Complexes as Efficient and Reusable Catalysts for the Carboxylative Cyclization of Unsubstituted Propargylic Derivatives. *ChemSusChem* **14**, 2367–2374 (2021).

107 Zhang, Y. *et al.* Controllable encapsulation of silver nanoparticles by porous pyridine-based covalent organic frameworks for efficient CO_2 conversion using propargylic amines. *Green Chem.* **24**, 930–940 (2022).

108 Short, R. P., Kennedy, R. M. & Masamune, S. An improved synthesis of (–)-(2*R*,5*R*)-2,5-dimethylpyrrolidine. *J. Org. Chem.* **54**, 1755–1756 (1989).

109 House, H. O. & Lee, L. F. New synthesis of 2-alkylpyrrolidines and 2-alkylpiperidines. *J. Org. Chem.* **41**, 863–869 (1976).

110 Gribkov, D. V. & Hultzsch, K. C. Hydroamination/Cyclization of Aminoalkenes Using Cationic Zirconocene and Titanocene Catalysts. *Angew. Chem. Int. Ed.* **43**, 5542–5546 (2004).

111 Zhang, Y., Yang, X., Yao, Q. & Ma, D. CuI/DMPAO-Catalyzed *N*-Arylation of Acyclic Secondary Amines. *Org. Lett.* **14**, 3056–3059 (2012).

112 González-Martínez, D., Gotor, V. & Gotor-Fernández, V. Stereoselective Synthesis of 1-Arylpropan-2-amines from Allylbenzenes through a Wacker-Tsuji Oxidation-Biotransamination Sequential Process. *Adv. Synth. Catal.* **361**, 2582–2593 (2019).

113 Pressnitz, D. *et al.* Asymmetric Amination of Tetralone and Chromanone Derivatives Employing ω-Transaminases. *ACS Catal.* **3**, 555–559 (2013).

114 Cho, J. H. & Kim, B. M. LiOH-mediated *N*-monoalkylation of α-amino acid esters and a dipeptide ester using activated alkyl bromides. *Tetrahedron Lett.* **43**, 1273–1276 (2002).

115 Yang, Q., Lai, Y.-Y., Xiao, W.-J. & Alper, H. Efficient synthesis of 4-vinyl α,β-unsaturated γ-lactams by ring-closing enyne metathesis reactions. *Tetrahedron Lett.* **49**, 7334–7336 (2008).

116 Aaseng, J. E., Melnes, S., Reian, G. & Gautun, O. R. Asymmetric catalytic aziridination of dihydronaphthalenes for the preparation of substituted 2-aminotetralins. *Tetrahedron* **66**, 9790–9797 (2010).

117 Kawada, T. *et al.* Asymmetric Transfer Hydrogenative Amination of Benzylic Ketones Catalyzed by Cp*Ir(III) Complexes Bearing a Chiral *N*-(2-Picolyl)sulfonamidato Ligand. *J. Org. Chem.* **87**, 8458–8468 (2022).

118 Gergel, S. *et al.* Engineered cytochrome P450 for direct arylalkene-to-ketone oxidation via highly reactive carbocation intermediates. *Nat. Catal.* **6**, 606–617 (2023).

119 Aleku, G. A. *et al.* Kinetic Resolution and Deracemization of Racemic Amines Using a Reductive Aminase. *ChemCatChem* **10**, 515–519 (2018).